Large Rivers
Geomorphology and Management

Edited by Avijit Gupta

School of Geography, University of Leeds, UK

and

Centre for Remote Imaging, Sensing and Processing,
National University of Singapore, Singapore

John Wiley & Sons, Ltd

Large Rivers

Large Rivers
Geomorphology and Management

Edited by Avijit Gupta

School of Geography, University of Leeds, UK

and

Centre for Remote Imaging, Sensing and Processing,
National University of Singapore, Singapore

John Wiley & Sons, Ltd

Other Wiley Editorial Offices

John Wiley & Sons Inc., 111 River Street, Hoboken, NJ 07030, USA

Jossey-Bass, 989 Market Street, San Francisco, CA 94103-1741, USA

Wiley-VCH Verlag GmbH, Boschstr. 12, D-69469 Weinheim, Germany

John Wiley & Sons Australia Ltd, 42 McDougall Street, Milton, Queensland 4064, Australia

John Wiley & Sons (Asia) Pte Ltd, 2 Clementi Loop #02-01, Jin Xing Distripark, Singapore 129809

John Wiley & Sons Ltd, 6045 Freemont Blvd, Mississauga, Ontario L5R 4J3, Canada

Wiley also publishes its books in a variety of electronic formats. Some content that appears in print may not be available in electronic books.

Anniversary Logo Design: Richard J. Pacifico

Library of Congress Cataloging-in-Publication Data

Gupta, Avijit.
Large rivers : geomorphology and management / Avijit Gupta.
p. cm.
Includes bibliographical references and index.
ISBN 978-0-470-84987-3 (cloth)
1. Rivers. 2. Geomorphology. 3. Environmental management. I. Title.
GB1205.G87 2007
551.48′3 – dc22
2007024257

British Library Cataloguing in Publication Data

A catalogue record for this book is available from the British Library

ISBN 978-0-470-84987-3

Typeset in 9/11 pt Times by SNP Best-set Typesetter Ltd., Hong Kong
Printed and bound in Great Britain by Antony Rowe Ltd, Chippenham, Wiltshire
This book is printed on acid-free paper responsibly manufactured from sustainable forestry in which at least two trees are planted for each one used for paper production.

Contents

Colour plates are grouped together at the end of the text. Where an illustration in the text is also reproduced in colour, this is noted in the text caption. Black and white copies are placed within the text for easy reference.

Preface

Fluvial geomorphology is based primarily on rivers of manageable dimensions. It is desirable to extend this coverage to the major rivers of the world, only certain members of which have been studied in detail and throughout their total length. It is currently difficult to recognize large rivers of the past from sedimentation patterns or to structure management policies for long international rivers. This book brings together a set of papers on large rivers of the world, possibly as the first introduction to a demanding subject. The emphasis is on geomorphology and sedimentology of large rivers and techniques for their measurement and management.

Present techniques such as remote sensing have made it easier to inspect rivers several thousand kilometres in length. As the papers in this book illustrate, we have started to explore the complicated issues of geomorphology, sedimentation pattern, and management of big rivers. A large river may flow across a range of environments. The Zambezi, for example, flows through alternating rock gorges and alluvial basins for a considerable length of its course. Such behaviour is seldom described in textbooks. A basic knowledge of the form and function of major rivers is necessary for managing large international rivers in heavy use. Climate-related changes may further complicate the picture in the future. Regional and currently popular names of rivers have been used as far as possible, although their modified versions are still in use and could not be avoided entirely. Examples include Ganga (Ganges) and Changjiang (Yangtze). The reader therefore will come across both names, the one regionally in use being more frequent.

Completion of this book has been a demanding task, and I am very grateful to the editorial and production units of John Wiley & Sons, Ltd for their remarkable patience, help, and encouragement. I should thank the contributors for the huge amount of hard data, detailed observation, and tightly structured generalization that have gone into the chapters. The chapters have been peer-reviewed by Vic Baker, Jim Best, John Boland, Ian Campbell, Zhongyuan Chen, Tom Dunne, Chris Fielding, Martin Gibling, Steve Goodbred, Gordon Grant, Ken Gregory, Avijit Gupta, Vishwas Kale, Jim Knox, David Leigh, Terry McCarthy, R.H. Meade, Leal Mertes, Andy Miller, Jim O'Connor, J. Runge, Jack Schmidt, S.K. Tandon, Peter Wilcock, Ellen Wohl, M.G. Wolman and Jamie Woodward.

Sadly, Leal Mertes died while the book was in preparation. Leal was tremendously enthusiastic about this compilation and co-authored two chapters. We hope she would have approved of the final product.

Avijit Gupta

To my friends, who at one time or another,
Have walked various rivers with me

Bert Swan, John Costa, Helen Fox,
Amit Dutt, Vishwas Kale, Fred Scatena,
Andy Miller and Rafi Ahmad

List of Contributors

Philip J. Ashworth
Division of Geography, School of the Environment, University of Brighton, Cockcroft Building, Lewes Road, Brighton BN2 4GJ, UK

Victor R. Baker
Department of Hydrology and Water Resources, University of Arizona, Tucson, AZ 85721-0011, USA

James L. Best
Department of Geology and Geography and Ven Te Chow Hydrosystems Laboratory, University of Illinois at Urbana – Champaign, 1301 W. Green St., Urbana, IL 61801, USA

David S. Biedenharn
Coastal and Hydraulics Laboratory, US Army Engineer Research and Development Center, ERDC, Vicksburg, MS 39180, USA

Michael D. Blum
Department of Geology and Geophysics, Louisiana State University, Baton Rouge, LA 70803, USA

John P. Bolte
Department of Bioengineering, Oregon State University, Corvallis, OR 97331, USA

Ian C. Campbell
Mekong River Commission, 364, MV Preah Monivong, Phnom Penh, Cambodia
Current address: School of Biological Sciences, Monash University, Victoria 3800, Australia

Zhongyuan Chen
State Key Laboratory for Estuarine and Coastal Research, East China Normal University, Shanghai 200062, People's Republic of China

Peter D. Clift
School of Geosciences, University of Aberdeen, Aberdeen AB24 3UE, UK

François Costard
UMR 8148 IDES, CNRS-Université Paris-Sud 11, 91405 Orsay Cédex, France

Fenton P.D. (Woody) Cotterill
Department of Geological Sciences and Department of Molecular and Cell Biology, University of Cape Town, Rondebosch 7701, South Africa

Muhammad Danish
National Institute of Oceanography, ST. 47 Clifton Block 1, Karachi, Pakistan

Roger P. Denlinger
Cascade Volcano Observatory, Vancouver, WA 98683, USA

Thomas Dunne
Bren School of Environmental Science and Management and Department of Earth Science, University of California, Santa Barbara, CA 93106, USA

Christopher R. Fielding
Department of Geosciences, 214 Bessey Hall, University of Nebraska-Lincoln, NE 68588-0340, USA

Emmanuèle Gautier
CNRS UMR 8591, Laboratoire de Géographie Physique and University Paris 8, 92195 Meudon Cédex, France

Robert F. Giegengack
Department of Earth and Environmental Science, University of Pennsylvania, Philadelphia, PA 19104, USA

Liviu Giosan
Geology and Geophysics, Woods Hole Oceanographic Institution, Woods Hole, MA 02543, USA

Gordon E. Grant
Pacific Northwest Research Station, USDA Forest Service, Corvallis, OR 97331, USA

Avijit Gupta
School of Geography, University of Leeds, Leeds LS2 9JT, UK and Centre for Remote Imaging, Sensing and Processing, National University of Singapore, Singapore 119260

Oliver P. Harmar
Halcrow Group Ltd., Arndale House, Otley Road, Leeds LS6 2UL and Industrial Research Fellow, School of Geography, University of Nottingham, Nottingham NG7 2RD, UK

Kazuaki Hori
Department of Environmental Science and Technology, Meijo University, Nagoya 468-8502, Japan

Asif Inam
National Institute of Oceanography, ST. 47 Clifton Block 1, Karachi, Pakistan

James C. Knox
Geography Department, University of Wisconsin, Madison, WI 53706-1491, USA

Michael D. Krom
School of Earth Sciences,University of Leeds, Leeds LS2 9JT, UK

Stephen T. Lancaster
Department of Geosciences, Oregon State University, Corvallis, OR 97331 USA

Dénes Lóczy
Department of Physical Geography, University of Pécs, Ifjúság útja 6, H-7624 Pécs, Hungary

Mark G. Macklin
Institute of Geography and Earth Sciences, University of Wales, Aberystwyth, Aberystwyth SY23 3DB, UK

T. Tamuka Magadzire
USGS FEWS NET Regional Representative for Southern Africa, c/o SADC Regional Remote Sensing Unit, SADC Food, Agriculture and Natural Resources Directorate, SADC Secretariat, Gaborone, P. Bag 0095, Botswana

Mike P.L. Main
Box 2265, Gaborone, Botswana

Robert H. Meade
Research Hydrologist Emeritus, US Geological Survey, MS 413, Box 25046, Federal Center, Denver, CO 80225-0046, USA

Leal A.K. Mertes
Department of Geography, University of California, Santa Barbara, CA 93106, USA

John D. Milliman
School of Marine Science, College of William & Mary, Gloucester Point, VA 23062, USA

Andy E. Moore
AMPAL (Pty) Ltd, Box 66, Maun, Botswana

Melissa R. Neave
Department of Geosciences, The University of Sydney, NSW 2006, Australia

C. Fred Pinkard
Coastal and Hydraulics Laboratory, US Army Engineer Research and Development Center, ERDC, Vicksburg, MS 39180, USA

Muhammad Moazam Rabbani
National Institute of Oceanography, ST. 47 Clifton Block 1, Karachi, Pakistan

Scott C. Rayburg
Riverine Landscapes Research Laboratory, University of Canberra, ACT 2601, Australia

Julie E. Roden
BG Group, 100 Thames Valley Park Drive, Reading RG6 1PT, UK

Jürgen Runge
Johann Wolfgang-Goethe Universität, FB 11: Institut für Physische Geographie and Zentrum für interdisziplinäre Afrikaforschung (ZIAF), Altenhöferallee 1, D-60438 Frankfurt am Main, Germany

Yoshiki Saito
Geological Survey of Japan, National Institute of Advanced Industrial Science and Technology (AIST), Tsukuba 305-8567, Japan

Maminul H. Sarker
Center for Environmental and Geographic Information Services (CEGIS), House No. 6, Road No. 23/C, Gulshan-1, Dhaka-1212, Bangladesh

John C. Schmidt
Department of Watershed Sciences, Utah State University, Logan, UT 84322-5210, USA

Stanley A. Schumm
Mussetter Engineering, Inc., Fort Collins, CO 80525, USA

Indra B. Singh
Department of Geology, Lucknow University, Lucknow 226007, India

Sunil K. Singh
Planetary Geosciences Division, Physical Research Laboratory, Navrangpura, Ahmedabad 380009, India

Rajiv Sinha
Engineering Geosciences Group, Department of Civil Engineering, Indian Institute of Technology, Kanpur 208016, India

Philip J. Soar
JBA Consulting, Magna House, South Street, Atherstone CV9 IDF, UK and Industrial Research Fellow, School of Geography, University of Nottingham, Nottingham NG7 2RD, UK

Ali Rashid Tabrez
National Institute of Oceanography, ST. 47 Clifton Block 1, Karachi, Pakistan

Muhammad Tahir
Fugro Geodetic Limited, 28-B, KDA Scheme #1, Karachi 75350, Pakistan

Sampat K. Tandon
Department of Geology, University of Delhi, Delhi 110007, India

Martin C. Thoms
Riverine Landscapes Research Laboratory, University of Canberra, ACT 2601, Australia

Colin R. Thorne
School of Geography, University of Nottingham, Nottingham NG7 2RD, UK

Jennifer Rose Wallick
DHI, Inc., 319 SW Washington St Suite 614, Portland, OR 97204, USA

Masataka Watanabe
Faculty of Environment and Information Studies, Keio University, Kanagawa 252-8520, Japan

Hugh B. Williams
7 Rothesay Road, Avondale West, Harare, Zimbabwe

Martin A.J. Williams
Geographical and Environmental Studies, University of Adelaide, Adelaide, South Australia 5005, Australia

Ellen E. Wohl
Department of Geosciences, Colorado State University, Ft Collins, CO 80523, USA

M. Gordon Wolman
Department of Geography and Environmental Engineering, Johns Hopkins University, Baltimore, MD 21218, USA

Jamie C. Woodward
School of Environment and Development, The University of Manchester, Manchester M13 9PL, UK

Hui Xu
Institute of Atmospheric Physics, Chinese Academy of Sciences, Beijing 100029, People's Republic of China

Kaiqin Xu
National Institute for Environmental Studies, Tsukuba 305-8506, Japan

Kehui Xu
School of Marine Science, College of William & Mary, Gloucester Point, VA 23062, USA

Zuosheng Yang
College of Marine Geosciences / Key Lab of Submarine Science and Exploration Technology, Ministry of Education, Ocean University of China, Qingdao 266003, People's Republic of China

1

Introduction

Avijit Gupta

School of Geography, University of Leeds, Leeds LS2 9JT, UK and Centre for Remote Imaging, Sensing and Processing, National University of Singapore, Singapore 119260

1.1 A BOOK ON LARGE RIVERS

Large rivers are important components of continental landforms. A number of them have been associated with the growth and development of human civilization in their fertile valleys. The structured water utilization in the Nile Valley is an excellent example. Several have been impounded, starting from the second quarter of the twentieth century. The Hoover Dam over the Colorado is one of the early huge engineering structures, the Three Gorges Dam over the Changjiang (Yangtze) the most recent one.

In spite of these rivers being physical marvels and resources utilized by a large number of people, our knowledge about their form, evolution or function remains limited. This is possibly due to logistical problems, as case studies in the fields of geomorphology, sedimentology or river ecology are generally on smaller rivers that are easier to investigate, model or manage. For example, direct measurements of sediment are not regularly available for a number of these big rivers, requiring indirect estimates of sediment load. Our knowledge of these rivers also varies. A lot more is known about the Mississippi or the Colorado than the Zambezi. The Nile has been measured for thousands of years but not the Congo. The Amazon is attracting a very large number of researchers from a wide range of institutions, countries, and specializations but such large-scale national or international endeavours are rare for other tropical rivers. Over the last four decades, a compilation of information on channel form, sediment, and mobility of the Lower Brahmaputra has built up, a dataset not available for its upper course. We have started to comprehend the interconnection between the flood pulse, sediment flux, and riverine ecology in these rivers. But the coverage is not uniform and for a number of major rivers our knowledge is inadequate for both generalization and planning. For example, at the current level of understanding, it is difficult to predict the effect of the expected climate changes on large rivers, a task that will undoubtedly become essential for the next generation of scholars.

This book is an attempt to bring together a number of papers on big rivers. It is not a complete coverage but provides an introduction to geomorphology and the management of rivers of large dimension. Certain rivers and topics have been hard to cover because of their complexity and location and a couple of the chapters originally planned did not arrive, but overall this is a unique volume not attempted before at this scale.

The book is designed in three sections. The first section is on the environmental requirements for creating and maintaining a large river. In that sense, the chapters included are valuable generalizations based on existing knowledge. The second section is a collection of case studies on big rivers flowing through a range of physical environments. The third section is on the measurement and management of large rivers and their basins. Almost all chapters have been rather demanding to write, but the end product is a bold pioneering volume that hopefully will generate enough interest and controversy to push the boundary of our knowledge related to large rivers. It may even contribute towards saving their channels and basins from both random and organized mismanagement.

Large Rivers: Geomorphology and Management, Edited by A. Gupta

1.2 WHAT IS A LARGE RIVER?

If we are to list the largest rivers in the world, all of us would probably list the same 15 or 20 rivers, but a proper definition is elusive. Potter, in his 1978 paper on the significance and origin of big rivers, listed four properties that could be considered for this purpose: size of the drainage basin, length of the river, volume of sediment transported, and water discharge. He used river length and drainage basin size to identify the 50 largest rivers of the world. All except one of these rivers were more than 10^3 km long and the smallest drainage basin was 10^5 km^2. These 50 streams collectively drain about 47% of the continental surface, excluding Greenland and Antarctica (Potter, 1978). Inman and Nordstrom (1971) listed rivers with drainage areas above 10^5 km^2, with the Amazon ranked as 1 and the Po as the last one to qualify at rank 58.

Quality data on the two other criteria of large rivers, discharge of water and especially discharge of sediment, are not always available. Meade (1996) listed the first 25 rivers for both water and average suspended sediment discharges to the coastal zone. It is difficult to determine the total sediment load of a large river and, as Meade has pointed out, bed load is especially difficult to measure. The two lists, however, do not coincide, as certain rivers such as the Zambezi or Lena carry a large water discharge but their sediment loads are low. Impoundments have reduced the sediment load of rivers such as the Mississippi-Missouri, and almost removed it for the Nile or the Colorado. Impoundments have also reduced the water discharge of a number of major rivers (Meade, 1996). The Huanghe now does not reach the sea for about half the year. A river that should be in the list because of its former glory may not qualify on current performance. Recently Hovius tabulated the morphometric, climatic, hydrologic, transport and denudation data for 97 river basins, all of which measured above 2.5×10^4 km^2 (Hovius, 1998). Miall raised the question of identifying big rivers of the past, and attempted to define the 'bigness' in rivers based on previous studies (Miall, 2006).

Qualitatively, therefore, a large river carries a very big discharge, is long, has a large drainage basin and, commonly, but not always, annually transports a large volume of sediment. Of these, a huge volume of water flowing down the channel is probably the commonest expectation of a large river in a natural state, but given the variations that occur among three other properties, a rigorous definition is impossible. Instead it is expedient to list the top twenty or so and base our discussion on their characteristics. Table 1.1, compiled from various sources, is a comparison of the top 24 rivers of the world, selected on basis of their discharge. The discharge figures are from Meade (1996). Other measurements have been derived from a range of sources that are listed below Table 1.1. These measurements, however, differ between sources, especially regarding the area of the basins which has been resolved by rounding off to 10^6 km^2. Even at this scale there are discrepancies. Given the scale, perhaps it is inevitable that different figures will be quoted by different authors. A relationship exists between river length and drainage basin areas (Leopold *et al*., 1964; Potter, 1978) but not between the other variables. Variations in basin geology, relief, and hydrology are responsible for the scatter.

The great length of these rivers allows them to flow across a range of environments. The Changjiang, Mekong, and Zambezi, for example, flow in and out of rock gorges into alluvial basins. Morphological and behavioural adjustments happen at each transition. The sequence of steep headwaters, a braided segment, a meandering channel through an alluvial floodplain, and a delta at the end as prescribed for rivers of a more manageable dimension may not hold. Other rivers may demonstrate significant hydrological variations along their courses. The Quaternary history may also be complicated with different kind of changes occurring at the mountainous headwaters, along the valley, and near the coast. In spite of their size, a number of big rivers have been anthropogenically modified out of their natural conditions.

1.3 THE BOOK AND ITS CONTENT

Certain characteristics and conclusions are repeated independently by different contributors throughout the book. Although the ages vary, large rivers could have been in existence for a long period. The Mississippi, for example, has a history going back to at least the Late Jurassic. The present course of a river, however, could be an assemblage of several subunits of different age and appearance. Formation and sustenance of big rivers are commonly associated with orogenic belts, the Upper Indus, for example, remains pinned in a suture zone for a considerable part of its course. Large rivers interestingly also occur in rift valleys and cratonic settings, and many transect more than one setting along their length. Neither the Congo nor the Danube arises from a high orogenic belt, and they traverse a range of structural environments that cause them to regionally adjust their forms and behaviour. Even in the wide alluvial valleys, crustal deformation and belts of transverse resistant lithology change the low gradient of rivers resulting repeatedly in channel form and behaviour changes. The most striking example is the structurally controlled Amazon flowing in an extremely wide valley

Table 1.1 Selected characteristics of 24 large rivers

River	Annual average water discharge (10^9 m^3)	Length (km)	Drainage basin area (10^6 km^2)	Current average annual suspended sediment discharge (10^6 t)
1. Amazon	6300	6000[a]	5.9[a]	1000–1300
2. Congo	1250	*4370*	*3.75*	43
3. Orinoco	1200	770[a]	1.1[a]	150
4. Ganga-Brahmaputra	970	*B-2900*	*1.06*	900–1200
		G-2525	*(B-0.63)*	
5. Changjiang	900	*6300*	*1.9*	480
6. Yenisey	630	5940[b]	2.62[b]	5
7. Mississippi	530	*6000*	*3.22*	210
8. Lena	510	*4300*	*2.49*	11
9. Mekong	470	*4880*	*0.79*	*150–170*
10. Paraná-Uruguay	470	3965[c]	2.6[c]	100
11. St Lawrence	450	3100[d]	1.02[d]	3
12. Irrawaddy	430	2010[e]	0.41[e]	260
13. Ob	400	>5570[b]	2.77[b]	16
14. Amur	325	4060[b]	2.05[b]	52
15. MacKenzie	310	4200[d]	2.00[d]	100
16. Zhujiang	300	2197[g]	0.41	80
17. Salween	300	2820[e]	0.27[e]	about 100
18. Columbia	250	2200[d]	0.66[d]	8
19. Indus	240	*3000*	*0.97*	50
20. Magdalena	240	1540	0.26	220
21. Zambezi	220	*2575*	*1.32*	20
22. Danube	210	*2860*	*0.82*	40
23. Yukon	195	3200[d]	0.83[d]	60
24. Niger	190	4100[f]	2.27	40

These figures vary between sources although perhaps given the size such variations are proportionally negligible. Discharge and sediment figures unless otherwise mentioned are from Meade (1996). Figures in italics are from chapters in this book. Other sources are indicated by superscripts: [a] Warne *et al*. (2002); [b] Koronkevich (2002); [c] Orfeo and Stevaux (2002); [d] Wohl (2002); [e] Gupta (2005); [f] Allen (1970); [g] Z. Chen, personal communication. Drainage basin areas rounded off to 10^6 km^2 to avoid discrepancies between various sources. Note that the Nile is 6500 km long but does not qualify for this table as its water and sediment discharges are relatively low.

filled with alluvium. Structural controls may exist on a continental scale that determines the primary location of the river in a downwarped plate tectonic setting. Within such a setting, structural control on a smaller scale also forces the river to change its direction, gradient, shape, and behaviour sharply, contributing to a series of regional variations on a scale of tens and hundreds of kilometres. Tectonics, climate and eustasy may control a long river in combination, each of these factors being significant in different parts of its course.

Rivers of this dimension obviously require large precipitation over their basins, which is met both in the monsoonal tropics and regions seasonally drained by meltwater floods from winter ice and snow. A large river therefore could be dependent on its headwater mountains for sustenance of its discharge. The headwater mountains, and in certain cases mountains at the head of major tributaries, also are the usual sources for the supply of sediment that travels down the channel to the mouth with short transfer times and long storage periods, especially when the sediment is stored in the floodplain. Sediment therefore arrives in the trunk stream via a restricted number of paths. Storage and remobilization of floodplain sediment influence the distribution and sustenance of regional plant and animal species. Isolated basins and gorges have given rise to speciation and origin of endemic organizations contributing rivers with diverse flora and fauna along their courses. Large rivers tend to build megadeltas, although, irrespective of the age of the rivers, the current megadeltas were formed in the Holocene. These deltas have experienced changes due to both natural and anthropogenic causes, the latter accelerating delta growth following human settlements in river basins. Such anthropogenic changes influence rivers even at the scale of the Yangtze.

Many major rivers have undergone extremely large shifts in discharge due to climate change or meltwater floods at the end of the Pleistocene and in Early Holocene.

These late Quaternary megafloods have altered drainage evolution and channel geometry in a number of rivers and the planetary pattern of water and sediment contribution to the oceans. Sediment from this time may still exist in the channel or the floodplain of the river. A major river may exist at the same location for a long period of time, but its present form tends to reflect forcing caused by tectonics, climate shifts, and sea level changes subsequent to origin; and, over the last several millenniums, anthropogenic activities in the drainage basin and the channel.

It is possible that evidence of deposition by large rivers like the Brahmaputra has not been noticed in sedimentary rocks or has been misinterpreted due to the huge scale. The reconstruction of rivers at this scale going back in geological time is therefore rather limited. An urgent need therefore exists to gather more and higher quality data on sedimentation by modern large rivers and to determine their preservation in older rocks.

The second section of the book (Chapters 8–21) is a collection of case studies on a number of rivers: Amazon, Mississippi, Colorado, Lena, Danube, Nile, Congo, Zambezi, Indus, Ganga, Brahmaputra, Mekong, and Changjiang. Several of these rivers have again been discussed elsewhere regarding specific aspects such as management, but these are important rivers and such repetition reflects reality. Although the book has been designed as a holistic unit, individual chapters can be read independently. An attempt was made to cover a wide range of geological and climatological environments, and although it has not been possible to include all the rivers originally planned, there is enough here to provide a very reasonable cross-section of the major river basins of the world. Two major points follow from these studies. First, a number of common characteristics, as summarized above and discussed in detail in the first section of the book (Chapters 2–7), show up in the case studies; and second, certain specific properties, such as structural control, high erosion rates or anthropogenic modification, may be significant enough for an individual large river to demand further discussions.

The third section of the book (Chapters 22–30) is on utilization, techniques, and management, although it has been expedient to base such discussions on individual rivers to some extent. The Nile has been used to connect a long history of hydraulic civilization with the physical characteristics of the river. Utilizing a major river as a resource by impoundment or other structural changes affects even huge rivers and several of the current biggest negative environmental impacts arise out of attempts to control or manage rivers. The scale of large rivers requires innovative tools for their study or modelling and techniques such as use of satellite imagery, channel geometry analysis, and mapping disturbances in the channel have been discussed. Even with satellite imagery it is extremely difficult for an individual to be familiar in detail with more than one long river which inhibits research. River management is a demanding task, and particularly so at this scale. The management policy and techniques not only have to take into consideration the physical and biological backgrounds concerning the entire catchment, channel, and floodplain but also, as rivers are intimately associated with people, the prevalent economic, social and political backgrounds. The technique of integrated water resources management (IWRM) is frequently proposed. As large rivers tend to flow in international basins, the political demand on management may override other expectations. As managing many of these rivers requires capacity-building in their basins, management could be very difficult.

Primarily, we need to know about large rivers and their basins covering all these aspects. This book is only a beginning and it is focused on the physical environment of rivers. It is absolutely crucial that subsequent volumes are produced to extend our knowledge of rivers at this scale, so that their sustainable management becomes feasible even in the future with climate change and sea level rise.

REFERENCES

Allen, J.R.L. (1970) Sediments of the modern Niger Delta: a summary and review. In: *Deltaic Sedimentation: Modern and Ancient* (J.P. Morgan, Ed.), Society of Economic Paleontologists and Mineralogists Special Publication 15, Tulsa, 138–151.

Gupta, A. (2005) Rivers of Southeast Asia. In: *The Physical Geography of Southeast Asia* (A. Gupta, Ed.), Oxford University Press, Oxford, 65–79.

Hovius, N. (1998) Controls of sediment supply by large river. In: *Relative Role of Eustasy, Climate, and Tectonism in Continental Rocks* (K.W. Shanley and P.J. McCabe, Eds), Society for Sedimentary Petrology Special Publication 59, Tulsa, 3–16.

Inman, D.L. and Nordstrom, C.E. (1971) On the tectonic and morphologic classification of coasts. *Journal of Geology*, 79, 1–21.

Koronkevich, N. (2002) Rivers, lakes, inland seas, and wetlands. In: *The Physical Geography of Northern Eurasia* (M. Shahgedanova, Ed.), Oxford University Press, Oxford, 122–148.

Leopold, L.B., Wolman, M.G. and Miller, J.P. (1964) *Fluvial Processes in Geomorphology*, W.H. Freeman, San Francisco.

Meade. R.H. (1996) River-sediment inputs to major deltas. In: *Sea-level Rise and Coastal Subsidence: Causes, Consequences, and Strategies* (J.D. Milliman and B.U. Haq, Eds), Kluwer, Dordrecht, 63–85.

Miall, A.D. (2006) How do we identify big rivers? And how big is big? *Sedimentary Geology*, 186, 39–50.

Orfeo, O. and Stevaux, J. (2002) Hydraulic and morphological characteristics of middle and upper reaches of the Paraná River (Argentina and Brazil). *Geomorphology*, 44, 309–322.

Potter. P.E. (1978) Significance and origin of big rivers. *Journal of Geology*, 86, 13–33.

Warne, A.G., Meade, R.H., White, W.A., Guevara, E.H., Gibeaut, J., Smyth, R.C., Aslan, A. and Tremblay, T. (2002) Regional controls on geomorphology, hydrology, and ecosystem integrity in the Orinoco Delta, Venezuela. *Geomorphology*, 44, 273–307.

Wohl, E.E. (2002) Rivers. In: *The Physical Geography of North America* (A.R. Orme, Ed.), Oxford University Press, Oxford, 199–216.

2

Geology of Large River Systems

Sampat K. Tandon[1] and Rajiv Sinha[2]

[1]*Department of Geology, University of Delhi, Delhi 110007, India*
[2]*Engineering Geosciences Group, Department of Civil Engineering, Indian Institute of Technology Kanpur 208016, India*

2.1 INTRODUCTION

River basins occupy about 69 % of the land area, transporting an estimated 19 billion tonnes of material annually, about 20 % of which is in solution (Nanson and Gibling, 2004). Figure 2.1 shows the location of the large rivers across the world defined on the basis of one or more of the following criteria: drainage area (A) = 800 000 km^2, river length (Lr) = 2500 km, average discharge (Q) = 7500 m^3 s^{-1}, and annual suspended and dissolved load = 100 mt (Hovius, 1998). Of the world's rivers, large rivers are significant because they are, now, and have been in the past, important links of the sediment transfer system from the continents to the world's ocean basins. Large rivers play a major role in sculpturing the topography of the earth.

In a classic paper, Potter (1978) indicated that most large rivers 'have large, long-lived deltas which have played a major role in both deep and shallow waters'. Most large rivers and their valleys have alluvial stratigraphic records that enable an understanding of their development on different timescales – century, millennial, tens of thousands of years, million and tens of millions of years. The subject of large rivers can be approached from different perspectives, from a modern perspective that emphasizes the hydrological, sediment transport and network organization of large rivers, and also from a stratigraphic perspective that emphasizes the reconstruction of ancient large river systems through the methods of sedimentary basin analysis.

Many of the great ancient civilizations were established in the vicinity of ancient large rivers. Large rivers are important constituents of the hydrological cycle; they not only possess inorganic constituents, but also support biotic systems. Huge deposits of coal within the fluvial Gondwana sequences emphasize the significance of fluvial deposits of ancient rivers. Apart from this, the placer deposits of large rivers are also economically significant as they may contain uranium, gold or diamonds. The deltas of large rivers are very important sites for vegetation growth, e.g. the Sundarbans delta at the mouth of the Ganga-Brahmaputra system.

This chapter reviews the origin and evolution of large rivers across the globe in a variety of tectonoclimatic settings. We assess geological criteria for the definition of large rivers. Maps of the distribution of modern large rivers in different tectonic settings and climatic regimes are used to throw light on their genesis and sustenance. Hydrological and sediment dispersal aspects of the large rivers have been discussed in the light of climatic variations and source area characteristics. A direct manifestation of sediment dispersal by large river systems is the sedimentary architecture developing below the alluvial plains, and not surprisingly, the large rivers display a strong variability in terms of their alluvial architecture. We describe some of these settings, including longitudinal trunk systems, radial fans, fan–interfan systems and interfluve settings, mostly with examples drawn from our own work in the Ganga plains. Many of the big rivers originate in active mountain belts and terminate in open oceans after draining through large alluvial plains. These systems are influenced by sea level changes, tectonics and climate change in different parts of their

Large Rivers: Geomorphology and Management, Edited by A. Gupta

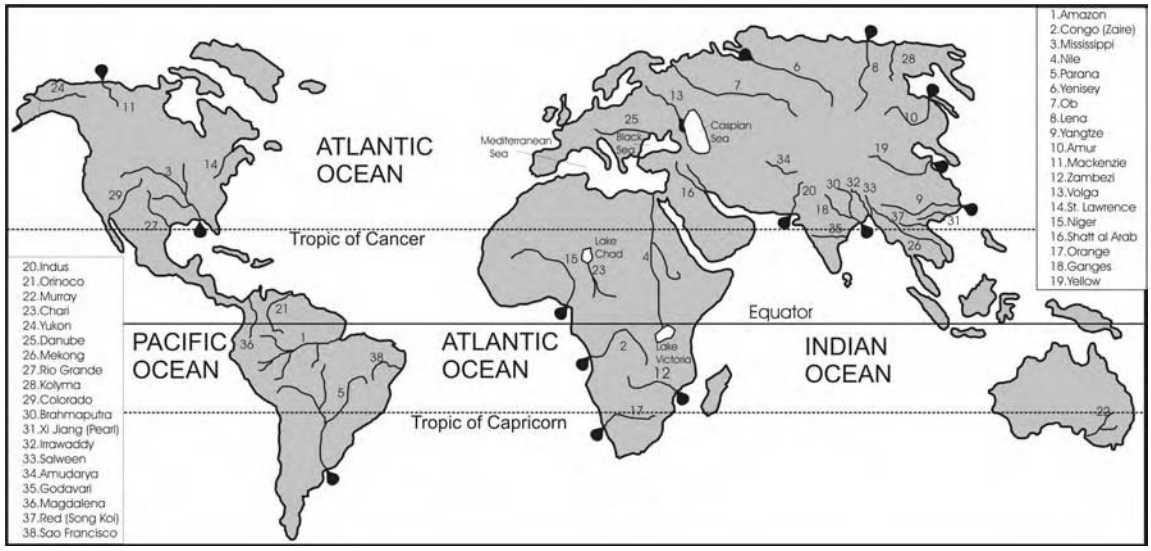

Figure 2.1 Major rivers of the world; numbers correspond to the river names as listed

catchments but the extent of these controls and their coupling are not well understood.

This review also highlights our limited understanding of the integrative aspects of large river systems.

2.2 TECTONIC SETTINGS OF LARGE RIVER SYSTEMS

Most modern large river systems have their headwaters in the uplifted zones of large orogens, and flow through extensive continental-scale cratonic areas. Location of large rivers and their positioning with reference to the global tectonic setting is shown in Figure 2.2. Large continental-scale masses such as those of the Indian (drained by the Ganga, Brahmaputra), N. American (Mississippi, Rio Grande), African (Congo, Zambezi, Orange) and Australian (Murray-Darling) Shields adjoining major compressional belts on the globe provide the necessary 'scale' constraints for the formation of these rivers, and their sustenance through a long period of time. These examples suggest common conditions for the origin of the large rivers. At the very minimum, there should be an uplifted zone and a bordering continental mass of considerable extent.

Continental areas such as Antarctica and Greenland are ice-covered and presently do not allow the formation of large rivers. There are areas such as New Zealand which are being uplifted extremely rapidly, and even though New Zealand has some very active rivers, the land area is too small for any 'large' rivers to form. This is true for all the volcanic arcs. There are upland areas under water, e.g. mid-ocean ridges which only reach the surface at isolated points such as Iceland. Also there are large river systems that have flowed entirely sub-ocean, e.g. the huge braided system of NAMOC (Hess *et al*., 2001), although this may have been generated in large part by catastrophic outflows of short duration. There is thus a link between the evolution of large river systems with the Wilson Cycle – the creation and destruction of super continents, such as Rodinia and Pangea. These super continents must have promoted the formation of large rivers and the size of these palaeocontinents may establish a rough maximum length and catchment area that large rivers could reach on Earth. At the present, the Earth has continental land areas large enough for big rivers to exist. In the Archaean, there may not have been enough continental area to allow for many large rivers to form. Thus, the formation of large rivers needs a long-term first-order relief structure aiding the transport of water from the uplifted zone to the ocean. Sufficient precipitation should fall in the basin area to sustain the large river systems, and the run-off coefficient of the terrain of the drainage basin should be high.

Recent works (Brookfield, 1998) have demonstrated that the large river systems of Asia have evolved through continental-scale tectonics (plate tectonics), modified by climate and local tectonic effects. In other words, rivers evolve with time because of the motion of plates on which they occur and because major rivers are related to global

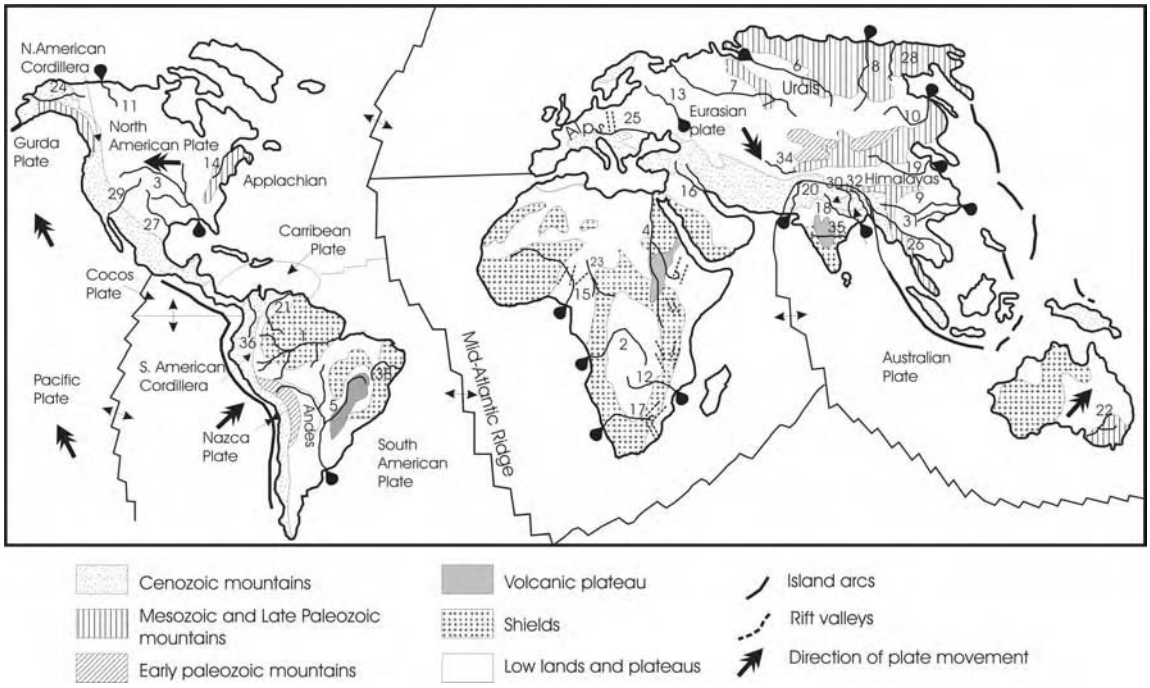

Figure 2.2 Tectonic setting of large rivers and their deltas. Major highlands of the world and margins of large plates are plotted (some other smaller plates are not shown). Arrow indicates the direction of plate movement. Numbers refer to rivers listed in Figure 2.1. Redrawn from Global Geomorphology, Summerfield, M.A., Longman: London, 1991, with permission from Pearson Education Ltd

tectonics and the hydrologic system. As mentioned earlier, the development of topography is the most important requisite for the development of large rivers which, in turn, is governed by the balance between forces generated by plate convergence and gravitational spreading (England and Housemen, 1988). Based on the basin-forming mechanism according to the principles of plate tectonics, three major settings of large rivers can be identified: (a) continental collision belts; (b) rift systems; and (c) cratonic settings. In terms of complexity of drainage type, further variations are recognized with respect to the orientation and location of the river valley in relation to the structural grain of the major tectonic features (Table 2.1).

2.2.1 Rivers in Continental Collision Belts

Continental collision belts are one of the most important sites for the creation of an uplifted zone. Once large continental masses have amalgamated, tectonic uplift processes may generate the catchment/drainage for the large rivers. Long-term denudation may generate/enlarge the river valleys. The river systems of South, Southeast and East Asia (Ganga, Brahmaputra, Indus, Mekong, Yangtze, etc.) are some of the best examples of this category related to the large scale deformation of the India-Asia collision (Figure 2.2). The precise tectonic situation and development of each system in the region varies significantly, and Brookfield (1998) has provided a detailed description of these river systems. The Yangtze, Mekong and Salween rise on the Tibetan Plateau, bend around the eastern Himalayan syntaxis, and run in deeply incised gorges before meeting the sea. It is believed that differential shear and clockwise rotation between the compressing Tibetan Plateau and Southeast Asia were responsible for the great sigmoidal bends of these rivers (Brookfield, 1998). The Brahmaputra and the Ganga have very deep gorges in the Higher Himalaya and may once have flowed longitudinally behind the Himalaya (Brookfield, 1993). Southward thrusting and massive frontal erosion of the Himalaya caused progressive truncation of the longitudinal courses of these rivers (Seeber and Gornitz, 1983). Several examples of river capture illustrate the longitudinal and lateral movements of the river systems, and one of the most dramatic examples is the truncation of the original

Table 2.1 Tectonic settings and morphological variability of large rivers

Tectonic setting	Description	Modern examples
Continental collision belt	Rivers formed in convergent plate boundaries associated with the development of orogenic belts	
Longitudinal foreland basin	Rivers having headwater in the mountain range at converging margin but have trunk stream flowing axial or longitudinal to the mountain range	Ganga, Paraná
Transverse systems	Rivers having headwater in the mountain range at converging margin and flow transverse to the structural grain across stable platform or shield	Amazon, Missouri-Mississippi
Intrabasinal setting	Rivers flowing within the mountain belts parallel to major structural trends until near their mouths	Mekong, Brahmaputra, Irrawaddy
Rift systems	River basins formed by creation of new relief in rift and rift-shoulder settings	Rio Grande
Cratonic settings	River systems formed by cratonic tectonic events unconnected to Wilson Cycle, e.g. doming associated with large igneous provinces	Lower Paraná, Orange

Tsangpo and Irrawaddy systems by the Brahmaputra River (Brookfield, 1998). The Lower Mekong River also shows evidence of river capture and headward erosion and diversion of its original course (Brookfield, 1998).

An interesting example of rivers in the compressional belt is the Shatt al Arab formed by the confluence of the Euphrates and the Tigris Rivers and draining the Mesopotamian plains (Bridges, 1990). The rivers rising in the Zagros mountains and following tortuous courses in deep gorges are often cited as examples of drainage antecedent to the Zagros mountains which formed in Miocene times and have been affected by strong thrusting and faulting in the Late Tertiary.

2.2.2 Rivers in Rift Settings

An alternate process of formation of large river basins may involve commencement of rifting and rift-shoulder systems by creation of new relief. Several examples of large rivers forming in rift settings in a continental interior exist, the most notable being the Rio Grande (Figure 2.2). The Rio Grande rift is a pull-apart structure, the formation of which began in early Miocene; the rifting first resulted in shallow basins with terrestrial input and a through-flowing drainage developed about 3 Ma ago perhaps due to uplift in the headwater region or due to a wetter climatic phase (Belcher, 1975; Chapin and Seager, 1975). Potter (1978) also suggested that the Rio Grande may exemplify a very early phase of rifting in a continental interior, long before any major subsidence and delta formation. Another example is the Congo River which rises on the western, elevated shoulder of the East African Rift, and drains in a transverse system to the Atlantic Ocean. Some rivers may occupy rifts in parts of their courses, and arguably, the Mississippi is one of these which enter a highly active fault zone with big earthquakes in Arkansas (Ervin and McGinnis, 1975). The Blue Nile, the high discharge tributary of the Nile River actually rises within the Ethiopian rift system, and over half of its 800 km course from Lake Tana to Khartoum is through a gorge which is over 1500 m deep over much of its length (Hurst and Phillips, 1931).

2.2.3 Rivers in Cratonic Settings

Large rivers in cratonic settings have formed through tectonic events unconnected to the Wilson Cycle. Such processes may include doming associated with large igneous provinces formed by mantle plumes (Cox, 1989). Many of the continental areas affected by mantle plumes during the Late Cretaceous characteristically remain topographically high due to crustal thickening caused by magmatic underplating (McKenzie, 1984). These high landmasses aid in the development of large rivers and one of the examples is the middle reaches of the Paraná River in southern Brazil before its confluence with the Paraguay River (Figure 2.2). The Serra Geral Formation (basalts and rhyolites) in the Paraná Basin is considered to form a relict dome, and a dome-flank drainage pattern is dominant in this part of the basin (Cox, 1989). Other examples of control by mantle plumes in the development of large continental drainage include the Orange and the Zambezi river systems associated with the Karoo province (Cox, 1989). However, there have been suggestions that most of the drainage basins cited as examples of dome-flank drainage may not be antecedent drainage lines (the centre point of the mantle plume hypothesis) but have been significantly affected by the surface uplift resulting from isostatic response to large denudational unloading during the late Cenozoic (Summerfield, 1990).

Apart from the cratonic rivers from mantle plume setting, there are several rivers on major cratons that currently drain parts of orogens that still have some elevation but are inactive or only slightly tectonically active. They could also, perhaps, be considered 'cratonic'. In North America, these include the Mississippi, Mackenzie, St Lawrence, and Yukon, all rising in the Cordillera or the Appalachians. In Europe, the Danube rises in the Black Forest, and passes some still active areas to the east. In Australia, this group includes drainage from the Great Dividing Range – the Murray, as well as Cooper Creek farther north which has a large drainage area but very low discharge (not plotted in Figure 2.1). In northern Asia, the Yenisey and the Lena rivers drain the Angara Shield and form a dissected plateau on the Archaean and Proterozoic rocks of Precambrian age. There is a limited area of coastal plain west of the Lena Basin and the shield rocks are exposed again in the Taimyr Peninsula to the north. The average relief of this area is 300–800 m which was developed following the Alpine Orogeny followed by Pleistocene glaciations (Bridges, 1990, p. 126). The shield also underlies the lowlands of the Ob River to the west but folded and faulted mountain belts of Lower Palaeozoic occur to the south and east (Figure 2.2). Another important river of this region is the Kolyma River rising in the Kolyma Range in northeast Asia, composed of Permian, Triassic and Jurassic rocks which are well dissected with higher parts having an alpine relief (Bridges, 1990). The Kolyma River drains through the Kolyma lowland, less than 50 m above sea level, which has a cover of unconsolidated Quaternary sediments with permafrost, and forms an estuary into the Arctic Ocean.

2.3 COMPLEXITY OF DRAINAGE TYPES

Two major drainage types with respect to the river orientation in relation to the structural grain are longitudinal and transverse systems (Potter, 1978; Miall, 1981). In the longitudinal system, the structural grain may be the axis of the foreland basin with a trunk stream flowing axial or longitudinal to the mountain range (foreland basin, Figure 2.3a). A typical example is the Ganga River which involved uplift of the Himalaya and separation of the aggradational basin from the eroded source area. The river basin occurs in the longitudinal, structurally controlled valleys, and the major river deposition is outside the orogenic belt but oriented parallel to the strike of the Himalaya. Another example of this category includes the Paraná River in Brazil. The main Paraná rises in the Precambrian rocks of the Brazilian Shield on the north and east whereas one of its major tributaries, the Salado River rises in the highlands of the eastern flank of the Andes (Petri and Fulfaro, 1983). The river flows parallel to the Mesozoic sandstone of the Caiua Formation to its left with a strongly asymmetric alluvial reach; the left bank continuously erodes the sandstones and the right bank builds a large floodplain (Stevaux, 1994).

In other situations, the river flows transverse to the structural grain across a stable platform or shield (Figure 2.3b), e.g. the Amazon and the Missouri. The Amazon has its headstream in the Andes fed by glacial lakes in Peru and flows across the Brazilian Shield before entering the Atlantic Ocean near Belém. The Amazon is guided by a structural low and a graben system near its mouth. The chief tributary of the Mississippi is the Missouri River which has its headwaters in the Rocky Mountains, and the combined Missouri-Mississippi system flows generally south to enter the Gulf of Mexico through a huge delta in southeast Louisiana. The southerly part of its course follows a tectonic zone that has a long history of activity (Potter, 1978).

Another useful way to characterize the large river systems is on the basis of hinterland characteristics, e.g. mountain-fed, foothills-fed, plains-fed or mixed-fed river systems (Sinha and Friend, 1994). Such genetic differences in river types are strongly reflected in terms of their morphology, hydrology, and sediment transport characteristics through the controls of precipitation and erosional history in their source areas. Mountain-fed rivers are generally multichannel, braided systems, characterized by discharge and sediment loads that are many times higher than those of the single-channel, sinuous foothills-fed and plains-fed river systems. They also transfer a large quantity of sediments from their high relief catchments to the plains, and many of them consequently form large depositional areas (megafans) where they enter the basin. The foothills-fed and plains-fed rivers derive their sediments from the foothills and from within the plains, and a large proportion of this material is re-deposited in the plains after local reworking. Most large rivers would be mountain-fed or foothills-fed systems (Figure 2.3c, d).

In a long-term history of the large river systems, the exact positioning and configuration may change from longitudinal to transverse systems and vice versa in response to hinterland tectonics (Miall, 1996). The axial rivers respond quite significantly to the changes induced by tectonic processes of the region, for example, the diversion of the Indus river flow from south-west to southwards due to the growth of the Salt Range and uplift of the piggyback basin behind it (Burbank and Beck, 1991). The Ganga foreland basin was properly established only in the Middle Miocene, after significant lithospheric flexure and subsidence of the basin. Several lines of evidence suggest that during the Middle Miocene to Middle Pleistocene

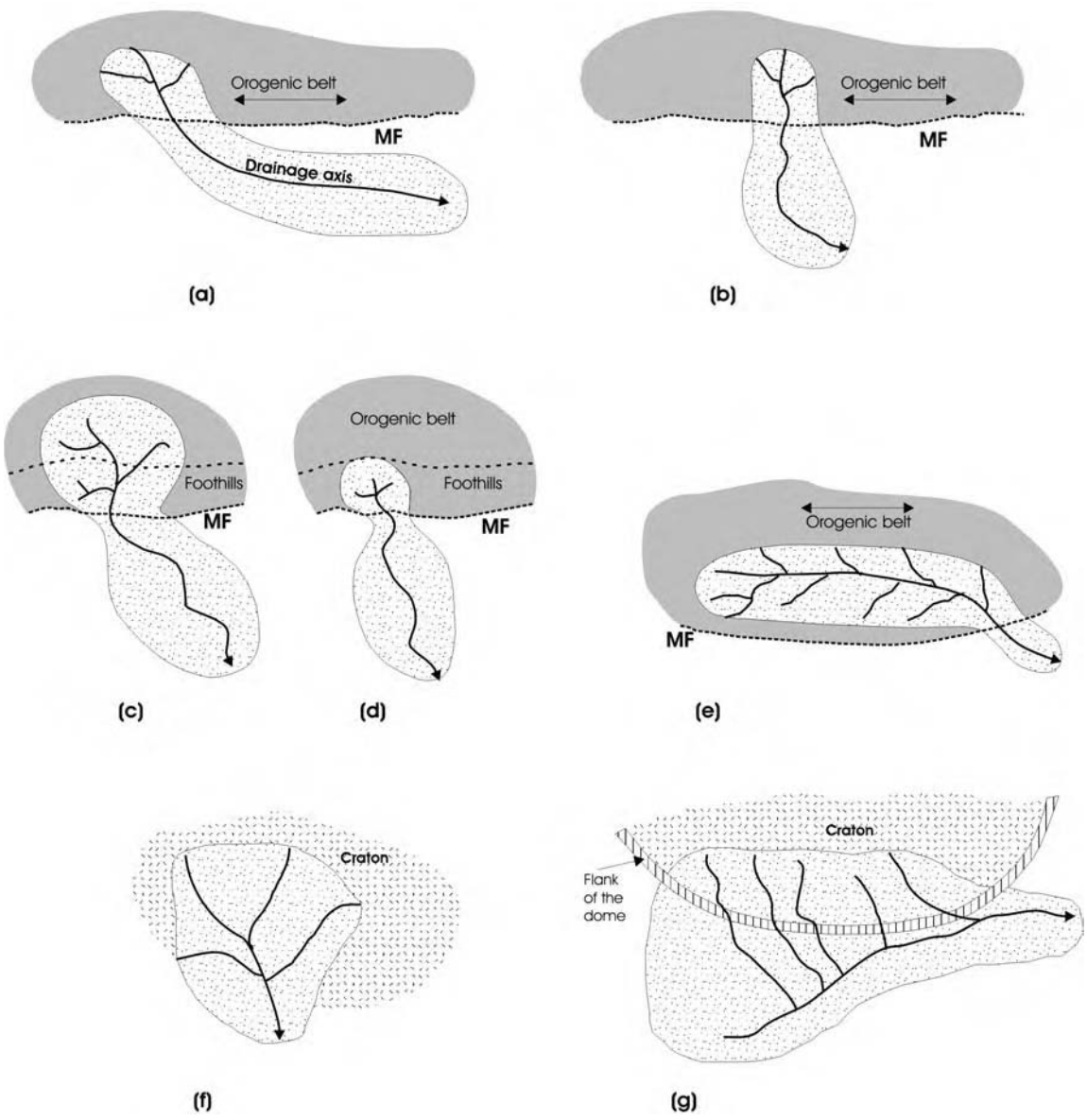

Figure 2.3 Complexity of drainage types of large river systems: (a) longitudinal trunk system; (b) transverse drainage; (c) mountain-fed system; (d) foothills-fed system; (e) confined in the mountain belt; (f) cratonic setting; (g) domal flank drainage. MF, Mountain front

(deposition of Lower to Upper Siwalik Group), the northern part of the Ganga Basin was uplifted and thrust basinwards, and the depocenter of the Ganga Basin shifted southward (cratonwards) in response to thrust loading in the orogen (Raiverman *et al*., 1983; Burbank, 1992; Burbank *et al*., 1996; DeCelles *et al*., 1998; Kumar *et al*., 2001). Covey (1986) applied the term 'under-filled basin' to the Ganga foreland basin at this time, when it represented a topographic low between the thrust belt (Himalaya) and the peripheral bulge. The under-filled condition developed due to an efficient transport system for the sediment supplied, which removed the bulk of the sediment to

the Ganga Delta and Bengal Fan. It has also been suggested that the Ganga foreland basin has been dominated by transverse river systems since the Pliocene due to erosionally driven uplift (symmetric subsidence of the foreland), whereas the Indus foreland basin has been dominated by longitudinal river systems due to tectonically driven uplift (asymmetric subsidence of the foreland) (Burbank, 1992). Large Plio-Pleistocene sediment fluxes combined with less asymmetric subsidence and uplift of the proximal foreland led to the progradation of the transverse drainage systems that displaced the Ganga River to the edge of the foreland basin. The present day position of the Ganga River is consistent with erosion-driven uplift in the adjacent Himalaya. Furthermore, the sediment accumulation rates generally exceeded the subsidence rates of the foreland throughout the history of the Ganga Basin (Burbank *et al*., 1996).

Many rivers flow along and within the structural grain of the fold belts until near their mouth (Figure 2.3e), and the most notable examples are the Mekong, the Brahmaputra, and the Irrawaddy. The Mekong has its marshy source on the Rup-sa Pass in the highlands of Tibet, where it rises as the Za Qu (Dza Chu) and flows generally south through Yunnan province in deep gorges and over rapids. Leaving Yunnan, the Mekong flows through or along the borders between Myanmar, Lao PDR and Thailand, finally reaching the Cambodian plains to form a large delta, most of which is in Vietnam. Barring the Cambodian plains, most of the river course lies within upland terrain. The Brahmaputra flows in deep gorges in the Tibet Himalaya for most of its course before debouching on to the plains of Bangladesh to form one of the world's largest deltas after meeting the Ganga.

Some rivers flow through stable platforms for most of their course and may not have their headwaters in an active mountain belt (Figure 2.3f). Examples include the Nile and the Niger Rivers which have their catchments in the uplifted parts of the shield (Figure 2.2). The Nile (Figure 2.2, no. 4), possibly the longest river in the world, has two branches, the White Nile from the equatorial east Africa and the Blue Nile from the Ethiopian Highlands, and both formed on the western flank of the East African Rift. Often referred to as 'inverted flow that goes downstream in going upstream' (Grimal, 1988), the Nile flows through a complex igneous terrain resulting in a series of rapids or cataracts before entering the wider northern valley and the delta region. The Niger River (Figure 2.2, no. 15) in western Africa has an unusual crescent-shaped course. Its source region in the Precambrian Guinean Shield is just 240 km from the Atlantic Ocean but the river flows away from the sea into the Sahara Desert and then takes a sharp right turn to southeast to flow into the Gulf of Guinea. It is believed that the present-day course of the Niger is a result of the merger of two independent systems, the Upper Niger and the Lower Negro due to drying of the Sahara in 4000–1000 BC (Gasse *et al*., 1990; Gasse, 2000).

Rivers owing their origin to mantle plumes (Figure 2.3g) tend to develop as dome-flank systems (Cox, 1989). The plume hypothesis (Burke *et al*., 1973; White and McKenzie, 1989) postulates that the fracturing of the domal structure formed by mantle plumes may produce rifts and volcanism. Cox (1989) suggested that the rivers rising close to the escarpment mark the flank of the remnant dome; they drain away from the continental edge and the failed arms of the rift system leads the drainage towards the new ocean. The Paraná River in southern Brazil and the Orange river in southeastern Africa related to the Serra do Mar and Cape Angola topographic highs are cited as examples of this type of drainage (Cox, 1989).

The tectonic setting of large rivers, coupled with catchment lithology and erosional history, is clearly reflected in the longitudinal profile of the river. A useful parameter is 'stream gradient index' (Hack, 1973), a function of slope and distance from source. In general, high gradient indices (implying high stream energy) would correspond to (a) a belt of resistant rocks, (b) a zone of differential uplift, or (c) erosional disequilibrium between two drainage systems. Conversely, low gradient indices would suggest (a) a belt of less resistant rocks, (b) zone of differential subsidence, or (c) depositional disequilibrium between two drainage systems (Brookfield, 1998). Relatively sudden changes of gradient (knickpoints) are generally interpreted to have been caused by tectonics and river capture. Several rivers in the Tibetan and Himalayan region display dramatic shifts in their longitudinal profiles which mark the reaction to major uplift and shear (Seeber and Gornitz, 1983; Brookfield, 1998).

2.4 LARGE RIVERS – CLIMATIC SETTINGS AND CLIMATIC VARIABILITY

Climatic effects on the development of large rivers are generally manifested through their control upon erosion processes. The two most important climatic factors influencing the drainage pattern include precipitation and temperature through their control on vegetation cover (Leopold *et al*., 1964; Gregory and Walling, 1973). Large rivers occur in areas of large annual rainfall such as the humid tropics (see Figure 2.4).

Precipitation depends upon latitude (air pressure), temperature, available moisture, atmospheric disturbances, landform barriers, frontal activity, air mass movement,

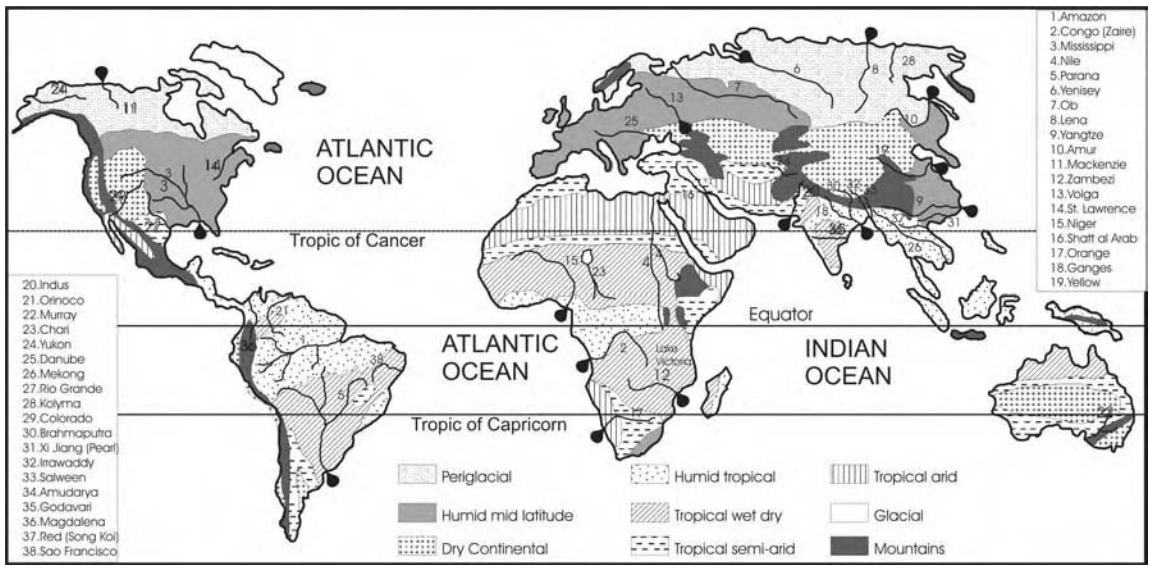

Figure 2.4 Large rivers – their climatic settings and climatic variability. Redrawn from Global Geomorphology, Summerfield, M.A., Longman: London, 1991, with permission from Pearson Education Ltd

and differential heating. For large rivers to form, adequate precipitation must fall in the source or headwater areas of the rivers so that the river has sufficient power to erode and develop the drainage network. Tropical latitudes are the zones of convergence of air streams and therefore the zones of maximum precipitation. Many large rivers today occur in the tropical regions.

An important control of precipitation in a region is a mountain barrier which generally forms the headwater areas of large rivers. Such barriers force the moisture-laden winds to ascend and thus cause precipitation. The precipitation is concentrated on the windward slope and a rain shadow is established on the leeward side of the mountain. In tropical areas, upper air subsidence disfavours precipitation but rain falls in these areas through orographic precipitation.

Glaciation has also affected several large rivers such as the Mississippi, Mackenzie, and St Lawrence to the extent of major diversions (Mississippi/St Lawrence system) and drainage reversal (Yukon). Continental glaciation, about 100 ka before present, blocked the Mississippi near Rock Island and diverted it to its present course farther to the west. The Mississippi River course has also been temporarily reversed by the earthquakes (1811 and 1812, ~8 on the Richter scale) along the New Madrid Fault Zone related to a failed rift that formed at the same time as the Gulf of Mexico. The Yukon River, one of the longest rivers in North America, originates in the Llewellyn Glacier at the southern end of Atlin Lake in British Columbia and has been strongly affected by glaciation throughout its history (Bridges, 1990). The Mackenzie River, the longest river in Canada (~1800 km) begins at Great Slave Lake in the Northwest Territories and flows north into the Arctic Ocean. The Mackenzie River freezes every year in October and melts in May and therefore the hydrology of the river is strongly affected by the glacio-fluvial processes.

It is now well established that the earth's climate has changed with time, and as a consequence, the response of large river systems to ongoing and future climate change has become a subject of intensive research. Climate change is caused by the combined effects of many forcing functions, and this leads to complexities in the natural response times of the various components of the earth's climate system, including those of large rivers. Ruddiman (2001) has emphasized large scale responses in terms of the presence of ice sheets at high latitudes, changes in strength of low-latitude monsoon circulations, the reaction of ice-free land surfaces outside monsoon regions, the flow of deep water and the movement of carbon among reservoirs in the climate system.

Climate variability in monsoonal settings has been investigated on various timescales (Prell and Kutzbach, 1987; Overpeck *et al*., 1996). It has been demonstrated that much of the considerable variability over the past 150 000 years occurs at orbital periodicities 'and all of the

paleo-climatic time series show four monsoon maxima that occur during interglacial conditions and coincide with the precession maxima and minima of the northern hemisphere summer radiation' (Prell and Kutzbach, 1987, p. 8411). Our understanding of the response of large river systems such as the Ganga to such changes is still not satisfactory. Goodbred (2003) has suggested that climate-related signals propagate downstream and show tight coupling between source area, catchment basin, and coastal and marine depocentres. However, the nature and amplitude of climate shift required to bring about a response in large dispersal systems is not fully understood. It is also not clear how the fluvial system is affected by increased sediment load and whether the sediment supply processes are threshold controlled. High sediment flux in the Early Holocene in many large systems such as the Ganga-Brahmaputra system, although documented by earlier workers, has not been mimicked so far in hydrological models by increase of precipitation alone (I. Overeem, personal communication). The importance of threshold processes such as landsliding and glacial sediment production remains to be established. Earlier studies on the response of the dispersal system to climate change on multimillennial timescales ($<10^4$ years) in a system-wide and contemporaneous manner require renewed assessment in view of the limited data on which these conclusions are based. Many of world's large rivers and deltas are concentrated in the monsoonal belt of Asia wherein the sediments stored in the system are vigorously mobilized and transported to the delta region, and therefore, provide a record of the source-to-sink response of the system (Goodbred, 2003). However, the long-term role of climate in these systems is not fully understood.

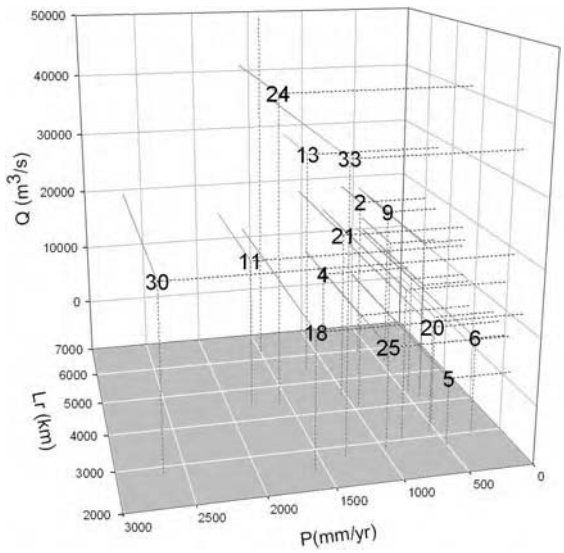

Figure 2.5 Characterization of large rivers on the basis of precipitation (P), length (Lr) and discharge (Q). (Numbers correspond to names of some of the rivers, see Fig. 2.4 for explanation.) The Amazon River has not been plotted due to scale constraints. Two distinct clusters can be recognized in terms of length, falling in the range 2000–3000 km and 4000–5000 km. Both precipitation and discharge parameters show significant variability

2.5 MODERN LARGE RIVERS – HYDROLOGY AND SEDIMENT DISPERSAL

Large rivers are hydrological systems with high magnitude basin areas, main channel lengths, and water and sediment discharges. Potter (1978) provided measurements for 50 large rivers of the world. Hovius (1998) compiled data on water discharge, sediment yield, sediment transport, and source area characteristics of 97 intermediate and large rivers (catchment area $>2.5 \times 10^4\,km^2$) from a variety of climatic, topographic, tectonic and geomorphic settings.

Figure 2.5 plots the length and the discharge of large rivers as a function of precipitation (the Amazon has been excluded from this plot due to scaling constraints). A large range in the precipitation regime of large rivers is obvious from this plot. In terms of length, several rivers fall within the 2000–3000 km range but a larger cluster is within the length 4000–5000 km range. Only two rivers are longer than 6000 km, namely the Nile and the Amazon (not plotted). Annual discharges of the large rivers are extremely variable. The discharges of the Nile and the Salween are as small as 3157 and 1460 $m^3\,s^{-1}$, respectively, whereas those of the Amazon and the Congo are 200 000 and 40 000 $m^3\,s^{-1}$. Several rivers fall in the range 10 000–20 000 $m^3\,s^{-1}$, including the Paraná, the Mississippi, the Brahmaputra, the Mekong and the Ganga.

Large rivers mobilize an enormous amount of sediments from their source areas, a part of which is accommodated within the basin and the rest is finally delivered to the oceans. Figure 2.6 shows plots for 38 large rivers listed by Hovius (1998) and highlights the hydrological and sediment supply characteristics of these rivers. Figure 2.6a shows that water discharge (Q) generally increases with drainage area (A). Three major exceptions are the Nile, the Colorado and the Rio Grande, which flow through tropical arid or tropical semi-arid climatic zones (Figure 2.3) for most parts of their course, leading to relatively low discharge. Figure 2.6b plots the drainage area and suspended/dissolved load, and a large scatter is generally interpreted to be a manifestation of varied precipitation

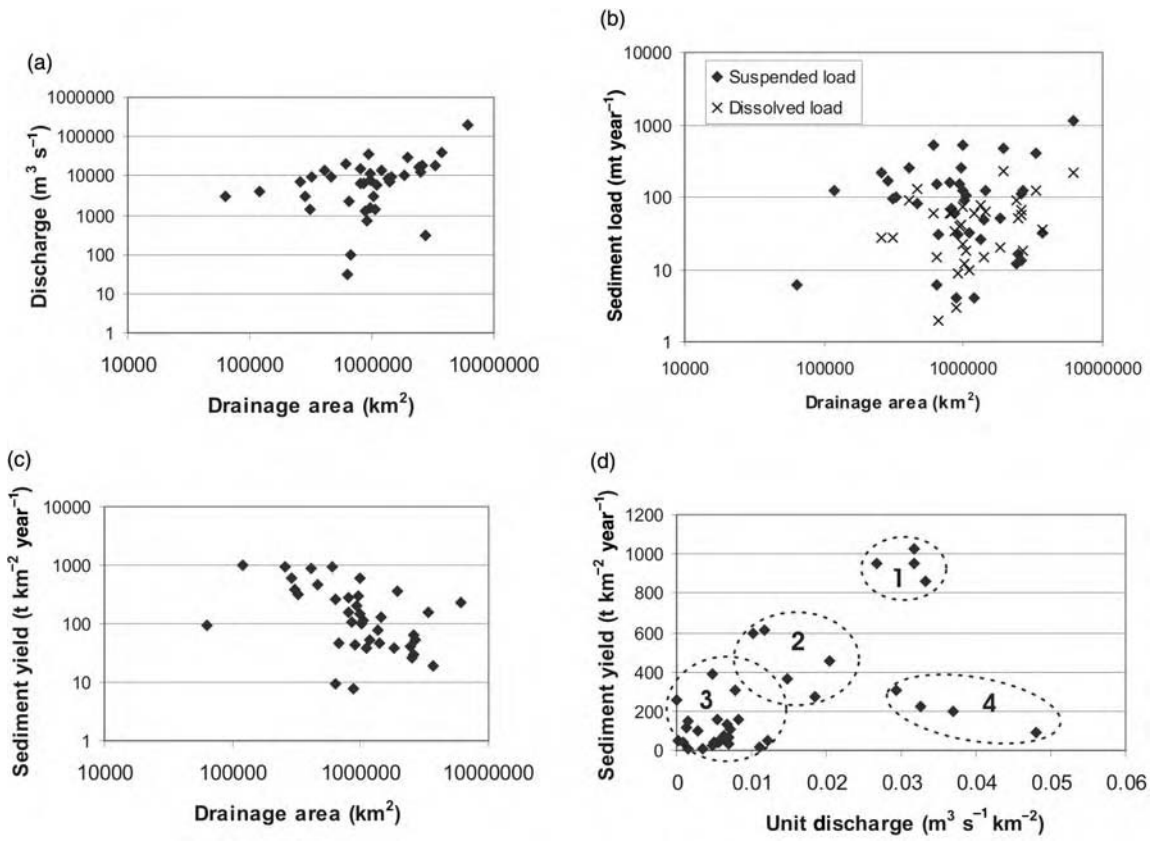

Figure 2.6 Drainage area, and discharge sediment of selected large rivers: (a) discharge vs drainage area; (b) sediment load vs drainage area showing large variability which is a function of precipitation and/or topographic characteristics; (c) sediment yield vs drainage area; (d) sediment yield vs unit discharge showing distinct clusters which are a function of tectonic setting of the hinterland of the rivers. Based on data from Hovius, 1998

characteristics and/or topographic aspects of the drainage basin (Hovius, 1998). A number of other studies have also suggested a weak correlation between denudation rate and precipitation (Ahnert, 1984; Pinet and Souriau, 1988) keeping in mind that many erosional processes are influenced by instantaneous precipitation rather than mean annual precipitation (Caine, 1980).

Figure 2.6c shows that sediment yield (based on sediment delivery to the river mouth) generally decreases with drainage area. Hovius (1998) found a better correlation and a broad zonation if the data are separated in terms of tectonic setting of the drainage basin. A plot of annual discharge and sediment load showed a very poor correlation. However, a plot of unit discharge (discharge per unit area) and sediment yield (Figure 2.6d) brings out interesting relationships. Cluster 1 with highest values of both unit discharge and sediment yield includes the Magdalena, Brahmaputra, Sông Hóng (Red), and Irrawaddy. The Magdalena transports ~250 million tonnes of sediment annually from the Columbian Andes, which corresponds to ~20% of the total sediment load of the Amazon system (Latrubesse *et al*., 2005). The Brahmaputra with an annual load of ~580 million tonnes ranks first among the world's rivers in terms of sediment yield (Figure 2.6d), a reflection of the continued high uplift rates of the Himalaya. The Sông Hóng and the Irrawaddy also have very high sediment production in their catchments.

Rivers such as the Ganga, Godavari, Mekong, Yangtze, and Pearl fall in Cluster 2. These rivers are essentially Himalayan drainages with high sediment production in active tectonic settings, except the Godavari which has high sediment yield in spite of its cratonic setting.

Both Clusters 3 and 4 represent situations of relatively low sediment yield at the river mouth. A large number of

rivers fall in Cluster 3 showing the lowest values of unit discharge which is self-explanatory. Cluster 4 shows the highest values of unit discharge with corresponding low values of sediment yield and includes four rivers, namely the Amazon, Orinoco, Sao Francisco, and Salween. Both the Orinoco and the Sao Francisco drain shields (Figure 2.2) but fall in humid mid-latitudes and tropical wet/dry climatic regimes respectively (Figure 2.4), which explains high discharges but low sediment production in their catchment. The inclusion of the Amazon and the Salween in this cluster seems to be a function of size. The Amazon is a very large fluvial network which stores a large part of its sediment load in its alluvial plains (tropical rainforest), and hence the sediment yield at its mouth is much lower. The Salween is a smaller system with an annual sediment load of ~100 million tonnes but with a discharge of $>9500\,m^3\,s^{-1}$.

Based on a regression model, Hovius (1998) suggested five estimator variables to explain the variance in global sediment yield, namely specific runoff, drainage area, maximum catchment height, mean annual temperature, and annual temperature range. However, they only explain about half of the observed variance. Hovius (1998) also pointed out that an important control of sediment supply/yield is the rate of uplift in the catchment, which essentially provides new material for erosion and which is not adequately reflected in most models of sediment yield. It is obvious that the catchments in active orogenic belts would have high sediment yields ($100–10\,000\,t\,km^{-2}$ $year^{-1}$) whereas the cratonic catchments would have much lower sediment yields ($<100\,t\,km^{-2}$ $year^{-1}$). Old orogenic belts would have moderate values of sediment yield ($<200\,t\,km^{-2}$ $year^{-1}$). In other words, the estimates of sediment yield provide an indirect indication of tectonic activity in the catchment. Recent studies (e.g. Lavé and Avouac, 2001) have provided means of very precise estimates of uplift in the Himalayan catchments, but the data are too scarce at this stage to develop any quantitative relationship between the uplift rate and sediment supply. The relative role of uplift rate in influencing the sediment supply compared with climatic and topographic variables is a currently debated topic and an integrated understanding is yet to emerge.

Two important issues need to be mentioned here with regard to the hydrological and sediment transport data. First, all of these data pertain to the modern settings. In ancient rivers, prior to the establishment of vascular plants which greatly assist in stabilizing land surfaces, it is probable that sediment yield from catchments was proportionally greater than at present. This transition is generally put at Late Silurian onwards, but vascular plants are now known earlier than this (Ordovician), although not seemingly in great abundance (Gibling, 2006). Second, the data represented in these plots include some anthropogenic influence due to increased agricultural practices and deforestation in the catchments, providing a range of variation amongst the large rivers in the world.

The rate of sediment supply along with change in accommodation space eventually controls the development of alluvial stratigraphy within the basin (Schlager, 1993; Shanley and McCabe, 1994; Hovius, 1998). Furthermore, many of the large rivers have formed significantly large deltas at their mouths, which mark the penultimate storage of sediments before final discharge into the deep sea. Sediment supply at the river mouth essentially reflects the integrated response of the entire river system, and the partitioning of sediments between the delta region and the deep sea will eventually control the stratigraphy of the continental margins. Goodbred and Kuehl (1999) provided first-order estimates of the sediment budgets of the Ganga-Brahmaputra system, which is ranked very high among the world's river systems in terms of sediment flux. They concluded that about 30% of the annual discharge is accommodated within the floodplains and delta plains, ~40% of the sediment load stays in the subaqueous delta, and the remaining 30% is transported to the deep-sea Bengal Fan. Such studies have important implications towards refinement of sequence stratigraphic models, and they support the earlier findings of Milliman and Syvtiski (1992) that the clastic sediment flux into the oceans from rivers may be overestimated because these have not taken into consideration the accommodation of a large volume of sediments in floodplains and delta plains.

2.6 VARIABILITY IN THE ALLUVIAL ARCHITECTURE OF LARGE RIVER SYSTEMS

The sedimentary record reveals a complex history of the erosional development and dynamics of large river systems. The very nature of a river system is to produce sediments which record the variability of the processes through time and space. The rock record, for example, frequently shows transitions from meandering to braided rivers, which is in line with the downstream variations of channel pattern in modern rivers as well as with temporal changes in morphology as a function of variable discharge and sediment load. Some understanding of the alluvial architecture evolving below modern river plains in a variety of settings is available, and we draw extensively from our own work (Gibling *et al*., 2005; Sinha *et al*., 2005a; Tandon *et al*., 2006) in the Ganga plains to illustrate the variability of alluvial stratigraphy of the large river systems under different climatic and geomorphic settings.

2.6.1 Longitudinal Trunk Systems

River systems like the Ganga and the Paraná are good examples of longitudinal systems. The Ganga flows parallel to the Himalaya after it debouches on to the plains for a major part of its course, before it reaches the Bay of Bengal. The fragmentary information available from the different reaches of the Ganga suggests that the upper reaches of the river has numerous gravel bars, and several metres of gravel deposits are the main element of the alluvial architecture (Figure 2.7a). The gravels disappear within about 20 km of its downstream journey from the

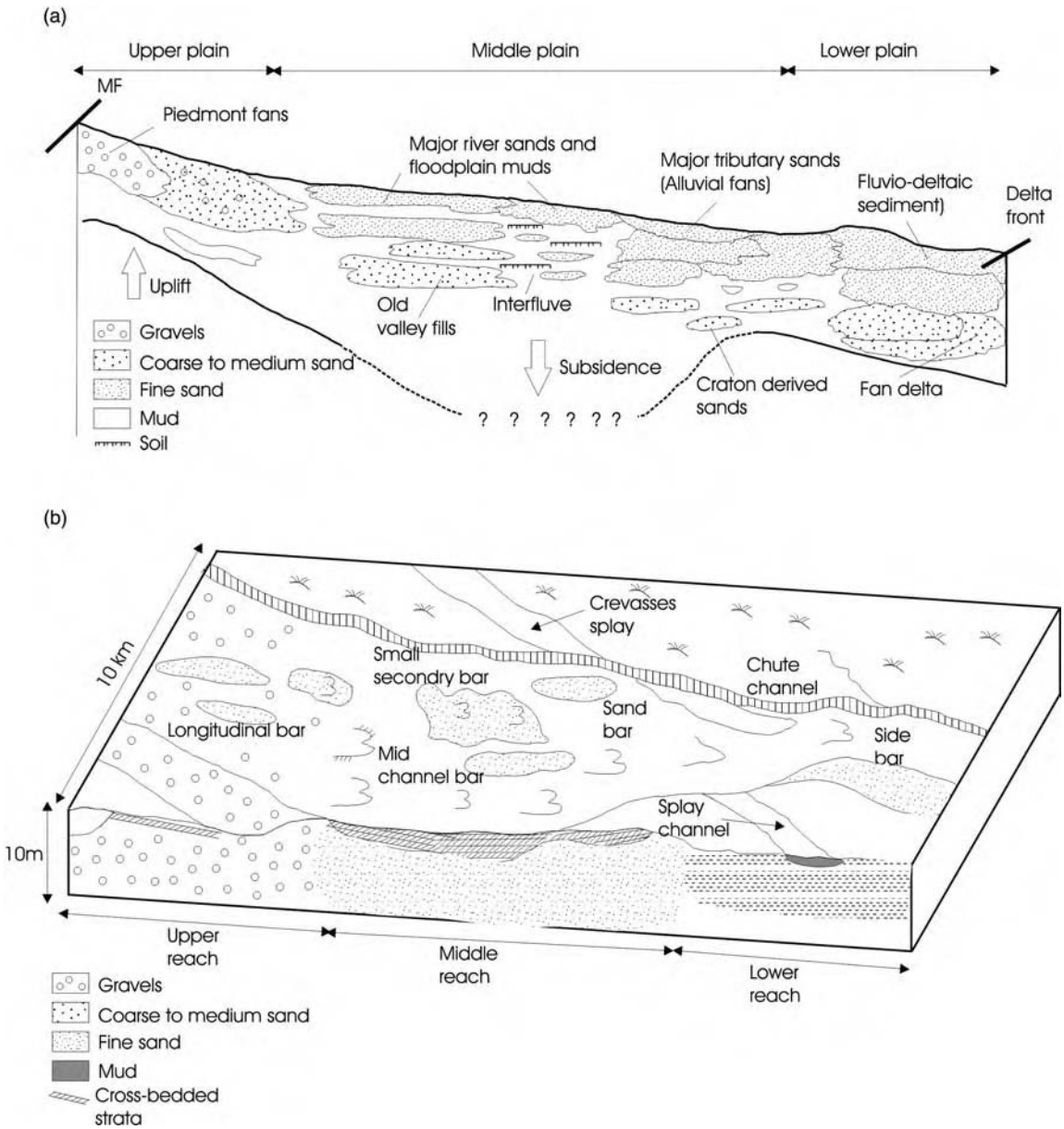

Figure 2.7 Variability in alluvial architecture of large rivers: (a) longitudinal trunk system; (b) radial fan; (c) fan–interfan system. Reproduced from Current Science, 84(8), Jain, Sinha, 1025–1033, Copyright (2003), Current Science Online; (d) interfluve. Reproduced from Journal of Sedimentary Research, 75(3), Gibling *et al*., 369–385, Copyright (2005), Society for Sedimentary Geology. MF, Mountain front

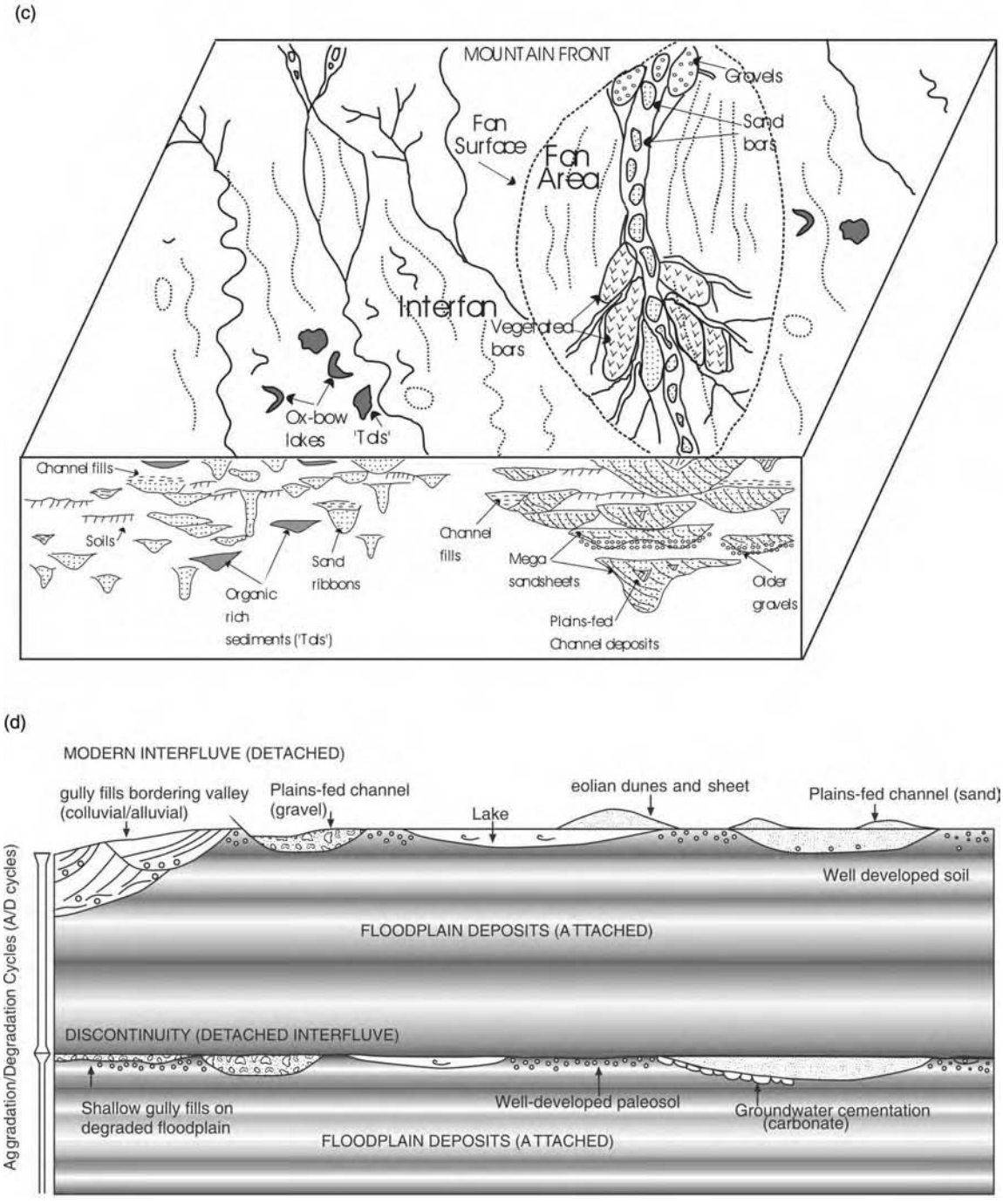

Figure 2.7 *Continued*

mountain front, and are replaced by coarse sands (Shukla *et al*., 2001) corresponding to the braided channel belt. The channel belts in the middle reaches of the Ganga show a mean grain size of fine to very fine sand in modern deposits, although layers of medium to coarse sand, 9–10 m thick, have been recorded in deeper valley fills (Sinha *et al*., 2005a; Tandon *et al*., 2006). These channel sands are separated by floodplain mud, 5–7 m thick, which are pedogenically altered, thus indicating switching of the main channel.

Very little information on alluvial architecture is available for the lower Ganga plains. Stratigraphic sections plotted by Umitsu (1993) and Goodbred and Kuehl (2000a) based on the borehole data suggest about 90 m of uninterrupted sand deposits. The upper sand bodies grade from medium sand close to the channel to fine sand away from it but the basal sediments are dominantly coarse sand. Such sequences and the absence of fine-grained deposits suggest the occupation of the present channel through much of the Quaternary (Goodbred and Kuehl, 2000a).

2.6.2 Radial Fans

The Kosi River, a major inland tributary of the Ganga in the Bihar plains is an excellent example of a radial fan. Most workers have recognized distinct zonal distribution of facies from upstream to downstream; four zones are recognized in Kosi megafan deposits (Singh *et al*., 1993), namely zone 1 (gravelly sandy, braided, 20 km), zone 2 (sandy, braided, 95 km), zone 3 (fine sand/mud, straight, 40 km) and zone 4 (fine sand/mud, meandering, 160 km). The three-dimensional architecture of megafan deposits consists of multi-storeyed sand-sheets (generally gravel in upper reaches), interbedded with overbank muddy layers (Figure 2.7b). The thickness and facies distribution varies from upstream to downstream. The sand sheets are typically 8–10 m thick and 16–20 m in the case of multi-storeyed bodies (Singh *et al*., 1993).

2.6.3 Fan–Interfan Setting

The alluvial plains between tributaries of the Ganga system in the eastern plains, namely the Gandak and the Kosi, exemplify transverse fan–interfan settings. Contrary to the understanding that the interfans represent rather subdued fluvial activity, the interfan areas in the eastern Ganga plains are occupied by active rivers, only smaller than the fan-generating rivers, with several being extremely dynamic showing decadal-scale avulsions (Jain and Sinha, 2004). The information available on the stratigraphy of the interfan area is very limited. Shallow alluvial architectural studies in the Gandak-Kosi interfan (Sinha, 1995; Jain and Sinha, 2003) showed that the top 2–3 m of the interfan area predominantly consist of muddy sequences, with narrow sand bodies defining former channel positions and very minor sandy layers defining crevasses (Figure 2.7c). More detailed studies in the Baghmati alluvial plains in north Bihar on the basis of subsurface records down to about 300 m show that 30–50 m thick mud-rich units including very thin sand layers (2–4 m) characterize the distal floodplain environment (Sinha *et al*., 2005b). Thin sands intercalated with mud may represent crevasse splay deposits or the occasional influx of sand-grade material into the floodplains. Sands in the top 50 m range from a few metres to 25 m thick and extend laterally for about 10 km, suggesting the presence of sand sheets below. It is likely that the present-day fan and interfan positions have interfingered in the past and the adjoining fans may also have contributed to the building of the alluvial architecture below the interfan areas. In the adjoining Sarda-Gandak interfan area, the top 10–20 m of sediments are also characterized by muddy sequences averaging thick medium sand layers (Chandra, 1993).

2.6.4 Interfluves

Many of the large river basins have active fluvial belts separated by wide interfluves that are currently not flooded by the rivers. As the major drainage axis of the rivers incise, distinctive interfluve discontinuities are generated across the floodplains. In coastal plains, such surfaces are generally recognized by well-developed palaeosols but the alluvial tracts may have several other manifestations of such discontinuities. The interfluve successions in the western and southern Ganga plains comprise a series of discontinuity-bounded sequences with alternating aggradational and degradational units (Figure 2.7d). The aggradational units are characterized by overbank mud and sand whereas the degradational units show gullied degradation surfaces, palaeosols, lacustrine mud, and aeolian silts. Age models for the successions show a first-order correlation between modelled precipitation changes and periods of incision and accumulation over 10^3–10^4 years. It has been inferred that the alluvial architecture in the western and southern Ganga plains has been governed by fluctuations in monsoonal precipitation (Gibling *et al*., 2005). Marine Isotope Stages (MIS) 3–5 appear to represent a period of strong fluvial activity. In the proximal interfluves, floodplain deposits capped by aeolian and lake deposits record reduced river activity after 27 ka before present as the region entered the Last Glacial Maximum. Channels elsewhere were filled with aeolian sediment and windblown shells at this time. In the distal interfluve cores, we record

50 m of floodplain deposits that date back to about 86 ka before present (Sinha *et al*., 2007). The distal interfluves appear to have been a site of floodplain accumulation from small plains-fed channels over this period, during which Himalayan and plains-fed channels appear to have occupied separate floodplain tracts, with large parts of the plains detached from the direct effects of the large rivers. The interfluve floodplains were sites of more intense pedogenesis, and accumulated through cycles of aggradation and soil formation, possibly in response to monsoonal fluctuations on a timescale of 10^3–10^4 years (Gibling *et al*., 2005).

It is worth pointing out that no megafans have developed in the western Ganga plains, in sharp contrast to the eastern Ganga plains discussed in the preceding section. Most rivers of the western Ganga plains are deeply incised, probably due to low sediment yields and high unit stream power (Sinha *et al*., 2005c). It is suggested that such hydrological differences in the river system have resulted in a marked geomorphic diversity across the plains (Sinha *et al*., 2005c; Tandon *et al*., 2006), and this contrast may have existed for a fairly long time because it probably reflects long-term precipitation gradients and tectonic patterns. There is a significant implication of such spatial inhomogeneity in geomorphic development in understanding fluvial response to climate change. Spatial or geographical differences in fluvial response due to global change in circulation patterns result in changes in discharge regimes (Blum and Törnqvist, 2000). However, it is also recognized (Sinha *et al*., 2005c) that significant inhomogeneities may also occur in areas separated by less than 1000 km in large river systems due to spatial differences in sediment supply governed by rainfall and tectonics. Given such inherent inhomogeneities, these areas would also respond differently to any change in global circulation pattern. In other words, they would have a 'differential sensitivity' (Blum and Törnqvist, 2000) to climate change. If such differential sensitivity has existed over a long timescale, this would be translated into variable alluvial architectural styles developing below the plains.

2.7 GROWTH AND DEVELOPMENT OF LARGE RIVER SYSTEMS

Large rivers evolve through geologic time; their growth and development is therefore intricately linked to (a) tectonic processes such as orogenesis, rifting and domal/plateau uplifts, and (b) long term climatic variability including precipitation trends. Large river systems are also influenced by the dynamic interaction between tectonism and erosion. Tectonic and climatic processes together influence uplift in mountain systems such as the Himalaya (Hodges *et al*., 1996; Beaumont *et al*., 2001; Wobus *et al*., 2003). The interplay between focused precipitation, erosion and uplift in response to unloading favour the sustenance of hinterland to basin slopes over geological timescales. Topographic barriers, for example, such as those associated with the Main Central Thrust in the Higher Himalaya, promote focused denudation and this acts as a positive feedback for the sustenance of this system of slope development, water and sediment supply – all factors that promote and nurture large river systems. A key region where these processes are being actively investigated is the Himalaya. The Indus, the Ganga and the Brahmaputra are considered antecedent to the main mountain building events in the Himalaya. The Himalayan foredeep preserves fluvial deposits belonging to at least ~30 million year old stratal sequences. Growth and development of the foredeep resulted in the formation of early and Middle Miocene large river systems, flowing southeastward to the Bay of Bengal. Major sand-dominated large rivers flowed in the Himalayan foreland, ~10 Ma ago. Burbank *et al*. (1996) indicated that at this time sandstone abundances doubled, fluvial discharges increased fivefold, and a major influx of detritus occurred. Tectonic loading associated with the Main Boundary Thrust led to the establishment of these large axially flowing sandy fluvial systems. Major reorganization of the western Himalayan river system took place after 5 million years ago (Clift and Blusztajn, 2005). Major tributaries of the Ganga in the Punjab were captured by the Indus. Either northeastward advance of the tributaries of the Indus resulted in the capture of the tributaries of the Ganga, or tectonic episodes of the Main Central Thrust and early Miocene uplift of the Salt Range may have caused this major drainage reorganization (Clift and Blusztajn, 2005). For the main part, hinterland tectonics and focused denudation because of uplift driven by erosional unloading appear to be the main influential factors in the growth and development of the large river system sourced in the Himalaya; base level changes modulate the large river system(s) in this region in a framework determined by coupled hinterland tectonic-climatic processes.

Cox (1989) has suggested the role of mantle plumes in the development of continental drainage patterns in the Deccan (India), southern Brazil, and the Karoo (Africa). According to Cox, 'characteristic drainage patterns indicating topographic doming associated with plume activity are still preserved after up to 200 Ma. Crustal thickening by magmatic differentiation is the most likely cause of the persistence of such features' (Cox, 1989, p. 873). In the above framework of domal uplift and rifting, some rivers are considered to be of great antiquity. For example, the

Orange system is considered to have originated in the Jurassic, about 190 Ma ago. Further, Cox (1989) has pointed out that the Orange is antecedent to the Cape-Angola high, and that it 'presumably originally flowed on into the general region of Buenos Aires lending weight to speculation about the possibility of other African rivers such as the proto-Congo flowing across South America'. Kent (1991) cited palaeoflow patterns in eastern India as evidence for long-lived drainage systems due to uplift associated with a mantle plume below eastern Gondwana. Preservation of dome flank drainages is partly related to the age of the volcanic province, but these are best preserved where the flat-lying volcanics or subvolcanic sediments are still preserved. The rift-related river systems flow at lower topographic levels in relation to the dome flank drainage, and can lengthen the system by river capture (Cox, 1989). A number of large rivers may also come together by joining of several streams by avulsion, stream capture, etc., and one of the best examples is the Zambezi, which is joined by more than six major tributaries including the Cuando and the Kafue in the upper and middle Zambezi, respectively.

Evidently the growth and developmental stages of large river systems follow different pathways in different settings. The evolutionary history of a large river system is complex and strongly dependent upon geologic and climatic factors. It is indeed a moot point that large river systems evolve from smaller systems, and in many cases their early history may stand obliterated. The modern large river channel system of a 'large river basin' represents a limited part of its long evolutionary history.

2.8 DURATION OF LARGE RIVER SYSTEMS AND THE ROCK RECORD

The question of the duration of the large river systems has been intensely debated in the literature and is normally defined from the date of its 'origin' to 'termination'. The issues regarding the origin of the large river systems have already been discussed in earlier sections. Potter (1978) commented on the determinants of the termination of large rivers as any large geological event such as a marine invasion, glacial event, and drastic change in precipitation regime or volcanic outpouring. However, many systems can be remarkably long-lived because such events may affect only a part of the system and the river can be rejuvenated after some interruptions in a more or less similar setting and location. The best cited example is the Mississippi dating back to 250 Ma which follows the axial zone of the Mesozoic-Cenozoic fill in the Mississippi Embayment which has been considered to be a manifestation of a reactivated rift initiated in the Late Precambrian (Ervin and McGinnis, 1975). There is probably no other river system in the world reported to have such longevity but there are a few others that may have existed for at least 100 Ma. A series of small deltas in the Tertiary of Texas mapped by Fisher and McGowen (1967) remarkably shows their spatial coincidence with several of the modern drainage systems such as the Colorado, the Brazos and the Trinity. Potter (1978) observed that this coincidence suggests a 'vertical persistence in time' of the ancient river systems. The ancient beginning of the Nile river has its origin in systems that traversed the Afro-Arabian swell as early as the Late Cretaceous, about 100 Ma ago (Hurst and Phillips, 1931) preserved as the Nubian Sandstones.

Many studies have reported large river deposits in the rock record and a detailed compilation of alluvial architecture of ancient channel bodies is provided by Gibling (2006). The Triassic (~200 Ma) Hawkesbury sandstone of the Sydney Basin in New South Wales, Australia is believed to represent the deposits of an unusually large braided river. Recent work (Miall and Jones, 2003) has estimated the magnitude of Hawkesbury channels and bars from the preserved architecture and suggested this to be somewhat smaller than the modern Brahmaputra system. The Siwalik Group of rocks (Miocene) in the Himalayan foreland basin is considered to have formed by rivers originating in the Himalaya flowing southward; the major sedimentation was in the form of megafans, very similar to those presently operating in the Ganga plains (Parkash *et al*., 1980; Kumar, 1993; Friend *et al*., 2001). The compilation of the rock record of river systems by Gibling (2006) also suggests that braided and low-sinuosity rivers were the dominant fluvial style through the geological time. In the Early to Mid-Palaeozoic, the development of vascular plants stabilized the land surface which was manifested in a much wider range of fluvial styles.

2.9 SEA LEVEL, TECTONIC AND CLIMATIC CONTROLS ON THE LARGE RIVER SYSTEMS

The processes controlling valley formation and filling in large river basins are extremely variable in space, and Figure 2.8 shows a simplified model, based on the Ganga system, to explain the spatial variation in valley generation. Tectonic and climatic effects are implicated in valley formation near the mountain front, where major faults are active. More broadly, tectonics also governs long-term subsidence and accumulation within the foreland basin, depending on distance from the thrust front and the complex topography of the underlying basement. The general lack of a proxy record for tectonic activity, however, hampers attempts to correlate alluvial architec-

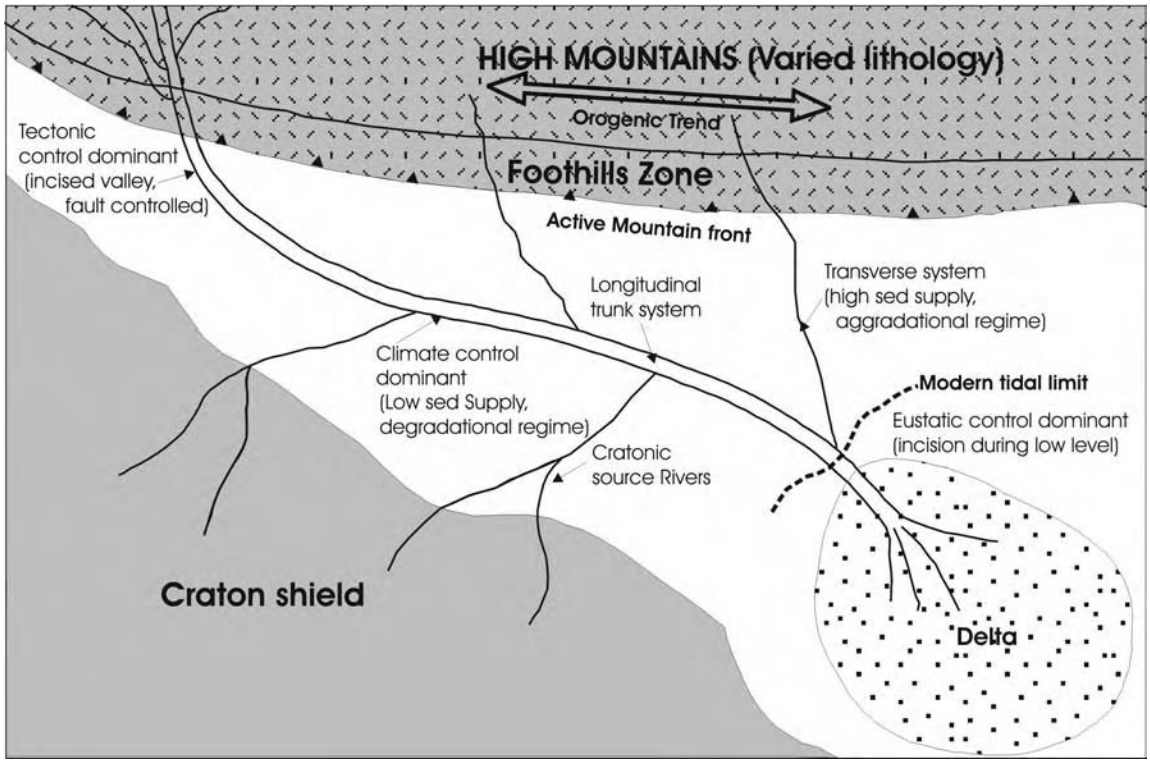

Figure 2.8 Sea-level, tectonic and climate control on valley formation for rivers like the Ganga. While both tectonics and climate controls are dominant near the mountain front, climate is an important factor away from the frontal region. Close to the sea front in the delta region, glacioeustasy exerts a key control in the valley formation and filling

ture with tectonic activity. Climate is an important factor away from the frontal region, where tectonic activity is reduced and subsidence rates are moderate. Glacioeustasy exerts a key control on valley incision and filling in the delta region.

Our studies in the Ganga system (Gibling *et al*., 2005; Sinha *et al*., 2005a; Tandon *et al*., 2006) along with those of Goodbred (2003) have shown that changes in southwest monsoon precipitation have affected all parts of the system over the past ~100 ka, from the foothills to the delta. In Himalayan valleys north of the eastern Ganga Plains, monsoon intensification has been linked to landslides and regolith removal, initially overwhelming the river's sediment transport capacity and causing aggradation, with subsequent erosion of material after about 7 ka (Pratt *et al*., 2002). Fluvial activity was greatly reduced during the Last Glacial Maximum (Cullen, 1981; Wiedicke *et al*., 1999; Goodbred, 2003) but subsequently intensified greatly. In consequence, sediment yield to the Ganga-Brahmaputra delta between 11 and 7 ka was more than double present rates (Goodbred and Kuehl, 2000b), and large volumes of sediment were transported to the Bengal deep-sea fan after about 13 ka, during a period of rapid sea-level rise (Weber *et al*., 1997). The subsidence rate also varied in the delta area, with especially rapid subsidence in the Sylhet Basin of Bangladesh (Goodbred and Kuehl, 2000b).

An important role for climate is also indicated from studies of deep-sea fan systems in southern Asia (Prins and Postma, 2000). Other factors that have affected discharge include meltwater fluctuations due to the growth and melting of Himalayan glaciers (Owen *et al*., 2002) and the activity of the northeast monsoon (Enzel *et al*., 1999). Additionally, there is local evidence for avulsion and river capture on the plains and in the headwaters (Wilhelmy, 1969; Parkash *et al*., 2000; Jain and Sinha, 2005; Roy and Sinha, 2005), caused in some cases by tectonic activity at mountain exits (Gupta, 1997) and by the intrinsic effect of sediment accumulation on megafans (Wells and Dorr, 1987).

The relationship between discharge of fluid and sediment is complex, with feedback loops, nonlinear responses, and response times that affect the system's sediment transport capacity in time and space (Bogaart *et al*., 2003). Knox (1993) noted that even modest climatic shifts may have huge effects on flood response and sediment yield. Within the Himalayan context, sediment pulses may reflect enhanced precipitation (Goodbred and Kuehl, 2000b; Pratt *et al*., 2002), but may also be independent of precipitation. For example, the 1950 Assam earthquake released 47 billion m^3 of sediment, which caused unprecedented floods as a result of channel aggradation and generated a wave of aggradation and subsequent degradation along the Brahmaputra River over a period of decades (Goswami, 1985). Depending on the balance between fluid and sediment availability and the energy available for erosion, rivers of the Ganga Plains may aggrade their channels and floodplains, or may incise or become underfit, detaching from the adjacent floodplains.

Hydrological changes in large river systems could be global due to phenomena that are widespread such as past glaciation or current ENSO events. Otherwise they may be linked to spatial variability in precipitation, sediment availability, distribution of snowmelt and vegetational effects, as well as the crossing of response thresholds. However, all parts of southern Asia are affected by the huge driver of the monsoon, and may be expected to show some degree of parallel response. Goodbred (2003) suggested that the Ganga system responds rapidly to fluctuations in fluid and sediment discharge in the headwaters, despite alluvial storage in the plains. He noted that sediment pulses recorded in the delta succession correspond in age with periods of sediment release in the headwaters, as well as with modelled precipitation maxima. Glacioeustatic changes in sea-level over the past 30 ka have clearly influenced the Ganga-Brahmaputra Delta. In the modern Ganga-Brahmaputra Delta region, Goodbred and Kuehl (2000b) documented two buried valleys extending for at least 350 km inland from the modern shoreline valley systems filled with at least 90 m of coarse- to fine-grained sand, coarsening upstream and thinning laterally. A boulder-rich layer underlying the valley fills has a slope much higher than that of the modern delta, suggesting that rivers were graded down to more than 100 m below present sea-level (Umitsu, 1993). A radiocarbon date of about 28 ka ^{14}C years BP (Umitsu, 1993) from below the boulder layer and dates from alluvium that post-dates the Last Glacial Maximum (LGM) suggest that the valleys filled during the lowstand of MIS 2 and the succeeding transgression, as sea-level rise promoted accommodation and backfilling.

Several studies have indicated that relative sea-level changes can impact large river systems and their deltas. As the sea level rises, freshwater/seawater interface is pushed landward, river gradient drops considerably and more accommodation space is created within the flooded reaches of the valley complex. Islam and Tooley (2004) suggested on the basis of lithostratigraphic and biostratigraphic data that the sedimentary environment within the Bengal Basin from Early Mid-Holocene until ca. 1750 BP was dominated by regional sea-level movements. They recognized five periods of marine to fluvial transitions during this period at a site (Panigati) ~100 km inland of the present-day tidal limit. Similarly, the Rhine extended some 800 km farther seaward from its present position during the LGM (Gibbard, 1988) and the terrace intersection of Pleniglacial terrace and Holocene deposits shifted landward by ~150 km as a result of Holocene sea level rise (Van Dijk *et al*., 1991). It has been demonstrated that the rate of sea-level rise also affects the channel pattern in the near-coast fluvial area. In the Rhine-Meuse delta a faster rate gave rise to low-energy, narrow anastomosing river pattern (7500–4000 ^{14}C years BP) whereas a slower rate resulted in dominance of low sinuosity meandering rivers (post-4000 ^{14}C years BP) (Törnqvist, 1993) although straight anastomosing channels continue to exist until present (Makaske, 2001). Low stream power was related to discharge and low gradients, and thus indirectly linked also to rapid sea-level rise (Makaske, 2001). Studies in the East China Sea (Wellner and Bartek, 2003) have also shown that sea-level changes during MIS 2 and 1, coupled with climate controlled water discharge, sediment supply, and shelf physiography controlled the valley fills in the region. During the sea level rise in late MIS 2, the upper parts of the drowned lowstand fluvial deposits were reworked into a valley-wide tidal bar and tidal sheet complex. This phase was followed by wetter climatic conditions during MIS 1 and a higher sediment delivery which resulted in burial and preservation of the lowstand fluvial deposits to a depth below the tidal effects.

2.10 CONCLUDING REMARKS

The development and growth of large river systems is strongly influenced by the interplay of climate, tectonics and source area characteristics. Many of the modern large rivers are confined within the tropics in monsoonal settings, obviously due to the high precipitation in these regions. The sustenance of first-order relief in the hinterland of the river systems is one of the prerequisites for the development of large rivers. The coupled effect of tectonics and climate is quite critical to sustain the large rivers. Mountain uplift and orographic precipitation are closely

interlinked. Focused denudation and erosion triggered by tectonics cause more uplift through isostatic effects, thereby sustaining the orographic precipitation (positive feedback system). Moreover, continued uplift and erosion provide continuity of slopes, resulting in high discharge and sediment transfer which, in turn, leads to valley enlargement.

A number of large rivers occur in the mid-latitude region, which has significantly different amount and distribution of precipitation compared with the tropics. The sustenance of large rivers in this region is likely to be related to the intensity and episodicity of the tectonic system.

Lithospheric flexure and subsidence play a major role in the development and the growth of large river systems. Collision belts and rift systems promote valley formation and create conduits for the transfer of water and sediment to the ocean. In cratonic areas also, relict domes related to mantle plume activity provide the necessary relief for the formation and sustenance of large rivers. Valleys of the large river systems occur in a variety of morphological settings, namely axial or transverse to the orogenic trend or confined within the mountain belt. The long-lived systems respond to changes in tectonic setting of the region, and may change spatial positions, altering the relative domains of axial and transverse systems.

Several issues related to the development of large rivers still remain unresolved. An improved understanding of sources and sustenance mechanisms of large rivers in a tectonics-climate coupled system remains a great challenge in the interdisciplinary domains of the earth sciences. Variations in annual sediment flux driven by climate through geological time, and its implications for sequence stratigraphic models, are intensely debated topics. A system-wide response of large river systems to climate change has been suggested by some workers, but the component-scale response of the system remains poorly understood and so does the propagation and transfer of the response from one component to another. We also need newer models of propagation of base level driven changes and an improved understanding of the interplay between the upstream propagation of base-level changes and downstream propagation of the source area related changes of large river systems.

ACKNOWLEDGEMENTS

We thank Avijit Gupta for inviting us to write this chapter and for bearing long delays. We have had several useful discussions with Martin Gibling during the writing of this chapter, which greatly benefited the scientific content. Several students helped in generating the diagrams and plots and we thank Sumit Kumar, Raj Kumar Mishra and Smita Swarup Swain for their efforts.

REFERENCES

Ahnert, F., (1984) Local relief and the height limits of mountain ranges. *American Journal of Science*, 284: 1035–1055.

Beaumont, C., Jamieson, R.A., Nguyen, M.H. and Lee, B., (2001) Himalayan tectonics explained by extrusion of a low-viscosity crustal channel coupled to focused surface denudation. *Nature*, 414: 738–742.

Belcher, R.C., (1975) The geomorphic evolution of the Rio Grande. *Baylor Geological Studies Bulletin* 29, 64 p.

Blum, M.D. and Törnqvist, T.E., (2000) Fluvial responses to climate and sea-level change: a review and look forward. *Sedimentology*, 47(Suppl.1): 2–48.

Bogaart, P.W., Van Balen, R.T., Kasse, C. and Vandenberghe, J., (2003) Process-based modelling of fluvial system response to rapid climate change – I. Model formulation and generic applications. *Quaternary Science Reviews*, 22: 2077–2095.

Bridges, E.M., (1990) *World Geomorphology*, Cambridge University Press, Cambridge.

Brookfield, M.E., (1993) Quaternary deposits along the Indus suture zone and evolution of Himalayan rivers. *Current Science*, 64(11 and 12): 903–907.

Brookfield, M.E., (1998) The evolution of the great river systems of southern Asia during the Cenozoic India-Asia collision: rivers draining southwards. *Geomorphology*, 22: 285–312.

Burbank, D.W., (1992) Causes of recent Himalayan uplift deduced from deposited patterns in the Ganga basin. *Nature*, 357: 680–683.

Burbank, D.W. and Beck, R.A., (1991) Models of aggradation versus progradation in the Himalayan foreland. *Geologische Rundschau*, 80: 623–638.

Burbank, D.W., Leland, J., Fielding, E., Anderson, R.S., Brozovic, N., Reid, M.R. and Duncan, C., (1996) Bedrock incision, rock uplift and threshold hillslopes in the northwestern Himalayas. *Nature*, 379: 505–510.

Burke, K.C., Kevin, J.F. and Dewey, J.F., (1973) Plume generated triple junction: key indicators in applying plate tectonics to old rocks. *Geology*, 81: 406–433.

Caine, N., (1980) The rainfall intensity-duration control of shallow landslides and debris flows. *Geografiska Annaler*, 62A: 23–27.

Chandra, S., (1993) Fluvial landforms and sediments in the north-central Gangetic plains, India. PhD Thesis, University of Cambridge, Cambridge.

Chapin, C.E. and Seager, W.R., (1975) Evolution of the Rio Grand Rift in the Socorro and Las Cruces areas. In: *Guide Book of the Las Cruces Country* (W.R. Seager, Ed.). New Mexico Geological Society, Socorro, NM, pp. 297–321.

Clift, P.D. and Blusztajn, J.S., (2005) Reorganization of the western Himalayan river system after five million years ago. *Nature*, 438: 1001–1003.

Covey, M., (1986) The evolution of foreland basins to steady state: the foreland basin of the Banda Orogen. *International Association of Sedimentology Special Publication* No. 8: 77–90.

Cox, K.G., (1989) The role of mantle plumes in the development of continental drainage patterns. *Nature*, 342: 873–877.

Cullen, J.L., (1981) Microfossil evidence for changing salinity patterns in the Bay of Bengal over the last 20 000 years. *Palaeogeography, Palaeoclimatology, Palaeoecology*, 35: 315–356.

DeCelles, P.G., Gehrels, G.E., Quade, J. and Ojha, T.P., (1998) Eocene-early Miocene foreland basin development and the history of Himalayan thrusting, western and central Nepal. *Tectonics*, 17: 741–765.

England, P.C. and Houseman, G.A., (1988) The mechanics of the Tibetan Plateau. *Philosophical Transactions of the Royal Society of London*, A326: 301–320.

Enzel, Y., Ely, L.L., Mishra, S., Ramesh, R., Amit, R., Lazar, B., Rajaguru, S.N., Baker, V.R. and Sandler, A., (1999) High-resolution Holocene environmental changes in the Thar desert, Northwestern India. *Science*, 284: 125–128.

Ervin, C.P. and McGinnis, L.D., (1975) Reelfoot rift: reactivated precursor of the Mississippi Embayment. *Geological Society of America Bulletin*, 86: 1287–1295.

Fisher, W.L. and McGowen, J.H., (1967) Depositional systems in the Wilcox Group of Texas and their relationship to occurrences of oil and gas. *Gulf Coast Association of the Geological Society*, 27: 105–125.

Friend, P.F., Raza, S.M., Geehan, G. and Sheikh, K.A., (2001) Intermediate-scale architectural features of the fluvial Chinji Formation (Miocene), Siwalik Group, northern Pakistan. *Journal of the Geological Society of London*, 158: 163–177.

Gasse, F., (2000) Hydrological changes in the African tropics since the last glacial maximum. *Quaternary Science Reviews*, 19(1–5): 189–211.

Gasse, F., Tehet, R., Durand, A., Gibert, E. and Fontes, J.C., (1990) The arid humid transition in the Sahara and the Sahel during the last deglaciation. *Nature*, 346(6280): 141–146.

Gibbard, P.L., (1988) The history of the great northwest European rivers during the past three million years. *Philosophical Transactions of the Royal Society of London*, 318: 559–602.

Gibling, M.R., (2006) Width and thickness of fluvial channel bodies and valley fills in the geological record: a literature compilation and classification. *Journal of Sedimentary Research*, 76(5–6): 731–770.

Gibling, M.R., Tandon, S.K., Sinha, R. and Jain, M., (2005) Discontinuity-bounded alluvial sequences of the southern Gangetic plains, India; aggradation and degradation in response to monsoonal strength. *Journal of Sedimentary Research*, 75(3): 369–385.

Goodbred S.L., Jr, (2003) Response of the Ganges dispersal system to climate change: a source-to-sink view since the last interstade. *Sedimentary Geology*, 162: 83–104.

Goodbred, S.L. and Kuehl, S.A., (1999) Holocene and modern sediment budgets for the Ganges Brahmaputra river system: evidence for highstand dispersal to flood-plain, shelf and deep-sea depocentres. *Geology*, 27(6): 559–562.

Goodbred, S.L. and Kuehl, S.A., (2000a) The significance of large sediment supply, active tectonism, and eustasy on margin sequence development: Late Quaternary stratigraphy and evolution of the Ganges-Brahmaputra delta. *Sedimentary Geology*, 133: 227–248.

Goodbred, S.L. and Kuehl, S.A., (2000b) Enormous Ganges-Brahmaputra sediment discharge during strengthened early Holocene monsoon. *Geology*, 28(12): 1083–1086.

Goswami, D.C., (1985) Brahmaputra River, Assam, India: physiography, basin denudation, and channel aggradation. *Water Resources Research*, 21: 959–978.

Gregory, K.J. and Walling, D.E., (1973) *Drainage Basin Form and Process*, John Wiley & Sons, Ltd, New York.

Grimal, N., (1988) *A History of Ancient Egypt*, Blackwell, London.

Gupta, S., (1997) Himalayan drainage patterns and the origin of fluvial megafans in the Ganga foreland basin. *Geology*, 25(1): 11–14.

Hack, J.T., (1973) Stream-profile analysis and stream gradient indices. *United States Geological Survey Journal of Research*, 1: 421–429.

Hess, R., Klaucke, I., Khodabaksh, S., Piper, D.J.W., Ryan, W.B.F. and NAMOC Study Group, (2001) Sandy submarine braid plains: potential deep water reservoirs. *American Association of Petroleum Geologists Bulletin*, 85: 1499–1521.

Hodges, K.V., Parrish, R.R. and Searle, M.P., (1996) Tectonic evolution of the central Annapurna Range, Nepalese Himalayas. *Tectonics*, 15(6): 1264–1291.

Hovius, N., (1998) Controls on sediment supply by large rivers. In: *Relative Role of Eustasy, Climate and Tectonism in Continental Rocks* (K.W. Shanley and P.J. McCabe, Eds.). SEPM Special Publication No. 59, Tulsa, OK, pp. 4–15.

Hurst, H.E. and Phillips, P., (1931) *The Nile Basin*. General Description of the Basin, 1. Government Press, Cairo.

Islam, M.S. and Tooley, M.J. (2004) Coastal and sea level changes during the Holocene in Bangladesh. *Quaternary International*, 55: 61–75.

Jain, V. and Sinha, R., (2003) River systems in the Gangetic plains and their comparison with the Siwaliks: a review. *Current Science*, 84(8): 1025–1033.

Jain, V. and Sinha, R., (2004) Fluvial dynamics of an anabranching river system in Himalayan foreland basin, Baghmati river, north Bihar plains, India. *Geomorphology*, 60:147–170.

Jain, V. and Sinha, R., (2005) Response of active tectonics on the alluvial Baghmati river, Himalayan foreland basin, eastern India. *Geomorphology*, 70(3–4): 339–356.

Kent, R., (1991) Lithospheric uplift in eastern Gondwana: evidence for a long-lived mantle plume system? *Geology*, 19: 19–23.

Knox, J.C., (1993) Large increases in flood magnitude in response to modest changes in climate. *Nature*, 361: 430–432.

Kumar, R., (1993) Coalescence megafan: multistorey sandstone complex of the late-orogenic (Mio-Pliocene) sub-Himalayan belt, Dehra Dun, India. *Sedimentary Geology*, 85: 327–337.

Kumar, S., Wesnousky, S.G., Rockwell, T.K., Ragona, D., Thakur, V.C. and Seitz, G.G., (2001) Earthquake recurrence and rupture dynamics of Himalayan Frontal Thrust, India. *Science*, 294: 2328–2331.

Latrubesse, E.M., Stevaux, J.C. and Sinha, R., (2005) Tropical rivers. *Geomorphology*, 70: 187–206.

Lavé, J. and Avouac, J.P., (2000) Active folding of fluvial terraces across the Siwalik Hills, Himalayas of central Nepal. *Journal of Geophysical Research*, 105(B3): 5735–5770.

Leopold, L.B., Wolman, M.G. and Miller, J.P., (1964) *Fluvial Processes in Geomorphology*. W.H. Freeman, San Francisco.

McKenzie, D.P., (1984) A possible mechanism for epeirogenic uplift. *Nature*, 307: 616–618.

Makaske, B., (2001) Anastomosing rivers: a review of their classification, origin and sedimentary products. *Earth Science Reviews*, 53: 149–196.

Miall, A.D., (1981) Alluvial sedimentary basins: tectonic setting and basin architecture. *Geological Association of Canada Special Paper*, 23: 1–33.

Miall, A.D., (1996) *The Geology of Fluvial Deposits*. Springer-Verlag, Berlin.

Miall, A.D. and Jones, B.G., (2003) Fluvial architecture of the Hawkesbury Sandstone (Triassic), Near Sydney, Australia. *Journal of Sedimentary Research*, 73: 531–545.

Milliman, J.D. and Syvitski, P.M., (1992) Geomorphic/ tectonic control of sediment discharge to the ocean: the importance of small mountainous rivers. *Journal of Geology*, 100: 525–544.

Nanson, G.C. and Gibling, M.R., (2004) Anabranching and anastomosing rivers. In: *Encyclopedia of Geomorphology* (A.S. Goudie, Ed.). International Association of Geomorphologists, Routledge, London, pp. 21–25.

Overpeck, J., Anderson, D., Trumbore, S. and Prell, W., (1996) The Southwest Indian monsoon over the last 18 000 years. *Climate Dynamics*, 12: 213–225.

Owen, L.A., Finkel, R.C. and Caffee, M.W., (2002) A note on the extent of glaciation throughout the Himalaya during the global Late Glacial Maximum. *Quaternary Science Reviews*, 21: 147–157.

Parkash, B., Sharma, R.P. and Roy, A.K., (1980) The Siwalik Group (molasse)–sediments shed by collision of continental plates. *Sedimentary Geology*, 25: 127–159.

Parkash, B., Kumar, S., Rao, M.S., Giri, S.C., Kumar, C.S., Gupta, S. and Srivastava, P., (2000) Holocene tectonic movements and stress field in the western Gangetic plains. *Current Science*, 79(4): 438–449.

Petri, S. and Fulfaro, V.J., (1983) Geologia da chapada dos Parcis, Mato Grosso, Brasil. *Revista Brasileria de Geociencias*: 274–282.

Pinet, P. and Souriau, M., (1988) Continental erosion and large scale relief. *Tectonics*, 7: 536–582.

Potter, P.E., (1978) Significance and origin of big rivers. *Journal of Geology*, 86: 13–33.

Pratt, B., Burbank, D.W., Heimsath, A. and Ojha, T., (2002) Impulsive alluviation during early Holocene strengthened monsoons, central Nepal Himalaya. *Geology*, 30: 911–914.

Prell, W.L. and Kutzbach, J.E., (1987) Monsoon variability over the past 150 000 years. *Journal of Geophysical Research*, 92: 8411–8425.

Prins, M.A. and Postma, G., (2000) Effects of climate, sea level, and tectonics unraveled for last deglaciation turbidite records of the Arabian Sea. *Geology*, 28: 375–378.

Raiverman, V., Kunte, S.V. and Mukherjea, A., (1983) Basin geometry, Cenozoic sedimentation and hydrocarbon prospects in northwestern Himalaya and Indo-Gangetic plains. *Petroleum Asia Journal*, 6: 67–97.

Roy, N.G. and Sinha, R., (2005) Alluvial geomorphology and confluence dynamics in the Gangetic plains, Farrukhabad-Kannauj area, Uttar Pradesh, India. *Current Science*, 88(12): 2000–2006.

Ruddiman, W.F. (2001) *Earth's Climate: Past and Future*. W.H. Freeman, San Francisco.

Schlager, W., (1993) Accommodation and supply – a dual control on stratigraphic sequences. *Sedimentary Geology*, 86: 111–136.

Seeber, L. and Gornitz, V., (1983) River profiles along the Himalayan arc as indicators of active tectonics. *Tectonophysics*, 92: 335–367.

Shanley, K.W. and McCabe, P.J., (1994) Perspectives on sequence stratigraphy of continental strata. *American Association of Petroleum Geologists Bulletin*, 78: 544–568.

Shukla, U.K., Singh, I.B., Sharma, M. and Sharma, S., (2001) A model of alluvial megafan sedimentation: Ganga megafan. *Sedimentary Geology*, 144: 243–262.

Singh, H., Parkash, B. and Gohain, K., (1993) Facies analysis of the Kosi megafan deposits. *Sedimentary Geology*, 85: 87–113.

Sinha, R., (1995) Sedimentology of Quaternary alluvial deposits of the Gandak-Kosi interfan, north Bihar plains. *Geological Society of India*, 46: 521–532.

Sinha, R. and Friend, P.F., (1994) River systems and their sediment flux, Indo-Gangetic plains, northern Bihar, India. *Sedimentology*, 41: 825–845.

Sinha, R., Tandon, S.K., Gibling, M.R., Bhattacharjee, P.S. and Dasgupta, A.S., (2005a) Late Quaternary geology and alluvial stratigraphy of the Ganga basin. *Himalayan Geology*, 26(1): 223–240.

Sinha, R., Gibling, M.R., Jain, V. and Tandon, S.K., (2005b) Sedimentology and avlusion patterns of the anabranching Baghmati river in the Himalayan foreland basin, India. *Special Publication of International Association of Sedimentologists*, 35: 181–196.

Sinha, R., Jain, V., Prasad Babu, G. and Ghosh, S., (2005c) Geomorphic characterization and diversity of the fluvial systems of the Gangetic plains. *Geomorphology*, 70: 207–225.

Sinha, R., Bhattacharjee, P., Sangode, S.J., Gibling, M.R., Tandon, S.K., Jain, M. and Godfrey, D., (2007) Valley and interfluve sediments in the southern Ganga plains, India: exploring facies and magnetic signatures. *Sedimentary Geology* doi:10.1016/j.sedgeo.2007.07.004.

Stevaux, J.C., (1994) The upper Parana river (Brazil): geomorphology, sedimentology and paleoclimatology. *Quaternary International*, 21: 143–161.

Summerfield, M.A., (1990) Geomorphology and mantle plumes (Scientific Correspondence). *Nature*, 344: 387–388.

Summerfield, M.A., (1991) *Global Geomorphology*. Longman, London.

Tandon, S.K., Gibling M.R., Sinha R., Singh V., Ghazanfari P., Dasgupta A., Jain M. and Jain V., (2006) Alluvial valleys of the Gangetic Plains, India: causes and timing of incision. In: *Incised Valleys in Time and Space* (B. Dalrymple, Ed.). SEPM Special Publication No. 85, Tulsa, OK, pp. 15–35.

Törnqvist, T.E., (1993) Holocene alternation of meandering and anastomosing fluvial systems in the Rhine-Meuse delta (central Netherlands) controlled by sea level rise and subsoil erodibility. *Journal of Sedimentary Petrology*, 63: 683–693.

Umitsu, M., (1993) Late Quaternary sedimentary environments and landforms in the Ganges delta. *Sedimentary Geology*, 83: 177–186.

Van Dijk, G.J., Berendsen, H.J.A. and Roeleveld, W., (1991) Holocene water level development in The Netherlands' river area: implications for sea level reconstruction. *Geologie en Mijnbouw*, 70: 311–326.

Weber, M.E., Wiedicke, M.H., Kudrass, H.R., Hubscher, C. and Erlenkeuser, H., (1997) Active growth of the Bengal Fan during sea-level rise and highstand. *Geology*, 25: 315–318.

Wellner, R.W. and Bartek, L.R., (2003) The effect of sea level, climate and shelf physiography on the development of incised valley complexes: a modern example from the East China Sea. *Journal of Sedimentary Research*, 73(6): 926–940.

Wells, N.A. and Dorr, J.N., (1987) Shifting of the Kosi river, northern India. *Geology*, 15: 204–207.

White, R.S. and McKenzie, D.P., (1989) The generation of volcanic continental margins and flood basalts. *Journal of Geophysical Research*, 94: 7685–7730.

Wiedicke, M., Kudrass, H.-R. and Hubscher, C., (1999) Oolitic beach barriers of the last Glacial sea-level lowstand at the outer Bengal shelf. *Marine Geology*, 157: 7–18.

Wilhelmy, H., (1969) The ancient river valley on the eastern border of the Indus Plain and the Sarasvati problem. *Zeitschrift für Geomorphologie*, 8: 76–93.

Wobus, C.W., Hodges Kip, V. and Whipple, K.X., (2003) Has focused denudation sustained active thrusting at the Himalayan topographic front? *Geology*, 31(10): 861–864.

3

Hydrology and Discharge

Ellen E. Wohl

Department of Geosciences, Colorado State University, Ft Collins, CO 80523, USA

3.1 HYDROLOGY OF LARGE RIVER BASINS

The climate and hydrology of each of the world's major river drainages are inherently diverse because these drainages cover such large areas that they encompass diverse atmospheric circulation patterns, geology, topography, vegetation, and land use. Diversity both within and between drainage basins means that drainage area–discharge relations cannot be extrapolated between regions. The arid Nile River drainage has a mean unit discharge of 0.001 $m^3 s^{-1} km^{-2}$, whereas the value for the similarly sized Congo River drainage is 0.011. Figure 3.1 schematically illustrates the magnitude of mean annual discharge at the mouth of major rivers.

The peak unit discharge of major rivers also reflects precipitation-generating mechanisms. Flash floods in small catchments reflect regional differences in rainfall intensity over short time spans; maximum 24-h precipitation intensities are on the order of 90 mm for arctic and subarctic regions (Church, 1988), but can reach 1870 mm in the tropics (Gupta, 1988). Peak unit discharges of major rivers do not begin to approach the peak unit discharges recorded for very small catchments around the world. Peak unit discharge for big rivers is typically less than 0.2 (Table 3.1). In contrast, catchments of less than 100 km^2 have recorded peak unit discharges of 46 in China, 114 in the United States (Costa, 1987), and 156 in the Himalaya (Starkel, 1972). However, the twentyfold variability in peak unit discharge listed in Table 3.1 reflects differences in precipitation generation associated with regional to hemispheric, atmospheric, and oceanic circulation patterns.

Hayden (1988) classified flood hydroclimatology by distinguishing baroclinic and barotropic climates. Baroclinic atmospheric conditions predominate at higher latitudes where contrasting air masses create intersecting gradients of pressure and temperature. Barotropic conditions are more common at tropical low latitudes where atmospheric pressure is constant on constant-density surfaces and horizontal thermal gradients are small. The dominant rain-producing mechanisms of baroclinic regions tend to be fronts where masses of air from different source regions converge. The frontal storms vary in size from several hundred kilometres to more than a thousand kilometres in diameter, and tend to move from west to east or southwest to northeast. The dominant rain-producing mechanisms in barotropic regions are the Intertropical Convergence Zone (ITCZ) where the trade winds converge, cyclonic systems, and orographic uplift. Larger river basins are proportionally more influenced by meteorologic patterns covering larger spatial and longer temporal scales, such as seasonal movements of the ITCZ, large fronts, or cyclones (Hirschboeck, 1988). Both annual precipitation and precipitation intensity values are greatest in equatorial and tropical latitudes, where tropical cyclones combined with orographic effects have produced the highest rainfall intensities on record (Lockwood, 1974). A drainage basin that includes high latitudes or high altitudes is likely to include substantial runoff from the melting of snow or glacial ice, in addition to rainfall.

Interannual variability in peak discharge does not correlate well with latitude and type of atmospheric conditions, but does correlate slightly with mean annual

Large Rivers: Geomorphology and Management, Edited by A. Gupta

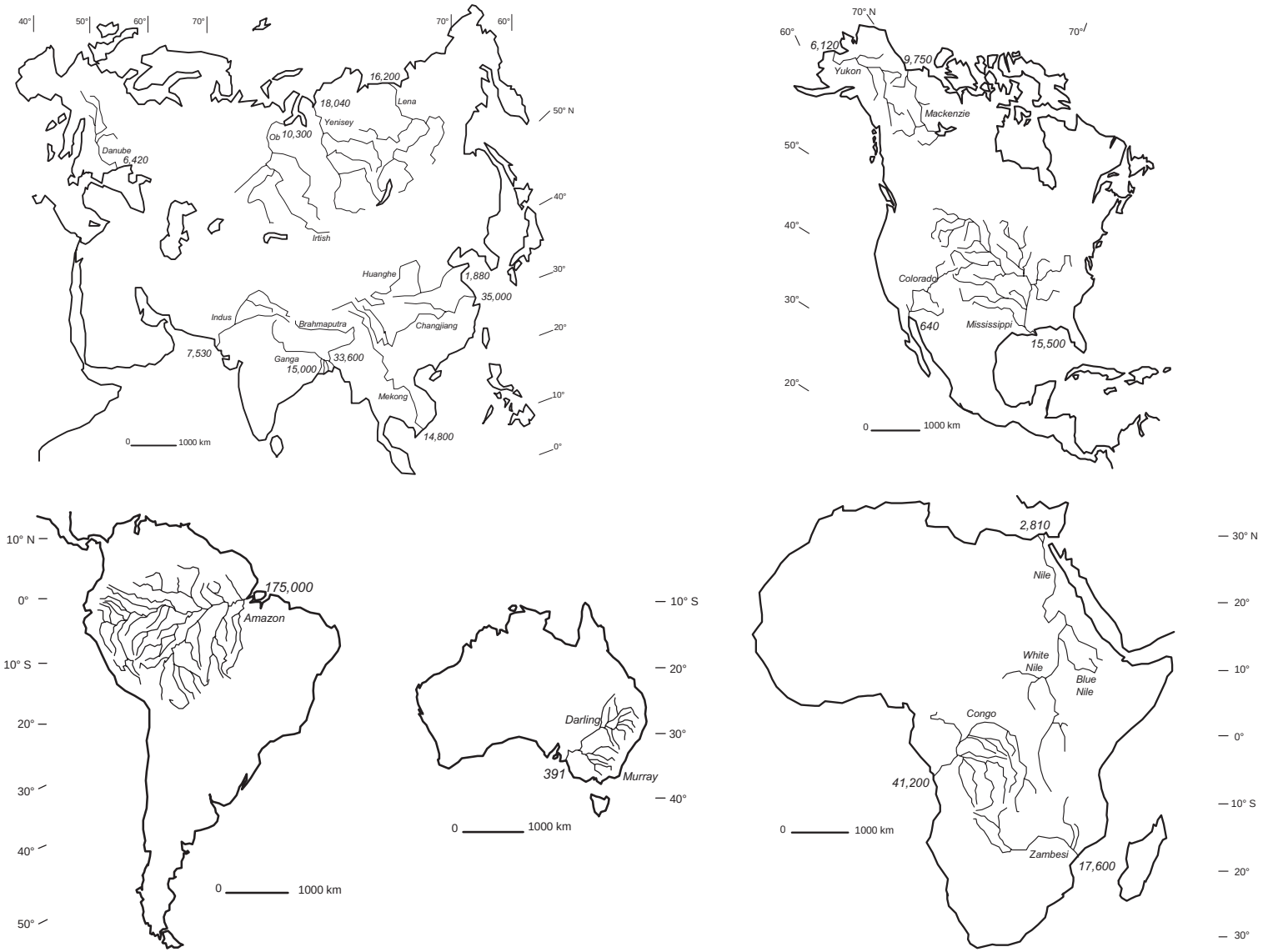

Figure 3.1 Maps showing location of rivers discussed in this chapter, plotted at the same scale. Number at the mouth of each river indicates mean annual discharge at the mouth

Table 3.1 Basic characteristics of the world's major river basins, listed from largest to smallest mean annual discharge

River basin	Drainage area (km^2)	Date: peak recorded discharge ($m^3 s^{-1}$) (damage area, km^2)	Peak unit discharge ($m^3 s^{-1} km^{-2}$)	Mean annual discharge ($m^3 s^{-1}$): [unit]	Annual volume of discharge (million $m^3 year^{-1}$)	Flood hydroclimatology[b]
Amazon	6 915 000	1953: 370 000[a] (4 640 000)	0.08	175 000 [0.025]	6 930 000	Tpz
Congo	3 822 000	1961: 80 830[a] (3 475 000)	0.02	41 200 [0.011]	1 250 000	Tsz
Changjiang	1 940 000	1870: 110 000 1954: 110 000	0.11	35 000 [0.018]	870 000	Tszo
Brahmaputra	580 000	1962: 72 748[a] (424 309)	0.17	33 600 [0.058]	612 500	Tszo
Yenisey	2 580 000	1959: 112 000[a] (2 440 000)	0.05	18 040 [0.007]	620 000	CSs**
Zambezi	1 331 000	1905: 17 000[a] (940 000)	0.02	17 600 [0.013]	106 000	Tsz
Lena	2 490 000	1967: 189 000[a] (2 430 000)	0.08	16 200 [0.006]	525 000	CSs**
Mississippi	3 230 000	1927: 84 000	0.03	15 500 [0.005]	562 000	TsuCpSe*
Ganga	952 000	1971: 65 072[a] (935 000)	0.07	15 000 [0.016]	180 000	Tszo
Mekong	811 000	1966: 31 400[a] (391 000)	0.08	14 800 [0.018]	667 000	Tpz
Ob	2 990 000	1979: 44 800[a] (2 430 000)	0.02	10 300 [0.003]	429 000	CSs**
Mackenzie	1 787 000	1972, 1977: 22 000[a] (1 570 000)	0.01	9 750 [0.006]	306 000	CSs**
Indus	1 165 000	1948: 20 050[a] (832 418)	0.02	7 530 [0.006]	109 000	Tszo
Danube	816 000	1970: 14 520[a] (807 000)	0.02	6 420 [0.008]	282 000	CpSe*
Yukon	850 000	1962: 24 049[a] (767 000)	0.03	6 120 [0.007]	140 000	CSs**
Nile	3 349 000	1878: 12 345	0.01	2 810 [0.001]	89 000	Tpu
Huanghe	752 443	1843: 33 000 (730 036)	0.04	1 880 [0.002]	46 400	TsuCpSe*
Colorado	640 000	1884: 8 424[a] (310 556)	0.03	640 [0.001]	20 000	Tsu
Murray-Darling	1 072 000	1974: 2 044[a] (991 000)	0.01	391 [0.001]	12 000	Tsu-Cp

[a] Indicates discharge not at river mouth.
[b] T, barotropic; C, baroclinic; p, perennial; s, seasonal; z, ITCZ; o, organized convection; u, unorganized convection; S, snow cover; s, seasonal snow cover; e, ephemeral snow cover; *, snow cover 10–50 days; **, snow cover 50 days or more: Tpz (perennially barotropic; ITCZ initiates precipitation and its north-south movement creates a dry and a wet season), Tsz (seasonally barotropic; ITCZ present for part of year), Tpu (perennially barotropic; tropical storms absent, but convective systems occur; semiarid or arid, orographic conditions important), TsuCpSe* (summer barotropic; winter snowfall; diverse weather and flooding in all seasons), CSs** (perennially baroclinic; modest precipitation from frontal cyclones; snowfall), Tszo (seasonally barotropic; ITCZ present for part of year; also organized convective systems), CpSe* (perennially baroclinic; frontal cyclones; winter snowfall), Tsu (summer barotropic, winter baroclinic; during summer, thunderstorm precipitation; during winter, fronts and cyclones; arid), and Cp (perennially baroclinic; flooding from frontal cyclone precipitation; often orographic enhancement; flooding at all seasons).
Sources: Czaya (1981), Gupta (1988), Hayden (1988), Herschy (1998), RivDIS (2003).

precipitation or mean annual runoff (Figure 3.2a). The more arid drainage basins have a much greater interannual variability than the drainage basins with greater precipitation totals. Substantial scatter complicates this relationship, however, as suggested by comparing the positions of the adjacent Yukon and Mackenzie River basins (Figure 3.2a). Annual variability in discharge, as indicated by coefficient of variation for mean monthly discharge, does not correlate with either latitude or mean annual precipitation (Figure 3.2b).

A portion of the interannual variability in both peak and total discharge for several of the world's largest rivers arises from atmospheric and oceanic fluctuations associated with the El Niño-Southern Oscillation (ENSO) circulation system. Approximately 10% of the annual variance in flow from the Amazon and the Congo, and 25% of the Nile's annual variance, is explained by ENSO (Amarasekera *et al.*, 1997). Flow volume from the Murray-Darling system is also negatively correlated with ENSO (Simpson *et al.*, 1993), and in the Colorado River basin both snowpack in the headwaters and rainfall from dissipating tropical storms lower in the basin are influenced by ENSO (Clark *et al.*, 2001).

The average annual hydrograph in the downstream portion of each major river basin is characterized by a strong seasonal peak, although the timing, duration, and peakedness of the period of high flow vary among basins (Figure 3.3). This presumably reflects both differences in runoff-generating mechanisms among basins, and differences in downstream conveyance of water. Mean annual precipitation tends to decrease downstream in arid and semiarid basins such as the Colorado, Nile, Murray-Darling, Huanghe and Indus. Flow in these drainages originates mostly in mountainous headwater regions, with

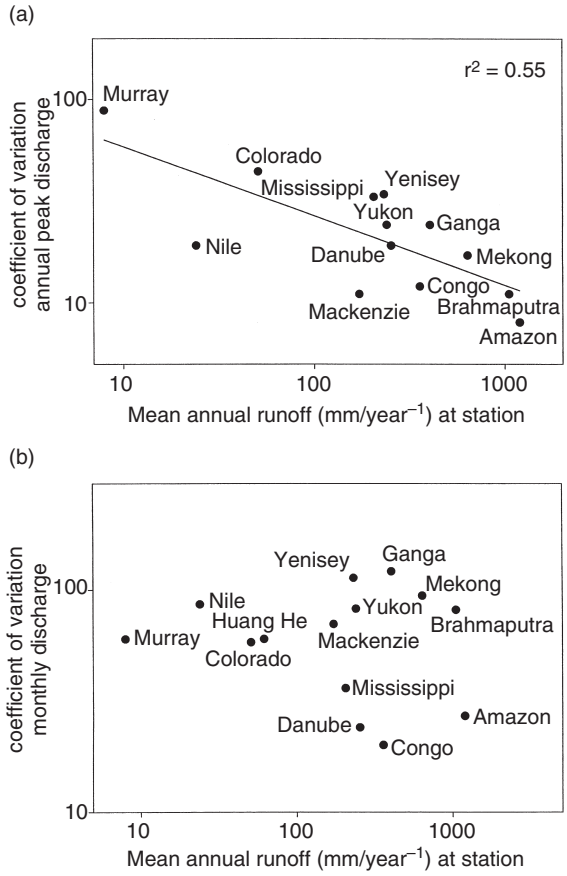

Figure 3.2 Coefficient of variation of (a) annual peak discharge and (b) monthly discharge versus mean annual runoff for selected rivers

precipitation and runoff pulses related to strongly seasonal effects such as snow (Colorado) or orographic monsoonal rainfall (Nile). In contrast, mean annual precipitation increases steadily downstream in basins such as the Amazon and the Changjiang (Yangtze).

Downstream conveyance processes have been substantially altered by flow regulation and channel alteration in most of the world's large rivers. Prior to the era of extensive dam construction and channelization, rivers such as the Nile and the Mississippi were famous for annually flooding thousands of hectares of bottomlands, as the Amazon still does today. Historical inundation extent and duration provide insight into the nature of both the annual hydrograph, and the terrain and aquatic ecosystems present in the lower portion of each river. Of the rivers covered in this chapter, the Amazon is certainly the champion flooder, with a floodplain up to 50 km wide that covers 300 000 km^2 for up to 11 months each year (Goulding, 1989; Mertes *et al.*, 1996; Dunne *et al.*, 1998; Smith, 1999). Yet even relatively low-discharge rivers such as the Murray-Darling system in Australia historically had extensive floods approximately every 2 years that lasted up to 6 months (Walker, 1994). Much of this historical flooding no longer occurs annually or regularly. Between 1950 and 1982, nearly 30 000 dams were constructed on the world's rivers, and by the early 1990s 13 % of the global river flow to the oceans had been dammed or diverted (Milliman, 1997).

The remainder of this chapter provides a brief summary of existing knowledge of the contemporary and post-glacial hydroclimatology and hydrology for each of 19 major river basins. These summaries include mention of human alterations of hydrology via flow regulation and diversion for river basins in which these activities have been substantial. The intent of the summaries is to introduce the hydrology of selected large rivers, most of which are discussed at greater length in subsequent chapters of this volume. The rivers are grouped into drainages lying primarily within the equatorial and tropical regions (Amazon, Congo, Zambezi); arid-region drainages (Nile, Indus, Colorado, Murray-Darling); mid-latitude rivers draining primarily humid temperate regions (Mississippi, Danube); rivers flowing south-southeast from the Himalaya (Ganges, Brahmaputra); rivers of Southeast and East Asia (Huanghe, Changjiang, Mekong); and high-latitude rivers (Ob, Yenisey, Lena, Mackenzie, Yukon). Although the rivers treated in this chapter could have been grouped differently, these subdivisions reflect characteristics of hydroclimatology, topography, and discharge shared within each group. The coverage in each river summary is uneven in level of detail because much more work has been conducted on some rivers than on others.

3.2 LARGE RIVERS OF THE EQUATORIAL REGIONS

The flood hydroclimatology of the major rivers of low latitudes, such as the Amazon, Congo, and Zambezi, minimizes variability in both monthly and annual peak discharge (Figure 3.2). Seasonally or perennially barotropic conditions dominate the climate of these drainages, and the ITCZ largely controls precipitation, which tends to be both abundant and intense. These conditions produce the world's largest annual volumes of discharge on the Amazon and Congo Rivers, which are also distinguished by huge drainage areas.

3.2.1 Amazon River

Flow within the Amazon drainage basin occurs at the largest scale. This single river contributes 20 % of total

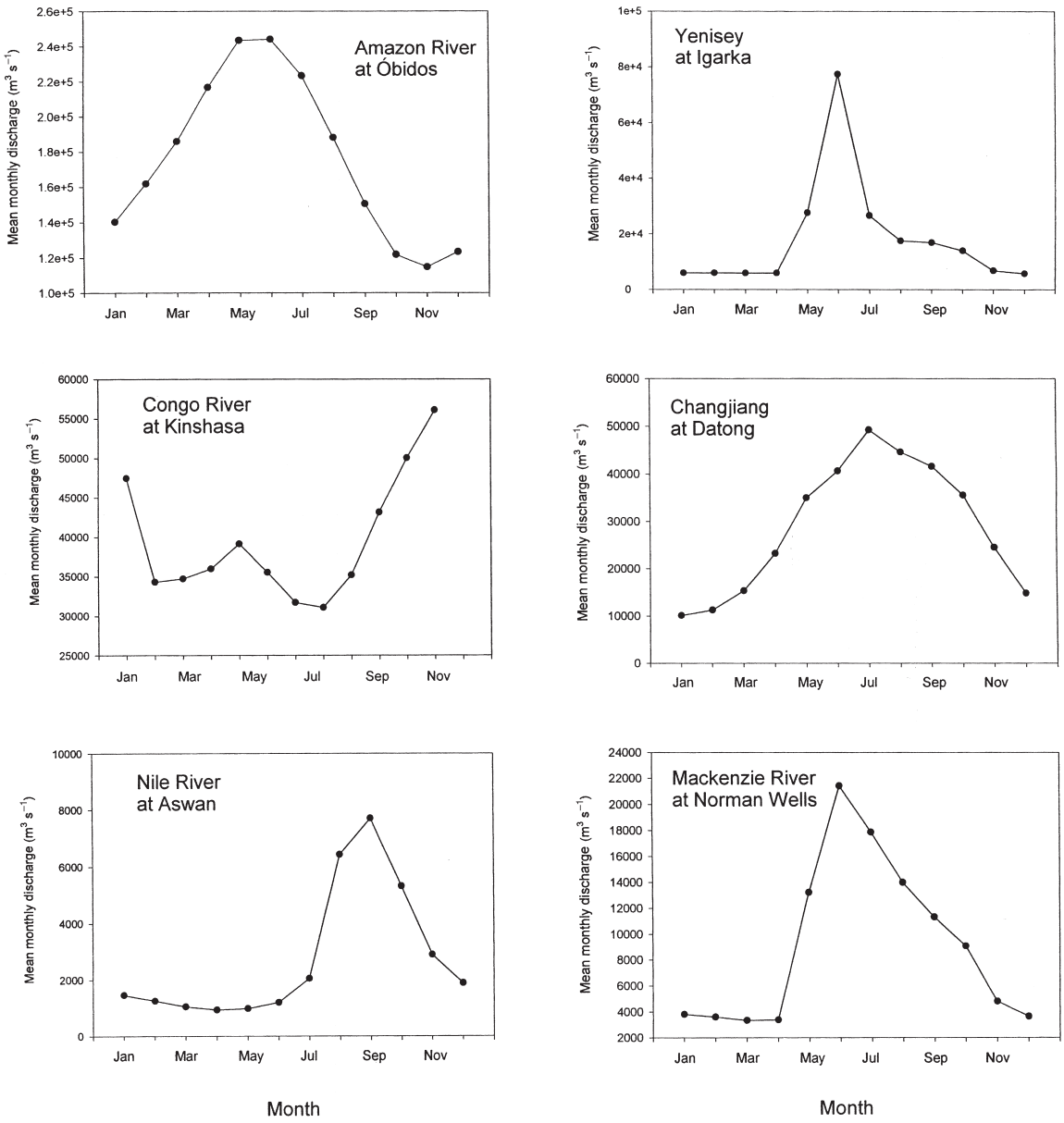

Figure 3.3 Average annual hydrographs for selected rivers. Scale of axis indicating discharge magnitude varies between plots

global river discharge to the oceans, and has the largest rainfall-runoff flood (Table 3.1) ever recorded (Richey *et al.*, 1989). Mean annual precipitation is highly variable across the basin, ranging from 7000 mm on the eastern side of the Andes (which includes snow), through more than 3500 mm in the northwest lowlands, to less than 2000 mm in the northeastern and southern parts of the basin (Jordan, 1989; Richey *et al.*, 1989). About half of the rain falling on the basin produces runoff; the remainder is recycled to the atmosphere via evapotranspiration from the dense vegetation covering most of the basin (Richey *et al.*, 1989).

The basin straddles the Equator, and fluctuations in the ITCZ induce wet and dry seasons in alternating portions

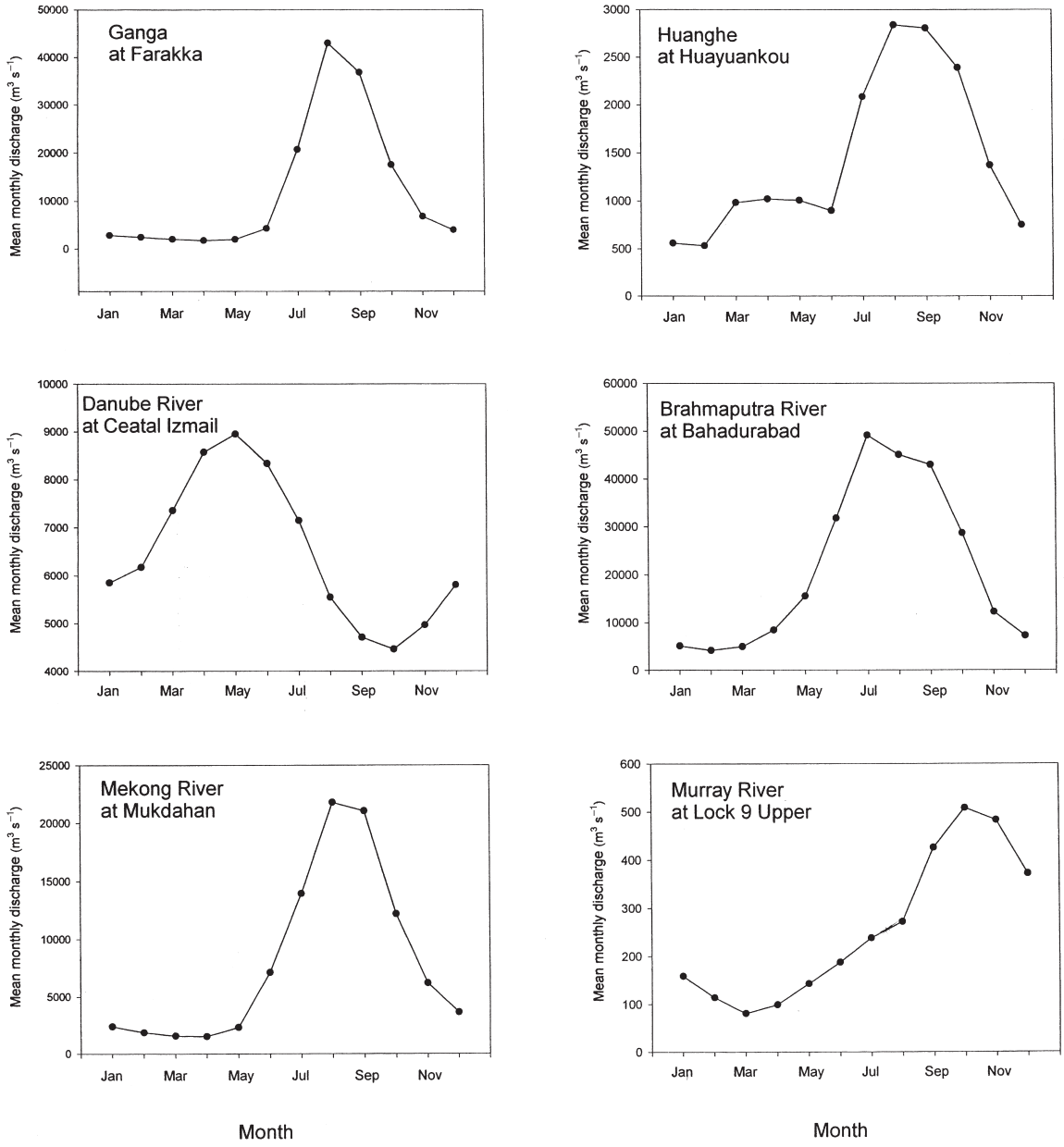

Figure 3.3 *Continued*

of the year across the northern and southern portions of the basin (dry June–August south of the Equator, and January–March north of the Equator). A 3-month phase lag in peak flows is present between north- and south-draining tributaries because of these seasonal differences in precipitation, as well as the large volume of water stored on the floodplain. Thirty per cent of the water in the mainstem Amazon is derived from water that passed through the floodplain (Richey *et al.*, 1989).

Existing data are too sparse and disputable to produce convergent views on late Quaternary palaeoecology and palaeohydrology in the Amazon basin (Kadomura,

1995). Palaeoecological and sedimentological evidence from the rainforest portion of the basin suggests dry phases during 6000–3000 years BP and 2700–400 years BP in the Brazilian Amazon (Sanford *et al.*, 1985), and 4300–4200 and 3800–3150 years BP in the Ecuadorian Amazon (Liu and Colinvaux, 1988), probably in relation to the ENSO circulation (Servant *et al.*, 1993). Freshwater influx to the Amazon cone during the period 13 600–6000 years BP peaked circa 9600 years BP, probably in association with deglacial pluvial activity (Showers and Bevis, 1988).

3.2.2 Congo River

The headwaters of the Congo River flow from hills and low tablelands across Equatorial Africa into a broad basin before reaching the Atlantic Ocean. The main control of precipitation over the equatorial and tropical regions of Africa is the seasonal migration of the ITCZ, whereas variability in monsoonal strength is determined by precessional forcing (Schneider *et al.*, 1997). In western Africa the ITCZ migrates seasonally from 5° N in the boreal winter to 20° N in the boreal summer, with a mean annual position around 13° N (Marret *et al.*, 2001). Mean annual precipitation across the Congo Basin is tied to this circulation pattern, and varies from 1600 mm in the northern portions of the basin, down to 600 mm elsewhere (Walling, 1996). The annual flood occurs in November–December, with a secondary peak in March–April (Walling, 1996). Approximately 10 % of the annual variance in Congo flow is explained by the ENSO circulation (Amarasekera *et al.*, 1997).

Thomas and Thorp (1996) suggest that higher flows occurred circa 10–8 ka BP in the Congo Basin. More site-specific information comes from pollen, foraminifera and isotopic records obtained via a core of the Congo Fan. This core suggests a major discharge pulse circa 13 calendar ka BP, in association with latitudinal migration of the ITCZ across the Congo Basin from its more southerly position during the last glacial maximum, leading to the extension of monsoonal conditions over the basin (Marret *et al.*, 2001). Data from the core also indicate abrupt and short-lived changes in the equatorial precipitation regime within the system of monsoonal dynamics operating over the Congo Basin.

3.2.3 Zambezi River

The Zambezi River heads in hills and low tablelands of tropical southern Africa, then flows east into the Indian Ocean. Rainfall is largely determined by the position of the ITCZ, which is at its southern limit over the Zambezi River basin during the austral summer (Walker, 1990). High discharges during March and low discharges during August–December dominate the annual flow regime of the Zambezi River basin, where mean annual precipitation varies from 1200 mm in the north down to 600 mm (Walling, 1996).

The more northerly position of the ITCZ during the last glacial maximum would have produced drier conditions over the Zambezi Basin (Walker, 1990), but little is known of late Quaternary changes in the basin's hydrology.

3.3 LARGE RIVERS OF THE DRYLANDS

Rivers of arid and semiarid regions are distinguished by generally low values of peak discharge per unit drainage area (Table 3.1) because some part of the basin does not effectively contribute surface runoff during peak discharges. The drylands rivers discussed here – the Nile, Indus, Colorado, and Murray-Darling – have mostly perennially or seasonally barotropic climates, except for the Murray-Darling basin. Convective storms and the orographic influence of topography are particularly important controls on precipitation in drylands drainages, although the ITCZ may also be important, as in the Indus Basin. Unless the headwaters lie in a region of consistently high precipitation, as is the case for the Blue and White Nile Rivers, interannual variability in peak discharge tends to be quite high for drylands rivers (Figure 3.2a).

3.3.1 Nile River

The Nile River has a relatively low annual volume of flow compared with other drainage basins of similar size (Table 3.1). This reflects the relatively low mean annual precipitation, which ranges from 0 to 1400 mm across the drainage basin (Kashef, 1981). The drainage basin includes two primary subdivisions in its headwaters, the Blue Nile to the east, and the White Nile to the west. The Blue Nile drains orographic monsoonal rainfall over the northern Ethiopian highlands, and it this region which generates the lower Nile's annual flood (Rossignol-Strick *et al.*, 1998). The main Nile floods during the northern hemisphere summer, when Ethiopia contributes 90–95 % of the total discharge. During the March–June low flow the White Nile contributes 75 % of the total discharge (Hassan and Stucki, 1987). A 1300-year record of floods indicates that magnitude variations result from differences in flow contribution from Equatorial Africa and Ethiopia (Hassan and Stucki, 1987). Large floods result from an increase in winter/early spring and late autumn precipitation in eastern Africa.

Flow in the Nile River basin is among the most highly regulated in the world. In addition to the High Aswan

Dam, completed in 1970 and capable of storing almost 2 years of average Nile discharge, other dams within the basin store more than 10 % of average annual flow (Collins, 1990). Massive diversion schemes such as the partially completed Jonglei Canal (projected to carry 43 million m^3 of water) will further alter the natural flow regime (Moghraby, 1982).

The White Nile is fed by overflow from Lakes Victoria and Albert, which stopped during the Last Glacial Maximum. The modern flow regime was established when overflow resumed between 13 000 and 12 000 years ago (Talbot *et al.*, 2000; Beuning *et al.*, 2002). Flows remained relatively high until 6000 years ago, with peak flooding episodes during the early to middle Holocene at circa 8400–8100, 7500 and 7000 years ago (Krom *et al.*, 2002). Flows declined with fluctuations, reaching a minimum circa 4500–4200 years ago, fluctuated at higher levels until 3100 years ago, then remained fairly low until 1000 years ago. These Holocene fluctuations were primarily driven by variations in the monsoonal circulation associated with movement of the ITCZ. The higher flows until 6000 years ago reflect a northward shift in the ITCZ and more precipitation in the Ethiopian highlands (Krom *et al.*, 2002). Equatorial contribution to Nile flow was greater from 1250 to 1480 AD, and lower during the Little Ice Age of 1480 to 1870 AD (Hassan and Stucki, 1987).

3.3.2 Indus River

The Indus River originates in the Himalaya and travels across 1200 km of lower elevation plains to reach the Arabian Sea (Ittekkot and Arain, 1986). The catchment has a tropical to subtropical climate characterized by very low precipitation; mean annual precipitation varies from greater than 1000 mm in the headwaters at 5000–7000 m elevation (Hewitt, 1998), to much lower values in the middle and lower basin; 200 mm in the south to as little as 76 mm in the north (Memon, 1969). Both precipitation and streamflow are highly variable and seasonal, as expected for an arid to semiarid region (Ahmad and Kutcher, 1992). Discharge in the river is highest during the May–October wet season as a result of both snowmelt in the headwaters, and rainfall. Despite the basin's aridity, the lower Indus has a floodplain up to 30 km wide, which was historically inundated for 3–4 months during the wet season. Flow in the basin is now extensively altered by dams, channelization and diversions (Ittekkot and Arain, 1986).

3.3.3 Colorado River

Peak annual flow in the Colorado River is dominated by spring–summer snowmelt from the Rocky Mountains in the catchment's headwaters. Precipitation also falls throughout the basin as winter frontal storms from the North Pacific; dissipating Pacific tropical cyclones that coincide with mid-latitude low-pressure troughs during autumn; and local convective thunderstorms (Ely *et al.*, 1993). Except for the very headwater regions, the catchment is arid or semiarid, with mean annual precipitation of 300 mm, and high interannual variability in precipitation and streamflow (Graf, 1985). Much of this variability results from El Niño circulation patterns, which produce drier conditions and lower snow water equivalents in the northern portion of the basin, and wetter conditions in the southern portion of the basin (Clark *et al.*, 2001).

Flow in the Colorado River basin is highly regulated for water storage and hydroelectric power generation. Diversion structures up to 10 m tall are common throughout the basin, and 19 large dams more than 20 m tall are present (Graf, 1985). Individual rivers within the drainage have a ratio of reservoir storage to annual water supply of 2.3 to 3.3, and the ratio of current streamflow to natural streamflow varies from 25 to 68 % (Riggs and Harvey, 1990).

Palaeoflood records derived from slackwater deposits indicate periods of larger floods that coincide with cool, moist climates and more frequent El Niño events during 4800–3600 years BP, circa 1000 years BP, and after 500 years BP, with marked decreases in flooding between 3600–2200 years BP and 800–600 years BP (Ely *et al.*, 1993). Palaeoflood records from the Grand Canyon indicate 10 floods exceeding 6800 $m^3 s^{-1}$, and one flood of 14 000 $m^3 s^{-1}$, during the past 4500 years (O'Connor *et al.*, 1994). The peak historic discharge from the region is 8500 $m^3 s^{-1}$.

3.3.4 Murray-Darling River

The Murray-Darling drainage is Australia's largest single drainage basin, covering 14 % of the continent's total land area (Walker, 1994). The Murray River drains west-northwest from the Australian Alps across a broad, low-relief basin where it is joined by the Darling River flowing southwest from the Great Dividing Range. Because the drainage is arid, it conveys only 5 % of Australia's runoff. The basin is mostly of low relief and below 200 m in elevation. The 2 % of the basin in highlands contributes 37 % of the flow. More than 85 % of the basin contributes no net surface runoff during most years (Herczeg *et al.*, 1993). Mean annual precipitation drops sharply from 1400 mm in the highlands, where it is winter-dominated, to 300 mm on the northwestern plains, where the precipitation falls predominantly during summer. Snowmelt from the Australian Alps also contributes to river flow (Crabb,

1988). Aridity and a strong influence from the ENSO circulation pattern create substantial annual and longer period fluctuations in flow of 3700 million m^3 to 48 000 million m^3 per year (see also Figure 3.2). High summer temperatures produce evaporation that exceeds rainfall in most of the basin. Of the two contributing drainages, the more southerly Murray River contributes the bulk of the discharge (Walker, 1994).

Approximately three-quarters of all irrigated agricultural lands in Australia lie within the Murray-Darling drainage basin (Walker, 1994). Flow in the basin is extensively regulated via dams and other structures, and irrigation diversions and consumptive uses have reduced mean annual flow by approximately one-third relative to flow volumes prior to European settlement of the region (Walker, 1994).

The wide alluvial plains of the Murray basin preserve palaeochannels that record a shift circa 15–13 ka ago from wide, large-amplitude meandering channels to smaller, deeper channels with smaller meander amplitude and wavelength that retain high sinuosity (Baker *et al.*, 1995).

3.4 RIVERS OF THE MID-LATITUDES

The rivers of the mid-latitudes of North America and Europe have climates in which diverse circulation patterns produce precipitation. Both the Mississippi and the Danube have winter snowfall, frontal storms, and convective storms. This mix of precipitation-generating mechanisms produces moderate interannual variability in peak discharge, and fairly low variability in monthly discharge (Figurs 3.2 and 3.3).

3.4.1 Mississippi River

The Mississippi River basin encompasses the humid temperate regions of the United States, and the semiarid grasslands and mountains of the central western part of the country. These dichotomies are reflected in the Mississippi's two primary tributary basins; the Ohio Basin drains from the east and provides most of the Mississippi's discharge, whereas the Missouri River drains from the west and provides the majority of the Mississippi's sediment load (Meade *et al.*, 1990). Mean annual precipitation across the basin varies from 250 mm in the western portion of the basin to 1500 mm near the mouth, and includes both snow and rain. High flows generally occur March–May and low flows during August–October. The most substantial floods of the past century were the 1927 flood on the lower river, and the 1993 flood in the upper basin. Both floods were caused by unprecedented, prolonged rains; late winter and spring rains in 1927, and summer rains in 1993.

As with most of the world's major rivers, hydrology and discharge in the Mississippi basin have changed substantially during the past two centuries in response to human impacts. Widespread land-use changes include clearing of forest cover, draining of wetlands, and urbanization. More than 13 000 km of levees have been built in the 208 000 km^2 of the upper river basin, and 65 % of the original wetlands have been drained. By 1950, a system of 29 locks and dams had been built along the upper river from St Louis to Minneapolis, and a 2.7 m navigation channel had been dredged from St Louis to Sioux City, Iowa (Watson and Biedenharn, 2000). Channelization and artificial meander cutoffs are widespread. Flood stages for constant discharge have increased 2–4 m over the past century at numerous locations in the Mississippi River basin, but sites without extensive river engineering do not exhibit such increases (Criss and Shock, 2001).

Post-glacial changes in the Mississippi River basin's discharge were dramatic because for 3000 years the drainage served as the primary meltwater conduit between the massive Laurentide Ice Sheet and the Gulf of Mexico. Between circa 14 000 and 11 000 years ago, approximately 18 million km^3 of meltwater flowed down the Mississippi (Brown and Kennett, 1998). Meltwater floods reached their peak between 12 600 and 12 000 years ago. Mississippi flow volumes diminished substantially after 11 000 years ago as the northward-retreating ice sheet uncovered the St Lawrence and other drainages that then began to convey meltwater to the Atlantic Ocean (Brown and Kennett, 1998).

Examination of palaeochannels in the upper Mississippi River drainage indicates a warmer, drier period of smaller floods circa 3300–5000 years ago. During this period the largest floods were of a magnitude that now recurs every 50 years (Knox, 1993). When the climate became cooler and wetter circa 3300 years ago, flood frequency increased; floods that now recur only approximately every 500 years became much more frequent, with a culmination in flood magnitude between about AD 1250 and 1450 (Knox, 1993).

3.4.2 Danube River

The Danube River flows south-southeast from the Alps of central-western Europe into the Black Sea. Mean annual precipitation is relatively consistent across the Danube Basin, from 1000 mm in the northwest to 950 mm in the southeast (Hotzl, 1996), although snowmelt from the Alps contributes more runoff in the upper basin, and summer rainfall contributes more runoff in the middle and lower

portions of the basin. The annual hydrograph reaches its highest levels from snowmelt during late spring and early summer (Hotzl, 1996).

Following Pleistocene deglaciation, lesser glacial advances occurred in the alpine headwaters of the Danube circa 8.6–8.0, 6.5–6.0, 5.3–5.0, 4.7–4.4, 3.3–3.0, 2.9–2.3, 1.8–1.3 and 1.0 ka BP (Starkel, 1995). Increases in runoff along the Black Sea margins are recorded in annual lake laminae at circa 2.1–1.9, 1.15–0.9 and 0.4–0.2 ka BC (Schwetz, 1978). Study of historical maps of the Danube's course suggest that ice floods and other types of flooding increased during the latter half of the eighteenth century, probably in association with the Little Ice Age (Pisut, 2002).

3.5 RIVERS DRAINING SOUTH FROM THE HIMALAYA

The great rivers draining south-southeast from the Himalayan massif have seasonally barotropic climates influenced by the ITCZ during a portion of the year, and by organized convective systems (Table 3.1). Monsoonal precipitation dominates discharge in both the Ganga and Brahmaputra drainages, with a lesser contribution from snowmelt. Interannual variability in peak discharge is moderate, but variability between months is high (Figure 3.2).

3.5.1 Ganga River

The Ganga heads in the Gangotri glacier of the Himalaya and is fed by glacier and snowmelt from these upper regions. A quarter of the Ganga's catchment lies within the Himalaya (Meybeck and Carbonnel, 1975). Peak flow occurs toward the end of the July–September southwest monsoon (Sarin and Krishnaswami, 1984), which brings 70–80% of the basin's total precipitation (Ansari *et al.*, 2000).

Much of the basin is occupied by the Ganga alluvial plain, one of the most densely populated regions on Earth. This region, which contains a third of India's population, also includes large agricultural areas that depend on the groundwater that forms one of the largest subsurface water repositories on the planet (Ansari *et al.*, 1999). Geomorphic surfaces on the plain record a river metamorphosis from meandering to braided during the last 25 ka, accompanied by decrease in grain size and discharge, and increase in sediment load (Singh *et al.*, 1990).

3.5.2 Brahmaputra River

Sixty per cent of the Brahmaputra River's drainage basin lies within the Himalaya, as compared with 25% for the Ganga River drainage (Meybeck and Carbonnel, 1975). The Brahmaputra begins to rise a month before the Ganga, during March–April, in response to snowmelt in the Himalaya. The Brahmaputra then peaks in late July or early August, whereas the Ganga peaks in late August or early September (Allison, 1998). Mean annual precipitation for both the Ganga and Brahmaputra drainages is 1520 mm. Precipitation across the Brahmaputra Basin varies from 5000 mm in the Himalaya to less than 2000 mm over the southeastern portion of the catchment. Monsoonal rains from June to September account for 60–70% of the annual rainfall in the central portion of the basin that lies in India (Goswami, 1998). The discharge peak in the Brahmaputra is produced by summer snowmelt in the Himalaya as well as heavy local rainfall in the summer monsoon (Thorne *et al.*, 1993).

Discharge in the Brahmaputra drainage basin decreased during the last glacial maximum as a result of a weakened monsoonal circulation and aridity in the headwaters (Goodbred and Kuehl, 2000). Discharge began to increase by 15 000 years ago, and the intensified early Holocene monsoon of circa 11 000–7000 years ago increased water and sediment discharge in the drainage. The immense Ganga-Brahmaputra Delta began to form circa 11 000 years ago as rising sea-level flooded the Bengal Basin and trapped most of the river's discharge on the inner margin (Goodbred and Kuehl, 2000).

3.6 RIVERS OF EAST AND SOUTHEAST ASIA

The great rivers of East Asia, which drain mostly the midlatitudes, have seasonally or perennially barotropic climates (Table 3.1). Snowfall produces some runoff in the headwaters of these basins, but rainfall associated with the movement of the ITCZ or other circulation patterns is a more important source of discharge. These rivers are characterized by moderate interannual variability in peak discharge, and high monthly discharge variability (Figure 3.2).

3.6.1 Huanghe

The Huanghe or Yellow River, sometimes known as China's sorrow because of its history of extensive flooding, heads on the Tibetan Plateau. The Plateau contributes more than half of the river's runoff, but 90% of the sediment load comes from the Loess Plateau of the middle basin, where mean annual precipitation decreases from 700 mm in the southeast to 200 mm in the northwest (Wan and Wang, 1994; Shi *et al.*, 2002). Approximately 70% of the middle and lower catchment's precipitation falls during the June–September wet season, when rain-

storm intensities may reach 1–3 mm min^{-1} (Wan and Wang, 1994). Ice floods may also occur during February–March (Li *et al*., 2002). Prior to 1950, the river overflowed its levees approximately twice every 3 years (Wang and Liang, 2000). However, flow in the river has been steadily decreasing during the past few decades as a result of both climatic change and, more importantly, diversions and flow regulation. Precipitation volumes during the 1980s and 1990s produced 20–50% less mean annual runoff than equivalent volumes during the 1950s and 1960s (Ren *et al.*, 2002). Prior to 1991, the river did not flow to the sea for up to 40 days each year. In 1997, this number reached 227 days, and the dry portion of the river bed extended nearly 700 km (Postel, 1999). The corresponding dramatic reduction in runoff and sediment entering the Huanghe river delta has created both ecological and engineering problems (Wang and Liang, 2000).

Historical records for the Huanghe cover a period of nearly 3000 years. During this timespan, five major changes of course occurred in the lower Huanghe. The period of artificial levee construction along the river covers nearly as long a timespan (Fuling, 1989). Slackwater deposits preserved along the middle reaches of the Huanghe record a peak discharge of 42 900 $m^3 s^{-1}$ at Xiaolangdi (6.94×10^5 km^2 catchment area), for which the largest historic discharge is 32 500 $m^3 s^{-1}$ in 1843 (Yang *et al.*, 2000).

3.6.2 Changjiang

The Changjiang heads on the Tibetan Plateau, flows south-southwest onto the Yunnan Plateau, then turns north again before flowing east across China's Red Basin and broad alluvial plains as it approaches the China Sea. The Changjiang's drainage is at the meeting point of the Indian and Pacific monsoons. Rainfall in the upper basin, along with snow and glacial melt in the Tibetan Plateau headwaters, produces about half of the Changjiang's discharge (Z. Chen *et al.*, 2001). Mean annual precipitation increases steadily down the Changjiang drainage basin, from 435 mm in the upper basin above Yichang, through 1396 mm in the central portion from Yichang to Hukuo, and 1644 mm in the lower basin. Much of the rain falls during the March–September wet season. Annual mean discharge from the upper basin has significantly decreased since the end of the nineteenth century, probably as a result of climatic warming and associated glacial retreat and increased evaporation (X. Chen *et al.*, 2001). The lower basin is also affected by extensive flow regulation and substantial water transfer capacity (up to 5000 $m^3 s^{-1}$) associated with large diversion projects (X. Chen *et al.*, 2001).

Numerous dams were constructed in the upper Changjiang catchment during the period of 1950 to 1980. More than 46 000 dams throughout the Changjiang Basin can now store an estimated 125 billion m^3 of water (Fu, 1998). Three Gorges Dam is the latest culmination in this history of flow regulation. The massive dam is 2.3 km in length and 185 m in height, with a difference of 112 m in the river level upstream and downstream from the dam. When the reservoir above the dam is full, it will extend more than 600 km upstream. When operated at the projected normal reservoir level of 175 m, the dam will have a total storage capacity of 39 billion m^3 of water (Fu, 1998).

Progradation of the Changjiang Delta has occurred since sea level stabilized circa 6–7 ka BP (Hori *et al.*, 2001). The progradation rate more than doubled abruptly circa 2 ka BP, but it is not clear whether this resulted from widespread land use or from a combination of land use and climatic cooling after the mid-Holocene.

3.6.3 Mekong River

In contrast to river basins in which the headwaters provide much of the total discharge, the 25% of the upper Mekong basin that lies within the Himalaya provides only 15% of the river's discharge (Meybeck and Carbonnel, 1975). Approximately 75% of the total discharge is supplied by monsoon rainfall across the basin, which stretches southward across alluvial lowlands to the South China Sea. Mean annual precipitation in the eastern basin is 2000 to 4000 mm, but falls to less than 1500 mm in parts of the western basin. Mean annual precipitation for the entire basin is 1672 mm according to the Mekong River Commission. The rivers of the Mekong Basin begin to rise in May and June as the southeastern monsoon winds begin. High flow occurs during August and September in the upper reaches of the rivers, and during September and October lower in the basin (Hori, 2000).

Very little is known of the post-glacial evolution of the Mekong River. The incised valley that formed along the lower river during the last glacial maximum filled during the subsequent rise of sea level, and a massive delta has formed during the past 6 ka. Unlike other Asian rivers where land use has resulted in substantially increased sediment yields, estimated sediment discharge to the Mekong Delta has been relatively constant for the last 3 ka (Ta *et al.*, 2002).

3.7 HIGH-LATITUDE RIVERS

The great rivers of the high latitudes, which drain North America or Eurasia because of the global distribution of

landmasses at high latitudes, have perennially baroclinic climates (Table 3.1). Although frontal cyclones can produce most precipitation across these drainages, runoff is dominated by snowmelt. These rivers have low to moderate interannual variability in peak discharge, and high monthly variability in discharge (Figure 3.2).

3.7.1 Ob, Yenisey and Lena Rivers

The Ob, Yenisey and Lena are the great rivers of the Siberian arctic. Mean annual precipitation averages 250–500 mm across their drainage basins. The annual hydrograph of these rivers rises quickly during the snowmelt period, and the floods of late May to early June generally carry half of the total annual flow (Smith and Alsdorf, 1998). Ice dams are particularly important sources of both contemporary and historical/Quaternary flooding on these rivers (Yamskikh *et al.*, 1999).

Maizels (1995) has characterized these rivers as having a five-stage pattern of drainage changes since the last glacial maximum. Drainage was substantially affected by the formation of ice-dammed lakes, and large-scale aggradation of glaciofluvial deltas characterized the period from at least circa 20 ka BP until between 14 and 9 ka BP. Lake drainage led to incision and the formation of one or more glaciofluvial, and later, fluvial terraces. Extensive aggradation occurred from circa 9 to 6.5 ka BP, followed by mid-Holocene erosion until circa 4.5 ka BP, then renewed aggradation. However, most of the Holocene was characterized by small-scale erosional episodes separated by longer periods of modest aggradation or stability (Maizels, 1995).

3.7.2 Mackenzie and Yukon Rivers

The Mackenzie River drains north to the Arctic Ocean from western headwaters in the Canadian Rockies and eastern headwaters in Canada's northern lakes. The Yukon River drains west to the Bering Sea from headwaters in the Canadian and Alaskan Cordillera. Mean annual precipitation across both basins ranges from 1000 mm in the mountains to less than 250 mm in the lowlands. Like the Siberian rivers described previously, the Mackenzie and Yukon rivers of the American arctic reach their maximum discharge during late spring–early summer snowmelt, and have secondary discharge peaks produced by summer frontal precipitation (Burn, 1995). Ice jamming during the spring breakup is an important process that can locally obstruct and elevate flow (Brooks, 2000). Discharge is very low during the winter months when the surface of the rivers is frozen (Burn, 1995).

Much of the physical character of the Mackenzie River valley derives from a series of temporary glacial lakes impounded by retreating ice during the last glacial maximum (Duk-Rodkin and Lemmen, 2000). The fine-grained sediments deposited in these lakes now contain large reservoirs of permafrost that are particularly susceptible to melting under projected scenarios of global warming. Melting of permafrost has the potential to substantially alter the river's hydrology and discharge regime, as well as channel morphology and sediment supply to the river (Dyke and Brooks, 2000).

The Mackenzie Valley was ice-free by 10 ka BP (Duk-Rodkin and Lemmen, 2000). Conditions were generally warmer and drier than present from circa 10–6 ka BP, cooler and wetter during 6–1 ka BP, and then progressively warmer during the past thousand years except for the Little Ice Age (Dyke and Brooks, 2000; MacDonald, 2000).

3.8 SUMMARY

The great rivers of the world both respond to existing topography and, particularly in their lower reaches, create their own topography and landscapes. During the last glacial maximum, many of these rivers responded to lowered sea level by incising into coastal plains and nearshore regions. Fluctuations in water and sediment supply associated with glacial advances and retreats, changing vegetation and hillslope stability, and precipitation patterns produced episodes of incision and aggradation that left terraces and relict channels along the rivers. Many of the world's great rivers experienced periods of extremely large discharge as headwater glaciers substantially melted at the end of the Pleistocene. During this period higher discharges occurred along rivers in the equatorial and tropical regions as a result of post-glacial migration of the ITCZ and establishment of the modern monsoonal circulation patterns. Stabilization of global sea levels circa 6000 years ago resulted in aggradation and changes in channel pattern along the lower reaches of major rivers. Establishment of ENSO circulation patterns at approximately the same time created fluctuations in precipitation and river discharge over periods of hundreds to thousands of years.

Changes in atmospheric composition are presently accelerating late Holocene warming trends. Simulation models and extrapolation from existing systematic records of precipitation and river discharge suggest that many of the great rivers are likely to see lower flow volumes in future as a result of global warming (Wohl, 2000). These changes are being overshadowed at present by the dramatic changes in river hydrology and discharge associated

with other human activities. The combined effects of flow regulation in association with dams and diversions, and alteration of channel geometry and mobility through channelization, construction of levees, draining of wetlands, construction of locks and dams, dredging for navigation, and channel stabilization, have caused river metamorphosis in even the world's largest rivers.

Each of the great rivers historically was a source of immense natural wealth through the extensive wetlands and rich alluvial plains that the river created and maintained with its cycles of flooding and channel movement. Most of these wetlands are now gone; drained, covered, isolated from the river channel, or poisoned with agricultural and industrial wastes. The Amazon provides an encouraging exception in that it represents a major river that still functions as it did historically. In contrast, heavily diverted rivers such as the Huanghe (Liu and Zheng, 2002), the Nile, the Colorado, and the Indus now cease to flow in their lower reaches for some portion of each year (Postel, 1999), and the delta of rivers such as the Colorado has essentially ceased to exist (Fradkin, 1981). Humans have not controlled the great rivers of the world in the sense of creating fully predictable river environments that can be readily manipulated, but we have certainly altered the hydrology and discharge of these river systems to an extent that compares with the great changes of the Quaternary.

ACKNOWLEDGEMENTS

V. Baker, L. Mertes and A. Gupta provided helpful reviews of this chapter.

REFERENCES

Ahmad, M. and Kutcher, G.P. (1992) Irrigation planning with environmental considerations: a case study of Pakistan's Indus Basin. *World Bank Technology Paper* No. 166, Washington, DC, 196 pp.

Allison, M.A. (1998) Geologic framework and environmental status of the Ganges-Brahmaputra delta. *Journal of Coastal Research*, 14, 826–836.

Amarasekera, K.N., Lee, R.F., Williams, E.R. and Eltahir, E.A.B. (1997) ENSO and the natural variability in the flow of tropical rivers. *Journal of Hydrology*, 200, 24–39.

Ansari, A.A., Singh, I.B. and Tobschall, H.J. (1999) Status of anthropogenically induced metal pollution in the Kanpur-Unnao industrial region of the Ganga Plain, India. *Environmental Geology*, 38, 25–35.

Ansari, A.A., Singh, I.B. and Tobschall, H.J. (2000) Role of monsoon rain on concentrations and dispersion patterns of metal pollutants in sediments and soils of the Ganga Plain, India. *Environmental Geology*, 39, 221–237.

Baker, V.R., Bowler, J.M., Enzel, Y. and Lancaster, N. (1995) Late Quaternary palaeohydrology of arid and semi-arid regions. In: *Global Continental Palaeohydrology* (K.J. Gregory, L. Starkel and V.R. Baker, Eds.). John Wiley & Sons, Ltd, Chichester, pp. 203–231.

Beuning, K.R.M., Kelts, K., Russell, J. and Wolfe, B.B. (2002) Reassessment of Lake Victoria-Upper Nile River paleohydrology from oxygen isotope records of lake-sediment cellulose. *Geology*, 30, 559–562.

Brooks, G.R. (2000) Streamflow in the Mackenzie valley. In: The Physical Environment of the Mackenzie Valley, Northwest Territories: A Base Line for the Assessment of Environmental Change (L.D. Dyke and G.R. Brooks, Eds.). *Geological Survey of Canada Bulletin*, 547, 153–166.

Brown, P.A. and Kennett, J.P. (1998) Megaflood erosion and meltwater plumbing changes during last North American deglaciation recorded in Gulf of Mexico sediments. *Geology*, 26, 599–602.

Burn, C.R. (1995) The hydrologic regime of Mackenzie River and connection of 'no-closure' lakes to distributary channels in the Mackenzie Delta, Northwest Territories. *Canadian Journal of Earth Sciences*, 32, 926–937.

Chen, X., Zong, Y., Zhang, E., Xu, J. and Li, S. (2001) Human impacts on the Changjiang (Yangtze) River basin, China, with special reference to the impacts on the dry season water discharges into the sea. *Geomorphology*, 41, 111–123.

Chen, Z., Li, J., Shen, H. and Zhanghua, W. (2001) Yangtze River of China: historical analysis of discharge variability and sediment flux. *Geomorphology*, 41, 77–91.

Church, M. (1988) Floods in cold climates. In: *Flood Geomorphology* (V.R. Baker, R.C. Kochel, and P.C. Patton, Eds.). John Wiley & Sons, Ltd, New York, pp. 205–229.

Clark, M.P., Serreze, M.C. and McCabe, G.J. (2001) Historical effects of El Nino and La Nina events on the seasonal evolution of the montane snowpack in the Columbia and Colorado River basins. *Water Resources Research*, 37, 741–757.

Collins, R.O. (1990) The *Waters of the Nile: Hydropolitics and the Jonglei Canal, 1900–1988*. Markus Wiener Publishers, Princeton, NJ, 441 pp.

Costa, J.E. (1987) A comparison of the largest rainfall-runoff floods in the United States with those of the People's Republic of China and the world. *Journal of Hydrology*, 96, 101–115.

Crabb, P. (1988) Managing the Murray-Darling basin. *Australian Geographer*, 19, 64–88.

Criss, R.E. and Shock, E.L. (2001) Flood enhancement through flood control. *Geology*, 29, 875–878.

Czaya, E. (1981) *Rivers of the World*. Cambridge University Press, Cambridge, 248 pp.

Duk-Rodkin, A. and Lemmen, D.S. (2000) Glacial history of the Mackenzie region. In: The Physical Environment of the Mackenzie Valley, Northwest Territories: A Base Line for the Assessment of Environmental Change (L.D. Dyke and G.R. Brooks, Eds.). *Geological Survey of Canada Bulletin*, 547, 11–20.

Dunne, T., Mertes, L.A.K., Meade, R.H., Richey, J.E. and Forsberg, B.R. (1998) Exchanges of sediment between the flood plain and channel of the Amazon River in Brazil. *Geological Society of America Bulletin*, 110, 450–467.

Dyke, L.D. and Brooks, G.R. (eds) (2000) Introduction. In: The Physical Environment of the Mackenzie Valley, Northwest Territories: A Base Line for the Assessment of Environmental change (L.D. Dyke and G.R. Brooks, Eds.). *Geological Survey of Canada Bulletin*, 547, 7–10.

Ely, L.L., Enzel, Y., Baker, V.R. and Cayan, D.R. (1993) A 5000-year record of extreme floods and climate change in the southwestern United States. *Science*, 262, 410–412.

Fradkin, P.L. (1981) *A River No More: the Colorado River and the West*. Knopf, New York, 360 pp.

Fu, S. (1998) A profile of dams in China. In: *The River Dragon has Come! The Three Gorges Dam and the Fate of China's Yangtze River and its People* (J.G. Thibodeau and P.B. Williams, Eds.). M.E. Sharpe, London, pp. 18–24.

Fuling, X. (1989) Evolution of the course of the lower Yellow River in past history. In: *Taming the Yellow River: Silt and Floods* (L.M. Brush, M.G. Wolman and H. Bing-Wei, Eds.). Kluwer, Dordrecht, pp. 545–555.

Goodbred, S.L. and Kuehl, S.A. (2000) Enormous Ganges-Brahmaputra sediment discharge during strengthened early Holocene monsoon. *Geology*, 28, 1083–1086.

Goswami, D.C. (1998) Fluvial regime and flood hydrology of the Brahmaputra River, Assam. In: *Flood Studies in India* (V.S. Kale, Ed.). Memoir No. 41, Geological Society of India, 53–75.

Goulding, M. (1989) *Amazon: the Flooded Forest*. Sterling Publishing Co., New York, 208 pp.

Graf, W.L. (1985) *The Colorado River: Instability and Basin Management*. Association of American Geographers, Washington, DC, 86 pp.

Gupta, A. (1988) Large floods as geomorphic events in the humid tropics. In: *Flood Geomorphology* (V.R. Baker, R.C. Kochel, and P.C. Patton, Eds.). John Wiley & Sons, Ltd, New York, pp. 301–315.

Hassan, F.A. and Stucki, B.R. (1987) Nile floods and climatic change. In: *Climate: History, Periodicity, and Predictability* (M. R. Rampino, J.E. Sanders, W.S. Newman and L.K. Konigsson, Eds.). Van Nostrand Reinhold, New York, pp. 37–46.

Hayden, B.P. (1988) Flood climates. In: *Flood Geomorphology* (V.R. Baker, R.C. Kochel and P.C. Patton, Eds.). John Wiley & Sons, Ltd, New York, pp. 13–26.

Herczeg, A.L., Simpson, H.J. and Mazor, E. (1993) Transport of soluble salts in a large semiarid basin: River Murray, Australia. *Journal of Hydrology*, 144, 59–84.

Herschy, R.W. (1998) Rivers. In: *Encyclopedia of Hydrology and Water Resources* (R.W. Herschy and R.W. Fairbridge, Eds.). Kluwer, Dordrecht, pp. 571–583.

Hewitt, K. (1998) Catastrophic landslides and their effects on the Upper Indus streams, Karakoram Himalaya, northern Pakistan. *Geomorphology*, 26, 47–80.

Hirschboeck, K.K. (1988) Flood hydroclimatology. In: *Flood Geomorphology* (V.R. Baker, R.C. Kochel, and P.C. Patton, Eds.). John Wiley & Sons Ltd, New York, pp. 27–49.

Hori, H. (2000) *The Mekong: environment and development*. United Nations University Press, Tokyo, 398 pp.

Hori, K., Saito, Y., Zhao, Q., Cheng, X., Wang, P., Sato, Y. and Li, C. (2001) Sedimentary facies and Holocene progradation rates of the Changjiang (Yangtze) delta, China. *Geomorphology*, 41, 233–248.

Hotzl, H. (1996) Origin of the Danube-Aach system. *Environmental Geology*, 27, 87–96.

Ittekkot, V. and Arain, R. (1986) Nature of particulate organic matter in the river Indus, Pakistan. *Geochimica et Cosmochimica Acta*, 50, 1643–1653.

Jordan, C.F. (ed.) (1989) *An Amazonian Rain Forest*. UNESCO, Paris, 176 pp.

Kadomura, H. (1995) Palaecological and palaeohydrological changes in the humid tropics during the last 20 000 years, with reference to equatorial Africa. In: *Global Continental Palaeohydrology* (K.J. Gregory, L. Starkel and V.R. Baker, Eds.). John Wiley & Sons, Ltd, Chichester, pp. 177–202.

Kashef, A.-A.I. (1981) The Nile – one river and nine countries. *Journal of Hydrology*, 53, 53–71.

Knox, J.C. (1993) Large increases in flood magnitude in response to modest changes in climate. *Nature*, 361, 430–432.

Krom, M.D., Stanley, J.D., Cliff, R.A. and Woodward, J.C. (2002) Nile River sediment fluctuations over the past 7000 yr and their key role in sapropel development. *Geology*, 2002, 71–74.

Li, W., Su, Y., Jiang, N. and Zhang, Y. (2002) Flood and flood control of the Yellow River. In: *Flood Defence 2002* (B. Wu, Z.Y. Wang, G. Wang, G.G.H. Huang, H. Fang and J. Huang, Eds.). Science Press, Beijing, pp. 1518–1522.

Liu, C. and Zheng, H. (2002) Hydrological cycle changes in China's large river basin: The Yellow River drained dry. In: *Climatic Change: Implications for the Hydrological Cycle and for Water Management* (M. Beniston, Ed.). Kluwer, Dordrecht, pp. 209–224.

Liu, K.B. and Colinvaux, B.A. (1988) A 5200-year history of Amazon rain forest. *Journal of Biogeography*, 15, 231–248.

Lockwood, J.G. (1974) *World Climatology: an Environmental Approach*. Edward Arnold, London, 330 pp.

MacDonald, G.M. (2000) Postglacial vegetation and climate. In: *The Physical Environment of the Mackenzie Valley, Northwest Territories: A Base Line for the Assessment of Environmental Change* (L.D. Dyke and G.R. Brooks, Eds.). Geological Survey of Canada Bulletin, 547, 57–63.

Maizels, J.K. (1995) Palaeohydrology of polar and subpolar regions over the past 20 000 years. In: *Global Continental Palaeohydrology* (K.J. Gregory, L. Starkel and V.R. Baker, Eds.). John Wiley & Sons, Ltd, Chichester, pp. 259–299.

Marret, F., Scourse, J.D., Versteegh, G., Jansen, J.H.F. and Schneider, R. (2001) Integrated marine and terrestrial evidence for abrupt Congo River palaeodischarge fluctuations during the last deglaciation. *Journal of Quaternary Science*, 16, 761–766.

Meade, R.H., Yuzyk, T.R. and Day, T.J. (1990) Movement and storage of sediment in rivers of the United States and Canada. In: *Surface Water Hydrology* (M.G. Wolman and H.C. Riggs, Eds.). Geological Society of America, Boulder, CO, pp. 255–280.

Memon, M.M. (1969) The soil and water resources of the lower Indus region. *Oriental Geographer*, 13, 41–52.

Mertes, L.A.K., Dunne, T. and Martinelli, L.A. (1996) Channel-floodplain geomorphology along the Solimões-Amazon

River, Brazil. *Geological Society of America Bulletin*, 108, 1089–1107.

Meybeck, M. and Carbonnel, J.P. (1975) Chemical transport by the Mekong River. *Nature*, 255, 134–136.

Milliman, J.D. (1997) Blessed dams or damned dams? *Nature*, 386, 325–326.

Moghraby, A.I. (1982) The Jonglei Canal – needed development or potential ecodisaster? *Environmental Conservation*, 9, 141–148.

O'Connor, J.E., Ely, L.L., Wohl, E.E., Stevens, L.E., Melis, T.S., Kale, V.S. and Baker, V.R. (1994) A 4500-year record of large floods on the Colorado River in the Grand Canyon, Arizona. *Journal of Geology*, 102, 1–9.

Pisut, P. (2002) Channel evolution of the pre-channelized Danube River in Bratislava, Slovakia (1712–1886). *Earth Surface Processes and Landforms*, 27, 369–390.

Postel, S. (1999) *Pillar of Sand: Can the Irrigation Miracle Last?* W.W. Norton and Company, New York, 313 pp.

Ren, L., Wang, M., Li, C. and Zhang, W. (2002) Impacts of human activity on river runoff in the northern area of China. *Journal of Hydrology*, 261, 204–217.

Richey, J.E., Nobre, C. and Dreser, C. (1989) Amazon River discharge and climate variability: 1903 to 1985. *Science*, 246, 101–103.

Riggs, H.C. and Harvey, K.D. (1990) Temporal and spatial variability of streamflow. In: *Surface Water Hydrology* (M.G. Wolman and H.C. Riggs, Eds.). Geological Society of America, Boulder, CO, pp. 81–96.

RivDIS (Global River Discharge). (2003) Dataset at http://www-eosdis.ornl.gov/daacpages/ rivdis.html.

Rossignol-Strick, M., Paterne, M., Bassinot, F.C., Emeis, K.-C. and DeLange, G.J. (1998) An unusual mid-Pleistocene monsoon period over Africa and Asia. *Nature*, 392, 269–272.

Sanford, R.L., Saldarriaga, J., Clark, K.E., Uhl, C. and Herrera, R. (1985) Amazon rain-forest fires. *Science*, 227, 53–55.

Sarin, M.M. and Krishnaswami, S. (1984) Major ion chemistry of the Ganga-Brahmaputra river systems, India. *Nature*, 312, 538–541.

Schneider, R.R., Price, B., Müller, P.J., Kroon, D. and Alexander, I. (1997) Monsoon related variations in Zaire (Congo) sediment load and influence of fluvial silicate supply on marine productivity in the east equatorial Atlantic during the last 200 000 years. *Paleoceanography*, 12, 463–481.

Schwetz, G.I. (1978) *Multi-centennial Changes of the Run-off of the Dniepr River*. Gidrometeoizdat, Leningrad (in Russian, cited in Starkel, 1995).

Servant, M., Maley, J., Turcq, B., Absy, M.L., Bernac, P., Fournier, M. and Ledru, M.P. (1993) Tropical forest changes during the late Quaternary in African and South American lowlands. *Global and Planetary Change*, 7, 25–40.

Shi, C., Zhang, D. and You, L. (2002) Changes in sediment yield of the Lower Yellow River basin of China during the Holocene. *Geomorphology*, 46, 267–283.

Showers, W.J. and Bevis, M. (1988) Amazon cone isotopic stratigraphy: evidence for the source of the tropical freshwater spike. *Palaeogeography, Palaeoclimatology, Palaeoecology*, 64, 189–199.

Simpson, H.J., Cane, M.A., Herczeg, A.L., Zebiak, S.E. and Simpson, J.H. (1993) Annual river discharge in southeastern Australia related to El Nino-Southern Oscillation forecasts of sea surface temperatures. *Water Resources Research*, 29, 3671–3680.

Singh, I.B., Bajpai, V.N., Kumar, A. and Singh, M. (1990) Changes in the channel characteristics of Ganga River during late Pleistocene-Holocene. *Journal Geological Society of India*, 36, 67–73.

Smith, L.C. and Alsdorf, D.E. (1998) Control on sediment and organic carbon delivery to the Arctic Ocean revealed with space-borne synthetic aperture radar: Ob River, Siberia. *Geology*, 26, 395–398.

Smith, N.J.H. (1999) *The Amazon Rain Forest: a Natural History of Plants, Animals, and People*. Oxford University Press, New York, 208 pp.

Starkel, L. (1972) The modelling of monsoon areas of India as related to catastrophic rainfall. *Geographia Polonica*, 23, 151–173.

Starkel, L. (1995) Palaeohydrology of the temperate zone. In: *Global Continental Palaeohydrology* (K.J. Gregory, L. Starkel and V.R. Baker, Eds.). John Wiley & Sons, Ltd, Chichester, pp. 233–257.

Ta, T.K.O., Nguyen, V.L., Tateishi, M., Kobayashi, I., Tanabe, S. and Saito, Y. (2002) Holocene delta evolution and sediment discharge of the Mekong River, southern Vietnam. *Quaternary Science Reviews*, 21, 1807–1819.

Talbot, M.R., Williams, M.A.J. and Adamson, D.A. (2000) Strontium isotope evidence for late Pleistocene reestablishment of an integrated Nile drainage network. *Geology*, 28, 343–346.

Thomas, M.F. and Thorp, M.B. (1996) The response of geomorphic systems to climatic and hydrological change during the Late Glacial and early Holocene in the humid and sub-humid tropics. In: *Global Continental Changes in the Context of Paleohydrology* (J. Branson, A.G. Brown and K.J. Gregory, Eds.). Geological Society Special Publication No. 115, London, pp. 139–153.

Thorne, C.R., Russell, A.P.G. and Alam, M.K. (1993) Planform pattern and channel evolution of the Brahmaputra River, Bangladesh. In: *Braided Rivers* (J.L. Best and C.S. Bristow, Eds.). Geological Society Special Publication No. 75, London, pp. 257–276.

Walker, K.J. (1994) *The Political Economy of Environmental Policy: an Australian Introduction*. University of New South Wales Press, Kensington, NSW, 349 pp.

Walker, N.J. (1990) Zimbabwe at 18 000 BP. In: *The World at 18 000 BP* (C. Gamble and O. Soffer, Eds.), v. 2, Low Latitudes. Unwin Hyman, London, pp. 206–213.

Walling, D.E. (1996) Hydrology and rivers. In: *The Physical Geography of Africa* (W.M. Adams, A.S. Goudie and A.R. Orme, Eds.). Oxford University Press, Oxford, pp. 103–121.

Wan, Z. and Wang, Z. (1994) *Hyperconcentrated Flow*. IAHR-AIRH Monograph, AA Balkema, Rotterdam, 290 pp.

Wang, Z.-Y. and Liang, Z.-Y. (2000) Dynamic characteristics of the Yellow River mouth. *Earth Surface Processes and Landforms*, 25, 765–782.

Watson, C.C. and Biedenharn, D.S. (2000) Comparison of flood management strategies. In: *Inland Flood Hazards: Human, Riparian and Aquatic Communities* (E.E. Wohl, Ed.). Cambridge University Press, Cambridge, pp. 381–393.

Wohl, E.E. (2000) Anthropogenic impacts on flood hazards. In: *Inland Flood Hazards: Human, Riparian and Aquatic Communities* (E.E. Wohl, Ed.). Cambridge University Press, Cambridge, pp. 104–141.

Yamskikh, A.F., Yamskikh, A.A. and Brown, A.G. (1999) Siberian-type Quaternary floodplain sedimentation: the example of the Yenisei River. In: *Fluvial Processes and Environmental Change* (A.G. Brown and T.A. Quine, Eds.). John Wiley & Sons, Ltd, Chichester, pp. 241–252.

Yang, D., Yu, G., Xie, Y., Zhan, D. and Li, Z. (2000) Sedimentary records of large Holocene floods from the middle reaches of the Yellow River, China. *Geomorphology*, 33, 73–88.

4

Transcontinental Moving and Storage: the Orinoco and Amazon Rivers Transfer the Andes to the Atlantic*

Robert H. Meade

Research Hydrologist Emeritus, US Geological Survey, MS 413, Box 25046, Federal Center, Denver, CO 80225-0046, USA

4.1 INTRODUCTION

Large rivers are massive conveyance systems for moving detrital sediment and dissolved matter across transcontinental distances. As Potter (1978a,b) pointed out a generation ago, the large eastward-flowing rivers of South America transfer sediment over thousands of kilometres, from the leading edge (active margin) to the trailing edge (passive margin) of a drifting continent. Matching these large spatial scales of movement are the temporal scales of alluvial storage, on the order of thousands of years, that retard the conveyance of sediment from original source to ultimate sink. In the post-Pleistocene Orinoco and Amazon River basins, the original sources have been the eastern slopes of the northern half of the Andean mountain ranges. The extensive alluvial plains of the Andean foreland basin and the large tracts of floodplain along the Amazon mainstem and some of its major tributaries are the depositories in which much of the Andean-derived sediment is stored – for periods of centuries, millennia, or longer – during its eastward journey. The ultimate sinks for these sediments ('ultimate' on a multimillennial timescale) are the lowermost floodplains and deltaic regions of the Amazon and Orinoco, and the thousand-and-a-half-kilometre Atlantic coastal zone that separates the mouths of these two great rivers.

All the major parts of the story that follows have been told previously (but mostly separately), especially in the publications by Dunne *et al.* (1998), Eisma *et al*. (1991), Johnsson *et al*. (1991), Meade (1994), Meade *et al.* (1985, 1990), Mertes *et al*. (1996), Nittrouer and DeMaster (1987), Nittrouer and Kuehl (1995), Nordin *et al*. (1994), Stallard (1995), Stallard *et al*. (1990) and Warne *et al.* (2002). This chapter recounts the major components of the story in downstream sequence, from west to east across the northern half of South America.

4.2 ANDEAN SOURCES AND ALLUVIAL STORAGE

The mountainous terranes of the Andes are the principal sources of the fluvial sediment carried by the Orinoco and Amazon Rivers. Alfred Russel Wallace (1853) gave the scientific literature its initial hint of this fact in his discussion of the distinctly different river types in the Amazon basin: 'white-water', 'black-water' and 'blue-water' (changed in later usage to 'clear-water'). Harald Sioli (1957), in a paper published a century after Wallace's book, went on to point out that the large white-water rivers (so-called because of their visibly large concentrations of suspended sediment) of Amazonia had their origins in the Andes or the Andean foothills. Ronald Gibbs reiterated

Large Rivers: Geomorphology and Management, Edited by A. Gupta

and substantiated this fact a decade later in his doctoral dissertation research (Gibbs, 1965, 1967), for which he travelled thousands of kilometres on local river boats, sampling the suspended-sediment concentrations of the Amazon and its tributaries. He measured the greatest concentrations in the tributaries that drained either the mountains themselves or the tributaries draining the Andean-derived second-generation sedimentary terranes of the foreland basin. Later work in the other major river basins of South America – the Paraná (Ritter, 1977a,b; Drago and Amsler, 1988), Magdalena (NEDECO, 1973; Winkley *et al.*, 1994) and Orinoco (Meade *et al.*, 1990) – have borne out this generality. Subsequent and more detailed work in the Amazon Basin (Meade *et al*., 1985; Guyot, 1993; Dunne *et al*., 1998) has shown that, while Gibbs was correct in principle, his numbers might have been too conservative. He estimated that 82% of the sediment carried by the Amazon was derived from the 12% of the drainage area that was underlain by the Andes. Our later measurements and estimates would credit more than 90% to the Andean source. And if we consider the recycled sedimentary deposits in the foreland basins as material of ultimate Andean origin, then we can say that virtually all the modern fluvial sediment in both the Amazon and Orinoco has been derived from the Andes.

The preponderance of fluvial sediment in the world's rivers, great and small, is derived from the regions of greatest tectonism (Milliman and Meade, 1983; Milliman and Syvitski, 1992). Nearly a third of the active fluvial sediment in the world, for example, is being transported seaward by the combination of rivers [Indus, Ganga, Brahmaputra, Irrawaddy, Salween, Mekong, Red (Sông Hóng), Yangtze (Changjiang)] that drain the furrows of the great tectonic collision between the Indian subcontinent and the rest of Asia. Although notable exceptions may be found in the shale outcroppings of the Northern Great Plains of the Mississippi valley and the Loess Plateau of the valley of China's Yellow River, most of the rest of the world's fluvial sediment is being produced in tectonically active regions such as the large islands of the western Pacific and the western edges of North and South America. Although many authors have generalized this correlation by constructing graphs relating sediment yield to topographic relief, it is well to remember that the observed relation is not so much with relief itself as with a numerically less specifiable property which is the degree of tectonism. Perhaps Milliman and Syvitski said it best:

> '. . . that elevation or relief is . . . only a surrogate variable for tectonism. . . . [,and] . . . the strong correlation between sediment and topographic relief may not indicate that the second is the cause of the first, but rather that both are caused by another factor less susceptible to numerical description – namely, tectonism. It is probably the entire tectonic milieu of fractured and brecciated rocks, oversteepened slopes, seismic and volcanic activity, rather than simple elevation/relief, that promotes the large sediment yields from active orogenic belts.'
>
> (Milliman and Syvitski, 1992: pp. 539–540)

The traveller through the Andes is struck by the prevalence of tectonically oversteepened slopes and fractured rocks, massive landslides, and sediment-glutted streams. US Naval Lieutenant Lardner Gibbon, while travelling down an interior Andean valley in Peru in 1851, noted:

> 'Our road lies through a rich valley, often four miles wide, and level as a floor. The mountains on both sides are dry and unproductive, except in the ravines. The half-yearly displacement of earth is very great; during the rainy season the mountain torrents come down from the summit loaded with soil. The Juaja river flows sluggishly and serpent-like through the whole length of the valley, and creeping through the Andes, suddenly rushes off at a rapid rate, as though sensible of its long journey, by the Ucayali and Amazon, to the Atlantic ocean. The bed of the river is half a mile wide, and in the wet season is probably eighteen feet deep.'
>
> (Gibbon, 1854)

Recent examples of catastrophic-scale sediment productions from Andean slopes underlain by tectonically influenced rocks (although neither example is from the Orinoco or Amazon basin proper) are the huge deposits set in motion by the November 1985 eruption of Nevado del Ruiz in the Andes of Colombia and the massive landslides and debris flows that devastated the northern coastal towns of Venezuela in December 1999 (Pierson *et al*., 1990; Larsen *et al*., 2001a,b).

As they leave their narrow mountain gorges, the streams coming off the Andes flow onto river beds that are self-made. Massive amounts of sediment brought down from the mountains become the substrates over which and through which the flowing waters, with their accompanying loads of even *more* sediment, must make their ways. Once off the Andean slopes and out of the confinement of mountain-girt channels, the river-borne sediment is likely to endure many episodes of confinement and occupy many rest stops and storage compartments before it reaches its ultimate destination.

During the last century, the scientific community of sedimentologists has shown much less concern for sedi-

ment storage than it has for sediment movement. From a temporal point of view, this preponderance of interest in movement over storage is oddly displaced. Any given particle of sediment in an active river system is, at any randomly selected instant, more likely, by factors of thousands or more, to be resting quietly in storage than to be actively in motion. This preponderance of interest likely betrays the preference of most sedimentologists for the physical aspects over the chemical aspects of river sedimentation. Interesting as the physical aspects of sediment movement certainly are, equally interesting are the chemical consequences of prolonged sediment storage. For in tropical river basins, the temporal scales of alluvial sediment storage overlap the temporal scales of soil weathering. As a consequence, many of the chemically less stable minerals and rock fragments that have been hydraulically deposited as solid sediment grains in the flood plains of tropical rivers become weathered *in situ* to the point that they lose their solidity, yield up their substance to the dissolved state, and are easily carried away, ion by ion or molecule by molecule, invisibly into the percolating ground waters and flowing rivers.

4.3 ORINOCO

The Orinoco River today drains most of Venezuela and about one-fifth the area of Colombia. Flowing during earliest Miocene times between the rising Andes to the west and the Guayana Shield to the east, the ancestral Orinoco most likely debouched northward into Caribbean waters near the present site of Lake Maracaibo (Díaz de Gamero, 1996). However, the rising of the easternmost cordillera of the Andes, and its continuation into the east-west-trending ranges along the Caribbean coast during Middle Miocene times, deflected the course of the river to the east and directly into the Atlantic Ocean along the northern edge of the exposed Guayana Shield (Figure 4.1).

The Orinoco is the most abundantly watered of the large river basins of the world. The fresh-water discharge at the Orinoco's mouth is twice that of the Mississippi, although the Orinoco drains an area only one-third as large. Averaged over their entire river basins, therefore, the landscapes of the Orinoco Basin are six times more abundantly watered than those of the Mississippi. Sediment discharge of the Orinoco, however, is less than half that of the pre-engineered Mississippi (that is, *before* the great dams were built on the Missouri River and other large tributaries; Meade, 1995: p.18). About half the fresh water discharged at its mouth by the Orinoco flows off the Guayana Shield, a terrane of ancient erosion-resistant rocks that yield virtually no sediment. The maps in Figure 4.2 show that, although the Orinoco derives its waters in approximately

(a)

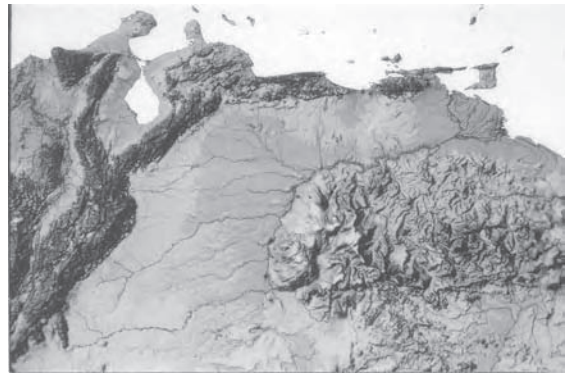

(b)

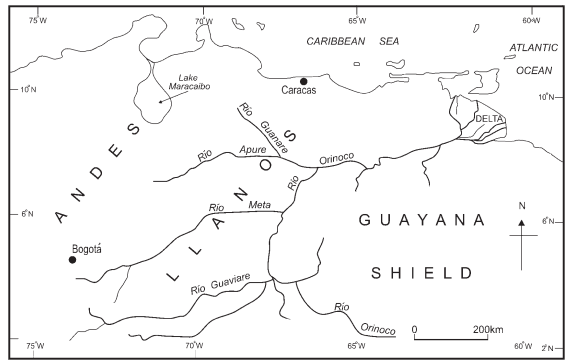

Figure 4.1 (a,b) Orinoco River basin of Venezuela and Colombia. Andes Mountains shown as dark areas along western edge. Lowland llanos (alluvial plains) separate Andes from highlands of Guayana Shield. Orinoco River flows for much of its length along border between llanos and shield. (a) Compiled from satellite imagery by Lisa Mae Olsen and Norman Bliss of US Geological Survey's EROS Data Center

equal measure from the right-side tributaries that drain the Guayana Shield and the left-side tributaries that drain the Andes, the only significant amounts of sediment are coming off the Andes.

Large alluvial plains, locally called 'llanos', have formed on the surfaces of the Andean forelands of Venezuela and Colombia. The llanos are built on materials that have been shed from the eastern slopes of the rising Andes since at least early Tertiary times. The alluvial plains slope gently away from the Andes, and halt only where their eastern distal edges abut the opposing slopes of the bedrocked Guayana Shield. Along this broadly clockwise-curving line of contact, the Orinoco River flows as a massive drain. On opposite banks of the great river, one can observe the encroachment of one of the world's

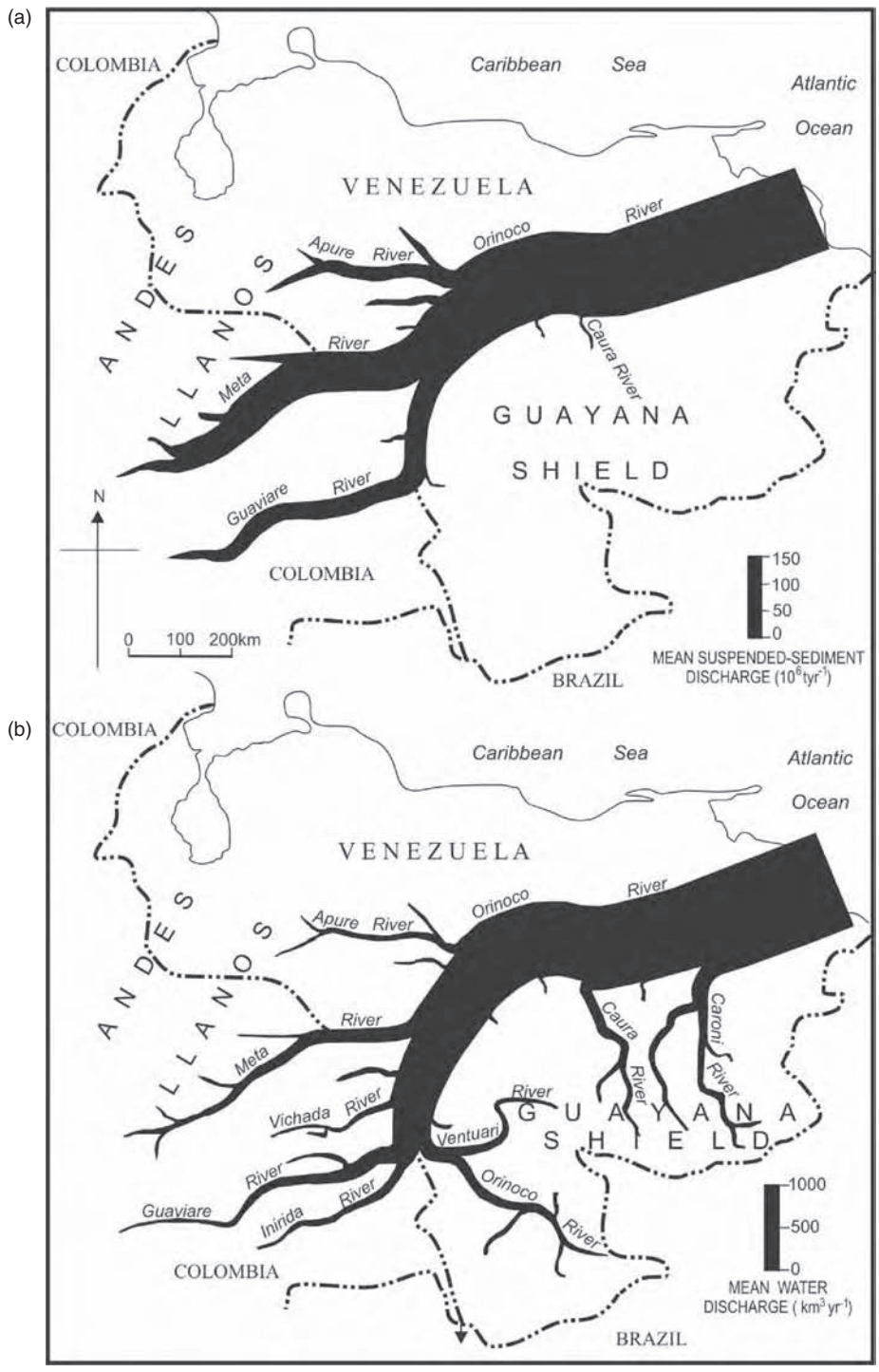

Figure 4.2 Average discharges of suspended sediment (a) and fresh water (b) in Orinoco River and its tributaries. Details of compilation given by Meade *et al.* (1990); for further hydrologic details, see also Nordin *et al*. (1994) and Pérez Hernández and López (1998)

youngest and most active landscapes, the llanos, onto the exposed edge of one of the world's oldest. The ancient landscapes of the Guayana Shield are developed on rocks, which, billions of years ago, formed part of the crystalline core of the supercontinent that we have come to call Gondwanaland.

In the transfer of sediment from the Andes to the Atlantic in the Orinoco River system, the llanos function as an immense storage compartment (Figure 4.3). Although sediment storage times range into the millions of years in the deep underlying sedimentary rocks of the Andean foreland, the processes of storage and remobilization that affect the compositions of sediment exposed on the surface of the llanos today operate mostly at timescales of centuries to millennia. Flowing out of the Andes, the streams shift their courses with great frequency, entraining, in the process, older sediment that had been previously deposited in the alluvial landscape, while leaving behind newer materials that had been brought more recently from the mountains. The effect of these repeated episodes of storage and remobilization can be seen in the mineral compositions of the sediments themselves. With increasing storage times in the alluvial soils of the Venezuelan llanos, the less stable mineral species and rock fragments become more weathered. With each successive episode of transport and intervening period of storage, in stepwise sequence down the gentle slope of the llanos between the Andean front and the mainstem Orinoco River, the sediment becomes more mature in composition. By the time most of the Andean-derived sands have been carried across the llanos, they have lost to solution most of the less stable constituents of their rock fragments, and consist of more than 90% quartz (Stallard *et al*., 1990; Johnsson *et al*., 1991). Andean-derived sands can therefore lose as much as a quarter of their original mass to solution, as their unstable grains are progressively dissolved out during successive episodes of storage and weathering in the alluvial soils of the llanos. Figure 4.4 shows the progressive deterioration of Andean-derived rock fragments and the consequent residual enrichment of quartz in sands being transported down the Guanare and Apure Rivers as they cross the western llanos of Venezuela.

4.4 AMAZON

4.4.1 Setting

The Amazon River today drains large parts of six of the countries (i.e. all but the Guianas) that occupy the northern half of South America. The downstream half of its great length flows from west to east along a lowland between two large cratons, the Guayana and Brazilian Shields (Figure 4.5), that became separated from the Pangaean supercontinent some hundred million years ago to form the ancient bedrock core of what is now South America. Most observers have surmised that, many tens of millions of years ago, the ancestral Amazon River must have flowed westward, in at least part of the same lowland through which it now flows eastward. A supporting supposition is that the rift zone along which South America became separated from Africa (pictured as analogous to the present East African Rift) was a highland from which the ancestral Amazon and other rivers flowed westward down to the sea. The rising of the Andes on the leading edge of the drifting South American continent eventually blocked the westward flow of the Amazon, perhaps (but not certainly) forming a large lake. Blocked from northward and southward flow by topographic obstructions of low but sufficient elevation in the developing Andean forelands, and strengthened by tributary waters from the forelands as well as from the eastern slope of the rising Andes, the Amazon found itself a passage between the shields through which it could flow eastward into the Atlantic Ocean. For a more engaging and stimulating discussion of the geologic history of the drainage of South America, see the paper by Potter (1997). See also the excellent chapter in this volume by Leal Mertes and Thomas Dunne (Chapter 8).

With only a single exception, the hydrographic dimensions and hydrologic parameters of the Amazon far exceed those of all other rivers on the planet. The exception is river length, the record for which is held by the Nile, only a few kilometres longer than the Amazon, according to the latest reliable reckonings (see Goulding *et al*., 2003: pp. 23–24). The total area drained by the Amazon is half again as large as that drained by the second-place Congo, and twice that drained by the third-place Mississippi. The quantity of fresh water discharged by the Amazon at its mouth is five times that of the second-place Congo, six times that of the third-place Orinoco, and twelve times that of the seventh-place Mississippi. (Ranking fourth through sixth in the discharge of fresh water to the coastal oceans are three Asian rivers: respectively, the combined Ganga-Brahmaputra, the Yangtze, and the Yenisey; Meade, 1996.) Two of the Amazon's tributaries, rio Madeira and rio Negro, themselves discharge more fresh water at their mouths than all but the Congo, Orinoco, and Yangtze.

The sediment load of the Amazon, measured at Óbidos near the point of maximum in-channel sediment discharge, averages about 1200 million tonnes per year. Only two other rivers of the world, both in Asia, discharge sediment quantities of this magnitude: the combined Ganga and

Figure 4.3 Oblique aerial photographs of the Venezuelan llanos, showing visual evidences of the distribution and storage of Andean-derived sediment. (a) View up small stream flowing out of Andes (mountains in clouds in distance) and onto llanos, showing meanders and active point bars as evidences of recent shifting of the self-made channel. (b) View up moderate-sized river flowing across central llanos. A more distant view, of a somewhat larger river than the one shown in (a). (c) Abandoned channels in central llanos, showing where rivers formerly flowed and where fluvial sediments are now stored. Approximately same scale as (b). Andes in clouds in far distance. (d) Eastern edge of llanos near the Apure-Orinoco confluence. View south. Middle-ground shows scroll marks developed on edge of llanos. In far distance is Río Orinoco (flowing to left), beyond which (far left) lie the ancient rocks of the Guayana Shield

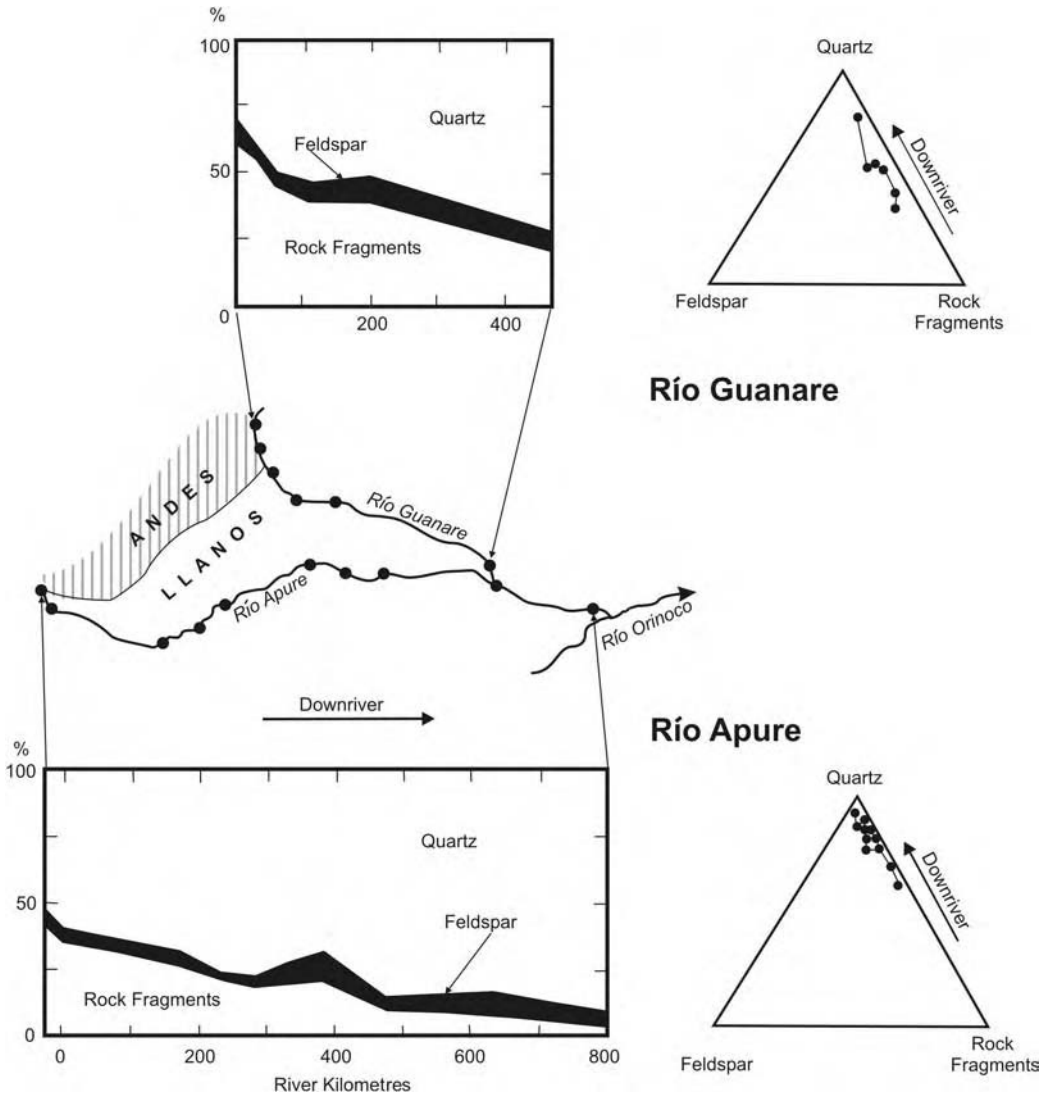

Figure 4.4 Graphs showing the progressive maturation in the mineral compositions of fluvial sands in streams crossing the northwestern llanos of Venezuela. Compiled by Mark Johnsson from supplementary supporting data (Geological Society of America Supplementary Data 91-33) of Johnsson *et al*. (1991)

Brahmaputra, which drain the Himalayas and share a delta in the Bay of Bengal, and the Yellow River (Huanghe) of China, which drains a vast loess plateau that has been subjected to thousands of years of artificially accelerated erosion. Since the completion of large dams at Sanmenxia and Xiaolangdi, however, the Yellow River no longer delivers its enormous sediment loads to its delta (Milliman *et al.*, 1987; Zhao *et al*., 1989; Zhou and Pan, 1994; Shi *et al*., 2002).

Figure 4.6 shows that, while most of the water in the Brazilian mainstem is gathered from the many rainfall-fed tributaries that drain the lowlands, virtually all the suspended sediment is derived from either the Andes of Peru via the Amazon mainstem or the Andes of Bolivia via the Madeira. Quantities portrayed in the figure are averages over the few recent decades of record. Water flows are cumulative and conservative – that is, the total outflow of fresh water at the mouth is the sum of all the tributary

(a)

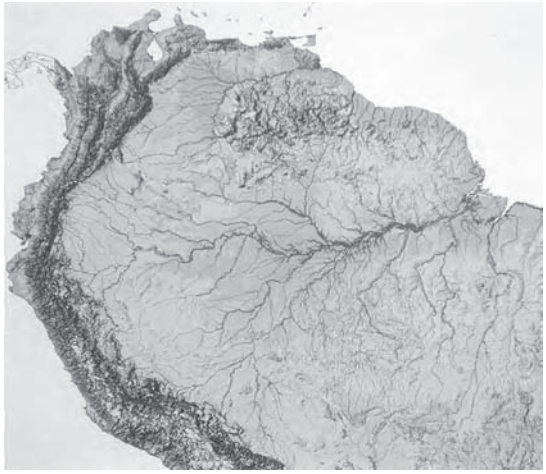

(b)

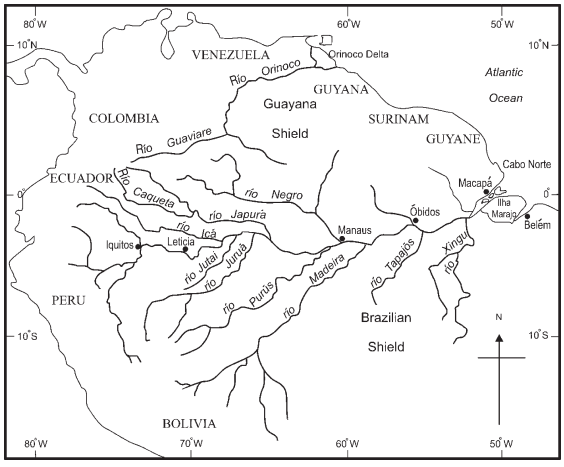

Figure 4.5 Amazon River basin in context of northern South America. Andes Mountains shown as dark area along western margin. Amazon mainstem flows almost due east from Iquitos, Peru, to the Atlantic Ocean. (a) Compiled from satellite imagery by Lisa Mae Olsen and Norman Bliss of US Geological Survey's EROS Data Center. Local usages for 'River' are 'Río' in Spanish-speaking countries and 'rio' in Portuguese-speaking Brazil

inputs. This assumes that the water that leaves the channel to cover the floodplains during the rising-water season is returned to the channel in the same quantities during the following falling-water season (Richey *et al.*, 1989). Suspended-sediment discharges, however, are not shown as conservative. Much of the sediment that leaves the channel in suspension in flood waters during the rising-water season is deposited on the floodplains before the waters are returned to the channel during the falling-water season. In the figure, this is shown especially in the lower Amazon, where large lakes on the floodplains are filling progressively with slowly accumulating sediment.

Similar diagrams constructed by Guyot (1993) for the Amazonian headwaters (Rio Madeira) of Bolivia show similar patterns of conservative water discharges and non-conservative suspended-sediment discharges. Guyot states that almost half the sediment brought down by headwater streams in the Andes of Bolivia is deposited in the foreland basin and on floodplains by the time the waters of rio Madeira flow out of Bolivia and into Brazil. The upper diagram in Figure 4.6, however, tells only part of the story. It does not show seasonal variations in the concentrations and discharges of suspended sediment (Meade, 1985; Meade *et al.*, 1985). Nor does it show the longer timescale exchanges of sediment between the channel and floodplains (Mertes *et al*., 1996; Dunne *et al*., 1998)

4.4.2 Storage and Remobilization of Floodplain Sediment

The floodplains of the Amazon retard the seaward progress of Andean sediment, much as do the llanos of the Orinoco. They provide storage compartments where Atlantic-bound sediment can rest for centuries or millennia and can remain sufficiently long for tropical soil-weathering processes to partially transform its mineral composition. The Amazon mainstem in Brazil alone is flanked by nearly 90 000 km^2 of floodplain area (Wolfgang Junk, quoted by Goulding *et al*., 2003: p. 46). A segment of one of the larger contiguous tracts of floodplain along the middle Amazon is shown in the side-looking-airborne-radar imagery in Figure 4.7. These vast tracts provide the most productive substrates and landscapes of lowland Amazonia: the flooded forests and riparian savannas, and the farms and ranches to which many of them have been converted (Junk, 1997; Junk *et al.*, 2000). The floodplains built of Andean-derived sediment are so distinctive (Sioli, 1951, 1984; Sternberg, 1956, 1975; Irion *et al*., 1997), especially when contrasted with those of sediment-poor lowland rivers of the Amazon region, that indigenous populations have long given them a special name, *várzea*. Owing to the regularity of the annual rise and fall of the river, the floodplains of the middle Amazon are constructed by slow vertical accretion, particle by particle, layer by layer, year by year, as the overflowing waters spread thin layers of new sediment over wide areas.

Thus are formed the habitats for a remarkable assemblage of plants and animals. Great trees whose roots and lower trunks are tolerant of months of inundation by several metres of flood water, rapidly growing grasses,

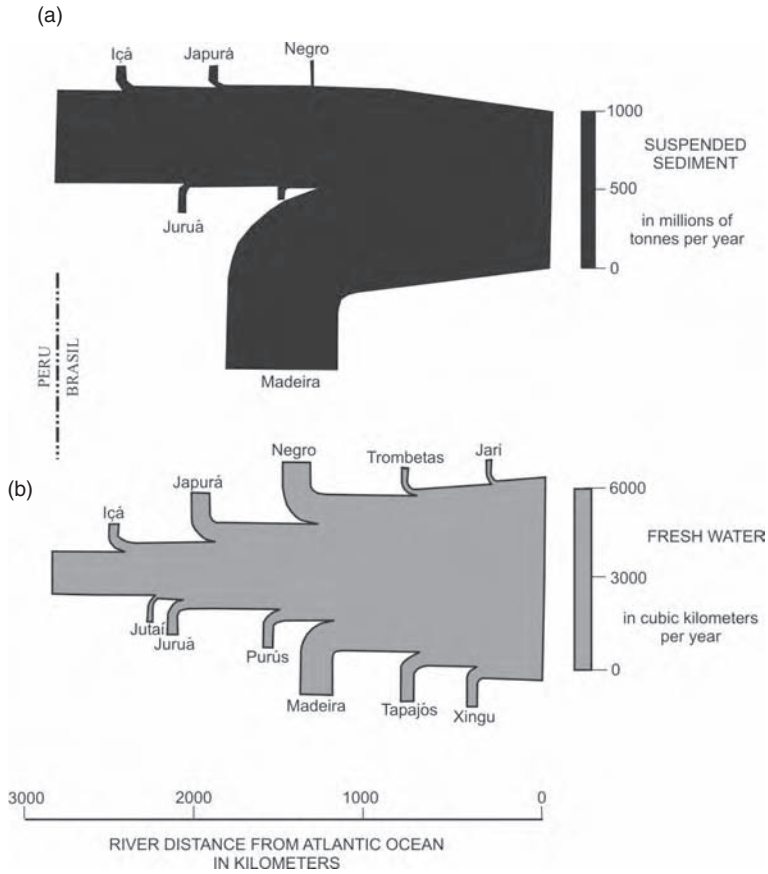

Figure 4.6 Average discharges of suspended sediment (a) and fresh water (b) in the mainstem channel of the Amazon River of Brazil. Suspended-sediment data from Dunne *et al.* (1998); fresh-water data from Carvalho and da Cunha (1998)

Figure 4.7 Side-looking-airborne-radar mosaic of large tract of floodplain between tributary rio Japurá and rio Solimões (local name for Amazon mainstem between Peru-Brazil border and confluence with rio Negro). River flow is from upper left to lower right. From Projeto RADAM (1973). This specific imagery has almost become a poster for large-scale changes in river-channel configuration: it was used, for example, as the dust-jacket picture for the book, *River Channel Changes* (Gregory, 1977). Since the time the imagery was collected (1971), the channel configurations here have continued to change. Within the last few years, for example, the narrow chute channel with the single near-perfect sine-curve meander that crossed the outer part of the neck of the great meander of rio Solimoes (left side of figure) has widened, deepened, and straightened itself sufficiently to become part of the preferred navigation channel used by ocean-going ships to reach the upper-river ports of Leticia, Colombia, and Iquitos, Peru (Jacson Miranda, Amazon river pilot, personal communication, 2001). Other large tracts of stored fluvial sediment on floodplains of the Amazon and Madeira Rivers are described by Latrubesse (2002), Latrubesse and Franzinelli (2002), and by Mertes and Dunne in their chapter in the present volume (Chapter 8)

and herbaceous aquatic species of a spectacular variety – all are adapted not only to the available spatial and nutritional niches of the floodplain, but to the annual transformations from emergent to submerged lands and back again, and, during the months of inundation, to the special rhythms of the flood pulse (Salo *et al.*, 1986; Junk and Piedade, 1997). Among the most interesting animal species that seasonally invade the flooded forests and grasslands along with the rising waters are the turtles and crocodilians, the fish (especially those that gather most of their year's food supply from forest trees during the inundation season), and the mammals (sloths that swim and flexible dolphins that navigate the shallow waters between the tree trunks) (Goulding, 1980; Best, 1984; Goulding *et al*., 1996; Araujo-Lima and Goulding, 1997). The more charismatic residents of the flooded *várzea* habitat, such as the giant water lily *Victoria amazonica* and the freshwater dolphin *Inia geoffrensis*, rank with monkeys and macaws as principal attractants for the local ecotourism industry.

But floodplains do not grow forever. Complementary to the slow upward accretionary growth of floodplains is their destruction and the consequent remobilization of their constituent sediment particles by bank erosion. As the Amazon and its tributaries meander along and across their valley bottoms, their channels are shifted laterally. Meander bends grow larger and larger in radius and circumference, forming longer and longer necks that eventually are cut off to re-shorten, at least momentarily, the overall channel length. All this lengthening, shifting, and re-shortening of channels remobilizes, in the process, considerable quantities of sediment. Thus is the vertical accretion of floodplains counterbalanced by the lateral erosion of their exposed banks.

This constant cycle of the laying down of floodplain sediment and its subsequent remobilization by the shifting river has become a grand metaphor for the chaotic and lacunae-plagued human history of the Amazon region. This metaphor had its most powerful expression in the spectacular prose penned a century ago by Euclides da Cunha, which has been revisited recently and insightfully by Suárez-Araúz (1999) and Slater (2002). Although his prose is notoriously difficult to render into English with simultaneous loyalty to both style and accuracy, a sample translation (mine) from Euclides da Cunha (1909) may perhaps whet the appetite of a more competent reader of Portuguese:

> 'The tumultuous inconstancy of the river manifests itself, moreover, in its interminable meanderings, hopelessly entangled, reading like the indecisive logbook of a lost wanderer, guessing at horizons, directing itself into all its principal courses or throwing itself into unexpected shortcuts. . . . It hurls itself through the drowned narrows of Óbidos in complete disregard of its ancient bed that yet today divines itself in the enormous pestilential floodplain, ganglionic with lakes, of Vila Franca; or goes, at other points, into unexpected "furos", to flow into its large affluents, making itself illogically tributary to its own tributaries, always untidy, disheveled, and fluctuating, destroying and building, reconstructing and devastating, extinguishing in an hour what was built over decades – like . . . a monster artist insatiably applying finishing touches, recomposing and endlessly restarting an indeterminate portrait. Such is the river; such is its history: subversive, unruly, incomplete.'

The quantities of sediment involved each year in the exchanges between channel and floodplain are enormous. In the Amazon Basin as a whole, the quantities of sediment exchanged between channels and floodplains far exceed the quantities of downriver flux shown in the upper diagram of Figure 4.6. In a 1500 km reach of the Amazon mainstem in Brazil (only about one-quarter of the overall mainstem length), the total exchanges – by the overbank accretion of floodplains or the remobilization of sediment by bank erosion – exceed the downriver fluxes of sediment (Figure 4.8). A simple linear extrapolation of this relation to the full length of the Amazon (especially the length fringed by large floodplains) allows us to estimate that annual exchanges of sediment between channels and floodplains must exceed the annual downchannel fluxes of sediment by a factor of at least three.

Residence time of sediment on the Amazon floodplains – the period between the time any given sediment particle may be deposited and the time it is remobilized by bank erosion – is commonly measurable in thousands of years. In their comprehensive assessment of the geomorphology of the Brazilian Amazon, Mertes *et al*. (1996) estimated mean recycling times on the order of 1000–2000 years for the floodplains between the mouths of rios Jutaí and Madeira. Local residence times in specific floodplain tracts will, of course, exceed these mean values, even to periods of time sufficiently long for tropical soil-weathering processes to transform some of the mineral compositions of the sediments. In the central Amazon of Brazil, Johnsson and Meade (1990) described floodplain sediments that had been stored inside a large meander bend (shown on the left side of Figure 4.7) for sufficient time to allow many of the lithic fragments to be weathered out of the sands and some of the less stable clay minerals to be weathered out of the finer fractions.

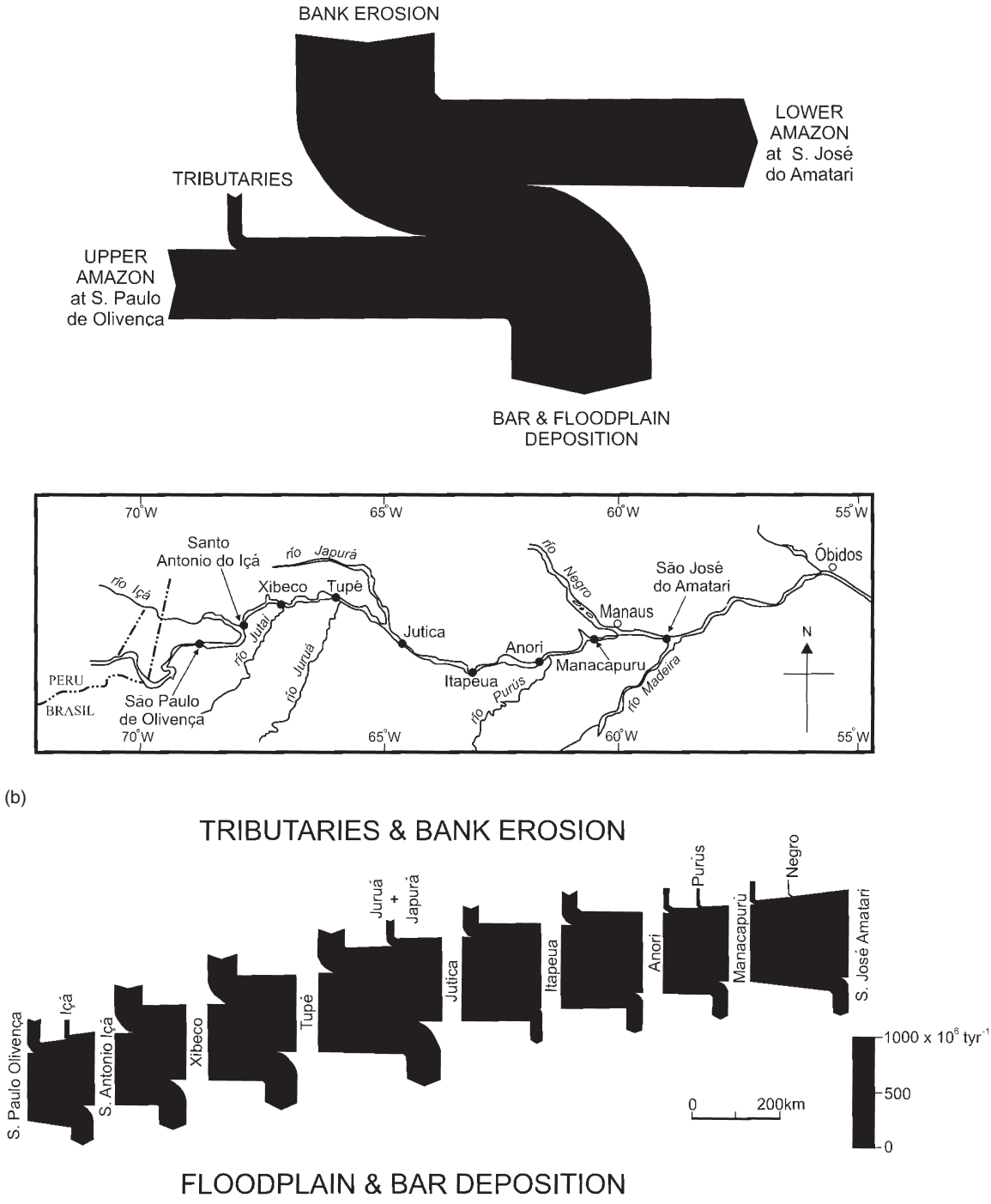

Figure 4.8 Diagrams showing average annual fluxes and exchanges of sediment between channels and floodplains of a 1500 km segment of the Amazon mainstem of Brazil, between the Peru-Brazil border and the confluence with rio Madeira. (a) Generalized diagram that shows schematically the averaged values for the entire 1500 km reach. Quantities of sediment exchanged through the erosion of banks and through deposition on point bars and floodplains significantly exceed the flux of sediment from upriver (including tributary inputs) or the flux continuing downriver. (b) An exploded version of (a), showing the individual sediment budgets for each of eight consecutive reaches of the mainstem Amazon between São Paulo de Olivença and São José do Amatarí. The upper left corners show the quantities of sediment contributed to the eight segments from bank erosion. The lower right corners show the quantities removed from the channel by overbank deposition onto floodplains and pointbars. Details of the calculations and compilations are given by Dunne *et al.* (1998)

A detailed look at the storage and remobilization of Amazonian floodplain materials, given in the context of average annual fluxes of sediment in the mainstem channel, is provided by the exploded lower diagram of Figure 4.8. The 'explosion' was made possible by a series of repeated measurements made at nine mainstem cross-sections and in five principal tributaries during the early 1980s (Meade, 1985; Richey *et al.*, 1986), giving us sufficiently accurate averages that we were able to break the diagram into eight segments. Within each segment – about 200 km of river length, defined between the regularly measured cross-sections – Dunne *et al.* (1998) were able to estimate the mean annual quantity of new sediment added to the floodplain and the mean annual quantity of sediment remobilized by bank erosion. By sweeping the eye more or less horizontally from left to right across the exploded diagram, the reader might gain the impression (or at least the supposition) that any given sediment particle moving downstream past São Paulo de Olivença (especially during high-water season when much sediment-laden water is flowing onto the floodplain) is likely to be carried out of the channel and be deposited on the floodplain before the thread of the water flow reaches São José do Amatari. Conversely, by looking upstream from the section at São José do Amatari, the reader might just as easily visualize the likelihood that any sediment particle passing through this cross-section (especially during falling-water season when river-bank collapse is maximal for the year) had come out of one of those eroding banks, rather than having been swept this year off an Andean slope somewhere in Peru or Ecuador.

In the Amazon system, we are able to look closely at such processes because of the general lack of engineering works along the river and the complete freedom this great river is still allowed in the making of its floodplains and the destruction of its banks. Most rivers in highly developed parts of the world (the Mississippi, for example) have been engineered to prevent or at least retard these processes: levees to prevent flooding, revetments to prevent bank erosion. In the Amazon, these natural processes are still visible, and their visibility is useful in understanding such issues as the fates of sediment-transported contaminants. Many of the contaminants in the world's river systems are transported as materials adsorbed onto sediment particles. Trace metals, many radionuclides and insecticides, for example, show a marked preference – by factors of thousands or more – for piggyback transport in the adsorbed state on sediment particles rather than as dissolved ions or molecules in true solution in the water. The fate of the sediment particles, therefore, determines the fates of many contaminants. This is sufficiently true that the contaminants in many polluted rivers can be used as tracers to follow the pathways and find the eventual resting places of the sediment particles.

Let us return to the exploded lower diagram of Figure 4.8 and consider some of its implications for the fates of sediment-transported contaminants in large rivers. We consider two scenarios, both of which are hypothetical and not based on any known or even suspected occurrence to date. Suppose that, somewhere along the Peruvian Amazon, a large quantity of polychlorinated biphenyls (PCBs) is spilled into the sediment-laden waters of the flowing mainstem river during, say, the rising-water season. The PCBs, as usual, are preferentially adsorbed onto the particles of suspended sediment. This being high-water season, the bulk of the sediment particles to which the PCBs are adsorbed will settle out of the overflowing waters and onto the floodplains before they reach the middle of the Brazilian Amazon. The sediment particles and their adsorbed PCBs will remain on the floodplains until they are remobilized by bank erosion or some other process. Because the disintegration time of PCBs (only 100–200 years) is so much shorter than the likely residence time of the sediment (millennia), the floodplains will have acted as 'decontamination depositories' for the PCBs. By the time the sediment is remobilized into the flowing waters of the river, the PCBs will have long since 'disappeared' by having been degraded into daughter compounds and carried away mostly in solution.

Let us now consider another, longer-lived, contaminant that is preferentially adsorbed onto sediment particles. Instead of PCBs, let us consider the highly toxic radionuclide, plutonium, which has a half-life in excess of 20 000 years. This hypothetical example postulates, as in the previous example of PCBs, a plutonium spill somewhere in the Peruvian Amazon, the complete adsorption of the plutonium onto sediment particles in the flowing river, and the complete removal from the flowing river of the plutonium-carrying particles by overbank deposition onto the floodplains of the middle Amazon. Because the bulk of the spilled plutonium is likely to have been adsorbed by the finest particles in suspension, and because their fineness will have allowed them to be transported long distances onto the floodplain before being deposited as overbank sediment, the plutonium-contaminated particles are likely to be remobilized by lateral bank erosion only after some decades, perhaps centuries, of storage. Some hundreds, perhaps thousands, of years after the original plutonium spill, these same sediment particles will be remobilized as the banks of the floodplains are eroded, and the City Fathers of Manaus will have no way of determining the source of (or being able to do anything about) the by-then-mysterious presence of plutonium in the river.

4.4.3 Sediment Storage in the Lowermost Amazon Valley

The lowermost Amazon River is herein defined as the reach between the farthest downstream river gauge on the mainstem at Óbidos and the estuarine embayment south of Macapá. In this 600 km reach, much river sediment apparently is being deposited on floodplains, especially in floodplain lakes. As the upper diagram in Figure 4.6 indicates, new sediment is being deposited on the lowermost floodplain at a significantly greater rate than the older deposits are being remobilized by bank erosion. This lowermost segment may be considered an upstream extension of the Amazon Delta – an area in which much sediment is being deposited in places where it is unlikely to be re-eroded under present-day conditions.

The lowermost reaches of most large rivers are difficult places in which to measure the fluxes of sediment. River hydrologists traditionally locate their farthest downstream gauges somewhere upriver of the influence of daily fluctuations in oceanic tides. In the Amazon this location is at Óbidos, some 700 km landward of the transition from fresh water to salt water. Even here, diurnal tidal fluctuations of a few centimetres may be observed during some weeks of lowest river stage (Oltman, 1968). Because hydrologists generally monitor day-to-day river discharges by continuously measuring river stages, any fluctuations (tidal or otherwise) in river level that are unrelated to fresh-water discharge will introduce errors.

Sediment fluxes are even more difficult to measure, and therefore subject to even greater errors. Sediment transport is sensitively determined by water velocity and by the slope of the river surface. In reaches affected by oceanic tides, river slope and velocity may change markedly from one hour to the next. In the estuary proper, water flows may even reverse directions. Appropriate measurements of sediment discharges in tidally affected river reaches therefore require a complex scheme of temporally frequent and spatially dense sampling (see, for example, Meade, 1969, 1972; Milliman *et al*., 1985; Kineke and Sternberg, 1995). Sediment fluxes in the lowermost Amazon, as shown in Figure 4.6, are estimated, partly by difference between measurements made both landward and seaward of this lowest reach. The farthest downstream measurements of sediment flux of any reliability are those at Óbidos. These measurements are derived from repeated discharge-weighted samples that were collected and composited through the full depth and across the full width of the Amazon River (Meade, 1985; Richey *et al.*, 1986). From a total of a dozen such measurements made at Óbidos at different seasons of the year and related to the typically simple sinusoidal hydrograph of river discharge there, Dunne *et al.* (1998) reported a mean annual sediment discharge of 1240 (±130) million tonnes.

This figure for the suspended-sediment discharge at Óbidos is certainly more correct than the estimate of 600 million tonnes per year reported recently by Naziano Filizola and his colleagues (Filizola, 1999; Seyler and Boaventura, 2001). Filizola computed this 'more recent' estimate from archived data on a set of about 20 samples collected at Óbidos during 1979–1983, and he apparently was unaware that these samples had been collected only a few tens of centimetres below the river surface. Such surficial sampling, in river waters 40–60 m deep, as they are at Óbidos (Figure 4.9), will not detect the greater concentrations of suspended sediment that are typical of deeper flowing waters. Consequently, the 'more recent' estimate of 600 million tonnes per year is too small by a factor of two.

4.5 THE AMAZON GOES TO SEA

Many photographs and satellite images show the areal distribution of turbid waters offshore of the mouth of the Amazon as the river debouches into the Atlantic Ocean. Vertical satellite images are presented by Curtin and Legeckis (1986), Geyer *et al.* (1996), and Kineke and Sternberg (1995), and an especially dramatic astronaut photograph has been published in the book by Apt *et al*. (1996: p. 152) and on the cover of the November 1996 issue of *National Geographic* magazine (Apt, 1996).

The astronaut photograph, taken during August 1985, is an oblique view that includes the curvature of the earth in the far distance. In the nearer distance, multiple plumes of lighter-coloured water show the ebb-tide extents of successive surges of sediment-laden Amazon River waters making their entries into the ocean. The diurnal range of oceanic tide is large here, usually on the order of 3 m (Geyer *et al.*, 1996). The 'fronts' of river water therefore surge considerably as they enter the Atlantic. The most prominent plume in the picture probably represents the ebbing river flow on the day of the photograph. More ragged-looking plume edges that float seaward of the latest plume most likely represent the remnants of previous ebb-tide pulses of seaward-flowing river waters. As the river waters are slowed by their entry into the ocean and their flow is reversed by the rising tides, most of their sediment particles gradually settle towards the sea floor. Kuehl *et al*. (1986) report that approximately half the quantity of sediment that passes Óbidos settles onto the sea bed of the continental shelf off the mouth of the Amazon River.

But this is not the end of the story. All the Andean sediment that the Amazon brings to the Atlantic does not end its journey here on the continental shelf of Brazil.

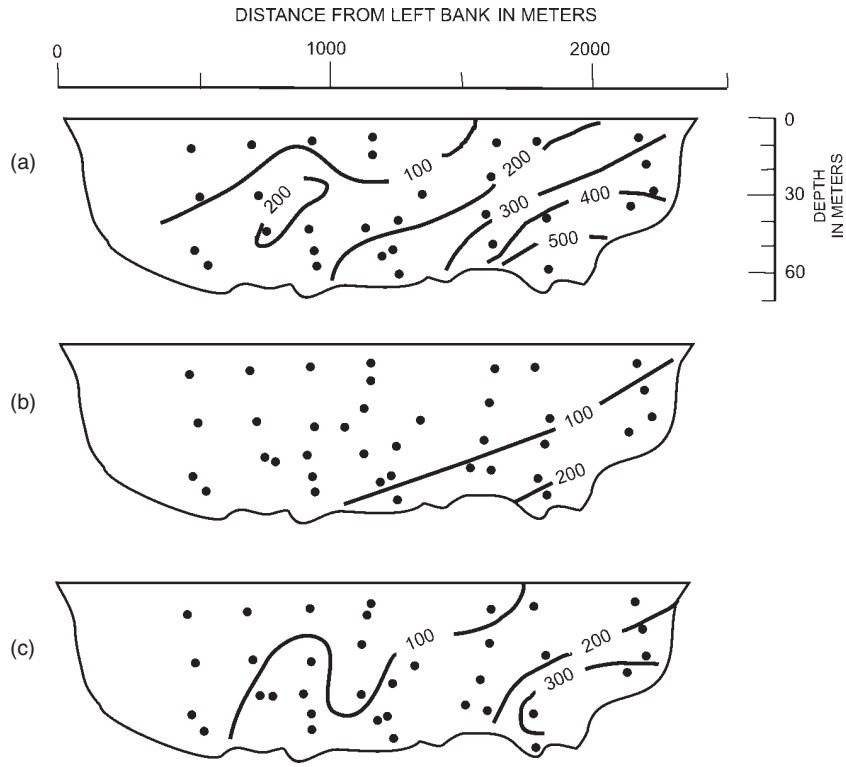

Figure 4.9 Cross-sections of rio Amazonas at Óbidos, 15 June 1976, showing vertical and lateral heterogeneity of suspended-sediment concentrations. Based on individual point-sample data. Viewer is facing downstream. Vertical distance scale is exaggerated 10 times relative to horizontal. (a) Total suspended sediment, in $mg\,l^{-1}$. (b) Suspended sand (>63 µm), in $mg\,l^{-1}$. (c) Suspended silt and clay (<63 µm), in $mg\,l^{-1}$. Data from Meade *et al.* (1979a); cross sections previously published by Eisma (1993, p. 33) and Meade (1994). Clearly shown is the increase in sediment concentration with increasing water depth, from which one may easily infer the unsuitability of surface-only sampling for accurate measurement of the total sediment discharge at Óbidos. Illustrations of similar differences in sediment concentration between surface waters and deeper waters in other Amazonian river cross sections have been published by Curtis *et al.* (1979) and Meade *et al.* (1979b)

Each of the images cited in the first paragraph of this section shows a band of turbid water along the coastline to the northwest of the large open mouth of the Amazon. A substantial proportion of the sediment that is discharged by the Amazon to the sea (perhaps as much as a fifth, or even a quarter, of the quantity that was transported past Óbidos) is being carried to the northwest around Cabo Norte, the promontory that marks the northern corner of the Amazon's estuarine embayment, and is being transported longshore and nearshore, under the influence of the North Brazil Current, along the northeastern coast of South America (Eisma *et al*., 1991).

The entrainment of the Amazon's sediment alongshore to the northwest is an episodic process. Timescales of alternating transport and storage range from diurnal (tidal) to at least centennial. During their slow progression to the northwest, the sediment-laden coastal waters are washed into and out of mangrove swamps and mudflats as the tides rise and fall. Along the Brazilian coast north and northwest of the Amazon mouth, century-scale episodes of shore erosion alternate with equivalent-scale episodes of coastal accretion. Farther downcurrent, hundreds of kilometres from the Amazon mouth, along the coasts of Guyane (French Guiana), Surinam, and Guyana, great mudbanks shift their ways gradually northwestward (Allison *et al*., 1995a,b, 2000).

Just how much Amazonian sediment is dispersed northwestward along the northeast coast of South America, and how far does it eventually travel? Perhaps an average as great as 200–250 million tonnes per year is carried around Cabo Norte. Along the first thousand kilometres alongshore downcurrent of Cabo Norte, much of the river-

derived sediment is carried into coastal wetlands and estuarine embayments, probably to reside there more or less permanently on a centuries-to-millennia timescale. Perhaps a quantity on the order of 100 million tonnes per year – half what is carried around Cabo Norte at the beginning of the northwestward trajectory, but still in excess of the sediment loads of all but a dozen of the world's largest rivers – reaches the outer coastline of the Orinoco Delta, some 1600 km downcurrent from the mouth of the Amazon.

Whatever the absolute quantity of Amazonian sediment that reaches the outer delta of the Orinoco, that quantity is greater than the amount supplied by the Orinoco River itself. By comparing the mineral compositions of recently deposited fine-grained sediments submerged on the outer Orinoco Delta with the distinctively different compositions of like-sized sediments from the two rivers, Eisma *et al.* (1978) were able to conclude that the outer-delta deposits were more Amazonian than Orinocoan. At its point of maximum sediment transport near the inner edge of its delta, the Orinoco River carries seaward an average of about 150 million tonnes per year. Most of this quantity is deposited in the inner and middle regions of the delta (Warne *et al.*, 2002). The quantity of Orinocoan sediment deposited on the outermost delta of the Orinoco therefore is apparently less than that of the more extensively traveled Amazonian materials deposited there.

In the astronaut photograph of the Orinoco delta region in Figure 4.10, the incoming Amazonian sediment may be seen as the turbid coastal water in the right third of the picture. It is attractive to speculate, in the light of the earlier discussions in this chapter, on the histories of the individual particles that cloud the waters of this incoming plume. Among the billions of particles suspended in this plume may well be a few that were detached recently from an Andean slope somewhere in Bolivia or Peru and, within less time than the span of a single year, were carried virtually nonstop for a distance of 5000 or 6000 km, down the Amazon River and along the Guiana coast to the Orinoco Delta. Much more likely, however, is that the particles now suspended in the plume shown in the eastern third of the picture have spent hundreds to thousands of years making their journeys from their Andean sources to this eventual sink. They are likely to have spent days or weeks in active river transport, centuries or millennia in storage after having been deposited on floodplains, before being remobilized, by bank erosion or channel shifting, into flowing water for another few days or weeks of riverine transport. This cycle of transport, deposition, remobilization, and re-deposition likely was repeated in the river multiple times until the particles passed out the Amazon mouth, around Cabo Norte, to continue their journey, through many more episodes of successive deposition and remobilization, northwestward along the South American coastline. All in all, the histories of most of these particles have comprised many long periods of storage in floodplains, coastal wetlands and mudbanks, punctuated by short bursts of downstream transport.

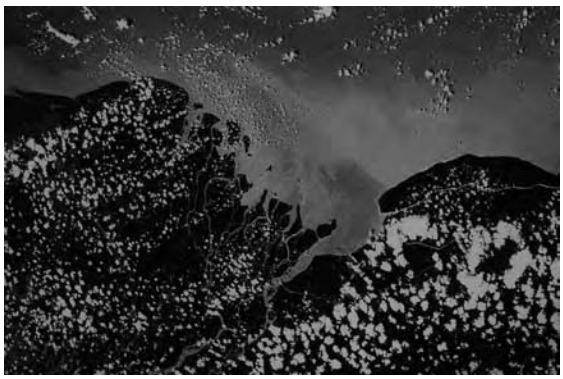

Figure 4.10 Astronaut photograph of Orinoco delta region. NASA photograph 51D-32-004, selected and generously supplied by Michael Helfert. Vertical or near-vertical view. Long dimension of photograph is 200 km. Main mouth of Orinoco River is in bottom centre. Land area in left half of photograph is Orinoco Delta. Coastal waters in right side of picture are made turbid by sediment carried alongshore from the mouth of the Amazon

4.6 CODA

In the eastern cordillera of the Andes of Colombia, about 3° latitude north of the Equator and nearly 75° longitude west of the Greenwich meridian, is a narrow divide between the headwaters of the Orinoco and those of the Amazon. From one side of the divide, water carries sediment into a small tributary of Río Guaviare, through which it eventually enters the Orinoco. From the other side of the divide, water carries sediment into and through a series of tributaries of Río Caquetá, which, as it flows out of Colombia and into Brazil, becomes rio Japurá, a principal tributary of the mainstem Amazon.

Now consider two soil particles that lay, some thousands of years ago, less than a metre apart – one on the Orinoco side of the divide and the other on the Amazon side – and began, during a heavy rainfall, their separate journeys downstream. What is the likelihood that these same two particles, after their diverging and circuitous journeys down their separate great rivers, now lie again within a few metres of each other, here on the floor of the continental shelf on the seaward edge of the delta of the

Orinoco? Such an outcome may be improbable – but not highly so. It is certainly not impossible. And a full consideration, beginning with their separation and concluding in their reunion, of the spatial and temporal trajectories of these two particles – in some aspects similar to each other and in others quite different – across thousands of kilometres of transport and during thousands of years of storage, amounts to no less than a grand mental excursion through the sedimentary processes by which the earth's surface recycles itself.

ACKNOWLEDGEMENTS

A thoughtful and energetic company of colleagues and coworkers has unfolded and told the story that is recounted in this chapter, and the most relevant names may be found among the authors and acknowledgees of the papers listed in the introductory paragraphs. Chief among those who consistently kept my sights highest during two decades of joyous potamologic pursuits on the Amazon and Orinoco were Tom Dunne, John Edmond, Georg Irion, Abel Mejía, Leal Mertes, Carl Nordin, David Pérez Hernández, Jeff Richey, and Bob Stallard.

REFERENCES

Allison, M.A., Nittrouer, C.A., and Kineke, G.C., (1995a) Seasonal sediment storage on mudflats adjacent to the Amazon River, In: *Geological significance of sediment transport and accumulation on the Amazon continental shelf*: *Marine Geology* (special issue) (C.A. Nittrouer and S.A. Kuehl, Eds.), v.125, nos 3 and 4, pp. 303–328.

Allison, M.A., Nittrouer, C.A., and Faria, L.E.C., Jr, (1995b) Rates and mechanisms of shoreface progradation and retreat downdrift of the Amazon River mouth, In: *Geological significance of sediment transport and accumulation on the Amazon continental shelf*: *Marine Geology* (special issue) (C.A. Nittrouer and S.A. Kuehl, Eds.), v. 125, nos 3 and 4, pp. 373–392.

Allison, M.A., Lee, M.T., Ogston, A.S., and Aller, R.C., (2000) Origin of Amazon mudbanks along northeastern coast of South America. *Marine Geology*, 163, 241–256.

Apt, J., (1996) Orbit – the astronauts' view of home: *National Geographic*. v.190, no. 5, pp. 2–27.

Apt, J., Helfert, M., and Wilkinson, J., (1996) *Orbit – NASA astronauts photograph the earth*. National Geographic Society, Washington, DC, 224 p.

Araujo-Lima, C., and Goulding, M., (1997) *So fruitful a fish: ecology, conservation and aquaculture of the Amazon's tambaqui*. Columbia University Press, New York, 191 p. (Also published in Portuguese: 1998, *Os frutos do tambaqui: Ecologia, conservação e cultivo na Amazônia*. Sociedade Civil Mamirauá, Tefé, 186 p.)

Best, R.C., (1984) The aquatic reptiles and mammals of the Amazon, In: *The Amazon: limnology and landscape ecology of a mighty tropical river and its basin* (H. Sioli, Ed.). Dr W. Junk, Dordrecht, pp. 371–412.

Carvalho, N.O., and da Cunha, S.B., (1998) Estimativa da carga sólida do rio Amazonas e seus principais tributários para a foz e oceano: uma retrospectiva. *A Água em Revista*, v. 6, no. 10, pp. 44–58.

Curtin, T.B., and Legeckis, R.V., (1986) Physical observations in the plume region of the Amazon River during peak discharge – I. Surface variability. *Continental Shelf Research*, v. 6, pp. 31–51. (Reprinted 1987 *in* Nittrouer, C.A., and DeMaster, D.J., Eds. *Sedimentary processes on the Amazon continental shelf*. Pergamon Press, Oxford, pp. 31–51.)

Curtis, W.F., Meade, R.H., Nordin, C.F., Jr, Price, N.B., and Sholkovitz, E.R., (1979) Non-uniform vertical distribution of fine sediment in the Amazon River. *Nature*, v. 280, pp. 381–383. (Portuguese translation published 1982, Distribuição vertical não uniforme de sedimento fino no rio Amazonas: *Acta Amazonica*, v. 12, pp. 697–700.)

da Cunha, E., (1909) *A margem da história*: Aillaud & Lellos, Lisbon. (Many subsequent reprints; e.g. 1999, Livraria Martins Fontes, São Paulo, 209 p. English translation by R. Sousa, (2006) *The Amazon*: *land without history*. Oxford University Press, Oxford, 96 p.)

Díaz de Gamero, M.L., (1996) The changing course of the Orinoco River during the Neogene: a review. *Palaeogeography, Palaeoclimatology, Palaeoecology*, 123, 385–402.

Drago, E.C., and Amsler, M.L., (1988) Suspended sediment at a cross section of the Middle Parana River: concentration, granulometry and influence of the main tributaries, In: *Sediment budgets* (M.P. Bordas and D.E. Walling, Eds.). *International Association of Hydrological Sciences Publication* 174, pp. 381–396.

Dunne, T., Mertes, L.A.K., Meade, R.H., Richey, J.E., and Forsberg, B.R., (1998) Exchanges of sediment between the flood plain and channel of the Amazon River in Brazil. *Geological Society of America Bulletin*, 110, 450–467.

Eisma, D., (1993) *Suspended matter in the aquatic environment*. Springer, Berlin, 315 p.

Eisma, D., van der Gaast, S.J., Martin, J.M., and Thomas, A.J., (1978) Suspended matter and bottom deposits of the Orinoco delta: turbidity, mineralogy and elementary composition. *Netherlands Journal of Sea Research*, 12, 224–251.

Eisma, D., Augustinus, P.G.E.F., and Alexander, C., (1991) Recent and subrecent changes in the dispersal of Amazon mud. *Netherlands Journal of Sea Research*, 28, 181–192.

Filizola, N.P., Jr, (1999) *O fluxo de sedimentos em suspensão nos rios da bacia Amazônica Brasileira*. Agencia Nacional de Energia Elétrica, Brasilia, 63 p.

Geyer, W.R., Beardsley, R.C., Lentz, S.J., Candela, J., Limeburner, R., Johns, W.E., Castro, B.M., and Soares, I.D., (1996) Physical oceanography of the Amazon shelf, In: *Oceanography of the Amazon continental shelf*: *Continental Shelf Research* (special issue) (C.A. Nittrouer and D.J. DeMaster, Eds.), v. 16, nos 5 and 6, pp. 575–616.

Gibbon, Lt L., (1854) *Exploration of the valley of the Amazon, made under the direction of the Navy Department, by Wm. Lewis Herndon and Lardner Gibbon, Part II*: U.S. House of

Representatives, 33d Congress, 1st Session, Executive no. 53, 339 p.

Gibbs, R.J., (1965) *The geochemistry of the Amazon River Basin*. University of California, San Diego, PhD dissertation, 96 p.

Gibbs, R.J., (1967) The geochemistry of the Amazon River system: Part I. The factors that control the salinity and the composition and concentration of the suspended solids. *Geological Society of America Bulletin*, 78, 1203–1232.

Goulding, M., (1980) *The fishes and the forest: explorations in Amazonian natural history*. University of California Press, Berkeley, 280 p.

Goulding, M., Smith, N.J.H., and Mahar, D.J., (1996) *Floods of fortune: ecology and economy along the Amazon*. Columbia University Press, New York, 193 p.

Goulding, M., Barthem, R., and Ferreira, E., (2003) *The Smithsonian atlas of the Amazon*. Smithsonian Institution, Washington, 255 p.

Gregory, K.J., Ed., (1977) *River channel changes*. John Wiley & Sons, Ltd, Chichester, 448 p.

Guyot, J.L., (1993) *Hydrogéochimie des fleuves de l'Amazonie bolivienne*. ORSTOM Editions, Paris, 261 p.

Irion, G., Junk, W.J., and de Mello, J.A.S.N., (1997) The large central Amazonian river floodplains near Manaus. Geological, climatological, hydrological and geomorphological aspects, In: *The central Amazon floodplain: ecology of a pulsing system* (W.J. Junk, Ed.). Springer, Berlin, pp. 23–46.

Johnsson, M.J., and Meade, R.H., (1990) Chemical weathering of fluvial sediments during alluvial storage: the Macuapanim Island point bar, Solimões River, Brazil. *Journal of Sedimentary Petrology*, 60, 827–842.

Johnsson, M.J., Stallard, R.F., and Lundberg, N., (1991) Controls on the composition of fluvial sands from a tropical weathering environment: sands of the Orinoco River drainage basin, Venezuela and Colombia. *Geological Society of America Bulletin*, 103, 1622–1647.

Junk, W.J., Ed., (1997) *The central Amazon floodplain: ecology of a pulsing system*. Springer, Berlin, 525 p.

Junk, W.J., and Piedade, M.T.F., (1997) Plant life in the floodplain with special reference to herbaceous plants, In: *The central Amazon floodplain: ecology of a pulsing system* (W.J. Junk, Ed.). Springer, Berlin, pp. 147–185.

Junk, W.J., Ohly, J.J., Piedade, M.T.F., and Soares, M.G.M., editors, (2000) *The central Amazon floodplain: actual use and options for sustainable management*. Backhuys, Leiden, 584 p.

Kineke, G.C., and Sternberg, R.W., (1995) Distribution of fluid muds on the Amazon continental shelf, In: *Geological significance of sediment transport and accumulation on the Amazon continental shelf*: *Marine Geology* (special issue) (C.A. Nittrouer and S.A. Kuehl, Eds.). v. 125, nos 3 and 4, pp. 193–233.

Kuehl, S.A., DeMaster, D.J., and Nittrouer, C.A., (1986) Nature of sediment accumulation on the Amazon continental shelf. *Continental Shelf Research*, 6, 209–225. (Reprinted 1987 *in* Nittrouer, C.A., and DeMaster, D.J., editors, *Sedimentary processes on the Amazon continental shelf*: Pergamon Press, Oxford, pp. 209–225.)

Larsen, M.C., Vásquez Conde, M.T., and Clark, R.A., (2001a) Flash-flood related hazards: landslides, with examples from the December 1999 disaster in Venezuela, In: *Coping with flash floods* (E. Gruntfest and J. Handmer, Eds.). Kluwer, Dordrecht, pp. 259–275.

Larsen, M.C., Wieczorek, G.F., Eaton, L.S., Morgan, B.A., and Torres-Sierra, H., (2001b) Venezuela debris-flow and flash-flood disaster of 1999 studied. *EOS*, *American Geophysical Union Transactions*, 82, 572–573.

Latrubesse, E.M., (2002) Evidence of Quaternary palaeohydrologic changes in middle Amazonia: the Aripuana-Roosevelt and Jiparaná 'fans'. *Zeitschrift für Geomorphologie*, Suppl., 129, 61–72.

Latrubesse, E.M., and Franzinelli, E., (2002) The Holocene alluvial plain of the middle Amazon River, Brazil. *Geomorphology*, 44, 241–257.

Meade, R.H., (1969) Landward transport of bottom sediments in estuaries of the Atlantic Coastal Plain. *Journal of Sedimentary Petrology*, 39, 222–234.

Meade, R.H., (1972) Transport and deposition of sediments in estuaries, In: *Environmental framework of coastal-plain estuaries* (B.W. Nelson, Ed.). *Geological Society of America Memoir* 133, pp. 91–120.

Meade, R.H., (1985) Suspended sediment in the Amazon River and its tributaries in Brazil during 1982–84. *US Geological Survey Open-File Report* 85-492, 39 p.

Meade, R.H., (1994) Suspended sediments of the modern Amazon and Orinoco Rivers, In: *Quaternary of South America* (M. Iriondo, Ed.). *Quaternary International*, v. 21, pp. 29–39.

Meade, R.H., (1995) Setting: geology, hydrology, sediments, and engineering of the Mississippi River, In: *Contaminants in the Mississippi River, 1987–92* (R.H. Meade, Ed.). *US Geological Survey Circular* 1133, pp. 13–28.

Meade, R.H., (1996) River-sediment inputs to major deltas, In: *Sea-level rise and coastal subsidence* (J.D. Milliman and B.U. Haq, Eds.). Kluwer, Dordrecht, pp. 63–85.

Meade, R.H., Nordin, C.F., Jr, Curtis, W.F., Mahoney, H.A., and Delaney, B.M., (1979a) Suspended-sediment and velocity data, Amazon River and its tributaries, June–July 1976 and May–June 1977. *US Geological Survey Open-File Report* 79-515, 40 p.

Meade, R.H., Nordin. C.F., Jr., and Curtis, W.F., (1979b) Sediment in rio Amazonas and some of its tributaries during the high-water seasons of 1976 and 1977. *Simpósio Brasileiro de Hidrologia, 3d, Anais*, v. 2, pp. 472–485.

Meade, R.H., Dunne, T., Richey, J.E., Santos, U. de M., and Salati, E., (1985) Storage and remobilization of suspended sediment in the lower Amazon River of Brazil. *Science*, 228, 488–490.

Meade, R.H., Weibezahn, F.H., Lewis, W.M., Jr, and Pérez Hernández, D., (1990) Suspended sediment budget for the Orinoco River, In: *El Río Orinoco como ecosistema/ The Orinoco River as an ecosystem* (F.H. Weibezahn, H. Alvarez and W.M. Lewis, Jr, Eds.). Impresos Rubel, Caracas, pp. 55–79.

Mertes, L.A.K., Dunne, T., and Martinelli, L.A., (1996) Channel-floodplain geomorphology along the Solimões-Amazon River,

Brazil. *Geological Society of America Bulletin*, v. 108, pp. 1089–1107.

Milliman, J.D., and Meade, R.H., (1983) World-wide delivery of river sediment to the oceans. *Journal of Geology*, 91, 1–21.

Milliman, J.D., and Syvitski, J.P.M., (1992) Geomorphic/tectonic control of sediment discharge to the ocean: the importance of small mountainous rivers. *Journal of Geology*, 100, 525–544.

Milliman, J.D., Shen, H.-T., Yang, Z.-S., and Meade, R.H., (1985) Transport and deposition of river sediment in the Changjiang estuary and adjacent continental shelf. *Continental Shelf Research*, 4, 37–45.

Milliman, J.D., Qin, Y.S., Ren, M.E., and Saito, Y., (1987) Man's influence on the erosion and transport of sediment by Asian rivers: The Yellow River (Huanghe) example. *Journal of Geology*, 95, 751–762.

NEDECO, (1973) *Río Magdalena and Canal del Dique Survey Project*. Netherlands Engineering Consultants, The Hague, 397 p.

Nittrouer, C.A., and DeMaster, D.J., Eds., (1987) *Sedimentary processes on the Amazon continental shelf*. Pergamon, Oxford, 379 p.

Nittrouer, C.A., and Kuehl, S.A., Eds., (1995) *Geological significance of sediment transport and accumulation on the Amazon continental shelf*: *Marine Geology* (special issue), v. 125, nos 3 and 4, pp.175–399.

Nordin, C.F., Mejía, A., and Delgado, C., (1994) Sediment studies of the Orinoco River, Venezuela, In: *The variability of large alluvial rivers* (S.A. Schumm and B.R. Winkley, Eds.). American Society of Civil Engineers, New York, pp. 243–265.

Oltman, R.E., (1968) Reconnaissance investigations of the discharge and water quality of the Amazon River. *US Geological Survey Circular* 552, 16 p.

Pérez Hernández, D. and López, J.L., (1998) Algunos aspectos relevantes de la hidrología del Río Orinoco, In: *El Río Orinoco – Aprovechamiento sustentable* (J.L. López Sánchez, I.I. Saavedra Cuadra and M. Dubois Martínez, Eds.). Universidad Central de Venezuela, Caracas, pp. 88–98.

Pierson, T.C., Janda, R.J., Thouret, J.-C., and Borrero, C.A., (1990) Perturbation and melting of snow and ice by the 13 November 1985 eruption of Nevado del Ruiz, Colombia, and consequent mobilization, flow, and deposition of lahars. *Journal of Volcanology and Geothermal Research*, 41, 17–66.

Potter, P.E., (1978a) Significance and origin of big rivers. *Journal of Geology*, 86, 13–33.

Potter, P.E., (1978b) Petrology and chemistry of modern big river sands. *Journal of Geology*, 86, 423–449.

Potter, P.E., (1997) The Mesozoic and Cenozoic paleodrainage of South America: a natural history. *Journal of South American Earth Sciences*, 10, 331–344.

Projeto RADAM, (1973) Mosaico semi-controlado de radar SA-20-Y-A: 1 sheet, scale 1: 250 000.

Richey, J.E., Meade, R.H., Salati, E., Devol, A.H., Nordin, C.F., Jr, and dos Santos, U., (1986) Water discharge and suspended sediment concentrations in the Amazon River: 1982–1984. *Water Resources Research*, 22, 756–764.

Richey, J.E., Mertes, L.A.K., Victoria, R.L., Forsberg, B.R., Dunne, T., Oliveira, E., and Tancredi, A., (1989) Sources and routing of the Amazon River floodwave. *Global Biogeochemical Cycles*, 3, 191–204.

Ritter, J.R., 1977a, Reconnaissance of sediment transport and channel morphology in the lower Río Bermejo basin, Argentina, with a section on reconnaissance of the lower Río Pilcomayo basin, Argentina and Paraguay. *US Geological Survey Open-File Report* 76-564, 41 p.

Ritter, J.R., 1977b, Reconnaissance of sedimentation in the Río Pilcomayo basin, May 1975, Argentina, Bolivia, and Paraguay. *US Geological Survey Open-File Report* 77-327, 34 p.

Salo, J., Kalliola, R., Häkkinen, I., Mäkinen, Y., Niemelä, P., Puhakka, M., and Coley, P.D., (1986) River dynamics and the diversity of Amazon lowland forest. *Nature*, 322, 254–258.

Seyler, P.T., and Boaventura, G.R., (2001) Trace elements in the mainstem Amazon River, In: *The biogeochemistry of the Amazon Basin* (McClain, M.E., Victoria, R.L., and Richey, J.E., Eds.). Oxford University Press, Oxford, pp. 307–327.

Shi, C.-X., Dian, Z., and You, L.-Y., (2002) Changes in sediment yield of the Yellow River basin of China during the Holocene. *Geomorphology*, 46, 267–283.

Sioli, H., (1951) Sobre a sedimentação na várzea do baixo Amazonas. *Instituto Agronómico do Norte Boletim Técnico* no. 24, pp. 45–65.

Sioli, H., (1957) Sedimentation in Amazonasgebiet. *Geologische Rundschau*, 45, 608–633.

Sioli, H., (1984) The Amazon and its main affluents: Hydrography, morphology of the river courses, and river types, In: *The Amazon – limnology and landscape ecology of a mighty tropical river and its basin* (H. Sioli, Ed.). Dr W. Junk, Dordrecht, pp. 127–165.

Slater, C., (2002) *Entangled Edens: visions of the Amazon*. University of California Press, Berkeley, 332 p.

Stallard, R.F., (1995) Tectonic, environmental, and human aspects of weathering and erosion: a global review using a steady-state perspective. *Annual Review of Earth and Planetary Science*, 23, 11–39.

Stallard, R.F., Koehnken, L., and Johnsson, M.J., (1990) Weathering processes and the composition of inorganic material transported through the Orinoco River system, Venezuela and Colombia, In: *El Río Orinoco como ecosistema/ The Orinoco River as an ecosystem* (F.H. Weibezahn, H. Alvarez and W.M. Lewis, Jr, Eds.). Impresos Rubel, Caracas, pp. 81–119. (Reprinted in 1991 in *Geoderma*, 51, 133–165.)

Sternberg, H.O., (1956) *A Água e o Homem na Várzea do Careiro*. Universidade do Brasil, Rio de Janeiro. (Second edition: 1998, published by Museu Paraense Emilio Goeldi, Belém, v. 1, 248 p. + Appendix; v. 2, 17 maps.)

Sternberg, H.O., (1975) *The Amazon River of Brazil*. Geographische Zeitschrift Beihefte, 40, 74 p.

Suárez-Araúz, N., (1999) Amazonian literature: a fountain of memory and amnesia. *Amazonian Literary Review*, issue 2, pp. v–xx.

Wallace, A.R., (1853) *A narrative of travels on the Amazon and Rio Negro, with an account of the native tribes, and observations on the climate, geology, and natural history of the Amazon Valley*. Reeve & Co., London. (The 2nd edition of 1889: Ward, Lock and Co., London, 363 p., has been reprinted numerous times, e.g., (1972) Dover Publications, New York.)

Warne, A.G., Meade, R.H., White, W.A., Guevara, E.H., Gibeaut, J., Smyth, R.C., Aslan, A., and Tremblay, T., (2002) Regional controls on geomorphology, hydrology, and ecosystem integrity in the Orinoco Delta, Venezuela. *Geomorphology*, 44, 273–307.

Winkley, B.R., Ordonez, J.I., Saenz, J.E., and Duque, R., (1994) The Magdalena River, Colombia, In: *The variability of large alluvial rivers* (S.A. Schumm and B.R. Winkley, Eds.). American Society of Civil Engineers, New York, pp. 139–160.

Zhao, Y.A, Pan, X.D., Fan, Z.Y., and Han, S.F., (1989) Sedimentation in the lower reaches of the Yellow River and its basic laws, In: *Taming the Yellow River: silts and floods* (L.M. Brush, M.G. Wolman and B.W. Huang, Eds.). Kluwer, Dordrecht, pp. 477–516.

Zhou, Z., and Pan, X.-D., (1994) Lower Yellow River, In: *The variability of large alluvial rivers* (S.A. Schumm and B.R. Winkley, Eds.). American Society of Civil Engineers, New York, pp. 363–393.

5

Greatest Floods and Largest Rivers

Victor R. Baker

Department of Hydrology and Water Resources, University of Arizona, Tucson, AZ 85721-0011, USA

5.1 INTRODUCTION

The last major deglaciation of planet Earth (the last portion of Marine Isotope Stage 2, from about 20 000 to 11 000 calendar years ago) produced huge fluxes of water from the wasting continental ice sheets. It has become increasingly apparent that much of this water was delivered as floods of immense magnitude and relatively short duration. These Late Quaternary megafloods, and the megafloods of earlier glaciation, had short-duration peak flows, comparable in discharge with the more prolonged fluxes of ocean currents. The unit of discharge for both ocean currents and megafloods is the sverdrup, equivalent to 1 million $m^3 s^{-1}$. Some outburst floods likely induced very rapid, short-term effects on Quaternary climates. The Late Quaternary megafloods also greatly altered drainage evolution and the planetary patterns of water and sediment movement to the oceans. Connected paths of glacial flood spillways occurred for all the great continental ice sheets, and that of the Eurasia ice sheets may have temporarily constituted the largest terrestrial river. As large as these terrestrial megafloods were, however, even larger flows, and a larger river occurred on the planet Mars.

5.2 HISTORICAL BACKGROUND

Up until the middle of the nineteenth century considerable progress was being made in scientific studies of the role of cataclysmic flooding in the geological evolution of river valleys. While some of these studies invoked a kind of biblical catastrophism, much of the work merely employed hypotheses of immense floods because they seemed to provide the best explanations for such features as scoured bedrock and accumulations of huge, water-transported boulders. This whole branch of science was seriously retarded because of the popularity of Charles Lyell's logically flawed notion of uniformitarianism. Lyell's methodology for geology resulted in an epistemological stigma for hypotheses invoking types and magnitudes of flood processes not directly observed today. The flaws in Lyell's doctrine of uniformitarianism were anticipated by the author of the term, Lyell's contemporary, William Whewell (see Baker, 1998). Most geologists ignored (or failed to understand) Whewell's insights, and uniformitarianism became imbedded into the subsequent practice of geology, greatly hindering progress on understanding the role of cataclysmic flooding in geological processes.

Two circumstances of the twentieth century produced a renaissance in cataclysmic flood studies. The first was the prolonged scientific controversy over the origin of the Channelled Scabland in the northwestern United States (Baker, 1981). Extending from the 1920s to the 1970s, the great 'scablands debate' eventually led to a general acceptance of the cataclysmic flood origin championed by J Harlen Bretz, a professor at The University of Chicago. The second important development was the discovery in the early 1970s of ancient cataclysmic flood channels on the planet Mars (e.g. Baker, 1978). The Martian outflow channels were produced by the largest known flood discharges, and their effects have been preserved for billions of years (Baker, 2001).

Based on Bretz's study of the Channelled Scabland, the distinctive erosional and depositional features of

Large Rivers: Geomorphology and Management, Edited by A. Gupta

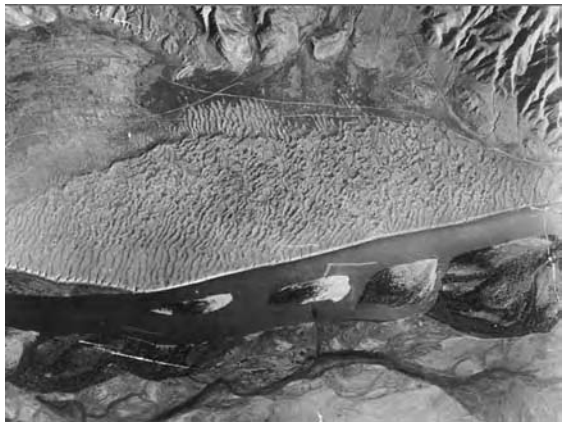

Figure 5.1 Aerial photograph of giant current ripples (gravel dunes) located near Kyzyl, Tuva. The ripples occur on a gravel bar just north of the Yenisei River (bottom of photograph) about 25 km southwest of Kyzyl. There are nearly 100 ripples on a bar 6 km in length. Ripple heights vary from 2 to 3 m. The photograph shows an area 6 × 4 km. The palaeoflood flow was moving from right (east) to left (west)

cataclysmic flooding are now well known. These include scabland bedrock erosion, streamlining of residual uplands, large-scale scour around flow obstacles, depositional bars, huge sediment fans, and giant current ripples (Figure 5.1). These features can be identified on orbital remote sensing images and by field reconnaissance. They can be used to discover and document cataclysmic flood effects on more river basins globally.

5.3 TERRESTRIAL GLACIAL MEGAFLOODS

Continental ice sheets that form during epochs of glaciation exert immense influences on water drainage across the land. Their huge loads depress the underlying land surface, and lakes form in the moats that surround ice sheets. They can block the lower courses of major rivers, impounding flow, and even diverting it into adjacent drainage basins. Meltwater from glacial margins may introduce huge discharges into land-surface depressions that hold much smaller lakes during nonglacial periods. The lakes may climatically alter water balances, promoting further glaciation by a kind of positive feedback. There are modern examples for all these situations, but the relatively small size and different thermal regimes of modern versus ice-age glaciers pose problems of extrapolation to the past conditions of major continental glaciation that favoured the development of glacial megalakes.

5.3.1 Cordilleran Ice Sheet

Very deep lakes can form when a glacier advances down a mountain valley to block a river. A famous example is Glacial Lake Missoula, which formed south of the Cordilleran Ice Sheet, in the northwestern United States. The Purcell Lobe of the Ice Sheet extended south from British Columbia to the basin of modern Pend Oreille Lake in northern Idaho. It thereby impounded the Clark Fork River drainage to the east, forming Glacial Lake Missoula in western Montana. At maximum extent this ice-dammed lake covered 7500 km^2, and held a water volume of about 2500 km^3 with a depth of 600 m at the dam. Repeated failures through subglacial tunnels are inferred to have occurred between about 17 500 and 14 500 calendar years ago (Waitt, 1985; Atwater, 1986). Cataclysmic failure of the ice dam impounding this lake resulted in discharges into the Columbia River system of up to about 20 sverdrups (O'Connor and Baker, 1992). As recognized by Baker and Bunker (1985), the multiple outburst events were of greatly differing magnitudes. About 15 exceeded 3 sverdrups, and at least one of these exceeded about 10 sverdrups in discharge (Benito and O'Connor, 2003). The largest failure or failures probably involved a different source mechanism than the subglacial tunnelling envisioned by Waitt (1985) because that mechanism yields discharges of only 1 to 2 sverdrups (Clarke *et al*., 1984).

The Snake River, a major tributary to the lower Columbia River, was impacted by the spilling of the Late Pleistocene Lake Bonneville, the mega-lake predecessor of the Great Salt Lake. This palaeolake achieved a maximum area of 52 000 km^2 and a volume of 7500 km^3 between about 22 000 and 17 500 calendar years ago. The lake filled to the level of a spill point in south-central Idaho, and then dropped 100 m as it eroded into the outlet, releasing the catastrophic Bonneville Flood down the Snake River (O'Connor, 1993).

Upon reaching the Pacific Ocean the Missoula floodwaters continued flowing down the continental slope as hyperpycnal flows and associated turbidity currents (Normark and Reid, 2003). The sediment-charged floodwaters followed the Cascadia submarine channel into and through the Blanco Fracture Zone and out onto the abyssal plain of the Pacific. As much as 5000 km^3 of sediment may have been carried and distributed as turbidites over a distance of 2000 km west of the Columbia River mouth (Figure 5.2).

5.3.2 Laurentide Ice Sheet

As the Laurentide Ice Sheet of central and eastern Canada retreated from its late Quaternary maximum extent, it was

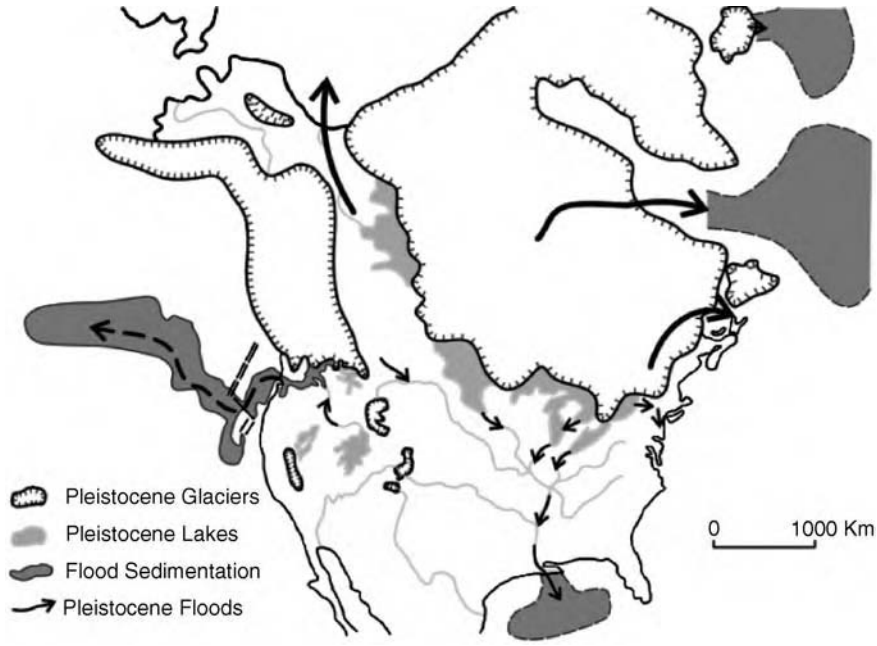

Figure 5.2 Sketch map of the late Pleistocene glacially diverted drainage systems of North America. Note the glacial flood augmentation of the Columbia, Mississippi, Hudson, Mackenzie, and St Lawrence Rivers. Other glacial megafloods occurred in Iceland and the Hudson Strait (upper right)

bounded to the south and west by immense meltwater lakes, which developed in the troughs surrounding the ice. As the lake levels rose, water was released as great megafloods, which carved numerous spillways (Figure 5.2) into the drainages of the Mississippi, St Lawrence, and Mackenzie Rivers (Kehew and Teller, 1994). Outbursts of meltwater into the Atlantic Ocean may have generated climate changes by influencing the thermohaline circulation of the North Atlantic Ocean (Teller *et al*., 2002).

The Laurentide Ice Sheet achieved its maximum extent during the Last Glacial Maximum about 20 000 years ago. The initial glacial retreat generated relatively small lakes because of the regional river drainage to the south, away from the ice front. The ice sheet surged and readvanced at times, leading to very complex history in the basins that now contain the Great Lakes. However, when the ice sheet retreated north of this area into the Canadian Shield, Lake Agassiz formed in the trough between the ice and drainage divides to the south and west, in parts of present-day North Dakota, Manitoba, and western Ontario. The Agassiz megalake seems to have initiated close to the time of the Younger Dryas cooling event, which began about 12 700 calendar years ago. One explanation for this cooling is diversion to the St Lawrence River of the Laurentide meltwater that previously flowed to the Gulf of Mexico via the Mississippi (Figure 5.2). The outflow of great quantities of freshwater into the North Atlantic disrupted the salinity gradient that drives the thermohaline circulation of the oceans by the formation of deepwater in the North Atlantic (Broecker and Denton, 1989).

As the southern margin of the Laurentide Ice Sheet retreated northward into the present Hudson Bay region, Lake Agassiz lowered by a succession of overflow or spill points (Teller *et al*., 2002), approximately as follows:

1. It drained southward via the Minnesota River to the Mississippi and Gulf of Mexico (about 12 000–13 000 years ago).
2. It then entered Lake Superior via a route near Thunder Bay.
3. It shifted to the northwest via the Clearwater Spillway to the Mackenzie River and the Arctic Ocean (about 11 000 years ago).
4. It then flowed eastward again to Lake Superior through a succession of spillways (about 10 000 years ago).
5. It shifted to the Ottawa River to the St Lawrence.
6. Finally it flowed to the Hudson Bay area (about 8400 years ago).

This 5000-year history resulted in lacustrine inundation at one time or other of 1.5 million km^2. Its maximum one-time extent was not achieved until a union occurred with glacial Lake Ojibway in northern Ontario about 8400 years ago. At this maximum, terminal stage, the resulting megalake covered about 840 000 km^2, and held about 160 000 km^3 of water (Leverington *et al*., 2002). This is double the volume of the largest modern lake, the Caspian Sea, but the palaeolake was highly unstable. It was dammed by remnants of the Laurentide Ice Sheet, severely weakened because of the influx of marine water into Hudson Bay. The stage was set for a massive subglacial outburst of the Lake Agassiz water through Hudson Strait into the Labrador Sea, a probable trigger for the 8400-year BP abrupt and widespread global climatic cooling event (Clarke *et al*., 2003). The maximum discharge for this event is estimated as 5 sverdrups (Clarke *et al*., 2004).

A variety of enigmatic landforms, involving water erosion and deposition, developed beneath the Laurentide Ice Sheet. These landforms include drumlins, Rogen moraines, large-scale bedrock erosional marks, and tunnel channels (valleys). Though commonly explained by subglacial ice deformational processes, the genesis of these features cannot be observed in modern glaciers that are much smaller than their Late Quaternary counterparts. Shaw (1996) explains the assemblage of landforms as part of an erosional/depositional sequence beneath continental ice sheets that precedes regional ice stagnation and esker formation with a phase of immense subglacial sheetfloods, which, in turn, follows ice-sheet advances that terminate with surging, stagnation and melt-out. Shaw proposes that peak discharges of tens of sverdrups are implied by the Late Quaternary subglacial landscapes of the southern Laurentide Ice Sheet. At least three major drainageways are envisioned: Cordilleran, Livingstone Lake, and Algonquin (Figure 5.3). Shoemaker (1995) provides some theoretical support for Shaw's model, though at smaller flow magnitude levels. Shaw's (2002) meltwater hypothesis for subglacial landscape development is a current source of considerable controversy among glacial geologists (e.g. Benn and Evans, 1998).

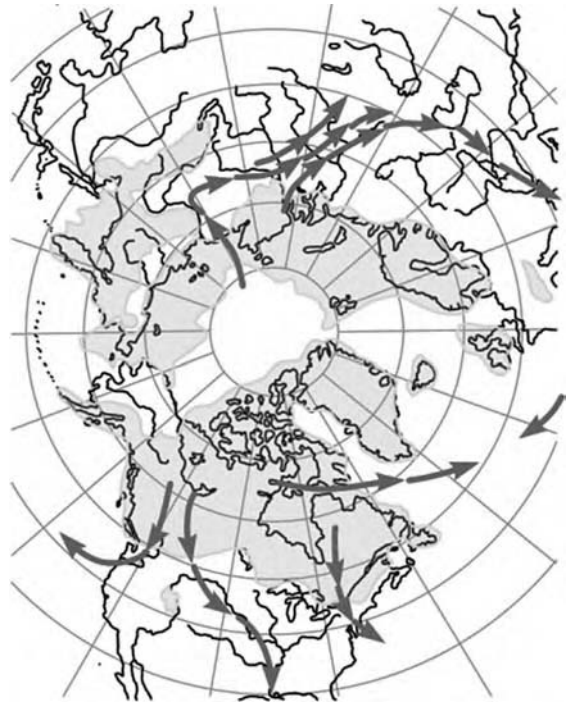

Figure 5.3 Hypothetical pattern of the northern hemisphere glacial megafloods (arrows) to full-glacial ice sheets. The North American pattern includes, from west to east (1) Shaw *et al*.'s (1999) controversial connection of subglacial Cordilleran Ice Sheet floods to the Channelled Scabland and the Pacific Ocean, (2) Shaw's (1996) 'Livingstone Lake Event' of Laurentide Ice Sheet subglacial megaflooding to the Gulf of Mexico, and (3) Shaw's (1996) 'Algonquin Event' of Laurentide Ice Sheet subglacial megaflooding to the Atlantic Ocean. The northern Laurentide Ice Sheet also had outbursts to the east through the Hudson Strait (Clarke *et al*., 2004). The Eurasia Ice Sheets are shown with a controversial maximal extent in the east proposed by Grosswald and Hughes (2002) and the immense cross-Asian pattern of megafloods proposed by Grosswald (1999)

5.3.3 Eurasia Ice Sheets

In the 1970s Mikhail G. Grosswald recognized that the Quaternary ice-sheet margins of northern Eurasia, like those of northern North America, held huge proglacial lakes, and great spillways developed for the diversion of drainage. Not only was meltwater diverted to the south-flowing Dneiper and Volga Rivers, but the great north-flowing Siberian Rivers, the Irtysh, Ob, and Yenisei were impounded by ice sheets that covered the modern Barents and Kara Seas. Though Grosswald's reconstructions created considerable controversy, recent work (e.g. Mangarud *et al*., 2001) shows that these impoundments and some of their related margins did indeed occur. Grosswald (1980) interpreted this blockage to be Late Weichselian in age (about 15 000–20 000 years ago). However, other work considers the event to have been Early Weischselian (Arkhipov *et al*., 1995), about 90 000 years ago, when ice-sheet growth was enhanced by the climatic influence of the ice-dammed lakes (Krinner *et al*., 2004).

The largest lake, named 'Mansi' (Figure 5.4), formed on the west Siberian plain. It is estimated by Mangarud

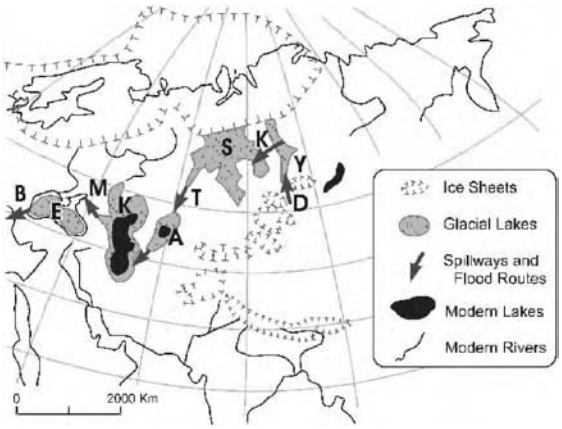

Figure 5.4 Sketch map of the late Pleistocene glacially diverted drainage system of central Asia. The various ice-dammed lakes, expanded lakes, and seas include: the Yenisei Lake (Y), Lake Mansi (S), the Aral Sea (A), the Kvalynian Lake (K), and the New Euxine Lake (E). These are connected by a series of spillways, as follows: Kas-Ket (K), Turgai (T), Manych (M), Bosporous (B), and Dardanelles (D)

et al. (2001) to have covered 600 000 km^2 at a surface elevation of 60 m. However, both Arkhipov *et al*. (1995) and Grosswald (1980) postulate a much larger palaeolake, about 1.2 million km^2 in area, with a volume of about 75 000 km^3 at a surface elevation of 128 m (Figure 5.5). This west Siberian megalake was the Asian equivalent of Agassiz. It drained southward, through the Turgai divide of north-central Kazakhstan, to the basin of the modern Aral Sea. The latter rose from its 1960 elevation of 53 m to 70 or 80 m, enlarging from 60 000 km^2 (1960 area) to about 100 000 km^2 in the Pleistocene. This palaeolake then drained southwestward through a spillway at its southwestern end, the Uzboi channel, into the basin of the modern Caspian Sea (Figure 5.4). Also fed by glacial meltwater from northern Europe via the Volga, the Caspian expanded to a Late Quaternary size over twice its modern extent. Known as the Khvalyn palaeolake, it inundated an area of 950 000 km^2, holding a volume of 135 000 km^3 at an elevation of 50 m (the modern Caspian level is –28 m). The Khvalyn palaeolake spilled westward through the Manych spillway into the Don River valley. The huge size of the Manych spillway, up to 35 km wide, implies that flows may have reached a peak of 10 sverdrups (Baker, 1996). This water spilled into the Sea of Azov, and through the Kerch Strait to the Euxine Abyssal Plain, which is the floor of the modern Black Sea.

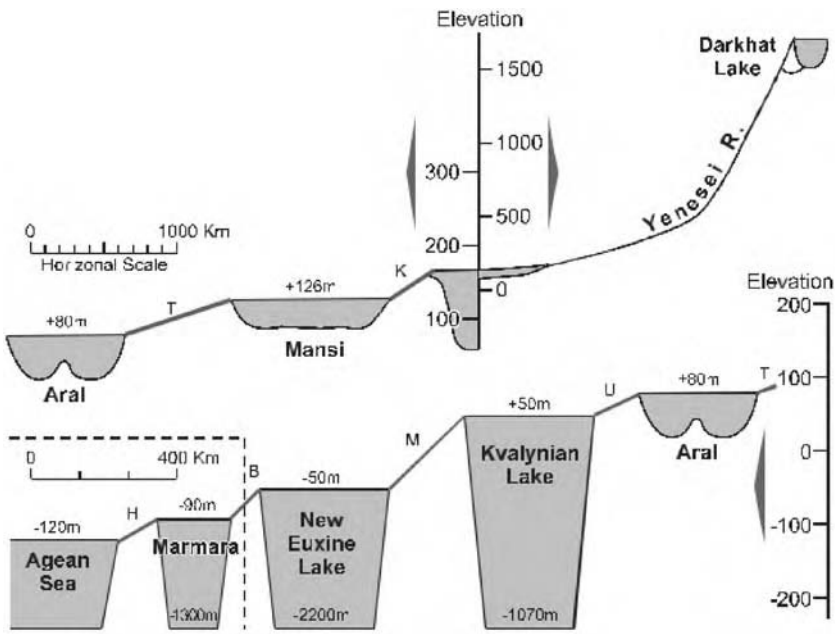

Figure 5.5 Schematic longitudinal profile of the late Pleistocene glacially diverted drainage system in central Asia. The various spillways comprising the system are designated by the same letters used in the sketch map in Figure 5.4

During the last glaciation, the Black Sea was isolated from the Mediterranean Ocean, and it filled with fresh water derived from the great system of glacially augmented rivers entering it from the north. About 18 000 years ago, this phase, called the New Euxine, had a well-developed freshwater faunal facies, showing that the Caspian was spilling through the Manych spillway. At times, so much freshwater entered that the megalake spilled into the Sea of Marmara, which, in turn, spilled via the Hellespont into the Agean and Mediterranean. The whole system of Asian spillways and megalakes (Figure 5.5) constituted a temporary river over 8000 km in length. It was Earth's largest river. Indeed, the late Quaternary of the northern hemisphere was a period of magafloods and megarivers (Figure 5.6).

Although Late Quaternary freshwater inundation of the Black Sea is well recognized, it is usually correlated to enhanced proglacial meltwater flow via the many rivers draining southward from the northern Eurasian Ice Sheets, as noted above. A recent controversy has arisen, however, over the marine influx to the Black Sea that occurred during rising Holocene sea level, which spilled Mediterranean water through the Hellspont and Bosporus, reaching the Black sea about 8000 years ago. One view (Ryan *et al*., 2003) holds that the global ocean rose to the level of a relatively shallow sill of the Bosporus outlet and catastrophically spilled into the Black Sea basin, which then was partly filled with freshwater to a level about 85 m below that of today. The resulting cataclysmic inundation presumably displaced a large human population in a calamity that they equate to the Noachian flood myth. An alternative view is that much of the Bosporus is underlain by freshwater facies of Late Pleistocene age, derived from the Black Sea. The minimal erosion of these sediments is not consistent with cataclysmic flooding leading to the overlying Holocene marine facies of Mediterranean origin.

Figure 5.6 Conventionally accepted pattern of late Pleistocene megafloods (arrows) in relation to northern hemisphere ice sheets and ice-marginal lakes

5.3.4 Central Asian Mountains

A number of cataclysmic flood landscapes are now recognized in the mountain areas of Central Asia. The best studied of these regions is the Altai Mountains of south-central Siberia (Carling *et al*., 2002). The Altai flooding derived from the Chuja-Kuray ice-dammed lake, which may have held as much as 1000 km^3 of water at a maximum depth of up to 900 m (Baker *et al*., 1993; Herget, 2005). Downstream of this ice dam the Chuja and Katun River valleys are characterized by immense gravel bars, emplaced by the flooding into various valley-side embayments. The bars are up to 5 km long and 120 m in height. The bar surfaces and associated run-up layers of flood-transported gravel indicate maximum flow depths of about 320 m. Flow modelling of the associated palaeoflood discharges retrodicts a peak flow of about 11 sverdrups and mean flow velocities of about 30 $m\,s^{-1}$ (Herget and Agatz, 2003).

Another region with extensive evidence of Late Quaternary megafloods is Tuva. The Tuvan palaeofloods derived from an ice-dammed lake in the Darkhat depression of north-central Mongolia (Grosswald and Rudoy, 1996). The palaeolake held about 250 km^3 of water with a depth of 200 m at its ice dam. The palaeoflooding entered the upper Yenisei River and it was remarkable for the emplacement of spectacular trains of giant current ripples (gravel dunes) near the Tuva capital city of Kyzyl (Figure 5.1).

In Kirgizstan, Lake Issyk-Kul, the world's second largest modern mountain lake, was transformed into an even larger ice-dammed lake during the last glaciation. Iceberg-emplaced landforms rise to 300 m above the present lake level (Grosswald *et al*., 1994). Spectacular erosion at the full-glacial lake outlet, Boam Canyon, indicates that the palaeolake failed by cataclysmic outburst

flooding. This flood emplaced an enormous outwash fan, extending 85 km from the mouth of Boam Canyon. A similar, but smaller fan occurs on the upper Yenisei River, where the Tuvan floods emerged from canyons of the West Sayan Mountains and entered the Abakan Basin. Another area of probable glacial cataclysmic flooding is Lake Baikal with a current area of 31 500 km^2 and a volume of 23 000 km^3. This huge lake may have expanded during full-glacial periods by ice blockages of its outlet, thereby raising its level of spill points.

5.4 EXTRATERRESTRIAL MEGAFLOODS AND MEGARIVERS

Fluvial-like landforms occur on at least five of the solar system bodies. The 'riverine' features of Venus and Earth's moon seem to have been produced by lava (Baker and Komatsu, 1999). The Venus channels are especially remarkable, with one having a length of 6800 km, thereby longer than any terrestrial river (Baker *et al*., 1992). Though a minority view, a submarine aqueous origin is still under consideration for the Venus channels (Jones and Pickering, 2003). The newly discovered channel networks on Saturn's moon Titan seem to have been caused by flowing hydrocarbons, perhaps liquid methane (Kerr, 2005). Only on Earth and Mars do aqueous processes seem responsible for the fluvial-like landscapes.

The surface of Mars preserves landforms associated with the largest known water floods. While most of these megafloods occurred more than one billion years ago, recent spacecraft images document a phase of outburst flooding and associated volcanism that seems no older than tens of millions of years (Berman and Hartmann, 2002: Burr *et al*., 2002). The megafloods that formed the Martian outflow channels had maximum discharges comparable with those of Earth's ocean currents and its thermohaline circulation (Baker, 2002). On both Earth and Mars, abrupt and episodic operation of these megascale processes are likely major factors in global climatic change. The Martian megafloods are hypothesized to have induced the episodic formation of a northern plains 'ocean', which, with contemporaneous volcanism, led to relatively brief periods of enhanced hydrological cycling on the land surface (Baker *et al*., 1991).

Parker *et al*. (1989) recognized that a number of Martian flood channels and valley networks were connected into a great 8000 km long system (Figure 5.7). The resulting flow path (Figure 5.8) connected the ancient glacial deposits of the South Polar Cap through various breached impact basins to the northern plains of Mars (Clifford and Parker, 2001). The northern plains would have been the site of a temporary ocean, the 'Oceanus

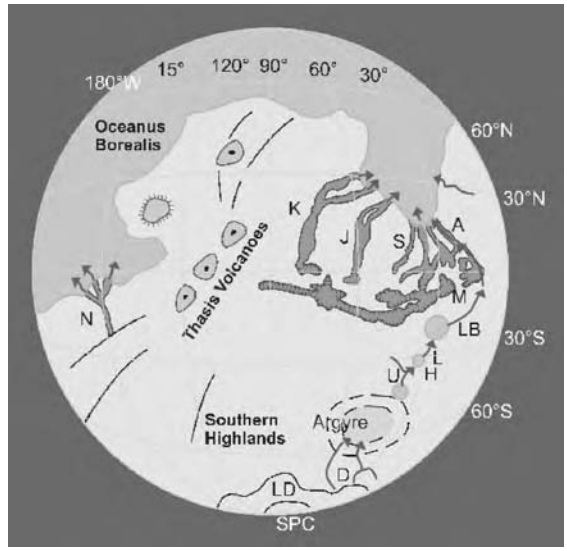

Figure 5.7 Sketch map of the western hemisphere of Mars, showing the 8000 km drainage system that extends to the northern plains ('Oceanus Borealis') from the layered deposits (LD) that underlie the South Polar Cap (SPC). Elements of the drainage include (from south to north): Dzigai Vallis (D), the Argyre impact basin, Uzboi Vallis (U), Holden Crater (H), Ladon Vallis (L), Ladon Basin (LB), Margaritifer Vallis (M), and Ares Vallis (A). Prominent outflow channels include Mangala Vallis (N), Kasei Vallis (K), Maja Valis (J), and Shalbatana Vallis (S)

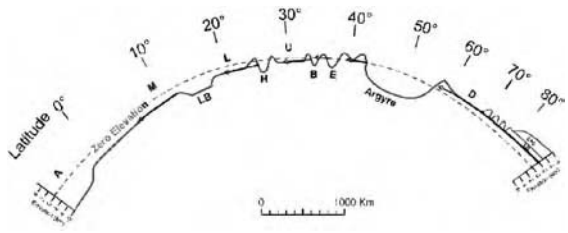

Figure 5.8 Schematic profile and cross-section along the 8000 km drainage system that extends from the south polar area (right) to the northern plains (left). Dzigai Vallis (D) heads in the polar layered deposits (LD) that underlies the South Polar Cap (SPC). Dzigai Vallis enters the Argyre impact basin, which drains northward through Hale (E) and Bond (B) craters to Uzboi Vallis (U). The latter heads to Holder Crater (H), Ladon Vallis (L), Ladon Basin (LB), Margeritifer Vallis (M), and Ares Vallis (A). Figure 5.7 is a sketch map of the same routing

Table 5.1 Properties of various terrestrial megafloods

Location	Lake area (km^2)	Lake volume (km^3)	Age (^{14}C yrs)	Peak discharge (Sverdrups)	References
L. Agassiz	840 000	160 000	7 700	5–10	Clarke *et al*. (1984)
L. Missoula	7 500	2 000	16 000	17	O'Connor and Baker (1992)
Chuya-Kuray	2 600	1 000	~17 000	18	Baker *et al*. (1993)
Livingstone	N/A	80 000	~15 000	60	Shaw (1996)
Darkhat	2 600	250	~17 000	0.4	Grosswald and Rudoy (1996)
Issyk-Kul	6 000	1 300	~17 000	1	Grosswald *et al*. (1994)
Bonneville	50 000	5 000	14 500	1	O'Connor (1993)

Borealis' of Baker *et al*. (1991). Comparable in length to the glacial spillway systems of Central Asia, this Martian river was remarkable for delivering water from one pole of Mars to the other, with resulting consequences for the climate. Thus, the greatest floods and the largest rivers for both Earth and Mars seem to have shared many features in common.

5.5 CONCLUSION

Of Earth's major rivers, a great many experienced the influence of megafloods associated with the margins of the great Pleistocene ice sheets. Especially in North America and Eurasia river basins, the invasions of glacial megafloods changed drainage patterns, enlarged valleys, and delivered huge fluxes of water and sediment to the oceans. Numerous spillways were flood-integrated into temporary rivers in parts of North America (the St Lawrence, Mackenzie, Yukon, Mississippi, and Columbia Rivers) and Eurasia (the Ob, Irtysch, Yenisei, Volga, and Dneiper Rivers). Some of these systems remained integrated after the flooding, but others were greatly changed. In North America, the ice-age spillways that had fed a megaflood-augmented Mississippi (Figure 5.2) were subsequently isolated by the capture of the Great Lakes drainage by the St Lawrence River. In Asia, the great megaflood river to the Mediterranean (Figure 5.6) was terminated by the post-glacial reestablishment of the northward flowing routes of the Lena, Yenisei, and Ob-Irtysch Rivers.

Discharges for the various ice-age megaflood rivers temporarily exceeded any known modern river flows (Table 5.1). Discharges on the order of 10 to 20 sverdrups occurred in the Channelled Scabland (Columbia River), the Siberian Altai (Ob River), and the Manych Spillway (Dneiper River). Even larger palaeoflood flows occurred on planet Mars, though the Martian palaeofloods are extremely ancient, occurring 10^8–10^9 years ago. The greatest known rivers were then generated by these floods. On Earth the greatest flood river may have been the system of late-glacial flood spillways extending about 8000 km from northern Siberia to the Mediterranean. On Mars a somewhat analogous system extended in very ancient time from the South Polar Ice Cap to a hypothesized Oceanus Borealis on the northern Plains. Conveying water from one pole to the other, over a distance of 8000 km, this great flood-river system was the Martian equivalent to Earth's ocean currents.

REFERENCES

Arkhipov, S.A., Ehlers, J., Johnson, R.G. and Wright, H.E., Jr (1995) Glacial drainage towards the Mediterranean during the Middle and Late Pleistocene. *Boreas*, 24, 196–206.

Atwater, B.F. (1986) Pleistocene Glacial-lake Deposits of the Sanpoil River Valley Northeastern Washington. *US Geological Survey Bulletin 1661*, 39 pp.

Baker, V.R. (1978) The Spokane Flood controversy and the Martian outflow channels. *Science*, 202, 1249–1256.

Baker, V.R. (1981) *Catastrophic Flooding: the Origin of the Channeled Scabland*. Hutchinson Ross, Stroudsburg, PA.

Baker, V.R. (1996) Megafloods and glaciation. In: *Late Glacial and Post Glacial Environmental Change* (I.P. Martini, Ed.). Oxford University Press, New York, 98–108.

Baker, V.R. (1998) Catastrophism and uniformitarianism: logical roots and current relevance. In: *Lyell: the Past is the Key to the Present* (D.J. Blundell and A.C. Scott, Eds.). Geological Society Special Publications, London, No. 143, 171–182.

Baker, V.R. (2001) Water and the Martian Landscape. *Nature*, 412, 228–236.

Baker, V.R. (2002) High-energy megafloods: planetary settings and sedimentary dynamics. In: *Flood and Megaflood Processes and Deposits: Recent and Ancient Examples* (I.P. Martini, V.R. Baker and G. Garzon, Eds.). International Association of Sedimentologists, Oxford, Special Publication No. 32, 3–15.

Baker, V.R. and Bunker, R.C. (1985) Cataclysmic late Pleistocene flooding from glacial Lake Missoula: a review. *Quaternary Science Reviews*, 4, 1–41.

Baker, V.R. and Komatsu, G. (1999) Extraterrestrial fluvial forms. In: *Varieties of Fluvial Form* (A.J. Miller and A. Gupta, Eds.). John Wiley & Sons, Ltd, Chichester, 11–30.

Baker, V.R., Benito, G. and Rudoy, A.N. (1993) Paleohydrology of late Pleistocene superflooding, Altai Mountains, Siberia. *Science*, 259, 348–350.

Baker, V.R., Strom, R.G., Gulick, V.C., Kargel, J.S., Komatsu, G. and Kale, V.S. (1991) Ancient oceans, ice sheets and the hydrological cycle on Mars. *Nature*, 352, 589–594.

Baker, V.R., Komatsu, G., Parker, T.J., Gulick, V.C., Kargel, J.S. and Lewis, J.S. (1992) Channels and valleys on Venus: a preliminary analysis of Magellan data. *Journal of Geophysical Research*, 97, 13421–13444.

Benito, B. and O'Connor, J.E. (2003) Number and size of last-glacial Missoula floods in the Columbus River valley between Pasco Basin, Washington and Portland, Oregon. *Geological Society of America Bulletin*, 115, 624–638.

Benn, D.I. and Evans, D.J.A. (1998) *Glaciers and Glaciation*. Arnold, London.

Berman, D.C. and Hartmann, W.K. (2002) Recent fluvial, volcanic, and tectonic activity on the Cerberus Plains of Mars. *Icarus*, 159, 1–17.

Broecker, W.S. and Denton, G.H. (1989) The role of ocean–atmosphere reorganizations in glacial cycles. *Geochimica Cosmochimica Acta*, 53, 2465–2501.

Burr, D.M., Grier, J.A., McEwen, A.S. and Keszthelyi, L. (2002) Repeated aqueous flooding from the Cerberus Fossae: evidence for very recently extant, deep ground water on Mars. *Icarus*, 159, 53–73.

Carling, P.A., Kirkbride, A.D., Parnachov, S., Borodavko, P.S. and Berger, G.W. (2002) Late Quaternary catastrophic flooding in the Altai Mountains of south-central Siberia: a synoptic overview and introduction to flood deposit sedimentology. In: *Floods and Megaflood Processes and Deposits: Recent and Ancient Examples* (I.P. Martini, V.R. Baker and G. Garzon, Eds.). International Association of Sedimentologists, Oxford, Special Publication No. 32, 17–35.

Clarke, G., Leverington, D., Teller, J. and Dyke, A. (2003) Superlakes, megafloods, and abrupt climate change. *Science*, 301, 922–923.

Clarke, G., Leverington, D., Teller, J. and Dyke, A. (2004) Paleohydraulics of the last outburst flood from glacial Lake Agassiz and the 8200 BP cold event. *Quaternary Science Reviews*, 23, 389–407.

Clarke, J.J., Mathews, W.H. and Pack, R.T. (1984) Outburst floods from glacial Lake Missoula. *Quaternary Research*, 22, 289–299.

Clifford, S.M. and Parker, T.J. (2001) The evolution of the Martian hydrosphere: implications for the fate of a primordial ocean and the current state of the northern plains. *Icarus*, 154, 40–79.

Grosswald, M.G. (1980) Lake Weichselian Ice Sheet of northern Eurasia. *Quaternary Research*, 13, 1–32.

Grosswald, M.G. (1999) *Cataclysmic Megafloods in Eurasia and the Polar Ice Sheets.* Scientific World, Moscow (in Russian).

Grosswald, M.G. and Hughes, T.J. (2002) The Russian component of an Arctic Ice Sheet during the Last Glacial Maximum. *Quaternary Science Reviews*, 21, 121–146.

Grosswald, M.G. and Rudoy, A.N. (1996) Quaternary glacier-dammed lakes in the mountains of Siberia. *Polar Geography*, 20, 180–198.

Grosswald, M.G., Kuhlke, M. and Fastook, J.L. (1994) Würm glaciation of Lake Issyk-Kul area, Tien Shan Mts: a case study in glacial history of central Asia. *GeoJournal*, 33, 273–310.

Herget, J. (2005) *Reconstruction of Pleistocene Ice-Dammed Lake Outburst Floods in the Altai Mountain, Siberia*. Geological Society of America Special Paper No. 386, 117 pp.

Herget, J. and Agatz, H. (2003) Modelling ice-dammed lake outburst floods in the Altai Mountains (Siberia) with HEC-RAS. In: *Palaeofloods, Historical Data and Climatic Variability: Applications in Flood Risk Assessment* (V.R. Thorndycraft, G. Benito, M. Barriendos and M.S. llasat, Eds.). Proceedings of the PHEFRA Workshop, Centro de Ciencias Medioamientales, Madrid, 171–181.

Jones, A.P. and Pickering, K.T. (2003) Evidence for aqueous fluid-sediment transport and erosional processes on Venus. *Journal of the Geological Society*, 160, 319–327.

Kehew, A.E. and Teller, J.T. (1994) History of the late glacial runoff along the southwestern margin of the Laurentide Ice Sheet. *Quaternary Sciences Reviews*, 13, 859–877.

Kerr, R.A. (2005) Titan, once a world apart, becomes eerily familiar. *Science*, 308, 330–331.

Krinner, G., Mangerud, J., Jacobson, M., Crucifix, M., Ritz, C. and Svendsen, J.L. (2004) Enhanced ice sheet growing in Eurasia owing to adjacent ice-dammed lakes. *Nature*, 427, 429–432.

Leverington, D., Mann, J.D. and Teller, J.T. (2002) Changes in the bathymetry and volume of glacial Lake Agassiz between 9200 and 7700 ^{14}C yr B.P. *Quaternary Research*, 57, 244–252.

Mangerud, J., Astakhov, V., Jacobsson, M. and Svendsen, J.I. (2001) Huge ice-age lakes in Russia. *Journal of Quaternary Research*, 16, 773–777.

Normark, W.R. and Reid, J.A. (2003) Extensive deposits on the Pacific Plate from Late Pleistocene North-American glacial lake bursts. *Journal of Geology*, 111, 617–637.

O'Connor, J.E. (1993) *Hydrology, Hydraulics and Sediment Transport of Pleistocene Lake Bonneville Flooding on the Snake River, Idaho*. Geological Society of America Special Paper 274, 83 pp.

O'Connor, J.E. and Baker, V.R. (1992) Magnitudes and implications of peak discharges from glacial Lake Missoula. *Geological Society of America Bulletin*, 104, 267–279.

Parker, T.J., Saunders, R.S. and Schneeberger, D.M. (1989) Transitional morphology in the west Deuteronilus Mensae region of Mars: implications for modification of the lowland/upland boundary. *Icarus*, 82, 111–145.

Ryan, W.B.F., Major, C.O., Lericolais, G. and Goldstein, S.L. (2003) Catastrophic flooding of the Black Sea. *Annual Reviews of the Earth and Planetary Sciences*, 31, 525–554.

Shaw, J. (1996) A meltwater model for Laurentide subglacial landscapes. In: *Geomorphology sans Frontieres* (S.B. McCann and D.C. Ford, Eds.). John Wiley & Sons, Ltd, New York, 182–226.

Shaw, J. (2002) The meltwater hypothesis for subglacial landforms. *Quaternary Science Reviews*, 90, 5–22.

Shaw, J., Munro-Stasiuk, M., Sawyer, B., Beaney, C., Lesemann, J.E., Musacchio, A., Rains, B. and Young, R.R. (1999) The Channeled Scabland: back to Bretz?, *Geology*, 27, 605–608.

Shoemaker, E.M. (1995) On the meltwater genesis of drumlins. *Boreas*, 24, 3–10.

Teller, J.T., Leverington, D.W. and Mann, J.D. (2002) Freshwater outbursts to the oceans from glacial Lake Agassiz and their role in climate change during the last deglaciation. *Quaternary Science Reviews*, 21, 879–887.

Waitt, R.B., Jr (1985) Case for periodic, colossal jokulhlaups from Pleistocene glacial Lake Missoula. *Geological Society of America Bulletin*, 96, 1271–1286.

6

Classification, Architecture, and Evolution of Large-river Deltas

Kazuaki Hori[1] and Yoshiki Saito[2]

[1]*Department of Environmental Science and Technology, Meijo University, Nagoya 468-8502, Japan*
[2]*Geological Survey of Japan, National Institute of Advanced Industrial Science and Technology (AIST), Tsukuba 305-8567, Japan*

6.1 INTRODUCTION

Many people imagine a river with a large drainage basin, channel length, or water discharge, or all three, when they hear the term *large river*. However, sediment discharge data are rarely reported. Here, we emphasize the role of sediment discharge in delta morphology, formation, and associated sedimentary processes.

Table 6.1 lists the large rivers of the world with water discharges of more than $10\,000\,m^3\,s^{-1}$, drainage basins larger than 1 million km^2, or a suspended sediment load of more than 100 million t $year^{-1}$. The locations of the mouths of these rivers are shown in Figure 6.1. Rivers with large sediment discharge occur mainly at low- to mid-latitudes in Asia and South America (Hori and Saito, 2003). Many of the world's largest rivers such as the Ganga (Ganges), Brahmaputra, Ayeyarwady (Irrawaddy), Mekong, Changjiang (Yangtze), and Huanghe (Yellow) are in Asia and have their sources in the high mountains of the Himalaya and the Tibetan Plateau. The high sediment load of these rivers reflects the large sediment production in their drainage basins caused by heavy rainfall driven by a monsoon climate and high relief produced by active crustal movements (Saito, 2001).

The rivers with large sediment discharge listed in Table 6.1 have formed megadeltas (deltas with very large areas) at their mouths (Table 6.2). Our understanding of deltas has been developed greatly by many studies on the Mississippi delta, a majority of which were published between the 1950s and the 1970s. These pioneering delta studies developed a number of concepts regarding delta formation, modern depositional processes at the mouths of rivers, and strata formation related to sea-level and climate changes (Coleman, 1981, 1988). Most textbooks on geomorphology and sedimentology generally use the Mississippi delta as a representative and standard example. However, Middleton (1991) pointed out that a majority of very large rivers in terms of sediment load currently occur on tide-dominated coasts, forming tide-dominated or tide-influenced deltas. Such deltas are less well known than their fluvial- or wave-dominated counterparts. Although the characteristics of many deltas in the world are different from those of the fluvial-dominated delta of the Mississippi (Figure 6.2a), detailed studies on other types of deltas were limited in number and such studies were internationally not well known before the 1980s. Studies of these deltas, however, have been published in local languages. For example, two useful books on the Huanghe Delta (Gao *et al*., 1989) and the Changjiang Delta (Yan and Xu, 1987) were published in Chinese with English abstract. Moreover, many of these deltas are located in developing countries, and research on these was slow to start. Since the late 1980s, however, many international research projects have been carried out and valuable information has been rapidly obtained. For instance, special issues of international journals have included papers on the Changjiang (Milliman and Jin, 1985), Huanghe (Keller and Prior, 1986), and Amazon

Large Rivers: Geomorphology and Management, Edited by A. Gupta

Table 6.1 Large rivers in the world in terms of suspended sediment load, water discharge, and drainage area

River	Average annual suspended load ($\times 10^6$ t)	River	Water discharge ($\times 10^4$ m^3 s^{-1})	River	Drainage area ($\times 10^6$ km^2)
Amazon	1200	Amazon	20.00	Amazon	6.15
Huanghe (Yellow)	1080	Zaire (Congo)	4.09	Zaire (Congo)	3.70
Ganga-Brahmaputra	1060	Orinoco	3.49	Mississippi	3.34
Changjiang (Yangtze)	480	Ganga-Brahmaputra	3.09	Nile	2.72
Mississippi	400 (210)	Changjiang (Yangtze)	2.85	Parana	2.60
Ayeyarwady (Irrawaddy)	260	Mississippi	1.84	Yenisey	2.58
Indus	250 (59)	Parana	1.80	Ob	2.50
Magdalena	220	Yenisey	1.78	Lena	2.43
Godavari	170	Lena	1.62	Changjiang (Yangtze)	1.94
Mekong	160	Mekong	1.49	Amur	1.86
Orinoco	150	St Lawrence	1.43	Ganga-Brahmaputra	1.59
Sông Hóng (Red)	130	Ayeyarwady (Irrawaddy)	1.36	Mackenzie	1.45
Narmada	125	Ob	1.22	Zambezi	1.40
Colorado	120 (0.1)	Amur	1.03	Volga	1.35
Nile	120 (0)			St Lawrence	1.19
Fly	115			Niger	1.11
				Shatt al Arab (Tigris-Euphrates)	1.05
				Orange	1.02

Suspended sediment load is after Milliman and Syvitski (1992). Modified from the Journal of Geology, 100, Geomorphic/tectonic control . . . , pp. 525–544, with permission from The University of Chicago. Water discharge and drainage area are after Hovius (1998). Load value in parentheses indicates post-dam values. Sediment loads of the Nile and Colorado Rivers have been decreased drastically by the construction of dam reservoirs (Milliman and Meade, 1983).

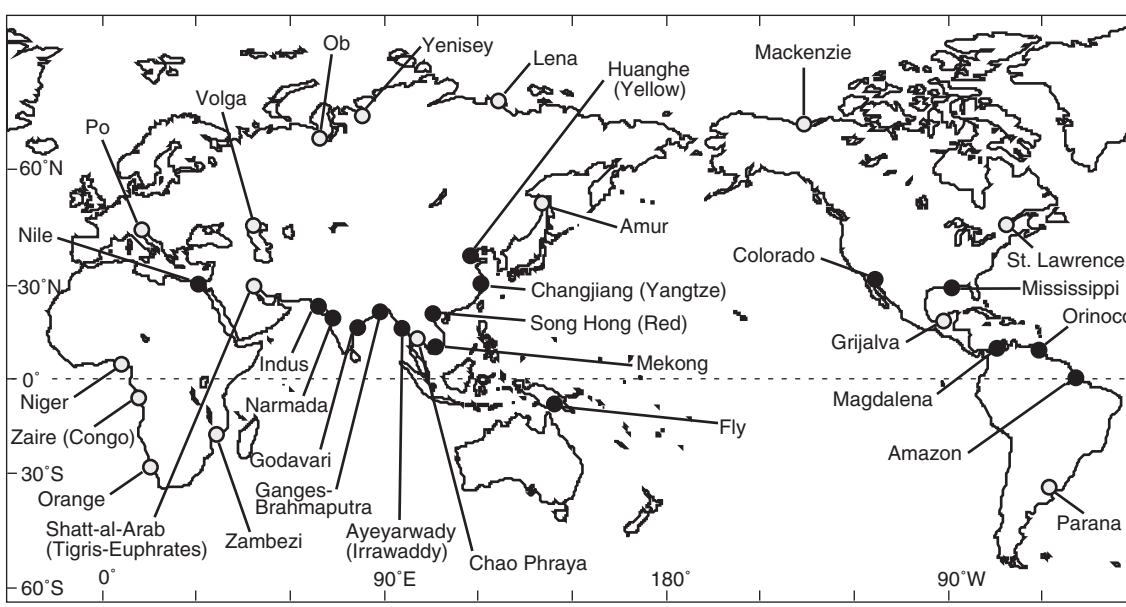

Figure 6.1 Map showing the locations of mouths of major large rivers. Solid circles indicate rivers with high sediment load listed in Table 6.1. Reproduced from J. Geogr., 112, K. Hori, Y. Saito, Morphology and sediments of large river deltas, 337–359, Copyright (2003) with permission from Tokyo Geographical Society

deltas (Nittrouer and DeMaster, 1986, 1996; Nittrouer and Kuehl, 1995).

This chapter focuses on major deltas built by large rivers with high sediment discharge and discusses their morphology, sedimentology, and evolution based mainly on data from recent studies. Readers can obtain general information on deltas by referring to the many summaries (Coleman and Wright, 1975; Coleman, 1981; Miall, 1984; Wright, 1985; Elliott, 1986; Bhattacharya and Walker, 1992; Davis, 1992; Suter, 1994; Galloway and Hobday, 1996; Hori and Saito, 2003).

Table 6.2 Delta areas of selected major river systems

River	Delta area (km^2)
Amazon	467 078
Ganga-Brahmaputra	105 641
Mekong	93 781
Changjiang (Yangtze)	66 669
Lena	43 563
Huanghe (Yellow)	36 272
Indus	29 524
Mississippi	28 568
Volga[a]	27 224
Orinoco	20 642
Ayeyarwady (Irrawaddy)	20 571
Niger	19 135
Shatt-al-Arab (Tigris-Euphrates)	18 497
Grijalva	17 028
Po	13 398
Nile	12 512
Sông Hóng (Red)	11 908
Chao Phraya	11 329

After Coleman and Wright (1975).
[a] The Volga River empties into the Caspian Sea.

6.2 DEFINITION OF A DELTA AND DELTA COMPONENTS

Elliott (1986) defined deltas as discrete shoreline protuberances formed where rivers enter oceans, semienclosed seas, lakes, or lagoons and supply sediment more rapidly than it can be redistributed by basinal processes. Other researchers have proposed definitions similar to this. Notably, Walker (1995) emphasized that deltas are formed by the advance of shorelines. Shoreline advance is very important for distinguishing deltas from estuaries, which also occur at river mouths (Boyd *et al*., 1992; Dalrymple *et al*., 1992). Fundamentally, deltas are regressive/prograding systems and estuaries are transgressive coastal depositional systems, according to the sedimentological definitions proposed by Boyd *et al*. (1992) and Dalrymple *et al*. (1992).

The well-known Gilbert-type delta is divided into three sedimentary facies from land to the receiving basin on the

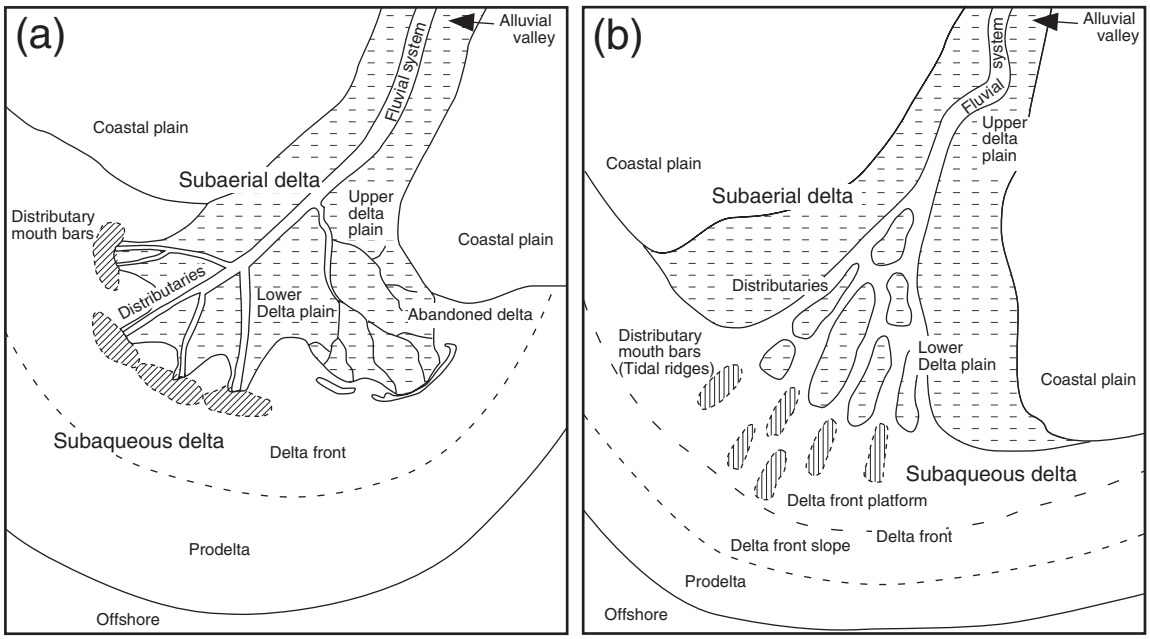

Figure 6.2 Basic delta environments: (a) fluvial-dominated delta (modified after Suter, 1994); (b) tide-dominated delta

basis of studies on Pleistocene fan deltas in Lake Bonneville (Gilbert, 1885, 1890; Allen, 1978), These are: topset beds with gentle slope, foreset beds with an inclination of 10–25°, and bottomset beds with gentle slope, which correspond to topset, foreset, and bottomset topography, respectively (Figure 6.3a). These terms are ordinarily applied to fan deltas and lacustrine deltas, which in cross-section exhibit a steep foreset between gentle bottomset and topset beds.

On the other hand, the major modern deltas discussed in this chapter, and deltas generally composed of fine-grained material, are usually divided according to sedimentary environments (Figure 6.3b and c). These deltas are divided into two parts in relation to sea level. The subaerial delta is the part of the delta above the low tide level, the subaqueous delta is the sector below this level. The subaerial delta is further subdivided into a 'lower delta plain' influenced by tides and an 'upper delta plain'

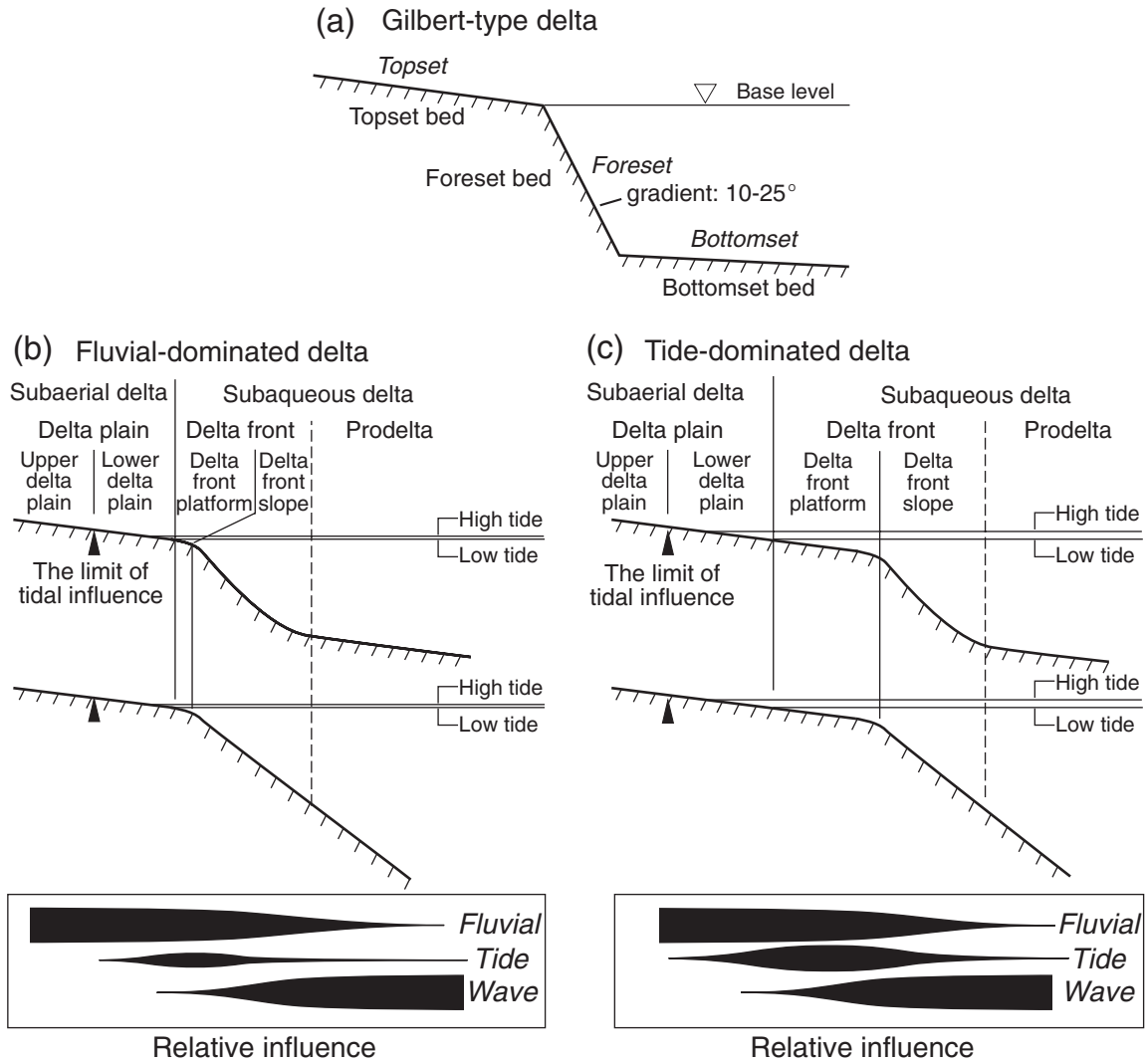

Figure 6.3 Components of deltas based on their morphology and sedimentary environment: (a) Gilbert-type delta; (b) fluvial-dominated delta; (c) tide-dominated delta. Reproduced from J. Geogr., 112, K. Hori, Y. Saito, Morphology and sediments of large river deltas, 337–359, Copyright (2003) with permission from Tokyo Geographical Society

above the tidal influence. The subaqueous delta is subdivided into the delta front and prodelta (Figures 6.2 and 6.3) (Wright, 1982; Suter, 1994; Thomas and Goudie, 2000). The delta front is the proximal part of deposition, where the sediment supplied to the delta from rivers accumulates most actively. A part of the delta-front sediment is carried by traction. Sand bodies built at distributary terminals are referred to as distributary-mouth bars (Figure 6.2). The prodelta lies seaward of the delta front as the distal part of deposition and its deposits are composed of fine silt to clay, transported in suspension. Delta studies, on the basis of analyses of sedimentary strata, have adopted the common terms delta plain, delta front, and prodelta, because the sediments deposited in each environment are easily distinguishable. Then delta front facies in ancient sedimentary rocks is identified as coarse-grained sediments. It is hard to estimate palaeo-delta morphology from ancient sediment. Therefore, this classification system is based on sediments and not directly on delta topography. On the other hand, modern delta front facies of large river deltas consists of sand for distributary channels and mouth bars, and fine-grained sediments for most of the delta front slope. Modern large river deltas receive 80–90 % fine-grained suspended load and 10–20 % coarse-grained (sandy) bed load (Milliman and Meade, 1983).

We discuss that relationship by referring to modern delta examples. Figures 6.4–6.6 illustrate the topography and sediment patterns in several major deltas of the world. The relationship between topographic cross-sections and sedimentary environments in the deltas as deduced from these data are illustrated schematically in Figure 6.3. The cross-sections are roughly grouped into two types on the basis of their characteristic features. One type shows a clear gradient change in cross-section near the boundary between the delta plain and delta front, that is, near the shoreline. The Mississippi Delta is of this type (Figure 6.3b). In the other type, this gradient change occurs far from the shoreline; the Amazon and Ganga-Brahmaputra Deltas are examples of this second type (Figure 6.3c). The delta front is subdivided into the 'delta front platform', which slopes very gently seaward, and the 'delta front slope', which slopes steeply seaward (Allen, 1965).

Both types have a gradient change near the boundary between the delta front and prodelta (Figure 6.3b and c). Nittrouer *et al*. (1986) and Kuehl *et al*. (1989) divided the subaqueous deltas of the Amazon and Ganga-Brahmaputra Rivers, which have a cross-section like that shown in Figure 6.3c, into topset, foreset, and bottomset, as for a Gilbert-type delta. The division corresponds to one based on sedimentary environments. The topset is the delta-front platform, the foreset is the delta-front slope, and the bottomset is the prodelta. As discussed above, the relationships between sedimentary environments and the morphology of deltas are grouped into three types for different sedimentary environments, as illustrated in Figure 6.3.

6.3 CLASSIFICATION OF DELTAS

A ternary diagram (Figure 6.7) originally proposed by Galloway (1975) is the best-known system for classifying deltas. It builds on a concept by Fisher (1969), who subdivided deltas into two major types: high-constructive and high-destructive deltas. Galloway (1975) focused on the relative intensities of fluvial and marine (tidal and wave) processes operating along deltaic coasts and classified deltas into thee end members. Fluvial-dominated deltas are typically elongated (Figure 6.2a); wave-dominated deltas have cuspate shorelines; and tide-dominated deltas display an estuary-like geometry (Figure 6.2b). By considering sediment grain size of delta deposits, Orton and Reading (1993) modified Galloway's ternary model and proposed a new classification system, which accounts for gravelly to muddy deltas. These classification systems are still meaningful because they help us understand the major processes acting on a delta and the resulting geometry and sediment facies.

On the other hand, Walker (1992) showed that a tide-dominated delta can be regarded as an estuary and asserted that the diagram by Galloway (1975) should be revized, because most large tide-dominated or tide-influenced deltas have estuary-like funnel-shaped river-mouth topography instead of convex coastal topography. However, Walker formulated his view without the benefit of many studies of tide-dominated deltas. Moreover, Walker may have failed to take into account that the shorelines of present-day tide-dominated deltas have become stable or have migrated landward as a result of a Holocene sea-level rise. Examples of prograding, tide-dominated Holocene deltas were not well studied until around 1990. However, Walker's assertion has promoted many recent studies of tide-dominated deltas.

Quantitative data on mean tidal range and mean wave height are used to classify coastal morphology, such as barrier or barrier-islands systems. A diagram based on qualitative data was proposed originally by Hayes (1979) and modified by Davis and Hayes (1984). Orton and Reading (1993) applied this diagram as well as Galloway's ternary diagram to delta classification. Bhattacharya and Giosan (2003) proposed an asymmetry index A for wave-influenced deltas to express the degree of dominance of marine versus fluvial factors quantitatively. This index is defined as the ratio between the net

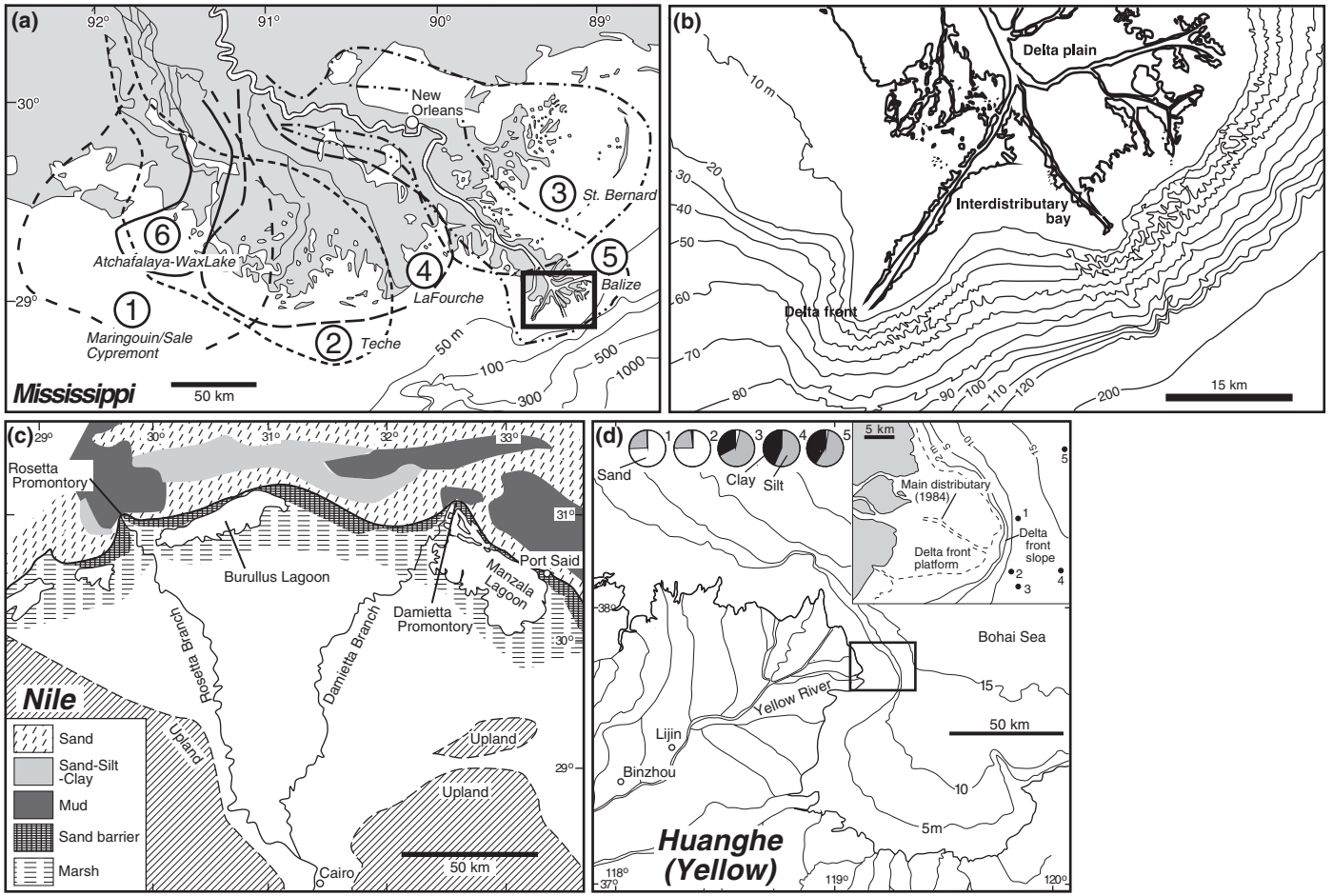

Figure 6.4 Wave-influenced (type 1) deltas: (a) and (b) Mississippi Delta. Modified from Journal of Coastal Research, Vol. 14, Coleman *et al*., Mississippi River delta: an overview, pp. 698–716, 1998, with permission from Coastal Education & Research Foundation. Circled numbers indicate the order of deposition of each lobe; (c) Nile. Modified from Marine Geology, Vol. 42, Coleman *et al*., Morphology and dynamic sedimentology of the Eastern Nile delta shelf, pp. 301–326, 1981, with permission from Elsevier and Geol. Soc. Spec. Publ., no. 41, Sestini, G. (1989) Nile Delta: a review of depositional environments and geological history. In Whateley, M.K.G. and Pickering, K.T. eds. Deltas: Sites and Traps for Fossil Fuels, 1989, with permission from The Geological Society; (d) Huanghe (Yellow). Modified from Geo-Marine Letters, Vol. 6, Bornhold *et al*., Sedimentary framework of the modern Huanghe (Yellow River) delta, pp. 77–83, 1986, with permission from Springer-Verlag GmbH and Geo-Marine Letters, Vol. 6, Prior *et al*., The subaqueous delta of the modern Huanghe (Yellow River), pp. 67–75, 1986, with permission from Springer-Verlag GmbH. The present mouth of the Huanghe (Yellow River) is located about 15 km southeastward of that of 1984

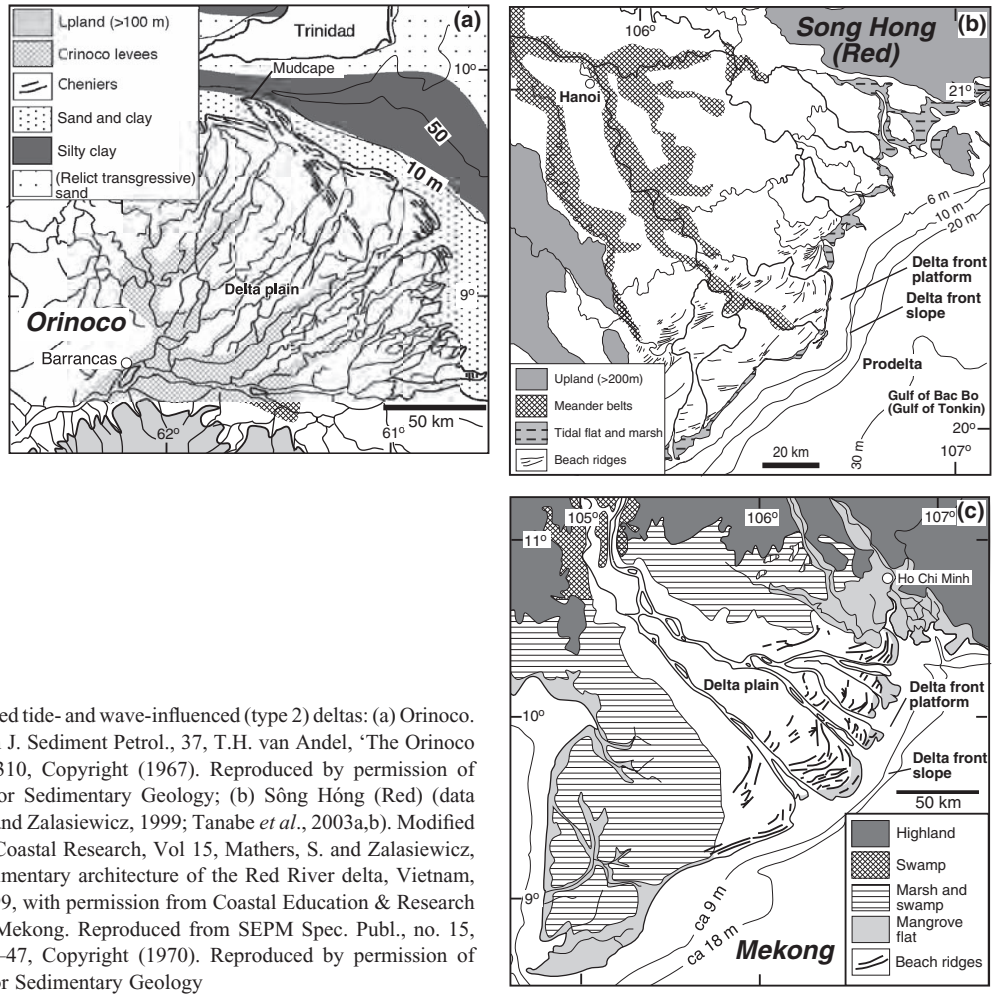

Figure 6.5 Mixed tide- and wave-influenced (type 2) deltas: (a) Orinoco. Reproduced from J. Sediment Petrol., 37, T.H. van Andel, 'The Orinoco delta. . . .', 297–310, Copyright (1967). Reproduced by permission of SEPM Society for Sedimentary Geology; (b) Sông Hóng (Red) (data source: Mathers and Zalasiewicz, 1999; Tanabe *et al*., 2003a,b). Modified from Journal of Coastal Research, Vol 15, Mathers, S. and Zalasiewicz, J., Holocene sedimentary architecture of the Red River delta, Vietnam, pp. 314–325, 1999, with permission from Coastal Education & Research Foundation; (c) Mekong. Reproduced from SEPM Spec. Publ., no. 15, J.P. Morgan, 31–47, Copyright (1970). Reproduced by permission of SEPM Society for Sedimentary Geology

longshore transport rate at the river mouth (in m^3 $year^{-1}$) and river discharge (in 10^6 m^3 $month^{-1}$). However, it is very hard to obtain the net longshore transport rate in a delta system. Moreover, the index does not seem to work well with tide-influenced deltas. Harris *et al*. (2003) classified Australian clastic coastal depositional systems by using quantified wave, tide, and river power.

In this paper, the quantitative indices, such as suspended sediment load, fluvial discharge, mean tidal range, and mean wave height were used to classify the major deltas built by large rivers with high sediment discharge. We plotted log mean tidal range/mean wave height versus log suspended sediment load, and log water discharge (Figure 6.8). If we recognize a delta as a sediment body at a river mouth accompanied with shoreline advance, all deltas should be influenced strongly by fluvial discharge and sediment load. Therefore, the well-known delta type 'fluvial-dominated' used in the ternary diagram (Galloway, 1975) is not adopted here. Instead, we conveniently classify the deltas shown in Figure 6.8 into three types on the basis of the coastal environment: wave-influenced (type 1); mixed wave- and tide-influenced (type 2); and tide-influenced (type 3). As pointed out by Middleton (1991), many rivers have their mouths along tide-influenced environments. Wave influences are more prominent than tidal influences at the Huanghe, Mississippi, and Nile deltas. Deltas plotting higher up in the diagrams tend to show greater contribution of the related rivers. In the next section, the morphology, sediment, and sediment accumulation rates of each type are described.

This classification is not based on sediment facies. When sediment deposition occurs only by river-flushing into a receiving basin, a delta must be classified as a fluvial-influenced high-constructive delta. However if such sediments are reworked and redeposited by waves and/or tides, it must be classified as a wave- or tide-

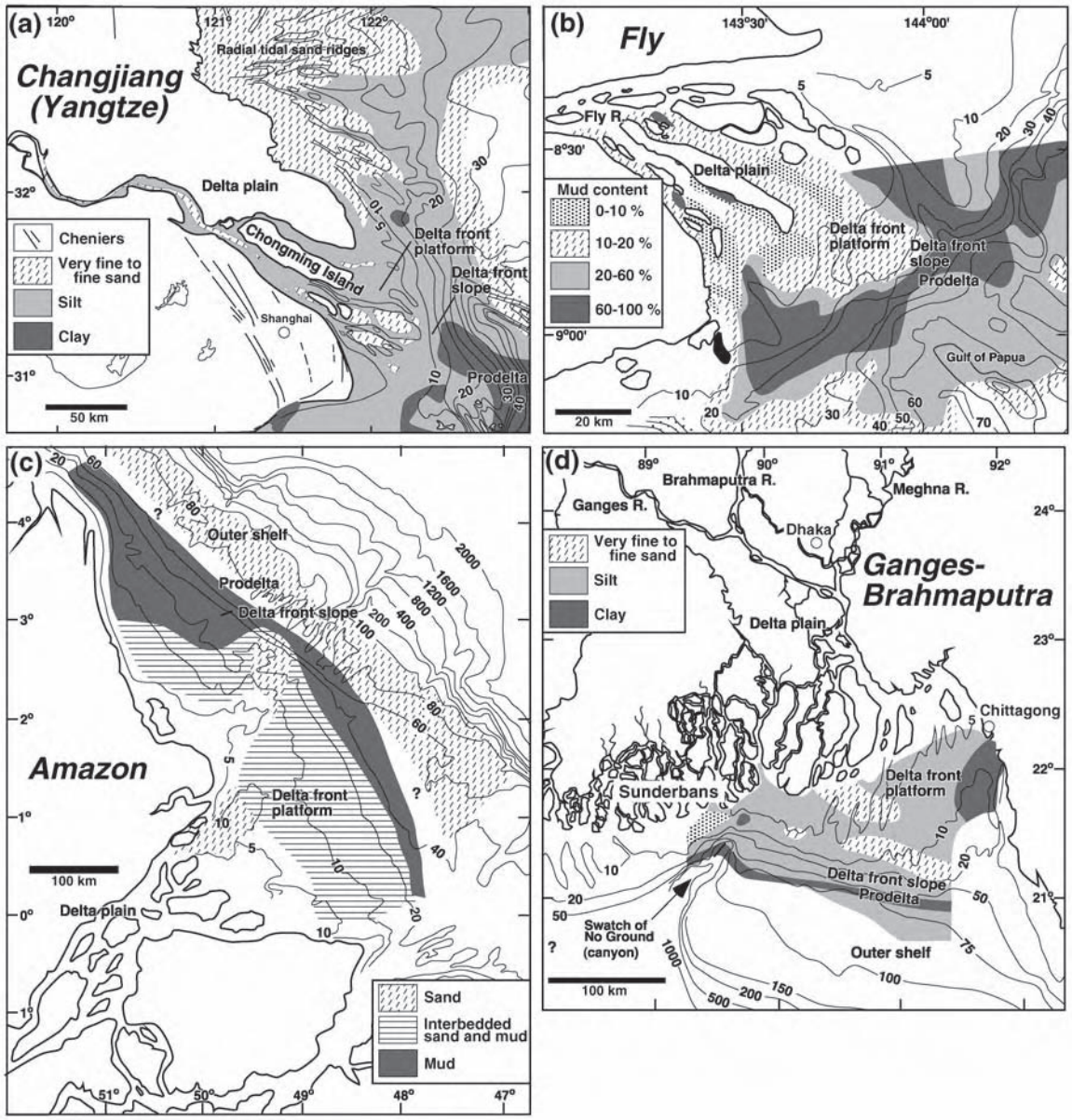

Figure 6.6 Tide-influenced (type 3) deltas: (a) Changjiang (Yangtze); (b) Fly; (c) Amazon; (d) Ganga (Ganges)-Brahmaputra. Modified from Sedimentary Geology, vol. 146, Hori *et al*., Architecture and evolution of the tide-dominated Changjiang (Yangtze) River delta, China, pp. 249–264, 2002, with permission from Elsevier

influenced destructive delta. There may be some wave- or tide-influenced constructive deltas. This classification is not designed to illustrate sedimentary processes and sediment preservation but rather delta morphology and evolution.

6.4 MORPHOLOGY AND SEDIMENT

6.4.1 Morphology

Figures 6.4–6.6 display the morphology and subaqueous sediment distribution of the deltas plotted in Figure 6.8,

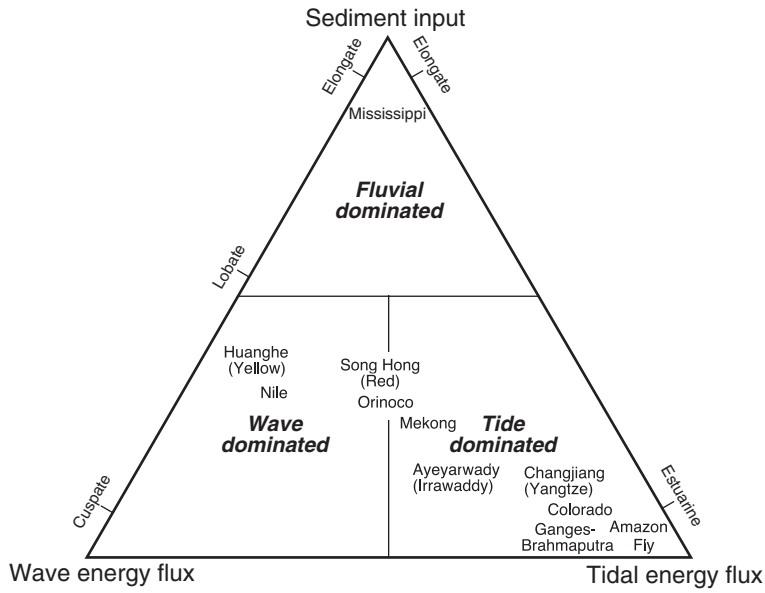

Figure 6.7 A classification of deltas in terms of relative amounts of fluvial, wave, and tide influence. Modified after Galloway (1975)

using data from earlier studies. The Colorado and Ayeyarwady Deltas are excluded because of lack of detailed information.

Type 1 (wave-influenced) deltas form shoreline protuberances where the rivers and their distributaries empty into the ocean. The width of the delta front platform is very small. In plan view, the Mississippi Delta exhibits bird's-foot topography. Natural levees have been built extending seaward along the main channel and distributary channels. An interdistributary bay occurs between the distributaries (Figure 6.4). Marshes and swamps are well developed on the delta plain (Kosters, 1989; Kosters and Suter, 1993).

The Nile delta shoreline is cuspate at the distributary mouths (Figure 6.4). However, shore-parallel beach ridges, barriers, and large lagoons occur between distributaries at the Nile Delta (Sestini, 1989) because the present local sea level is at its highest Holocene position (Warne and Stanley, 1993; Nakada and Okuno, 2000). Therefore, true deltaic features are found only at the river mouths, and transgressive coastal features have developed in other parts of the Nile Delta.

The Huanghe has built an elongated delta at its mouth because of its extremely large sediment load and the shallow receiving basin in the Bohai Sea. Judging only from the river-mouth shape, this delta would be interpreted as a fluvial-dominated delta. However, the delta coast, except at the present river mouth, is being eroded by wave action. Although the delta lobe that formed after AD 1855 and whose apex is near Lijin, is cuspate to lobate in shape, older delta lobes to its north and south are characterized by relatively smooth shorelines and chenier (shell) ridge development. The present high sediment discharge of the Huanghe has resulted from human activities in its drainage basin, estimated sediment discharge of more than 1000 years ago being an order of magnitude lower than that at present. Therefore, the Huanghe delta has developed from a wave-dominated delta to a more fluvial-dominated delta on a millennial timescale as a result of human activities (Saito *et al*., 2000, 2001). However, if we look at the whole delta system of the Huanghe, including surrounding chenier plains, which were the locations of former delta lobes, the whole Huanghe Delta should be regarded as a wave-influenced delta. Current bird's-foot delta lobes will be eroded after the movement of a river course. Due to recent human activities, such as dam construction, sediment discharge has been sharply reduced, resulting in severe erosion along the entire Huanghe delta coastline (Yang *et al*., 1998; Saito, 2001).

Type 2 (mixed wave- and tide-influenced) deltas are characterized by not only many bifurcations of the mainstream that begin around the apex of the delta but also groups of subparallel or diverging beach and chenier

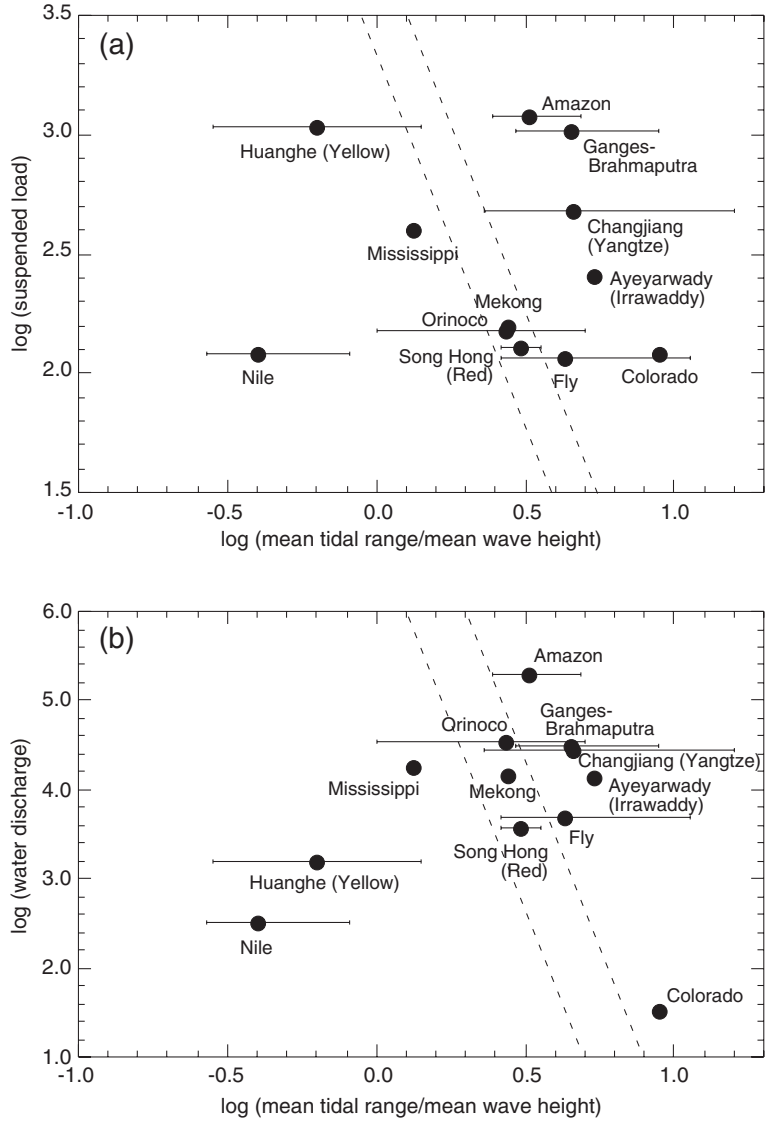

Figure 6.8 Coastal environments for major large-river deltas plotting log (mean tidal range/mean wave height) versus: (a) log (suspended load); and (b) log (water discharge). The dashed lines dividing the three groups (wave-influenced, mixed tide- and wave-influenced, and tide-influenced deltas) were drawn by eye

ridges along the shorelines (Nguyen *et al*., 2000; Warne *et al*., 2002) (Figure 6.5). Although beach ridges are not observed inland on the Mekong delta plain, series of beach ridges are common in its seaward part (Nguyen *et al*., 2000). Similar beach ridge distribution patterns are found in the Sông Hóng (Red River) and Orinoco Deltas (van Andel, 1967; Mathers and Zalasiewicz, 1999). This pattern reflects the increased wave influence that accompanies delta progradation (Ta *et al*., 2002a, b; Tanabe *et al*., 2003d).

Although both the Mekong and Sông Hóng have built type 2 deltas facing the South China Sea, the shoreline shape of each delta differs in detail. The Sông Hóng Delta is convex in the river-mouth area. Notably, sediment reworked by waves forms hooked spits on either side of the river mouth. In contrast, the shoreline is not convex at

the mouths of the Mekong, although delta progradation is occurring overall.

Natural levees and scroll bar topography along distributaries are well developed on the subaerial delta plain of the Orinoco (van Andel, 1967). Estuary-like topography is found along the eastern coast, where fluvial and tidal influences are dominant. However, chenier ridges and mudcapes occur locally along the northern coasts because of strong northwestward longshore currents (Warne *et al*., 2002). Mudcapes are rounded, elongate, fine-grained promontories that are typically 5–10 km wide and as long as 100 km. They have formed along the coast of South America from the mouth of the Amazon to the Orinoco River mouth under the strong influence of the Guiana Current (Allison *et al*., 1995).

Type 3 (tide-influenced) deltas exhibit estuary-like, funnel-shaped river-mouth topography (Figure 6.6, Amazon, Ganga-Brahmaputra, Changjiang, and Fly Rivers). Delta front platforms of tide-dominated deltas are wider than those of the other types of deltas (Nittrouer *et al*., 1986). The river mouths are characterized by multiple distributaries and islands. Distributary channels build elongated, sandy, distributary-mouth bars roughly parallel to the channels. Such bars were called 'tidal ridges' by Dalrymple (1992). Distributaries with bars forming at their seaward ends are the active principal distributaries. Over time, the bars develop, merge with other bars, and are finally abandoned (Wang *et al*., 1981). Sand shoals and islands between distributaries originated as abandoned bars.

Muddy intertidal flats also develop well along shorelines of type 3 deltas. Several chenier ridges are found in the southern Changjiang delta plain (Liu and Walker, 1989; Yan *et al*., 1989). The southwestern Ganga-Brahmaputra delta plain is characterized by a broad mangrove lowland with well-developed tidal creeks, known as the Sunderbans (Umitsu, 1987; Allison and Kepple, 2001).

6.4.2 Sediments and Sediment Facies

Sediments transported to the ocean by the large rivers draining the continents are 80–90% fine-grained suspended load and 10–20% coarse-grained (sandy) bed load (Milliman and Meade, 1983). In most of the deltas discussed in this chapter, clay- to silt-sized particles dominate in the prodelta sediments, and silt- to sand-sized particles compose the delta front and river or tidal channel sediments in general.

Prodelta sediments are usually intercalated with silt stringers and thin shell beds, and are highly bioturbated regardless of delta type. The shell beds result mainly from storms. Storm events provide coarse-grained sediments to the prodelta.

Alternating sand and mud layers occur commonly in delta front sediments, and some of the sand layers may display cross or parallel lamination (Coleman, 1981; Kuehl *et al*., 1982; Coutellier and Stanley, 1987; Harris *et al*., 1993). Studies of modern delta front sediments in the Amazon and Ganga-Brahmaputra Deltas have shown that interbedded or interlaminated sand and mud are formed under the strong influence of tides, especially neap–spring tidal cycles (Segall and Kuehl, 1994; Jaeger and Nittrouer, 1995). Sandy layers form by erosion and bedload transport during spring tides, whereas muddy layers are produced under relatively low-energy conditions during neap tides (Jaeger and Nittrouer, 1995). Tidal currents also contributed to the formation of the sand–mud couplets that have been observed in the Holocene Changjiang delta sediments, because some sand layers display bidirectional cross laminations (Hori *et al*., 2001a), and ripples were found on the seabed of the delta front by a side-scan sonar survey (Chen and Yang, 1993). On the other hand, seasonal changes in surface wave energy may have resulted in the interbedded sand and mud layers in the delta front sediments of the Fly River, because each annually deposited, sand–mud layer pair is about 2 cm thick, which is compatible with the mean annual sedimentation rate of about 1.7 cm at the delta front (Harris *et al*., 1993). Surface wave energy causes sandy, bioturbated lag deposits to form during the trade wind season (March–November), and then low surface wave activity during the northwest monsoon (December–March) results in a mud drape being deposited, covering the sand deposits.

Sediments of varying grain size texture, reflecting delta topography, fluvial, tide, and wave interactions, and climatic conditions, compose the delta plain. At the Mississippi Delta, bioturbated silt to fine sand has accumulated in natural levees and crevasse splays along the distributaries, while muddy organic-rich sediments are found in swamps and marshes between the distributaries (Coleman, 1981). In the outer delta plain of the Nile, fine- to medium-grained sand with molluscan shells are deposited in beach ridges, and dunes and mud have accumulated in lagoons under the strong influence of waves (Coutellier and Stanley, 1987). Similar sediment facies have been reported from the Mekong Delta (Ta *et al*., 2002a). Thinly laminated sand and mud layers with included plant roots occur commonly in tidal flats of type 3 deltas (Hori *et al*., 2001a) and backmarsh or tidal flat facies behind beach ridges of type 2 deltas (Ta *et al*., 2002a). Peaty facies, originating from mangroves, are common in deltas located in tropical to subtropical zones, such as the Sông Hóng, Mekong, Ganga-Brahmaputra and Fly deltas.

Delta progradation results in a typical facies succession: prodelta, delta front, and delta plain facies, in ascending order. In general, an upward-coarsening succession of prodelta to delta front sediments is overlain by an upward-fining succession of uppermost delta front to delta plain sediments. The coarsest and most well-sorted deposits usually occur in the boundary zone between delta front slope and delta front platform or at distributary-mouth bars (Coleman, 1981; Hori *et al*., 2002; Ta *et al*., 2002a) because these are the zones of highest energy, and fine sediments are reworked offshore. As wave influence increases, a foreshore facies develops in the upper to middle intertidal zone, and beach ridge and dune facies overlie this facies. Therefore, the succession of delta front to delta plain deposits comprise a fining-upward delta front platform facies overlain by a coarsening-upward foreshore/beach ridge/dune facies (Ta *et al*., 2002a). Moreover, significant wave influence results in a succession very similar to a strand plain, which is characterized by upper shoreface to foreshore/backshore facies. In contrast, muddy flats and mangrove forests occur commonly in the intertidal zone of tide-dominated deltas and result in upward-fining successions (Hori *et al*., 2002; Walsh and Nittrouer, 2004). Upward-coarsening and upward-fining successions may be obscured by extraordinary fluvial influence. The Huanghe mouth may receive a huge sediment discharge, of about 4–5 billion tonnes of sediment, during a period of several days when an extremely heavy flood occurs (Ren and Shi, 1986). This unusual sediment influx probably results in various facies successions characterized by both coarsening- and fining-upward successions in the delta front sediments of borehole cores (Saito *et al*., 2000).

Although this typical succession occurs commonly within active subaerial deltas, some deltas display different successions. For example, the Nile Delta displays the typical succession only around Manzala Lagoon and the Rosetta Branch (Figure 6.4) (El Askary and Frihy, 1986; Coutellier and Stanley, 1987; Frihy and Stanley, 1987; Arbouille and Stanley, 1991; Chen *et al*., 1992; Stanley and Warne, 1993). Because the sea level has continued to rise along the Nile deltaic coast, probably owing to glacial-isostasy, a barrier–lagoon system, a typical transgressive coastal depositional system, is found along most of the coast except at the distributary mouths, which receive much larger sediment discharges. Thus, the distribution of the typical facies succession is influenced strongly by relative sea-level changes. In addition, other important factors controlling the facies succession are the extent of landward marine influence reached at maximum transgression and the location, form, and depth of any valleys incised as the relative sea level dropped.

6.4.3 Sediment Accumulation Rates

Scruton (1960) estimated the sediment accumulation rate of the Mississippi delta by comparing bathymetrical changes between 1874 and 1940 and found that the accumulation rates at the upper delta front were ten or more times larger than those found toward the delta plain and prodelta. Similar results were obtained for the progradation of the Southwest Pass, Mississippi River Delta by using historic maps and borings acquired along the channel (Gould, 1970; Coleman, 1988). These results are consistent with the typical longitudinal S-shaped profile of a delta comprising gentle/steep/gentle gradients. At the delta front, where the delta gradient is steepest, sedimentation rates increase and show maximum values (Masuda and Saito, 1995).

In addition to such calculations of accumulation rates from topographical changes, many studies, after the 1980s, directly measured accumulation rates of delta sediments by using various radionuclides, such as ^{234}Th (half-life, 24.1 days), ^{210}Pb (half-life, 22.3 years), and ^{137}Cs (half-life, 30.2 years) (e.g. Amazon: Kuehl *et al*., 1982, 1986, 1996; Changjiang: McKee *et al*., 1983; DeMaster *et al*., 1985; Fly: Harris *et al*., 1993, 1996; Baker *et al*., 1995; Walsh and Nittrouer, 2004; Ganga-Brahmaputra: Kuehl *et al*., 1989, 1997; Allison *et al*., 1998; Goodbred and Kuehl, 1998; Michels *et al*., 1998; Allison and Kepple, 2001). Sedimentation rates of the Ganga-Brahmaputra Delta have been measured by radiochemical techniques (^{137}Cs and ^{210}Pb) combined with evaluation of seismic profiles. In the subaerial delta, accumulation rates are the largest in the fluvial braidbelt and adjacent floodplain, decrease rapidly with distance from the main channel, and increase again in low-lying distal basins called 'beel' (Allison *et al*., 1998; Goodbred and Kuehl, 1998). In the subaqueous delta, high accumulation rates, ~5–7 cm year^{-1}, are observed near the centre of the delta front slope. Sedimentation rates decrease toward the prodelta to less than 0.3 cm year^{-1} (Kuehl *et al*., 1997; Michels *et al*., 1998). Similar results have been reported for the Amazon subaqueous delta. Large accumulation rates as high as ~10 cm year^{-1} occur near the outer topset and foreset regions corresponding to the delta front (30–60 m water depth). Accumulation rates are ~2 cm year^{-1} in the bottomset (prodelta) region and are negligible on the outer shelf, where relict sands are exposed (Kuehl *et al*., 1985, 1986). Walsh and Nittrouer (2004) shows the relationship between sediment facies and accumulation rates of a bank-channel system of the Fly River Delta, and the significance of episodic sedimentation.

Accumulation rates of deltaic sediments vary considerably on different timescales. McKee *et al*. (1983) reported

that on a 100-day timescale, the deposition rate of muddy prodelta sediments of the Changjiang Delta, 4.4 cm month^{-1}, based on ^{234}Th data, are an order of magnitude higher than the rate of 5.4 cm year^{-1} (0.45 cm month^{-1}) reported on a 100-year timescale, based on ^{210}Pb data. The difference is probably because most of the sediments deposited at the prodelta on a 100-day timescale are later transported southward by winter storms and a strong coastal current (McKee *et al*., 1983). This example suggests that both short-term deposition rates and accumulation rates calculated from preserved sedimentary strata are very important for understanding sedimentary processes and strata formation. Similar problems on preservation potential of intertidal sediments of a delta system are reported from the Chanjiang Delta (Li *et al*., 2000) and the Fly River Delta (Walsh and Nittrouer, 2004).

The radiocarbon dating method is used most frequently to analyze borehole sediments taken from deltas on centennial to millennial timescales. In particular, accelerator mass spectrometry (AMS) dating has quickly become very popular, because it allows very small samples of material found in borehole sediments to be dated. Changes in accumulation rates can be calculated from a single borehole core from which a number of radiocarbon ages are available (Nakai and Nakamura, 1988), enabling us to discuss the relationship between accumulation rates and the sedimentary environment at the borehole site. In addition, palaeoaltitude and palaeo-water depth at the site can be estimated by comparing the accumulation curves with the sea-level curve in the study area (Saito, 1995).

Recently, many studies have applied this method to the investigation of Asian deltas (Huanghe: Saito *et al*., 2000; Changjiang: Hori *et al*., 2001a, 2001b, 2002; Sông Hóng: Tanabe *et al*., 2003a, b; Hori *et al*., 2004; Mekong: Ta *et al*., 2001, 2002a, b; Tanabe *et al*., 2003d; Chao Phraya: Tanabe *et al*., 2003c). The relationship between sedimentary environments and their accumulation rates can be determined from a radiocarbon-dated borehole core. Moreover, isochrons can be drawn between several radiocarbon-dated borehole cores shown in longitudinal cross-sections. These isochrons roughly show longitudinal profiles of past land and submarine topographies. Thus, it becomes possible to estimate the delta progradation rate, the sedimentation rate in each sedimentary environment, and past topographic slopes.

6.5 DELTA EVOLUTION

6.5.1 Response to Holocene Sea-Level Change

Deltas develop well at river mouths during regressive phases (Boyd *et al*., 1992). By analyzing radiocarbon ages of the basal or near-basal sediments of the world's deltas, Stanley and Warne (1994) and Warne and Stanley (1995) showed that delta initiation occurred worldwide after about 8500–6500 year BP, and concluded that the initiation was controlled principally by the declining rate of the Holocene sea-level rise. Sediment supply from rivers overtook accommodation created by sea-level rise after that period.

The relative sea-level change after delta initiation differs significantly among deltas because of hydro-isostatic effects (Nakada *et al*., 1991), tectonic uplift or subsidence, and/or sediment compaction (Roberts *et al*., 1994). Thus, the response of deltas to relative sea-level changes differs markedly. The highest Holocene sea level, approximately 2–3 m higher than that at present, occurred about 6000 years BP at the inner part of the Changjiang Delta, which is located far from the former ice sheets; since then, the sea level has gradually fallen to its present level as a result of hydro-isostatic effects. The coastal zone of the Changjiang Delta has a different sea-level curve (Chen and Stanley, 1998) also due to hydro-isostatic effects (Nakada *et al*., 1991). The evolution of the Changjiang Delta reflects those sea-level changes: an aggradational system developed during the slow rise of sea level from 8000 to 6000 years BP, and a progradational system developed after 6000 years BP, when the sea level had almost stabilized (Hori *et al*., 2002). A similar evolutionary pattern has been reported for the Sông Hóng (Hori *et al*., 2004) and Mekong (Ta *et al*., 2005) Deltas.

In contrast, the present sea level is the highest Holocene sea level at the Mississippi and Nile Deltas. The Mississippi River has built six major delta complexes, including the Teche, St Bernard, and LaFourche complexes (Figure 6.4) (Kolb and van Lopik, 1958; Frazier, 1967; Roberts, 1997). Boyd *et al*. (1989) estimate that the two delta complexes Maringouin/Sale Cypremont and Teche, formed during overall transgressive periods, driven mainly by the relatively rapid sea-level rise before 3500 years BP, and that the other complexes developed during the following sea-level stillstand. In particular, the former two complexes developed a delta plain only during stillstands or slow rise in sea level after rapid rise in sea level (Boyd *et al*., 1989).

Holocene sea-level changes have had a great impact on the accumulation pattern of delta deposits. Accommodation is still being added at deltas, such as the Nile and Ganga-Brahmaputra Deltas, where on a millennial timescale the sea level has continued to rise. Thus, at these deltas, fluvial sediments are actively accumulating on the delta plain (Goodbred and Kuehl, 2000a). Constant accumulation rates can be expected in a borehole core recovered from the delta plain of a delta that has been built

under a steadily rising sea level (Figure 6.9b). In reality, no Holocene deltas have experienced a constant sea-level rise since their initiation about 8000 years BP. However, sea level has remained relatively stable or has fallen gradually since the mid-Holocene at most Asian deltas. Accommodation has increased little on these delta plains from the mid-Holocene to the present, and sediments supplied by the rivers have mainly caused delta progradation. Therefore, a series of age–depth plots at borehole sites on these deltas show a trajectory that resembles that depicted in Figure 6.9a, reflecting delta progradation under a stable sea level. Low gradient at delta front platform and prodelta makes slow accumulation and high gradient at delta front slope high accumulation. This trajectory does not indicate constant sedimentation rates for all sedimentary environments. Thus, the current state of the Nile and Ganga-Brahmaputra Deltas is similar to the aggradational phases of other Asian deltas during 8000–6000 years BP. At present, sediment deposition in the delta plain of the Ganga-Brahmaputra delta shows a very high accumulation rate on a centennial scale; about one-third of the sediment supply from the rivers contributes to the aggradation of the delta plain. This delta is therefore a good example of a modern analogue of an aggradational/progradational delta during a slow rise in sea level.

Recently, it has been argued that most radiocarbon dates in Holocene sequences are older than should be reasonably expected because of the influence of old carbon during sediment storage and reworking such as prevail in fluvial and delta plains (Stanley and Chen, 2000; Stanley and Hait, 2000; Stanley, 2001). These investigators assume that delta sedimentation rates have been constant since about 7000 years BP, when delta initiation occurred worldwide. However, this idea does not account for landform and sedimentation processes of the subaqueous delta or for differences in relative Holocene sea-level changes among regions.

6.5.2 Changes in the Course of a River Channel and of its Distributaries

River-channel shift (e.g. avulsion), an important process in fluvial sedimentology and geomorphology (Jones and Schumm, 1999), is closely linked to delta formation. The relationship between such shifts and delta formation has been discussed in relation to the Mississippi and Huanghe Deltas. River-channel shifts have caused widespread switching of active delta complexes (delta superlobes) in the Mississippi Delta at a frequency of once every 1000–2000 years (Frazier, 1967; Roberts, 1997). The ages of some complexes were re-evaluated by ^{14}C dates from the tops of peat beds underlying clayey overbank deposits (Törnqvist *et al*., 1996). The results show that the beginnings of the St Bernard and LaFourche delta complexes are 1000–2000 years younger than the well-known ages previously inferred by Frazier (1967). The new ages are in agreement with those from archaeological sites on the lobes. An active delta complex is abandoned when

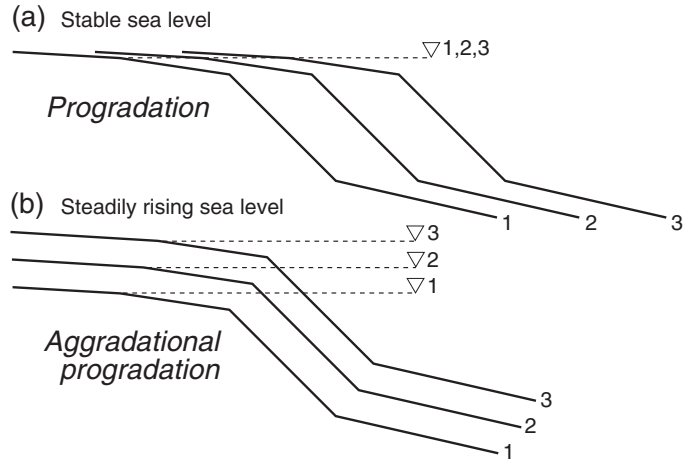

Figure 6.9 Evolution of deltas in response to sea-level changes: (a) stable sea level; and (b) steadily rising sea level. Each profile displays a longitudinal cross-section. Solid and dashed lines represent isochrons and sea levels at successive times 1, 2, and 3, respectively. Reproduced from J. Geogr., 112, K. Hori, Y. Saito, 'Morphology and sediments of large river deltas', 337–359, Copyright (2003) with permission from Tokyo Geographical Society

avulsion or stream capture occurs. The abandoned delta complex is then sequentially transformed into an erosional headland with flanking barriers, a transgressive barrier island arc, and finally an inner-shelf shoal, as reworking of the sediments by waves and subsidence of the delta surface overwhelm fluvial processes after the abandonment (Penland *et al*., 1988) (Figure 6.2a). Avulsion has occurred frequently near Kaifeng, 500 km upstream from the Huanghe mouth, resulting in changing of river-mouth locations (Saito *et al*., 1994). As a result, 10 delta complexes have developed over the past 6000 years (Xue, 1993; Saito *et al*., 2000). Chenier ridges characterize the coastal and delta plains of abandoned delta complexes.

Distributary shifts of the Huanghe and Mississippi Rivers have caused the locations of active delta lobes to change within a delta complex (Frazier, 1967; Xue, 1993) (Figure 6.10a). Numerous sediment borings have also revealed changes in the locations of delta lobes of the northeastern Nile Delta (Coutellier and Stanley, 1987). Moreover, each delta lobe of the Mississippi Delta may comprise one or more subdeltas, and smaller crevasse or overbank splays have developed at the mouths of secondary channels that diverge from major distributaries (Coleman and Gagliano, 1964).

Short-term and long-term processes both cause a river channel shift (e.g. avulsion) (Smith, 2003; Stouthamer, 2004). In short-term processes, large floods are the most common triggers for an avulsion (Jones and Schumm, 1999). Most avulsion in the Huanghe is caused by hydrological flooding (Xue, 1993). Base level change (e.g sea-level rise), climatic change, and tectonic movements are the representative long-term processes. Recently, Lowrie and Hamiter (1995) proposed that Mississippi delta lobe switching might be related to minor eustatic sea-level oscillations. Careful interpretation is required because only autochthonous processes, for example, a reduction in the channel gradient resulting from continued progradation, can cause such switching.

As described above, a type 2 delta, such as that of the Orinoco, has groups of beach and chenier ridges (Figure 6.5). Moreover, natural levees fringing distributary channels are well developed on the delta plain. Determining the precise ages of these components is necessary to evaluate the relationship between distributary shifts and coastal evolution.

In contrast, the Changjiang Delta (type 3) has not been affected by avulsion, because a single, deep, stable river channel is present in the lower reaches (Hori *et al*., 2002). However, the evolution of distributary channels has been important. Distributary channels have formed and been abandoned commonly in the Changjiang Delta (Figure 6.10b). The North Branch, located north of Chongming Island (Figure 6.6a), was the major distributary before the eighteenth century, although it transports little fluvial

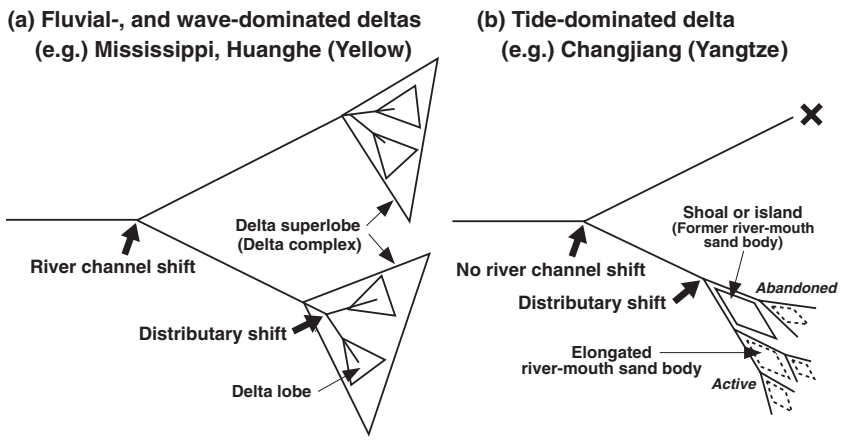

Figure 6.10 Schematic illustration of delta switching. (a) Wave-influenced deltas show widespread switching of delta superlobes (delta complex) and delta lobes because of channel avulsion. (b) Tide-influenced deltas do not show such switching because of the presence of a single, deep, stable river channel. However, the formation and abandonment of distributary channels occur commonly in tide-dominated deltas, resulting in the formation of river-mouth sandbars at the seaward ends of these channels. Modified from Sedimentary Geology, Vol. 146, Hori *et al*., Architecture and evolution of the tide-dominated Changjiang (Yangtze) River delta, China, pp. 249–264, 2002, with permission from Elsevier

sediment now (Chen *et al*., 1985). The active distributary channel at present is the South Channel, which has bifurcated into the North and South passages. River-mouth sandbars are being actively built at the seaward ends of these channels. These river-mouth sandbars will evolve into sand shoals/islands, which will separate new distributary channels. A similar phenomenon has been reported for the Fly Delta (Dalrymple *et al*., 2003). Discharge variation among distributary channels contributes greatly to subaqueous delta evolution of type 3 deltas (Figure 6.10b).

Avulsion also has a close relationship with sea-level changes and accommodation space of deposition. The rise of sea level induces sediment deposition in river channels and flooding, resulting in sediment deposition in levees and flood plains (e.g. Ganga-Brahmaputra Delta). Millennial sea-level changes must be impacting not only delta evolution and sediment deposition, but also avulsion.

6.5.3 Coastal Environment Change Related to Delta Progradation

When delta formation began at 8000–6000 years BP, many river mouths opened into embayments as a result of transgression caused by the rapid postglacial sea-level rise. Delta progradation then gradually filled the bay, until finally the delta was on an open coast. Analyses of drilled cores from the Mekong Delta show that the deltaic facies changed from those of a tide-dominated delta to those of a mixed tide- and wave-dominated delta around 3000 years BP as the delta prograded and the gradient of the delta front gradually steepened (Ta *et al*., 2002a, b; Tanabe *et al*., 2003d). The results are harmonious with the distribution of rows of beach ridges, which are found only along the present coasts. The Mekong example shows that the delta became more influenced by waves and storms as it prograded and the coast became more open and exposed. Thus, delta progradation changes the river-mouth environment, which, in turn, influences the deltaic topography and sediment facies. Delta evolution from a tide-dominated delta in a bay to a mixed tide- and wave-dominated delta facing an open coast may occur frequently during a sea-level highstand.

A similar environmental change can be found as a result of the evolution of a bayhead delta in a lagoon or an estuary lying behind a barrier (Dalrymple *et al*., 1992). The bayhead delta fills the lagoon and eventually reaches the coast during a regression phase, where it will also be affected more by wave influences. The São Francisco of South America and the Rhone and Po of Europe have such a history.

6.6 PROBLEMS OF SEDIMENT SUPPLY

6.6.1 Estimation of Past Sediment Discharge

When considering the transfer of sediment from the land to the sea, it is important to estimate past sediment discharge quantitatively either from the rate of advance of the delta front or by calculating the total sediment volume of a delta. In particular, data from the 1960s–1970s (Milliman, 1991) show that Asian rivers used to contribute more than 40% of world's total sediment discharge to the sea. However, this disproportionate contribution was not the natural state of affairs, but resulted from widespread human influence, such as deforestation or farming in drainage basins, over the past 2000–2500 years (Milliman and Syvitski, 1992).

Hori *et al*. (2001a) analyzed borehole samples taken from the Changjiang Delta and showed that the rate of delta front progradation doubled after ca. 2000 years BP, compared with the rate before 2000 years BP. This change to a rapid progradation rate correlates with the active extension of the subaerial delta (Wang *et al*., 1981; Chen, 1998). The increase in the progradation rate reflects the change in sediment supply to the river mouth. The causes of this active progradation may have been an increase in sediment production in the drainage basin from widespread human interference (Chen *et al.*, 1985) or a decrease in deposition in the middle reaches, which are characterized by extensive flood plains and a large number of natural lakes (Hori *et al*., 2001a). Calculations of the amount of marine sediment deposited by the Huanghe during the Holocene suggest that the sediment load of the river became an order of magnitude greater after 1000 years BP than it had been before that time (Milliman *et al*., 1987; Xue, 1993; Saito *et al*., 2001). This change was caused principally by increased cultivation of the Loess Plateau, where erosion occurs easily. The Huanghe is a striking example of a drastic increase in sediment load being caused by human activities in the drainage basin.

Taking into consideration the large increases in farming and deforestation activities, particularly in southern Asia and Oceania, during the last 1000–2000 years, Milliman and Syvitski (1992) estimated that pristine sediment discharge prior to extensive human influence was less than half the present level of about 20 billion t year^{-1}. However, the rate of delta front progradation of the Mekong Delta, the largest delta in Southeast Asia, does not suggest an increase in sediment discharge during the last 3000 years (Ta *et al.*, 2002b). Tanabe *et al.* (2003c) estimated the average rate of sedimentation of the Chao Phraya Delta, Thailand, by calculating the total sediment volume of the delta, and found it to be nearly the same as the present total sediment load from the Chao Phraya and

Mae Klong Rivers, suggesting that the sediment discharge has been roughly constant during delta formation. Goodbred and Kuehl (2000b) analyzed chronostratigraphic data from the Ganga-Brahmaputra deltaic deposits and estimated that the mean sediment load of the rivers has been relatively stable since about 7000 years BP. Judging from these examples, we believe that Milliman and Syvitski (1992) may have overestimated the effect of human activities on sediment yield. Recently, Syvitski (2001, 2003) estimated that global sediment delivery is at present about 18–24 billion t year^{-1}, but we need more data on pristine sediment discharge to confirm this estimate.

6.6.2 Sediment Budgets in Deltas and Sediment Supply to the Oceans

Estimates of sediment inputs from the world's rivers to its oceans were based mainly on data collected at gauging stations upstream from river mouths (Milliman and Meade, 1983; Milliman and Syvitski, 1992). In fact, many gauging stations of large rivers are situated hundreds of kilometres from the shoreline. A part of the sediment load can be assumed to be stored in the extensive floodplains and subaerial deltas that lie between the stations and the river mouths.

Many studies have attempted to quantify the partitioning of the sediment load of the Ganga-Brahmaputra Rivers among floodplains, subaerial and subaqueous deltas, continental shelf, and deep sea (Kuehl *et al*., 1997; Allison, 1998b; Allison *et al*., 1998; Goodbred and Kuehl, 1998, 1999; Michels *et al*., 1998). Goodbred and Kuehl (1999) estimated that the recent sediment load (approximately 1×10^9 t year^{-1}), through a main gauging station ~300 km inland of the coast, is distributed as follows: about 30% of the load is deposited on the subaerial delta and floodplains, about 40% is sequestered by the subaqueous delta, and the remaining 30% is transported to the deep sea (Bengal deep-sea fan) (Weber *et al*., 1997; Kudrass *et al*., 1998) through a submarine canyon called 'Swatch of No Ground.' Therefore, only about 70% of the sediment load that passes through the station reaches the ocean.

The Amazon River transports an average suspended-sediment load of 1.2×10^9 t year^{-1} past Óbidos, the farthest downstream gauging station. One-quarter of the suspended sediment is stored along the lower reaches and on the delta plain, about half is deposited on the subaqueous delta and the adjacent shelf, and about one-fifth is carried to the Orinoco subaqueous delta by longshore currents (Meade, 1994). The suspended load of the Huanghe is also deposited in large part on the delta plain, and the remaining load, approximately 70–90%, reaches the coast (Saito and Yang, 1994). In particular, during flood events, most of the sediment discharge is deposited on the floodplain and the delta plain, resulting in a decrease in sediment transport to the sea.

We should interpret data on the sediment discharges of the large rivers reported previously as sediment delivery not to the oceans but to the delta regions. Judging from the above examples, 10–30% of sediment load passing the farthest downstream gauging stations are trapped in delta plains of subaerial deltas and river channels. Subaerial and subaqueous deltas at the large rivers may trap 70–80% of sediment load passing the farthest downstream gauging stations.

6.7 CONCLUDING REMARKS

This chapter has reviewed the characteristics of the large-river deltas in terms of their geomorphology and sedimentology, based mainly on recent studies. In conclusion, we would like to mention two points that should be examined in the near future. First, we should integrate quantitative data on different timescales in order to understand modern sedimentary processes and establish a hierarchy of strata formation. Accumulation rates determined from dates obtained by various radiometric methods give valuable information for such integrated studies. Second, we should clarify changes in depositional systems that occurred before and after delta initiation in detail. Present deltas have formed largely since the rate of postglacial sea-level rise decreased. It is particularly important to consider changes that occurred during transgressive–regressive transitions in order to differentiate deltas from estuaries.

Human activities, such as dam construction and water- and land-use changes in drainage basins, substantially affect large rivers (Coleman and Roberts, 1989; Stanley and Warne, 1998; Woodroffe, 2000; Saito, 2001). At present, 30% of the global sediment flux is trapped behind large reservoirs (Vörösmarty *et al*., 1997). In particular, numerous serious problems have arisen recently regarding Asian rivers, for example, water shortages and coastal erosion in the case of the Huanghe (Yang *et al*., 1998), the construction of the Three Gorges Dam on the Changjiang, and reservoir construction, saline intrusion into groundwater, and cutting of mangroves for shrimp farm aquaculture along the Mekong (Umitsu, 2001), coastal erosion of the Sông Hóng Delta (Haruyama and Phai, 2002), and arsenic contamination in groundwater and coastal erosion in the Ganga-Brahmaputra Delta (Allison, 1998a; Umitsu, 2001). Deltaic lowlands in Asia are particularly important regions because of the many rapidly growing megacities located on them and because most of Asia's population and most of the rice paddies in the world are concentrated there. It is expected that

comprehensive studies on these deltas will be performed with international participation. For example, intensive studies of Asian deltas began in 2003 under the auspices of a new research project, IGCP-475 'Deltas in the Monsoon Asia-Pacific Region: DeltaMAP.'

ACKNOWLEDGEMENTS

This study was financially supported by a Grant-in-Aid from the Scientific Research Project of the Ministry of Education, Culture, Sports, Science and Technology of Japan and by the Global Environment Research Fund of the Ministry of the Environment of Japan. The authors are deeply grateful to Dr Avijit Gupta for his kind invitation to contribute to this special book. We thank Zhongyuan Chen and Steve Goodbred for critical and constructive comments that improved the manuscript. This study is part of the UNESCO/IUGS-supported International Geoscience Programme (IGCP) Project No. 475, 'Deltas in the Monsoon Asia-Pacific Region: DeltaMAP' and APN project on Mega-Deltas of Asia.

REFERENCES

Allen, J.R.L. (1965) Late Quaternary Niger delta, and adjacent areas: sedimentary environments and lithofacies. *Am. Assoc. Petrol. Geol. Bull.*, 49, 547–600.

Allen, J.R.L. (1978) Deltaic sediments. In: *Encyclopedia of Sedimentology* (Encyclopedia of Earth Science Series; v. 6) (R.W. Fairbridge and J. Bourgeois, Eds.). Dowden, Hutchinson & Ross, Inc., Stroudsburg, PA, pp. 235–240.

Allison, M.A. (1998a) Geologic framework and environmental status of the Ganges-Brahmaputra delta. *J. Coastal Res.*, 14, 826–836.

Allison, M.A. (1998b) Historical changes in the Ganges-Brahmaputra delta front. *J. Coastal Res.*, 14, 1269–1275.

Allison, M.A. and Kepple, E.B. (2001) Modern sediment supply to the lower delta plain of the Ganges-Brahmaputra River in Bangladesh. *Geo-Mar. Lett.*, 21, 66–74.

Allison, M.A., Nittrouer, C.A. and Faria, L.E.C. Jr (1995) Rates and mechanisms of shoreface progradation and retreat downdrift of the Amazon River mouth. *Mar. Geol.*, 125, 373–392.

Allison, M.A., Kuehl, S.A., Martin, T.C. and Hassan, A. (1998) Importance of flood-plain sedimentation for river sediment budgets and terrigenous input to the oceans: insights from the Brahmaputra-Jamuna River. *Geology*, 26, 175–178.

Arbouille, D. and Stanley, D.J. (1991) Late Quaternary evolution of the Burullus lagoon region, north-central Nile delta, Egypt. *Mar. Geol.*, 99, 45–66.

Baker, E.K., Harris, P.T., Keene, J.B. and Short, S.A. (1995) Patterns of sedimentation in the Fly River Delta. In: *Tidal Signatures in Modern and Ancient Sediments* (B.W. Flemming and A. Bartholoma, Eds.). Spec. Publ. Int. Assoc. Sedimentol. no. 24, pp. 193–211.

Bhattacharya, J.P. and Walker, R.G. (1992) Deltas. In: *Facies Models: Response to Sea Level Change* (R.G. Walker and N.P. James, Eds.). Geological Association of Canada, St Johns, NF, pp. 157–177.

Bhattacharya, J.P. and Giosan, L. (2003) Wave-influenced deltas: geomorphological implications for facies reconstruction. *Sedimentology*, 50, 187–210.

Bornhold, B.D., Yang, Z.S., Keller, G.H., Prior, D.B., Wiseman, W.J., Jr, Wang, Q., Wright, L.D., Xu, W.D. and Zhuang, Z.Y. (1986) Sedimentary framework of the modern Huanghe (Yellow River) delta. *Geo-Mar. Lett.*, 6, 77–83.

Boyd, R., Suter, J. and Penland, S. (1989) Relation of sequence stratigraphy to modern sedimentary environments. *Geology*, 17, 926–929.

Boyd, R., Dalrymple, R. and Zaitlin, B.A. (1992) Classification of clastic coastal depositional environments. *Sed. Geol.*, 80, 139–150.

Chen, J., Zhu, H., Dong, Y. and Sun, J. (1985) Development of the Changjiang estuary and its submerged delta. *Cont. Shelf Res.*, 4, 47–56.

Chen, W. and Yang, Z. (1993) Study of subaqueous slope instability of the modern Changjiang River delta. In: *Proceedings of the 1993 PACON China Symposium, Estuarine Coastal Processes* (D. Hopley and Y. Wang, Eds.). Resource Exploration and Management, Shanghai, pp. 133–142.

Chen, X. (1998) Changjiang (Yangtze) River delta, China. *J. Coastal Res.*, 14, 838–858.

Chen, Z. and Stanley, D.J. (1998) Sea-level rise on eastern China's Yangtze delta. *J. Coastal Res.*, 14, 360–366.

Chen, Z., Warne, A.G. and Stanley, D.J. (1992) Late Quaternary evolution of the northwestern Nile Delta between the Rosetta Promontory and Alexandria, Egypt. *J. Coastal Res.*, 8, 527–561.

Coleman, J.M. (1981) *Deltas: Processes of Deposition and Models for Exploration*. Burgess Publishing Co., Minneapolis, MN.

Coleman, J.M. (1988) Dynamic changes and processes in the Mississippi River delta. *Geol. Soc. Am. Bull.*, 100, 999–1015.

Coleman, J.M. and Gagliano, S.M. (1964) Cyclic sedimentation in the Mississippi River deltaic plain. *Gulf Coast Assoc. Geol. Soc. Trans.*, 14, 67–80.

Coleman, J.M. and Roberts, H.H. (1989) Deltaic coastal wetlands. *Geologie en Mijnbouw*, 68, 1–24.

Coleman, J.M. and Wright, L.D. (1975) Modern river deltas: variability of processes and sand bodies. In: *Deltas, Models for Exploration* (M.L. Broussard, Ed.). Houston Geological Society, Houston, TX, pp. 99–149.

Coleman, J.M., Roberts, H.H. and Stone, G.W. (1998) Mississippi River delta: an overview. *J. Coastal Res.*, 14, 698–716.

Coleman, J.M., Roberts, H.H., Murray, S.P. and Salama, M. (1981) Morphology and dynamic sedimentology of the Eastern Nile delta shelf. *Mar. Geol.*, 42, 301–326.

Coutellier, V. and Stanley, D.J. (1987) Late Quaternary stratigraphy and paleogeography of the eastern Nile Delta, Egypt. *Mar. Geol.*, 77, 257–275.

Dalrymple, R.W. (1992) Tidal depositional systems. In: *Facies Models: Response to Sea Level Change* (R.G. Walker and N.P.

James, Eds.). Geological Association of Canada, St Johns, NF, pp. 195–218.

Dalrymple, R.W., Zaitlin, B.A. and Boyd, R.A. (1992) A conceptual model of estuarine sedimentation. *J. Sediment. Petrol.*, 62, 1130–1146.

Dalrymple, R.W., Baker, E.K., Harris, P.T. and Hughes, M.G. (2003) Sedimentology and stratigraphy of a tide-dominated, foreland-basin delta (Fly River, Papua New Guinea). In: *Tropical Deltas of Southeast Asia – Sedimentology, Stratigraphy, and Petroleum Geology* (H.W. Posamentier, F.H. Sidi, H. Darman, D. Nummedal and P. Imbert, Eds.). SEPM Spec. Publ. no. 76, pp. 147–173.

Davis, R.A., Jr. (1992) *Depositional Systems: an Introduction to Sedimentology and Stratigraphy*, 2nd edition. Prentice Hall, Harlow.

Davis, R.A., Jr and Hayes, M.O. (1984) What is a wave-dominated coast? *Mar. Geol.*, 60, 313–329.

DeMaster, D.J., McKee, B.A., Nittrouer, C.A., Qian, J. and Cheng, G. (1985) Rates of sediment accumulation and particle reworking based on radiochemical measurements from continental shelf deposits in the East China Sea. *Cont. Shelf Res.*, 4, 143–158.

El Askary, M.A. and Frihy, O.E. (1986) Depositional phases of Rosetta and Damietta promontories on the Nile delta coast. *J. African Earth Sci.*, 5, 627–633.

Elliott, T. (1986) Deltas. In: *Sedimentary Environments and Facies* (H.G. Reading, Ed.), Blackwell Scientific, Oxford, pp. 113–154.

Fisher, W.L. (1969) Facies characterization of Gulf Coast Basin delta systems, with some Holocene analogues. *Gulf Coast Assoc. Geol. Soc. Trans.*, 19, 239–261.

Frazier, D.E. (1967) Recent deltaic deposits of the Mississippi River: their development and chronology. *Gulf Coast Assoc. Geol. Soc. Trans.*, 17, 287–315.

Frihy, O.E. and Stanley, D.J. (1987) Texture and coarse fraction composition of Nile Delta deposits: facies analysis and stratigraphic correlation. *J. African Earth Sci.*, 7, 237–255.

Galloway, W.E. (1975) Process framework for describing the morphologic and stratigraphic evolution of deltaic depositional systems. In: *Deltas, Models for Exploration* (M.L. Broussard, Ed.). Houston Geological Society, Houston, TX, pp. 87–98.

Galloway, W.E. and Hobday, D.K. (1996) *Terrigenous Clastic Depositional Systems: Applications to Fossil Fuel and Groundwater Resources*, 2nd edition. Springer-Verlag, Berlin.

Gao, S., Li, Y., An, F.T., Wang, Y.M. and Yan, F.H., eds. (1989) *Formation of Yellow River Delta and Sedimentary Environment*. China Science Press, Beijing (in Chinese with English abstract).

Gilbert, G.K. (1885) The topographic features of lake shores. *US Geol. Surv., 5th Ann. Rept*, 69–123.

Gilbert, G.K. (1890) Lake Bonneville. *US Geol. Surv. Monogr*. 1.

Goodbred, S.L., Jr and Kuehl, S.A. (1998) Floodplain processes in the Bengal Basin and the storage of Ganges-Brahmaputra river sediment: an accretion study using ^{137}Cs and ^{210}Pb geochronology. *Sediment. Geol.*, 121, 239–258.

Goodbred, S.L., Jr and Kuehl, S.A. (1999) Holocene and modern sediment budgets for the Ganges-Brahmaputra River system: evidence for highstand dispersal to flood-plain, shelf, and deep-sea depocenters. *Geology*, 27, 559–562.

Goodbred, S.L., Jr and Kuehl, S.A. (2000a) The significance of large sediment supply, active tectonism, and eustasy on margin sequence development: Late Quaternary stratigraphy and evolution of the Ganges-Brahmaputra delta. *Sediment. Geol.*, 133, 227–248.

Goodbred, S.L., Jr and Kuehl, S.A. (2000b) Enormous Ganges-Brahmaputra sediment discharge during the strengthened early Holocene monsoon. *Geology*, 28, 1083–1086.

Gould, H.R. (1970) The Mississippi delta complex. In: *Deltaic Sedimentation: Modern and Ancient* (J.P. Morgan, Ed.). SEPM Spec. Publ. no. 15, pp. 3–30.

Harris, P.T., Baker, E.K., Cole, A.R. and Short, S.A. (1993) A preliminary study of sedimentation in the tidally dominated Fly River Delta, Gulf of Papua. *Cont. Shelf Res.*, 13, 441–472.

Harris, P.T., Pattiaratchi, C.B., Keene, J.B., Dalrymple, R.W., Gardner, J.V., Baker, E.K., Cole, A.R., Mitchell, D., Gibbs, P. and Schroeder, W.W. (1996) Late Quaternary deltaic and carbonate sedimentation in the Gulf of Papua foreland basin: response to sea-level change. *J. Sediment. Res.*, 66, 801–819.

Harris, P.T., Heap, A.D., Bryce, S.M., Porter-Smith, R., Ryan, D.A. and Heggie, D.T. (2003) Classification of Australian clastic coastal depositional environments based upon a quantitative analysis of wave, tidal, and river power. *J. Sediment. Res.*, 72, 858–870.

Haruyama, S. and Phai, V.V. (2002) Coastal change in the Southern Song Hong Delta. *J. Geogr.*, 111, 124–132 (in Japanese with English abstract).

Hayes, M.O. (1979) Barrier island morphology as a function of tidal and wave regime. In: *Barrier Islands from the Gulf of St Lawrence to the Gulf of Mexico* (S.P. Leatherman, Ed.). Academic Press, New York, pp. 1–27.

Hori, K. and Saito, Y. (2003) Morphology and sediments of large river deltas, *J. Geogr.*, 112, 337–359 (in Japanese with English abstract).

Hori, K., Saito, Y., Zhao, Q., Cheng, C., Wang, P., Sato, Y. and Li, C. (2001a) Sedimentary facies and Holocene progradation rates of the Changjiang (Yangtze) delta, China. *Geomorphology*, 41, 233–248.

Hori, K., Saito, Y., Zhao, Q., Cheng, C., Wang, P., Sato, Y. and Li, C. (2001b) Sedimentary facies of the tide-dominated paleo-Changjiang (Yangtze) estuary during the last transgression. *Mar. Geol.*, 177, 331–351.

Hori, K., Saito, Y., Zhao, Q. and Wang, P. (2002) Architecture and evolution of the tide-dominated Changjiang (Yangtze) River delta, China. *Sediment. Geol.*, 146, 249–264.

Hori, K., Tanabe, S., Saito, Y., Haruyama, S., Nguyen, V. and Kitamura, A. (2004) Delta initiation and Holocene sea-level change: example from the Song Hong (Red River) delta, Vietnam. *Sediment. Geol.*, 164, 237–249.

Hovius, N. (1998) Controls on sediment supply by large rivers. In: *Relative Role of Eustasy, Climate, and Tectonism in Continental Rocks* (K.W. Shanley and P.J. McCabe, Eds.). SEPM Spec. Publ. no. 59, pp. 3–16.

Jaeger, J.N. and Nittrouer, C.A. (1995) Tidal controls on the formation of fine-scale sedimentary strata near the Amazon river mouth. *Mar. Geol.*, 125, 259–281.

Jones, L.S. and Schumm, S.A. (1999) Causes of avulsion: an overview. In: *Fluvial Sedimentology VI* (N.D. Smith and J. Rogers, Eds.). Spec. Publ. Int. Assoc. Sedimentol. no. 28, pp. 171–178.

Keller, G.H. and Prior, D.B., eds. (1986) Huanghe (Yellow River) Delta. *Geo-Mar. Lett.*, 6, 63–120.

Kolb, C.R. and van Lopik, J.R. (1958) *Geology of the Mississippi River deltaic plain, southeastern Louisiana*. US Army Engineer Waterways Experiment Sta., Vicksburg, MS, Tech. Rept.

Kosters, E.C. (1989) Organic-clastic facies relationships and chronostratigraphy of the Barataria interlobe basin, Mississippi delta plain. *J. Sediment. Petrol.*, 59, 98–113.

Kosters, E.C. and Suter, J.R. (1993) Facies relationships and systems tracts in the late Holocene Mississippi delta plain. *J. Sediment. Petrol.*, 63, 727–733.

Kudrass, H.R., Michels, K.H., Wiedicke, M. and Suckow, A. (1998) Cyclones and tides as feeders of a submarine canyon off Bangladesh. *Geology*, 26, 715–718.

Kuehl, S.A., Nittrouer, C.A. and DeMaster, D.J. (1982) Modern sediment accumulation and strata formation on the Amazon continental shelf. *Mar. Geol.*, 49, 279–300.

Kuehl, S.A., Nittrouer, C.A., DeMaster, D.J. and Curtin, T.B. (1985) An overview of sedimentation on the Amazon continental shelf. *Geo-Mar. Lett.*, 4, 207–210.

Kuehl, S.A., DeMaster, D.J. and Nittrouer, C.A. (1986) Nature of sediment accumulation on the Amazon continental shelf. *Cont. Shelf Res.*, 6, 209–225.

Kuehl, S.A., Hariu, T.M. and Moore, W.S. (1989) Shelf sedimentation off the Ganges-Brahmaputra river system: evidence for sediment bypassing to the Bengal fan. *Geology*, 17, 1132–1135.

Kuehl, S.A., Nittrouer, C.A., Allison, M.A., Faria, L.E.C., Dukat, D.A., Jaeger, J.M., Pacioni, T.D., Figueiredo, A.G. and Underkoffler, E.C. (1996) Sediment deposition, accumulation, and seabed dynamics in an energetic fine-grained coastal environment. *Cont. Shelf Res.*, 16, 787–815.

Kuehl, S.A., Levy, B.M., Moore, W.S. and Allison, M.A. (1997) Subaqueous delta of the Ganges-Brahmaputra river system. *Mar. Geol.*, 144, 81–96.

Li, C., Wang, P., Fan, D., Dang, B. and Li, T. (2000) Open coast intertidal deposits and their preservation potential: a case study from east-central China. *Sedimentology* 47, 1039–1051.

Liu, C. and Walker, H.J. (1989) Sedimentary characteristics of cheniers and the formation of the chenier plains of East China. *J. Coastal Res.*, 5, 353–368.

Lowrie, A. and Hamiter, R. (1995) Fifth and sixth order eustatic events during Holocene (fourth order) highstand influencing Mississippi delta-lobe switching. In: *Holocene Cycles: Climate, Sea Levels, and Sedimentation* (C.W. Finkl, Jr, Ed.). J. Coastal Res., Spec. Issue no. 17, 225–229.

Masuda, F. and Saito, Y. (1995) Characteristics of sedimentary facies and strata formation during progradation. *Gekkan Chikyu*, 17, 671–674 (in Japanese).

Mathers, S. and Zalasiewicz, J. (1999) Holocene sedimentary architecture of the Red River delta, Vietnam. *J. Coastal Res.*, 15, 314–325.

McKee, B.A., Nittrouer, C.A. and DeMaster, D.J. (1983) Concepts of sediment deposition and accumulation applied to the continental shelf near the mouth of the Yangtze River. *Geology*, 11, 631–633.

Meade, R.H. (1994) Suspended sediments of the modern Amazon and Orinoco Rivers. *Quat. Int.*, 21, 29–39.

Miall, A.D. (1984) Deltas. In: *Facies Models* (R.G. Walker, Ed.), 2nd edition. Geoscience Canada, Reprint Series 1, Toronto, ON, pp. 105–118.

Michels, K.H., Kudrass, H.R., Hubscher, C., Suckow, A. and Wiedicke, M. (1998) The submarine delta of the Ganges-Brahmaputra: cyclone-dominated sedimentation patterns. *Mar. Geol.*, 149, 133–154.

Middleton, G.V. (1991) A short historical review of clastic tidal sedimentology. In: *Clastic Tidal Sedimentology* (D.G. Smith, G.E. Reinson, B.A. Zaitlin and R.A. Rahmani, Eds.). Can. Soc. Petrol. Geol., Memoir 16, ix–xv.

Milliman, J.D. (1991) Flux and fate of fluvial sediment and water in coastal seas. In: *Ocean Margin Processes in Global Change* (R.F.C. Mantoura, J.-M. Martin and R. Wollast, Eds.). John Wiley & Sons, Ltd, Chichester, pp. 69–89.

Milliman, J.D. and Jin, Q., eds. (1985) Sediment Dynamics of the Changjiang Estuary and the Adjacent East China Sea. *Cont. Shelf Res.*, 4, 1–251.

Milliman, J.D. and Meade, R.H. (1983) World-wide delivery of river sediment to the oceans. *J. Geol.*, 91, 1–21.

Milliman, J.D. and Syvitski, J.P.M. (1992) Geomorphic/tectonic control of sediment discharge to the oceans: the importance of small mountain rivers. *J. Geol.*, 100, 525–544.

Milliman, J.D., Qin, Y.S., Ren, M.-E. and Saito, Y. (1987) Man's influence on the erosion and transport of sediment by Asian rivers: the Yellow River (Huanghe) example. *J. Geol.*, 95, 751–762.

Morgan, J.P. (1970) Depositional processes and products in the deltaic environment. In: *Deltaic Sedimentation: Modern and Ancient* (J.P. Morgan, Ed.). SEPM Spec. Publ. no. 15, pp. 31–47.

Nakada, M. and Okuno, J. (2000) Holocene sea-level changes and glacio-hydroisostasy. *Bull. Geol. Survey Japan*, 51, 269.

Nakada, M., Yonekura, N. and Lambeck, K. (1991) Late Pleistocene and Holocene sea-level changes in Japan: implications for tectonic histories and mantle rheology. *Palaeogeogr., Palaeoclimatol., Palaeoecol.*, 85, 107–122.

Nakai, N. and Nakamura, T. (1988) *Radiocarbon dating*. Mem. Geol. Soc. Japan no. 29, pp. 235–252 (in Japanese with English abstract).

Nittrouer, C.A. and DeMaster, D.J., eds. (1986) Sedimentary Processes on the Amazon Continental Shelf. *Cont. Shelf Res.*, 6, 1–379.

Nittrouer, C.A. and Kuehl, S.A., eds. (1995) Geological Significance of Sediment Transport and Accumulation on the Amazon Continental Shelf. *Mar. Geol.*, 125, 175–399.

Nittrouer, C.A. and DeMaster, D.J., eds. (1996) Oceanography of the Amazon Continental Shelf. *Cont. Shelf Res.*, 16, 551–841.

Nittrouer, C.A., Kuehl, S.A., DeMaster, D.J. and Kowssmann, R.O. (1986) The deltaic nature of Amazon shelf sedimentation. *Geol. Soc. Am. Bull.*, 97, 444–458.

Nguyen, V.L., Ta, T.K.O. and Tateishi, M. (2000) Late Holocene depositional environments and coastal evolution of the Mekong River Delta, Southern Vietnam. *J. Asian Earth Sci.*, 18, 427–439.

Orton, G.J. and Reading, H.G. (1993) Variability of deltaic processes in terms of sediment supply, with particular emphasis on grain size. *Sedimentology*, 40, 475–512.

Penland, S., Boyd, R. and Suter, J.R. (1988) Transgressive depositional systems of the Mississippi delta plain: a model for barrier shoreline and shelf sand development. *J. Sediment. Petrol.*, 58, 932–949.

Prior, D.B., Yang, Z.S., Bornhold, B.D., Keller, G.H., Lin, Z.H., Wiseman, W.J., Jr, Wright, L.D. and Lin, T.C. (1986) The subaqueous delta of the modern Huanghe (Yellow River). *Geo-Mar. Lett.*, 6, 67–75.

Ren, M.-E. and Shi, Y.L. (1986) Sediment discharge of the Yellow River (China) and its effect on the sedimentation of the Bohai and the Yellow Sea. *Cont. Shelf Res.*, 6, 785–810.

Roberts, H.H. (1997) Dynamic changes of the Holocene Mississippi River delta plain: the delta cycle. *J. Coastal Res.*, 13, 605–627.

Roberts, H.H., Bailey, A. and Kuecher, G.J. (1994) Subsidence in the Mississippi River delta – important influences of valley filling by cyclic deposition, primary consolidation phenomena, and early diagenesis. *Gulf Coast Assoc. Geol. Soc. Trans.*, 44, 619–629.

Saito, Y. (1995) High-resolution sequence stratigraphy of an incised-valley fill in a wave- and fluvial-dominated setting: latest Pleistocene–Holocene examples from the Kanto Plains of central Japan. In: *Sequence Stratigraphy: Toward a New Dynamic Stratigraphy* (Y. Saito, K. Hoyanagi and M. Ito, Eds.). Mem. Geol. Soc. Japan no. 45, pp. 76–100.

Saito, Y. (2001) Deltas in Southeast and East Asia: their evolution and current problems. In: *Global Change and Asia Pacific Coast* (N. Mimura and H. Yokoki, Eds.). Proceedings of APN/SURVAS/LOICZ Joint Conference on Coastal Impacts of Climate Change and Adaptation in the Asia–Pacific Region: APN & Ibaraki University, pp. 185–191.

Saito, Y. and Yang, Z. (1994) The Huanghe River: its water discharge, sediment discharge, and sediment budget. *J. Sed. Soc. Japan*, no. 40, 7–17.

Saito, Y., Ikehara, K., Katayama, H., Matsumoto, E. and Yang, Z. (1994) Course shift and sediment discharge changes of the Huanghe recorded in sediments of the East China Sea. *Chishitsu News*, no. 476, 8–16 (in Japanese).

Saito, Y., Wei, H., Zhou, Y., Nishimura, A., Sato, Y. and Yokota, S. (2000) Delta progradation and chenier formation in the Huanghe (Yellow River) Delta, China. *J. Asian Earth Sci.*, 18, 489–497.

Saito, Y., Yang, Z.S. and Hori, K. (2001) The Huanghe (Yellow River) and Changjiang (Yangtze River) deltas: a review on their characteristics, evolution and sediment discharge during the Holocene. *Geomorphology*, 41, 219–231.

Scruton, P.C. (1960) Delta building and the deltaic sequence. In: *Recent Sediments, Northwest Gulf of Mexico* (F.P. Shepard and T.H. van Andel, Eds.). American Association of Petroleum Geologists, Tulsa, OK, pp. 82–102.

Segall, M.P. and Kuehl, S.A. (1994) Sedimentary structures on the Bengal shelf: a multi-scale approach to sedimentary fabric interpretation. *Sediment. Geol.*, 93, 165–180.

Sestini, G. (1989) Nile Delta: a review of depositional environments and geological history. In: *Deltas: Sites and Traps for Fossil Fuels* (M.K.G. Whateley and K.T. Pickering, Eds.). Geol. Soc. Spec. Publ. no. 41, pp. 99–127.

Smith, N.D. (2003) Avulsion. In: *Encyclopedia of Sediments and Sedimentary Rocks* (G.V. Middleton, Ed.). Kluwer Academic Publishers, Dordrecht, pp. 34–36.

Stanley, D.J. (2001) Dating modern deltas: progress, problems, and prognostics. *Ann. Rev. Earth Planet Sci.*, 29, 257–294.

Stanley, D.J. and Chen, Z. (2000) Radiocarbon dates in China's Holocene Yangtze delta: record of sediment storage and reworking, not timing of deposition. *J. Coastal Res.*, 16, 1126–1132.

Stanley, D.J. and Hait, A.K. (2000) Deltas, radiocarbon dating, and measurements of sediment storage and subsidence. *Geology*, 28, 295–298.

Stanley, D.J. and Warne, A.G. (1993) Nile Delta: recent geological evolution and human impact. *Science*, 260, 628–634.

Stanley, D.J. and Warne, A.G. (1994) Worldwide initiation of Holocene marine deltas by deceleration of sea-level rise. *Science*, 265, 228–231.

Stanley, D.J. and Warne, A.G. (1998) Nile Delta in its destruction phase. *J. Coastal Res.*, 14, 794–825.

Stouthamer, E. (2004) Avulsion. In: *Encyclopedia of Geomorphology* (A.S. Goudie, Ed.), Volume 1, Routledge, Cambridge, p. 44.

Suter, J.R. (1994) Deltaic coasts. In: *Coastal Evolution: Late Quaternary Shoreline Morphodynamics* (R.W.G. Carter and C.D. Woodroffe, Eds.). Cambridge University Press, Cambridge, pp. 87–120.

Syvitski, J.P.M. (2001) Supply and flux of sediment along hydrological pathways: anthropogenic influences at the global scale. *LOICZ News Letter* no. 20, 4–7.

Syvitski, J.P.M. (2003) Supply and flux of sediment along hydrological pathways: research for the 21st century. *Global and Planetary Change* 39, 1–11.

Ta, T.K.O., Nguyen, V.L., Tateishi, M., Kobayashi, I. and Saito, Y. (2001) Sedimentary facies, diatom and foraminifer assemblages in a late Pleistocene–Holocene incised-valley sequence from the Mekong River delta, Bentre Province, southern Vietnam: the BT2 core. *J. Asian Earth Sci.*, 20, 83–94.

Ta, T.K.O., Nguyen, V.L., Tateishi, M., Kobayashi, I. and Saito, Y. (2002a) Sediment facies and Late Holocene progradation of the Mekong River Delta in Bentre Province, southern Vietnam: an example of evolution from a tide-dominated to a tide- and wave-dominated delta. *Sediment. Geol.*, 152, 313–325.

Ta, T.K.O., Nguyen, V.L., Tateishi, M., Kobayashi, I., Tanabe, S. and Saito, Y. (2002b) Holocene delta evolution and sediment discharge of the Mekong River, southern Vietnam. *Quat. Sci. Rev.*, 21, 1807–1819.

Ta, T.K.O., Nguyen, V.L., Tateishi, M., Kobayashi, I. and Saito, Y. (2005) Holocene delta evolution and depositional models of the Mekong River Delta, southern Vietnam. In: *River Deltas – Concepts, Models and Examples* (L. Giosan and J.P. Bhattacharya, Eds.). SEPM Spec. Publ., no. 83, pp. 453–466.

Tanabe, S., Hori, K., Saito, Y., Haruyama, S., Doanh, L.Q., Sato, Y. and Hiraide, S. (2003a) Sedimentary facies and radiocarbon dates of the Nam Dinh-1 core from the Song Hong (Red River) delta, Vietnam. *J. Asian Earth Sci.*, 21, 503–513.

Tanabe, S., Hori, K., Saito, Y., Haruyama, S., Vu, V.P. and Kitamura, A. (2003b) Song Hong (Red River) delta evolution related to millennium-scale Holocene sea-level changes. *Quat. Sci. Rev.*, 22, 2345–2361.

Tanabe, S., Saito, Y., Sato, Y., Suzuki, Y., Sinsakul, S., Tiyapairach, N. and Chaimanee, N. (2003c) Stratigraphy and Holocene evolution of the mud-dominated Chao Phraya delta, Thailand. *Quat. Sci. Rev.*, 22, 789–807.

Tanabe, S., Ta, T.K.O., Nguyen, V.L., Tateishi, M., Kobayashi, I. and Saito, Y. (2003d) Delta evolution model inferred from the Mekong Delta, southern Vietnam. In: *Tropical Deltas of Southeast Asia – Sedimentology, Stratigraphy, and Petroleum Geology* (H.W. Posamentier, F.H. Sidi, H. Darman, D. Nummedal and P. Imbert, Eds.). SEPM Spec. Publ. no. 76, pp. 175–188.

Thomas, D.S.G. and Goudie, A., Eds. (2000) *The Dictionary of Physical Geography*, 3rd edition. Blackwell, Oxford.

Törnqvist, T.E., Kidder, T.R., Autin, W.J., van der Borg, K., de Jong, A.F.M., Klerks, C.J.W., Snijders, E.M.A., Storms, J.E.A., van Dam, R.L. and Wiemann, M.C. (1996) A revised chronology for Mississippi River subdeltas. *Science*, 273, 1693–1696.

Umitsu, M. (1987) Late Quaternary sedimentary environment and landform evolution in the Bengal Lowland. *Geogr. Rev. Japan*, 60B, 164–178.

Umitsu, M. (2001) Influence of sea-level rise on deltas in Asia. In: *Sea-Level Rise and Asian Coast* (M. Umitsu and Y. Hirai, Eds.). Kokon, Tokyo, pp. 16–34 (in Japanese).

van Andel, T.H. (1967) The Orinoco delta. *J. Sediment. Petrol.*, 37, 297–310.

Vörösmarty, C.J., Meybeck, M., Fekete, B. and Sharma, K. (1997) The potential impact of neo-Castorization on sediment transport by the global network of rivers. Human impact on erosion and sedimentation. *IAHS Publication*, 245, 261–273.

Walker, R.G. (1992) Facies, facies models and modern stratigraphic concepts. In: *Facies Models: Response to Sea Level Change* (R.G. Walker and N.P. James, Eds.). Geological Association of Canada, St Johns, NF, pp. 1–14.

Walker, R.G. (1995) *Clastic sedimentology seminar*. Japan National Oil Corporation Technology Research Center, Chiba, pp. 21–42.

Walsh, J.P. and Nittrouer, C.A. (2004) Mangrove-bank sedimentation in a meso-tidal environment with large sediment supply, Gulf of Papua. *Mar. Geol.*, 208, 225–248.

Wang, J., Guo, X., Xu, S., Li, P. and Li, C. (1981) Evolution of the Holocene Changjiang delta. *Acta Geol. Sin.* 55, 67–81.

Warne, A.G. and Stanley, D.J. (1993) Archaeology to refine Holocene subsidence rates along the Nile delta margin, Egypt. *Geology*, 21, 715–718.

Warne, A.G. and Stanley, D.J. (1995) Sea-level change as a critical factor in development of basin margin sequences: new evidence from Late Quaternary record. In: *Holocene Cycles: Climate, Sea Levels, and Sedimentation* (C.W. Finkl, Jr, Ed.). *J. Coastal Res.*, Spec. Issue no. 17, 231–240.

Warne, A.G., Meade, R.H., White, W.A., Guevara, E.H., Gibeaut, J., Smyth, R.C., Aslan, A. and Tremblay, T. (2002) Regional controls on geomorphology, hydrology, and ecosystem integrity in the Orinoco Delta, Venezuela. *Geomorphology*, 44, 273–307.

Weber, M.E., Wiedicke, M.H., Kudrass, H.R., Hubscher, C. and Erlenkeuser, H. (1997) Active growth of the Bengal Fan during sea-level rise and highstand. *Geology*, 25, 315–318.

Woodroffe, C.D. (2000) Deltaic and estuarine environments and their Late Quaternary dynamics on the Sunda and Sahul shelves. *J. Asian Earth Sci.*, 18, 393–413.

Wright, L.D. (1982) Deltas. In: *The Encyclopedia of Beaches and Coastal Environments* (M.L. Schwartz, Ed.). Hutchinson Ross Publishing Co., Stroudsburg, PA, pp. 358–369.

Wright, L.D. (1985) River Deltas. In: *Coastal Sedimentary Environments* (R.A. Davis, Jr, Ed.), 2nd revised expanded edition. Springer-Verlag, Berlin, pp. 1–76.

Xue, C. (1993) Historical changes in the Yellow River delta, China. *Mar. Geol.*, 113, 321–329.

Yan, Q. and Xu, S., eds. (1987) *The Recent Yangtze Delta Deposits*. East China Normal University Press, Shanghai (in Chinese with English abstract).

Yan, Q., Xu, S. and Shao, X. (1989) Holocene cheniers in the Yangtze delta, China. *Mar. Geol.*, 90, 337–343.

Yang, Z.S., Milliman, J.D., Galler, J., Liu, J.P. and Sun, X.G. (1998) Yellow River's water and sediment discharge decreasing steadily. *EOS, Trans. Am. Geophys. Union*, 79, 589–592.

7

Sedimentology and Stratigraphy of Large River Deposits: Recognition in the Ancient Record, and Distinction from 'Incised Valley Fills'

Christopher R. Fielding

Department of Geosciences, 214 Bessey Hall, University of Nebraska-Lincoln, NE 68588-0340, USA

7.1 INTRODUCTION

The deposits of large rivers have been of interest to geologists for some time, although studies of the ancient have perhaps suffered from a lack of substantial data on which to base interpretations. The importance of big rivers in delivering sediment to Earth's oceans, and in depositing substantial continental, deltaic, slope and base-of-slope sediments, was emphasized by Audley-Charles *et al*. (1977) and Potter (1978). Both of these landmark papers also emphasized the role of regional plate tectonics and local structure in controlling the location, size and longevity of the World's big rivers. If these parameters can be predicted from the statistics of modern rivers, such information might be valuable in evaluating the rock record, in particular in the exploration for resources of oil, gas and water. Predictive geological tools are likely to be all the more valuable the older the rocks are, and thus the more likely it is that original drainage basin geometry has been modified and partially destroyed by tectonic upheaval.

Potter (1978) defined a 'big river' as having one or more of the following: (1) a large drainage basin; (2) a long course; (3) a large volume of sediment in transport; (4) a large fluid discharge (Figure 7.1). From these criteria, it follows that such rivers will also be characterized by having a large cross-sectional area, at least in downstream portions. The big rivers of the World drain a disproportionately large area of the present-day continents, and supply a disproportionately high percentage of suspended sediment to the oceans (Table 7.1). Potter (1978) reasoned that if climates and the hypsometry of the continents have occupied similar ranges over geological time, then these relationships should also characterize the geological record. In the light of recent research, however, it is evident that climates and the distribution of climates have varied considerably over geological time, as have the areas and topographic profiles of the continents. Furthermore, there is now a greater appreciation of the coupling between tectonics and climate via the construction of mountain ranges. Also, before the advent of modern remote-sensing technologies, data on the fluid and solids discharge from the World's big rivers were relatively scarce, because of the difficulties involved in obtaining representative samples without danger to the samplers. Accordingly, Potter (1978) used drainage area and river length as principal variables in characterizing big rivers. More recent analyses (e.g. Milliman and Meade, 1983; Milliman and Syvitski, 1992; Hovius, 1998) incorporate a larger, if still incomplete, database on fluid and solids discharge.

The large rivers of the modern World are also those that transport the highest volumes of sediment to the oceans

Large Rivers: Geomorphology and Management, Edited by A. Gupta

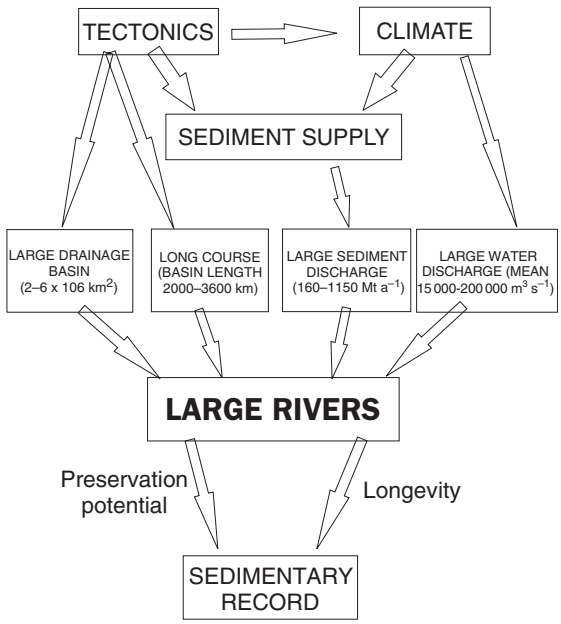

Figure 7.1 Conceptual framework for large rivers and their deposits. Statistics from Hovius (1998)

(Table 7.1, and see data tabulated by Hovius, 1998). The role of sediment supply as an independent variable in determining stratigraphic architecture has been underestimated in the recent past. Renewed research on the inter-relationships among climate, sea-level change and sediment supply has led to the recognition of complex feedbacks (see review by Blum and Törnqvist, 2000). Hovius (1998) has shown that sediment yield from continental catchments is primarily a function of the erosion rate in the source area. Hovius (1998) determined five primary controls on erosion/denudation rate: drainage area, maximum height of catchment, specific runoff, mean annual temperature and temperature range. Milliman and Syvitski (1992) and Mulder and Syvitski (1996), on the basis of similar analyses, derived statistically significant relationships between discharge and basin area, and between sediment load and a basin area/slope function. An additional factor that is difficult to quantify is the lithology of material constituting the source of sediment in a river system, specifically the erodibility of the substrate. A good example of this control is given by the Huanghe (Yellow River), which derives much of its large suspended sediment load from the extensive loess plateau of central China (Xu, 2002).

From the above, it will be evident that the World's largest rivers should have their headwaters in topographically elevated, and likely tectonically active, mountain ranges, and indeed most do. The highest potential for the

Table 7.1 Selected properties of some of the World's large rivers (with ranking up to 10 values in parentheses)

River	Drainage area (km^2)	Basin length (km)	Suspended sediment[a] ($Mt\,a^{-1}$)	Mean discharge ($m^3\,s^{-1}$)
Amazon	6 150 000 (1)	3310 (2)	1150 (1)	200 000 (1)
Amur	1 855 000 (10)	2455 (7)	52 (–)	10 300 (–)
Brahmaputra	610 000 (–)	1270 (–)	520 (3)	19 300 (5)
Congo	3 700 000 (2)	2020 (–)	33 (–)	40 900 (2)
Ganga	980 000 (–)	1560 (–)	524 (2)	11 600 (–)
Godavari	287 000 (–)	920 (–)	170 (9)	2 920 (–)
Indus	960 000 (–)	1610 (–)	250 (7)	7 610 (–)
Irrawaddy	410 000 (–)	1420 (–)	260 (6)	13 600 (–)
Lena	2 430 000 (8)	2525 (6)	12 (–)	16 200 (9)
Mackenzie	1 488 000 (–)	2270 (8)	125 (–)	9 830 (–)
Magdalena	260 000 (–)	1050 (–)	220 (8)	6 980 (–)
Mekong	810 000 (–)	2950 (3)	160 (10)	14 900 (10)
Mississippi	3 344 000 (3)	2220 (10)	400 (5)	18 400 (6)
Nile	2 715 000 (4)	3600 (1)	125 (–)	317 (–)
Ob	2 500 000 (7)	2530 (5)	16 (–)	12 200 (–)
Orinoco	945 000 (–)	1550 (–)	150 (–)	34 900 (3)
Parana	2 600 000 (5)	2175 (–)	112 (–)	18 000 (7)
Yangtze	1 940 000 (9)	2730 (4)	480 (4)	28 500 (4)
Yenisey	2 580 000 (6)	2250 (9)	13 (–)	17 800 (8)

[a] Mean annual value.
Date from Hovius (1998).

development of large rivers lies marginal to contractional orogenic belts, the next highest in continental rift zones, then older orogens and lastly stable cratons (see Hovius, 1998, Figure 4, for a succinct summary). It follows, therefore, that knowledge of the tectonic setting and palaeogeography of an ancient drainage basin might provide some predictive opportunities to geologists seeking natural resources reservoired in fluvial sandstones. That said, recent field and modelling studies have suggested that long-term stability in sediment export from drainage basins may be achieved in some circumstances, have attributed this to the storage and remobilization of alluvium within the drainage basin, and have suggested that this phenomenon may buffer drainage systems against environmental change (Phillips, 2003). Sediment storage during periods of excess yield might be expected to facilitate the preservation of fluvial channel bodies, all the more so in larger basins where there is a greater capacity for storage (e.g. Allison *et al*., 1998; Goodbred and Kuehl, 1998). The issue of preservation potential is complex, since a variety of studies have shown this to be a function of the long-term aggradation-incision history and avulsion frequency of a system (e.g. Mackey and Bridge, 1995), factors that are essentially scale-invariant. Nonetheless, preservation of the deposits of a large river system will be more likely the longer-lived the system (see below).

Mulder and Syvitski (1996) proposed that during glacio-eustatic lowstands of sea-level, continental drainage systems will become reorganized into fewer, larger systems that merge onto the exposed continental shelf into giant river systems. They also cite the merged palaeo-drainage systems of northwest Europe during the Pleistocene glaciations as an example of this phenomenon. Many case studies of Quaternary river systems, such as those on the Gulf Coast of the USA, however, have emphasized channel incision and extension rather than coalescence (e.g. Suter and Berryhill, 1985; Anderson *et al*., 1996), and these processes have become embedded in recent sequence stratigraphic models (e.g. Van Wagoner *et al*., 1990; Posamentier and Allen, 1999). The term 'vacuum cleaner model' has been coined to describe the situation where sediment supply is derived from distal portions of the drainage basin by the excavation of a valley system (Blum and Törnqvist, 2000). However, Blum and Törnqvist (2000) argue that many major river systems of the Quaternary World did not behave in this manner during the Pleistocene glacio-eustatic cycles of sea-level change. Rather, they exhibited a more complex record of aggradation and degradation (Blum and Törnqvist, 2000). These rivers conform more to a 'conveyor belt model', whereby sediment is delivered from the entire drainage basin and does not necessitate excavation of a deep, extensive valley. This alternative is also supported by a variety of modelling studies, many of which emphasize the effects of varying depositional gradient (Summerfield, 1985; Leeder and Stewart, 1996; Talling, 1998; Paola, 2000; van Heijst and Postma, 2001; Meijer, 2002).

These apparent disparities between glacio-eustatic sea-level cyclicity and fluvial response may result from the variability in system response to regional climate change. Leeder *et al*. (1998) show that a single cycle of global climate change may produce differing responses, for instance in sediment yield, in different regions of the World. Leeder *et al*. (1998) also emphasize the distinction between nonuniform sediment supply in spatial terms and unsteady sediment supply on a temporal frame. Both factors may complicate patterns of fluvial response to climate change, specifically in terms of the resulting stratigraphic record. Indeed, Allen and Hovius (1998) point out that in tectonically active hinterlands where sediment flux is controlled by landslides, the rate of tectonic uplift is the principal control, independent of climate. It is likely, then, that sediment supply to big river systems is a complex function that varies spatially and temporally in response to a variety of stimuli.

Longevity of river courses is another factor relevant to the geological evaluation of ancient big rivers. Many of the present World's big rivers are remarkably long-lived, having persisted through major changes in climate, tectonic activity and consequent changes in physiography. Potter (1978) cites the Mississippi as a classical example of such a system that occupied a similarly located and oriented basin for over 300 Ma. The Mississippi may be an extreme example, but there are numerous cases of river systems active over at least tens of millions of years (e.g. Gulf Coast USA rivers: Fisher and McGowen, 1967; Galloway and Hobday, 1996; Amazon: Putzer, 1984; Ganga-Brahmaputra: Lindsay *et al*., 1991; Vaal-Orange: Jacob *et al*., 1999). Many, if not most, of these long-lived systems are located along, and oriented parallel to, major fractures in the continental crust that have been reactivated at intervals throughout geological time (e.g. Youssef, 1968, and see Potter, 1978). Such long-lived fluvial systems are also well-represented in the geological record, for example in the Carboniferous of North America (Gibling *et al*., 1992; Archer and Greb, 1995), and northern Britain (Guion and Fielding, 1988; Leeder, 1988; Rippon, 1996).

This chapter draws comparisons between big river systems in the modern and those from the ancient, in terms of external geometry and dimensions, internal lithology, sedimentary structure and architecture. It examines issues of scale, problems of diagnosis, confusion in the literature over the distinction between channel deposits of large rivers and 'incised valley fills', and considers predictive

opportunities for resource exploration. The chapter draws the conclusion that many large fluvial sediment bodies in the rock record that have recently been interpreted or reinterpreted as incised valley fills may be trunk channel fills of large rivers formed independently of forcing through base-level change.

7.2 SEDIMENTOLOGY AND STRATIGRAPHY OF MODERN BIG RIVERS

Data on the distribution of lithofacies, and their stacking arrangements, in modern large rivers is still not abundant, despite the increasing research over the past two decades. The understanding of modern big river stratigraphy clearly lags behind geomorphological and hydrological studies, and is notably insufficient compared with the many accounts of ancient counterparts already in the literature (see review by Miall, 1996). The paucity of data has been partly a logistical problem, in that acquisition of data from large rivers in high flow stage has until recently been virtually impossible without considerable danger to personnel and equipment. Accordingly, sedimentologists have found it more convenient, time-effective and safer to focus on smaller fluvial systems. Techniques for acquiring subsurface geophysical data are restricted either to waterborne seismic reflection methods, which cannot typically resolve the fine detail of subsurface stratification, or to largely land-based methods such as ground-penetrating radar and electrical resistivity. Rivers with extremely variable discharges, therefore, are best-suited to geophysical investigations, because their beds are at least partially exposed at low stage. In the last 10 years, however, increasing use has been made of instruments such as the Acoustic Doppler Current Profiler (ADCP) in combination with high-resolution echo-sounders and Differential Global Positioning System (DGPS) to derive detailed measurements of three-dimensional flow structure, suspended sediment concentration and bed form in certain large rivers (e.g. McLelland *et al*., 1999; Ashworth *et al*., 2000).

The most obvious characteristic of big rivers is, of course, their dimensions, as well as those of resulting sediment bodies. Bristow (1987) estimated that the sand body formed by the modern Brahmaputra River will be 40 m thick and 20 km wide, and that of the Amazon is likely to be comparable in size (Mertes *et al*., 1996; Vital *et al*., 1998; Archer, 2005). Many other rivers fall in the same order of magnitude as these two examples. Massive changes in discharge, flow depth and bed condition are recorded from large rivers. For example, changes in water surface elevation of up to 8 m are common in the Brahmaputra/Jamuna River of Bangladesh (Coleman, 1969; Bristow, 1987; Ashworth *et al*., 2000), and up to 12 m in the Amazon (Mertes *et al*., 1996; Archer, 2005). Although some large modern rivers (such as the Amazon) occupy bedrock-floored trenches perhaps scoured at times of lowered sea-level, it is important to note that these are clearly scaled to modern discharge levels. They are, furthermore, morphologically distinct from larger-scale 'incised valleys' formed during sea-level lowstand, and from braidplains formed by lateral amalgamation of rivers, such as the Canterbury Plains of New Zealand: (e.g. Leckie, 1994, 2003; Browne and Naish, 2003). Those engaged in interpreting the rock record must be aware of these distinctions.

Modern large rivers span the spectrum of planform type, with many examples of each major style. The question then arises: is the stratigraphy of a big river deposit simply a scaled-up version of that of a smaller planform equivalent? Since the geomorphic elements of big rivers are similar to those of smaller rivers, it might be tempting to assume that the resulting stratigraphies will also be similar. A review of the (admittedly limited) literature on the topic of stratigraphy of modern big rivers suggests that there are few differences not accounted for by simple comparison (Figure 7.2). Studies of large rivers and their sediments have determined that the hierarchy of depositional and geomorphic elements operates similarly to smaller rivers. Scale invariance in geomorphological properties and some sedimentological characteristics has recently been shown for braided rivers by Best *et al*. (2003) and Sambrook-Smith *et al*. (2005). At a process-bedform level, scale invariance is also demonstrated from studies of catastrophic confined outflows such as the Quaternary deposits of the Channelled Scablands of the western USA (Baker, 1973) and of the Altai Mountains of Siberia (Carling, 1996).

In the large, braided Brahmaputra/Jamuna River of Bangladesh, bedforms (notably dunes) are scaled to water depth in local, 'third-order' channels, bars are scaled to the width of major anabranches, and major, metastable mid-channel islands are scaled to the height of bankfull discharge and the width of the primary channel (Thorne *et al*., 1993). Bedforms can therefore be considered as 'mesoforms', bars as 'macroforms' and larger features such as metastable islands as 'megaforms' in the classification scheme of Jackson (1975) and Church and Jones (1982). Features that can be similarly assigned to a hierarchical scale classification have also been observed in large, low sinuosity, meandering and anastomosing systems. Ashley (1990) noted that subaqueous dunes (including so-called 'megaripples') may form over a variety of scale, and in large rivers may reach several metres in height as they are scaled to water depth (Julien and Klaassen, 1995; Leclair

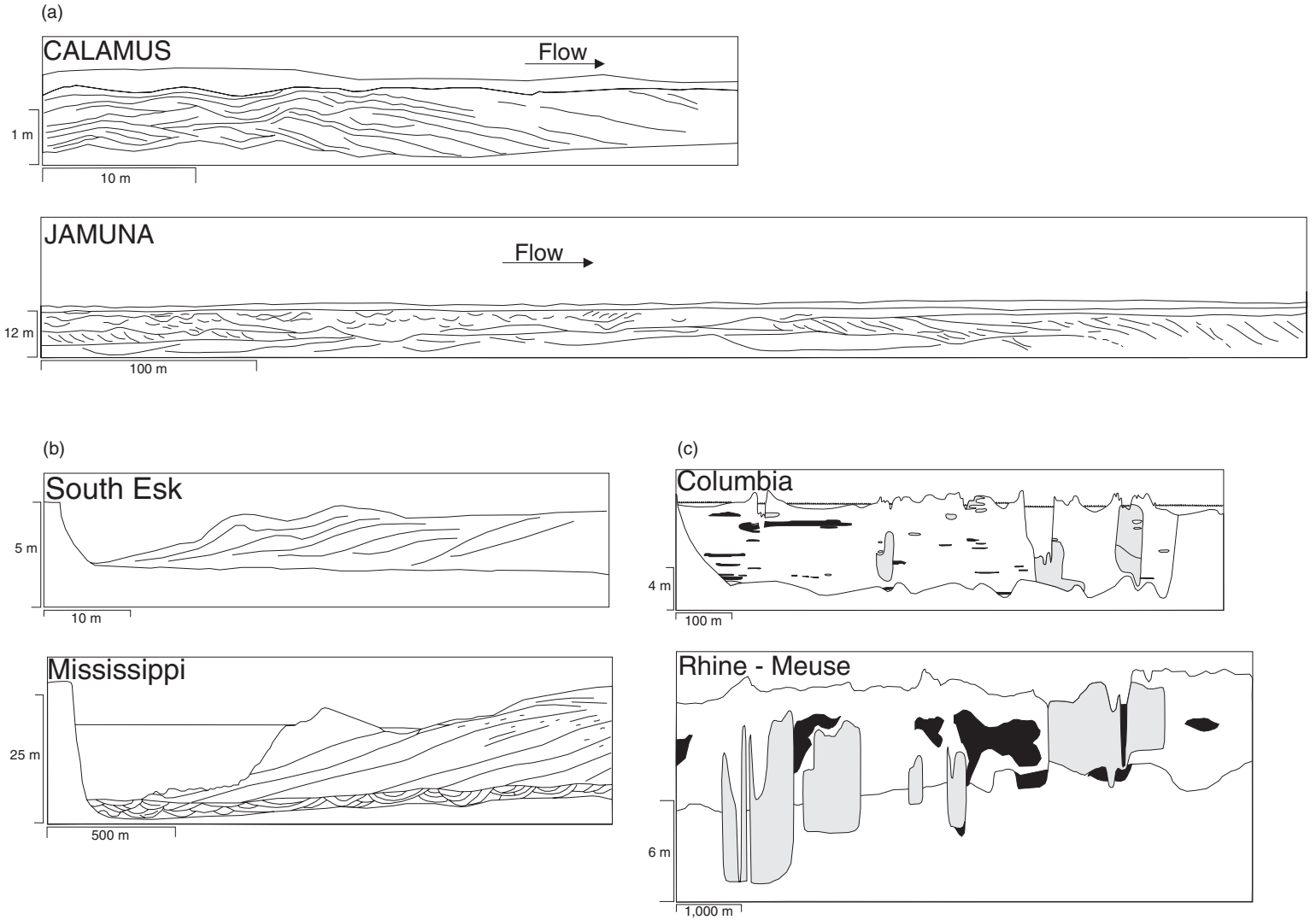

Figure 7.2 Scale drawings to illustrate scale invariance in the facies architecture of river sediment bodies. Examples of three different planforms are shown (a, braided; b, meandering; and c, anastomosed), with a similarly oriented cross-section from a small example shown adjacent to a cross-section from a large example. Note the similarity in internal structure in each case. Braided examples are sections parallel to flow direction, whereas those for meandering and anastomosed rivers are perpendicular to flow direction. On anastomosed sections, grey shading is channel sand bodies, black is peat. Data from Bridge *et al*. (1998: Calamus), Best *et al*. (2003: Jamuna), Bridge *et al*. (1995: South Esk), Jordan and Pryor (1992: Mississippi), Makaske *et al*. (2002: Columbia) and Berendsen and Stouthamer (2001: Rhine-Meuse)

and Bridge, 2001). One characteristic of many modern, and hence ancient, big rivers might therefore be the abundance of large-scale cross-bedding (sets 2 m+ in thickness, since preserved set thickness has been shown to be ca. 35 % of original dune height: LeClair and Bridge, 2001). Cross-sets several metres in thickness might also be common in such situations, but are more likely to be the product of channel/bar-scale processes. An issue relevant to sedimentological interpretation in such cases, however, is that the dimensions of dunes (mesoforms) formed at high flow stage may exceed those of bars (macroforms) active at lower stage. Furthermore, since the size of macroforms and megaforms might be up to an order of magnitude larger than in smaller rivers, determination of external geometry and internal architecture in such cases would require laterally extensive outcrops (cf. Bristow, 1987; Singh *et al*., 1993; Shukla *et al*., 1999). Nonetheless, it should be possible to separate deposits of dunes from those of bars by reference to the depth of contemporaneous channels. As a general observation, dunes seem to be the most common bedform on the floors of large, braided and low sinuosity river channels.

A further potential characteristic of big river deposits is the abundance of deep scours in the bed of rivers. Scours up to 40 m deep have been recognized from the Brahmaputra (Bristow, 1987, 1993; Best and Ashworth, 1997; Ashworth *et al*., 2000) and lower Amazon Rivers (Vital *et al*., 1998), and an extraordinary 80 m deep in the Yangtze (Saito *et al*., 2001) and 100 m deep in the middle Amazon (Sioli, 1984). Such features might be recorded in ancient channel sandstone bodies by either a highly erosional basal surface with several tens of metres of relief or major scour forms (deep troughs) within the sediment body. These scours are particularly common at channel confluences and might therefore be most abundant in the deposits of multichannel fluvial systems (Bristow *et al*., 1993; Tiwari *et al*., 2001). Again, though, the ratio of scour depth to mean channel depth seems to be similar to that of smaller rivers, demonstrating another aspect of scale invariance (see Sambrook-Smith *et al*., 2005).

Among braided and low sinuosity rivers, studies of the Brahmaputra/Jamuna River are by far the most advanced and potentially useful to the geological community (Coleman, 1969; Bristow, 1987, 1993; Thorne *et al*., 1993; Flood Action Plan 24, 1996; Ashworth *et al*., 2000; Best *et al*., 2003, 2007). Best *et al*. (2003) have used Ground-Penetrating Radar to investigate the subsurface of a large mid-channel braid bar (3 km long, 1 km wide, 12 m high) on the Jamuna River. They recognize four radar facies, interpreted as: (1) large-scale, cross-stratification (sets up to 8 m thick, >100 m wide) recording cross-channel migration of bar margins; (2) trough cross-sets up to 4 m thick and 300 m wide, deposited from large, sinuous-crested dunes; (3) small-scale trough cross-stratification, the product of smaller, sinuous-crested dunes; and (4) mud drapes. Best *et al*. (2003, 2007) conclude that the bar grew by propagation of a downstream-accreting slipface, vertical accretion through stacking of dunes on the bar stoss and top, and lateral accretion of bar margins during falling stage of major flow events. Together with other observations (e.g. Bristow, 1987 on the Brahmaputra; Bridge *et al*., 1998 on the Calamus River of Nebraska; and Lunt and Bridge, 2004 on the Sagavinirktok River of Alaska) this demonstrates that a significant portion of sediment accretion on braid bars of any scale is transverse to the channel direction. Many other big rivers might be expected to display comparable patterns of bar accretion and migration [e.g., the lower Yellow River (Zhou and Pan, 1994) and the Rio Orinoco and Magdalena River in northernmost South America (Nordin and Perez-Hernandez, 1989; McKee, 1989; Nordin *et al*., 1994; Winkley *et al*., 1994)]. The high variance distributions of bedform orientations measured by Shukla *et al*. (1999) from large bars of the Ganga River are probably typical of such situations (Bridge, 1985, 1993).

Large meandering rivers also appear from available data (e.g. Jordan and Pryor, 1992) to be scaled-up equivalents of smaller meandering streams (Figure 7.2). The lithology of individual large meandering channel fills is generally more heterogeneous than in braided and low-sinuosity fills (Fisk, 1944; Jordan and Pryor, 1992; Saucier, 1994; Dietrich *et al*., 1999; Guccione *et al*., 1999). The primary internal architectural features are lateral accretion surfaces, which as they extend from the top of the point bar to the channel thalweg are scaled to bankfull flow and therefore are megaforms. Although lateral accretion is also an important process in braided rivers (see above), the systematic lateral accretion patterns characteristic of meandering rivers will in most cases give rise to a distinctively different cross-sectional channel-fill architecture. At a smaller scale, unit bars (macroforms) are common on the lower parts of point bars, and as with braided and low sinuosity rivers dunes seem to be the most common mesoform on channel floors. For example, on a point bar of the Mississippi River, Jordan and Pryor (1992) documented trains of nearly straight-crested dunes (‘sand waves’) up to 5 m high, with barchanoid dunes up to 6 m high in the thalweg (see also Harbor, 1998) and also on the uppermost part of the bar. These features formed cross-bedding on a variety of scales (sets up to at least 5 m thick: Jordan and Pryor, 1992).

Fielding *et al*. (1999) have conducted Ground-Penetrating Radar surveys over large sand and gravel-dominated point bars in the upper Burdekin River of

northeastern Australia (channels <25 m deep, 300–400 m wide), which were at times covered by sinuous-crested dunes up to 3 m in height. The internal architecture of the sand-dominated section comprises high-angle cross-bedding in sets up to 3 m thick, low-angle cross-bedding (?antidunal), planar bedding, and scour surfaces (including trough-like scours <5 m deep). Little preserved evidence of lateral accretion surfaces was found, leading Fielding *et al*. (1999) to suggest that deposits of such extremely variable-discharge systems could be mistaken for those of braided rivers in the ancient (see also Gupta *et al*., 1999 on the meandering Narmada River in India). In rivers such as these, the entire alluvium is likely to be mobile during major flow events, an interpretation confirmed for the meandering upper Burdekin River by Fielding *et al*. (1999).

Large anastomosing rivers such as parts of the Magdalena in Colombia (Smith, 1986; Winkley *et al*., 1994) and of the Rhine-Meuse in the Netherlands (Törnqvist, 1993; Törnqvist *et al*., 1993; Berendsen and Stouthamer, 2001) also seem to represent scaled-up equivalents of smaller systems (Figure 7.2). Törnqvist (1993) noted that the sand bodies produced by anastomosing and meandering rivers in the Rhine-Meuse complex could be discriminated on the basis of cross-sectional dimensions, with those of anastomosing river reaches characterized by relatively narrow but thick units. The three-dimensional geometries and facies relationships of the Rhine-Meuse system are directly comparable to those of the Columbia and other smaller anastomosing rivers where the depositional model was first formulated (Smith and Smith, 1980; Makaske *et al*., 2002). The internal architecture of individual channels (each hundreds of metres wide and <15 m deep, in the case of the big rivers) appears to be simple, with symmetrical filling patterns favoured, but it must be noted that virtually no geophysical or other architectural data are yet available.

7.3 SEDIMENTOLOGY AND STRATIGRAPHY OF ANCIENT BIG RIVERS

Numerous papers have been published describing large fluvial lithosomes in the rock record, and interpreting them as the products of large rivers (Figure 7.3). Representatives of all the major planform styles have been recognized, some rather more convincingly than others. Nonetheless, the only common characteristics that emerge are: (1) the large external dimensions of sediment bodies (tens of metres thick, several kilometres wide); (2) the presence of deep, basal and internal erosional surfaces; and (3) large scale-cross-bedding (5 m+ sets). This in turn suggests strongly that scale invariance may be present in a range of geomorphic and depositional elements of alluvial systems. The following selective review is not intended to be an exhaustive survey but rather to highlight and illustrate the features common to interpreted ancient big river deposits. Some of the examples given have been the subject of published disputes over interpretation, highlighting the issues of perception raised in this review.

One of the best-known ancient big river deposits is the Triassic Hawkesbury Sandstone (Figure 7.3a) of the Sydney Basin in eastern Australia (Conaghan, 1980; Rust and Jones, 1987; Miall and Jones, 2003). The interpretation now generally accepted for this enigmatic sheet sandstone (up to 290 m thick and outcrop area ca. 20 000 km^2: Rust and Jones, 1987) involves deposition in a succession of large, braided rivers analogous to the modern Brahmaputra River (Conaghan and Jones, 1975; Rust and Jones, 1987; Miall and Jones, 2003). Despite the general consensus on interpretation, it is worth mentioning that the same outcrops have also previously been interpreted as the deposits of a marine barrier/tidal delta system (Conolly, 1969; Conolly and Ferm, 1971), and as aeolian dunes within a coastal barrier system (Ashley and Duncan, 1977). Rust and Jones (1987) summarize the objections to these alternative interpretations.

The Hawkesbury Sandstone, which crops out spectacularly in coastal cliffs and road cuts around Sydney (Figure 7.3a), comprises a series of sandstone sheets, internally composed of stratified sandstone, massive sandstone, and mudrock in a 67 : 30 : 3 ratio (Rust and Jones, 1987). The stratified sandstone facies assemblage contains abundant large-scale cross-bedding (sets <7.5 m thick), deep erosional scour surfaces and bank collapse scours (<11 m deep), and abandoned channel forms (<18 m deep), while the massive sandstone facies assemblage contains deposits of major bank collapses and associated high-concentration sand flows. Rust and Jones (1987) proposed a large, braided river system as the origin for the Hawkesbury Sandstone, and voiced general agreement with the earlier proposal of Conaghan and Jones (1975) for a Brahmaputra-like system.

In an alluvial architectural study utilizing extensive coastal cliff exposures, Miall and Jones (2003) suggested that Hawkesbury channels were (conservatively) 5–10 m deep, with channel confluence scours to 20 m deep. They concluded that the scale of features in the Hawkesbury Sandstone was smaller than the modern Brahmaputra/Jamuna, though the comparison depends very much on the choice of dimensions used. Those cited for the portion of the Jamuna studied by Best and Ashworth (1997) are directly comparable with the Hawkesbury (mean channel depth 6 m, scours to 30 m).

Upper Carboniferous successions in the Appalachians and adjacent areas of eastern USA have also been the

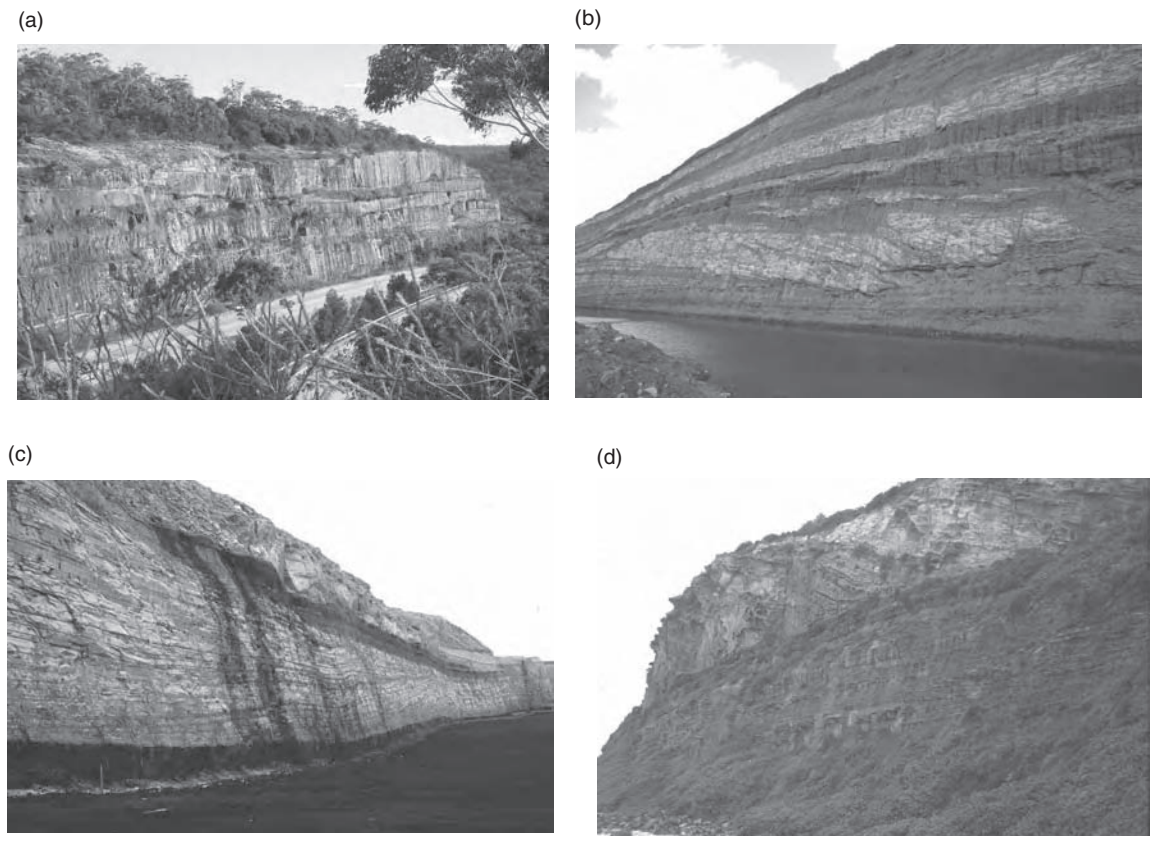

Figure 7.3 Examples of ancient big river deposits from the Permian and Triassic systems of eastern Australia. (a) View of the Triassic Hawkesbury Sandstone in an expressway cutting north of Sydney, New South Wales. The exposed section, ca. 80 m high, comprises several stacked channel sandstone bodies separated by thin and laterally discontinuous fine-grained intervals (now covered by grey concrete). (b) View of the Goonyella coal mine in central Queensland, showing a laterally accreted channel body and final plug fill within the Upper Permian Moranbah Coal Measures (face ca. 45 m high). (c) View of the Moura coal mine in central Queensland, showing a laterally accreted fluvial channel sandstone in the Upper Permian Baralaba Coal Measures (face is ca. 40 m high). (d) View of the Upper Permian Redhead Conglomerate at Redhead Beach in central New South Wales, showing a laterally accreted fluvial channel conglomerate/sandstone body in the upper part of the cliff (total cliff height ca. 70 m). The vertical extent of lateral accretion surfaces in the channel bodies shown in (b)–(d) demonstrate that all are single channel fills, and therefore despite their considerable thickness should not be considered as incised valley fills

subject of alternative interpretations. Thick, quartzose sandstones in the lower Pennsylvanian (Westphalian A) Lee Formation were originally interpreted as arising from shoreline reworking of fluvial sands in a series of barrier coastline systems (Ferm and Horne, 1979; Cecil and Englund, 1989). Wizevich (1992, 1993), however, in a detailed sedimentological analysis of the quartzose sandstone bodies, found channel forms, and a variety of simple and compound cross-bedding (sets <6 m thick) interpreted as the products of dunes organized into large-scale, downstream-accreting macroforms. Wizevich (1992) came to the conclusion that these sandstones were deposited in large, deep (10–20 m), low-sinuosity rivers, and cited the Brahmaputra and Orinoco as analogues (see also Greb and Chesnut, 1996).

Thick sandstone- and conglomerate-dominated bodies in the Upper Permian of eastern Australia have also caused considerable controversy. These are laterally extensive (at least 1–2 km) and thick (<40 m) units containing large-scale dipping bedding surfaces that extend from the top to the base of individual bodies (Figure 7.3b–d). Previous interpretations have included deposition in Gilbert-type

deltas (Conaghan, 1981; Hunt and Hobday, 1984), and crevasse splays or crevasse sub-deltas (Johnson, 1984; Flood and Brady, 1985; Galloway and Hobday, 1996; Herbert, 1997). However, by analysing the dip azimuths of major bedding surfaces relative to the migration directions of smaller-scale structures as given by cross-bedding and other structures, Fielding *et al*. (1993) and Fielding and Alexander (2001) showed that these bodies were the deposits of large, meandering rivers. The large-scale dipping surfaces were identified as lateral accretion surfaces, and thus channel megaforms. Many of these channel sandstones contributed to, or themselves constitute the principal axial drainage conduits within a large Late Permian foreland basin, the Bowen–Gunnedah–Sydney Basin System (Fielding *et al*., 2001; Esterle and Sliwa, 2002). Some of these channels contain upright, *in situ* tree fossils, which Fielding and Alexander (2001) interpreted as indicators of highly variable discharge caused by a strongly seasonal palaeoclimate. The plethora of alternative interpretations for these rocks suggests that those who worked on these rocks could not conceptualize meandering channels of such dimensions, yet they are no larger than many modern meandering rivers such as the Mississippi and Fly Rivers. Examples of similarly large ancient meandering river and estuarine channel deposits are to be found in the Cretaceous McMurray Formation of Canada, among many others (e.g. Mossop and Flach, 1983; Muwais and Smith, 1990; Strobl *et al*., 1997).

7.4 DISCUSSION: ANCIENT BIG RIVER DEPOSITS VS 'INCISED VALLEY FILLS'

One of the major impacts of the recent resurgence of sequence stratigraphy has been the reinterpretation of many large fluvial lithosomes in the rock record as 'incised valley fills'. According to the sequence stratigraphic model, incised valleys form during lowstands of relative sea-level (the term 'relative' having been added to acknowledge that geodynamic factors may exert as important controls on stratigraphy as the volume of water in oceanic basins), and are filled progressively during the succeeding rise in relative sea-level. Many such reinterpretations seem to be based on circular arguments, however, and the diagnostic criteria for recognizing such valley fills are equivocal. In particular, given the dimensional (width <20 km, depth tens of metres) and other characteristics of modern big rivers summarized in this chapter, one may ponder whether some interpreted 'incised valley fills' may simply be the deposits of large ancient rivers (particularly given the longevity of many modern and ancient systems). The key issue here is the primary formative mechanism for an ancient fluvial 'sand' body, that is, whether it owes its origin to the intrinsic properties of a drainage system or to sea-level drawdown (regardless of whether or not cycles of relative sea-level change were experienced during the life of the channel).

It is worth briefly considering the definitions of 'incised valley fills' adopted by recent workers. A review by Schumm and Ethridge (1994) shows that the traditional geomorphological definition of an alluvial valley is of a linear topographic low fashioned by erosion and occupied along its lowest point by a stream the dimensions of which are orders of magnitude smaller than those of the valley. However, many of the features interpreted as valley fills in the rock record from outcrop and subsurface data (especially seismic reflection data) show erosional relief at a scale similar to the dimensions of the channel fills occupying those erosional features (see examples in Schumm and Ethridge, 1994). Furthermore, the characteristic V-shaped cross-sectional morphology shown by Schumm and Ethridge (1994) is not evident in most of these recent interpretations, rather the basal erosion surface is generally flat to somewhat irregular, with steep sides. Many such cases may be merely incised (or entrenched) channels or channel belts, rather than valley fills. New insights into the relationships between fluvial valleys and the channels contained within them are coming to light using large, three-dimensional seismic reflection datasets ('seismic geomorphology': e.g. Posamentier, 2001).

Why do these distinctions matter? They matter both to the scientific interpretation of ancient successions and to exploration for natural resources in such successions, because from the interpretation of an incised valley fill follows many other assumptions and predictions concerning the distribution of sediment body types in a basin fill. Thus, important decisions, both scientific and commercial, hinge upon the correct interpretation of fluvial deposits.

From an exploration perspective, if a series of thick fluvial channel sandstones are interpreted as overlying a sequence boundary, then this can form the basis for reservoir prediction in the subsurface (e.g. Hampson *et al*., 1999b). Firstly, one would expect to find concentrations of reservoir sandstone bodies at the same stratigraphic horizon regionally, and furthermore, this encourages exploration in the basinward equivalents of these strata for slope wedge and fan deposits formed in deeper water during the fall and lowstand of relative sea-level. Of course, if the series of sandstone bodies rather records an array of large trunk channels that avulsed to different positions over a period of time, then the above exploration philosophy is invalid and misleading.

It is worth reviewing the diagnostic criteria for recognizing incised valley fills in the rock record, as summarized by Hampson *et al*. (1997): (1) the basal erosion

surface that records the lowstand of relative sea-level (the 'sequence boundary') must be of regional (basin-wide) extent; (2) facies associations overlying the basal erosion surface should be markedly different from those below the surface; (3) the erosional unconformity should remove underlying strata, which may be preserved beneath interfluve areas of the sequence boundary; and (4) incised valley fills have a distinctive internal architecture that is commonly multi-storey, and that records the progressive rise in base-level through the filling of the valley. The first of these criteria is crucial and probably the only one that is truly diagnostic. This criterion is also very difficult to satisfy unequivocally, however, because it requires that any correlation of a surface between outcrops or subsurface data points demonstrates absolute equivalence, and this is difficult to do in heterogeneous successions. Disparity in facies associations cannot be viewed as diagnostic of base-level fall in a continental, fluvial setting, and any erosion surface will, by definition, involve removal of underlying strata. Furthermore, any fluvial sediment body formed by processes that include a component of aggradation and avulsion may be multi-storey (Miall, 1996; Bridge, 2003), and progressively-rising base-level may be simply a function of channel abandonment in a subsiding basin. So, of the criteria listed above, only the regional extent of the basal 'sequence boundary' is diagnostic. Based on studies of the modern Jamuna River in Bangladesh, Best and Ashworth (1997) have suggested further that to confirm an incised valley fill interpretation requires evidence of basal scour that is at least five times the mean depth of the formative channel.

It is also fair to say that not all incised channels are incised valleys, and for that matter not all incised channels are a consequence of base-level lowering. The last glacial lowstand channel of the Burdekin River in northeastern Australia, which has been traced across the Great Barrier Reef shelf (Fielding *et al*., 2003, 2005), has incised or entrenched a body comprising in most places only a single channel fill with local evidence of older channel scour remnants and of limited lateral accretion. For reasons of scale, this cannot be considered as a valley fill, even though it was formed in response to sea-level lowering during the last glacial cycle. Similarly, Figure 7.3b–d shows examples of large alluvial channel fills from the Permian of eastern Australia that could potentially be the consequence of base-level lowering. Because the lateral accretion surfaces in these bodies span the entire vertical thickness of the body in each case, however, they must be regarded as channel fills and not valley fills, whatever their origin.

If one accepts that valleys are geomorphic features at a larger scale than channels and channel belts, then scale becomes important, at least within a given system. Valleys should be tens to hundreds of metres deep and kilometres to tens of kilometres in width (Dalrymple *et al*., 1994; Schumm and Ethridge, 1994), but more importantly if an incised channel complex is an order of magnitude larger than other such channel bodies within the same succession, or is otherwise out of context while also satisfying the other criteria listed (e.g., those in the Pennsylvanian cyclothems of the Midcontinent USA: Archer and Feldman, 1995; Feldman *et al*., 1995; Bowen and Weimer, 2003), then an incised valley interpretation can be justified.

Examples of these issues can be found in the Euro-American Upper Carboniferous systems alluded to earlier in this chapter. Upper Carboniferous (Pennsylvanian, in the North American usage) coal-bearing successions of eastern USA (Archer and Greb, 1995) and northwest Europe (Guion and Fielding, 1988; Leeder, 1988) contain a record of large and long-lived fluvial dispersal systems. Both areas contain thick, multi-storey fluvial channel sandstones, and although many authors believe these bodies to be trunk channels of major rivers (e.g. Archer and Greb, 1995; Greb and Chesnut, 1996; Greb *et al*., 2004), they have also been recently interpreted as incised valley fills (Aitken and Flint, 1994, 1995, 1996, in the Appalachians; Flint *et al*., 1995; Hampson, 1995; Hampson *et al*., 1996, 1997, 1999a,b in northwest Europe). The criteria and the quality of data used to develop these interpretations vary from study to study, however, and several of the incised valley fill interpretations have been challenged.

In the Appalachian Basin of Kentucky, thick, multi-storey fluvial sandstone bodies 5–20 km wide and <20 m thick throughout the Lower and Middle Pennsylvanian were interpreted as incised valley fills by Aitken and Flint (1994, 1995). Finer-grained and palaeosol-bearing facies laterally equivalent to these bodies in outcrops were interpreted as 'interfluve' surfaces recording the lateral extension of the sequence boundary in between incised valleys by Aitken and Flint (1996). However, exposures are not sufficiently extensive as to allow physical correlation over large distances and the interfluve facies are not sufficiently distinctive (e.g. palaeosols of unique chroma and hue, or thin sandstone beds with persistent vertical succession of sedimentary structures) as to allow their correlation between outcrops, rendering any diagnosis of regional extent questionable. Furthermore, the palaeosols record predominantly waterlogged surfaces (gleysols) with some indications of temporary, partial drainage, and not the deep drainage and intense oxidation that would surely accompany a base-level drop of tens of metres in a humid, tropical climate. Indeed, widespread and well-developed palaeosols are recorded throughout the Pennsylvanian

record of Midcontinent USA (e.g. Joeckel, 1994) with evidence for increasingly well-drained landscapes upward through the Pennsylvanian (Joeckel, 1999). Such palaeosols were not found in the outcrops examined by Aitken and Flint (1996). Furthermore, Greb *et al*. (2004) concluded that it is not possible to trace sequence boundaries unambiguously through these formations, and indeed chose to define genetic stratigraphic units based on more readily correlatable flooding surfaces.

Archer and Greb (1995) and Greb and Chesnut (1996) proposed that the large, incised fluvial bodies record the trunk channels of long-lived, Amazon-scale fluvial drainage systems, and also recognized more sheet-like but otherwise similar fluvial sandstones that were characteristic of different positions within the drainage basin. These authors allow for the influence of sea-level fluctuation in the accumulation of the thick fluvial sandstones, but crucially do not invoke sea-level fall as the principal factor leading to their formation (i.e. do not regard them as incised valley fills). This is an important distinction, because elsewhere within the 'cyclothemic' Pennsylvanian record of the eastern and central USA large, complexly filled valley forms are unquestionably preserved. These bodies are anomalously coarse-grained and outsized in the context of their enclosing facies and distinct from the otherwise minor evidence of fluvial activity in these units. They contain clear evidence of one or more cycles of regression and subsequent transgression within their fills, and are thus more readily interpreted as the product of cycles of sea-level fluctuation (e.g. Archer and Feldman, 1995; Feldman *et al*., 1995; Bowen and Weimer, 2003; Feldman *et al*., 2005).

In the United Kingdom, Flint *et al*. (1995) have reinterpreted several large fluvial sandstone bodies in the Upper Carboniferous as incised valley fills. Among them are bodies that can be mapped in detail from coal mine and exploration data, and outcrops. As with the Appalachian outcrops, however, the scale of the sandstone bodies is well within the scale range of big rivers (sandstone bodies 20–30 m thick, unknown width). It is difficult to demonstrate that basal erosion surfaces were forced by sea-level drop and not merely channel floors with deep scours, and interfluves are essentially impossible to identify and trace over any distance. Once again, palaeosols indicate predominantly gleyed conditions despite well-drained palaeosols having been recorded in basin-marginal locations by Besly and Fielding (1989). Furthermore, Guion *et al*. (1995) and Rippon (1996) have demonstrated via careful mapping that the margins of these sandstone bodies are not incised but rather are aggradational, and that some channels were long-lived, spanning two or more depositional cycles as defined by major coal seams.

One potentially profitable way of assessing the origin of large channel bodies is to plot distributions of channel belt width against thickness for a given formation or succession (Figure 7.4). In Figure 7.4a, the distribution of major channel bodies in the Westphalian Coal Measures of the Durham coalfield in Northeast England shows a more or less linear distribution with the exception of one body that is anomalously thick (the Westphalian B 'Low Main Post'). Outcrop data indicate that this body is incised, and multi-storey (Fielding, 1986), and it is clearly anomalously thick in the context of other similar bodies within the succession. This out-of-context sandstone body might therefore be a candidate for an incised valley fill. Figure 7.4b shows channel belt width vs thickness data for the Late Permian German Creek and Moranbah Coal Measures of Queensland, Northeast Australia (Falkner and Fielding, 1993). Here, the virtually linear distribution is also offset by a single anomalous data point that records an unusually thick and wide body, shown from opencut mine exposure to have incised margins. In this case, however, mapping of channel sandstones bodies across the coalfield by Esterle and Sliwa (2002) has demonstrated that this body is in fact the trunk channel of a massive, basin-axial dispersal system that operated within the northern Bowen Basin. The suspicion therefore remains that the Low Main Post of the Durham coalfield might be another such trunk channel.

7.5 CONCLUSION

There is an urgent need for more and higher quality data on the sedimentology of the World's large rivers. Significant logistical and technological challenges must be overcome in order to meet these needs. Available data suggest that sediment bodies of large, low sinuosity, braided, meandering and anastomosed rivers are largely scaled-up equivalents of their smaller counterparts. This in turn suggests there is a scale invariance in fluvial systems with respect to their component geomorphic and depositional elements. Numerous examples of large river deposits have been recognized in the rock record, with dimensions and internal characteristics that are comparable with well-known modern big rivers. The cross-sectional dimensions of sediment bodies of the World's big rivers are such that they may be readily mistaken for incised valley fills, formed during a cycle of lowering and rising of relative sea-level. A more rigorous application of criteria is necessary in order to provide reliable diagnosis of incised valley fills. Criteria that in combination can be considered reliably diagnostic of a sequence boundary within continental fluvial successions are: (1) that the surface can be traced over large distances, ideally between basins; (2) that a

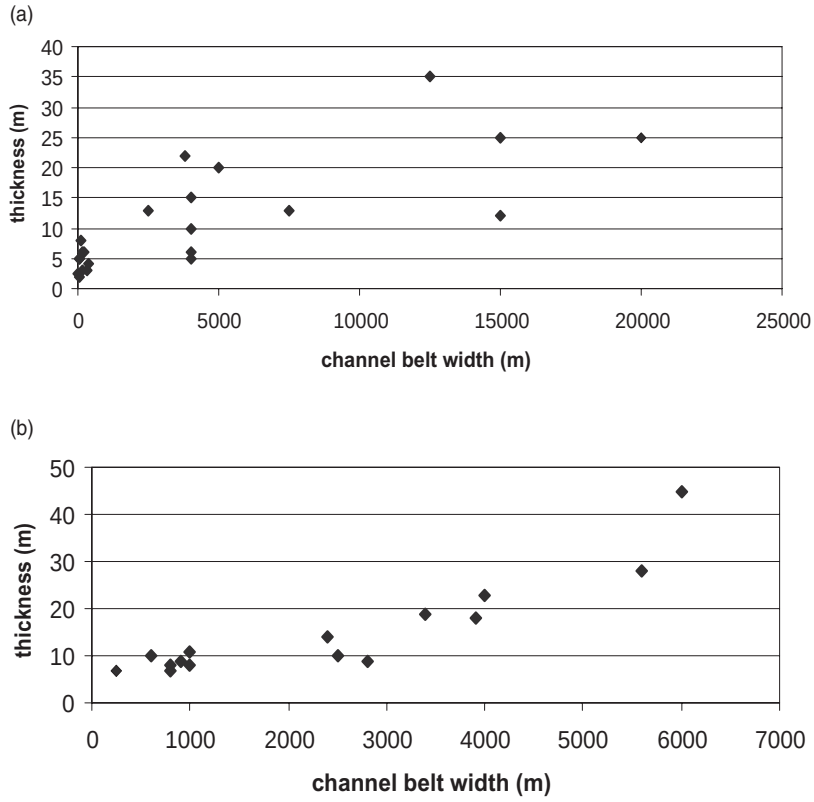

Figure 7.4 Crossplots of channel belt width against thickness for (a) Upper Carboniferous Durham Coal Measures of NE England (Fielding, 1986) and (b) Upper Permian Moranbah and German Creek Coal Measures of Queensland, Australia (Falkner and Fielding, 1993). One prominent outlier is evident on each plot that could be candidates for incised valley fills on the basis of their exceptional thicknesses. For different reasons, however, both are believed to record trunk channels of large, ancient river systems. See text for further discussion

compound channel body is at a higher order of scale than others in the same succession or is otherwise out of context; and (3) that the basal erosion surface of that body show scour at least five times deeper than the mean depth of the formative channel.

ACKNOWLEDGEMENTS

I am grateful to Jim L. Best, R. Matt Joeckel and Sampat K. Tandon for their insightful reviews, particularly to Jim for sharing with me his ideas and data on scale invariance in fluvial systems. Cody Jacobs at UNL assisted in the preparation of diagrams.

REFERENCES

Aitken, J.F. and Flint, S.S. (1994) High-frequency sequences and the nature of incised-valley fills in fluvial systems of the Breathitt Group (Pennsylvanian), Appalachian foreland basin, eastern Kentucky. In: *Incised-valley Systems: Origin and Sedimentary Sequences* (R.W. Dalrymple, R. Boyd and B.A. Zaitlin, Eds.), SEPM Special Publication 51, Tulsa, 353–368.

Aitken, J.F. and Flint, S.S. (1995) The application of high-resolution sequence stratigraphy to fluvial systems: a case study from the Upper Carboniferous Breathitt Group, eastern Kentucky, USA. *Sedimentology*, 42, 3–30.

Aitken, J.F. and Flint, S.S. (1996) Variable expressions of interfluvial sequence boundaries in the Breathitt Group (Pennsylvanian), eastern Kentucky, USA. In: *High Resolution Sequence Stratigraphy: Innovations and Applications* (J.A. Howell and J.F. Aitken, Eds.), Geological Society of London Special Publication 104, London, 193–206.

Allen, P.A. and Hovius, N. (1998) Sediment supply from landslide-dominated catchments: implications for basin-margin fans. *Basin Research*, 10, 19–35.

Allison, M.A., Kuehl, S.A., Martin, T.C. and Hassan, A. (1998) Importance of flood-plain sedimentation for river sediment

budgets and terrigenous input to the oceans: insights from the Brahmaputra-Jamuna River. *Geology*, 26, 175–178.

Anderson, J.B., Abdulah, K., Sarzalejo, S., Siringin, F. and Thomas, M.A. (1996) Late Quaternary sedimentation and high-resolution sequence stratigraphy of the East Texas shelf. In: *Geology of Siliciclastic Shelf Seas* (M. de Batist and P. Jacobs, Eds.), Geological Society of London Special Publication 117, London, 95–124.

Archer, A.W. (2005) Review of Amazonian depositional systems. In: *Fluvial Sedimentology VII* (M. Blum, S.B. Marriott and S.F. LeClair, Eds.), International Association of Sedimentologists Special Publication 35, Oxford, 17–39.

Archer, A.W. and Feldman, H.R. (1995) Incised valleys and estuarine facies of the Douglas Group (Virgilian): implications for similar Pennsylvanian sequences in the US Mid-continent. In: *Sequence Stratigraphy of the Mid-Continent* (N. Hyne, Ed.), Tulsa Geological Society, Tulsa, OK, 119–145.

Archer, A.W. and Greb, S.F. (1995) An Amazon-scale drainage system in the Early Pennsylvanian of central North America. *Journal of Geology*, 103, 611–628.

Ashley, G.M. (1990) Classification of large-scale subaqueous bedforms: a new look at an old problem. *Journal of Sedimentary Petrology*, 60, 160–172.

Ashley, G.M. and Duncan, I.J. (1977) The Hawkesbury Sandstone: a critical review of proposed environmental models. *Journal of the Geological Society of Australia*, 24, 117–119.

Ashworth, P.J., Best, J.L., Roden, J.E., Bristow, C.S. and Klaassen, G.J. (2000) Morphological evolution and dynamics of a large, sand braid-bar, Jamuna River, Bangladesh. *Sedimentology*, 47, 533–555.

Audley-Charles, M.G., Curray, J.R. and Evans, G. (1977) Location of major deltas. *Geology*, 5, 341–344.

Baker, V.R. (1973) Paleohydrology and sedimentology of Lake Missoula flooding in eastern Washington. *Geological Society of America, Special Paper*, 144, Boulder.

Berendsen, H.J.A. and Stouthamer, E. (2001) *Palaeogeographic Development of the Rhine-Meuse Delta, The Netherlands*, Van Gorcum, Assen, 1–268.

Besly, B.M. and Fielding, C.R. (1989) Palaeosols in Westphalian coal-bearing and red-bed sequences, central and northern England. *Palaeogeography, Palaeoclimatology, Palaeoecology*, 70, 303–330.

Best, J.L. and Ashworth, P.J. (1997) Scour in large braided rivers and the recognition of sequence stratigraphic boundaries. *Nature*, 387, 275–277.

Best, J.L., Ashworth, P.J., Bristow, C.S. and Roden, J. (2003) Three-dimensional sedimentary architecture of a large, mid-channel sand braid bar, Jamuna River, Bangladesh. *Journal of Sedimentary Research*, 73, 516–530.

Best, J.L., Ashworth, P.J., Sarker, M.H. and Roden, J.E. (2007) The Brahmaputra-Jamuna River, Bangladesh. In: *Large Rivers: Geomorphology and Management* (A. Gupta, Ed.), John Wiley & Sons, Ltd, Chichester, 395–433.

Blum, M.D. and Tornqvist, T.E. (2000) Fluvial responses to climate and sea-level change: a review and look forward. *Sedimentology*, 47 (Suppl. 1), 2–48.

Bowen, D.W. and Weimer, P. (2003) Regional sequence stratigraphic setting and reservoir geology of Morrow incised-valley sandstones (lower Pennsylvanian), eastern Colorado and western Kansas. *American Association of Petroleum Geologists Bulletin*, 87, 781–815.

Bridge, J.S. (1985) Palaeochannel patterns inferred from alluvial deposits: a critical evaluation. *Journal of Sedimentary Petrology*, 55, 579–589.

Bridge, J.S. (1993) The interaction between channel geometry, water flow, sediment transport, erosion and deposition in braided rivers. In: *Braided Rivers* (J.L. Best and C.S. Bristow, Eds.), Geological Society of London Special Publication 75, London, 13–71.

Bridge, J.S. (2003) *Rivers and Floodplains: Forms, Processes and Sedimentary Record*. Blackwell, Oxford, 491 p.

Bridge, J.S., Alexander, J., Collier, R.E.Ll., Gawthorpe, R.L. and Jarvis, J. (1995) Ground-penetrating radar and coring used to study the large-scale structure of point bar deposits in three dimensions. *Sedimentology*, 42, 839–852.

Bridge, J.S., Collier, R.E.Ll. and Alexander, J. (1998) Large-scale structure of Calamus River deposits revealed using ground-penetrating radar. *Sedimentology*, 45, 977–985.

Bristow, C.S. (1987) Brahmaputra River: channel migration and deposition. In: *Recent Developments in Fluvial Sedimentology* (F.G. Ethridge, R.M. Flores and M.D. Harvey, Eds.), SEPM Special Publication 39, 63–74.

Bristow, C.S. (1993) Sedimentary structures exposed in bar tops in the Brahmaputra River, Bangladesh. In: *Braided Rivers* (J.L. Best and C.S. Bristow, Eds.), Geological Society of London Special Publication 75, Bath, 277–289.

Bristow, C.S., Best, J.L. and Roy, A.G. (1993) Morphology and facies models of channel confluences. In: *Alluvial Sedimentation* (M. Marzo and C. Puigdefabregas, Eds.), International Association of Sedimentologists Special Publication 17, Oxford, 91–100.

Browne, G.H. and Naish, T.R. (2003) Facies development and sequence architecture of a late Quaternary fluvial-marine transition, Canterbury Plains and shelf, New Zealand: implications for forced regressive deposits. *Sedimentary Geology*, 158, 57–86.

Carling, P.A. (1996) Morphology, sedimentology and palaeohydraulic significance of large gravel dunes, Altai Mountains, Siberia. *Sedimentology*, 43, 647–664.

Cecil, C.B. and Englund, K.J. (1989) Origin of coal deposits and associated rocks in the Carboniferous of the Appalachian Basin. In *Coal and Hydrocarbon Resources of North America, 2, 28th International Geological Congress Field Trip Guidebook T143*, American Geophysical Union, Washington, DC, 84–88.

Church, M. and Jones, D. (1982) Channel bars in gravel-bed rivers. In: *Gravel Bed Rivers* (R.D. Hey, J.C. Bathurst and C.R. Thorne, Eds.), John Wiley & Sons, Ltd, Chichester, 291–324.

Coleman, J.M. (1969) Brahmaputra River: channel processes and sedimentation. *Sedimentary Geology*, 3, 129–239.

Conaghan, P.J. (1980) The Hawkesbury Sandstone: gross characteristics and depositional environment. *Geological Survey of New South Wales Bulletin* 26, 188–253.

Conaghan, P.J. (1981) Lacustrine (Gilbert) deltas in the Permian coal measures of eastern Australia and India: implications for the widespread hydroponic origin and deep-water diagenesis of Gondwana coals. *Advances in the Study of the Sydney Basin*, Abstracts, 16th Symposium, University of Newcastle, Newcastle, NSW, 6–9.

Conaghan, P.J. and Jones, J.G. (1975) The Hawkesbury Sandstone and Brahmaputra: a depositional model for continental sheet sandstone. *Journal of the Geological Society of Australia*, 22, 275–283.

Conolly, J.R. (1969) Models for Triassic deposition in the Sydney Basin. *Geological Society of Australia Special Publication*, 2, 209–223.

Conolly, J.R. and Ferm, J.C. (1971) Permo-Triassic sedimentation patterns, Sydney Basin, Australia. *American Association of Petroleum Geologists Bulletin*, 55, 2018–2032.

Dalrymple, R.W., Boyd, R. and Zaitlin, B.A. (1994) History of research, valley types and internal organization of incised-valley systems: introduction to the volume. In: *Incised Valley Systems: Origin and Sedimentary Sequences* (R.W. Dalrymple, R. Boyd and B.A. Zaitlin, Eds.), SEPM Special Publication 51, Tulsa, 3–10.

Dietrich, W.E., Day, G. and Parker, G. (1999) The Fly River, Papua New Guinea. In: *Varieties of Fluvial Form* (A.J. Miller and A. Gupta, Eds.), John Wiley & Sons, Ltd, Chichester, 345–376.

Esterle, J.S. and Sliwa, R. (2002) *Bowen Basin Supermodel 2000*, CSIRO Australia Exploration and Mining Report 976C, Brisbane, 1–196.

Falkner, A.J. and Fielding, C.R. (1993) Quantitative facies analysis of coal-bearing sequences in the Bowen Basin, Australia: applications to reservoir description. In: *The Geological Modelling of Hydrocarbon Reservoirs and Outcrop Analogues* (S.S. Flint and I.D. Bryant, Eds.), International Association of Sedimentologists Special Publication 15, 81–98.

Feldman, H.R., Gibling, M.R., Archer, A.W., Wightman, W.G. and Lanier, W.P. (1995) Stratigraphic architecture of the Tonganoxie Paleovalley Fill (Lower Virgilian) in northeastern Kansas. *American Association of Petroleum Geologists Bulletin*, 79, 1019–1043.

Feldman, H.R., Franseen, E.K., Joeckel, R.M. and Heckel, P.H. (2005) Impact of longer-term modest climate shifts on architecture of high-frequency sequences (cyclothems), Pennsylvanian of Midcontinent USA. *Journal of Sedimentary Research*, 75, 350–368.

Ferm, J.C. and Horne, J.C. (Eds) (1979) *Carboniferous Depositional Environments in the Appalachian Region*, Carolina Coal Group, Department of Geology, University of South Carolina, Columbia, 1–760.

Fielding, C.R. (1986) Fluvial channel and overbank deposits from the Westphalian of the Durham coalfield, NE England. *Sedimentology*, 33, 119–140.

Fielding, C.R. and Alexander, J. (2001) Fossil trees in ancient fluvial channel deposits: evidence of seasonal and longer-term climatic variability. *Palaeogeography, Palaeoclimatology, Palaeoecology*, 170, 59–80.

Fielding, C.R., Alexander, J. and McDonald, R. (1999) Sedimentary facies from ground-penetrating radar surveys of the modern, upper Burdekin River of north Queensland, Australia: consequences of extreme discharge fluctuations. In: *Fluvial Sedimentology VI* (N.D. Smith and J. Rogers, Eds.), International Association of Sedimentologists Special Publication 28, 347–362.

Fielding, C.R., Falkner, A.J. and Scott, S.G. (1993) Fluvial response to foreland basin overfilling: the Late Permian Rangal Coal Measures in the Bowen Basin, Queensland, Australia. *Sedimentary Geology*, 85, 475–497.

Fielding, C.R., Sliwa, R., Holcombe, R.J. and Jones, A.J. (2001) A new palaeogeographic synthesis for the Bowen, Gunnedah and Sydney Basins of eastern Australia. In: *Eastern Australasian Basins Symposium* (K.C.Hill and T. Bernecker, Eds.), Petroleum Exploration Society of Australia Special Publication, Australasian Institute of Mining and Metallurgy, Melbourne, 269–278.

Fielding, C.R., Trueman, J.D., Dickens, G.R. and Page, M. (2003) Anatomy of the buried Burdekin River channel across the Great Barrier Reef shelf: how does a major river operate on a tropical mixed siliciclastic/carbonate margin during sea level lowstand? *Sedimentary Geology*, 157, 291–301.

Fielding, C.R., Trueman, J.D., Dickens, G.R. and Page, M. (2005) Geomorphology and internal architecture of the ancestral Burdekin River across the Great Barrier Reef shelf, northeast Australia. In: *Fluvial Sedimentology VII* (M.D. Blum, S.B. Marriott and S.F. LeClair, Eds.), International Association of Sedimentologists Special Publication 35, 321–347.

Fisher, W.L. and McGowen, J.H. (1967) Depositional systems in the Wilcox Group of Texas and their relationship to occurrence of oil and gas. *Transactions of the Gulf Coast Association of Geological Societies*, 27, 105–125.

Fisk, H.N. (1944) *Geological Investigation of the Alluvial Valley of the Lower Mississippi River*. US Army Corps of Engineers, Mississippi River Commission, 1–78.

Flint, S.S., Aitken, J.F. and Hampson, G. (1995) Application of sequence stratigraphy to coal-bearing, coastal plain successions: implications for the UK Coal Measures. In: *European Coal Geology* (M.K.G. Whateley and D.A. Spears, Eds.), Geological Society of London Special Publication 82, London, 1–16.

Flood Action Plan 24; Delft Hydraulics and DHI. (1996) FAP24 River Survey Project, Final Report, Main Volume, Annexes and Special Reports (prepared for FPCO), Dhaka, Bangladesh.

Flood, P.G. and Brady, S.A. (1985) Origin of large-scale cross-beds in the Late Permian coal measures of the Sydney and Bowen Basins, eastern Australia. *International Journal of Coal Geology*, 5, 231–245.

Galloway, W.E. and Hobday, D.K. (1996) *Terrigenous Clastic Depositional Systems*, 2nd Edn, Springer-Verlag, Berlin, 1–489.

Gibling, M.R., Calder, J.H., Ryan, R., van de Poll, H.W. and Yeo, G.M. (1992) Late Carboniferous and Early Permian drainage patterns in Atlantic Canada. *Canadian Journal of Earth Sciences*, 29, 338–352.

Goodbred, S.L. and Kuehl, S.A. (1998) Floodplain processes in the Bengal Basin and the storage of Ganges-Brahmaputra river

sediment: and accretion study using ^{137}Cs and ^{210}Pb geochronology. *Sedimentary Geology*, 121, 239–258.

Greb, S.F. and Chesnut, D.R. (1996) Lower and Middle Pennsylvanian fluvial to estuarine deposition, central Appalachian basin: effects of eustasy, tectonics and climate. *Geological Society of America Bulletin*, 108, 303–317.

Greb, S.F., Chesnut, D.R. and Eble, C.F. (2004) Temporal changes in coal-bearing depositional sequences (Lower and Middle Pennsylvanian) of the central Appalachian Basin, USA. In: *Sequence Stratigraphy, Paleoclimate, and Tectonics of Coal-bearing Strata* (J.C. Pashin and R.A. Gastaldo, Eds.), American Association of Petroleum Geologists Studies in Geology, Tulsa 51, 89–120.

Guccione, M.J., Burford, M.F. and Kendall, J.D. (1999) Pemiscot Bayou, a large distributary of the Mississippi River and a possible failed avulsion. In: *Fluvial Sedimentology VI* (N.D. Smith and J. Rogers, Eds.), International Association of Sedimentologists Special Publication 28, 211–220.

Guion, P.D. and Fielding, C.R. (1988) Westphalian A and B sedimentation in the Pennine Basin. In: *Sedimentation in a Synorogenic Basin Complex: the Upper Carboniferous of Northwest Europe* (B.M. Besly and G. Kelling, Eds.), Blackie, Glasgow, 153–177.

Guion, P.D., Banks, N.L. and Rippon, J.H. (1995) The Silkstone Rock (Westphalian A) from the east Pennines, England: implications for sand body genesis. *Journal of the Geological Society of London*, 152, 819–832.

Gupta, A., Kale, V.S. and Rajaguru, S.N. (1999) The Narmada River, India, through time and space. In: *Varieties of Fluvial Form* (A.J. Miller and A. Gupta, Eds.), John Wiley & Sons, Ltd, Chichester, 113–143.

Hampson, G.J. (1995) Discrimination of regionally extensive coals in the Upper Carboniferous of the Pennine Basin, UK, using high resolution sequence stratigraphic concepts. In: *European Coal Geology* (M.K.G. Whateley and D.A. Spears, Eds.), Geological Society of London Special Publication 82, London, 79–97.

Hampson, G.J., Elliott, T. and Flint, S.S. (1996) Critical application of high resolution sequence stratigraphic concepts to the Rough Rock Group (Upper Carboniferous) of northern England. In: *High Resolution Sequence Stratigraphy: Innovations and Applications* (J.A. Howell and J.F. Aitken, Eds.), Geological Society of London Special Publication 104, London, 221–246.

Hampson, G.J., Elliott, T. and Davies, S.J. (1997) The application of sequence stratigraphy to Upper Carboniferous fluvio-deltaic strata of the onshore UK and Ireland: implications for the southern North Sea. *Journal of the Geological Society of London*, 154, 719–733.

Hampson, G.J., Stollhofen, H. and Flint, S.S. (1999a) A sequence stratigraphic model for the Lower Coal Measures (Upper Carboniferous) of the Ruhr district, north-west Germany. *Sedimentology*, 46, 1199–1231.

Hampson, G.J., Davies, S.J., Elliott, T., Flint, S.S. and Stollhofen, H. (1999b) Incised valley fill sandstone bodies in Upper Carboniferous fluvio-deltaic strata: recognition and reservoir characterization of southern North Sea analogues. In: *Petroleum Geology of Northwest Europe* (A.J. Fleet and S.A.R. Boldy, Eds.), Proceedings of the 5th Conference, Geological Society of London, London, 771–788.

Harbor, D.J. (1998) Dynamics of bedforms in the lower Mississippi River. *Journal of Sedimentary Research*, 68, 750–762.

Herbert, C. (1997) Relative sea level control of deposition in the Late Permian Newcastle Coal Measures of the Sydney Basin, Australia. *Sedimentary Geology*, 107, 167–187.

Hovius, N. (1998) Controls on sediment supply by large rivers. In: *Relative Role of Eustasy, Climate, and Tectonics in Continental Rocks* (K.W. Shanley and P.J. McCabe, Eds.), SEPM Special Publication 59, Tulsa, 3–16.

Hunt, J.W. and Hobday, D.K. (1984) Petrographic composition and sulphur content of coals associated with alluvial fans in the Permian Sydney and Gunnedah Basins, eastern Australia. In: *Sedimentology of Coal and Coal-Bearing Sequences* (R.A. Rahmani and R.M. Flores, Eds.), International Association of Sedimentologists Special Publication 7, Oxford, 43–60.

Jackson, R.G. (1975) Hierarchical attributes and a unifying model of bedforms composed of cohesionless material and produced by shearing flow. *Geological Society of America Bulletin*, 86, 1523–1533.

Jacob, R.J., Bluck, B.J. and Ward, J.D. (1999) Tertiary-age diamondiferous fluid deposits of the lower Orange River valley, southwest Africa. *Economic Geology*, 94, 749–758.

Joeckel, R.M. (1994) Virgilian (Upper Pennsylvanian) paleosols in the upper Lawrence Formation (Douglas Group) and its Snyderville Shale Member (Oread Formation, Shawnee Group) of the northern Midcontinent, USA: pedologic contrasts in a cyclothem sequence. *Journal of Sedimentary Research, Section A*, 64, 853–866.

Joeckel, R.M. (1999) Paleosol in Galesburg Formation (Kansas City Geoup, Upper Pennsylvanian), northern Midcontinent, USA: evidence for climate change and mechanisms of marine transgression. *Journal of Sedimentary Research*, 69, 720–737.

Johnson, D.P. (1984) Development of Permian fluvial coal measures, Goonyella, Australia. In: *Sedimentology of Coal and Coal-Bearing Sequences* (R.A. Rahmani and R.M. Flores, Eds.), International Association of Sedimentologists Special Publication 7, Oxford, 149–162.

Jordan, D.W. and Pryor, W.A. (1992) Hierarchical levels of heterogeneity in a Mississippi River meander belt and application to reservoir systems. *American Association of Petroleum Geologists Bulletin*, 76, 1601–1624.

Julien, P.Y. and Klaassen, G.J. (1995) Sand-dune geometry of large rivers during floods. *Journal of Hydraulic Engineering*, 121, 657–663.

Leckie, D.A. (1994) Canterbury Plains, New Zealand – implications for sequence stratigraphic models. *American Association of Petroleum Geologists Bulletin*, 78, 1240–1256.

Leckie, D.A. (2003) Modern environments of the Canterbury Plains and adjacent offshore areas, New Zealand – an analog for ancient conglomeratic depositional systems in nonmarine and coastal zone settings. *Bulletin of Canadian Petroleum Geology*, 51, 389–425.

Leclair, S.F. and Bridge, J.S. (2001) Quantitative interpretation of sedimentary structures formed by river dunes. *Journal of Sedimentary Research*, 71, 713–716.

Leeder, M.R. (1988) Devono-Carboniferous river systems and sediment dispersal from the orogenic belts and cratons of NW Europe. In: *The Caledonian-Appalachian Orogen* (A.L. Harris and D.J. Fettes, Eds.), Geological Society of London Special Publication 38, London, 549–558.

Leeder, M.R. and Stewart, M.D. (1996) Fluvial incision and sequence stratigraphy: alluvial responses to relative sea-level fall and their detection in the geologic record. In: *Sequence Stratigraphy in British Geology* (S.P. Hesselbo and D.N. Parkinson, Eds.), Geological Society of London Special Publication 103, London, 25–39.

Leeder, M.R., Harris, T. and Kirkby, M.J. (1998) Sediment supply and climate change: implications for basin stratigraphy. *Basin Research*, 10, 7–18.

Lindsay, J.F., Holliday, D.W. and Hulbert, A.G. (1991) Sequence stratigraphy and the evolution of the Ganges-Brahmaputra delta complex. *American Association of Petroleum Geologists Bulletin*, 75, 1233–1254.

Lunt, I.A. and Bridge, J.S. (2004) Evolution and deposits of a gravelly braid bar, Sagavinirktok River, Alaska. *Sedimentology*, 51, 415–432.

Mackey, S.D. and Bridge, J.S. (1995) Three-dimensional model of alluvial stratigraphy: theory and application. *Journal of Sedimentary Research*, B65, 7–31.

Makaske, B., Smith, D.G. and Berendsen, H.J.A. (2002) Avulsions, channel evolution and floodplain sedimentation rates of the anastomosing upper Columbia River, British Columbia, Canada. *Sedimentology*, 49, 1049–1071.

McKee, E.D. (1989) Sedimentary structures and textures of Rio Orinoco channel sands, Venezuala and Colombia. *US Geological Survey Water Supply Paper* 2326B, 1–23.

McLelland, S.J., Ashworth, P.J., Best, J.L., Roden, J. and Klaasen, G.J. (1999) Flow structure and transport of sand-grade suspended sediment around an evolving braid bar, Jamuna River, Bangladesh. In: *Fluvial Sedimentology VI* (N.D. Smith and J. Rogers, Eds.), International Association of Sedimentologists Special Publication 28, Oxford, 43–57.

Meijer, X.D. (2002) Modelling the drainage evolution of a river-shelf system forced by Quaternary glacio-eustasy. *Basin Research*, 14, 361–377.

Mertes, L.A.K., Dunne, T. and Martinelli, L.A. (1996) Channel-floodplain geomorphology along the Solimoes-Amazon River, Brazil. *Geological Society of America Bulletin*, 108, 1089–1107.

Miall, A.D. (1996) *The Geology of Fluvial Deposits: Sedimentary Facies, Basin Analysis and Petroleum Geology*, Springer-Verlag, New York, 1–582.

Miall, A.D. and Jones, B.G. (2003) Fluvial architecture of the Hawkesbury Sandstone (Triassic), near Sydney, Australia. *Journal of Sedimentary Research*, 73, 531–545.

Milliman, J.D. and Meade, R.H. (1983) World wide delivery of river sediment to the oceans. *Journal of Geology*, 91, 1–21.

Milliman, J.D. and Syvitski, J.P.M. (1992) Geomorphic/tectonic control of sediment discharge to the ocean: the importance of small, mountainous rivers. *Journal of Geology*, 100, 525–544.

Mossop, G.D. and Flach, P.D. (1983) Deep channel sedimentation in the Lower Cretaceous McMurray Formation, Athabasca Oil Sands, Alberta. *Sedimentology*, 30, 493–509.

Mulder, T. and Syvitski, J.P.M. (1996) Climatic and morphologic relationships of rivers: implications of sea-level fluctuations on river loads. *Journal of Geology*, 104, 509–523.

Muwais, W.K. and Smith, D.G. (1990) Types of channel-fills interpreted from dipmeter logs in the McMurray Formation, northeast Alberta. *Bulletin of Canadian Petroleum Geology*, 38, 53–63.

Nordin, C.F. Jr and Perez-Hernandez, D. (1989) Sandwaves, bars and wind-blown sands of the Rio Orinoco, Venezuala and Colombia. *US Geological Survey Water Supply Paper* 2326A, 1–74.

Nordin, C.F. Jr, Mejia, A. and Delgado, C. (1994) Sediment studies of the Orinoco River, Venezuala. In: *The Variability of Large Alluvial Rivers* (S.A. Schumm and B.R. Winkley, Eds.), American Society of Civil Engineers Press, New York, 243–265.

Paola, C. (2000) Quantitative models of sedimentary basin filling. *Sedimentology*, 47 (Suppl. 1), 121–178.

Phillips, J. (2003) Alluvial storage and the long-term stability of sediment yields. *Basin Research*, 15, 153–163.

Posamentier, H.W. (2001) Lowstand alluvial pypass systems: incised vs. unincised. *American Association of Petroleum Geologists Bulletin*, 85, 1771–1793.

Posamentier, H.W. and Allen, G.P. (1999) Siliciclastic sequence stratigraphy – concepts and applications. *SEPM Concepts in Sedimentology and Paleontology*, 7, 1–210.

Potter, P.E. (1978) Significance and origin of big rivers. *Journal of Geology*, 86, 13–33.

Putzer, H. (1984) The geological evolution of the Amazon Basin and its mineral resources. In: *The Amazon – Limnology and Landscape Ecology of a Mighty Tropical River and its Basin* (H. Sioli, Ed.), Monographiae Biologicae, 56, Junk, Dordrecht, 15–46.

Rippon, J.H. (1996) Sand body orientation, palaeoslope analysis and basin-fill implications in the Westphalian A-C of Great Britain. *Journal of the Geological Society of London*, 153, 881–900.

Rust, B.R. and Jones, B.G. (1987) The Hawkesbury Sandstone south of Sydney, Australia: Triassic analogue for the deposit of a large, braided river. *Journal of Sedimentary Petrology*, 57, 222–233.

Saito, Y., Yang, Z.S. and Hori, K. (2001) The Huanghe (Yellow River) and Changjiang (Yangtze River) deltas: a review on their characteristics, evolution and sediment discharge during the Holocene. *Geomorphology*, 41, 219–231.

Sambrook-Smith, G.H., Ashworth, P.J., Best, J.L., Woodward, J. and Simpson, C.J. (2005) The morphology and facies of sandy braided rivers: some considerations of scale invariance. In: *Fluvial Sedimentology VII* (M. Blum, S.B. Marriott and S.F. LeClair, Eds.), International Association of Sedimentologists Special Publication 35, Oxford, 145–158.

Saucier, R.T. (1994) *Geomorphology and Quaternary Geologic History of the Lower Mississippi Valley*. US Army Corps of Engineers, Vicksburg, MS, 1–364 (2 volumes).

Schumm, S.A. and Ethridge, F.G. (1994) Origin, evolution and morphology of fluvial valleys. In: *Incised-valley Systems: Origin and Sedimentary Sequences* (R.W. Dalrymple, R. Boyd and B.A. Zaitlin, Eds.), SEPM Special Publication 51, Tulsa, 11–27.

Shukla, U.K., Singh, I.B., Srivasatava, P. and Singh, D.S. (1999) Paleocurrent patterns in braid-bar and point-bar deposits: examples from the Ganga River, India. *Journal of Sedimentary Research*, 69, 992–1002.

Singh, H., Parkash, B. and Gohain, K. (1993) Facies analysis of the Kosi megafan deposits. *Sedimentary Geology*, 85, 87–113.

Sioli, H. (1984) The Amazon and its main affluents: hydrography, morphology of the river courses, and river types. In: *The Amazon – Limnology and Landscape Ecology of a Mighty Tropical River and its Basin* (H. Sioli, Ed.), Monographiae Biologicae, 56, Junk, Dordrecht, 127–165.

Smith, D.G. (1986) Anastomosing river deposits, sedimentation rates and basin subsidence, Magdalena River, northwestern Colombia, South America. *Sedimentary Geology*, 46, 177–196.

Smith, D.G. and Smith, N.D. (1980) Sedimentation in anastomosed river systems: examples from alluvial valleys near Banff, Alberta. *Journal of Sedimentary Petrology*, 50, 157–164.

Strobl, R.S., Wightman, D.M., Muwais, W.K., Cotterill, D.K. and Yuan, L.P. (1997) Geological modeling of McMurray Formation reservoirs based on outcrop and subsurface analogues. In: *Petroleum Geology of the Cretaceous Manville Group, Western Canada* (S.G. Pemberton and D.P. James, Eds.), Canadian Society of Petroleum Geologists Memoir 18, Calgary, 292–311.

Summerfield, M.A. (1985) Plate tectonics and landscape development on the African continent. In: *Tectonic Geomorphology* (M. Morisawa and J. Hack, Eds.), Allen and Unwin, Boston, 27–51.

Suter, J.R. and Berryhill, H.L. Jr. (1985) Late Quaternary shelf-margin deltas, northwest Gulf of Mexico. *American Association of Petroleum Geologists Bulletin*, 69, 77–91.

Talling, P.J. (1998) How and where do incised valleys form if sea-level remains above the shelf edge? *Geology*, 26, 87–90.

Thorne, C.R., Russell, A.P.G. and Alam, M.K. (1993) Planform pattern and channel evolution of the Brahmaputra River, Bangladesh. In: *Braided Rivers* (J.L. Best and C.S. Bristow, Eds.), Geological Society of London Special Publication 75, London, 257–276.

Tiwari, G.S., Tiwari, R.N. and Singh, K.N. (2001) Architecture of geomorphic surfaces associated with migration and confluence of Ganga and Jamuna River channels, Allahabad, U.P. *Geological Survey of India Special Publication* 65, Calcutta, 147–152.

Törnqvist, T.E. (1993) Holocene alternation of meandering and anastomosing fluvial systems in the Rhine-Meuse delta (central Netherlands) controlled by sea-level rise and subsoil erodibility. *Journal of Sedimentary Petrology*, 63, 683–693.

Törnqvist, T.E., van Ree, M.H.M. and Faessen, E.L.J.H. (1993) Longitudinal facies architectural changes of a Middle Holocene anastomosing distributary system (Rhine-Meuse delta, central Netherlands). *Sedimentary Geology*, 85, 203–219.

Van Heijst, M.W.I.M. and Postma, G. (2001) Fluvial response to sea-level changes: a quantitative, analogue, experimental approach. *Basin Research*, 13, 269–292.

Van Wagoner, J.C., Mitchum, R.M., Campion, K.M. and Rahmanian, V.D. (1990) Siliciclastic sequence stratigraphy in well logs, cores and outcrops. *American Association of Petroleum Geologists Methods in Exploration Series*, 7, 1–55.

Vital, H. Statteger, K., Posewang, J. and Theilen, F. (1998) Lowermost Amazon River: morphology and shallow seismic characteristics. *Marine Geology*, 152, 277–294.

Winkley, B.R., Ordonez, J.I., Saenz, J.E. and Duque, R. (1994) The Magdalena River, Colombia. In: *The Variability of Large Alluvial Rivers* (S.A. Schumm and B.R. Winkley, Eds.), American Society of Civil Engineers Press, New York, 139–160.

Wizevich, M.C. (1992) Sedimentology of Pennsylvanian quartzose sandstones of the Lee Formation, central Appalachian Basin: fluvial interpretation based on lateral profile analysis. *Sedimentary Geology*, 78, 1–47.

Wizevich, M.C. (1993) Depositional controls in a bedload-dominated fluvial system: internal architecture of the Lee Formation, Kentucky. *Sedimentary Geology*, 85, 537–556.

Xu, J.X. (2002) Implication of relationships among suspended sediment size, water discharge and suspended sediment concentration: the Yellow River basin, China. *Catena*, 49, 289–307.

Youssef, M.I. (1968) Structural pattern of Egypt and its interpretation. *American Association of Petroleum Geologists Bulletin*, 52, 601–614.

Zhou, Z.D. and Pan, X.D. (1994) Lower Yellow River. In: *The Variability of Large Alluvial Rivers* (S.A. Schumm and B.R. Winkley, Eds.), American Society of Civil Engineers Press, New York, 363–393.

8

Effects of Tectonism, Climate Change, and Sea-level Change on the Form and Behaviour of the Modern Amazon River and its Floodplain

Leal A.K. Mertes[1†] *and Thomas Dunne*[2]

[1]*Department of Geography, University of California, Santa Barbara, CA 93106, USA*
[2]*Bren School of Environmental Science and Management and Department of Earth Science, University of California, Santa Barbara, CA 93106, USA*

8.1 BACKGROUND

The theory of how continental-scale rivers respond to global or regional change is not yet well developed. Large rivers record influences that are not apparent in the form and behaviour of most small streams. The sizes of their channels and floodplains require that large sediment fluxes and therefore long time periods are required for changes in morphology, in particular those resulting from perturbations induced by the Last Glacial Maximum. Crustal deformation and excavation of resistant materials can significantly perturb the small gradients of continental-scale rivers, thereby changing flow directions, channel gradients and sinuosity, alongstream patterns of sediment transport capacity, channel patterns, migration rates, and floodplain construction. The extraordinarily low gradients of continental-scale lowland rivers allowed the effects of Quaternary sea-level changes to propagate far inland. For example, the furthest upstream incision during low sea stands for the Mississippi River appears to have reached Baton Rouge, approximately 360 km upstream of the mouth (Saucier, 1981; Schumm, 1993). Finally, large drainage basins cause strong, complex interactions between rivers and their floodplain. Their protracted flood hydrographs force long overbank flow seasons, which together with the fine texture of suspended sediment loads, imposed by low gradients, induce intense overbank sedimentation in many reaches.

These distinctive characteristics of large rivers result ultimately from the long-term interplay of geology and climate, although large-scale land use and river engineering increasingly affect some large rivers. The Amazon River, however, is still free of recognizable anthropogenic influence. Thorne (1994) noted that changes in these external forcings can result in changes in the watershed morphology and the dimensions of valleys, the hydrology and the nature of the material in transport, the channel geometry, channel pattern, and the rate and type of channel migration. Potter (1978) drew attention to the direct influence of plate tectonics on the locations and topographic and lithologic frameworks of continental-scale rivers, but also acknowledged that some basinwide impacts result from climatic and sea-level change. Schumm (1993) also illustrated how climatic changes or tectonic deformation could affect an entire river system depending on the scale and trend of the perturbation. By dividing the landscape

[†] Deceased.

Large Rivers: Geomorphology and Management, Edited by A. Gupta

into erosional uplands, alluvial valleys, and coastal plains many researchers (e.g. Schumm, 1977; Thorne, 1994) have been able to interpret landform evidence for changes in tectonics, base level, and climate in the context of the processes likely to dominate fluvial processes in different types of river reaches.

Potter (1978) illustrated how continental-scale tectonic deformation controls the physiographic setting of large rivers, in that most large rivers are located in structural lows or continental rifts and flow into oceans off the trailing edges of continents. However, the upstream penetration of the effects of base-level change can be complicated by local deformation, as well as the river's ability to adjust slope, planform, width–depth ratios, or roughness (Schumm, 1993). Thus, Wright (1977), McGinnis *et al*. (1993), Thorne (1994), Talling (1998) and Woolfe *et al*. (1998) showed that whether a reduction in base level causes channel and valley incision depends on the type of river and coastal margin, and the pattern of base-level change. Talling (1998) suggested that for most coastal regions the shelf edge typically has not been sub-aerially exposed and that incision would be compensated for within the shelf region. The limits to upstream incision are typically alternate adjustments of the bed and banks of the river (Schumm, 1993) and are reported to extend a few tens to hundreds of kilometres upstream.

In this chapter, we review these geologic and climatic effects on the modern form and behaviour of the Amazon River and its valley, using the best available, but sometimes sparse, information on the geologic and structural setting of the system. Our survey is essentially an update or elaboration of the pioneering interpretations by Sioli (1957, 1984), Tricart (1975, 1977), and Klammer (1984). The stratigraphy of recent sediments is not yet well-established due to a paucity of information on dates throughout the basin sediments (e.g. Räsänen *et al*., 1991). In contrast, the pre-Quaternary stratigraphy is well documented because of oil exploration and has been used to determine the position of large-scale structures along the river corridor. New information is provided here on the potential impact of ancient structures on the current channel gradient and on valley configuration in the reaches of the river downstream of the Negro River confluence. The modern conditions of the climate, hydrology, geomorphology, and sediment transport are described and compared with the differences to be expected due to climate fluctuations during the late Quaternary, the only period for which any palaeoclimatic data exist at this time. Based on recently acquired acoustic subsurface surveys of incision depths, we also present an estimate of the incision of the Amazon mainstem during the lowered sea level of the Last Glacial Maximum, and discuss the implications of the imposed steeper slope on sediment transport and the transfer of sediment to the Amazon Cone, which is an active depocenter only during periods of lower sea-level. We also discuss the impact of postglacial sea-level rise on current sedimentation of the floodplain.

8.2 AMAZON BASIN CHARACTERISTICS

The physiography of the 7 million km^2 Amazon Basin has been in place since the Miocene uplift of the Andes Range, and is dominated by mountains in the west, vast lowlands in the east, and modest highlands in the north and south (Figures 8.1 and 8.2). The long (1–4 km), steep slopes (averaging about 35°) of the Andes, comprised mainly of marine and volcaniclastic sedimentary rocks metamorphosed to varying degrees, grade into an active fold-and-thrust belt and a downwarped foreland basin. The highlands in the north and south of the Basin are developed mainly on crystalline rocks of the Guiana and Brazilian Shields. In the axial trough of the central basin extending towards the ENE, the landscape is dominated by fluvial processes along some of the world's largest rivers. This largely unglaciated basin supports a remarkably uniform forest cover interspersed with savannas, though large swaths of the forest cover have been removed from the southern and eastern margins of the basin in recent decades.

The mountain valleys contain steep, bedrock- and gravel-bedded channels, which transition to meandering sand channels on entering the foreland basin (Figure 8.2b) and the central Amazon trough (Figure 8.2c–e). The centre of the basin is occupied by Tertiary and Quaternary lacustrine and alluvial deposits of sands and silts, often weathered to clays, and dissected into a landscape of short hillslopes (0.05–0.5 km) under a thick forest cover. The Holocene Amazon floodplain is incised into the centre of this depression and contains a complex pattern of channels of various scales with scroll bars and levees, and lakes in channel cutoffs, backswamps, and other depressions (Figure 8.2c–e). Large tributary-mouth lakes (Figure 8.2e) are dammed by the alluvium of the main channel in the eastern half of the basin. The estuarine reach of the Amazon (Figure 8.2f) contains a delta plain downstream of which the river flows around several large islands. Tidal influence extends nearly 1000 km upstream into the estuary (near Óbidos, see Figure 8.1) due to the low river gradient.

Although the modern physiography of the Amazon valley is dominated by the collisional setting associated with the rise of the Andes, which affects the flow direction and dominant sediment source of the river, other long-term effects associated with ancient tectonic settings,

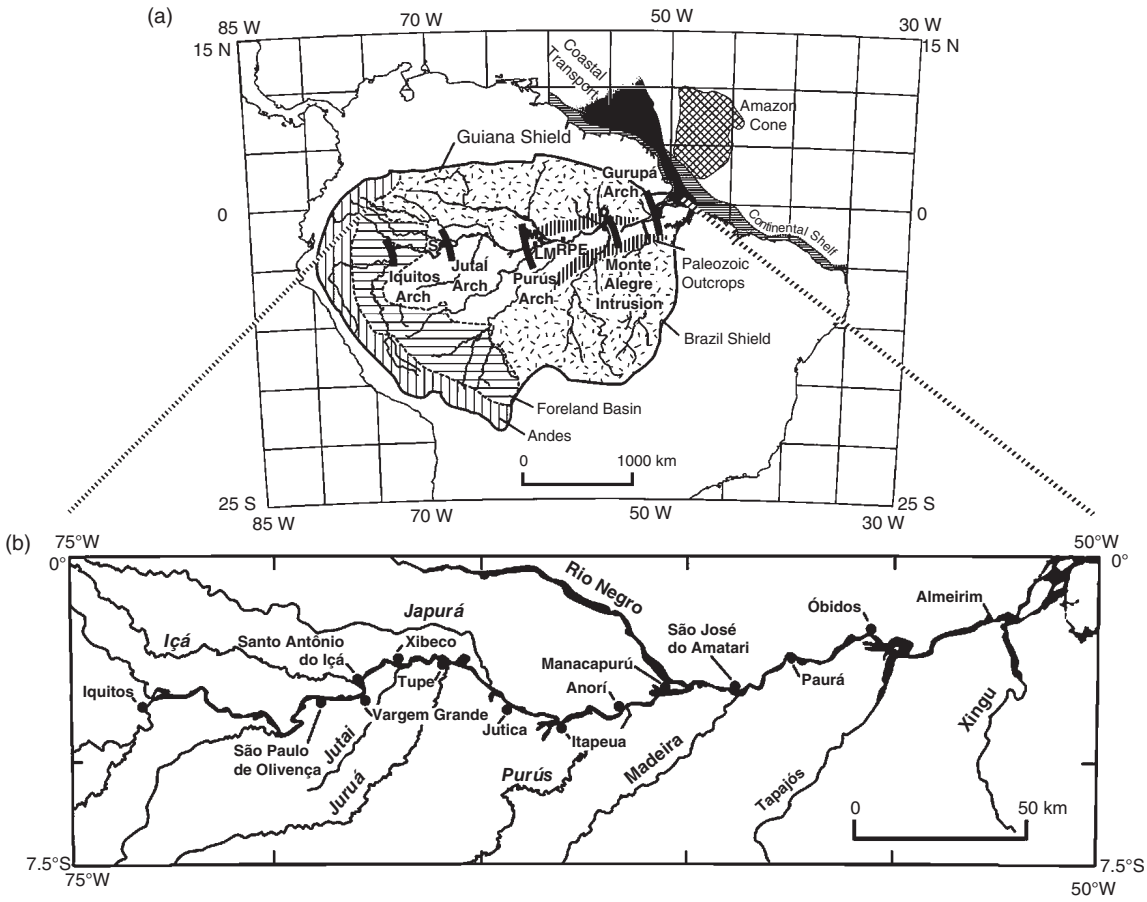

Figure 8.1 (a) Generalized map of lithologic zones and structural features in the Amazon Basin. The axial traces of the four intracratonic arches that traverse the axis of the main Amazon channel are marked. The Monte Alegre 'Intrusion' is described in the geological literature as a structural high that brings Palaeozoic sandstones to the surface of the Amazon valley. Lago Manacapurú (LM) and Rio Preto da Eva (RPE) are referred to in the text. The direction of coastal transport from the modern river is illustrated schematically. (b) The Amazon River and its major tributaries, showing sediment sampling stations and locations of river reaches referred to in the text and in other figures. Upstream of the Negro confluence the river is known as the Solimoes River in Brazil; downstream of the confluence in Brazil and upstream in Peru, the river is known as the Amazon. Also marked are the positions of three gauge locations São Paulo de Olivença (S), Manacapurú (M), and Óbidos (Ó). Figure modified with permission from the Geological Society of America Bulletin, vol. 110, Dunne *et al*., Exchanges of sediment between the flood plain and channel of the Amazon River in Brazil, pp. 450–467, 1998. Geological Society of America

climate change, and base-level change also continue to imprint the form and behaviour of the Amazon River. During the Late Cenozoic, climate has alternated between cooler-drier and warmer-wetter states, and sea level has oscillated by more than 100 m. Both the tectonic deformation and the base-level changes have extensive effects because the valley gradients in the large lowland rivers of Amazônia are measured in only centimetres per kilometre.

8.3 LITHOLOGIC AND TECTONIC INFLUENCES ON THE MODERN AMAZON

8.3.1 First-Order Basin-Scale Influences

Potter (1978) highlighted the tectonic construction of the Amazon Basin between the Andean arc at the leading edge of the South American Plate and a graben which localizes the river mouth on the trailing edge of the continent. Since the Miocene rise of the Andes the generally low

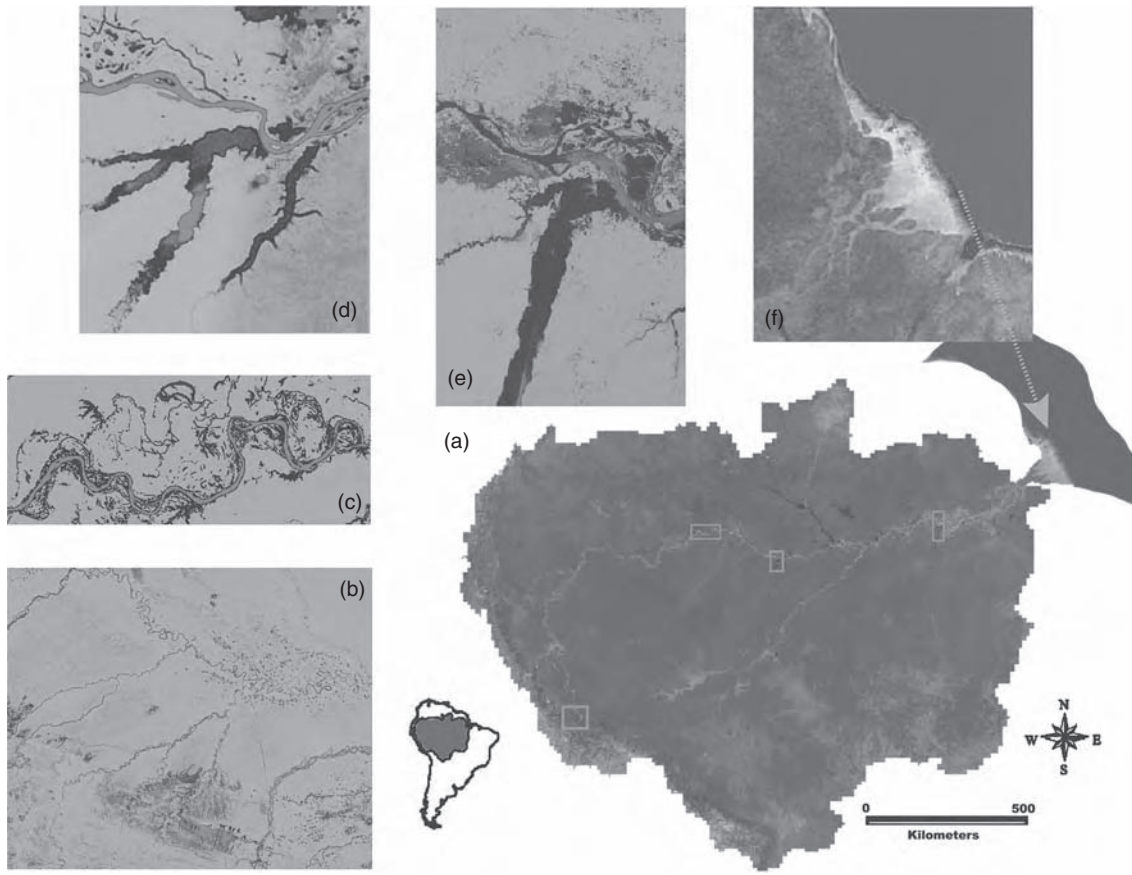

Figure 8.2 (See also colour plate section.) Regional patterns of channel-floodplain and coastal properties. Processed remote sensing images of Amazon Basin derived from MODIS (a and f) true-colour composite and Landsat TM and ETM (b–e). Processing for the Landsat data involved application of spectral mixture analysis (Adams *et al*., 1995) yielding landscape gradients among turbid water (red to purple), clear water (blue) and tropical forest (green and blue-green). (a) True-colour MODIS image shows the basin boundary and locations in clockwise rotation (downstream) from most western site for images (b)–(d). The confluence of the Negro River with the Solimões River creating the Amazonas River can be observed as the large black water river between the boxes delineating images (d) and (e). (b) Assembly of rivers flowing off the eastern slope of Andes. The large meandering tributary flowing NW to SE is the Madre de Dios River, one of the larger tributaries to the Beni River and eventually the Madeira River. Other rivers exhibit braiding and oxbow lakes associated with intensive bar formation and channel migration. The bright red colour indicates high turbidity in all of the channels. The large rectangular red area near the base of the mountain front indicates the location of extensive thinly vegetated or bare alluvium, probably in the form of substantial floodplain and fan deposits that extend for 10–20 km. (c) The most sinuous reach in the Brazilian Amazon (Mertes *et al*., 1996) showing remarkable large-amplitude bends and complex intersections of floodplain channels. The complex scroll topography is representative of large areas of the central Amazon floodplain in Brazil. In the north-central portion of the image the only oxbow on the central Amazon that is scaled to the main channel bend size (30–40 km across) can be observed as a very clear (blue) lake. An oxbow in the making is observed in the modern cutoff developing at the Fonte Boa bend, the most eastern meander on the image. The former floodplain channel on the south side of this bend has been actively capturing more water over at least the past 150 years according to historical accounts of the position and nature of this channel. Earlier accounts (Bates, 1864; Herndon, 1853) indicate that the main channel of the river flowed around the sharp bend and that the small town of Fonte Boá was 1.2 km from the main river on a narrow and slowly migrating side channel. The main channel has now migrated more rapidly towards the town and the side channel has widened, requiring dismantling of some of the Fonte Boa water front in the 1980s. (d) Coari Lake with the Amazon River cutting across the former mouth of the Coari River (at 4°8′S 64°50′W) due to an avulsion that formed the relatively sharp bend with the single island in the middle of the lake. The avulsion occurs at the eastern end of a south-trending tilted zone, first described by Tricart (1977). Turbid water can be observed entering the lake at the upstream ends of the three larger branches. The river is straighter in this section than upstream, the scroll-bar topography of the floodplain becomes smoother, and lakes increasingly become rounder downstream. (e) The mouth bay of the Tapajós River showing the NE–SW trending fracture pattern and also the tremendous size (tens of km across) of a ria lake. The surface sediment concentrations in the Amazon main channel are lower (darker red and tending towards purple) in this downstream image than in (b)–(d). The river is anastomosing through this reach and large round lakes on the floodplain can be differentiated from ria lakes and the smaller, narrower lakes observed upstream. (f) The delta region of the Amazon River showing the transfer of the sediment plume (orange-brown) nearly 100 km out to sea. Also visible is the northerly dispersion of the sediment plume due to tidal circulation and wave action. In the SW corner of the image a black rectangle indicates the location of the ria lake at the mouth of the Xingú River

topographic zone linking the Andean foreland with the graben on the Atlantic coast focused the drainage of this exceptionally large and wet region towards the east. Thus, the fundamental characteristic of the Amazon River as the world's largest with a significant sediment input being spread only from its upstream end through an extensive lowland was set by plate tectonics. Certain other aspects of this tectonic setting, at a range of scales, also affect the form and behaviour of the modern river, as outlined below.

Stratigraphic evidence from deep cores indicates that the main Amazon valley is underlain by a 6000-m-deep east–west trending sag in the crust between the Guiana and Brazilian Shields (Figures 8.1 and 8.3) that leads into a graben, the Marajó Rift, at the eastern end of the basin (Caputo, 1984). The structural sag appears to have first developed in response to Palaeozoic rifting (Caputo, 1984), and to have been reactivated during the Triassic separation of South America and Africa, and the mouth and lower Amazon valley downstream of Manaus appear to be localized by an aulacogen (Potter, 1978). Although the Amazon trough has been present since the Palaeozoic, significant eastward flow of water commenced with the Miocene uplift of the Andes. The mineralogical composition of Early Miocene deposits in northwestern Amazônia indicates that sediment was being transported from the Guiana and Brazilian Shields towards the southeast and the northeast, respectively, at that time (Hoorn *et al*., 1995, Figure 1).

As the Andes Range was thrust over the western portion of the Brazilian craton in the Middle Miocene, sedimentation occurred in a marine embayment, connected to the ocean first through the Orinoco foreland and later through the Lake Maracaibo lowland (Hoorn, 1994; Hoorn *et al*., 1995; Räsänen *et al*., 1995, p. 387). Marine sediments were eventually covered by swamp, lake and fluvial deposits, dominated by crevasse splays. The resulting sedimentary ramps gradually allowed drainage and sediment transport from the mountain range to escape eastward and connect with the current estuary through a process and chronology that have not yet been documented. Damuth and Kumar (1975) suggested that the transcontinental drainage system was eventually established when rapid clastic sedimentation began on the carbonate platform of the Amazon continental shelf between 8 and 15 Ma ago. Rossetti *et al*. (2005) provide a sedimentary interpretation of the post-Miocene evolution of the basin drainage, suggesting that drainage to the east was established only 40 ka ago, but it seems unlikely that this evidence reflects anything more than a temporary reversal of drainage.

The Andes and the adjacent fold-and-thrust belt of the Sub-Andes cover only about 800 000 km^2 of the basin, and consist primarily of high relief zones of sedimentary and igneous rocks, metamorphosed to varying degrees (Putzer, 1984). The Eastern Cordillera of the Bolivian Andes appear to have eroded at rates of 0.1–0.5 mm a^{-1} (median = 0.25 mm a^{-1}) over the past 10^6–10^7 yr (Safran *et al*., 2006) and of 0.04–1.35 mm a^{-1} (median = 0.30 mm a^{-1}) over the past 10^3–10^4 yr (Safran *et al*., 2005). Thus, the mountain range has been supplying 500–600 Mt of sediment per year into the Amazon Basin throughout the Late Cenozoic, though in the past few decades at least a north–south trending series of foreland basins east of the range has been trapping approximately half of this flux (Guyot, 1993). Since the foreland basins immediately east of the Andes are subsiding in response to loading by the Andes and by sediments shed from them, river gradients across the foreland are only a few cm km^{-1}, so that only sediment finer than about 0.5 mm escapes into the lowland Amazon Basin. The flow and sediment leaving this foreland basin complex are conveyed to the ocean by rivers that generally follow the ENE-trending axial trough of the central Amazon. Sediment that accumulates in the foreland basins causes rapid, large-scale bar building and channel shifting (Räsänen *et al*., 1987, 1990, 1992).

The surface rocks within the main Amazon trough range in age from Cretaceous east of the Amazon-Negro confluence (Figure 8.1), becoming generally younger towards the Andes (Rossetti *et al*., 2005, Figure 1). There is also a general trend from lacustrine to more fluvial units at the surface toward the Andes (Rossetti *et al*., 2005). These deposits are poorly consolidated argillaceous siltstones and sandstones, and are deeply weathered with high contents of iron oxide coated kaolinite. The Holocene floodplain of the modern mainstem Amazon, covering approximately 90 000 km^2 (Sippel *et al*., 1992), lies between discontinuous terraces that are generally about 5–15 m above the regularly inundated surface, except in reaches where higher terraces are interpreted as due to recent uplift. The Holocene deposits consist of medium sand and finer sediments, weathering to clay complexes dominated by vermiculite and smectite (Johnsson and Meade, 1990). The mineral composition of these sediments matures downstream from the Andes due to concentration of quartz by weathering of the originally high lithic and feldspar-rich components in floodplain sediments and terraces together with a small influx of quartz from the rivers draining the shields (Franzinelli and Potter, 1983).

The Brazil and Guiana Shields, flanking the central Amazon trough, are developed on Precambrian crystalline rocks, deeply weathered on low-gradient terrains with long hillslopes (~1–2 km) but interrupted by steeper slopes with thin soils on upstanding granite and diabase intrusions and by the edges of extensive platforms of younger

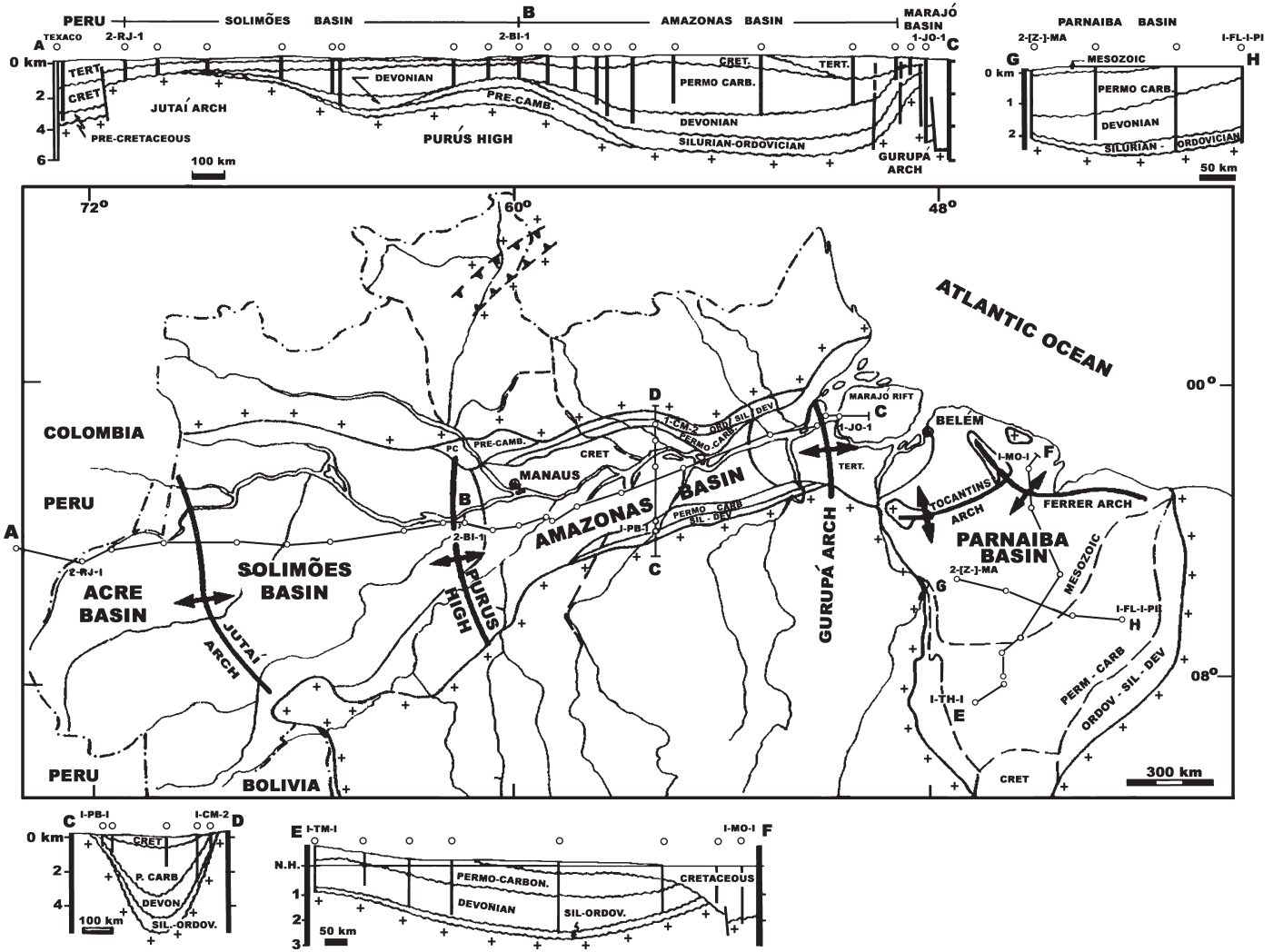

Figure 8.3 Structural framework of the Solimões, Amazonas, and Parnáiba Palaeozoic Basins according to Caputo (1984). The stratigraphy and structure outlined in this illustration correspond with maps and information provided also by Nunn and Aires (1988) and Petri and Fúlfaro (1988) and the locations of several of the structural highs are marked on Figure 8.1

sedimentary rocks. The main contribution of the shields to the behaviour of the modern Amazon River is to supply a huge discharge of water and a small addition of sediment from their low-gradient landscapes covered with forested, water-stable, kaolinitic, iron-rich soils. The sediment supplies to the rivers on these shields are generally much lower than their transport capacity, so that the rivers frequently flow on bedrock, and rapids are common except in downstream reaches where the tributaries flow in the alluvium-filled axial Amazon trough.

8.3.2 Second-Order Transverse Structures

Figures 8.1 and 8.3 portray a secondary scale at which the tectonics of the Amazon Basin affects the form and behaviour of the modern river. Between the Peru–Brazil border and the Atlantic Ocean four major structural arches lie transverse to the main Amazon trough and are named the Iquitos, Jutaí (Carauari), Purús, and Gurupá Arches from west to east (Figure 8.1). A fifth structure, the Monte Alegre Intrusion, which brings Palaeozoic sedimentary rocks to the surface, was identified by Caputo (1984, Figure 18), Nunn and Aires (1988), and Petri and Fúlfaro (1988, Figure I-4). Sediment cores and seismic surveys show that formations in each basin pinch out in the vicinity of the structural highs (Figure 8.3). The stratigraphy of these deposits indicates that the Jutaí and Purús Arches have been areas of relief since the Palaeozoic (Caputo, 1984) and the Iquitos and Gurupá Arches first evolved during the Mesozoic (Putzer, 1984; Dumont and Garcia, 1991). For the basins between the Iquitos and Purús Arches and south of the Jutaí Arch, Caputo (1991) presented evidence for substantial tectonic deformation. Although no detailed analysis was provided, Caputo (1991, p. 249) suggested that the 'stresses that generated the structures along the Solimões megashear [also generated] other similar structures at distances far to the east in the Amazon Basin'. Driscoll and Karner (1994) predicted that post-Miocene loading of sediment on the Amazon Fan should have caused flexural uplift parallel to the coast near the mouth of the river. They calculated uplift of 40–50 m along the coastal margin, coinciding with the position of the Gurupá Arch. The Iquitos Arch probably results from lithospheric flexure due to the loading of the Andes (Caputo, 1991). Dumont *et al*., (1990) and Dumont and Garcia (1991) concurred with this view and also concluded that, after alternate periods of uplift and subsidence, the Iquitos Arch has been uplifted since the beginning of the Quaternary, resulting in terraces 30 m above present river floodplains.

It is not known whether the other arches and the graben formed in the aulacogen in the east are currently deforming, although Milliman and Barretto (1975) dated oolitic limestones that lie below their depth of formation on the continental shelf, even after correcting for eustatic sea-level changes, and they calculated crustal subsidence averaging 28 mm a^{-1} between 16 and 21 ka. There was no evidence of deformation since that time. However, the Andean orogeny has altered the structural character of the entire Amazon Basin, and the impact of this orogenic loading may extend east of the Iquitos Arch in the form of reactivation of structural features that originally developed in response to earlier plate movements and attendant stresses. Possible mechanisms for reactivation and therefore continued uplift of cratonic arch structures include thermal rejuvenation, new horizontal stresses, long-term viscous relaxation, or new extensional faulting (Nunn, 1990). Fluvial sedimentation in the intervening basins may also have played a part by creating compensating crustal flexure. The effect of these transverse structures on modern river form and behaviour will be described below.

8.3.3 Fracture Patterns

The effect of large-scale fractures on drainage patterns throughout the tributary network of the Amazon Basin has been described by several authors. Drainage networks oriented in a northeast and northwest direction (Figure 8.2d and e) appear to reflect deep-seated basement fracturing that has continued to disturb the overlying sedimentary rocks (Sternberg and Russell, 1952). The presumption is then that the fracture networks have been exploited by some combination of weathering and channel erosion. Tricart (1977) also proposed that the presence of enormous lakes (Figure 8.2d and e) at the mouths of several Amazon tributaries (e.g. Negro, Tapajós, and Xingú) is in part due to subsidence along these northeast and northwest trending faults. Franzinelli and Igreja (2002) interpreted the alignment of the Lower Negro River as being controlled largely by a NW–SE tectonic lineament that is a segment of a major tectonic transcurrent dextral megasystem of the Amazon Basin. Intersecting sets of faults have formed sunken crustal blocks and depressions along a half-graben, which is inundated to an average depth of 20 m and a width of up to 20 km. The low supply of fine-grained sediment from the forested shield of the Negro Basin is flushed through the inundated fault-lined depression with only small amounts of sand storage along the margins. Most of the channel margin consists of cliffs of cohesive lacustrine sediments. The lack of bed material load exposes bedrock on the channel bed. An archipelago of long, narrow islands, consisting mainly of silt and clay runs parallel to the

banks; their origin is often interpreted as due to the presence of faults (Franzinelli and Igreja, 2002), but the mechanism by which such fine-grained sediment has become stabilized in this reach remains unclear. Leenheer and Santos (1982) suggested that the stabilization of these sediments might be due to flocculation; kaolinitic clays, which comprise a large proportion of these sediments, are known to be especially susceptible to flocculation in highly acidic water, like that of the Rio Negro, where pH values commonly fall in the range of 4–5. Franzinelli and Igreja (2002) suggest that these sediments are deposited in lakes sheltered by levees of sand that are deposited as lateral bars along upfaulted strips of the underlying bedrock.

A tilted fault block between the Jutaí and Purús arches was recognized by Tricart (1977) on morphological grounds in both the floodplain and the adjacent upland. Tricart recognized that upstream of Lake Coari (at 4°8′S 64°50′W in Figure 8.2d), the Amazon runs along and undermines a high terrace on its southern bank for a distance of more than 200 km. South of this escarpment, small river networks all drain towards the south, away from the Amazon, and many are beheaded. North of the river, a wide terrace and floodplain sequence slopes gradually towards the south (northwest corner of Figure 8.2d). At the southeastern end of this reach, the Amazon makes a sharp turn to the south, abandoning an alluvial reach of floodplain that continues the trend of its upstream reach towards the northeast (lighter green zone in Figure 8.2d). The tilted fault block recognized by Tricart is only one example of a larger array of evidence for neotectonic activity along the central and eastern Amazon valley interpreted by Iriondo (1982) and Iriondo and Sugio (1981). Latrubesse and Franzinelli (2002) interpreted changes in alignment of straight reaches of the Solimões/Middle Amazon main channel as reflecting recent activity on a set of NW–SE and SW–NE trending fractures, originally mapped from river and lake alignments by Sternberg and Russell (1952). They also mapped a 160 km long series of depressions, now occupied by lakes and smaller channels, including the lower Purús River, and interpreted the morphological evidence as indicating a massive avulsion of the Amazon main channel from the southern margin of the Holocene floodplain to the northern side, coinciding with a wide V-shaped, sunken tectonic block (Figure 8.4) controlled by NW and NE lineaments and filled with Holocene sediments. They estimated the age of the avulsion as approximately 1 ka. The Purús River has a high-sinuosity meandering pattern throughout most of its lowland, but its confluence with the Solimões River is approached through an almost straight channel along the southeastern margin of the proposed tectonic block. At present, the Purús cuts through the lake-filled silt and clay-rich Solimões floodplain, but has developed almost no alluvial plain of its own (Latrubesse and Franzinelli, 2002).

Inferences that structure and tectonic activity are influencing the channel-floodplain systems in the Amazon Basin have been based primarily on sparse stratigraphic and geomorphic evidence, rather than on instrumental measurements of crustal movements. Sternberg and Russell (1952) listed the dates of several earthquakes reported in the basin since the seventeenth century. Without precise geodetic or seismic measurements it is not yet possible to prove that there has been recent tectonic movement. However, interpretations of various channel and other landscape features are consistent with recent or continuing deformation.

Figure 8.5 suggests some intriguing new evidence that the tectonics of the axial graben of the Amazon trough may continue to affect the alignment of the modern river and its entire Holocene floodplain on the scale of 100–150 km reaches. Nunn and Aires (1988) reported gravity measurements for the lower Amazon region (Figure 8.5a) between 61° W and 54° W, approximately 780 km east from the Purús Arch to the reach immediately downstream of the Monte Alegre Intrusion in Figure 8.1. Approximately 6000 m of sediment lie in the Palaeozoic basin, but in detail, the pattern of gravity anomalies in the eastern half of Figure 8.5a is characteristic of the asymmetric structures (Figure 8.5d–e) commonly observed in continental rift zones (Faulds and Geissman, 1992) for which the East Africa Rift System is the type example (Morley *et al*., 1992; Scholz, 1995). Rift zones often comprise ‘a series of half-graben basins linked end-to-end along the axis of the rift’ (Scholz, 1995, p. 1680). The thickest accumulations of sediment are usually closest to the bounding faults at the downslope end of steeply dipping depositional planes. The individual asymmetric basins are typically linked across the rift through areas of higher and more horizontal surfaces named either ‘accommodation’ or ‘transfer’ zones ranging in length from 50 to 150 km (Morley, 1989, 1990; Faulds and Geissman, 1992; Scholz, 1995). The transfer zones in the Amazon Rift, visible on Figure 8.5a, are approximately 100 km long. The deepest portions of the cross-sections in Figure 8.5 are centrally located in the west, asymmetrically located in the north near cross-section C–C', and then shifted to the south near cross-section D–D'. Although the asymmetry in Figures 8.5D and 8.5E is partly the product of the chosen orientation of cross-sections C–C' and D–D', the radial cross-sections are also asymmetric at these locations (Figure 8.5a).

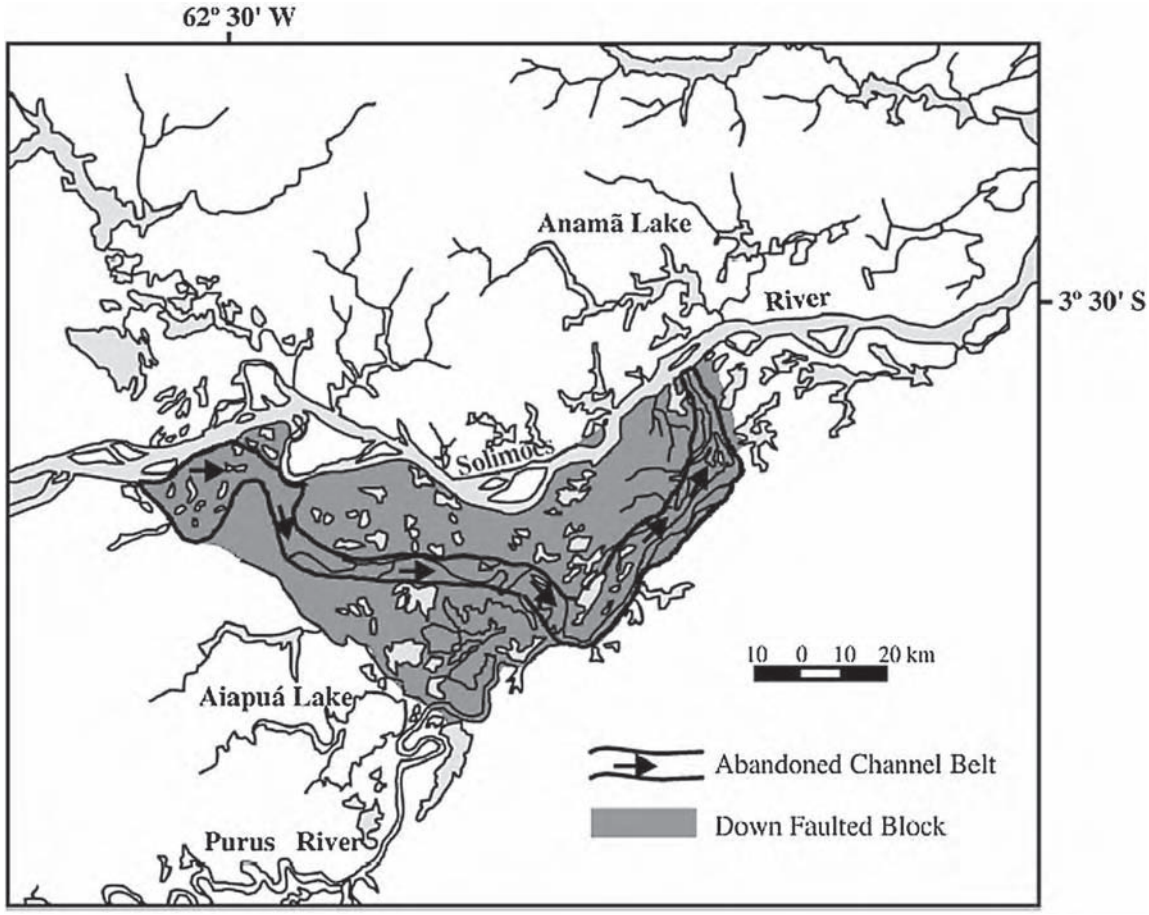

Figure 8.4 Reconstruction by Latrubesse and Franzinelli (2002) of the former alignment of the Solimões-Amazon River near the Purús River confluence. A belt of channels and lakes and the lower Purus River channel occupy a former path of the Solimões-Amazon River abandoned by avulsion upstream of the confluence with the Purus. Figure reprinted from Geomorphology, vol. 44, Latrubesse, E.M., Franzinelli, E., The Holocene alluvial plain of the middle Amazon River, Brazil, pp. 241–257, 2002, with permission from Elsevier

As the Amazon approaches this graben from the west, the river flows ~100 km north of the graben axis and does not appear to be influenced by the structure where the sedimentary basins are symmetrical (cross-section A–A' and B–B', Figure 8.5b and c). However, at longitude 57°20′W, the river intersects the expected location of a transfer zone between two depositional basins in the graben, and the alignment of the valley changes dramatically towards an ESE trend and the river crosses its entire Holocene valley. After impinging on the cohesive sediments of the southern margin of the valley, the river suddenly changes direction again and flows directly back to the north side of its valley as it encounters the location of the next downstream transfer zone near cross-section C–C'. The river and its Holocene valley then continue eastward outside of the influence of the graben until they reach the estuary. The drainage systems of the active Africa Rift System exhibit similar asymmetric patterns (e.g. Scholz, 1995; Upcott *et al*., 1996). The mechanism by which deep-seated accommodation of crustal stresses propagates to the surface to influence river alignments remains unknown and speculative, but presumably is related to the same kind of subtle land surface tilting that seems to be responsible for the tilting of the valley upstream. It may provide an explanation for the otherwise surprising observation that the Amazon undergoes two dramatic

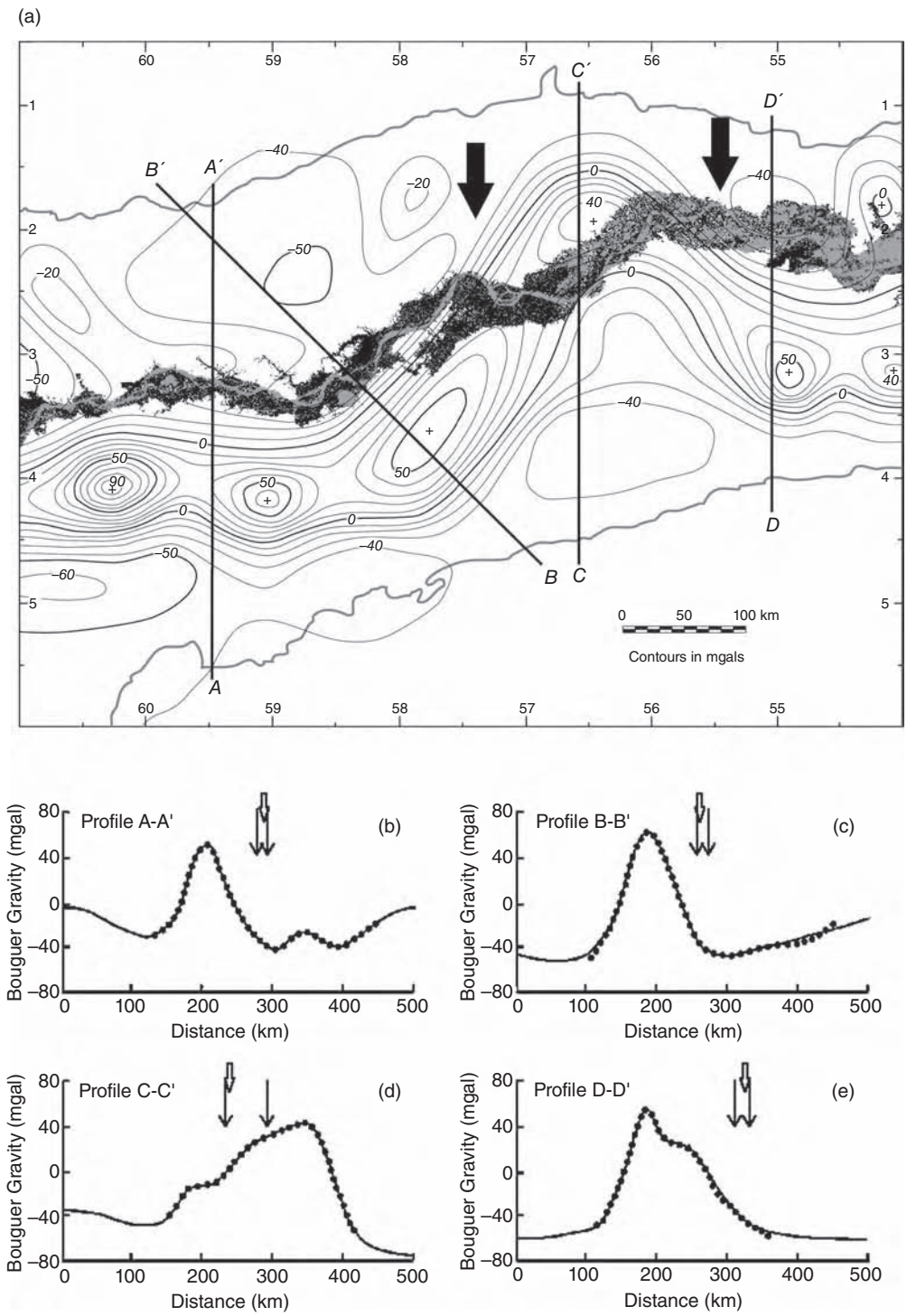
(a)
A
A´
B
B´
C
C´
D
D´
Contours in mgals
0 50 100 km
Profile A-A'
(b)
Profile B-B'
(c)
Profile C-C'
(d)
Profile D-D'
(e)
Bouguer Gravity (mgal)
Distance (km)

Figure 8.5 (a) Map of the Amazon floodplain (shaded image) overlaid on a Bouguer gravity map of the region, in which large positive gravity anomalies are directly proportional to depth of sediment in crustal basins. The Holocene Amazon channel and floodplain (shaded in grey) were mapped from a geo-referenced, classified mosaic of Landsat images. Between the two vertical arrows the channel crosses the valley from the north edge to the south edge and then crosses back to the northern edge of the valley. These transits occur where the valley crosses two transfer zones of the underlying graben. The gravity map is reproduced from Nunn, J.A., Aires, J.R., Gravity anomalies and flexure of the lithosphere at the middle Amazon basin, Brazil, Journal of Geophysical Research, vol. 93, pp. 415–428, 1988, by permission of American Geophysical Union (b–e) Bouguer anomalies for the cross-sections marked A-A' (b), B- B' (c), C- C' (d), and D- D' (e) from Nunn and Aires (1988, their Figures 4 and 6c). The asymmetry of the structure is most pronounced in (d) and (e) between which exists a transfer zone. The arrows at the top of each graph indicate the edges of the Amazon valley and the position of the river channel in between. Modified from Nunn, J.A., Aires, J.R., Gravity anomalies and flexure of the lithosphere at the middle Amazon basin, Brazil, Journal of Geophysical Research, vol. 93, pp. 415–428, 1988, by permission of American Geophysical Union

excursions across its entire floodplain in the illustrated reach, a change of alignment that is not repeated along the entire river course.

8.3.4 Structural Influences on Amazon River Geomorphology

There is considerable variation of inundation and sedimentation processes and of channel and floodplain form and behaviour along the central Amazon trough. Some of the local variations in channel alignment have been referred to above because they provide the evidence for the tectonic influences on landform evolution. What follows is a survey of the geomorphological impacts, other than alignment, of the various tectonic influences introduced above.

The increase in drainage area between the foreland basin and tidewater results in a large increase in discharge as runoff drains from the Amazon lowland and shields. The mean annual flow of the Solimões at São Paulo de Olivença near the Peru–Brazilian border (drainage area 940 000 km^2) is 45 600 $m^3 s^{-1}$ (1275 mm a^{-1}) and the mean annual flood is 64 000 $m^3 s^{-1}$. At Óbidos (4 640 000 km^2), these flows are 170 000 $m^3 s^{-1}$ (960 mm a^{-1}) and 237 000 $m^3 s^{-1}$. The average annual sediment flux is 616 Mt a^{-1} at São Paulo and 1240 Mt a^{-1} at Óbidos after 715 Mt a^{-1} are supplied by the Madeira River and 117 Mt a^{-1} by the other tributaries (Dunne *et al*., 1998). These measured sediment yields are considerably larger than the rates of sediment production calculated from geochronological methods for the Bolivian Andes during the last few thousand and few million years (Safran *et al*., 2005, 2006). Similarly, transport calculated from river sediment sampling in Bolivia indicates high rates of sediment supply for the past few decades. Aalto *et al*. (2006) calculated erosion rates averaging 0.65 mm a^{-1} (~1400 Mt a^{-1}) for 47 Andean basins in Bolivia, sampled by Guyot (1993), and 2300–3100 Mt a^{-1} when the measurements were extrapolated to the rest of the Amazonian Andes on the basis of a statistical analysis of basin topography. Yet, a determined ground and satellite search for land-use effects on sediment yield was not successful (Aalto *et al*., 2006). We do not yet understand the significance of the differences in these estimates of sediment supply to the Amazon for different time periods. The river transports this load through its Holocene floodplain, which is generally incised more than 10 m below the surrounding landscape of Tertiary and Quaternary sediments. Large exchanges of sediment between channel and floodplain occur during this transit, and several hundred Mt a^{-1} enter long-term storage, especially in the lower Amazon floodplain (Dunne *et al*., 1998). Considering that system-wide exchanges of sediment between channels and floodplains may exceed downriver sediment fluxes by a factor of two or more (Dunne *et al*., 1998; also Chapter 4), even small perturbations in the rates at which sediment is added to or eroded from the floodplains are likely to confound any calculations of sediment budgets based solely on in-channel sediment fluxes.

Several studies of foreland basin geomorphology in Peru and Bolivia invoke tectonic deformation as a primary cause for development of terrace sequences through alternating river aggradation and incision and channel migration (e.g. Dumont and Garcia, 1991; Dumont *et al*., 1991). There are at least two sets of terraces in the Brazilian Amazon that record a preferred pattern of river migration which may indicate local tilting, instead of base-level or climatic change. Between the Japurá and Amazon channels (Figure 8.2c) and then north of the Japurá River at the same longitude, terraces exist that from north to south apparently decrease in elevation and show decreased weathering of what are probably older channel deposits (their surfaces show scroll bars), thus indicating a consistently younger age from north to south (Klammer, 1984; Irion *et al*., 1995). Therefore, these sets of terraces indicate that both the Japurá and Amazon channels have been migrating steadily to the south for tens to hundreds of

millennia in response to valley tilting caused by local tectonic deformation (Tricart, 1977).

The gradient of the Solimões-Amazon channel varies along the river in concert with the pattern of structures transverse to the river valley (Figure 8.1). Figure 8.6 demonstrates several associations between these transverse structural features and changes of river gradient. The horizontal black bars in Figure 8.6b indicate average water-surface gradients for 11 river reaches calculated from radar altimeter readings of low-water elevation (see Dunne *et al*., 1998 for details). These changes in gradient correlate with water-surface gradients calculated from flow velocity profiles, and have been recorded on a higher spatial and temporal resolution through radar altimetry over an entire annual hydrograph (Birkett *et al*., 2002). The bars in Figure 8.6 demonstrate that the river becomes steeper as it approaches the Jutaí and Purús Arches and the Monte Alegre Intrusion and then its gradient declines downstream of each structure. The increases in gradient are associated with narrowing of the floodplain and decreases in channel sinuosity across the structural highs (Mertes *et al*., 1996) as the river impinges on high, cohesive banks, suggesting recent incision of older floodplain. A fourth zone of increased gradient lies in the vicinity of the tilted fault block recognized by Tricart (1977), in the range 1000–1400 km downstream of Iquitos in Figure 8.6b, where the Amazon also appears to have been shortened and steepened by autocapture and tilting of the valley floor towards the south-southeast. The gradient then decreases between kilometres 1400 and 1700 as the river flows along the southern margin of its valley away from the tilted reach.

The variation of channel gradients and floodplain widths along the modern Amazon continue to influence the modern patterns of sediment transport (Dunne *et al*., 1998), long-term sediment accumulation, and floodplain morphology (Mertes *et al*., 1996). Where the river crosses structural highs, the resulting downstream sequence of changes in floodplain width, channel sinuosity, gradient, and migration rate are associated with patterns in the various sediment transport processes between the channel and floodplain and along the river, determining net alongstream transport and storage. The pattern is complicated slightly by net scour downstream of the large flow increment of the sediment-poor Negro (Dunne *et al*., 1998, p. 465).

Mertes *et al*. (1996) illustrated the association between variations of channel gradient and the character of the channel and floodplain. The main channel of the Amazon is anastomosing throughout its Brazilian reach with a sinuosity of 1.0–1.2 along most of its course (Figures 8.7–8.12). Anabranches are common along the river, apparently the remnants of flow switching. When bends occur, however, they have half-wavelengths of 10–15 km and amplitudes of 15–25 km upstream of the Negro confluence (Figures 8.7–8.9). Downstream of the Negro, bends are generally less sinuous and longer (Figures 8.10 and 8.11) with poorly defined half-wavelengths of 30–50 km and amplitudes of 10–50 km. The characteristic size of bends in a river as large as the Amazon (Dury, 1964; Leopold *et al*., 1964), as well as the valley tilting and realignments described above, ensure that the river frequently encounters the cohesive terrace materials bordering its Holocene floodplain, creating scalloped terrace edges (Figure 8.10) and straightened channel courses (Figure 8.8).

In addition to the main channel, the floodplain contains a dense network of channels with discharges that are less than an order of magnitude smaller than that of the main river. The larger, deeper ones tend to remain connected to the main channel in the low-flow season while many of the smaller ones become stagnant, though remain flooded. The width of the largest floodplain channels generally increases in the downstream direction from 800 to 2000 m, although floodplain channels about 100 m wide occur in every reach (Mertes *et al*., 1996, Figure 8.13). As the main channel, anabranches, and floodplain channels migrate, scroll bars are left behind on the floodplain surface. In the downstream reaches the scroll bars tend to be longer, farther apart, and straighter than the upstream bars. The outer scroll bars were originally formed by the main channel, but many of the inner scroll bars were deposited in the bends of floodplain channels, which are significantly smaller than the bends of the main Amazon channels (Mertes *et al*., 1996). Downstream of the Madeira River confluence the scroll bars are less distinct and tend to be almost straight along their preserved lengths.

Where the river crosses a structural high such as the Jutaí Arch (Figure 8.7) or the Purús Arch (Figure 8.8), the river runs along cohesive terrace materials and is almost straight for considerable distances, the floodplain is relatively narrow, scroll bars are confined to the immediate channel margins, channel migration rates are small, and floodplain lakes are relatively rare. In low-gradient reaches between the arches, floodplains are wide with large-scale river movement or avulsion that builds scroll bars and anabranches in the Solimões (Figure 8.9). Downstream of the Negro confluence, the wide floodplains in low-gradient reaches such as Figures 8.10 and 8.11 have anabranches, leveed distributary channels with deltas built into floodplain lakes, and considerable floodplain complexity.

The wider floodplains contain a complex mosaic of lakes, lake deposits, and fluvial overbank deposits. In reaches upstream of the Purús arch, where the floodplain is widest, the lakes are generally small and are confined

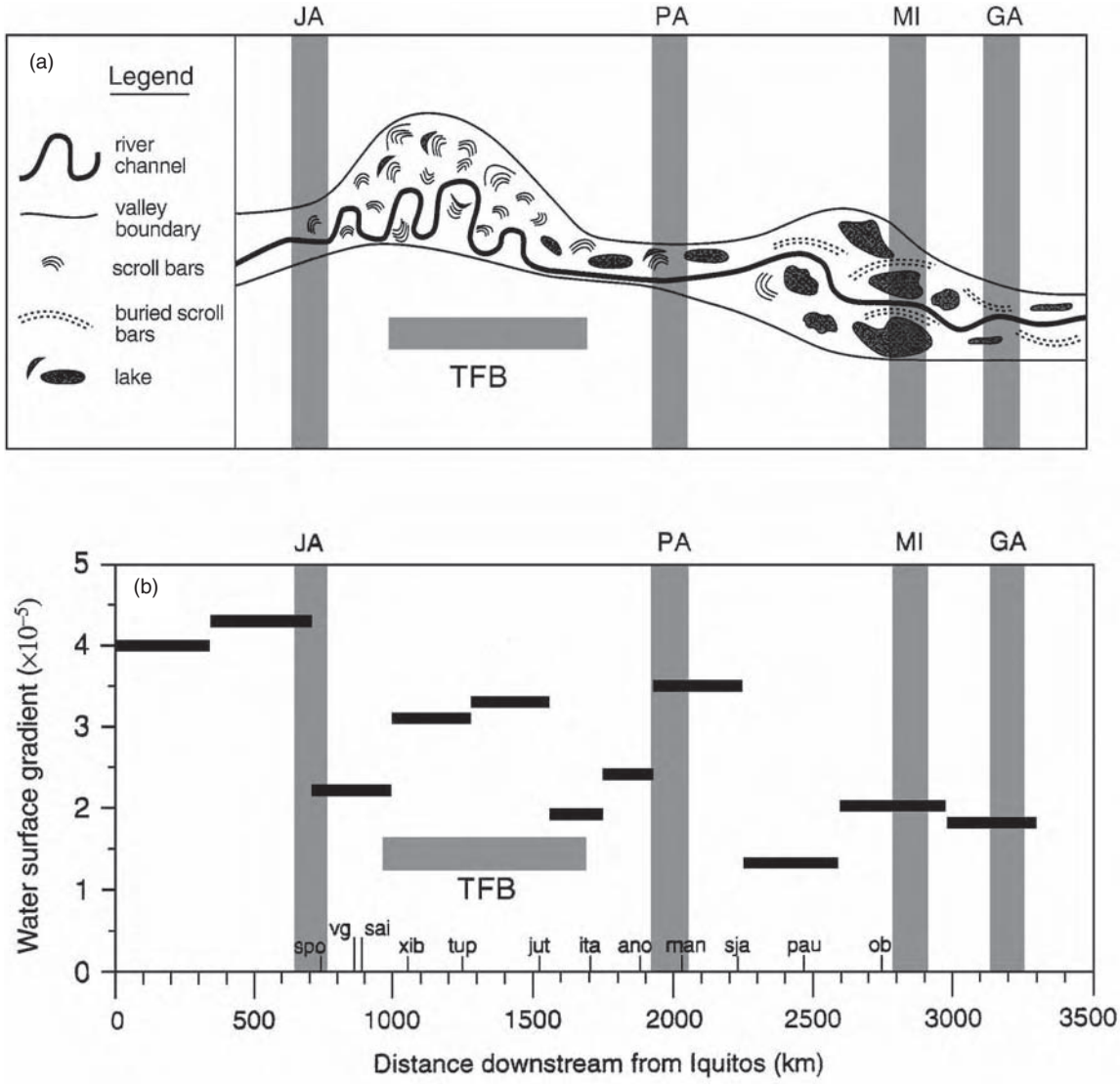

Figure 8.6 (a) Schematic illustration of the relation between geomorphic and structural features of the lower Amazon valley. The four vertical bars indicate the approximate locations of the axes of arches and structural highs mapped by Petri and Fúlfaro (1988) and Caputo (1991): JA, Jutaí Arch; PA, Purús Arch: MI, Monte Alegre Intrusion and ridge; GA, Gurupá Arch. TFB, the approximate extent of a tilted fault block proposed by Tricart (1977). Reproduced with permission from Geological Society of America Bulletin, vol. 110, Dunne *et al*., Exchanges of sediment between the flood plain and channel of the Amazon River in Brazil, pp. 450–467, 1998. Geological Society of America. (b) Water-surface gradient at low flow along a 3200 km long reach of the Amazon River, based on radar altimetry measurements collected during low water between 27 July and 9 August 1978 for 32 sites. Details on data acquisition and analysis are described by Dunne *et al*. (1998). Abbreviations on the abscissa refer to sediment sampling stations, gauging stations, and reaches referred to in the text and other figures. Corresponding to Figure 8.1 are São Paulo de Olivença (spo), Manacapurú (man), and Óbidos (obi). Reproduced with permission from Geological Society of America Bulletin, vol. 110, Dunne *et al*., Exchanges of sediment between the flood plain and channel of the Amazon River in Brazil, pp. 450–467, 1998. Geological Society of America

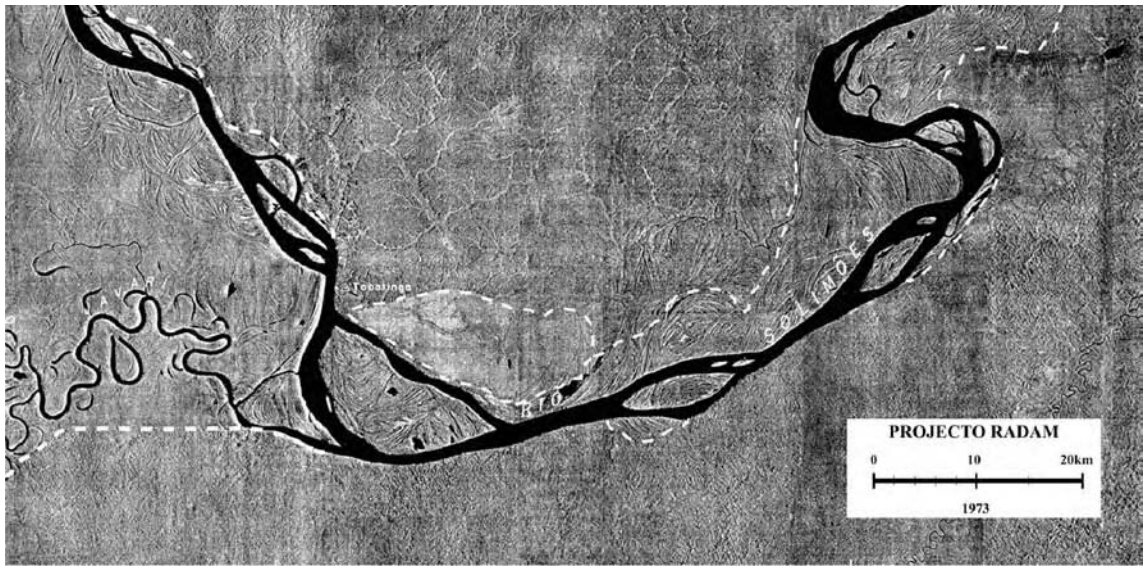

Figure 8.7 The Solimões River reach centred approximately at 69°45′W where the river crosses the Jutaí Arch, approximately at 550 km on Figure 8.6b. The floodplain with scroll bar topography is generally less than 10 km wide, and the channel impinges on cohesive terrace materials throughout most of the reach. The dashed white curves indicate the approximate position of the boundary between the modern floodplain and the higher terrain that has not been alluviated probably since the late Tertiary and has been eroded by dendritic drainage networks. The closed dashed polygon north of the river in the central portion of the image is probably an older portion of the floodplain on which the scroll bars, channels, and narrow lakes that dominate the modern floodplain have been diffused by either erosion or overbank sedimentation. Source: radar image from the Radambrasil Project

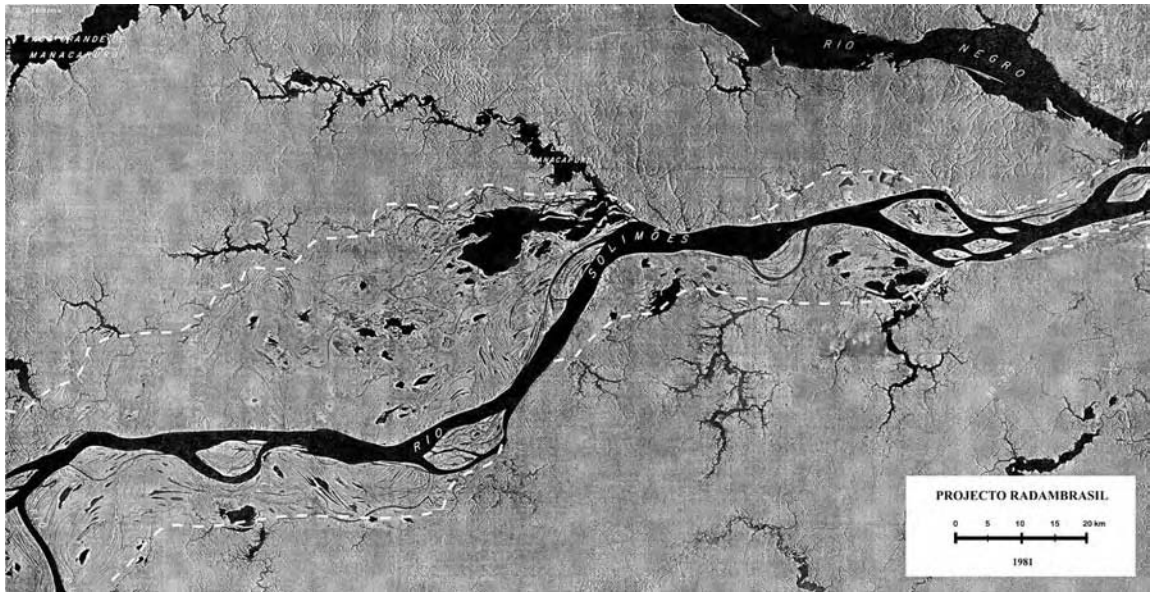

Figure 8.8 The Solimões River reach between the Purús (lower left corner) and Negro (upper right corner) confluences, centered approximately at 60°45′W near Manacapurú at 2030 km in Figure 8.6b. The dashed white curves indicate the approximate position of the boundary between the modern floodplain and the higher terrain that has not been alluviated probably since the late Tertiary and has been eroded by dendritic drainage networks. Small, sediment-poor streams draining from the Tertiary sediments across the floodplain margins are dammed by the rapid alluviation of the mainstem floodplain. The Solimoes-Amazon River is crossing the Purús Arch in the eastern half of the image, and the floodplain is narrow and the channel steep (around 2000 km on Figure 8.6b). Source: radar image from the Radambrasil Project

Figure 8.9 The Solimões River reach centred on 66°45′W downstream of the River Jutaí confluence at 1100 km on Figure 8.6b. In the tilted fault block reach between the Jutaí and Purús Arches, the floodplain is wide, allowing the development of large meanders, extensive scroll bars, and an abandoned oxbow lake. The dashed white curves indicate the approximate position of the boundary between the modern floodplain and the higher terrain that has not been alluviated probably since the late Tertiary and has been eroded by dendritic drainage networks. The ages of the various surfaces within the Quaternary floodplain are generally unknown. Source: radar image from the Radambrasil Project

Figure 8.10 The Amazon River reach centred at 57°45′W approximately at 2450 km on Figure 8.6b, ~150 km downstream of the Madeira River confluence. The floodplain is 40–50 km wide and includes scroll bar topography near the river and irregular lake networks farther from the channel. The dashed white curves indicate the approximate position of the boundary between the modern floodplain and the higher terrain that has not been alluviated probably since the late Tertiary and has been eroded by distinctive drainage networks. Sediment-poor tributaries draining from the Guiana Shield and Tertiary sediments across the floodplain margins are dammed by the rapid alluviation of the mainstem floodplain. Source: radar image from the Radambrasil Project

Figure 8.11 The Amazon River reach centred at 56°15′W approximately at 2650 km on Figure 8.6b. The floodplain appears to be 'underfilled' with a large area of lakes separated from the channel by narrow scroll bars and levees that are almost straight. Small channels entering these lakes from the main channel or from tributaries build leveed channels and small deltas into the lakes. The dashed white curves indicate the approximate position of the boundary between the modern floodplain and the higher terrain that has not been alluviated probably since the late Tertiary and has been eroded by distinctive drainage networks. Sediment-poor tributaries draining from the Guiana Shield and Tertiary sediments across the floodplain margins are dammed by the rapid alluviation of the mainstem floodplain. Source: radar image from the Radambrasil Project

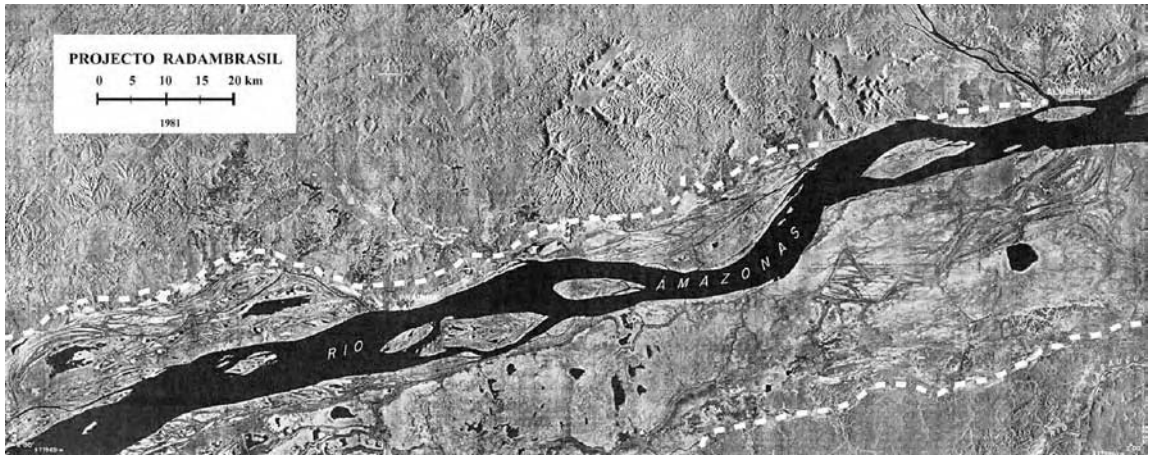

Figure 8.12 The Amazon River reach centred at 53°15′W approximately at 3050 km on Figure 8.6b. Downstream of the Monte Alegre Intrusion the river is constructing a delta plain (between the dashed white curves) with rapidly shifting mid-channel bars and a floodplain that contains very few lakes. The absence of strongly developed scroll bars at the surface suggests intensive overbank sedimentation. Source: radar image from the Radambrasil Project

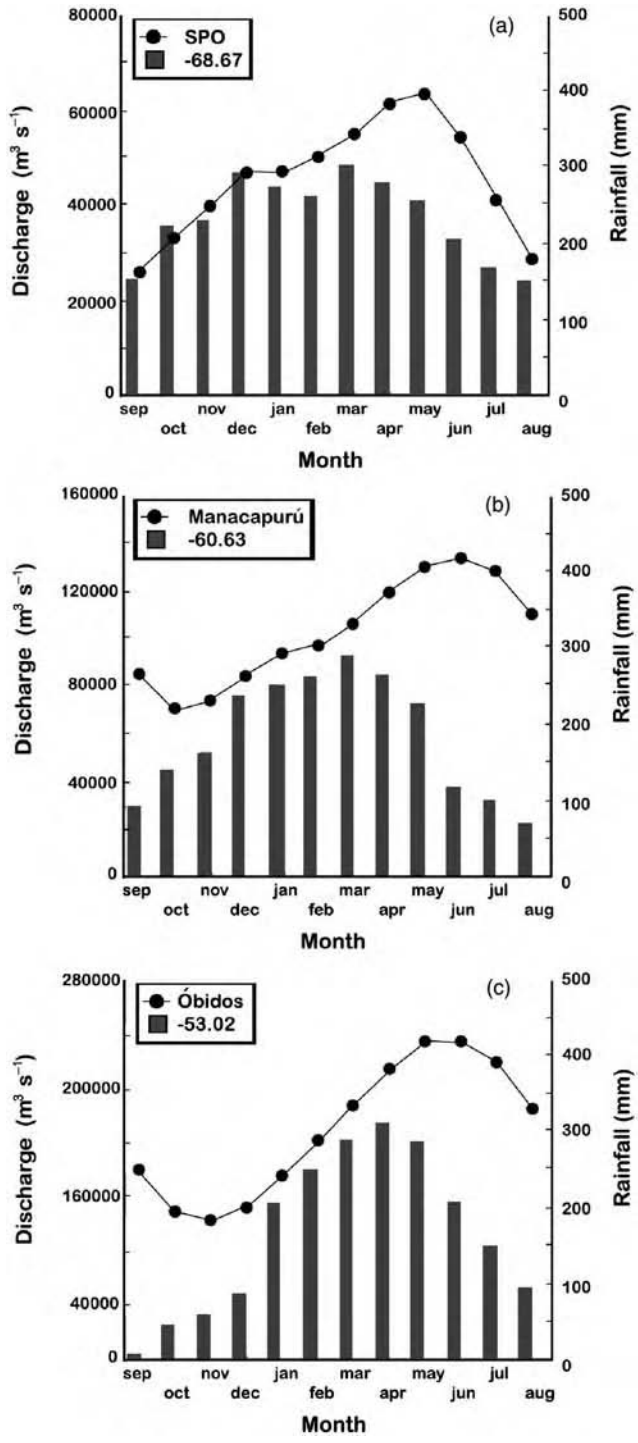

Figure 8.13 Typical monthly hyeto- and hydrographs along the mainstem Amazon River. Monthly rainfall totals are interpolated from maps of average values for 1972–1996, based on data from rainfall stations distributed across the basin. (Data supplied by the Brazilian Water Resources Agency ANEEL). Position along the river is indicated in degrees of longitude. Discharge is based on mean monthly average flows for gauges as reported by Richey *et al*. (1986) and shown in the legend for gauges at (a) SPO, (b) Manacapurú, and (c) Óbidos (locations shown on Figure 8.1)

to narrow swales between scroll bars. In contrast, the larger lakes tend to be in the downstream reaches, regardless of floodplain width, and have less well defined boundaries. The largest lakes are just downstream from Óbidos and are as much as 65 km across (Melack, 1984). The alongstream pattern in a number of lakes is irregular, however. The number of lakes increases between 1000 km and 1700 km downstream of Iquitos (see Figure 8.6), approximately in the reach from Xibeco to Itapeua, then decreases in the downstream direction to São José do Amatari (2228 km), increases again after the Madeira River confluence (2300 km), and then the lakes disappear just downstream from the Tapajós River (2900 km). The modern floodplain transitions to the estuary through a delta plain downstream of the Tapajós and Xingú ria mouths and the Gurupá Arch, where the number and size of islands and lakes decrease dramatically as overbank flows intensify sedimentation (Figure 8.12). In the lower Amazon valley, tectonic influences on gradient interact with the effects of postglacial sea-level rise to control the patterns of alluviation (see later).

The impacts of tectonics on the landscape of the Amazon River and its valley are subtle, but widespread. At the largest scale, they result from the geological constitution and deformation of the continent that impose a path and a distribution of water and sediment loads on the river. At smaller scale, they result from the fact that such a large river has very low gradients, and frequently encounters lithological constraints from surrounding geological materials, including its own weathered, cohesive terraces. We have outlined a schematic model for the eastern Amazon main channel and valley that illustrates the spatial correlation between the narrowing of the alluvial valley as the river crosses structural highs and the gradual widening of the valley on the downstream limb of these features. In addition, new evidence in Figure 8.5 extends the interpretation that the position and alignment of the Amazon channel, even in the lowland reaches, continues to be strongly influenced by deep geologic structures. Therefore, the overall effect of intracratonic tectonic deformation and ancient rift structures on the continental-scale Solimões-Amazon River in Brazil is to create a landscape where, on the scale of hundreds of kilometres, the main river is entrenched, confined in its valley, is straight, and relatively immobile.

8.4 INFLUENCE OF CLIMATE CHANGE ON THE AMAZON RIVER

The modern hydroclimatology of the Amazon Basin is dominated by the shifting of the Intertropical Convergence Zone (ITCZ) (Hjemfelt, 1978; Salati *et al*., 1979; Hayden, 1988) with the Andean region also being affected by the South Atlantic Convergence Zone (SACZ) (Liebmann *et al*., 1999; Seluchi and Marengo, 2000). The climate is also impacted by changes in sea-surface temperature as the SACZ moves seasonally (Liebmann *et al*., 1998; Uvo and Graham, 1998; Uvo *et al*., 2000; Liebman and Marengo, 2001). With these influences, precipitation is fairly uniformly distributed across the basin with modest orographic effects in the west. Overall the basin receives 2000–2500 mm of rain annually. The lowest rates occur in the extreme northeastern and southern parts of the basin (~2000 mm a^{-1}) with 3500 mm a^{-1} in the northwest lowlands and local maxima up to 7000–8000 mm a^{-1} on the lower eastern slopes of the Andes in Peru. Precipitation maxima are limited to the lowermost 500–1000 m of the Andes, above which precipitation generally declines with increasing elevation.

The seasonality of rainfall is driven by the movement of the ITCZ, generating a rainy season that begins in the southern half of the basin in November and December and in the northern half of the basin almost 2 months later. The alongstream pattern of rainfall is illustrated with the hyetographs and compared with the river hydrograph in Figure 8.13. The hydrograph is unimodal, damped and delayed by the size and length of the basin channel network, the storage capacity of the large floodplain wetlands which exceed 100 000 km^2, and the temporal offset between tributary inputs from the northern and southern hemispheres (see Richey *et al*., 1989a for tributary hydrographs). Statistical analyses of trends in the historical record (most notably the 100-year record at Manaus) show that there has been no secular regime change. For example, any impacts of deforestation on flow patterns are not yet sufficient to produce trends in the flow record of the Amazon (Marengo, 1995; Marengo *et al*., 1998). However, Costa *et al*. (2003) have shown that clearing and pasturing of 49% of a shrub-covered 175 000 km^2 catchment within the Tocantins River Basin in the relatively dry (1600 mm a^{-1} rainfall) southeastern Amazon has resulted in a 24% increase in annual runoff despite annual rainfall remaining statistically unchanged in the same period.

Precipitation and river flow are affected by the strength of the El Niño – Southern Oscillation (ENSO). Richey *et al*. (1989b) showed that in the period 1906–1985 low annual flows of the Amazon at Manaus occurred during El Niño years when ocean circulation anomalies associated with ENSO modify both the intensity and location of the energy source for atmospheric heating and circulation (Aceituno, 1988; Molion, 1990). The main convection centre shifts to the central Pacific and weakens over the central Amazon, reducing rainfall (Foley *et al*., 2002). Molion (1990) quoted reductions of up to 1.8 standard

deviations in rainy season totals in the northwest Amazon Basin and 0–1.2 standard deviations in the central and eastern portions of the basin. More recent studies have added regional detail in general agreement with this picture. Generally speaking, El Niño years are drier and warmer than normal in Amazonia. Foley *et al*. (2002) demonstrated that changes are stronger over the northern portion of the basin (generally north of 4° S latitude) with an average 4.8% (120 mm a^{-1}) reduction in rainfall in El Niño years and an average increase of 8.5% (215 mm a^{-1}) during La Niña conditions. This northern region also experiences an increase in annual runoff averaging 18%. In the south, changes are generally smaller. By contrast, the southwest Amazon Basin, at 10° S latitude and closer to the perturbed offshore area of the East Pacific, shows an increase of up to 1.2 standard deviations in rainy season rainfall during the cold phase of the ENSO, causing widespread landsliding and flooding in the Beni River system (Ronchail, 1998). River flows and sedimentation patterns are sensitive to even subtle shifts in the ENSO circulation. For example, the Mamore River floodplain, immediately south of the Beni, spans a transitional region of climate response to the ENSO (Coelho *et al*., 2002), which seems to have migrated in the early 1970s. Before 1970, rainfall was high during La Niña, but after 1970 this effect disappeared (Ronchail, 1998), and floods have decreased with an abrupt reduction in the frequency of overbank sedimentation in the foreland basin reach of the Mamore (Aalto *et al*., 2003). Thus, climatic fluctuations of this scale can affect inundation and sedimentation processes, but no morphological effects on the river system have yet been recognized. It is not clear whether the onset of 'ENSO-like' conditions about 7000 years ago (Martin *et al*., 1993) had any impacts apart from the changes in lake levels, vegetation changes recorded in pollen profiles, and sedimentation records from which the climatic change was interpreted.

During the glacial periods, glaciers expanded in the Andes, and colder climates prevailed over the Amazon Basin. The timing of the Last Glacial Maximum in the Andes and the Amazon Basin has been assigned various dates by people working with differing kinds of evidence. Clapperton (1993) suggested a date of around 27 ka with glaciers extending nearly 1000 m lower in elevation on the eastern faces of the ranges, indicating a temperature decline of about 5 °C. Smith *et al*. (2005a) used a broader definition of 34–21 ka, during a period of complex changes by glaciers in varying topographic settings that was wetter than at present on the Altiplano. Baker *et al*. (2001a), using various sedimentary properties of cores from Lake Titicaca, set the end of the LGM at 21 ka set within a period from 26–15 ka when the Altiplano was wetter than at present. Stable isotopes from Peruvian ice cores imply that Last Glacial Maximum (LGM) high-altitude temperatures were 8–12 °C cooler than present-day temperatures (Thompson *et al*., 1995, 2000). Detailed chronologies and field mapping of glacial deposits in three valleys of the Peruvian and Bolivian Andes led Smith *et al*. (2005a) to conclude that the maximum lowering of snowlines was varied within a range of 300–1000 m, implying only a 2–4 °C lowering of mean annual temperature. A broader survey of the tropical Andes (Smith *et al*., 2005b) revealed a snowline depression of 300–1350 m with local topographic and precipitation effects complicating any generalizations. Colinvaux *et al*. (1996) interpreted the shift of Andean taxa into the lowland Amazon along the Equator near 67° W to indicate a cooling of 5–8 °C. Palaeo-ground temperatures in northeastern Brazil, estimated from noble gas concentrations in groundwater dated with ^{14}C, indicate a cooling of at least 5 °C (Stute *et al*., 1995), in line with both the majority of snowline interpretations and vegetation reconstructions in the region (see below). These same geochemical results indicated that warming began around 13 ka. There is no evidence for glaciation in the shields in the north and south of the basin.

The history of precipitation across the basin appears to have been more complex. Early interpretations of a drier glacial climate in Amazônia relied mainly on geomorphic evidence of relict dune fields (Tricart, 1975, 1985; Clapperton, 1993) around the margins of the Basin. More recently, the sedimentology, mineralogy, chemistry, and palynology of lake sediments have provided the basis for palaeoclimatic reconstructions, although the number of lake studies remains small for such a vast area with significant regional differences to be anticipated in weather systems. Constraints on the amount of datable material in cores and the precision of some methods leave uncertainties about the synchronicity of changes recorded in various regions.

The Bolivian Altiplano at 70° W (Baker *et al*., 2001b) and the north-central Amazon lowland at the Equator and 67° W (Bush *et al*., 2002) were both relatively wet during 22–18 ka, after an exceptionally dry period from 35 to 27 ka (Bush *et al*., 2002). Baker *et al*. (2001a, b) have also suggested that throughout the Late Glacial and Holocene, including the particularly cold Younger Dryas episode, wet periods in the Andes and lowland Amazonia were simultaneous with periods of cold sea-surface temperatures in the tropical Atlantic Ocean. This millennial-scale alternation with warmer and drier periods has continued in the recent history of the region. On the eastern slopes of the Andes, cooling lowered the tree line by 1200–1500 m and led to taxa from higher and drier regions penetrating the western Amazon lowland (Van der

Hammen, 1974; Liu and Colinvaux, 1985; Bush *et al*., 1990; Colinvaux *et al*., 1996; Colinvaux and De Olivera, 2000). Baker *et al*. (2001a,b) and Bush *et al*. (2002) recognized humid conditions during most of this period in the central and northwestern Amazon Basin, with the Andes drying immediately after the Last Glacial Maximum (15–13 ka), according to Baker *et al*. (2001a). On the other hand, Seltzer *et al*. (2000) concluded that arid conditions prevailed in Andean Peru in the Late Glacial and Early Holocene, followed by wet conditions in the Middle and Late Holocene. Siffedine *et al*. (2001) also accumulated evidence for a drying of Lake Titicaca on the Altiplano (16° S 69° W) during the LGM. This contradiction remains unresolved until hydroclimatic processes in the region are clarified.

However, even in the driest period, centred around 33 ka, the forest cover in the central lowland and western slopes of the Amazon Basin remained continuous, despite the fact that cooler, fluctuating temperatures probably led to a more open forest structure and composition. Bush *et al*. (2002) estimated that during this driest period the annual rainfall could have decreased by as much as 30 % without breaking the continuity of the forest cover. Pollen records described by Frost (1988) confirm the continuity of forest cover in the Andean foothills of eastern Ecuador throughout the Holocene, despite the evidence for severe dry periods (Baker *et al*., 2001a), although the composition of these forests changed frequently.

There is more uncertainty about the history of precipitation in the northern, eastern, and southern parts of the Amazon Basin. Pollen records from the central Amazon Basin during the Holocene (Absy, 1979) and from the periphery of the Basin over a longer period (Van der Hammen, 1974; Van der Hammen *et al*., 1992a,b; Servant *et al*., 1993; Van der Hammen and Absy, 1994) show intermittent dominance of grass pollen, which has been interpreted as evidence for a change to savanna conditions. This result from cores in the central lowland has been questioned because it conflicts with other data described above and might be the result of local changes in inundation hydrology (Räsänen *et al*., 1991). However, the shallow lakes cored by Van der Hammen and Absy (1994) and Servant *et al*. (1993) at Carajás in eastern Amazonia are located on a plateau with a present-day rainfall of 1500–2000 mm a^{-1} and a strong 3-month dry season. The site is occupied by evergreen forest with patches of deciduous trees and grassland on thin, rocky soils in the surrounding region, so it seems reasonable that it should be a sensitive indicator of any drying. Servant *et al*. (1993) reported that in the Late Glacial (22–13 ka), after recording forest cover for at least 10 000 years, the lake dried up and recorded low amounts of tree pollen before and after the hiatus. Independent studies of geochemical and petrographic studies from small lakes in the same region essentially confirmed these results and documented oscillations between wet and drier periods throughout the Holocene once wetter conditions were re-established after 15.4 ka.

Van der Hammen and Absy (1994) recorded savanna pollen in Rondônia (9° S 63° W) around 18.5 ka, after a wetter forested period, and at Carajás and in the Guiana region in Late Glacial time, suggesting that the eastern and southeastern arc of the Amazon Basin margin, currently occupied by open evergreen forest with a significant dry season, probably experienced savanna conditions in Late Glacial time before reforestation as the climate became generally wetter and warmer at the beginning of the Holocene. If so, there must have been a strong gradient between this drying region and Bush's site at 67° W on the Equator at this time. Van der Hammen and Absy (1994) estimated that reductions of precipitation of 500–1000 mm a^{-1} (~25–40 %) would explain the distribution of forest and savanna pollen records. This interpretation took no account of the documented atmospheric cooling on moisture effectiveness before 13 ka, which makes it even more difficult to reconcile the savanna pollen with rainfall estimates. The Carajás site should also be expected to have responded sensitively to the Holocene rainfall fluctuations that Baker *et al*. (2001a) projected across the Amazon Basin. Additional Holocene climate reconstructions based on pollen records from the southwestern Amazon Basin (Campbell and Frailey, 1984) show fairly consistent oscillations of pollen that were also interpreted to represent changes from moist tropical to savanna climates (see Dickinson and Virji, 1987, for review). Haberele and Maslin (1999) analyzed pollen from the Amazon Fan and found very little long-term variation in both savanna-type and lowland rain forest taxa in the glacial-age sediments. However, they accepted as reasonable the Bush (1994) and Van der Hammen and Absy (1994) estimates of a 25 % reduction of rainfall during glacial times, producing a reduction of about 30 % in the forest cover of the Amazon Basin in an arc stretching around the eastern and southern margins of the Basin. Behling and Hooghiemstra (2001) reviewed the Late Quaternary history of tropical South American savannas north and south of the Amazon, and concluded that during the full-glacial period, savannas both north and south of the Equator expanded, reflecting markedly drier conditions. Behling (2002) concluded that 'The Amazon rainforest area must have been reduced'.

Maslin and Burns (2000) used the oxygen isotope record of planktonic foraminifera in a core from the western Amazon Fan to interpret the history of Amazon discharge since 14 000 ka. They estimated that discharge

declined from about 80% of the present value at 14 ka to at most 60% of the modern value at 12 ka, and then began a steady increase throughout the Holocene. This interpretation of aridity in the cold Younger Dryas is in general agreement with the Altiplano interpretations of Seltzer *et al*. (2000) and the interpretation of aridity in the eastern Amazon (Servant *et al*., 1993), but it remains at odds with the claim by Baker *et al*. (2001a,b) and Bush *et al*. (2002) associating relative wetness with the LGM in the Andes and northwesterly parts of the Basin. The exact temporal and mechanistic correspondence between these changes is still unclear, but they are at variance with the claim that wet–dry periods are synchronous across the Basin in response to sea-surface temperatures (Baker *et al*., 2001a,b).

The regional differences, temporal offsets, and contradictions between some of the interpretations of Quaternary palaeoclimate make it difficult to draw conclusions about the probable condition of the Amazon River during this period. The lowering of temperature would have lowered evapotranspiration at a time when precipitation was apparently relatively high in the Andes and glaciers and glacial runoff increased. Thus, glaciers expanded, and it is reasonable to expect that both runoff and sediment transport into the Andean tributaries of the Amazon increased. An approximate reconstruction of the area glaciated indicates several tenfold greater coverage than at present. Hallet *et al*. (1996, Figure 3E) compared sediment yields between glaciated and nonglaciated basins in Alaska, Norway and Iceland, and concluded that climatic conditions favourable for the expansion of temperate valley glaciers tend to increase both mechanical and chemical denudation rates. It is likely, therefore, that at the Last Glacial Maximum (LGM) the Andes shed more runoff and sediment into the foreland basins to the east. Notwithstanding the high sediment trapping efficiency of these basins at present, it is likely that the sediment load of the lowland Amazon and Madeira Rivers was higher than modern values during the LGM.

However, by far the larger portion of modern discharge of the Amazon is generated in the lowland, especially in the northwestern part of the Basin. High runoff from the western part of the Basin at and soon after the LGM would contribute to transporting the high sediment load downstream and into the floodplain before any drying around 14 ka. Interpretations of aridity in the eastern Amazon and surrounding regions (Servant *et al*., 1993; Van der Hammen and Absy, 1994) at the LGM require an extraordinary reduction in precipitation because the accompanying 5–6 °C decrease in temperature would reduce evapotranspiration. Unfortunately, reconstructions of discharge records do not yet extend back to the LGM. It remains difficult to explain how the flow of the river could be reduced very much in a cooler climate, even if precipitation declined in the lowland.

At the same time, thinning of the vegetation cover in the lowland and surrounding shields probably increased erosion slightly. The sediment yield of the modern Niger River Basin, which has a large proportion of savanna cover, is about 33 $t\,km^{-2}\,a^{-1}$ (drainage area 1.2 million km^2, with an internal basin that probably reduces the sediment yield; runoff of 160 $mm\,a^{-1}$), whereas the modern forested Congo Basin (3.8 million km^2; 340 $mm\,a^{-1}$ of runoff) yields 11 $t\,km^{-2}\,a^{-1}$ of sediment (Milliman and Syvitski, 1992). Our own sediment sampling in large rivers of the forested central Amazon lowland (Dunne *et al*., 1998) indicates sediment yields of 11 $t\,km^{-2}\,a^{-1}$ for the Negro River Basin (0.69 million km^2; 1350 $mm\,a^{-1}$) and 4 $t\,km^{-2}\,a^{-1}$ for the Jutaí River Basin (0.053 million km^2; runoff = 2380 $mm\,a^{-1}$). Although it is likely that land use has affected the yields of the Niger more than those of the forest-dominated basins, these measurements suggest that forested continental interiors yield less sediment than lowland savannas. We expect, therefore that at the LGM the extra-Andean Amazon Basin supplied slightly more sediment to the river with a lower runoff than is the case today. Mousinho de Meis (1971) interpreted colluvial wedges of sediment at the base of hillslopes across the Amazon lowlands as evidence for aggradation caused by a reduction of runoff with an increase in sediment supply. A return to wetter conditions would have provoked erosion of these deposits. It is not known how much of this extra sediment load was trapped within the Amazon lowland, but the process quantified by Dunne *et al*. (1998) and Aalto *et al*. (2003) suggest that some accelerated floodplain sedimentation was likely in the foreland basin and between the tectonic arches further downstream. However, the lower Amazon, downstream of the Negro, was severely affected by the other main influence of glaciation, namely sea-level decline.

8.5 INFLUENCE OF SEA-LEVEL CHANGES ON THE AMAZON RIVER AND FLOODPLAIN

In the modern era, a surprisingly small proportion of the Amazon's sediment supply reaches the continental shelf. Aalto *et al*. (2006) estimated that the Andes shed approximately 2300–3100 $Mt\,a^{-1}$ to the Amazon Basin. Yet only about 1400 $Mt\,a^{-1}$ of this sediment enters the lowland Amazon from the Solimões (Peruvian) and Madeira (Bolivian) tributaries, and only 1240 $Mt\,a^{-1}$ reach tidewater at Óbidos. A sediment budget for the coastal region estimated by Mertes and Dunne (1988) indicated net deposition of 400–500 $Mt\,a^{-1}$ of sediment in the reach between

Óbidos and the Atlantic Ocean. The mass balance numbers include the estimated sediment discharge at Óbidos of 1240 Mt a^{-1} (Meade *et al*., 1985; Dunne *et al*., 1998), the sum of deposition on the continental shelf of 610–650 Mt a^{-1} (Kuehl, *et al*., 1986), and the rate of along-shelf sediment transport of 100–200 Mt a^{-1} estimated by Augustinus (1982). Motivation for the budget calculation was based initially on the geomorphic observation that the spatial density of lakes on the floodplain surface declines dramatically downstream of Óbidos (Klammer, 1984; Mertes, 1985) and the comment by a Brazilian river boat captain that this is the worst reach in the Amazon to navigate, because 'sand bars are always shifting around everywhere'. This coastal-zone sediment budget agrees essentially with estimates by Eisma, *et al*. (1991) and Nittrouer *et al*. (1995).

Sedimentation in the estuary and offshore zone must have been very different during the LGM. Sioli (1957) was the first to propose that when sea level was 120 m lower than the present level during the Late Wisconsinian regression, the lower Amazon River and the lower reaches of its tributaries incised their beds in response to the lower base level. During the Holocene sea-level rise, the incised valleys began to fill with sediments, but those tributaries without Andean sediment sources were unable to keep pace with the rate of vertical accretion of the mainstem Amazon, resulting in impoundment of river-mouth lakes, or *rias*. Results of ^{14}C dating of sediments in these ria lakes show that there were changes in rates of sedimentation that may have been related to changes in lake level (Irion, 1982, 1984). Irion suggested that the presence of oxidized organic layers intermixed with unoxidized lacustrine sediments indicated fluctuations in lake level that may have been caused by base level changes as sea level fluctuated during the Late Pleistocene. Rias exist throughout the Amazon Basin along the main stem (Figure 8.2d and e) and tributaries, as far as 3000 km from the mouth of the Amazon (Irion, 1984), and were used by Sioli to suggest that incision progressed upstream to 65° W. However, Tricart (1977) interpreted rias upstream of the Negro confluence as due to neotectonic tilting of fault blocks. This second hypothesis agrees with the proposed mechanism for ria development in western Amazonia, which includes drainage derangement due to channel migration and tectonic deformation and does not require significant base-level changes (Neller *et al*., 1992; Dumont, 1993).

The lowered sea level during the LGM appears to have steepened the gradient of the Amazon sufficiently to pass the larger sediment load and to incise the channel and floodplain of the lower Amazon. The elevation of the incised bed can be roughly estimated from measurements made by Müller *et al*. (1995) and Irion *et al*. (1995), who used acoustic measurements to document buried river channels in two water bodies along the margin of the lower Amazon valley near Lago Manacapurú (LM) and at the mouth of Rio Preto da Eva (RPE) (see Figure 8.1 for locations). From these images Müller *et al*. (1995) and Irion *et al*. (1995) concluded that the water surface of the Amazon River probably dropped 20–25 m below its current level during the last glacial period when sea level was 120 m lower. Our analysis of these same acoustic images and data on river water-surface gradient and average low-water depth (Mertes *et al*., 1996) indicate that the river bed lay about 12 m below its present level at the RPE site, assuming that the water depth was essentially the same during the lower sea stand (Figure 8.14). At the LM site the bed was approximately 5 m below present level after the water depth (12–14 m) is subtracted. Additional data from Lake Calado, 80 km upstream of Manaus indicate approximately the same amount of incision (Keim *et al*., 1999), and the carbon-dated sequence of sediment suggests that the rate of vertical accretion averaged about 3.7 mm a^{-1} from 9500 to 7600 ka, and ≤2.8 mm a^{-1} between 7600 and at least 3000 ka. The Amazon attained its current elevation in this reach some time after 3000 ka. Assuming that channel incision and postglacial sedimentation at these floodplain-margin sites reflect the bed elevation of the nearby main channel, we extrapolated from them to calculate the geometry of the LGM channel bed and of the wedge of postglacial sedimentation (Figure 8.14).

Using these acoustic surveys of buried channel beds and the low-water river depth and water-surface slope we calculated the depth of incision below the present bed level at the LGM (Figure 8.14). Water-surface gradients for the lower Amazon River range between 1 and 3 cm km^{-1} for low-water conditions (Dunne *et al*., 1998). From these slopes and a zero reference elevation at the coastline, we calculated the water-surface elevation for sites along the modern river at low water (Figure 8.14). The low-water surface elevation calculated for the Manaus gauge by this method is approximately 23 m, which is intermediate between measured elevations for minimum river stage (17.8 ± 1.8 m) and maximum river stage (27.7 ± 1.2 m) surveyed from benchmarks near the port of Manaus gauge (J. Moody and R.H. Meade, US Geological Survey, unpublished data). The modern bed elevation profile was calculated by subtracting average low-water depths from the calculated water-surface elevations, ignoring bar-pool topography of the bed (Figure 8.14).

Several assumptions were required to estimate the bed incision for a sea level of −120 m at the LGM. We assumed that incision below the present bed (and thus postglacial sedimentation) varied linearly along the lower Amazon

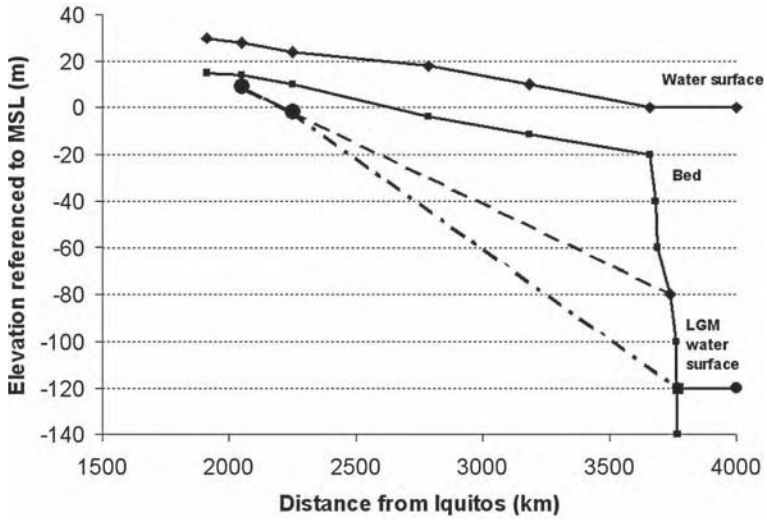

Figure 8.14 Modern water surface elevation, modern bed elevation, and incised bed elevation for the mainstem Amazon River during a lower sea level of −120 m during the Last Glacial Maximum. Calculation based on two measurements of bed incision reported by Müller *et al*. (1995) for Lago Manacapurú (LM) and Rio Preto da Eva (RPE). Water surface elevations and bed elevations based on data reported by Mertes *et al*. (1996). Modern coastal shelf profile based on cross section B as reported by Nittrouer *et al*. (1986). If the channel-bed gradient defined by the two incised bed elevations (large dots) is extrapolated downstream to the coast, the channel bed intersects the shelf edge at a depth of −80 m with a gradient of 5.5 cm km^{-1}. Alternatively, if the two incised sites are connected with an elevation of −120 m at the shelf edge, the predicted gradient is 9.4 cm km^{-1}. These two projections reflect the current range of uncertainty in defining the wedge of postglacial sedimentation. A low-water river depth of 20 m of water was assumed at the coastal boundary and at the shelf edge

valley. The incision depths calculated for the two floodplain-margin sites (Müller *et al*., 1995) were assumed to represent conditions in the nearby main river (up to 20 km distance). We then made two estimates of the incision profile. First, the incision depths from 12 to 5 m over the 200 km between the RPE and LM sites were assumed to fix the incised channel bed slope, which was extrapolated upstream and downstream along the northern arm of the Amazon mouth to the edge of the continental shelf, mapped by Nittrouer *et al*. (1986, Figure 1, transect B). The projected incised elevation is −80 m at the shelf edge, 60 m below the current bed, indicating a channel-bed slope of about 5.5 cm km^{-1}, for the lower Amazon, compared with about 2 cm km^{-1} today. A separate projection was made by connecting the two incised bed sites with an LGM sea level of −120 m at the shelf edge (Figure 8.14). The estimation is therefore very approximate and needs to be refined with additional subsurface data, but is sufficient for our current purpose.

The projected incision depth reaches zero approximately 140 km upstream of the LM site, approximately 1700 km from the coast near 62° W. This estimated upstream limit of base-level effects during the LGM lies in the area influenced by the Purús Arch. Upstream of the arch, the disturbances of drainage patterns interpreted by Latrubesse and Franzinelli (2002), shown in Figure 8.4 and by Tricart (1977), and the ria form of Lake Coari (Figure 8.2d) may thus reflect neotectonic effects upstream of the arch while the distribution of rias downstream of this reach reflects the eustatic effect on incision suggested by Sioli (1957) and Klammer (1984).

If the depths of postglacial sediment accumulation in Figure 8.14 are combined with an average width of 50 km for the Holocene floodplain (Figure 8.5a), deposition of approximately 2400–4000 km^3 of sediment is indicated since sea-level began to rise. This assumed width ignores the fact that the modern floodplain narrows downstream, that the incised valley might have been wider at the shelf edge, and that some sedimentation occurred in the Pará arm of the river south of Marajó Island (Figure 8.2f). However, Milliman *et al*. (1975) report that this latter channel is floored mainly by quartz and kaolinite and has a low sediment input and a large flow increment (~10^4 m^3 s^{-1}) from the Tocantins River. If an approximate date of 12 000 years BP is taken for the onset of rapid postglacial sea-level rise, an average annual accumulation of 200–330 M m^3 a^{-1}

(~300–500 Mt a^{-1}) is indicated in the estuary and lower river valley. The estimate is, of course, linearly sensitive to the assumption of the width of the valley-floor incision. Interestingly, this is more or less the same rate (400–500 Mt a^{-1}) that Mertes *et al*. (1996) estimated for the modern rate of sedimentation within the estuary. They also suggested on morphological grounds that most of the present accumulation is occurring on the delta plain (Figure 8.12) near the mouth of the Xingu River. The average vertical accretion rate at the coast indicated by this reconstruction is 5–8 mm a^{-1} (Figure 8.14); Vital and Stattegger (2000) measured a rate of 6 mm a^{-1} on carbon-dated sediments from the past millennium approximately 100–150 km from the coast.

It appears, therefore that the Amazon River carries sufficient load to effect the incomplete sedimentation of the floodplain that is evident from the floodplain topography of the lower valley. Figures 8.10 and 8.11 show that downstream of the River Madeira confluence the Amazon channel is lined by complex levees and almost straight scroll bars that confine the river. Sedimentation in the floodplain occurs through vertical accretion of fine sediment and avulsion of floodplain channels that emerge from the main channel and from tributaries to build leveed courses and small deltas into and across lakes. Most of the numerous lakes are irregularly shaped, though some are long and narrow between old scroll bars, levees, and blocked floodplain channels. The large area of lakes indicates the incomplete nature of the response to glacial-age evacuation, possibly intensified by continuing subsidence of the graben. Klammer (1984) recognized fragments of older floodplain from the pattern and texture of channel networks eroded into their surfaces. These fragments lie at almost the same elevation as the depositional surface of the modern floodplain, indicating that the pre-glacial floodplain elevation is being re-established in the lower Amazon valley. Upstream of the Negro confluence, the modern floodplain is at or above its pre-glacial level.

Klammer (1984) also used the distribution and surface texture of flat patches of high ground along the Amazon and its eastern tributaries to argue for extensive terrace formation at elevations from 10 to 180 m above modern river levels. He mapped these features on aerial photos and interpreted them as evidence for base level control by higher, fluctuating sea levels throughout the late Cenozoic. Klammer measured their elevations by ground survey and photogrammetry and grouped them into 9–10 classes throughout the central and eastern Amazon Basin. He then qualitatively correlated these elevation groups with fluvial and coastal terraces that have been classified as eustatic on other continents. This evidence remains to be evaluated with more ground surveys and dating methods, but Klammer (1984, pp. 76–77) used them to argue for widespread eustatic control of floodplain and terrace formation throughout the late Cenozoic, and to reject the influence of neotectonics. Irion (1984) shared this interpretation and claimed that during the postglacial transgression a huge lake formed in the Amazon lowland and extended upstream to Santa Rita do Weil, 600 km downstream of Iquitos, the vicinity of the Jutaí Arch (Figure 8.6). Evaluation of this interpretation awaits more extensive stratigraphic evidence.

The sedimentary deposits of the inner coastal region are dominated by inner-shelf mud deposits in the form of a sub-aqueous delta (Kuehl *et al*. 1986; Nittrouer *et al*., 1986). Off the coast, downstream from the Amazon Canyon is the Amazon Cone (Figure 8.1), which is one of the world's largest deep-sea fans. It extends approximately 1200 km down fan from the mouth of the river (Pirmez *et al*., 1997) to depths approaching 5000 m. It began to form approximately 8 to 15 million years ago (Damuth and Kumar, 1975). Sediment transported from the basin during sea stands lower than –80 m was apparently deposited directly onto the Amazon Cone (Damuth and Kumar, 1975; Milliman, *et al*., 1975). According to isotopic dating of the sediments, glacier-age rates of sedimentation on the cone averaged metres per year with the intervening interglacials with high sea level showing only centimetres per year of accumulation (ODP Leg 155 Scientific Drilling Party, 1995). The development of the fan is described as a series of 'repeated cycles of levee progradation and upfan avulsion [that] produce laterally shingled channel-levee systems' (Hiscott, *et al*., 1997, pp. 13–14). Manley and Flood (1988) suggested that these levee complexes were deposited during individual episodes of lower sea level, and that the different locations and volumes of the levee complexes represent a record of individual glacial periods. These ideas have been confirmed by dating of the deposits that shows consistent dates throughout individual levee complexes (Piper *et al*., 1997). In particular, the Upper Levee Complex (ULC) is now known to have been deposited entirely during oxygen isotope stages 2–4 of the latest Pleistocene (Piper *et al*., 1997). Manley and Flood (1988) calculated that the volume of the ULC is approximately 24 000 km^3. This accumulation volume and a 65 000-year duration for the three Wisconsinian isotope stages yields an average accumulation rate of ~550 Mt a^{-1} with as much as 4000 km^3 (Figure 8.14) originating from the lower valley during the sea level regression, which would lower the supply rate from the river to the cone to ~450 Mt a^{-1}. This amount of rock material is equivalent to an average erosion rate of 0.38 mm a^{-1} for the 800 000 km^2 of the Amazonian Andes. This value is close to the median of the cosmogenic isotope estimated erosion rates

(0.30 mm a^{-1}) for the Bolivian Andes (Safran *et al*. 2005) during the Holocene, and supports the idea that if corrections could be made for the trap efficiency of the foreland basin, and possibly of the lowland floodplain, the late Pleistocene erosion rate of the Andes would be greater than the Holocene rates and the fission-track measurements of exhumation (averaging 0.25 mm a^{-1}) over the last few millions of years (Safran *et al*., 2006). The reason for the higher modern sediment supply from the Andes (Aalto *et al*., 2006) and to the estuary (Dunne *et al*., 1998) remains a mystery.

8.6 CONCLUSION

In the Amazon Basin tectonic setting, climate change, and sea-level fluctuations have interacted during the Late Cenozoic and particularly the Late Quaternary to affect the conditions of sediment transport, erosion, deposition, and thus the channel and floodplain form throughout the mainstem valley. The tectonic setting comprises the rapidly eroding Andean cordillera, the deforming foreland basin, ancient crystalline shields, subsiding lowlands that converge on ancient rift structures, and a wide coastal plain and shelf region affected by isostatic adjustments to sediment loading on the Amazon Cone. Several authors have noted the effects of neotectonic deformation on river alignments (e.g. Figure 8.4), and new geomorphic evidence (Figure 8.5) suggests that between the Purús Arch and Monte Alegre Intrusion (Figure 8.1) ancient structures in the form of asymmetric depositional rift segments, control the modern position of the Amazon valley. Most striking is that the valley appears to be prevented from crossing the rift structure except at transfer zones in a manner similar to drainage patterns along the East African Rift system. Satellite information (Figure 8.6b) has allowed definition of channel gradients along the Amazon, showing the continuing effect of ancient transverse structures on the width of the floodplain and the sinuosity and gradient of the channel. In turn, these changes of floodplain width and channel gradient affect the transport of sediment and its exchange between channel and floodplain, as reflected by modern measurements of river hydrology, hydraulics, sediment transport, and channel change. From the measured sediment delivery to the estuary it appears that fluvial transport in the Holocene could have re-established a channel-floodplain system in the lowermost 1500–1700 km of the valley in response to postglacial sea-level rise, but that this sediment delivery and channel-floodplain construction was, and continues to be, modulated by ancient tectonic structures affecting sediment transport through the Andean foreland basins (Guyot *et al*., 1988; Guyot, 1993; Aalto *et al*., 2003) and the mainstem valley (Dunne *et al*., 1998) and the response to postglacial eustatic sea level rise. These structures affect the trap efficiency of the sediment dispersal system, and therefore the rate at which the lower Amazon responds to sea-level rise and supplies sediment to the shelf.

Direct effects of Late Quaternary climate change on the modern Amazon are harder to discern. The expanded glacial cover in the Andes and thinning of vegetation in the lowland probably resulted in an increased sediment yield, still overwhelmingly from the mountain range. Whether or not sediment production increased or decreased due to climate change, the signal may not have moved efficiently through the entire river system. The foreland basins would have acted as a partial sink, as they do today, and it is reasonable to expect that the rate of floodplain sedimentation there would have increased during glacial expansions. Any signal of increased sediment yield from hillslopes in the lowlands and on the shields due to thinning of vegetation would be difficult to distinguish along the larger rivers, especially the main Amazon channel because its sediment load is dominated by Andean inputs, and lowland tributary supplies are overwhelmed by massive exchanges with floodplain sediments. Any accelerated sedimentation may become apparent as terraces along tributaries (Latrubesse, 2002, 2003; Latrubesse and Franzinelli, 1998; Latrubesse and Kalicki, 2002) and colluvial deposits at the base of hillslopes (Mousinho de Meis, 1971) are systematically mapped and dated.

Effects of LGM sea-level fluctuations on the evacuation and postglacial accumulation of sediment appear to have extended upstream to about the location of the Purús Arch, and the floodplain and estuary of the lower Amazon continue to accumulate hundreds of millions of tonnes of sediment per year. The resulting topography of the floodplain remains ‘unfilled’ with extensive lakes and an intricate pattern of leveed distributary channels that disperse sediment away from the main channel. The pattern of sediment accumulation in this evacuated reach continues to be affected by subtle variations of gradient associated with tectonic structures, and perhaps by continuing subsidence of the entire estuarine graben.

The remarkable conclusion from all of these analyses is that the imprint of tectonic deformation and basin structure at both coarse and fine scales appears to have been a dominant influence on past and present conditions of sediment transport, and channel and floodplain development, even though direct evidence for active deformation in the eastern basin is missing. The massive deposition rates associated with the rivers in the foreland basin show the dramatic influence of the tectonics associated with the Andean orogeny (Guyot, 1993). Moving towards the east, the influences of the ancient aulacogen on the valley

boundary, channel alignment, and channel gradient are particularly striking along the lowland Amazon. The tectonic framework of the river controls its sediment supply and the trap efficiency of its floodplains, and thus the rate at which the river can respond to glacial-age sea-level fluctuations by constructing a channel and filling its valley with a complex floodplain and delta plain within the estuary.

ACKNOWLEDGEMENTS

Contribution number 139 of the CAMREX Project, directed by J. E. Richey, University of Washington. Jeff Richey and Robert Meade directed the sediment sampling and helped us enormously with interpretation of sediment transport data within the CAMREX Project. This work was supported by NSF grants BSR-8107522 (for the CAMREX Project) and EAR-0309688, and NASA/EOS Project NAGW-2652 and NASA/LBA Project NAGW-5233.

REFERENCES

Aalto, R.E., Maurice-Bourgoin, L., Dunne, T., Montgomery, D.R., Nittrouer, C.A., and Guyot, J.L., (2003) Episodic sediment accumulation on Amazonian floodplains influenced by El Niño/Southern Oscillation, *Nature*, 425, 493–497.

Aalto, R.E., Dunne, T., and Guyot, J.L., (2006) Geomorphic controls on Andean denudation, *Journal of Geology*, 114, 85–99.

Absy, M.L., (1979) *A palynological study of Holocene sediments in the Amazon Basin*: Amsterdam, University of Amsterdam, 76 p.

Aceituno, P., (1988) On the functioning of the Southern Oscillation in the South America Sector Part I: surface climate, *Monthly Weather Review*, 116, 505–524.

Adams, J.B., Sabol, D.E., Kapos, V., Almeida, R., Roberts, D.A., Smith, M.O., and Gillespie, A.R., (1995) Classification of multispectral images based on fractions of endmembers – application to land-cover change in the Brazilian Amazon, *Remote Sensing of Environment*, 52(2), 137–154.

Augustinus, P.G.E.F., (1982) Coastal changes in Suriname since 1948. Future of roads and rivers in Suriname and neighboring region: Paramaribo, Suriname, Delft University of Technology, pp. 329–338.

Baker, P.A., Seltzer, G.O., Fritz, S.C., Dunbar, R.B., Grove, M.J., Tapia, P.M., Cross, S.L., Rowe, H.D., and Brodas, J.P., (2001a) Tropical precipitation for the past 25 000 years, *Science*, 291, 640–643.

Baker, P.A., Rigsby, C.A., Seltzer, G.O., Fritz, S.C., Lowensteink, T.K., Bacher, N.P., and Veliz, C., (2001b) Tropical climate changes at millennial and orbital timescales on the Bolivian Altiplano, *Nature*, 409, 698–701.

Bates, H.W., (1864) *The Naturalist on the River Amazon*: Berkeley, CA, University of California Press, p. 465.

Behling, H., (2002) South and southeast Brazilian grasslands during Late Quaternary times: a synthesis, *Palaeogeography, Palaeoclimatology, Palaeoecology*, 177, 19–27.

Behling, H. and Hooghiemstra, H., (2001) Neotropical savanna environments in space and time: Late Quaternary interhemispheric comparisons. In: *Interhemispheric Climate Linkages* (V. Markgraf, Ed.). San Diego, Academic Press, pp. 307–323.

Birkett, C.M., Mertes, L.A.K., Dunne, T., Costa, M.H., and Jasinski, M.J., (2002) Surface water dynamics in the Amazon Basin: application of satellite radar altimetry, *Journal of Geophysical Research*, doi: 10.1029/2001JD000609, 04.

Bush, M.B., (1994) Amazonian speciation: a necessarily complex model, *Journal of Biogeography*, 21, 5–17.

Bush M.B.,Weimann M., Piperno D.R., Liu K.-B. and Colinvaux, P.A., (1990) Pleistocene temperature depression and vegetation change in Ecuadorian Amazonia, *Quaternary Research*, 34, 330–345.

Bush, M.B., Miller, M.C., De Oliveira, P.E., and Colinvaux, P.A., (2002) Orbital forcing signal in sediments of two Amazonian lakes, *Journal of Paleolimnology*, 27, 341–352.

Campbell, K.E., Jr, and Frailey, C.D., (1984) Holocene flooding and species diversity in Southwestern Amazonia, *Quaternary Research*, 21, 369–375.

Caputo, M.V., (1984) Stratigraphy, tectonics, paleoclimatology and paleogeography of northern basins of Brazil, Department of Geological Science, University of California, Santa Barbara, p. 583.

Caputo, M.V., (1991) Solimões megashear: intraplate tectonics in northwestern Brazil, *Geology*, 19, 246–249.

Clapperton, C., (1993) *Quaternary Geology and Geomorphology of South America*. New York, Elsevier, p. 779.

Coelho, C.A.S., Uvo, C.B., and Ambrizzi, T., (2002) Exploring the impacts of the tropical Pacific SST on the precipitation patterns over South America during ENSO periods, *Theoretical and Applied Climatology*, 71, 185–197.

Colinvaux P.A. and De Oliveira P.E., (2000) Palaeoecology and climate of the Amazon basin during the last glacial cycle. *Journal of Quaternary Science*, 15, 347–356.

Colinvaux, P.A., De Oliveira, P.E., Moreno, J.E., Miller, M.C., and Bush, M.B., (1996) A long pollen record from Lowland Amazonia: forest and cooling in glacial times, *Science*, 274, 85–88.

Costa, M.H., Botta, A., and Cardillo, J.A., (2003) Effects of large-scale changes in land cover on the discharge of the Tocantins River, Southeastern Amazonia, *Journal of Hydrology*, 283, 206–217.

Damuth, J.E., and Kumar, N., (1975) Amazon Cone: morphology, sediments, age, and growth pattern, *Geological Society of America Bulletin*, 86, 863–878.

Dickinson, R.E., and Virji, H., (1987) Climate change in the humid tropics, especially over the last twenty thousand years. In: *The Geophysiology of Amazonia* (R.E. Dickinson, Ed.). New York, John Wiley & Sons, Ltd, pp. 91–101.

Driscoll, N.W., and Karner, G.D., (1994) Flexural deformation due to Amazon Fan loading: a feedback mechanism affecting sediment delivery to margins, *Geology*, 22, 1015–1018.

Dumont, J.F., (1993) Lake patterns as related to neotectonics in subsiding basins: the example of the Ucamara Depression, Peru, *Tectonophysics*, 22, 69–78.

Dumont, J.F., and Garcia, F., (1991) Active subsidence controlled by basement structures in the Marañon basin of northeastern Peru, Fourth International Symposium on Land Subsidence, International Association of Hydrological Sciences, pp. 343–350.

Dumont, J.F., Lamotte, S., and Kahn, F., (1990) Wetland and upland forest ecosystems in Peruvian Amazonia: plant species diversity in the light of some geological and botanical evidence, *Forest Ecology and Management*, 33/34, 125–139.

Dumont, J.F., Deza, E., and Garcia, F., (1991) Morphostructural provinces and neotectonics in the Amazonian lowlands of Peru, *Journal of South American Earth Sciences*, 4(4), 373–381.

Dunne, T., Mertes, L.A.K., Meade, R.H., Richey, J.E., and Forsberg, B.R., (1998) Exchanges of sediment between the flood plain and channel of the Amazon River in Brazil: *Geological Society of America Bulletin*, 110(4), 450–467.

Dury, G.H., (1964) Principles of underfit streams, *US Geological Survey Professional Paper* 452–A, 67 pp.

Eisma, D., Augustinus, P.G.E.F., and Alexander, C., (1991) Recent and subrecent changes in the dispersal of Amazon mud, Netherlands *Journal of Sea Research*, 28, 181–192.

Faulds, J.E., and Geissman, J.W., (1992) Implications of paleomagnetic data on Miocene extension near a major accommodation zone in the Basin and Range Province, northwestern Arizona and southern Nevada, *Tectonics*, 11, 204–227.

Foley, J.A., Botta, A., Coe, M.T., and Costa, M.H., (2002) El Niño-Southern Oscillation and the climate, ecosystems and rivers of Amazonia, *Global Biogeochemical Cycles*, 16(4), 1132.

Franzinelli, E. and Igreja, H., (2002) Modern sedimentation in the Lower Negro River, Amazonas State, Brazil, *Geomorphology*, 44, 259–271.

Franzinelli, E. and Potter, P.E., (1983) Petrology, chemistry, and texture of river sands, Amazon basin system, *Journal of Geology*, 91(1), 23–29.

Frost, I., (1988) A Holocene sedimentary record from Anañgucocha in the Ecuadorian Amazon, *Ecology*, 69, 66–73.

Guyot, J.L., (1993) *Hydrogéochimie des fleuves de l'Amazonie bolivienne: Collection Etudes & Thèses*, Paris, Editions de l'ORSTOM, 261 p.

Guyot, J.L., Bourges, J., Hoorelbecke, R., Roche, M.A., Calle, H., Cortes, J., and Barragan Guzman, M.C., (1988) Exportation de matières en suspension des Andes vers l'Amazonie par le Rio Beni, Bolivie, Sediment Budgets, International Association of Hydrological Sciences Publication 174, pp. 443–451.

Haberle, S.G., and Maslin, M.A., (1999) Late Quaternary vegetation and climate change in the Amazon Basin based on a 50 000 year pollen record from the Amazon Fan, ODP Site 932, *Quaternary Research*, 51, 27–38.

Hallet, B., Hunter, L., and Bogen, J., (1996) Rates of erosion and sediment evacuation by glaciers: A review of field data and their implications, *Global and Planetary Change*, 12, 213–235.

Hayden, B.P., (1988) Flood climates. In: *Flood Geomorphology* (V.R. Baker, R.C. Kochel and P.C. Patton, Eds.). New York, John Wiley & Sons, Ltd, pp. 13–26.

Herndon, W.L., (1853) Exploration of the Valley of the Amazon, made under the direction of the Navy Department by Herndon, W.L. and Gibbon, L., Part I: US Senate 32d Congress, 2d Session, Executive no. 36, 414 p.

Hiscott, R.N., Hall, F.R., and Pirmez, C., (1997) Turbidity-current overspill from the Amazon Channel: texture of the silt/sand load, paleoflow from anisotropy of magnetic susceptiblity, and implications for flow processes. In: *Ocean Drilling Program Initial Reports* (L.C. Peterson, Ed.), 155. College Station, TX, Ocean Drilling Program, pp. 53–78.

Hjemfelt, A.T., (1978) Amazon basin hydrometeorology, *Journal of the Hydraulics Division of the American Society of Civil Engineers*, 104, 887–897.

Hoorn, C., (1994) An environmental reconstruction of the palaeo-Amazon River system (Middle-Late Miocene, NW Amazonia), *Palaeogeography, Palaeoclimatology, Palaeoecology*, 112, 187–238.

Hoorn, C., Guerrero, J., Sarmiento, G.A., and Lorente, M.A., (1995) Andean tectonics as a cause for changing drainage patterns in Miocene northern South America, *Geology*, 23(3), 237–240.

Irion, G., (1982) Mineralogical and geochemical contribution to climatic history in central Amazonia during Quaternary time, *Tropical Ecology*, 23, 76–85.

Irion, G., (1984) Sedimentation and sediment of Amazonian rivers and evolution of the Amazonian landscape since Pliocene times. In: *The Amazon: Limnology and landscape ecology of a mighty tropical river and its basin* (H. Sioli, Ed.). Dordrecht, Dr W. Junk Publishers, pp. 201–214.

Irion, G., Müller, J., Nunes de Melho, J., and Junk, W.J., (1995) Quaternary geology of the Amazonian Lowland, *Geo-Marine Letters*, 15, 172–178.

Iriondo, M.H., (1982) Geomorfologia da planicie Amazônica. In: *Atas do Simposio do Quaternia no Brasil, 4th*. Rio de Janeiro, Associação Brasileira de Estudos do Quaternário, pp. 323–348.

Iriondo, M.H., and Sugio, K., (1981) Neotectonics of the Amazon plain, *International Quaternary Association Neotectonic Commission Bulletin*, 4, 72–78.

Johnsson, M.J., and Meade, R.H., (1990) Chemical weathering of fluvial sediments during alluvial storage: the Macuapanim Island point bar, Solimões River, Brazil, *Journal of Sedimentary Petrology*, 6(6), 827–842.

Keim, G., Irion, G., Behling, H., Junk, W.J., and Nunes de Mello, J., (1999) The sediment deposits of Lago Calado, a ria lake in Central Amazonia (Brazil), as indicator for postglacial water level rise of the Amazon River. In: Manaus '99, Proceedings of a Symposium, Manaus, Brazil (Abstract on CD-ROM).

Klammer, G., (1984) The relief of the extra-Andean Amazon basin. In: *The Amazon: Limnology and landscape ecology of a mighty tropical river and its basin* (H. Sioli, Ed.). Dordrecht, Dr W. Junk Publishers, pp. 47–84.

Kuehl, S.A., DeMaster, D.J., and Nittrouer, C.A., (1986) Nature of sediment accumulation on the Amazon continental shelf: *Continental Shelf Research*, 6(112), 209–225.

Latrubesse, E., (2002) Evidence of Quaternary paleohydrological changes in middle Amazonia: the Aripuanã/Roosevelt and Jiparana fans like systems. *Zeitschrift für Geomorphologie*, 129, 61–72.

Latrubesse, E., (2003) The Late Quaternary paleohydrology of large South American fluvial systems. In: *Palaeohydrology: Understanding Global Change* (K. Gregory and G. Benito, Eds.). Chichester, John Wiley & Sons, Ltd, pp. 193–212.

Latrubesse, E.M. and Franzinelli, E., (1998) Late Quaternary allnvial sedimentation in the Upper Negro basin, Amazonia, Bazil: paleohydrological implications. In: *Paleohydrology and Environmental Change* (G. Benito, V.R. Baker and A.J. Gregory, Eds.). Chichester, John Wiley & Sons Ltd, pp. 259–271.

Latrubesse, E., and Franzinelli, E., (2002) The Holocene alluvial plain of the middle Amazon River, Brazil, *Geomorphology*, 44, 241–257.

Latrubesse, E and Kalicki, T., (2002) Late Quaternary Paleohydrology of the Purús river, Amazon, Brazil. *Zeitschrift für Geomorphologie*, 129, 41–59.

Leenheer, J.A., and Santos, U. de M., (1982) Considerações sobre os processos de sedimentação na água preta ácida do rio Negro (Amazônia Central), *Acta Amazônica*, 12(2), 343–355.

Leopold, L.B., Wolman, M.G., and Miller, J.P., (1964) Fluvial Processes in Geomorphology, San Francisco, W.H. Freeman, 504 pp.

Liebmann, B., and Marengo, J.A., (2001) Interannual variability of the rainy season and rainfall in the Brazilian Amazon basin, *Journal of Climate*, 14, 4308–4318.

Liebmann, B., Marengo, J.A., Glick, J.D., Kousky, V.E., Wainer, I.C., and Massambani, O., (1998) A comparison of rainfall, outgoing longwave radiation, and divergence over the Amazon Basin, *Journal of Climate*, 11, 2898–2909.

Liebmann, B., Kiladis, G.N., Marengo, J.A., Ambrizzi, T., and Glick, J.D., (1999) Submonthly convective variability over South America and the South Atlantic convergence zone, *Journal of Climate*, 12(7), 1877–1891.

Liu, K., and Colinvaux, P.A., (1985) Forest changes in the Amazon Basin during the last glacial maximum, *Nature*, 318, 556–557.

Manley, P.L., and Flood, R.D., (1988) Cyclic sediment deposition within the Amazon deep-sea fan, *American Association of Petroleum Geologists Bulletin*, 72, 912–925.

Marengo, J.A., (1995) Variations and change in South American streamflow, *Climatic Change*, 31, 99–117.

Marengo, J.A., Tomasella, J., and Uvo, C.R., (1998) Trends in streamflow and rainfall in tropical South America – Amazonia, eastern Brazil, and northwestern Peru, *Journal of Geophysical Research-Atmospheres*, 103(D2), 1775–1783.

Martin, L., Fournier, M., Mourquiary, P., Sifeddine, A., Turca, B., Absy, M.L., and Flexor, J.-M., (1993) Southern oscillation signal in South American palaeoclimatic data of the last 7000 years, *Quaternary Research*, 39, 338–346.

Maslin, M.A., and Burns, S.J., (2000) Reconstruction of the Amazon Basin effective moisture availability over the past 14 000 years, *Science*, 290, 2285–2287.

McGinnis, J.P., Driscoll, N.W., Karner, G.D., Brumbaugh, R.W., and Cameron, N., (1993) Flexural response of passive margins to deep-sea erosion and slope retreat: implications for relative sea-level change, *Geology*, 21, 893–896.

Meade, R.H., Dunne, T., Richey, J.E., Santos, U. de M., and Salati, E., (1985) Storage and remobilization of suspended sediment in the lower Amazon River of Brazil, *Science*, 228, 488–490.

Melack, J.M., (1984) Amazon floodplain lakes: shape, fetch, and stratification, *International Association of Theoretical and Applied Limnology Proceedings*, 22, 1278–1282.

Mertes, L.A.K., (1985) Floodplain development and sediment transport in the Solimões-Amazon River, Brazil: Seattle, WA, University of Washington, p. 108.

Mertes, L.A.K., and Dunne, T., (1988) Morphology and construction of the Solimões-Amazon River floodplain, Chapman Conference – On the fate of particulate and dissolved components within the Amazon dispersal system: River and ocean: Charleston, S C, American Geophysical Union, pp. 82–86.

Mertes, L.A.K., Dunne, T., and Martinelli, L.A., (1996) Channel-floodplain geomorphology along the Solimões-Amazon River, Brazil, *Geological Society of America Bulletin*, 108, 1089–1107.

Milliman, J.D., and Barretto, H.T., (1975) Relict magnesian calcitic oolite and subsidence of the Amazon shelf, *Sedimentology*, 22, 137–145.

Milliman, J.D., and Syvitski, J.P.M., (1992) Geomorphic/tectonic control of sediment discharge to the ocean: the importance of small mountainous rivers, *Journal of Geology*, 100, 525–544.

Milliman, J.D., Summerhayes, C.P., and Barretto, H.T., (1975) Quaternary sedimentation on the Amazon continental margin: a model, *Geological Society of America Bulletin*, 87, 610–614.

Molion, L.C.B., (1990) Climate variability and its effects on Amazonian hydrology, *Interciência*, 15, 367–372.

Morley, C.K., (1989) Extension, detachments, and sedimentation in continental rifts (with particular reference to East Africa), *Tectonics*, 8, 1175–1192.

Morley, C.K., (1990) Transfer zones in the East African Rift system and their relevance to hydrocarbon exploration in rifts, *American Association of Petroleum Geologists Bulletin*, 74, 1234–1253.

Morley, C.K., Cunningham, S.M., Harper, R.M., and Wescott, W.A., (1992) Geology and geophysics of the Rukwa Rift, East Africa, *Tectonics*, 11, 69–81.

Mousinho de Meis, M.R., (1971) Upper Quaternary process changes of the middle Amazon area, *Geological Society of America Bulletin*, 82, 1073–1087.

Müller, J., Irion, G., Nunes de Melho, J., and Junk, W.J., (1995) Hydrological changes of the Amazon during the last glacial-interglacial cycle in central Amazonia (Brazil), *Naturwissenschaften*, 82, 232–235.

Neller, R.J., Salo, J., and Räsänen, M.E., (1992) On the formation of blocked valley lakes by channel avulsion in upper Amazon foreland basins, *Zeitschrift für Geomorphologie*, 36, 401–411.

Nittrouer, C.A., Curtin, T.B., and DeMaster, D.J., (1986) Concentration and flux of suspended sediment on the Amazon continental shelf, *Continental Shelf Research* 6, 151–174.

Nittrouer, C.A., Kuehl, S.A., Sternberg, R.W., Figueiredo, A.G., Jr, and Faria, L.E.C., (1995) An introduction to the geological significance of sediment transport and accumulation on the Amazon continental shelf, *Marine Geology*, 125, 177–192.

Nunn, J.A., (1990) Relaxation of continental lithosphere: an explanation for late Cretaceous reactivation of the Sabine Uplift of Louisiana-Texas, *Tectonics*, 9, 341–359.

Nunn, J.A., and Aires, J.R., (1988) Gravity anomalies and flexure of the lithosphere at the middle Amazon basin, Brazil, *Journal of Geophysical Research*, 93, 415–428.

ODP Leg 155 Scientific Drilling Party (1995) Drilling the fantastic Amazon Fan, *Geotimes*, pp. 18–19.

Petri, S., and Fúlfaro, V.J., (1988) Geologia do Brasil. In: *São Paulo, Editoria da Universidade de São Paulo*, (Paulo, E. de U. dos S., Ed.). Biblioteca de Ciencias Naturais, pp. 631.

Piper, D.J.W., Flood, R.D., Cisowski, S., Hall, F., Manley, P.L., Maslin, M., Mikkelsen, N., and Showers, W., (1997) Synthesis of stratigraphic correlations of the Amazon Fan. In: *Ocean Drilling Program Initial Reports* (L.C. Peterson, Ed.), v. 155, College Station, TX, Ocean Drilling Program, pp. 595–609.

Pirmez, C., Flood, R.D., Baptiste, J., Yin, H., and Manley, P.L., (1997) Clay content, porosity and velocity of Amazon Fan sediments determined from ODP Leg 155 cores and wireline logs, *Geophysical Research Letters*, 24, 317–320.

Potter, P.E., (1978) Significance and origin of big rivers, *Journal of Geology*, 86, 13–33.

Putzer, H., (1984) The geological evolution of the Amazon basin and its mineral resources. In: *The Amazon: Limnology and Landscape Ecology of a Mighty Tropical River and its Basin* (H. Sioli, Ed.). Dordrecht, Dr W. Junk Publishers, pp. 15–46.

Räsänen, M.E., Salo, J., and Kalliola, R., (1987) Fluvial perturbance in the western Amazon basin: regulation by long-term sub-Andean tectonics, *Science*, 238, 1398–1401.

Räsänen, M.E., Salo, J., Jungner, H., and Pittman, L.R., (1990) Evolution of the western Amazon lowland relief: impact of Andean foreland dynamics, *Terra Nova*, 2, 320–332.

Räsänen, M.E., Salo, J., and Jungner, H., (1991) Holocene floodplain lake sediments in the Amazon: ^{14}C dating and palaeoecological use, *Quaternary Science Reviews*, 10, 363–372.

Räsänen, M.E., Neller, R.J., Salo, J., and Jungner, H., (1992) Recent and ancient fluvial deposition systems in the Amazonian foreland basin, Peru, *Geology Magazine*, 129, 293–306.

Räsänen, M.E., Linna, A.M., Santos, J.C.R., and Negri, F.R., (1995) Late Miocene tidal deposits in the Amazonian foreland basin, *Science*, 269, 386–389.

Richey, J.E., Meade, R.H., Salati, E., Devol, A.H., Nordin, C.F., Jr, and Santos, U. d. M., (1986) Water discharge and suspended sediment concentrations in the Amazon River: 1982–1984, *Water Resources Research*, 22, 756–764.

Richey, J.E., Mertes, L.A.K., Dunne, T., Victoria, R., Forsberg, B.R., Tancredi, A., and Oliveira, E., (1989a) Sources and routing of the Amazon River flood wave, *Global Biogeochemical Cycles*, 3, 191–204.

Richey, J.E., Nobre, C., and Deser, C., (1989b) Amazon River discharge and climate variability: 1903–1985, *Science*, 246, 101–103.

Ronchail, J., (1998) Variabilité pluviométrique en Bolivie lors des phases extrêmes de l'oscillation australe du Pacifique (1950–1993). *Bulletin l'Institut Français d'Etudes Andines*, 27, 687–698.

Rossetti, D de F., Mann de Toledo, P., and Góes, A.M., (2005) New geological framework for Western Amazonia (Brazil) and implications for biogeography and evolution, *Quaternary Research*, 63, 78–89.

Safran, E.B., Bierman, P.R., Aalto, R.E., Dunne, T., Whipple, K.X, and Caffee, M., (2005) Erosion rates driven by channel network incision in the Bolivian Andes, *Earth Surface Processes and Landforms*, 30(8), 1007–1024.

Safran, E.B., Blythe, A., and Dunne, T., (2006) spatially variable exhumation rates in orogenic belts: an Andean example, *Journal of Geology*, 114, 665–681.

Salati, E., Dall'Olio, A., and Matsui, E., (1979) Recycling of water in the Amazon Basin: an isotopic study, *Water Resources Research*, 15, 1250–1258.

Saucier, R.T., (1981) Current thinking on riverine processes and geologic history as related to human settlement in the southeast, *Geoscience and Man*, 22, 7–18.

Scholz, C.A., (1995) Deltas of the Lake Malawi Rift, East Africa: seismic expression and exploration implications, *American Association of Petroleum Geologists Bulletin*, 79, 1679–1697.

Schumm, S.A., (1977) *The Fluvial System*. New York, John Wiley & Sons, Ltd, p. 388.

Schumm, S.A., (1993) River responses to baselevel change: Implications for sequence stratigraphy, *Journal of Geology*, 101, 279–294.

Seltzer, G.O., Rodbell, D.T., and Burns, S.J., 2000. Isotopic evidence for late Quaternary climatic change in tropical South America, *Geology*, 28, 35–38.

Seluchi, M.E., and Marengo, J.A., (2000) Tropical-midlatitude exchange of air masses during summer and winter in South America: climatic aspects and examples of intense events, *International Journal of Climatology*, 20, 1167–1190.

Servant, M., Maley, J., Turcq, B., Absy, M.L., Brenac, P., Fournier, M., and Ledru, M.-P., (1993) Tropical forest changes during the Late Quaternary in African and South American lowlands, *Global and Planetary Change*, 7, 25–40.

Siffedine, A., Martin, L., Turq, Volkmer-Ribeiro, C., Soubiès, F., Campello Cordeiro, R., Sugio, K., (2001) Variations of the Amazonian rainforest environment: a sedimentological record covering 30 000 years, *Palaeogeography, Palaeoclimatology, Palaeoecology*, 168, 221–235.

Sioli, H., (1957) Sedimentation im Amazonasgebiet, *Geologicsche Rundschau*, 168, 608–633.

Sioli, H., (1984) The Amazon and its main affluents: Hydrography and morphology of the river courses, and river types. In:

The Amazon: Limnology and Landscape Ecology of a Mighty Tropical River and its Basin (H. Sioli, Ed.): Dordrecht, Dr W. Junk Publishers, pp. 127–165.

Sippel, S.J., Hamilton, S.K., and Melack, J.M., (1992) Inundation area and morphometry of lakes on the Amazon River floodplain, Brazil, *Archiv für Hydrobiologie*, 123, 385–400.

Smith, J.A., Seltzer, G.O., Farber, D.L., Rodbell, D.T., and Finkel, R.C., (2005a) Early Local Last Glacial Maximum in the Tropical Andes, *Science*, 308, 678–681.

Smith, J.A., Seltzer, G.O., Rodbell, D.T. and Klein, A.G., (2005b) Regional synthesis of last glacial maximum snowlines in the tropical Andes, South America, *Quaternary International*, 138–139, 145–167.

Sternberg, H.O'.R., and Russell, R.D., (1952) Fracture patterns in the Amazon and Mississippi valleys, Proceedings, 8th General Assembly and 17th International Congress: Washington, DC, International Geographical Union, pp. 380–385.

Stute, M., Forster, M., Friischkorn, H., Serejo, A., Clark, J.F., Schlosser, P., Broecker, W.S., and Bonani, G., (1995) Cooling of tropical Brazil during the Last Glacial Maximum, *Science*, 269, 379–383.

Talling, P.J., (1998) How and where do incised valleys form if sea level remains above the shelf edge?, *Geology*, 26, 87–90.

Thompson, L.G., Mosley-Thompson, E., Davis, M.E., Lin, P.N., Henderson, K.A., Coledai, J., Bolzan, J.F., and Liu, K.B., (1995) Late-Glacial stage and Holocene tropical ice core records from Huascaran, Peru, *Science*, 269, 46–50.

Thompson L.G., Mosley-Thompson, E., and Henderson, K.A., (2000) Ice-core palaeoclimate records in tropical South America since the Last Glacial Maximum, *Journal of Quaternary Science*, 15(4), 377–394.

Thorne, J., (1994) *Constraints on riverine valley incision and the response to sea-level change based on fluid mechanics, Incised-valley systems: origin and sedimentary sequences*, SEPM Special Publication no. 51, Tulsa, pp. 29–43.

Tricart, J., (1975) Influence des oscillations climatiques récentes sur le modelé en Amazonie Orientale (Région de Santarém) d'après les images radar latéral, *Zeitschrift für Geomorphologie*, 19, 140–163.

Tricart, J., (1977) Types de lits de fluviaux en Amazonie brésilienne, *Annales de Géographie*, 473, 1–54.

Tricart, J., (1985) Evidence of Upper Pleistocene dry climates in northern South America. In: *Environmental Change and Tropical Geomorphology* (T. Spencer, Ed.). London, George Allen and Unwin, pp. 197–217.

Upcott, N.M., Mukasa, R.K., and Ebinger, C.J., (1996) Along-axis segmentation and isostasy in the Western rift, East Africa, *Journal of Geophysical Research*, 101, 3274–3268.

Uvo, C.B., and Graham, N.E., (1998) Seasonal runoff forecast for northern South America: a statistical model, *Water Resources Research*, 34, 3515–3524.

Uvo, C.B., Tolle, U., and Berndtsson, R., (2000) Forecasting discharge in Amazonia using artificial neural networks, International *Journal of Climatology*, 20, 1495–1507.

Van der Hammen, T., (1974) The Pleistocene changes of vegetation and climate in tropical South America, *Journal of Biogeography*, 1, 3–26.

Van der Hammen, T., and Absy, M.L., (1994) Amazonia during the last glacial, *Palaeogeography, Palaeoclimatology, Palaeoecology*, 109, 247–261.

Van der Hammen, T., Duivenvoorden, J.F., Lips, J.M., Urrego, L.E., and Espejo, N., (1992a) Late Quaternary of the middle Caquetá River area (Colombian Amazonia), *Journal of Quaternary Science*, 7(1), 45–55.

Van der Hammen, T., Urrego, L.E., Espejo, N., Duivenvoorden, J.F., and Lips, J.M., (1992b) Late-glacial and Holocene sedimentation and fluctuations of river water level in the Caquetá River area (Colombian Amazonia), *Journal of Quaternary Science*, 7(2), 57–67.

Vital, H., and Stattegger, K., (2000) Lowermost Amazon River: evidence of late Quaternary sea-level fluctuations in a complex hydrodynamic system, *Quaternary International*, 72, 53–60.

Woolfe, K.J., Larcombe, P., Naish, T., and Purdon, R.G., (1998) Lowstand rivers need not incise the shelf: an example from the Great Barrier Reef, Australia, with implications for sequence stratigraphic models, *Geology*, 26, 75–78.

Wright, L.D., (1977) Sediment transport and deposition at river mouths: a synthesis, *Geological Society of America Bulletin*, 88, 857–868.

9

The Mississippi River System

James C. Knox

Geography Department, University of Wisconsin, Madison, WI 53706-1491, USA

9.1 INTRODUCTION

The Mississippi River system drains approximately 3 224 600 km^2 representing about 41% of the 48 contiguous United States and a small area of two Canadian provinces (Figure 9.1). The Mississippi River system is exceeded in length only by the Amazon and Nile Rivers and is exceeded in drainage basin area only by the Amazon, Congo, and Nile basins (Schumm and Winkley, 1994). Quaternary age glacial deposits underlie much of the drainage basin north of the Ohio River on the eastern side of the Mississippi River and north of the Missouri River on the western side of the Mississippi River (Figure 9.2). A loess cover of one to several metres thick covers much of the basin represented by pre-Wisconsin (~ pre-isotope stage 4) age glaciations as well as in unglaciated areas along the margins of the major rivers that carried sediment-laden glacial meltwater (Bettis *et al*., 2003). Aeolian sand sheets and dune complexes are common in the Great Plains region west of the Missouri River involving the upper and central drainage basins of the Red, Canadian, Arkansas, Republican, and Platte Rivers (Holliday *et al*., 2002) (Figure 9.1). Phanerozoic sedimentary rocks that range in age from earliest Palaeozoic to late Tertiary underlie most of the drainage basin, but Proterozoic crystalline rocks are locally and regionally present in areas of structural highs. The modern configuration of the drainage basin north of the Ohio and Missouri Rivers strongly reflects influences of repeated Quaternary glaciations. The exact location of the northern Mississippi River pre-glacial drainage divide remains imprecise although it is generally accepted that much of the headwater drainage of the Missouri River upstream of southeastern South Dakota drained northward to Hudson Bay prior to Quaternary glaciations (Figures 9.1 and 9.2) (Thornbury, 1965).

Four large tributaries account for more than 90% of the present-day Mississippi River drainage basin. These tributaries include the: Missouri (~45%), Upper Mississippi (~17%), Ohio (~15%), and the Arkansas (~15%). Less than one-fourth of the water and sediment contributions to the lower Mississippi River occurs downstream of the entrance of the Ohio River. Inputs to the lower Mississippi River under present day conditions involve disproportionately large contributions of water from the Ohio River and a disproportionately large influx of sediment from the Missouri River. A late 1920s study, prior to the construction of numerous large dams in the Mississippi River basin, showed that the mean annual discharge of the Ohio River represented about 43% of the whole Mississippi River system mean annual discharge in spite of representing only about 15% of the whole Mississippi River drainage basin (Swenson, 1938). The same study showed that the mean annual discharge of the Missouri River drainage basin, which represents about 45% of the whole Mississippi River drainage basin area, contributed only about 14% of the total mean annual discharge of the whole Mississippi River drainage basin (Swenson, 1938). However, during glacial times, the Ohio, upper Mississippi River, and Missouri River all contributed large inputs of water and sediment to the Lower Mississippi River.

9.2 CENOZOIC DRAINAGE EVOLUTION

Most of the topography and drainage of the Mississippi River system has developed within relatively recent

Large Rivers: Geomorphology and Management, Edited by A. Gupta

Figure 9.1 The Mississippi River drainage basin drains more than 3.2 million km^2 representing about 41% of the contiguous 48 United States and a small area of two Canadian provinces

geologic time. For example, downstream of the mouth of the Ohio River, the Mississippi River flows within a region of broad crustal down-warping known as the Mississippi Embayment (Figure 9.3). Downwarping was present in the late Cretaceous and the area received major sedimentation during the Tertiary and Quaternary Periods (Hinze and Braile, 1988). Coleman (1988) stated that the Mississippi River system has been active since at least the late Jurassic and has been delivering large volumes of sediments to the Gulf of Mexico from Cretaceous times to the present. Ages of valley fills and their relations with regional stratigraphy indicate that many deeply incised bedrock valleys in mid-continent North America probably were not present as recently as the late Pliocene (2–3 million years ago) (Knox, 1982; Anderson, 1988; Trowbridge, 1921). The Mississippi River basin has undergone significant uplift during the past few million years even though this mid-continent location on the North American craton is normally perceived as a region of relative geomorphic stability. The amount of uplift over the past 10 million years in the central part of the basin on the eastern Great Plains has been estimated to range between 100 and 500 m, whereas uplift of the Rocky Mountains on the western edge of the drainage basin has been estimated to range between 1.5 and 2.0 km during the same interval (Gable and Hatton, 1983). On the other hand, an analysis of post-depositional tilting of 17.5–5.0 million year old gravel of the Ogallala Group distributed from western Nebraska near the longitude of the eastern border with Colorado to near the eastern edge of the Rocky Mountains in southeastern Wyoming indicated a differential uplift across that part of the western plains of only about 680 m (McMillan *et al*., 2002). Major uplift in the Rocky Mountain region on the western margin of the Mississippi River drainage basin led to extensive sediment production and alluviation of the Great Plains by eastward flowing rivers

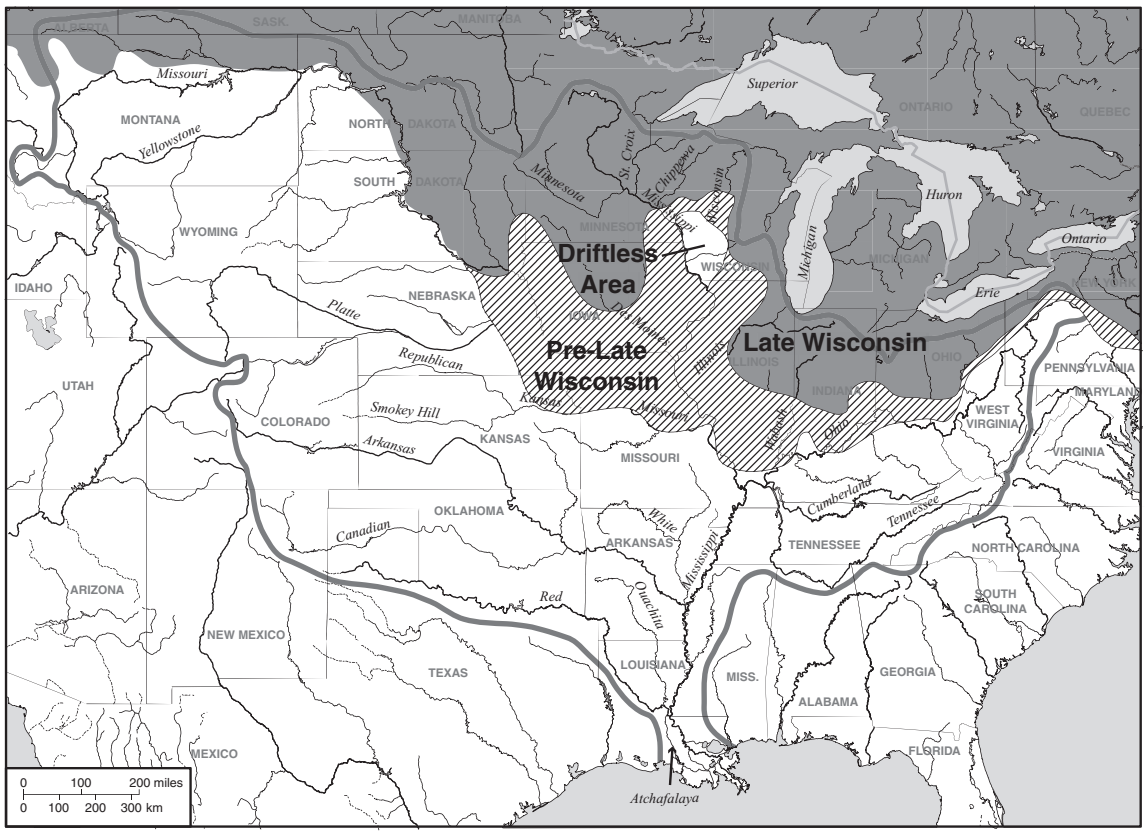

Figure 9.2 Quaternary age continental glaciation has occurred within the Mississippi River basin within areas that mostly lie north of the Ohio and Missouri Rivers except for small areas in northeastern Kansas and eastern Nebraska and the unglaciated Driftless Area of southwestern Wisconsin and northwestern Illinois. The Late Wisconsin (isotope stage 2) glacial advance into the Mississippi River drainage basin began about 26 000 ^{14}C years BP and generally began its retreat out of the drainage basin about 14 000 ^{14}C years BP (16 800 calendar years BP) (Mickelson and Colgan, 2004). See text for a discussion of estimated ages for the pre-Late Wisconsin glaciations

that were tributary to the ancestral Mississippi River located in the mid-continent. The occurrence of Rocky Mountain-derived sediments on Iowa uplands on the eastern side of the modern Missouri River is evidence that the present southward-flowing Missouri River between the states of Iowa and Nebraska was not present during this alluviation (Witzke and Ludvigson, 1990). Patterns of loess deposition between Nebraska and Iowa indicate that a southward-flowing Missouri River was established there at least by the time of Illinoian glaciation (isotope stages 6–8), but it remains unclear which Pre-Illinoian glaciation may have been responsible for establishing the southward drainage orientation. Elsewhere, a large pre-glacial tributary drainage system located east of the present Mississippi River flowed westward toward the modern Mississippi River. This drainage, known as the Teays-Mahomet preglacial valley system, is a former deeply entrenched large river that flowed from south-eastern Ohio westward across north-central Indiana and central Illinois, to join the ancient Mississippi River in the mid-continent (Melhorn and Kempton, 1991). Here, near the head of the Mississippi Embayment, the west-ward flowing Teays-Mahomet drainage converged with the eastward flowing drainage from the Rocky Mountain front. The location of this convergence shows that the main-channel Mississippi River in its middle and lower reaches has been in the same general location since at least early Cenozoic time.

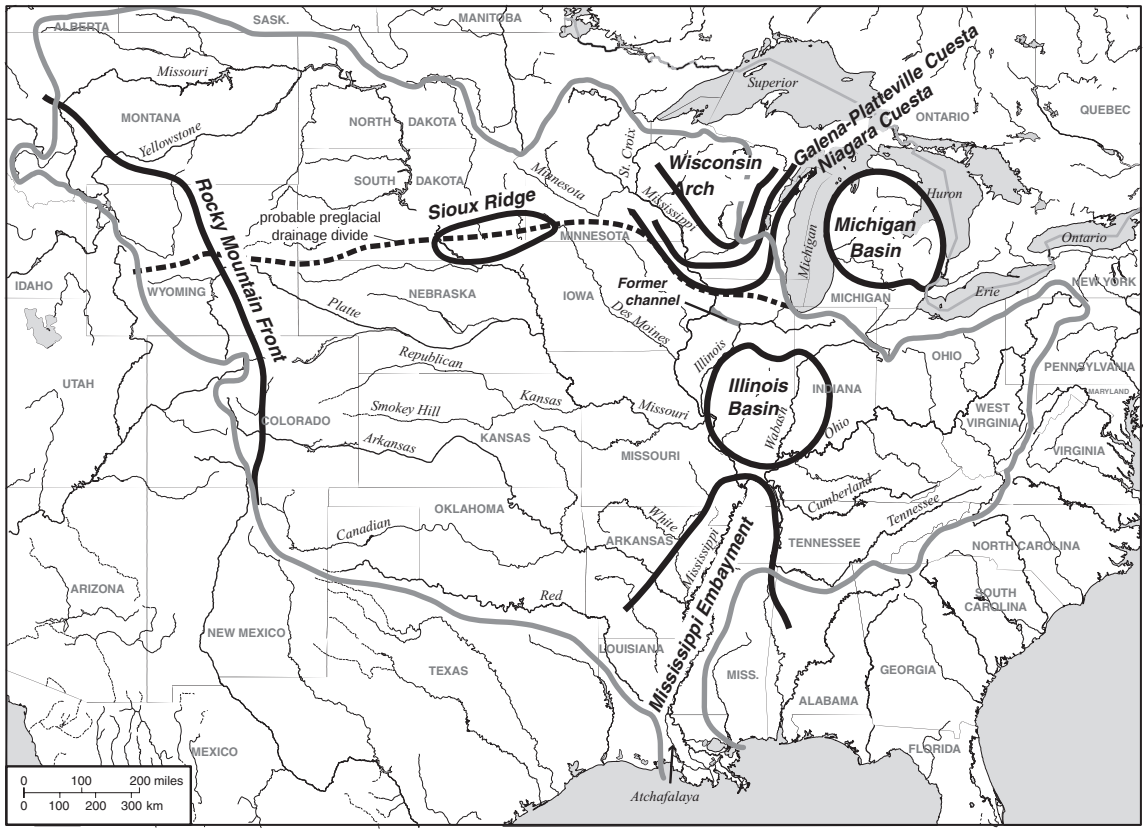

Figure 9.3 Major structural features within and near the Mississippi River drainage basin. (Data source for structure phenomena: Hinze and Braile, 1988). The former channel in northwestern Illinois represented the course of the upper Mississippi River prior to its diversion by outflow from a proglacial lake in front of the southwestward advancing Late Wisconsin (isotope stage 2) glacier about 20 300 ^{14}C years BP (24 000 calendar years BP). The outflow incised the present channel along the western border of Illinois southwestward to where it joined the ancient Iowa River system. The pre-glacial northern boundary of the Mississippi River drainage basin differed significantly from its modern boundary. Palaeo drainage features suggest the former boundary may have extended westward across northern Illinois along the Niagara Cuesta to northeast Iowa where it turned northwestward along the same cuesta to southeast Minnesota. There it apparently extended westward across southern Minnesota to the structural high of the quartzite Sioux Ridge and then southwestward across southern South Dakota and central Wyoming to the Rocky Mountains

9.3 INFLUENCE OF QUATERNARY GLACIATIONS

In contrast to the relative geographic stability for location of the lower Mississippi River, the headwaters of the upper Mississippi River system appear to have experienced considerable modifications during the last 2.5–3.0 million years in response to regional advances and retreats by continental glaciers. Comparison of modern drainage patterns with regional geologic structures and with orientations of remnant preglacial buried valley segments indicates that the continental glaciers considerably modified the northern drainage basin boundary of the Mississippi River system. The exact pre-Quaternary northern drainage divide is unknown, but regional geologic structures suggest that it followed an east–west trend along the Niagara cuesta in northern Illinois, thence northwesterly along the same cuesta in northeast Iowa, followed by a westerly course across southern Minnesota to the area of the Sioux Arch in southern South Dakota, then west-southwestly to the Rocky Mountain Front (Figure 9.3). The drainage represented by the upper Missouri, Yellowstone, and other tributaries in the Dakotas flowed north to

Hudson Bay prior to glacial modification of the region (Thornbury, 1965).

The effects of Quaternary glaciers and their associated deposits also account for most of the anomalous relations between geologic structures and geographic locations of the upper Mississippi River main channel. The Mississippi River along the western borders of northwestern Illinois and southwestern Wisconsin is incised across dolomite cuestas rather than being deflected by them. It is therefore said to be 'out of accordance with structure' (Anderson, 1985, 1988) (Figure 9.3). As recently as late Cretaceous time (60–65 million years ago), drainage in the present northern upper Mississippi River valley along western Wisconsin was apparently southwestward from the Wisconsin Arch toward the Cretaceous Ocean then located in a north–south alignment in the North American mid-continent (Hallberg *et al*., 1985; Molenaar and Rice, 1988). This early drainage pattern is suggested by regional gradients for Cretaceous age stream gravels associated with former southwestward-flowing channels whose deposits now cap various upland divides in southwestern Wisconsin, southeastern Minnesota, and northeastern Iowa. Mineralogical properties of the gravels indicate an origin in Precambrian crystalline rock highlands associated with the Wisconsin Arch in northern Wisconsin (Figure 9.3). The origin and distribution of these upland fluvial gravels is evidence that a southward-flowing Mississippi River, as occurs today between the states of Wisconsin to the east and Minnesota and Iowa to the west, was not present then.

The incision of the Mississippi River and the development of a relatively narrow gorge across the cuestas along southwestern Wisconsin and northwestern Illinois apparently occurred since the first glaciers invaded the region between 2.5 and 3.0 million years ago. Deep weathering profiles of apparent Miocene age, as young as about 15–5 million years, are associated with a former low relief erosion surface that pre-dates the deep incision of the Upper Mississippi Valley (Dury and Knox, 1971). Drainage of Quaternary proglacial lakes across preglacial drainage divides apparently was a principal cause of river incision through the cuestas. Glacial outwash gravel from a northwesterly source direction occurs on bluff tops along the eastern side of the Mississippi River in southwestern Wisconsin and northwestern Illinois and probably was deposited prior to incision of the river gorge (Willman and Frye, 1969; Knox, 1985a; Willman *et al*., 1989). Glacial sediment in buried, incised valleys of northeastern Iowa is estimated to be about 500 000 years old (Hallberg *et al*., 1985), while glacial related sediment at the mouth of the Wisconsin River on a strath 60 m above the Mississippi River bedrock valley floor and 135 m below the adjacent upland ridge is at least about 790 000 years old (Knox and Attig, 1988). These ages support the idea that major valley incision here probably had occurred within the early Quaternary, and at least before about 800 000 years ago.

The Missouri, upper Mississippi, and Ohio tributary basins have experienced continental glaciations several times during the last 2–3 million years. Because details of glaciations older than about 300 000 years are not well understood, the classic four-stage model of Quaternary glaciations has been abandoned (Boellstorff, 1978; Hallberg, 1986; Roy *et al*., 2004). The early Quaternary stage names of Nebraskan and Kansan have been replaced with a simple Pre-Illinoian (pre-isotope stage 8) designation to reflect the occurrence of at least six glaciations prior to 300 000 years ago in western Iowa and Nebraska. Very little is known about the effects of Pre-Illinoian glaciations in influencing drainage in the Mississippi River drainage basin. The Illinoian glaciation (isotope stages 6–8), which occurred between about 300 000 and 130 000 years ago (Johnson, 1986), temporarily diverted the Mississippi River out of its existing course in northern Illinois. The Illinoian glacier expanded southwestward across Illinois into eastern and southeastern Iowa and diverted meltwater flow and the Mississippi River over the uplands and around the western edge of the ice sheet in eastern Iowa (Hallberg, 1980). The Pre-Illinoian Mississippi River flowed southeastward across northwestern Illinois to the present Illinois River and then southward along the present Illinois River to the present Mississippi River near the confluence with the Missouri River (Figure 9.3). The Illinoian age diversion was temporary and the Mississippi River returned to its Pre-Illinoian course across northern Illinois following retreat of Illinoian glacial ice from the region. The Illinoian glaciation also diverted the Mississippi River on Illinois' western border at a few other locations and explains anomalous narrow valley widths and bedrock rapids that occurred along the extreme southeastern Iowa reach of the river prior to impoundment by a dam about a century ago (Willman and Frye, 1970). Glaciers of Wisconsin age (during isotope stage 3) began to influence the Mississippi River by about 55 000 ^{14}C years BP (Leigh and Knox, 1994). During late Wisconsin glaciation (isotope stage 2), about 20 350 ^{14}C years BP (~24 000 calendar years BP), westward expansion of the glacier in northern Illinois again blocked the Mississippi River and resulted in a large northwestern Illinois lake (Curry, 1998). This proglacial lake drained over the uplands on its southwest margin and subsequently incised a new course for the Mississippi River along the present boundary between Illinois and Iowa from the lake's former location to approximately the mouth of the Iowa River

system where the flow joined an ancestral valley of the ancient Iowa River system (Curry, 1998) (Figure 9.3). Ages of alluvial fill underlying terraces in the Mississippi Valley near the confluence with the Missouri and Illinois Rivers indicate that the middle reach, upper Mississippi River continued to aggrade after the diversion until at least about 18 800 ^{14}C years BP (22 300 calendar years BP), but soon after began a series of cuttings and fillings (Hajic *et al*., 1991). Local reaches of the upper Mississippi River and its tributaries northward of the late Wisconsin terminal moraine in Wisconsin and Minnesota have morphologies and topography that reflect processes associated with movement and subsequent stagnation of glacial ice (Figures 9.1 and 9.2). These reaches also include floodplain and valley lakes that resulted from the post-glacial melt-out of massive ice-blocks that had been buried in proglacial outwash.

During the Wisconsin Stage of glaciation the Mississippi River system drained nearly the entire southern margin of the continental (Laurentide) ice sheet (Wright, 1987). The upper Mississippi, Missouri, and Ohio Rivers contributed massive volumes of glacial meltwater and glacial outwash to the Lower Mississippi Valley. The massive aggradation by sand and gravel extended onto the continental shelf and into the Mississippi sedimentation cone in the Gulf of Mexico (Autin *et al*., 1991). While it was formerly believed that a lowering of base level by as much as 100 m or more during a low sea level of full glacial periods produced incision of the Lower Mississippi Valley upstream to near the head of the embayment (Fisk, 1944), it is now generally accepted that upstream incision due to lowering of sea level probably was restricted to only the most downstream few hundred km of the river (Autin *et al*., 1991).

9.4 PROGLACIAL LAKES AND EXTREME FLOODS

By about 14 000 ^{14}C years BP (16 800 calendar years BP) a general northward retreat of the southern margin of the Late Wisconsin (isotope stage 2) continental glacier was underway and large proglacial lakes were forming between the ice sheet and former ice front positions. The runoff regime for much of the upper Mississippi River system, where runoff was filtered through these proglacial lakes, shifted from dominance by aggradation to dominance by degradation at this time because these lakes served as sediment traps and released water of relatively low sediment concentration to the downstream river system. Furthermore, many outlets of proglacial lakes failed catastrophically and released large magnitude erosive floods into downstream valleys (Teller, 1987). One of the largest such floods occurred from Glacial Lake Agassiz, a proglacial lake that is believed to have originated some time after about 11 700 ^{14}C years BP (11 670 calendar years BP) in the eastern Dakotas, western Minnesota, and southern Canada between the northern drainage basin divide of the Mississippi River and the retreating ice front (Teller and Clayton, 1983). Glacial Lake Agassiz clearly originated after 12 100 ^{14}C years BP (14 100 calendar years BP) because ages of wood buried in or below glacial till in north-central Iowa indicate that active glacial ice was still present at this time in the north-central Iowa region south of the southern limit of Glacial Lake Agassiz sediments (Kemmis *et al*., 1981). Glacial Lake Agassiz drained into the Minnesota River and subsequently into the upper Mississippi River in southeastern Minnesota. Estimates of maximum flood magnitudes from Glacial Lake Agassiz have ranged from as high as 1 000 000 $m^3 s^{-1}$ (Matsch, 1983) to about 50 000 $m^3 s^{-1}$ (Wiele and Mooers, 1989). The last meltwater discharge through the southern outlet of Glacial Lake Agassiz to the Mississippi River occurred between about 9900 and 9400 ^{14}C years BP (11 250 and 10 600 calendar years BP) (Fisher, 2003). A discharge of 42 000 $m^3 s^{-1}$ has been estimated for outflow during this interval (Licciardi *et al*., 1999). Elsewhere along the upper Mississippi River, near its confluence with the Wisconsin River, stratigraphic and morphologic evidence of former palaeochannel dimensions input into a one-dimensional flow model indicated an estimated late-glacial palaeoflood discharge as large as 30 000 $m^3 s^{-1}$ (Knox, 1999). A radiocarbon age of 13 545 ^{14}C years BP (16 300 calendar years BP) from the base of a palaeochannel cut by this flood indicates the flood predates the origin of Glacial Lake Agassiz by 1850 ^{14}C years (~2600 calendar years) (see following paragraph). This large palaeoflood most likely was related to rapid drainage of Glacial Lake Duluth, a large proglacial lake that is the predecessor of modern Lake Superior. Glacial Lake Duluth delivered floods to the upper Mississippi River via the St Croix River. Discharges from this proglacial lake have been estimated to range from 30 000 to 45 000 $m^3 s^{-1}$ (Carney, 1996). Streamlined landforms shaped by a former mega-flood or mega-floods are common in both the St Croix and upper Mississippi Rivers along western Wisconsin. The evidence for an upper Mississippi River large flood about 13 545 ^{14}C years BP (16 300 calendar years BP) is consistent with stratigraphic evidence in the Gulf of Mexico that indicates deposition associated with a Mississippi River super-flood about 13 400 ^{14}C years BP (~16 000 calendar years BP) (Aharon, 2003). Nevertheless, flood magnitudes undoubtedly attenuated rapidly downstream from their proglacial lake sources. Observations of flood attenuations downstream from historical dam breaks show that after travelling about 100 km the peak

discharge magnitude is commonly 10% or less of the outlet discharge (Costa, 1988). However, it is difficult to verify previous downstream attenuations of former proglacial floods on the Mississippi River because many of the large tributaries of the upper Mississippi, upper Missouri, and Ohio Rivers contributed similar large flood inputs. The catastrophic failure of an ice dam associated with Glacial Lake Wisconsin, a central Wisconsin proglacial lake with a maximum depth of 50 m and a length of 115 km long, produced an extreme flood or floods that flowed to the Mississippi River via the lower Wisconsin River (Figure 9.1). The maximum magnitude of the Glacial Lake Wisconsin flood is estimated to have been about 170 000 $m^3 s^{-1}$ at the outlet, but was reduced by attenuation to between 36 000 and 57 000 $m^3 s^{-1}$ about 100 km downstream of the breach and about 50 km upstream of the Wisconsin River's mouth at the Mississippi River (Clayton, 2000). Farther south, the 'Kankakee floods' that were derived from proglacial Lake Michigan and adjacent smaller proglacial lakes, rapidly drained into the upper Mississippi River via the Illinois River between about 16 000 and 15 500 ^{14}C years BP (19 100–18 500 calendar years BP) (Willman and Frye, 1970). Large floods associated with rapid drainage of proglacial lakes also characterized northern headwater tributaries of the Ohio and Missouri River basins where drainage of the southern margin of the Late Wisconsin age continental ice sheet was occurring (Teller, 1987).

Channel incision undoubtedly was promoted both by catastrophic floods and by sustained high magnitude average meltwater discharges whose sediment loads were relatively low. The upper Mississippi River and the lower reaches of its tributaries were still actively aggrading as late as about 14 300 ^{14}C years BP (17 135 calendar years BP). That age was obtained by the present author for a horizon of fluvially deposited snail shells buried 4.3 m below a southwest Wisconsin terrace surface whose elevation represented the maximum level of upper Mississippi River aggradation at the end of the late Wisconsin (isotope stage 2). Major entrenchment apparently occurred quickly following ice retreat in the upper Mississippi Valley because the basal age of a channel incised about 34 m below the level of maximum late Wisconsin alluviation is 13 545 ± 85 ^{14}C years BP (~16 300 calendar years BP) at a site about 75 km upstream of the Wisconsin River junction with the Mississippi River (Knox, 1999). This rapid incision appears to be related to major outflow from Glacial Lake Duluth delivered to the Mississippi River via the St Croix River. Elsewhere, the depth of incision following Glacial Lake Agassiz drainage to the Mississippi River reached 85 m in southeastern Minnesota (Wright, 1987). Teller (1990) estimated average discharge from the Mississippi River to the Gulf of Mexico, resulting from precipitation and meltwater during the deglaciation interval, to be about 98 200 $m^3 s^{-1}$ between about 14 000 and 13 500 ^{14}C years BP (16 900 and 16 300 calendar years BP) and about 51 600 $m^3 s^{-1}$ by 11 500 to 11 000 ^{14}C years BP (13 450 to 13 000 calendar years BP) He concluded that between about 10 000 and 9500 ^{14}C years BP (11 500 and 10 700 calendar years BP) average flow to Gulf was about 42 000 $m^3 s^{-1}$, but subsequently decreased to about 17 400 $m^3 s^{-1}$ until approximately 8000 ^{14}C years BP (9000 calendar years BP). It is interesting that Teller's estimated magnitude of 17 400 $m^3 s^{-1}$ for two episodes of reduced flow to the Gulf of Mexico during the Pleistocene to Holocene transition is approximately equivalent to the average discharge of about 18 000 $m^3 s^{-1}$ to the Gulf of Mexico during the modern period of instrumentation (Schumm and Winkley, 1994).

9.5 RESPONSE OF THE LOWER MISSISSIPPI VALLEY TO UPPER VALLEY GLACIATION AND FLOODING

The Lower Mississippi Valley lowland (Embayment region) extends over a distance of about 780 km from the Mississippi-Ohio River confluence to the Gulf of Mexico (Figures 9.3 and 9.4). The width of the lowland containing late Wisconsin and Holocene alluvium ranges from about 40 to 200 km and the present floodplain is about 84 m above sea level at the upstream end (Autin *et al*., 1991; Saucier, 1994b). The period of late Wisconsin glaciation was associated, in the lower Mississippi Valley, with a wide braided river that was transporting sand and gravel into the Gulf of Mexico (Schumm and Brakenridge, 1987; Wright, 1987; Autin *et al*., 1991; Saucier, 1994a, b). Extensive alluvial proglacial outwash whose surfaces contain remnant braided channel systems remain along the western margin of the valley in the Western Lowlands and at Macon Ridge (Figure 9.4). Recent application of optically stimulated luminescence (OSL) dating methodology to Lower Mississippi Valley alluvial deposits confirms the conclusions of several earlier investigators that channel incision and channel belt abandonment occurred during a period of sea level rise when meltwater discharge to the lower Mississippi River increased (Rittenour, 2002). These results further refute the idea that trends of aggradation or degradation throughout the lower valley have been dominated by changes in base level related to rising and falling sea level during the Quaternary. As previously noted, the greatest responses to base level influences apparently were limited to the most downstream few hundred kilometres of the lower Mississippi River (Autin *et al*., 1991; Saucier, 1994b), but full upstream

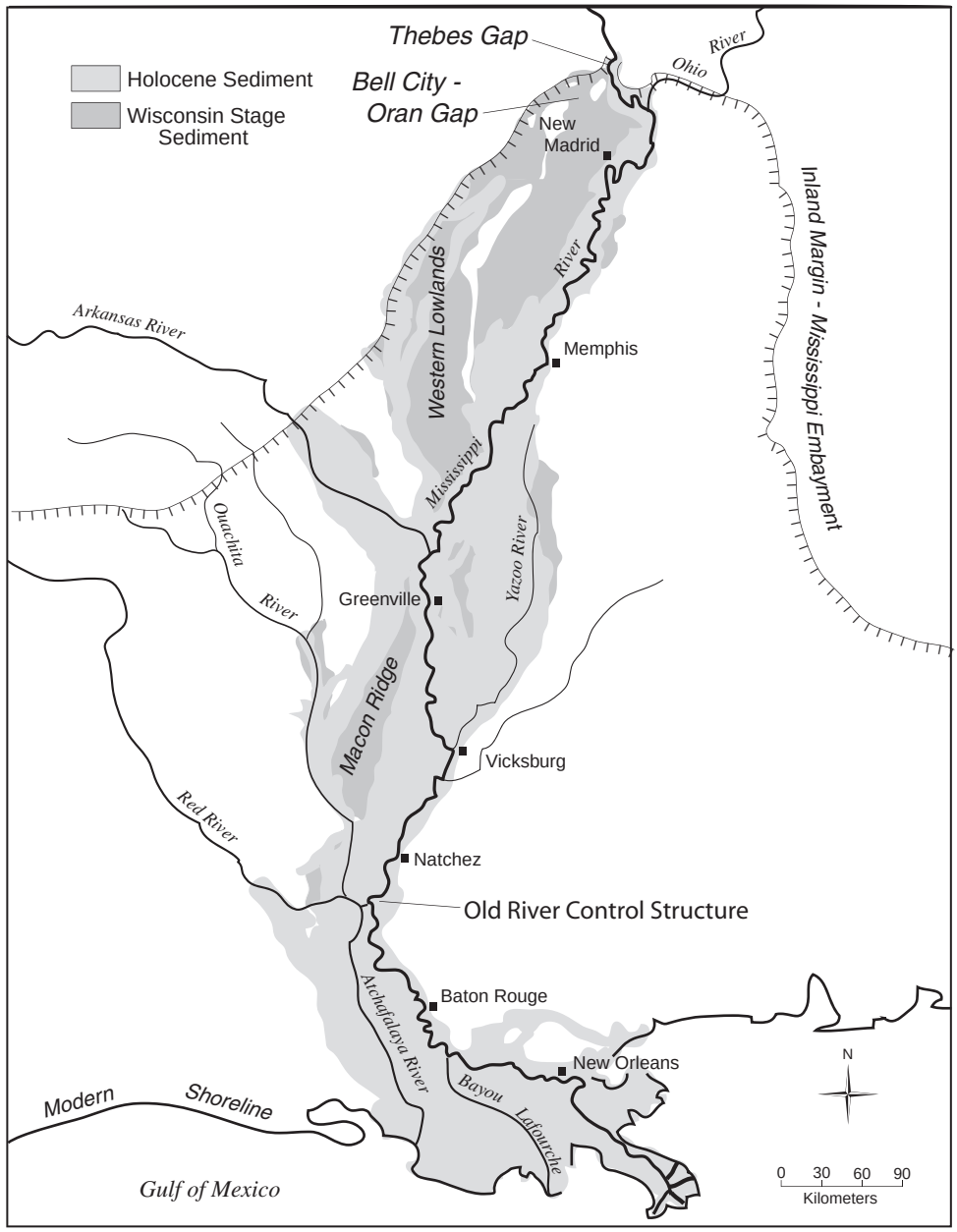

Figure 9.4 Wisconsin and Holocene alluvial deposits in the lower Mississippi River valley (modified from Autin *et al*., 1991). The Mississippi River flowed in a course along the Western Lowlands until about 16 300 ^{14}C years BP (19 500 calendar years BP) when a series of late glacial outburst floods caused the river to be diverted across low ridges, first at the Bell City-Oran Gap and later at Thebes Gap. The 'Old River Control Structure' is a flow regulation facility that consists of a series of gates that control the flow of water from the Mississippi River into the Atchafalaya River. This structure and a nearby companion structure were built to prevent the Atchafalaya River from capturing the lower Mississippi River due to the Atchafalaya River's steeper gradient, lower elevation, and more direct route to the Gulf of Mexico (McPhee, 1989)

aggradation effects due to Holocene sea level rise may extend approximately twice this distance. For example, Blum and Törnqvist (2000) used the intersection of the modern floodplain and the floodplain surface associated with the last glacial maximum to define the upstream extent of coastal onlap due to sea-level rise for the lower Mississippi River and they concluded that the influence of Holocene sea-level rise on upstream aggradation ranges between 300 and 400 km. The gradient of the lower Mississippi River during glacial times was clearly much steeper than the modern and late Holocene gradients. Respective OSL ages of about 19 700–17 800, 16 100–15 000, and 12 500–12 100 OSL years ago for near-surface sediments that represent three prominent levels of relict braided channel belts in the northern sector of the lower valley confirm hypothesized late Wisconsin ages (isotope stage 2) for these deposits and support an idea that the surfaces were abandoned when adjacent floodplain surfaces were incised by meltwater and/or by large magnitude floods following catastrophic failure of outlets for large proglacial lakes (Rittenour *et al*., 2003). These results show that early mapping, which placed Quaternary alluvium and landforms within the classic four-stage model of Quaternary glaciations and which assigned Holocene ages to the relict braided stream deposits in the northern Lower Mississippi Valley, were erroneous (Fisk, 1944).

The displacement of the late Wisconsin Mississippi River from its position in the Western Lowlands along the western side of the Lower Mississippi Valley in southeastern Missouri and eastern Arkansas to its present position along the eastern margin of the valley is thought to have resulted from an avulsion created by extreme late Wisconsin floods associated with rapid drainage of proglacial lakes (Blum *et al*., 2000). An abrupt decrease in flow competency after about 16 300 ^{14}C years BP (19 500 calendar years BP) is suggested by sedimentological changes in sediments of the Western Lowlands and it has been hypothesized that this sedimentological shift resulted from flow diversion and incision of the Mississippi River across a low ridge first at the Bell City-Oran Gap and later at Thebes Gap (Royall *et al*., 1991; Saucier, 1994a; Knox, 1996) (Figure 9.4). Blum *et al*. (2000) studied alluvial deposits in the gaps and concluded that the Bell City-Oran Gap was the primary course of the Mississippi River during the entire Wisconsin stage of glaciation, and that the Thebes Gap location of the modern Mississippi River was established in earliest Holocene time. The most likely floods that contributed to the shift in river location include the Kankakee Flood(s) which emanated from outlet failure of a large proglacial lake at the southern margin of present Lake Michigan between about 16 000 and 15 500 ^{14}C years BP (19 100–18 500 calendar years BP) (Willman and Frye, 1970) and the Glacial Lake Agassiz floods that occurred between about 11 700 and 9400 ^{14}C years BP (13 700–10 600 calendar years BP) (Teller, 1990; Leverington *et al*., 2000; Fisher, 2003). Another possible contributing catastrophic flood may have been Glacial Lake Duluth (predecessor of modern Lake Superior) which drained catastrophically via the St Croix and upper Mississippi Rivers (Knox, 1999). However, given the tendency for outbreak flood magnitudes to rapidly attenuate downstream, floods derived from far northern tributaries of the upper Mississippi River seem less likely sources for this diversion.

The lower Mississippi River has been characterized by a meandering morphology during the Holocene. The shift from the late Wisconsin braided morphology apparently began near the mouth about 12 000 ^{14}C years BP (14 000 calendar years BP) and reached the head of the lower valley near the Ohio River junction by about 9000 ^{14}C years BP (10 200 calendar years BP) (Autin *et al*., 1991; Saucier, 1994b). Several distinct meander belts have developed during the Holocene. Lateral and vertical scouring by the Mississippi River during meander belt formation removed tens of metres of late Wisconsin sand and gravel and replaced these deposits with inset point-bar and natural levee alluvium consisting mainly of clay, silt, and fine sand and fills of silt and clay in abandoned channels (Autin *et al*., 1991). Holocene backswamp environments have accumulated from 10 to 35 m of sediment deposited during overbank flooding (Autin *et al*., 1991). Thickness of the deposits increases downstream in the Lower Mississippi Valley.

9.6 THE MISSISSIPPI RIVER SYSTEM DURING THE HOLOCENE

9.6.1 Climate and Vegetation Changes

Alluvial activity in the Mississippi River system during the Holocene has been strongly influenced by fluvial adjustments to late Pleistocene sedimentation and erosion and also strongly influenced by climate and vegetation changes. The deep entrenchment of late Wisconsin alluvial fills in the main valley of the upper Mississippi River Valley was initiated by runoff from proglacial lakes, and by large floods from many of these lakes, when their outlets failed catastrophically as warmer Holocene climates approached. The entrenchment of the main valley produced a lowered base level for tributaries that, in response, incised their massive deposits of alluvial and colluvial sediments that had accumulated during late Wisconsin glacial and periglacial climates. Consequently, in the reach of the upper Mississippi River along

Wisconsin's western border, massive Holocene alluvial fans accumulated at tributary mouths and, in turn, the fans typically have displaced the main channel Mississippi River toward the opposite valley side where it has remained throughout Holocene time. The rapid sedimentation of the alluvial fans locally dammed the main valley and in some cases produced a series of river lakes similar to those in the upper reaches of the Mississippi drainage system in Minnesota and at Lake Pepin upstream of the junction with northwestern Wisconsin's Chippewa River (Wright, 1987). Along western Wisconsin, the Holocene remobilization of sediment from tributaries has been associated with at least 15–20 m of progressive Holocene alluviation in the main valley upper Mississippi River (Knox, 1999). The Holocene sedimentation is progressively burying low relief, unpaired terraces that formed during downcutting at the late-glacial to post-glacial transition. Consequently, the magnitude of Holocene aggradation varies from 0 m for higher terrace surfaces not yet subject to flooding to as much as 20+ m overlying surfaces associated with the maximum depth of incision at the late-glacial to post-glacial transition. It is unknown how much of the upper Mississippi River system in other regions has experienced this sequence of sediment redistribution, but it is likely that it occurred elsewhere in the upper Missouri and upper Ohio River drainages because similar glacial-fluvial activity is apparent for these drainage basins.

The large scale vegetation biomes that characterize the Mississippi River drainage basin had approached their modern locations by about 9000 ^{14}C years BP (10 000 calendar years BP) (Bartlein *et al*., 1984; Webb *et al*., 1993; Baker, 2000). In spite of the general relative geographic stability of the biomes during the Holocene, the prairie-forest ecotone not only fluctuated in response to modest climate changes, but ecotone movements have not been entirely synchronous across the Mississippi River drainage basin. Nevertheless, the environmental changes in the regions of the ecotone are symbolic of the climate and vegetation shifts that were influencing much of the Mississippi River drainage basin. Therefore, Holocene environmental changes in the ecotonal region are used in the following to represent the broader scale major climate shifts that have influenced fluvial activity in the Mississippi River drainage basin.

During the Holocene, most of the Missouri River tributary system and much of the upper reaches of Mississippi River tributaries that drain the southern Great Plains have been dominated by grasslands, while the upper Mississippi River in Wisconsin and east-central Minnesota, the Ohio River basin, and much of the lower Mississippi Basin east of the Great Plains have been dominated by forest (Figure 9.5). This vegetation cover was prevalent until the nineteenth century when widespread vegetation cover removal for cropland and grazing occurred across the drainage basin (Knox, 2002). The prairie-forest ecotone, which respectively crosses the Mississippi River in both northwestern and southwestern Illinois, is associated with major seasonal air mass boundaries (Bryson, 1966; Bryson and Wendland, 1967). Bryson (1966) showed that the grassland region is influenced more than half of an average year by relatively dry, mild air masses of Pacific origin. Elsewhere, in the forest region of the upper Mississippi River drainage basin in Wisconsin, he found that more than half of the average year is dominated by Arctic-derived or Pacific-derived air masses having a more northerly trajectory, or by mixtures of the two. The forest region to the southeast of the grasslands was shown to be dominated by relatively warm and moist air masses of tropical origin during more than half of the average year (Bryson, 1966). Although Holocene climatic changes occurred throughout the Mississippi River system, the relative hydrologic impacts of these climate shifts were much greater for tributaries draining the western side of the Mississippi River because runoff and sediment yields are more responsive in grassland and steppe vegetation areas than in forest areas (Dendy and Bolton, 1976; Langbein and Schumm, 1958).

The results of many palaeoclimatic investigations throughout the region of the upper Mississippi and Missouri River drainages indicate that maximum dryness associated with grassland expansion during the Holocene progressed eastward from the Great Plains with maximum Holocene dryness occurring between about 8000 (9000 calendar years BP) and 5000–4000 ^{14}C years BP (5700–4400 calendar years BP) near the Mississippi River headwaters in north-central Minnesota (Wright, 1992; Dean, 1997). Farther to the southeast, in northeastern Iowa and southern Wisconsin, maximum Holocene dryness occurred later between about 5000 and 3000 ^{14}C years BP (5700 and 3150 calendar years BP) (Winkler *et al*., 1986; Wright, 1992; Baker *et al*., 1996, 2002). Still farther southeastward, the eastward extent of the prairie grassland in Illinois was greater at about 3000 ^{14}C years BP (3150 calendar years BP) than it had been at 7000 ^{14}C years BP (7850 calendar years BP), the time of approximate maximum eastward penetration of the grassland-forest ecotone in east-central Minnesota. Proxy climate data collected and analyzed by others indicate that climatic conditions during the late middle Holocene in the southern Wisconsin – northeastern Iowa region involved a warming of about 1.5 °C above the preceding period and that mean annual precipitation then was about 15% less than modern (Bartlein *et al*., 1984; Winkler *et al*., 1986; Baker *et al*., 1996; Denniston *et al*., 1999a). These climatic changes in

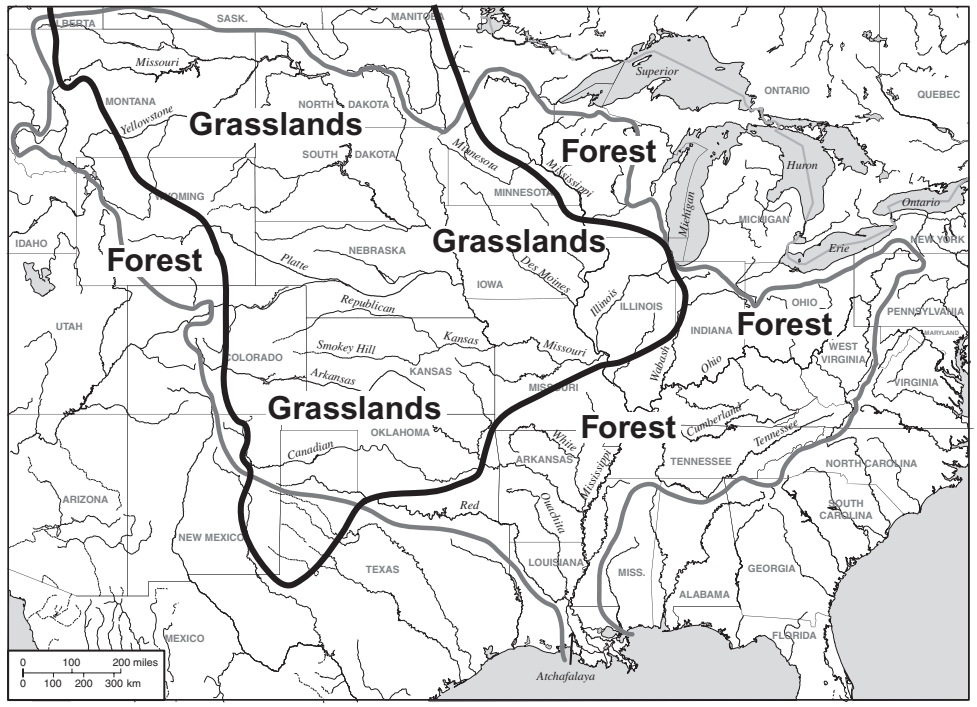

Figure 9.5 Prior to Euro-American settlement prairie grasslands dominated most of the Missouri River drainage basin and most of the middle and upper sectors of the Arkansas drainage basin. Farther east, the lower Mississippi Valley, the Ohio River drainage basin, and a significant part of the upper Mississippi drainage basin were then dominated by forest vegetation. The heavy black line approximates the modern location of the grassland–forest border

the upper Mississippi River valley were strongly associated with changes in magnitudes and frequencies of floods as shown in the section below on Holocene flooding.

Holocene environmental changes representing the core region for the western tributaries of the Mississippi River have recently been summarized for southeastern Nebraska and other areas of the mid-continent (Baker, 2000). This summary indicates that southeastern Nebraska experienced maximum Holocene aridity between about 8500 and 5800 ^{14}C years BP (9500 and 6600 calendar years BP) when components of upland forest disappeared and conditions were sufficiently dry that even riparian woodlands were stressed. Another extremely dry phase with similar biotic associations apparently occurred between about 3100 and 2700 ^{14}C years BP (3300–2800 calendar years BP) It is noteworthy that between about 5800 and 3100 ^{14}C years BP (6600 and 3300 calendar years BP), when maximum dryness was occurring on the eastern edge of the grasslands in northeastern Iowa, southern Wisconsin, and central Illinois, dryness in southeastern Nebraska eased and riparian woodlands flourished again. Landscape cover in southeastern Nebraska approached modern conditions by about 2700 ^{14}C years BP (2800 calendar years BP). Elsewhere, investigations of fossil isotopes of ^{13}C in cave stalagmites of southern Missouri and northern Arkansas, along with other climate proxies such as pollen and vertebrate fossils, indicate that the middle Holocene climate was considerably drier than at present with establishment of prairie grasslands by about 7500 ^{14}C years BP (8350 calendar years BP) and maximum effective dryness occurred between about 5300 and 4500 ^{14}C years BP (6100–5100 calendar years BP) (Denniston *et al*., 1999b, 2000). Deciduous forest apparently replaced grasslands as the dominant vegetation between about 4500 and 3000 ^{14}C years BP (5100 and 3200 calendar years BP), but drier conditions on the southern ecotone returned between about 3000 and 1500 ^{14}C years BP (3200 and 1400 calendar years BP) and allowed rejuvenation of prairie dominance that in turn was followed by deciduous forest dominance since about 1500 ^{14}C years BP (1400 calendar years BP) (Denniston *et al*., 2000). Comparison of ages and directions of climate/vegetation shifts among sites

along the northern and southern sectors of the southern ecotone show that timing of maximum dryness in the Missouri-Arkansas region is broadly similar to the timing of maximum Holocene dryness that occurred in central and western Minnesota. However, as previously noted, maximum dryness in northeastern Iowa, southern Wisconsin, and east-central Illinois apparently occurred between about 5000 and 3000 ^{14}C years BP (5700 and 3150 calendar years BP) when sites on the northeastern and southeastern margins of the grasslands were retreating from maximum dryness. While ages that denote prominent directional shifts in climate and vegetation are broadly similar across the mid-continent, local responses differ as might be expected with different regimes of large scale atmospheric circulation regimes.

9.6.2 Holocene Alluvial Episodes

Rates of erosion and sedimentation in grassland environments are sensitive even to relatively modest changes in climate (Langbein and Schumm, 1958; Dendy and Bolton, 1976). Figure 9.5 shows that more than half of the Holocene pre-agriculture Mississippi River drainage basin was grassland, including most of the western tributaries and the Illinois region to the east of the Mississippi River. The high sensitivity of grasslands to climate change is confirmed by alluvial chronologies for various tributaries from within the Mississippi River drainage basin. Recognition of widespread synchroneity across these chronologies has often met with skepticism because of a common belief that many factors other than climate and vegetation also strongly influence fluvial activity. Observations that erosion and sedimentation in tributaries and trunk streams are often out-of-phase (Antevs, 1955; Schumm, 1965), and that episodes of cutting and filling often depend on geomorphic thresholds such as slope stability or that multiple episodes of cutting and filling can be triggered by a single downcutting event (Schumm, 1977; Patton and Schumm, 1981), are explanations commonly offered against widespread synchroneity. Clearly these sorts of processes mask and complicate recognition of the forcing effects of climate change on alluvial chronologies, and they underscore that singular erosional and depositional events are not necessarily related to an external forcing effect such as climate. On the other hand, broad trends that involve episodes of active cutting and filling or active lateral channel migration punctuated with episodes of relative stability, are evidence of long-term systematic changes in the relative intensity of fluvial activity. An illustration is the mid-continent tendency for widespread early Holocene valley aggradation when climatic conditions became warmer and drier and late Wisconsin woodland was replaced by grassland (Knox, 1983). Mandel's (1995) comprehensive compilation of radiocarbon ages of alluvial sediments in the central US Great Plains led him to remark: 'Although there are some variations in the pattern and timing of erosion and sedimentation during the Holocene, regional synchroneity is indisputable.' A comparison of alluvial chronologies between basins along a 600 km transect from presently semiarid southwestern Kansas to presently subhumid central Iowa showed similar basin-wide patterns of Holocene erosion and deposition (Bettis and Mandel, 2002). The comparative analysis by Bettis and Mandel showed that between about 11 000 and 8000 ^{14}C years BP (13 000 and 8900 calendar years BP) valley alluviation was widespread, but punctuated by slow alluviation and/or stability about 10 000 ^{14}C years BP (11 400 calendar years BP). They found, on the other hand, that between about 8000 and 5000 ^{14}C years BP (8900 and 5700 calendar years BP) net erosion and sediment remobilization dominated in small valleys, while net sedimentation dominated in large, main valleys, and episodic aggradation occurred on alluvial fans. They found that for the late Holocene, after about 5000 ^{14}C years BP (5700 calendar years BP), alluvial fans were dominated by widespread stabilization, while net sediment deposition occurred on floodplains of small valleys, and net aggradation slowed on floodplains in large valleys. Alluvial chronologies from elsewhere in the Great Plains grasslands and ecotone region of the mid-continent region are broadly supportive of the conclusions presented by Bettis and Mandel (Brakenridge, 1981; Knox *et al*., 1981; Knox, 1983, 1996, 1999; McDowell, 1983; Johnson and Martin, 1987; May, 1989, 1992, 2003; Martin, 1992; Baker *et al*., 2000). Furthermore, farther south, ages for discontinuities in alluvial chronologies from Mississippi River tributaries in northern Mississippi (Grissinger *et al*., 1982) and the Duck River tributary of the lower Tennessee River in western Tennessee (Brakenridge, 1984), are also broadly similar to those of the upper Mississippi Valley and Great Plains.

9.6.3 Holocene Flood Episodes in the Upper Mississippi Valley

Systematic examination of long-term variations of Holocene floods has been undertaken only for a regional sector of the upper Mississippi River system. Results of these studies show that long-term variations in flood magnitudes, both in small tributaries of less than ten to a few hundred km^2 and for the main channel upper Mississippi River of 120 000–205 000 km^2 drainage area, are strongly related to the Holocene climate changes described in the preceding section (Knox, 1999, 2000, 2003). Since the

methodologies used for reconstructing these palaeoflood histories have been described in references cited above, only the general patterns of Holocene flood variability will be described here (Figure 9.6). A late Holocene history of large overbank floods on small tributaries in southwestern Wisconsin was reconstructed by computing competent depths of flood waters required to transport the largest cobbles and/or boulders deposited on floodplains during former large overbank floods, and depths were then expressed as a ratio to the normal bankfull depth at each respective site (Figure 9.6a) (Knox, 1993). The average magnitude for the interval separating the upper and lower

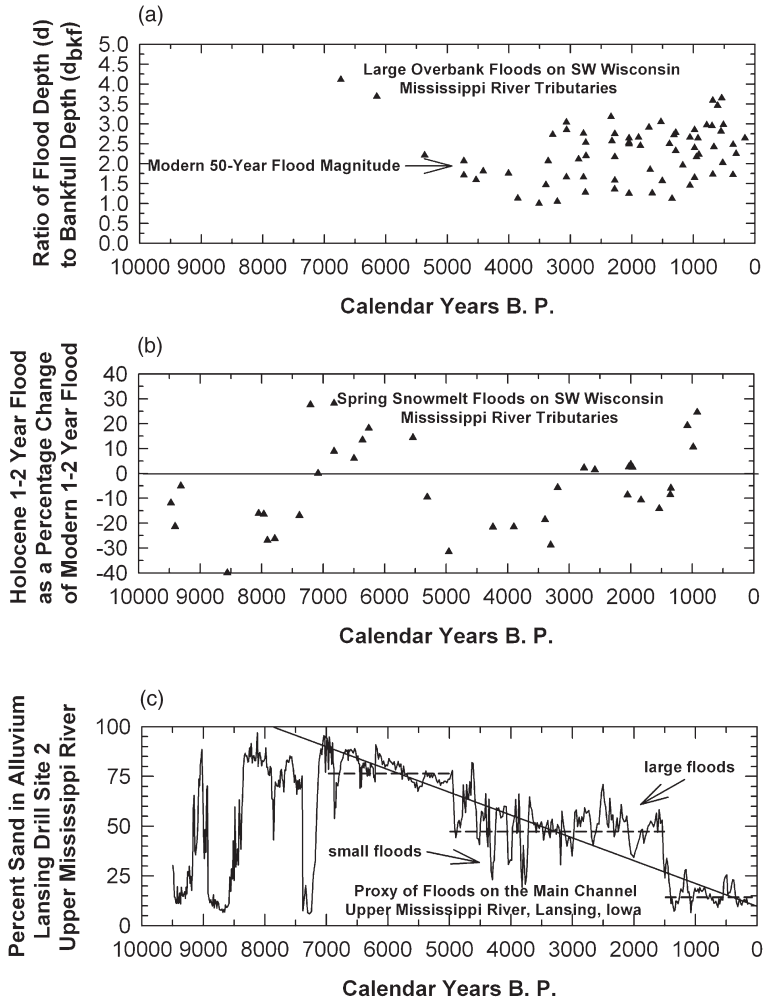

Figure 9.6 Proxy palaeoflood histories, for southwestern Wisconsin sites in the upper Mississippi River Valley, show that Holocene floods have varied in a very episodic fashion that is strongly related to changes of climate. For example, a prominent warm and dry climatic episode between about 5000 and 3000 years ago in the area represented by the above sites affected floods on small tributaries as well as the main channel upper Mississippi River. The largest overbank floods on small tributaries with drainage areas between a few km^2 to a few hundred km^2 show that flood magnitudes then generally did not exceed a stage equivalent to twice their associated modern local bankfull stage. These overbank floods between 5000 and 3000 years ago rarely exceeded a magnitude of a modern flood of an annual recurrence probability of 2% (50-yr flood). Estimated magnitudes of small, high frequency floods of 1–2 recurrence probability determined from coring relict cutoff alluvial channels also indicate that the warm and dry climatic episode between about 5000 and 3000 years ago were small, reaching from 15 to 25% smaller than their modern counterparts. [Data sources: (a) Knox, 1993; (b) Knox, 1985b, 2000; (c) Knox, 2003.] See text for discussion and explanation of flood proxies

95th percentile confidence intervals is 0.6 for the flood ratio and about 870 calendar years for age. These large overbank floods on tributaries are mainly produced during summer heavy rains associated with slow-moving or stalled cold fronts involving the collision of polar and tropical derived air masses. A Holocene record of floods of 1–2 years recurrence probability was reconstructed by computing discharge magnitudes required to fill relict cut-off channels to their former bankfull stages indicated by tops of lateral accretion sediments preserved in relict point bar sediments (Figure 9.6b). Either spring snowmelt or common summer rainstorms account for most bankfull stage floods in this region. Ages for relict channels were determined, either directly by radiocarbon dating of wood from basal channel sediments, or indirectly by a sediment depth – radiocarbon age relationship for overbank sediments. The standard error of estimate for the latter was about 1000 calendar years, and the standard error for the reconstructed bankfull discharge is estimated to be 25–30% (Knox, 1985b). Holocene variations in large overbank floods on the main channel upper Mississippi River are currently under investigation, and an exemplary Holocene flood record is shown in Figure 9.6c (Knox, 2003). This proxy record is based on the percentage of sand in the total sediment fraction of overbank flood deposits on the upper Mississippi River floodplain. Because stratigraphic signatures of overbank floods are also influenced by flood durations, as well as flood stage magnitudes and sediment concentrations, the sedimentary record represents a general approximation of past floods (Benedetti, 2003). Radiocarbon dating has shown that this reach of the Upper Mississippi valley has experienced progressive aggradation throughout the Holocene. The proxy is based on the relation that large floods of high energy deposit larger amounts and coarser sand than small floods which deposit smaller amounts of sand and finer sand. Large overbank floods on the upper Mississippi River are dominated by snowmelt runoff, but excessive spring and summer rainfalls occasionally also result in large floods as illustrated by the 'Great Flood of 1993' (Knox, 1988; Parrett *et al*., 1993). The trend line in Figure 9.6c was fitted by least-squares regression and represents a fining-upward tendency for this floodplain site. However, the overall fining-upward trend is composed of step-like subset trends shown by the dashed lines superimposed on Figure 9.6c. The breaks between subsets probably reflect changes in land surface area subject to flooding as progressive alluvium overtops and buries low terraces. Nevertheless, the relative temporal patterns for sand anomalies are broadly similar for both sets of trends. Sand percentages that plot above either the solid or dashed trend lines indicate large floods of high energy, whereas small floods of low energy transport lesser amounts of sand to the floodplain and plot below the trend lines. The general pattern for flood departures from average is the same for both comparisons. The estimated ages in Figure 9.6 used the conversions of Stuiver *et al*. (1998) to transform radiocarbon ages to calendar years BP Ages for plotting positions were then determined from the statistical regression equation that regressed predicted calendar years BP from depths of radiocarbon samples. The equation was significant at $P < 0.0001$, with a standard error of 340 years.

The Holocene variations in upper Mississippi Valley floods imply a very non-stationary behaviour for the means and variances in the flood series (Figure 9.6). Comparison of the three flood records shows both similarities and differences among the three flood series that reflect diversity in types of floods that dominate the respective series. The anomalous large variations in sand represented in the pre-7000 calendar years BP portion of the upper Mississippi River record shown on Figure 9.6c may be an unreliable characterization of flooding then because these large variations probably reflect in large part the remobilization of massive deposits of colluvium and alluvium that had accumulated in tributaries during periglacial and glacial climatic conditions immediately prior to the Holocene. Alternatively, there may have been more spatial variability in the loci of overbank deposition on the youthful early Holocene floodplain. Furthermore, since the age calibration was based on 11 radiocarbon ages, the oldest being 6370 calendar years BP, the early Holocene scaling also may be unreliable due to anomalous large inputs of sediment from tributaries during that period.

A prominent similarity between the three Holocene flood records occurs between about 4800 and 3100 ^{14}C years BP (5500–3300 calendar years BP) when all three proxies suggest an episode of smaller floods. Climate conditions at this time, according to fossil proxy climate indicators presented by others (Bartlein *et al*., 1984; Winkler *et al*., 1986; Baker *et al*., 1996), involved an increase of 1.5 °C in mean annual temperature above the preceding period and a reduction of the mean annual precipitation to a magnitude of about 15% less than the modern period. Isotopic analyses of $\delta\,^{13}$C and $\delta\,^{18}$O from northeast Iowa cave stalagmites also indicate that cool season precipitation probably predominated during this generally dry climate episode (Denniston *et al*., 1999a). Sampling of former large overbank floods in small tributaries representing this period showed that flood stages were generally smaller than a magnitude equivalent to about twice the local bankfull stage depth. This implies, on the basis of comparison with modern flood depths, that the largest overbank floods for these sites were generally smaller than

magnitudes of modern floods having a 2% chance recurrence probability (Figure 9.6a). The large upper Mississippi River also was experiencing generally smaller floods then, but the most noteworthy aspect of upper Mississippi River flooding in this period was a dramatic increase in short-term variability involving frequent fluctuations between moderately large floods and extremely small floods. Many of these large floods probably resulted from spring rains falling earlier than normal on melting snow, similar to occurrences of moderately large to very large floods that have been produced by combined rain and snowmelt during anomalously warm recent decades. Nevertheless, while these anomalous warm periods are characterized by extreme short-term variability involving high frequencies of both moderately large floods as well as high frequencies of very small floods, floods on the average tend to be smaller during warm and dry episodes than during cool and moist episodes. This is because frequent dry years with little precipitation and reduced runoff dominate the average conditions of these warm episodes. The relationship also is influenced by the tendency of cool and more moist climate episodes to be associated with greater snow cover (a principal cause of upper Mississippi River floods) and the tendency for cooler climate episodes to favour increased runoff due to relatively lower evapotranspiration losses for antecedent river basin conditions.

All three proxy flood records show an abrupt shift to larger floods about 3100 ^{14}C years BP (3300 calendar years BP) which is consistent with a return to somewhat cooler and more moist climates (Bartlein *et al*., 1984; Winkler *et al*., 1986; Baker *et al*., 1996). Although there are some indications of similarities in flooding variability among the three records during the last three millennia, too few data are available to support clear relations (Figure 9.6c). The pattern of large overbank floods on southwestern Wisconsin tributaries shows only modest change during the last three millennia, although there is weak evidence of an overall shift upward in flood magnitudes between about 1100 and 400 ^{14}C years BP (1000 and 500 calendar years BP). Data are too few to determine whether this trend ended or increased after about 500 years ago. Comparison of snowmelt-dominated floods on the small tributaries (Figure 9.6b) against those on the main upper Mississippi River (Figure 9.6c) suggests a weak out-of-phase relation. This is most apparent for the period between about 1775 and 1555 ^{14}C years BP (1700–1500 calendar years BP) when the 1–2 years recurrence frequency floods on small tributaries were about 10% smaller than modern counterparts, but overbank floods on the main upper Mississippi River were then larger than average. Several independent studies involving climatic proxies developed by others have shown that drought conditions were widespread across mid-continent North America beginning about 1650 years ago and these dry episodes locally lasted up to three centuries (Woodhouse and Overpeck, 1998). A high frequency of warm and dry climate with early spring rain on melting snow may account for the out-of-phase relation between floods on the small tributaries versus those on the main channel upper Mississippi River. This is because snowmelt runoff normally occurs too slowly to produce large floods in small headwater drainages, but the simultaneous combined, widespread snowmelt runoff from the many small tributary systems produces large or very large floods on big river systems such as the upper Mississippi River (Knox and Daniels, 2002). As previously noted, most floods on the upper Mississippi River, including large floods, involve runoff from snowmelt. Seasonally warm winters and springs often favour rainfall on melting snow, and this probably is the principal explanation for the high variability and frequent large floods during warm climate episodes. Warm periods also favour an increased incidence of such air masses in the region and this process also contributes to the patterns of clustered floods described above. The linkage between frequent large palaeofloods and past warm climates is consistent with the anomalous high frequency of large floods on the upper Mississippi River that have occurred since about AD 1950 (Olsen *et al*., 1999; Knox, 2000). However, prolonged and heavy summer rains also occasionally produce large summer floods on the upper Mississippi River as occurred during the Great Flood of 1993 (Parrett *et al*., 1993). Large summer floods typically involve stalled or slow-moving frontal systems with a persistent influx of low latitude air masses in which water vapour content is very high.

In summary, the sedimentological proxy used here to identify large floods in the upper Mississippi River's alluvial stratigraphic record does not permit exact quantitative assignment of flood magnitudes and recurrence probabilities. However, comparisons of stratigraphic units for the large Holocene palaeofloods against thicknesses and textures of stratigraphic units associated with large historical floods that have known discharges and recurrence probabilities indicate that the large palaeofloods were at least equivalent to or larger than modern floods of 50- to 100-year recurrence probabilities. The proxy record of late Holocene overbank floods on the upper Mississippi River indicates a tendency for floods to be slightly smaller but much more variable with frequent moderately large floods punctuated by very small floods during prolonged warm episodes compared with floods being larger and less variable during prolonged cool episodes. This pattern is particularly evident in Figure 9.6c which shows an episode of moderate to relatively large floods between about 7850 and 4800 ^{14}C years BP (7000 and 5500 calendar years BP),

followed by an episode of highly variable but somewhat smaller floods between about 4800 and 3100 ^{14}C years BP (5500 and 3300 calendar years BP), then returning to generally larger floods after about 3100 ^{14}C years BP (3300 calendar years BP). The respective local effective climatic conditions during these three episodes involved modest shifts from cool/moist to warm/dry and back to cool/moist during the same times (Baker *et al*., 2002). However, as previously noted above for shorter timescales, there also has been a strong tendency toward increased extreme short-term variability involving frequent occurrences of moderately large floods during warm climate episodes. Furthermore, there is some evidence to support the idea that occurrences of very large floods are especially favoured during times of rapid climate change. Overall, noteworthy large or moderately large upper Mississippi River floods occurred about 4150, 2500–2200, 1850–1550, 1325, 1120–860, and 570–310 ^{14}C years BP (4700, 2500–2200, 1800–1500, 1280, 1000–750, and 550–400 calendar years BP). Some of the upper Mississippi River floods apparently were coincident with widespread large floods elsewhere in the Mississippi River system because ages of about 4700, 3500, 3000, 2000, 1200, and 300 calendar years BP have been associated with megafloods interpreted from the marine record of the northern Gulf of Mexico (Brown *et al*., 1999).

9.6.4 Lower Valley Alluvial Responses to Upper Valley Holocene Environmental Change

A little more than three-fourths of the drainage basin of the Mississippi River is geographically located upstream of the head of the Mississippi Embayment at the southern tip of Illinois, and slightly over 60 % of the drainage basin is represented by the Missouri and Upper Mississippi subsystems (Figure 9.7). Late nineteenth century instrument

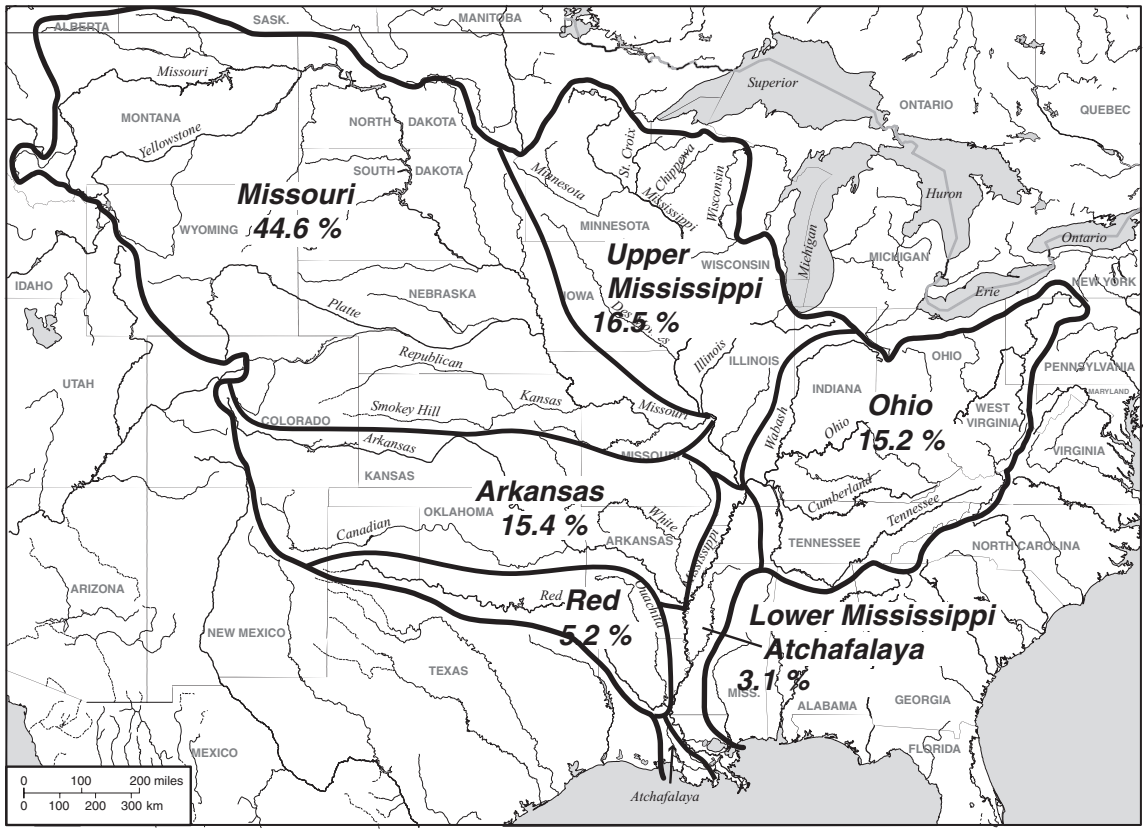

Figure 9.7 Approximately three-fourths of the drainage area of the Mississippi River system occurs upstream of the head of the lower Missississsippi River valley which begins below the entry point of the Ohio River. Present day lower Mississippi River flow is dominated by discharge from the Ohio River system and by large sediment loads from the Missouri River system

observations indicated the semiarid Missouri River basin, prior to modification by dams and reservoirs, contributed about 84% of the suspended sediment delivered to the head of the lower Mississippi River even though it represented only about 45% of the total Mississippi River system (Keown *et al*., 1986). This sediment load ignores relatively modest additional contributions from small basins between the mouth of the Missouri River and the Mississippi River confluence with the Ohio River. The high magnitude sediment loads from this region, and the relatively similar broad-scale alluvial chronologies and ages of alluvial discontinuities for the many areas of the eastern Great Plains and central sectors of the upper Mississippi River valley that were noted previously, imply that evolution of lower Mississippi River Holocene meander belts and delta lobes might be related. Five Holocene meander belts and five delta lobes have been recognized in the lower Mississippi Valley (Autin *et al*., 1991) (Figure 9.8). Although attempts have been made to correlate activation ages of these lower valley landforms with alluvial chronologies and floods in upper valley drainages (Knox, 1996), such correlations have been viewed as questionable because of the combination of poor age control for the lower valley landforms, coupled with the integrated inputs from so many diverse upstream sources, and unknown system thresholds and feedbacks. Surficial mapping coupled with floodplain borings and radiocarbon dating of overbank alluvium near the Old River control structure in Louisiana and elsewhere in the lower Mississippi Delta indicated avulsions have been common and that individual avulsions can produce geomorphologic feedbacks that last from hundreds to as long as a few thousand years (Törnqvist *et al*., 1996; Aslan *et al*., 1998). Coleman (1988) reported that Mississippi River delta lobes have switched locations of deposition on an average of about once every 1500 years. Coleman indicated that each lobe covers an area of about 30 000 km^2 and that the lobes have an average thickness of about 35 m.

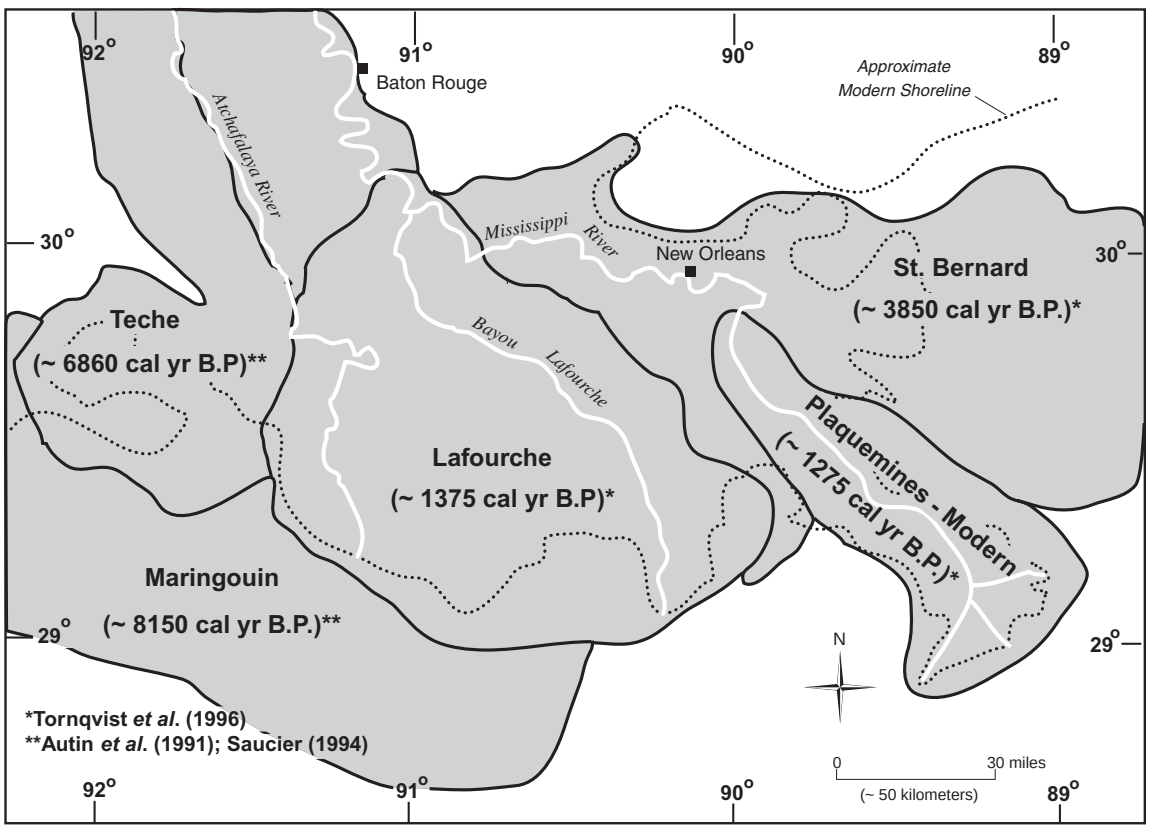

Figure 9.8 Entry of the Mississippi River into the Gulf of Mexico has involved five different major sedimentary deltas during the Holocene

The potential of large floods to trigger an avulsion leads to questions regarding whether responses of lower valley floods and sediment loads to upstream climate changes could influence lower valley avulsions. The strong influence of Great Plains and upper Mississippi valley drainage systems to influence loads of water and sediment to the lower Mississippi River valley, and the demonstrated sensitivity of these upstream areas to even relatively modest changes of climate during the Holocene, suggest that possible relations are worthy of further investigation. Hydrologic and sedimentologic data collected during four cruises at high water on the Mississippi River indicated that about 84% of the mean annual discharge and 88% of the mean annual sediment load delivered to the lower Mississippi River is provided by the Missouri, upper Mississippi, and Ohio tributary systems (Moody and Meade, 1993). These percentages, which ignore minor inputs from the Ouachita and Red River basins that represent about 5% of the Mississippi River system area, illustrate the importance of water and sediment loads from the upper valley to strongly influence fluvial activity in the lower valley. Possible relations between shifts in alluvial delta positions in the lower Mississippi Valley and climate change are more than mere academic interest. The Mississippi River might abandon the Plaquemines-Modern delta in favor of a shorter, more direct route to the Gulf via the Atchafalaya River if natural causes were left to their own (Figures 9.4 and 9.8). The expected capture area is in the vicinity of the Old River Control Structure shown on Figure 9.4, but capture is also probable if levees were to fail in other nearby areas.

The likely capture of the lower Mississippi River by the Atchafalaya River during a large flood or series of large floods, if natural causes were left in control, was recognized at least as early as 1804 (McPhee, 1989, p. 40). The modern Red and Ouachita Rivers flow into the Atchafalaya River adjacent to the Mississippi River in east central Louisiana (Figure 9.1). The Red River, before human intervention, flowed directly into the Mississippi at a former large meander now known as Old River. An early nineteenth century log jam removal on the lower Red River, coupled soon after with the artificial Old River meander cut-off for navigation improvements, ultimately resulted in diversion of the Red and Ouachita River flows into the Atchafalaya River and thereby increased the likelihood that the Atchafalaya River would capture the lower Mississippi River. After the diversion, a flow connection between the Red-Atchafalya River and the Mississippi River was maintained through the Old River meander for navigation interests. Because the Atchafalya was somewhat lower and possessed a steeper more direct route to the Gulf of Mexico, the Atchafalaya progressively captured more and more of the flow from the Mississippi River through the Old River and would have eventually captured most of the flow if natural forces were allowed to continue. A concise history of the issues and background associated with possible capture and attempts to control the course and flow of the lower Mississippi River has been presented by McPhee (1989). The information presented here extracts a few of the key events and actions identified by McPhee. He noted that by the mid-twentieth century, about 30% of the Mississippi River flow was passing into the Atchafalaya River via the Old River cut-off river meander. It was believed that full capture would occur by AD 1975 if intervention were not undertaken, and this belief resulted in the United States Congress ordering the US Corps of Engineers to prevent such a capture while at the same time maintaining AD 1950 proportions of Mississippi River flow diversions into the Atachafalaya River via the Old River. The 'Old River Control Structure' was completed in 1954 in response to the charge by the US Congress, but this structure came close to failing during a large flood in 1973 (McPhee, 1989). Although several other lower Mississippi River flow diversion projects have been implemented in recent years, including another auxiliary flow control near the 'Old River Control Structure', many scientists and engineers remain concerned that it is only a matter of time before a super-flood exceeds the integrity of these controls.

9.7 MORPHOLOGY OF THE MISSISSIPPI RIVER

9.7.1 Upper Mississippi River

The longitudinal profile of the Mississippi River does not possess a smooth concave-upward morphology that is typical of most large alluvial rivers (Figure 9.9). The upper Mississippi River from its headwater source in the Lake Itasca area in northern Minnesota to its junction with the Ohio River at Cairo, Illinois is notably convex and comprised of a series of distinct reaches that reflect the complex influence of Quaternary glaciations in the region. Most of this convexity results from a shortening of the middle section of the river caused by diversion from its former course across northwestern Illinois to the present Illinois River and thence southwestward to where the Illinois River joins the present Mississippi River. The convexities, as occur in the rock gorges between Fulton and Rock Island along northwestern Illinois, between Fort Madison and Keokuk along southeastern Iowa, and the Thebes Gap reach along southwestern Illinois, have resulted from Quaternary diversions and incisions of the Mississippi River across bedrock uplands. Consequently, the modern river flows on resistant bedrock in these reaches. Figure 9.9

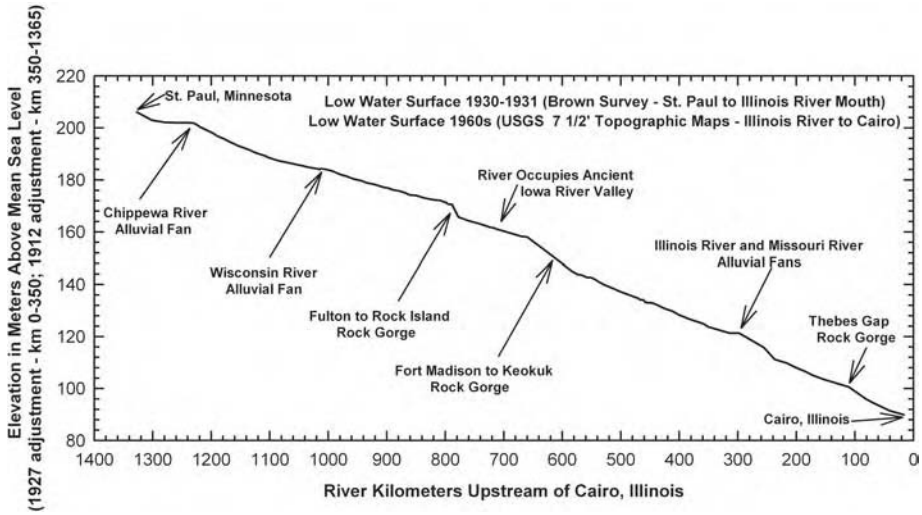

Figure 9.9 Longitudinal profile of the low water surface on the upper Mississippi River between St Paul, Minnesota and Cairo, Illinois. (Data sources: Brown, 1931; US Geological Survey 7.5 min topographic quadrangles)

shows that other local convexities in the longitudinal profile of the upper Mississippi River are the result of alluvial fans that have formed where tributaries have introduced an abundance of Holocene sediment. For example, large alluvial fans occur at the mouths of the Chippewa, Wisconsin, Illinois, and Missouri Rivers.

The upper Mississippi River can be divided into reaches of similar geomorphology with the number of reaches reflecting the scale of generalization that is needed. For example, 10 different geomorphic reaches were recognized for the upper Mississippi River from near the mouth of the Minnesota River to the mouth of the Ohio River in a recent study of the cumulative effects of 29 locks and dams (West Consultants Inc., 2000). The last of the locks and dams was constructed in 1940. For present purposes, the entire upper Mississippi River can be generalized into four general segments. The first is the river headwaters, downstream from its source in north-central Minnesota at Lake Itasca to approximately the mouth of the Minnesota River. Through much of this course, the Mississippi River meanders through a late Wisconsin age (isotope stage 2), low relief morainic topography with numerous lakes and marshes. Here the river is characterized by a relatively low gradient and with intense meandering. Farther downstream in the lower half of this headwater segment, where sandy proglacial outwash sediment becomes more common along with other glacial deposits, the river takes on a straighter and steeper morphology. Segment one of the upper Mississippi River has experienced the least amount of historical modification compared with the other three, mainly because the hydraulic dimensions are not sufficient to allow passage of large boats and because much of this reach is located in an area where, traditionally, there has been less need for shipping agricultural and manufacturing products. Nevertheless, the first system of reservoirs built in the US by the Corps of Engineers involved the construction between 1883 and 1912 of six dams in the headwaters of this segment (Anfinson, 2003, p. 90).

An island-braided system represents most of the pre-regulated second segment that extends from the Minnesota River mouth downstream to the head of the former Rock Island rapids in the Fulton to Rock Island rock gorge of northwestern Illinois (Figure 9.9). Very large quantities of sandy bedload introduced from tributaries along this reach account for the numerous islands and a former wide shallow morphology that existed prior to artificial constriction. The 1866 Rivers and Harbors Act passed by the US Congress directed the US Corps of Engineers to survey the upper Mississippi River between St Anthony Falls, Minnesota, a short distance upstream of the mouth of the Minnesota River, and the Rock Island Rapids. This event marked the beginning of widespread efforts by the Corps of Engineers to modify the river for navigation improvement upstream of the Rock Island Rapids (Anfinson, 2003). The first dredging and snag removals to improve the navigability of the river for steamboats began in 1868, and a Corps of Engineers officer in charge of improvements in the early 1870s reported that it was almost impossible to keep the river

open due to so many sandbars in the channel between the Rock Island Rapids and the mouth of the Chippewa River in northwestern Wisconsin (Anfinson, 2003, p. 44). The narrative journal of Henry R. Schoolcraft also attests to the numerous sand bars in the river below the mouth of the Chippewa River. He noted on 4 August 1820 that below the Chippewa mouth, '. . . the Mississippi has an increased width, and contains a great number of small willow and cottonwood islands, and the navigation is rendered more difficult, on account of the innumerable sand bars . . .' (Williams, 1992, p. 216). The principal means used for increasing depth of flow to improve navigation between the 1860s and the early 1930s involved supplementing dredging of sand bars with constructing rock and brush dams (wing dams) along the channel margins and constructing closing dams to prevent flow into side channels and backwater sloughs. The wing dams, which rose above the normal low water surface, induced sedimentation that eventually became colonized by vegetation when the level of sedimentation exceeded the low water stage. While the constriction of flow by these mechanisms initially facilitated the development of a navigation channel that was at least 1.4 m in depth and, later, development of a 1.8 m minimum depth navigation channel, the occurrences of low water during drought years and the constant need for dredging of sand bars led to demands for a deeper channel. Anfinson (2003, p. 146) reported that during the 28 years that the 1.4 m channel was maintained, the Corps of Engineers and their contractors built about 1900 wing and closing dams representing a length of 540 km if laid end to end. He noted that new and higher wing and closing dams were added during the following era of the 1.8 m minimum depth channel. In addition the Corps armoured an extensive amount of shoreline with willow mats and rock to minimize bank erosion in local reaches. Nevertheless, by the 1920s it was understood that the 1.8 m minimum depth channel would be inadequate to facilitate reliable and cost-effective shipping on the upper Mississippi River and a proposal was made to develop a new navigation channel with a 2.75 m minimum depth (Anfinson, 2003, pp. 219–222). This controversial proposal provoked much debate between the Corps of Engineers, environmentalists, the business community including farmers, the railroad industry, politicians, and others. The 2.75 m channel project finally was passed by the US Congress in June 1930 and signed and authorized by President Hoover on July 3, 1930. However, further hearings and limitations of funds delayed construction activity. About one-third of the construction had been completed by 1935 and the opening of the last lock and dam did not occur until March 12, 1940 (Anfinson, 2003, p. 274). The final system included 29 new and pre-existing locks and dams between St Louis, Missouri and St Paul, Minnesota. These structures converted the island braided segment two and the meandering and straight reaches of segment three of the upper Mississippi River, between the mouth of the Missouri River and the mouth of the Minnesota River, into a series of stepped pools. The cumulative effects of the 2.75 m channel project were studied in the late 1990s (West Consultants Inc., 2000). Results from this investigation indicated that, compared with pre-locks and dams conditions, the width of the main channel is narrower in the upstream part of almost every pool because of placement of dredged materials and natural sedimentation along the channel margins. On the other hand, main channel width was found to be considerably wider in the lower portion of most pools due to water impoundment upstream of the dams. Analyses of long-term suspended sediment records indicated that suspended sediment loads on the upper Mississippi River have been experiencing a decreasing trend since the mid-1940s and this, in addition to the scouring effects of several recent large floods, may be the explanation why river cross-section data representing the period since the mid-1950s indicate modest net channel degradation along most of the pools from south of the Wisconsin River to just upstream of the alluvial fan effect of the Illinois and Missouri Rivers (West Consultants Inc., 2000).

The third and rather complex segment of the upper Mississippi River extends from the head of the Rock Island Rapids to the mouth of the Missouri River at St Louis, Missouri (Figure 9.9). The complexity of this reach, which involves both straight and meandering subreaches, results from the late Quaternary diversion and incision of the river across two major bedrock uplands, from its intersection with and location within ancient valleys downstream of the rock gorges, and from large suspended sediment load inputs from tributaries that drain landscapes covered by thick, easily eroded, loess deposits. The large suspended sediment load contributes significantly to numerous islands as deposition of sediment during high stage flows is enhanced by vegetation on islands and bars. Sediment yields from tributaries tend to increase in a southward direction across the upper Mississippi River drainage basin because the area south of the late Wisconsin glacial boundary is characterized by relatively steep hillslopes and thick and relatively easily eroded loess deposits in comparison with that part of the upper Mississippi River drainage basin that lies north of the late Wisconsin glacial boundary (Figure 9.2). Tributaries such as the Iowa River, Des Moines River, and Illinois River have experienced especially high suspended sediment loads under intensive row crop agriculture since the

middle and late nineteenth century. Modern sediment yields under agricultural land use for segment three Mississippi River tributaries range between 200 and 500 times greater than yields from segment one tributary drainage basins in the extreme northern part of the upper Mississippi River drainage basin where forest cover is abundant (UMRB Committee, 1970; Nielsen *et al*., 1984). The relatively steep gradient of the river downstream from the Keokuk Rock Gorge to the mouth of the Missouri River reflects in large part the relatively coarse and large bedload introduced by the Des Moines River (Figures 9.2 and 9.9) (West Consultants Inc., 2000). The bed load for most reaches of upper Mississippi River segments two and three is predominantly sand, but fine gravel is sometimes sampled below the Des Moines River confluence to the Missouri confluence (West Consultants Inc., 2000). The rapids in the two rock gorges were frequent impediments to steamboat navigation in the pre-regulated river. The Corps of Engineers began blasting rock from the lower rapids in 1838 and over the following year opened a channel about 15 m wide, 1.2 m deep, and 6.5 km long through the most obstructive section, and they began a similar effort on the Rock Island Rapids in 1856 (Anfinson, 2003, pp. 25–26). Navigation problems associated with the lower rapids in the Keokuk Rock Gorge were resolved when the rapids were submerged in 1913 after closure of a dam at Keokuk, Iowa, a short distance upstream of the Des Moines River mouth. The rapids between Fulton and Rock Island, Illinois also were ultimately submerged following completion of a dam at Rock Island as part of the 2.75 m channel project. The large islands that characterize the river downstream of the rock gorges result from the large suspended sediment load of silt whose deposition is promoted by terrestrial vegetation on floodplain and island surfaces during overbank flows. Island occurrences are also favoured by the widening of the valley and floodplain downstream of the gorges where flow expansion and partial deposition of the relatively large sediment load are common.

The fourth segment of the upper Mississippi River extends downstream from the mouth of the Missouri River to the Ohio River mouth at the southern tip of Illinois. This reach is today commonly referenced as the 'open river' section because there are no locks and dams associated with its course. Meander scars on the floodplain and low terraces show that previous Holocene morphologies of the open-river segment once involved a greater meandering behaviour than is currently present. However, West Consultants Inc. (2000, p. 189) cited a study by others who concluded that the position of the river has changed little in the last 200 years. The introduction of wing and closing dams, as noted for segments two and three, further ensured the relative geographic stability for the open river segment. However, the open river segment, especially in its upper reaches, has experienced major downcutting of the channel bed and erosion of sediment that previously had been deposited adjacent to wing dams. This erosion is directly related to reduction in the overall sediment load since closure of five large dams on the Missouri River in the 1950s and 1960s and to the closure in the same general period of other large dams in the Kansas River tributary to the Missouri River (Keown *et al*., 1986; Meade *et al*., 1990). The steep upper portion of segment four results from its beginning on the alluvial fans formed at the mouths of the Missouri and Illinois Rivers (Figure 9.9). The Thebes Gap Rock Gorge, about 120 km upstream from the Ohio River mouth, also resulted from a flow diversion and river incision through a low pass in a bedrock ridge. Because of the greater volume of water at this downstream river segment, rapids and navigation restrictions were never the type of problem experienced upstream in segment three of the upper Mississippi River.

9.7.2 Lower Mississippi River

The overall longitudinal profile of the lower Mississippi River floodplain from its head at the Ohio River mouth downstream to about 40 km north of Vicksburg, Mississippi shows relatively little convexity or concavity, except at the local reach scale (Schumm *et al*., 1994) (Figure 9.4). The generally straight and relatively steep profile apparently reflects the need for a relatively steep energy gradient to transport the large volume of sandy bed load. Farther downstream, modest concavity is present as the river grades to sea level in the Gulf of Mexico. In spite of the downvalley relatively straight profile of the floodplain, considerable reach to reach variability existed prior to meander cutoffs that were human made for navigation purposes (Schumm *et al*., 1994). Schumm *et al*. (1994) divided the pre-regulated lower Mississippi River between the mouth of the Ohio and the 'Old River Control Structure' (Figure 9.4) into 24 geomorphic reaches. Local influences, including outcrops of Tertiary age bedrock, Pleistocene gravel, clay plugs contained in old meander cutoffs, and at least two zones of major surface deformation by tectonic uplift, contributed to abrupt differences in river width and sinuosity between local reaches whose upstream and downstream boundaries were commonly associated with marked changes of floodplain slope (Schumm *et al*., 1994). Tectonic activity, associated with modest regional uplift and faulting, has influenced sinuosity and meander orientations in the area near and downstream of New Madrid, Missouri and particularly in the

general area between Greenville and Vicksburg, Mississippi (Figure 9.4). Schumm *et al*. (1994) observed from an 1821 river survey that the pre-regulated lower Mississippi River between the mouths of the Ohio River and Red River did not conform to general hydraulic geometry relations because the bankfull channel width showed a progressive downstream decrease and other downstream hydraulic geometry variables were subject to strong local reach controls. Comparison of the 1821 river morphology with river morphology documented in later surveys of 1880 and 1915 showed that the relative stability of river morphology for the lower Mississippi River was very strongly associated with modest changes in valley slope. Steeper floodplains and steeper valley gradients were associated with greater bank erosion facilitated by adjustments in sinuosity. On average, straight reaches were associated with low valley slopes and tended to accommodate changes through adjustments in channel width. The comparison by Schumm *et al*. (1994) of river morphology between the three early surveys showed that the lower Mississippi River between the mouths of the Arkansas and Red Rivers experienced more changes in sinuosity and river cross-section morphology than the upstream segment between the mouths of the Arkansas and Ohio Rivers. They attributed this difference as probably due to the large inputs of medium texture sand and increased discharge from the Arkansas River. The surveys in 1880 and 1915 showed that bankfull width had approximately doubled since the 1821 survey, and Schumm *et al*. attributed this change to human activities in the Ohio River and upper Mississippi River drainage basins and to clearing of bank vegetation along the lower Mississippi River. A recent investigation of differences in channel slope and stream power between pre-cutoff (1880s–1930s) and post-cutoff (1943–1992) conditions indicated that post-cutoff channel steepening probably has significantly increased local channel bed erosion and transport of bedload sediment (Biedenharn *et al*., 2000). The authors of this study suggested that the relative stability of the lower Mississippi River could be characterized as ranging from '. . . dynamic equilibrium in the farthest upstream reaches through severe degradation to dynamic equilibrium in the middle reaches, and aggradation in the lowest reaches.' They suggest that changes in stream power that evolved from changes in stream slope have promoted adjustments in incoming bed material load to each reach and these changes explain the recent evolutionary morphologic trends for the lower Mississippi River (Biedenharn *et al*., 2000).

Significant human impacts on the lower Mississippi River began in the early eighteenth century when levees were built at New Orleans for flood protection. New Orleans was proclaimed safe from flooding in 1727 following levee construction, but this claim proved to be false as waters overflowed the area during large floods in 1735 and 1785 (McPhee, 1989). Levees along the lower Mississippi were initially about 1 m high, but today exceed 10 m (Winkley, 1994). Levee development expanded rapidly because of the desire to protect plantation riverfront properties and because, later, it was viewed as the principal way to protect valuable agricultural lands while at the same time concentrating the flow to maintain a self-scouring and an effective navigation channel. McPhee (1989) stated that nearly continuous levees lined the lower Mississippi River in southern Louisiana by 1828. He noted that by the mid-1850s levees along many sections of the lower Mississippi River averaged about 2 m height and that the confinement of flows was resulting in ever higher and higher flood stages along the river. Increasing flood related problems along the lower Mississippi River eventually resulted in the US Congress creating the Mississippi River Commission in 1879. For the next nearly half century the Commission promoted the use of levees as the principal means to prevent destructive floods in the lower valley, and this policy ultimately led to construction of 2400 km of levees along the lower Mississippi River (McPhee, 1989). The great lower Mississippi River flood of 1927 involved disastrous levee breaks in many places along the lower valley from Cairo, Illinois to southern Louisiana. Although the 1927 flood is commonly perceived as the record flood on the lower Mississippi River, McPhee (1989) indicated that the volume of the 1927 high water was not the extreme as perceived, but rather the 1927 flood disaster was the result of a breakout of a large amount of water that had been confined between levees. Nevertheless, this flood led to re-examination of the 'levees only' policy for flood protection along the lower Mississippi River and to the development of a new and current management system that includes construction of dams and reservoirs in tributaries and spillway structures that can divert water out of the main channel into storage basins and alternate pathways of drainage (McPhee, 1989). These diversions include Bonnet Carre spillway on the east bank about 50 km upstream of New Orleans and the Old River control and Auxiliary control structures which divert flow into the Atchafalaya River (Figure 9.4).

The construction of levees constrained much of the flooding within the channel and minimized inundation of the wide floodplain of the lower valley. Winkley estimated that modern levees now contain about 50% or more of the higher flows on a much narrower floodplain. A 1932 Corps of Engineers study, summarized by Winkley (1994), estimated that about 2 mm of floodplain sedimentation

occurred with each flood. However, between 1937 and 1989, sedimentation within the floodplain between levees, as indicated by average banktop elevations, occurred at a rate of about 2.4 cm year^{-1} (Winkley, 1994). Decreasing suspended sediment loads, in concert with the elimination of overbank flows related to construction of artificial levees, have been identified as major contributors to wetland losses in coastal Louisiana (Kesel, 1988, 1989). Kesel found that relatively little sediment enters the lower Mississippi River from its adjacent floodplain because artificial revetment structures have minimized bank caving and promoted sediment storage in channel bars (Kesel, 2003). He argues that these changes have contributed significantly to the recent degradation of the channel bed in the lower Mississippi River in Louisiana. Winkley (1994) reported that in 1885 the Corps of Engineers began protecting river banks to prevent meander cutoffs on the lower Mississippi River and dredging of crossings between meander bends to improve navigation. He noted that natural cutoffs documented in early river surveys showed that the lower Mississippi River had continually varied its length by as much as 77 km during the period 1765 to 1930, but a decision to artificially develop cutoffs in 1929 resulted in 16 cutoffs which reduced the river length by 243 km by 1943. The relative shortening was distributed unevenly whereby the decrease in length was about 12% for the entire lower Mississippi River, but shortening of 40% occurred between the mouths of the Arkansas and Yazoo tributaries (Winkley, 1994). The increased slope induced by shortening further aggravated the unstable character of this reach. Additional shortening of the lower Mississippi River by another 88 km was induced by dredging chute channels across bars, but because the river continually attempted to re-establish its natural pre-cutoff length, the net shortening between 1930 and 1975 was only 235 km (Winkley, 1994). While levee construction, meander cutoffs, and bank revetment projects since 1930 were promoted to stabilize the lower Mississippi River for improvement of navigation, Winkley reported that many unstable and maintenance-prone reaches could not be satisfactorily improved with the availability of funds and materials in spite of enormous investment. Winkley reported that the various stabilization projects have ironically led to a general increase in top bank widths and channel bed erosion for most of the lower Mississippi River upstream of the Old River control structure near the mouth of the Red River (Figure 9.4). Winkley attributed the inability of the Mississippi River to convey its full sediment load, resulting in net bed aggradation downstream of the Old River control structure, as due to diversion of about 25% of all Mississippi River flows into the Atchafalaya since 1962.

9.8 MODERN HYDROLOGY

9.8.1 Climate, Runoff, and Floods

The present-day Mississippi River drainage basin, representing more than 3.2 million km^2, is dominated in the eastern one-half by relatively humid climates in the upper Mississippi, Ohio, and main valley lower Mississippi subdrainage basins, while the western one-half is dominated by relatively semiarid climates in the Missouri, Arkansas, and Red River subdrainage basins. Large differences between winter and summer temperatures are characteristic of this continental drainage basin. A relatively steep latitudinal gradient is characteristic of January (winter) daily average temperatures which range from about +10 °C near the mouth of the basin in Louisiana to −10 °C across the northern portion of the drainage basin extending from Montana to Wisconsin (Figure 9.10a). For the same transect, a much flatter latitudinal gradient is characteristic of July (summer) daily average temperatures when the range varies from about +28 °C in the Lower Mississippi valley to about +20 °C near the headwaters of the upper Mississippi River in northern Minnesota (Figure 9.10b). Annual precipitation for most of the Mississippi River drainage basin decreases both northward and especially from east to west (Figure 9.10c). The depth of average annual precipitation exceeds 140 cm near the mouth of the basin in Louisiana and exceeds 100 cm over most of the Ohio River drainage basin, but drops to less than 60 cm over most of the Missouri River and western Arkansas River basins on the Great Plains. The combination of very warm summers, with a sharp east to west reduction in precipitation across the Red, Arkansas, and Missouri River tributaries, results in a dramatic east to west reduction in average annual runoff across the western one-half of the Mississippi River drainage basin (Figure 9.10d). The gradient is abruptly reversed at the Rocky Mountains front in a narrow fringe along the western margin of the Mississippi River drainage basin. The depth of average annual runoff ranges between 30 and 60 cm over most of the Ohio River drainage basin and exceeds 60 cm in the southern Appalachian Mountains tributaries of the Tennessee River along the southeastern margin of the Ohio River drainage basin. Most of the upper Mississippi River system is associated with depths of average annual runoff between 10 and 30 cm with the lesser amounts occurring in a westward direction. Depths of average annual runoff decrease westward for all latitudes from about 10 cm along the eastern sector of the Great Plains to only 1 cm at the longitude of central South Dakota and west-central Nebraska. Runoff remains low across the western Great Plains, but then increases abruptly in the

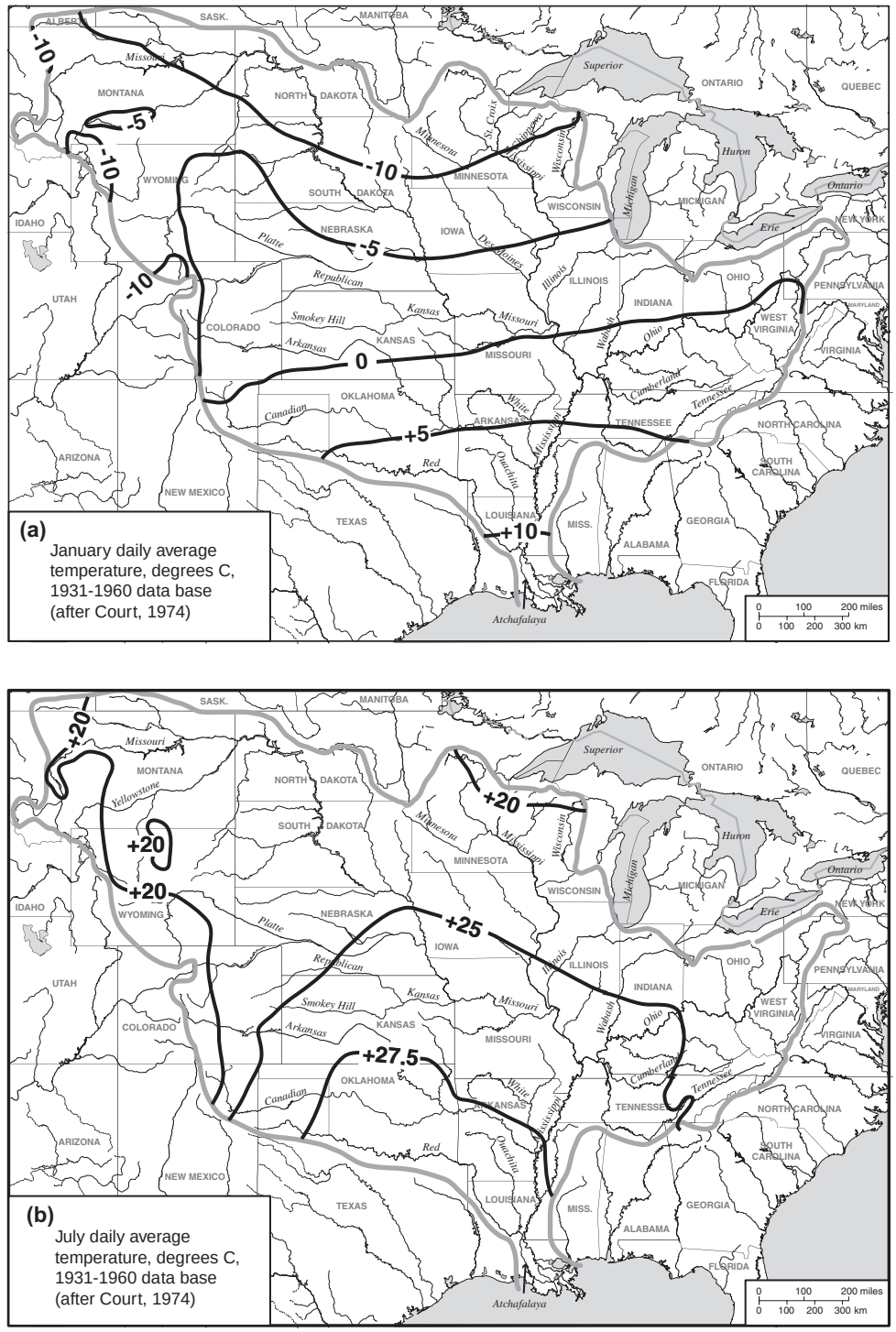

Figure 9.10 (a, b) Temperature, (c) precipitation, and (d) runoff in the Mississippi River drainage basin. (Data sources: Court, 1974; Riggs and Harvey, 1990)

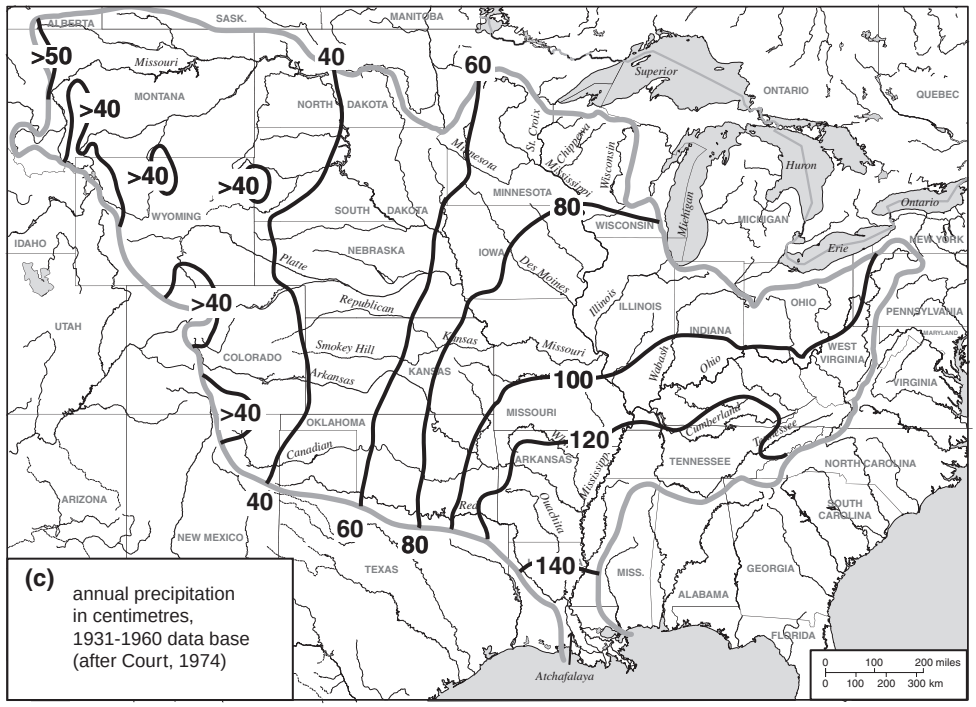

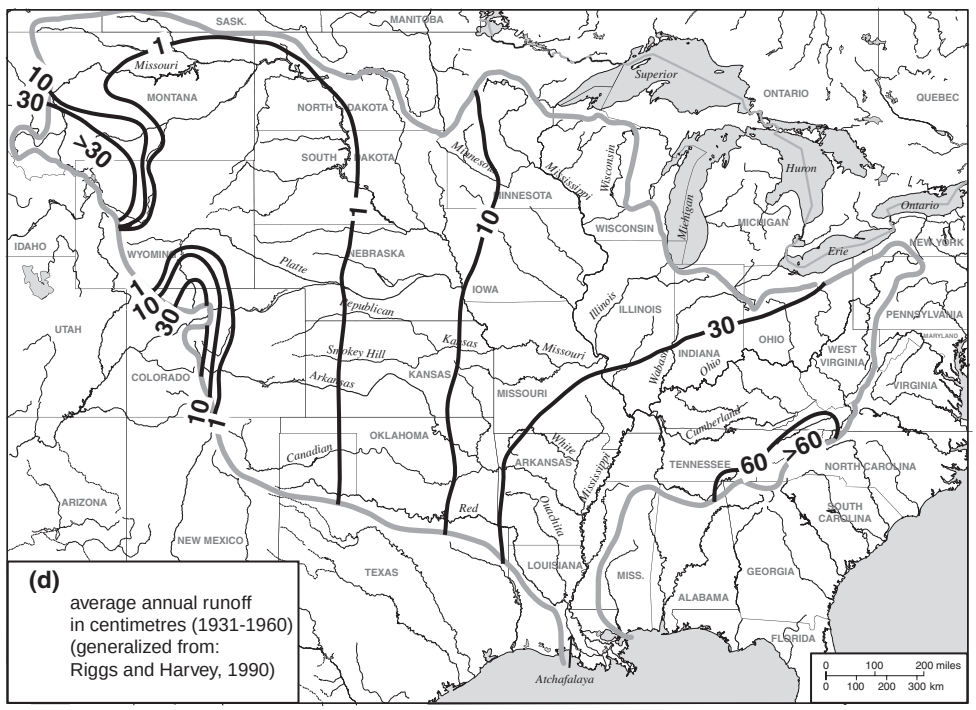

Figure 9.10 *Continued*

highlands of the Rocky Mountains on the western margin of the Mississippi River Basin.

The disproportionate contribution of average annual runoff from the humid sector of the Mississippi River system also is evident from magnitudes of historical annual peaks of flood runoff. Figure 9.11, for example, shows that since the early nineteenth century the largest flood magnitude on the Missouri River at Hermann,

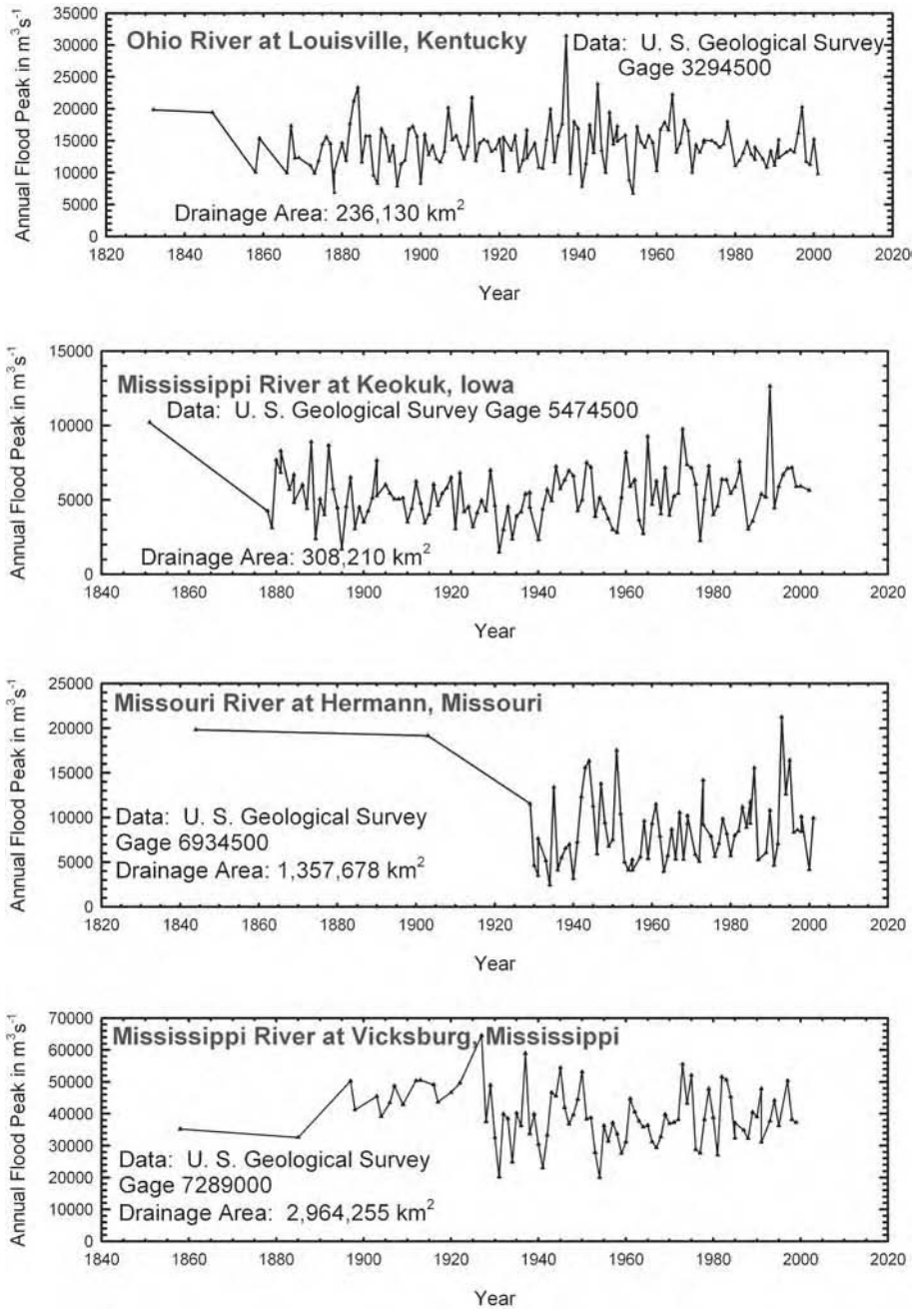

Figure 9.11 Annual maximum flood series at selected sites in the Mississippi River drainage basin

Missouri, with an upstream drainage area of about 1.36 million km^2, was about 22 000 m^3 s^{-1}, but the Ohio River at Louisville, Kentucky with a drainage area of only 0.24 million km^2 has experienced a flood greater than 30 000 m^3 s^{-1} as well as many large floods whose magnitudes are comparable with the largest floods for the much larger Missouri River drainage basin at Hermann. Time series of average daily discharge for four sites on the main channel upper and lower Mississippi further illustrate the dominant role of the Ohio River to control discharge along the lower Mississippi River (Figure 9.12). Note that the patterns of variability and ranges of daily discharge for the Memphis gauge near the head of the lower valley and upstream of the Arkansas tributary, whose drainage area is nearly equivalent to that of the Ohio River, differ only modestly from average daily discharges for the Vicksburg gauge located at the head of the lower one-third of the lower valley and downstream of the Arkansas tributary (Figure 9.4). Furthermore, the Ohio River gauge at Louisville is located upstream of the Tennessee and Cumberland River drainages which also contribute major additional inputs from the Ohio River system to flows on the lower Mississippi River (Figure 9.1). The upper Mississippi River at Keokuk, Iowa, where the contributing drainage area is about 0.31 million km^2 and significantly larger than the 0.24 million km^2 drainage area upstream of Louisville on the Ohio River, has historically experienced smaller floods than the Ohio River at Louisville. The Great Flood of 1993 on the upper Mississippi River at Keokuk, Iowa experienced a discharge of 12 000–13 000 m^3 s^{-1} for which application of standard statistical methodology indicated this flood approximated a magnitude expected once in 500 years (Pitlick, 1997; Knox, 2000). However, flood magnitudes of 12 000–13 000 m^3 s^{-1} have been exceeded numerous times on the Ohio River at Louisville for the same period of record (Figure 9.11).

9.8.2 Dams: Flow Modification and Sediment Storage

The twentieth century witnessed the construction of many large dams and reservoirs throughout the Mississippi River basin. The dams on the upper Mississippi River described above had little impact on reducing magnitudes of large floods and only modest influence on sediment storage there because nearly all of these dams were designed such that gates are raised to a fully open position during large floods. However, elsewhere dams have generally reduced the variability in flows, including reductions in magnitudes of flood peaks. Furthermore most of the dams have greatly reduced the amount of sediment moving downstream in the river system. A series of dams constructed under the auspices of the Tennessee Valley Authority began in the 1930s to provide downstream flood protection, generate hydroelectric power, and provide economic assistance to a region especially affected by the Great Economic Depression of the 1930s, greatly altered the flow hydrology of the Tennessee River system (Miller *et al*., 1996). Figure 9.13 shows that the natural range for magnitudes of annual maximum floods since records began in 1867 and until the mid-1930s on the Tennessee River at Chattanooga, Tennessee commonly approached 8000 m^3 s^{-1}, while four floods were much larger than this magnitude. However, since construction of upstream Tennessee Valley Authority dams, most magnitudes for annual maximum floods are less than 6000 m^3 s^{-1} and only one flood has approached 8000 m^3 s^{-1} (Figure 9.13). Prior to construction of major dams, only three floods smaller than about 3000 m^3 s^{-1} occurred under natural conditions between 1867 and the mid-1930s, but since then annual maximum floods have dropped below 3000 m^3 s^{-1} 12 times (Figure 9.13). The temporary storage of runoff behind dams typically results in trapping and storing much of a river's normal sediment load in the reservoirs upstream of dams (Meade *et al*., 1990). A 6-year US Geological Survey record of suspended sediment load on the Tennessee River at Chattanooga showed that the annual suspended sediment discharge was 10.5 million tonnes in 1938, but following upstream dam closures, approximate magnitudes of annual suspended sediment loads in millions of tonnes, dropped over 5 years of monitoring to 6.2 in 1937, 5.2 in 1938, 4.2 in 1939, 1.3 in 1940, and 0.8 in 1941.

The twentieth century was associated with construction of many dams on rivers of the sub-humid to semi-arid western tributaries of the Mississippi River. In almost all cases these dam closures were followed by major downstream reductions in natural flow variability that also led to significant changes in channel morphology. An example of well-documented morphologic change by this process is the Platte River system, which once was the classic example of a wide, shallow, braided river (Schumm, 1977; Williams, 1978; Collier *et al*., 1996). The modern Platte River is much narrower than it was before human disturbance because of the reduction in magnitudes of floods and reduction in sediment load. Downstream effects of dams on the upper Missouri River were briefly noted in the context of post-dam downstream erosion in the open river segment of the upper Mississippi River, but the dramatic impacts of these dams warrant additional commentary. The Missouri River dams were constructed to provide water for irrigation, for hydroelectric power generation, and for augmenting downstream flows during the warm season to improve river navigation. Meade *et al*. (1990) commented that construction of these five large dams on

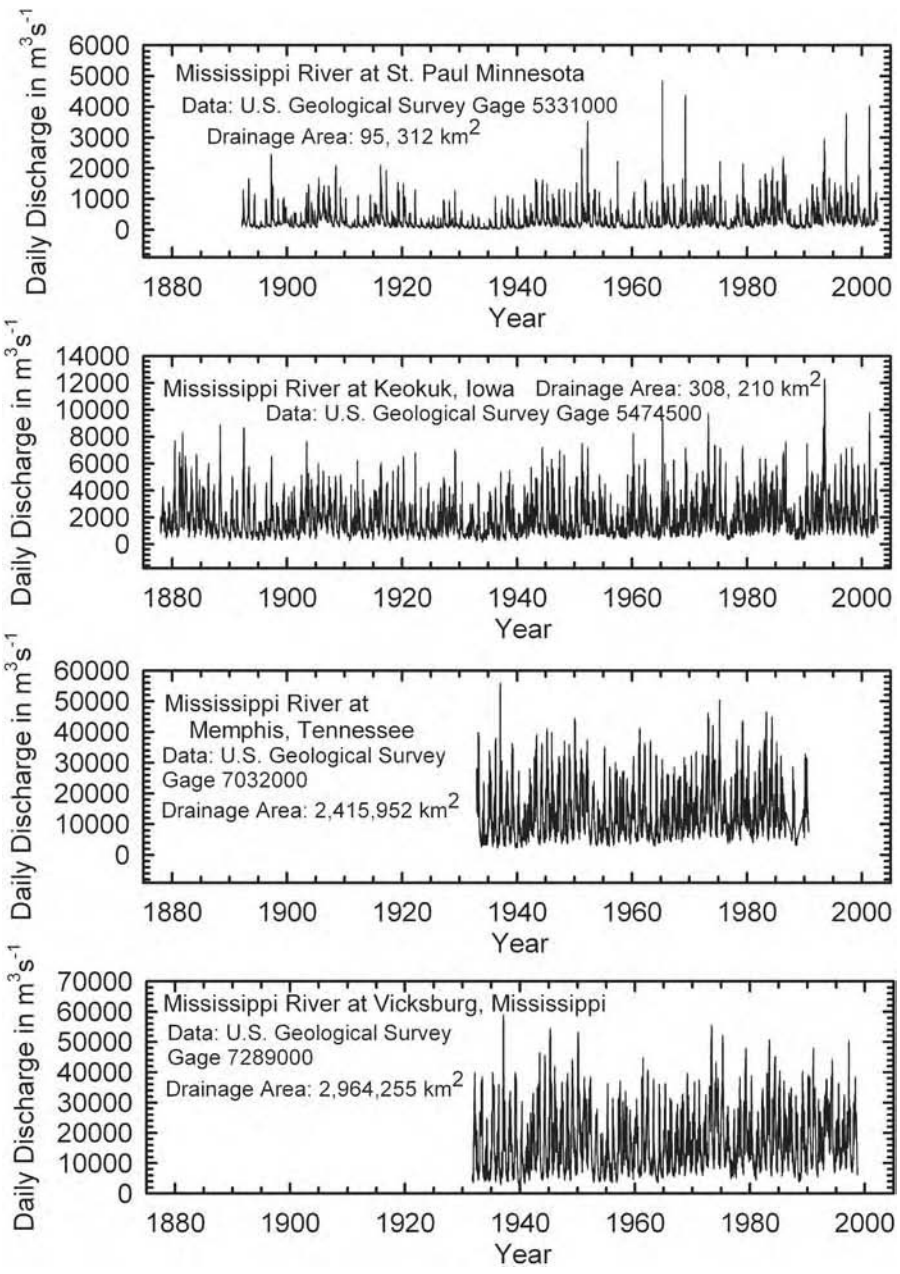

Figure 9.12 Time series of average daily discharge for sites along the Mississippi River. Note the large increase in discharge at the Memphis gauge which reflects the contribution of the Ohio River that enters the Mississippi River a short distance upstream

the Missouri River in South Dakota and North Dakota between 1953 and 1963 virtually stopped the flow of sediment to the downstream Missouri River. The record of daily average discharges for the river gauge at Nebraska City, Nebraska located about 280 km downstream of the most downstream of the five large dams, and about 50 km downstream of the mouth of the Platte River, shows that the dams had a dramatic impact on flow variability

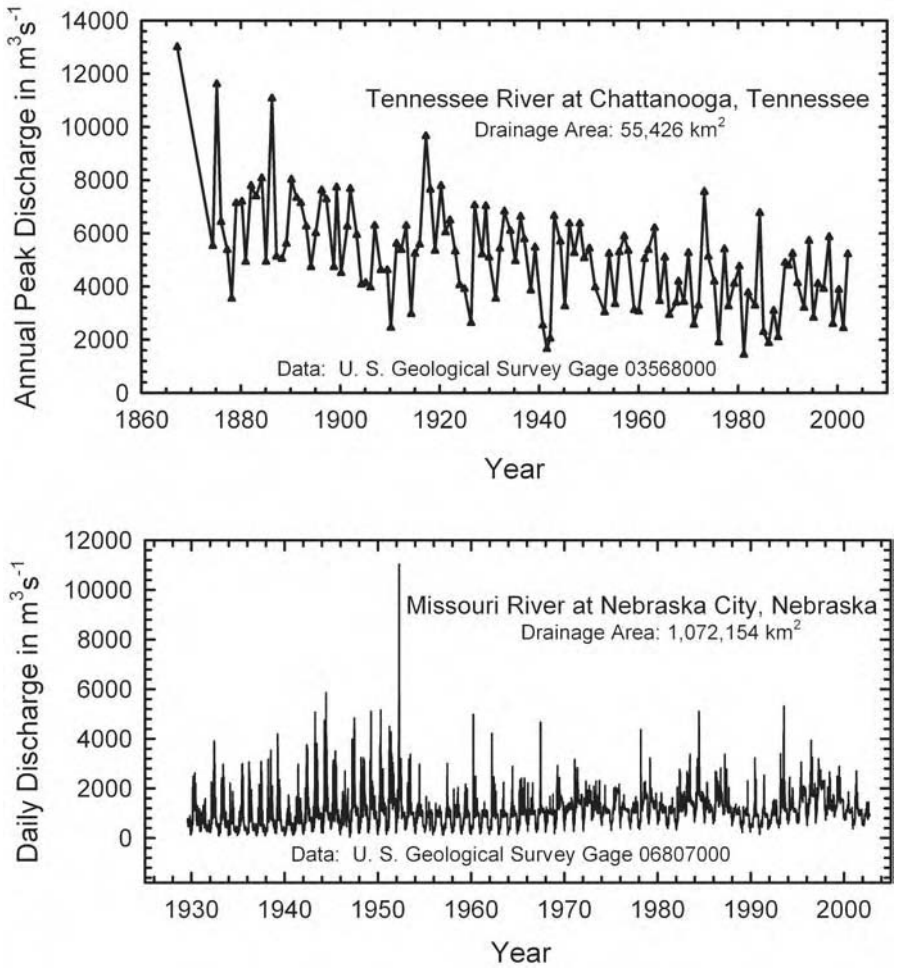

Figure 9.13 Dams reduce flood peaks and flow variability for downstream river discharges. Dams on the Tennessee River upstream of Chattanooga are part of the Tennessee Valley Authority's complex of dams which are carefully regulated to facilitate multiple uses including power generation. Consequently, because of relatively modest water use requirements and because the Tennessee River drains a region of abundant runoff (Figure 9.10), the reduction in flow variability is not as severe here as it is for the Missouri River at Nebraska City, Nebraska. The Missouri River drains a much drier environment where annual runoff is meager compared with the Tennessee River (Figure 9.10). The storage of upper Missouri River water behind five large dams for irrigation and power generation results in a major reduction in downstream flow variability that is further affected by a modest increase in low stage flows to assist navigation interests

(Figure 9.13). Here, the normal range of short-term flow variability was radically reduced after closures while the average low stage flows were increased for much of the year to facilitate navigation on the lower river. Because the downstream Missouri River had developed a pre-dam energy gradient and cross-section morphology that was adapted to transport very high volumes of both suspended and bedload sediments, flows since dam closures have been erosive causing significant instability and degradation of channel margins along the lower Missouri River. Reduced inputs of sediment to the lower Missouri were further exacerbated by construction of a series of similar large dams during the same general period in the Kansas River basin, a large downstream western tributary to the lower Missouri River (Figure 9.1). Keown *et al*. (1986) indicated that the downstream instability of the channel

due to loss of the normal sediment load from the upper Missouri and the Kansas River systems led to placement of numerous bank revetment structures and spur dikes to minimize impacts by erosive currents. Keown *et al*. (1986) estimated that the average annual suspended sediment load at Hermann, Missouri, on the lower Missouri River about 150 km upstream of the river's mouth, was about 289.2 million tonnes prior to beginning the construction of major dams in 1953, but decreased to about 78.4 million tonnes after 1967 when construction of the series of major dams in the upstream drainage basin had been completed.

Because the Missouri River has been the principal contributor of sediment to the lower Mississippi River during Holocene and modern times, the large reduction in sediment load caused by dams and by various channel stabilization structures is strongly reflected in the lower Mississippi River. Figure 9.14 shows that the annual suspended sediment loads in the Mississippi River immediately downstream of the Missouri River mouth dropped from 250–375 million tonnes prior to upstream dam closures to maximum loads of 150–180 million tonnes after closure. Farther downstream, near the 'Old River Control Structure,' the Mississippi River's suspended sediment load dropped from a maximum of about 500 million tons immediately prior to upstream dam closures to about 150–300 million tonnes after dam closures in the 1950s and 1960s (Figure 9.14). Present-day average sediment discharges to the Gulf of Mexico are estimated to be about one-half of average magnitudes that occurred prior to 1953 (Keown *et al*., 1986; Meade *et al*., 1990). Contemporary and historical inputs of water and sediment to the lower Mississippi River at the head of the Lower Mississippi Valley have been dominated respectively by the Ohio and Missouri River tributaries (Keown *et al*., 1986). A short instrumentation period in the late nineteenth century, prior to construction of dams and reservoirs, indicated the humid climate Ohio River drainage with about 15% of the total Mississippi River drainage basin area contributed about 60% of the average discharge and about 16% of the suspended sediment load to the Mississippi River at the confluence at the head of the lower Mississippi River (Keown *et al*., 1986). Similar late nineteenth century observations showed that the semi-arid Missouri River, draining about 45% of the total Mississippi River system, contributed about 84% of the suspended sediment delivered to the head of the lower Mississippi River (Keown *et al*., 1986). The Missouri percentage ignores relatively modest additional contributions from small basins of the upper Mississippi River basin between the mouth of the Missouri River and the Mississippi River confluence with the Ohio River. Mostly because of upstream dams, the present-day sediment discharges to the Gulf of Mexico by the Mississippi River are less than half of pre-1953 levels (Meade *et al*., 1990; Moody and Meade, 1993). Keown *et al*. (1986) estimated that the annual sediment yield of the Mississippi River basin is about 815–820 million tonnes, but the proportion of the yield passing into the Gulf of Mexico declined from about 395 million tonnes prior to 1963 to about 230 million tonnes today. Erosion of wetlands in the Mississippi Delta and Gulf Coast shoreline erosion have been directly correlated with these large reductions in sediment load from the Mississippi River (Kesel, 1988, 1989, 2003).

9.9 THE MISSISSIPPI RIVER SYSTEM: SUMMARY AND OUTLOOK

The Mississippi River drainage basin encompasses more than 3.2 million km^2 involving about 41% of the 48 contiguous United States and small areas of two Canadian provinces. A little more than 200 years ago the drainage basin had been little affected by human activities, except in localized areas of Native American settlements (Butzer, 1990; Denevan, 1992; Doolittle, 1992; Knox, 2002). The drainage basin in the mid-eighteenth century in the east and the mid-nineteenth century in the west was only beginning to experience modification of its natural mosaic of forest and grasslands by logging, agricultural, and other land settlement. Forests dominated most of the tributaries on the eastern side of the Mississippi River except in central and northern Illinois where prairie grasslands prevailed (Williams, 1989). Forest cover also dominated the southern sector of the drainage basin in southern Missouri, Arkansas and Louisiana as well as highlands along the headwaters in the Rocky Mountains and local highlands in the Northwestern Great Plains. Elsewhere, prairie grasslands dominated much of the landscape. The westward advancing wave of Euro-American settlement between about 1750 and 1850 greatly altered the natural land cover. By the end of the twentieth century, the approximate average land use for the entire Mississippi River drainage basin was 33% cropland, 24% grazing land, 32% forest and woodlands, 2% urban, and the remaining 9% scattered in various other small categories (US Water Resources Council, 1978). Table 9.1 shows that modern land uses vary significantly among the major tributaries with cropland ranging from a low of 17% in the Tennessee River drainage basin to a high of 57% in the upper Mississippi River drainage basin. Similarly, grazing land varies from a low of about 10% in the upper Mississippi River drainage basin to a high of 50% in the Missouri River drainage basin. As might be anticipated from regional climatic and physiographic differences, forest and woodlands range from a low of 9% in the

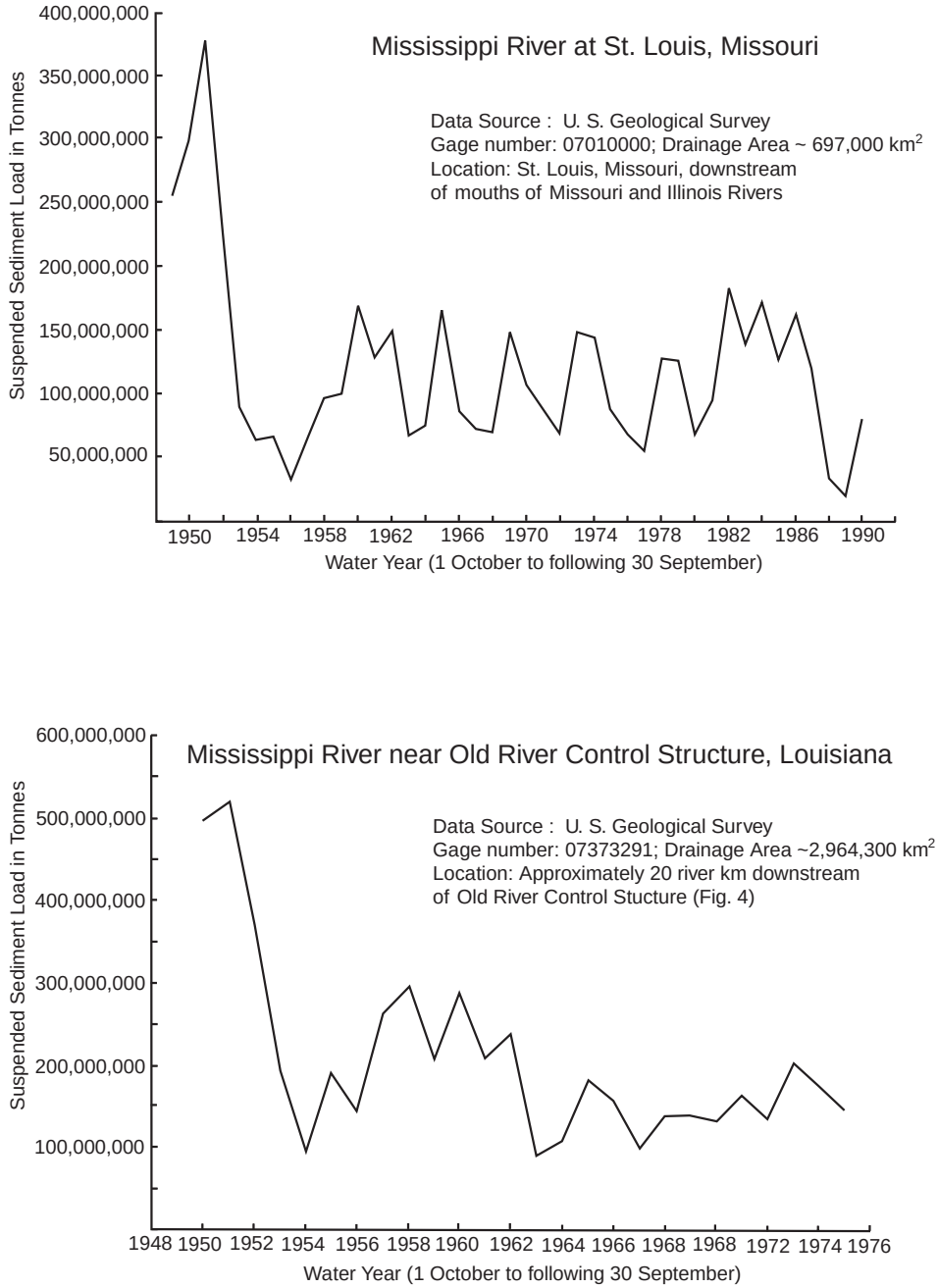

Figure 9.14 The dramatic reduction in suspended sediment load on the middle and lower Mississippi River after about 1953 reflects a series of dam closures in the Missouri River basin that began then and continued into the 1960s (Keown *et al*., 1986; Meade *et al*., 1990)

Table 9.1 Percentages of land uses in the Mississippi River drainage basin

Subdrainage basin name	Cropland (%)	Grazing land (%)	Forest and woodland (%)	Urban (%)	Other land uses (%)
Ohio River upstream of the Tennnessee River	32.4	13.8	42.5	3.3	8.0
Tennessee River	16.6	13.3	54.1	2.5	13.5
Upper Mississippi River	56.7	10.3	21.7	1.9	9.4
Lower Mississippi River	31.6	15.4	42.0	1.4	9.6
Missouri River	32.6	50.0	9.2	0.4	7.8
Arkansas-White-Red Rivers	28.8	43.1	21.7	1.1	5.3
Entire Mississippi River Basin	33.1	24.3	31.9	1.8	9.2

Data source: US Water Resources Council, 1978.

semi-arid low relief Great Plains Missouri River drainage basin to a high of 54% in the humid and hilly Tennessee River drainage basin.

The Mississippi River enters the twenty-first century as a system heavily modified by human activities. Historical soil erosion associated with accelerated runoff in areas of cropland have led to sub-basin average topsoil losses of 15–20 cm or more in areas with extensive agriculture cropland (Knox, 2002). Although agriculturally related wind erosion has been equally destructive of topsoil in the semi-arid western tributaries to the Mississippi River, this erosion has not directly impacted the Mississippi River water and sediment loads in the same way as accelerated runoff and accelerated sediment loads associated with running water (Knox, 2002). Inputs of agriculturally related, water transported sediment to the tributaries and main channel Mississippi River appear to have peaked in the late nineteenth and early twentieth centuries prior to extensive land conservation measures and prior to the introduction of commercial fertilizers and other chemicals that allowed improvements in cropping practices (Knox, 2001, 2002). An example of decreased rates of upland soil erosion in agricultural areas since the early twentieth century is illustrated by the response of soil erosion to changing land use practices in the loess covered hilly region along the upper Mississippi River in northeast Iowa, southwest Wisconsin, and southeast Minnesota (Argabright *et al*., 1996). Argabright *et al*. estimated that the average annual rate of soil loss in 1930 on land in row crops, small grains, and rotation meadow was about $33.4\,t\,ha^{-1}\,year^{-1}$, but that subsequent better land conservation practices decreased losses to $17.5\,t\,ha^{-1}\,year^{-1}$ by 1982 and to $14.1\,t\,ha^{-1}\,year^{-1}$ by 1992. These changes are reflected in long-term variations in tributary drainage basin sediment budgets (Trimble, 1983, 1993).

In spite of reductions in both runoff and soil erosion related to improvements in land conservation practices, and in spite of the storage of runoff and sediments by dams and reservoirs, flooding and pollution by sediments and human-related chemicals remain major problems in the Mississippi River system. Three factors contribute to this situation. First, a major historical increase in drainage density has occurred throughout the northern sector of the Mississippi River drainage basin, northward of the late Wisconsin age glacial ice extent (Figure 9.2). Much of the topography northward of the late Wisconsin glacial terminus was poorly drained and characterized by extensive wetlands prior to Euro-American settlement (McCorvie and Lant, 1993). The artificial drainage of much of this landscape introduced a highly efficient, hydraulically smooth, drainage network that rapidly transmits runoff from the landscape. A second factor involves construction of levees that have disconnected the main channel Mississippi River from its natural floodplain for all but the more extreme floods. Extreme floods, as occurred on the middle reach of the upper Mississippi River and lower reach of the Missouri River in 1993, occasionally overtop or break levees to reconnect with the natural storage of the river's formerly active floodplain. Today, high levees occur along much of the lower third of the upper Mississippi River valley and throughout most of the lower Mississippi River valley as well as along the lower reaches of several major tributaries. The constrictions of flows by levees and other structures have been shown to increase magnitudes of upper Mississippi River flood stages for flood discharges of a given return frequency (Pinter *et al*., 2001, 2002). The combination of upstream channelization and downstream levee constriction of the Mississippi River also has resulted in lower Mississippi River discharges transporting abnormally high concentrations of pollutants. For example, the heavy rainfall and severe flooding during the summer of 1993, over the region of intense agricultural cultivation in the upper Mississippi River valley, transported extraordinarily large amounts of agricultural chemicals into

the Mississippi River and subsequently into the Gulf of Mexico (Goolsby *et al*., 1993). A third factor that seems to be contributing to flooding and sustained high levels of sediment pollution is related to climate change. Analyses of flood records that represent the upper Mississippi River and Missouri River have shown an upward trend in the recurrence frequency of large floods since about 1950 (Olsen *et al*., 1999; Knox, 2000). While this upward trend probably results from effects related both to climate change and the other human factors described above, the role of climate change is clearly apparent. This is because annual maximum floods on small tributaries have been decreasing in recent decades as might be expected with historical trends in improving land conservation, while at the same time the main channel upper Mississippi River has been experiencing an opposite trend toward more frequent large floods (Knox, 2000). The large upper Mississippi River floods result from the systematic integration of runoff from its many tributaries as occurs during snowmelt or long-duration stalled frontal systems such as in 1993. Consequently, changes over widespread areas affecting precipitation amounts and snowmelt can significantly influence Mississippi River floods. It is noteworthy that regions represented by the upper Mississippi River and northeastern upper Missouri River drainage basins have experienced recent upward trends in both annual precipitation as well as the amount of precipitation being delivered in large magnitude rainfalls (Karl and Knight, 1998; Knapp, 1994). Furthermore, in concert with global warming, the diurnal temperature range has been decreasing over most of the Mississippi River drainage basin and annual minimum temperatures have been getting higher, especially in the northern Missouri River and upper Mississippi River drainage basins (Easterling *et al*., 1997, 2000). The higher temperatures have resulted in early spring rains falling on melting snow packs, which in turn have contributed to recent large floods on the upper Mississippi River as occurred during 2001. A study of upper Mississippi River floods during past warm climate episodes of the Holocene is currently in progress and results are indicating these warm episodes also were characterized by anomalous high frequencies of large floods that separated intervening short periods of very small floods and probable droughts (Knox, 2003). The similarities between climate and flooding characteristics during regional warming since the mid-twentieth century and regional warming and climate and flooding characteristics during the late Holocene suggests that the upper Mississippi River might anticipate increased year-to-year variations in flow volumes and stage magnitudes in response to anticipated continued global warming in the twenty-first century. At present there is insufficient information to speculate how hydrologic responses to anticipated global warming might affect other parts of the Mississippi River system. The large capacity of the lower Mississippi River channel normally allows it to accommodate volumes of flood runoff from the upper Mississippi and Missouri River tributaries, but when flooding in either or both of these rivers combines with a large flood from the Ohio River system, serious flooding becomes a possibility along the lower Mississippi River. At present relatively little is known about how climate change might influence the joint probabilities of flooding from the Ohio River in combination with major flooding from the Missouri and upper Mississippi Rivers. More research on this subject seems especially warranted given the concerns about preventing the diversion of the lower Mississippi River into the Atchafalya during a large flood in the lower Mississippi Valley.

ACKNOWLEDGEMENTS

Information assembled for this manuscript was facilitated in part by support from US National Science Foundation, Earth System History Award ATM-0112614 and in part by support from an Evjue-Bascom research award from the University of Wisconsin, Madison. Review comments by Ken Gregory, Avijit Gupta, David Leigh, and Joe Mason, and cartographic assistance by Richard Worthington are gratefully acknowledged.

REFERENCES

Aharon, P., (2003) Meltwater flooding events in the Gulf of Mexico revisited: implications for rapid climate change during the last deglaciation. *Paleoceanography*, 18(4): 3.1–3.14.

Anderson, R.C., (1985) Preglacial drainage in the Upper Mississippi Valley region. In: *Pleistocene Geology and Evolution of the Upper Mississippi Valley* (R.S. Lively Ed.). Minnesota Geological Survey, St Paul, MN, Winona, MN, pp. 9–10.

Anderson, R.C., (1988) Reconstruction of preglacial drainage and its diversion by earliest glacial forebulge in the upper Mississippi Valley region. *Geology*, 16: 254–257i.

Anfinson, J.O., (2003) *The River We Have Wrought: A History of the Upper Mississippi*. University of Minnesota Press, Minneapolis, MN, 365 pp.

Antevs, E., (1955) Geologic-climatic dating in the West. *American Antiquity*, 20: 317–335.

Argabright, M.S., Cronshey, R.G., Helms, J.D., Pavelis, G.A. and Sinclair, H.R., (1996) Historical changes in soil erosion 1930–1992: the northern Mississippi Valley loess hills, US Department of Agriculture, Natural Resources and Conservation Service, Historical Notes No. 5, Washington, DC, 92 pp.

Aslan, A., Autin, W.J., Blum, M.D. and Broussard, T.J., (1998) Late Holocene Mississippi and Red River avulsion in

Louisiana. Geological Society of America Abstracts with Programs, 30(7): 294.

Autin, W.J., Burns, S.F., Miller, B.J., Saucier, R.T. and Snead, J. I., (1991) Quaternary geology of the Lower Mississippi Valley. In: *Quaternary Nonglacial Geology: Conterminous* (R.B. Morrison Ed.). US Geological Society of America, Boulder, CO, pp. 547–582.

Baker, R.G., (2000) Holocene environments reconstructed from plant macrofossils in stream deposits from southeastern Nebraska, USA. *Holocene*, 10(3): 357–365.

Baker, R.G., Bettis, E.A., Schwert, D.P., Horton, D.G., Chumbley, C.A., Gonzalez, L.A., Reagan, M.K., (1996) Holocene paleoenvironments of northeast Iowa. *Ecological Monographs*, 66: 203–234.

Baker, R.G., Bettis, E.A., Fredlund, G.G. and Mandel, R.D., (2000) Holocene environments of the central Great Plains: Multi-proxy evidence from alluvial sequences, southeastern Nebraska. *Quaternary International*, 67: 75–88.

Baker, R.G., Gonzalez, L.A., Strickland, L.E., Krieg, J.R., Bettis, E.A., Denniston, R.F., (2002) Holocene paleoenvironments in southeastern Minnesota – chasing the prairie-forest ecotone. *Palaeogeography, Palaeoclimatology, Palaeoecology*, 177(1–2): 103–122.

Bartlein, P.J., Webb, T.I. and Fleri, E., (1984) Holocene climatic change in the northern Midwest: pollen-derived estimates. *Quaternary Research*, 22: 361–374.

Benedetti, M.M., (2003) Controls on overbank deposition in the upper Mississippi River. *Geomorphology*, 56: 271–290.

Bettis E.A. and Mandel, R.D., (2002) The effects of temporal and spatial patterns of Holocene erosion and alluviation on the archaeological record of the central and eastern Great Plains, USA. *Geoarchaeology*, 17(2): 141–154.

Bettis E.A., Muhs, D.R., Roberts, H.M. and Wintle, A.G., (2003) Last glacial loess in the conterminous USA. *Quaternary Science Reviews*, 22: 1907–1946.

Biedenharn, D.S., Thorpe, C.R. and Watson, C.C., (2000) Recent morphological evolution of the lower Mississippi River. *Geomorphology*, 34: 227–249.

Blum, M.D. and Törnqvist, T.E., (2000) Fluvial responses to climate and sea-level change: a review and look forward. *Sedimentology*, 47(1): 2–48.

Blum, M.D., Guccione, M.J., Wysocki, D.A., Robnett, P.C. and Rutledge, E.M., (2000) Late Pleistocene evolution of the lower Mississippi River valley. *Geological Society of America Bulletin*, 112(2): 221–235.

Boellstorff, J., (1978) North American Pleistocene stages reconsidered in light of probable Pliocene-Pleistocene continental glaciation. *Science*, 202: 305–307.

Brakenridge, G.R., (1981) Late Quaternary floodplain sedimentation along the Pomme de Terre River, southern Missouri. *Quaternary Research*, 15: 62–76.

Brakenridge, G.R., (1984) Alluvial stratigraphy and radiocarbon dating along the Duck River, Tennessee: Implications regarding flood-plain origin. *Geological Society of America Bulletin*, 95: 9–25.

Brown, P., Kennett, J.P. and Ingram, B.L., (1999) Marine evidence for episodic Holocene megafloods in North America and the northern Gulf of Mexico. *Paleoceanography*, 14(4): 498–510.

Brown, W.N. Inc., (1931) *Upper Mississippi River: Hastings, Minnesota to Grafton, Illinois, Survey 1929 to 1930*. Williams and Heintz Co., Washington, DC.

Bryson, R.A., (1966) Air masses, streamlines, and the boreal forest. *Geographical Bulletin*, 8: 228–269.

Bryson, R.A. and Wendland, W.M., (1967) Tentative climatic patterns for some late-glacial and post-glacial episodes in central North America. In: *Life, Land, and Water* (W.J. Mayer-Oakes, Ed.). University of Manitoba Press, Winnipeg, MB, pp. 271–298.

Butzer, K.W., (1990) The Indian legacy in the American landscape. In: *The Making of the American Landscape* (M.P. Conzen, Ed.). Unwin Hyman, Boston, pp. 27–50.

Carney, S.J., (1996) Paleohydrology of the western outlets of Glacial Lake Duluth. MS Thesis, University of Minnesota, Duluth, Duluth.

Clayton, J.A., (2000) The drainage of Glacial Lake Wisconsin: reconstruction of a late Pleistocene catastrophic flooding episode. MS Thesis, University of Wisconsin, Madison, Madison, WI, 138 pp.

Coleman, J.M., (1988) Dynamic changes and processes in the Mississippi River delta. *Geological Society of America Bulletin*, 100: 999–1015.

Collier, M., Webb, R.H. and Schmidt, J.C., (1996) Dams and rivers: primer on the downstream effects of dams. *US Geological Survey Circular* 1126, Washington, DC, 94 pp.

Costa, J.E., (1988) Floods from dam failures. In: *Flood Geomorphology* (V.R. Baker, R.C. Kochel and P.C. Patton, Eds.). John Wiley & Sons, Ltd, New York, pp. 439–463.

Court, A., (1974) The climate of the conterminous United States. In: *Climates of North America* (R.A. Bryson and F.K. Hare, Eds.). Elsevier Scientific, Amsterdam, pp. 193–341.

Curry, B.B., (1998) Evidence at Lomax, Illinois, for Mid-Wisconsin (~40 000 yrs B.P.) position of the Des Moines Lobe and for diversion of the Mississippi River by the Lake Michigan Lobe (20 350 yrs B.P.). *Quaternary Research*, 50: 128–138.

Dean, W.E., (1997) Rates, timing, and cyclicity of Holocene eolian activity in north-central United States: evidence from varved lake sediments. *Geology*, 25: 331–334.

Dendy, F.E. and Bolton, G.C., (1976) Sediment yield-runoff-drainage area relationships in the United States. *Journal of Soil and Water Conservation*, 31: 264–266.

Denevan, W.M., (1992) The pristine myth: the landscape of the Americas in 1492. *Annals of the Association of American Geographers*, 82: 369–385.

Denniston, R.F., Gonzalez, L.A., Asmerom, Y., Baker, R.G., Reagan, M.K., Bettis, E.A., (1999a) Evidence for increased cool season moisture during the middle Holocene. *Geology*, 27(9): 815–818.

Denniston, R.F., Gonzalez, L.A., Semken, H.A., Asmerom, Y., Baker, R.G., Recelli-Snyder, H., Reagan, M.K., Bettis, E.A., (1999b) Integrating stalagmite, vertebrate, and pollen sequences to investigate Holocene vegetation and climate change in the southern Midwest. *Quaternary Research*, 52: 388–392.

Denniston, R.F., Gonzalez, L.A., Asmerom, Y., Reagan, M.K. and Recelli-Snyder, H., (2000) Speleothem carbon isotopic records of Holocene environments in the Ozark Highlands, USA. *Quaternary International*, 67: 21–27.

Doolittle, W.E., (1992) Agriculture in North America on the eve of contact: a reassessment. *Annals of the Association of American Geographers*, 82: 286–401.

Dury, G.H. and Knox, J.C., (1971) Duricrusts and deep-weathering profiles in southwestern Wisconsin. *Science*, 174: 291–292.

Easterling, D.R., Horton, B., Jones, P.D., Peterson, T.C., Karl, T. R., Parker, D.E., Salinger, M.J., Razuvayev, V., Plummer, N., Jamason, P. and Folland, C.K., (1997) Maximum and minimum temperature trends for the globe. *Science*, 277: 364–367.

Easterling, D.R., Meehl, G.A., Parmesan, C., Changnon, S.A., Karl, T.R. and Mearns, L.O., (2000) Climate extremes: observations, modeling, and impacts. *Science*, 289: 2068–2074.

Fisher, T.G., (2003) Chronology of glacial Lake Agassiz meltwater routed to the Gulf of Mexico. *Quaternary Research*, 59: 271–276.

Fisk, H.N., (1944) *Geological investigation of the alluvial valley of the Lower Mississippi River*, US Army Corps of Engineers, Mississippi River Commission, Vicksburg, MS.

Gable, D.J. and Hatton, T., (1983) Maps of vertical crustal movements in the United States over the last 10 million years. US Geological Survey: Map I-1315, 2 sheets, scale 1 : 5 000 000 and 1 : 10 000 000, 25 p.

Goolsby, D.A., Battaglin, W.A. and Thurman, E.M., (1993) Occurrence and transport of agricultural chemicals in the Mississippi River basin, July through August 1993. *US Geological Survey Circular* 1120-C: 1–22.

Grissinger, E.H., Murphey, J.B. and Little, W.C., (1982) Late-Quaternary valley-fill deposits in north-central, Mississippi. *Southeastern Geology*, 23(3): 147–162.

Hajic, E.R., Johnson, W.H. and Follmer, L.R., (1991) Quaternary Deposits and Landforms, Confluence Region of the Mississippi, Missouri, and Illinois Rivers, Missouri and Illinois: Terraces and Terrace Problems, Midwest Friends of the Pleistocene 38th Field Conference. Illinois State Geological Survey, Urbana, IL, pp. 1–106.

Hallberg, G.R., (1980) Pleistocene stratigraphy in east-central Iowa. Technical Information Series No. 10, 10. Iowa Geological Survey, Iowa City, IA, 168 pp.

Hallberg, G.R., (1986) Pre-Wisconsin glacial stratigraphy of the cerntral plains region in Iowa, Nebraska, Kansas, and Missouri. *Quaternary Science Reviews*, 5: 11–15.

Hallberg, G.R., Witzke, B.J., Bettis, E.A. and Ludvigson, G.A., (1985) Observations on the evolution and age of the bedrock surface in eastern Iowa. In: *Pleistocene Geology and Evolution of the Upper Mississippi Valley* (R.S. Lively, Ed.). Minnesota Geological Survey, Winona, MN, pp. 15–19.

Hinze, W.J. and Braile, L.W., (1988) Geophysical aspects of the craton: US In: *Sedimentary Cover – North American Craton* (L.L. Sloss, Ed.). US Geological Society of America, Boulder, CO, pp. 5–24.

Holliday, V.T., Knox, J.C., Running IV, G.L., Mandel, R.D. and Ferring, C.R., (2002) The Central Lowlands and Great Plains. In: *The Physical Geography of North America* (A.R. Orme, Ed.). Oxford University Press, Oxford, pp. 335–362.

Johnson, W.C. and Martin, C.W., (1987) Holocene alluvial-stratigraphic studies from Kansas and adjoining states of the east-central Plains. In: *Quaternary Environments of Kansas* (W.C. Johnson, Ed.). Kansas Geological Survey, Lawrence, KS, pp. 109–122.

Johnson, W.H., (1986) Stratigraphy and correlation of the glacial deposits of the Lake Michigan Lobe prior to 14 ka BP. *Quaternary Science Reviews*, 5: 17–22.

Karl, T.R. and Knight, R.W., (1998) Secular trends of precipitation amount, frequency, and intensity in the United States. *Bulletin of the American Meteorological Society*, 79: 231–241.

Kemmis, T.J., Hallberg, G.R. and Lutenegger, A.J., (1981) Depositional environments of glacial sediments and landforms on the Des Moines Lobe, Iowa. Iowa Geological Survey Guidebook Series No. 6, Iowa City, IA, 132 pp.

Keown, M.P., Dardeau, E.A.J. and Causey, E.M., (1986) Historic trends in the sediment flow regime of the Mississippi River. *Water Resources Research*, 22(11): 1555–1564.

Kesel, R.H., (1988) The decline in the suspended load of the lower Mississippi River and its influence on adjacent wetlands. *Environmental Geology and Water Sciences*, 11(3): 271–281.

Kesel, R.H., (1989) The role of the Mississippi River in wetland loss in southeastern Louisiana, USA. *Environmental Geology and Water Sciences*, 13(3): 183–193.

Kesel, R.H., (2003) Human modifications to the sediment regime of the lower Mississippi River flood plain. *Geomorphology*, 56(3–4): 325–334.

Knapp, H.V., (1994) Hydrologic trends in the upper Mississippi River Basin. *Water International*, 19(4): 199–206.

Knox, J.C., (1982) Quaternary history of the Kickapoo and Lower Wisconsin River Valleys, Wisconsin. In: *Quaternary History of the Driftless Area* (J.C. Knox, L. Clayton and D.M. Mickelson, Eds.). Wisconsin Geological and Natural History Survey, Madison, WI, pp. 1–65.

Knox, J.C., (1983) Responses of river systems to Holocene climates. In: *Late Quaternary Environments of the United States: Volume 2, The Holocene* (H.E. Wright Jr, Ed.). University of Minnesota Press, Minneapolis, pp. 26–41.

Knox, J.C., (1985a) Geologic history of valley incision in the Driftless Area. In: *Pleistocene Geology and Evolution of the Upper Mississippi Valley* (R.S. Lively, Ed.). Minnesota Geological Survey, St Paul, Winona, MN, pp. 5–8.

Knox, J.C., (1985b) Responses of floods to Holocene climatic change in the Upper Mississippi Valley. *Quaternary Research*, 23(3): 287–300.

Knox, J.C., (1988) Climatic influence on Upper Mississippi Valley floods. In: *Flood Geomorphology* (V.R. Baker, R.C. Kochel and P.C. Patton, Eds.). John Wiley & Sons, Ltd, New York, pp. 279–300.

Knox, J.C., (1993) Large increases in flood magnitude in response to modest changes in climate. *Nature*, 361: 430–432.

Knox, J.C., (1996) Late Quaternary upper Mississippi River alluvial episodes and their significance to the lower Mississippi River system. *Engineering Geology*, 45(1–4): 263–285.

Knox, J.C., (1999) Long-term episodic changes in magnitudes and frequencies of floods in the Upper Mississippi River Valley. In: *Fluvial Processes and Environmental Change* (A.G. Brown and A.G. Quine, Eds.). John Wiley & Sons, Ltd, Chichester, pp. 255–282.

Knox, J.C., (2000) Sensitivity of modern and Holocene floods to climate change. *Quaternary Science Reviews*, 19(1–5): 439–457.

Knox, J.C., (2001) Agricultural influence on landscape sensitivity in the Upper Mississippi River Valley. *Catena*, 42(2–4): 193–224.

Knox, J.C., (2002) Agriculture, erosion, and sediment yields. In: *The Physical Geography of North America* (A.R. Orme, Ed.). Oxford University Press, Oxford, pp. 482–500.

Knox, J.C., (2003) North American paleofloods and future floods: responses to climatic change. In: *Palaeohydrology: Understanding Global Change* (G. Benito and K.J. Gregory, Eds.). John Wiley & Sons, Ltd, London, pp. 143–164.

Knox, J.C. and Attig, J.W., (1988) Geology of the Pre-Illinoian sediment in the Bridgeport Terrace, Lower Wisconsin River Valley, Wisconsin. *Journal of Geology*, 96: 505–513.

Knox, J.C. and Daniels, J.M., (2002) Watershed scale and the stratigraphic record of large floods. In: *Ancient Floods, Modern Hazards: Principles and Applications of Paleoflood Hydrology* (P.K. House, R.H. Webb, V.R. Baker and D.R. Levish, Eds.). American Geophysical Union, Washington, DC, pp. 237–255.

Knox, J.C., McDowell, P.F. and Johnson, W.C., (1981) Holocene fluvial stratigraphy and climatic change in the Driftless Area, Wisconsin. In: *Quaternary Paleoclimate* (W.C. Mahaney, Ed.). Geo Books, Norwich, pp. 107–127.

Langbein, W.B. and Schumm, S.A., (1958) Yield of sediment in relation to mean annual precipitation. *American Geophysical Union Transactions*, 39: 1076–1084.

Leigh, D.S. and Knox, J.C., (1994) Loess of the Upper Mississippi Valley Driftless Area. *Quaternary Research*, 42: 30–40.

Leverington, D.W., Mann, J.D. and Teller, J.T., (2000) Changes in the bathymetry and volume of Glacial Lake Agassiz between 11 000 and 9300 ^{14}C yr B.P. *Quaternary Research*, 54: 174–181.

Licciardi, J.M., Teller, J.T. and Clark, P.U., (1999) Freshwater routing by the Laurentide Ice Sheet during the last deglaciation. In: *Mechanisms of Global Climate Change at Millennial Time Scales* (P.U. Clark, R.S. Webb and L.D. Keigwin, Eds.). Geophysical Monograph 112. Ameican Geophysical Union, Washington, DC, pp. 177–201.

Mandel, R.D., (1995) Geomorphic controls of the Archaic record in the Central Plains of the United States. In: *Archaeological Geology of the Archaic Period in North America* (E.A. Bettis, Ed.). Geological Society of America Special Paper 297, Boulder, pp. 37–66.

Martin, C.W., (1992) Late Holocene alluvial chronology and climate change in the central Great Plains. *Quaternary Research*, 37: 315–322.

Matsch, C.L., (1983) River Warren, the southern outlet of Glacial Lake Agassiz. In: *Glacial Lake Agassiz* (J.T. Teller and L. Clayton, Eds.). Geological Association of Canada, St Johns, New Foundland, pp. 231–244.

May, D.W., (1989) Holocene alluvial fills in the South Loup River Valley, Nebraska. *Quaternary Research*, 32: 117–120.

May, D.W., (1992) Late Holocene valley-bottom aggradation and erosion in the South Loup River Valley, Nebraska. *Physical Geography*, 13(2): 115–132.

May, D.W., (2003) Properties of a 5500-year-old flood-plain in the Loup river Basin, Nebraska. *Geomorphology*, 56: 243–254.

McCorvie, M.R. and Lant, C.L., (1993) Drainage district formation and the loss of Midwestern wetlands, 1850–1930. *Agricultural History*, 67: 13–39.

McDowell, P.F., (1983) Evidence of stream response to Holocene climate change in a small Wisconsin watershed. *Quaternary Research*, 19: 231–244.

McMillan, M.E., Angevine, C.L. and Heller, P.L., (2002) Postdepositional tilt of the Miocene-Pliocene Ogallala Group on the western Great Plains: Evidence of late Cenozoic uplift of the Rocky Mountains. *Geology*, 30(1): 63–66.

McPhee, J., (1989) *The Control of Nature*. Farrar, Straus, and Giroux, New York, 272 pp.

Meade, R.H., Yuzyk, T.R. and Day, T.J., (1990) Movement and storage of sediment in rivers of the United States and Canada. In: *Surface Water Hydrology, the Geology of North America* (M.G. Wolman and H.C. Riggs, Eds.), V. 0-1. Geological Society of America, Boulder, CO, pp. 255–280.

Melhorn, W.N. and Kempton, J.P. (Editors), 1991. *Geology and hydrogeology of the Teays-Mahomet bedrock valley system*, Special Paper 258. Geological Society of America, Boulder.

Mickelson, D.M. and Colgan, P.M., (2004) The southern Laurentide Ice Sheet. In: *The Quaternary Period in the United States* (A.R. Gillespie, S.C. Porter and B.F. Atwater, Eds.). Developments in Quaternary Science, Vol. 1. Elsevier, Amsterdam, 1–16.

Miller, B.A., Whitlock, A. and Hughes, R.C., (1996) Flood management – the TVA experience. *Water International*, 21(3): 119–130.

Molenaar, C.M. and Rice, D.D., (1988) Cretaceous rocks of the Western Interior Basin. In: *Sedimentary Cover – North American Craton* (L.L. Sloss, Ed.). US Geological Society of America, Boulder, CO, pp. 77–82.

Moody, J.A. and Meade, R.H., (1993) Hydrologic and sedimentologic data collected during four cruises at high water on the Mississippi River and some of its tributaries. US Geological Survey Open File Report 92–651, 227 pp.

Nielsen, D.N., Rada, R.G. and Smart, M.M., (1984) Sediments of the Upper Mississippi River: their sources, distribution, and characteristics. In: *Contaminants in the Upper Mississippi River: Proceedings of the 15th Annual Meeting of the Mississippi River Research Consortium* (J.G. Wiener, R.V. Anderson and D.R. McConville, Ed.). Butterworth Publishers, Toronto, pp. 67–98.

Olsen, J.R., Stedinger, J.R., Matalas, N.C. and Stahkhiv, E.Z., (1999) Climate variability and flood frequency estimation for

the upper Mississippi and lower Missouri Rivers. *Journal of the American Water Resources Association*, 35: 1509–1523.

Parrett, C., Melcher, N.B. and James Jr, R.W., (1993) Flood discharges in the Upper Mississippi River Basin, 1993. *US Geological Survey Circular* 1120A, pp.1–14.

Patton, P.C. and Schumm, S.A., (1981) Ephemeral-stream processes: Implications for studies of Quaternary valley fills. *Quaternary Research*, 15: 24–43.

Pinter, N., Thomas, R. and Wlosinski, J.H., (2001) Assessing flood hazard on dynamic rivers. *EOS, Transactions, American Geophysical Union*, 82(31): 333, 338–339.

Pinter, N., Thomas, R. and Wlosinski, J.H., (2002) Reply to comment on 'assessing flood hazard on dynamic rivers'. *EOS, Transactions, American Geophysical Union*, 83(3 Sept 2002): 397–398.

Pitlick, J., (1997) A regional perspective of the hydrology of the 1993 Mississippi River Basin floods. *Annals – Association of American Geographers*, 87(1): 135–151.

Riggs, H.C. and Harvey, K.D., (1990) Temporal and spatial variability of streamflow. In: *Surface Water Hydrology, The Geology of North America* (M.G. Wolman and H.C. Riggs, Eds.), Volume O-1. Geological Society of America, Boulder, CO, pp. 81–96.

Rittenour, T.M., (2002) OSL Chronology of fluvial response to deglaciation in the Lower Mississippi Valley. Geological Society of America Abstracts with Programs, 34(7): 367.

Rittenour, T.M., Goble, R.J. and Blum, M.D., (2003) An optical age chronology of Late Pleistocene fluvial deposits in the northern lower Mississippi valley. *Quaternary Science Reviews*, 22: 1105–1110.

Roy, M., Clark, P.U., Barendregt, R.W., Glasmann, J.R. and Enkin, R.J., (2004) Glacial stratigraphy and paleomagnetism of late Cenozoic deposits of the north-central United States. *Geological Society of America Bulletin*, 116(1/2): 30–41.

Royall, P.D., Delcourt, P.A. and Delcourt, H.R., (1991) Late Quaternary paleoecology and paleoenviroonments of the Central Mississippi Alluvial Valley. *Geological Society of America Bulletin*, 103: 157–170.

Saucier, R.T., (1994a) Evidence of late glacial runoff in the Lower Mississippi Valley. *Quaternary Science Reviews*, 13: 973–981.

Saucier, R.T., (1994b) *Geomorphology and Quaternary geologic history of the Lower Mississippi Valley*: Volume 1. US Army Corps of Engineers, Vicksburg, MS, 1–364 pp.

Schumm, S.A., (1965) Quaternary paleohydrology. In: *The Quaternary of the United States* (H.E. Wright Jr and D.G. Frey Eds.). Princeton University Press, Princeton, NJ.

Schumm, S.A., (1977) *The Fluvial System*. John Wiley & Sons, Ltd, New York, 338 pp.

Schumm, S.A. and Brakenridge, G.R., (1987) River responses. In: *North America and Adjacent Oceans during the Last Deglaciation* (W.F. Ruddiman and H.E. Wright Jr, Eds.). The Geology of North America, Volume K-3. Geological Society of America, Boulder, CO, pp. 221–240.

Schumm, S.A. and Winkley, B.R., (1994) The character of large alluvial rivers. In: *The Variability of Large Alluvial Rivers* (S.A. Schumm and B.R. Winkley, Eds.). American Society of Civil Engineers, NY, pp. 1–9.

Schumm, S.A., Rutherfurd, I.D. and Brooks, J., (1994) Pre-cutoff morphology of the lower Mississippi River. In: *The Variability of Large Alluvial Rivers* (S.A. Schumm and B.R. Winkley, Eds.). American Society of Civil Engineers, New York, NY, pp. 13–44.

Stuiver, M., Reimer, P.J. and Braziunas, T.F., (1998) High-precision radiocarbon age calibration for terrestrial and marine samples. *Radiocarbon*, 40(3): 1127–1151.

Swenson, B., (1938) The Ohio and Mississippi River floods of January–February 1937. *Monthly Weather Review* (Suppl. No. 37): 1–55.

Teller, J.T., (1987) Proglacial lakes and the southern margin of the Laurentide Ice Sheet. In: *North America and Adjacent Oceans during the Last Deglaciation* (W.F. Ruddiman and H.E. Wright Jr, Eds.). The Geology of North America. Volume K3. Geological Society of America, Boulder, CO, pp. 39–69.

Teller, J.T., (1990) Volume and routing of late-glacial runoff from the southern Laurentide Ice Sheet. *Quaternary Research*, 34: 12–23.

Teller, J.T. and Clayton, L., (1983) *Glacial Lake Agassiz*. Special Paper 26. Geological Association of Canada, St Johns, NF, 451 pp.

Thornbury, W.D., (1965) *Regional Geomorphology of the United States*. John Wiley & Sons, Ltd, New York, 609 pp.

Törnqvist, T.E., Kidder, T.R., Autin, W.J., van der Borg, K., de Jong, F.M., Klerks, C.J.W., Snijders, E.M.A., Storms, J.E.A., van Dam, R.L. and Wiemann, M.C., (1996) A revised chronology for Mississippi River subdeltas. *Science*, 273: 1693–1696.

Trimble, S.W., (1983) A sediment budget for Coon Creek basin in the Driftless Area, Wisconsin, 1853–1977. *American Journal of Science*, 283: 454–474.

Trimble, S.W., (1993) The distributed sediment budget model and watershed management in the Paleozoic Plateau of the upper Midwestern United States. *Physical Geography*, 14: 285–303.

Trowbridge, A.C., (1921) *The Erosional History of the Driftless Area*, University of Iowa Studies in Natural History. University of Iowa, Iowa City, IA, pp. 1–127.

Upper Mississippi River Basin (UMRB) Committee, (1970) Volume III, Appendix G, Fluvial Sediment, Upper Mississippi River Comprehensive Basin Study, Minneapolis, MN.

US Water Resources Council, (1978) *The Nation's Water Resources – The Second National Water Assessment*, Volume A-4, Streamflow Conditions, US Water Resources Council, Washington, DC, 255 p.

Webb, T., Bartlein, P.J., Harrison, S.P. and Anderson, K.H., (1993) Vegetation, lake levels, and climate in eastern North America for the past 18 000 years. In: *Global Climates since the Last Glacial Maximum* (H.E. Wright Jr, J.E. Kutzbach, T. Webb, W.F. Ruddiman, F.A. Street-Perrott and P.J. Bartlein, Eds.). University of Minnesota Press, MN, pp. 415–467.

West Consultants Inc., (2000) *Upper Mississippi River and Illinois Waterway Cumulative Effects Study*, Bellevue, WA.

Wiele, S. and Mooers, H.D., (1989) Glacial River Warren: steady state and peak discharge. Geological Society of America Abstracts with Programs, 21: A60.

Williams, G.P., (1978) The case of the shrinking channels – the North Platte and Platte Rivers in Nebraska. *US Geological Survey Circular* 781, Washington, DC, 48 pp.

Williams, M., (1989) *Americans and Their Forests: A Historical Geography*. Cambridge University Press, Cambridge, 599 pp.

Williams, M.L., (1992) *Schoolcraft's Narrative Journal of Travels*. Michigan State University Press, East Lansing, MI, 520 pp.

Willman, H.B. and Frye, J.C., (1969) High-level glacial outwash in the Driftless Area of Northwestern Illinois. Circular 440, Illinois State Geological Survey, Urbana, IL.

Willman, H.B. and Frye, J.C., (1970) Pleistocene Stratigraphy of Illinois, 94. Illinois State Geological Survey Bulletin 94, Urbana, IL, 204 pp.

Willman, H.B., Glass, H.D. and Frye, J.C., (1989) Glaciation and origin of the geest in the Driftless Area of Northwestern Illinois. Circular 535, Illinois State Geological Survey, Urbana, IL.

Winkler, M.G., Swain, A.M. and Kutzbach, J.E., (1986) Middle Holocene dry period in the northern midwestern United States: lake levels and pollen stratigraphy. *Quaternary Research*, 25: 235–250.

Winkley, B.R., (1994) Response of the lower Mississippi River to flood control and navigation improvements. In: *The Variability of Large Alluvial Rivers* (S.A. Schumm and B.R. Winkley, Eds.). American Society of Civil Engineers, New York, NY, pp. 45–74.

Witzke, B.J. and Ludvigson, G.A., (1990) Petrographic and stratigraphic comparisons of sub-till and inter-till alluvial units in western Iowa: implications for development of the Missouri river drainage. In: *Holocene Alluvial Stratigraphy and Selected Aspects of the Quaternary History of Western Iowa* (E.A. Bettis, Ed.). Midwest Friends of the Pleistocene Field Conference Guidebook, pp. 119–143.

Woodhouse, C.A. and Overpeck, J.T., (1998) 2000 years of drought variability in the central United States. *Bulletin of the American Meteorological Society*, 79: 2693–2714.

Wright, H.E. Jr, (1987) Synthesis: the land south of the ice sheets. In: *North America and Adjacent Oceans during the Last Deglaciation, the Geology of North America* (W.F. Ruddiman and H.E. Wright Jr, Eds.). Geological Society of America, Boulder, CO, pp. 479–488.

Wright, H.E. Jr, (1992) Patterns of Holocene climatic change in the Midwestern United States. *Quaternary Research*, 38: 129–134.

10

The Colorado River

John C. Schmidt

Department of Watershed Sciences, Utah State University, Logan, UT 84322-5210, USA

10.1 INTRODUCTION

Although of modest size by the standard of total flow, the Colorado River is significant on other accounts. Once referred to as the Colorado River of the West to distinguish it from a Texas stream one-fifth its size, the river of concern here drains parts of six intermountain states, as well as small parts of California and Mexico (Figure 10.1). Construction of large reservoirs and diversions, beginning in the early twentieth century, fueled growth of this region. Today, the Colorado River has the largest ratio of reservoir storage to mean annual flow of any large basin in North America (Hirsch *et al*., 1990). There are substantial consumptive demands placed on the river; diversions deliver water to urban areas whose total population exceeds 30 million, including Los Angeles, the second largest urban area in the United States, and Las Vegas, the United States' fastest growing city. Nearly 2 million people now live on the Colorado River's delta and adjacent areas.

Dam construction achieved international prominence with completion of Hoover Dam in 1936 (Stevens, 1988) and reached its climax in the early 1960s with completion of the six dams of the Colorado River Storage Project (CRSP) (Martin, 1989). Proposals for and construction of other dams in the watershed led to political battles that gave rise to the modern American environmental movement (Harvey, 1994; Pearson, 2002). Environmental concerns at the end of the twentieth century led to establishment of several river rehabilitation programs. Today, these programs attempt to resolve the competing needs of consumptive water use, hydroelectric power production, and protection and recovery of unique endemic fisheries.

The river has a famous history of river-based scientific exploration (Powell, 1875; Westwood, 1992), and many fundamental concepts of geomorphology arose from observations made in the watershed in the late 1800s (Newberry, 1861, 1876; Powell, 1875; Gilbert, 1876, 1877; Dutton, 1880, 1881, 1882). The Colorado Plateau portion of the Colorado River basin is one of the most scenic areas of the United States, and has the country's densest concentration of federally protected areas, including the national parks or monuments of Arches, Bryce, Black Canyon of the Gunnison, Canyonlands, Capitol Reef, Dinosaur, Grand Canyon, Grand Staircase-Escalante, and Zion. Elsewhere in the Colorado Plateau are national parks and monuments protecting prehistoric archaeology, including Canyon de Chelly, Chaco Canyon, and Mesa Verde. The reservoirs also attract significant recreational visitation. Annual visitation at Lake Mead and Glen Canyon National Recreation Areas was 9.7 million in 2003.

The delta and estuary of the Colorado River are only replenished in years of unusually large runoff. Approximately 10% of the pre-development stream flow now crosses the border to Mexico, an amount set by international treaty, and most of this is diverted for irrigation and does not reach the sea. The reduction in stream flow, and conversion of much of the delta to agricultural fields, transformed a 'jaguar-infested jungle' in the 1920s (Leopold, 1949) to a 'barren salt encrusted tidal flat' in the 1960s (Glenn *et al*., 2001a). A small part of the delta ecosystem has recovered in response to occasional years of high runoff since the early 1980s, thereby inspiring a bi-national effort to rehabilitate this unique ecosystem.

Large Rivers: Geomorphology and Management, Edited by A. Gupta

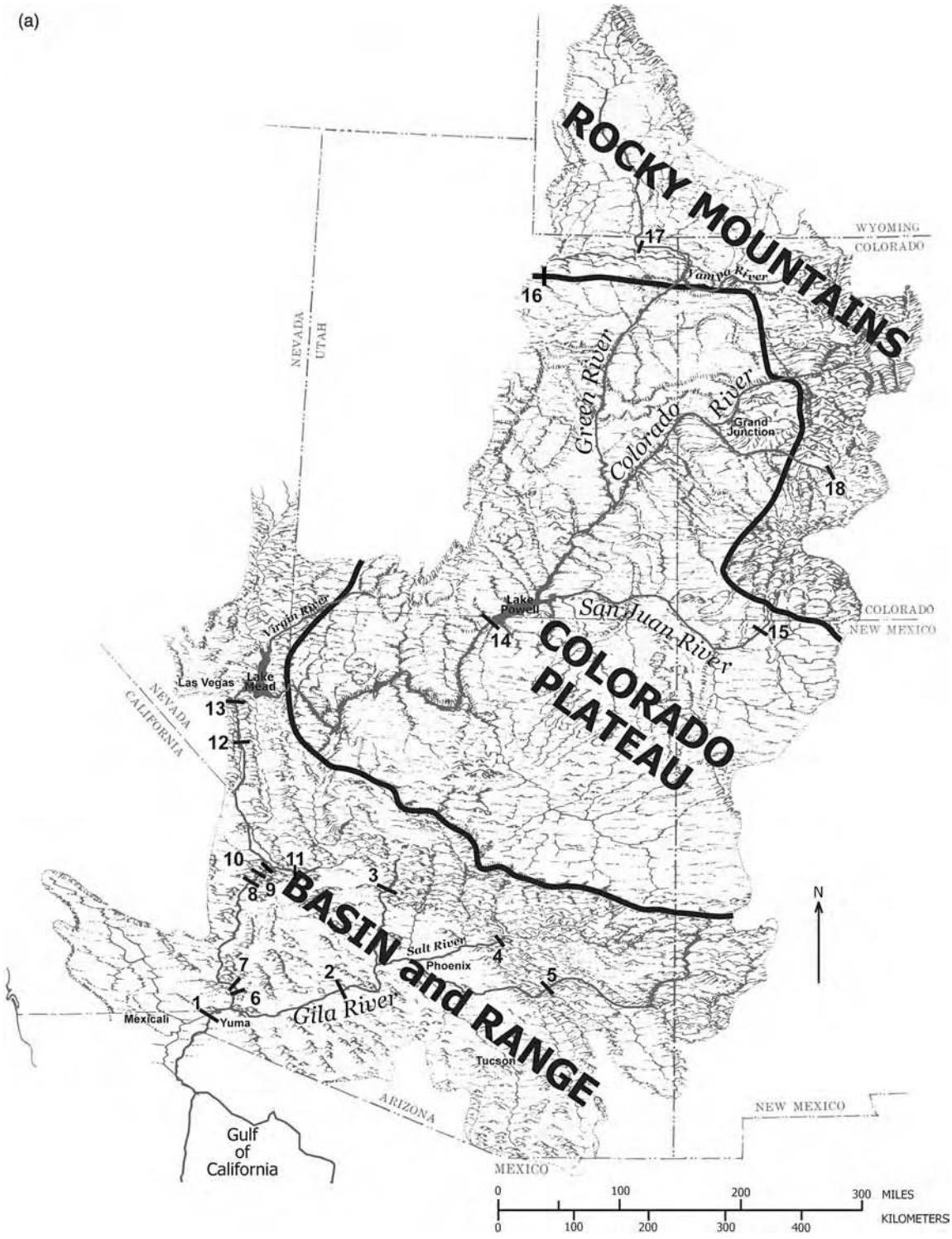

Figure 10.1 Map of the Colorado River basin and its principal landforms. Background block diagram is from Hunt (1969). (a) Major streams and dams of the Colorado River basin and the three major physiographic provinces that occur in the basin. Table 10.1 lists the names and characteristics of these dams. (b) Boundaries of the sections of each physiographic province, as defined by Graf (1987). Numbers on this figure refer to place names and letters refer to units of the National Park system described in text

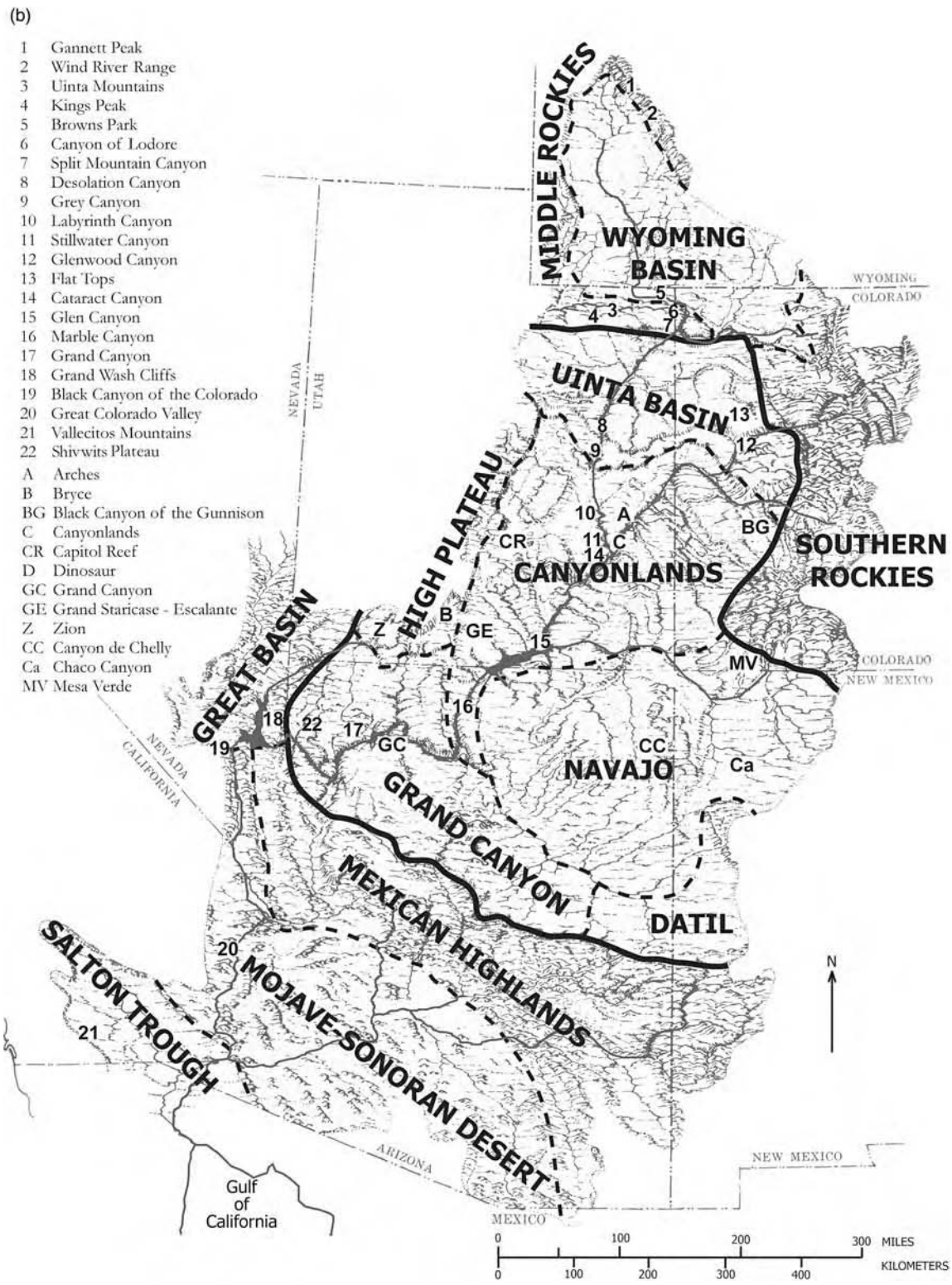

Figure 10.1 *Continued*

Table 10.1 Major dams of the Colorado River basin. The dams listed here are those on the main stem of the Colorado River in the Lower Basin, and all other dams whose storage capacity exceeds $1.0 \times 10^6\,m^3$

Name of dam (name of river)	Date of first completion/date of most recent reconstruction	Type of structure and structural height of dam (m)	Name of reservoir if different from name of dam	Storage capacity ($\times 10^6\,m^3$)[a]
Lower Basin				
Mainstem Colorado River				
(1)[b] Morelos	1950			
(6) Laguna	1909	gravity 3		1.97
(7) Imperial	1938	gravity 26		197
(8) Palo Verde	1957	gravity 20		1.23
(9) Headgate Rock	1942	gravity 21	Moovalya	24.7
(10) Parker	1938	arch 98	Havasu	764
(12) Davis	1953	gravity 61	Mohave	2240
(13) Hoover	1936	arch 222	Mead	37300
Tributary basins				
(2) Painted Rock (Gila)	1960	gravity 55		5960
(3) New Waddell (Agua Fria)	1938/1993	gravity 134	Pleasant	1370
(4) Theodore Roosevelt (Salt)	1911	arch 87		1920
(5) Coolidge (Gila)	1929	arch 77	San Carlos	1320
(11) Alamo (Bill Williams)	1968	gravity 88		1850
Upper Basin				
(14) Glen Canyon (Colorado)	1964	arch 216	Powell	35600
(15) Navajo (San Juan)	1963	gravity 123		2450
(16) Soldier Creek (Strawberry)	1909/1973	gravity 83	Strawberry	1390
(17) Flaming Gorge (Green)	1964	arch 153		4940
(18) Blue Mesa (Gunnison)	1966	gravity 119		1160

[a] Includes dead storage.
[b] Number corresponds to location in Figure 10.1.
Data are from the national inventory of dams (US Army Corps of Engineers, 1996).

The purpose of this chapter is to describe the geomorphic and hydrologic attributes of the river, the changes that have occurred in these attributes over time, the relationship of these attributes to the dependant ecological and human systems, and the efforts made to reverse undesired environmental trends.

10.2 PHYSIOGRAPHY

> 'The Colorado River. . . . , has its sources in alpine lakes fed by everlasting snows. These streams. . . . have a strange, eventful history as they pass down through gorges, tumbling in cascades and cataracts, until they reach the hot, arid plains of the Lower Colorado, where the waters that were so clear above empty as turbid floods into the Gulf of California. . . . The general course of the river is from north to south and from great altitudes to the level of the sea. Thus it runs "from the land of snow to the land of sun."'
>
> (Powell, 1875)

The Colorado River drains an area of about $75 \times 10^6\,km^2$, about 15% of the conterminous United States. The headwaters are in the middle and southern Rocky Mountains (Figure 10.1). These streams generally drain south and west, in some places crossing mountain ranges in deep canyons, and eventually join to form the three primary upper basin branches of the drainage network. The upper Colorado (once called the Grand), Green, and San Juan Rivers flow south and west across the great uplifted structural block of the Colorado Plateau and join to form the mainstem Colorado River in southeastern Utah. Most of the mainstem's course across the Colorado Plateau is confined within spectacular, deep canyons, including the 400 km long, 1000–1500 m deep Grand Canyon. Downstream, the river crosses the broad basins and isolated mountain ranges of the Basin and Range. The Gila River is the one long tributary whose course is wholly within the Basin and Range. The Gila River's headwaters are in the Mexican Highlands of west-central New Mexico. The Gila crosses the Sonoran Desert before joining the

mainstem at the head of the Colorado River delta in the Salton Trough. The Salton Trough includes the delta and two large closed basins, the Salton Sink in the United States and the Laguna Salada in Mexico. The delta ecosystem once covered an area of more than 7700 km^2 (Glenn *et al*., 2001).

10.2.1 Description of the Green and Colorado Rivers, from Headwaters to the Sea

The distance between the headwaters of the Green River in the Wind River Range and the Gulf of California is about 2900 km, the longest along-channel distance in the network. John Wesley Powell traversed much of this distance in an epic boating journey in 1869 (Powell, 1875), and Fletcher (1997) walked and boated the entire distance at the end of the twentieth century. The physiography of this traverse is typical of routes downstream along other headwater tributaries, in that the river course alternates between long, deep canyons and short, open valleys.

The Green River's most upstream sources are on the west side of the Continental Divide of the Wind River Range, including the slopes of Gannett Peak, Wyoming's highest at 4229 m (Figure 10.2). Here, streams carry the melt of snowfields and glaciers, occupy the floors of glacial troughs, and are dammed by Pleistocene moraines where they exit the mountains. The Green River itself flows from the northwestern end of the Wind River Range, and tributaries draining other parts of the range, as well as the nearby Wyoming Range, join the mainstem in the Wyoming Basin. This intermontane basin is the largest in the Rocky Mountains. In the centre of the basin is the 40-m tall Fontenelle Dam, forming the 33 km long Fontenelle Reservoir, the most upstream mainstem reservoir in the Green River basin. Further south, the Green River has eroded canyons along the northern edge of the Uinta Mountains, an east–west trending range that is the most southerly of the middle Rocky Mountains and includes Utah's highest point, Kings Peak, at 4123 m. Here, the 150 m high Flaming Gorge Dam creates a 150 km long reservoir. Downstream, the Green River flows to the east through deep canyons and the open valley of Browns Park, before turning abruptly to the south and crossing the Uintas through the Canyon of Lodore (Figure 10.3). For the next 70 km, the river flows through a series of canyons and parks formed by smaller anticlines and synclines (Figure 10.4).

Figure 10.2 Photograph of glacial ice along the Continental Divide near Gannett Peak in the Wind River Range, in the headwaters of the Green River. (Reproduced with permission from Michael Collier)

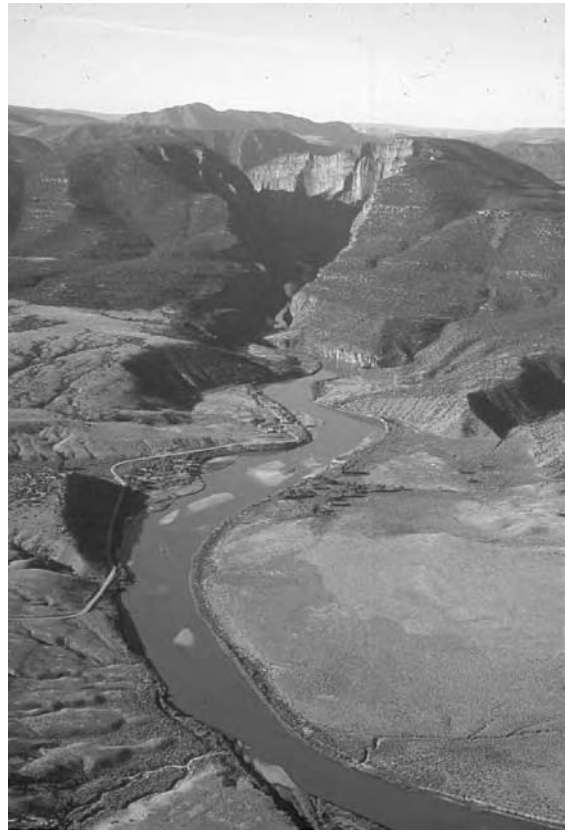

Figure 10.3 Photograph of the Gates of Lodore, where the Green River flows across the eastern Uinta Mountains in northwestern Colorado. Browns Park is in the foreground. View is downstream. (Reproduced with permission from Michael Collier)

Figure 10.4 Photograph of the Green River in Island and Rainbow Parks, Dinosaur National Monument. The view is downstream and the river breaches the anticline of Split Mountain in the distance. (Reproduced with permission from Michael Collier)

Figure 10.5 Photograph of the Green River in the restricted meandering section of the Uinta Basin. Flow is from left to right. Embayments in the lee of sand bars provide nursery habitat for the Colorado pikeminnow and floodplain lakes provide nursery habitat for razorback suckers. (Reproduced with permission from Michael Collier)

Figure 10.6 Photograph of fixed meanders of the Green River in Stillwater Canyon in Canyonlands National Park. Flow is from left to right. (Reproduced with permission from Michael Collier)

Upon leaving Split Mountain, the most downstream of these canyons, the Green River enters the Uinta Basin section of the Colorado Plateau. Here, the Green River flows in a relatively wide alluvial valley (Figure 10.5). Further downstream, the valley narrows in Desolation, Grey, Labyrinth, and Stillwater Canyons, and fixed meanders are common (Figure 10.6). The confluence of the Green and upper Colorado Rivers occurs deep within Canyonlands National Park; the channel banks are bedrock, and there is virtually no alluvial valley (Figure 10.7). For the next 800 km, the Colorado River is confined within a series of narrow canyons: Cataract, Glen, Marble, and Grand (Figure 10.8), before entering the Basin and Range. More than 300 km of lower Cataract and Glen Canyons are now inundated by Lake Powell reservoir, and the most downstream 70 km of Grand Canyon are inundated by the upstream end of Lake Mead reservoir. Grand Canyon

Figure 10.7 Photograph of the confluence of the Green and Colorado Rivers in Canyonlands National Park. The Green River is in the foreground and the upper Colorado River enters from above and right. (Reproduced with permission from Michael Collier)

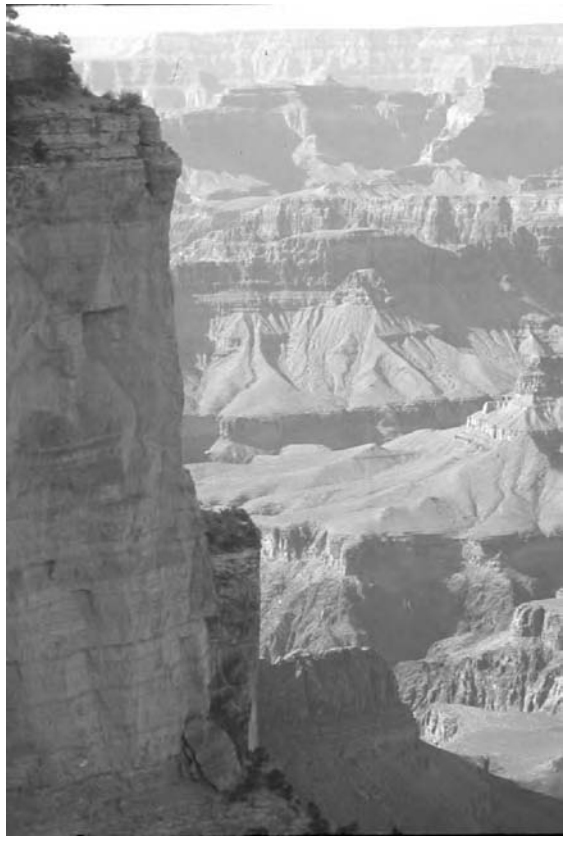

Figure 10.8 Photograph of the Grand Canyon. View is towards the north rim. The Colorado River is in the lower part of the photograph. The ages of bedrock range from 2100 million years old Proterozoic metamorphic and igneous rock at the canyon bottom to 200 million years old Permian sedimentary rocks at the canyon rim

abruptly ends at the fault zone scarp of the Grand Wash Cliffs.

Downstream in the Basin and Range, the Colorado River initially flows to the east for about 130 km across north–south trending mountain ranges and intervening valleys. This segment is now inundated by Lake Mead. Subsequently, the river turns to the south, flows through 60 km long Black Canyon, and enters the Lower Colorado River Trough (Figure 10.9). For about 800 km, the river follows the trend of extensional basins including 180 km of the Great Colorado Valley and crosses a few mountain ranges in short canyons before reaching the head of its delta. Much of this distance is now channelized, confined within levees or inundated by reservoirs and lined by recreational developments and homes. Large pumps in Lake Havasu reservoir divert more than one-third of the river's average flow to aqueducts destined for southern California and central Arizona. At Imperial Dam, most of the remaining flow is diverted to the All American and Yuma Main Canals and only a small base flow continues to Mexico.

The channel is entirely dewatered at Morelos Dam. The next 100 km is intermittent, confined within 6 m high earthen levees, and only receives agricultural and municipal return flows. The Rio Hardy, a former distributary channel of the delta, delivers saline agricultural runoff to the Colorado at the head of the intertidal zone, and the Colorado River is again perennial from this point to the Gulf of California (Figure 10.10).

10.3 AGE OF THE RIVER

> 'To reach the Gulf of California, the river and most of its tributaries must cross many mountains and high plateaus which are structural barriers of resistant rocks. No other river in the Western Hemisphere crosses so many. Not only does the river cross mountain barriers, it must also cross the Colorado Plateau, a tremendous structural block covering more than half the drainage basin; the plateau has been uplifted and tilted northeast against the river.'
>
> (Hunt, 1969)

Geologists have pondered the establishment and evolution of the drainage network for more than a century, and especially focused on the mechanisms and timing of the

Figure 10.9 Photograph of a relatively natural part of the lower river in the the Lower Colorado River Trough, downstream from Ehrenberg, Arizona. Flow is from top to bottom. (Reproduced with permission from Michael Collier)

Figure 10.10 Photograph of the Colorado River where it meets the Gulf of California. (Reproduced with permission from Michael Collier)

various crossings of tectonic structures. Most geomorphic research has been on explaining how the Colorado River established its course across the Grand Canyon section of the Colorado Plateau, which is the highest part of that physiographic region. The Colorado Plateau is composed of a thick sequence of flat-lying and relatively undeformed sedimentary rocks that generally dip to the north, against the course of the river. Metamorphic and igneous rocks are only exposed in a few deep canyons. Basalts occur in scattered areas of volcanism in the southern half of the region.

There have been two fundamentally contrasting views about the age of the river (Hunt, 1969; Lucchitta, 2003). The view held in the mid-twentieth century was that the drainage network was established in the early Tertiary and subsequently evolved as one coherent network (Powell, 1875; Dutton, 1882; Blackwelder, 1934; Longwell, 1936, 1946). The more recent perspective is that parts of the network were established at different times and that the Grand Canyon is among the youngest segments. Although the latter view is now generally accepted, the absolute ages and mechanism of drainage establishment are debated.

The timing of establishment of drainage across the Grand Canyon section is constrained by the youngest non-fluvial deposits in the present Colorado River valley and the oldest fluvial deposits that contain sediments or fossils from the upper basin. Faulting that ultimately created more than 2000 m of structural relief between the Colorado Plateau and Basin and Range began before the Grand Canyon was eroded. Dating of lavas on the western scarp of the Shivwits Plateau indicates that the Grand Wash Cliffs existed in essentially their present form 9.1 mya (million years ago) (Lucchitta and Jeanne, 2001). In contrast, excavation of western Grand Canyon had not begun 6 mya, based on the distribution and basal contact of Shivwits Plateau lavas of that age (Lucchitta and Jeanne, 2001), the distribution of gravels derived from central Arizona that occur north and south from Grand Canyon (Lucchitta and Jeanne, 2001), and the existence of the 6 mya freshwater Hualapai Limestone at the base of the Grand Wash Cliffs (Faulds *et al*., 2001). The sources of water for some the freshwater lakes in which the limestones formed were springs issuing from Colorado Plateau aquifers and/or streams locally draining the Grand Wash Cliffs.

Since there are few preserved fluvial deposits in the erosional landscape of Grand Canyon, most of the evidence about the onset of drainage establishment comes from deposits further downstream. This evidence suggests that the Colorado River cut Grand Canyon beginning 5.6–5 mya. Evidence includes basalts and tuffs interbedded with gravels yielding ages of 5 mya (tuff in the Bouse formation; Spencer *et al*., 2001), 4.7 mya (basalt flows near Grand Wash; Howard *et al*., 2000), 4.4 mya (Sandy Point basalt lava in the southern Grand Wash trough; Faulds *et al*., 2001), and 4.3–5 mya (Imperial Formation in the Salton Trough; Johnson *et al*., 1983). The Bouse Formation consists of an upwardly coarsening sequence of marl, siltstone, cross-bedded sandstone, and gravels that are interpreted to represent the first arrival of the Colorado River into a series of freshwater lakes in the Lower Colorado River Trough (Spencer *et al*., 2001). Marine shells in some Bouse sediments initially led researchers to

believe that the Colorado River first emptied into a proto-Gulf of California that extended much farther north, but it is now thought more plausible that the lower river established its course by a downstream-progressing sequence of lake spillover that integrated originally distinct basins (Spencer and Pearthree, 2001).

There are several hypotheses for the processes whereby the Colorado River established its course to form the Grand Canyon. Earlier researchers suggested antecedence (Powell, 1875) or superposition (Dutton, 1882). Several workers proposed integration of two drainage networks by stream capture of an older upstream channel in the eastern Grand Canyon region by a smaller, steep stream whose headwaters migrated to the east from the Grand Wash Cliffs (McKee *et al*., 1967; McKee and McKee, 1972; Lucchitta, 1972, 2003). Blackwelder (1934) suggested that the Kaibab Plateau was eroded by lake spillover from the east, and Meek and Douglass (2001), Scarborough (2001), and Spencer and Pearthree (2001) have recently found speculative support for this hypothesis.

Hamblin (1994) estimated that incision of Grand Canyon was largely complete by 1.2 mya, but more recent work suggests that downcutting continued later in the Quaternary (Dalrymple and Hamblin, 1998). Estimates of incision rates during the past 500 000 years vary over nearly a sixfold range: between 70 and 140 m my^{-1} (Pederson *et al*., 2002), 120 and 400 m my^{-1} (Davis *et al*., 2001), and 70 and 400 m my^{-1} (Lucchitta *et al*., 2001).

In contrast to the relatively recent age of the Grand Canyon, fluvial sediments in western Colorado and eastern Utah indicate that the general patterns of drainage in the upper basin are much older. Drainage west from the Rocky Mountains, similar to modern drainage directions, created late Oligocene fluvial sedimentary rocks. Lava flows in the Flat Tops north from Glenwood Canyon indicate than an ancestral Colorado River began to carve a broad valley sometime after 20 mya (Kirkham *et al*., 2001).

The river system did not incise at a uniform rate. Variability in estimates of incision rates of the mainstem and its tributaries are partly due to different dating techniques that span different time periods, but the rates differ sufficiently to indicate real variation in time and space. Kirkham *et al*. (2001) estimated that the incision rate of the upper Colorado River into Glenwood Canyon was 24 m my^{-1} between 7.7 and 3 mya, but greatly increased to about 240 m my^{-1} since 3 mya. Incision rates of the Colorado River in the Canyonlands section of the Colorado Plateau are approximately 180–500 m my^{-1} and are as great as 400 m my^{-1} in some tributaries (Hanks *et al*., 2001; Marchetti and Cerling, 2001; Willis and Biek, 2001).

10.4 GRADIENT, VALLEY WIDTH, AND CHANNEL FORM IN THE COLORADO PLATEAU

> 'We are three quarters of a mile in the depths of the earth, and the great river shrinks into insignificance as it dashes its angry waves against the walls and cliffs that rise to the world above. . . . We have an unknown distance yet to run, an unknown river to explore. What falls there are, we know not; what rocks beset the channel, we know not; what walls rise over the river, we know not.'
>
> (Powell, 1875)

The Holocene longitudinal profiles of the Green, upper Colorado, and mainstem include a number of convexities, such as at the upstream ends of Lodore, Desolation, Glenwood, Cataract, and Marble Canyons (Figure 10.11). The relative roles of neotectonics, bedrock hardness, and tributary-derived sediment in causing these convexities is debated. Mackley and Pederson (2004) showed a strong correlation between rock hardness and gradient for Glen, Marble, and Grand Canyons. Karlstrom and Kirby (2004) hypothesized that longitudinal convexities are inherited knickpoints associated with differential uplift.

Although the role of neotectonics and bedrock hardness are debated, the correlation between debris flows and steep gradients of the modern river is very strong. All of the steep segments occur in canyons where debris flows deliver coarse material to the mainstem, supporting the view that convexities occur at the transition from flat-gradient alluvial to steep-gradient debris fan-dominated segments. Leopold (1969) reported that 50% of the total elevation loss of the Colorado River in Grand Canyon, as surveyed in 1923, took place in only 9% of the downstream distance, and Magirl *et al*. (2005) found that 66% of the total drop, as measured in 2000, occurred in the same distance. The importance of debris flows and associated rapids in controlling stream gradient has been demonstrated at several spatial scales: for a single rapid (Kieffer, 1985; Webb *et al*., 1988, 1999), for Grand Canyon (Dolan *et al*., 1978; Graf, 1979; Howard and Dolan, 1981), and for the Green River (Graf, 1979; Grams and Schmidt, 1999; Elliott, 2002). Further evidence of the role of debris flows comes from the fact that the modern river is only in contact with bedrock at a few places. The unconsolidated fill of the Colorado River in Grand Canyon varies between 0 and 45 m, based on hydroacoustic and side-scan sonar surveys, geophysical records, observations of bedrock islands in the channel, and borings at proposed dam sites (Anima *et al*., 1998; Schmidt *et al*., 2004).

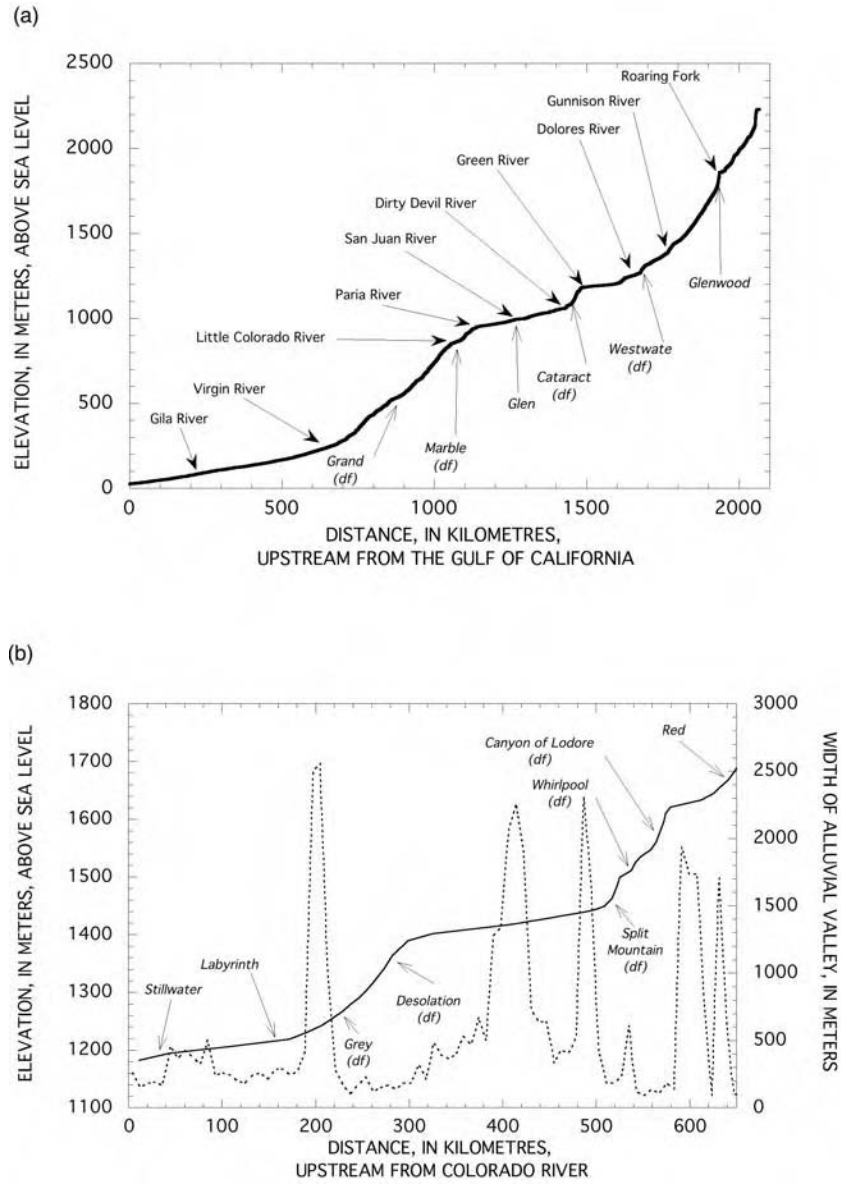

Figure 10.11 Graphs showing (a) longitudinal profile of the Colorado River between the Southern Rocky Mountains and the Gulf of California and (b) the longitudinal profile (solid line) and width of the alluvial valley (dashed line) of the Green River in Colorado and Utah

Although the role of bedrock as a control on gradient is debated for the Colorado River and its largest tributaries, there is a clear relationship between rock strength and width of these alluvial valleys. Narrow valleys occur where the river level rocks are relatively strong, whereas wide alluvial valleys exist where there are weak rocks at river level (Harden, 1990; Grams and Schmidt, 1999; Elliott, 2002; Mackley and Pederson, 2004). Thus, the valley of the Colorado River does not progressively increase in width in the downstream direction. Instead, the sequence in which wide and narrow valleys occur is determined by the sequence of lithologies encountered at river

level which in turn results from the geologic history of the region.

The range of valley widths and the degree to which they affect channel form and gradient leads to three categories of channel/valley conditions – wide valleys, narrow valleys with flat gradients, and narrow valleys with steep gradients. The latter condition occurs in debris fan affected canyons. These three conditions are associated with three general classes of channel form: restricted meanders (*sensu* Ikeda, 1989), fixed meanders (*sensu* Ikeda, 1989), and fan-eddy complexes (Schmidt and Rubin, 1995). In restricted meanders, the channel shape is typically unaffected by bedrock except at the outer margins of the meander belt where the planform and channel cross-section are distorted (Figure 10.5). In fixed meanders, the channel and valley meander wavelength are essentially the same, the valley is relatively narrow, and the channel encounters bedrock at the outside of most bends (Figure 10.6). The channel in restricted and fixed meandering segments includes permanent islands and bank-attached compound bars; permanent islands are rare in fixed meandering reaches. Thalweg and bar substrate is typically sand, although gravel bars occur in some segments. Typically, bank-attached compound bars occur on alternating sides of the river.

In debris fan-affected canyons, coarse debris from steep ephemeral channels partially blocks the mainstem, forming rapids in the narrow, shallow, bouldery channel. Channel organization in debris fan-affected canyons is centred on the fan-eddy complex. These complexes are composed of a sequence, ordered downstream, of: (1) ponded backwater upstream from rapids; (2) rapid; (3) recirculating flow zones immediately downstream where channel cross-section widens; and (4) gravel/cobble bars downstream from the recirculation zones (Figure 10.12).

Figure 10.12 Photograph of a fan-eddy complex in the Green River in Grey Canyon. Flow is from bottom to top. Flow is ponded upstream from the debris fan that constricts the channel. Downstream from the fan, an eddy bar is exposed and this bar was inundated by recirculating flow during the preceding flood. At top right is a mid-channel gravel bar. Reproduced with permission from Michael Collier

10.5 HYDROLOGY: PRE-DAM

> 'All winter long snow falls on its mountain-crested rim, filling the gorges, half burying the forests, and covering the crags and peaks with a mantle woven by the winds from the waves of the sea. When the summer sun comes this snow melts and tumbles down the mountain sides in millions of cascades. A million cascade brooks unite to form a thousand torrent creeks; a thousand torrent creeks unite to form half a hundred rivers beset with cataracts; half a hundred roaring rivers unite to form the Colorado, which rolls, a mad, turbid stream, into the Gulf of California.'
>
> (Powell, 1875)

The Colorado River watershed is customarily divided, scientifically as well as administratively, into the Upper Basin and Lower Basin, with the dividing point occurring immediately downstream from the confluence of the Paria and Colorado Rivers, near Lees Ferry, Arizona (Figure 10.13). This point was defined by the Colorado River Compact of 1922. The Compact was the first inter-state compact negotiated in the United States, and it established regional allocations for consumptive water use by dividing the basin into two parts. The Upper Basin includes the region where runoff originates, and the Lower Basin is the region where water is withdrawn and now consumed in large amounts.

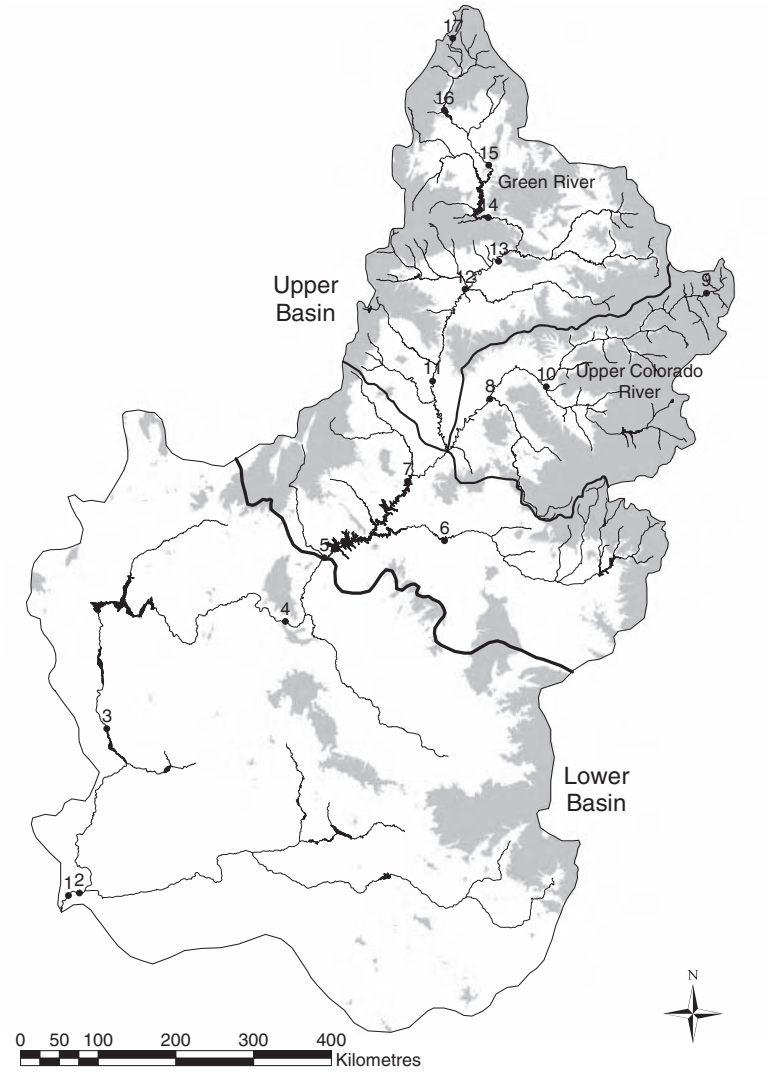

Figure 10.13 Map showing the Colorado River basin, shaded areas higher than 2000 m elevation, and gauging stations referred to in the text. 1, Colorado River at northern international border (NIB). 2, Colorado River at Yuma, AZ. 3, Colorado River at Topock, CA. 4, Colorado River near Grand Canyon, AZ. 5, Colorado River at Lees Ferry, AZ. 6, San Juan River near Bluff, UT. 7, Colorado River at Hite, UT. 8, Colorado River at Cisco, UT. 9, Colorado River at Hot Sulphur Springs, CO. 10, Gunnison River near Grand Junction. 11, Green River at Green River, UT. 12, Green River near Ouray, UT. 13, Green River at Jensen, UT. 14, Green River near Greendale, UT. 15, Green River at Green River, WY. 16, Green River near Fontenelle, WY. 17, Green River at Warren Bridge, near Daniel, WY

Stream-flow measurement in the basin by the US Geological Survey (USGS) began in 1889 with the establishment of a gauge on the Gila River at Buttes, Arizona (LaRue, 1916), and a network of gauges was subsequently created to provide data with which to plan water development. Suspended-sediment measurements were made to help in reservoir design. Iorns *et al*. (1964, 1965) provided a comprehensive compilation of the stream flow and sediment transport data collected in the Upper Basin prior to the construction of large dams.

A hydrographic feature of the basin in common with other rivers that traverse extensive downstream arid regions is the disproportionate role of the mountain headwaters in supplying most of the mainstem flow (Figure 10.14).

Mean annual runoff in the Rocky Mountains is between 300 and 1000 mm (Riggs and Wolman, 1990), and 54% of the total annual mainstem flow past Lees Ferry is already in the stream system in the upstream 15% of the basin, as measured at headwater gauges. Average runoff from these headwater basins is about 200 mm, whereas gauges in the remaining 85% of the Upper Basin have unit runoff less than 50 mm. There are few tributaries that enter the mainstem in the Lower Basin, and historically the Gila River had a modest average flow in relation to Upper Basin tributaries.

Mainstem stream flow is primarily derived from snowmelt. Prior to the construction of large dams, the peak flow typically occurred between late May and late June. Spring melt first began in the central Colorado Plateau and melt occurred later in the middle Rocky Mountains. This pattern is illustrated for water year 1952 in Figure 10.15. The initial rise of the spring flood in 1952 was caused by melting of snow in the central Colorado Plateau. Rise of the Green River's annual flood began in early April, as measured at Ouray and Green River, Utah. Runoff derived

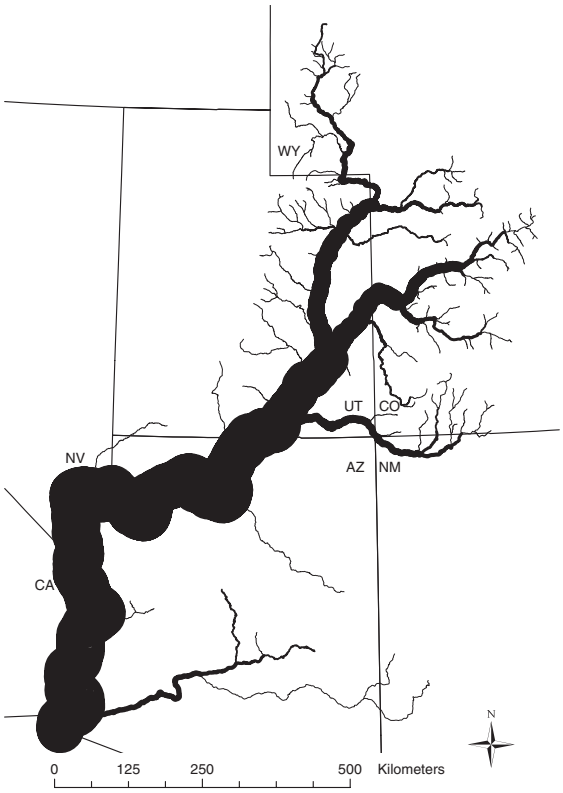

Figure 10.14 Map showing the relative amounts of stream flow in different segments of the pre-dam Colorado River system. The majority of stream flow originated in the Rocky Mountains. The width of river segments is proportional to the widest line segment, which is 510 $m^3 s^{-1}$ at the US – Mexico border. Data compiled from Iorns *et al.* (1964) and gauging records of the US Geological Survey

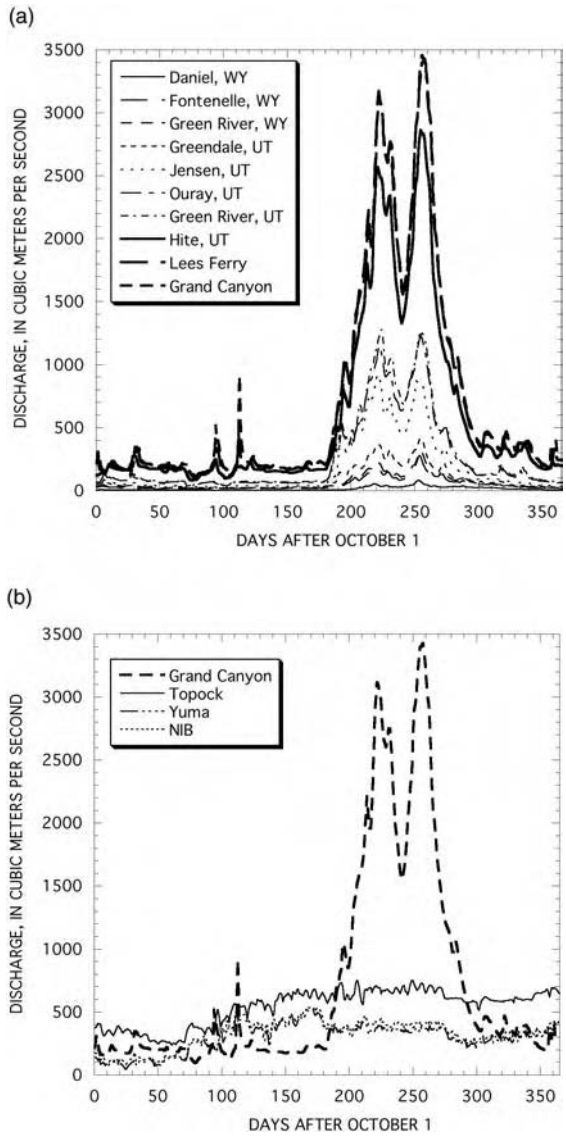

Figure 10.15 Graphs showing downstream changes in stream flow in the Green and Colorado Rivers in 1952. (a) Stations upstream from Lake Mead reservoir. (b) Stations in the Lower Basin. Stream flow at the Grand Canyon gauge is shown in both parts for comparison. Stream flow at Topock, Yuma and the NIB are affected by Hoover and Parker Dams and by diversions. Station locations are shown in Figure 10.13

from snowmelt in the middle Rocky Mountains occurred a month later, as measured at Daniel, Fontenelle, and Green River, Wyoming. Large increments of stream flow were added to the river system at major tributary confluences, as illustrated by the increase between the Greendale and Jensen gauges and the increase between the Green River, Utah, and Hite gauges. The former increase was caused by inflow from the Yampa River and the latter by inflow from the upper Colorado River. Further downstream, stream flow did not increase significantly – flow at Hite, Lees Ferry, and Grand Canyon was nearly the same.

The Colorado River system has experienced times of drought and periods when runoff was high (Figure 10.16). The dendrohydrologic record of the Colorado River at Lees Ferry has been extended back to 762 (Fig. 10.16). The mean annual runoff for the period 1490 to 2005 is estimated between 17.7 and 18.1 $\times$ 10^9 m^3 (Woodhouse *et al*., 2006). This value is less than the 20×10^9 m^3 annual runoff that was measured early in the twentieth century when the Colorado River Compact was negotiated and demonstrates that there is less water available for distribution among the Colorado River basin states than was assumed by Compact negotiators. Severe sustained drought has the potential to greatly reduce stream flow at Lees Ferry and greatly strain the water delivery infrastructure on which municipalities and agriculture depend. The lowest 25-year mean stream flow occurred between 1130 and 1154 and was less than 84% of the observed mean annual flow between 1906 and 2004 (18.5×10^9 m^3) (Meko *et al*., 2007). There is a 10% probability that the true mean of this medieval period drought was as low as 79% of the 20th century mean.

Wet and dry cycles are also evident in the palaeoflood record for Arizona and southern Utah. This record has been extended back in time to 5600 years before present (BP), 10 times further that the dendrohydrologic record (Ely *et al*., 1993). The largest floods in the region occurred at times of cool, moist climate and frequent El Nino events, such as between 4800 and 3600 years BP, around 1000 years BP, and since 500 years BP. O'Conner *et al*. (1994) estimated that the largest mainstem flood during the past 4500 years in the Grand Canyon was approximately 14 000 m^3 s^{-1}, based on dated slack-water sediments and one-dimensional flow modelling near Lees Ferry. The largest measured flood at Lees Ferry occurred in 1921 and was 4810 ± 570 m^3 s^{-1}; a flood of 5950 ± 850 m^3 s^{-1} occurred in 1884, based on measurements of water stage (Topping *et al*., 2003).

Modern stream gauging recorded a shift from the large runoff of the first 25 years of the twentieth century to less runoff in mid-century, as well as a subsequent era of regulated stream flow following dam construction (Figure 10.17a, c, d). The climatically driven shift from early century to mid-century stream flow led to lower magnitude floods of shorter duration and involving less total runoff (Allred and Schmidt, 1999).

Historically, the Colorado River delta was flooded annually between May and July, and flows the rest of the year were much lower. The long-term average flow to the delta was 18.5×10^9 m^3 (Pontius, 1997).

10.6 HYDROLOGY: POST-DAM

> 'Yesterday the Colorado River was a natural menace. Unharnessed it tore through deserts, flooded fields, and ravaged villages. It drained the water from the mountains and plains, rushed it through sun-baked thirsty lands, and dumped it into the Pacific Ocean – a

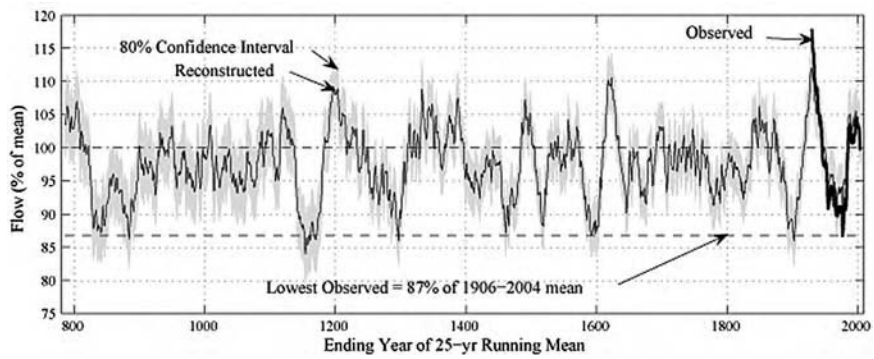

Figure 10.16 Graph showing time series of 25-year running mean of reconstructed flows at Lees Ferry, Arizona, plotted as a percentage of the mean of observed flows for the period 1906–2004 (18.53×10^9 m^3). Horizontal dashed line is lowest 25-year running mean of observed flows, which is the period 1953–1977. Figure is from Meko *et al*. (2007) and reproduced with permission of the authors

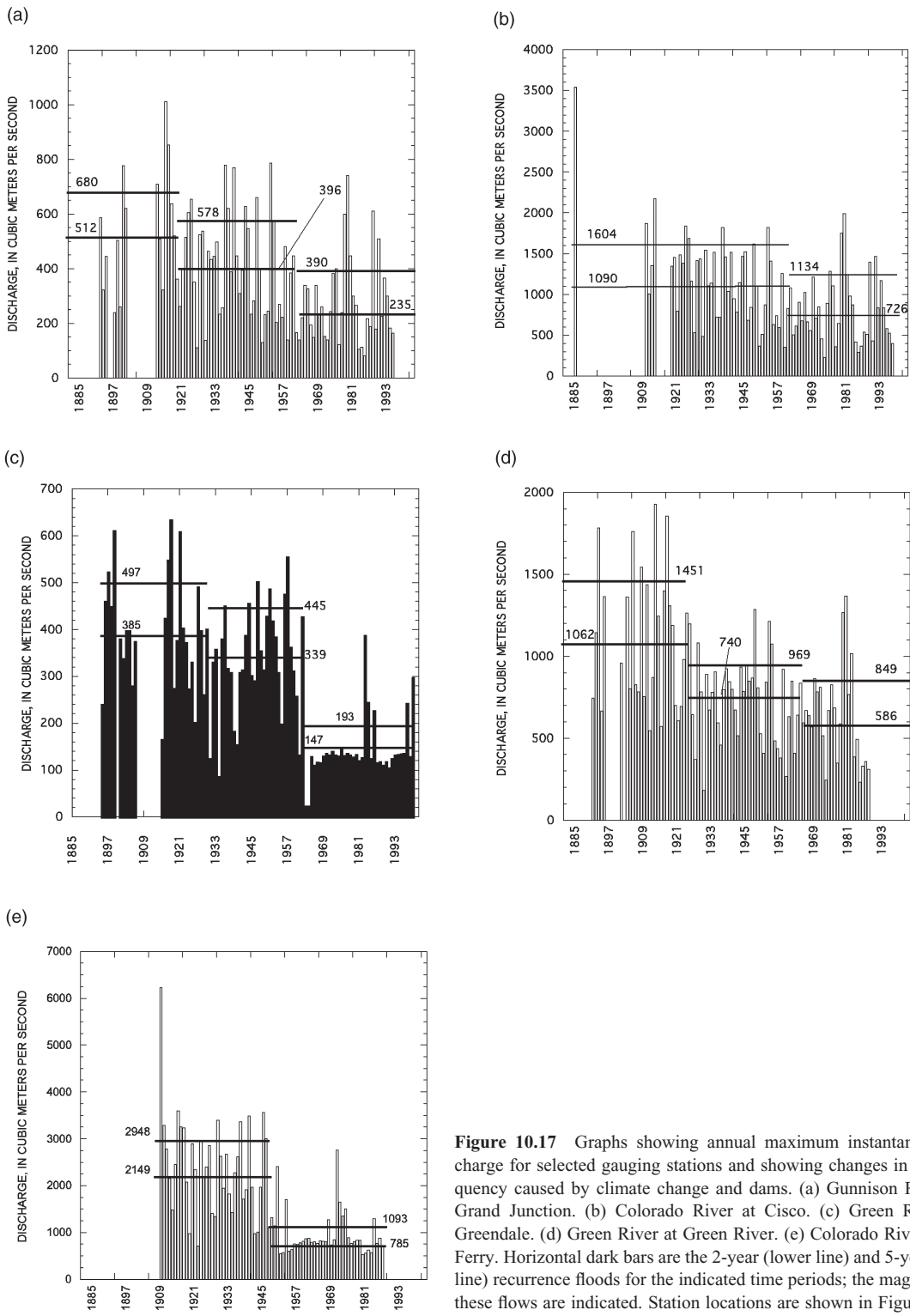

Figure 10.17 Graphs showing annual maximum instantaneous discharge for selected gauging stations and showing changes in flood frequency caused by climate change and dams. (a) Gunnison River near Grand Junction. (b) Colorado River at Cisco. (c) Green River near Greendale. (d) Green River at Green River. (e) Colorado River at Lees Ferry. Horizontal dark bars are the 2-year (lower line) and 5-year (upper line) recurrence floods for the indicated time periods; the magnitudes of these flows are indicated. Station locations are shown in Figure 10.13

> treasure lost forever. Man was on the defensive. He sat helplessly by to watch the Colorado River waste itself, or attempted in vain to halt its destruction. Today this mighty river is recognized as a national resource. It is a life giver, a power producer, a great constructive force.'
>
> (US Department of the Interior, 1946)

The transformation of the natural flow regime caused by reservoirs and diversions is profound (Figure 10.18). The total volume of reservoir storage is now $114 \times 10^9\,m^3$ (92.8×10^6 ac-ft), which is nearly seven times the long-term mean annual flow at Lees Ferry (Figure 10.19). Total basin consumptive uses have increased from about $4 \times 10^9\,m^3$ (4×10^6 ac-ft) to about $15 \times 10^9\,m^3$ (12×10^6 ac-ft), about 90% of the long-term average annual flow at Yuma. Upper Basin consumptive uses are about $5 \times 10^9\,m^3$ (4×10^6 ac-ft), or about 30% of the long-term average annual flow at Lees Ferry (Table 10.2).

10.6.1 Upper Basin

Major construction of dams in the Upper Basin began in the 1950s. Total basin reservoir storage increased dramatically in 1963 when the CRSP was completed (Table 10.1). The magnitude of hydrologic alteration is much less than in the Lower Basin. Total reservoir storage upstream from Lake Powell is 1.8 times the mean annual flow at Lees Ferry, and there are relatively few segments where flood magnitudes have been dramatically reduced. The only segments in which flood reduction is comparable with the alterations downstream from Glen Canyon or Hoover Dams are the 100 km between Flaming Gorge Dam (Figure 10.17c) and the Yampa River, the San Juan River immediately downstream from Navajo Dam, and smaller streams downstream from large diversions. The latter situation is illustrated by the hydrologic changes of the upper Colorado River at Hot Sulphur Springs, Colorado (Figure 10.20a), downstream from large trans-basin diversions beneath the Continental Divide. Elsewhere and including the mainstem of the upper Colorado River (Figure 10.17b), the magnitude of post-dam flood reduction is 25% or less.

10.6.2 Lower Basin

Regulation of stream flow began earlier in the Lower Basin. The first major storage dam was Theodore Roosevelt Dam on the Salt River, tributary of the Gila River, and was completed in 1911. The hydrology of the lower Colorado River was fundamentally changed by construction of Hoover Dam, when the basin-wide ratio of reservoir storage to flow increased from less than 0.5 to about 2.7. The hydrology was further altered when Glen Canyon Dam was completed. Thereafter, the annual spring flood was greatly decreased (Figures 10.15b and 10.17e) and the magnitude of base flows increased (Figure 10.20f, g, h), because river managers attempt to route all stream flow through power plant turbines and provide high steady base flows to facilitate diversion.

The dramatic nature of these changes is illustrated by the releases from Glen Canyon Dam (Figure 10.21), where dam releases diurnally vary in response to hourly changes in electricity demands that are greatest during the daytime between Monday and Friday. Total dam releases are largest in January and August when demand for electricity for heating and air conditioning, respectively, is greatest.

Stream flows into the delta were first significantly affected by construction of the Alamo diversion at the international border, described below. The greatest change occurred when Hoover Dam was completed. No flows entered the delta between the 1930s and early 1980s when all excess stream flow not committed to diversion was stored in Lakes Mead or Powell. During this 50-year period, the only flows that reached the Gulf of California were irrigation return flows.

During years of average runoff, releases from Hoover Dam occur in volumes that barely fulfill water diversion needs of the Colorado River Aqueduct to southern California, the Central Arizona Project Canal, the All American Canal, other smaller diversions, and treaty commitments. The high discharges occur between March and August, much different than the natural regime (Figure 10.20h). Downstream from the All American Canal (Figure 10.20i), a base flow of about $30\,m^3\,s^{-1}$ is released to Mexico, and there is no semblance of the pre-dam regime. This flow fulfills the requirements of the 1944 Treaty, officially called the *United States – Mexico Treaty on the Utilization of Waters of the Colorado and Tijuana Rivers and of the Rio Grande*. This treaty commits the United States to deliver $1850 \times 10^6\,m^3$ of water each year, of which at least $1678 \times 10^6\,m^3$ is to be delivered at the Northerly International Border (NIB) (Hundley, 1966). The NIB is the line of latitude that separates the states of Baja California and California.

The base flow release to Mexico is entirely diverted at Morelos Dam, a run-of-the-river diversion dam with no effective storage. Stream flow in the 100 km between Morelos Dam and the confluence with the Rio Hardy is intermittent. In years of high basin-wide runoff and full upstream reservoirs, releases from Hoover Dam sometimes exceed those needed for diversion or are in excess of Morelos' diversion capacity, which is $226\,m^3\,s^{-1}$. In such years, stream flow from the United States enters the

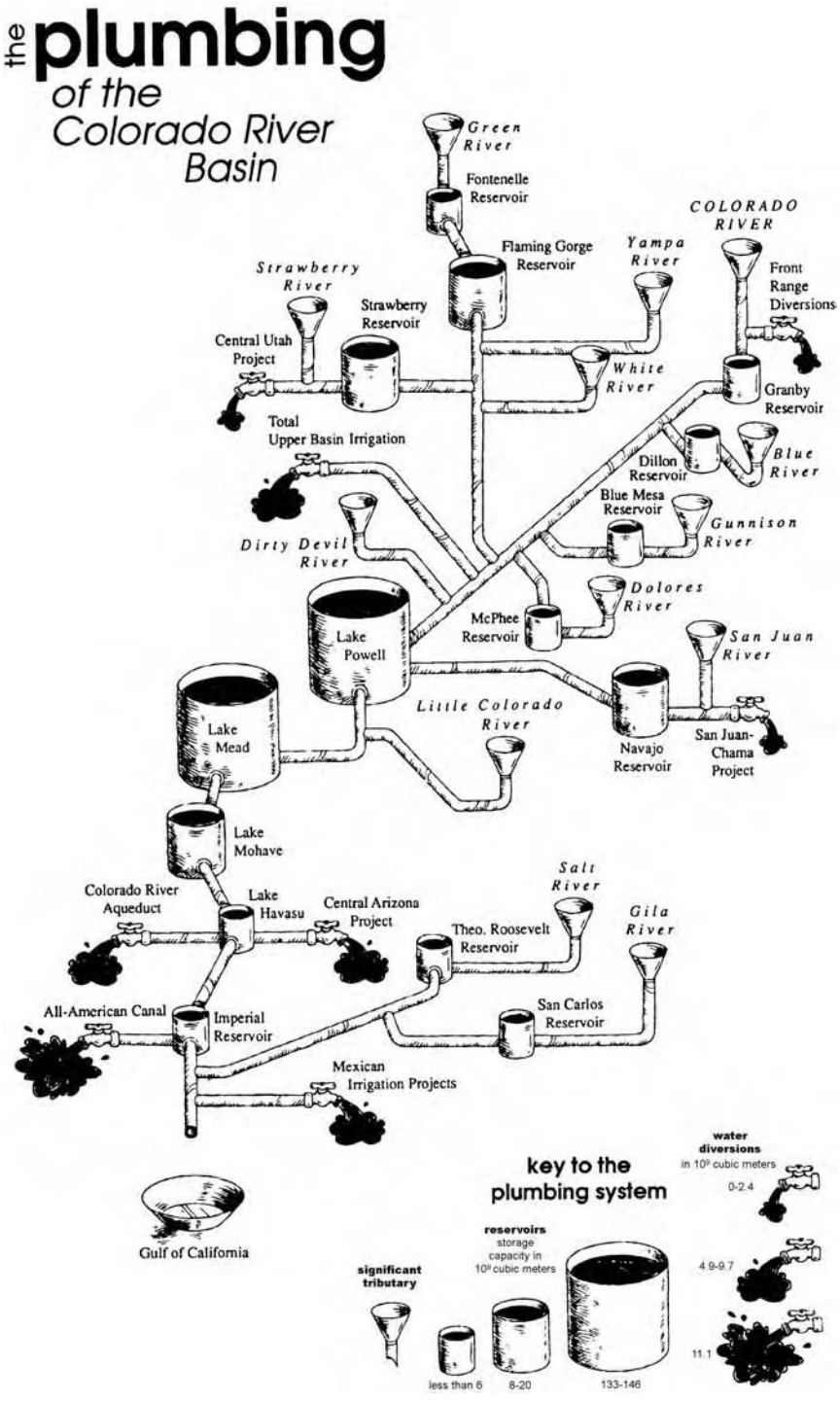

Figure 10.18 Diagram showing distribution of reservoirs and diversions of the Colorado River system, depicted as a plumbing system. (Illustration by L. Dore and C. McKnight, reprinted with permission of High Country News)

delta; such flows occurred five times between 1972 and 2002 (Mueller and Marsh, 2002). Downstream from the Rio Hardy, the Colorado River is again perennial.

10.7 PRE-DAM AND POST-DAM SEDIMENT YIELD AND SEDIMENT TRANSPORT

> 'Before leaving the terraces we may with advantage pause to contemplate the great lesson which lay open to us. The subject of the lesson is EROSION. The geologist, seeing that around a considerable part of the periphery of the Grand Canon district the Eocene and Mesozoic strata suddenly terminate in great cliffs facing the Carboniferous platform, would at once conclude that these strata formerly reached beyond their present boundaries. But how far?. . . . The area of maximum denudation is from 13 000 to 15 000 square miles, and the average thickness of the strata removed from it was about 10 000 feet.'
>
> (Dutton, 1882)

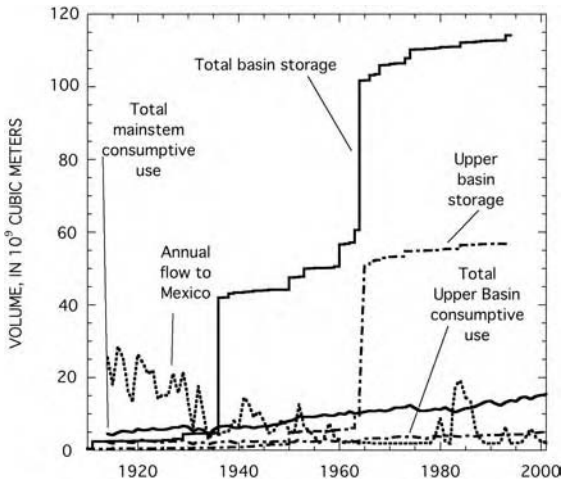

Figure 10.19 Graph showing change in cumulative reservoir storage in the Colorado River basin, the Upper Basin, total basin wide mainstem consumptive use and total Upper Basin consumptive use

The Colorado River delivered about 100×10^6 tonnes $year^{-1}$ of fine sediment to the Gulf of California in the beginning of the eighteenth century, prior to extensive European settlement (Meade *et al*., 1990). Only the Mississippi River delivered more sediment from North America to the sea.

The major source of fine sediment to the Colorado River is the Colorado Plateau, downstream from the river's major source of water in the Rocky Mountains. Thus, the average concentration of fine sediment increases as stream flow moves from the water-producing basin rim to the interior, sediment-producing desert. Of the estimated pre-dam sediment load, approximately 20% came from the upper Colorado River, 27% from the Green River, and 20% from the San Juan River (Figure 10.22). The rest came from watersheds of the southern Colorado Plateau, such as the Dirty Devil, Escalante, Paria, Little Colorado, and Virgin Rivers, even though these streams deliver insignificant amounts of stream flow.

Despite the large sediment loads of the pre-dam Colorado River, the high slope and relatively narrow width of the river was such that transport capacity exceeded supply in many of the canyons (Topping *et al*., 2000). Evidence for this is the hysteresis of the annual transport relation at many

Table 10.2 Legal allocations of the water and actual uses in the Colorado River Basin

	Legal allocation (ha m)	Upper Basin allocation if mean annual flow at Lees Ferry is 1 726 900 ha m[b]	Upper Basin allocation if mean annual flow at Lees Ferry is 1 480 200 ha m[b]	Average consumptive uses and loses, 1981–85[c]	Average consumptive uses and loses, 1986–90[c]
Mexico	185 025			203 770	199 827
Arizona	345 380			131 980	216 730
California	542 740			555 820	612 310
Nevada	37 005			12 580	16 900
Arizona	6 168	6 168	6 168	5 180	4 810
Colorado	51.75%[a]	363 880	235 600	245 960	258 790
New Mexico	11.25%[a]	78 940	51 810	46 500	43 540
Utah	23%[a]	161 590	104 850	81 040	93 380
Wyoming	14%[a]	98 680	64 140	40 950	61 920

[a] Percentage of total Upper Basin allocation, as agreed upon in the Upper Basin Compact of 1948.
[b] MacDonnell *et al*. (1995).
[c] Available at <www.usbr.gov/>.

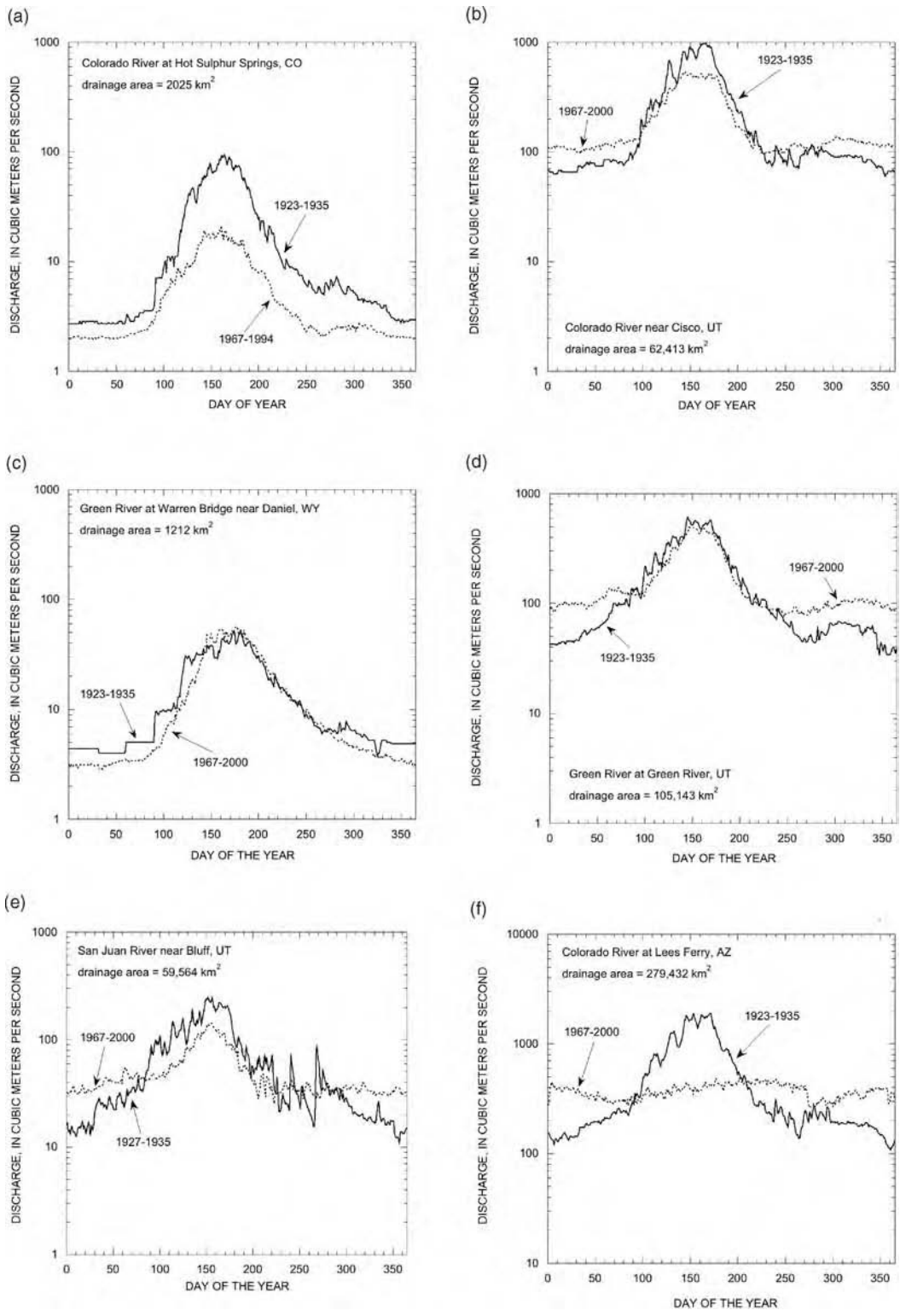

Figure 10.20 Graphs showing median hydrographs of mean daily discharge at selected stations in the Colorado River basin for representative pre-dam and post-dam periods. (a) Colorado River at Hot Sulphur Springs, CO. (b) Colorado River near Cisco, UT. (c) Green River at Warren Bridge near Daniel, WY. (d) Green River at Green River, UT. (e) San Juan River near Bluff, UT. (f) Colorado River at Lees Ferry, AZ. (g) Colorado River near Grand Canyon, AZ. (h) Colorado River near Topock, CA and below Davis Dam. (i) Colorado River at and below Yuma, AZ. Station locations are shown in Figure 10.13

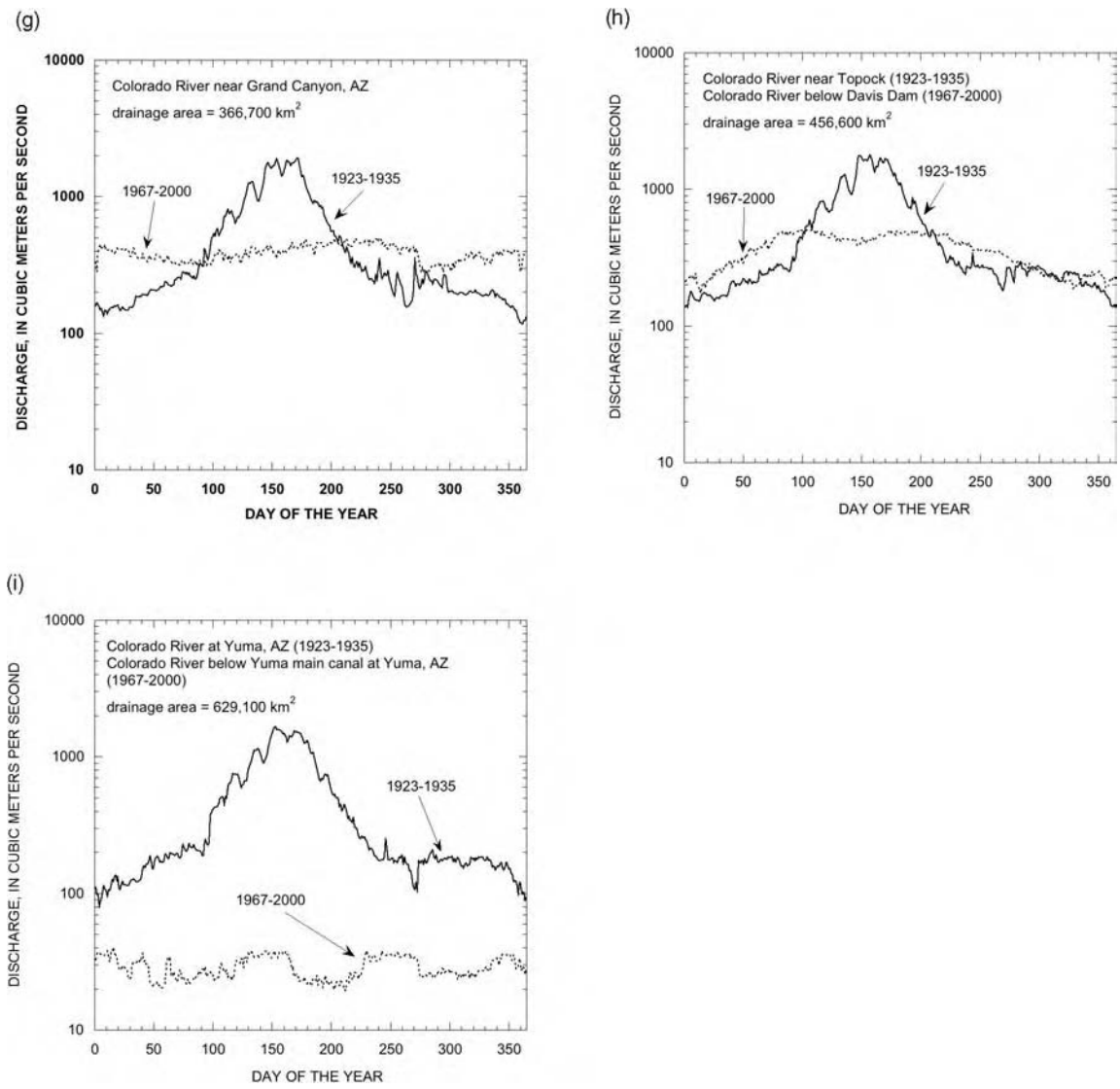

Figure 10.20 *Continued*

gauging stations, where the concentration of suspended sediment is much greater on the rising limb of the annual snowmelt hydrograph than on the falling limb (Figure 10.23). Hysteresis manifests itself also in the sedimentology of flood deposits. Rubin *et al*. (1998) showed that pre-dam, as well as post-dam, Colorado River flood deposits in Grand Canyon typically coarsen upward, because grain size increases as concentration and supply decrease.

The large reservoirs of the Colorado River basin trap the entire upstream sediment load. Releases from every large dam have no sediment, and suspended sediment loads only increase downstream where tributaries supply sediment to the regulated rivers. Annual sediment loads at Topock, located about 60 km downstream from Hoover Dam, decreased to about 10×10^6 Mg year^{-1} after completion of Hoover Dam (Figure 10.24). Completion of Glen Canyon Dam caused a decrease of about 99.5% in the amount of fine sediment entering Grand Canyon and the annual load past the Grand Canyon gauge decreased 81 to 85% (Topping *et al*., 2000). Today, sediment delivery to the delta is essentially zero.

River segments with drastically decreased sediment supply are much shorter in the Upper Basin than in the Lower Basin, because there are many undammed

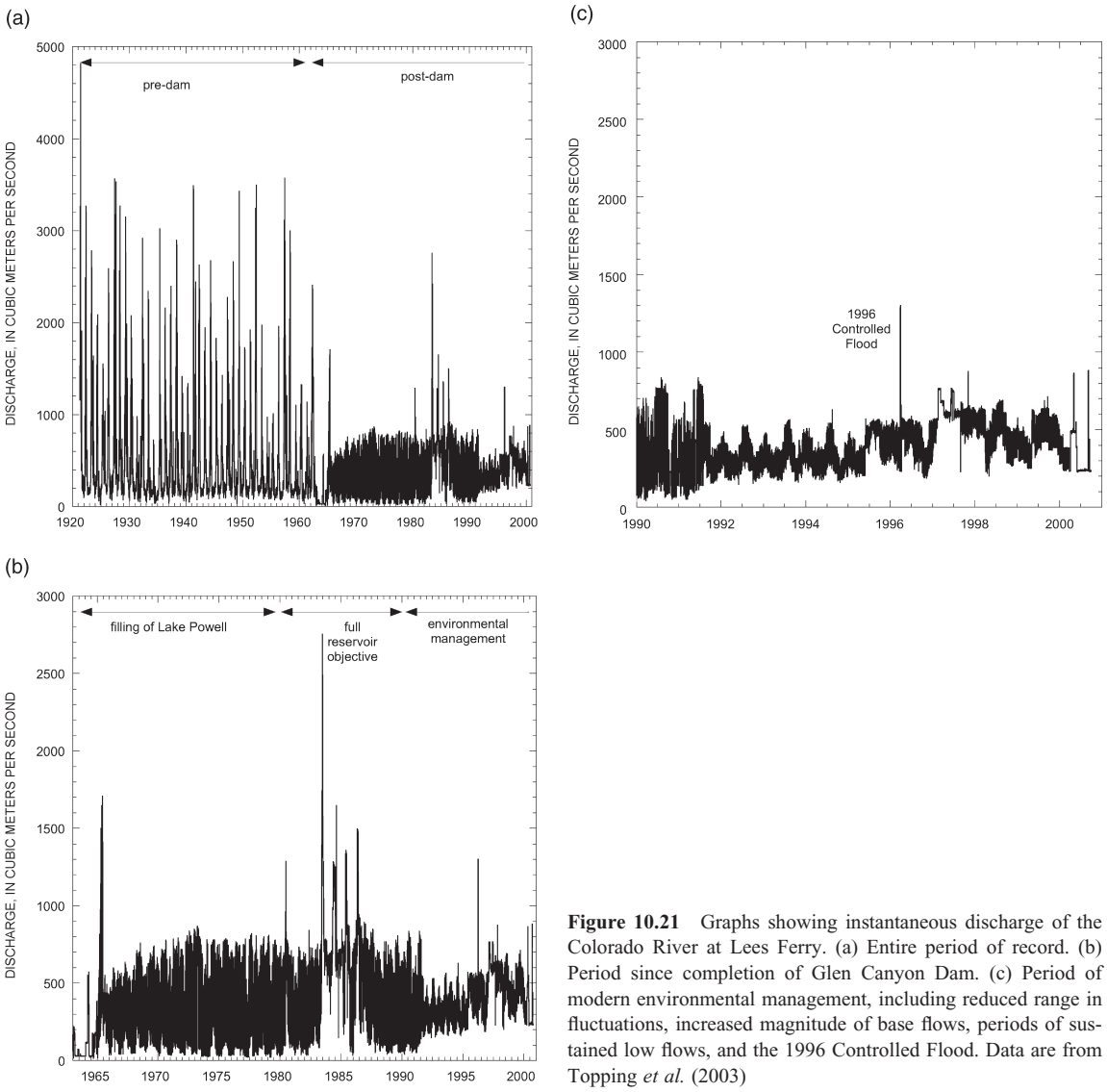

Figure 10.21 Graphs showing instantaneous discharge of the Colorado River at Lees Ferry. (a) Entire period of record. (b) Period since completion of Glen Canyon Dam. (c) Period of modern environmental management, including reduced range in fluctuations, increased magnitude of base flows, periods of sustained low flows, and the 1996 Controlled Flood. Data are from Topping *et al.* (2003)

tributaries that enter the upper Colorado, Green, and San Juan Rivers. For example, unregulated tributaries of the Green River downstream from Flaming Gorge Dam deliver sufficient sediment to the river such that the mean annual load at Jensen has only decreased by about 50% and the load at Green River, Utah, has decreased by between 35 and 50%. Annual sediment load of the upper Colorado River at Cisco decreased by about 20%, because most of the dams in the upper Colorado River basin are small and are in the headwaters, upstream from sediment sources.

10.8 CHANNEL ADJUSTMENT AND CHANGE DURING THE TWENTIETH CENTURY

> 'My plans depended on the state of the main Colorado below Morelos Dam. If it still flowed, I'd keep rafting south. But if, as seemed likely, the river petered out, I had three options: attempt to raft the Rio Hardy through the irrigation system; walk to the sea along the delta's eastern edge; or walk in or near the old and mostly dry riverbed . . .'
>
> (Fletcher, 1997)

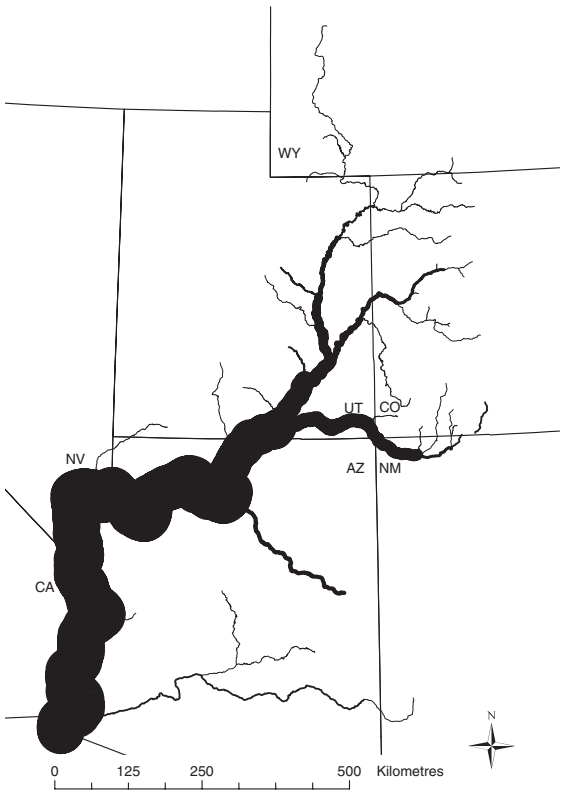

Figure 10.22 Map showing the relative amounts of suspended sediment in transport in the pre-dam river system. These data are the estimates of Iorns *et al.* (1965) for the period 1937–1955 and USGS gauging stations for the lower river for the same period. The width of river segments is proportional to the widest line segment, which is 15.3×10^6 metric t year^{-1} for the lower river

Given the magnitude of change in the water and sediment flux, it is not surprising that the channels of the Colorado River system are very different today than they were at the turn of the twentieth century. The mainstem and its large Upper Basin tributaries can be approximately divided between the completely transformed section downstream from Hoover Dam and the generally 'wild' section upstream (Figure 10.25). The wild condition of the Upper Basin largely results from the long, inaccessible canyons and relatively few people who live along the river. The largest city in the Upper Basin, Grand Junction, only had a population of 42 000 in 2000. The exceptions to the wild condition of the Upper Basin are where river segments have been transformed to reservoir or where there are short reaches in wide valleys that are channelized or have levees. In contrast, the lower Colorado River has been extensively channelized, dredged, and has levees. The delta has been completely altered, and the Salton Trough has been transformed into the Salton Sea and the irrigated fields of the Imperial and Mexicali Valleys.

10.8.1 The Delta

Historically, the delta encompassed approximately 7700 km^2 (Luecke *et al*., 1999). Descriptions of the region at the beginning of the twentieth century record tremendous biodiversity and abundance:

> '. . . a vast gallery forest of cottonwood (*Populus fremontii*) and willow (*Salix gooddingii*) in the north, interspersed with wetlands containing cattail (*Typha domengensis*) and common reed (*Phragmites australis*) in low areas and mesquite (*Prospis glandulosa and P. pubescens*) bosques on higher terraces. Large expanses of salt tolerant vegetation such as salt bush (*Atriplex spp*.), salt grass (*Distichlis spicata*), and arrowweed (*Pluchea sericea*) were found throughout the delta. . . . The endemic salt grass, *D. palmeri*, dominated the estuarine zone. Beaver, jaguars and deer were still found in the delta when Leopold visited [in the 1920s].'
>
> (Glenn *et al*., 2001)

The distributary channels of the delta created a virtual maze.

> 'The channel is circuitous. . . . Slues branch in every direction, and many of them might mislead a person unacquainted with the localities. . . . The water is perfectly fresh, of a dark red color, and opaque from the quantity of mud held in suspension. The width of this portion of the river varies from one-eighth to half a mile. The course is exceedingly tortuous. The depth of the channel is from eight to twenty feet, but bars are frequently encountered where there are not more than two feet of water.'
>
> (Ives, 1861)

Channels changed course frequently.

> 'The shifting of the channel, the banks, the islands, the bars is so continual and so rapid that a detailed description, derived from the experiences of one trip, would be found incorrect, not only during the subsequent year, but perhaps in the course of a week, or even a day.'
>
> (Ives, 1861)

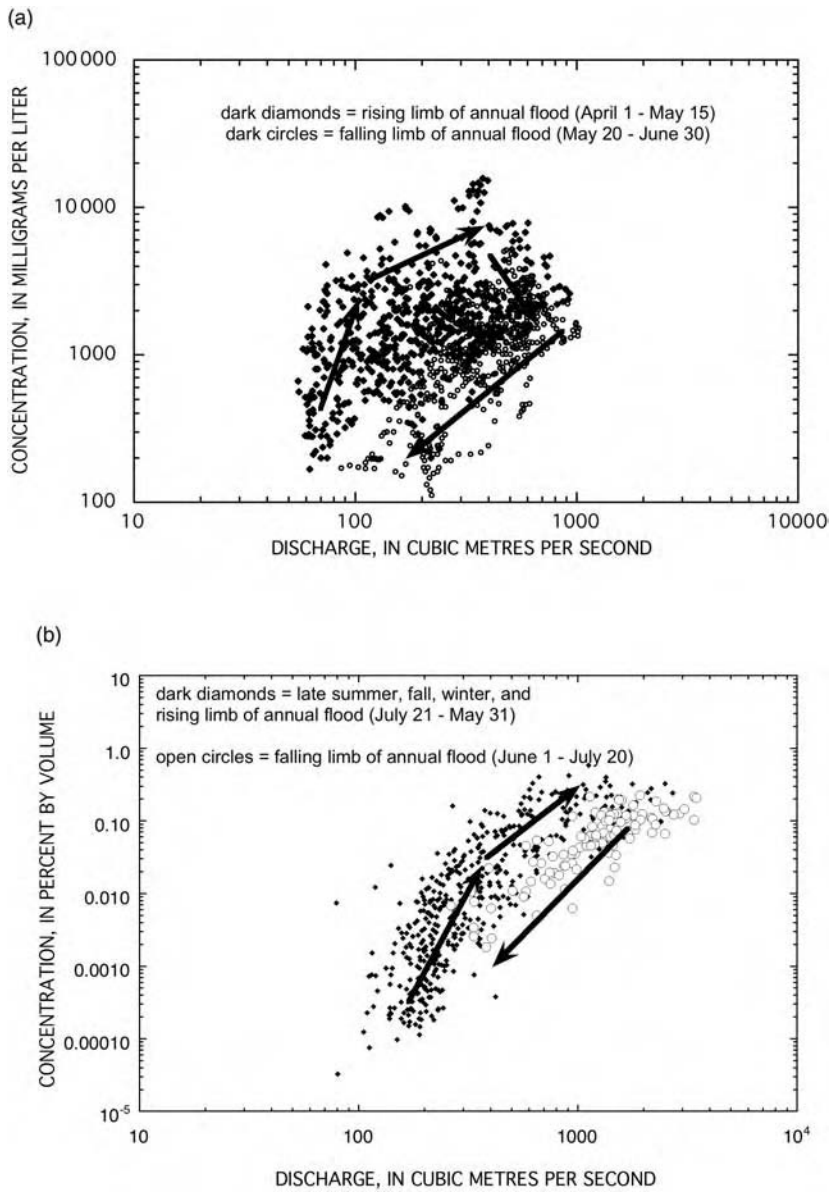

Figure10.23 Graphs showing hysteresis in sediment transport relations (a) in the Green River at Jensen (Grams and Schmidt, 2002) and (b) in the Colorado River near Grand Canyon (Topping *et al.*, 2000). In each case, concentrations are higher on the ascending limb of the annual flood. Arrows indicate generalized hysteresis pattern. [(a) Reprinted from Geomorphology, Vol. 44, Schmidt, J.C., Grams, P.E., Streamflow regulation and multilevel flood plain formation: channel narrowing on the aggrading Green River in the eastern Uinta Mountains, Colorado and Utah, pp. 337–360, 2002, with permission from Elsevier]

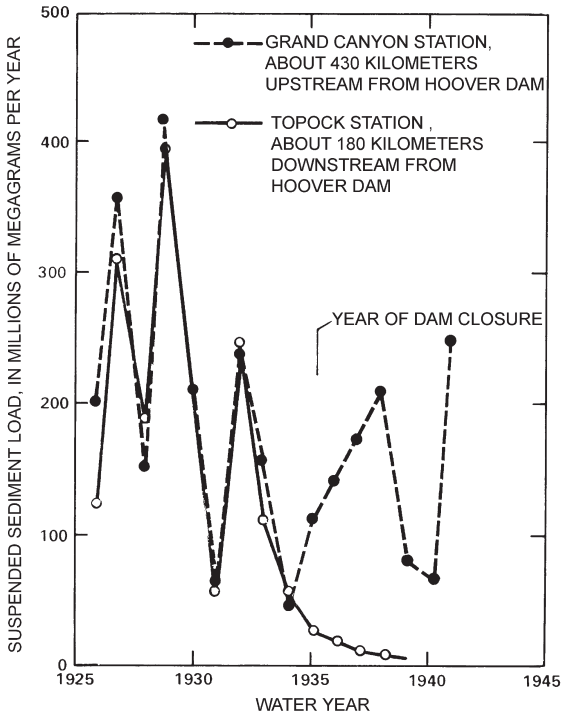

Figure 10.24 Graph showing variation in annual suspended-sediment loads before and after closure of Hoover Dam at a station upstream from the dam (Grand Canyon) and downstream from the dam (Topock). (From Williams and Wolman, 1984, Figure 2. Courtesy of the United States Geological Survey)

Today, the delta is a very different place. Between Morelos Dam and the Rio Hardy, the river is confined within levees, and the delta's extent is about 600 km^2, less than a tenth of its former area (Luecke *et al*., 1999). In the northern part of the delta, the area beyond the levees is mostly irrigated farm fields or cities. All of the flow in normal runoff years is diverted, but some irrigation return flow and municipal effluent enters the channel (Cohen *et al*., 2001). Vegetation is dominated by salt cedar (*Tamarix ramosissima*), but there are cohorts of native trees that were established in the years of surplus runoff.

The Rio Hardy is perennial due to agricultural return flows. The confluence of the Rio Hardy with the Colorado also marks the approximate northern limit of the intertidal zone, and the channel downstream from this point is perennial. Tides at the north end of the Gulf of California are as large as 8 m. The distance between the levees widens towards the sea, and there are numerous, braided channels. Most of the vegetation here is a vast monoculture of salt cedar thickets, with denser stands near the river channels.

The downstream intertidal zones are dominated by salt grass or cattails. Part of the east bank of this zone includes the Cienega de Santa Clara, the largest cattail marsh in the Sonoran Desert. This marsh is primarily maintained by agricultural waste water from the Welton-Mohawk Irrigation District in Arizona via the main outlet drain extension canal.

The marine part of the delta received almost no freshwater between 1935 and 1981, and salinities are now typically between 35 and 45% in years of average basin-wide runoff (Alvarez Borrego *et al*., 1975, cited by Glenn *et al*., 2001b). Increased salinity reversed the circulation in the northern part of the Gulf of California (Lavin and Sanchez, 1999). When less dense pre-dam stream flow entered the estuary, it remained on the surface of the Gulf and induced a northward bottom flow of denser, more saline marine water. Carbajal *et al*. (1997) estimated that the freshwater mixing zone extended 60 km south from the river's mouth. Today, estuarine circulation is driven by evaporation of marine water at the river mouth that generates dense, saline bottom flow to the south, the reverse direction of that which had previously occurred.

No fine sediment is delivered to the modern delta, and waves and strong tidal currents are eroding the older beach deposits (Carriquiry and Sanchez, 1999). Erosion of sands and muds has left shell-rich chenier beach deposits that are more than 40 km long along the western edge of the delta (Kowalewski and Flessa, 1995).

10.8.2 The Imperial Valley and Salton Sea

The 160 km passage west from Yuma Crossing to the next reliable water source at the base of the Vallecitos Mountains was the most difficult part of the overland Southern Emigrant Route to California (deBuys, 1999). Nevertheless, pioneers and explorers of that time deduced what was already known in the oral history of the resident Indian tribes – that the depression of the Salton Sink was below sea level and occasionally had been filled by a lake. Blake (1857) reported that a Cahuilla Indian:

> '. . . chief gave an account of a tradition they have of a great water which covered the whole valley and was filled with fine fish. There was also plenty of geese and ducks. Their fathers lived in the mountains and used to come down to the lake to fish and hunt. The

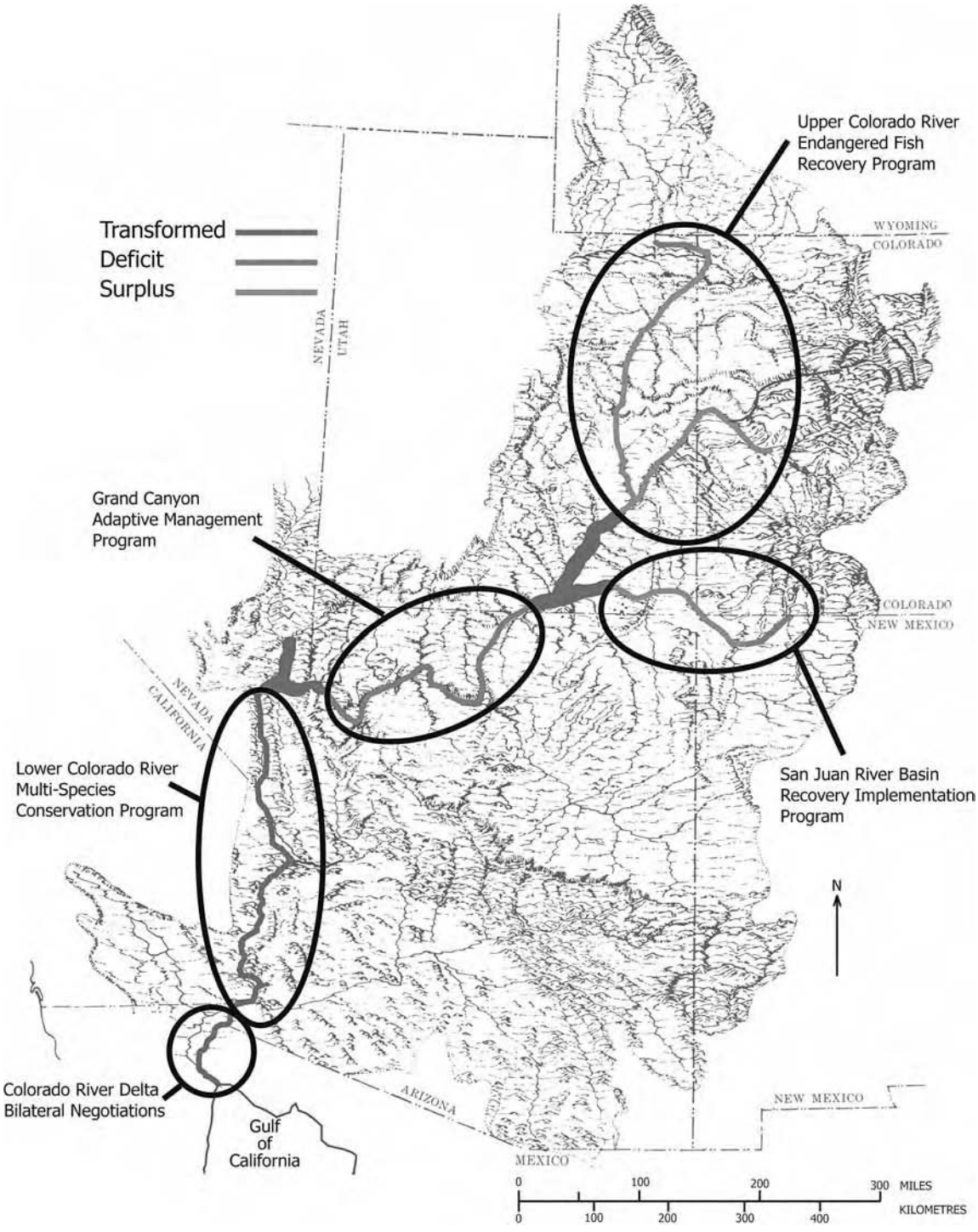

Figure 10.25 Map showing the style of channel adjustment of major streams of the Colorado River basin. Map also shows areas of concern of various river management programs. The lower river, labelled as transformed, includes several reservoirs, channelized reaches, and relatively short naturalized reaches that are typically in sediment deficit. Note the long length of the sediment deficit segment in Grand Canyon. See text for explanation and data sources. Background block diagram is from Hunt (1969)

> water gradually subsided '*poco*,' '*poco*,' (little by little), and their villages were moved down the mountains, into the valley it had left. They also said that the waters once returned very suddenly and overwhelmed many of the people and drove the rest back to the mountains. . . .'
>
> (Blake, 1857, p. 98)

Geological and archaeological evidence supports the legend; discoloured rocks form a horizontal band of a high water mark, tufa deposits occur below the high water mark, 300- to 1000-year-old fish traps occur below the high water mark, constructed from rocks, and high elevation beach deposits sometimes contain charred remains of fish species endemic to the mainstem of the Colorado River (Mueller and Marsh, 2002). The lake would have been 175 km long and nearly 100 m deep (Wilke, 1980). The lake intermittently occurred in the late 1800s. Emigrants were surprised to find a 100-km-long lake in the Sink in 1862. H. W. Patton confirmed the link between the Colorado River and the Salton Sink by boating from Yuma to the Sink during the flood of 1891 (deBuys, 1999).

The irrigation potential due to the elevation head between the abundant water of the Colorado River and the desert of the Salton Sink was apparent to the earliest observers (Blake, 1857). Construction of a diversion into the Salton Sink was completed in 1902, setting off an influx of settlement to the renamed Imperial Valley. The diversion point was originally immediately north from the NIB but was subsequently moved south from the NIB to alleviate sedimentation and political problems. The Alamo, or Imperial, Canal routed water into the abandoned delta distributary channel that Patton had floated a few years earlier – the Alamo River. In 1905, the Colorado River broke through the diversion, and most of the river flowed unimpeded into the Salton Sink until 1907, thereby forming the Salton Sea.

The All American Canal was consrtructed in the 1930s and began delivering water to the Imperial Valley in 1941 from a diversion point at Imperial Dam. The canal was built in response to flood, siltation, political, and management problems with the Alamo Canal and is entirely within the United States.

Although initial expectations were that the Salton Sea would eventually evaporate, irrigation return flow and municipal waste has maintained the lake to the present. In response, the submerged parts of the Salton Sink were permanently set aside as a drainage reservoir (deBuys, 1999). The fishery and wildlife that were stocked or took advantage of this reservoir have evolved with ever increasing salinity and pollution levels.

10.8.3 The Lower River

The earliest human use of the lower Colorado River and of the Gila River has been documented to about 1000 AD in canals unearthed in the construction of modern Phoenix and surrounding communities of central Arizona. This irrigation system included small storage reservoirs and hundreds of kilometres of canals that probably represent the largest area in North America irrigated prior to European contact (Mueller and Marsh, 2002).

Quechan Indians lived along the Colorado River near Yuma Crossing, and extensively farmed the floodplain and terraces. In years of drought, they are known to have carried water to their crops with clay pots, but these people did not practice irrigation in any other form (deBuys, 1999). Fort Yuma was established in 1851, and it was initially supplied by sternwheel steamboats that carried freight that had been transferred to them from ocean vessels that anchored at Port Isabella, at the head of the Gulf of California (deBuys, 1999).

Steamboats plied the entire length of the lower Colorado as far upstream as the Virgin River. Navigation upstream from Yuma was difficult and most easily accomplished at flood stage. At low flow, Hardyville, modern Bullhead City, was the upstream head of navigation. In the canyons, boats were winched over rapids with pulleys. At flood stage, parts of the lower river were more than 3 km wide, but at low flow, the channel was shallow and braided. Steamboat traffic in the delta ceased in 1877 when the transcontinental railroad reached Yuma (Mueller and Marsh, 2002). Traffic between the Yuma railhead and upstream mines and settlements continued until 1909 when 3 m high Laguna Dam, immediately upstream from Yuma, was completed.

Completion of Hoover Dam transformed about 150 km of the Colorado River into reservoir. Subsequent construction of other dams (Table 10.1) transformed nearly half the lower Colorado River to reservoir. Much of the remaining river was straightened, dredged, and confined by levees such that it more resembles a canal (Figure 10.26).

Degradation of the bed of the lower Colorado River has been extensive. Maximum degradation was 4.25 m downstream from Parker Dam, 5.65 m downstream from Davis Dam, and 7.45 m downstream from Hoover Dam in 1975 (Williams and Wolman, 1984). Bed degradation has disconnected the river from its former floodplain, and wetlands and riparian forests only occur where they are artificially maintained by pumps and levees. Today's river is seldom more than 150 m wide, where it was once more than 3 km wide at flood stage.

Figure 10.26 Aerial photographs showing the Colorado River just downstream from Needles, CA, taken in (a) 1938 and (b) 2000. Arrows indicate the same place in the (a) and (b). [(a) Photograph courtesy of the United States Geological Survey (Mueller and Marsh, 2002)]

10.8.4 The River System within the Colorado Plateau

Dams control the flux of water and sediment of each of the large Upper Basin tributaries where they enter the Colorado Plateau. The main stem Colorado is controlled by Glen Canyon Dam, located just upstream from the head of Marble Canyon. Geomorphic changes in the various river segments are largely determined by the relative degree to which the water and sediment flux are controlled, because direct manipulation of the channel and floodplain is rare.

Channel adjustment in segments where transport capacity exceeds supply

Sediment deficit segments exist immediately downstream from each large dam. The length of each segment varies greatly and depends on (1) the relative reduction of the pre-dam transport capacity, (2) reduction in the pre-dam sediment supply, and (3) location of downstream tributaries that supply the main stem with sediment. The longest sediment deficit segment is downstream from Glen Canyon Dam. Sediment deficit can be measured at least 170 km

downstream (Topping *et al*., 2000), and sediment deficit may exist the entire 400 km downstream to Lake Mead. In contrast, sediment deficit probably does not exist more than 40 km downstream from Flaming Gorge Dam (Grams and Schmidt, 2005).

The relative amount of sediment eroded from the bed and the banks in deficit segments depends on the size of bed material in relation to the post-dam flood regime. Where the bed material is relatively small, such as in fixed meander segments, incision has occurred. Where a significant part of the bed is very coarse, as in debris fan-affected canyons, incision has not occurred but fine sediment has been eroded from recirculation zones.

Bed degradation downstream from Glen Canyon Dam is restricted to the 25 km segment that had a sand and gravel bed prior to dam construction. Here, pools were eroded about 6 m and riffles about 3 m (Grams *et al*., 2007). Water surface elevation at a reference discharge of $150\,m^3\,s^{-1}$ is now about 2.3 m lower near the dam than it was prior to construction, and the gradient has decreased about 25% (Grams *et al*., 2007). The extensive bed degradation removed the original sand bed, and the present bed is established in what had been the underlying gravels (Figure 10.27). Today's channel is somewhat narrower and deeper than the pre-dam channel. Bed incision and reduction in flood magnitude caused abandonment of the former floodplain, and this surface is no longer inundated.

In debris fan-affected segments, there is little evidence for systematic bed degradation under conditions of sediment deficit, such as in Red Canyon downstream from Flaming Gorge Dam (Grams and Schmidt, 2007) or in Marble Canyon (Schmidt *et al*., 2004). Some evidence indicates that the coarse-grained deposits that form rapids are aggrading (Graf, 1980; Webb *et al*., 1999; Magirl *et al*., 2005). Since rapids constitute the hydraulic control on water surface elevation, stage-discharge relations do not change. Bathymetric and bed imaging, as well as estimates of pre-dam sediment storage, indicate that the bed is now depleted of fines and is dominated by gravel and coarse material (Schmidt *et al*., 2004).

Fine sediment has been removed from recirculation zones in Grand Canyon. The area of exposed sand at base flow was approximately 25% smaller in the 1990s than in the pre-dam era, and the thickness of sand irreversibly lost in some recirculation zones exceeds 2 m (Schmidt *et al*., 2004). Loss of sand from recirculation zones is due to wind deflation and fluvial erosion during post-dam base flows. Long-term trends are illustrated by the historical changes at Badger Creek Rapids, 40 km downstream from Glen Canyon Dam, where nearly 2 m of sand has been deflated from a prominent sand bar and other bars have been scoured away (Figure 10.28).

Channel adjustment in segments where capacity is less than supply

Available evidence indicates that parts of the Green River (Andrews, 1986; Grams and Schmidt, 2005) and upper Colorado River (VanSteeter and Pitlick, 1998) are in a

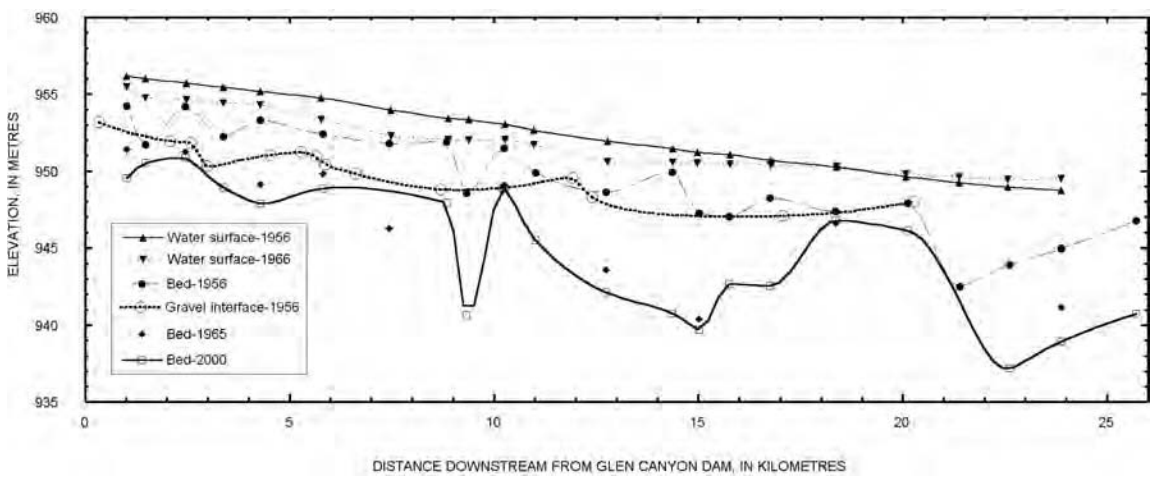

Figure 10.27 Graph showing bed degradation downstream from Glen Canyon Dam. In 1956, the bed had about 2 m of sand overlying gravel, whereas in 2000 bed degradation has scoured the channel entirely into the gravel (Grams *et al*., 2007). (Courtesy of the United States Geological Survey)

Figure 10.28 Photographs of Badger Creek Rapids, taken from the cliffs above the Colorado River. Flow is from right to left. Note the extensive areas of bare sand that have been extensively eroded. (a) Photograph taken by Tad Nichols in July 1956. (b) Photograph taken by R.H. Webb on October 4, 1991. Photographs are from the USGS photo archives of R.H. Webb. The dark circle on both photos is of the same talus block. The elevation of the surrounding sand is approximately 2 m lower in (b)

condition of sediment surplus, and these channels have narrowed and simplified. The Green River is between 10 and 25% narrower than it was at the beginning of the twentieth century, as measured in Browns Park (Grams and Schmidt, 2005), the canyons of the eastern Uinta Mountains (Grams and Schmidt, 2002), in the Uinta Basin (Lyons *et al*., 1992), near Green River, UT (Allred and Schmidt, 1999), and further downstream (Graf, 1978). Similar trends were measured on the Duchesne River in northeastern Utah (Gaeuman *et al.*, 2003, 2005) and on the upper Colorado River downstream from the Gunnison River (Van Steeter and Pitlick, 1998).

Graf (1978) argued that most of the narrowing was due to the invasion of salt cedar, and Andrews (1986) argued that most narrowing was due to the sediment surplus condition induced by Flaming Gorge Dam. Subsequent detailed analysis of gauging station records, aerial photographs, and dendrogeomorphic evidence indicates that about half of the narrowing is due to a combination of climate change and salt cedar invasion at mid-century and half to dam construction (Allred and Schmidt, 1999). In the Canyon of Lodore, eddy bars are now overgrown by salt cedar and have been incorporated into the active floodplain (Figure 10.29). Near Green River, Utah, two inset deposits record the mid-century and post-dam narrowing episodes (Figure 10.30).

10.9 IMPLICATIONS OF HYDROLOGIC, SEDIMENT TRANSPORT, CHANNEL CHANGE, AND TEMPERATURE TO THE ENDEMIC FISHERY

> 'The air was balmy, no wind blew, and a universal quiet prevailed when suddenly Jack uttered several exclamations not entirely in harmony with the moment. He thought his precious hook was caught on a snag. Pulling gently in order not to break his line the snag lifted with it and presently he was astounded to see, not the branch of a tree or a water-logged stick, but the head of an enormous fish appear above the

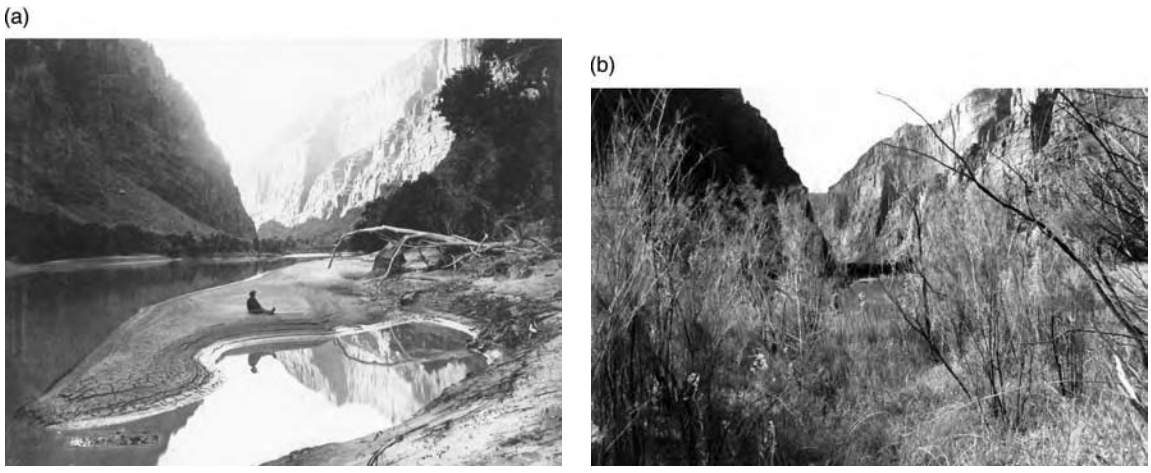

Figure 10.29 Photographs showing channel narrowing caused by aggradation and invasion of riparian vegetation at a sand bar in the Canyon of Lodore, Green River. (a) Photograph taken by E.O. Beaman on June 1, 1871, at river kilometre 78 in the Canyon of Lodore. View is downstream. (b) Repeat photograph taken August 22, 1993. The deep channel that separated the eddy bar from the bank near the large rock is now completely filled (Grams and Schmidt, 2002). (Reprinted from Geomorphology, Vol. 44, Schmidt, J.C., Grams, P.E., Streamflow regulation and multilevel flood plain formation: channel narrowing on the aggrading Green River in the eastern Uinta Mountains, Colorado and Utah, pp. 337–360, 2002, with permission from Elsevier)

> surface. Had there been some splashing he would have been prepared for the extraordinary sight but the monster came with barely a wriggle as if he did not know what it was to be caught. He was successfully landed in the middle cabin of the boat, which was empty except for some water, and lay there unhurt as if it were the natural place for him. Casting again another of the same kind came forth and then a third. The longest appeared to be the length of the cabin, as he floated in the water, and that was four feet. He was at least thirty or thirty-six inches with a circumference of fifteen inches. . . . These fish are now called Colorado River salmon. The flesh was white and they seemed to us good eating.'
>
> (Dellenbaugh, 1908)

The Colorado River basin's native fishery is unique and composed of relatively few species. The watershed has the highest degree of endemism of any large basin in North America; 74% of the native fish species occur there and nowhere else (Miller, 1959). The delta estuary contained more than 75 marine species, but only nine species were native to the lower Colorado River, representing four families of freshwater species and two marine species that frequently invaded the river (Mueller and Marsh, 2002). Fourteen species were native to the Upper Basin.

Four mainstem endemic species are endangered: bonytail (*Gila elegans*), humpback chub (*Gila cypha*), razorback sucker (*Xyrauchen texanus*), and Colorado pikeminnow (*Ptychocheilus lucius*) (Minckley and Deacon, 1991). The bonytail is the largest of the chubs that live in the basin, and was the most common that lived in the main channel. There are few remaining, and little is known about its life history. Humpback chub (Figure 10.31) do not migrate long distances and live as separate populations in debris fan-affected canyons in the basin (Muth *et al.*, 2000). The largest and most stable population is in Grand Canyon, near the confluence of the Colorado and Little Colorado Rivers (Valdez and Ryel, 1997). This uniquely shaped and highly specialized fish has a streamlined, robust body and a pronounced dorsal hump. Upper Basin populations occur in Cataract Canyon of the main stem, Black Rocks and Westwater Canyons of the upper Colorado, Desolation and Grey Canyons of the Green River, and the Yampa Canyon.

Razorback suckers (Figure 10.32) were once distributed between Mexico and Wyoming, and were most abundant in the Lower Basin, including the lower Gila River (Muth *et al.*, 2000). This is the largest and most robust of several suckers that live in the basin, and can weigh up to 8 kg (Marsh and Mueller, 2002). Today, there are a few discrete populations in the Upper Basin, and the largest population

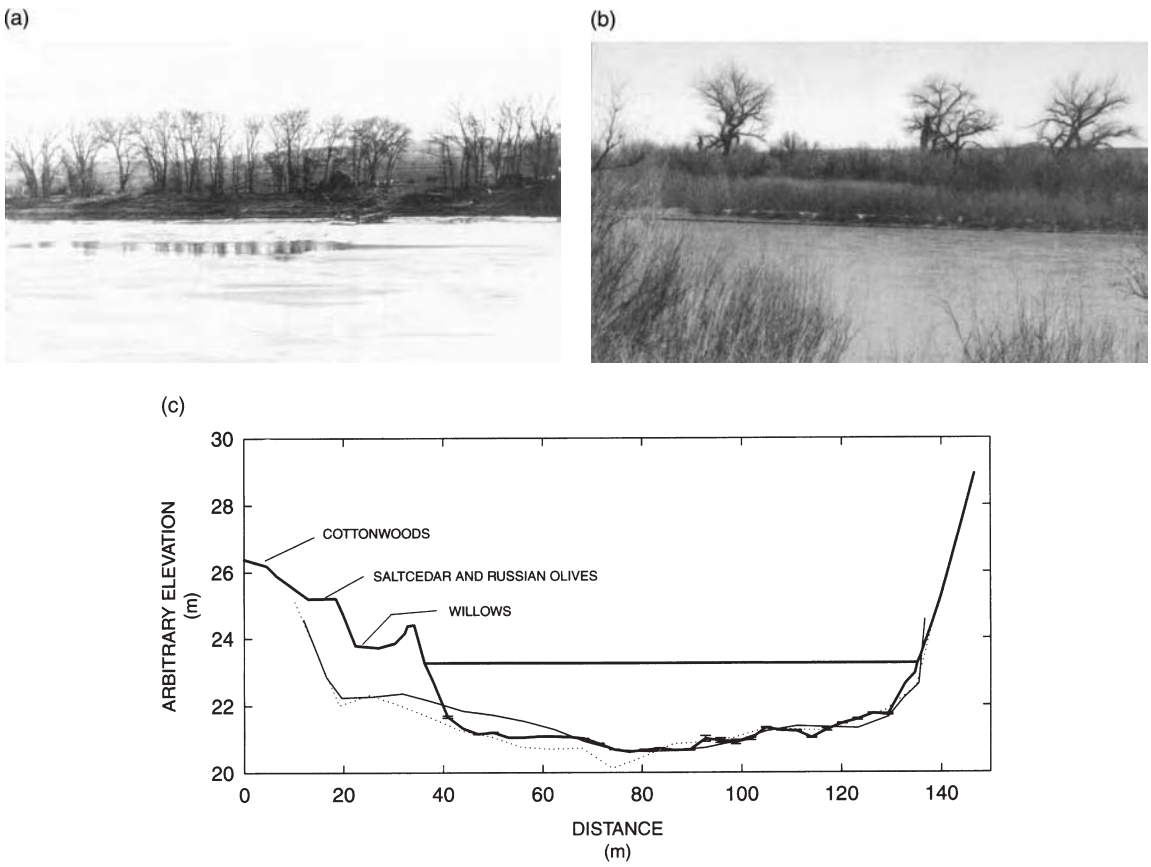

Figure 10.30 Photographs showing channel narrowing of the Green River approximately 9 km downstream from the town of Green River, UT. Matched photographs of the old ferry/cableway: (a) December 5, 1911, photo looking east at ferry/cableway; (b) 1997 match; (c) Cross-section with approximately 6× vertical exaggeration. The thick solid line is the cross-section surveyed in spring 1997, the thin line is from May 1928, and the dotted line is from June 1912, as determined from discharge measurement data. Note that very little change occurred in width between 1912 and 1928. Note that the modern willow and salt cedar floodplain levels are not present in the 1911 photos. [(a) Courtesy of the United States Geological Survey; (b,c) from Allred and Schmidt (1999)]

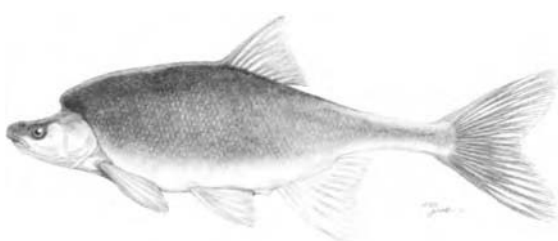

Figure 10.31 Drawing of a humpback chub. (Courtesy of the United States Geological Survey)

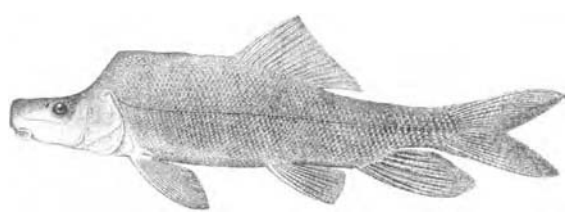

Figure 10.32 Early drawing of a razorback sucker from Jordan (1891). (Courtesy of the United States Geological Survey)

now occurs in the Lower Basin in Lake Mohave Reservoir where there is little or no natural recruitment.

The Colorado pikeminnow (Figure 10.33) is the largest minnow in North America and the top native predator. It was historically abundant in the Lower Basin and delta but was extirpated from these areas. Today, its only viable population is in the Green River (Gilpin, 1993), and there are smaller populations in the upper Colorado and San Juan Rivers. Individuals grew longer than 1 m and weighed as much as 20 kg (Minckley, 1973). Fish longer than 0.8 m or heavier than 10 kg are rarely encountered. The largest of these are probably older than 40 years.

These species are adapted to the wide range of flows, high sediment loads, and geomorphic organization of the pre-development river. Construction of dams throughout the watershed adversely affected the native fishery, because the annual range of flows was reduced, the magnitude of floods decreased, sediment delivery to the channel system was lowered, lentic habitats were converted to reservoirs, spawning and rearing areas were inundated, and passage by migratory species was blocked.

Operations of existing dams have direct effects on the remaining populations of these species. For example, the location and timing of spawning and subsequent larval drift of the Colorado pikeminnow in the Upper Basin are closely tied to the annual hydrologic regime and the distribution of aquatic habitats (Muth *et al.*, 2000). These fish spawn in gravel bars on the descending limb of the annual snowmelt flood in 2- to 3-km meandering reaches of the lower Yampa River, the Green River in Grey Canyon, and the upper Colorado River in Grand Valley. Larvae emerge after less than a week of incubation and passively drift downstream to low-gradient, sand-bedded meandering reaches where bank-attached alternate bars emerge as the annual flood recedes. Low velocity zones occur in the lee of these bars (Figure 10.5), and these backwaters are the nursery habitats for this species in their first year of life. Alterations in the magnitude and rate of recession of the annual flood affect the downstream rate of larval transport and the availability and stability of nursery habitats (Schmidt and Brim Box, 2004).

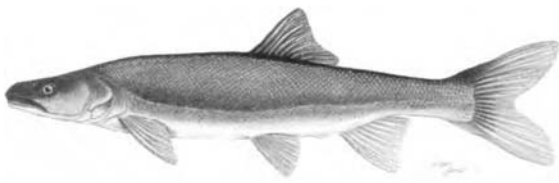

Figure 10.33 Drawing of a Colorado pikeminnow. (Courtesy of the United States Geological Survey)

Razorback suckers are affected by the magnitude of the annual flood and changes in floodplain geomorphology. The species spawns on the ascending limb of the annual flood and its larvae are swept into inundated floodplains that provide nursery and rearing habitat. Disconnection of the channel from its floodplain due to channel incision or flood reduction impede the species' survival.

Dams also change the downstream temperature regime. For example, pre-dam temperatures of the Colorado River in Grand Canyon ranged between 0 and 29 °C. River temperatures no longer vary seasonally but instead are determined by the temperature of the reservoir hypolimnion where water is typically withdrawn into the penstocks that lead to the power plant. In most summers, water temperatures are between 8 and 10 °C in the Grand Canyon ecosystem. Most native species require temperatures exceeding 16 °C for successful spawning, and the consistently cold water released from the dams impedes reproduction (Stanford and Ward, 1989). Thus, long river segments are no longer usable for spawning.

Dams not only affect the native fishery by the direct alterations in hydrology, sediment transport, or changes in habitat, but also by encouraging introduction of non-native warm water centrarchid game species into reservoirs. The existence of constant cold temperatures and gravel bedded streams in sediment deficit segments encouraged introduction of trout. Non-native reservoir warm-water species have moved into rivers and now fill ecological niches similar to those filled by the remaining native species, and non-native cold-water species fill new ecological niches. Some of the non-native species are predatory or compete with native species. In Grand Canyon, mechanical removal of trout that prey on humpback chub began in 2003 near the Little Colorado River confluence.

The increase in salinity in the delta due to near-cessation of freshwater flows has partly contributed to the decline of two marine species – the totoaba (*Totoaba macdonaldi*) and the vaquita, or Gulf of California harbor porpoise (*Phocoena sinus*). The totoaba is a steel-blue fish that grows up to 2 m and 135 kg, supported a commercial fishery until 1975, and is listed as endangered by Mexico. The vaquita is the world's smallest marine mammal and most endangered porpoise; it is listed as endangered by Mexico and is listed as 'critically endangered' by the International Union for the Conservation of Nature (Pitt, 2001). Increasing salinity is thought to have degraded the totoaba's spawning and rearing habitats and affected the vaquita in unknown ways (Glenn *et al.*, 2001b). However, these species are also affected by overfishing, secondary catch in shrimp nets, and poaching.

10.10 ENVIRONMENTAL MANAGEMENT OF THE MODERN RIVER

A number of environmental management programs have been created in response to the social pressures and legal requirements to protect and recover endangered fish or restore attributes of the pre-dam riverine ecosystem (Figure 10.25). The US federal government plays a large role in managing these programs, because they are primarily driven by the need of the federal government to comply with the Endangered Species Act of 1973 (ESA), which prohibits federal agencies from jeopardizing the survival of species. Typically, representatives of the affected state and tribal governments, and some private interests, also participate in these programs. They include the Upper Colorado River Endangered Fish Recovery Program (UCR recovery program), the San Juan River Basin Recovery Implementation Program (SJRIP), the Grand Canyon Adaptive Management Program (GCAMP), and the Lower Colorado River Multi-Species Conservation Program (MSCP).

In each case, program mandates do not include changes in existing agreements concerning water allocation. For example, the SJRIP seeks to:

> '. . . protect and recover endangered fishes in the San Juan River basin while water development proceeds in compliance with all applicable Federal and State laws. . . . Nothing in the Program shall be construed to affect the right to use water under any Federal or state law or permit, Federal contract, treaty, interstate compact or the right of any party in any adjudication proceeding to determine rights to use water or to contract for water.'
>
> (San Juan River Basin Recovery Implementation Program, 2004)

Program mandates in the Upper Basin are also constrained by the CRSP enabling legislation that mandates that these dams exist for the purpose of 'regulating flow . . . , storing water for beneficial consumptive use . . . , control of floods . . . and for the generation of hydroelectric power' (US Chapter 203, Public Law 485) Thus, these species recovery programs are challenged to protect or rehabilitate pre-dam native riverine ecosystems while accommodating the infrastructure and water use patterns that caused ecosystem transformation in the first place.

The focus of the UCR recovery program is protection and recovery of the endangered fishery. The UCR program was established in 1988 and concerns the watersheds of the upper Colorado and Green Rivers. The program was created, because lawsuits to protect the endemic fishery threatened to halt new water projects. The program partners are four agencies of the federal government, the states of Colorado, Utah, and Wyoming, three organizations that advocate for water development, one organization that advocates for hydroelectric power production, and two nongovernmental environmental groups. The program budget between 1989 and 2000 was nearly US$82 million, 88% of which was funded by the federal government (Upper Colorado River Endangered Fish Recovery Program, 2004). Approximately 60% of the budget was spent on quantifying and obtaining in-stream flows or in rehabilitating habitats. Some of these efforts resulted in changes in dam operations to simulate floods, augmentation or stabilization of base flows, reduction of the daily range of hydroelectric peak power production, and improvement of irrigation canal efficiency in order to reduce the magnitude of diversions.

The SJRIP has a similar history and diversity of partners that include four federal agencies, the states of Colorado and New Mexico, and four Indian tribes. The SJRIP was established partly to mitigate adverse impacts of the US$500 million Animas-La Plata project in southwestern Colorado, scheduled for completion in 2009 (Animas La Plata Project, 2004).

The MSCP is a proposed 50-year, US$620 million program that specifically targets protection of six federally listed species (US Bureau of Reclamation Lower Colorado Region, 2004). In contrast to the Upper Basin programs that focus specifically on endangered fish, the MSCP also focuses on endangered or threatened birds, reptiles, and plants. Half of the cost of the program will be paid for by the federal government and half by the states of Arizona, California, and Nevada. One part of the MSCP is creation of 33 km^2 of new riparian, marsh, and aquatic habitat along the 1150 km lower river.

10.10.1 The Glen Canyon Dam Adaptive Management Program

Although not the most costly program in the basin, the GCDAMP is well known by river managers and scientists because of the program's commitment to scientifically based adaptive management. The initial research phase began in 1983 by the Bureau of Reclamation (BoR) in partial settlement of a lawsuit that required more extensive assessment of the environmental effects of the dam. In 1992, the Grand Canyon Protection Act (GCPA) was signed into law, thereby creating the GCDAMP and the Grand Canyon Monitoring and Research Center (GCMRC), which provides monitoring, modelling, and scientific guidance to the GCDAMP. Similar to the other environmental management programs, the GCDAMP includes represen-

tatives of diverse interests, including five federal agencies, the seven signatory states of the Colorado River Compact, five Indian tribes, two environmental organizations, two recreational groups, and the Colorado River Electrical Energy Distribution Association.

The laws that guide the GCDAMP are diverse, because they include the CRSP enabling legislation, ESA requirements, and the mandate of the GCPA. Meeting all of these requirements and mandates may be impossible. The humpback chub is the only remaining endangered fish in Grand Canyon, and recovery of this species is one focus of management. However, the GCPA significantly expands the scope of environmental river management. The GCPA requires that Glen Canyon Dam also be operated so as to 'protect, mitigate adverse impacts to, and improve the values for which Grand Canyon National Park and Glen Canyon National Recreation Area were established, including . . . natural and cultural resources and visitor use.' These provisions thereby give the National Park Service (NPS) an important role in advising BoR on dam operations. Since the mission of the NPS is to 'preserve unimpaired the natural and cultural resources and values . . . for the future enjoyment, education, and inspiration of this and future generations' the goals of the GCDAMP include restoration of a range of ecosystem attributes of the pre-dam river, as well as pursuit of the traditional water development and power production objectives.

The resources that are the subject of these goals include relicts of the pre-dam river and artifacts of post-dam conditions (Schmidt *et al.*, 1998). Pre-dam resources include attributes of the pre-dam riparian and aquatic ecosystem and the flow and sediment transport conditions in which those ecosystems developed. Post-dam resources are those elements of the ecosystem that flourished because of reduced flood magnitude, increased base flows, greatly reduced sediment transport, bed degradation, and colder river temperatures, and include an introduced non-native trout sport fishery. Although some scientific oversight committees have suggested that maintenance and recovery of pre-dam resources ought to be the only guide to environmental river management in Grand Canyon, the GCDAMP has chosen to attempt maximization of pre-dam and post-dam resources.

The 1996 controlled flood

The intentional release of 7 days of a steady 1274 $m^3 s^{-1}$ from Glen Canyon Dam beginning March 26, 1996, was unprecedented in the Colorado River basin. Prior to this event, dam releases in the basin had only exceeded power plant capacity in years of unexpectedly high inflow and full reservoir conditions (Figure 10.21). There were two long-standing objectives for staging an intentional flood: redistribute sand to higher elevations along the channel margin and provide a disturbance to the aquatic and riparian ecosystem (Schmidt *et al.*, 1999). The flood had been planned for the four previous years, but political and management considerations had prevented high dam releases in prior years.

The controlled flood was of short duration and small magnitude in the context of pre-dam flows (Figure 10.21c). The magnitude of the controlled flood was less than the pre-dam 1.25-year recurrence flood for the period 1922 to 1962 (Schmidt *et al.*, 2001). The duration of the controlled flood was short and the difference between flood magnitude and recessional base flow was less than in those pre-dam years when similar magnitude floods occurred. However, the controlled flood was large in relation to post-dam flows. The flood had a recurrence of 5.1 years and was the largest flow since 1986. Although observations of the flood's impact immediately upon flood recession were positive (Collier *et al.*, 1997), subsequent studies showed that geomorphic changes that were of positive resource benefit were short-lived (Schmidt, 1999; Rubin *et al.*, 2002) and biological changes were insignificant (Valdez *et al.*, 1999). However, important scientific insights concerning sediment transport and storage were made that led to significant revision of dam management paradigms (Schmidt, 1999; Rubin *et al.*, 2002). These insights were: (1) the realization of the extreme degree of sediment deficit that exists in the Grand Canyon ecosystem; (2) the relatively fast rate at which fine sediment is transported downstream after it is initially delivered from tributaries; and (3) the role of elevated base flows in transport. The flood remains a benchmark event in the history of river management, however, simply because it occurred.

Between 1996 and 2004, other flow regimes were released from Glen Canyon Dam (Figure 10.21c). The objectives of these flows were to manage the scant fine sediment delivered into Marble and Grand Canyons and to reverse the continued loss of fine-sediment deposits along the channel margin (Rubin *et al.*, 2002). These flows included month-long periods of sustained low flows and small floods less than power plant capacity. In November 2004, a peak flow of 1175 $m^3 s^{-1}$ was released for 60 h. The purpose of the low flows was to restrict fine sediment transport immediately after the delivery of fine sediment from tributaries, and the purpose of the floods was to redistribute this sediment from the channel bed to the banks. None of the flow regimes prior to November 2004 were effective in reversing the loss of fine sediment in the Grand Canyon ecosystem, and the results of the November 2004 flood were not know at the time of this writing.

10.10.2 Opportunities for Recovery of the Delta Ecosystem

By the early 1980s, after a 50-year period when no flow from the United States entered the delta, Fradkin (1981) declared that the Colorado River was, 'A river no more.' The delta had become a vast, barren mudflat. In the mid-1980s, however, occasional floodwaters passed through the delta, sparking ecosystem recovery and the re-establishment of wetlands and riparian areas. Today, there are 600 km^2 of functioning delta that provide habitat for five species considered endangered by Mexico and five species of birds considered threatened. The endangered species are the desert pupfish (*Cypranodon macularius*), Yuma clapper rail (*Rallus longorostris yumanensis*), bobcat (*Felis rufus*), vaquita, and totoaba (Pitt, 2001). The delta is considered a critical link in the Pacific Flyway, utilized by hundreds of thousands of migrating Western Hemisphere birds.

These, and other values, inspired 35 US and Mexican environmental groups to form a coalition that advocates for protection and rehabilitation of the delta (Pitt *et al.*, 2000). The Defenders of Wildlife and 15 other environmental groups filed a lawsuit alleging that the US fails to comply with the ESA by ignoring the impacts of its dams and diversions on delta ecosystems. In 2001, the US and Mexico began a process to consider delta rehabitation by jointly sponsoring the Colorado River Delta Symposium in Mexicali.

Preliminary studies indicate that significant ecosystem recovery might occur if a surprisingly small amount of fresh water input were re-established to the delta. Cohen *et al.* (2001) showed that native trees and marsh plants are supported by agricultural return flows which recharge alluvial aquifers and wetlands. Zamora-Arroyo *et al.* (2001) estimated that a once-in-4-year, 3-month duration spring flow of $3 \times 10^8 m^3$ at 80–120 $m^3 s^{-1}$ is sufficient to establish new cohorts of native trees in the upstream half of the delta. Pitt *et al.* (2000) recommended an additional small perennial flow of $4 \times 10^7 m^3 year^{-1}$. The total of these recommendations is 0.5% of the mean annual for of the Colorado River, yet there is substantial political opposition to these proposals (Pitt, 2001).

10.11 THE FUTURE

The demands on the Colorado River's water and power continue to grow. Population growth and demand for water is increasing in Utah, Colorado, and New Mexico, thereby increasing the demand for trans-basin diversions from the Upper Basin. At the same time, the population of those areas served by Lower Basin diversions increases at a high rate. At present, dams in the Colorado River basin have a combined generating capacity of 4425 MW (Pontius, 1997), and this electricity provides a critical component to the regional supply, especially during high demand periods (Figure 10.34). Efforts to recover species and rehabilitate segments of the river system constrain the ability to produce hydroelectric power and cost money. These efforts may have cumulative impacts on regional power production, and efforts to rehabilitate the delta ecosystem have the potential to affect the quantity of water diverted to Arizona and California. The potential cumulative impacts of species or ecosystem rehabilitation suggest that it is appropriate to compare the costs and benefits of environmental river management in different parts of the basin.

10.11.1 The Delta and Lower River

The lower river and delta have been transformed by flood control at Hoover Dam, large diversions, channelization, levees, and bed degradation. The flow regime of the modern river in no way resembles that of 100 years ago, and the channel at the international border is that of a small stream. Restoration, defined as the return of an ecosystem to its pre-disturbance condition (National Research Council, 1992) is for all intents and purposes impossible, due to the human population and economy pressures of southern California and central and southern Arizona. Thus, rehabilitation of small parts of the Lower Colorado River is probably the only possible objective for environmental river management. This is the modest and appropriate goal of the MSCP.

Efforts to restore the delta ecosystem are in their infancy. For more than 50 years, Mexico and the United States have pledged to protect the delta, but governmental support of necessary research has been nearly absent and no in-stream flows have yet been dedicated to the delta (Pitt, 2001). Drought in the watershed at the beginning of the twenty-first century heightened focus on full utilization of stream flow for off-stream uses. Proposals to invest any water for recovery of the delta remain controversial and speculative, at best.

10.11.2 The Grand Canyon Ecosystem

The Grand Canyon segment of the Colorado River is a crucible for resolving competing needs among relict riverine resources, artifact riverine resources, and utilitarian demands for hydropower and water supply. The requirements of the Colorado River Compact dictate a minimum transfer of water from Lake Powell to Lake Mead each

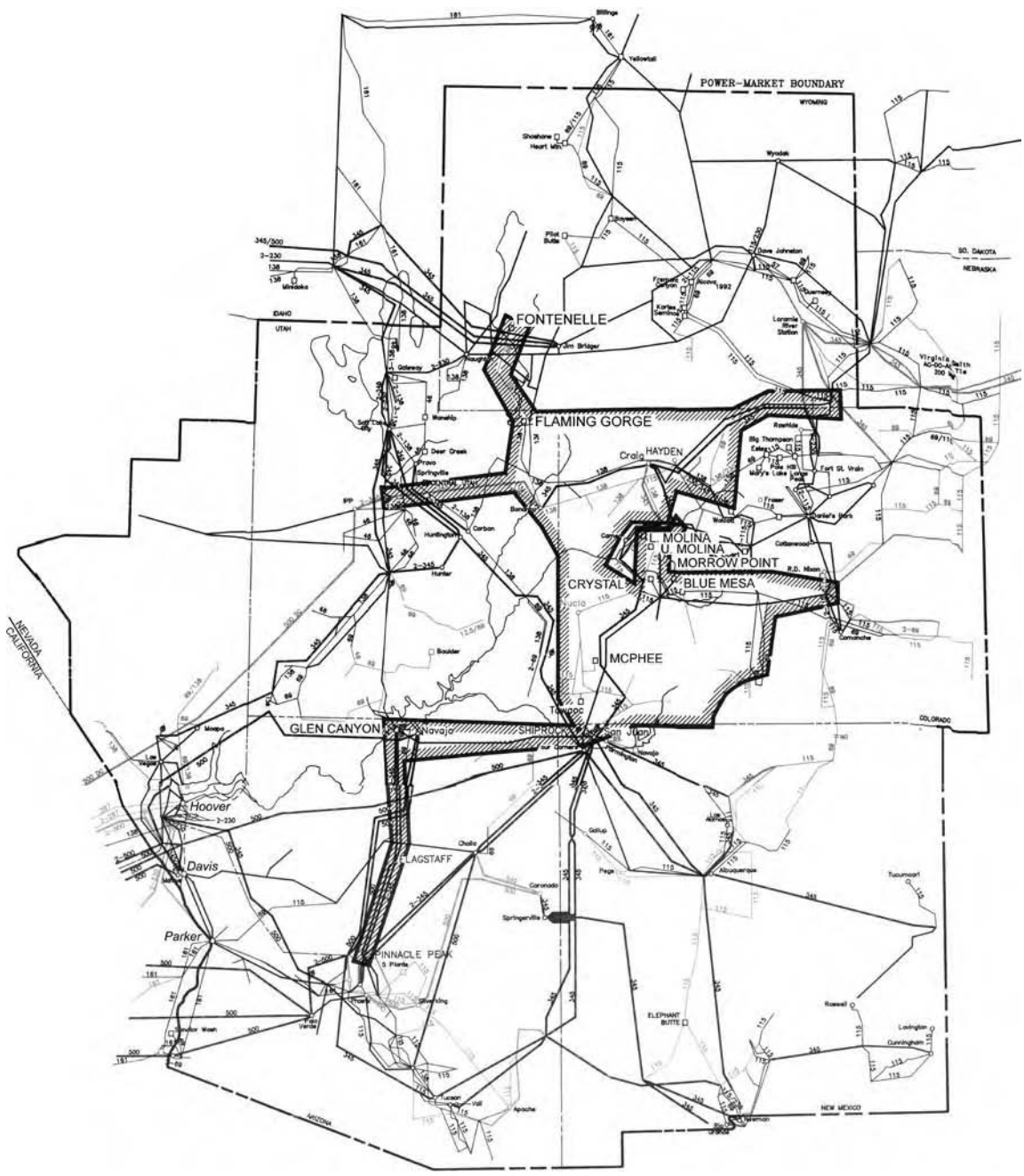

Figure 10.34 Map showing the interconnected transmission system that distributes hydroelectric power produced at federal dams of the Upper Basin (US Department of the Interior, 1995). This transmission system is integrated with federal and privately owned thermal power plants as well. Upper Basin powerplants at federal dams are shown in bold capitalized lettering. Major powerplants at federal dams in the Lower Basin are shown in bold and italized lettering. The grid network represents the transmission lines. The area enclosed in the hatched region is the portion of the electricity grid specifically controlled by the federal government. This area is called the Western Area Upper Colorado Control Area

year, the effect of which is to eliminate sustained low flows in Grand Canyon, regardless of the existence of drought conditions in the Upper Basin. There are few floods, because the regional importance of power produced at Glen Canyon Dam dictates that all possible flows are routed through the power plant.

Use of floods that exceed power plant capacity, such as occurred in 1996 in Grand Canyon, will probably always be controversial. Harpman (1999) estimated that the economic cost of the 1996 controlled flood, in terms of lost hydropower production, was US$2.5 million, resulting in a 3.3% decline in the economic value of hydropower generated at the dam that year. Water available for floods may become more difficult to obtain as consumptive uses in the Upper Basin, especially trans-basin diversions, increase.

The existence of relict and artifact environmental values in Grand Canyon also challenges the development of an achievable rehabilitation plan for the river. Restoration to pre-disturbance conditions is impossible so long as the GCDAMP chooses to manage for relict resources that benefit from floods as well as artifact resources that do not benefit from floods and that did not exist in the river corridor prior to Glen Canyon Dam (Schmidt *et al.*, 1998). Unless the national political consensus changes, it is difficult to imagine a scenario wherein true restoration becomes a management objective, because such a plan would require dismantling Glen Canyon Dam and destroying artifact resources. Instead, the GCDAMP will probably continue to attempt to meet a wide range of competing, and perhaps mutually exclusive, management objectives.

An emerging issue in the Grand Canyon regards the possibility of by-passing fine sediment around Glen Canyon Dam. The scientific community has reached the consensus that restoration is probably impossible without augmenting the Grand Canyon ecosystem with fine sediment (Rubin *et al.*, 2002). A 1986 survey of Lake Powell showed that there were about $1.07 \times 10^9\,m^3$ (868 000 ac-ft) of fine sediment that had been deposited in the reservoir since its creation, representing a 3.2% decrease in total storage capacity in 23 years (US Department of the Interior, 1995). At that rate, sediment will reach the level of the penstocks in 300–500 years. Since the 400 km downstream from the dam are in fine-sediment deficit, environmental organizations and river scientists (Rubin *et al.*, 2002) have called for consideration of the feasibility of routing fine sediment from the reservoir deltas downstream. Such a plan, if implemented, would be controversial because of its potential adverse impact on the artifact tail water trout fishery and on reservoir storage in Lake Mead.

10.11.3 The Upper Basin

Rehabilitation opportunities in the Upper Basin are much greater, largely because there is more available water and there are few segments that are in sediment deficit. The relatively large amount of stream flow remaining in the river system is due to the fact that the Colorado River Compact requires that a significant amount of stream flow continue downstream to the Lower Basin diversions. Thus, the Colorado River Compact guarantees a significant in-stream flow for the Green and upper Colorado Rivers. The additional volume of water available for consumptive Upper Basin use is uncertain, because the Compact stipulates the amount of water that must pass to the Lower Basin (MacDonnell *et al.*, 1995). However, there is probably between 0.2 and $2.7 \times 10^9\,m^3$ (0.175 and 2.200×10^6 ac-ft) of water that can still be consumed in the Upper Basin annually.

The only severely dewatered stream segments in the Upper Basin are the San Juan River and those immediately downstream from trans-basin diversions. Elsewhere, the objectives of species recovery can be met with reintroduction of higher magnitude floods that do not jeopardize the downstream delivery of water to the Lower Basin. These floods are of much less economic impact in lost power production than are changes at Glen Canyon Dam, because the upstream dams are much smaller.

Decommissioning large dams in the Upper Basin has been suggested, and there is significant publicity generated by some environmental organizations regarding Glen Canyon Dam. However, federal agencies have not begun any studies to evaluate such action. There are other dams in the basin that provide less storage and power generation and where loss of these uses might not adversely affect the regional economic infrastructure, such as Fontenelle and Flaming Gorge Dams on the Green River.

10.12 CONCLUSION

The Colorado River has evolved during the past 20 million years, and changes continue to the present. Its Grand Canyon formed in the last 5 million years when the present drainage network became fully integrated. A primary attribute of the watershed is that the areas of highest unit runoff are on the exterior rim of the basin in the middle and southern Rocky Mountains. In contrast, sediment yield increases greatly in the middle of the basin, and sediment loads transported by the mainstem increase greatly downstream. Great floods have passed through the drainage network, and there have been decadal periods of extreme drought and water abundance.

The presence of the Colorado River in an arid region near areas destined for large population growth and

agricultural development encouraged the construction of diversions and dams. The cumulative impact of human activities since about 1900 is of a similar magnitude to the natural geomorphic and ecological processes of thousands of preceding years.

The first such efforts were on the lower river in the Basin and Range and ultimately led to the construction of numerous dams, as well as to dredging, straightening of the channel, and construction of levees along much of the lower river. Since water laws in the western United States give priority to the earliest users of water, the presence of one of the oldest, and largest, diversions in the basin guarantees that stream flow from the Upper Basin continues throughout nearly the entire length of the stream network. This diversion began as the Alamo diversion at the international border, and now is fulfilled by the All American Canal diversion upstream from Yuma. Other large diversions in the Lower Basin supply coastal southern California and central and southern Arizona and further guarantee that water from the Upper Basin passes downstream.

In contrast, the rest of the basin is much less impacted by dams and diversions, even though the size of all reservoirs in the basin greatly exceeds the mean annual flow. There are long river segments between each reservoir, and some of these segments are in a condition of sediment surplus. The longest sediment deficit segment is the Grand Canyon ecosystem, and efforts to rehabilitate fine sediment deposits there have generally been unsuccessful.

The endemic fishery evolved to take advantage of the unique hydrology and sediment transport characteristics of the Colorado River. This fishery has declined greatly during the same period that fish passage was blocked and the hydrology and sediment transport regime were changed by these dams and diversions. Protection and recovery of endangered species are the objectives of many environmental management programs, and the traditional techniques for managing water resource supplies are now constrained. The test of the future concerns the ability to recover species that evolved in a flow and sediment transport regime that has been fundamentally altered, where such alterations have been fundamental to the population and economic growth of the region.

REFERENCES

Allred, T.M. and J.C. Schmidt. (1999) Channel narrowing by vertical accretion along the Green River near Green River, Utah. *Geological Society of America Bulletin* 111(12): 1757–1772.

Alvarez Borrego, S., B.P. Flores Baez and L.A. Galindo Bect. (1975) Hidrologia del Alto Golfo de California II. Conditicionnes durante inveierno, primavera yverano. *Ciencias Marinas* 2: 21–36.

Andrews, E.D. (1986) Downstream effects of Flaming Gorge Dam on the Green River, Colorado and Utah. *Geological Society of America Bulletin* 97(8): 1012–1023.

Anima, R.J., M.S. Marlow, D.M. Rubin and D.J. Hogg. (1998) Comparison of sand distribution between April 1994 and June 1996 along six reaches of the Colorado River in Grand Canyon, Arizona. US Geological Survey Open-File Report 98–141, 33 p.

Animas La Plata Project. (2004) Web site http://www.usbr.gov/uc/progact/animas.

Blackwelder, E. (1934) Origin of the Colorado River. *Geological Society of America Bulletin* 45: 551–566.

Blake, W.P. (1857) Geological report, Part 2 in United States Senate executive document 78, 32nd Congress, 2d Session, Reports on Explorations and Surveys to Ascertain the Most Practicable and Economical Route for a Railroad from the Mississippi River to the Pacific Ocean, volume 5 'Reports on Routes in California to connect with the routes near the thirty-fifth and thirty-second parallels explored by Lt R.S. Williamson, Corps of Topographical Engineers, in 1853.'

Carbajal, N., A. Sousa and R. Durazo. (1997) A numerical model of the ex-ROFI of the Colorado River. *Journal of Marine Systems* 12: 17–33.

Carriquiry, J.D. and A. Sanchez. (1999) Sedimentation in the Colorado River delta and Upper Gulf of California after nearly a century of discharge loss. *Marine Geology* 158: 125–145.

Cohen, M.J., C. Henges-Jeck and G. Castillo-Moreno. (2001) A preliminary water balance for the Colorado River delta, 1992–1998. *Journal of Arid Environments* 49: 35–48.

Collier, M.P., R.H. Webb and E.D. Andrews. (1997) Experimental flooding in Grand Canyon. *Scientific American* 276: 82–89.

Dalrymple, G.B. and W.K. Hamblin. (1998) K-Ar of Pleistocene lava dams in the Grand Canyon in Arizona. *Proceedings of the National Academy of Science* 95: 9744–9749.

Davis, S.W., M.E. Davis, I. Lucchitta, T.C. Hanks, R.C. Finkel and M. Caffee. (2001) Erosional history of the Colorado River through Glen and Grand Canyons, In: *Colorado River Origin and Evolution*, (R.A. Young and E.E. Spamer, Eds.). Grand Canyon, AZ, Grand Canyon Association, pp. 135–139.

deBuys, W. (1999) *Salt dreams: land and water in low-down California*. Albuquerque, University of New Mexico Press, 307 p.

Dellenbaugh, F.S. (1908) *A canyon voyage, the narrative of the Second Powell expedition*. Tucson, The University of Arizona Press, 277 p.

Dolan, R., A. Howard and D. Trimble. (1978) Structural control of the rapids and pools of the Colorado River in the Grand Canyon. *Science* 202: 629–631.

Dutton, C.E. (1880) *Report on the Geology of the High Plateaus of Utah*. Washington, DC, US Geographical and Geological Survey of the Rocky Mountain Region, 307 p.

Dutton, C.E. (1881) The physical geology of the Grand Canyon region. *US Geological Survey, 2nd Annual Report*, pp. 47–166.

Dutton, C.E. (1882) Tertiary history of the Grand Canyon region. *US Geological Survey Monograph* 2, 264 p.

Elliott, C.M. (2002) Relationships between tributary catchments, valley-bottom width, debris-fan area and mainstem gradient on the Colorado Plateau: a case study in Desolation and Gray Canyons on the Green River. Logan, Utah State University Department of Geology Masters thesis, 120 p.

Ely, L.L., Y. Enzel, V.R. Baker and D.R. Cayan. (1993) A 5000-year record of extreme floods and climate change in the southwestern United States. *Science* 262: 410–412.

Faulds, J.E., M.A. Wallace, L.A. Gonzalez and M.T. Heizler. (2001) Depositional environment and paleogeographic implications of the late Miocene Hualapai Limestone, northwestern Arizona and southern Arizona, In: *Colorado River Origin and Evolution*, (R.A. Young and E.E. Spamer, Eds.). Grand Canyon, AZ, Grand Canyon Association, pp. 81–87.

Fletcher, C. (1997) *River, one man's journey down the Colorado, source to sea*. New York, Vintage Books, 400 p.

Fradkin, P. (1981) *A river no more: the Colorado River and the west*. New York, Knopf, 360 p.

Gaeuman, D.A., J.C. Schmidt and P.R. Wilcock. (2003) Evaluation of in-channel gravel storage with morphology-based gravel budgets developed from planimetric data. *Journal of Geophysical Research* 108(F1): 2-1–2-16.

Gaeuman, D.A., J.C. Schmidt and P.R. Wilcock. (2005) Complex channel responses to changes in stream flow and sediment supply on the lower Duchesne River, Utah. *Geomorphology* 64: 185–206.

Gilbert, G.K. (1876) The Colorado Plateau province as a field for geological study. *American Journal of Science* 12: 16–24, 85–103.

Gilbert, G.K. (1877) *Report on the Geology of the Henry Mountains*. Washington, DC, Geographical and Geological Survey of the Rocky Mountain Region, 160 p.

Gilpin, M. (1993) *A population viability analysis of the Colorado squawfish in the upper Colorado River basin*. Report of Department of Biology, University of California, San Diego to US Fish and Wildlife Service, Denver.

Glenn, E.P., C. Lee and C. Valdes-Casillas. (2001a) Introduction. *Journal of Arid Environments* 49: 1–4.

Glenn, E.P., F. Zamora-Arroyo, P.L. Nagler, M. Briggs, W. Shaw and K. Flessa. (2001b) Ecology and conservation biology of the Colorado River delta, Mexico. *Journal of Arid Environments* 49: 5–15.

Graf, W.L. (1978) Fluvial adjustments to the spread of tamarisk in the Colorado Plateau region. *Geological Society of America Bulletin* 89: 1491–1501.

Graf, W.L. (1979) Rapids in Canyon rivers. *Journal of Geology* 87: 533–551.

Graf, W.L. (1980) The effect of dam closure on downstream rapids. *Water Resources Research* 16: 129–136.

Graf, W.L., editor. (1987) *Geomorphic systems of North America*. Boulder, CO, Geological Society of America Centennial Special Volume 2, 643 p.

Grams, P.E. and J.C. Schmidt. (1999) Geomorphology of the Green River in the eastern Uinta Mountains, Dinosaur National Monument, Colorado and Utah, In: *Varieties of Fluvial Form*, (A.J. Miller and A. Gupta, Eds.). Chichester, John Wiley & Sons, Ltd, pp. 81–111.

Grams, P.E. and J.C. Schmidt. (2002) Streamflow regulation and multi-level flood plain formation: channel narrowing on the aggrading Green River in the eastern Uinta Mountains, Colorado and Utah. *Geomorphology* 44: 337–360.

Grams, P.E. and J.C. Schmidt. (2005) Equilibrium or indeterminate? Where sediment budgets fail: sediment mass balance and adjustment of channel form, Green River downstream from Flaming Gorge Dam, Utah and Colorado. *Geomorphology* 71: 156–181.

Grams, P.E., J.C. Schmidt and D.J. Topping. (2007) The rate and pattom of bed incision and bank adjustment on the Colorado River in Glen Canyon downstream from Glen Canyon Dam, 1956–2000. *Geological Society of America, Bulletin* 119: 556–575.

Hamblin, W.K. (1994) Late Cenozoic lava dams in the western Grand Canyon. *Geological Society of America Memoir* 183: 331–376.

Hanks, T.C., I. Lucchitta, S.W. Davis, M.E. Davis, R.C. Finkel, S.A. Lefton and C.D. Garvin. (2001) The Colorado River and the age of Glen Canyon, In: *Colorado River Origin and Evolution*, (R.A. Young and E.E. Spamer, Eds.). Grand Canyon, AZ, Grand Canyon Association, pp. 129–133.

Harden, D.R. (1990) Controlling factors in the distribution and development of incised meanders in the central Colorado Plateau. *Geological Society of America Bulletin* 102: 233–242.

Harpman, D.A. (1999) The economic cost of the 1996 controlled flood, In: *The Controlled Flood in Grand Canyon*, (R.H. Webb *et al.*, Eds.) Washington, DC, AGU Geophysical Monograph 110, pp. 351–357.

Harvey, M.W.T. (1994) *A Symbol of Wilderness: Echo Park and the American conservation movement*. Albuquerque, University of New Mexico Press, 368 p.

Hirsch, R.M., J.F. Walker, J.C. Day and R. Kallio. (1990) The influence of man on hydrologic systems, In: *Surface Water Hydrology*, (M.G. Wolman and H.C. Riggs, Eds.). Boulder, CO, Geological Society of America, The Geology of North America, vol. O-1, pp. 329–359.

Howard, A.D. and R. Dolan. (1981) Geomorphology of the Colorado River in Grand Canyon. *Journal of Geology* 89: 269–297.

Howard, K.A., J.E. Faulds, L.S. Beard and M.J. Kunk. (2000) Reverse-drag folding across the path of the antecedent early Pliocene Colorado River below the mouth of the Grand Canyon: implications for plateau uplift. Geological Society of America abstracts with programs 32(7): 41.

Hundley, N., Jr. (1966) *Dividing the Waters: a century of controversy between the United States and Mexico*. Los Angeles, University of California Press, 266 p.

Hunt, C.B. (1969) Geologic history of the Colorado River. *US Geological Survey Professional Paper* 669-C: 59–130.

Ikeda, H. (1989) Sedimentary controls on channel migration and origin of point bars in sand-bedded meandering rivers, In *River meandering*, (S. Ikeda and G. Parker, Eds.). Washington, DC, American Geophysical Union, pp. 51–68.

Iorns, W.V., C.H. Hembree, D.A. Phoenix and G.L. Oakland. (1964) Water resources of the Upper Colorado River basin – basic data. *US Geological Survey Professional Paper* 442, 1036 p.

Iorns, W.V., C.H. Hembree and G.L. Oakland. (1965) Water resources of the Upper Colorado River basin – technical report. *US Geological Survey Professional Paper* 441, 370 p.

Ives, J.C. (1861) Report on the Colorado River of the West, explored in 1857 and 1858 by Lieutenant Joseph C. Ives, Corps of Topographical Engineers, under the direction of the Office of Explorations and Surveys: A.A. Humphreys, Captain Topographical Engineers, in charge, by order of the Secretary of War, 36th Congress, 1st Session, Senate, Executive Document. Washington, DC, Government Printing Office.

Johnson, N.M., C.B. Officer, N.D. Opdyke, G.D. Woodward, P.K. Zeitler and E.H. Lindsay. (1983) Rates of late Cenozoic tectonism in the Vallecito-Fish Creek basin, western Imperial Valley, California. *Geology* 11: 664–667.

Jordan, D.S. (1891) Report of explorations in Utah and Colorado during the summer of 1889, with an account of the fishes found in each of the river basins examined. *Bulletin of the US Fish Commissioner* 9: 1–40.

Karlstrom, K.E. and E. Kirby. (2004) Colorado River system of the southwestern US: longitudinal profiles, differential incision and a hypothesis for Quaternary tectonism at both ends. Geological Society of America Annual Meeting Abstract http://gsa.confex.com/gsa/2004AM/finalprogram/abstract_80893.htm.

Kieffer, S.W. (1985) The 1983 hydraulic jump in Crystal Rapid: implications for river-running and geomorphic evolution in the Grand Canyon. *Journal of Geology* 93: 385–406.

Kirkham, R.M., M.J. Kunk, B. Bryant and R.K. Streufert. (2001) Constraints on timing and rates of late Cenozoic incision by the Colorado River in Glenwood Canyon, Colorado: a preliminary synopsis, In: *Colorado River Origin and Evolution*, (R.A. Young and E.E. Spamer, Eds.). Grand Canyon, AZ, Grand Canyon Association, pp. 113–116.

Kowalewski, M. and K.W. Flessa. (1995) Comparative taphonomy and faunal composition of shelly cheniers from northeastern Baja California, Mexico. *Ciencias Marinas* 21: 155–177.

LaRue, E.C. (1916) Colorado River and its utilization. *US Geological Survey Water-Supply Paper* 395, 231.

Lavin, M.F. and S. Sanchez. (1999) On how the Colorado River affected the hydrography of the upper Gulf of California. *Continental Shelf Research* 19: 1545–1560.

Leopold, A. (1949) *A Sand County Almanac*. New York, Oxford University Press, 226 p.

Leopold, L.B. (1969) The rapids and the pools – Grand Canyon. *US Geological Survey Professional Paper* 669-D: 131–145.

Longwell, C.R. (1936) Geology of the Boulder Reservoir floor, Arizona-Nevada. *Geological Society of America Bulletin* 47: 1393–1476.

Longwell, C.R. (1946) How old is the Colorado River? *American Journal of Science* 244(12): 817–835.

Lucchitta, I. (1972) Early history of the Colorado River in the Basin and Range province. *Geological Society of America Bulletin* 83: 1933–1948.

Lucchitta, I. (2003) History of the Grand Canyon and of the Colorado River in Arizona, In: *Grand Canyon Geology*, (S.S. Beus and M. Morales, Eds.). New York, Oxford University Press, pp. 260–274.

Lucchitta, I. and R.A. Jeanne. (2001) Geomorphic features and processes of the Shivwits Plateau, Arizona, and their constraints on the age of western Grand Canyon, In: *Colorado River Origin and Evolution*, (R.A. Young and E.E. Spamer, Eds.). Grand Canyon, AZ, Grand Canyon Association, pp. 65–69.

Lucchitta, I., G.H. Curtis, M.E. Davis, S.W. Davis, T.C. Hanks, R.C. Finkel and B. Turrin. (2001) Rates of downcutting of the Colorado River in the Grand Canyon region, In: *Colorado River Origin and Evolution*, (R.A. Young and E.E. Spamer, Eds.). Grand Canyon, AZ, Grand Canyon Association, pp. 155–157.

Luecke, D.F., J. Pitt, C. Congdon, E. Glenn, C. Valdes-Casillas and M. Briggs. (1999) *A Delta Once More: Restoring Riparian and Wetland Habitat in the Colorado River Delta*. Washington, DC, Environmental Defense Publications, 51 pp.

Lyons, J.K., M.J. Pucherelli and R.C. Clark. (1992) Sediment transport and channel characteristics of a sand-bed portion of the Green River below Flaming Gorge Dam, Utah. *Regulated Rivers: Research & Management* 7: 219–232.

MacDonnell, L.J., Jr, D.H. Getches and W.C. Hugenberg Jr. (1995) The law of the Colorado River: coping with severe sustained drought. *Water Resources Bulletin* 31(5): 825–836.

Mackley, R.D. and J. Pederson. (2004) Relating rock strength controls to large-scale variations in the Colorado River's profile, Glen and Grand Canyons, UT and AZ. Geological Society of America Annual Meeting Abstract. http://gsa.confex.com/gsa/2004AM/finalprogram/abstract_77705.htm.

Magirl, C., R.H. Webb and P.G. Griffiths. (2005) Changes in the water surface profile of the Colorado River in Grand Canyon, Arizona between 1923 and 2000. *Water Resources Research* 41, W05021, doi: 10.1029/2003WR002519.

Marchetti, D.W. and T.E. Cerling. (2001) Bedrock incision rates for the Fremont River, tributary of the Colorado River, In *Colorado River Origin and Evolution*, (R.A. Young and E.E. Spamer, Eds.) Grand Canyon, AZ, Grand Canyon Association, pp. 125–127.

Martin, R. (1989) *A Story that Stands like a Dam, Glen Canyon and the Struggle for the Soul of the West*. New York, Henry Holt and Company, 354 p.

McKee, E.D. and E.H. McKee. (1972) Pliocene uplift of the Grand Canyon region: time of drainage adjustment. *Geological Society of America Bulletin* 83(7): 1923–1932.

McKee, E.D., R.F. Wilson, W.J. Breed and C.S. Breed. (1967) Evolution of the Colorado River in Arizona. *Museum of Northern Arizona Bulletin* 44, 67 p.

Meade, R.H., T.R. Yuzyk and T.J. Day. (1990) Movement and storage of sediment in rivers of the United States and Canada, In: *Surface Water Hydrology*, (M.G. Wolman and H.C. Riggs, Eds.). Boulder, CO, Geological Society of America, The Geology of North America, vol. O-1, pp. 255–280.

Meek, N. and J. Douglass. (2001) Lake overflow: an alternative hypothesis for Grand Canyon incision and development of the

Colorado River, In: *Colorado River Origin and Evolution*, (R.A. Young and E.E. Spamer, Eds.). Grand Canyon, AZ, Grand Canyon Association, pp. 199–204.

Meko, D.M., C.A. Woodhouse, C.A. Baisan, T. Knight, J.J. Lukas, M.K. Hughes and M.W. Salzer. (2007) Medieval drought in the upper Colorado River Basin. *Geophysical Research Letters* 34, L10705, doi: 10.1029/2007GL029988.

Miller, R.R. (1959) Origin and affinities of the freshwater fish fauna of western North America, In: *Zoogeography*, (C.L. Hubbs, Ed.). Washington, DC, American Association for the Advancement of Science, pp. 187–222.

Minckley, W.L. (1973) *Fishes of Arizona*. Phoenix, Arizona Game and Fish Department.

Minckley, W.L. and J.E. Deacon, editors. (1991) *Battle against extinction: native fish management in the American West*. Tucson, The University of Arizona Press, 517 p.

Mueller, G.A. and P.C. Marsh. (2002) Lost, a desert river and its native fishes: a historical perspective of the lower Colorado River. Information and Technology Report USGS/BRD/ITR–2002–0010. Denver, US Government Printing Office, 69 p.

Muth, R.T., L.W. Crist, K.E. LaGory, J.W. Hayse, K.R. Bestgen, T.P. Ryan, J.K. Lyons and R.A. Valdez. (2000) Flow and temperature recommendations for endangered fishes in the Green River downstream of Flaming Gorge Dam. Final Report, Upper Colorado River Endangered Fish Recovery Program Project FG-53.

National Research Council, (1992) *Restoration of Aquatic Ecosystems*. Washington, DC, National Academy Press, 552 p.

Newberry, J.S. (1861) Colorado River of the West. *American Journal of Science* 33: 387–403.

Newberry, J.S. (1876) *Geological report of the exploring expedition from Santa Fe, New Mexico, to the junction of the Grand and Green rivers of the great Colorado of the West in 1859*. Washington, DC, US Government Printing Office, 159 p.

O'Conner, J.E., L.L. Ely, E.E. Wohl, L.E. Stevens, T.S. Melis, V.S. Kale and V.R. Baker. (1994) A 4500-year record of large floods on the Colorado River in the Grand Canyon, Arizona. *Journal of Geology* 102: 1–9.

Pearson, B.E. (2002) *Still the Wild River Runs: Congress, the Sierra Club and the fight to save Grand Canyon*. Tucson, The University of Arizona Press, 246 p.

Pederson, J., K. Karlstrom, W. Sharp and W. McIntosch. (2002) Differential incision of the Grand Canyon related to Quaternary faulting – constraints from U-series and Ar/Ar dating. *Geology* 30: 739–742.

Pitt, J. (2001) Can we restore the Colorado River delta? *Journal of Arid Environments* 49: 211–220.

Pitt, J., D. Luecke, M. Cohen, E. Glenn and C. Valdes-Casillas. (2000) Two countries, one river: managing ecosystem conservation in the Colorado River delta. *Natural Resources Journal* 40: 819–864.

Pontius, D. (1997) *Colorado River Basin Study*. Final Report to the Western Water Policy Review Advisory Commission, 132 p.

Powell, J.W. (1875) *Exploration of the Colorado River of the West and its Tributaries, 1869–1872*. Washington, DC, US Government Printing Office, Smithsonian Institute Publication, 291 p.

Riggs, H.C. and M.G. Wolman. (1990) Introduction, In: *Surface Water Hydrology*, (M.G. Wolman and H.C. Riggs, Eds.). Boulder, CO, Geological Society of America, The Geology of North America, vol. O-1, pp. 1–9.

Rubin, D.M., J.M. Nelson and D.J. Topping. (1998) Relation of inversely graded deposits to suspended-sediment grain-size evolution during the 1996 Flood experiment in Grand Canyon. *Geology* 26: 99–102.

Rubin, D.M., D.J. Topping, J.C. Schmidt, J. Hazel, M. Kaplinski and T.S. Melis. (2002) Recent sediment studies refute Glen Canyon Dam hypothesis. *EOS* 83(25): 273–278.

San Juan River Basin Recovery Implementation Program. (2004) Web site <http://southwest.fws.gov/sjrip/>.

Scarborough, R. (2001) Neogene development of Little Colorado River valley and eastern Grand Canyon: field evidence for an overtopping hypothesis, In: *Colorado River Origin and Evolution*, (R.A. Young and E.E. Spamer, Eds.). Grand Canyon, AZ, Grand Canyon Association, pp. 207–212.

Schmidt, J.C. (1999) Summary and synthesis of geomorphic studies conducted during the 1996 controlled flood in Grand Canyon, In: *The Controlled Flood in Grand Canyon*, (R.H. Webb *et al.*, Eds.). Washington, DC, AGU Geophysical Monograph 110, pp. 329–341.

Schmidt, J.C. and D.M. Rubin. (1995) Regulated streamflow, fine-grained deposits and effective discharge in canyons with abundant debris fans, In: *Natural and Anthropogenic Influences in Fluvial Geomorphology*, (J.E. Costa, A.J. Miller, K.W. Potter and P.R. Wilcock, Eds.). Washington, DC, AGU Geophysical Monograph 89, pp. 177–195.

Schmidt, J.C. and J. Brim Box. (2004) Application of a dynamic model to assess controls on age-0 Colorado pikeminnow distribution in the middle Green River, Colorado and Utah. *Annals of the Association of American Geographers* 94(3): 458–476.

Schmidt, J.C., R.H. Webb, R.A. Valdez, G.R. Marzolf and L.E. Stevens. (1998) Science and values in river restoration in the Grand Canyon. *Bioscience* 48: 735–747.

Schmidt, J.C., E.D. Andrews, D.L. Wegner, D.T. Patten, G.R. Marzolf and T.O. Moody. (1999) Origins of the 1996 controlled flood in Grand Canyon, In: *The Controlled Flood in Grand Canyon*, (R.H. Webb *et al.*, Eds.). Washington, DC, AGU Geophysical Monograph 110, pp. 23–36.

Schmidt, J.C., R.A. Parnell, P.E. Grams, J.E. Hazel, M.A. Kaplinski, L.E. Stevens and T.L. Hoffnagle. (2001) The 1996 controlled flood in Grand Canyon: hydrology, hydraulics, sediment transport and geomorphic change. *Ecological Applications* 11(3): 657–671.

Schmidt, J.C., D.J. Topping, P.E. Grams and J.E. Hazel. (2004) System-wide changes in the distribution of fine sediment in the Colorado River corridor between Lees Ferry and Bright Angel Creek, Arizona. Logan, UT, Department of Aquatic, Watershed and Earth Resources, Utah State University, Final Report to the Grand Canyon Monitoring and Research Center, 99 p.

Spencer, J.E. and P.A. Pearthree. (2001) Headward erosion versus closed-basin spillover as alternative causes of Neogene capture

of the ancestral Colorado River by the Gulf of California, In: *Colorado River Origin and Evolution*, (R.A. Young and E.E. Spamer, Eds.). Grand Canyon, AZ, Grand Canyon Association, pp. 215–219.

Spencer, J.E., L. Peters, W.C. McIntosh and P.J. Patchett, (2001) $^{40}Ar/^{39}Ar$ geochronology of the Hualapai limestone and Bouse formation and implications for the age of the lower Colorado River, In: *Colorado River Origin and Evolution*, (R.A. Young and E.E. Spamer Eds.). Grand Canyon, AZ, Grand Canyon Association, pp. 89–91.

Stanford, J.A. (1994) *Instream flows to assist the recovery of endangered fishes of the upper Colorado River basin*. National Biological Survey Biological Report 24, 47 p.

Stanford, J.A. and J.V. Ward. (1989) Serial discontinuities in a Rocky Mountain river.I. Distribution and abundance of *Plecoptera*. *Regulated Rivers: Research and Management* 3: 169–175.

Stevens, J.E. (1988) *Hoover Dam, an American Adventure*. Norman, University of Oklahoma Press, 326 p.

Topping, D.J., D.M. Rubin and L.E. Vierra, Jr. (2000) Colorado River sediment transport 1. natural sediment supply limitation and the influence of Glen Canyon Dam. *Water Resources Research* 36(2): 515–542.

Topping, D.J., J.C. Schmidt and L.E. Vierra, Jr. (2003) Computation and analysis of the instantaneous-discharge record for the Colorado River at Lees Ferry, Arizona – May 8, 1921, through September 30, 2000. *US Geological Survey Professional Paper* 1677, 118 p.

Upper Colorado River Endangered Fish Recovery Program. (2004) Web site <http://coloradoriverrecovery.fws.gov/>.

US Army Corps of Engineers. (1996) Water control infrastructure: national inventory of dams [CD-ROM]. Federal Emergency Management Agency, Washington, DC.

US Bureau of Reclamation Lower Colorado Region. (2004) Web site <http://www.usbr.gov/lc/>.

US Department of the Interior. (1946) *The Colorado River, a natural menace becomes a national resource*. Report prepared under general supervision of the Bureau of Reclamation, 295 p.

US Department of the Interior. (1995) Final environmental impact statement, operation of Glen Canyon Dam, Colorado River Storage Project.

Valdez, R.A. and R. Ryel. (1997) Life history and ecology of the humpback chub in the Colorado River in Grand Canyon, Arizona, In: Proceedings of the Third Biennial Conference on the Colorado Plateau Denver, National Park Service, pp. 3–31.

Valdez, R.A., J.P. Shannon and D.W. Blinn. (1999) Biological implications of the 1996 controlled flood, In: *The Controlled Flood in Grand Canyon*, (R.H. Webb *et al.*, Eds.). Washington, DC, AGU Geophysical Monograph 110, pp. 343–350.

Van Steeter, M.M. and J. Pitlick. (1998) Geomorphology and endangered fish habitats of the upper Colorado River, 1. Historic changes in streamflow, sediment load and channel morphology. *Water Resources Research* 34: 287–302.

Webb, R.H., P.T. Pringle, S.L. Reneau and G.R. Rink. (1988) Monument Creek debris flow, 1984, implications for formation of rapids on the Colorado River in Grand Canyon National Park. *Geology* 16: 50–54.

Webb, R.H., T.S. Melis, P.G. Griffiths and J.G. Elliott. (1999) Reworking of aggraded debris fans, In: *The Controlled Flood in Grand Canyon*, (R.H. Webb *et al.*, Eds.). Washington, DC, AGU Geophysical Monograph 110, pp. 117–130.

Westwood, R.E. (1992) *Elwyn Blake's Colorado River Expeditions*. Reno, University of Nevada Press, 259 p.

Wilke, P.J. (1980) Prehistoric weir fishing on recessional shorelines of Lake Cahuilla, Salton basin, southeastern California. Bishop, CA, *Proceedings of the Desert Fishes Council*, vol. 11, pp. 101–102.

Williams, G.P. and M.G. Wolman. (1984) Downstream effects of dams on alluvial rivers. *US Geological Survey Professional Paper* 1286, 83 p.

Willis, G.C. and R.F. Biek. (2001) Quaternary incision rates of the Colorado River and major tributaries in the Colorado Plateau, Utah, In: *Colorado River Origin and Evolution*, (R.A. Young and E.E. Spamer, Eds.). Grand Canyon, AZ, Grand Canyon Association, pp. 119–123.

Woodhouse, C.A., S.T. Gray and D.M. Meko. (2006) Updated streamflow reconstructions for the Upper Colorado River Basin. *Water Resources Research* 42, W05415, doi: 10.1029/2005WR004455.

Zamora-Arroyo, F., P. Nagler, M. Briggs, D. Radtke, H. Rodriquez, J. Garcia, C. Valdes, A. Huete and E. Glenn. (2001) Regeneration of native trees in response to flood releases from the United States into the delta of the Colorado River, Mexico. *Journal of Arid Environments* 49: 163–171.

11

The Lena River: Hydromorphodynamic Features in a Deep Permafrost Zone

François Costard[1] and Emmanuèle Gautier[2]

[1]*UMR 8148 IDES, CNRS-Université Paris-Sud 11, 91405 Orsay Cédex, France*
[2]*CNRS UMR 8591, Laboratoire de Géographie Physique and University Paris 8, 92195 Meudon Cédex, France*

11.1 INTRODUCTION

With a mainstem exceeding 4300 km in length and more than 500 tributaries totalling 60 000 km, the Lena River is one of the major fluvial hydrosystems in the world occupying the 11th place among the largest rivers (Figure 11.1).

Due to its huge basin (2.49×10^6 km^2), the Lena River represents a very important contribution to the Laptev Sea, bringing annually 525 km^3 of water (15 % of total freshwater flow into the Arctic Ocean; Shiklomanov *et al*., 2000), between 12 and 17 million t of suspended load, and 49 million t of dissolved substances (Lopatin, 1952; Antonov, 1960; Lvovitch, 1971; Gordeev and Sidorov, 1993). From its source in the Baïkal range (20 km west from the Baikal Lake) to the Arctic Ocean, the river flows northeast and north in Siberia, receiving water and sediment supplies from its main tributaries: the Vitim, Olyokma, Aldan and Viliuy Rivers. The two last rivers are the longest ones with 2270 and 2650 km in length, respectively. Just before pouring into the Laptev Sea, the Lena develops 150 branches (with three main channels carrying 70 % of the discharge), forming a large delta (30 000 km^2) that supports abundant wildlife.

Given its length and south–north orientation, the Lena crosses several latitudinal belts, and its basin exhibits a great diversity of flora and fauna. The boreal forest (taiga) represents a vast preserved ecoregion covering 83 % of the basin and spanning over 20° of latitude. Downstream of the Arctic Circle, the landscape is dominated by the Arctic tundra. The Siberian taiga and tundra still preserve pristine habitats and the Lena Basin exhibits at least 28 species of mammal, 285 species of bird, 43 of fish, and about 4000 insect species. Regarding the flora, 1831 species of vascular plants, 526 species of moss, more than 550 species of lichen, and more than 510 species of mushroom have been listed for only the Yakutia latitudes (60–73° N) crossed by the Lena River. Therefore, the Lena River floodplain and delta are host to many protected areas, the most extensive being the Lena Delta Nature Reserve (the largest protected area in Russia).

The Lena River is an important waterway, navigable for almost all its length. Yakutsk (the most important town of the Lena Basin), Olekminsk, Lensk, Kirensk, and Osetrovo are the biggest ports on the river. Yakutsk is the capital of the Sakha Republic (Yakutia), the largest republic in the Russian Federation.

11.2 DESCRIPTION OF THE LENA DRAINAGE BASIN

The Lena Basin occupies the eastern half of the Siberian Craton, with an Archaean continental nucleus that is exposed in the Aldan and Anabar Shields. The drainage area of the Lena consists of three major tectonic units. In the south-western upper basin, the Baikal and Mongolo-Okhotsk folded region is composed of gneiss, schists,

Large Rivers: Geomorphology and Management, Edited by A. Gupta

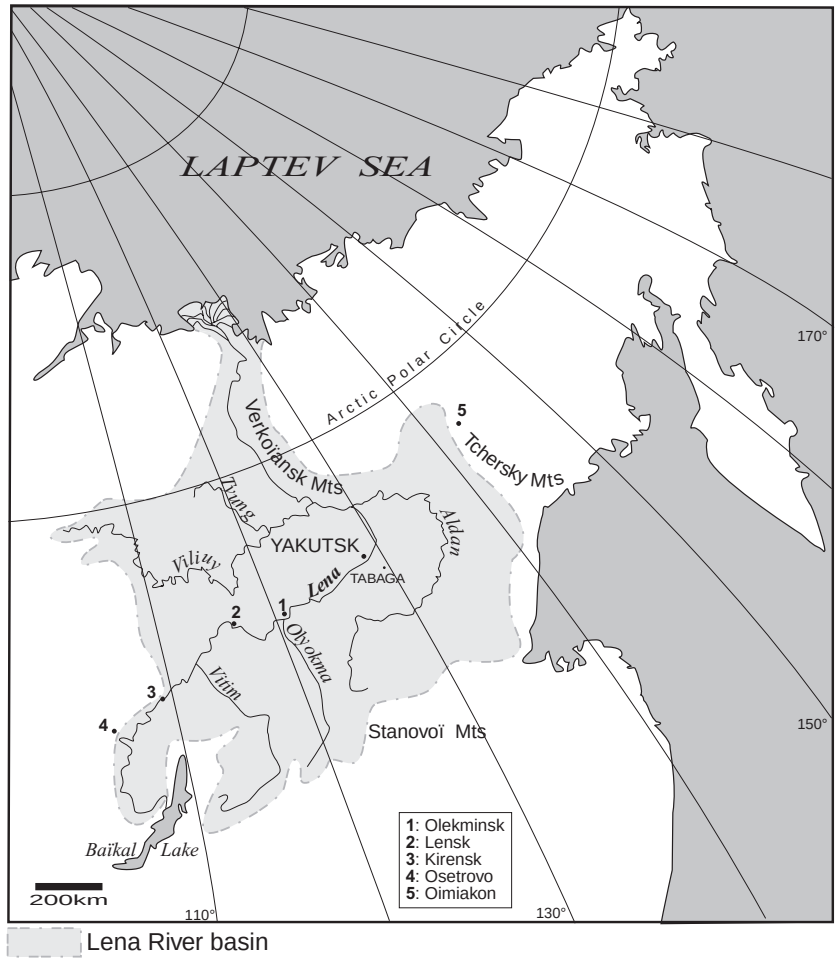

Figure 11.1 Location map of the Lena River

quartzites and marble/limestone of Proterozoic age. The Aldan Shield in the south-eastern zone, consists of Archean and Proterozoic crystalline and metamorphic rocks. In the central and lower parts of the basin, the Siberian Platform is covered by diversified sediments several kilometres thick, associated with both marine transgressions and continental deposits. These include Precambrian, Cambrian and Late Cretaceous limestones and dolomites, detrital sandstones and shales of Devonian and of Jurassic to Cretaceous age including important salt and coal-bearing sequences, and Quaternary lacustrine-glacial and alluvial deposits. Two other units limit the basin. The north-western zone of the basin (upper basin of the Viliuy) belongs to the Siberian Traps (Permian to Triassic volcanic rocks). The Verkhoyano-Kolimean folded region forms the eastern divide with Late Palaeozoic, Triassic and Jurassic sedimentary complex (Gordeev and Sidorov, 1993; Huh *et al*., 1998; Peregovich *et al*., 1999).

In the upper valleys, the Lena and its tributaries are incised in the Trans-Baikal Highlands and the Archaean Aldan Shield. Flowing through narrow valleys, on relatively steep gradients, the rivers transport mainly cobbles, gravel and coarse sands. This mountainous topography is accompanied by a relatively wet climate, with a maximum of 800–1000 mm of precipitation, the mean annual precipitation for the basin being below 400 mm (Antonov, 1967). The plateaux of the Siberian Platform induce a marked change in the topography and fluvial landforms: incised in the plateaux, the river occupies the bottom of the valley with a single wide channel. Locally, the channel divides

into two branches, separated by an elongated island. Upstream of Yakutsk, the floodplain widens and the river develops a multichannel pattern, numerous channels surround very large sand bars and forested islands. The river longitudinal gradient is sharply reduced (0.0001), and the sediment observed on the bars consists of medium and fine sands (D_{50}: 250 µm; Gautier and Costard, 2000). The Aldan River is a higher energy system, transporting cobble (D_{50}: 13 cm; Gautier and Costard, 2000) and finer gravel up to the junction with the main river. Downstream of the Viliuy River junction, the Lena turns north and keeps this direction up to the Laptev Sea. The floodplain is asymmetric, the right side of the river being flanked by the Verkoiansk Mountains, while on the left side, the floodplain can be more than 20 km wide with numerous anastomosed channels, swamps, and thermokarstic lakes. The Lena River in Yakutia exhibits four main Pleistocene terraces composed of silty and sandy materials. The Bestyakh, Tyungyulyu, Abalakh and Magan Terraces are 55–75 m, 65–100 m, 115–135 m and 155–175 m above the river respectively. The terraces are covered by loess-like silt mantles.

This northward course is accompanied by a climatic gradient of decreasing temperature and precipitation.

11.3 A PERIGLACIAL ENVIRONMENT

The Lena River is particularly interesting for its spectacular floods controlled mostly by periglacial dynamics. Along most of its course, the Lena River crosses the Yakutia, a region well known for its lowest temperature records (−72 °C) as well as for its maximum thickness of permafrost (1500 m). Permafrost is perennially frozen ground at a temperature under 0 °C for more than 2 years continuously. Thus, the strongly continental climate together with the permafrost creates a periglacial environment. Temperature and precipitation decrease following a southwest – northeast gradient. In central and northern Siberia, low temperature (mean annual temperature at Yakutsk of −10.2 °C), average annual precipitation (800 mm in the southwestern part of the basin decreasing to 190 mm $year^{-1}$ in central Siberia), high evaporation (180 mm $year^{-1}$) and sublimation rates are characteristics of a very cold and dry climate, even if the summer is warmer (19 °C in July) and relatively wetter (Katasonow and Soloviev, 1969).

Much of central Yakutia has not been glaciated. However, continental ice sheet and alpine glaciers almost surrounded the interior of Yakutia during the period of glacial maxima (Péwé, 1991). The lack of extensive ice sheets during the Pleistocene, together with a thin snow cover, favoured the development and the preservation of deep permafrost. The whole basin is underlain by continuous permafrost, except the southern zone where the permafrost is discontinuous with thickness varying between 25 and 100 m. The maximum depth of frozen soil in Oïmiakon (Yakutia) is about 1500 m and the thickness of the average Siberian permafrost is about 350 m (Anisimova *et al*., 1973). The active layer is around 0.5–2.5 m in thickness. The temperature of continuous permafrost at the depth of minimum annual seasonal change varies from −5 to −13 °C (Péwé, 1991). Unfrozen ground is nevertheless present under the bed of the Lena River and its tributaries as taliks (soil without ground-ice) of varying depths and sometimes as isolated taliks.

11.4 FLOODPLAIN, DELTA AND PERIGLACIAL LANDFORMS

Along the Lena floodplain, the permafrost exhibits a large amount of massive ice and ice wedges. Its subsequent thawing has produced a large variety of cold climate landforms. Fluvial thermokarst can appear under various forms such as collapsed pingos, beaded rivers, and especially, alases (Soloviev, 1973). The alases are mainly developed as flat-floored and deep-sided depressions by the preferential thawing of massive icy beds. Their coalescence produces a mature alas valley. The floor of an alas exhibits a chaotic topography of collapsed masses with temporary ponds. The irregularly backwearing of alas slopes favours the production of thermocirques and landslides. Alases have a length between 100 m and 15 km but commonly reach 1 km. Their depth varies between 3 m and 40 m (Soloviev, 1963). Alluvial thermokarst is essentially concentrated in the Pleistocene alluvial plains of Central Yakoutia (Czudek and Demek, 1970). Thus, 40–50 % of plains of the Central Yakoutia have been covered by the alases.

At the mouth of the Lena River, the subaerial delta is about 28 500 km^2. It is frozen for about 7 months of the year. The delta is characterized by many drained lakes, and by a large number of anastomosing channels and sand bars (Figure 11.2). Its tundra surface exhibits various patterned ground and thermokarst alases. The large Lena basin delivers a huge quantity of water and sediments during the flood season in the delta region. As a consequence, the inclusion of freshwater discharges into the Arctic sea via the Lena River affect the ocean circulation near the river mouth.

11.5 FLUVIAL DYNAMICS AND LANDFORMS

Due to its periglacial environment and its south-to-north course, the Lena River exhibits very specific hydrodynamic features. In terms of mean water discharge, the river

Figure 11.2 The Lena Delta in summer, Landsat 7 image. Note the thermokarstic lakes. USGS EROS Data Center Satellite Systems Branch. Width of the image: 220 km. Source: Landsat.org, Center for Global Change and Earth Observations, Michigan State University (http://landsat.org)

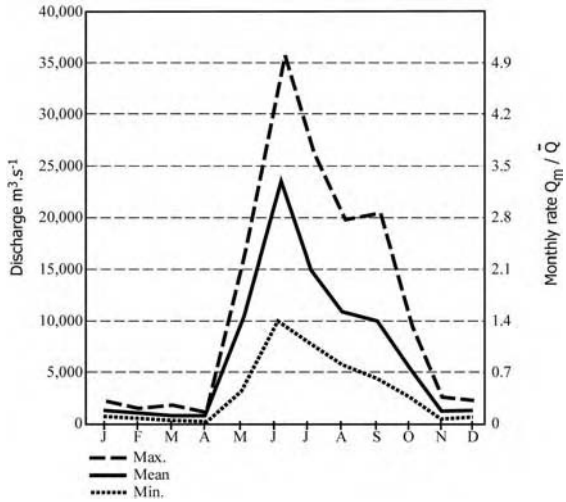

Figure 11.3 Regime of the Lena River. Tabaga gauging site, 1927–1980. (Geographie Physique et Quatenaire, 54, 327–342, Costard and Gautier, 2000. Reproduced by permission of Les Presses de I'Universite de Montreal)

does not represent a major hydrosystem, mainly because of the dry climate and the lack of important basin groundwater resources. At Yakutsk, the mean annual discharge is 7000 $m^3 s^{-1}$, and 16 600 $m^3 s^{-1}$ at Kusur, in the lower valley. This represents a moderate specific discharge of 7.88 $l s^{-1} km^{-2}$ in central Siberia and 6.8 in the lower valley (7.46 $l s^{-1} km^{-2}$ for its alter ego, the Aldan River). Several tributaries, the Viliuy River for example, show lower specific discharge (3 $l s^{-1} km^{-2}$). Rain and groundwater in the southern basin and snow in the northern basin are the main inputs to the Lena River. Near the Arctic Circle, the role of groundwater in the river supply becomes less significant because of the increasing thickness of the permafrost.

The hydrology of the Lena and its tributaries is characterized by an extremely episodic flow regime (Figure 11.3), mainly controlled by rapid snowmelt during spring (Gautier and Costard, 2000). Continuous low water level during the Siberian winter reflects the strong control exerted by the climate: the discharge in Yakutia is very low for 6–7 months. The freeze-up of the rivers begins in the middle of October and a continuous ice cover can be observed at the beginning of November in the middle and lower sections. The ice thickness increases downstream: 0.5 m in the upper branches, 2 m in central Siberia, and more than 3 m in the north where the ice cover persists for more than 240 days $year^{-1}$. The discharge drops to its lowest value at the end of winter, a few weeks before the flood (Gautier and Costard, 2000). The thick ice cover makes the river a road for trucks during the long winter.

On the Lena, the spring ice break-up migrates progressively downstream. It begins in late April in the upper basin, occurs during the second half of May just south of Yakutsk and progressively moves downriver in June. Thus, the time lag can be 50 days between the upper and lower valley. A very high proportion of the annual discharge occurs during the short break-up and flood period of about 1 month. During the flood, the mean annual discharge reaches 25 000 $m^3 s^{-1}$ at Tabaga near Yakutsk (Figure 11.3) but it can undergo a marked inter-annual variability. Downstream, because of the contribution from the Aldan River, the flood discharge can be about 50 000 $m^3 s^{-1}$, with a maximum exceeding 100 000 $m^3 s^{-1}$ (May 1966, May 2001). The presence of ice-jams and log-jams contributes to sudden rises in water level, leading to the rapid inundation of the floodplain, and sometimes of the first terrace above the floodplain. Such natural dams can elevate the water level up to 8–10 m. In May 2001, the region experienced its worst flooding in 100 years, with hundreds of thousands of people being affected by the floodwaters. Explosives were detonated in many places to dislodge

blocks of ice that were backing up rivers and exacerbating flooding. The city of Yakutsk was partly submerged by this catastrophic flooding where the water rose 19 m above the critical level. This event was caused by a combination of an exceptionally harsh winter and an unusually warm spring. The water temperature and the discharge increase simultaneously from May to June (from 1 to 5 °C and the discharge is multiplied by a factor of 2.3). In contrast, from June to July, the water temperature is still increasing up to 12 °C while the discharge decreases by a factor of 1.6.

Upstream of Yakutsk, the floodplain width is 2–4 km wide, which increases downstream of the town to 10–25 km. The fluvial system develops a multiple-channels pattern accompanied by very large forested islands. Two topographic levels (5–6 m and 8–10 m) occur on the islands and the floodplain above the low water level. These surfaces are submerged during different flood magnitudes, the same observation has been made on the Yenissei River (Yamskikh *et al*. 1999).

In central Yakutia the river consists of a large number of shallow and wide channels that are between several hundred metres and 3 km in width (Figures 11.4 and 11.5). These multiple channels enclose large islands (from 1 to 5 km in length) and large sandy bars. The secondary channels carry water during the high water levels but rapidly run dry by the end of July. The decrease in discharge, related to the lack of significant groundwater inflow, makes navigation extremely difficult and dangerous. During the summer, the river is a strategic economic axis: huge boats exporting the natural resources of Siberia (coal, wood etc.) to the Arctic Ocean benefit from a very short period of favourable conditions, between the end of the ice break-up and the low water stage.

Numerous anastomosed branches represent another type of channel observed in the islands and floodplain. These channels are several tens of metres wide, and often sinuous. A certain number of them are not directly connected with a main channel, and may even disappear downstream without outlets. These anastomosed channels, flooded during the peak discharge, are rapidly dewatered. These characteristic channels can be associated with three main factors controlling the fluvial dynamics of the Lena: the brevity of the efficient discharge, the formation and rapid destruction of the log- and ice-jams, and the very low gradient of the river (0.0001). A great number of topographic depressions occupied by lakes or swamps can also be observed on the floodplain and islands.

This fluvial system may be compared with anabranching rivers, which are multiple channels separated by permanent alluvial islands (Smith 1986; Knighton and Nanson, 1993; Nanson and Knighton, 1996). The regime

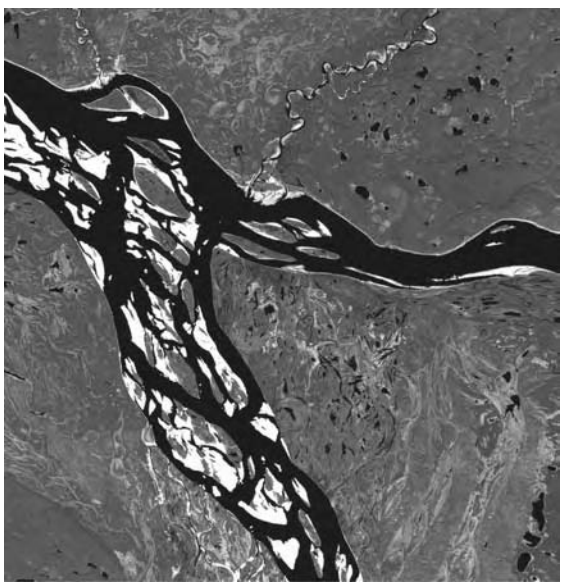

Figure 11.4 The Lena River at the Aldan junction in summer, Landsat image. Width of the image: 45 km. Source: Landsat.org, Center for Global Change and Earth Observations, Michigan State University (http://landsat.org)

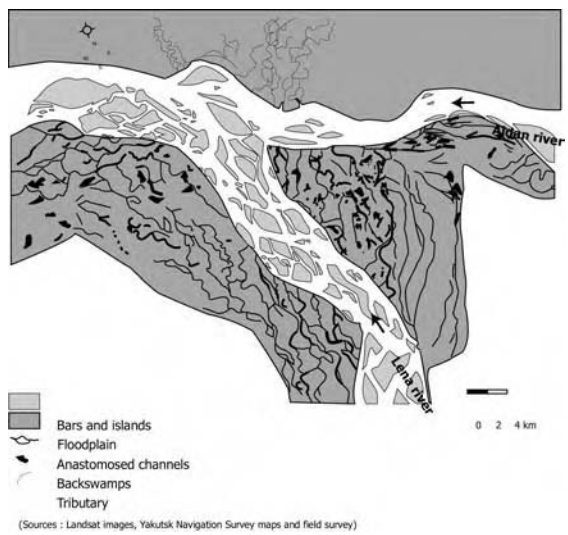

Figure 11.5 Fluvial landforms of the Lena River at the Aldan junction. (Geographie Physique et Quatenaire, 54, 327–342, Costard and Gautier, 2000. Reproduced by permission of Les Presses de l'Universite de Montreal)

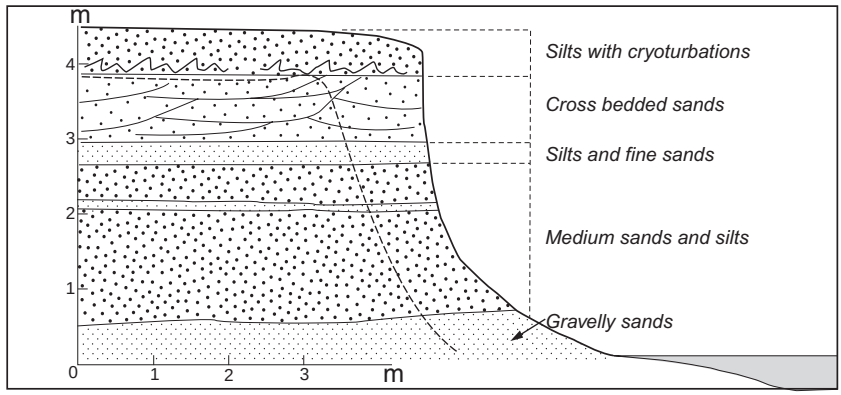

Figure 11.6 Section in the Lena River of a frozen river bank (63°25′N–129°25′E)

of the anabranching systems maximizes bed-sediment transport under very low gradient and efficient discharges. The low specific stream power of the Lena River and its tributaries is due to their very gentle gradient. Therefore, the sediment load (mainly sandy deposits) does not migrate over long distances downstream and is accumulated on wide bars, long islands and anastomosed branches (Gautier and Costard, 2000).

Specific deposits bordering the main active channels could be associated with the log-jams and ice-jams that generate major sedimentation processes. Sedimentary sequences located along channel margins have a certain number of common sedimentary features: sub-horizontal layers at the base consist of well-sorted medium sands which are covered by silts and sands showing marked cross stratifications (Figure 11.6).

At the beginning of the outburst flood, the river transports great quantities of ice and tree logs that create local jams. The conjunction of several elements explains the jam formation: (i) the thickness (up to 2 m) of the river ice during the winter; (ii) the density of the vegetation on the islands and the floodplain, which provides a great quantity of logs transported during the flood and which favours the formation of jams on the lateral margins. The accumulation of ice and logs causes a transitory rise in the water level, before the jam breaks. This mechanism involves the 're-routing' of the water of the channel towards the plain or across an island, thus creating a new channel inlet. In the channel inlet thus formed, sediments are similar to those of the nearby active channels. Marked cross stratifications are associated with the progradation of the sand and silt. The breaking of the log- and ice-jams initiates the mechanism of avulsion and the deposition of specific sedimentary features on the channel margins. Only the sudden increase in the water energy makes it possible to explain the presence of these sands on the high parts of the islands and channel margins. However, as a consequence of the brevity of this particular phenomenon, the inlet of the channel is rarely prolonged downstream (Figure 11.7). Moreover, the very low gradient determines that the hydraulic power is also limited. Thus the mechanism of avulsion is frequently blocked in its initial stage. Finally, it can be supposed that the jam-breaks and their associated deposits occur over a surface that is still frozen.

Figure 11.7 Inlet of an anastomosed channel on the Lena River. The size of the channel decreases downstream. Photo: E. Gautier, 1997

An interesting comparison could be made with the study conducted by Smith and Pearce (2002) on the Milk River (Alberta and Montana) where channel ice-jams also reroute river water across meander lobes and erode gullies. In this case, the ice-jams force flow to avulse, forming a gully that initiates a new channel. Thus a complete avulsion occurs. Smith and Pierce (2002) also

describe scour holes in the Milk River floodplain that are formed by water vortices beneath and between ice blocks.

11.6 THERMAL EROSION AND ITS IMPACT ON THE FLUVIAL FORMS

Thermal erosion refers to erosion by water combined with its thermal effect on frozen ground. During the flood season, the river water induces the propagation of a thawing line within the frozen riverbank. Thawing of the ice within a porous medium reduces the strength of the thawed sediments and produces easily removable uncemented ground material. This explains why thermal erosion is more effective than pure mechanical erosion. But this is only true for noncohesive sediments (Jahn, 1975).

Fast bank retreats are observed when thermal and mechanical erosion are jointly at work. With a relatively high discharge, the thawed sediments are swept away. During the thawing period, the river is constantly in direct contact with the permafrost and induces both thermal and mechanical erosion. Are (1983) calculated a mean 6.5 m annual retreat of the riverbanks. He has observed exceptional bank retreats of 19–24 m year^{-1} (40 m year^{-1} at the head of islands) on the Lena River. A diachronic study (1967–2001) of the middle Lena River fluvial forms on the basis of satellite images illustrates clearly the efficiency of the bank erosion and its spatial distribution. Two main results can be highlighted.

The main channel bank retreat can be considered as low or moderate: 3–4 m year^{-1} that represents only 0.05–0.1 % of the channel width. This erosion does not allow the channel to migrate. The channel remained stable during the study period. Higher values have been observed (14–18 m year^{-1}), but they affect only short sections of the river, especially those located upstream of major junctions in relation to active deposition on bars. It can also be noticed that anastomosed branches remain remarkably stable.

The heads of islands undergo strong erosion with mean values of 12 m year^{-1} and maximal values reach 20 m (near Yakutsk and just upstream of the junction with the Aldan River), and a exceptional rate of 40 m was measured locally over a very short stretch (Figure 11.8). Therefore, the islands are the most mobile mesoforms in the river.

During flooding, thermal erosion may have produced thermo-erosive niches which contributed to the disequilibrium of the bank by thermokarstic subsidence (Walker, 1983), resulting in subsequent large slumps along the riverbanks (Figure 11.9). The water level does not seem to be the primary factor behind the corresponding level of thermo-erosive niches. Various field observations indicate the variation of the thermo-erosive niches at various scales as a function of the lithologic discontinuities. Some of these variations in the niching rate have been identified as resulting from the existence of main discontinuities between sand and silt.

Figure 11.8 Recession of riverbanks by thermal erosion between 1969 and 2002 along the Lena at the latitude of Yakutsk city

These stratified banks of fine and coarse sediment may lead to characteristics bank morphology. Thermo-erosive niches seems to be particularly well developed at the interface. River bed and terraces are mostly capped with 10–35 m of silt. These river banks show sandy material usually overlain by silt-clay. Such banks have a coarse noncohesive substratum and a relatively more cohesive

Figure 11.9 Thermo-erosive niches along the Lena River. Height of the river bank 22 m. Photo: F. Costard, 1997

top stratum. In most places, the deepest thermo-erosive niches usually corresponds to the interface between these two kinds of materials.

11.7 IMPACT OF CLIMATIC CHANGE ON THE HYDROSYSTEM

Global air surface temperature has increased 0.6 °C over the last century and climate models project a 1.4–5.8 °C global surface air temperature increase in the 21st century, with a particularly strong effect on Arctic zones (IPCC, 2001; Serreze, *et al*., 2002). In the Lena Basin, according to Yang *et al*. (2002), the annual mean temperature has increased about 1.3 °C since 1930. This warming is characterized by a progressive inter-seasonal change: the winter temperature (November–March) has increased by 1.9–3.8 °C over the last six decades, and spring temperature (April and May) by 0.7–1.4 °C. Related to the cold-season temperature change, a remarkable thinning of the river ice cover at Kusur station has been discovered by Yang *et al*. (2002). The ice cover was 20–30 cm thinner during 1970–1980 than during the 1950s or 1960s. In central Siberia (near Yakutsk), Fedorov and Konstantinov (2003) observed a pronounced increase of the mean annual air temperature since the early 1980s, the temperature varied between −10 °C and −11 °C for the 1930–1980 period whereas it has reached −8.8 °C since 1992. The summer temperature shows the same trend. Positive anomalies of the soil temperature and permafrost temperature over the last two decades accompanied by a deepening of the active layer accelerate the extension and subsidence of thermokarstic depressions (Pavlov, 1994; Serreze *et al*., 2002; Federov and Konstantinov, 2003).

The climatic change strongly influences the behaviour of the river. Peterson *et al*. (2002), studying the six largest Eurasian Arctic rivers (including the Lena), calculated an annual average rate of increase in water volume of 2.0 ± 0.7 km^3, an approximate 7% increase. The change of the active layer depth influences the most important groundwater supply to the river bed, the river flow is also reinforced by winter precipitation increase (of about 12 mm) and the earlier thawing. These factors in conjunction explain a strong winter and spring discharge increase (November–May, +27–90%) and Yang *et al*. (2002) underline that the highest floods registered in May were associated with positive temperature anomalies.

11.8 CONCLUSION

The Lena River is one of the major fluvial hydrosystems in the world. By its length and its south–north orientation, the Lena crosses a wide latitudinal range, and its basin exhibits a great diversity of flora and fauna. The Lena is particularly interesting for the relationships between climate, permafrost, and hydrologic dynamics in its channel. The extremely episodic flow regime, controlled mainly by rapid snowmelt during spring, generates characteristic fluvial forms and processes. During the flood season, the river water propagates a thawing line within the frozen riverbank. When thermal and mechanical erosion are jointly at work, bank retreats of 25–40 m $year^{-1}$ occur locally. The floodplain width can be up to 25 km wide and include a variety of thermokarstic landforms due to the local melting of the continuous permafrost. The fluvial system has developed a multichannel anabranching pattern accompanied by very large forested islands. Sediment transport is thus optimized on very low gradients and short efficient discharges. The Arctic is a climatically sensitive region, and recent studies clearly emphasize the current warming and the associated hydrologic impacts. Positive anomalies of the soil temperature and permafrost temperature over the last two decades accompanied by a deepening of the active layer have deeply influenced the river which functions with high discharge during the flood season. The increasing winter and spring discharges may accelerate the retreat of the riverbanks and thereby partially destabilize the fluvial dynamics of the system.

REFERENCES

Anisimova, N.P., Nikitina, N.M., Piguzova, U.M. and Shepelyev, V.V., (1973) Water sources of Central Yakutia – Guidebook, 47 p. In: Proceedings, 2nd International Conference on Permafrost, Yakutsk, URSS, National Academy of Sciences, Washington, DC, 783 p.

Antonov, S., (1960) Delta reki Leny. *Trudy Okeanographitcheskiy Comissyi. Ak. Nauk. SSSR*, 6: 25–34.

Antonov, V.S., (1967) *The Mouth Area of the Lena* (the Hydrographic Review). Gidrometeoizdat, Leningrad, 440 p.

Are, F.E., (1983) Thermal abrasion on coasts, pp. 24–28. In: Proceedings, 4th International Conference on Permafrost, Fairbanks, Alaska, National Academy Press, Washington, DC, 1524 p.

Czudek, T. and Demek, J., (1970) Thermokarst in Siberia and its influence on the development of lowland relief. *Quatern. Res.*, 1: 103–120.

Fedorov, A. and Konstantinov, P., (2003) Observations of surface dynamics with thermokarst initiation, Yukechi site, Central Yakutia, pp. 239–243. In: Proceedings, 8th International Conference on Permafrost, Zurich, Switzerland, Balkema, 660 p.

Gautier, E. and Costard, F., (2000) Les systèmes fluviaux à chenaux anastomosés en milieu périglaciaire: la Léna et ses principaux affluents en Sibérie Centrale. *Géograph. Phys. Quatern.*, 54/3: 327–342.

Gautier, E., Brunstein, D., Costard, F. and Lodina, R., (2003) Fluvial dynamics in a deep permafrost zone: the case of the middle Lena river (Central Yakutia), pp. 271–275. In: Proceedings, 8th International Conference on Permafrost, Zurich, Switzerland, Balkema, 660 p.

Gordeev, V.V. and Sidorov, I.S., (1993) Concentrations of major elements and their outflow into the Laptev Sea by the Lena river. *Mar. Chem.*, 43: 33–45.

Huh, Y., Tsoi, M.Y., Zaitsev, A. and Edmond, J.M., (1998) The fluvial geochemistry of the rivers of Eastern Siberia: I. Tributaries of the Lena river draining the sedimentary platform of Siberian craton. *Geochim. Cosmochim. Acta*, 62(10): 1657–1676.

Intergovernmental Panel on Climate Change (IPCC) 2001. The specific basis. In: *Contribution of Working Group 1 to the Third Assessment Report of the IPCC* (Houghton, J.T. *et al*., Eds.), Cambridge University, Press, Cambridge.

Jahn, A., (1975) *Problems of the Periglacial Zone*, PWN-Polish Scientific Publishers, Warsaw, 223 p.

Katasonov, E.M. and Soloviev, P.A., (1969) Guide to trip in Central Iakoutia. In: *Palaeogeography and Periglacial Phenomena*, International Symposium, Iakutsk, 87 p.

Knighton, A.D. and Nanson, G.C., (1993) Anastomosis and the continuum of channel pattern. *Earth Surf. Proc. Landforms*, 18: 613–625.

Lopatin, G.V., (1952) River Loods in the USSR (in Russian). *Vses. Geogr. Ovo. Novia Ser. 14. Nauka*, Moscow, 336 p.

Lvovitch, M.I., (1971) *Rivers of the USSR* (in Russian). Mysl, Moscow, 349 p.

Nanson, G.C. and Knighton, A.D., (1996) Anabranching rivers: their cause, character and classification. *Earth Surf. Proc. Landforms*, 21: 217–239.

Pavlov, A.V., (1994) Current change of climate and permafrost in the Arctic and Subarctic of Russia. *Permafrost Periglacial Proc.*, 5: 101–110.

Peregovich, B., Hoops, E. and Rachold, V., (1999) Sediment transport to the Laptev Sea (Siberian Arctic) during the Holocene – evidence from the heavy metal composition of fluvial and marine sediments. *Boreas*, 28: 205–214.

Peterson, B.J., Holmes, R.M., McClelland, J.W., Vörösmarty, C.J., Lammers, R.B., Shiklomanov, A.I., Shiklomanov, I.A. and Rahmstorf, S., (2002) Increasing river discharge to the Arctic Ocean. *Science*, 298: 2171–2173.

Péwé, T.L., (1991) Origin and character of loesslike silt in unglaciated south-central Yakutia, Siberia, USSR. *US Geological Survey Professional Paper* 1262, 46 p.

Serreze, M.C., Bromwich D.H., Clark M.P., Etringer A.J., Zhang T. and Lammers R., (2002) The large scale hydroclimatic of the terrestrial Arctic drainage. *J. Geophys. Res.*, 108(D2).

Shiklomanov, I.A., Shiklomanov, A.A.I., Lammers, R.B., Peterson, B.J. and Vorosmarty, C.J., (2000) The dynamics of river water inflow to the Arctic Ocean, pp. 281–296. In: The Fresh Water Budget of the Arctic Ocean, Proceedings of the NATO Advanced Research Workshop, Tallin, Estonia, 27 April–1 May 1998, Kluwer, Dordrecht.

Smith, D.G., (1986) Anastomosing river deposits sedimentation rates and basin susbsidence, Magdalena river, Northwestern Columbia, South America. *Sediment. Geol.*, 46: 177–196.

Smith, D.G. and Pearce C.M., (2002) Ice jam-caused fluvial gullies and scour holes on northern river flood plains. *Geomorphology*, 42: 85–95.

Soloviev, P.A., (1963) Alasny doliny Jakutii, pp. 80–83. In: *Conditions and Peculiarities of Permafrost Development in Siberia and North-East*, Moscow Academy of Sciences, Yakutsk Permafrost Institute, 90 p.

Soloviev, P.A., (1973) Thermokarst phenomena and landforms due to frost heaving in Central Yakutia. *Biul. Peryglac.*, 23: 135–155.

Walker, H.J., (1983) Erosion in a permafrost dominated delta, pp. 1344–1349. In: Proceedings, 4th International Conference on Permafrost, Fairbanks, Alaska, National Academy Press, Washington, DC, 1524 p.

Yamskikh, A.F., Yamskikh, A.A. and Brown, A.G., (1999) Siberain-type Quaternary floodplain sedimentation: the example of the Yenisei river, pp. 241–252. In: *Fluvial Processes and Environmental Change* (Brown, A.G. and Quine, T.A., Eds.), John Wiley & Sons, Ltd, Chichester, 413 p.

Yang D., Kane D.L., Hinzman L.D., Zhang X., Zhang T. and Ye H., (2002) Siberain Lena River hydrologic regime and recent change. *J. Geophys. Res.*, 107(D23).

12

The Danube: Morphology, Evolution and Environmental Issues

Dénes Lóczy

Department of Physical Geography, University of Pécs, Ifjúság útja 6, H-7624 Pécs, Hungary

12.1 INTRODUCTION

The Danube, the second longest river (2860 km) in Europe, is truely an international river. Not surprisingly, it is known by various names: Donau (German), Dunaj (Slovakian), Duna (Hungarian), Dunav (Southern Slavic), Dunarea (Romanian), Dunaj (Ukrainian), Danubius (Latin), Ister (Greek). The name Danubius is of Celtic origin ('danu' meaning 'fast-flowing river') and probably refers to a river gorge cutting through the Swabian or the Franconian Jura.

The Danube is the only major European river that follows a general west to east course and, thus, transports water from high mountains with snow cover in winter and basins of abundant rainfall towards the drier parts of the continent's humid temperate zone. Its basin (Figure 12.1) extends over 817 000 km^2, covering most of the Eastern Alps, the eastern slopes of the Black Forest, the southern slopes of Swabian-Franconian Jura (Alb), the Swabian-Bavarian Basin (Alpine Foreland), the south-western section of the Bohemian Forest, the minor basins of the Austrian Alpine Foreland, the Vienna Basin, the eastern half of Czecho-Moravian Hills, the Carpathians, the Carpathian Basin, the Dinaric Range, the low mountains of Serbia, the northern slopes of the Balkan Range, the Romanian Plain and the western and northern slopes of the Dobrogea Hills. The highest point in the watershed is Piz Bernina (4049 m) in the Eastern Alps. More than 1000 km^2 of the catchment in the Eastern Alps is glaciated, and glacial meltwater is an important source of discharge for the 15 major right-bank tributaries. There are 20 major left-bank tributaries to the Danube, mostly fed by rainfall. Frequent changes in present-day river behaviour point to a highly variable physical environment.

The Danube functions as a reserve for drinking, industrial and irrigation water; a source for generating electricity; an artery for navigation, an area for recreation. It is also an embodiment of scenic beauty and a source of inspiration for writers (Jules Verne's novel 'Le pilote du Danube'), poets (the Hungarian Attila József's philosophical poem 'By the Danube'), and composers (Johann Strauss' waltz 'The Blue Danube').

12.2 WATER AND SEDIMENT

The annual water discharge of the Danube to the Black Sea amounts to 191 km^3 (6047 $m^3 s^{-1}$; Malciu, 2000). The remarkable increase in the mass of water along the Austrian section is demonstrated in the difference between mean discharges above the confluence with the Inn (2230 river km, 625 $m^3 s^{-1}$) and at Vienna (number 8 in Figure 12.1, 1920 $m^3 s^{-1}$). A moderate input is derived from the northern sector of the Carpathian Basin (at Bratislava, number 9, 2080 $m^3 s^{-1}$, at Budapest, number 12, 2340 $m^3 s^{-1}$). The discharge of the Danube increases downstream from contributions by the Drava, the Tisza and, particularly, the Sava (at Orşova, number 20, 5600 $m^3 s^{-1}$). Only a modest increase (Duna, 1998) occurs along the Romanian–Bulgarian border (at Galaţi, just below number

Large Rivers: Geomorphology and Management, Edited by A. Gupta

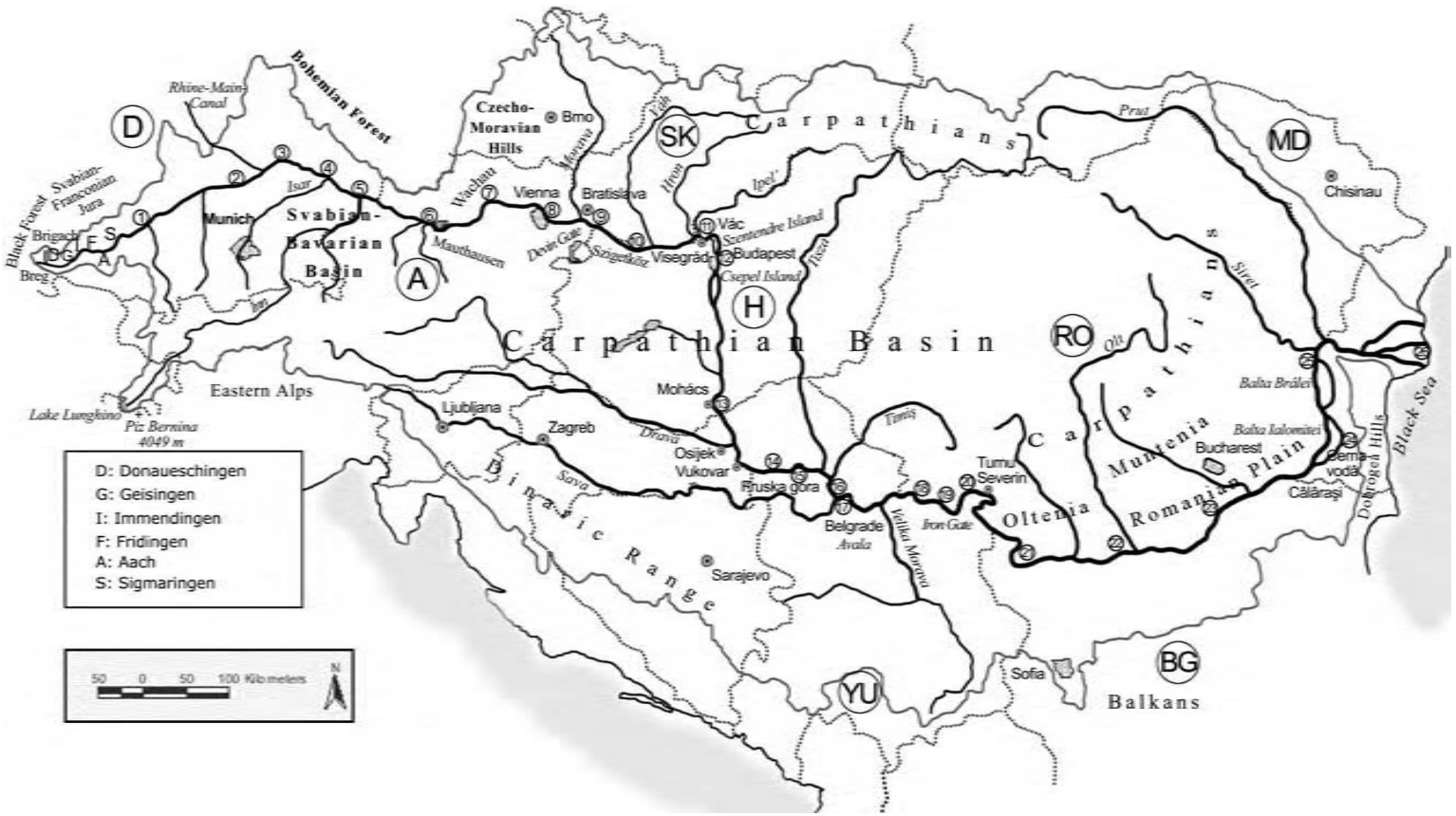

Figure 12.1 The Danube catchment. All geographical names mentioned in the text [major tributaries, gauging stations (1–26 as numbered in Table 12.1), the Danubian countries and macroregions] are indicated on this map. Capital lettters within circles indicate countries

25 in Figure 12.1, 6430 $m^3 s^{-1}$). The absolute maximum recorded discharge to the Black Sea was more than 35 000 $m^3 s^{-1}$ in 1897 (DDBRA, 2000). For mean water discharge at the mouth the Danube ranks twenty-second among the rivers of the world (Czaya, 1981). Remarkably, an increase in annual discharges at stations of the upper section coincides with a decrease along the Serbian and Romanian reaches. Thus, the contrast between the 'humid' and 'arid' parts of the subbasins is increasing.

Taken as a whole the Danube cannot be considered a mountain river unlike some of its tributaries. Its bed drops not more than 680 m (almost 80 % in the Upper Danube) and, except for the irregularities caused by gorges, it has a graded longitudinal section (Figure 12.2). The pre-dam average bed slope was 0.00025 in the Iron Gate Gorge (Lászlóffy, 1965). However, it drops below 0.00004 along the lowland reaches of the Romanian–Bulgarian border, and 0.00001 for the last 500 km.

The river hydrograph mostly depends on the temperate climate of the catchment, and floods along the tributaries of the Upper Danube and right-bank tributaries from the Alps. Two periods of flooding are usually observed: early spring and early summer (Lóczy and Juhász, 1997). Sudden snowmelt along the Upper Danube may cause ice-jam floods in early spring particularly along the Austrian and Hungarian section (like in Buda in 1838). Early summer 'green' floods (so-called because of the green twigs and branches that are carried by the river) are associated with the precipitation maximum on the Upper Danube catchment, often coinciding in time with the melting of Alpine glaciers. The lowest water stages are observed in autumn and winter.

The channel conditions along the Danube are variable. The hydraulic radius is very large in gorges with narrow channels (particularly in the Iron Gate at Đerdap, where the channel width is only 170 m). It is low in the broad channels of the lowlands. At Belgrade, number 17 in Figure 12.1, the channel is almost 1 km wide and before entering gorges upstream at Đerdap, (number 20) its width is more than 2 km. The maximum measured river depth is at the damsite of Đerdap (>75 m). The channel is highly variable along reaches where flow regulations and artifacts like bridges have strongly modified natural channel shape. At Budapest the river is only 3 m deep at some locations, while at Liberty Bridge it is >10 m. Maximum current velocity is 5–6 m s^{-1} during floods along the upper section. At Budapest the mean current velocity is 0.5 m s^{-1}, amounting to 2.5 m s^{-1} at exceptionally high water levels.

Various estimates exist for the sediment transported in the Danube (Table 12.1). The data refer to readings taken after the major flow regulation activities and confirm the general lowland character of the river. Suspended load prevails over bedload. The amounts have been reduced by hydroelectric dams constructed on the Danube and its tributaries (Kraus-Kalveit and Pannonhalmi, 2001). Bedload has been reduced to a very small fraction (often a tenth or twentieth) of the values during the 1960s in the upper section. Today, suspended solids do not occur in concentrations above 50 mg l^{-1} (ICPDR, 2002). At present, average total load at the apex of the delta is estimated as 67–80 million tonnes (Domokos *et al*., 2000) or as 51.7 million t $year^{-1}$, averaged over 1858–1988 (Malciu, 2000). The extreme values recorded are 162 million t in 1941 and 19.8 million t in 1921 (DDBRA, 2000). Intensive

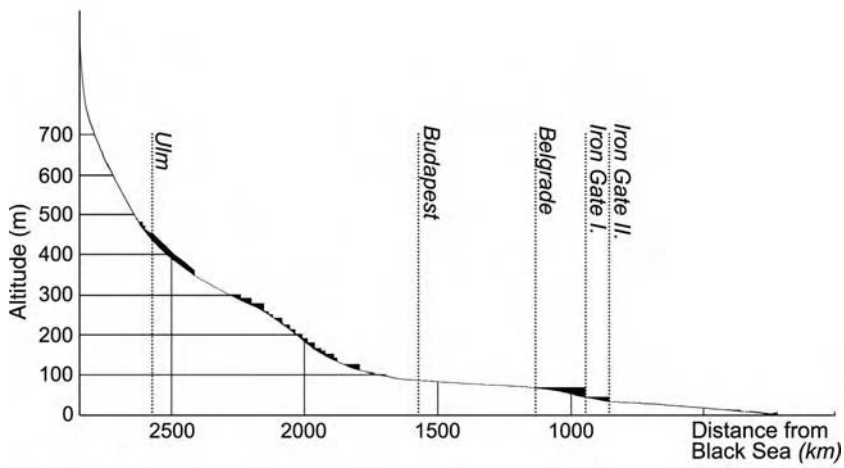

Figure 12.2 The longitudinal profile of the Danube with impounded reaches (after Pécsi, 1959)

Table 12.1 Proportions of the estimated bedload and suspended load transport along the Danube after low-flow regulations after Lászlóffy, 1965

No.[a]	Locality	River km from mouth	Bedload			Suspended load	
			Annual average (million tonnes)	Average grain size (mm)	Maximum grain size (mm)	Annual average (million tonnes)	Specific load ($mg\,l^{-1}$)
1	Ulm	2586	0.03/	14	65	0.26	72
2	Ingolstadt	2458	0.15/0.03[b]	17	65	0.96/0.40[b]	100/42[b]
3	Regensburg	2376	0.04	7	120	1.0	74
4	Hofkirchen	2257	0.06	10	100	1.1/0.055[b]	55/8[b]
5	Passau	2225	0.70	30	150	3.9/0.35[b]	88/6[b]
6	Linz	2135	0.54	20	100	4.0/0.34[b]	87/10[b]
7	Stein–Krems	2004	0.72	18	110	4.5/0.46[b]	87/11[b]
8	Vienna	1934	1.07/ca. 0.4[b]	11	80	4.7/0.048[b]	79/10[b]
9	Bratislava	1869	0.90	10	70	7.3/1.21[b]	113/13[b]
10	Gönyü	1791	0.05	3	35	6.5/0.37[b]	99
11	Nagymaros	1695	0.02	2	30	10/0.91[b]	135
12	Budapest	1647	0.01/–[b]	2/–[b]	30/–[b]	11/1.46[b]	149/18[b]
13	Mohács	1447	0.04/–[b]	1/–[b]	2/–[b]	15/1.3[b]	199/38[b]
14	Bogojevo	1367	0.05	1/–[b]	2/–[b]	18/1.68[b]	191/42[b]
15	Novi Sad	1255	0.01	1/–[b]	1/–[b]	18	191
16	Zimun	1173	–	–	–	33	271
17	Belgrade	1171	0.05	1	2	40	239
18	Baziaş	1072	0.10	5	60	44	250
19	Drencova	1015	0.03	2	30	45	255
20	Orşova	955	–	–	–	45	255
21	Calafat	795	–	–	–	46	261
22	Corabia	630	–	–	–	52	292
23	Giurgiu	493	–	–	–	66	357
24	Cernavodă	300	–	–	–	70	375
25	Brâila	170	–	–	–	70	375
26	Sulina	0	–	–	–	76	380

[a] Numbers listed are the locations shown in Figure 12.1.
[b] Updated with new data (from various sources) after barrage constructions.

deposition occurs along the Kilia (Chilia) distributary at the delta, where extensive shoals build up. However, the amount of annual suspended sediment was reduced to 30 million t between 1981 and 1990.

The Danube freezes in cold winters. Ice conditions can be illustrated by the long-term averages observed at Bratislava, with river ice occurring in 94% and ice-jams in 32% of years. The average duration of drift ice is 30–40 days, usually between mid-December and early February. On average, the first ice on water is recorded on 15 November and the last on 15 April.

12.3 HEADWATERS OF THE DANUBE

In the time of the great explorations the location of the sources of major rivers in remote parts of the Earth presented a real challenge for scientists. Although it is located in the heart of Europe, the true source of the Danube remained a mystery for a long time. The spring in the park of the Fürstenberg castle of Donaueschingen regarded as the source ('Donauquelle') since the Romans, is in reality just a place where a minor headwater issues. The Danube rises from two streams (Figure 12.3): the Brigach, that rises at 1125 m above sea level near the village of Hirzbauernhof; and the Breg, which takes its origins from numerous small springs in a swamp meadow at an altitude of 1078 m in the northern side of the hill Brend (1148 m). As the Breg is longer than the Brigach, this small watercourse is rightfully considered the uppermost reach of the Danube. However, the name Danube only applies to the river from the confluence at Donaueschingen, ca. 45 km downstream.

Both headwaters rise in the area of the central intrusion of Upper Carboniferous (ca. 320 Ma old) granite surrounded by a paragneiss. This surface was subsequently eroded to a plain, and covered by fluvial and marine sediments during the Triassic and Jurassic. As a result of an uplift during the Miocene, the strata acquired an easterly

Figure 12.3 The channelized Breg and the braided Brigach join to form the Danube below Donaueschingen, Germany (photograph by Lóczy)

Figure 12.4 Percolation of water underground at Immendingen. The river bed is dry for an average of 55 days in a year (photograph by Lóczy)

dip of 7–15° and was significantly denuded. Rapid uplift and differential erosion in the Pliocene produced the Swabian-Franconian escarpments, cut across by the Danube headwaters. The streams transport small boulders and small shards of granite.

Drainage systems may be named after the longest headwater or alternatively after the one with the highest discharge. In the latter sense the Danube system originates from the Inn, a major tributary (length 510 km; catchment area 26 100 km^2) rising from a tarn (Lake Lunghino) in the Rhaetian Alps, Graubünden, Switzerland with a mean discharge of 730.8 $m^3 s^{-1}$ at its confluence with the Danube at Passau (number 5, Figure 12.1). Its whitish colour indicates that it also transports more suspended sediment (clay particles from Tertiary sediments and silt from Quaternary till) than the Danube.

12.4 THE DANUBE: A DESCRIPTION

The river is commonly divided into three parts. The Upper Danube ends at the narrow passage of the Devín Gate, the Middle Danube stretches downstream to the Iron Gate, and the Lower Danube flows through the lowland beyond and the delta. The upper section is traditionally identified with the occurrence of salmonid fishes, the middle section with barbel *(Barbus barbus)*, and the lower lowland reaches with bream *(Abramis brama)*. The delta is characterized by a brackish water biota. Pristine or rather semi-natural conditions are restricted to very short stretches of the Danube and its tributaries.

12.4.1 The Upper Danube in Germany and Austria

An extraordinary phenomenon occurs at a short distance below the confluence of the headwaters. The Danube regularly loses water to the Rhine system. Downstream of Geisingen the river breaks through the Swabian Jura in a picturesque gorge. This valley section originates from the time when the Jurassic limestones were still covered by the easily erodible Alpine molasse (>15 Ma ago). The palaeo-Danube formed large meanders, which with the uplift of the Swabian Jura, were incised into the limestone. Swabian Jura is a source of the Danube's coarse gravel (Table 12.1).

The Swabian Jura, the largest karst region (ca. 5000 km^2) in Europe (Geyer and Gwinner, 1984), is a low plateau of Malm Limestone with a retreating 200 to 300 m high escarpment above the Neckar (a tributary to the Rhine), but with usually much gentler slopes towards the south where a marginal flexure forms its topographic boundary. Karstic processes began to operate at least 15 Ma ago, when uplift with southeastward tilting started. The extensive caves and underground passages (estimated total volume 50 million m^3), opening to the surface in ponors, are responsible for the percolation of Danube water deep into the subsurface and eventually into the Rhine system (Hötzl, 1996). Thus, the Rhine extends its drainage area underground, capturing more and more of the Danube catchment.

Bedding planes and joints in Oxfordian or Kimmeridgian limestones broadened by karstic process also occur in the Danube bed itself and, consequently, the channel may dry up entirely for months as happened at Immendingen in 1874, 1911, 1921, 1928 and 1943, and recently almost every year. Between Immendingen (Figures 12.4 and 12.5) and Fridingen, loss of water underground is calculated at 4 $m^3 s^{-1}$ as the total for several sites of percolation. The water follows underground passages for 12–

Figure 12.5 The Aachquelle, a spring of abundant discharge in Germany (photograph by Lóczy)

20 km and reappears in springs of abundant yield towards the south-east. The most important one among the 12 springs is Aachtopf at Aach (Figures 12.4 and 12.5). It is the largest in Germany (medium yield 8.59 $m^3 s^{-1}$; maximum 24.10 $m^3 s^{-1}$; minimum 1.31 $m^3 s^{-1}$).

In 1877 an experiment with 20 t of rock salt used as a tracer indicated that the catchment of the Danube is linked to that of the Rhine through underground karst passages. Following the 15% overall slope of the passages, it took 60 h until the underground stream of ca. 195 $m h^{-1}$ velocity reached the surface in the Aachtopf spring. Further tracer experiments (Werner *et al*., 1997) revealed that about two-thirds of its water yield derives from the Danube. The springwater feeds a stream (Radolfzeller Ach) which flows into Lake Constance, part of the Rhine catchment.

Along the uppermost section (until Linz in Austria, number 6, Figure 12.1) downcutting channels are typical (Figure 12.3). The entrenched meanders between Geisingen and Sigmaringen, however, indicate that the earlier slope was lower.

At Sigmaringen, the eastern gate to the Danube Gorge, the river leaves the Swabian Jura, enters the Swabian-Bavarian Basin, and cuts a broad valley along the southern marginal flexure of the mountains. The first two significant right-bank tributaries are the Iller (68 $m^3 s^{-1}$ discharge at confluence) and the Lech (118 $m^3 s^{-1}$), which have built an extensive elevated surface of Upper Molasse sands and gravels during the Eopleistocene (ca. 1 Ma ago) and Early Pleistocene glaciations (0.7–0.4 Ma ago, Emiliani isotope stages 16–10) (Löscher, 1976; Jerz, 1995). Both the coarse glacial deposits and the underlying beds of upper freshwater molasse are excellent aquifers. Coarse fraction of the glacial deposits has increased the grain size of the Danube sediment.

At Regensburg (number 3, Figure 12.1), the northernmost point of its valley, the Danube meanders broadly following the moderate subsidence (maximum 16 m over 10 ka) of the Alpine Foreland (Buch, 1989). Downstream of Regensburg the rivers from the Alps (the Isar with 176 $m^3 s^{-1}$ discharge and the Inn with 730 $m^3 s^{-1}$) deposit their load to form large alluvial fans and broad terraces. An important feature of this section on the Danube is the large-scale asymmetry of the location of the river, the channel being forced by tributaries carrying huge amounts of bedload towards the northern margin of the Swabian-Bavarian Basin.

After receiving its largest tributary the Inn at Passau, the Danube enters the Linz Basin and follows the northern margin of the Austrian Alpine Foreland. Alpine tributaries of high discharge and sediment load, the Traun (150 $m^3 s^{-1}$), the Enns (230 $m^3 s^{-1}$), and the Ybbs (42 $m^3 s^{-1}$), maintain the asymmetry of the catchment mentioned above (Figure 12.1).

Tectonic control increases along the Austrian section as small plains alternate with constricted passages along the Danube. At the Enns confluence the Mauthausen Gate separates the Linz Basin from the Machland where crystalline gravels are deposited transported by a large number of streams from the southern spurs of the Bohemian Forest. This first basin that shows considerable sedimentation, is followed by one of the most spectacular gorges of the Danube, the Wachau. Then follows the largest depression that the river crosses along the Austrian section, the Vienna Basin. Here a 220 m thick middle Pliocene to Holocene alluvial sequence overlies deep Lower Miocene to Lower Pliocene marine sediments.

12.4.2 The Middle Danube (Slovakia, Hungary and Serbia)

In the Devín Gate (Porta Hungarica) between the Leitha Mountains and the Little Carpathians, where eight terraces have been identified (Mahr and Šajgalik, 1979), the river enters the Pannonian Basin (the largest of all the Danubian basins) and crosses its north-western and central parts. The Little Hungarian Plain is a focus of drainage network (Pécsi and Schweitzer, 1995). The palaeo-Danube built a double alluvial fan in the Little Hungarian Plain (Pécsi, 1959) below its confluence with the main river of Moravia, the Morava (105 $m^3 s^{-1}$ mean discharge and large amounts of suspended load, Table 12.1) at Bratislava. On this alluvial fan two meandering distributary channels have formed two large islands: the Szigetköz (375 km^2) bordered by the Moson Danube on the Hungarian side and the Žitný ostrov (in Hungarian: Csallóköz, 1600 km^2) bordered by the 128 km long Lesser Danube on the Slovak side. The Old Danube has a braided channel. River competence decreases rapidly along the present-day river bed on gravel. At the upper tip of the Szigetköz interfluve maximum grain size is 15–20 mm and at the lower one 5 mm. The environment along this section has been fundamentally altered by the construction of the Gabcíkovo Barrage (see below).

Before barrages were constructed on the Danube, coarse bedload arrived via the major left-bank tributaries, the Váh (190 $m^3 s^{-1}$ mean discharge) and the Hron (58 $m^3 s^{-1}$). A major right-bank tributary, the Rába (80 $m^3 s^{-1}$) with its confluence at Győr (near number 10, Figure 12.1) in contrast only transports suspended load. In the terraced valley east of Győr the Danube flows in a braided channel with numerous shoals built of the Váh and Hron deposits. A mineralogical study (Pécsi-Donáth, 1958) revealed the diverse composition of the middle Pleistocene terraces, remnants of the older alluvial fan of the Danube: quartz, quartzite, lydite, Alpine and Tatran (Carpathian) granites, gneisses, mica schists, fine-grained sandstones, menilites (liver opals), various limestones and dolomites. Minerals of volcanic origin (feldspar, muscovite, amphibolite, and pyroxene grains) are common and increase again in amount as the river leaves the Danube Bend near Budapest.

A dramatic change takes place when the Danube arrives at the andesitic Visegrád and Börzsöny Mountains range (volcanic activity dated to 15.5–14 Ma BP). The Danube in the Visegrád Gorge is 300 m wide and at least 5 m deep. Seven terraces are identified in the horseshoe-shaped bend of the Danube. At the town of Vác (river km 1680) the north–south stretch begins in the Great Hungarian Plain, the largest and driest of the Danubian basins. The anastomosed river of the Pleistocene is indicated by extensive islands, the largest being the Szentendre (gravel) and the Csepel Islands (coarse sand). The present river is different with meanders and point bars. The river follows the tectonic Buda Thermal Line, which gives rise to hot springs (even on the channel bed) and the famous baths of Budapest. Even before the construction of the Austrian hydroelectric plants, gravel transport in the Danube did not reach further downstream than immediately beyond Budapest (Table 12.1). Pécsi (1959) concluded that the Danube deposited a 15–20 m thick alluvial sequence here during the Holocene, based on his investigation of several floodplain and terrace cross-sections.

South of Budapest the Danube receives no major tributary for more than 250 km. The striking valley asymmetry continues. On the right bank the high undercut loess bluffs of the Mezőföld occur in contrast to the flat alluvial left bank. South of Mohács the Danube leaves Hungary marking the boundary between Croatia and Serbia (Jankovič and Jovičič, 1994). The three largest tributaries along this section differ in their water and sediment discharges. The Drava (696 km length, 622 $m^3 s^{-1}$ mean discharge) flows into the Danube east of Osijek (upstream of number 14, Fig. 12.1). Along its upper reaches it transports a large amount of bedload, but only some sand and suspended silt and clay reach the Danube (Bendeffy, 1979). The longest tributary, the Tisza (962 km channelised length), discharges a long-term average of 995 $m^3 s^{-1}$ water at the confluence of Titel (near number 15, Figure 12.1), while the Sava of almost the same length (940 km) yields 1800 $m^3 s^{-1}$ at Belgrade. As opposed to the suspended fine silt of the 'blonde' (light-coloured) Tisza, the Sava brings walnut-sized limestone and ophiolite boulders from the Dinaric Mountains. An even greater contrast is found between the sediment loads of the next left-bank tributary, the Timiş (104 $m^3 s^{-1}$ mean discharge), and a right-bank one, the Velika Morava (the second river of this name, 244 $m^3 s^{-1}$). The former transports very fine sand and silt, while >10 cm diameter volcanic gravels travel down the Velika Morava (Bendeffy, 1979).

The discharge of the Danube rises to 5840 $m^3 s^{-1}$, allowing it to cope with the increased load. In the southernmost Great Hungarian Plain the river is forced to turn east first at Vukovar by the Palaeozoic metamorphics of Fruška Gora (539 m) and again near Belgrade by the Avala Laccolith (511 m).

Leaving the Pannonian Basin, the river crosses the arc-shaped Southern Carpathians–Serbian Ore Mountains in the 145 km long narrow reaches between Bazias (number 18, Figure 12.1) and Turnu Severin. The first in this series of gorges, Đerdap, is separated by an embayment into a

Figure 12.6 The deepest gorge on the Danube: the Iron Gate on the Romanian–Serbian border. (Reproduced with permission from Attila Nagy)

small and a large gorge. Jurassic limestone is exposed on 250–300 m high walls on both sides. The mean water level after damming is 77 m, but the deepest points of large potholes in the rocky river bed are about 7–8 m above sea level. Leaving the Orşova Basin and merging with the Cerna (virtually the only typically Carpathian tributary of the Danube), the Danube enters the Iron Gate (Porţile de Fier) Gorge (Orghidan, 1966; Figure 12.6), the last of this series of gorges.

12.4.3 The Lower Danube (Romania, Bulgaria and Ukraine)

Below the Iron Gate occurs large-scale deposition. The river proceeds in large bends towards the south and turns east again south of Vidin. In the Vidin embayment the grain size of alluvium ranges from clay to sand, indicating an eventful but not yet properly studied river history.

Only 3.3 % of the Danubian catchment is in Bulgaria. Along the right bank stretches the 130 m high steep margin of the Danubian Tableland of Bulgaria (502 m maximum altitude) (Dinev and Mishev, 1980). A relatively significant tributary along this section is the Iskâr (368 km long, 8646 km^2 catchment area, and 55 $m^3 s^{-1}$ mean discharge). Like other tributaries, it crosses the ranges of the Balkan Mountains in two gorges but reaches the Danube in braided channels. The tributaries from the Romanian Plain are larger (the Olt having the highest discharge, 215 $m^3 s^{-1}$) and show both meandering and braided patterns.

A system of five major terraces has been identified on the Romanian side (Popp, 1974). Moving downstream, the number of terraces is reduced to only one at Câlâraşi (300 river km). The marshy Holocene floodplain (called 'lunca' in Romanian) is 8–12 km wide along the western section and broadens to 20 km at Câlâraşi. It is dotted by numerous oxbow lakes.

The river terraces in Bulgaria are more than 20 m thick sand and gravel above the typical floodplain features of long parallel sand ridges locally called 'gredove' (meaning 'beams') and blown sand dunes of 8–10 m (maximum 15 m) height and 0.5 km length. Their greyish yellow sands are not cemented. Where finer deposits allow the formation of more fertile alluvial soils (e.g. in the Pobrezhe region near Ruse in Bulgaria), irrigated arable cultivation is typical.

Today the Danube flows along the southern margin of the Romanian Plain in an asymmetric valley as a braided sand channel 300–1600 m wide at low water (Dinev and Mishev, 1980). Navigation is hindered by several fords, the shallowest being 0.9 m deep. There are 97 islands of various size along this section where sediment accumulates, followed downstream by a meandering Danube.

In the eastern half of the Romanian Plain, in Muntenia, yazoo rivers are typical at 10–20 km distance from the Danube. The present river system evolved following the gradual subsidence of the Siret confluence area as well as the building of natural levees of 5–10 m height. At the town of Cernavodă (number 24, Figure 12.1) the river approaches the Black Sea but the eroded mass of Dobrogea Hills forces it to turn north at Câlâraşi only 40 km from the sea. The Dobrogea Hills rise to 467 m to form a flat surface of Palaeozoic granites and phyllites as well as Mesozoic carbonate rocks and Quaternary loess presenting a barrier to river flow since their uplift during Neogene times.

West of the Dobrogea Hills the anastomosed Danube has large marshy islands (Balta Ialomiţei, Balta Brăilei) at the confluences of major tributaries. At the major river port of Galaţi it turns again in an easterly direction and receives the last major tributaries, the Siret (255 $m^3 s^{-1}$ mean discharge) and the Prut (76 $m^3 s^{-1}$). Their sources are in the eastern and northeastern Carpathians. The arid hills of Romania and Moldova (specific runoff below 50 mm $year^{-1}$ or 1.51 $s^{-1} km^{-2}$) along the middle and lower reaches only provide a very small amount of suspended load to the Danube (Table 12.1).

12.5 THE DANUBE DELTA

The town of Tulcea is at the head of a typical arcuate delta of 4345 km^2 area. Modern maps (Figure 12.7) only show three main distributary channels [Chilia (Kilia), Sfântu Gheorghe (St George) and Sulina] but five to seven of them have been reported in Greek antiquity. The large-

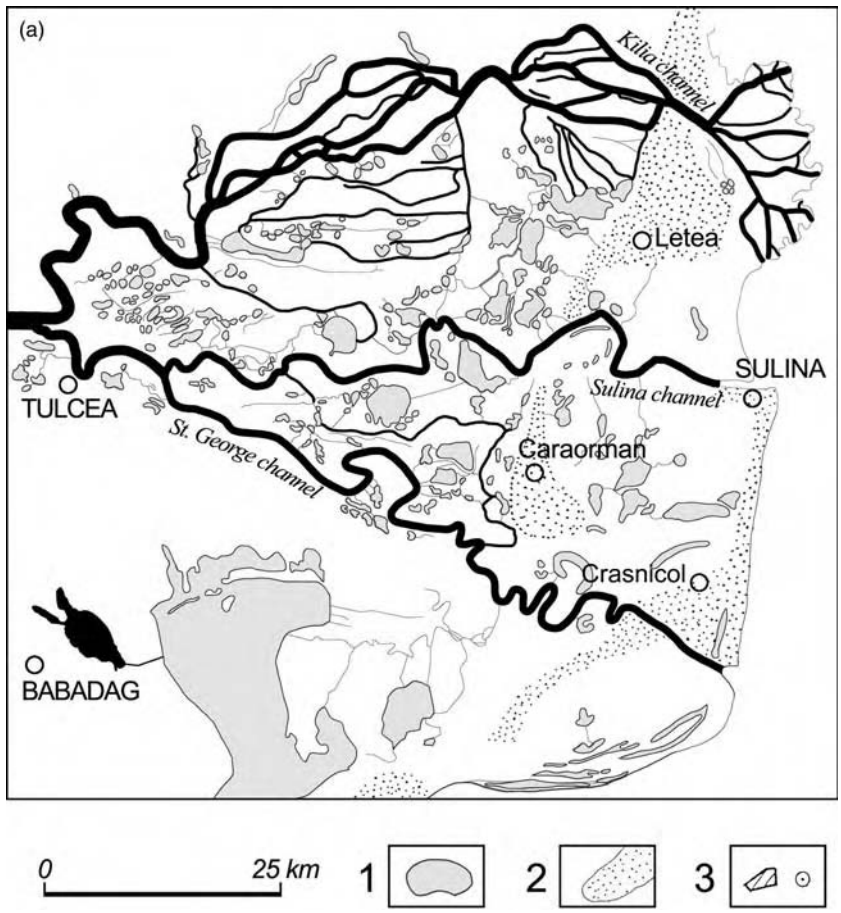

Figure 12.7 The Danube delta. (a) Earlier stage (after Hartley, 1887) and (b) current stage (after Romanescu, 1996). 1, lagoons, lakes; 2, sand dunes on barrier islands, beaches; 3, settlement. [(b) Reprinted from Zeitschrift für Geomorphologie Supplement-Band 106, Romanescu, Gh., 1996, with permission from Gebr. Borntraeger Verlagsbuchhandlung]

scale mapping project of the Danube by Marsigli (1726) shows five branches. The Delta is a mosaic of shallow lakes and channels. Recent measurements confirm that the total length of natural watercourses (1743 km) roughly equals that of man-made canals (1753 km) in the delta. Lakes of maximum 4 m depth make up 258 km^2 (8% of delta area), the largest being the Dranov (20 km^2) and Red Lakes (Lacul Roşu, 14.5 km^2; DDBRA, 2000). Several elongated freshwater lakes outside the Delta resulted from rapid deposition that blocked north to south running watercourses.

A truly amphibian landscape, the Delta has only 9% of its area permanently above water. Only sand dunes are higher than 10 m. Natural levees, up to 4.2 m height and 100–250 m wide (highest in the south and along the three main distributary channels), make up 6% of the Delta area, two-thirds of the more elevated surfaces (DDBRA, 2000). Crevasse splays are common. About a fifth is below the Black Sea mean level and more than half (54.6%) is between 0 and 1 m altitude. About 75% of the surface deposits are fine to very fine sand but the low slope of the prograding delta is muddy (Coleman *et al*., 1986).

12.5.1 Delta Habitats and Environmental Problems

Biodiversity is remarkable in the Danube Delta but threats to it are also high. The most common habitat types are:

- aquatic habitats (freshwater watercourses and lakes, brackish and saltwater coastal lagoons);

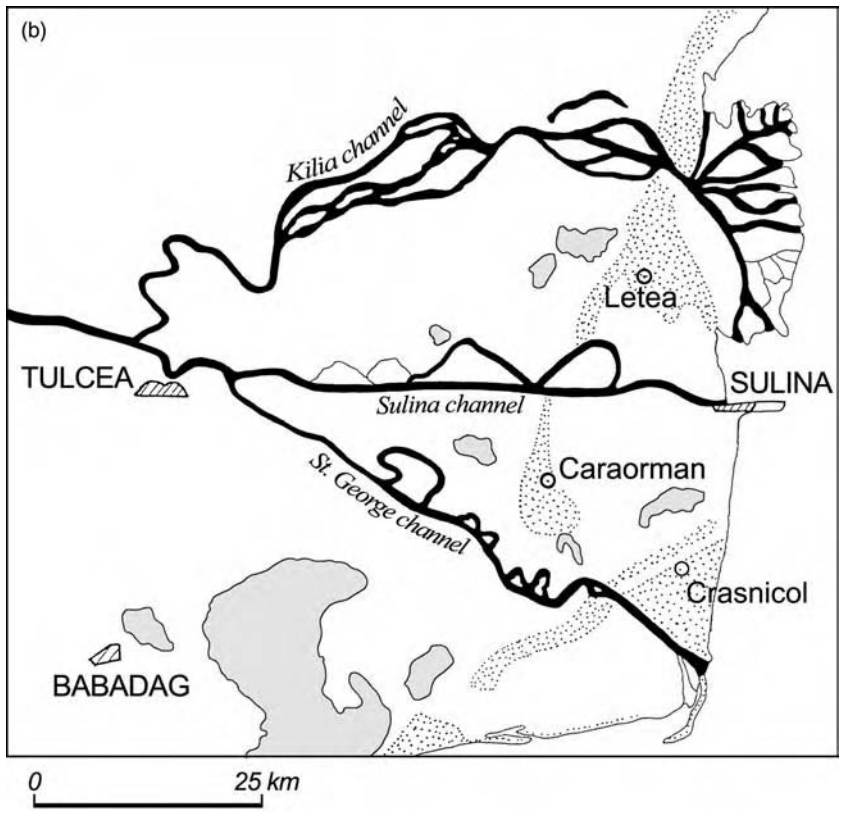

Figure 12.7 *Continued*

- regularly flooded small islands ('plaur');
- other wetlands (reed beds and willow stands);
- riparian (willow and poplar) forests;
- wet and dry meadows;
- sand and mud beaches;
- shrubs;
- barren land and man-made habitats (human settlements; agricultural and forested polders; poplar plantations and fish ponds).

The filling of lakes with organic-rich substances leads to the formation of extensive floating organic mats (Figure 12.8), a special feature of the Delta.

The Danube Delta Biosphere Reserve (6792 km^2) was established in 1991 and approved as a Ramsar site and a Natural World Heritage Site by UNESCO (DDBRA, 2000). Protection was extended over the Ukrainian part of the delta in 1998 (Vadineanu and Voloshyn, 1999). There are 2840 km^2 of reed beds in Romania alone. In the ca. 460 km^2 wetlands of the Ukrainian delta, 240 of the total 320 bird species (cormorants, pelicans, geese etc.) live. It is also one of the last refuges of the European mink (*Mustela lutreola*), the wildcat, the freshwater otter, the globally threatened monk seal (*Monachus monachus*), and certain reptiles.

The Delta is an extremely valuable buffer zone between the Danube Basin and the Black Sea (UNEP, 1991). Environmental pressure is very high. There are four primary causes of the decline in delta ecosystems (Pringle *et al*., 1993):

- the high nutrient yields of the Danube leading to eutrophication (algal blooms);
- channelization, floodplain drainage, and the impacts of engineering works (damming, dredging): reduction or elimination of natural freshwater and sediment recharge leading to coastal erosion (17 m shoreline retreat per year);

Figure 12.8 Floating vegetation on one of the lakes in the Danube Delta. (Copyright Danube Delta Biosphere Reserve Authority, Romania)

- intensive agriculture (35 000 km^2 agricultural land) next to the Danube channel and in the delta itself and aquaculture (2440 km^2 of fish farms) causing pollution (pesticides, herbicides and fertilizers; mercury and heavy metals from industrial sources);
- groundwater salinization (salt content locally reaching 800 mg l^{-1}).

The rising sea level (0.128 cm year^{-1} as averaged between 1933 and 1998) also contributes to salt water intrusion and coastal erosion (Malciu, 2000). Land loss is estimated as high as 11.5 km^2 year^{-1} (DDBRA, 2000). As the Sulina (number 26, Figure 12.1) branch was developed into a waterway (straightened and dredged), it lost its links with wetlands that carried high filtering capacity. It now delivers pollutants in a concentrated form to the Black Sea.

The environmental deterioration of the Danube Delta has a deleterious influence also on the Black Sea ecosystem. In the 1990s the chemocline (the upper boundary of oxygen-poor deep water) of the Black Sea rose from 170 to 110 m below the surface in a few years (Pringle *et al.*, 1993).

12.6 THE EVOLUTION OF THE VALLEY OF THE DANUBE

12.6.1 The Upper Section

A striking feature of the Upper Danube section was the drainage modification over several million years during the Neogene.

The catchments of three major European rivers, the Danube, the Rhine and the Rhône, developed simultaneously after the last marine inundation (the Burdigalan Molasse Sea) that ceased at least 16 Ma ago. The controlling tectonic processes were associated with the uplift of the Alps and the gradual subsidence of the Upper Rhine Rift Valley. The uplift of the Alps involved the accumulation of a molasse sequence (6500 m deep to the south and thinning out towards the north) in the Northern Alpine Foreland Basin, that consists of lower marine molasse, lower freshwater molasse, upper marine molasse and upper freshwater molasse (Habbe, 1994). The Vosges and Black Forest mountains rose bounding the southward extending Upper Rhine Rift Valley resulting in the retreat of the Molasse Sea. The Palaeo-Danube appeared in the Middle Miocene (15 Ma ago), draining the Alpine Foreland towards the east (Figure 12.9a). It was located along the cliffed coastline of the former Molasse Sea in a broad 'molasse trough' across an intricate system of sluggishly meandering rivers and extensive flat lakes among scattered molasse hills under humid tropical climate and lush vegetation (Niedermeier, 1995). The watershed between the Palaeo-Danube and the Palaeo-Rhône was aligned along the southern extension of the Black Forest. Testimony to this oldest course of the river is provided by the highest (and thus oldest) of the nine terraces, ca. 245 m above the present-day mean water level (Fischer, 1989).

Later the main direction of this indeterminate east-flowing drainage suddenly changed direction through 180° towards the west or south-west (Figure 12.9b). This change has been associated with both regional tilting, i.e. more intensive uplift in the east (Villinger, 1986), and disturbances caused by the meteorite impact that formed the Ries crater at Nördlingen 14.8 ± 0.6 Ma ago (Kavasch, 1992). The ejecta reshaped relief and drainage pattern within a large radius, filling up valleys, blocking previously existing watercourses into extensive lakes, and adding certain rivers like the ancient Main to the Danube system.

It is not known for how long the west-flowing Palaeo-Danube survived. It is widely accepted, however, that by the late Badenian (ca. 8 Ma ago) an eastward-flowing draining system developed again. The headwaters to the west were probably the Aare and the Valais Rhône, and for this reason the axial river is called the Aare-Danube

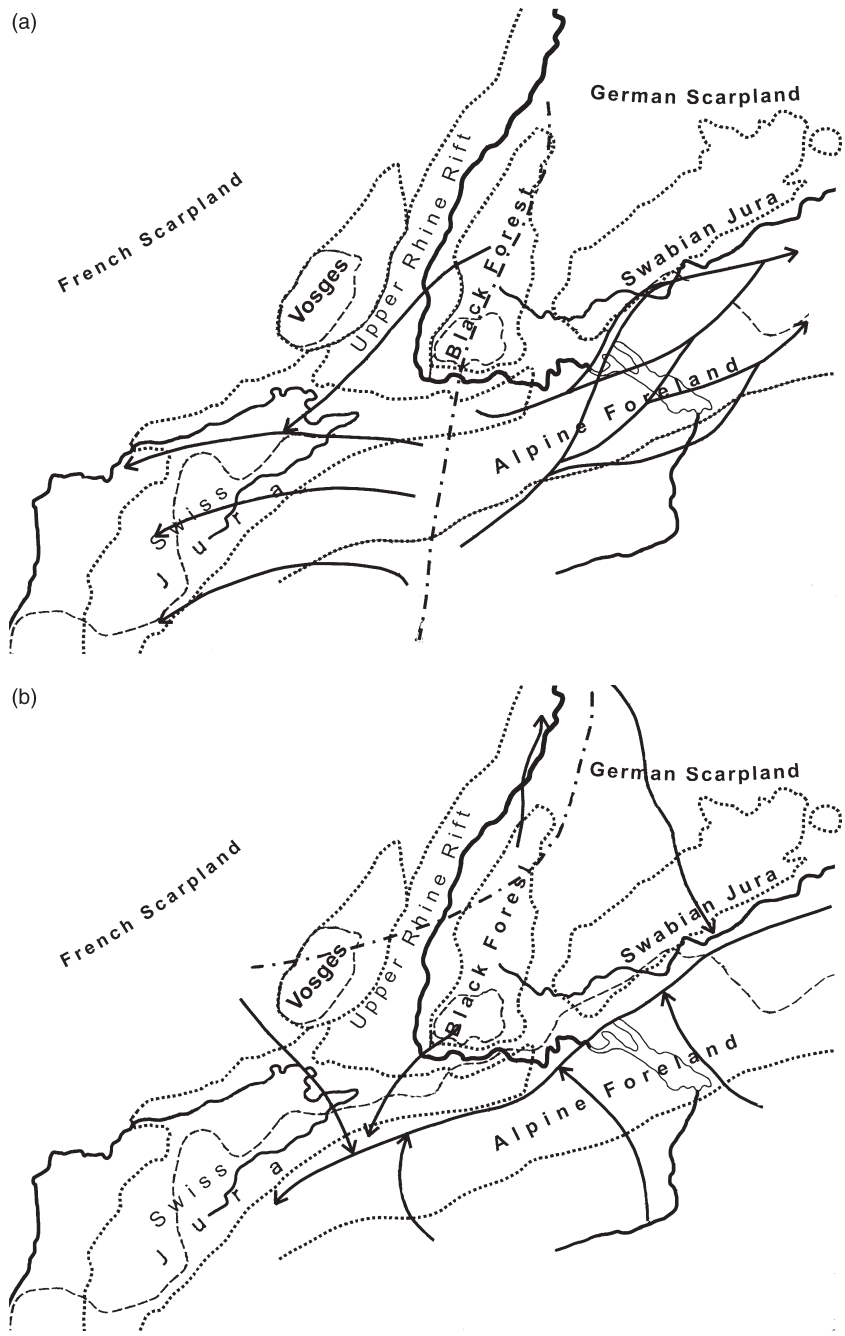

Figure 12.9 Stages in the development of the upper reaches of the Palaeo-Danube (redrawn after Liniger, 1966; Tillmanns, 1984; Villinger, 1986, 1998). (a) Middle Miocene (early Badenian); (b) Middle Miocene (late Badenian); (c) Late Miocene (Sarmatian)–Early Pliocene; (d) Late Pliocene; (e) Middle Pleistocene

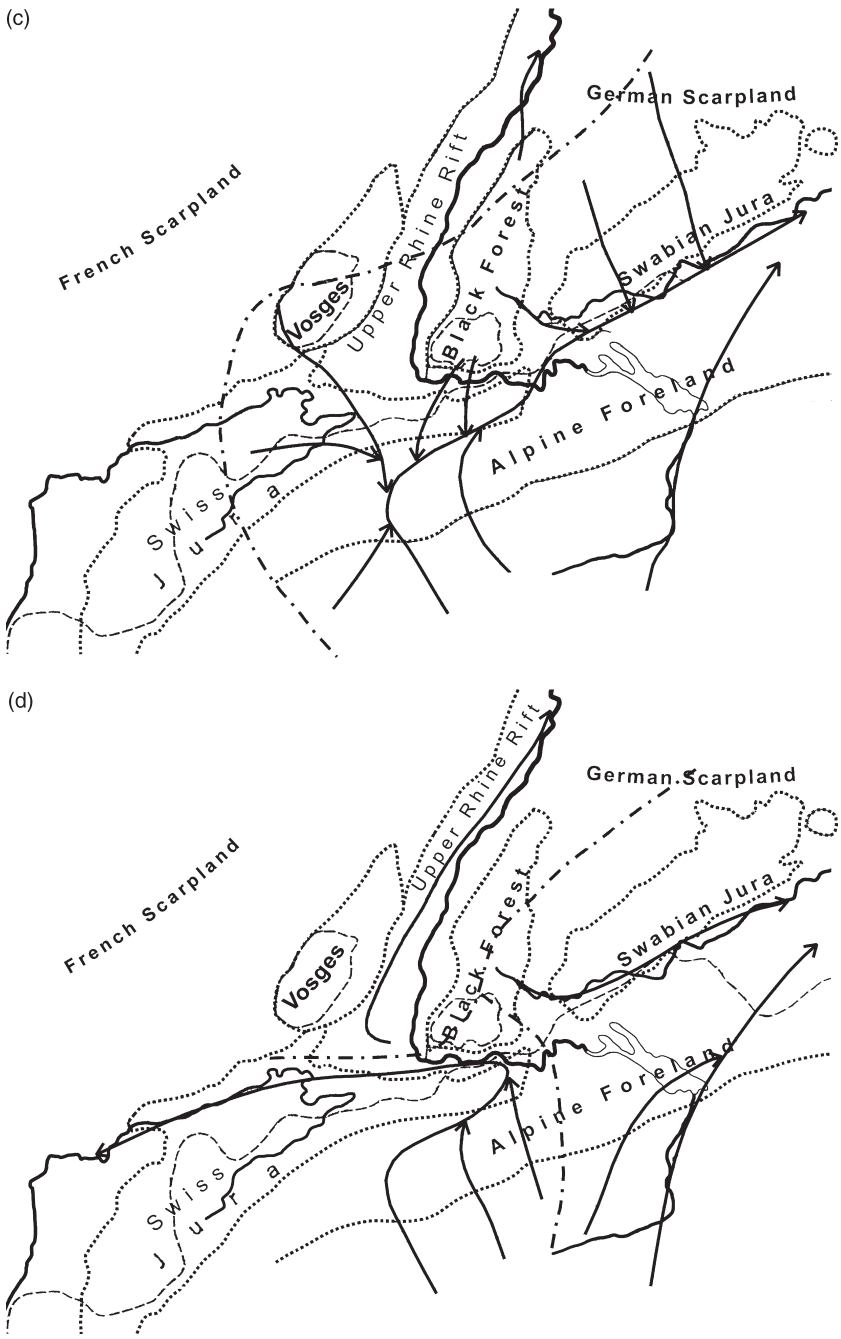

Figure 12.9 *Continued*

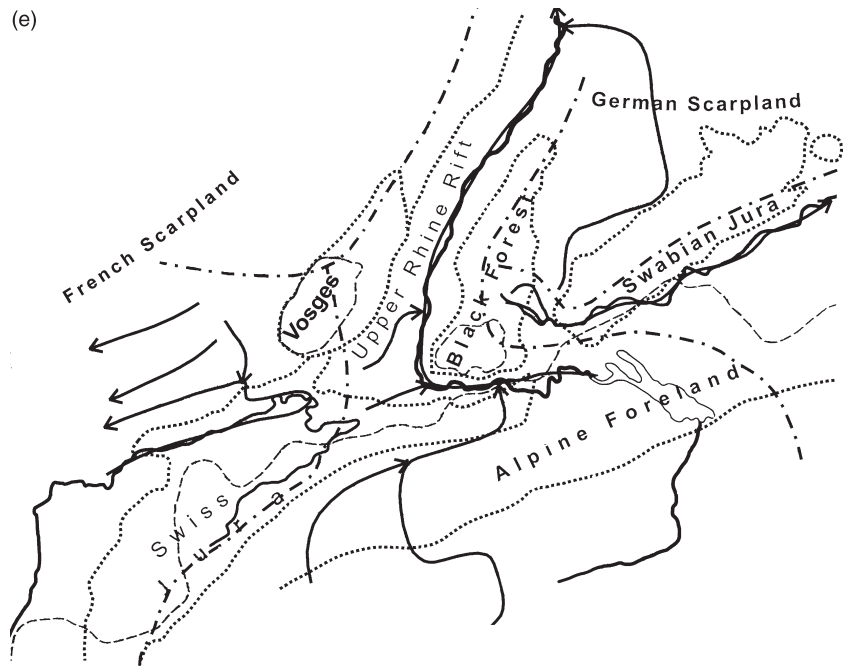

Figure 12.9 *Continued*

(Figure 12.9c; Domokos *et al.*, 2000). Most of its discharge, however, was contributed by the Alpine Rhine, a major right-bank tributary (Villinger, 1986). Where exactly the Alpine Rhine joined the Danube is still a subject of controversy. The Wutach area (Habbe, 1994), Ehingen (Villinger, 1998) or Ulm (Liniger, 1966) all have been suggested. The reconstruction of the courses of southern tributaries is more difficult as subsequent glacial or glaciofluvial processes have probably obliterated older topography. In the Sarmatian the Aare-Danube was primarily fed by watercourses from the southern Vosges and southern Black Forest as well as by those flowing from the present-day Neckar catchment in the south-east direction across the Swabian Jura (Figure 12.9c). Sands and gravels at 70–250 m above the present-day Wutach river attest to an ancient tributary of the Aare-Danube, the so-called Feldberg-Danube, which drained the central and southern Black Forest (Villinger, 1986). The predecessors of the present-day Danube headwaters, the Breg and the Brigach, probably also existed as early as the Late Miocene. At that time the Upper Rhine Rift Valley did not yet extend to the south beyond the Colmar–Kaiserstuhl volcano–Emmendingen line (Figure 12.9c). Thus, most of the Black Forest region drained to the Palaeo-Danube system (Tillmanns, 1984).

By the late Pliocene (ca. 3 Ma ago) intensive uplifting of the Black Forest region blocked the Aare-Danube and the river turned to the north-east and began to follow more or less its present course. The headwaters of the Rhine extended southwards rapidly through headward erosion. The differentiation of topography at the southern end of the Upper Rhine Rift Valley went on. The Swiss Jura was rapidly uplifting and the Aare-Danube was unable to keep pace with this tectonic change. It had to find a new drainage route to the west (Figure 12.9d). The resulting Aare-Doubs drained the western section of the Alpine Foreland into the Mediterranean Sea (Liniger, 1966; Labhart, 1987). Thus, the Rhône Basin gained substantially in area at the expense of the Danube catchment. Evidence for the shift of drainage is found in the Sundgau terrace of sands and gravels of 20 m thickness west of Basel, originating from the Valais Alps and the Bern Mittelland (Labhart, 1987).

The regression of Rhine headwaters reached the Swiss Jura by the very end of the Pliocene (Piacenzan, ca. 2.5 Ma ago, Figure 12.9e) and captured the Upper Aare, which became a north-flowing tributary of the Rhine system (Rutte, 1987). The Alpine Rhine, flowing through the Lake Constance, and the Feldberg-Danube remained in the Danube system (Liniger, 1966). Either during the late Eopleistocene (ca. 1.5 Ma ago; Liniger, 1966), or much

later, in the Middle Pleistocene (Tillmanns *et al.*, 1983), the Alpine Rhine was also diverted into the Rhine system. Advancing Alpine glaciers and gravel-depositing southern tributaries caused the Danube to shift its channel in the Pleistocene, changing catchment boundaries and producing undercut cliffs (Villinger, 1986). About 15–20 ka ago the lower Wutach captured the upper section of the Feldberg-Danube, fed by a glacier to the Rhine (Hebestreit *et al.*, 1993). The five terraces along the upper Wutach correspond to the recession stages of this glacier. The stream deepened its valley floor 150–200 m in order to cause one of the most recent large-scale river beheadings in Europe (Hebestreit *et al.*, 1993).

By the end of the Pleistocene the present drainage pattern in the source area of the Danube had taken shape. During postglacial times higher discharges led to the stabilization of drainage lines by incision. The complicated story, however, has not yet come to an end. The relief between the valley floor of the Danube (678 m above sea level at Donaueschingen) and that of the Rhine (345 m at the confluence with the Aare) clearly indicates that the capture of the uppermost Danube section is foreseeable in the geologically near future. This will happen through the headward erosion of a misfit stream rapidly approaching the present-day Aitrach in the Blumberg dry gap along the valley of the one-time Feldberg-Danube.

Quartz gravels transported from the Aare–St Gotthard Massive along the southern margin of the Swabian Jura provide evidence that once the Danube flowed at the top level of the cliffs of the last (Molasse) sea and formed its valley through rapid incision (80 m over the first half of the Pleistocene) into the molasse deposits. The massive accumulations of molasse constantly recharged by right-bank tributaries from the Eastern Alps caused a shift towards anastomosing pattern and also prevented the river from taking a more southerly course. This accumulation even promoted the undercutting of the southern margin of the Jura.

The most significant shift of the river course along the section above the Ulm took place at Ehingen (515 m above sea level), where in the Middle Pleistocene the Danube abandoned its previous course along the cliff line of the Swabian Jura and occupied its present valley shaped by small streams south of the Hochsträß molasse hills (Villinger, 1986). The Palaeo-Danube valley is in the process of being filled by two small misfit streams (the Schmiech and the Blau).

Another instance of major channel shifting is attested by one of the longest abandoned Danube valley sections in the basin, the present Wellheim and Altmühl valley (Fischer, 1991). It was first occupied immediately after the Ries meteorite impact and again by the so-called Alb-Danube ca. 4 Ma ago. The channel shifted to the north over the molasse-mantled Malm sequence; its meanders continued to incise deeply into the uplifting Franconian Jura tableland of hard Malm limestone after the molasse cover had been denuded. The evolution of this superimposed valley is reconstructed on the basis of sands and gravels in high position, 100–140 m above the valley floor (Niedermeier, 1995). The Danubian origin of the valley is evidenced by the presence of typical mineral components (radiolarite, lydite) of terrace sediments (Glatthaar and Liedtke, 1988). During the isotope stage 4 (ca. 200 ka ago) the Danube changed course again and occupied the floor of a collapsed karst polje with west-retreating springs for several millennia. Later the channel shifted to its more southerly location that it uses at present. Major abandoned Danube valley sections have been described by German geomorphologists in the eastern half of the Bavarian Basin (Jerz, 1995). Investigation of loess profiles reveals a more southerly course in the oldest Pleistocene (Strunk, 1989). Studies on the river mechanism (Buch, 1988a,b) reveal the difficulties of correlating intervals of intensive incision and sediment accumulation with interglacials and glacials, respectively. The last pleniglacial (isotope stage 4) and late glacial (isotope stage 2) were characterised by deep incision, while accumulation in braided and anastomosing systems occurred in the Early Holocene. The alternation of narrow valley sections with small partial basins along the course of the river seem to be a stronger regulating force than the alternation of glacial and interglacial climatic conditions – a feature which becomes even more marked along the Austrian section.

Further channel changes during the Plio-Pleistocene have been reconstructed for the Danube section along the Austrian Alpine Foreland. The spectacular Strudengau Gorge, cut in Palaeozoic rocks, was occupied by the Danube only in the later stages of the Pliocene (Fink, 1966). The ancient river followed a more northerly course across the Bohemian Forest (BOKU, 2000). It joined the picturesque and narrow Wachau Gorge, which has undergone a similar antecedent evolution. Intensive Pleistocene subsidence explains that the thickest alluvial accumulations are found in the Tulln and Vienna Basins, separated by the Vienna Gate (at Klosterneuburg). Along the Austrian section natural flow and sediment transport patterns have been fundamentally changed by the recent impoundment of the river (Figure 12.1). The Alpine foreland is characterized by a clearly distinguishable geomorphic surface at 330–400 m elevation (Fink, 1966). In all probability, this marks the level where the ancient Danube began to flow ca. 5.5 Ma ago, at first in a broad valley to the south of its present-day course (across St Pölten), away from the Strudengau, with virtually no incision. Later the

gradual uplift of the mountain margin and the simultaneous downcutting of the river and its tributaries produced a spectacular series of terraces (Figure 12.10). During the repeated semiarid to arid climatic spells anastomosing systems prevailed and gravels and sands (terrace treads) accumulated at high elevations. The lower erosion surfaces of the Alpine foreland described in classic papers (Fink, 1966) – the early 'Levantine' (Upper Pliocene) at 260–270 m and the broadest late 'Levantine' (Eopleistocene) at 200–220 m – may also be related to the action of the Palaeo-Danube.

In the Vienna Basin subsidence took place in a complicated pattern, adjusted to several foci of limited extension. This explains why the river turned north, then east,

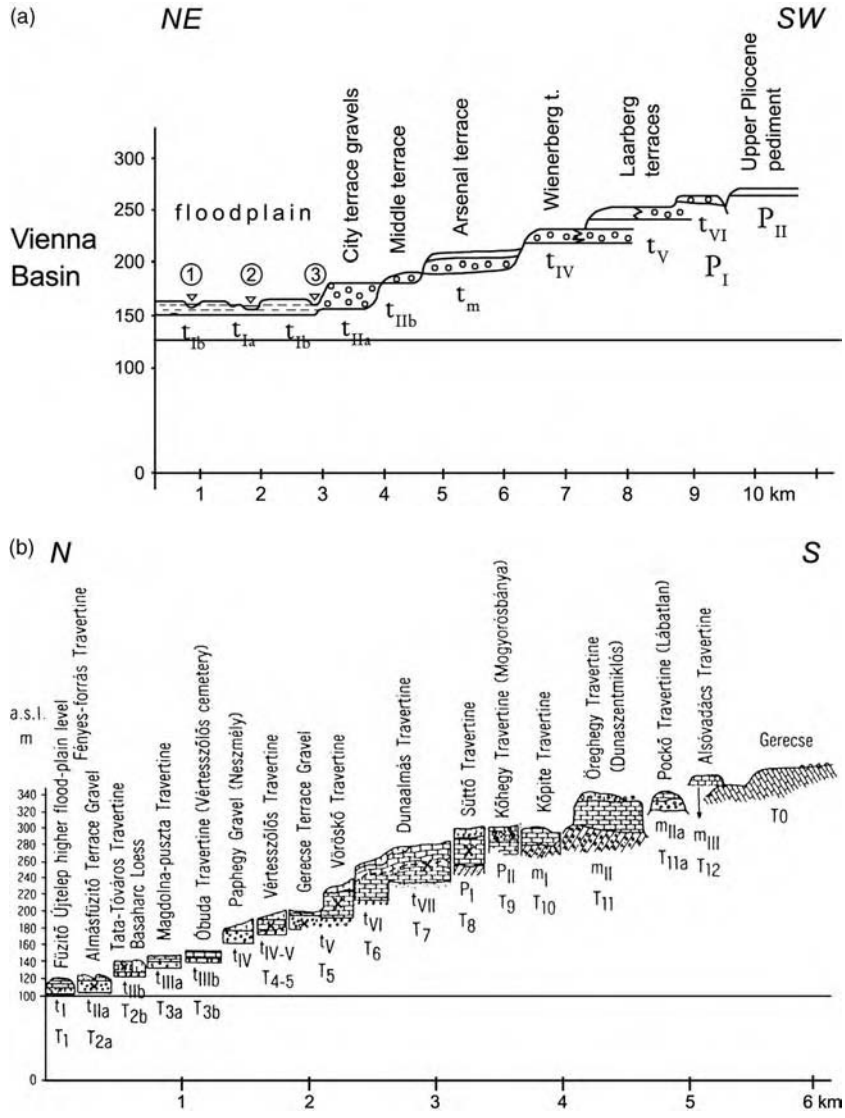

Figure 12.10 Terraces in the Vienna Basin (a, after Fink, 1972) and in the Danube Bend (b, after Pécsi *et al.*, 1988). t_I–t_{VII}, Danube terraces covered by travertine horizons (T_1–T_7) and loess; P_I–P_{II}, Pliocene pediment surfaces covered by travertines (T_8–T_9); m_I–m_{II}, Upper Miocene raised beaches covered by travertines (T_{10}–T_{12}); T_0, older surface of planation. [(b) From Neogene and Quaternary geomorphological surfaces and lithostratigraphical units in the Transdanubian Maintains, Pécsi *et al.*, 1988, with permission from F. Schweitzer]

and occupied the present-day Vienna Gate only at a later date in the Pleistocene. The eastern border of the basin may have been a row of islands separating it from the basins of the brackish eastern Paratethys. The oldest member of the terrace system (Laarberg terrace, 230–250 m altitude), dated early Pleistocene, is followed by other Pleistocene terraces (Fink, 1972). The Holocene level is ca. 5 m above the mean water level of the Danube (157 m altitude).

12.6.2 The Middle Section

Recently, it has been proposed that the development of modern drainage network in the spacious Carpathian or Middle Danubian Basin was interrupted by a marked spell of arid climate at the beginning of the Pliocene (ca. 5 Ma ago; Schweitzer, 1997), coincident with the Messinian Salinity Crisis. Thus, the evolution of the present drainage could only resume during times of red clay formation under humid climate (4.5–3.3 Ma). From that time on the ancient Danube – along with the Tisza – became a main hydrographic axis in the Basin.

There are three possible locations where the Palaeo-Danube may have entered the Carpathian Basin at various times (Figure 12.11): the Ebenfurth or Sopron Gate (south-west of the Leitha Mountains), the Bruck Gate (north-east of the same mountains, now occupied by the Leitha River) and the Porta Hungarica (Devín Gate) between the Alps (Hainburg Block) and the (Little) Carpathians. The river was relocated from one gate to the other in this sequence, producing two main alluvial fans. The older one (Figure 12.11b) has its apex in the Bruck Gate and the younger (Figure 12.11c) in the Devín Gate. According to conservative estimates the Danube had deposited almost 90% of its annual 400 000 to 600 000 million m^3 of bedload in the fan before channelization (Pécsi, 1959). Under natural conditions (studied in detail for the period 1712–1886 by Pišút, 2002) the high-energy river showed intensive lateral erosion. The key mechanisms of channel planform change were avulsions and meander migration leading to chute and neck cutoffs. The adjustment of the river to human interventions and major floods resulted first in large-scale meandering and then in the development of an anastomosing–meandering pattern.

The massive gravel accumulation on the western margin of the Little Hungarian Plain at Parndorf is currently attributed to the enormous drop in slope

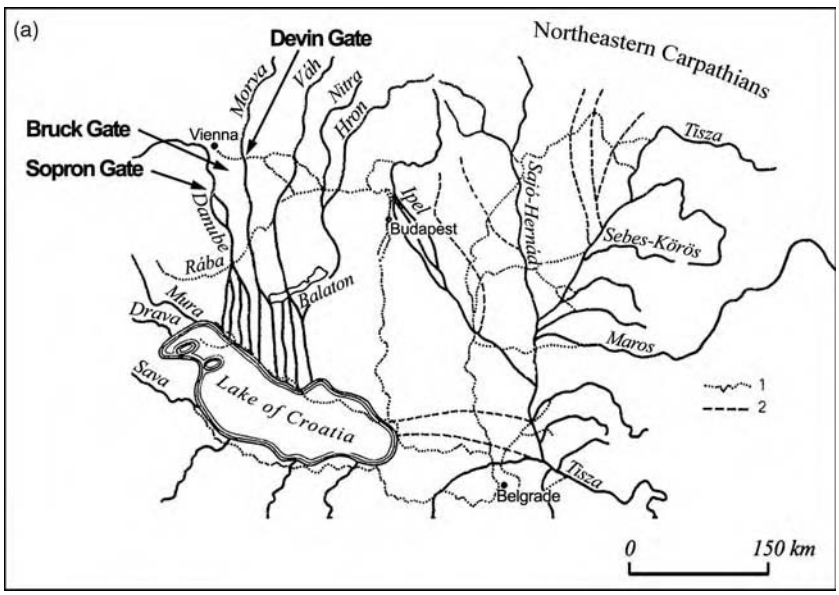

Figure 12.11 The reconstructed ancient drainage of the Carpathian Basin. (a) End of Pliocene (after Sümeghy, 1953); (b) Early Pleistocene; (c) middle of last glaciation (both after Borsy and Félegyházi, 1983). [(a) Reprinted from Annual Report of the Hungarian Geological Institute for 1951, Sümeghy, J., Issues concerning the Pliocene and Pleistocene stratigraphy in Hungarian basins, 1953, with permission of the Geological Institute of Hungary. (b, c) Reprinted from Reconstructed ancient drainage of the Carpathian Basin, Borsy, Félegyházi, Copyright (1983) with permission from Dr E. Félegyházi]

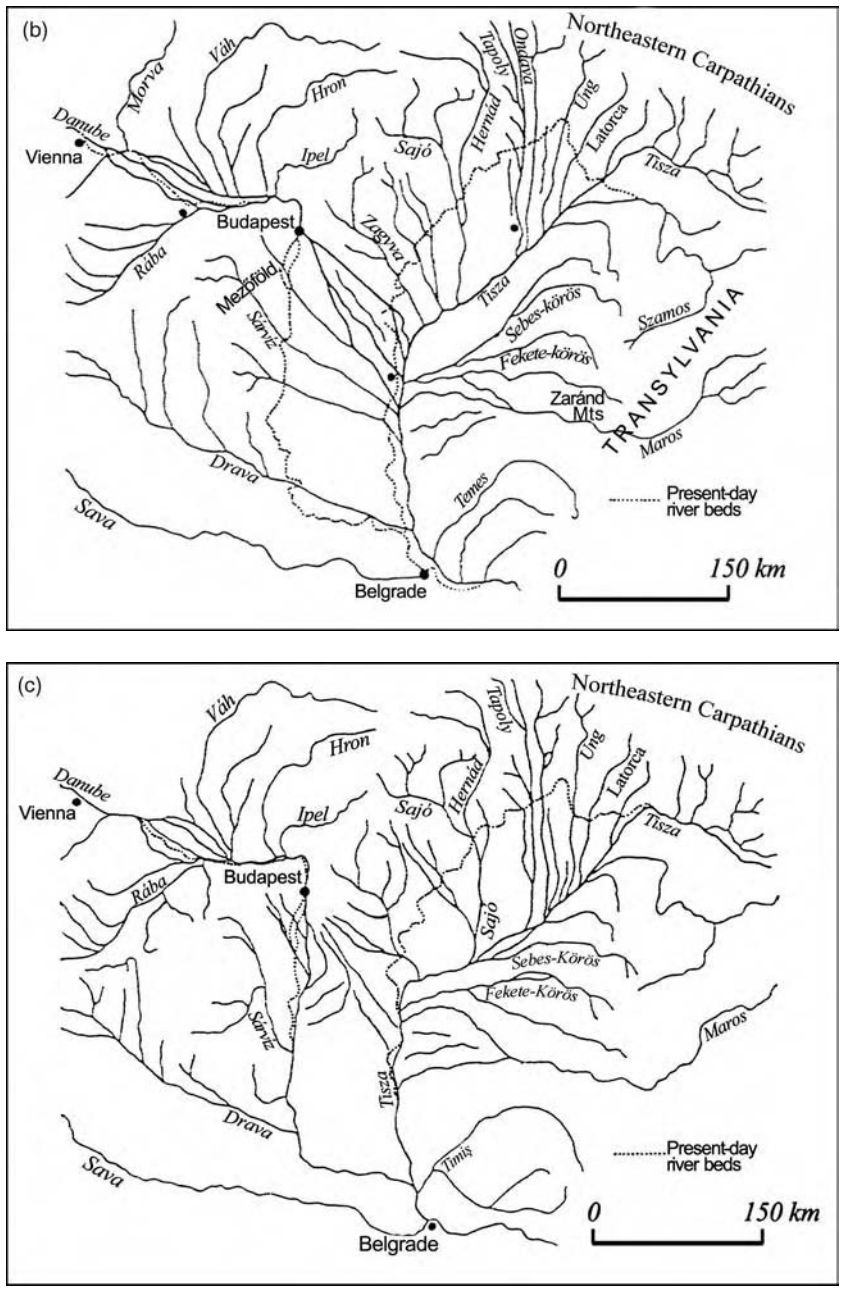

Figure 12.11 *Continued*

downstream of the gates to the Carpathian Basin, whose floor at the time was 2000 m deeper than that of the Vienna Basin.

During the late Pliocene, the ancient Danube may have had a north to south course along the margin of the subalpine gravel mantles of Transdanubia into the last remnant of the Pannonian Inland Lake, the Slavonian–Serbian Lake (as originally proposed by Sümeghy, 1953; Figure 12.11a). The attempts to convincingly reconstruct subsequent courses across the Trans-Danubian Range (in the

Mór Graben) or even across Lake Balaton Basin (Mike, 1991) have failed.

The origin of the picturesque Visegrád Gorge or Danube Bend has been the subject of debates among Hungarian geomorphologists for more than a century (Pécsi, 1959, 1999). The occurrence of the Danube here is now placed in the late Miocene or early Pliocene, opposed to the previous view that it only happened during the later Pliocene or the Pleistocene (Korpás, 1998). The gorge has been regarded as antecedent, superimposed or both by various scientists (Karátson, 2002). The antecedent hypothesis seems to be more probable as valley formation kept pace with the 200–300 m uplift during the Pleistocene and – according to the terraces identified – incision was interrupted. The U-planform of the Bend is now explained by a volcanic reconstruction with the river occupying the interior of an eroded double caldera. Limestone occurrences are identified as patchy coral reef deposits instead of remnants of a continuous marine cover sequence. Recent large mammal finds as well as large boulders in the deltaic deposits indicate that river may have been an active eroding and accumulating agent as early as the second half of the Miocene. The Miocene age of the deltaic deposits is supported by the overlying travertine accumulations dated from mollusc and vertebrate finds (Schweitzer and Scheuer, 1986). It seems probable that while some late Miocene rivers coming from the North-western Carpathians (not necessarily the predecessor of the Danube) were depositing along the shore zone of the retreating Pannonian inland sea, the Visegrád Gorge functioned as a strait in the centre of a volcanic archipelago between the inundated Little and Great Hungarian Plains over a longer time span. The subsequent tectonic movements along the Hungarian Mountain Range explain the variable altitudes of delta, alluvial fan, and terrace deposits along the present-day river. Climatic fluctuations may only have had a secondary importance (Pécsi, 1999).

The marked mineral composition of Danubian deposits permitted the tracing of the ancient courses of the river in the Great Hungarian Plain (Borsy and Félegyházi, 1983; Borsy, 1990). During the Pleistocene the Danube built a vast alluvial fan covering most of the present-day Danube–Tisza Interfluve (Figure 12.11). The sands of the alluvial fan were partially redeposited by aeolian processes during drier periods. In the early Pleistocene the Palaeo-Danube followed a north-west–south-east course probably occupying the late Pliocene channel of the river Ipel'/Ipoly (Figure 12.11a). Carrying a heavy and coarse sediment load from the rapidly uplifting mountains and accommodating it in a channel of high width/depth ratio, the river formed an anastomosing system (Figure 12.11b). Over the early and middle Pleistocene a gradual westward shift of this drainage system took place, probably promoted by dry interglacial climates as well as more abundant water recharge from the karst mountains of Transdanubia (Lóczy *et al.*, 1989). The channel rotated almost 20° to the west. In postglacial times intensified incision followed (Somogyi, 1983) and the anastomosing system was considerably reduced in size (Figure 12.11c). However, its survival to historical times is attested by two residual hills with alluvial and loess mantles on the Danube–Tisza Interfluve (Solti-halom 124 m; Tétel-halom 114 m). The floodplain features and deposits of the Sárköz embayment provide further evidence that the river once followed even more westerly courses than today.

South of Budapest the rate of bluff retreat can be reconstructed from archaeological evidence (Lóczy *et al.*, 1989) that suggests 5–15 m channel shifts per 100 years. The frequency of channel bars supports the view that braiding was common before flow regulation. Today, however, a clear meandering tendency is displayed. The Kalocsa–Mohács depression of 25 km diameter and 80 m depth with sands and gravel fill is held responsible for the westward relocation of the main channel during the Pleistocene. The depression is an eastward extension of a tectonic graben with rejuvenated horizontal and vertical movements (Jaskó and Krolopp, 1991).

12.6.3 The Lower Section

The Iron Gate, like the Danube Bend in Hungary, was also previously assumed to have originated from a river capture. Now it is recognized as an antecedent valley. During the various stages of the Pliocene it was a strait between the Pannonian and Moesian basins of the Paratethys Sea. The floor of potholes up to 75 m deep reach below present sea level here.

The evolution of the Romanian (Walachian) Lowlands was controlled by tectonic movements and marine transgressions. Subsidence in the younger Rhodanian orogenic phase took place along fault-lines along the Siret River in a north to south direction and also at right angles to that, meeting at the town of Galaţi, a seismically still active area. The uneven depression was filled by Miocene–Pliocene marine and lacustrine sediments and with a 350 m thick Quaternary series mostly carried by the south-flowing Carpathian rivers. The Danube gradually occupied this area following the west to east marine regression (Popp, 1974). The history of geomorphic evolution of this area is so closely intertwined with the changes in the level of the Black Sea that it cannot be reconstructed until we know more about the connection between the Black Sea and the Mediterranean (Aksu *et al.*, 2002).

12.6.4 The Delta

The level of the Black Sea was 60–130 m lower during the glacial times. The entire delta sequence of the present time accumulated during the Holocene. Delta formation started in the Early Holocene, 9000–8500 years ago (Panin *et al.*, 1983), immediately following the assumed catastrophically rapid infilling of the Black Sea Basin (Ryan *et al*., 1997). Recent findings from optical luminescence analyses, however, indicate a more recent date, ca. 5200 years (Giosan *et al.*, 2006). Probably this younger age also implies a higher rate of erosion in the Danube Basin during the late Holocene. The previous chronology, strongly based on ^{14}C dating of bivalves and associated with sea-level changes (Panin *et al*., 1983), is now questioned (Giosan *et al*., 2005). Three stages of delta evolution have been identified: a gulf, a lagoon and a delta phase (Popp, 1974). Different authors, however, have attributed different dates to the individual stages (Panin, 1989). The most recent reconstruction of the delta development suggests stable relative sea levels (fluctuations limited to a range of +1.5 m and −2 m) in the region for the second half of the Holocene. Local submergences, which influenced delta evolution, have been attributed to local subsidences (Giosan *et al*., 2005, 2006).

As a result of the southward directed longshore drift (Giosan *et al.*, 1998), the first barrier of the gulf developed ca. 5200 years ago (Giosan *et al*., 2006). The line of the past barrier islands matches the current Letea-Caraorman-Crasnicol sand dune complex (*grinduri*) of 45–55 m thickness and a maximum altitude of 12.4 m (Figure 12.7). The first delta was built by the present St George Branch. Later it became inactive and a nothern distributary (Sulina) and delta lobe began to develop 3600 years ago, and at the latest, expanded until 1800 years before present (Giosan *et al.*, 2006). Subsequently new distributaries and young delta sequences were created around the delta periphery: the second Sfântu Gheorghe Branch to the south and the northernmost distributary at Chilia that were formed in three stages from ca. 2000 years ago to historical times. A new set of barrier islands with steep sea faces developed, the youngest forming between 1500 and 600 years ago near the ancient Greek town of Istria towards the southern limit of the delta (Giosan *et al*., 2006). Wave action eroded and reworked the older delta lobes. Coastal erosion is the characteristic process today all along the coast south of the Chilia lobe which is maintained by the high water and sediment discharges of this 300–700 m wide distributary.

12.7 HUMAN IMPACTS

In this long and densely inhabited region, human activities have inevitably left their mark on the Danube and its riparian landscape.

12.7.1 A Brief History of Channelization

Navigation on the Danube has always been a serious problem. Although the first towing paths were carved into the cliffs of the Iron Gate Gorge under Emperor Trajan around 100 AD, regular traffic was started by the Danube Steamboat Navigation Company (DDSG) only in 1837. When the Turks controlled the Sulina channel of the Delta, they compelled every outgoing vessel to tow a large rake to stir up silt to enable the current to carry it out to the open sea (Hadfield, 1986). Later, after its foundation in 1856, the European Commission of the Danube encouraged the removal of sandbanks from the delta distributaries. In those days the river was described as: ‘Fast and difficult down to Vienna, with rapids and sandbanks, it remained fast to Komárom in Hungary, though because of shoals below Pressburg (Bratislava) this part of the river was in 1879 said to be fully navigable only for 202 days a year. Beyond Komárom it is navigable to the Carpathian Gorge, after which it spreads out on the flatlands towards the delta’ (Hadfield, 1986: 167–168). Today the Danube is navigable with small vessels to Ulm (2586 km from the mouth), with ships above 1300 t volume to Regensburg (river km 2379).

Flood control, however, has been an even stronger motivation for human intervention (Somogyi, 2000). At the beginning (in the thirteenth century) unconnected dykes were built along several reaches of the river (Stancíkova, 2001). The end of the eighteenth century and the beginning of the nineteenth century saw the first planned regulation measures. At first only settlements, later agricultural fields, were protected from flooding. A major stage was medium-flow regulation (Table 12.2) later supplemented by low-flow regulation indispensable for improving navigation or the undisturbed release of floating ice. The Fertő-Hanság water system in northwestern Hungary used to be linked to the Danube but it was detached and drained during the 1950–1960 channelization (Erdélyi, 1994). A natural disaster followed: peat resources desiccated into muck, were eroded and burnt spontaneously.

The Ferenc Canal was built in the south of the Great Plain in 1795–1802 to connect the Tisza with the Danube. Due to the westward channel shifts of the Danube, however, it had to be extended in 1851–1868 to reach the

Table 12.2 A summary of medium-flow regulation of the Danube

Section	Date of main activities	Reduction of river length (%)	Measures
Upper Danube in Baden-Württemberg	1820–1890	−73	Channel straightening, cut-offs, flood-control dykes, bank stabilization
In Bavaria	1826–1867	−15	Channel straightening, cut-offs, flood-control dykes, bank stabilization, channel deepening by dredging and explosions
In Austria	1850–1914	ca. −15	By-channel closures, bank stabilization, flood-control dykes, training walls
Middle Danube in Hungary	1871–1914	−18	Flood-control dykes, by-channel closures, cut-offs, bank stabilization, groynes, confluence relocations, protecting walls along urban sections
In Serbia	1894–1977	ca. −10	Flood-control dykes, bank stabilization, groynes
Lower Danube in Romania/Bulgaria	No regulation	–	Only dredging and some bank stabilization, flood-control dykes
Danube Delta (Sulina branch)	1860–1901	−30	Straightening, dredging, longitudinal structures, canal building

Based on UNESCO, 1999.

river. The lock at the town of Bezdan is claimed to be the first concrete lock in Europe. Along the Upper Danube the navigable Vienna flood canal (3 m deep, 305 m wide and 16 km long) was completed by 1866.

The Iron Gate remained as the most dangerous gorge to pass. Between 1833 and 1837 Hungary built the so-called Széchenyi Road with a 2 km long and 3 m deep shipping canal and between 1895 and 1898 the 2.5 km long Sip Canal, stone-pitched on both sides. On the Serbian bank rails were laid to allow a heavy steam locomotive to haul barges up (Hadfield, 1986). It could not solve all problems. For instance, infamous rocks like Ada Kaleh, rapids, and swift currents continued to present a threat to shipping. Some rocks were blown up but a final solution was only reached when the river was dammed in the Iron Gate between 1964 and 1972 to generate 2136 MW of electricity. Iron Gate II dam followed 80 km downstream in the 1980s (Hadfield, 1986).

As the barrage at Nagymaros has not been built (see below), the rock sill at Gönyü (Little Hungarian Plain section) at 0.9 m depth survives as the last major single natural obstacle to navigation along the Danube. On the other hand, although the wreckage of the eight bridges destroyed by American bombers along the former Yugoslav section were removed from the channel by 2002, it is reported in the newspapers that there are still nine locations where bombs and rockets lie in the river bed. A temporary pontoon bridge in Novi Sad also hinders navigation.

It had been long planned to connect the Danube with the Black Sea port, Constanţa, saving 380 km en route. The 64.2 km long, 90 m wide and 7 m deep canal completed by 1984 leaves the Danube at Cernavodă and shortens the distance to the sea by 400 km (Dragomirescu, 1993).

Regulating the Danube has resulted in increased channel incision along the whole length of the river. The dredging just above Budapest (with the removal of 25 million m^3 of gravels and sand) led to the thinning of gravel beds. These beds, which were 4–7 m thick in the 1960s, were eroded to 1–4 m thickness in the 1990s. The channel incision of 1.6 m was beneficial for navigation but was undesirable from other aspects (loss of the filtering capacity of gravel beds; uneven river bed; depressions in bed filled with toxic deposits; Erdélyi, 1994).

Contradictory opinions exist regarding impacts of river flow regulations and drainage measures. With an increasing emphasis on the presevation of wetland habitats in natural conditions and a decreasing demand for agricultural land, their benefits are often underestimated against their negative consequences. For example, losses to fishery as valuable fish species would require a higher range of water level fluctuation or secondary alkalization of soils in the floodplains (Somogyi, 2000). Regulation measures still continue but with a changed emphasis. Today the strongest motivation is river restoration for preservation of wildlife (Gewässerdirektion Donau/Bodensee, 2001).

12.7.2 The Rhine–Main–Danube Canal

The 171 km long Main–Danube Canal was started in 1959 and was completed by 1992. It is the key section of the main European waterway, the Rhine–Main–Danube navigation route of 3500 km total length. It mostly follows the old Ludwig Canal, established at the order of King Ludwig I of Bavaria between 1836 and 1845 (Hadfield, 1986), which is 172 km long, has 100 locks and can accommodate 100 tonne barges. In order to overcome the 175 m rise above the Main and the 68 m drop to the Danube, 15 lock systems had to be built along the Main–Danube Canal. The required depth is 3.5–4 m and the width is 40 m; for comparison, the corresponding data along the Danube between Kelheim and Passau are 2.8–3 m and 50–100 m, respectively. The Canal is navigable by vessels of up to 110 m length, 11.4 m width, 2.8 m load draught and 2800 tonnes capacity.

Each kilometre of the canal cost 27.5 million DM (at 1992 reckoning). It was cheaper than railway construction (ca. 36 million DM km^{-1}) but somewhat more expensive than building a motorway (ca. 20 million DM km^{-1}) (Die Rhein–Main–Donau–Wasserstraße, 1992). The investment, however, proved to be profitable as freight transport grew to 6.77 million tonnes by 1998. In 1999 this trend was interrupted by the bombing of Yugoslavia.

12.7.3 A Recent Example of Damming the Danube: the Gabcíkovo Barrage in Slovakia

Since the completion of the Kachlet dam in 1927, the 69 reservoirs and hydroelectric plants established in the Danube Basin (Figure 12.1) fundamentally transformed environmental conditions. Some of these generated heated debates.

The environmentally controversial engineering structure under discussion resulted from a Czechoslovak–Hungarian agreement signed in 1977 (Bravard, 1986; Nemerkényi, 1990). Now it comprises a barrage at Gabcíkovo (river km 1819) in Slovakia with a hydroelectric plant (720 MW capacity) and two navigation locks, the Čunovo weir and reservoir of 40 km^2 area and 3.5 m depth and a 29 km long navigation canal. The implementation of the large-scale barrage system is only partial. The planned lower barrage at Nagymaros has not been built and the large reservoir at Dunakiliti remains unused because in October, 1992 the Slovaks diverted the main Danube discharge into the navigation canal on their own territory. The lawsuit at the International Court in The Hague continues. One of the issues to be decided is how to share water between the two countries. According to an agreement made in 1995, 250–350 $m^3 s^{-1}$ water is released into the Old Danube channel as opposed to 2100 $m^3 s^{-1}$ before construction and 20 $m^3 s^{-1}$ (40–50 $m^3 s^{-1}$ before damming) into the Moson Danube.

A strong argument against the barrage has been that it damages the valuable groundwater reservoir of the Szigetköz (Erdélyi, 1994). The Danube is estimated to recharge the groundwater for an area of 910 km^2 in Hungary above Győr. Groundwater reserves amount to 5.4 km^3 in Hungary and 13 km^3 in Slovakia, primarily not recharged through vertical infiltration but laterally as groundwater flow (Lehoczky, 1979). While groundwater flow in alluvial gravels used to be rapid, on average 3.8 to 10.3 $m^3 s^{-1}$ (particularly in the north-west), it is assumed that river dams may cause siltation and the clogging of this flow in the long run. Connection with the karst water reservoir of the Trans-Danubian Mountains is also assumed (Erdélyi, 1994). Thus, huge freshwater reserves are affected.

When the Danube enters the Carpathian Basin from Austria, it has First Class water quality by the Hungarian standards. Below the Morava confluence it becomes Fourth Class, i.e. the worst category (Erdélyi, 1994). The diversion of most of the discharge has reduced the opportunity of filtering out contaminants through groundwater flow. Along the Rajka–Szob reach increased pollution associated with suspended load comes from Slovakia. The improvement of sewage treatment is indispensable for avoiding damage.

The pattern of the fluvial landscape reflects a highly uneven distribution of fine sediment cover (floodplain deposits) above sand-and-gravel point bars and, thus, great variations in the groundwater table depth and the availability of capillary water for crops (Góczán and Lóczy, 1990; Lóczy and Balogh, 1990). The diversion of most of the discharge into the navigation canal resulted in an increased range of groundwater level fluctuation in a zone next to the Danube, and dropping levels (at most –6 m) away from it. In order to prevent the lowering of groundwater to the gravel beds, an engineering structure, an underwater weir with fish ramp, was built across the channel. Experience shows that it successfully improves water recharge for the floodplain. A monitoring system to follow changes in groundwater level and quality is in operation.

12.7.4 Pollution

The Danube catchment lies across 14 countries, a distribution that underlines the importance of its transboundary influence (Literáthy, 2001). The water quality of the Danube has been investigated recently on several occasions. Here follows a summary of findings of the most recent survey (Literáthy, 2001; ICPDR, 2002). Conductivity measurements indicated increased salt contents only

Table 12.3 Average high- and low-water heavy metal concentrations ($mg\,l^{-1}$) in Danube water at Budapest

	At high water	At low water	Permissible limit (Class I water quality in Hungary)
Total dissolved elements	290	320	–
Pb	0.002	0.002	0.005
Mn	0.04	0.06	–
Cd	0.0003	0.0004	0.0005
Co	0.0009	0.0011	0.02

Measured by Z. Szalai in 2000.

below the confluences of the Tisza and the Sava Rivers. In the delta of the Danube salt concentrations (chloride and sulfate anions and sodium and magnesium cations) rose from 290 $mg\,l^{-1}$ (annual average for the period 1961–1970) to 400 $mg\,l^{-1}$ (1981–1990) (ICPDR, 2002). As far as nutrients are concerned, organic nitrogen contents remain constant all along the river. Phosphorus (orthophosphate-P and total P) shows only a moderate increase in Danube water but not in bottom sediments downstream. Heavy metals (particularly arsenic, copper and nickel) are observed in high concentration at the confluences of Bulgarian tributaries (Lom, Iskâr and Timok) but they occur in amounts close to limit values along the middle section too, particularly during low water stages (Table 12.3). Arsenic, chromium, mercury, lead and zinc concentrations were above the German quality targets even in the sediments of the Iron Gate Reservoir. The highly variable flow patterns result in major variations if cross-section middle values are compared with those near the banks where up to 50–70% increase was measured along the Hungarian section (Literáthy, 2001).

The most dangerous pollutants are organic compounds of industrial, agricultural and municipal origin (ICPDR, 2002). Even earlier surveys, such as the one led by J.-Y. Cousteau in 1991–92 (Cousteau Equipe, 1993) demonstrated high oil pollution in the river. The concentrations of polyaromatic hydrocarbons were particularly high in mussels collected from Middle Danube tributaries. Among pesticides the main source of atrazine to the Danube was found to be the Sava River (0.78 $\mu g\,l^{-1}$ maximum concentration).

12.7.5 How Much is the Danube Worth?

Evaluations have been made earlier for the ecological, nutrient load reduction, and rehabilitation potentials of the channel and floodplain of the Danube. A major trend in the development of land evaluation, however, is to express the value of natural potentials (including water and riparian resources) in monetary terms (Avis *et al.*, 2000). Although the economics of natural resources is difficult to establish, the first attempt has already been carried out (Andreasson-Gren and Groth, 1995). Based primarily on ecosystem productivity and substitutability, the average economic value of the Danube floodplains is estimated at £383 ha^{-1} $year^{-1}$. Since the total floodplain area is ca. 1.7 million ha, its value adds up to £650 million $year^{-1}$.

Internationally coordinated human utilization, carefully designed channel, floodplain and ecosystem restoration measures and the appropriate operation of the Trans-National Monitoring Network (TNMN) are needed to preserve or improve environmental quality and natural wealth along this major cultural river of Europe.

REFERENCES

Aksu, A.E., Mudie, P.J., Rochon, A., Kaminski, M.A., Abrajano, T. and Yasar, D. (2002) Persistent Holocene Outflow from the Black Sea to the Eastern Mediterranean Contradicts Noah's Flood Hypothesis. *GSA Today*, May, 4–10.

Andreasson-Gren, M. and Groth, K.H. (1995) Economic Evaluation of Danube Floodplains. WWF International Discussion Paper, Gland, Switzerland.

Avis, Ch., Tydeman, Ch. and Royo Gelabert, E. (2000) *What role for water pricing? Ten actions for internalising sustainability*. World Wide Fund for Nature, Brussels, 18 p.

Bendeffy, L. (1979) A Duna medrében görgetett hordalék eredete és kőzetminősége (Origin and lithology of Danubian bedload). *Földrajzi Értesítő* 28(1–2), 73–89.

BOKU. (2000) Geomorphologische Besonderheiten in Österreich und in den Alpen. Universität für Bodenkultur, Vienna, 7 p. http://homepage.boku.ac.at/h9440283/ggeomorp.htm

Borsy, Z. (1990) Evolution of the alluvial fan of the Alföld. In: *Alluvial Fans: a Field Approach* (A.H. Rachocki and M. Church, Eds). John Wiley & Sons, Ltd, Chichester, pp. 229–248.

Borsy, Z. and Félegyházi, E. (1983) Evolution of the network of watercourses in the end of the Pleistocene to our days. *Quaternary Studies in Poland* 4, 115–125.

Bravard, J.P. (1986) Gabčíkovo: un grand project et une controverse. *Revue de Géographie de Lyon* 74(1), 19–41.

Buch, M.W. (1988a) Spätpleistozäne und holozäne fluviale Geomorphodynamik im Donautal zwischen Regensburg und Straubing. *Regensburger Geographischen Schriften* 21, 240 p. + Suppl.

Buch, M.W. (1988b) Zur Frage einer kausale Verknüpfung fluvialer Prozesse und Klimaschwankungen im Spätpleistozän und Holozän – Versuch einer geomorphodynamischer Deutung von Befunden von Donau und Main. *Zeitschrift für Geomorphologie* 70, 131–162.

Buch, M.W. (1989) Late Pleistocene and Holocene development of the Danube Valley east of Regensburg. In: *Landforms and Landform Evolution in West Germany* (F. Ahnert, Ed.). *Catena*, Cremlingen-Destedt, pp. 279–287 (CATENA Supplement 15).

Coleman, J.M., Roberts, H.H. and Huh, O.K. (1986) Chapter 5. Deltaic Landforms. Plate D-2: Danube River Delta, Romania. In: Internet vesion of *Geomorphology from Space* (N.M. Short, Ed.). NASA, Distributed Active Archive Center, Goddard Space Flight Center, Greenbelt, MD. 2 p. http://daac.gsfc.nasa.gov/DAAC_DOCS/geomorphology/GEO_5/GEO_PLATE_D-2.html

Cousteau Equipe. (1993) The Danube . . . for whom and for what? Cousteau Equipe's Final Report, Paris.

Czaya, E. (1981) *Ströme der Erde*. – Verlag für Kunst und Wissenschaft, Leipzig. 212 p.

DDBRA. (2000) Danube Delta Biosphere Reserve. Danube Delta Biosphere Reserve Authority, Tulcea, Romania, 25 p. http://www.ddbra.ro

Die Rhein–Main–Donau–Wasserstraße. (1992) Schiffahrtsverein Deutschland, 2 p. http://www.schiffahrtsverein.de/wasserstr.htm

Dinev, L. and Mishev, K. (1980) *B'lgariya kratka geografiya* (A Short Geography of Bulgaria). D'rzhavno izdatelstvo Nauka i izkustvo, Sofiya, 351 p.

Domokos, M., Neppel, F. and Somogyi, S. (2000) Paläogeographische Geschichte der Donau und ihres Einzugsgebietes. *Hydrologie und Wasserbewirtschaftung* 44(4), 172–183.

Dragomirescu, S. (1993) Hydroelectricity in the Romanian Carpathians. *GeoJournal* 29(1), 31–39.

Duna (Danube). (1998) *In Magyar Nagylexikon* (Hungarian Macroencyclopaedia) 6. Csen–Ec. Magyar Nagylexikon Kiadó, Budapest, pp. 833–838.

Erdélyi, M. (1994) *Hydrogeology of the Hungarian upper Danube section (before and after damming the river)*. Hungarian Natural History Museum, Budapest, 115 p.

Fink, J. (1966) Die Paläogeographie der Donau. In: *Limnologie der Donau* (Liepolt, R. Ed.) 2. Schweitzerbart'sche Buchhandlungverlag, Stuttgart, pp. 1–50.

Fink, J. (1972) Die Terrassen im Wiener Stadtgebiet. Blätter zur Physische Geographie. Manuskript. Vienna, 87/1972.

Fischer, K. (1989) The landforms of the German Alps and the Alpine Foreland. In: *Landforms and Landform Evolution in West Germany* (F. Ahnert, Ed.). *Catena*, Cremlingen-Destedt, pp. 69–83 (CATENA Supplement 15).

Fischer, K. (1991) Flußgeschichte und Reliefgenese im Norden und Osten des Nördlinger Rieses. In: *Rieser Kulturtage Dokumentation 1990*, Nördlingen, Vol. VIII, pp. 60–82.

Gewässerdirektion Donau/Bodensee. (2001) Aktionsplan Durchgängigkeit baden-württembergische Donau und Breg. Riedlingen, 15 p. +3 Anlagen (Lebensraum Donau Erhalten–Entwickeln).

Geyer, O. and Gwinner, M. (1984) Die Schwäbische Alb und ihr Vorland. *Sammlung Geologischer Führer*, Vol. 67. 3. Auflage. Gebrüder Bornträger, Berlin, 275 p.

Giosan, L., Bokuniewicz, H.J., Panin, N. and Postalache, I. (1998) Longshore sediment transport pattern along the Romanian Danube Delta Coast. *Journal of Coastal Research* 15, 859–871.

Giosan, L., Donnelly, J.P., Vespremeanu, E.I. and Buonaiutu, F.S. (2005) River delta morphodynamics: Examples from the Danube delta. In: *River Deltas – Concepts, Models and Examples* (L. Giosan, and J.P. Bhattacharya, Eds). Society for Sedimentary Geology Special Publication 83, 87–132.

Giosan, L., Donnelly, J.P., Constantinescu, S., Filip, F., Ovejanu, I., Vespremeanu-Stroe, A., Vespremeanu, E.I. and Duller, G.A.T. (2006) Young Danube delta documents stable Black Sea level since the middle Holocene: Morphodynamics, paleogeographic and archaeological implications. *Geology* 34(9), 757–761. doi: 10.1130/G22587.1.

Glatthaar, D. and Liedtke, H. (1988) Untersuchungen in Wellheimer Trockental – Die Anlage des Schutterengtales (südl. Fränkische Alb). *Berichte zur deutschen Landeskunde* 62, 67–82.

Góczán, L. and Lóczy, D. (1990) The Slovak–Hungarian Barrage System on the Danube river and its environmental implications. *Geographia Polonica* 58, 89–98.

Habbe, K.A. (1994) Das deutsche Alpenvorland. In: *Physische Geographie Deutschlands* (H. Liedtke, and J. Marcinek, Eds). Perthes, Gotha, pp. 439–475.

Hadfield, Ch. (1986) World Canals: Inland Navigation Past and Present. Facts on File Publications, New York, 432 p.

Hartley, Ch.A. (1887) Cartes du Delta du Danube et plan comparatifs de l'embouchure et des sections fluviales du bras de Sulina. Commission Européenne du Danube, Leipzig, Plats I–IV.

Hebestreit, C., Schiedek, T., Bauer, M. and Pfaffenberger, C. (1993) Zeitmarken der Wutacheintiefung – Terassenkorrelation, Terrassenstratigraphie und Kalktuffe. *Jahresbericht und Mitteilungen Oberrheinischer Geologischer Verein*, Neue Folge 75, Stuttgart, pp. 291–312.

Hötzl, H. (1996) Origin of the Danube-Aach systems. *Environmental Geology* 27, 87–96.

ICPDR. (2002) Joint Danube Survey: 2581 km along the Danube. Technical Report. English summary. International Convention for the Protection of the Danube River Basin, 26 p.

Jankovič, D. and Jovičič, M. (eds) 1994. The Danube in Yugoslavia: contamination, protection and exploitation. Belgrade, 219 p.

Jaskó, S. and Krolopp, E. (1991) Negyedidőszaki kéregmozgások és folyóvízi üledékfelhalmozódás a Duna-völgyben Paks és Mohács között (Quaternary crustal movements and fluvial sedimentation in the Danube valley between Paks and Mohács). *A Magyar Állami Földtani Intézet Évi Jelentése az 1989. évről* (Report of Hungarian State Geological Survey for 1989), pp. 65–84.

Jerz, H. (1995) Bayern. In: *Das Quartär Deutschlands* (L. Benda, Ed.). Gebrüder Borntraeger, Berlin, pp. 296–326.

Karátson, D. (2002) *Magyarország földje. Kitekintéssel a Kárpát-medence egészére* (Land of Hungary with an Outlook to the Whole Carpathian Basin). Magyar Könyvklub, Budapest, 555 p.

Kavasch, J. (1992) Meteoritenkrater Ries. *Ein geologischer Führer*. 10. Mehrfach überarbeitete Auflage. Ludwig Auer Verlag, Donauwörth, 112 p.

Korpás, L. (ed.) (1998) Magyarázó a Börzsöny és a Visegrádi-hegység földtani térképéhez, 1 : 50 000 (Memoir to the 1 to 50 000 Geological Map 'Börzsöny and Visegrád Mountains'), 20 p.

Kraus-Kalveit, I. and Pannonhalmi, M. (2001) *Vom Rhein zur ungarischen Donau*. I–II. Ministry of the Environment and Forestry, Rhineland–Palatinate, Mainz.

Labhart, T.P. (1987) *Geologie der Schweiz*. 4. Auflage. Hallwag Verlag, Hamburg.

Lászlóffy, W. (1965) Die Hydrographie der Donau (Der Fluß als Lebensraum). In: *Limnologie der Donau 1* (R. Liepolt, Ed.). Schweitzerbart'sche Buchhandlungverlag, Stuttgart, pp. 16–57.

Lehoczky, J. (1979) The Danube river quality alterations in the course of natural infiltration. Proceedings, Third Conference on Water Quality and Technology, Technical University, Budapest, pp. 1–14.

Liniger, H. (1966) Das plio-altpleistozäne Flußnetz der Nordschweiz. *Regio basiliensis* 7, 158–177.

Literáthy, P. (2001) Laboratory Quality Management for Improving Water Pollution Monitoring of Transboundary Rivers – the Case of the Danube River Basin. Water Resources Research Centre (VITUKI), Budapest, 13 p.

Lóczy, D. and Balogh, J. (1990) Geo-ecological mapping in Hungary from satellite imagery. *Zeitschrift für Geomorphologie*, Suppl. 80, 7–16.

Lóczy, D. and Juhász, Á. (1997) Hungary. In: *Geomorphological Hazards of Europe* (C. Embleton, and C. Embleton-Hamann, Eds). Elsevier, Amsterdam, pp. 243–262.

Lóczy, D., Balogh, J. and Ringer, Á. (1989) Landslide hazard induced by river undercutting along the Danube. Geografia Física e Dinamica Quaternaria, Suppl. II, 5–11.

Löscher, M. (1976) Die präwürmzeitlichen Schotterablagerungen in der nördlichen Iller-Lech-Platte. *Heidelberger Geographische Arbeiten* 45, 157 p.

Mahr, T. and Šajgalik, J. (1979) Vývoj, zloženie a vlasnosti štvrtohorných sedimentov zapadnej casti Bratislavy (Development, Composition and Properties of Quaternary Sediments in the W of Bratislava). *Geologické práce*. Správy 73(1), 161–172 (English summary).

Malciu, V. (2000) Implications of accelerated sea-level rise (ASLR) for Romania. Proceedings of SURVAS Expert Workshop on European Vulnerability and Adaptation to Impacts of Accelerated Sea-Level Rise (ASLR), Hamburg, 19–21 June 2000, pp. 23–24.

Marsigli, L.F. (1726) *Pannonico-mysicus observationibus*, Vols I–VII. The Hague.

Mike, K. (1991) *Magyarország ősföldrajza és felszíni vizeinek története* (Palaeogeography of Hungary and the History of its Rivers and Lakes). Aqua, Budapest, 698 p.

Nemerkényi, A. (1990) Die Staustufe Gabčíkovo-Nagymaros an der Donau. *Geographische Rundschau* 42(6), 346–350.

Niedermeier, H. (1995) Flußgeschichte unserer Heimatlandschaft I. Die Urdonau. II. Die erste Laufverlegung der Donau. Freiherr-von-Ickstatt-Schule, Ingolstadt, 10+8 p. http://www.geocities.com/Athens/Olympus/6370/archaeol/donau-1.htm, . . . /donau-2.html

Orghidan, N. (1966) Die Donau und das Eiserne Tor. Revue Roumaine, *Serie Géographie* 10(1), 29–37.

Panin, N. (1989) Danube delta. Genesis, evolution and sedimentology. *Revue Roumaine de Géologie, Géophysique, Géographioe* 33, 25–36.

Panin, N., Panin, S., Herz, N. and Noakes, J.E. (1983) Radiocarbon dating of Danube delta deposits. *Quaternary Research* 19, 249–255.

Pécsi, M. (1959) *A magyarországi Duna-völgy kialakulása és felszínalaktana (Zusammenfassung: Entwicklung und Morphologie des Donautales in Ungarn)*. Akadémiai Kiadó, Budapest, 345 p.

Pécsi, M. (1999) Fluvial landforms. In: *Landform evolution studies in Hungary* (M. Pécsi, Ed.). Akadémiai Kiadó, Budapest, pp. 67–72.

Pécsi, M. and Schweitzer, F. (1995) The development of the Hungarian lowland and upland section of the Danube valley. In: Schirmer, W. (ed.) Quaternary Field Trips in Central Europe. INQUA 14th International Congress, August 3–10, 1995, Berlin, Vol. 1. Regional field trips. Verlag Friedrich Pfeil, Munich, pp. 305–310, 316–317.

Pécsi, M., Scheuer, Gy. and Schweitzer, F. (1988) Neogene and Quaternary geomorphological surfaces and lithostratigraphical units in the Transdanubian Mountains. In: *Paleogeography of Carpathian Regions* (M. Pécsi, and L. Starkel, Eds). Geographical Research Institute Hungarian Academy of Sciences, Budapest, pp. 11–42.

Pécsi-Donáth, É. (1958) Dunaterasz-kavicsok görgetettségi vizsgálata (Study of roundness of gravels from Danube terraces). *Földtani Közlöny* 88(1), 57–75.

Pišút, P. (2002) Channel evolution of the pre-channelized Danube River in Bratislava, Slovakia (1712–1886). *Earth Surface Processes and Landforms* 27, 369–390.

Popp, N. (1974) A Duna negyedkori fejlődéséről alkotott szintézis általános eredményei Romániában (A Synthesis of Research on the Quaternary Evolution of the Danube in Romania). *Földrajzi Értesítő*, 23(1), 19–25.

Pringle, C., Vellidis, G., Heliotis, F., Bandacu, D. and Cristofor, S. (1993) Environmental problems of the Danube Delta. *American Scientist* 81, 350.

Romanescu, Gh. (1996) L'évolution hydrogéomorphologique du delta du Danube. Etape Pleistocene–Holocene inférieur. *Zeitschrift für Geomorphologie* Suppl. 106, 267–295.

Rutte, E. (1987) *Rhein, Main, Donau: Wie – wann – warum sie wurden*. Eine geologische Geschichte. Jan Thorbecke Verlag, Sigmaringen, 154 p.

Ryan, W.B.F., Pitman III, W.C., Major, C.O., Shimkus, K., Moskalenko, V., Jones, G.A., Dimitrov, P., Görür, N., Sakinç, M. and Yuce, H. (1997) An abrupt drowning of the Black Sea shelf. *Marine Geology* 138, 119–126.

Schweitzer, F. (1997) On late Miocene–early Pliocene desert climate in the Carpathian Basin. *Zeitschrift für Geomorphologie*, Suppl. 110, 37–43.

Schweitzer, F. and Scheuer, Gy. (1986) The role of travertines in the geomorphological, paleohydrogeological and geochronological research of the Upper Cainozoic. In: *Pollution and Water Resources* (G. Halasi-Kun, Ed.). Columbia University, New York, pp. 71–90.

Somogyi, S. (1983) A magyar folyóhálózat szakaszjelleg típusai (Types of river reaches in Hungary). *Földrajzi Közlemények* 31(108), 220–229.

Somogyi, S. (ed.) 2000. *A XIX századi folyószabályozások és ármentesítések földrajzi és ökológiai hatásai* (Geographical and ecological impacts of flow regulation and drainage in the 19th century). Geographical Research Institute, Hungarian Academy of Sciences, Budapest, 302 p.

Stancíkova, A. (2001) *A Duna szabályozása* (Regulation of the Danube). Vízügyi Közlemények 83(3), 451–472.

Strunk, H. (1989) Aspects of the Quaternary in the Tertiary hills of Bavaria. In: *Landforms and Landform Evolution in West Germany* (F. Ahnert, Ed.). Catena, Cremlingen-Destedt, pp. 289–295 (CATENA Supplement 15).

Sümeghy, J. (1953) *Medencéink pliocén és pleisztocén rétegtani kérdései* (Issues concerning the Pliocene and Pleistocene stratigraphy in Hungarian basins). Annual Report of the Hungarian Geological Institute for 1951, Budapest, pp. 83–109.

Tillmanns, W. (1984) Die Flussgeschichte der oberen Donau. *Jahresheft des geologischen Landesamts Baden-Württemberg, Freiburg im Breisgau* 26, 99–202.

Tillmanns, W., Brunnacker, K. and Löscher, M. (1993) Erläuterungen zur Geologischen Übersichtskarte der Aindlinger Terrassentreppe zwischen Lech und Donau. *Geologica Bavaria*, Munich 85, 31 p.

UNEP. (1991) World Heritage Sites. Danube Delta Biosphere Reserve. Protected Areas Programme, UNEP World Conservation Monitoring Centre, Cambridge, 11 p.

UNESCO. (1999) *The Danube and its Basin – a Hydrologic Monograph*. Followup Volume 5. The Danube River Bed Conditions. Regional Cooperation of the Danube Countries in the frame of the International Hydrological Programme of UNESCO. VÚVH, Bratislava, 186 p.

Vadineanu, A. and Voloshyn, V. (eds) (1999) The Danube Delta Biosphere Reserve Romania/Ukraine. National UNESCO–MAB Committee of Romania, Bucharest, and National UNESCO–MAB Committee of Ukraine, Kyiv, 46 p.

Villinger, E. (1986) Untersuchungen zur Flussgeschichte von Aare-Donau/Alpenrhein und zur Entwicklung des Malm-Karsts in Südwestdeutschland. Jahresheft des geologischen Landesamts Baden-Württemberg, *Freiburg im Breisgau* 28, 297–362.

Villinger, E. (1998) Zur Flussgeschichte von Rhein und Donau in Südwestdeutschland. *Jahresbericht und Mitteilungen Oberrheinischer Geologischer Verein*, Neue Folge 75, Stuttgart, pp. 291–312.

Werner, A., Hötzl, H., Käss, W. and Maloszewski, P. (1997) Interpretations of Tracer Experiments in the Danube–Aach System, Western Swabian Alb, Germany, with analytical models. In: *Karst Waters and Environmental Impacts* (Y. Günay, and J. Johnson, Eds). Balkema, Rotterdam, pp. 153–160.

13

The Nile: Evolution, Quaternary River Environments and Material Fluxes

Jamie C. Woodward[1], Mark G. Macklin[2], Michael D. Krom[3] and Martin A.J. Williams[4]

[1]*School of Environment and Development, The University of Manchester, Manchester M13 9PL, UK*
[2]*Institute of Geography and Earth Sciences, University of Wales, Aberystwyth, Aberystwyth SY23 3DB, UK*
[3]*School of Earth Sciences, University of Leeds, Leeds LS2 9JT, UK*
[4]*Geographical and Environmental Studies, University of Adelaide, Adelaide, South Australia 5005, Australia*

13.1 INTRODUCTION

The Nile Basin contains the longest river channel system in the world (>6500 km) that drains about one tenth of the African continent. The evolution of the modern drainage network and its fluvial geomorphology reflect both long-term tectonic and volcanic processes and associated changes in erosion and sedimentation, in addition to sea level changes (Said, 1981) and major shifts in climate and vegetation during the Quaternary Period (Williams and Faure, 1980). More recently, human impacts in the form of land use change over the last few millennia and large dam construction over the last hundred years or so, have had major impacts on the hydrology and sediment budget of the Nile Basin. The river basin straddles 35° of latitude (4° S to 31° N) encompassing a wide variety of climates, river regimes, biomes and terrains – from the Equatorial lakes plateau of the White Nile headwaters to the delta complex in the Eastern Mediterranean Sea (Figure 13.1). It is unique among the large exotic rivers of the world in that today it flows for almost 2700 km through the Sahara Desert without any significant perennial tributary inputs. Of all the world's rivers with catchments greater than 1 million km^2, the Nile has the lowest specific discharge, 0.98 litres s^{-1} km^{-2} at Aswan (Shahin, 1985) – although base flows and the summer flood were significantly higher in the early Holocene (Adamson *et al*., 1980; Williams *et al*., 2000; Woodward *et al*., 2001; Krom *et al*., 2002) as well as during previous interglacial and interstadial periods (Williams *et al*., 2003). The true desert Nile begins in central Sudan at Khartoum (15° 37′N 32° 33′E) on the Gezira Plain where the Blue Nile and the White Nile converge (Figure 13.1). These two systems, and the tributary of the Atbara to the north, are all large rivers in their own right with distinctive fluvial landscapes and process regimes. The Nile has a total catchment area of around 3 million km^2 (Figure 13.1 and Table 13.1).

The Nile Basin supports a vast range of ecosystems (Rzoska, 1976) and has played a central role in the development of a rich diversity of cultures (Wendorf *et al*., 1976; Welsby, 1998, 2001; Shaw, 2003). It has been an important corridor for the movement of people and animals throughout the Quaternary and the lower Nile and delta saw the rise of the Kingdoms of Egypt (Davies and Friedman, 1999) and their great irrigation-based civilization (Hassan, 1988). Today over 180 million people live within the basin and about half this number are almost totally dependent on Nile flows for economic and domestic needs. While much of the basin is sparsely populated, rapidly growing urban centres, most notably Cairo (population >16.5 million) and greater Khartoum (population >6 million) – and extensive tracts of agricultural land on the valley floor and delta – are heavily or totally reliant

Large Rivers: Geomorphology and Management, Edited by A. Gupta

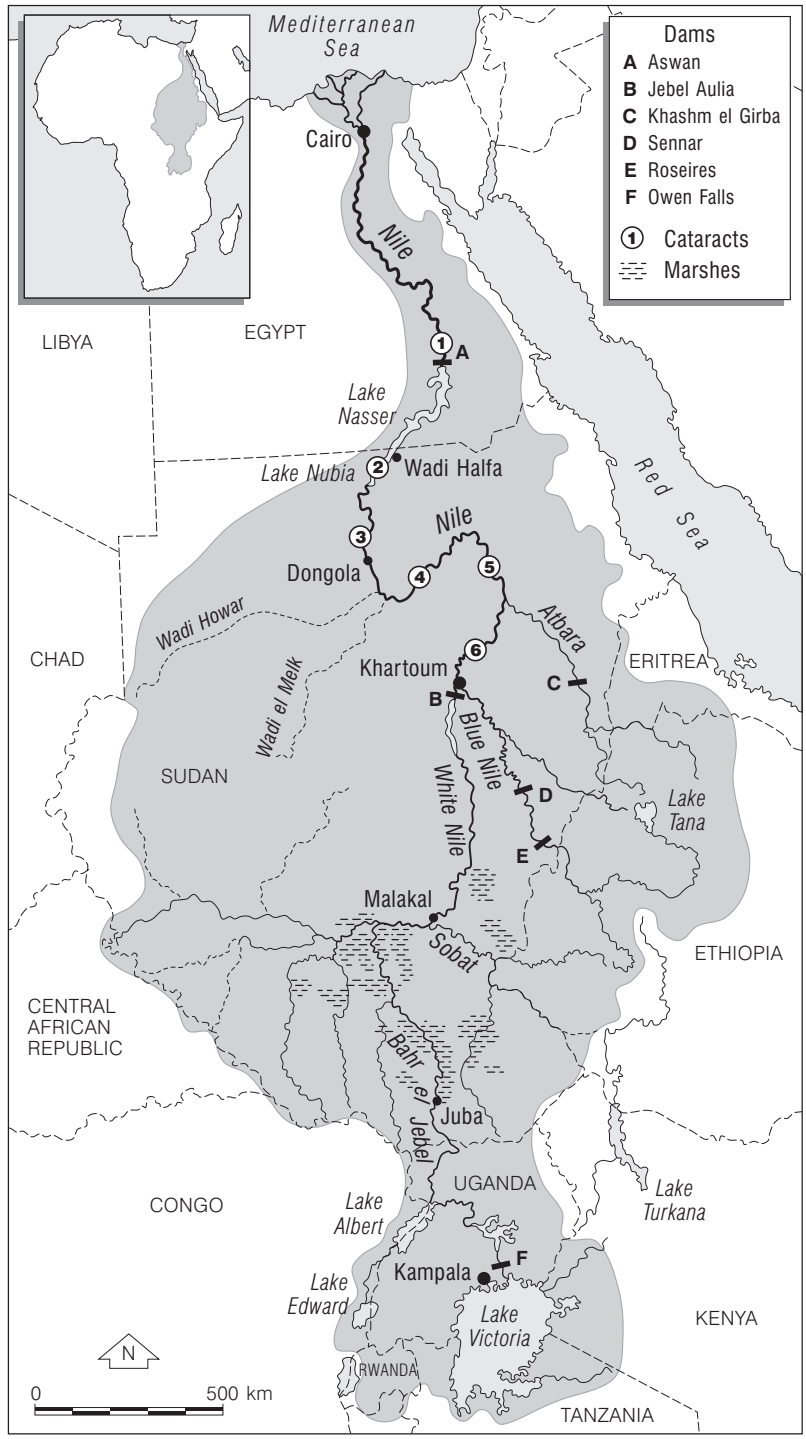

Figure 13.1 Map of the Nile Basin showing the drainage network, basin states, and major dams

Table 13.1 Geographical, hydrological, and water resource data for each of the 10 countries of the Nile Basin (based on sources in UNEP, 2000)

Country	Area of country within the Nile basin (km^2) and its percentage of the total basin area (in parentheses)	Average rainfall across the basin in each country for minimum and maximum years (mm)	Internal renewable water resources (IRWR) (km^3 $year^{-1}$)	Actual renewable water resources (ARWR) (km^3 $year^{-1}$)	The dependency ratio = the percentage difference between the ARWR and the IRWR	Population in the Nile Basin in 1990 (millions) with the percentage of the country's population in the basin (in parentheses)
Burundi	13 260 (0.4)	895 to 1570	3.6	3.6	0	3 204 (58)
DR Congo	22 143 (0.7)	875 to 1915	935	1019	8.2	1 838 (4)
Egypt	326 751 (10.5)	0 to 120	1.7	58.3	96.9	47 599 (85)
Eritrea	24 921 (0.8)	240 to 665	2.8	8.8	68.2	0.918 (30)
Ethiopia	365 117 (11.7)	205 to 2010	110	110	0	19 454 (35)
Kenya	46 229 (1.5)	505 to 1790	20.2	30.2	33.1	9 129 (32)
Rwanda	19 876 (0.7)	840 to 1935	6.3	6.3	0	5 731 (72)
Sudan	1 978 506 (63.6)	0 to 1610	35	88.5	77.3	20 893 (74)
Tanzania	84 200 (2.7)	625 to 1630	80	89	10.1	4 878 (16)
Uganda	231 366 (7.4)	395 to 2060	39.2	66	40.9	15 999 (75)
Total	3 112 369 (100)					129 643

on Nile flows for irrigation and power generation. The population of Egypt (>65 million in 2001) is expected to double by 2050 and it already uses the largest share of the annual water budget. The spatial pattern of rainfall inputs across the Nile Basin is highly variable and because Sudan and Egypt abstract the greatest volumes for irrigation – and have the highest water resource dependency ratios (Table 13.1) – the allocation and use of Nile waters continues to be a highly charged political issue within the 10 basin states (Howell and Allan, 1994).

The dominant water resource management and flood control strategy of the twentieth century saw the development of major river impoundments in the basin (Figure 13.1). Over the same period, as the population of Egypt and its irrigation schemes grew apace, the allocation and use of Nile waters emerged as a source of major international political tension (Collins, 1990; Howell and Allan 1994) and Nile Waters Treaties were signed in 1929 and 1959. The first phase of construction of the Aswan High Dam was completed in 1964 (the final phase ended in 1971) and other major twentieth century dams include the Jebel Aulia (1937) on the White Nile and the Roseires Dam (1966) on the Blue Nile (Figure 13.1). Since the long-term flow records for the Nile exhibit considerable annual variability (Hassan, 1981; Sutcliffe and Lazenby, 1994), the major water storage schemes hold considerable strategic importance for water resource management, power generation and flood control. These schemes are partly a response to the fact that most of the flows are generated in headwater areas that cover only about 20% of the basin. Local water resources are minimal in the arid and semi-arid regions of Egypt and Sudan (Table 13.1) and evaporation and seepage losses are high in this part of the basin (UNEP, 2000). The Merowe Dam near the fourth cataract in northern Sudan is expected to be completed in 2008 and it will treble the nation's hydropower capacity. Hydroelectric output from the Aswan High Dam never lived up to expectations owing to seepage losses and serious underestimates of evaporation losses. The Merowe project will create the first dam on the main Nile in Sudan and will involve the resettlement of 50 000 people as well as the loss of many archaeological sites (Askouri, 2004).

This chapter reviews the evolution of the river and its present day hydrology and fluvial geomorphology. It also summarises the response of the Nile Basin to Late Pleistocene and Holocene climatic changes as this provides important context for the contemporary fluvial environments of the basin. The suspended sediment budget of the basin and offshore regions is also discussed and the impacts of the major water resource management developments on water and sediment fluxes are assessed.

13.2 NILE BASIN RIVER ENVIRONMENTS

According to Said (1981) the Nile Basin encompasses five major regions that differ from one another in structure and geological history (Figures 13.1 and 13.2). These are listed below and the characteristic fluvial environments of each region are briefly described:

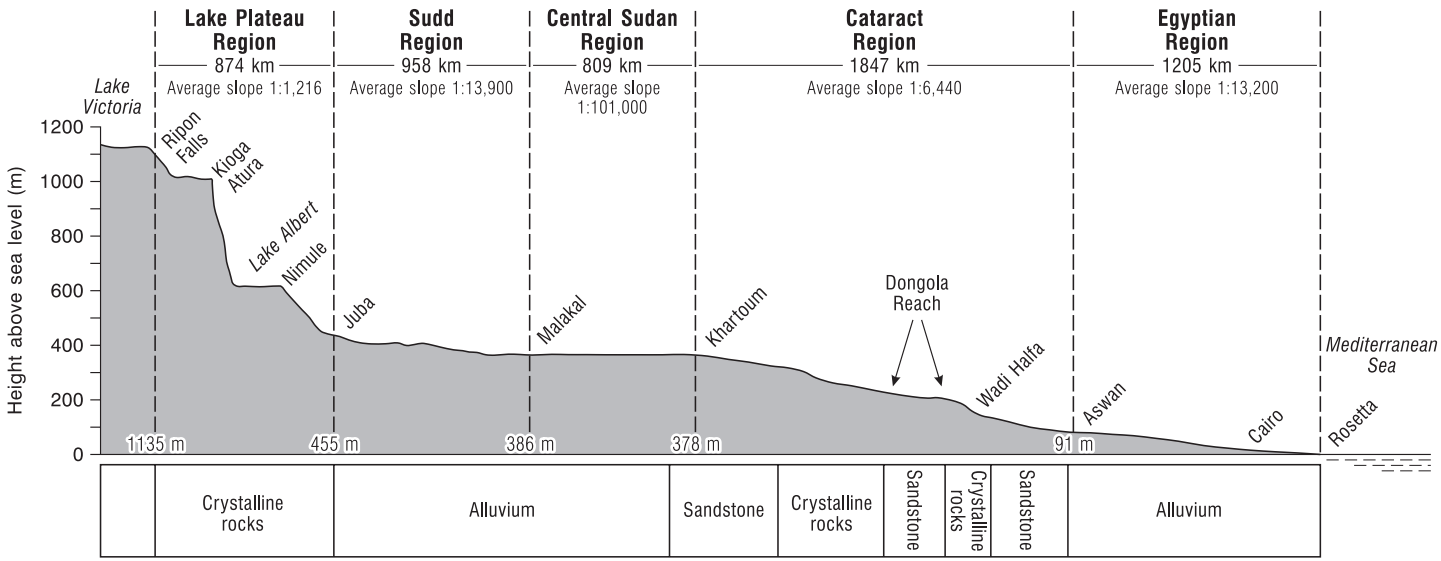

Figure 13.2 Long profile of the Nile from the White Nile headwaters to the Mediterranean Sea (after Said, 1994). Note that the Blue Nile is not shown

(1) The Equatorial lake plateau in the White Nile headwaters with densely forested, tropical catchments with perennial flow regimes.
(2) The Sudd region and central Sudan with low gradient floodplains, extensive swamplands and broad channel belts and low suspended sediment concentrations.
(3) The Ethiopian Highlands forming the headwaters of the Blue Nile and the Atbara with deep ravines, unstable slopes, entrenched steep gradient gravel bed streams with highly seasonal flows and high sediment loads.
(4) The great bends and cataracts of the desert Nile with ephemeral tributary wadi systems and alluvial fans in the arid lands of Sudan and Egypt and the cataracts and vast alluvial reaches of the main Nile with a strongly modified flow and sediment regime downstream of the Aswan High Dam.
(5) The Egyptian region including the low gradient delta complex with its large distributaries, promontories and lagoons, heavily modified drainage and dense network of irrigation canals.

Marked contrasts are evident in the hydrology and fluvial geomorphology of each of the five regions. Distinctive large river valley-floor environments are present in each region and these reflect the strong regional variations in topography, tectonic setting, climate, hydrology, vegetation, sediment supply and other factors. The legacy of Quaternary sediments and landforms on the valley floor is also apparent in many parts of the basin and these may exert an important influence on contemporary fluvial processes and on the chemical and physical properties of alluvial soils, especially soil permeability and soil salinity (Williams *et al*., 2000). These contrasts in river basin dynamics pose a wide range of catchment management issues and the nature and extent of the human impact and use of river-related resources varies markedly across the Nile basin.

13.3 EARLY ORIGINS AND THE LATE MIOCENE AND PLIOCENE NILE

Several detailed reviews of the evolution of the Nile drainage basin have been published in recent decades (Adamson and Williams, 1980; Williams and Williams, 1980; Said, 1981, 1993; Adamson *et al*., 1993). These document the development of the modern drainage configuration following the influence of major tectonic phenomena – including the rifting of East Africa – climatic changes and other factors. Adamson and Williams (1980) and Adamson *et al*., (1993) have examined the structure and tectonic history of the Nile Basin and neighbouring regions and have related these geological phenomena to the organization of the drainage network, to the location of major sedimentary basins, and to major changes in the former extent of the catchment. They argue that tectonic events of great antiquity – probably dating to the Pan-African orogenic event (~550 Ma) or earlier – have been influential in shaping the Nile Basin and the courses of the large river channel systems that form the modern catchment. The watershed of the present Nile and its relationship to the major rift zones and other large river systems to the east and west of the upper and middle Nile is shown in Figure 13.3. The courses of large rivers including the Bahr el Jebel, the Blue Nile, the Atbara, the main Nile and many tributaries are influenced by dominant linear structures including dykes, joints, faults and major geological contacts (Adamson and Williams, 1980; Adamson *et al*., 1993).

13.3.1 The Late Miocene Nile Canyon in Egypt

The severing of the connection between the North Atlantic Ocean and the Mediterranean Sea at the end of the Miocene (around 6.5 million years BP) led to the onset of the Messinian Salinity Crisis – arguably one of the most dramatic series of environmental changes recorded in recent Earth history (Hsu *et al*., 1973). The evaporation of the Mediterranean Sea and the shift to saline desert conditions across its former marine basins had profound impacts on the large river systems of the region including the Nile. The fall in base level in the Eastern Mediterranean led to large-scale fluvial incision and, according to Hsu *et al.* (1973), the Nile carved a deep bedrock canyon to ca. 570 m below present sea level at Cairo and to −170 m at Aswan – some 1000 km upstream from the present coastline. This fall in elevation of about 400 m between Aswan and Cairo for the Late Miocene Nile Valley compares with a fall of around 70 m for the modern Nile over the same distance. Figure 13.4 shows a block diagram of the Eonile Canyon from the area of present-day Cairo to the dried out basin of the Late Miocene Mediterranean. Said (1981) has called this Late Miocene river *The Eonile.* Recently, Le Pichon *et al.* (2005) have estimated that the canyon was about 1100 km long and 1900 m deep. Further downstream the Late Miocene Nile created a series of fans in the region of the North Delta Embayment (more than 4000 m below modern sea level) where evaporites accumulated in the distal areas of these fan complexes under arid climatic conditions (Figure 13.4). Said (1981: 99) has argued that the course of this river was determined by the tectonic framework of the region at the time and he observes that this was

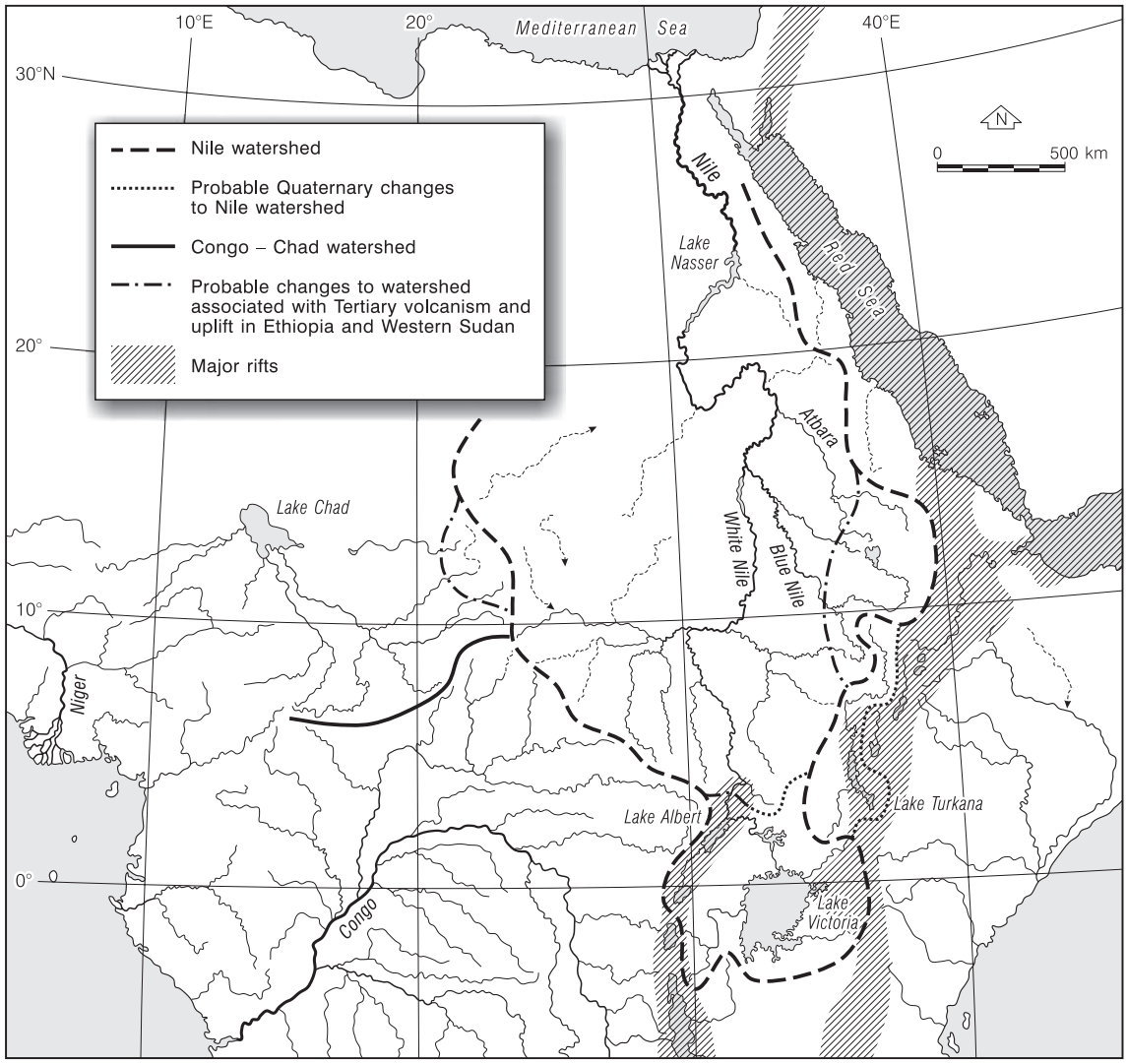

Figure 13.3 The drainage network of central and northeastern Africa showing the Congo, Chad, Niger and Nile river basins and the present and former extent of the Nile watershed. The major zones of Tertiary rifting are also shown (after Adamson and Williams, 1980)

> 'the first time in the history of the drainage of the elevated lands of Egypt that the river followed a defined and deep gorge which distinguishes it from the alluviating and shallow rivers of the pre-late Miocene drainage systems which preceded the Nile system.'

It is interesting to note that the Late Miocene Nile Canyon was longer and deeper that the Grand Canyon of the Colorado River (see Chapter 10; Table 13.2) and this phase of fluvial erosion generated an estimated 70 000 km^3 of sediment in less than 3 million years (Said, 1981). This represents about 20% of the total mass of sediment in the Nile Cone (Said, 1981). Estimates vary, with McDougall *et al.* (1975) suggesting a maximum volume for the Nile cone of ~200 000 km^3. Other large river systems draining to the Mediterranean Sea including the Po and Rhone also cut deep canyons at this time (Ryan and Cita, 1978).

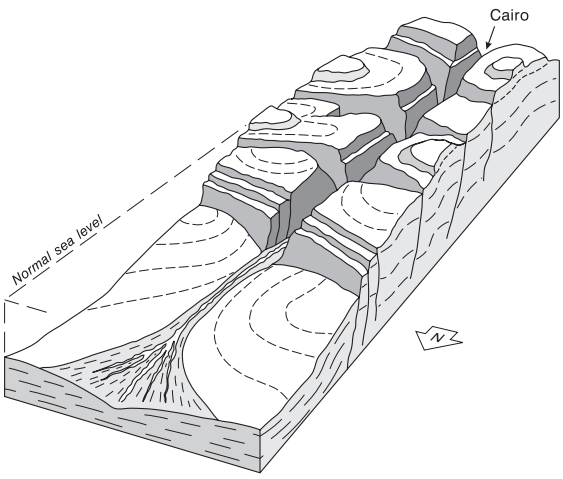

Figure 13.4 Schematic reconstruction of the Nile Canyon showing the main channel and tributary gorges cut by the Egyptian Nile drainage during the Late Miocene (Messinian) salinity crisis. See Table 13.2 and text for estimates of the main canyon's dimensions. Reprinted from The Geological Evolution of the River Nile, Said, R., page 151, Copyright (1981). With kind permission of Springer Science and Business Media

Table 13.2 A comparison of the modern Grand Canyon in Arizona with estimates for the size of the Late Miocene Nile Canyon. Reprinted from the Geological Evolution of the River Nile, Said R., pp 151. Copyright (1981). With kind permission of Springer Science and Business Media

	Grand Canyon, Arizona, USA, Colorado River	Eonile Canyon, Egypt (Late Miocene)
Width (km)	10–20	10–20
Length (km)	320	1300
Depth (m)	2080	2500
Gradient	1 : 625	1 : 400
Age	Early Miocene to present	Late Miocene
Formation time (years)	*ca*. 20 million	*ca*. 3 million

Higher sea levels during the Pliocene resulted in the creation of a long narrow marine gulf in the Nile Valley that reached as far south as Aswan. The marine sediments of the Early Pliocene filled about one third of the depth of the Eonile canyon (Said, 1981). The Late Pliocene Nile saw a shift from marine to brackish conditions with a load of fine-grained sediments derived from local wadi systems – the Egyptian Red Sea Hills were an important source of sediment at this time. This period saw the complete infilling of the Eonile canyon (Said, 1981) as the freshwater zone moved northwards towards the modern Mediterranean coastline.

13.3.2 The Integrated Nile

Much debate has surrounded the antiquity of the integrated Nile Basin that exists today and the nature and timing of the connections between the Egyptian Nile and the major headwater basins of the White Nile and Blue Nile (Figure 13.3). Adamson (1982) has reviewed the development of ideas on this topic during the 1960s and 1970s. Williams and Williams (1980) point out that while there is some evidence for a Late Cretaceous drainage link between Sudan and Egypt, the earliest firm evidence of Nile flow from the Ethiopian Highlands to the Mediterranean Sea (via Sudan and Egypt) dates to the Early Pleistocene. Tertiary tectonic events associated with the rifting of Africa and the separation of Arabia created the high elevation sub-basins of the Nile and determined its northward course to the Mediterranean Sea (Adamson, 1982; Adamson *et al*., 1993). Williams and Williams (1980) and Adamson (1982) have argued that the Nile has been transporting water and sediment from the Ethiopian Highlands to the Mediterranean since 'well back into the Tertiary' and they point to the microfossil and mineralogical evidence in the sediments of the Nile Cone – as well as the huge volume of those sediments – as evidence for a very early integration of sub-Saharan drainage with the Egyptian Nile. Part of their argument was based on the rough equivalence in the volume of rock eroded from the Ethiopian headwaters of the Nile (McDougall *et al*., 1975) and that of the Nile Cone. Adamson and Williams (1980: 251) have argued that, while climatic and tectonic events may have periodically interrupted the connection, the integrated Nile Basin is as old as the Tertiary rifting of Africa. Butzer and Hansen (1968: 6), however, contend that the Nile hydrographic system as we know it today is of comparatively recent age – they have argued that the White Nile and the Blue Nile catchments did not connect with the Saharan Nile before the Early Pleistocene. It is difficult to reconcile this latter view with the presence of sapropels in the pre-Quaternary marine record of the Eastern Mediterranean Sea as most workers agree that elevated flood flows from the Blue Nile Basin are a key ingredient for their formation (Rossignol-Strick *et al*., 1982).

More recent work has shown that the lower White Nile is relatively young, and flows across the floor of a very large lake that occupied its valley around 400 000 years BP (Williams *et al*., 2003). The age of the Blue Nile is harder to estimate. Some 2 km of uplift in the past 8 Ma initiated or accelerated the incision that gave rise to the Blue Nile Gorge, which dissects horizontal Trap Series

basalts of Upper Oligocene age (McDougall *et al*., 1975). It is clear from a wide range of sources that the Nile Basin watershed has expanded and contracted throughout its history (Figures 13.3 and 13.4). However, while the existence of several large, separated river basins at some stage in its early development is now widely accepted, reliable geochronological and stratigraphical data on their age and extent are not yet available for periods before the Late Pleistocene, apart for the lower White Nile (Williams *et al*., 2003).

13.4 THE LATE PLEISTOCENE AND HOLOCENE NILE

Fluctuations in the climate and hydrology of tropical Africa during the Quaternary exerted an important influence on the behaviour of the Nile sediment system. During the cold stages of the Pleistocene low lake levels reflect a decrease in precipitation as the expanded ice sheets cooled the global oceans and monsoon intensity fell (Hulme, 1994). These changes were driven by Milankovitch forcing of global climate and the precession signal was an especially important influence on tropical rainfall dynamics. The influences of eustatic changes in Quaternary sea level driven by changes in ice volume were not propagated upstream of the lower Nile in Egypt.

The Nile Basin contains a wide range of sedimentary archives that preserve information about Pleistocene and Holocene environments. Lacustrine sequences from lake basins of various sizes form the most detailed and well dated of these records (e.g. Gasse *et al*., 1980; Stager *et al*., 1997). The alluvial sedimentary record is also important, but most of the work in the Nile Basin has been conducted in Sudan and Egypt and, in general, the depositional records tend to be much more fragmented and less well dated than the lake sediment records (Butzer, 1980; Said, 1981). An exception is the lower White Nile, where an alluvial record extending back at least 240 ka is reasonably well preserved due to very gentle gradients and minimal erosion (Williams *et al*., 2003). In some areas the Late Pleistocene and Early Holocene fluvial geomorphology is well preserved and large-scale valley floor landforms point to the existence of very different fluvial environments at these times. Figure 13.5 shows the changing fluvial geomorphology of the lower White Nile valley during the global Last Glacial Maximum (LGM) (ca. 18–20 000 ^{14}C years BP), the Early Holocene (ca. 7000 ^{14}C years BP) and the present day. In a series of papers, Adamson *et al*. (1980), Williams and Adamson (1980) and Williams *et al*. (2000) have reviewed the Late Quaternary history of the Nile and its main tributaries and their findings, along with the outcomes of recent work on the Holocene records in the Nile Delta (Krom *et al*., 2002) and in northern Sudan (Woodward *et al*., 2001) are briefly summarized below. Note that all ages in the following section are uncalibrated radiocarbon ages unless otherwise stated.

13.4.1 20 000 to 12 500 ^{14}C Years BP

The early part of this period coincides with the global LGM of Marine Isotope Stage 2. This was a dry period across much of the Nile Basin with colder conditions than present and rapid erosion in the Ethiopian Highlands where the tree line was probably about 1000 m lower than at present during the coldest phases of the Pleistocene. In very general terms, during the global LGM the main channels of the Blue Nile and desert Nile were characterized by net aggradation and sediments were deposited on the valley floor in a braided river environment dominated by sandy bar complexes with some fine gravel. Adamson *et al.* (1980) have argued that discharges at this time were much reduced – perhaps amounting to only about 10–20 % of the modern Nile flows. The increased sediment supply to the fluvial system at this time resulted from a decrease in vegetation cover in the Ethiopian Highlands leading to slope instability and gully and sheet erosion. The hillslope environments and fluvial geomorphology of the Blue Nile Basin during the global LGM are shown in Figure 13.6. Small glaciers were present on the highest mountains in Ethiopia and periglacial activity was widespread in these uplands. It is likely that the LGM flow regime in the Blue Nile Basin was even more seasonal than at present (Williams and Adamson, 1980).

During this period the regime of the White Nile was also highly seasonal and with very low flows and even periods of complete drying out for all or part of the year (Williams *et al*., 2000). This is a key contrast with the modern White Nile system. This flow regime was the product of lower Equatorial rainfall during the Late Pleistocene and the absence of a connection with Lake Victoria. Thus, the White Nile in Sudan became isolated from its Equatorial headwaters in Uganda, and, as noted above, it is the White Nile that is presently responsible for maintaining the perennial flow of the main Nile, especially during drought years. With greater aridity at this time the valley floor of the White Nile was characterized by extensive active aeolian dune systems derived from the sandy fluvial bed load and these were large enough to block the channel zone in some reaches (Figures 13.5 and 13.7). The dunes are typically aligned north to south and it is likely that some of the discharge may have continued to flow north through the dune complexes (Williams and Adamson, 1980). The Late Pleistocene White Nile in central Sudan

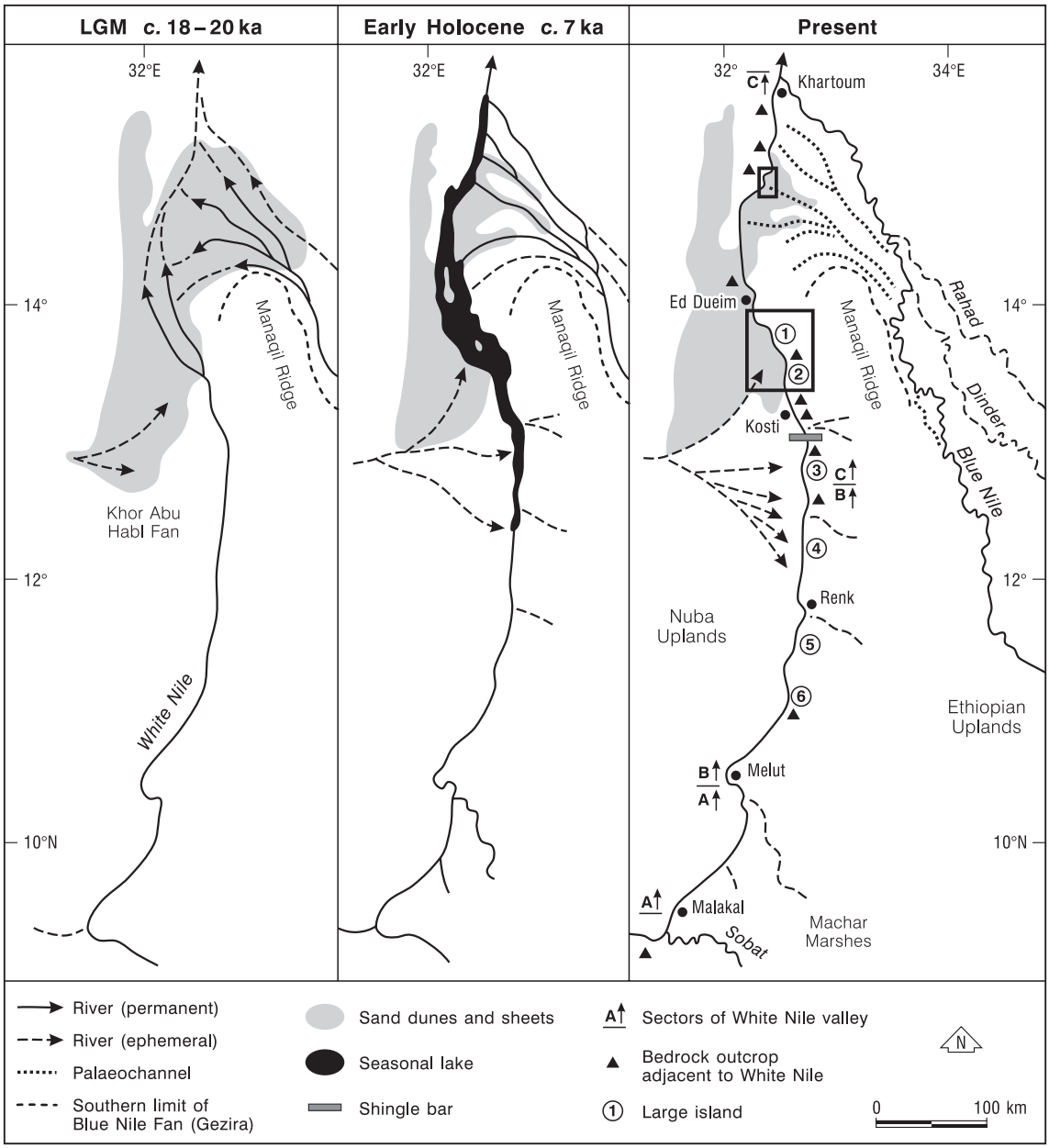

Figure 13.5 The geomorphology of the middle and lower reaches of the White Nile during the global Last Glacial Maximum, the Early Holocene and present day. Note that the dates are in radiocarbon years before present. The geomorphology of the reaches demarcated by the boxes on the present Nile is shown in more detail in Figure 13.7. Reprinted from Global and Planetary Change, 26, M.A.J. Williams *et al*., Late Quaternary . . . White Nile, pages 305–316, Copyright (2000), with permission from Elsevier

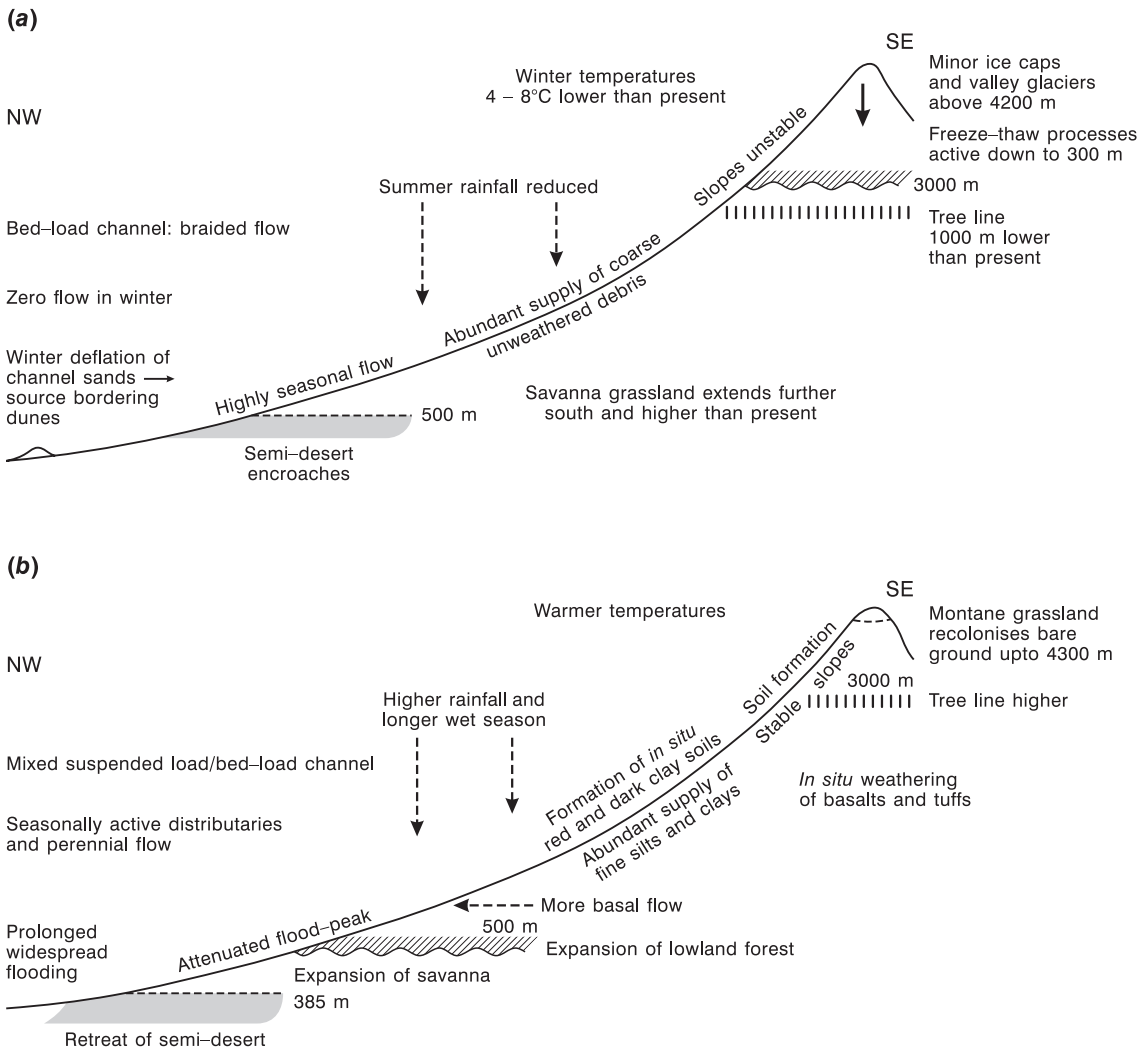

Figure 13.6 Geomorphological processes in the Blue Nile Basin during (a) the global Last Glacial Maximum and (b) the Early Holocene (after Williams and Adamson, 1980)

saw a range of large scale fluvio-aeolian interactions with each process regime providing sediment for aeolian or fluvial transport and there is a good deal of evidence for aeolian modification of fluvial landforms and vice versa. These process interactions would have been in evidence on a seasonal basis and in the longer term. Williams *et al*. (2000: 310) have argued that flood discharges were highly variable in the White Nile valley during this period, and seasonal ponding of runoff behind dunes and mobile sand bars would have created a fluvial landscape similar to that of the central Niger valley today. It is also important to appreciate that for much of the Late Pleistocene, flood waters and suspended sediments from the Blue Nile were conveyed via a series of distributaries across the Gezira fan (upstream of the confluence at Khartoum) and into the reaches of the lower White Nile (Figure 13.5). This has produced complex alluvial sedimentary records in this large confluence zone.

13.4.2 12 500 to 5000 ^{14}C Years BP

Shortly after about 12 500 ^{14}C years BP enhanced rainfall in the tropics led to the overflow of Lake Victoria and Lake Albert (Figure 13.1 and Table 13.4) leading to 'dra-

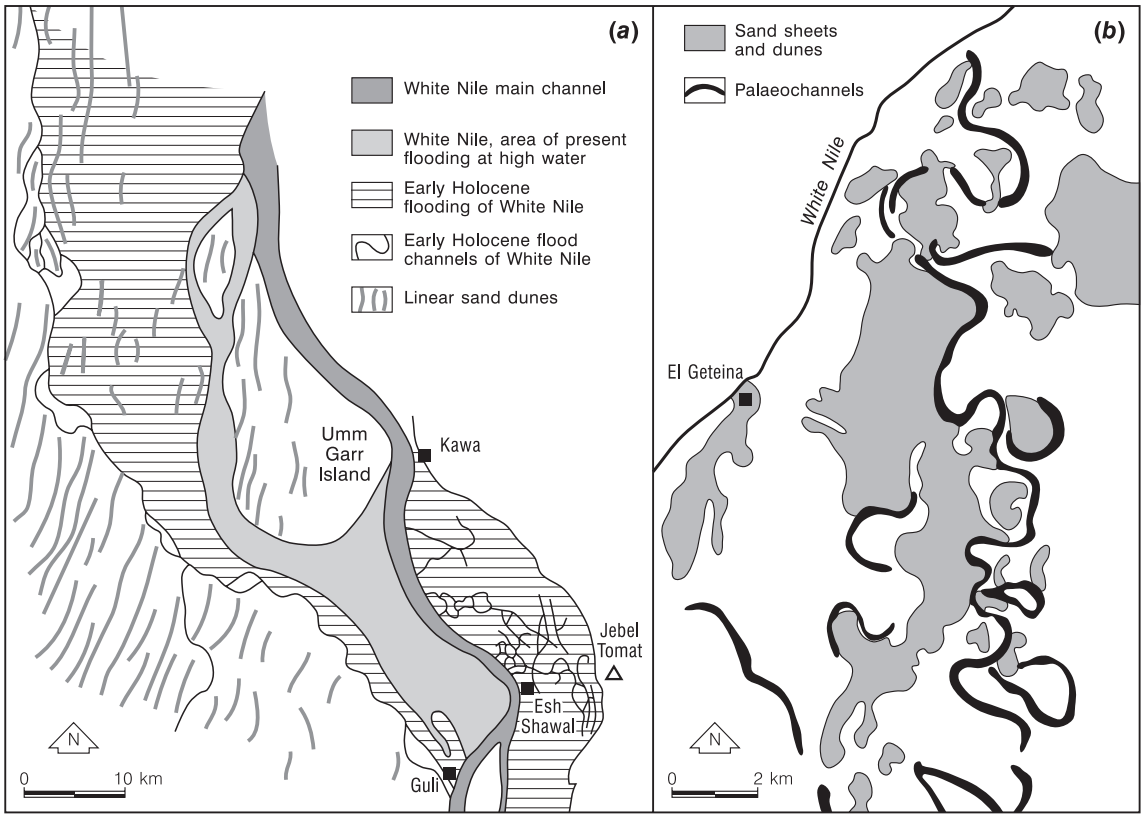

Figure 13.7 Geomorphological maps of the lower White Nile floodplain showing large-scale fluvial landforms relating to higher discharges in the Early Holocene and aeolian dunes representing more arid periods and much lower flows. (a) Reaches near Esh Shawal. (b) Reaches near El Geteina. See Figure 13.5 for locations. Reprinted from Global and Planetary Change, 26, M.A.J. Williams *et al.*, 'Late Quaternary . . . White Nile', pages 305–316, Copyright (2000), with permission from Elsevier.

matic and enduring changes in the lower White Nile valley' (Williams *et al*., 2000: 310). The onset of the modern discharge regime in the Nile Basin can be traced back to the beginning of this Late-glacial and early Holocene wet phase around 12 000 ^{14}C years BP (Talbot *et al*., 2000). An increase in regional humidity and a shift to a perennial flow regime led to stabilization of the dune systems on the White Nile valley floor by vegetation. In some areas the dunes were buried beneath low energy fine-grained fluvio-lacustrine clays (Figures 13.5 and 13.7). By about 11 500 to 11 000 ^{14}C years BP, the White and Blue Niles conveyed very large flood discharges and this produced a very extensive inundated area in the lower White Nile valley (Figure 13.5). This inundated area was about 4 to 5 m higher and 20 to 40 km wider than present and led to the deposition of fine-grained sediments over an extensive area of the lower White Nile valley (Williams *et al*., 2000). The reaches near Esh Shawel record a sequence of extensive Late Pleistocene linear sand dunes that were partly reworked by fluvial processes and partly buried beneath the fluvio-lacustrine sediments that were laid down across much of the valley floor when these reaches were inundated by the extensive terminal Pleistocene White Nile lake (Figure 13.7a) (Williams *et al*., 2000). Further north on the western margins of the Gezira Plain near El Geteina, well-preserved and highly sinuous palaeochannels of terminal Pleistocene and Early Holocene age are evident (Figure 13.7b).

After ca. 12 000 ^{14}C years BP, the climate became much wetter in the Ethiopian Highlands as the summer monsoon

increased in intensity and water fluxes from the Blue Nile headwaters increased. This resulted in an increase in vegetation cover and widespread slope stability and soil formation and a net decrease in sediment flux from the Blue Nile Basin. The geomorphology of the early Holocene Blue Nile is summarized in Figure 13.6. In the lower reaches of the Blue Nile the main channel incised into the valley floor leaving a series of perched palaeochannels on the surface of the Gezira fan complex (Figure 13.5). On the main Nile in northern Sudan, over 15 km to the east of the modern channel, large palaeochannel belts have been dated by OSL to the Early Holocene with the oldest ages >7000 calendar years BP (Woodward *et al*., 2001). Some of these palaeochannels are associated with Neolithic sites in the Northern Dongola Reach (Welsby, 2001) and represent high discharges at this time. During the early Holocene humid phase, the northern front of monsoonal rainfall extended about 700 km further north than present producing lake basins in the Sahara (Ritchie *et al*., 1985), recharging groundwaters and feeding seasonal flows in local wadi systems in northern Sudan. More extensive river systems also supplied water and sediment to the Nile in the Early and Middle Holocene including the Wadi Howar Basin that drained a large catchment in western Sudan (Figure 13.1) until it dried out around 4500 ^{14}C years BP (Pachur and Kropelin, 1987).

This general model is supported by work in the Nile Delta by Foucault and Stanley (1989). They showed that the contrasts in lithology between the White Nile and Blue Nile headwaters produces suspended sediment loads in these rivers with distinctive heavy mineral assemblages. Analysis of sediments from delta cores spanning the last 40 000 years or so have shown that the heavy mineral suite reflects changes in the relative contributions of sediment from the Blue Nile and the White Nile and provides a more or less continuous record of sediment source variations in the major Nile tributaries.

13.4.3 5000 ^{14}C Years BP to Present

Over the last five millennia or so the climate in much of the Nile Basin has become increasingly dry with the development of conditions that are comparable with the present. Detailed records of environmental change from this period in the arid zone of northern Sudan have been recovered from former lake basins in the Sahara Desert (e.g. Ritchie *et al*., 1985). This period saw the establishment of the exotic Nile that flows through the arid lands of northern Sudan and Egypt without any significant tributary inputs downstream of the Atbara.

Recent work in the Dongola Reach of northern Sudan (Figure 13.8) has revealed dramatic changes in valley floor geomorphology and human use of the river environment during the Neolithic, Kerma (ca. 2500 to 1500 calendar years BC), and later periods (Woodward *et al*., 2001; Welsby *et al*., 2002). Extensive systematic survey of the valley floor has recorded over 450 new archaeological sites and many of these are closely associated with former channels of the Nile up to 18 km to the east of the modern Nile. Geomorphological research and OSL dating of the Holocene alluvial record has shown that these palaeochannel belts were active during the Neolithic and Kerma periods (Macklin and Woodward, 1998, 2001). Decreasing Nile flows after ca. 2500 calendar years BC resulted in major changes in the settlement pattern on the valley floor with all archaeological sites located close to the palaeochannel systems. However, by the middle of the first millennium BC, all permanent settlements had become concentrated in the west along the banks of the course of the modern river (Welsby, 2001; Welsby *et al*., 2002).

Krom *et al.* (2002) have shown that the sedimentary record in the delta can provide a more or less continuous record of changing catchment behaviour for much of the Holocene. Figure 13.9 is a strontium isotope record from a sediment core taken from Manzala Lagoon in the Nile Delta. Sediments from the Blue Nile Basin derived from young volcanics and other rocks contain low strontium isotope ratios. The ancient shield terrains of the White Nile headwaters yield sediments with higher strontium isotope ratios and this contrast provides a valuable basis for establishing a long-term record of the changing provenance of fluvial sediment deposited in the delta. The form of the strontium isotope curve reflects changing environments in the Nile headwaters and, in general terms, provides a proxy for Nile flows and sediment flux for the last 7000 years or so (Krom *et al*., 2002). The lower part of the record shows high flows in the Early Holocene Nile that correlate with some of the large palaeochannel forms in the White Nile Valley (Figure 13.7). This part of the record reflects a significant flux of sediment from the White Nile Basin. The steep fall in the curve down to ca. 4200 calendar years BP reflects a progressive increase in sediment flux from the Ethiopian Highlands as Nile flows declined following a decrease in monsoon intensity and a reduction in vegetation cover in the Blue Nile headwaters. Krom *et al*. (2002) and Stanley *et al*. (2003) have argued that these strontium isotope minima provide the first geological data showing a catastrophic decline in Nile flows that may have led to the demise of the Old Kingdom (Bell, 1971). The central part of the record (after 4200 calendar years BP) shows fluctuating Nile flows up to around 1500 calendar years BP when the record may be partly influenced by enhanced sediment yields from Ethiopia following deforestation. In general terms the record shows a long

Figure 13.8 Geomorphology of the Nile channel complex in the Dongola Reach in northern Sudan at low flow. (a) A large sand bar and thick channel margin flood deposits. (b) A flood channel to the east of the main Nile. View looking downstream in each case. Photographs taken by Jamie Woodward in February 1997

term drying trend during the course of the Holocene and one with the tantalizing prospect of linking it to the long historical flood records.

13.5 RECORDS OF NILE RIVER BEHAVIOUR IN THE EASTERN MEDITERRANEAN SEA

The marine sedimentary record in the Eastern Mediterranean provides a valuable record of the long-term behaviour of the River Nile (Rossignol-Strick *et al*., 1982) because long-term changes in the flux of water and sediment from the Blue and White Nile Basins have exerted an important influence on oceanographic and sedimentation dynamics. The sedimentary record in the Eastern Mediterranean is punctuated by the occurrence of dark, organic rich layers known as sapropels (Stanley, 1978; Rohling, 1994; Thomson *et al*., 1999). These distinctive sediments range in thickness from a few millimetres to tens of centimetres and represent episodes of stratification and deep-water stagnation (when organic material was not broken down) and a net increase in biological productivity – which increases the flux of organic matter to the sea floor. Periods of enhanced discharge from the Nile have been shown to correspond with periods of sapropel deposition as the floodwaters created a freshwater layer across the surface of the Eastern Mediterranean. Indeed, Rossignol-Strick *et al.* (1982: 3) have argued that if the discharge of the Late-glacial Nile was 2.5 times greater than today (similar to the present Zambezi), it could have produced a 25 m deep freshwater layer across the surface of the Levantine and Ionian basins in only 15 years. Recent work by Williams *et al.* (2003) has shown that times of very high flow in the White Nile over the past 240 ka that have been dated by OSL show a good correlation with the dated sapropel record in the Mediterranean.

13.6 THE MODERN NILE: HYDROLOGY AND GEOMORPHOLOGY

The climate and hydrology of the modern Nile Basin ranges from Equatorial in the White Nile headwaters to hyperarid in the desert region of northern Sudan and Egypt. Thus, for much of its course, the Nile is an exotic river. Despite its large area, on average, runoff from the Nile Basin accounts for only around 2 % of the total runoff from the African continent (UNESCO, 1978). In fact it ranks fifth behind the Congo, Niger, Ogooue and Zambezi Rivers for mean annual runoff (Table 13.3). Data presented in UNESCO (1978) show that the Congo River is

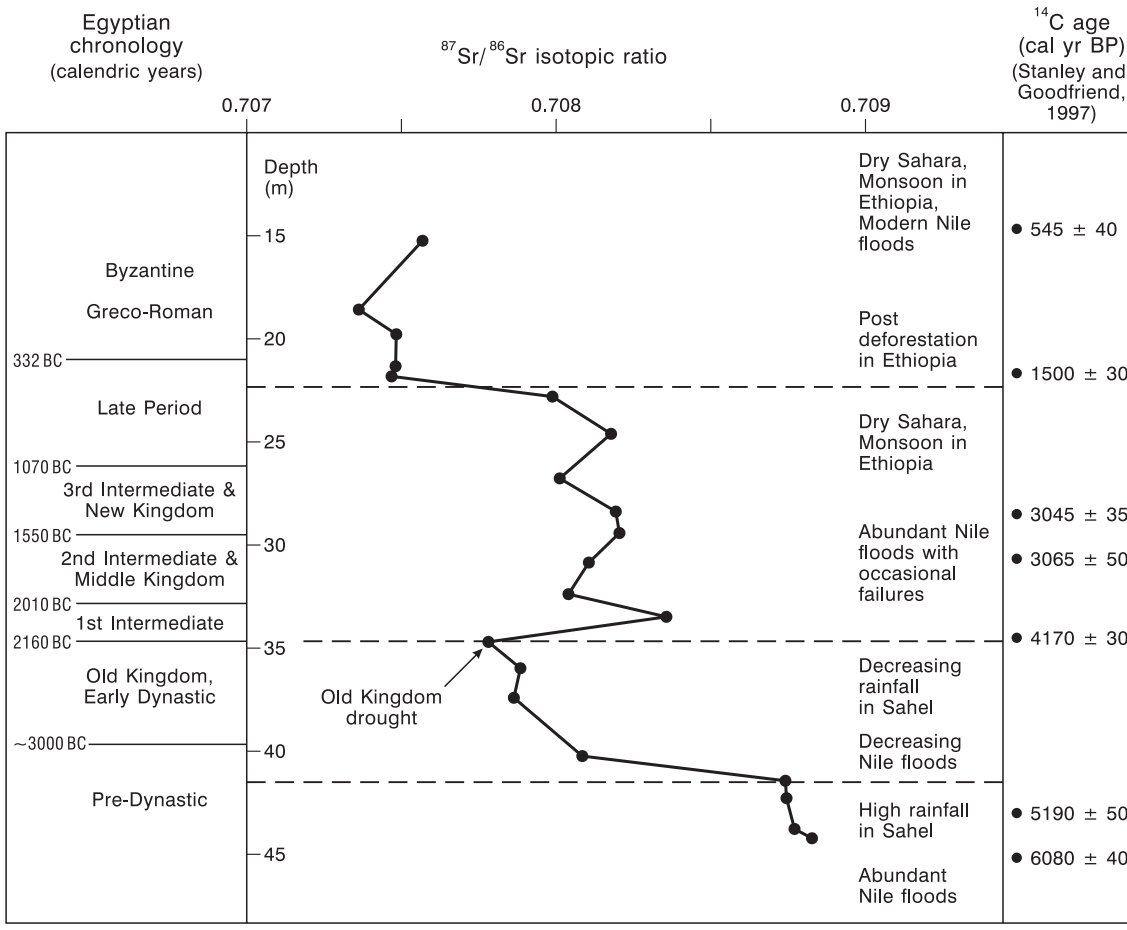

Figure 13.9 The strontium isotope record from the Nile Delta (Manzala Lagoon) showing the fluctuations in Nile flows for much of the Holocene. Note that the dates in the far right column are given in calibrated radiocarbon years before present. See text for discussion. Reproduced from Geoarchaeology: An International Journal, 18 (3), Stanley, D.-J., Krom, M.D., Cliff, R.A. and Woodward, J.C., Nile flow failure at the end of the Old Kingdom Egypt: strontium isotopic and petrologic evidence, 395–402, Copyright (2003), John Wiley & Sons., Inc

the most significant of the large African rivers in terms of water flows with the highest mean annual runoff of 1414 km^3 which compares with 73 km^3 for the Nile (Table 13.3).

13.6.1 The White Nile Basin

The southern headwaters of the White Nile lie in the Equatorial lakes region of east-central Africa (Figures 13.1 and 13.2). This part of the basin is formed in ancient uplifted and rifted rocks of Precambrian age in Kenya, Uganda and the Democratic Republic of Congo (DRC).

Table 13.3 Runoff data for the largest rivers on the African continent (after UNESCO, 1978 and Walling, 1996)

River	Mean annual runoff		Contribution to total external runoff from Africa (%)
	(mm)	(km^3)	
Congo	370	1414	38.0
Niger	128	268	7.2
Ogooue	732	149	4.0
Zambezi	80	106	2.8
Nile	25	73	2.0
Sanaga	503	68	1.8
Volta	103	41	1.1

The uplifted terrains of the western rift form the watershed with the eastern headwaters of the Congo River (Figure 13.3). The highest point in the Nile basin is Mount Stanley (5109 m) in the Ruwenzori Mountain range between Lake Edward and Lake Albert on the border between the DRC and Uganda. The geological evolution of this area is complex and it was subjected to tectonic movements related to the African Rift system during Tertiary and Quaternary times (Said, 1981). The drainage of the Lakes Plateau region into the Nile Basin followed regional uplift and the formation of Lake Victoria. Prior to this the region's drainage appears have formed part of the eastern headwaters of the Congo River (Said, 1981) (Figure 13.3). Figure 13.2 shows the long profile of the White Nile with its steep gradient reaches in the Lake Plateau region with large waterfalls and rapids between Ripon Falls (1135 m) and Juba (455 m) – a distance of some 874 km. Downstream of Juba the White Nile is a very low gradient system with an average slope of 1 : 13 900 in the Sudd Region and 1 : 101 000 between Malakal and Khartoum in its middle and lower reaches where it flows across the aggraded floor of the ~400 ka mega-lake (Williams *et al*., 2003) (Figures 13.2 and 13.5). The Sudd overlies a vast alluvial fan, hence its relatively steep gradient. The extensive low-lying alluvial plain of the Sudd region extends for over 220 km on either side of the modern river channel complex (Said, 1981).

Rainfall in the White Nile Basin varies markedly between the Lake Victoria catchment (with annual rainfall of <2000 mm) and the arid and semi-arid environments in central Sudan with values of about 175 mm year^{-1} at Khartoum and 800 mm year^{-1} near Malakal. The western mountains of the Lake Plateau are extremely wet with around 360 rain days and over 5000 mm of precipitation each year (Said, 1993). The hydrology of the White Nile headwaters is strongly influenced by the presence of large lakes and swamps and the main lakes and swamps in the Nile basin are listed in Table 13.4. These water bodies cover an area approaching 130 000 km^2. Lake Victoria, which is the second largest freshwater lake in the world, is by far the largest (ca. 67 000 km^2) and exerts an important control on White Nile discharge (Tate *et al*., 2001). Annual flows into Lake Victoria of about 20 km^3 year^{-1} are typical. This inflow is made up from 7.5 km^3 year^{-1} from the Kagera River (which forms the border between Rwanda and Tanzania), 8.4 km^3 year^{-1} from north-east Kenya, 3.2 km^3 from the Serengeti of Tanzania and 1–2 km^3 year^{-1} from the swamplands of north-west Uganda (Howell *et al*., 1988; FAO, 1997). The Ripon Falls in Uganda form the only outlet from Lake Victoria. The volume of the outflows (ca. 40 km^3 year^{-1}, Table 13.4) – which feed the Victoria Nile – is very sensitive to precipitation inputs to the Lake Victoria Basin as evaporation rates do not vary greatly from year to year. The Victoria Nile flows into Lake Albert via Lake Kioga (Figure 13.1).

A dominant characteristic of the White Nile flow regime is that the seasonal variability of flows is highly damped by storage in lakes and swamps. The Sudd Region downstream of Juba contains a huge area of swamplands (Figure 13.10) and evaporation from these water bodies is a very significant component of the water balance. Typical evaporation losses from this part of the White Nile Basin are

Table 13.4 Long-term water balance data for lakes and swamps in the Nile Basin for various periods of the twentieth century (after Sene *et al*., 2001). The monitoring periods are approximations in some cases

Water body	Area (km^2)	Monitoring period	Active storage (km^3)	Nile inflow (km^3 year^{-1})	Local runoff (km^3 year^{-1})	Outflow (km^3 year^{-1})	Direct rainfall (km^3 year^{-1})	Evaporation (km^3 year^{-1})
Kagera swamps	3 000	1940–1973	3.8	0.0	8.1	6.3	3.0	4.8
Lake Victoria	67 000	1925–1990	208.4	0.0	25.9	40.0	121.3	107.2
Lake Kioga	6 270	1970–1973	23.8	40.0	3.0	42.1	9.1	10.0
Lakes George and Edward	2 500		0.8	0.0	3.6	2.6	3.5	4.5
Lake Albert	5 400	1970–1973	28.1	42.1	6.2	45.1	5.4	8.6
Albert-Sudd reach swamps	380							
Sudd swamps	22 400	1961–1980	60.5	50.3	0.0	21.4	19.3	48.2
Machar marshes	3 200	1950–1955		0.0	1.4	0.1	6.0	7.3
Bahr el Ghazal swamps	<16 600	1942–1986		0.0	11.3	0.3	9.5	20.5
Lake Tana	3 000	1928–1937		0.0	3.9	4.0	3.8	3.7
Totals	<129 750				63.4		180.9	214.8

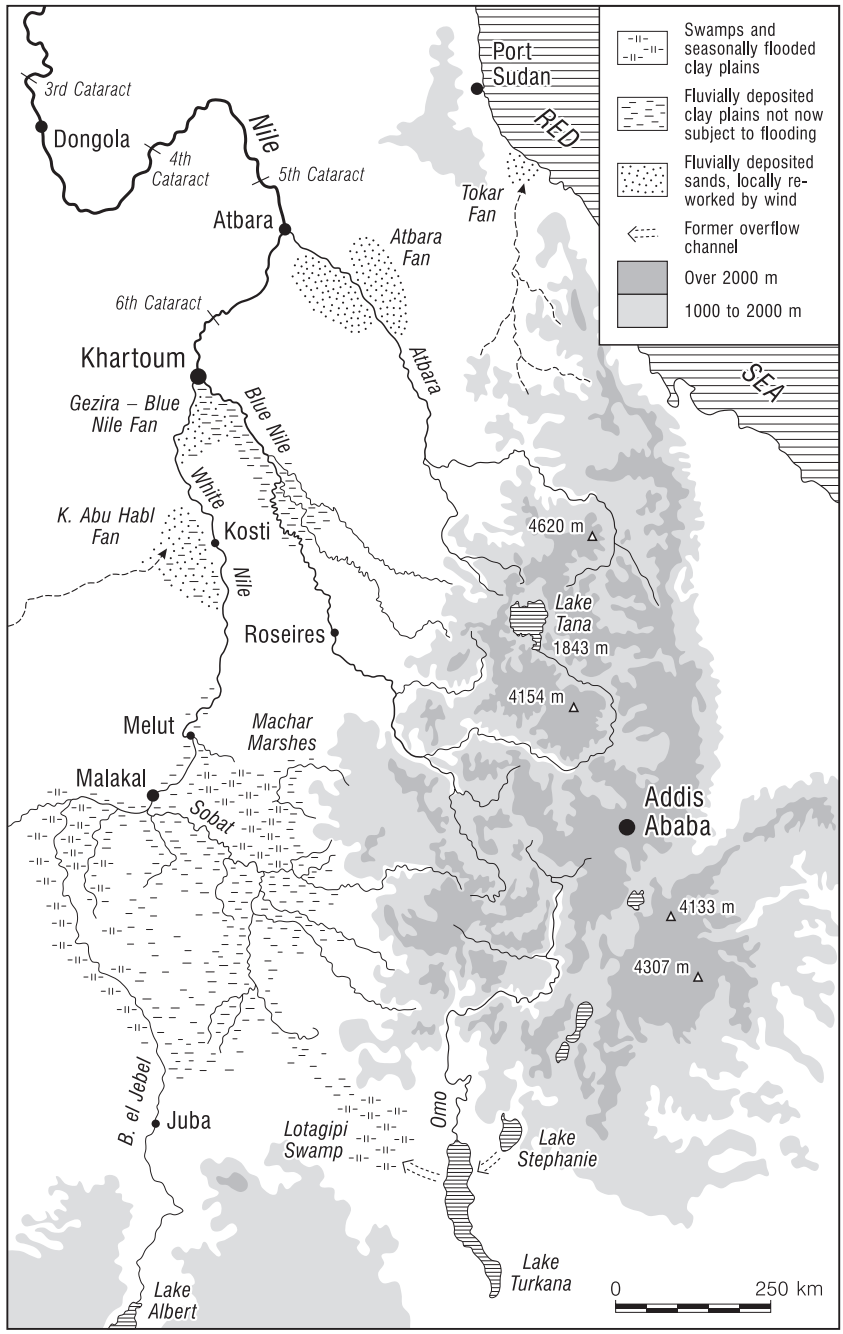

Figure 13.10 Geomorphological map of the Blue Nile and Atbara River basins and the middle and lower reaches of the White Nile. Note the large-scale areas of fan sedimentation in the lower reaches of each of these basins (after Williams and Adamson, 1980). The Sudd region is also shown upstream of Malakal on the White Nile (see Figure 13.2)

shown in Table 13.5. According to Howell *et al.* (1988), between 1905 and 1980 the mean annual water loss to evaporation and evapotranspiration in the Sudd region was 16.9 km^3 and this represents about 51.2% of the fluvial input to the area as recorded on the White Nile at Mongalla. The Sudd region has an extremely low gradient and contains a series of natural channels that flow through permanently waterlogged swamps flanked by seasonally flooded grasslands. The Sudd stretches over 900 km from Juba to Malakal (Figures 13.2 and 13.10) and hydrological assessments have shown that the evaporation losses are greatest in those years when inflows are highest and the inundated areas expand to cover a much greater area (Howell *et al*., 1988). High levels of rainfall in the lakes region of the White Nile headwaters in the 1960s and 1970s led to a significant increase in the perennial swamp area in the Sudd from 2700 km^2 in 1952 to 16 200 km^2 in 1980. Downstream of the Sudd Region, between Malakal and Khartoum, the Nile falls only 8 m over a distance of about 809 km with a mean average gradient of less than 1 cm km^{-1}. The climate becomes drier to the north and these reaches do not contain swamps and permanent water bodies. Downstream of the Sobat River junction there are no major tributary inputs south of Khartoum (Figure 13.1). The White Nile below Malakal is gently incised forming a broad and shallow alluvial channel that commonly bifurcates around the mid-channel bars and islands that are common in these reaches (Williams *et al*., 1982). The channel planform of the White Nile upstream of the ~400 ka mega-lake bed differs from that of the river where it flows along the former lake floor but has yet to be studied in detail.

13.6.2 The Blue Nile and Atbara Basins

The headwaters of the Blue Nile and the Atbara River lie in the highlands of Ethiopia and these upland fluvial systems contain steep river channels with coarse boulder beds that flow within deep gorges. Figure 13.10 shows those parts of the Ethiopian Highlands lying above 2000 m and the deeply dissected drainage network that feeds the main tributaries of the Blue Nile and Atbara rivers. Incision of these uplands was initiated by regional uplift during the Late Oligocene to Miocene, the Late Pliocene and the Late Pleistocene (McDougall *et al*., 1975). This created a superimposed drainage network from a cover of Oligocene to Miocene age basalts into Mesozoic limestone and sandstone and granite and metamorphic rocks of Precambrian age (Williams and Williams, 1980). Note that several tributaries of the Sobat River drain the southern part of this region before traversing low gradient swamplands in central Sudan and eventually joining the White Nile upstream of Malakal (Figure 13.10).

Downstream of Khartoum the flood hydrology of the main Nile is dominated by runoff from the Blue Nile and the Atbara (Table 13.6) and the climate and hydrology of their catchments are dominated by the influence of the summer monsoon. Rainfall and runoff in the Upper Blue Nile catchment (176 000 km^2) are strongly seasonal and many tributary channels do not convey flows in the dry season from November to May (Conway, 2000). The Upper Blue Nile has a mean annual discharge of 48.5 km^3 (1912–1997) and inter-annual variability in flows is controlled by the intensity of the monsoon and by ENSO, with low flow during years of strongly negative Southern Oscillation Index, at least in the past hundred years, and conversely (Whetton *et al*., 1990). Precipitation dynamics in the Blue Nile and Atbara headwaters are influenced by three main mechanisms (Conway, 2000):

(1) the summer monsoon;
(2) tropical upper easterlies;
(3) local convergence in the Red Sea coastal region.

About 70% of the annual rainfall in the Blue Nile headwaters of Ethiopia falls between June and September declining from 2000 mm in the southwest to less than 1000 mm in the northeast (Conway, 2000). The lower

Table 13.5 Water balance of the Sudd region for various periods of the twentieth century (after Howell *et al*., 1988 and FAO, 1997)

Period	Annual discharge at Mongalla (km^3)	Annual outflow from swamps (km^3)	Annual losses (km^3)	%
1905–1960	26.8	14.2	12.6	47.0
1961–1980	50.3	21.4	28.9	57.5
1905–1980	33.0	16.1	16.9	51.2

Table 13.6 Mean annual discharges for the major basins of the Nile as reported by Williams *et al.* (1982)

River basin	Discharge (km^3)	Peak flow (%)	Low flow (%)
White Nile	27.5	10	83
Blue Nile	51.0	68	17
Atbara	12.5	22	0
Main Nile	91		
Ethiopian Highlands	63.5	90	17

Blue Nile has a catchment area of about 324 530 km^2 (Shahin, 1985) and its flow regime is also characterized by highly seasonal flows and marked inter-annual variability. On average about 85% of annual flow of the Blue Nile is concentrated into one third of the year between July and October. The 1900 to 1982 gauging station records for the Blue Nile at Khartoum show a mean monthly range in discharge from 9 to 8834 m^3 s^{-1} with a mean of 1513 m^3 s^{-1}. The flow regime of the Atbara exhibits even greater seasonality and the river is commonly dry from December to May with very low flows in November and June. Between 1912 and 1982 the mean discharge in the Atbara at the Kilo 3 station (69 000 km^2) for the month of August ranged from 533 to 4928 m^3 s^{-1} with an average figure of 2002 m^3 s^{-1}.

The Ethiopian Highlands are strongly dissected and the Blue Nile flows in a narrow, steep-sided valley for much of its course. Between its source at Lake Tana (1829 m) and the Sudan border – a distance of about 850 m (Figure 13.10) – the Blue Nile falls 1350 m at a mean gradient of 0.0016. From the border to Khartoum (374 m), a distance of some 900 km, the gradient is much more subdued (0.00013) (Williams *et al*., 1982). This change in channel gradient indicates that much of the coarser bed load materials derived from the granites, basalts and sandstones of the Ethiopian Highlands now probably lie below the fine-grained sediments of the Gezira Fan Formation (Figure 13.10) – a body of sediment forming the large low-angle inland alluvial fan of radius ~300 km that lies upstream of Khartoum between the lower reaches of the Blue and White Niles (Williams *et al*., 1982). Extensive areas of fan deposits in the lower gradient reaches of the Atbara and Blue Nile Basins are shown in Figure 13.10 and these represent significant long-term sediment sinks. In its lower reaches the Blue Nile is a narrow and deep, single channel system incised into the Holocene and Pleistocene alluvial sediments of its former floodplain.

13.6.3 The Confluence Zone and the Desert Nile from Khartoum to the Mediterranean

A key function of the major water bodies in the Upper White Nile Basin is the maintenance of the perennial base flow of the desert Nile from November to June when the Blue Nile and Atbara are not in flood (Figure 13.11a). The ratio of peak monthly flow to minimum monthly flow is typically 40 : 1 in the Blue Nile and 5 : 2 in the White Nile. The Blue Nile flood reaches its peak in late August to early September with a rise in stage of about 10 m above its low season flow at Khartoum. The White Nile flood peak arrives later and is much lower (ca. +2 m) – but lasts from late September until January (Williams *et al*., 2000) (Figure 13.11a). Before the construction of large dams this contrast in flood stage at the confluence resulted in the

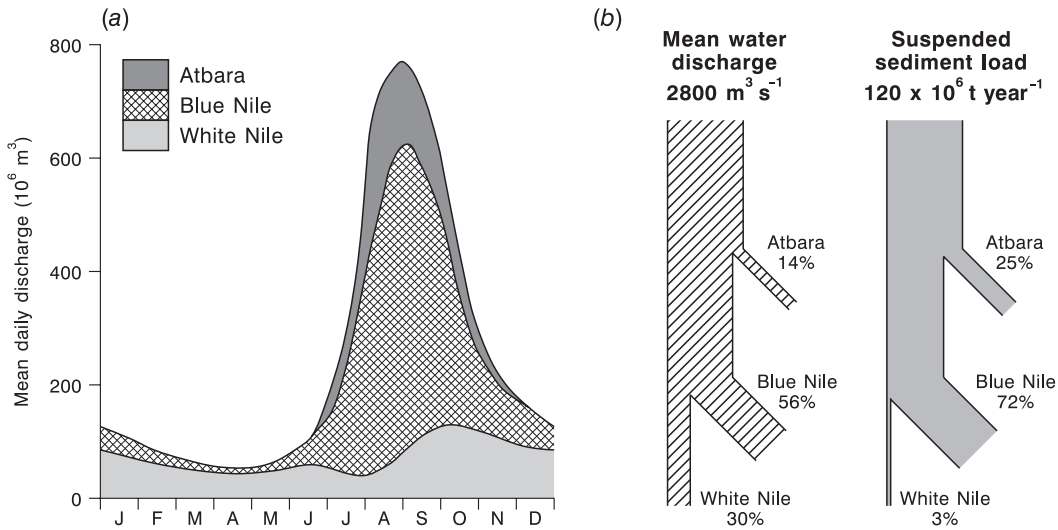

Figure 13.11 (a) Typical annual flow regime of the pre-impoundment Nile at Aswan showing the contributions from the three major tributary basins. Reproduced from The Nile: a General Account of the River and the Utilization of Its Waters, H.E. Hurst, Discharge of the Nile at Aswan, 1952, Constable and Company, London. (b) The discharge and suspended sediment budget of the Nile. Reprinted by permission from Macmillan Publishers Ltd: Nature, 339, 6219, Alain Foucault, Daniel Jean Stanley, Late Quaternary palaeoclimatic oscillations in East Africa recorded by heavy minerals in the Nile delta, pages, 44–46, Copyright (1989)

formation of a seasonal lake that extended for more than 300 km upstream of Khartoum along the White Nile floodplain (Williams *et al*., 2000). The width of this lake ranged from 1 to 7 km.

The six cataracts of the main desert Nile lie in the reaches between Khartoum (378 m) and Aswan (91 m) over a distance of 1847 km where the channel falls over 280 m (Figure 13.2). The great bends of the Nile are perhaps the most distinctive feature of the channel between the sixth and second cataracts (Figure 13.1). Adamson and Williams (1980) have suggested that the great bend that incorporates the sixth, fifth and fourth cataracts is a product of updoming and volcanic activity in the Bayuda area where evidence for volcanic flows and volcanic cones is extensive. These authors also point out that the prominent dykes and lineaments that are oriented ENE and SSE correspond with the course of the Nile as it bends around the Bayuda dome (Figure 13.3). The bedrock reaches account for about 30% (565 km) of the channel length between Khartoum and Aswan, where the steeper gradient cataract reaches are formed in resistant crystalline rocks (Said, 1981). Between the cataracts lie low gradient basins where softer Nubian sandstones have been eroded to provide accommodation space for expanses of Pleistocene and Holocene alluvial sediments (Figure 13.8). One example is the Dongola Reach of northern Sudan where the eastern side of the valley floor is flanked by a low relief Holocene floodplain complex with well preserved palaeochannel belts up to 18 km from the modern channel of the Nile (Macklin and Woodward, 2001; Woodward *et al*., 2001). Extensive aeolian dune systems are present in this reach and there is evidence in some reaches of large scale wind erosion of the Holocene alluvial record (Welsby *et al*., 2002).

Many of the large African rivers have flow records that extend back into the nineteenth century because gauging stations were established during the colonial era. Uniquely, the Nile has a long-term historical flood series that extends back to 622 AD at the Roda Island gauge at Cairo and these data have been analysed by many scholars (Brooks, 1927; Fraedrich *et al*., 1997). Modern discharge measurements on the Nile began in 1869 at Khartoum and in 1870 at Aswan. The flow records for the twentieth century show significant variability – the maximum water yield of 120 km^3 was recorded in 1916 while 1984 registered a minimum value of 42 km^3. Between 1870 and 1984 the Nile at Aswan had a mean monthly discharge of 2700–2800 $m^3 s^{-1}$ (Figure 13.11b). El-Manadely *et al*. (2002) report that the average yearly discharge of the Nile at Aswan is 84 km^3. It has been estimated that about half of the annual discharge released from the Aswan High Dam reaches the delta and this represents about 34–35 km^3 in an average year (Sharaf El Din, 1977; Stanley, 1996). Approximately one third of the flow reaching the delta is lost via evapotranspiration and infiltration to groundwater while another third drains slowly through irrigation channels and canals. Thus, as Stanley (1996) has pointed out, only about one third of the discharge that passes Cairo actually reaches the Mediterranean Sea. The last 'normal' flood discharge in the Nile was in 1964 and the flux of water to the Mediterranean between 1961 and 1973 is shown in Figure 13.12a. Note the marked decline in the annual peak of the controlled releases from Aswan and the shift in the timing of peak from summer (natural) to winter (controlled).

Before the completion of the Aswan High Dam in 1964 the annual Nile flood exerted an important influence on the hydrographic conditions and the pattern of circulation in the Eastern Mediterranean Sea up to about 80 km from the coast and to a maximum depth of ca. 150 m (Sharaf El Din, 1977). During the flood season (August to October) the salinity of the Mediterranean Sea fell from about 39 to <30 ppm at the near shore surface (Sharaf El Din, 1977). The huge particulate and solute loads associated with the floodwaters formed a vital role in the biology of the marine environment.

13.7 THE SUSPENDED SEDIMENT BUDGET

This section examines the contemporary suspended sediment budget of the basin upstream of the delta complex. Suspended sediment concentrations and loads have been measured at several stations on the Egyptian Nile – especially in the decades leading up to the planning and construction of the Aswan High Dam – but continuous long-term records are not presently available in the scientific literature. A good deal of the early work is documented in Volume IX of *The Nile Basin* (Hurst *et al*., 1959). The suspended sediment load of the Nile is rather modest in comparison with its basin area. Milliman and Syvitski (1992) quote a value of 120 million tonnes $year^{-1}$ for the average annual pre-Aswan High Dam load and a mean annual sediment yield of 40 t $km^{-2} year^{-1}$ (Table 13.7). The sediment loads of many of the large rivers of Africa that drain the ancient shield terrains of the tropical interior are also low by world standards (Table 13.7).

It is important to appreciate that sediment production and sediment delivery vary markedly in the major tributary basins and marked spatial and temporal (annual and seasonal) variability in suspended sediment flux is a key feature of the fluvial geomorphology of the basin. Suspended sediment concentrations and loads are subject to considerable annual variation. According to Abu El-Ata (1978) the annual sediment load of the Nile at Aswan has

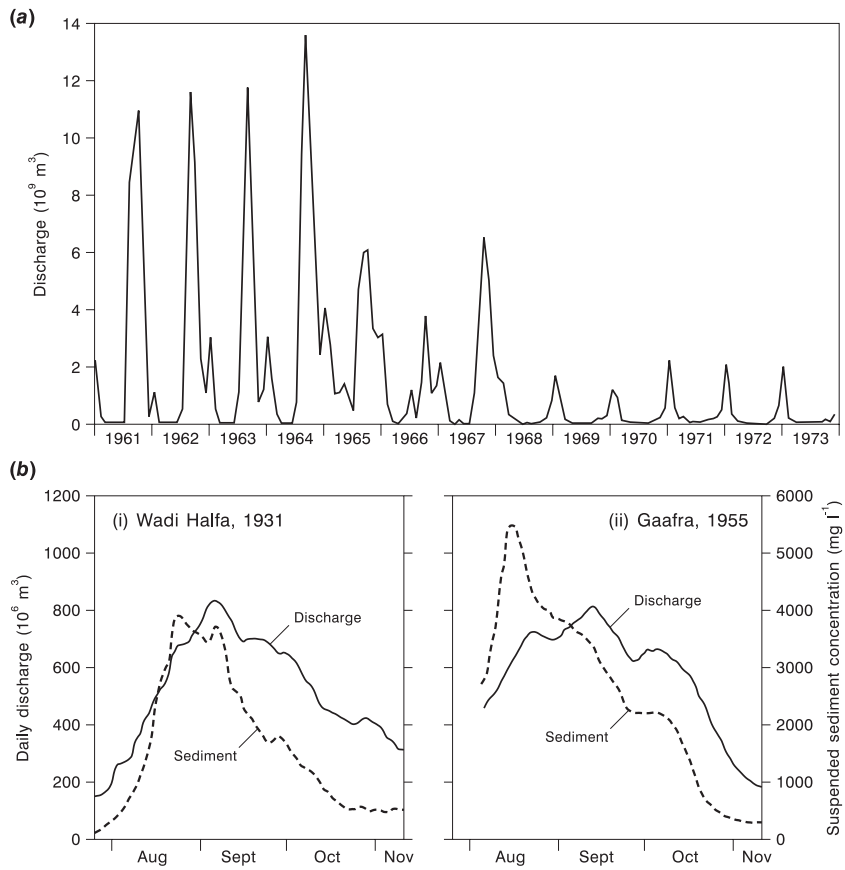

Figure 13.12 (a) The pre- and post-impoundment flow regime at Aswan between 1961 and 1973. Reprinted from Limnology and Oceanography, 22, 2, Sharaf El Din. Copyright (1977) by the American Society of Limnology and Oceanography, Inc. (b) Discharge and suspended sediment concentration series for summer floods on the main Nile at Wadi Halfa (1931) and Gaafra (1955). Reprinted from Hydrology of the Nile Basin, Developments in Water Science 21, Mamdouh Shahin, page 460, Copyright (1985), with permission from Elsevier

Table 13.7 The suspended sediment loads and yields of some large African rivers (from Milliman and Syvitski, 1992). The pre-impoundment loads are given in parentheses and these values have been used for the yield estimates

River	Basin area ($\times 10^6$ km^2)	Sediment load ($\times 10^6$ t year^{-1})	Sediment yield (t km^{-2} year^{-1})
Nile	3.00	0 (120)	40
Congo	3.80	43	11
Orange	0.89	17 (89)	100
Niger	1.20	40	33
Zambezi	1.40	20 (48)	35
Limpopo	0.41	33	80

varied between 50 and 228 million tonnes. Due to the erodible upland terrains, high sediment supply and high runoff, much of the suspended sediment load measured at Aswan derives from the highlands of Ethiopia. In fact, together the Blue Nile and Atbara contribute on average about 97% of the Nile's annual suspended sediment load (with about 72% from the Blue Nile and 25% from the Atbara) and the White Nile the remaining 3.0% (Figure 13.11b) (Foucault and Stanley, 1989). Suspended sediment flux is dominated by the summer flood in the Blue Nile and Atbara catchments. For example, with a peak flow to low flow ratio of 40 : 1, and typical mean August and June sediment concentrations of 4000 and 100 mg l^{-1} respectively, the Blue Nile can transport up to 1600 times

more sediment during the summer floods than at the end of the dry season (Williams *et al*., 1982: 119).

The White Nile drains the resistant rocks of the Equatorial plateau and these terrains have much lower erodibility and a more effective cover of protective vegetation in contrast to the deeply dissected Blue Nile headwaters. Consequently, suspended sediment concentrations are much lower in the floodwaters of the White Nile and the lower gradient White Nile is a much less efficient suspended sediment delivery system (Figure 13.11b). A significant proportion of its suspended sediment load is also trapped in the swamps and marshes of the Sudd region in the middle White Nile reaches. The Sudd swamps also act as an efficient biochemical filter, since the solute concentration of the river on leaving the Sudd is equal to that on entering it, despite the loss of half the original flow volume through evapotranspiration and seepage (Williams and Adamson, 1973). In the main Nile at Aswan the sediment wave tends to peak in August before the main flood peak and several weeks may separate these two events. The suspended sediment concentrations for the summer flood of 1955 at Gaafra (near Aswan) peak at over 5500 mg l^{-1} in mid-August and then decline steadily to <500 mg l^{-1} by the end of October (Figure 13.12b). Many of the suspended sediment sampling programmes have tended to focus on the flood season and the major findings of this work on the main Nile in Egypt have been reported by Shahin (1985) and may be summarized as follows:

- The mean annual pre-impoundment flux of suspended sediment at Aswan was about 125 million tonnes.
- Approximately 98% of the annual suspended sediment load is transported during the flood season from August to November and suspended sediment concentrations may range from about 100 to >5800 mg l^{-1} during this period (Figure 13.12b).
- The relationship between suspended sediment concentration and water discharge shows a clear tendency for clockwise hysteresis with sediment concentration rising rapidly and peaking before the main flood peak (Figure 13.12b).
- Typical particle size distributions for samples of the suspended load at Aswan contained 30% clay, 45% silt and 25% sand – and the proportion of sand tended to increase as the flood season progressed. Samples of suspended sediment collected from the delta region of Lake Nasser displayed a mean particle size distribution with 30% fine sand, 40% silt and 30% clay (El-Manadely *et al*., 2002).

Data on bed load flux in the Nile Basin are extremely scarce but Shahin (1985) reports that studies in the pre-Aswan High Dam period showed that bed load sediment transport accounted for only about 1–2% of the total load. Thus it became customary to consider the suspended sediment load as the total load. One would expect a significant flux of coarse bed load material in the steep and flashy headwater streams of the Blue Nile and Atbara basins. Indeed, as mentioned above, Williams *et al.* (1982: 117) speculate that much of the coarser bed load materials eroded from the granites, sandstones and basalts of Ethiopia now probably form the base of the Gezira Formation to the south of Khartoum (Figure 13.10), a surmise consistent with drilling records.

13.7.1 Reservoir Sedimentation

While there are still key gaps in our understanding of basin-wide sediment dynamics in the Nile, some of the most useful information on recent suspended sediment fluxes derives from repeat bathymetric surveys of the large artificial reservoirs. Furthermore, because they form very effective sediment traps, these reservoirs form an important component of the suspended sediment budget of the Nile Basin. As the Ethiopian Highlands are the main source of suspended sediment in the basin, the river systems draining this region have witnessed some of the most severe sediment management problems since the construction of large dams.

The Roseires Dam (1966) on the Blue Nile and the Khashm el Girba Dam (1964) on the Atbara River (Figure 13.1) both encountered major problems with sedimentation within a decade of their construction (Elsheikh *et al*., 1991). The Roseires Dam was built close to the Ethiopian border to store Blue Nile water for irrigation use in central Sudan. According to these authors, the storage capacity of the Roseires reservoir (3.02×10^9 m^3) had fallen by 18% after 10 years and 21% after 15 years – while the capacity of the Khasm el Girba reservoir fell by 25.4% after 7 years of operation and by 42.3% after 12 years. Bathymetric survey showed that 540 million m^3 of sediment had been deposited in the Roseires reservoir between 1966 and the 1975/1976 hydrological year – giving a mean annual value for sediment deposition of about 54 million m^3 for this period. The total volume of deposited sediment had increased to 640 million m^3 by 1980/81 (Elsheikh *et al*., 1991).

In the Ethiopian headwaters of the Blue Nile and Atbara Rivers, mean annual rates of soil loss today amount to about 40 t ha^{-1} (2 mm $year^{-1}$) on mountain slopes, but attain rates of over 300 t ha^{-1} (15 mm $year^{-1}$) during cultivation years, or some 5–10 times more than in non-mountainous areas (Hurni, 1999). In many areas the increasing demand for land has meant a reduction in fallow to virtually zero

and an expansion of the area under cultivation. In one region in Gojjam Province the area cultivated rose from 40% in 1957 to 77% in 1995, while natural forest land decreased from 27% to 0.3% (Hurni, 1999). These rates of accelerated soil erosion can be compared with long-term denudation rates for the catchment. The mean rate of geological erosion over the past 23.5 Ma was 0.01 mm year^{-1} in the Ethiopian headwaters of the Blue Nile (Williams and Williams, 1980). The rate of erosion in the Blue Nile headwaters during the 70 years before completion of the Aswan High Dam was 0.12–0.24 mm year^{-1}. In contrast, in the 1970s annual soil loss from parts of the Ethiopian Plateau was roughly 0.4–1.0 mm year^{-1}. This represents a two orders of magnitude increase in the rate of soil loss – a rate that is much faster than corresponding rates of soil formation.

Removal of forest in the seasonally wet tropical uplands of Ethiopia has changed the local hydrological balance, resulting in reduced infiltration, increased runoff and increased soil loss. The downstream effects are equally significant and in this instance are not confined to Ethiopia. By 1996, the capacity of the Roseires reservoir had been reduced by almost 60% by the influx of sediment from the Ethiopian uplands and that at Khashm el Girba on the Atbara, by 40% (Swain, 1997). It thus appears that deforestation in the headwaters of the Blue Nile and Atbara Rivers during the past 40 years has triggered a wave of accelerated soil loss from cultivated land and has led to siltation of reservoirs many hundreds of kilometres downstream.

Lake Nasser and Lake Nubia (the latter is the Sudanese sector of the reservoir behind the Aswan High Dam) (Figure 13.1) have a maximum surface area of 600 km^2 and this equates to a maximum storage capacity of 162 km^3. El-Manadely *et al*. (2002) have described the nature of the three storage zones in the reservoir:

(1) the dead storage zone – used for sediment accumulation up to 147 m asl – with a maximum capacity of 31 km^3;
(2) the live storage zone – 147 to 175 m asl – with a maximum capacity of 90 km^3;
(3) the flood-buffer storage zone – 175 to 182 m asl – with a capacity of 41 km^3.

Stanley (1996: 191) has described the sediment deposition in Lake Nasser as 'the New Nile delta' and by the mid-1990s this rapidly growing feature was about 200 km long, 12 km wide and about 40 m thick – extending northwards to Abu Simbel. When the annual flood reaches Lake Nubia, the flow velocity falls from >1.0 m s^{-1} to about 0.02 m s^{-1} (Shahin, 1985). Thus, the trap efficiency in the Aswan High Dam is close to 100% and under normal conditions only the finest fractions of the suspended load are transported to the downstream portion of the reservoir. The total volume of deposited sediment between 1964 and 1998 has been estimated to be 3.5 km^3 and 90% of this sediment is within the Sudanese side of the reservoir (El-Manadely *et al*., 2002). This estimate is based on a series of re-surveys of the original Nile river channel bed levels and valley floor cross-sections that were conducted before the construction of the dam. The last major sedimentation survey was carried out in 1998 when 15 cross-sections were surveyed in the reservoir's delta between 487 and 337.5 km upstream of the dam and the results are shown in Figure 13.13a. Comparison of the pre-reservoir bed levels and the 1998 survey shows that net sediment deposition ranges from ca. 2.4 m (at cross-section 23) to a maximum of 60.2 m at cross-section 6 (Figure 13.13a) (El-Manadely *et al*., 2002). It is important to appreciate that the width of the cross-sections (CS) increases from 300 m at CS 23 to 4100 m at CS 26 to 9300 m at CS 22 (Figure 13a) and this widening leads to a decrease in flow competence.

Suspended sediment concentrations in this part of Lake Nasser/Nubia based on samples collected in July 1978 and May 1998 are shown in Figure 13.13b and reflect this decrease in flow velocity moving northwards along the delta complex. The 1998 samples contain maximum mean suspended sediment concentrations of 172 mg l^{-1} (487 m upstream of the dam) and this value declines steadily to less than 50 mg l^{-1} around 150 km further down reservoir (El-Manadely *et al*., 2002). A general fining of the suspended sediment load accompanies the decline in sediment concentration. Mean clay content increases from around 30% at the entrance to Lake Nasser to >70% over the same distance. The survey work by El-Manadely *et al.* (2002), based on the calculated volume of sediment deposited between 1964 and 1998 in the Lake Nasser delta, gives an estimate of 310 years for the lifetime of the dead storage zone allocated for sediment accumulation (31 km^3) in Lake Nasser. These researchers also point out that significant volumes of sediment may be transported down reservoir towards the dam when large flood events follow a sustained period of low flows because this results in net erosion of some parts of the Lake Nasser delta complex. A further modification to the sediment budget of this vast reservoir will follow the completion of the new dam at Merowe on the fourth cataract as this will result in a marked reduction in suspended sediment flux to Lake Nasser/Nubia.

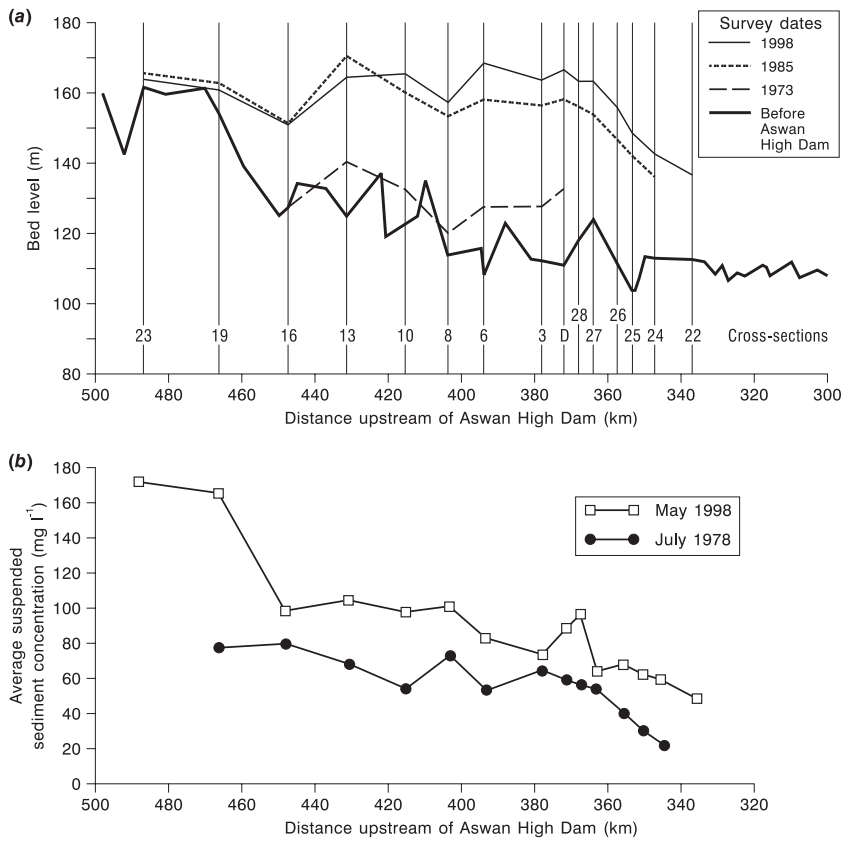

Figure 13.13 (a) Patterns of sediment deposition in Lake Nasser in 1973, 1985 and 1998. (b) Suspended sediment concentrations in Lake Nasser based on sampling programmes in July 1978 and May 1998. (a, b) Reprinted from Lakes and Reservoirs, 7, El-Manadely, M.S. Abdel-Bary, R.M., El-Sammany, M.S. Ahmed, T.A., Characteristics of the delta formation resulting from sediment deposition in Lake Nasser, Egypt, pages 81–86, Copyright (2002), with permission from Blackwell Publishing

13.7.2 Suspended Sediment Dynamics Downstream of the Aswan High Dam

The trap efficiency of Lake Nasser/Nubia is close to 100% and this has created a dramatic shift in sediment dynamics and geomorphological processes in the reaches downstream of the Aswan High Dam. The sluices of the dam are opened periodically to maintain main channel flows for navigation, irrigation and for hydroelectric power. Between 1965 and 1973 the mean flux of suspended sediment passing through the Aswan High Dam was estimated to be about 2.5 million tonnes (Shahin, 1985). Stanley and Wingerath (1996) state that about 98% of the sediment load (mainly silt and fine sand) that had previously been transported to the delta and the Mediterranean Sea is deposited in Lake Nasser/Nubia and clay-sized material (<2 μm) is now the major particulate fraction transported from the reservoir behind the Aswan High Dam to the downstream reaches of the Egyptian Nile. Stanley and Wingerath (1996) have studied the clay mineralogy of Nile sediments to assess the impact of dam construction on the composition of the suspended load. The clay fraction of suspended sediments entering Lake Nasser contains a large proportion of smectite (~70%) with some kaolinite (<25%) and illite (<10%) reflecting the composition of the volcanic terrains in the Blue Nile headwaters. However, the proportion of kaolinite increases to ~70% in the clay-rich suspended load downstream of the dam as changes to the sediment budget increase the significance of other sources of kaolinite. This clay mineral is blown into the reservoir from the desert and washed in from wave erosion of the reservoir margins. It is also introduced into the main

channel by clear water erosion of valley floor sediments and rocks downstream of the dam. Stanley and Wingerath (1996) argue that the kaolinite trace can be used to monitor the impoundment-related alterations to river flows and sediment composition. These impoundment-induced changes to the regional sediment budget from Lake Nasser to the delta are summarized in Figure 13.14.

13.8 THE NILE DELTA AND THE EASTERN MEDITERRANEAN

13.8.1 The Delta and Coastal Zone

The modern Nile Delta began forming in the early Holocene about 7500 ^{14}C years BP and is the largest depocentre in the Mediterranean region (Stanley and Warne, 1993). For much of this time the delta complex was built up by a series of large distributaries that conveyed water and sediment across the delta and to the coast. Nine major channel systems have been identified in the Holocene deposits of the northern delta and between two and five of these were active at any one time (Sestini, 1992; Stanley and Warne, 1993; Stanley, 1996). Today, downstream of Cairo, the Nile divides into two main distributaries – the Rosetta and Damietta channels and these flow to the north-west and north-east, respectively, where they have formed marked promontories at the coast (Figure 13.15a). These two distributaries have been the main conduits for water and sediment flux to the coast since the end of the nineteenth century. The delta covers an area of around 22 000 km^2 and the distance from Cairo to the coast is about 160 km. The rate of alluvial sedimentation on the delta and the floodplain of the lower Nile before 1964 has been estimated to be 60 to 150 mm century^{-1} with a mean rate of 0.8 mm year^{-1} (Shahin, 1985).

Since the closure of the Aswan High Dam in 1964, the main sources of suspended sediment downstream of Aswan have been fluvial erosion of the river channel margins and direct inputs of aeolian dust. In fact, suspended sediment concentrations greater than 850 mg l^{-1} have been recorded in Nile flows at Cairo since the closure of the dam (Stanley, 1996). However, only a very small proportion of this material actually reaches the coast because the delta's large barrages and the very high density of drainage canals and irrigation channels form a vast and very efficient network for trapping sediment. Figure 13.15b provides a graphic illustration of the human impact on the drainage network on the delta. Many of the larger artificial channels drain into the deltas wetlands and lagoons so that sediment delivery to the coast is further reduced (Stanley, 1996).

The coastal zone of the delta extends from east of Alexandria to Port Said – a distance of about 240 km. The main features of the coastline are the Rosetta and Damietta promontories and the broad Burullus headland between them that was created by sediment delivered from the former Sebennitic branch of the Nile about 6500 ^{14}C years BP (Orlova and Zenkovitch, 1974; Frihy *et al*., 2003) (Figure 13.15a). Since the completion of the Aswan High Dam, coastal erosion and sediment redistribution have been major concerns and, in very general terms, the actively prograding delta has been replaced by an eroding coastal plain (Stanley and Warne, 1993; Frihy *et al*., 2003). The eroding promontories are the principal sources of sediment for the coastal zone. Rates of shoreline change have been estimated from beach surveys and Frihy and Komar (1993) reported maximum rates of retreat along the Rosetta promontory of 106 m year^{-1} with rates of 10 m year^{-1} and 7 m year^{-1} at the Damietta and Burullus promontories, respectively. Zones of sediment accretion were identified within the embayments between the promontories with a maximum shoreline advance averaging about 13 m year^{-1}. Research by Frihy and co-workers over the last two decades has shown that the sediment budget at the coast can be viewed as a series of regional littoral sedimentation cells that extend from Alexandria to Akko on the northern margin of Haifa Bay, Israel. Each cell contains a coherent system of sediment sources, fluxes and sinks (Frihy *et al*., 2003).

13.8.2 Sediment Supply to the Eastern Mediterranean Sea

The Nile has been the major supplier of suspended sediment to the Eastern Mediterranean Sea since Late Miocene times until the construction of the Aswan High Dam. In the Late Quaternary and Holocene marine sedimentary record across the region, sands of Nile provenance have been identified in the Nile Cone and along the margins of Israel, while finer grained sediments (clays) have been traced as far north as Turkey (Stanley and Wingerath, 1996). While the Nile was the dominant supplier of fine-grained particulate material to the Levantine basin up to 1964, aeolian dust from the Sahara has long formed a very significant component of the Eastern Mediterranean marine sediment budget. Krom *et al*. (1999) have used strontium isotopes (^{87}Sr/^{86}Sr) to map the dispersal of Nile-derived suspended sediments across the Levantine basin to establish those parts of the marine environment that will be most affected by the trapping of sediment in the Aswan High Dam. Their results are shown in Figure 13.16. It is clear that Nile-derived sediment is dispersed widely across the Levantine basin with the highest values (>80 %) to the east of the Nile Cone and towards the coast of Israel following transport by easterly-directed surface currents

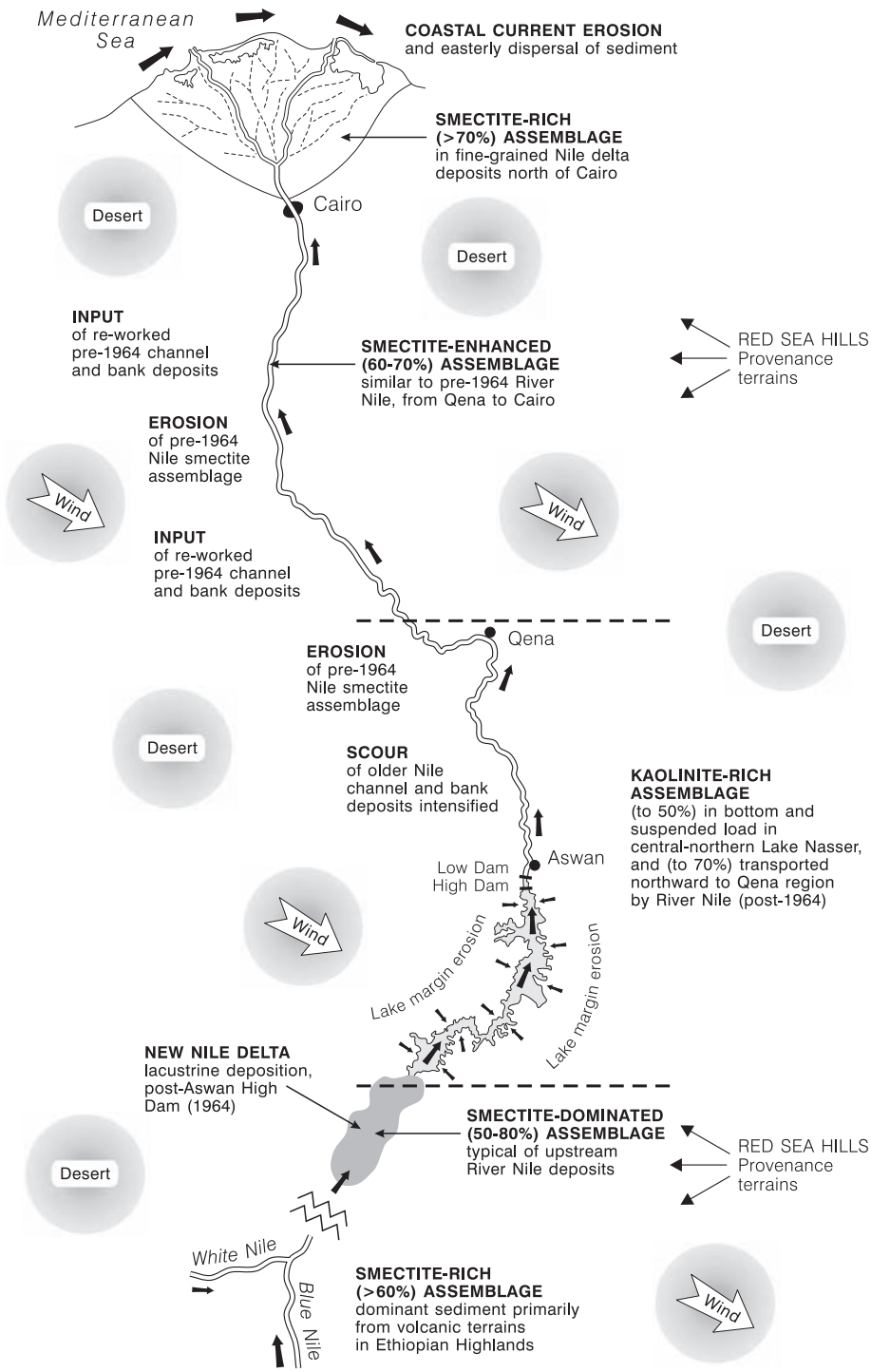

Figure 13.14 Geomorphological processes and the suspended sediment budget in the desert Nile (between Khartoum and the Mediterranean Sea) in relation to the sources and flux of kaolinite-rich sediments before and after the construction of the Aswan High Dam. See text for explanation. Reprinted from Marine Geology, 133, 1, D.J. Stanley and J.G. Wingerath, Nile sediment dispersal altered . . . , pages 1–9, Copyright (1996), with permission from Elsevier

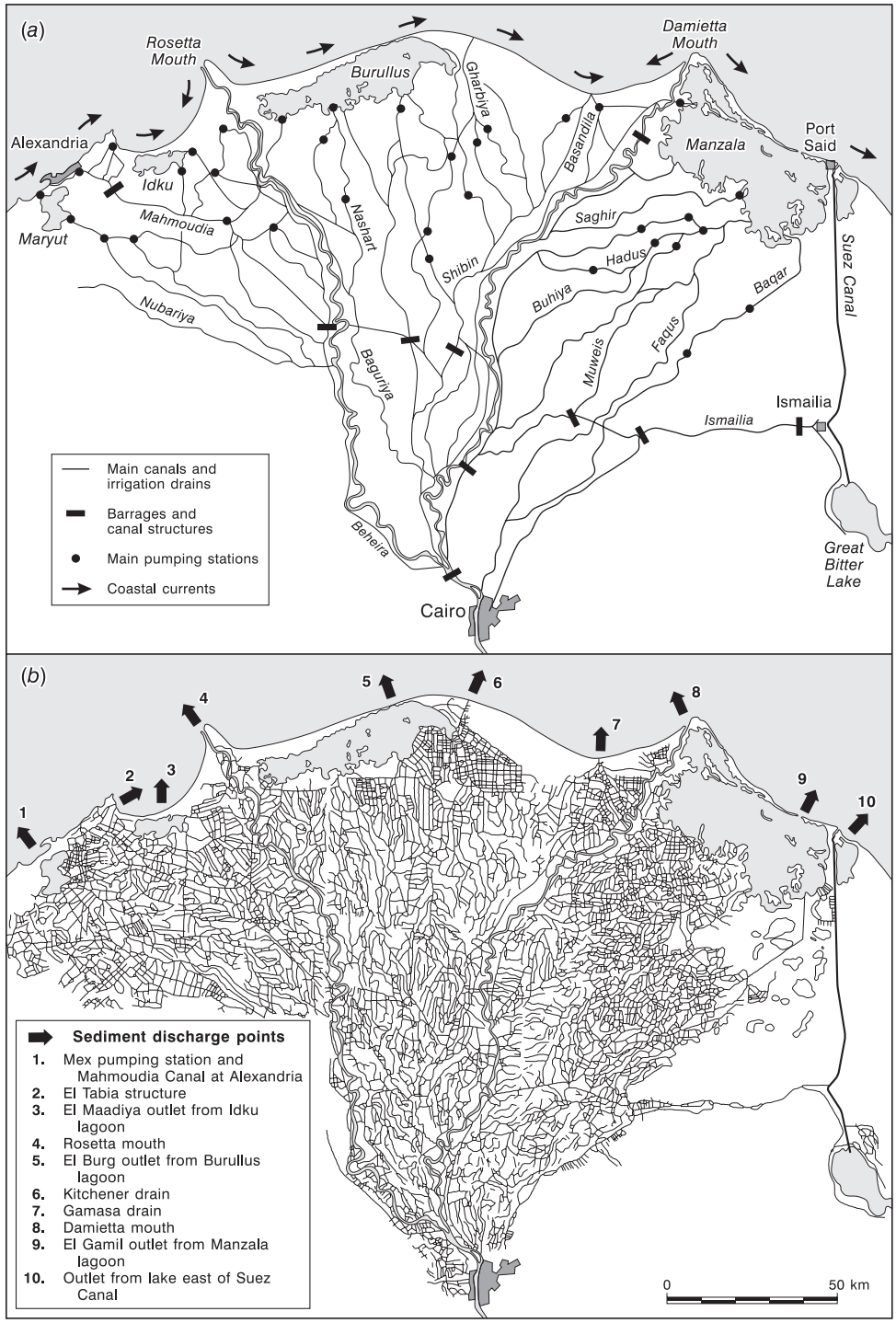

Figure 13.15 (a) The major geomorphological features and canals and pumping stations of the Nile delta and coastline. The arrows show the direction of major coastal currents and associated sediment flux. The main barrages on the delta are also shown. (b) Map of the delta showing more than 10 000 km of irrigation canals and drains. This map is based on charts produced by the Defence Mapping Agency (1970–1993). This area represents the most intensively modified portion of the Nile drainage basin. (a, b) Reprinted from Marine Geology, 129, 3–4, Daniel Jean Stanley, Nile delta extreme case of . . . , pages 189–195, Copyright (1996), with permission from Elsevier

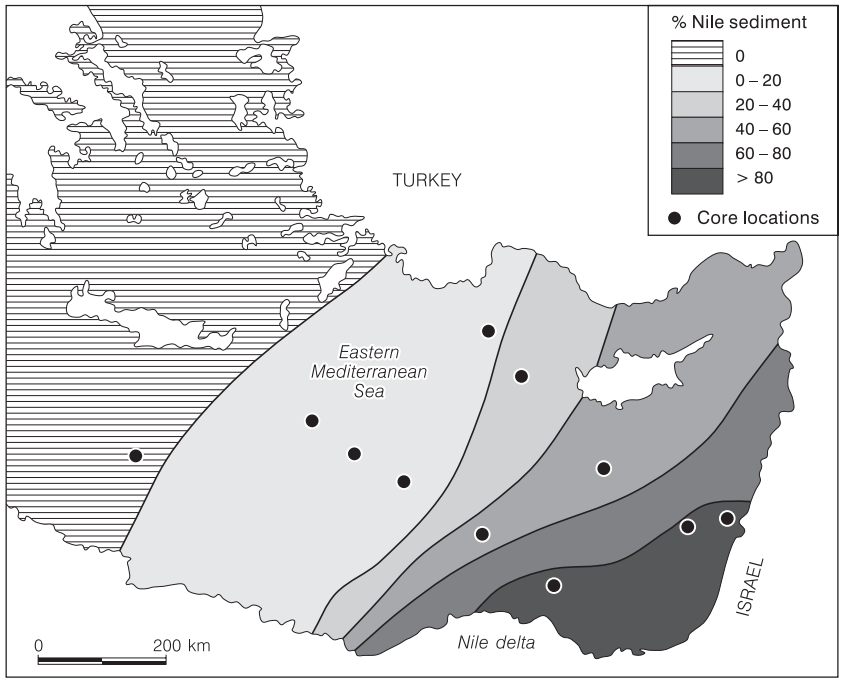

Figure 13.16 The pattern of Nile sediment dispersal in the Eastern Mediterranean Sea based on strontium isotope source tracing. The map shows the percentage of Nile-derived particulate matter in each area. Reprinted from Marine Geology. 155, 2–4, Krom *et al*., The characterization of Saharan . . . , pages 319–330, Copyright (1999), with permission from Elsevier

(Krom *et al*., 1999). The pattern of Nile-derived sediment distribution mapped by Krom and his co-workers showed that Nile sediment was more widely distributed than previously thought and the Aswan High Dam has changed the sedimentation dynamics across much of the Levantine basin. The bulk of the rest of the fine-sediment fraction on the sea floor was made up of aeolian dust from the Sahara. The long-term impacts of this change in sediment quality on the geochemistry and biology of the marine benthic environment are not known. Krom *et al*. (1999) point out that because Nile particulate matter may play an important role in the removal of phosphate by adsorption from the deep waters of the marine environment – another consequence of the Aswan High Dam may be a phosphate-driven increase in productivity in the Eastern Mediterranean Sea (Krom *et al*., 1991).

13.9 RIVER BASIN MANAGEMENT AND GLOBAL CHANGE

It is clear from this review that any discussion of the contemporary fluvial geomorphology and hydrology of the modern Nile Basin must be set within an appropriate historical context of Pleistocene and Holocene environmental change. Profound changes in river behaviour took place during these periods as fluctuations in Equatorial rainfall and monsoon intensity resulted in marked changes in flow regimes and flow volumes, sediment supply and river channel planform and floodplain sedimentation style. For example, in the central and lower reaches of the White Nile valley the large palaeochannels of the Early Holocene Nile lie adjacent to extensive aeolian dune systems providing a graphic illustration of the impact of shifts in Quaternary climate from wetter to drier modes. The Blue Nile has also seen dramatic changes in water and sediment flux during the Late Pleistocene and Holocene. Furthermore, recent research on Holocene sequences in the desert Nile of northern Sudan (Woodward *et al*., 2001; Welsby *et al*., 2002) and in the delta (Krom *et al*., 2002; Stanley *et al*., 2003) has shown that Nile flows and riparian environments can change *abruptly* and with potentially catastrophic consequences for local populations.

The scale of the Nile Basin and the marked basin-wide contrasts in river environments discussed in this chapter present a wide range of resource management issues and it is not possible to discuss them in detail here. The primary

concerns of the ten riparian states are water storage and allocation for irrigation and hydropower generation. The essence of the political conflict surrounds the conflict between the desires of the 'upstream' basin states to fully exploit the potential offered by Nile flows in their own territories, with the needs of the downstream users – particularly Egypt. The Nile Waters Treaty of 1959 allows the Sudan to abstract up to 18.5 $km^3 year^{-1}$ – this is about 22 % of the estimated mean Nile flow of 84 $km^3 year^{-1}$ that formed the basis of the agreement. The rest of the flow is accounted for by the allocation to Egypt and losses to seepage and evaporation (Sene *et al*., 2001). Egypt has the lowest concentration of arable land per head of population of any African state and this has led to more intensive farming methods and to the expansion of the cultivated area through year-round irrigation both on the delta and in the Nile Valley. Political tensions over water allocations for the basin states resurfaced in early 2004 with a meeting of the Nile Basin Initiative in Uganda. The riparian states upstream of Egypt and Sudan aim to develop their hydroelectric potential and the drought-prone lands of Ethiopia and Eritrea have plans for large-scale irrigation schemes of their own. The Nile Basin Treaty of 1929 states:

> 'Without the consent of the Egyptian government, no irrigation or hydroelectric works can be established on the tributaries of the Nile or their lakes, if such works can cause a drop in water level harmful to Egypt.'

Sutcliffe and Lazenby (1994) have reviewed the hydrological data requirements for planning the management of water resources in the Nile Basin. They emphasize the importance of accurate and consistent long-term hydrological records for the development of an effective basin-wide resource management plan. They also highlight the need for more efficient use of irrigation waters in Egypt and Sudan. Over the last century or so the dominant basin-wide strategy for the management of water resources in the Nile Basin has been the construction of large dams and reservoirs. The major water resource development projects are shown in Figure 13.17. The major reservoirs provide essential storage to serve the ever-growing and year-round irrigation demands in Egypt and Sudan. Storage losses to sedimentation are a significant management issue in the Atbara and Blue Nile Basins and a basin-wide sediment monitoring and management strategy is needed (Sutcliffe and Lazenby, 1994). The Jonglei Canal project in the Sudd (Figure 13.17) remains unfinished due to ongoing conflicts and political problems in Sudan (Howell *et al*., 1988). This scheme was intended to reduce evaporation losses in the swamplands and to increase the net water yield of the White Nile Basin. However, caution is needed when draining major wetlands. For example, Williams and Adamson (1973) have argued that some of the potential consequences of draining part of the Sudd include exposure of saline soils, an increase in channel bank erosion downstream, and a change in water chemistry.

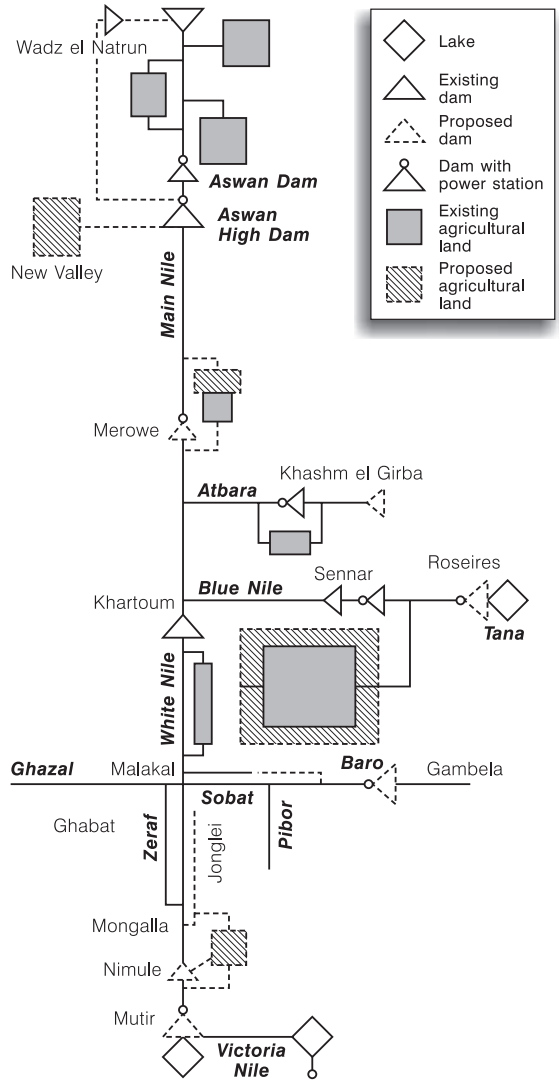

Figure 13.17 Major water resource development projects in the Nile Basin (after Newson, 1992). The Merowe Dam project on the main Nile in Sudan is under construction (Askouri, 2004). Reprinted from Dams, People and Development, Hussein M. Fahim, Copyright (1981) and Land, Water and Development, M.D. Newson, Copyright (1992). London, Routledge

Sutcliffe and Lazenby (1994) have pointed out that the issue of climate change and its effect on water discharge is especially important in the Nile Basin because the low

runoff coefficients associated with the rainfall regime suggest that even a modest change in precipitation will have a disproportionate effect on runoff. They cite the average long-term runoff value of just 55 mm at the Dongola gauging station in northern Sudan (19° N) to illustrate this point. The Nile comprises highly contrasting tributary basins but runoff from each is sensitive to changes in rainfall and this is why marked fluctuations in river flows on the main Nile have been recorded in the past (Sutcliffe and Lazenby, 1994).

The long historical discharge records for the Nile (Hassan, 1981) and the richness of the archaeological and Quaternary sedimentary records mean that this basin provides a unique context for the study of global climate change and its impact upon the hydrology and sediment dynamics of a large river and its population. Recent work in the Nile Basin has suggested that the river system can change rapidly and flow volumes from both the Blue Nile and the White Nile can decrease abruptly (Krom *et al*., 2002). The long flood records have been interrogated to explore the relationship between changes in the global climate system (e.g. monsoon intensity and ENSO) and Nile flood magnitude. Over the last decade or so researchers have attempted to predict the impact of various global climate change scenarios on Nile flows and flood regime (Sene *et al*., 2001), but the complexity and scale of the basin have proved to be problematic in many modelling studies (Hulme, 1994; Tate *et al*., 2001). Understanding the dynamics of the Nile Basin is a major challenge for hydrologists, geomorphologists and river basin planners. The uncertainty surrounding the nature and impact of global change and its potential impact on Nile flows is a major concern – especially in Egypt (Conway and Hulme, 1996) – and casts a large shadow over the politics of water sharing agreements in the basin. If we are to improve our understanding of how the Nile might respond to future changes in global climate, we also need to consider fluctuations in water and sediment fluxes (and the forcing factors responsible) over a range of Holocene and Pleistocene timescales and across the entire catchment (Krom *et al*., 2002). It is also important to investigate long-term interactions between climate change and the human use of river-based resources. This can only be achieved by carefully integrating information from both cultural and geological archives (Woodward *et al*., 2001). The broader significance of these research agendas for other large river systems is now clear. As Adamson (1982: 233) observed in a discussion of Late Quaternary environmental change in the Nile Basin written over two decades ago:

> '. . . climate in the future will undoubtedly oscillate between the extreme limits which the whole Nile basin has so recently experienced. An understanding of the past behaviour of such a river system as the Nile, and of its depositional legacy in the Sudan and Egypt, is therefore of both local and world-wide interest.'

ACKNOWLEDGEMENTS

We would like to thank Nick Scarle (School of Environment and Development, The University of Manchester) for expertly drawing the maps and diagrams. We also thank Avi Gupta and the two referees for their helpful reviews.

REFERENCES

Abu El-Ata, A. (1978) *Egypt and the Nile after the High Aswan Dam*. Ministry of Irrigation and Land Reclamation, Egypt.

Adamson, D.A. (1982) The integrated Nile. In: *A Land Between Two Niles: Quaternary Geology and Biology in Central Sudan* (M.A.J. Williams and D.A. Adamson, Eds.). A.A. Balkema, Rotterdam, 221–234.

Adamson, D.A. and Williams, F. (1980) Structural geology, tectonics and the control of drainage in the Nile basin. In: *The Sahara and The Nile: Quaternary Environments and Prehistoric Occupation in Northern Africa* (M.A.J. Williams and H. Faure, Eds.). A.A. Balkema, Rotterdam, 225–252.

Adamson, D.A., Gasse, F., Street, F.A. and Williams, M.A.J. (1980) Late Quaternary history of the Nile. *Nature*, 288, 50–55.

Adamson, D., McEvedy, R. and Williams, M.A.J. (1993) Tectonic inheritance in the Nile basin and adjacent areas. *Israel Journal of Earth Sciences*, 41, 75–85.

Askouri, A. (2004) A Culture Drowned. *World Rivers Review*, 19(2), 8–9.

Bell, B. (1971) The Dark Ages in Ancient History. I. The First Dark Age in Egypt. *American Journal of Archaeology*, 75(1), 1–26.

Brooks, C.E.P. (1927) Periodicities in the Nile floods. *Memoirs of the Royal Meteorological Society*, 2, 9–26.

Butzer, K.W. (1980) Pleistocene history of the Nile Valley in Egypt and Lower Nubia. In: *The Sahara and The Nile: Quaternary Environments and Prehistoric Occupation in Northern Africa* (M.A.J. Williams and H. Faure, Eds.). A.A. Balkema, Rotterdam, 253–280.

Butzer, K.W. and Hansen, C.L. (1968) *Desert and River in Nubia: Geomorphology and Prehistoric Environments at the Aswan Reservoir*. Madison, University of Wisconsin Press.

Collins, R.O. (1990) *The Waters of the Nile, Hydropolitics and the Jonglei Canal 1900–1988*. Clarendon Press, Oxford.

Conway, D. (2000) The climate and hydrology of the Upper Blue Nile River. *The Geographical Journal*, 166(1), 49–62.

Conway, D. and Hulme, M. (1996) The impacts of climate variability and future climate change in the Nile Basin on water resources in Egypt. *Water Resources Development*, 12(3), 277–296.

Davies, W.V. and Friedman, R. (1999) *Egypt.* The British Museum, London, 224 pp.

El-Manadely, M.S., Abdel-Bary, R.M., El-Sammany, M.S. and Ahmed, T.A. (2002) Characteristics of the delta formation resulting from sediment deposition in Lake Nasser, Egypt: approach to tracing lake delta formation. *Lakes and Reservoirs: Research and Management*, 7, 81–86.

Elsheikh, S., Kaikai, A. and Andah, K. (1991) Intensive sediment transport from the Upper Nile Basin and water resources management in Sudan. In: *Hydrology for the Water Management of Large Rivers* (F.H.M. van de Ven, D. Gutknecht, D.P. Loucks and K.A. Salewicz, Eds.). IAHS Publication No. 201, 291–300.

FAO (1997) *Irrigation Potential in Africa: A Basin Approach*. FAO Land and Water Bulletin 4. Food and Agriculture Organisation, Rome.

Foucault, A. and Stanley, D.J. (1989) Late Quaternary paleoclimatic oscillations in east Africa recorded by heavy minerals in the Nile Delta. *Nature*, 339, 44–46.

Fraedrich, K., Jiang, J., Gerstengarbe, F. and Werner, P. (1997) Multiscale detection of abrupt climate changes: application to River Nile flood levels. *International Journal of Climate Change*, 17, 1301–1315.

Frihy, O.E. and Komar, P.D. (1993) Long-term shoreline changes and the concentration of heavy minerals in beach sands of the Nile delta, Egypt. *Marine Geology*, 115, 253–261.

Frihy, O.E., Debes, E.A. and El Sayed, W.R. (2003) Processes reshaping the Nile delta promontories of Egypt: pre- and post protection. *Geomorphology*, 53, 263–279.

Gasse, F., Rognon, P. and Street, F.A. (1980) Quaternary history of the Afar and Ethiopian Rift Lakes. In: *The Sahara and The Nile* (M.A.J. Williams and H. Faure, Eds.). A.A. Balkema, Rotterdam, 361–400.

Hassan, F.A. (1981) Historical Nile floods and their implications for climate change. *Science*, 212, 1142–1145.

Hassan, F.A. (1988) Climatic change, Nile floods and civilization. *Nature and Resources*, 34(2), 34–40.

Howell, P.P. and Allan, J.A. (Eds.) (1994) *The Nile: Sharing a Scarce Resource*. Cambridge University Press, Cambridge.

Howell, P., Lock, M. and Cobb, S. (Eds.) (1988) *The Jonglei Canal: Impact and Opportunity.* Cambridge University Press. Cambridge.

Hsu, K.J., Ryan, W.B.F. and Cita, M.B. (1973) Late Miocene desiccation of the Mediterranean. *Nature*, 242, 239–243.

Hulme, M.A. (1994) Global climate change and the Nile basin. In: *The Nile: Sharing a Scarce Resource* (P.P. Howell and J.A. Allan, Eds.). Cambridge University Press, Cambridge, 139–162.

Hurni, H. (1999) Sustainable management of natural resources in African and Asian mountains. *Ambio*, 28(5): 382–389.

Hurst, H.E. (1952) *The Nile*. Constable, London.

Hurst, H.E., Black, R.P. and Simaika, Y.M. (1959) *The Nile Basin, Volume IX: The hydrology of the Blue Nile and Atbara and the Main Nile to Aswan with some reference to projects*. Nile Control Department Paper No. 12, Government Printing Offices, Cairo Egypt.

Krom, M.D., Brenner, S., Kress, N., Gordon, L.I. (1991) Phosphorous limitation of primary productivity in the Eastern Mediterranean Sea. *Limnology and Oceanography*, 36(3), 424–432.

Krom, M.D., Cliff, R.A., Eijsink, L.M., Herut, B. and Chester, R. (1999) The characterization of Saharan dusts and Nile particulate matter in surface sediments from the Levantine basin using Sr isotopes. *Marine Geology*, 155, 319–330.

Krom, M.D., Stanley, J.D., Cliff, R.A and Woodward, J.C. (2002) River Nile sediment fluctuations over the past 7000 years and their key role in sapropel development. *Geology,* 30(1), 71–74.

Le Pichon, X., Clauzon, G. and Bellier, O. (2005). Ouverture de la Méditerranée Occidentale et épisode messinien: implications pour la tectonique du sud de la France. Abstracts, *College de France Conférences publiques*, CEREGE, Aix-en-Provence.

Macklin, M.G. and Woodward, J.C. (1998) Alluvial architecture and OSL dating of Holocene palaeochannels in the Northern Dongola Reach of the Nile, Sudan. *Sudan and Nubia,* 2. The British Museum (SARS), London, 22–26.

Macklin, M.G. and Woodward, J.C. (2001) Holocene alluvial history and the palaeochannels of the River Nile in the Northern Dongola Reach. In: *Life on the Desert Edge: Seven Thousand Years of Settlement in the Northern Dongola Reach, Sudan* (D.A. Welsby, Eds.) (Volume 1). The Sudan Archaeological Research Society Publication No. 7, London, 7–13.

McDougall, I., Morton, W.H. and Williams, M.A.J. (1975) Age and rates of denudation of Trap Series basalts at Blue Nile gorge, Ethiopia. *Nature*, 254, 207–209.

Milliman, J.D. and Syvitski, J.P.M. (1992) Geomorphic/Tectonic control of sediment discharge to the ocean: the importance of small mountainous rivers. *The Journal of Geology*, 100, 525–544.

Newson, M.D. (1992) *Land, Water and Development*. London, Routledge.

Orlova, G. and Zenkovitch, V. (1974) Erosion of the shores of the Nile delta. *Geoforum*, 18, 68–72.

Pachur, H.J. and Kropelin, S. (1987) Wadi Howar: paleoclimatic evidence from an extinct river system in the southeastern Sahara. *Science*, 237, 298–300.

Ritchie, J.C., Eyles, C.H. and Haynes, C.V. (1985) Sediment and pollen evidence for an early to mid Holocene humid period in the eastern Sahara. *Nature*, 314, 352–355.

Rohling, E.J. (1994) Review and new aspects concerning the formation of Mediterranean sapropels. *Marine Geology*, 122, 1–28.

Rossignol-Strick, M., Nesteroff, V., Olive, P. and Vergnaud-Grazzini, C. (1982) After the deluge: Mediterranean stagnation and sapropel formation. *Nature*, 295, 105–110.

Ryan, W.B.F. and Cita, M.B. (1978) The nature and distribution of Messinian erosional surfaces – indicators of a several kilometer deep Mediterranean in the Miocene. *Marine Geology*, 27, 193–230.

Rzoska, J. (Ed.) (1976) *The Nile: Biology of an Ancient River*. W. Junk Publishers, The Hague, 417 pp.

Said, R. (1981) *The Geological Evolution of the River Nile.* Springer-Verlag, New York, 151 pp.

Said, R. (1993) *The River Nile: Geology, Hydrology and Utilization*. Pergamon Press, Oxford. 320 pp.

Said, R. (1994) Origin and evolution of the Nile. In: *The Nile: Sharing a Scarce Resource* (P.P. Howell, and J.A. Allan, Eds.). Cambridge University Press, Cambridge, 17–26.

Sene, K.J., Tate, E.L. and Farquharson, F.A.K. (2001) Sensitivity studies of the impacts of climate change on White Nile Flows. *Climatic Change*, 50, 177–208.

Sestini, G. (1992) Implications of climate change for the Nile delta. In: *Climatic Change and the Mediterranean* (L. Jeftic, J.D. Milliman and G. Sestini, Eds.). Edward Arnold, New York, 535–601.

Shahin, M. (1985) *Hydrology of the Nile Basin.* Elsevier, Amsterdam, 575 pp.

Sharaf El Din, S.H. (1977) Effect of the Aswan High Dam on the Nile flood and on the estuarine and coastal circulation pattern along the Mediterranean Egyptian coast. *Limonology and Oceanography*, 22, 194–207.

Shaw, I. (Ed.) (2003) *The Oxford History of Ancient Egypt.* Oxford University Press, Oxford, 540 pp.

Stager, J.C., Cumming, B. and Meeker, L. (1997) A high resolution 11 400-year diatom record from Lake Victoria, East Africa. *Quaternary Research*, 47, 81–89.

Stanley, D.J. (1978) Ionian Sea sapropel distribution and late Quaternary palaeoceanography in the eastern Mediterranean. *Nature*, 274, 149–152.

Stanley, D.-J. (1996) Nile delta: extreme case of sediment entrapment on a delta plain and consequent coastal land loss. *Marine Geology*, 129, 189–195.

Stanley, D.J. and Warne, A.G. (1993) Nile delta: recent geological evolution and human impact. *Science*, 260, 628–634.

Stanley, D.J. and Wingerath, J.G. (1996) Nile sediment dispersal altered by the Aswan High Dam: the kaolinite trace. *Marine Geology*, 133, 1–9.

Stanley, D.J. and Goodfriend, G.A. (1997) Recent subsidence of the northern Suez Canal. *Nature*, 388, 335–336.

Stanley, D.J., Krom, M.D., Cliff, R.A. and Woodward, J.C. (2003) Nile flow failure at the end of the Old Kingdom Egypt: strontium isotopic and petrologic evidence. *Geoarchaeology: an International Journal*, 18 (3), 395–402.

Sutcliffe, J. and Lazenby, J. (1994) Hydrological data requirements for planning Nile management. In: *The Nile: Sharing a Scarce Resource* (P.P. Howell and J.A. Allen, Eds.). Cambridge, Cambridge University Press, 163–192.

Swain, A. (1997) Ethiopia, the Sudan and Egypt: The Nile River dispute. *Journal of Modern African Studies*, 35, 674–694.

Talbot, M.R., Williams, M.A.J. and Adamson, D.A. (2000) Strontium isotope evidence for Late Pleistocene re-establishment of an integrated Nile drainage system. *Geology*, 28, 343–346.

Tate, E.L., Sene, K.J. and Sutcliffe, J.V. (2001) A water balance study of the upper White Nile basin flows in the late nineteenth century. *Hydrological Sciences Journal*, 46(2), 301–318.

Thomson, J., Mercone, D., de Lange, G.J. and van Santvoort, P. J.M. (1999) Review of recent advances in the interpretation of eastern Mediterranean sapropel S1 from geochemical evidence. *Marine Geology*, 153, 77–89.

UNEP (2000) *Water Sharing in the Nile River Valley*. Project GNV011: Using Remote Sensing for the Sustainable Use of Natural Resources. UNEP, Geneva, 85 pp.

UNESCO (1978) *World Water Balance and Water Resources of the Earth*. UNESCO Studies and Reports in Hydrology No. 25, Paris.

Walling, D.E. (1996) Hydrology and Rivers. In: *The Physical Geography of Africa* (W.M. Adams, A.S. Goudie and A.R. Orme, Eds.). Oxford, Oxford University Press, 103–121.

Welsby, D.A. (1998*) The Kingdom of Kush: The Napatan and Meroitic Empires*. Markus Weiner Publishers, Princeton.

Welsby, D.A. (2001) *Life on the Desert Edge: Seven Thousand Years of Settlement in the Northern Dongola Reach, Sudan*. The Sudan Archaeological Research Society Publication No. 7, London (two volumes).

Welsby, D.A., Macklin, M.G. and Woodward, J.C. (2002) Human responses to Holocene environmental changes in the Northern Dongola Reach of the Nile, Sudan. In: *Egypt and Nubia: Gifts of the Desert* (Renée Friedman, Ed.). The British Museum Press, London, 28–38.

Wendorf, F., Schild, R. and Issawi, B. (1976) *Prehistory of the Nile Valley*. New York, Academic Press.

Whetton, P., Adamson, D.A. and Williams, M.A.J. (1990) Rainfall and river flow variability in Africa, Australia and East Asia linked to El Niño – Southern Oscillation events. In: *Lessons for Human Survival: Nature's record from the Quaternary. Geological Society of Australia Symposium Proceedings* (P. Bishop, Ed.), l 1, 71–82.

Williams, M.A.J. and Adamson, D.A. (1973) The physiography of the central Sudan. *Geographical Journal,* 139, 498–508.

Williams, M.A.J. and Adamson, D.A. (1980) Late Quaternary depositional history of the Blue and White Nile rivers in central Sudan. In: *The Sahara and The Nile: Quaternary Environments and Prehistoric Occupation in Northern Africa* (M.A.J. Williams and H. Faure, Eds.). A.A. Balkema, Rotterdam, 281–304.

Williams, M.A.J. and Faure, H. (Eds.) (1980) *The Sahara and The Nile: Quaternary Environments and Prehistoric Occupation in Northern Africa*. A.A. Balkema, Rotterdam, 607 pp.

Williams, M.A.J. and Williams, F.M. (1980) Evolution of the Nile Basin. In: *The Sahara and The Nile: Quaternary Environments and Prehistoric Occupation in Northern Africa* (M.A.J. Williams and H. Faure, Eds.). A.A. Balkema, Rotterdam, 207–224.

Williams, M.A.J., Adamson, D.A. and Abdulla, H.H. (1982) Landforms and soils of the Gerzira: A Quaternary legacy of the Blue and White Nile rivers. In: *A Land Between Two Niles: Quaternary Geology and Biology of the Central Sudan* (M.A.J. Williams and D.A. Adamson, Eds.). A.A. Balkema, Rotterdam, 111–142.

Williams, M.A.J., Adamson, D., Cock, B. and McEvedy, R. (2000) Late Quaternary environments in the White Nile region, Sudan. *Global and Planetary Change*, 26, 305–316.

Williams, M.A.J., Adamson, D., Prescott, J.R. and Williams, F.M. (2003) New light on the age of the White Nile. *Geology*, 31, 1001–1004.

Woodward, J.C., Macklin, M.G. and Welsby, D.A. (2001) The Holocene fluvial sedimentary record and alluvial geoarchaeology in the Nile Valley of Northern Sudan. In: *River Basin Sediment Systems: Archives of Environmental Change* (D.R. Maddy, M.G. Macklin and J.C. Woodward, Eds.). A.A. Balkema, Rotterdam, 327–356.

14

The Congo River, Central Africa

Jürgen Runge

Johann Wolfgang Goethe-Universität, FB 11: Institut für Physische Geographie and Zentrum für interdisziplinäre Afrikaforschung (ZIAF), Altenhöferallee 1, D-60438 Frankfurt am Main, Germany

14.1 INTRODUCTION

The Congo, with a length of 4374 km, is the second longest river in Africa after the Nile and one of the longest in the world. Its huge drainage basin covers 3 747 320 km^2 (Devroey, 1951) including all of the Democratic Republic of Congo (former Zaire, Congo-Kinshasa), parts of Angola, Zambia, Tanzania, Burundi, Central African Republic (CAR), Cameroon, and Republic of Congo (Congo-Brazzaville) (Figure 14.1).

The Congo River and its tributaries have been traditional migration pathways for humans for centuries. There is archaeological evidence of early societies at the northern rain forest–savanna margin of the western Congo Basin (Iliffe, 1995). South of the Congo mouth the medieval Kongo Kingdom has been identified. Between 400–100 BC and 1600 AD, Bantu-speaking settlers moved from west to east along rivers (Iliffe, 1995; Wotzka, 1995), crossing the inner Congo region almost up to the Lomami River (Figure 14.1).

The arrival of the Portuguese in 1482–1484 and the subsequent rise of the slave trade weakened the early kingdoms and led to a final breakdown at the end of the seventeenth century (Wiese, 1980). Further European exploration took place in the 1870s when the missionary David Livingstone and the journalist Henry Morton Stanley travelled throughout the Congo Basin, mainly following the Congo River network. Kisangani, the former Stanleyville, an important eastern harbour on the Congo River, was founded in 1883. During Victorian times, Central Africa was considered to be the 'Heart of darkness'. This view was immortalized by Joseph Conrad's popular novel in 1902.

The Congo River remained important as a navigable waterway and a natural national border between Brazzaville (Republic of Congo) and Kinshasa (Democratic Republic of Congo), the former Léopoldville, during the Belgian colonial era and until recent times. In 1997, the Zairian dictator Mobutu fled Kinshasa, crossing the Congo River to escape the advancing army of Laurent D. Kabila. President Kabila was killed shortly after, in 2001, by his own supporters, and was subsequently replaced by his son, Joseph Kabila, who has tried since then to lead the Central African country, which has been economically and politically devastated for several years.

14.2 THE COURSE OF THE CONGO RIVER

The Congo River [known as the Zaire River during the Mobutu regime (1971–1997)], originates at an altitude of 1400–1500 m in the savanna highlands of the copper province Shaba in the southeast of the DR Congo. The complex sources of the Congo consist of several small headwater streams, swamps and lakes. Commonly, the upper course of the stream as far as Kisangani is called 'Lualaba' or 'Congo-Lualaba' (Figure 14.1).

The course of the Congo-Lualaba River follows a unique pattern, forming a very complex fluvial system (Figure 14.2). The river takes about 4000 km to drop 1500 m (Table 14.1). Tertiary and Pleistocene tectonic movements and heterogeneous bedrock within the

Large Rivers: Geomorphology and Management, Edited by A. Gupta

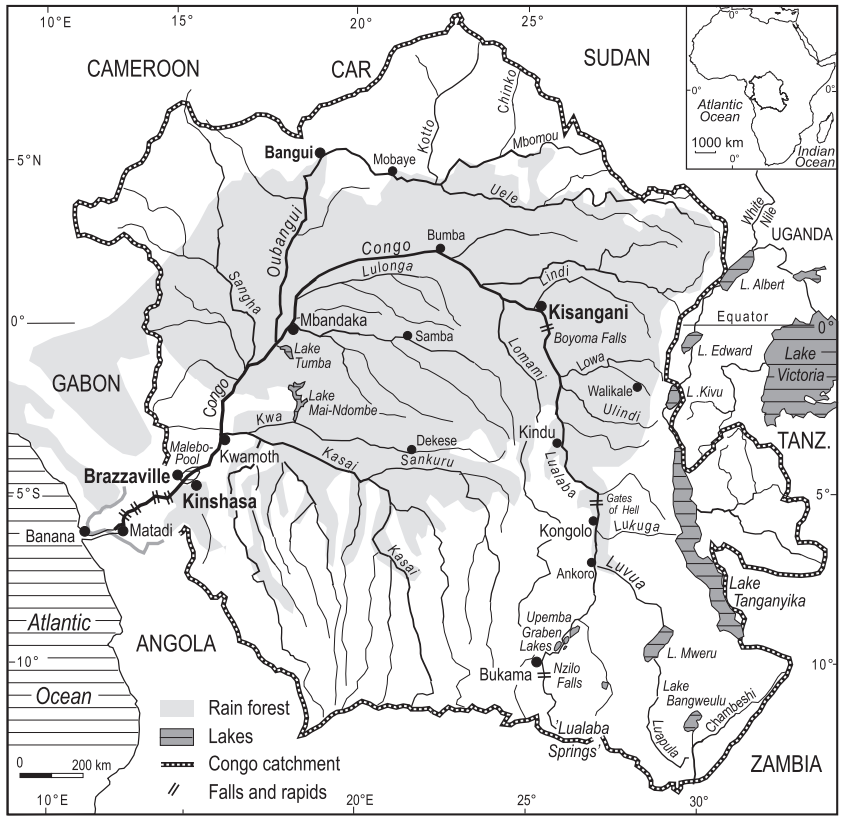

Figure 14.1 Location map of the Congo Basin. Reproduced from National Geographic Magazine, 180, No. 5, R. Caputo, Zaire River – Lifeline for a Nation, 11, Copyright (1991), National Geographic Magazine

catchment have given rise to a stepped topography with strong downcutting close to the source region at Nzilo Falls and again above the mouth at Livingstone Falls (Figure 14.3). Drainage near the Shaba Highland and the Western Rift Rise (Walikale, Mitumba Mountains, Figures 14.1 and 14.8) between Bukama and Kisangani is strongly influenced by warping and faulting (graben) and shows clear signs of tectonic control. In contrast, the middle course from Kisangani to Kinshasa is dominated by gentle, broad and anastomosing sand-silt stretches.

Leaving the Congo-Zambezi watershed, the Lualaba flows first west, and then north, and subsequently crosses through a ridge and hogback topography on the Shaba Highland (Likasi and Kolwezi Plateau) to enter the Nzilo Gorge with a large waterfall (Figure 14.5). Here the river has formed a strongly incised, 300–400 m deep, narrow valley, passing close to the town of Bukama into the SW–NE oriented Upemba Graben (Figure 14.1). From there it meanders across an enormous (30–180 km) graben, through a series of marshy lakes (Kabwe, Kabele, Mulenda, Upemba, Lukanga, Kisale, Kalombwe, Zimbambo, Kabamba) [Operational Navigation Chart (ONC), maps M4, N4, 1983, 1987, Figures 14.1 and 14.4]. Between Bukama and Kongolo, a distance of over 600 km, the Lualaba has been navigable for smaller vessels up to 40 tonnes. Due to fluvial dynamics and lack of maintenance, such as dredging since the 1960s, only episodic navigation during the rainy season with higher discharge is currently possible (Wiese, 1980).

The Lualaba leaves the graben in a northeastern direction along a steeper gradient. At Ankoro it receives the second main easterly headstream: the Luvua River. The Luvua has its source in northern Zambia by the Chambeshi River, which first drains southwest into the Lake Bangweulu swamp area. From there it exits as the Luapula River, flows northwards and forms the Congolian-Zambian border for some 300 km, before discharging into Lake Mweru. It emerges from Lake Mweru as the

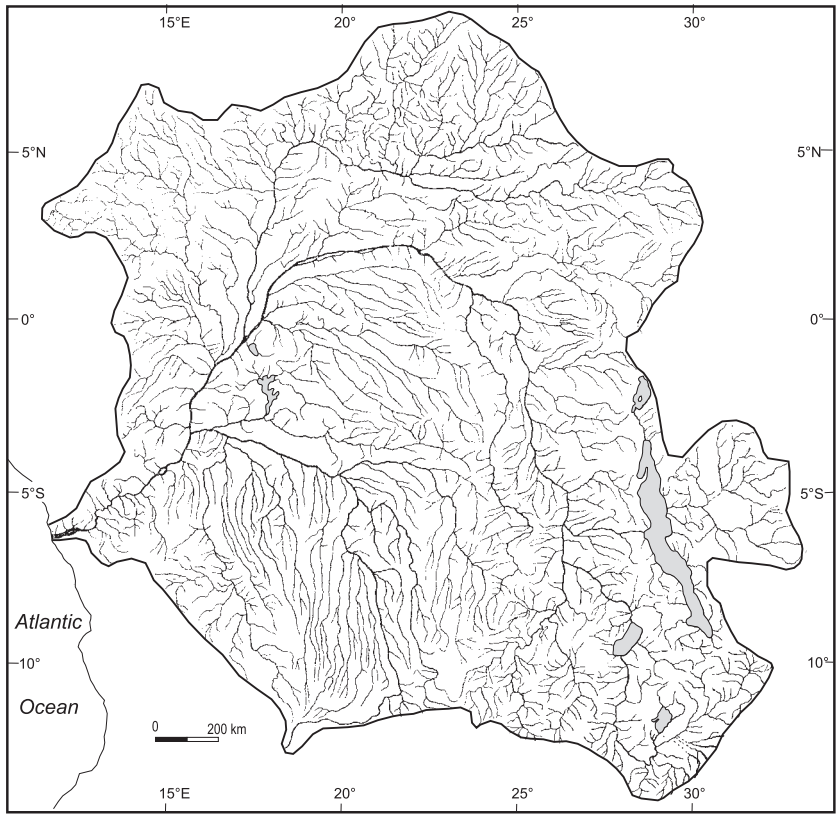

Figure 14.2 Drainage net, Congo Basin. Reproduced from Le Congo Physique, 3eme Edition, M. Robert, Copyright (1946), with permission from Presse Universitaires de France

Table 14.1 Gradient of the Congo River for selected sites

Site	Distance from mouth (km)	Distance between sites (km)	Gradient ($m\,km^{-1}$)	Elevation (m)
Lualaba springs	4372			1435
Nzilo	3975	397	0.59	1231
Bukama	3695	280	2.37	567
Kongolo	3055	640	0.052	533
Kindu	2705	350	0.2	461
Ubundu	2390	315	0.802	435
Kisangani	2240	150	0.28	393
Kinshasa	498	1742	0.066	277
Kwamuntu-Itimbiri	455	43	1.21	225
Manyanga	365	90	0.366	192
Isangila	236	129	0.16	171
Matadi	148	88	1.85	7.5
Banana	0	148	0.05	0

Source: modified from Robert, 1946.

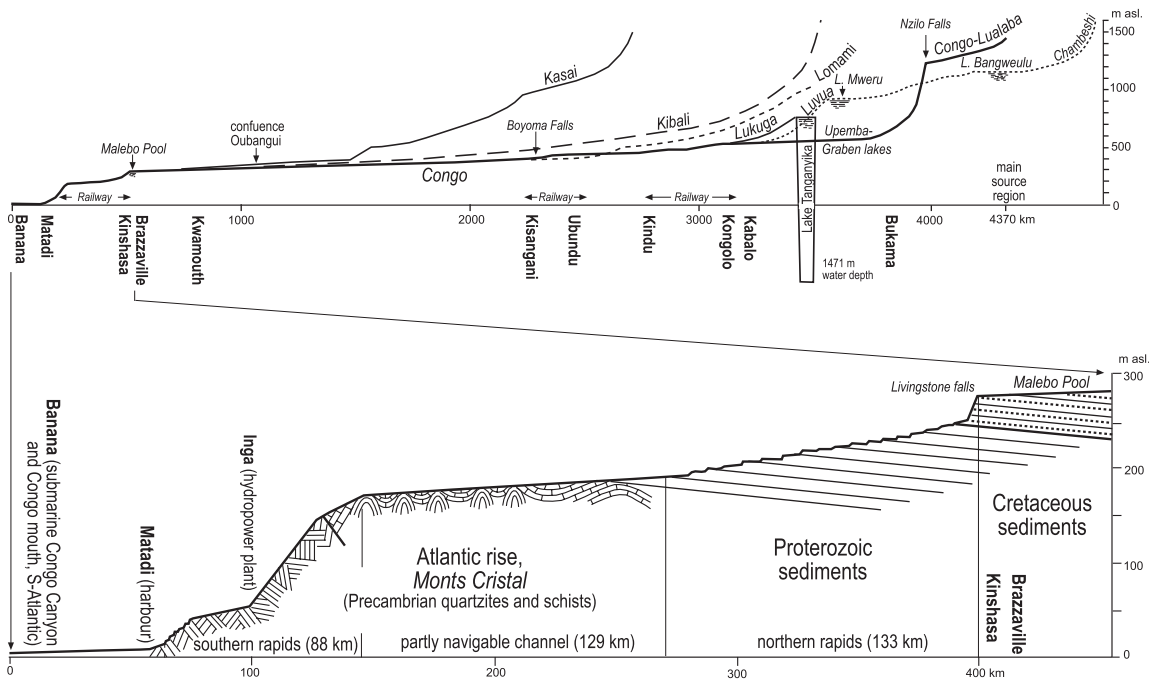

Figure 14.3 Longitudinal profiles of the Congo-Lualaba and the enlarged profile for the lower Congo course between Malebo Pool and Banana. Reproduced from Le Congo Physique, 3eme Edition, M. Robert, Copyright (1946), with permission from Presse Universitaires de France

Luvua River and reaches its confluence with the Lualaba about 320 km northwest.

A further important tributary to the Congo-Lualaba drainage system is the Lukuga River which begins from Lake Tanganyika (Figures 14.1 and 14.2) and joins the Lualaba north of Kabalo (6° 03′ S/26° 54′ E, 527 m asl). The Lukuga exit at Kalémie (5° 56′ 40″ S/29° 12′ 10″ E, 768 m asl) on the western shores of Lake Tanganyika has been subject of much discussion among hydrologists, as the discharge and the fluvial activity of this river is strongly dependent on lake level variations (Devroey, 1935; Veatch, 1935; Lepersonne, 1978).

From Kabalo onwards, between 25° and 27° E, the Lualaba River flows mainly north. North of Kongolo (5° 23′ 10″ S/27° 00′ 40″ E, 523 m) the character of the Lualaba changes with augmented discharge and the presence of many rapids and a deep and narrow gorge called the 'Gates of Hell' (Figure 14.1, 'Ports d'enfer'; Robert, 1946) along its course. A railway line from Kongolo to Kindu serves this non-navigable section. Further downstream between Kindu (2° 57′ 10″ S/25° 55′ 45″ E, 442 m) and Ubundu (0° 22′ 25″ S/25° 28′ 30″ E, 414 m) the river widens and shallows. Only small vessels can be used along this section.

The majority of tributaries joining the upper Lualaba enter from the east (Figures 14.1 and 14.2), draining the western slopes of the Central African Rift valley. On average, rainfall in excess of 2000 mm falls annually on these slopes (Bultot, 1971; Runge, 2001). Rivers like the Ulindi, Lowa and Maiko contribute to a significant increase of the Congo-Lualaba's discharge before Kisangani at 373 m asl (Bultot, 1971).

A further section with rapids, cataracts and falls (Boyoma Falls, Figure 14.1) follows between Ubundu and Kisangani, where the river crosses the Equator for the first time. A railway from Kisangani harbour to Ubundu passes this non-navigable section. Kisangani, once the industrial hub in the eastern Congo Basin, marks the end of the Lualaba River, the Congo's upper course, and the beginning of the 'true' Congo River, the 'lifeline of [the Congolese] nation' (Caputo, 1991).

At Kisangani the economically important inland water traffic connection (1742 km) to Kinshasa begins. Larger vessels up to 800 tonnes (Wiese, 1980) take up to 2 or 3 weeks to reach Kisangani from the capital. Because of the war in Central Africa, which has been going on since the mid 1990s, Kisangani harbour was closed in 1998, and was only recently reopened in August 2003.

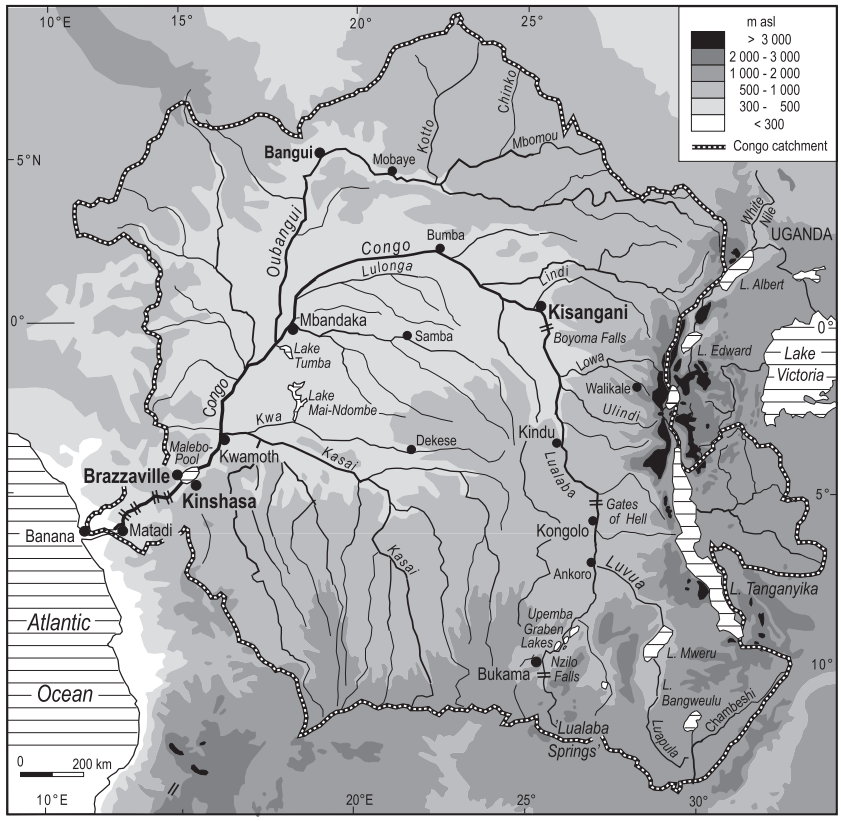

Figure 14.4 Morphology and elevation within the Congo River catchment. Reproduced from Le Congo Physique, 3eme Edition, M. Robert, Copyright (1946), with permission from Presse Universitaires de France

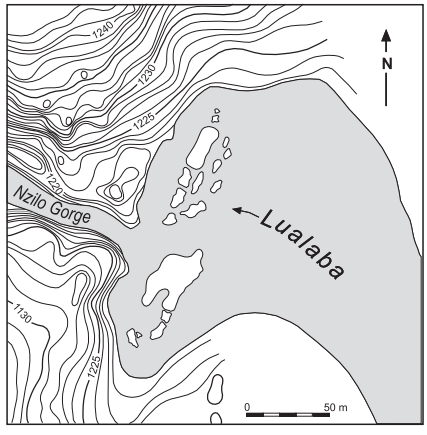

Figure 14.5 Topographic sketch map of the Nzilo Gorge south of Bukama, the upper Congo-Lualaba. Reproduced from Le Congo Physique, 3eme Edition, M. Robert, Copyright (1946), with permission from Presse Universitaires de France

This helps to provide goods to the remote areas of the Congo Basin.

Below Kisangani, the Congo changes its course to flow in a huge arc, first to the north-west (Bumba), and later to the west. It then crosses the Equator again in a south-west direction close to Mbandaka (Figure 14.1). Below Kisangani the Congo is uninterrupted by falls or rapids. The river bed is characterized by anastomosing river channels with extended sand bars and is in places up to 16 km wide (Figure 14.6). Huge colonies of aquatic vegetation, such as invasive water hyacinths (*Eichornia crassipes* Holms; Robyns, 1955; Mengho, 1994), and papyrus (Robert, 1946) locally cover the river and impair navigation.

Many large tributaries originating from (1) north of the Equator, the Oubangui (Runge and Nguimalet, 2005), Mongala, and Itimbiri, and (2) the central and south Congo Basin, the Kasai (Devroey, 1939), Lulonga, and Lomami, substantially increase the discharge of the middle Congo.

As these rivers partly drain semi-humid catchments with alternating dry and rainy seasons on both sides of the Equator, the discharge regime of the Congo River shows a relatively constant flow round the year (Bultot and Dupriez, 1987). The region below the Oubangui confluence is an extended zone of year-round inundation.

Below the confluence with the Oubangui and the Sangha River the Congo crosses the savanna-covered Batéké Plateau between Bolobo and Kwamoth. The river is again deeply incised (up to 50 m) and forms a box-shaped valley within the aeolian sands of the former Mega-Kalahari. The thickness of the sands reach a depth of about 80 m at Brazzaville (Schwartz, 1988). Within this 50-km long rectangular valley segment, the river bed narrows significantly to 1.5–2.5 km from its 16 km upstream width. At Kwamoth, another large tributary from the left, the Kasai River, joins the Congo. The Congo widens again below this confluence to form a near-oval lake, 24 to 28 km in diameter, with several islands. This is the Malebo Pool (formerly Stanley Pool). The capitals of Brazzaville and Kinshasa are located on a stepped series of fluvial terraces near flat surfaces on both sides of the Pool. This site with two big towns facing each other on either side of the Congo is an important hub for traffic and trade in Central Africa (Figure 14.7**)**.

The lower course of the Congo River, 498 km long, starts at the western edge of the Malebo Pool (Figure 14.3) where the river narrows again to cross an uplifted Precambrian mountain chain known as the Monts Cristal or the Atlantic Rise (Cahen *et al*., 1984). The Congo descends 267 m in a three-staged section of 66 falls and rapids to the harbour of Matadi (Robert, 1946). The first cascades (Livingstone Falls) with a height of 40 m are located shortly after the Pool, separating the interior of Central Africa from the Atlantic coast. With the exception of a partly navigable stretch of 129 km (Figure 14.3), railways and roads are used to pass this non-navigable lower section.

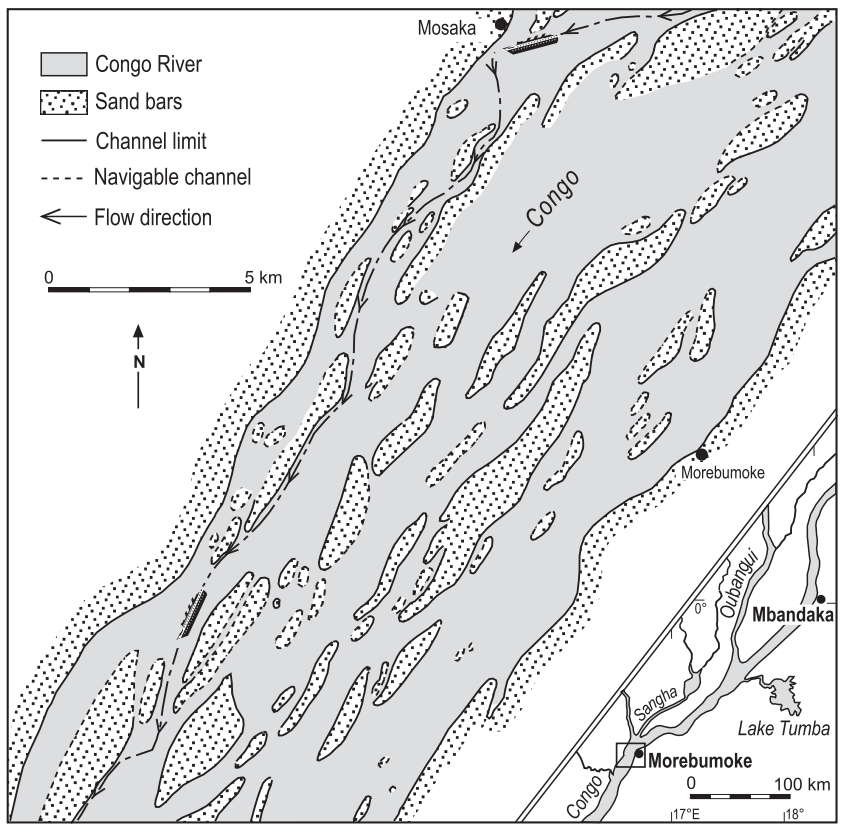

Figure 14.6 Sketch map of the Congo River (middle course) south of Mbandaka. A wide river bed with extended sand bars is typical for this part of the course. Reproduced from Le Congo Physique, 3eme Edition, M. Robert, Copyright (1946), with permission from Presse Universitaires de France

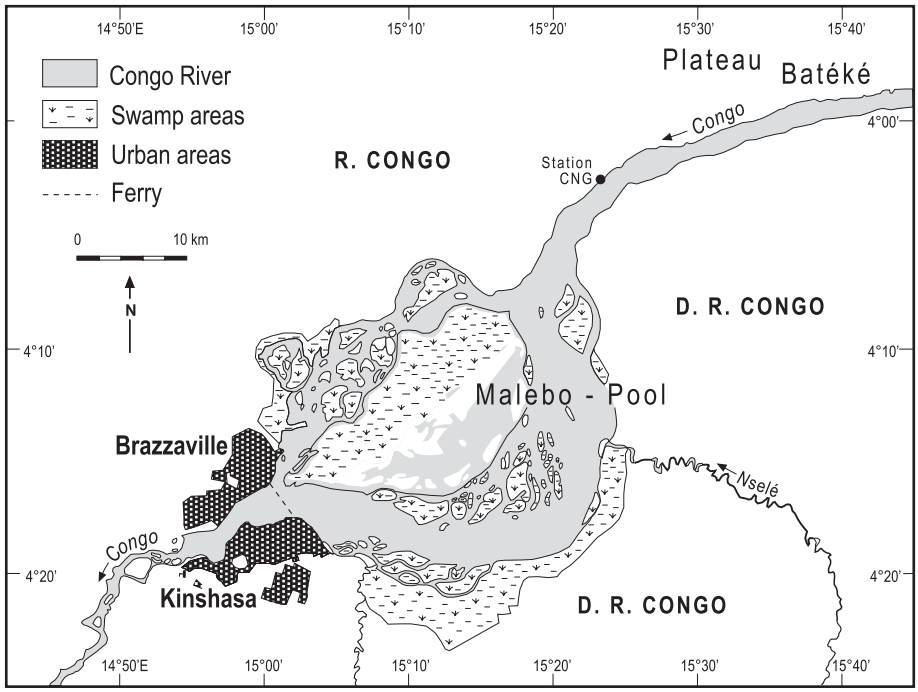

Figure 14.7 Malebo Pool in the western part of the Congo Basin forms a remnant of a Pliocene Congo lake dammed by the uplift of the Atlantic Rise (redrawn and modified from IGN topographic map 1 : 200 000, SB-33-IV, Brazzaville, République Populaire du Congo, Paris, Brazzaville, 1948–78, partly revised 1981)

From Matadi to the Atlantic (134 km) the Congo River becomes part of an estuarine coast. The river's bed is narrow and incised up to 250 m into outcropping quartzites. This section shows a winding pattern with huge whirlpools (Devil's Cauldron); in places shallow water and rocky outcrops interrupt navigation for ocean-going vessels. Further downstream, the Congo widens up to 19 km with numerous active, huge sand bars that require regular dredging to keep a navigable channel open. At Boma, still 100 km from the mouth, the Congo becomes a tidal river with an average tidal range of 140 cm (Bultot, 1971). Some 70 km further downstream, the Congo's deep sea fan and submarine Plio-Pleistocene (?) canyon extend into the river mouth. The latter can be followed down to 3000 m water depth on the continental shelf. Its sediments can be identified up to 1000 km away from the coast. The Congo River finally enters the Atlantic Ocean between a shallow cliff coast near Banana (DR Congo) and a long sand bar at Sharks Point (Angola). The freshwater surface plume of the river can be recognized up to 800 km away from its mouth, and a huge sediment-bearing plume stretches up to 20 km into the Atlantic (Jansen *et al*., 1984).

Table 14.2 Hypsometric structure of the Congo Basin

Elevation (m asl)	Percentage of drainage area (location)
0–300	0.51 (coastal plain)
>300–500	26.64 (central Congo Basin)
>500–1000	49.89 (Asande Rise, Atlantic Rise)
>1000–2000	22.18 (Angola, Shaba Highland, Lunda Rise)
>2000–3000	0.77 (Western Rift slopes, Mitumba)
>3000–5000	0.01 (Mitumba Mountains, Ruwenzori)

Source: modified from Robert, 1946.

14.3 GEOLOGY AND GEOMORPHOLOGY OF THE CONGO BASIN

14.3.1 The Central Congo Basin

The central basin is generally flat, between 300 and 500 m in elevation (Table 14.2, Figure 14.4), and covered by unconsolidated Cenozoic sediments. The basin is framed by extensive elevated (500–2000 m) flat to hilly landforms (rises), geologically consisting of deeply weathered Mesozoic and Precambrian rocks. The drainage net in the centre gives the appearance of a counterclockwise convergence.

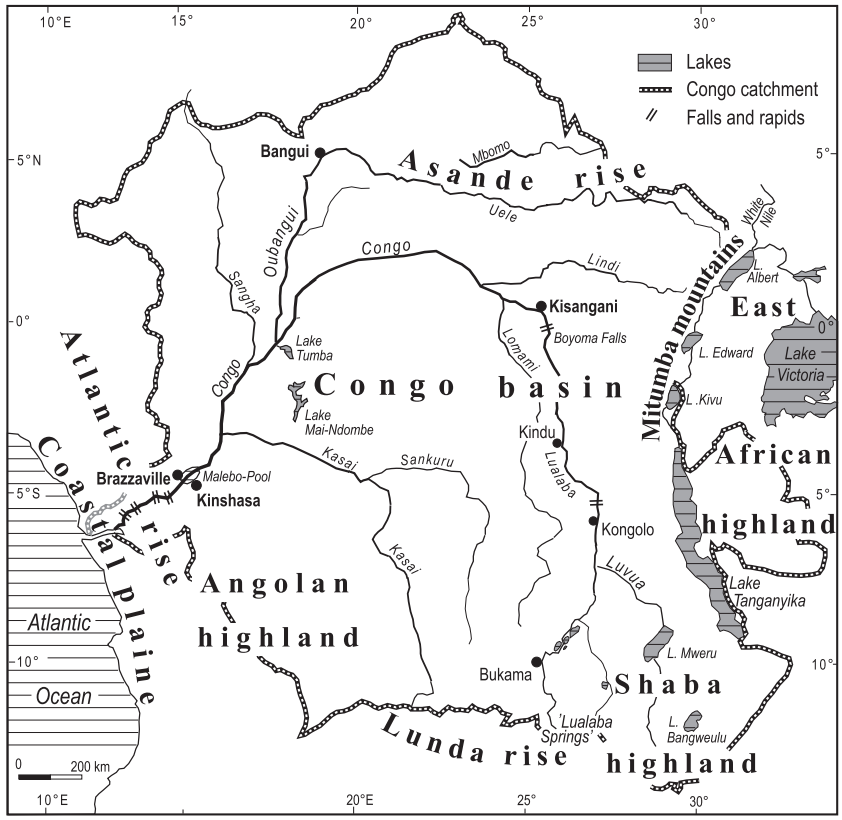

Figure 14.8 General landforms of the Congo Basin

The shape of the approximately 1000 km wide central Congo Basin is round to oval (Figures 14.1 and 14.4), which earlier gave rise to the hypothesis of a former, enormous, so-called 'Congo Lake' (Cornet, 1894). Subsequent more detailed studies on the sediments within the basin, however, indicated deposition under nonlacustrine, temporarily semi-arid environmental conditions (de Ploey *et al*., 1968; Republique du Zaire, 1974). Sediments overlying the Congo Craton and building up this basin are mainly of Carboniferous to Permian or Mesozoic age. The basin was originally a nearly horizontally level area. Later, it was deepened by epeirogenic crustal movements and subsequent deformation while progressively more sediment was deposited over it (Lepersonne, 1978; Petters, 1991). The widespread sandy to clayey 'Lualaba-Lubilash' strata correspond to the Mesozoic South African 'Karoo sequence' (Veatch, 1935), more recently known as the Karoo Supergroup. In the eastern Congo Basin, close to Walikale (Figure 14.1), glacial deposits such as tillites and dropstones derived from drifting icebergs of the Permo-Carboniferous 'dwyka' glaciation outcrop at the surface (Série de Lukuga, Série de Walikale, W1, Figure 14.9; Boutakoff, 1948; Runge, 2001). Renier (1951) identified imprints of Permian coal forming gymnosperms of the genera *Gangamopteris* and *Noeggerathiopsis* (Série de Walikale, W2, W4) within dark laminated clays and soft schists.

Deep drillings at Dekese (1856 m) on the southern limit of the basin, at Samba (2039 m) (République du Zaire, 1974), and the oil exploration site Mbandaka-I (4350 m) (Figure 14.1), provide an indication of the morphology and total sediment thickness of the Congo Basin. At Mbandaka, Permian to Carboniferous sediments (Série de Lukuga) are at 2100 m depth, whereas east of Kisangani these formations outcrop (Figure 14.9). Precambrian schists and quarzitic sandstones occur below 2887 m. The granitic basement of the Congo Craton lies below 4350 m (REGIDESO, 1985). Host bedrock sediment thickness throughout the basin can be expected to vary between 1000 and 4000 m.

The flat to undulating part of the basin in the centre has been covered by rain forest since a period of severe aridification during the Last Glacial Maximum (LGM) when the

Figure 14.9 The Lowa River, a right bank tributary to the Congo-Lualaba which drains the western Central African Rift slopes. The photo shows low discharge in July 2002 with outcropping Permo-Carboniferous sandstone and claystone (Série de Walikale). Photograph by J. Runge

forest was replaced by savanna vegetation (Runge, 2001). At the surface, Tertiary and Quaternary sediments, clayey and sandy alluvium of fluvial origin predominate and reach a thickness of 90–200 m (Evrard, 1957; REGIDESO, 1985). The low central part of the Congo Basin (300–500 m asl) or *cuvette centrale* in French, is surrounded by elevated landforms known as rises (swells) and tectonic structures (including grabens). The basin is flanked by the Asande Rise to the north, the Atlantic Rise to the west, the Angolan and Shaba Highlands to the south, and the Western Rift slopes to the east (Figures 14.4 and 14.8).

14.3.2 The Asande Rise

An almost imperceptible transition from the interior basin to the north takes place along the Asande Rise located north of the Equator. The vast ferruginous and 'cuirassed' (in Central Africa known as *lakéré*) planation surface is mainly in the catchment of the Oubangui River (Figure 14.1). Towards north it carries wooded savanna, and south of it a mosaic of high woody biomass and patches of tropical forests in an area of 1600–1800 mm annual rainfall (Bultot, 1971; Boulvert, 1996).

The Asande Rise is characterized by Precambrian magmatic and metamorphic rocks with extended greenstone belts. Radiometric age determinations within the Upper Congo (Zaire) granitoid massif at Moto and at Matundu provided ages of 2840 (Cahen *et al.*, 1984) and 3200 million years (Lavreau, 1982). Within the Central African Republic, the 75 000 km^2 Mbomou amphibole-gneiss complex represents one of the oldest units (3200–2900 million years) of the Congo Craton (Lavreau, 1982). The margins of the slightly upwarped Mbomou Gneiss are covered by weathering-resistant Proterozoic sediments like metamorphosed limestones and quarzitic sandstones (Boulvert, 1996). The northern tributaries of the Oubangui (e.g. the Kotto River) cross these fractured sandstone escarpments in numerous waterfalls such as the Chutes de Kotto (Mainguet, 1972; Runge, 2001).

14.3.3 The Atlantic Rise

The western limit between the Congo Basin and the Atlantic Ocean, the Atlantic Rise, is an uplifted composite mountain range associated with the West Congo orogen that consists of at least four episodes of mountain-building. It stretches almost parallel to the coast through Gabon, Congo and Angola for more than 1300 km. Its west–east extension varies between 150 and 375 km. The oldest tectonically stressed granites, charnockites, mixtites, quartzites and schists of the rise are supposed to be linked to the Eburean orogeny (locally called Kimezian) dated by Cahen *et al*. (1984) to 2088 million years. A later period of plate collision and marginal deformation of the western Congo Craton (Cahen *et al.*, 1984) occurred during the Middle (1500–1400 million years, known as Zandinian) and in the Upper Proterozoic at 1030 Ma (Mayumbian). At the transition to the Palaeozoic, between 734 and 450 million years, the existing structures were refolded by pan-African orogenesis. Subsequently, the morphologically outstanding Palaeozoic mountain chain was totally eroded to resemble a peneplain during the Gondwana times. At the outset of the Tertiary, mainly from the Oligocene to the Miocene (35–20 million years), epirogenetic movements again caused the geomorphological accentuation of this zone of already multiple-folded belts. Later, probably during the Pliocene, the Atlantic Rise seems to have dammed the course of the Congo River leading to the formation of a large lake in the western Congo Basin that nowadays still survives as the Malebo Pool (Figure 14.7). It has been argued that two other inland lakes some 250 km northeast of the Pool at Brazzaville and Kinshasa (Lake Tumba and Lake Mai-Ndombe, Figure 14.1) could have been part of this Pliocene Congo lake. However, their outline and morphology suggest that these lakes are more due to submergence of fluvially formed lows, and less of a primary damming by the uplift of the Atlantic Rise (Veatch, 1935; Wiese, 1980; Runge, 2001).

14.3.4 The Angolan and Shaba Highlands

The change in landscape from the southern Congo Basin to the Angolan and Shaba Highlands (Lunda Rise, Figure 14.4) is more strongly expressed morphologically than the transition to the northern Asande Rise. Metamorphosed, slightly upwarped basement rocks, known as the Kasai Shield (Cahen and Snelling, 1966), outcrop at an elevation of 1000–1800 m between 7°–11° S and 22°–24°30′ E. Rock ages vary from the Late Archaic to the Early Proterozoic. The ages of regional granite, gneiss, migmatite and gabbro were radiometrically determined to be 3400, 2820 and 2000 million years (Cahen and Snelling, 1966; Cahen *et al.,* 1984). The subsequently intruded 'Lulua-Complex' containing over 6000 m thick metasediment and also basic lava has radiometric ages between 1155 and >1400 million years (Cahen *et al.*, 1984). Further east, towards the Shaba Highlands, folded Palaeozoic (Silurian to Carboniferous) sediments occur, rich in raw materials (especially copper) and known as the Katanga-System (Robert, 1940). The Angolan and the Shaba Highlands are characterized by alternating wet and dry seasons and 1200–1500 mm of annual rainfall. The average temperature is several degrees lower than that within the central Congo Basin because of the elevation, and open savanna woodland is common. To the south, denser Miombo forests with grasslands, typical of river headwaters or dambos, characterize the landscape.

14.3.5 The Western Rift Rise

Upwarping and transform faulting between Central and Eastern Africa during the Miocene (25 Ma), favoured the development of fracture tectonism, strong uplift and volcanic eruptions in the remote parts of the eastern Congo Basin. The evolution of the Western or the Central African Rift Valley caused a rearrangement of local catchments, base levels and of drainage directions. There is evidence for an early Pliocene lake (Lake Obweruka) 550 km long, expanding in a north–south direction (Pickford *et al*., 1993), which was subsequently separated into today's smaller freshwater lakes of Kivu, Edward, and Albert. This has to be seen in the context of a continent-wide shift of divides between East and Central Africa (Schlüter, 1997).

In the eastern Congo, within the Ituri and the Kivu provinces, the granite-dominated Mitumba mountain chain was uplifted to a height of over 3000 m. This higher local relief resulted in a high gradient and erosivity that changed the character and the influx of right bank tributaries to the Congo-Lualaba drainage system. Rift tectonics on westerly exposed slopes towards the Congo Basin resulted in an increase in annual precipitation to 2400 mm (Runge, 2001). The eastern Congo Basin carries dense tropical rain forest between 400 and 1400 m (Figure 14.9).

14.4 EVOLUTION OF THE CONGO RIVER

The Congo-Lualaba River bends in a wide curve that crosses the Equator twice. Initially it flows in a south–north direction. Then from Kisangani downstream it curves northwest and then west. The final stretch is a southwesterly curve. The basin drainage net shows a convergence of the tributaries on the main river, the entire net curving in a counterclockwise direction (Figure 14.2). Many of the tributaries join the main river in the Lake Tumba, Lake Mai-Ndombe, and Malebo Pool area (Figure 14.1).

The south to north orientation of the streams on the Angolan Highland, the Lunda Rise, and the Shaba Plateau indicates that the original drainage direction of the proto-Congo was from south to north and then slightly northwest towards the current Lake Chad Basin. The Asande Rise of the north, which underwent planation many years ago, was not morphologically pronounced until early to mid-Tertiary, and the Congo used to follow a northwesterly direction, approximately along the Kisangani–Bumba line (Figure 14.1). No morphological evidence has been produced demonstrating the route of the proto-Congo. Even satellite imagery shows no signs of a previous but no longer active river channel, probably due to intense and continued terrestrial weathering and denudation, which removed evidence of fluvial morphological remnants like palaeochannels and alluvia from the surface. Perhaps further information on this topic might be revealed by more detailed studies on possible fluvial deposits of a proto-Congo system within the widespread iron crusts (*cuirasse* or *lakéré)* on the Asande Rise (Boulvert, 1983, 1996).

Another hypothesis suggests that the palaeo-Congo partly followed the current drainage channels on the Asande Rise (Figure 14.8), occupying the course of the present upper to middle part of the Oubangui River between Mobaye and Bangui (Figure 14.1). A Precambrian graben trending in a north-west direction close to Bangui (Cornacchia and Giorgi, 1986) could have acted as a gateway for this large river, allowing it to flow towards the Lake Chad Basin.

The altering of the course of the Congo, first to a western and then a southwestern direction, was probably initiated during the Miocene–Pliocene transition, when strong tectonic movements with rifting and volcanism on the eastern margin of the Congo Basin triggered the morphologic accentuation of the previously shallow rises by their significant uplift and the subsidence of the central basin. The uplift of the western Atlantic Rise against the flow of the river dammed the Congo, building up a shallow interior lake of Malebo Pool (Figure 14.7).

The explanation as to how the Congo managed to reach the Atlantic Ocean for a second time is controversial. As

the lower course of the Congo is relatively rectilinear, Cahen (1954) proposed a capture of the lake by a pre-existing antecedent valley created by tectonic activity, which was subsequently reactivated to drain the lake. A second hypothesis (Veatch, 1935) assumed a regressive, two-stage erosion sequence moving inland from the Atlantic coast, cutting through all of the Atlantic Rise and finally capturing and draining the interior lake. As the rocks of the Monts Cristal are resistant to fluvial erosion and the available time to cut through the structure was relatively short, it seems that Cahen's hypothesis is more likely than Veatch's suggestion. In any case, the capture and subsequent outflow of the Pliocene Congo Lake was a single, high energy geomorphic event.

14.5 THE FLOW REGIME OF THE CONGO

Hydrological data on the Congo River are often limited to documents that date back to the colonial times and for a brief period after that (Bultot, 1971). Many Congolese gauging stations, mainly those in rural areas, were abandoned after independence. However, research institutions like ORSTOM/IRD continued hydrologic measurements at several locations, so certain long-term records are available (Olivry and Boulègue, 1995; Laraque *et al.*, 2001).

The seasonal runoff pattern of the Congo River with contributing discharges from its tributaries is strongly determined by (1) annual rainfall characteristics of this basin located across the Equator and (2) the complex environmental nature of the basin as described in the two previous sections. The source region in the Shaba Highland (Figure 14.8) shows a seasonal wet and dry regime with an average annual rainfall of 1200 mm. The middle and parts of the lower Congo Basin (draining between Kindu and Mbandaka on the river) receive 1800–2400 mm of rainfall a year with almost no dry season (Bultot, 1971). Annual surface runoff was estimated by Bultot (1971) to be 900 mm for the basin's centre and 200–400 mm for the source region of the river. Average annual rainfall, evaporation, and surface runoff for the Congo catchment was calculated to be 1527, 1196 (78% of the rainfall), and 331 mm (Bultot, 1971).

Therefore, two flow regimes can be identified for the basin, depending on geographical location (Bultot, 1971; Breitengross, 1972). A clear single-peak annual discharge distribution occurs for the streams originating in semi-humid regions with contrasting wet and dry seasons. North of the Equator, the Oubangui River shows a marked maximum discharge between September and November, and a strongly reduced discharge between February and April (Runge and Nguimalet, 2005). To the south, below 5° S, the Congo-Lualaba, Luvua and Luapula Rivers show a single peak but in different period (Figure 14.10), the peak in discharge occurring between March and May and the significantly lower discharge between September and November (Bultot, 1971). The second type of flow regime has a double discharge peak. This runoff pattern is shown by gauging stations in the central Congo Basin, such as at Kinshasa and Brazzaville. As the Congo's catchment consists of both seasonal and equatorial climates, the flow regime of the main river is more complex, collecting runoff from different sources. The average annual discharge of the Congo (Figure 14.11), measured over 27 years (1932–1959) at Kinshasa, is 46 200 $m^3 s^{-1}$ (Bultot, 1971). The highest discharge recorded was 64 900 $m^3 s^{-1}$. High discharges occur between November and December–January when the rainy season runoff from the north arrives via the Oubangui to reach the confluence with the Congo south of Mbandaka. From April to June the river's discharge increases due to the augmented flows from the southern basin (Figure 14.10). This causes a smaller, second discharge peak at Kinshasa. A low discharge period is between July and August (Figure 14.11) with a minimum discharge (Q_{min}) of 23 500 $m^3 s^{-1}$ at Kinshasa (Bultot, 1971). Apart from the influx of discharge arriving from the northern and southern catchment areas, regular and high tropical rainfall (1800–2400 mm per year) falls on the central Congo Basin significantly reducing the variability in flow (Breitengross, 1972).

The spatiotemporal relationship between the geographical location of the catchment and the total size of the respective drainage area is illustrated in Figures 14.10 and 14.11. Differences in annual discharge of the sub-catchments such as the single and two-peaked drainage pattern at Kinshasa-East (3 747 320 km^2 draiange area), Kisangani (974 330 km^2), Kindu (810 440 km^2) and Bukama (63 090 km^2) are clear when plotted on a logarithmic scale (Figure 14.11). Annual variability of the Congo's discharge at Kinshasa is low, Q_{max}/Q_{min}= 2.8, but it is 11.9 in the upper Lualaba upstream from Kindu. Even more significantly, this ratio rises to 23.6 upstream from Bukama. The headwaters obviously experience high runoff variability (Figure 14.11).

14.6 SOLID, SUSPENDED, AND DISSOLVED LOAD

Early estimates of the Congo's suspended and dissolved load were not systematically determined. Individually chosen locations along the river and the use of surface water samples resulted in a wide range of values. For the entire basin, Meybeck (1976) calculated annual denudation rates of 13.2 t km^{-2} and 11.7 t km^{-2} for solid and dissolved materials respectively. This computes to an annual total of 47 million tonnes of suspended and dissolved load discharged by the Congo in the Atlantic. Using geochemical

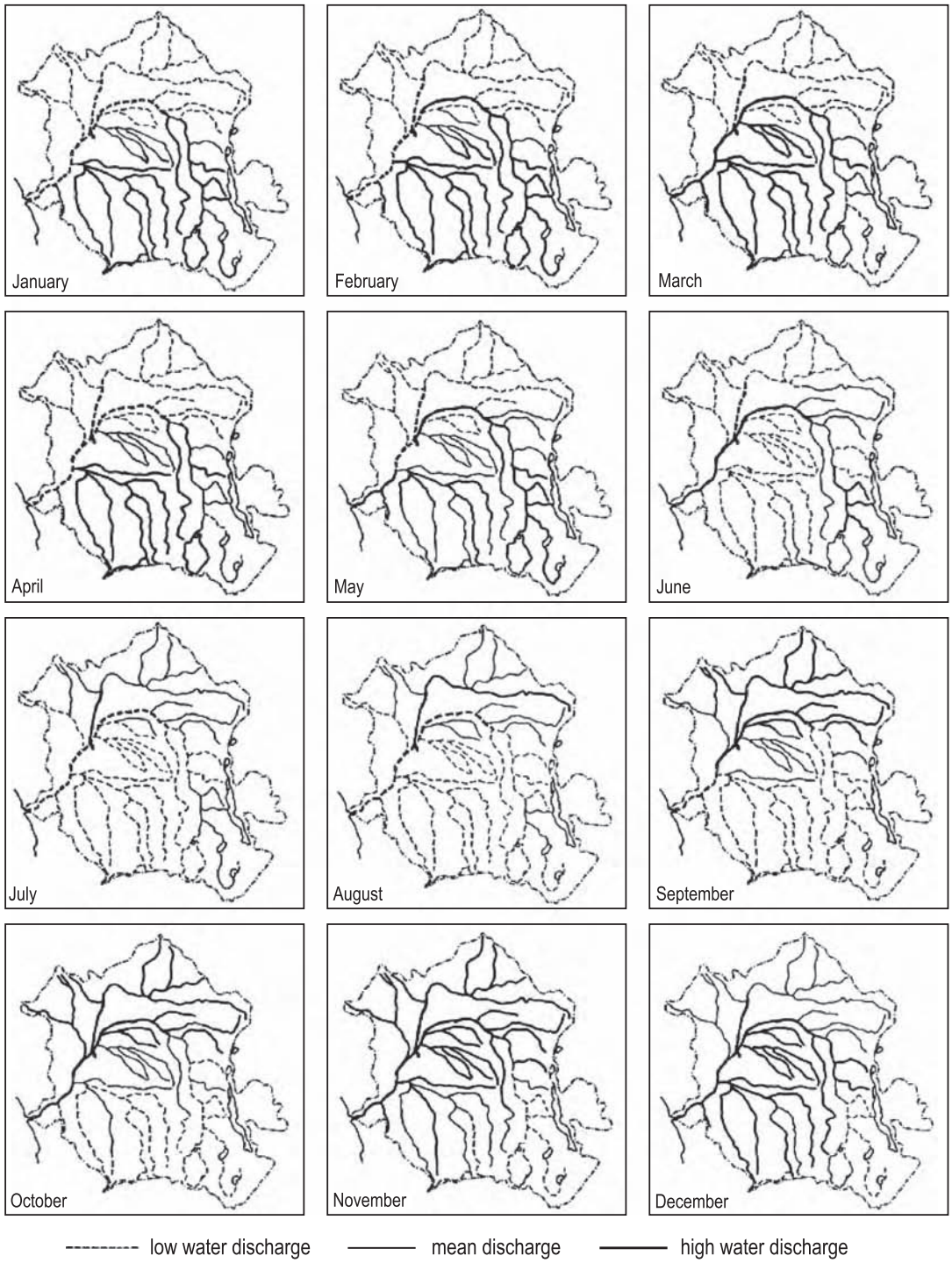

Figure 14.10 Hydrological regimes in the Congo Basin from January to December. Reproduced from Mitteilungen der Geographischen Gesellschaft in Hamburg, J.P. Breitengross, 60, pp. 18–19, 1972, with permission from Geographic Society in Hamburg

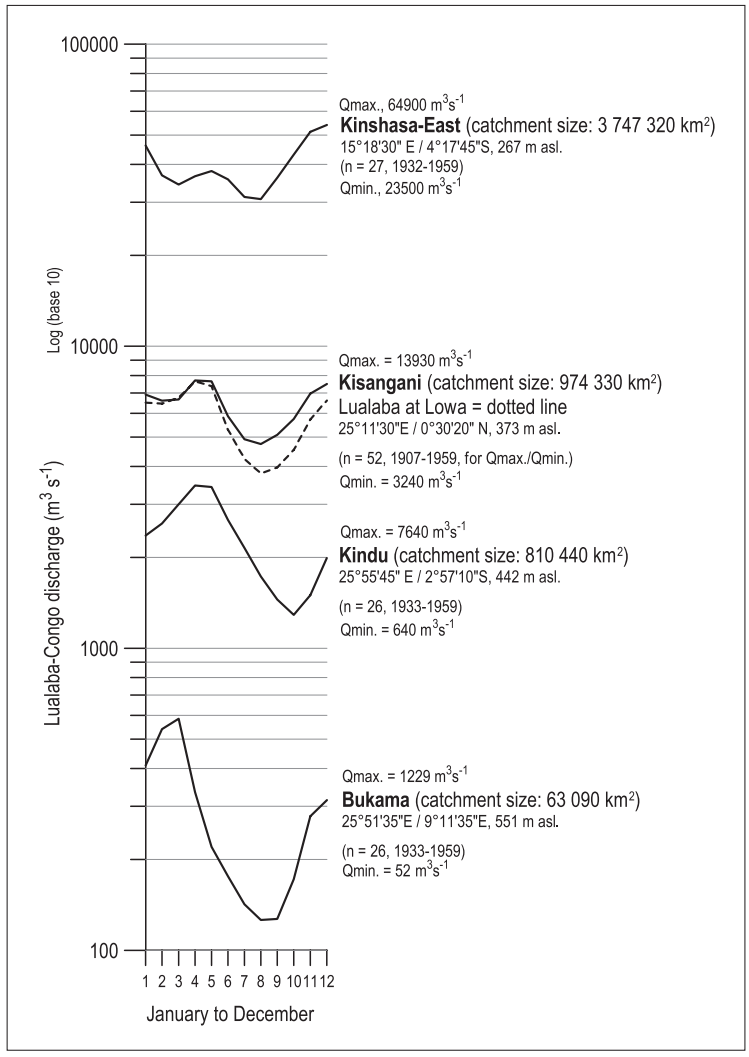

Figure 14.11 Mean annual discharge of the Congo River for selected gauging stations (source: Bultot, 1971)

techniques, Probst *et al*. (1992) calculated a total of 39–44 million tonnes of dissolved load for the Oubangui and the Congo at Brazzaville between 1987 and 1989. Regular measurements were carried out by French researchers in the Republic of Congo from 1987 to 1992 (Station CNG, Figure 14.7). Laraque *et al.* (1995) estimated an average annual Congo discharge of 37 700 $m^3 s^{-1}$ at Brazzaville and a total fluvial sediment and solute output from the Congo Basin of 91.8 million tonnes. This is twice the estimate of others. This yearly load is made up of 7.9 million tonnes of sand, 22.8 of silt and clay, and 61.1 of dissolved material.

Particle diameters of suspended load show a median range between 0.16 and 3 µm (fine clay to fine silt). The coarser silt fraction (up to 50 µm) contains abundant organic fragments. The content of organic matter in the Congo River is high during both low and high discharges (Delaune *et al*., 1995). The high discharge peak of organic matter may be caused by bank erosion in the rainy season. The suspended material also contains significant amounts of kaolinite, amorphous silica, phytoliths, illite and iron hydroxides. An influx of smectites is present (Delaune *et al*., 1995). The average annual concentration of the

Congo's suspended sediment load is 76.2 mg l^{-1}, rather low when compared with other large rivers (Laraque *et al.*, 1995).

Most of the dissolved load of the Congo is either silica or bicarbonate. Mean pH value of the Congo water is 7.01 (standard deviation 0.56). Electrical conductivity of 37.5 mS at Brazzaville correlates well ($r^2 = 0.83$) to the overall content of SiO_2 including all other cations and anions. The silica content (average values 10 mg l^{-1}) is positively correlated to discharge but is statistically less significant. Other major elements such as Na, Mg, Ca and HCO_3 demonstrate a significant negative correlation to discharge (Sondag *et al*., 1995). The Oubangui River that partly drains Precambrian limestone areas contributes a large proportion of the carbonates to the water of the Congo.

Basinwise, the Congo is an exceptionally clean system. The long-lasting political and economic stagnation in the former Republic of Zaire (now the Democratic Republic of Congo) allowed only a few active industrial centres to continue, resulting in almost no seriously degraded ecosystem along the river's banks. The Congo remains a surprisingly unpolluted river (World Bank, 2002). Waste water, received from urban and industrial areas of Kinshasa and Brazzaville, flows through the Lower Congo over the relatively short distance of 400 km to the sea. The turbulent flow of the Congo along this segment, caused by numerous falls, rapids and cataracts between Kinshasa and Matadi (Figure 14.3) raises the self-purification capacity of the stream.

14.7 THE CONGO MOUTH AND THE SUBMARINE CANYON

Some 30 km before the Congo enters the sea at Banana, the river deepens and transforms into an east–west oriented, elongated submarine valley, an enormous canyon deeply incised into the continental shelf of western Central Africa. Stallibrass (1887) and Buchanan (1887) were the first to report the existence of this geomorphic feature close to the Congo mouth. During 1925–1927, the German research vessel 'Meteor' explored the shape of the Congo Canyon in more detail (Veatch and Smith, 1939). Recent high resolution bathymetric data (GEBCO Digital Atlas, 1994–1997) allow a detailed geomorphic study (Figure 14.12).

The submarine canyon of the Congo is over 400 km long, down to a water depth of 3000–3200 m. About 130 km of the canyon's channel cuts through the continental shelf, where it reaches depths between 480 m (Banana) and 1000–1200 m at the outer shelf margin (Figure 14.12). An early hypothesis proposed that the canyon was formed by subaerial fluvial erosion of the Congo during glacial times when the sea level was low. Since during the LGM sea level was only 110–130 m lower than present, the eustatically initiated modification of the river's base level

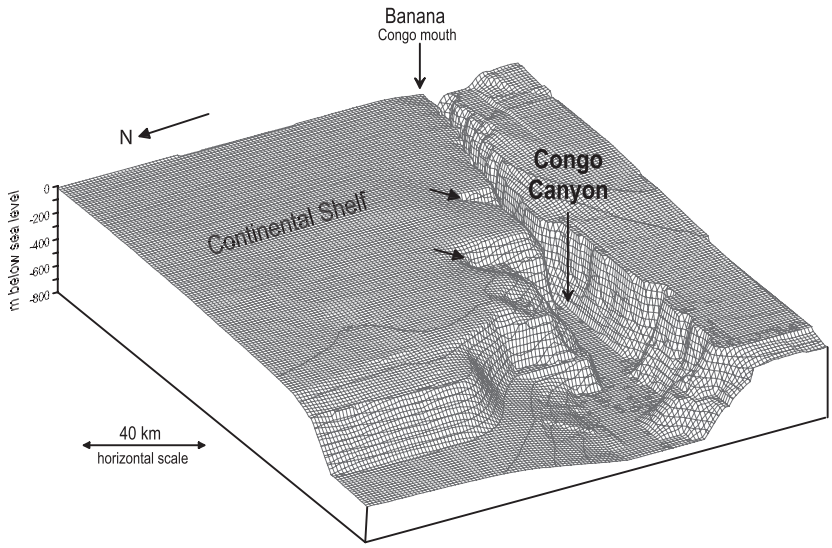

Figure 14.12 Digital elevation model (DEM) of the Congo submarine canyon west of Banana (isobaths from GEBCO Digital Atlas, 1994–1997; design J. Runge)

was not sufficient to form such a canyon. Also the 'collapse' of the Pliocene Congo Lake due to an early Quaternary capture scenario may not have been effective enough to erode the submarine valley and canyon.

The canyon of the Congo is strikingly straight without any submarine tributaries, indicating a possible tectonic origin. Especially noteworthy are some channels at right-angles to the trend of the canyon, north–south stretching sections of obviously downslope sagged material that strongly suggest gravity-based processes (see arrows in Figure 14.12). Submarine sliding was involved, probably triggered by local tectonic activities. Subsequently, turbidity currents on the steep continental shelf and slope could have initiated the development of this large submarine geomorphic form. Not only is there a natural predisposition of the Atlantic shelf region near the Congo mouth to tectonism, but the annual fluvial solid load of over 30 million tonnes deposited on the shelf (section 14.6) may also have encouraged tectonic activities and the formation of the canyon (Bourgoin *et al.*, 1963; Giresse, 1978, 1980).

14.8 THE CONGO RIVER AND ITS ECONOMIC IMPORTANCE

From a natural resource perspective the Democratic Republic of Congo is a potentially rich country. However, the Gross National Product (GNP) for 2001 is only $3.85 billion, corresponding to a mean annual income of $85 per person. Foreign debts of the Congo came to $9606 billion in 2002 (Indongo-Imbanda, 2003). The industrial concentrations of the Democratic Republic of Congo are located in three areas: the capitals of Kinshasa and Brazzaville at Malebo Pool, the urban centre of the eastern basin Kisangani, the mining region of Shaba (Katanga) in the southeast (Figure 14.1).

For the two industrial hubs on the Congo's banks, the stream and its tributaries provide a large inland navigation waterway with a total length of about 15 000 km (Wiese, 1980). Due to seasonally low discharge of the smaller tributaries, only part of the complete river network can be used for year-round navigation. The main operators of river steamers between Kinshasa-Brazzaville and Kisangani on the Congo, between Kinshasa and Ouesso on the Sangha, and to Bangui in the Central African Republic along the Oubangui River, are government enterprises and smaller privately owned shipping companies. The biggest navigation enterprises are the ATC (Agence Transcongolaise de Communications) and the SOCATRAF (Société Centrafricaine des Transport Fluviaux), who in 1989 transported almost 70 % of all goods on the Congo, Sangha and Oubangui (Mengho, 1994). The traditional means of waterway transport used by most of the riverside people is still the canoe (pirogue). Because few all-weather roads exist within the Congo Basin, the use of canoes for transporting goods like charcoal, wood, palm-oil kernels, cassava, bananas, and cotton is often the only way to link remote villages to towns and cities.

The economic use of the Congo River for navigation is locally restricted by falls and rapids. The non-navigable stretch of 350 km between Matadi and Kinshasa (Figure 14.3) is a major barrier that prevents the direct access of ocean-going vessels to Kinshasa – a significant disadvantage for infrastructure and economy. The estuarine ports at Matadi, Boma and their associated railways take over the function of a deep sea harbour for Kinshasa. Although the new harbour at Banana was originally planned as a more effective hub for goods going to Kinshasa and to the interior of the Congo Basin, it functions more as a transit port for ocean-going vessels, and is not really the gateway to the Congo.

The use of the Congo River for transporting goods is strongly dependent on the reliable operation of railways, which circumnavigate falls and rapids. The railway network in the former Belgian Congo measured 4644 km in 1945 (Robert, 1946). By 1994, it expanded to 5138 km, which rendered possible a transport combination of inland waterways and railways. During the last half-century some of the Congolese railway lines have been abandoned. Those still operating are often in bad condition, and can therefore only provide a restricted contribution to the economic growth of the Democratic Republic of Congo.

The Congo River has a large hydroelectric potential. Almost 91 % of the Democratic Republic of Congo's electricity comes from hydropower plants, only 9 % being generated by the combustion of oil and coal. The total energy-producing capacity reached 4.3 GW in 1997 (Energy Information Administration, 2003). The biggest hydropower facility is at Inga Falls, located some 40 km upstream from Matadi (Figure 14.3). The Inga hydroelectric facility was originally set up in 1972 (Inga I). At that time it was planned to extend the capacity of the Inga powerplant progressively until the end of the twentieth century. The long-running civil war and the economic crisis in the Congo prevented this mega-project from completion. However, recently there have been new initiatives to restart the building of the 2000 MW Inga II plant and the 40 000 MW 'Grand Inga' hydropower facility which would cost about $6 billion. When finished, the site will consist of 52 separate electricity generating units which will have a combined capacity 10 times greater than Lake Aswan in Egypt. Such a hydroelectric scheme in the Congo would be utilized primarily for exporting power to other African regions (Pearce, 2002). Generation facilities at Kinshasa and local energy production in the eastern

Kivu region have also been planned (Energy Information Administration, 2003). On a basin-wide perspective, however, hydroelectric technology is still underdeveloped in spite of Congolese government initiatives.

14.9 CONCLUSION

The Congo Basin and the Congo River together possess significant natural resources. However, a long period of mismanagement, lack of information, and continuous political crisis (civil war) together have hindered any economic growth within this potentially rich Central African region. Currently, apart from generation of hydroelectricity, the Congo River is used mainly in the area of infrastructure and transport. As there is no direct access to the sea because of rapids and falls in the lower course, a well-organized and effective railway network is as important as good river vessels. Frequent accidents involving river steamers and ferries with hundreds of victims, as for example happened in March, May and November of 2003, indicate that there is still much work to do to guarantee passengers safety on this traditional Central African highway.

Lack of industrial and agricultural activity along its banks still keeps the Congo River relatively unpolluted. The amount of suspended sediment is low. In future, if increased economic growth is to contribute significantly to regional welfare, such development should arrive with environmental sustainability. For the rain forest-covered basin of the Congo River, it will be of special importance to manage energy, water, wood, and other natural resources in an integrated fashion to ensure their long-term sustainability (World Bank, 1997).

ACKNOWLEDGEMENTS

I would like to express my gratitude to Mrs Ursula Olbrich, Frankfurt, who designed the figures for this paper. My sincere thanks go to Gerry Garland, Avijit Gupta, Ellen Wohl and Jamie Woodward, who reviewed the manuscript and supplied many helpful comments to improve this contribution.

REFERENCES

Boulvert Y. (1983) Carte Pédologique de la République Centralafricaine à 1 : 1.000.000. *ORSTOM Not explic* 100: 1–126.

Boulvert Y. (1996) Etude géomorphologique de la République Centralafricaine. Carte 1 : 1.000.000 en deux feuilles ouest et est. *ORSTOM Not explic* 110: 1–258.

Bourgoin V., Reyre D., Magloire P. and Krichewsky M. (1963) Les canyons sous-marins du Cap Lopez. *Cah océan* 15: 372–387.

Boutakoff N. (1948) Les formations glaciaires et postglaciares fossilifères, d'âge permo-carbonifère (Karroo inférieur) de la région de Walikale (Kivu, Congo belge). *Mém Inst Géol Univ Louvain* 9, 2: 1–122.

Breitengross J.P. (1972) Saisonales Fliessverhalten in großflächigen Flusssystemen. Methoden zur Erfassung und Darstellung am Beispiel des Kongo (Zaire). *Mitt Geogr Ges Hamburg* 60: 1–92.

Buchanan J.Y. (1887) On the land slopes separating continents and Ocean basins especially those on the west coast of Africa. *Scot Geol Mag* 3: 217–238.

Bultot F. (1971) Atlas climatique du bassin congolais. *Publ Inst Nat étud agro Congo (INEAC, Rép. Démocrat. Congo)*: 1–4.

Bultot F. and Dupriez G.L. (1987) Niveau et débits du fleuve Zaire à Kinshasa (Régime-Variabilité-Prévison). *Acad Roy Sc d'Outre-Mer Cl Sc Techn Mém 4* 6, 2: 1–49.

Cahen L. (1954) *Géologie du Congo Belge*. H. Vaillant Carmanne, Liège, 1–450.

Cahen L. and Snelling N.J. (1966) *The Geochronology of Equatorial Africa*. North-Holland Publishing Company, Amsterdam, 195 p.

Cahen L., Snelling N.J., Delhal J. and Vail J.R. (1984) *The Geochronology and Evolution of Africa*. Clarendon Press, Oxford, 512 p.

Caputo R. (1991) Lifeline for a nation – Zaire River. *Nat Geogr Mag* 180, 5: 5–35.

Cornet J. (1894) Les formations post-primaires du bassin du Congo. *Soc Geol Belge Mém* 21: 251–258.

Cornacchia M. and Giorgi L. (1986) Les séries Précambriennes d'origine sédimentaire et volcano-sédimentaire de la République Centrafricaine. Données nouvelles sur la Géologie de la Région de Bangui. *Mus Roy Afr Centr Ann Sér 8, Sc Géol* 93: 1–33.

Delaune M., Jouanneau J.M. and Harle J. (1995) Granulometrie et mineralogie des suspensions particulaires des fleuves Congo et Oubangui. In: *Grands bassins fluviaux périatlantiques: Congo, Niger, Amazone* (J.C. Olivry and J. Boulègue, Eds.). *Coll Sém* 69–82, ORSTOM, Paris.

de Ploey J., Lepersonne J. and Stoops G. (1968) Sédimentologie et origine des sables de la série des sables ocre et de la série des 'grès polymorphes' (système du Kalahari) au Congo. *Geol Wetens* 61: 1–72.

Devroey E.J. (1935) Le problème de la Lukuga. Exutoire du Lac Tanganika. *Inst Roy Colon Belge Sec Sc Techn Mém Coll 8* I, 1: 1–127.

Devroey E.J. (1939) Le Kasai et son bassin hydrographique. Goemaere, Imprimeur du Roi, Bruxelles, 339 p.

Devroey, E.J. (1951) Notice de la carte des eaux superficielles du Congo belge et du Ruanda-Urundi. *Acad Roy Sc Outre-Mer* 340: 1–7.

Energy Information Administration (2003) http://www.eia.doe.gov (20.11.2003).

Evrard P (1957) Les recherches géophysiques et géologique et les travaux de sondage dans la Cuvette congolaise. *Acad Roy Sc Colon Belge Mém 8 NS VII fasc* 1: 3–62.

GEBCO Digital Atlas (1994–1997) British Oceanographic Data Centre. Data on CD ROM, Birkenhead, UK.

Giresse P. (1978) Le contrôle climatique de la sédimentation marine et continentale en Afrique Centrale Atlantique à la fin du Quaternaire. Problèmes de corrèlation. *Palaeogeogr., Palaeoclim., Palaeoecol.* 23: 57–88.

Giresse P. (1980) Carte sédimentologique du plateau continental du Congo. *ORSTOM Not explic* 85: 1–24.

Iliffe J. (1995) *Africans. The History of a Continent*. Cambridge University Press, Cambridge, 435 p.

Indongo-Imbanda I. (2003) Kongo-Kinshasa. http://www.kongo-kinshasa.de (10.11.2003).

Jansen J.H.F., Van Weering T.C.E., Gieles R. and Van Iperen J. (1984) Late Quaternary oceanography and climatology of the Zaire-Congo fan and the adjacent eastern Angola basin. *Netherl J Sea Res* 17: 201–249.

Laraque A., Bricquet J.P., Olivry J.C. and Berthelot M. (1995) Transport Solides et dissous du fleuve Congo (Bilan de six années d'observations). In: *Grands bassins fluviaux périatlantiques: Congo, Niger, Amazone* (J.C. Olivry and J. Boulègue, Eds.). *Coll Sém* 133–145, ORSTOM, Paris.

Laraque A., Mahé G., Orange D. and Marieu B. (2001) Spatio-temporal variations in hydrological regimes within Central Africa during the 20th century. *J Hydrology* 245: 104–117.

Lavreau J. (1982) Etude géologique du Haut-Zaire. Genese et evolution d'un segment lithospherique archeen. Musée Royale de l'Afrique Centrale. *Ann Sér 8 Sc Géol* 88: 1–116.

Lepersonne J. (1978) Structure géologique du bassin intérieur du Zaire. *Acad Roy Sc Outre-Mer Classe Sc Nat Médic SN* 20: 21–27.

Mainguet M. (1972) Le modelé des grès. Problèmes généraux, Tome I. *IGN-Etudes de photo-interprétation* 1–227.

Mengho M.B. (1994) Les ports et les transports fluviaux dans la Cuvette congolaise (Rép. du Congo). *Cah Outre-Mer* 47, 187: 253–269.

Meybeck M. (1976) Total mineral dissolved transport by world major rivers. *Hydrol Sci Bull* 21: 265–284.

Olivry J.C. and Boulègue J. (Eds.) (1995) *Grands bassins fluviaux périatlantiques: Congo, Niger, Amazone*. *Coll Sémin* 1–520, ORSTOM, Paris.

Operational Navigation Chart (ONC) (1983) sheet N-4 Angola, Mozambique, Zaire, Zambia, Zimbabwe; scale 1 : 1 000 000. Defense Mapping Agency, Washington, DC.

Operational Navigation Chart (ONC) (1987) sheet M-4 Angola, Burundi, Rwanda, Tanzania, Uganda, Zaire; scale 1 : 1 000 000. Defense Mapping Agency, Washington, DC.

Pearce F. (2002) Africa states betray World Summit pledges by launching mega-projects. *New Scientist* 28 September: 5.

Petters S.W. (1991) Regional Geology of Africa. *Lect Not in Earth Sci* 40: 1–722.

Pickford M., Senut B. and Hadoto D. (1993) Geology and palaeobiology of the Albertine Rift valley, Uganda-Zaire. *CIFEG Occas Publ* 24: 1–190.

Probst J.L., Nkounkou R.R., Krempp G., Briquet J.P., Thiébaux J.P. and Olivry J.C. (1992) Dissolved major elements exported by the Congo and the Ubangi rivers during the period 1987–1989. *J Hydrology* 135: 237–257.

REGIDESO (1985) Etude sur les domaines hydrogéologiques du Zaire, Travaux de forage, Regie de distribution d'eau, Kinshasa (unpublished).

Renier A. (1951) Notes sur la flore des couches de la Lukuga de la Région de Walikale (Kivu). *Mem Inst Géol Univ Louvain* 9: 1–11.

République du Zaire (1974) Notice explicative de la carte géologique du Zaire au 1 : 2 000 000. Dép Min, Dir Géol 1–67.

Robert M. (1940) La Géologie du Katanga. Le système du Kundelungu et le système schisto-dolomitique. *Comité Spéc Katanga* 8: 1–108.

Robert M. (1946) *Le Congo Physique* (3è édition). Presse Universitaires de France, Liège, 449 p.

Robyns J. (1955) Le genre Eichornia, spec. *Eichornia crassipes* (jacinthe d'eau) au Congo Belge. *ARSC Bull NS* 1116–1137.

Runge J. (2001) Landschaftsgenese und Paläoklima in Zentralafrika. *Relief, Boden, Paläoklima* 17: 1–294.

Runge J. and Nguimalet C.R. (2005) Physiogeographic features of the Oubangui catchment and environmental trends reflected in discharge and floods at Bangui 1911–1999, Central African Republic. *Geomorphology*, 70: 311–327.

Schlüter T. (1997) Geology of East Africa. *Beitr Region Geol Erde* 27: 1–484.

Schwartz D. (1988) Histoire d'un paysage: Le Lousséké. Paléoenvironnements Quaternaires et podzolisation sur sables Batéké. *Ed ORSTOM Etud Thès* 1–285.

Sondag F., Laraque A. and Riandey C. (1995) Chimie des eaux du fleuve Congo à Brazzaville et de l'Oubangui à Bangui (années 1988 à 1992). In: *Grands bassins fluviaux périatlantiques: Congo, Niger, Amazone* (J.C. Olivry and J. Boulègue, Eds.). *Coll Sém* 121–131, ORSTOM, Paris.

Stallibras E. (1887) Deep-sea sounding in connection with submarine telegraphy. *J Soc Telegr Engl* 16: 479–511.

Veatch A.C. (1935) Evolution of the Congo Basin. Memoir. *Geol Soc Am* 3: 1–183.

Veatch A.C. and Smith P.A. (1939) Atlantic submarine valleys of the United States and the Congo submarine valley. *Geol Soc Am Spec Pap* 7.

Wiese B. (1980) Zaire-Landesnatur, Bevölkerung, Wirtschaft. *Wiss Länderk* 15: 1–360.

World Bank (1997) Challenges for Environmentally Sustainable Development. *Findings Africa Region* 78. http://www.worldbank.org/afr/findings/english/find78htm (01.11.2003).

World Bank (2002) World Development Indicators, Freshwater. http://www.worldbank.org (01.11.2003).

Wotzka H.P. (1995) Studien zur Archäologie des zentralafrikanischen Regenwaldes. Die Keramik des inneren Zaire-Beckens und ihre Stellung im Kontext der Bantu-Expansion. *Africa Praehist* 6: 1–582.

15

The Zambezi River

Andy E. Moore[1], Fenton P.D. (Woody) Cotterill[2], Mike P. L. Main[3] and Hugh B. Williams[4]

[1]*AMPAL (Pty) Ltd, Box 66, Maun, Botswana*
[2]*Department of Geological Sciences and Department of Molecular and Cell Biology, University of Cape Town, Rondebosch 7701, South Africa*
[3]*Box 2265, Gaborone, Botswana*
[4]*7 Rothesay Road, Avondale West, Harare, Zimbabwe*

15.1 INTRODUCTION

The Zambezi rises with considerable modesty in north-west Zambia from a small spring on the gentle upland of the Southern Equatorial Divide – the watershed that separates the river from north-west-flowing tributaries of the Congo (Figure 15.1). For some 30 km, the Zambezi headwaters flow to the north, towards the Congo, but then the course swings to the south-west, around a low ridge of Karoo sandstone known as Kalene Hill. This direction is maintained for a further 200 km into Angola before the river finally turns south-eastwards to the Indian Ocean. It is with such indecision that southern Africa's largest river commences its course.

The Zambezi can be divided into three major segments, each having a distinctive geomorphological unity (Wellington, 1955). The first of these extends from the headwaters to Victoria Falls; the second from the Falls to the edge of the Mozambique coastal plain, which commences below Cahora Bassa Gorge; while the third comprises the stretch traversing the coastal plain (Figure 15.2). The aim of this chapter is to provide a description of the Zambezi, with particular focus on the contrasting geomorphological character of these three sectors of the river. It will be demonstrated that these differences are not accidental, but closely reflect the evolution of the Zambezi by processes of river piracy over a period extending back to before the disruption of Gondwana around 120 Ma.

The evolution of the Zambezi River has had a major influence on the distribution of riverine plant and animal species. River captures have not only been important in facilitating species dispersions but, particularly in the Plio-Pleistocene, have also led to the disruption of formerly continuous populations, providing a driving force for speciation. Dating the timing of species divergence, using genetic markers, offers the potential to refine our understanding of the chronology of major river captures.

Parts of the Zambezi have a long history of human occupation, but there are also underpopulated areas that represent some of the world's last major remaining wilderness areas, in large measure because of the barrier to settlement posed by the tsetse fly. However, measures to control the tsetse fly are progressively reducing this barrier, and these wilderness areas are coming under increasing population pressure. Several large dams, which have been constructed along the Zambezi and its tributaries to provide hydroelectrical power, have had major ecological impacts on the Zambezi system. Additional impoundments that are planned will require that careful management plans be put in place to satisfy the competing demands for the river's finite resources. This in turn demands a refined understanding of the hydrology and ecology of the system. While a detailed overview of these aspects is beyond the scope of this chapter, salient issues will be highlighted.

Large Rivers: Geomorphology and Management, Edited by A. Gupta

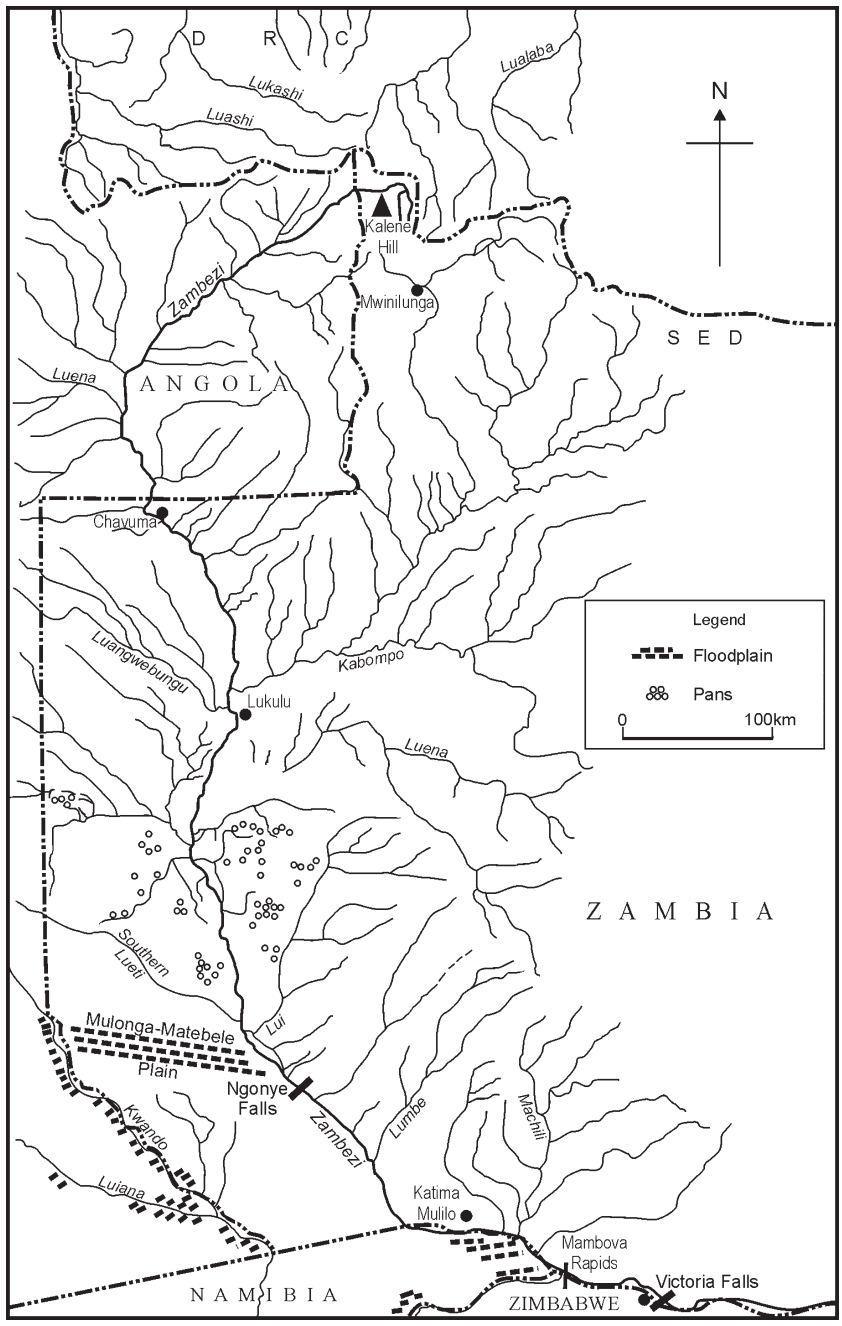

Figure 15.1 The Upper Zambezi system. Triangle shows the position of Kalene Hill. Note that the Southern Equatorial Divide (SED) forms the southern boundary of the Democratic Republic of Congo (DRC) with Angola and Zambia

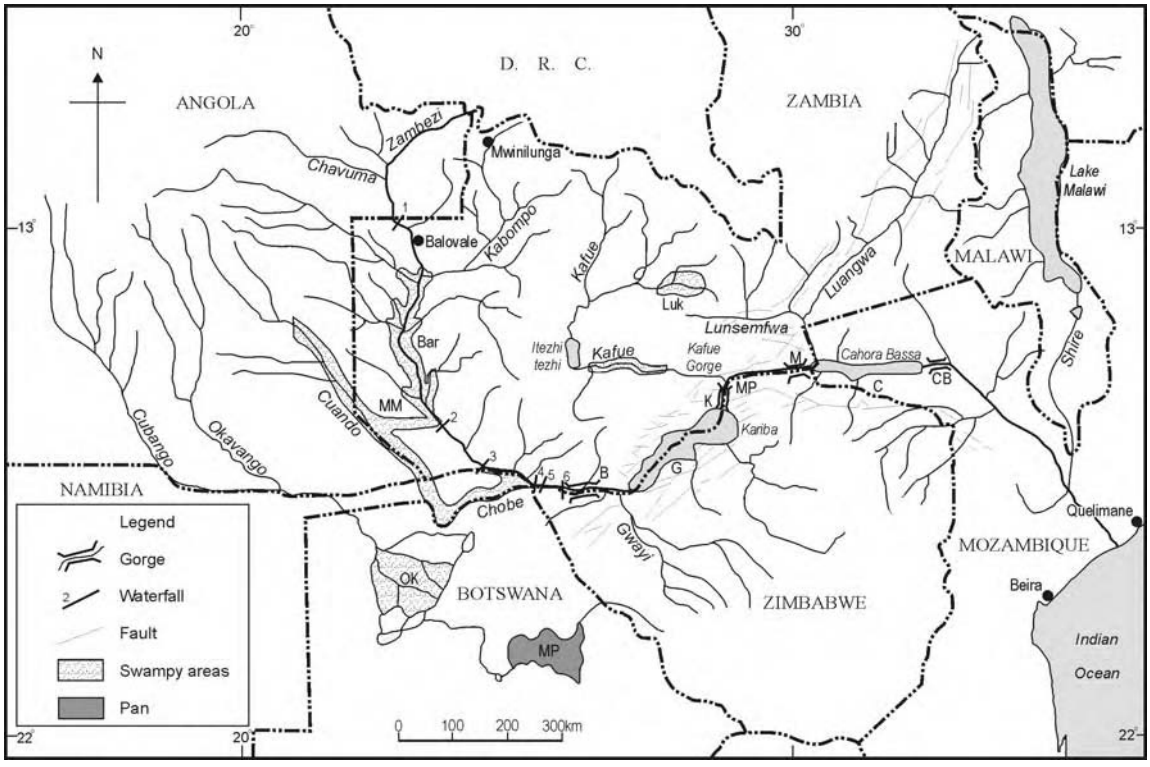

Figure 15.2 The Zambezi drainage system, adapted from Nugent (1990) and large dams. Note that the Linyanti and Chobe floodplains (both marked Chobe in this figure) are shown in detail in Figure 15.14. Rift basins: G, Gwembe Trough (mid-Zambezi Basin); MP, Mana Pools Basin; C, Chicoa or Cahora Bassa Basin. Gorges: B, Batoka Gorge; K, Kariba Gorge; M, Mupata Gorge; CB, Cahora Bassa Gorge. Rapids and Falls: 1, Chavuma; 2, Ngonye Falls; 3, Katima Mulilo; 4, Mambova; 5, Katombora; 6, Victoria Falls. Floodplains: Bar, Barotse floodplain; Luk, Lukanga; MM, Mulonga-Matebele. OK, Okavango Delta. Pans: MP, Makgadikgadi Pans

15.2 THE ZAMBEZI RIVER SYSTEM

The Zambezi River system and the locations of major dams are illustrated in Figure 15.2, while Figure 15.1 shows the major headwater tributaries. The upper reaches of the river are incised into Precambrian basement rocks that form the South Equatorial Divide. A little above the confluence with the west bank Lungwebungu tributary, which rises in the Angolan highlands, the Upper Zambezi widens into the Barotse floodplain (Figure 15.3). This is a very low gradient stretch of shallow, languid water, some 180 km in length, and 30 km in maximum width during periods of peak flood, which extends to just above Ngonye Falls (Figure 15.4). Most of this section of the river traverses unconsolidated sands (loosely referred to as the Kalahari Sand) that cap the Tertiary-age Kalahari Formation.

Figure 15.3 Barotse floodplain. Photograph reprinted with permission from Mike Main

Figure 15.4 Ngonye Falls. Upper Zambezi. Photograph reprinted with permission from Mike Main

Figure 15.5 Victoria Falls. Photograph reprinted with permission from Mike Main

The flats to the east of the Barotse floodplain are marked by a belt of numerous pans, up to 4 km in largest diameter. Some of these are perennially filled with water, while others are fed by springs rising from their margins. A number of lines of pans are also found to the west of the Barotse floodplain, although these are in general much smaller than those fringing the eastern margin. Many of the pans are aligned with shallow grassy valleys, known as dambos, which are bounded by gently sloping, densely vegetated interfluves. The hydrological regime of dambos is characterized by a persistently high water table that produces anaerobic soils, which in turn prohibits tree growth. Perennial water persists in shallow pools, shrouded in tall grass cover, throughout all but the most severe droughts. This makes the dambos the sponges that structure much of the Zambezi catchment. It is in fact hard to locate a minor tributary of the Upper Kafue, Upper Zambezi or Cuando Rivers whose runoff cannot be attributed to these dambos (White, 1976). Zambezian grasslands constitute the single largest unit mapped in the Zambezian phytochorion (see Section 15.6), which reflects the spatial dominance of floodplains and dambos (White, 1983).

Water flow into the dambos, downslope from the interfluves, has concentrated finer grained minerals into these moist sponges and created clayey soils, enriched in humus derived from the very luxuriant plant growth. The anaerobic grassland associated with dambos and larger floodplains of the Zambezian plateau is the single most widespread vegetation type in the Upper Zambezi Basin (White, 1976). The rich soils and availability of water makes the pans and dambos an important focus of agriculture (McFarlane, 1995). In terms of both edaphic and ecological criteria, the Upper Zambezi stands apart from the world's rivers because much of its catchment is comprised of dambos.

Below the Ngonye Falls, a little downstream of the southern end of the Barotse Floodplain (Figure 15.4), the gradient of the Zambezi steepens, and the river begins to incise into Karoo-age basalts and sediments that form the sub-Kalahari bedrock, creating a series of rapids. These anticipate the end of the leisurely course of the Upper Zambezi, which terminates abruptly where the river plunges some 100 m along the 1700 m length of the Victoria Falls, or Mosi-a-tunya – The-Smoke-That-Thunders – as they are more aptly known by their vernacular name (Figure 15.5).

Figure 15.6 illustrates the gradient of the section of the Zambezi River above and below Victoria Falls. The 340 km stretch from the Ngonye Falls to Victoria Falls, which constitutes the lower portion of the Upper Zambezi, has an average gradient of 0.00024. A second geomorphologically distinct section of the river, designated the Middle Zambezi (Wellington, 1955), commences immediately below the falls. Karoo-age basalts and sediments and subordinate Precambrian crystalline basement rocks constitute the bedrock over most of this stretch of the river. It is characterized by a markedly steeper gradient (0.0026) than the section above the falls (Figure 15.6), and initially follows a turbulent course through a series of narrow zigzag gorges before swinging abruptly to the east into the 100 km long Batoka gorge (Figure 15.7). The latter narrows at the Chimamba Rapids, some 30 km further downstream,

> 'where the whole volume of the great Zambezi converges into a simple pass, only some 50 or 60 feet in width, shuddering, and then plunging for 20 feet in a massive curve that seems in its impact visibly to tear the grim basaltic rocks asunder (and) one learns better than from the feathery spray-fans of the Victoria Falls what force there is in the river and wonders no longer at the profundity of the gorge . . .'
>
> (Lamplugh, 1907)

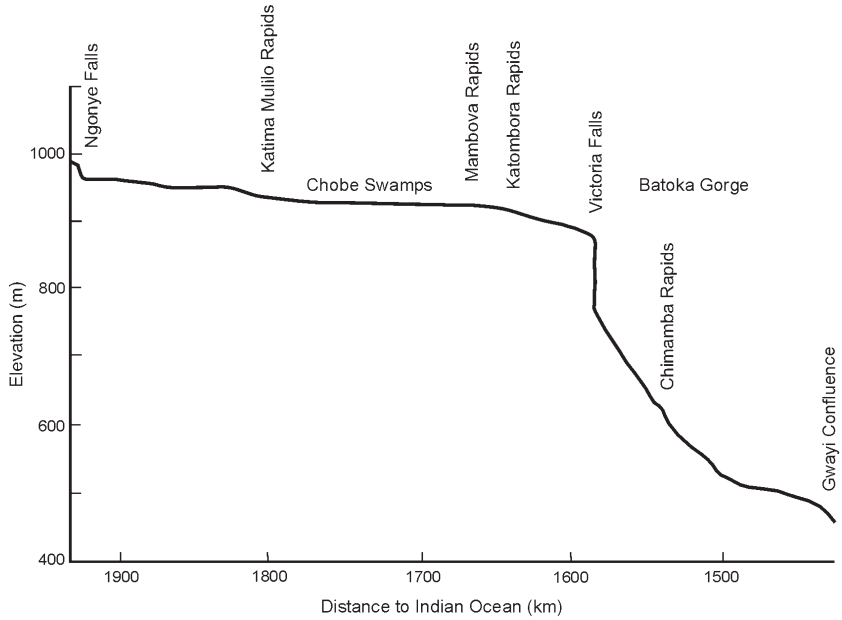

Figure 15.6 Zambezi River profile across the boundary between the upper and middle sections of the river (modified after Nugent, 1990)

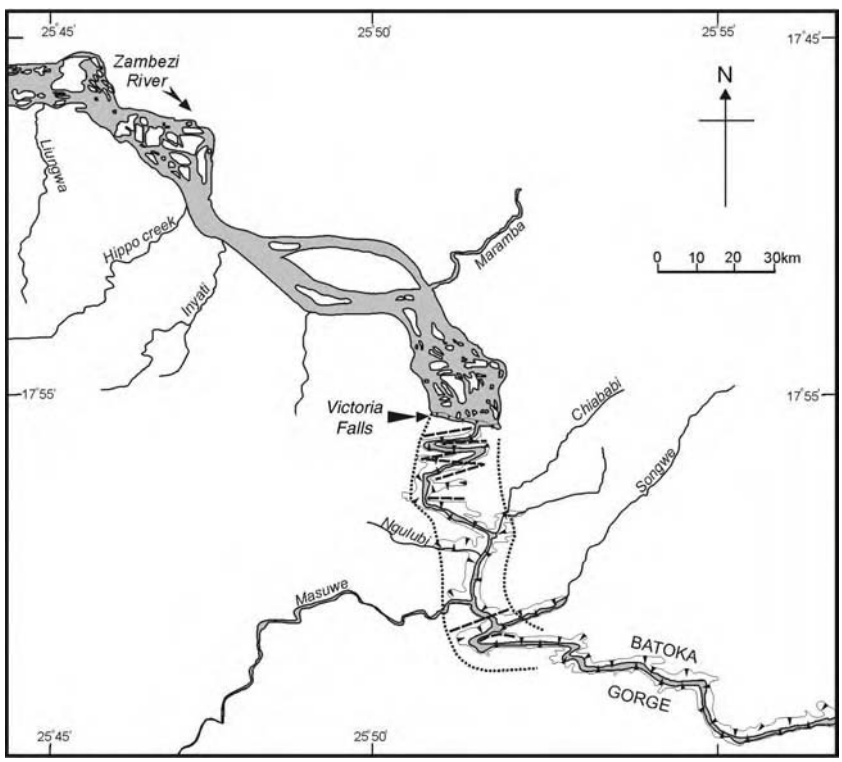

Figure 15.7 Geomorphology of the Zambezi River in the vicinity of Victoria Falls (from 1:50 000 topographical sheet 1725D4 (Victoria Falls). Dashed line on either side of the gorge below the Falls marks a low escarpment, interpreted to represent the original bank of the Zambezi prior to river capture (Wellington, 1955). The sharp deflection of the Zambezi from a southerly to an easterly course immediately below the confluence with the Songwe was inferred to mark the capture elbow where the Middle Zambezi beheaded the Upper Zambezi (Wellington, 1955). Reproduced from South African Journal of Geology, Vol. 104, Moore A.E., Larkin P.A., Drainage evolution in south-central Africa since the break-up of Gondwana, pp. 47–68, 2001, with permission of Geological Society of South Africa

The Chimamba Rapids also mark a sharp break in gradient of the river within the succession of gorges below Victoria Falls (Figure 15.6).

Below the Batoka Gorge, the Zambezi widens into one of the world's finest wildernesses, flowing through a series of broad basins, in places several kilometers in width, and known, in a downstream direction, as the Kariba (or Gwembe), Mana Pools and Chicoa (or Cahora Bassa) basins (Figures 15.2 and 15.8). These are linked by the narrow defiles of the Kariba and Mupata Gorges (Figure 15.9) – not as long or dramatic as the Batoka, but filled by a dark, powerful current, many mysterious eddies, and a haunting, pervasive silence that lingers long after the river enters the broad reaches of the lower basin. Much of the flat valley and steep escarpments in Zambia and Zimbabwe bordering the mid-Zambezi have been set aside as safari and controlled hunting areas. In combination, they stretch from Lake Kariba to the eastern reaches of Lake Cahora Bassa (Figure 15.2). Part of this region, comprising Mana Pools, Sapi and Chewore, stands out as one of the important remaining wilderness areas in the savannas of Africa, and is appropriately designated as a world heritage site (Frost *et al.*, 2002).

Downstream of the Chicoa Basin, the river flows through one last gorge – the Cahora Bassa, before entering an indolent stretch of the river known as the Lower Zambezi, which traverses the Cretaceous and Tertiary sedimentary cover of the low-lying (0–400 m) Mozambique coastal plain. The lower reaches of the river, below the Shire confluence (Figure 15.2), forms a huge 100 km long floodplain-delta system of oxbows, swamps, and multichannel meanders (Figure 15.10). The modern river empties into the Indian Ocean between Beira and Quelimane, but abandoned distributary channels of the delta are located along the entire 290 km distance between these two cities. Because of the shallow sloping shelf, this area

Figure 15.9. Mupata Gorge. Photograph reprinted with permission from Mike Main

Figure 15.8 Wide Zambezi at Mana Pools. Photograph reprinted with permission from Mike Main

Figure 15.10 Zambezi floodplain and delta. Photograph reprinted with permission from Mike Main

of the coastline has, at 6.4 m, the highest tidal range on the continent. Given the low-lying hinterland, tides can reach 40–50 km inland. Low-lying ridges, extending parallel to the coast, up to 30 km inland, mark past strandlines associated with former higher sea-level stands (Main, 1990). The rich alluvial soils along the river have been utilized for intensive agriculture. On the south bank is the large Marromeu Game Reserve, coastally fringed by extensive mangroves and low-lying dune forest. This was once famous for its large herds of buffalo, (*Syncerus caffer*) but the wildlife was severely depleted during the hostilities prior to and immediately after Mozambique independence. The recovery of Mozambique's wildlife is a slow process, but shows signs of some local successes.

The Zambezi has a number of important tributaries, which constitute major rivers in their own right. The most westerly of these is the Cuando (or Kwando), which follows a south-easterly course as far as the Botswana–Namibia border, where it veers sharply northeastwards, to link with the Zambezi via the Linyanti-Chobe floodplain (Figure 15.2). The mid-section of the Cuando is a floodplain, comparable with the Barotse floodplain, and linked to the latter by a broad belt of alluvium termed the Mulonga-Matebele Plain (Figure 15.1), which is subject to flooding in the wet season (Thomas and Shaw, 1991).

The Kafue is a north bank tributary with headwaters on the Southern Equatorial Divide. It initially flows in a general southwesterly direction towards the Upper Zambezi, but the course veers sharply eastwards in the vicinity of a broad floodplain known as the Kafue Flats. This tributary links with the Mana Pools Basin of the Middle Zambezi below the deeply incised Kafue Gorge (Figure 15.2).

The Luangwa River flows in a general south-westerly direction over most of its length – an unusual orientation for a major tributary of an east-draining river. The course veers sharply to the south-south-east a little above the confluence with the Zambezi in the upper reaches of the Chicoa Basin (Figure 15.2).

The mid-Zambezi has a number of relatively minor south bank tributaries, which rise on the central Zimbabwe divide. Their upper reaches flow in a general north-westerly direction that, like the orientation of the Upper Luangwa, is anomalous for tributaries of a major east-draining river. The major tributary of the Lower Zambezi is the Shire, which flows southwards from its headwaters in Lake Malawi, in Malawi (Figure 15.2).

15.3 HYDROLOGY

The Zambezi is some 2575 km in length from the headwaters to the coastal delta, and has a catchment area of 1.32 million km^2 that includes portions of eight countries (Nugent, 1990). This makes it the largest river in southern Africa, with a cumulative mean annual flow of the main stream and tributaries of approximately 97 km^3 (Table 15.1, Figure 15.11a). This is broadly comparable with the flow of the Nile, but an order of magnitude less than the

Table 15.1 Flow data used in Figure 15.11

Country	Sub catchment	Hydropower (km^3 year^{-1})	Irrigation (km^3 year^{-1})	Industry and primary (km^3 year^{-1})	Land use change (km^3 year^{-1})	1995 yield (km^3 year^{-1})	Mean flow (km^3 year^{-1})	Place
Angola	Upper Zambezi	0.00	0.00	–0.01	0.12	19.90	19.90	Chavuma
Angola	L. Bungo and Luanginga	0.00	0.00	–0.01	0.09	5.47	25.37	
Zambia	Kabompo	0.00	0.00	0.00	0.13	7.74	33.11	Mongu
Zambia	Barotse and Chobe	0.00	–0.02	–0.04	0.14	3.62	36.73	Victoria Falls
Zimbabwe	Kariba	–4.09	–0.19	–0.23	0.49	2.53	39.26	Kariba Dam
Zambia	Kafue	–0.06	–0.33	–0.13	1.02	8.89	48.15	Mana Pools
Zambia	Luangwa	0.00	–0.03	–0.14	1.29	16.34	64.49	Zumbo
Zim./Moz.	C. Bassa	–1.21	–0.23	–0.12	0.66	4.14	68.63	C. Bassa Dam
Malawi/ Tanzania	L. Malawi and Shire	0.00	–0.41	–0.45	5.70	20.12	95.65	Caia
Moz.	Delta and Tete	0.00	–0.26	–0.16	1.84	8.04	96.79	Sea
	Totals	–5.36	–1.47	–1.29	11.48	96.79		

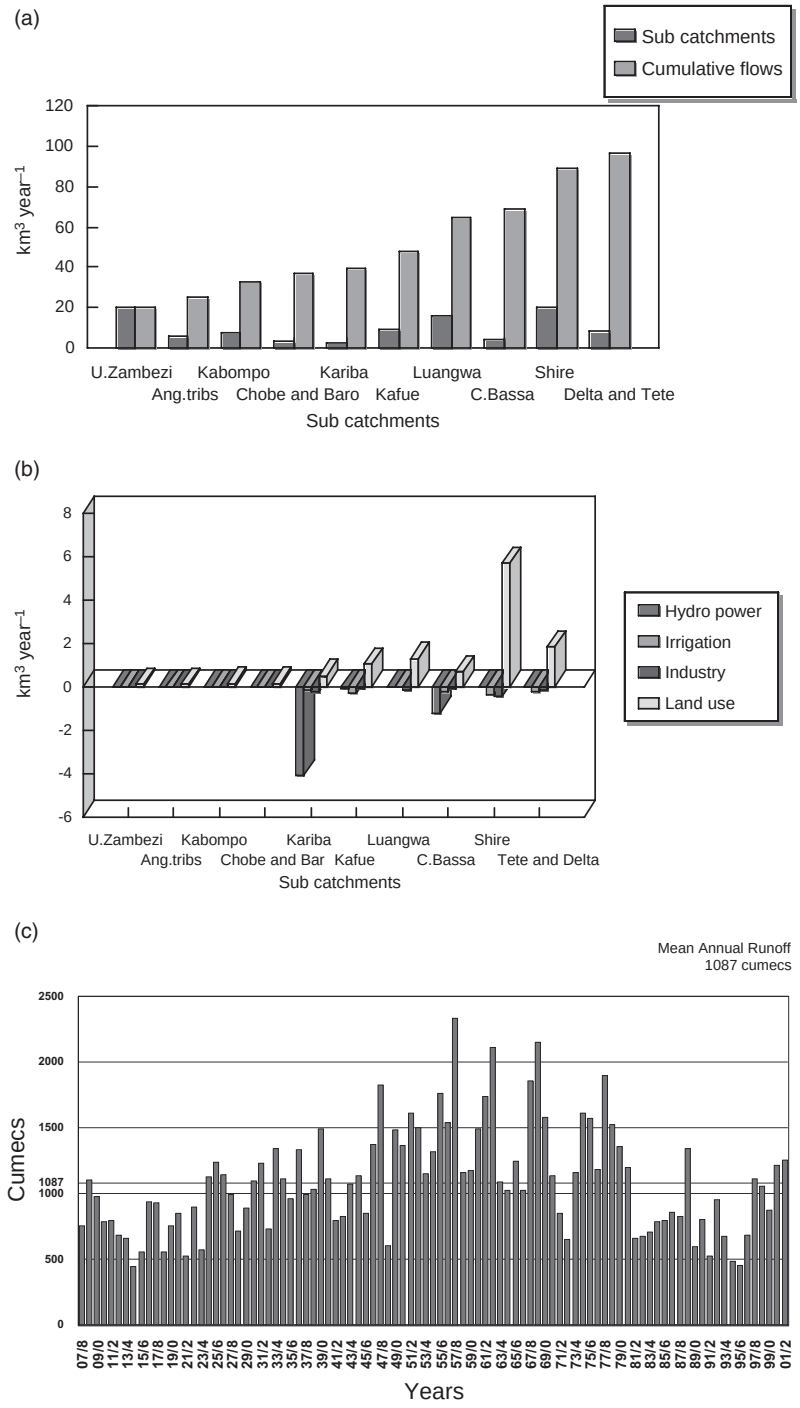

Figure 15.11 (a) Mean and cumulative annual flow of the Zambezi and major tributaries. (b) Utilization of water from the Zambezi and major tributaries. (c) Mean annual flows of the Zambezi River measured at the Victoria Falls station (1907–2002)

annual flow of the Congo, which in turn has a mean annual flow that is an order of magnitude less than that of the Amazon.

The hydrology of the Zambezi catchment is determined by the interplay of a variety of factors. The annual variation of rainfall in summer is due to the Intertropical Convergence Zone between the North-east Monsoon and the South-east Trades for the Middle and Lower Zambezi, and the Congo air boundary between the South-west Monsoon and the South-east Trades for the Upper Zambezi. The further south the two boundaries move, the greater the total delivery of rainfall. In winter these two climatic boundaries move north, resulting in drier conditions across the Zambezi Basin. Rainfall by and large increases from south to north (600–1300 mm), so that the largest contribution to runoff comes from the northern tributaries.

The hydrology of the Zambezi is further influenced by water exploitation by different users. The catchment as a whole is relatively undeveloped so that off-take by irrigation, industrial and domestic users only amounts to some 3% of the total flow of the Zambezi. The use by hydroelectric power, due to the net evaporation from the large reservoirs of Kariba and Cahora Bassa Dams and, to a lesser extent, of the Kafue Gorge Dam, amounts to just over 5% of the Zambezi flow. However usage by these sectors is more than offset by the increased runoff due to changes in land use, particularly since the middle of the last century (Davies, 1986). Thus, for example, preliminary calculations, based on research by the Wallingford Research Station on Lake Malawi (Price *et al.*, 1998), indicates that increased runoff caused by the clearing of natural forests in the Shire catchment, has meant the level of Lake Malawi in the early 1990s was 1 m higher than it would have been otherwise. Figure 15.11b and Table 15.1 summarize these sector and land use totals, and the resultant mean annual flows are shown in Figure 15.11a.

Mean monthly flows at four different stations (Figure 15.2) on the Upper Zambezi are given in Table 15.2. The annual variation in rainfall between dry winters and wet summers produce high flows in February–April and then progressively lower flows up to a November minimum (Table 15.2). The annual flooding is however buffered by the natural flood regulatory capacity of the floodplains developed on the major headwater tributaries. The most important of these are the Barotse and Chobe floodplains in the upper Zambezi, the Kafue Flats on the Kafue River and Elephant Marsh on the Shire River (Figure 15.2). Flow has been further affected by the construction of major dams (Figure 15.2) on the Zambezi (Kariba and Cahora Bassa) and on the Kafue (Itezhi tezhi and Kafue Gorge).

Records of water level from the hydrological station at Victoria Falls, taken since 1907 are illustrated in Figure 15.11c. These indicate lower than normal years for 1907–1946, above normal for the years 1947–1981, and again below normal for 1982–1997. A major flood of 1958, during the construction of Kariba Dam, followed heavy rains in the upper catchment and also the local catchment below Victoria Falls. A coffer dam was overtopped and a road bridge washed away – at its peak some 9000 $m^3 s^{-1}$ were passing over the Victoria Falls. In magnitude it was equivalent to the 1 in 100 year flood, which in turn is roughly half the probable maximum flood of 21 000 $m^3 s^{-1}$. McCarthy *et al.* (2000) tentatively interpret the variation

Table 15.2 Zambezi River: mean monthly flows ($m^3 s^{-1}$)

Station Period (years)	Chavuma 1959/60–2001/02	Lukulu 1950/51–2001/02	Katima Mulilo 1967/68–2001/02	Victoria Falls 1951/52–2001/02
Oct.	68	271	306	293
Nov.	94	310	320	297
Dec.	228	468	430	438
Jan.	655	803	678	686
Feb.	1411	1294	1211	1184
Mar.	2031	1645	2374	2175
Apr.	1770	1523	3129	3007
May.	684	944	2427	2613
Jun.	310	575	1326	1621
Jul.	188	434	691	845
Aug.	124	361	467	519
Sep.	83	306	364	376
Mean annual	637	745	1144	1171

Drainage area: Chavuma (75 500 km^2), Lukulu (206 500 km^2), Katimo Mulilo (337 300 km^2), Victoria Falls (507 200 km^2). See Figure 15.2 for station locations.

in annual flows of the Zambezi to show an apparent oscillation between periods of good years and poor years in an approximately 80 year cycle.

Long-term changes in the Zambezi flow regime are broadly mirrored in the Okavango River. Historical accounts of flooding of the Okavango Delta suggest average to above average outflows for the period 1849–1900, followed by limited outflow with some good years for the period 1900–1951. Outflow from the Delta for the 1960s and 1970s was above normal and the outflow for the 1980s and early 1990s below normal (McCarthy *et al.*, 2000).

Figure 15.12 Wall of the Kariba Dam. Photograph reprinted with permission from Mike Main

15.4 ECOLOGICAL IMPACT OF MAJOR DAMS

The densely vegetated floodplains such as the Barotse and Chobe (Upper Zambezi) and the Kafue Flats (Figures 15.1 and 15.2), with their shallow gradients, form natural sediment traps that greatly reduce the material supplied to the lower reaches of the river system. These floodplains as a consequence form major wetlands that provide important wildlife refuges, particularly for fish, avifauna and water-dependent mammals, including hippopotamus and the lechwe and sitatunga antelopes. Fish migrate into the inundated grasslands of the floodplains during the floods, spawn, and their fry utilize the rich plankton and benthic communities which develop after nutrient release from decomposing organisms drowned by the floodwaters. Readily accessible stretches of the Zambezi and major tributaries, such as the Barotse floodplain, provide a reliable perennial water source, and are thus an important focus for human settlement and agricultural activity (Davies, 1986).

There have been marked changes to the ecology and utilization of the Zambezi River system as a result of the construction of several major dams, such as Kariba (Figure 15.12) and Cahora Bassa on the middle Zambezi, and the Itezhi tezhi and Kafue Gorge Dams on the Kafue (Figure 15.2). These impoundments had a major impact on the economy of the region. Thus, they represent an important source of hydroelectricity for the whole subcontinent, where there is a rapidly rising demand for power. The introduction of the Lake Tanganyika sardine *Limnothrissa miodon* (colloquially known as 'kapenta') into Lake Kariba in 1967 has formed the basis of an important fishing industry. Against all expectations, this fish survived discharge via the Kariba turbines and sluice gates, as well as a journey of several hundred kilometres to colonise Cahora Bassa, where it now also forms the basis of an important fishing industry (Davies, 1986; Jackson, 2000). The large dams have also become the focus of an important tourist industry.

Nevertheless, these economic benefits have come at considerable human and ecological costs. The construction of Lake Kariba led to the displacement of about 50 000 members of the Tonga tribe which had inhabited the area since about 1100 AD, while about 25 000 people were relocated as a result of the construction of Cahora Bassa. These displacements have led to serious community disturbances, major psychological upsets and emotional problems in the attempt to adapt to new terrain and a new way of life, and bitterness and resentment that rankles to this day (Davies, 1986).

The dams have also had severe ecological impacts on the major floodplains, as a result of the reduction of the supply of water and sediment. The resultant contraction of these wetlands impacts particularly on fish, avifauna and water-dependent antelope species, and are only marginally offset by the added wetlands of the lake shallows (Davies, 1986). This is well illustrated by the collapse in numbers of the semi-aquatic Kafue lechwe (*Kobus kafuensis*), which is endemic to the Kafue flats, following construction of the Itezhi-tezhi Dam. Today, this species is confined to a fragment of the former range, with a decline from an estimated population of 350 000 at the turn of the twentieth century to less that 30 000 today (Cotterill, 2005). It has also been estimated that the closure of Cahora Bassa led to a 70 % reduction of the supply of sediment to the lower reaches of the river, and that this could lead to severe erosion of the Zambezi Delta, threatening both agricultural activity and the important Marromeu wilderness area. During the annual floods prior to construction of the dams, the drowned grasslands of the delta were protected from overgrazing, and thus able to regenerate. The virtual elimination of the natural flooding regime has disturbed this important ecological dynamic.

It may also be responsible for the present marked die-off of the coastal mangroves, and the catastrophic decline of the coastal shrimp-fishing industry (Davies, 1986). The latter author notes that a major problem in quantifying the ecological effects of the construction of the major dams was the lack of baseline environmental data prior to their construction.

15.5 EVOLUTION OF THE ZAMBEZI RIVER SYSTEM

It has long been appreciated that the configuration of the Zambezi and tributaries has evolved over time, and that the modern course of the river reflects the interplay of a complex history of geomorphic events. Our understanding of these evolutionary processes rests, in large measure, on remarkably perceptive early pioneering work of du Toit (1927, 1933), Dixey (1945), Wellington (1955), and Bond (1963); and more recent studies by Cooke (1980) and Thomas and Shaw (1991). This section briefly reviews some of the broader lines of evidence for the initiation and subsequent geomorphic evolution of the Zambezi system.

Major changes in the geometry of the Zambezi River system are indicated by the following lines of evidence:

1. The sharp changes in direction of the courses of the Cuando, Kafue, and Luangwa (Figure 15.2) strongly suggest capture elbows.
2. The upper Luangwa drains to the south-west, while south bank tributaries of the Zambezi, which rise on the central Zimbabwe divide, drain to the north-west (Figure 15.2). Moore *et al.* (2007) note that these orientations are most unusual for tributaries of a major east-flowing river, and suggest that these drainage lines were originally in accord with a west-flowing, Karooage fluvial system. Palaeocurrent directions in fluvial Triassic (Karoo) sediments in the Zambezi valley indicate westerly sediment transport directions (Oesterlen and Milsteed, 1994; Shoko, 1998), consistent with this interpretation.
3. The sedimentary sequence on the Mozambique plain between Maputo and Beira, and offshore deposits to the east of this plain (Dingle *et al.* 1983) reflect changes in sediment supply by the major eastward-draining southern African rivers, and provides a timescale for dating important river captures (Moore and Larkin, 2001).
4. Much of the western portion of Africa between the Orange River and the Congo is blanketed by a veneer of sediments of upper Cretaceous to Tertiary age (Figure 15.13). Isopach studies of these sediments have identified a number of deep pre-Kalahari valleys, which are inferred to mark the position of former drainage lines.
5. The occurrence of a high proportion (41%) of fish species common to the middle Zambezi and Limpopo Rivers (see Figure 15.13e for location of the latter drainage) indicates that they have been linked at some stage. The native fish fauna of the Upper Kafue (a tributary of the Middle Zambezi) is very similar to the Upper Zambezi, only less speciose. Of the 64 species of fishes recorded in the Upper Kafue, only two are absent from the Upper Zambezi (Gaigher and Pott, 1973; Bowmaker *et al.*, 1978; Skelton, 1993, 1994). This points to a former link between the Kafue and Upper Zambezi. Paired populations of riverine plant species on the Zambezi and Limpopo (Moore, 1988) could also be explained by a former link between these two rivers.

Based on lines of evidence such as those summarized above, Moore and Larkin (2001) postulated the following broad sequence of evolutionary changes in the Zambezi River system.

In the early Cretaceous, following the opening of the Atlantic Ocean at approximately 120 Ma, the Okavango, Cuando and Upper Zambezi were the major south-east-flowing headwaters of the Palaeo-Limpopo River system (Figure 15.13a). The Upper Zambezi was probably linked to the Limpopo via the Shashe River, which is over 1 km in width near the confluence of the latter two rivers, indicating a marked overfit with the ephemeral modern flow regime.

The Kafue was originally a major southwest-flowing east bank tributary of the Upper Zambezi. The Palaeo-Chambeshi, whose headwaters included rivers that are today part of the upper Congo system, formed the upper reaches of the palaeo-Kafue. The sharp change in course of the modern Kafue, where it enters the western end of the Kafue Flats, (Figure 15.2) is interpreted as a capture elbow (Dixey, 1945; Bond, 1963). The former course of the lower Kafue is marked by a 2 km wide wind gap in the modern divide with the Zambezi at the western end of the Kafue Flats, and a belt of alluvium, underlain by coarse, current-bedded fluvial gravels, between the Kafue Flats and the Machili Basin (Dixey, 1945; Thomas and Shaw, 1991). The location of the Machili River and Basin is shown in Figures 15.1 and 15.14. The Digital Elevation Model (DEM) image presented in Figure 15.15 clearly illustrates how the alluvium associated with the Machili Basin extends northeast across the line of the Upper Zambezi into northern Botswana.

Moore and Larkin (2001) inferred that the Luangwa originally continued on the southwesterly course of the

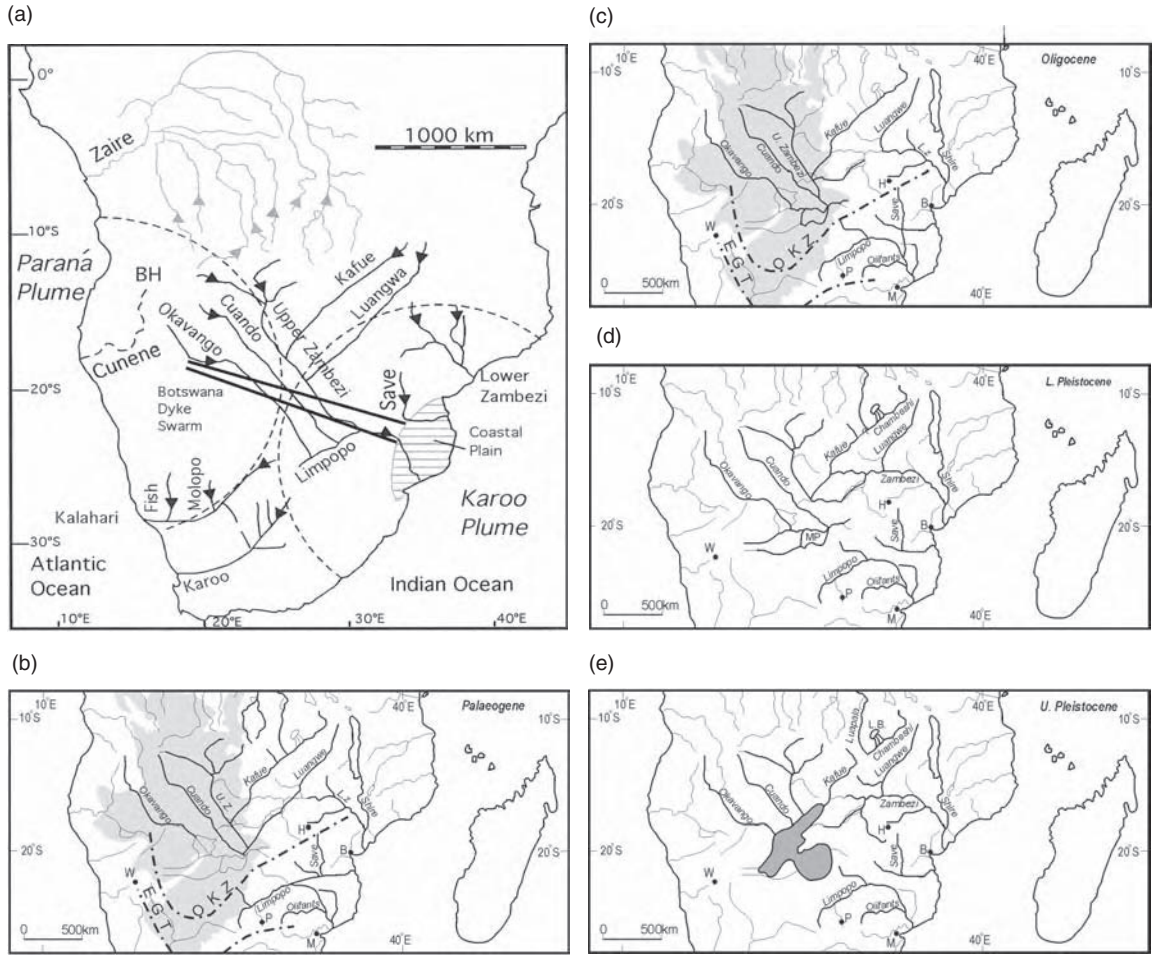

Figure 15.13 (a) Drainage system in south-central Africa based on reconstructions by de Wit (1999) and Moore and Larkin (2001). Dotted lines show the inferred extent of the areas affected by updoming by the Karoo and Paraná Plumes, respectively (after Cox, 1989). (b) Faint lines, modern drainage lines; heavy lines, reconstructed drainage lines for period; LZ, Lower Zambezi; OKZ, Ovambo-Kalahari-Zimbabwe flexure axis (after Moore, 1999). City locations as follows: B, Beira; H, Harare; M, Maputo; P, Pretoria; W, Windhoek. Grey tone shows modern distribution of Kalahari Group sediments. End-Cretaceous to early Tertiary flexuring across the OKZ Axis severed the link between the Limpopo and Cubango-Okavango, Cuando and Upper Zambezi–Luangwa–Kafue. During the Palaeocene and Eocene, the latter three rivers formed a major endoreic system, which terminated in the Kalahari Basin, and contributed to deposition of the Kalahari Group sediments. Lower Palaeogene isopachs on the Mozambique margin (Dingle *et al*., 1983) indicate southward displacement of the mouth of the Shire. (c) Abbreviations as for (b). Headward erosion of the lower Zambezi, inititated by crustal flexuring along the OKZ Axis, resulted in the capture of the Luangwa. The resultant lowering of the Luangwa base level, coupled with increased flow in the Lower Zambezi, initiated headward erosion towards the point of capture, and incision of the Cahora Bassa Gorge. (d) MP, Makgadikgadi Pans. Other abbreviations as for (b). Continued headward erosion of the Lower Zambezi led successively to capture of the Mana Pools Basin and the Gwembe Trough (location of Lake Kariba). These captures in turn initiated incision of the Mupata and Kariba Gorges, respectively. Incision of the Batoka Gorge was initiated once the Middle Zambezi beheaded the Upper Zambezi in the Early Pleistocene. (e) Grey tone shows Lake Palaeo-Makgadikgadi. LB, Lake Bangweulu; other abbreviations as for (b). Displacement along the major north-east-trending Linyanti and Chobe Faults temporarily severs the link between the Upper and Middle Zambezi, and diverts the flow of the Kafue and Zambezi into Lake Palaeo-Makgadikgadi, which filled to the 945 m shoreline level. Diversion of the headwaters of these rivers is reflected by a break in erosion in the Batoka Gorge. The timing of diversion of the Upper Zambezi into Lake Palaeo-Makgadikgadi cannot be accurately dated, but is estimated to be Early Pleistocene (Cotterill, 2006a). (a) Reproduced from South African Journal of Geology, Vol. 105, Moore A., Blenkinsop T., The role of mantle plumes in the development of continental-scale drainage patterns: The southern African example revisited, pp. 353–360, 2002, with permission from Geological Society of South Africa. (b–e) Reproduced from South African Journal of Geology, Vol. 104, Moore A.E. Larkin P.A., Drainage evolution in south-central Africa since the break-up of Gondwana, pp. 47–68, 2001, with permission of Geological Society of South Africa

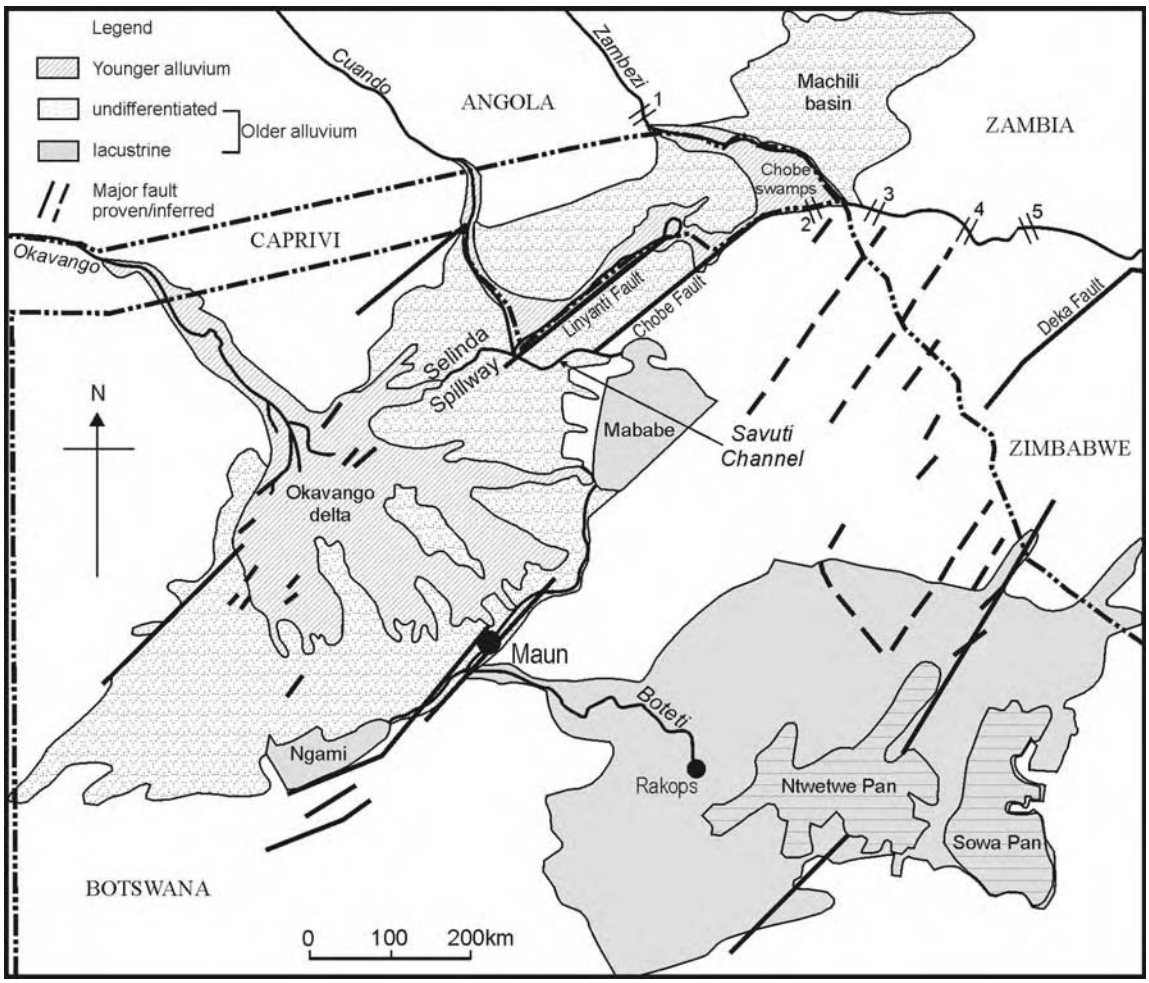

Figure 15.14 The distribution of alluvial and lacustrine sediments in north-eastern Botswana and southern Zambia. The alluvium of the Machili Basin probably extends further to the north-east as far as the Kafue Flats (Thomas and Shaw, 1991). Limits of the older alluvium reflect the approximate extent of Lake Makgadikgadi associated with the 945 m shoreline. This comprised two subsidiary basins, linked via a narrow neck along the Boteti River valley (Thomas and Shaw, 1991). Note that the south-west–north-east trending basin, which was subsequently partially covered by the Okavango Delta, is strongly fault-controlled. The younger alluvium (horizontal lining) is associated with the floodplain of the Okavango Delta and the fault-bound Linyanti and Chobe floodplains. Numbers 1–5 denote positions of rapids and falls: 1, Katima Mulilo; 2, Mambova; 3, Katombora; 4, Victoria Falls; 5, Chimamba Rapids. Reproduced from South African Journal of Geology, Vol. 104, Moore A.E., Larkin P.A., Drainage evolution in south-central Africa since the break-up of Gondwana, pp. 47–68, 2001, with permission of Geological Society of South Africa

upper reaches of the river, via the fault-bound Gwembe Basin. A deep pre-Kalahari valley, which straddles the Botswana–Zimbabwe border and located on a projection of this southwesterly line, was interpreted to be a relict of the original Luangwa–Gwembe course. This is consistent with the suggestion by Moore *et al.* (2007) that the Luangwa, which is floored by Karoo sediments, is a relict of a Karoo-age drainage system that pre-dated the break-up of Gondwana.

The major lower Cretaceous Zambezi-Limpopo River system entered the Mozambique coastal plain via a line of crustal weakness that was exploited by a major west–north-west trending dyke swarm. Reeves (1978) proposed that the dyke swarm was emplaced into the failed arm of

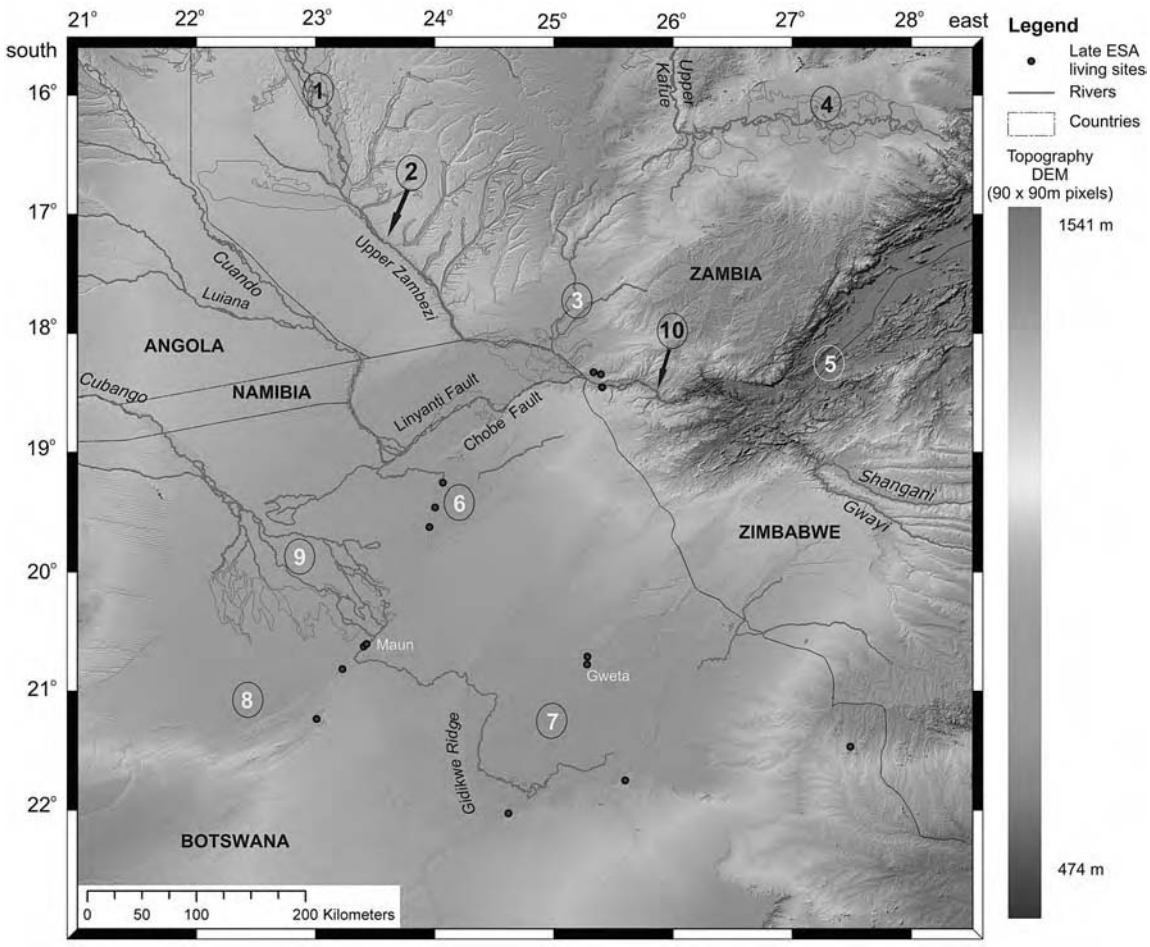

Figure 15.15 (See also colour plates.) DEM image illustrating the subdued topography extending from the Machili Flats, across the line of the Upper Zambezi River, south-west into the area formerly covered by the greater Palaeo-Lake Makgadkigadi. This reflects alluvium supplied by the upper Chambeshi-Kafue system, which was formerly linked to the Upper Zambezi via the Machili Flats. Locations: 1, Barotse Floodplain; 2, Ngonye (Sioma) Falls; 3, Machili Flats; 4, Kafue Flats, formerly occupied by Pleistocene Lake Patrick; 5, Gwembe Trough (Lake Kariba); 6, Mababe depression, 7, Makgadikgadi depression; 8, Ngami depression; 9, Okavango Delta; 10, Victoria Falls. Early Stone Age (ESA) living sites (Robbins and Murphy, 1998; McFarlane and Segadika, 2001) in the Makgadikgadi Basin depicted by circles

a triple junction associated with the disruption of Gondwana. The exit of the Save River to the Mozambique coastal plain was also closely linked to the line of crustal weakness exploited by the dyke swarm (Moore and Blenkinsop, 2002). During the lower Cretaceous, the Lower Zambezi constituted a subsidiary coastal drainage system with the Shire as a major north bank tributary. Geophysical evidence (Nairn *et al.*, 1991) shows that the Lower Zambezi course is controlled by major rift faulting. This reconstruction of the proto-Zambezi River system is consistent with the view expressed by Potter (1978) that rifts control the location of long-lived drainages.

The initiation of the early post-Gondwana drainage system in south-central Africa, described above, can be understood in terms of the model proposed by Cox (1989). He envisaged that doming of the subcontinent occurred over major mantle plumes (the Paraná and Karoo plumes) linked to the disruption of Gondwana, and considered responsible for triggering the eruption of the Karoo and Etendeka flood basalts in the east and west of the subcon-

tinent, respectively. The elevated ground over the plumes in turn, provided the headwaters for a new post-Gondwana drainage system. Moore and Blenkinsop (2002) demonstrated that there was a major reorganization of the drainage system on the subcontinent immediately prior to or at the time of disruption of Gondwana, consistent with Cox's proposal. They ascribed the initiation of an early Cretaceous proto-Zambezi-Limpopo drainage towards the Indian Ocean (Figure 15.13a) to updoming of the subcontinent over Paraná plume, which post-dated the ~180 Ma Karoo plume. The rectilinear pattern of this early river system, with parallel south-east and south-west trending river courses (Figure 15.13a), points to an important structural influence, superimposed on the primary role of the mantle plumes in determining the post-Gondwana drainage system.

The palaeo-Limpopo drainage system was disrupted (Figure 15.13b) by end-Cretaceous to early Tertiary crustal flexuring of the subcontinent along an arcuate line termed the Okavango–Kalahari–Zimbabwe (OKZ) Axis by Moore (1999) (modified after the Kalahari–Rhodesian Axis of du Toit, 1933). Uplift along this flexure severed the link between the Lower Limpopo and the former south-east-flowing headwater tributaries. These tributaries, including the Zambezi, now became a senile endoreic drainage system that supplied sediment to the inland Kalahari Basin (Figure 15.13b).

The lower Tertiary flexure along the OKZ Axis was responsible for the rejuvenation of the coastal Lower Zambezi, initiating aggressive headward erosion, and ultimately the capture of the Palaeo-Luangwa (Figure 15.13c). The sharp change in course of the latter from south-westerly to south-south-easterly, just above the modern confluence with the Zambezi (Figure 15.2) is interpreted as a capture elbow. The timing of this capture is not well constrained, but Moore and Larkin (2001) tentatively suggest an Oligocene age in order to account for the thick sedimentary sequence of this vintage on the Mozambique coastal margin. The lowering of the Luangwa base level following this capture, coupled with increased flow in the lower Zambezi, would have accelerated the process of headward erosion. This led to the deep incision of the Cahora Bassa Gorge, to link the Lower and Middle Zambezi River systems.

Continued headward erosion of the rejuvenated, and now predatory Zambezi River led to successive captures of the Mana Pools and Gwembe Basin during the Neogene. These captures were achieved via the successive incision of the Mupata and Kariba Gorges. The resultant lowering of the base level of the Middle Zambezi caused the reversal in flow of this section of the river, which previously flowed to the south-west.

Ultimately headward erosion cut across the line of the Upper Zambezi diverting the flow of this river from the endoreic Kalahari Basin into the Middle Zambezi, to re-establish the link to the Indian Ocean (Figure 15.13d). This capture thus provided the link between the gentle-gradient upper and steeper middle sections of the river. The result was a major lowering of the base level of the Upper Zambezi, and a dramatic increase in flow to the middle and lower sections of the river. This triggered rapid headward erosion by the Middle Zambezi into the Karoo-age Batoka basalts, probably strongly influenced by east–west structural controls, and incision of the deep, 101 km length of the Batoka Gorge. Wellington (1955) suggests that the capture elbow is marked by the point where the Zambezi swings from a southerly to easterly flow direction immediately below the confluence with the Songwe, and some 10 km below the modern line of Victoria Falls (Figure 15.7). Between the modern falls and the Songwe confluence, the Zambezi flows through a zigzag series of narrow gorges with either east-north-easterly or west-north-westerly orientations. The northern edges of these gorges are interpreted to represent earlier positions of the falls, controlled by faults and fracture lines (Wellington, 1955). The Devil's cataract, on the western edge of the modern line of the falls is generally considered to mark the point where a new line of falls will develop.

The timing of the capture of the Upper Zambezi is not well constrained. However, Derricourt (1976) notes that high level gravels, now isolated from 110 m to >250 m above the Zambezi, were laid down by the river before and during the upstream migration of the falls (Clark, 1950). Gravels above the eastern end of the Batoka Gorge are tentatively ascribed a lower Pleistocene age, suggesting that the capture was of a similar vintage.

Following the early Pleistocene capture of the Upper Zambezi by the Middle Zambezi, there was a complex series of drainage reorganizations in the area surrounding the point where the boundaries of Botswana, Zimbabwe, Zambia and Namibia meet (locally termed the Four Corners Area). The low relief of the area (an undulating plain generally between 900 and 1100 m in altitude), coupled with tectonic activity along faults with a north-east–south-west orientation (Figure 15.7), transverse to the major drainage lines (Reeves, 1972), played a major role in these changes to the drainage system.

Evidence for these changes comes from fossil lacustrine deposits and landforms in northern Botswana (Figure 15.14). The Ntwetwe and Sowa Pans (together referred to as the Makgadikgadi Pans) are relics of a major lake, enclosed at the 945 m level by a variety of fossil shoreline features. The lacustrine deposits associated with the

Makgadikgadi Pans are linked, via the Boteti River, to an extensive fault-bound south-west–north-east stretch of alluvium, which extends across the Zambezi River into the Machili Basin, to the western edge of the Kafue Flats. The alluvium associated with the Machili Basin that stretches across the Zambezi is illustrated in the DEM image shown in Figure 15.15.

These alluvial deposits provide evidence for a former major inland lake, termed Lake Palaeo-Makgadikgadi (Thomas and Shaw, 1991), with a surface area of the order of 120 000 km^2 (Figures 15.13e and 15.14). Grove (1969) calculated that it is not possible to account for the existence of a lake of such proportions by any realistic increase in precipitation. He demonstrated rather, that a body of water of this size could only be maintained by inflow from the Zambezi River. The implication is that the Zambezi was at some stage diverted from its modern course to the south-west, into northern Botswana. A ferricrete bar across the Zambezi, just above Victoria Falls (Clark, 1950), attests to an episode of sub-aerial exposure of the river bed, consistent with this interpretation. The extension of the alluvium into the Machili Basin and to the Kafue flats (Figures 15.14 and 15.15) suggests that the Kafue may have also emptied into this major lake. A less extensive lake (Lake Caprivi) is recorded by fossil shorelines at the 936 m level associated with the Mababe and Ngami depressions (Shaw and Thomas, 1988). These authors suggest that this lake post-dated the Lake Palaeo-Makgadikgadi at the 945 m level, although it also required inflow from the Zambezi. They note that fossil shorelines on the Makgadikgadi Pan at elevations of 920 m and 912 m may have been maintained by overflow from Lake Caprivi via the Boteti.

Dating of the 945 m lake level, and thus the timing of the diversion of the Zambezi into northern Botswana, is not well constrained. ^{14}C ages for shells and calcretes associated with the 945 m shoreline range from 10 000 to 50 000 years BP – the upper limit of the dating technique (Thomas and Shaw, 1991). Unfortunately, the significance of these ages is difficult to interpret, as calcretes often reflect multiple episodes of carbonate precipitation. McFarlane and Segadika (2001) describe an archaeological site with Early Stone Age (ESA) tools on the floor of the Makgadikgadi Pans between the 945 and 920 m shoreline levels. These Acheulian artifacts require that the lake is at least earlier than the end of the ESA, now considered to be at least 300 ka – and likely to be even older (Barham and Smart, 1996; McBrearty and Brooks, 2000). An older age for palaeo-lake Makgadikgadi would be consistent with evidence from the Batoka Gorge presented by Derricourt (1976). He suggested that the break in river profile at the Chimamba Rapids, 40.71 km downstream of the Victoria Falls, reflects a mid-Pleistocene break in the erosion. Diversion of the Zambezi into the Makgadikgadi Pans in northern Botswana could account for this break in erosion. It would also explain the sub-aerial formation of the ferricrete on the floor of the Zambezi above Victoria Falls. This in turn requires that the point of diversion of the river into northern Botswana was upstream of the Falls. Recent reappraisal of these events reveals the ferricrete and Chimamba rapids testify to not one, but two, discrete breaks in erosion of the Batoka gorge, which concur with the complex history of tenures of successive palaeolakes in northeast Botswana (Cotterill, 2006a; Cotterill and Moore, in preparation).

The exact mechanism responsible for diverting the Zambezi into northern Botswana is not well understood, but probably involved an interplay between tectonic movement associated with the Chobe Fault, which crosses the line of the Zambezi upstream of Victoria Falls (Figure 15.14), and sedimentation in the Chobe floodplain. Present day seismic activity in northern Botswana (Reeves, 1972), with epicentres defining a north-east–south-west swath, broadly parallel to the fault lines, in northern Botswana, indicates that they are still active.

Uplift along the Linyanti Fault (Figure 15.14) diverted the Cuando from a former south-easterly course (across northern Botswana) to the north-east to link with the Zambezi via the Linyanti-Chobe floodplain. Similarly, uplift along the Chobe Fault initiated sedimentation by the Zambezi, lowering the grade of the river, and leading to the development of the Chobe floodplain. The younger sediment associated with these floodplains overlie earlier deposits that extend north-east, via the Machili Basin towards the Kafue Flats, and southwest into northern Botswana beneath the modern alluvial deposits of the Okavango Delta.

The sharp change of the course of the Kafue to the east in the area of the Kafue Flats is interpreted to be a capture elbow (Dixey, 1945; Bond, 1963) where the upper reaches of the river were captured by a north bank tributary of the Middle Zambezi. Headward erosion of the latter is logically ascribed to the lowering of base level of the Middle Zambezi following capture of the Mana Pools Basin by the Lower Zambezi. The deep Kafue Gorge, a little above the confluence with the Middle Zambezi, would reflect accelerated erosion associated with this base level lowering, coupled with the enhanced flow resulting from the capture of the headwaters. Although the timing of the capture is not well constrained, recent fieldwork has identified a lacustrine sequence of carbonate sediments that reflect the former existence of a major lake (designated Lake Patrick), with an estimated former area of 17 000 km^2, that covered most of the Kafue Flats during early to

mid-Pleistocene times (Simms, 2000). More fieldwork is required to refine our understanding of the origin and duration of Lake Patrick. However, it may have been initiated by faulting across the Palaeo-Kafue that severed the former link to the Upper Zambezi. If so, the Kafue Flats floodplain is probably a relict of this lake, which would have been drained following capture by a Middle Zambezi tributary. Lake Patrick, and the later Kafue Flats floodplain are thus interpreted to reflect the early stages of river piracy in an area of low relief before the upper sections of the river had graded to the lowered base level. The evidence therefore tentatively suggests a mid-Pleistocene age for beheading of the Upper Kafue and subsequent capture by the Middle Zambezi.

The Chambeshi River, to the north-east of the Kafue headwaters, follows a south-westerly course before swinging sharply to the north, becoming the Luapala – a headwater tributary of the Congo River (Figure 15.13e). This sharp change in course suggests a capture elbow, and that the Chambeshi originally constituted the headwaters of the Kafue (Figure 15.13c). As yet, it is not possible to date this capture with any confidence, but the relative timing is discussed ahead in relation to the dispersal and modern distribution of closely related species of lechwe antelopes, and of the tigerfish (*Hydrocynus vittatus*).

Williams (1986) suggested that the formation of the Barotse floodplain was linked to tectonic uplift. While the precise nature of this uplift is not well understood, many of the east bank Zambezi tributaries in the south of the floodplain (Figure 15.1) exhibit remarkably linear north-east–south-west courses, parallel to the major faults to the south. This suggests that the Barotse floodplain developed as a result of a lowering of the gradient caused by faulting across the line of the Upper Zambezi, coupled with the resultant sedimentation. Clark (1950) describes a ferricrete bar with embedded Middle Stone Age (MSA) lithic artifacts on the Zambezi riverbed above Ngonye Falls. This attests to a period of sub-aerial exposure, pointing to impoundment of the river above the falls. A minimum age of 300 000 years on early MSA tools (Barham and Smart, 1996; McBrearty and Brooks, 2000) indurated in the ferricrete likely underestimates the impoundment. The resultant decrease in river gradient would, in turn, have lowered base-levels of the Upper Zambezi tributaries. Because of the low relief of the area, this would have disrupted these drainages, with lines of dambos and pans marking their original courses.

The Cuando floodplain probably has a tectonic origin similar to that suggested for the Barotse floodplain. The Cuando and Barotse floodplains are linked via the Matebele-Mulongo plain (Figure 15.1), which, from DEM images, appears to be an abandoned channel that originally linked the upper Cuando and the upper Zambezi. Wellington (1955) notes that outflow from the Okavango into the Linyanti (lower Cuando), and thence into the Zambezi, sometimes occurs via the Selinda spillway (Figure 15.14). He interprets this to reflect the incipient stages of capture of the Okavango by the Zambezi.

Patterns in distributions of certain fishes in the modern Zambezi testify to the radical changes in the landscape that forged its modern configuration. This geophysical evolution simultaneously enriched its biota. An excellent example is the tigerfish, *H. vittatus*, which is among the most charismatic of African fishes. Adapted to tropical conditions, this ferocious predator is widely distributed through much of the continent's freshwaters (Figure 15.16). The species is believed to have originated in the Congo Basin; and thereafter it dispersed through south-central Africa southwards as far as southern Mozambique, and Mpumalanga and Kwa-Zulu-Natal in South Africa. Bell-Cross (1965) hypothesized that the most likely dispersal route out of the Congo Basin was into Upper Zambezi headwaters from the Kasai. This occurred only after the Kasai, a north-flowing Congo tributary, captured an easterly flowing headwater of the Upper Zambezi. Thereafter tigerfish dispersed far and wide south of the Southern Equatorial Divide.

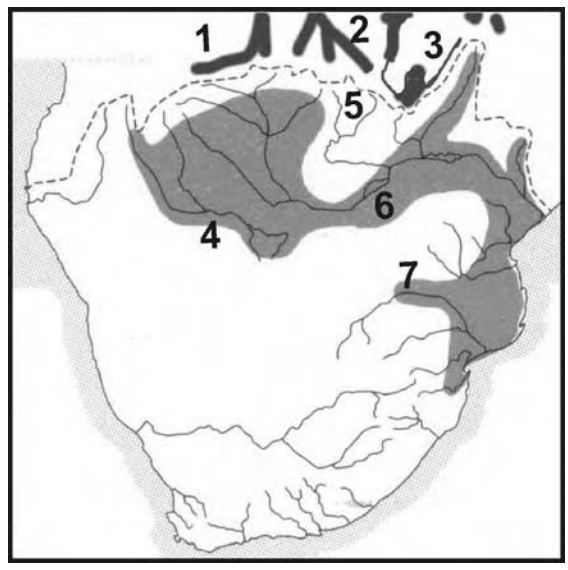

Figure 15.16 Distribution of the tigerfish (*Hydrocynus vittatus*). Dark grey: tributaries of the Congo River (1, Kasai; 2, Lufira; 3, Upper Chambeshi-Luapula). Lighter grey: drainages south of the Southern Equatorial Divide (4, Okavango; 5, Kafue; 6, Zambezi; 7, Limpopo)

Their movements have, nonetheless, been contained downstream of distinct waterfalls; and two conspicuous gaps in their modern distribution (Figure 15.16) are especially interesting. These highlight, and indeed reinforce, our insights into recent geomorphological evolution of the Zambezi and neighbouring drainage. Tigerfish are absent from the Shire River (and thus Lake Malawi) above the Shire Falls. A similar physical barrier in the Kafue Gorge, has prevented its invasion of the Upper Kafue system (Jubb, 1952; Skelton, 1994). Yet, the occurrence of tigerfish in adjacent Katanga and northern Zambia (especially the Lufira, Chambeshi, Luapula and Upper Lualaba Rivers) points to invasion of the Zambezi, only after the Chambeshi had become a Congo tributary; and equally when the Upper Kafue no longer flowed south-west and had been pirated by the Middle Zambezi creating the Kafue Gorge. We can conclude that the Kasai beheaded an Upper Zambezi tributary geologically recently. Clearly, it has followed on the breakup of the Palaeo-Chambeshi system. Therefore, the invasions by tigerfish (and several other Congo fish species) into the Upper Zambezi and adjacent rivers on the south-central African plateau occurred relatively recently in the Pleistocene (Cotterill, 2006a).

15.6 DRAINAGE EVOLUTION AND SPECIATION

The Zambezian region, and in particular the Upper Zambezi Basin, hosts a rich flora and fauna, making the area one of the world's 'hotspots' in terms of biodiversity and endemic species (White, 1965, 1983). This diversity is in turn a reflection of pulses of speciation and the evolution of many endemic organisms in the roughly 5 million years since the end of the Miocene. Examples of the rich biota of the Upper Zambezi are presented below, and the factors responsible for driving speciation are then considered. These underline the close link between evolutionary and geological processes.

The Upper Zambezi Basin lies in the centre of the Zambezian phytochorion (centre of plant endemism). At 3.77 million km^2, this phytochorion is the largest of all of Africa's nine principal centres of plant evolution. Its significance is exemplified in the occurrence of 53% endemic species of flowering plants in a total flora of no less than 8500 species (White, 1983). The headwaters of the Upper Zambezi lie within Africa's richest region of flowering plants – the Katanga-Bemba region of the Zambezian phytochorion. The magnitude of this richness can be gauged by the statistic of at least 180 endemic species of flowering plants recorded only in the degree square in which the Upper Kafue River rises (12° S; 29° E). This zone of uniqueness extends along the Southern Equatorial Divide (Figures 15.1 and 15.2): from north-east Angola across the source of the Zambezi in the Ikelenge pedicle (the narrow, north-oriented finger of land in the extreme north-west of Zambia) through Katanga and northern Zambia, and east to Lakes Tanganyika and Malawi (Linder, 2001). No less than 3000 species of flowering plants have been recorded within this Katanga-Bemba region (Malaisse, 1997).

The dambos associated with the Upper Zambezi have been a focus of major speciation, with an abundance of cryptophytic plants – or geoxylic suffrutices – aptly named underground trees because almost all the trunk and stems of these plants are buried. No less than 102 species in 55 genera of 30 families have been recorded in catchments of the Upper Zambezi, especially on the Kalahari sands. The closest relatives to many of these cyptophytes are large savanna trees. In fact besides their very different growth forms, these pairs of species (one a large tree, the other an inconspicuous suffrutex) are often very difficult to tell apart (White, 1976).

This richness of endemic plants in the Zambezian region is complemented in the fauna. This can be seen in better studied insect groups, especially the Lepidoptera. Beautiful butterflies of the genus *Charaxes* (Nymphalidae) include endemic species whose larvae feed on Zambezian plants such as *Brachystegia* (Henning, 1988). The Upper Zambezian headwaters is further characterized by a notable richness in fishes, dragonflies and reptiles, as well as certain mammals and birds. Thus, several birds are restricted to the dambos and floodplains of the Upper Zambezi. These include three species of longclaw (Fulleborn's, Grimwood's and Rosy-chested); White-throated francolin (*Pediperdix albogularis meinertzhageni*) endemic to the wide dambos of the Upper Zambezi and eastern Angola; and several cryptic species of passerine birds – especially cisticolas, including the aptly named Dambo Cisticola (Cotterill, 2006b). Another interesting example of speciation is the explosive evolution of molerats, revealed by recent research across western and central Zambia, with no less than 17 different chromosome forms, comprising six recognized species, (van Daele *et al.*, 2004). The most charismatic of the mammals is the puku (*Kobus vardoni*). The range of this dambo specialist is centred on the Zambezian region.

The endemism is further illustrated by the fragmented distributions of five isolated species of lechwe across south-central Africa. These semi-aquatic antelope are respectively endemic to Bangweulu (Black lechwe, *Kobus smithemani*), Kafue Flats (Kafue lechwe, *K. kafuensis*), with the apparently more widely distributed Red lechwe (*K. leche*) in the Okavango-Linyanti and Upper Zambezi floodplains. Roberts' lechwe (*K. robertsi*) occurred in

floodplains of the Kalungwishi and Luongo Rivers between Lakes Bangweulu and Mweru, but is now extinct. The recently described Upemba lechwe (*K. anselli*) (Cotterill, 2005) endemic to the Kamalondo depression (in the Upemba swamps of the Democratic Republic of Congo, over 300 km north of the Southern Equatorial Divide) is especially interesting, because its distribution indicates former links with rivers across a much wider area. Equally interesting, is an isolated population of lechwes in central Angola, on the northern side of the Southern Equatorial Divide in swamps in the headwaters of the Cuanza and Luando Rivers, which eventually flow into the Atlantic Ocean. These lechwes have therefore speciated across an archipelago of wetlands represented today in across the upper Congo, Okavango and Upper Zambezi drainage systems (Cotterill, 2004, 2005).

Several determinants can be singled out for not only just a high richness of species but also evolution of so many endemics, especially in the subregions (Barotse and Katanga-Bemba) within the Zambezi Basin. One has involved vicissitudes in climate, which especially through the Pleistocene, caused habitats to expand and contract sequentially. Evidence for these climatic fluctuations comes from major east–west *alab* dunes in south-western Zambia, north-western Zimbabwe and straddling the northern border between Botswana and Namibia. These dunes reflect at least three different episodes when the climate was considerably more arid than at present (Lancaster, 2000). During Pleistocene interglacials, moist evergreen forests, rich in Guineo-Congolian plants were widespread. Fragments of these forests are today restricted to headwaters of the Zambezi and Congo Rivers and along the plateau ridges. This history of expansion and contraction of evergreen forest in response to climatic change accounts for some of the speciation, but not all.

The formation and then fragmentation of wetlands by river piracy, particularly during the Pleistocene, has been an equally significant agent of pulses of speciation. Drainage evolution of the Palaeo-Chambeshi system has been invoked as the primary cause of the recent evolution of the molerats (van Daele *et al.*, 2004). The influence of river piracy is particularly well illustrated by speciation of the Lechwe antelopes. Originally, ancestral lechwe populations would have occurred more widely along the Okavango, Upper Zambezi and Palaeo-Chambeshi catchments. There is strong evidence for the last-mentioned formerly draining much of Katanga and north-east Zambia and linked with the Kafue (Figure 15.13d), although it is now part of the Congo Basin (Figure 15.13e). Contiguous habitat of these widely distributed aquatic antelopes was fragmented subsequently by late Plio-Pleistocene river piracy, leading to speciation in discrete wetlands (Cotterill, 2004, 2005). The isolated lechwe population in central Angola, discussed previously, is plausibly explained by headwater capture of originally south-flowing drainages by the Cuanza River. Generic studies, soon to be formally published, reveal these different lineages of antelopes were first isolated in the Middle Pleistocene, and thus refine the dating of river piracy events (Cotterill, 2006a).

The speciation of birds and plants endemic to dambos suggests that these habitats in Barotseland may have been important refuges during Pleistocene interpluvials when the surrounding vegetation was much more arid. Many of the larger moisture dependent savanna trees (e.g. *Parinari* and *Syzygium*) would have retreated far north as components of mesic savannas. The dominant vegetation across the Zambezian plateau in arid interpluvials was likely similar to the central Kalahari today, with arid adapted trees in valleys and grassy dunes (Barham, 2000). The current coexistence of *Parinari capensis* and *P. curatellifolia* along dambo margins in south-central Africa represents a remarkable circumstance that provides a snapshot of species' contractions and dispersions in the dynamics of palaeoenvironment.

The dramatic radiation of geoxylic suffrutices, or 'underground trees' across the Upper Zambezi valley (the area known as Barotseland) has been ascribed to the interplay of a number of factors. White (1976) notes that their characteristic habit is seasonally waterlogged anerobic grassland, mostly on extremely oligotrophic (nutrient-poor) Kalahari sands. This habitat forms as a result of the high water table in summer, and is particularly characteristic of the edges of the dambos that fringe the Upper Zambezi. Large trees are unsuited to this environment as their roots do not survive in waterlogged anaerobic conditions. White (1976) suggests that it was these inhospitable conditions that provided the trigger for large woodland tree species to adopt the suffretex growth form, leading to speciation. He inferred that such speciation appears recent, most likely Pleistocene, and that this pulse of diversification '. . . merely sharpened the edges of taxa which began their differentiation a very long time before . . .' (White, 1976: 67).

White (1976) however noted that such evolution is unlikely to have taken place by woodland tree species invading the dambos under stable conditions – they would simply not survive to colonize such an inhospitable environment. Rather, the more likely scenario has entailed gradual evolution of suffretex adaptations by these plants to correspondingly slow changes in their environments. So it appears that these Zambezian suffrutices tracked formation of the dambos. White (1976) further suggested that the latter in turn formed in response to the effects of tectonism in an area of low relief. This prescient suggestion is consistent with the proposed evolution of the

Barotse floodplain and associated dambos by faulting across the line of the river, as discussed in an earlier section. The resulting lowering of river gradients in turn initiated high summer water tables. The geoxylic suffrutices of the Barotseland area thus provide a fine illustration of geological processes driving speciation.

15.7 CULTURAL AND ECONOMIC ASPECTS

ESA artifacts recovered along the course of the Zambezi and its tributaries (Dixey, 1945; Clark, 1950; Derricourt, 1976) attest to lengthy human occupation of the Zambezi Basin. It has been suggested that in the Plio-Pleistocene, the mosaic of woodlands and dambos on the Zambezian plateau would have provided a suitable habitat for hominins that, despite the present lack of fossil remains, may have flourished in this area. The underground forests of cryptophytes would have been a most reliable food resource for hominins with requisite knowledge: a widespread and abundant source of carbohydrates (especially starch) in Zambezian dambos that extends into woodlands on Kalahari sand. Indeed, today, the San hunter-gatherers possess an intimate and indeed encylopaedic knowledge of a wealth of edible plants, including these particular cryptophytes. Acknowledgement of the potentially important role of the Zambezian region in human evolution places some ecogeographical objectivity to dominant entrenched views of hominin evolution. These focus on South and East Africa, with special devotion to the 'East side story' founded in the abundant fossil deposits of the East African Rift (O'Brien and Peters, 1999).

Today, human economics and culture are intimately linked to the changing character and seasonal cycles of the Zambezi. This is strikingly exemplified on the Barotse floodplain of western Zambia, which is home to the Lozi, who have their origins in the great Lunda-Luba Empire of the Congo Basin and probably arrived in these parts in the late seventeenth century. Comparative isolation allowed them to develop instruments of government that helped the nation exist as a political entity for more than 200 years and to have survived 40 years of domination by a migrant Sotho group, in the nineteenth century. Historically, the Lozi witnessed the first tentative steps of foreigners crossing the continent: Arab traders from Zanzibar, Mambaris (slavers) from what would become Angola, and Livingstone's double crossing of the continent in the late 1850s.

Inasmuch as people are shaped by the land in which they live, so the life and lore of the Lozi reflects the annual surges of the Zambezi's waters. Each year, high rainfall on the watershed impels the Zambezi to rise above its low banks and to begin its inundation of the great plains of western Zambia. Grasses, stimulated by the abundance of moisture, put on a sustained spurt of growth, which outpaces the rising flood. In this way a carpet of green shades the entire plain, sometimes standing a metre or more above it, creating the illusion of limitless meadow. The Lozi, who are pastoralists and agriculturalists, move ahead of the waters to the higher land that demarcates the eastern edge of the floodplains and return with their cattle and hoes when the waters recede. Centuries have shaped an elaborate and extremely colourful ceremony that marks these events.

Kuomboka is the annual ceremonial departure of the Lozi king and his counsellors from the flooded plains to the dry mainland. It symbolizes the king's leadership and the loyalty of his people and recognizes the dominating role of the annual flood in the lives of the Lozi. The move by boat is from the island of Lealui over 10 km from the mainland at Mongu. Royalty travel in splendid barges poled by bare-chested Indunas. The inhabitants, forbidden to leave before the king, follow in numerous smaller vessels.

To announce Kuomboka, the Maoma, or royal drums, are sounded a day or two before and, being heard from 15 km, echo through the night in dramatic style. Kuomboka itself is an unforgettable spectacle with reds, black, white and greens swirling in a kaleidoscope of dizzying, merging colours. Fleets of wooden canoes, the stately passage of Nalikwanda and Notila (the royal barges), the swift and sleek 'spy boats' that quest for passage and safety ahead of the procession all add to an extraordinary sight, unchanged since long before colonial times. One hundred and twenty men pole the great barge on which the royal orchestra, composed of drums and Lozi xylophones, fills the air with a deep and throbbing rhythm. It is an occasion of splendour, of colour, but, above all, a celebration of seasonable pulse of the river itself.

15.8 CONCLUSION

The readily accessible stretches of the Zambezi and its major tributaries provide a reliable perennial water source and thus an important focus of human settlement. Demands from humans have increased, and now increasingly determine the future of the flow regimes, and the riparian neighbourhood of the Zambezi. Less and less of its course escapes these demands and growing impacts. The first really major perturbation was the construction of the Kariba and Cahora Bassa Dams, creating two major manmade lakes. Two more – at Batoka and Mupata – are planned.

The major theme running though this chapter is the intimate link between geological, ecological, and evolu-

tionary processes. A clear understanding of these interwoven threads is critical to developing management plans for the Zambezi system as a whole. The large areas set aside as wilderness areas in the mid-Zambezi are coming under increasing pressure – from poaching, demands of tourism and, in accessible areas, demands for agricultural land. The war waged over several decades against the tsetse fly has greatly reduced this natural barrier to settlement of wild areas, as exemplified in the Dande, Sebungwe and Urungwe catchments of the mid-Zambezi in northern Zimbabwe. The widespread use of persistent pesticides in exterminating the tsetse fly has also conferred expensive environmental impacts (Douthwaite and Tingle, 1994). These impacts are compounded by the spread of rural subsistence agriculture across large areas of previously sparsely populated semi-arid savanna following elimination of the tsetse fly (du Toit and Cumming, 1999). These pressures require a balancing of aesthetic and economic concerns with ecological and geological constraints.

ACKNOWLEDGEMENTS

Spike McCarthy, Avijit Gupta and an anonymous referee are thanked for constructive suggestions that have improved the text considerably. Basher Attwell, Rob Cunliffe, Vivi Jedeikan and Tim Lynam are thanked for introducing the first author to the haunting wilderness of the Middle Zambezi and its memories of many changes since the far-off days of Gondwana. This is AEON Publication Number 45.

REFERENCES

Barham, L. (2000) The palaeobiogeography of central Africa. In: *The Middle Stone Age of Zambia, South Central Africa* (L. Barham, Ed.). Western Academic and Specialist Press, Bristol, 223–236.

Barham, L. and Smart, P.L. (1996) An early date for the Middle Stone Age of central Zambia. *J. Human Evol.* 30, 287–290.

Bell-Cross, G. (1965). Physical barriers separating the fishes of the Kafue and middle Zambezi river systems. *Fish. Res. Bull. Zambia* 4, 97–98.

Bond, G. (1963). Pleistocene environments in southern Africa. In: *African Ecology and Human Evolution* (F.C. Howell and F. Bouliere, Eds.). Viking Fund Publications in Anthropology. Aldine, Chicago, 308–334.

Bowmaker, A.P., Jackson, P.N. and Jubb, R.A. (1978). Freshwater fishes. In: *Biogeography and Ecology of Southern Africa* (M.J.A. Werger, Ed.). W.H. Junk, The Hague, 1181–1230.

Clark, J.D. (1950). *The Stone Age Cultures of Northern Rhodesia*. Southern African Archaeological Society, Claremont.

Cooke, H.J. (1980). Landform evolution in the context of climatic change and neo-tectonism in the middle Kalahari of northern central Botswana. *Trans. Inst. Br. Geographers* 5, 80–99.

Cotterill, F.P.D. (2004). Drainage evolution in south-central Africa and vicariant speciation in Swamp-dwelling weaver birds and Swamp flycatchers. *The Honeyguide* 25(1), 7–25.

Cotterill, F.P.D. (2005). The Upemba Lechwe, *Kobus anselli*: an antelope new to science emphasizes the conservation importance of Katanga (south-central Africa). *J. Zool. London* 265**,** 113–132.

Cotterill, F.P.D. (2006a). The evolutionary history and taxonomy of the *Kobus leche* species complex of south-central Africa in the context of Palaeo-drainage dynamics. PhD Thesis, University of Stellenbosch.

Cotterill, F.P.D. (2006b). Taxonomic status and conservation importance of the avifauna of Katanga (Southeast Congo Basin) and its environs. *The Ostruch* 77, 1–21.

Cox, K.G. (1989). The role of mantle plumes in the development of continental drainage patterns. *Nature* 342, 873–876.

Davies, B.R. (1986). The Zambezi River system. In: *The Ecology of River Systems* (B.R. Davies and K.F. Walker, Eds.). Dr W. Junk, Dordrechk, 225–267.

Derricourt, R.M. (1976). Retrogression rate of the Victoria Falls and the Batoka Gorge. *Nature* 264, 23–25.

de Wit, M.C.J. (1999). Post-Gondwana drainage and the development of diamond placers in western South Africa. *Econom. Geol*. 94, 721–740.

Dingle, R.V., Siesser, W.G. and Newton, A.R. (1983). *Mesozoic and Tertiary Geology of Southern Africa*. A.A. Balkema, Rotterdam, 375 pp.

Dixey, F. (1945) The geomorphology of Northern Rhodesia. *Proc. Trans. Geol. Soc. S. Afr*. 47, 9–45.

Douthwaite, R.J. and Tingle, C.C.D. (1994). *DDT in the Tropics: the Impact on Wildlife in Zimbabwe of Ground-spraying for Tsetse Fly Control.* Natural Resources Institute, Chatham.

du Toit, A.L. (1927). The Kalahari. *S. Afr. J. Sci*. 24, 88–101.

du Toit, A.L. (1933). Crustal movements as a factor in the evolution of South Africa. *S. Afr. Geogr. J*. 16, 3–20.

du Toit, J.T. and Cumming, D.H.M. (1999) Functional significance of ungulate diversity in African savannas and the ecological implications of the spread of pastoralism. *Biodiver. Conserv.* 8, 1643–1661.

Frost, P. H., Timberlake, J. R. and Chidumayo, E. (2002). Miombo-mopane woodlands and grasslands. In: *Wilderness: Earth's Last Wild Places* (P. Robles Gil, Ed.). Cemex Conservation International, Washington, DC, 182–204.

Gaigher, I.G. and Pott, R.Mc.C. (1973). Distribution of fishes in southern Africa. *S. Afr. J. Sci.* 69, 25–27.

Grove, A.T. (1969). Landforms and climatic change in the Kalahari and Ngamiland. *Geogr. J*. 135, 191–212.

Henning, S. P. (1988). *The Charaxinae Butterflies of Africa*. Aloe Books, Frandsen.

Jackson, P. N. B. (2000**)** Freshwater fishery research organisations in central and eastern Africa: a personal reflection, *Trans. Roy. Soc. S. Afr*. 55, 1–81.

Jubb, R. A. (1952) A note on the distribution of the *Hydrocynus vittatus* Castelnau, the well known tigerfish of the Zambezi and Limpopo rivers. *S. Afr. J. Sci*. 49, 50–51.

Lamplugh, G.W. (1907) Geology of the Zambezi basin around Batoka Gorge. Q. *J. Geol. Soci.* 63, 150.

Lancaster, N. (2000). Eolian deposits. In: *The Cenozoic of Southern Africa* (T.C. Partridge and R.R. Maud, Eds.). Oxford Monographs on Geology and Geophysics 40, 73–87.

Linder, H.P. (2001). Plant diversity and endemism in sub-Saharan tropical Africa, *J. Biogeogr.* 28, 169–182.

Main, M. (1990). *Zambezi. Journey of a River*. Southern Book Publishers, 313 pp.

Malaisse, F. (1997). *Se Nourrir en Forêt Claire Africaine: Approache écologique et nutrionnelle*. Presses Agronomiques de Gembloux, Gembloux.

McBrearty, S. and Brooks, A.S. (2000). The revolution that wasn't: a new interpretation of the origin of modern human behaviour. *J. Human Evol.* 39, 453–563.

McCarthy, T.S., Cooper, G.J.R., Tyson, P.D. and Ellery, W.N. (2000). Seasonal flooding in the Okavango Delta, Botswana – recent history and future prospects. *S. Afr. J. Sci.* 96, 25–33.

McFarlane, M.J. (1995). *Pans and dambos of Western Province, Zambia*. Backstopping mission, August 15–30, 1995. Department of Agriculture, Ministry of Agriculture, Food and Fisheries, Mongu, Western Province, Zambia. Open File Report.

McFarlane, M.J. and Segadika, P. (2001). Archaeological evidence for the reassessment of the ages of the Makgadikgadi. *Botswana Notes Rec.* 33, 83–90.

Moore, A.E. (1988). Plant distribution and the evolution of the major river systems in southern Africa. *S. Afr. J. Geol*. 91, 346–349.

Moore, A.E. (1999). A reappraisal of epeirogenic flexure axes in southern Africa. *S. Afr. J. Geol.* 102, 363–376.

Moore, A.E. and Blenkinsop, T (2002). The role of mantle plumes in the development of continental-scale drainage patters: the South African example revisited. *S. Afr. J. Geol.* 105, 353–360.

Moore, A.E. and Larkin, P.A. (2001). Drainage evolution in south-central Africa since the break-up of Gondwana. *S. Afr. J. Geol.* 104, 47–68.

Moore, A.E., Ait-Kaci, A. and Bouamar, H. (2007). A glacial ancestry for the Karoo-age Somabula alluvial gravels: implications for drainage evolution in Zimbabwe from the Permian to present 109, 625–636.

Nairn, A.E.M., Lerche, I. and Lliffe, J.E. (1991). Geology, basin analysis, and hydrocarbon potential of Mocambique and the Mocambique Channel. *Earth Sci. Rev.* 30, 81–124.

Nugent, C. (1990). The Zambezi River: tectonism, climatic change and drainage evolution. *Palaeogeogr*. *Palaeoclimat*. *Palaeoecol*. 78, 55–69.

O'Brien, E.M. and Peters, C.R. (1999). Landforms, climate ecogeographic mosaics, and the potential for hominid diversity in Pliocene Africa. In: *African Biogeography, Climate Change, and Human Evolution* (T.G. Bromage and F. Schrenk, Eds.). Oxford University Press, Oxford, 115–137.

Oesterlen, P.M. and Millsteed, B.D. (1994). Lithostratigraphy, palaeontology, and sedimentary environments of the western Cabora Bassa Basin, Lower Zambezi Valley, Zimbabwe. *S. Afr. J. Geol*. 97, 205–224.

Potter, P.E. (1978). Significance and origin of big rivers. *J. Geol.* 86, 13–33.

Price, D.J., Calder, I.R., and Hall, R.I. (1998) *Water Balance of African Lakes*. Institute of Hydrology, Wallingford, 72 pp.

Reeves, C.V. (1972). Rifting in the Kalahari? *Nature* 237, 95–96.

Reeves, C.V. (1978). A failed Gondwana spreading axis in southern Africa. *Nature* 273**,** 222–223.

Robbins, L.H. and Murphy, M.L. (1998). The Early and Middle Stone Ages of Botswana. In: *Pitswa Mmung, The Archaeology of Botswana* (P. Lane, A. Raid and A. Segobye, Eds.). Pulsa Press and Botswana Society, Gaborone, 50–64.

Shaw, P.A. and Thomas, D.S.G. (1988). Lake Caprivi: a late Quaternary link between the Zambezi and middle Kalahari drainage systems. *Zeischr. Geomorphol.* 32, 329–337.

Shoko, D.S.M. (1998). The tectono-sedimentary relationships within the Cabora Bassa basin, Zambezi Rift, with special emphasis on the Dande Sandstone Formation. PhD Thesis, University Zimbabwe, 312 pp. plus appendices.

Simms, M.F. (2000). Appendix A. Preliminary report on Lake Patrick. In: Barham, L. *Middle Stone Age of Africa*. Western Academic and Specialist Press, Bristol, 275–280.

Skelton, P.H. (1993). *A Complete Guide to the FreshwaterFishes of southern Africa.* Tutorial Press, Harare, 388 pp.

Skelton, P.H. (1994). Diversity and distribution of freshwater fishes in east and southern Africa. *Ann. Mus. Centr. Zool*. 275, 95–113.

Thomas, D.S.G. and Shaw, P.A. (1991). *The Kalahari Environment*. Cambridge University Press, Cambridge, 284 pp.

van Daele, P.A.A. G., Dammann, P., Meier, J.L., Kawalika, M., Van de Woestijne, C. and Burda, H. (2004) Chromosomal diversity in mole-rats of the genus *Cryptomys* (Rodentia: Bathyergidae) from the Zambezian region: with descriptions of new karyotypes. *J. Zool. Lond*. 264, 317–326.

Wellington, J.H. (1955). *Southern Africa – a Geographic Study*. *Volume 1, Physical Geography*. Cambridge University Press, Cambridge, 528 pp.

White, F. (1965). The savannah woodlands of the Zambezian and Sudanian Domains: an ecological and phytogeographical comparison. *Webbia* 19, 651–681.

White, F. (1976). The underground forests of Africa: a preliminary review. *Singapore Gardeners Bull.* 24, 57–71.

White, F. (1983). *The Vegetation of Africa. A descriptive memoir to accompany the UNESCO/AETFAT/UNSO vegetation map of Africa.* Unesco, Paris.

Williams, G.J. (1986). A preliminary Landsat interpretation of the relict landforms of western Zambia. In: *Geographical Perspectives on Development in Southern Africa* (G.J. Williams and A.P. Wood, Eds.). Commonwealth Geographical Bureau, James Cooke University, Queensland, 23–33.

16

The Geographic, Geological and Oceanographic Setting of the Indus River

Asif Inam[1], Peter D. Clift[2], Liviu Giosan[3], Ali Rashid Tabrez[1], Muhammad Tahir[4], Muhammad Moazam Rabbani[1] and Muhammad Danish[1]

[1]*National Institute of Oceanography, ST. 47 Clifton Block 1, Karachi, Pakistan*
[2]*School of Geosciences, University of Aberdeen, Aberdeen AB24 3UE, UK*
[3]*Geology and Geophysics, Woods Hole Oceanographic Institution, Woods Hole, MA 02543, USA*
[4]*Fugro Geodetic Limited, 28-B, KDA Scheme #1, Karachi 75350, Pakistan*

16.1 INTRODUCTION

The 3000 km long Indus is one of the world's larger rivers that has exerted a long lasting fascination on scholars since Alexander the Great's expedition in the region in 325 BC. The discovery of an early advanced civilization in the Indus Valley (Meadows and Meadows, 1999 and references therein) further increased this interest in the history of the river. Its source lies in Tibet, close to sacred Mount Kailas and part of its upper course runs through India, but its channel and drainage basin are mostly in Pakistan. Recent geological and geophysical information suggests that the Indus River system was initiated shortly after the collision between the Indian and Eurasian Plates prior to 45 million years ago (Clift *et al.*, 2001). The seasonal Indus drains an elevated and tectonically active upper basin that lies across western Tibet, the Himalaya, and the Karakoram. The Indus received water and sediment from a number of large tributaries. These are the Shyok, Shigar, Gilgit and Kabul from the north, and the Jhelum, Chenab, Ravi, Beas and Sutlej from the eastern plains of Punjab. It is the rains of the south-west monsoon of Asia that largely fill the Indus River although most of the run-off north of the Tarbela Dam comes from snow and ice melt. About 37% of the Karakoram Mountains and about 17% of the Himalaya in the upper basin carry glaciers (Tarar, 1982). The Indus, Jhelum and Chenab Rivers are the major sources of water for the Indus Basin Irrigation System (IBIS).

Seasonal and annual river flows both are highly variable (Ahmad, 1993; Asianics, 2000). Annual peak flow occurs between June and late September, during the southwest monsoon. The high flows of the summer monsoon are augmented by snowmelt in the north that also conveys a large volume of sediment from the mountains.

The 970 000 km^2 drainage basin of the Indus ranks the twelfth largest in the world. Its 30 000 km^2 delta ranks seventh in size globally. Much of the modern delta plain is rather arid, with swampy areas being restricted to the immediate neighbourhood of tidal channels and coastal plains that undergo tidal flooding. The wave power at the delta coast is about 13 $J\,s^{-1}$ per unit crest width, the fourth most powerful in the world. It rises to 950 $J\,s^{-1}$ (the highest in the world) at the offshore water depth of 10 m (Pakistan Water Gateway, 2003). Offshore, the sediment discharged by the Indus has produced the vast Indus submarine fan, about 5 million km^3 in volume (Naini and Kolla, 1982), second only to the Bengal Fan built by the Ganga-Brahmaputra Rivers.

One of the oldest known civilizations developed in the Indus Basin about 5000 years ago thriving on the waters provided by the Indus until weakening of the monsoon

Large Rivers: Geomorphology and Management, Edited by A. Gupta

probably drove this settlement into extinction (Possehl, 1997). The waters of the Indus River and its tributaries are heavily utilized for irrigation in this relatively arid area and the river is a lifeline for the economy and culture of the region (Fahlbusch *et al*., 2004). Around 25% of the modern drainage comprises irrigated crop land. The high population density of the Indus basin (145 people km^{-2}) results in major anthropogenic impacts. More than 90% of the original forests within the drainage basin have now been lost. Moreover, a number of dams and reservoirs in the basin have been constructed for flood control and electricity generation, which in turn have strikingly modified the channel and behaviour of the river.

16.2 THE DRAINAGE BASIN

16.2.1 Geology

The geology of the Indus drainage is largely shaped by the collision between the Indian Plate with mainland Asia, starting at around 50 million years ago. India is the last but largest of a series of continental blocks that rifted away from the southern super-continent of Gondwana, crossing the equatorial Tethys Ocean to form a collage of continental terrains that were stitched together to form the continent we see today. During the late Mesozoic the southern edge of Asia was characterized by north-dipping subduction and development of an Andean-type magmatic arc, whose roots can be seen today in the Hindu Kush and Karakoram. Around 120 million years ago a volcanic arc, similar to the modern day volcanic chains of Tonga or the Marianas in the western Pacific began to form within the Tethys Ocean south of palaeo-Eurasia. As subduction continued and destroyed the oceanic crust between this arc and mainland Asia it eventually collided with the active Asia margin at around 90 Ma. The oceanic 'arc' rocks, now exposed in Kohistan, were strongly deformed during their amalgamation with Eurasia. Despite this collision, north-dipping subduction of the Tethys and associated magmatic activity continued, with younger granite bodies, now exposed in Kohistan, intruding the deformed arc.

The Himalaya largely comprises the deformed northern edge of the Indian continental plate. Prior to collision India lay in equatorial latitudes and fine-grained sediments, especially limestones, dominated the shelf and slope regions. As India began to collide with Asia sedimentation changed quickly to sandstones as new mountain belts were uplifted and eroded. Along the line of collision between India and Eurasia, known as the Indus Suture Zone, a sequence of sandstones and shales document the start of mountain uplift and the birth of the Indus River. Although the northward motion of India slowed after the start of collision with Eurasia the subcontinent has continued to move northward into Asia since that time. In so doing India generated the major mountain ranges we see today. The northern edge of India was buried, deformed and heated before being brought back rapidly to the surface due to erosion, but also driven by extensional faulting triggered by the collapse of the giant mountains under their own weight. The Greater Himalaya represents the remains of the deformed northern edge of India that was intruded by granite bodies and then dramatically uplifted around 22 million years ago. As the compressional deformation migrated further south into the Indian Plate with time, new ranges have been uplifted in the Lesser Himalaya and their foothills.

Continued tectonic activity and erosion from the valleys has allowed the surrounding ranges to be uplifted to great heights. The most dramatic example of this is the peak of Nanga Parbat, located close to the Indus south of Kohistan. Nanga Parbat has been uplifting at rates of >1 cm $year^{-1}$ over recent geological times, one of the fastest such rates known anywhere in the world. Nanga Parbat also lies in a special location within the Himalayas, as east of this massif the ranges run NW–SE, while to the west they turn NE–SW. Nanga Parbat appears to mark the western edge of the colliding Indian Plate.

In contrast, the plains of Sindh and the Pakistan Shelf itself were formed in Late Cretaceous times, after about 70 million years ago, as India separated from the Seychelles. The gradual subsidence and sedimentation that have characterized the shelf and slope south-east of Karachi contrasts with the coastal and marine geology to the west. In practice Karachi lies close to a modern plate boundary. The central and eastern Arabian Sea is part of the Indian Plate and has been moving north relative to Arabia along the Owen and Murray Ridges, similar to the Chaman Fault in western Pakistan, along which the Indian block is moving north relative to Afghanistan.

16.2.2 Hydrology

The regional climate is arid to semi-arid with seasonal precipitation and significant variability. Mean annual rainfall is low, ranging from <100 mm over the lower plains to about 500 mm upstream in Lahore. Rainfall is much higher in the mountains, reaching almost 2000 mm in the frontal Himalayan Ranges. About 60% of precipitation is received during the south-west monsoon (July–September). The summer temperature everywhere in the plains is high, rising above 40 °C, resulting in a high evaporation rate. The mean annual evaporation in the upper Indus plain is more than 1500 mm, a figure that rises to over 2000 mm in the lower plains. The lower Indus,

especially the delta section, carries an extremely reduced discharge and sediment load which at times do not reach the delta shore face.

16.3 THE RIVER

The Indus is sourced at 5182 m elevation, on the northern slopes of Mount Kailash in the Gangdise Range of Tibet near Lake Mansarowar, close to the source of another major river, the Brahmaputra. The Indus River then flows north-west through the high plateau area of Ladakh into Kashmir (Figure 16.1). The river continues west-north-west past Skardu where it is joined by the Shyok at an elevation of 2730 m. Subsequently, the Indus partially circumvents the northern flanks of the Nanga Parbat-Haramosh Massif, where it first turns north along the Raikot Fault, then west, and finally south-west where the Gilgit River flows into the Indus from the west at an elevation of 1515 m. A number of past slope failures have wholly or partially blocked the river at times, even giving rise to catastrophic dam-failure floods downstream (Shroder, 1993). Cosmogenic dating of surfaces cut and abandoned by the river indicates that the Indus deepens its course at an extremely rapid pace between 2 and 12 mm $year^{-1}$ in the gorge section near Nanga Parbat (Burbank *et al*., 1996). In the same area Hancock *et al*. (1998) found the Indus capable of removing blocks of rock measuring up to 70 cm during the annual peak flow. They associated rock abrasion to the fifth power of local flow velocity and suggested that abrasion happens mainly by suspended sediment. Their measurement of annual abrasion using drill holes was ≤4 mm, which is an order of magnitude higher than the rates derived from cosmogenic nucleii as the long-term average. It is, however, evident that a very large amount of sediment, part of which is coarse, comes out of the upper Indus due to high erosive rates, periodic floods, and steep gradient of the river.

Figure 16.1 Indus River eroding Indus Molasse, Ladakh, about 1200 km upstream from the Indus Delta. (Photograph: P. Clift)

The river continues in the general south-western direction through a hilly tract as far as Durband, upstream of Tarbela, the location of a major dam of the Indus. Upstream of the Tarbela Dam, the river is deflected to the east in a loop. The Indus receives water near Tarbela through the Siran, a small and extremely seasonal stream that drains the alluvial lands of Mansehra, Abbotabad, and a part of Haripur. Downstream of Tarbela, the landscape changes and the Indus flows in a broad valley for about 50 km downstream where it reaches the Attock Gorge, cut through the compressional Trans-Indus Ranges. The gorge is 160 km upstream of Kalabagh where the plains start at an elevation of 242 m. Downstream of Kalabagh, the Indus flows for another 1600 km to the Arabian Sea. The Indus crosses the Salt Range at Kalabagh.

The upper Indus is a braided stream interrupted by gorges as it flows through the Karakoram, Kohistan, and Himalaya Ranges. The five major tributaries from the east (the Jhelum, Chenab, Ravi, Beas, and Sutlej) join the Indus River immediately downstream of Panjnad at Mithankot. These rivers drain the Lesser and Greater Himalaya and account for much of the sediment flux to the Arabian Sea. Flowing through the agricultural and densely populated Punjab, these rivers are of great importance to the agricultural productivity of the region. The Kabul River, the largest western tributary joins the Indus River near Attock, bringing material eroded from the Hindu Kush and the western Kohistan mountains. About 8 km above the Jinnah Barrage (Figure 16.2), the Soan River draining 12 400 km^2 of highly eroded Rawalpindi, Jhelum, and Attock districts, joins the Indus. It continues to be braided in its upper course in the plains until it reaches the southern Sindh region where it becomes a meandering stream. Downstream of Mithankot, a number of abandoned courses of the Indus can be recognized. Major avulsions of the river took place well above the delta, preferentially around Kashmore and Sehwan and old courses can be traced toward the Indus Delta in the lower Sindh.

16.4 EVOLUTION OF THE INDUS RIVER

Clift *et al.* (2001) showed that the Indus River was formed shortly after the collision between the Indian and the Eurasian Plates prior to 45 million years ago. The Indus is considered as one of the oldest documented rivers. The earliest Indus is older than the uplift that formed the Greater Himalaya during the Early Middle Miocene,

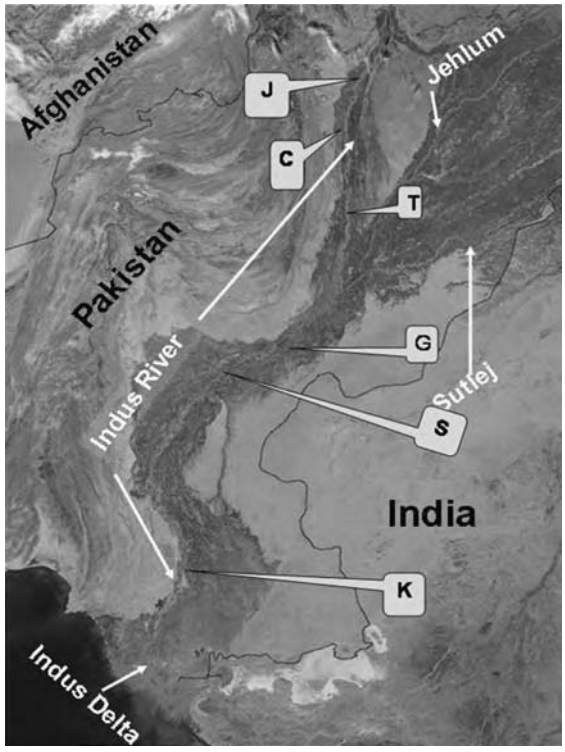

Figure 16.2 Satellite image of Pakistan, with Indus River and its drainage area. Major barrages are marked: K, Kotri; S, Sukker; G, Guddu; T, Taunsa; C, Chasma; J, Jinnah. (Image from NASA Visible Earth)

around 25–20 million years ago (Searle and Owen, 1999), and the river has followed a similar course along the Indus-Tsanpo Suture Zone in southern Tibet and Ladakh since then. According to Qayyum *et al*. (2001) two parallel west-flowing streams were in existence during the Eocene, one north and the other south of the Himalaya. These rivers jointly formed the Katawaz Delta at the western margin of the Katawaz Ocean, an embayment of the larger Tethys Ocean. The northern stream they recognized as the palaeo-Indus. The sediments of the Katawaz Delta were then axially fed into the Khojak submarine fan towards the west, now accreted and exposed in the ranges of the Makran accretional complex in Pakistan and southeast Iran.

The main stream of the Indus River has not shown much deviation from its past course in spite of tectonic events such as the uplift of the Sulaiman Range west of Punjab that displaced the main stream about 100 km towards the east since the Early Eocene. Subsequent growth of the Sulaiman Range must have pushed the course of the Indus southward by 200–300 km (Clift, 2002). Najman *et al.* (2003) interprets that 18 million years ago the palaeo-Indus first followed its modern course, cutting south through the Himalaya and into the foreland basin. According to Clift (2002), it has been flowing in approximately the same location since then. Shroder and Bishop (1999) were of the opinion that the Indus River was flowing somewhat north and well to the west of its present location during the late Cenozoic, but was captured and diverted to the south close to the Nanga Parbat massif of today as a result of extensional structures and downfaulted topography across the Kohistan Ladakh island arc terrain.

Using isotope data to trace evolving provenance Clift and Blusztajn (2005) have shown that the source of the sediment reaching the Arabian Sea changed sharply after 15 million years ago. The sudden increase in very radiogenic sediment into the Indus River was interpreted to reflect large-scale drainage capture of the Punjabi tributaries into the Indus shortly after 15 million years ago. The reason for the large-scale transfer of drainage from the Ganga to the Indus is not clear but was probably linked to regional subsidence in Pakistan caused by uplift of the Salt Ranges during the Pliocene.

In the restricted migration of the main channel, the Indus differs from several other large rivers. For example, the Nile (Said, 1981), Colorado (Elston and Young, 1991), and Amazon (Hoom *et al.*, 1995) all have present courses that differ from their past locations during the Late Miocene or later periods following regional uplift in their basins. The Indus remained pinned in the suture zone and flowing along an active strike-slip plate boundary within its foreland. The Indus therefore is located in an active tectonic region but without significant change in course through time.

Larger changes, however, are seen near its mouth. Since the last glacial maximum (about 20 000 years ago), the location of the main depositional lobe of the Indus Delta and the main channel had shifted significantly westward four times until it came to occupy its present course (Kazmi, 1984). The Indus River and its delta are prevented from moving further west by the uplifting ranges running north from Karachi.

16.5 THE INDUS DELTA

During the Holocene, the Indus has formed a vast deltaic complex in southern Sindh, most of which has been abandoned due to frequent natural channel avulsions. Much of the alluvial plain from the modern delta coast to north of Sukkur (Figure 16.2) has probably been formed during the last deglacial period and the Holocene, when the Indus

River filled its own valley system that was incised during the last sea level low-stand (Kazmi, 1984). Several remnants of the pre-deltaic relief composed of Eocene limestone outcrop within the delta. A relic feature of the pre-Holocene relief is the Indus Canyon (Figure 16.3), which is erosional in its upper part on the shelf and slope, where no levees are present (von Rad and Tahir, 1997). Because of the high sea-level stand, the impact of fluvial sediment is not strong enough to maintain a supply of coarse sediment to the deep-sea. The delta extends to the east into the Great Rann of Kutch, a vast mudflat area that is invaded by storm surges during the summer monsoon. The Rann of Kutch is probably a former gulf of the Arabian Sea that has been filled by deltaic deposition (Malik *et al*., 1999; Rajendran and Rajendran, 2001 and references therein).

The lobate delta of the Indus formed under arid climate conditions under important but highly variable river discharge, a moderate tidal range, extremely high wave energy, and a strong monsoonal wind system. The relatively coarse grade of the river sediments and the fact that most sediment is delivered in phase with summer monsoon wind setup that promotes retention of sand close to the shore was proposed to have favoured rapid expansion of the subaerial delta (Wells and Coleman, 1984). However, high silt and low carbonate contents in surface sediments on the modern Indus shelf (Nair *et al*., 1982; Khan *et al.*, 1993) show that sediments from the Indus River are dominant to depths of ~60–70 m. Geophysical and core data near the Indus Canyon show only patches of a thin veneer of Holocene sediments suggesting that the outer shelf has been largely nondepositional during the Holocene (Rasul, 1992; Prins *et al.*, 1995; von Rad and Tahir, 1997). The modern coastline is dissected by numerous tidal creeks that are reworked remnants of former river channels. The intricate network of creeks once supported one of the largest mangrove systems in the world. Dispersal of sediments delivered to the Arabian Sea by the river is accomplished by tidal and wind-driven currents. Tides are semidiurnal with a tidal range at the Karachi gauge of

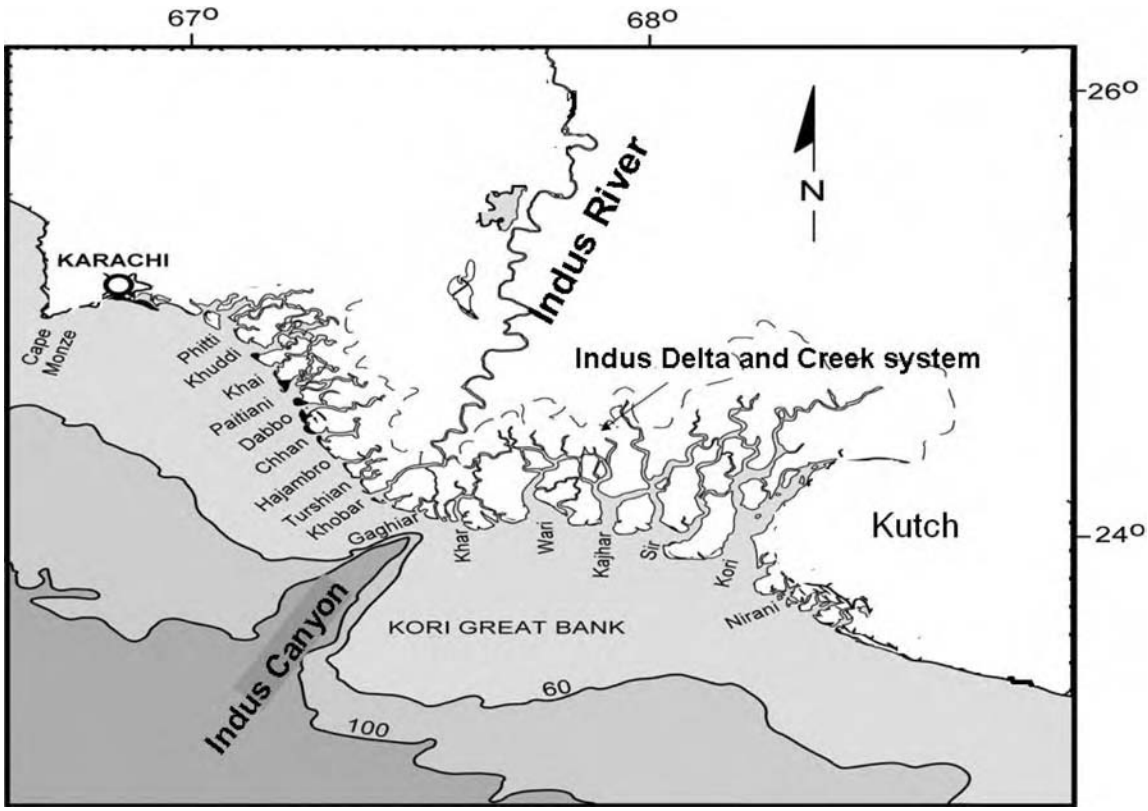

Figure 16.3 Lower Indus River with a network of major creeks and offshore bathymetric features (modified from Giosan *et al.*, 2006)

2.7 m. Measurements near Karachi show that the mean current switches from south-westerly during the summer monsoon to north-easterly during the winter monsoon (Rizvi *et al.*, 1988). The Indus Canyon is also presumed to have played a role in preventing the subaqueous delta from developing by capturing and funnelling sediment towards the Indus submarine fan (Islam, 1959; Nair *et al*., 1982; Wells and Coleman, 1984). The Indus shelf exhibits a clear compound clinoform morphology (Giosan *et al.*, 2006). Accumulation and erosion occurred primarily on the nearshore clinoform that extends along the entire delta coast from the shoreline to the 15–25 m water depth. At the active Indus mouths, the nearshore clinoform has built directly into the Indus Canyon, where sedimentation rates exceeded 50 cm $year^{-1}$. A second clinoform developed offshore between 30 and 90 m water depth is composed of three distinct lobes (Giosan *et al.*, 2006).

Abandoned Indus delta channels have been reworked by tides all along the coast into dendritic tidal creeks (Figure 16.3). The tidal creek network appears to be most extensive and mature east of the present Indus mouths (Khobar, Gaghiar) towards Kutch, where the coast has a dissected appearance typical of tide-dominated deltas. The wide channels of this eastern delta plain (Khar, Wari, Kajhar, Sir, and Kori) penetrate deep inland, leading to flooding of wide areas of the lower delta plain and the Rann of Kutch during the summer monsoon (Figure 16.3). The deltaic coast from Karachi to the river mouths exhibits a dense, less mature tidal channel network. A stronger wave influence along this part of the coast compared with further east is suggested by the frequent occurrence of drumstick-shaped barrier islands (Figure 16.4), typical of island systems significantly influenced by both waves and tides (Stutz and Pilkey, 2002).

16.6 SUBMARINE INDUS SYSTEM

Seaward of its delta, the Indus is transformed into a complex and spectacular distributory system which has created the world's second largest submarine fan in the Arabian Sea. The basic elements of this vast distributary system are deeply incised Indus Canyon, pronounced

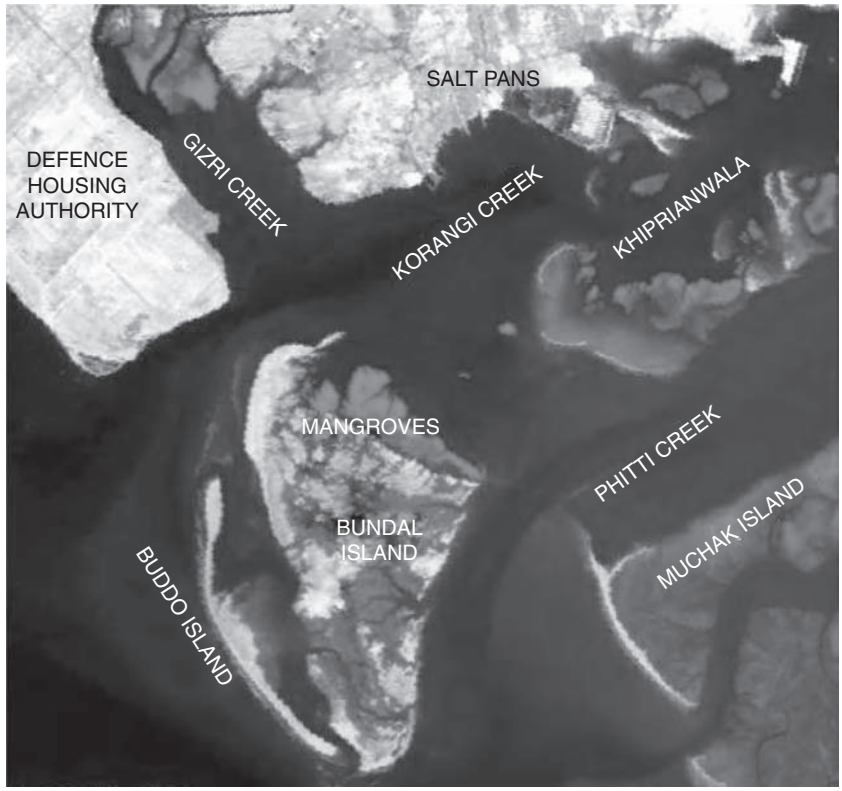

Figure 16.4 Satellite image of the barrier islands off the Indus Delta (NIO Report, 2001)

bathymetric channel-levee systems of various orders, and low-lying terminal sand lobes and sheets. The morphological features of this submarine 'fluvial' system exhibit striking similarities, both in shape and position, with morphological features of mature fluvial systems such as intricate meanders accompanied by neck and chute cut-offs, levee and crevasse-splay deposits, point bars, a full range of straight, meandering and braided channel patterns, gooseneck or convex down-valley asymmetric loops, anabranching and bifurcation channel patterns (Ayub, 1992).

The modern Indus Canyon commences close to the delta coast, about 3.5 km from mouth of the Gaghir Creek and in the water depths approximately 20 m and then progressively deepens seaward across the continental shelf and slope region with a maximum relief of about 1030 m in the shelf break vicinity. Along its approximately 185 km long traverse its average width is about 8 km and it shows a broad north-westward bend in the outer shelf and slope area (von Rad and Tahir, 1997).

The Indus Canyon, like many other large riverfed canyons, is considered to have been initiated and progressively developed by the extension of the channel of the Indus River over the subaerial continental shelf exposed during the Quaternary low sea levels and deposition of sediments at outer shelf/upper slope where turbidity currents and mass wasting processes eroded backward to carve the canyon during the glacial and interglacial times/periods/events.

At its mouth in the lower slope water depths of 1400 to 1500 m the canyon widens to 20 km (Coumes and Kolla, 1984) and transforms to large channel-levee systems of predominantly depositional/aggradational character, and progressively becomes transitional to erosional in the lower order distributary system further downfan. The youngest large channel extends to as far as 500 km up to the Upper Indus fan area where a radial pattern of small-order distributary channel-levee systems emanate.

The large channels are typically 300–400 m deep and 6–10 km wide near the foot of the continental slope, where they start, and decrease both in depth (100 to 120 m) and width (<2 km) in the distal part in the upper fan, between 2900 and 3300 m water depths. These are characterized by 10–30 km wide and up to 1100 m thick individual levee (overbank) deposits which attain a relief up to 800 m from the surrounding fan surface.

The average dimensions of small channels also progressively decrease downfan. The channel depths vary from 80 to 20 m, and widths become less than 2 km. The widths of individual levee deposits range from 20 km to 5 km and the height of levees from 60 m to about 5 m. In the extreme lower reaches, the small channels are devoid of levees and are entrenched below the fan surface. All the channels of higher and smaller order systems meander with variable sinuousity along their respective courses.

The turbidity currents are considered the main process of transporting the terrestrial sediments of the Indus River through this intricate and vast network of canyon-channel-levee complexes, to the farthest parts of the Indus Fan. There were at least two other complexes active earlier during the late Miocene and Pliocene times that are comparable with the modern Indus canyon-channel-levee complex of Pleistocene age, but only one canyon-large channel system was active at a time (Kenyon *et al.*, 1995). Thus numerous channel-levee complexes extensively migrated both in time and space, vertically as well as laterally, and ultimately coalesced and stacked resulting in the formation of voluminous Indus Fan deposits.

Thus, in fact the journey of the Indus River that started at the heights of about 5000 m in a geologically dynamic land region ends at the placid depths of about 4500 m in the Arabian Sea.

16.7 WATER MANAGEMENT

The water of the Indus has been used for six millennia from the Harappan period to the present through a series of different historical regimes and often in an organized fashion. The last half of the twentieth century, however, has seen the transfer to very large-scale management of the water system. Currently about 60 % of the Indus water is estimated to be used for irrigation, supplying water to more than 161 800 km^2, about 80 % of Pakistan's agricultural fields (Iftikhar, 2002). More than 150 000 km^2 of farmland is irrigated, giving rise to the highest national irrigated to rain-fed land ratio (4 : 1).

Pakistan depends on irrigation for producing 90 % of its food and other crops (World Bank, 1992; Asianics, 2000). This requires three major storage reservoirs, 19 barrages or headworks, and 43 major canals with a total conveyance length of 57 000 km. There are 89 000 watercourses with a running length of more than 1.65 million km.

The construction of the barrages and canals has, over the years, led to a systematic removal of water from the Indus (Table 16.1). According to several early estimates, construction of barrages, dams, and link canals has reduced the annual freshwater flow downstream from >150 billion m^3 to less than 45 billion m^3 (Keerio and Bhatti, 1999). The actual effect of the engineered diversions from the Indus River, however, is much more alarming, especially regarding the future conditions in the delta (Inam *et al.,* 2004). The subsurface hydrology of the basin is also affected. Between 1972 and 1997 the contribution of groundwater to irrigated agriculture nearly doubled in

Pakistan, from 32 billion m^3 $year^{-1}$ to 62. Next year it declined to 50 billion, equivalent to 38% of the surface water diversion. Engineering structures across the river have also reduced the sediment load travelling down the Indus. The annual sediment load of the pre-engineered Indus varied between 270 and 600 million t (Milliman *et al*., 1984). It is a fraction of that at present.

Table 16.1 Major dams and barrages on the Indus River

Structure	Year of construction	Maximum discharge capacity ($m^3 s^{-1}$)
Tarbela Dam	1976	18 386
Mangla Dam	1967	24 630
Ghazi Barotha Hydropower project	2004	500 000
Jinnah Barrage	1946	950 000
Chashma Barrage	1971	1 100 000
Taunsa Barrage	1959	750 000
Guddu Barrage	1962	1 200 000
Sukkur Barrage	1932	1 500 000
Kotri Barrage	1955	875 000

Modified after Pakistan Water Gateway (2003).

Most of the lower Indus basin is flat and the natural drainage flow is gradual allowing a rise in the water table. The prevalent canal irrigation system has resulted in large-scale problems of water logging and salinity. Approximately 60% of the aquifer underlying the IBIS is of marginal to brackish quality.

To mitigate the menace of rising groundwater and the associated problem of waterlogging and salinity, a network of drainage canals was constructed within the Indus Basin to drain groundwater directly to the Arabian Sea. The drainage system has been less effective due to low gradient of the flat topography and has in fact resulted in the intrusion of sea water to about 80 km upstream (Panhwar, 1999). Sea water intrusion is much worse during the south-west monsoon (Figure 16.5).

The increase in salinity due to depleting fresh water contribution by the Indus River has reduced the suitability of the delta for the cultivation of red rice, the production of exotic fruit, and raising of livestock. The mangrove ecosystem is being degraded, and the mangroves are now virtually monospecific and comparatively stunted with losses of about 2% $year^{-1}$. Degradation of the mangroves is due to a combination of water flow reductions and direct human destruction and over use. The major changes in river flow below Kotri have affected the ecology in the

Figure 16.5 One of the drainage canals in the Indus deltaic area of Keti Bandar where the sea water is entering irrigated land through a defective gate

lower Sindh and the coastal areas significantly, besides adversely affecting agricultural production.

The human population in and around mangrove forests on the Sindh coast is estimated to total 1.2 million people, nearly 900 000 of whom reside in the Indus Delta (Salman, 2002). Of these, a predominantly rural population of more than 135 000 depends on mangrove resources for their livelihoods (Shah, 1999). Reductions in freshwater inflows have had tangible impacts on mangrove ecology, and on the fish populations that rely on them for breeding and habitat. At least three-quarters of the rural population of the delta depend, directly or indirectly, on fishing as their main source of income, and most of Pakistan's commercial marine fishery operates in and around the mangrove creeks on the coast of Sindh Province. A large proportion of fish and crustaceans spend at least part of their life cycle in the mangroves, or depend on food webs originating there (Meynell and Qureshi, 1993).

The effect of anthropogenic alteration in the delta is reflected in the reduced water and sediment discharge downstream of the Kotri Barrage (Figure 16.6) near the delta. Prior to the construction of major dams and barrages along the Indus River, the recorded average annual discharge of water and sediment downstream of Kotri Barrage was 107 billion m^3 and 193 million t, respectively. The major decline in the water and sediment discharges to the delta occurred after the commissioning of the Mangla Dam (1967) and the Tarbela Dam (1976). From 1998 onwards, water and sediment discharges have declined at an alarming pace below Kotri Barrage, especially when the rainfall has been low.

The effect of the engineered structures on the Indus River water discharge can be measured by the number of days with no flow below Kotri Barrage. There was not a single day with zero flow before Kotri Barrage was constructed in 1955 (Figure 16.7). Zero-flow days were observed during 1962–1967, the maximum number in a year rising to 100. This increased to 250 days in the year in the post-Kotri and post-Mangla period (1967–1975). The present situation is even more alarming due to the current trend in low rainfall in the basin of the Indus River. At present, the Indus flows downstream of the Kotri Barrage for only 2 months: August–September. A discharge of less than 1 billion m^3 was observed downstream of the Kotri Barrage for the last couple of years (Inam *et al.*, 2004). As a consequence braiding and sand bars have become common in the river south of Kotri. Sediment passing down the system tends to be deposited in the section below Kotri rather than maintaining the growth of the delta (Figure 16.8).

16.8 THE INDUS DOLPHINS

One of the most threatened dolphins in the world is the freshwater species known as the Indus River dolphin or *Bhulan*, which lives in the Indus. The dolphins of

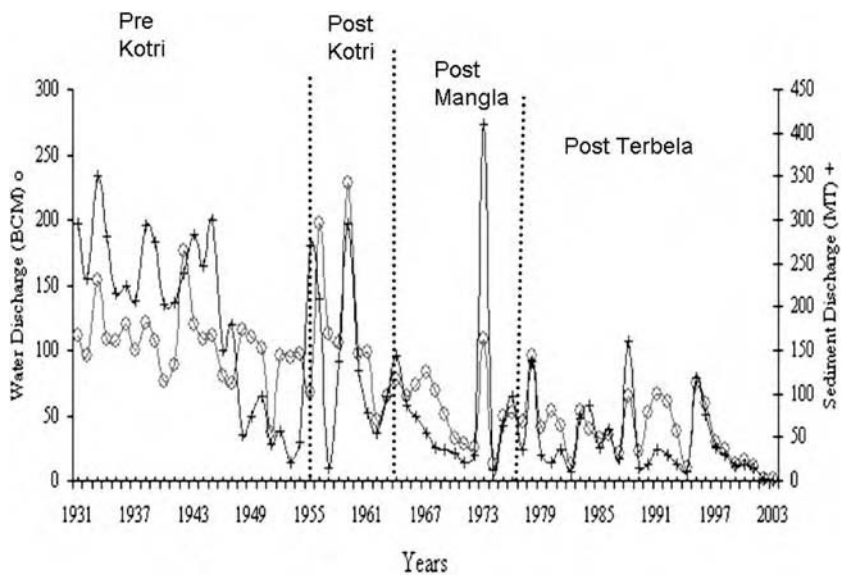

Figure 16.6 Variation in water and sediment discharge below Kotri (modified from Milliman *et al*., 1984)

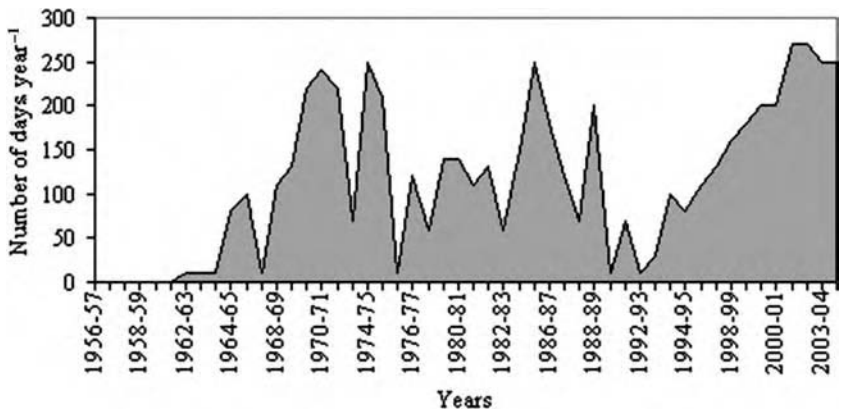

Figure 16.7 Numbers of days per season with zero flow downstream of Kotri Barrage (modified from Asianics, 2000)

Figure 16.8 Isolated water ponds downstream of the Kotri Barrage can be seen during most of the year. The flow of water downstream of the Kotri Barrage results in the catastrophic resuspension of fine sediments deposited on the dried river bed

the Indus and the Ganga rivers are unusual among the five most endangered species as these are functionally blind. Impassable irrigation barrages on the Indus River have trapped the dolphins into small populations. More than 600 dolphins are trapped between Guddu and Sukkur barrages, and progressively moving upstream, about 250 recorded between Taunsa and Guddu and less than 100 between Chashma to Taunsa. In the lower Indus, a 500 km long river sector between Sukkur and Kotri barrages has less than 20 dolphins. The low numbers probably are due to extraction of water from the river for irrigation, leaving a very low dry-season discharge through the area.

16.9 ENVIRONMENTAL CHANGES

Over time, the rich flora and fauna attracted settlements directly to the banks of the Indus and also along the numerous canals and distributary channels off it. During the eighteenth and nineteenth centuries, large volumes of water and sediment were discharged round the year through the delta. Two river ports, Keti Bandar and Shah Bandar, used to handle all imports and exports between Sindh and Bombay. The coastal agricultural areas near Keti Bandar, Kharo-Chan, and Shah Bandar produced rice which was the main export crop. Seaborne cargo traffic in transit to the upper Sindh was transported by boats. In general, the area was prosperous and the socioeconomic condition of the residents was very good. During the south-west monsoon, the boat traffic remained suspended as the vessels could not enter the delta due to the storminess of the wet monsoon. The drastic reduction of the water and sediment discharges down the Indus following the construction of Kotri Barrage in 1955 resulted in the loss of several hundred square kilometres of fertile land. The once prosperous port area of Keti Bandar was reduced to a fishing village and the population was forced to change their age old profession of farming to fishing and also to migrate to other parts of the delta in search of fresh water and shelter from saline intrusions. The anthropogenic impact of upstream water and sediment blockage resulted in the shrinkage of the active delta and also stunted the growth of the mangrove forest (Figure 16.9).

16.10 HUMAN-INDUCED CHANGES IN THE INDUS DELTA

The lack of environmental awareness led to any release of water to the Indus Delta being considered as wastage. The

Figure 16.9 The mangrove forest along the Indus Delta is rapidly diminishing due to the scarcity of fresh water and decline in the sediment contribution from the Indus River

Table 16.2 Rapidly declining water and sediment discharges downstream of the Kotri Barrage

Period	Average annual water discharge ($10^9 m^3$)	Average annual sediment discharge ($10^9 t$)
1931–1954	107	193
1955–1962	126	149
1963–1967	72	85
1968–1976	47	82
1977–1997	45	51
1993–2003	10	13

Source: Irrigation Department, Government of Pakistan (unpublished).

Table 16.3 Post-dam construction variations in sediment and water discharge downstream of the Kotri Barrage

Period	Average annual water discharge ($10^9 m^3$)	Average annual sediment discharge ($10^9 t$)
Pre-Kotri Barrage	110	184
Post Kotri Barrage	68	85
Post Mangla	47	82
Post Terbela	37	43

Source: Irrigation Department, Government of Pakistan (unpublished).

Indus Delta itself was perceived as a wasteland of mudflats, creeks, and mangroves (Asianics, 2000). The effect of anthropogenic changes in the fluvial regime by the construction of the dams and barrages on the Indus River can be seen in the historic records of sediment and water discharge to the Indus Delta. The average annual water and sediment discharges during 1931–1954 were $107 \times 10^9 m^3$ and $193 \times 10^9 t$, respectively. This discharge rate, over the years dropped to $10 \times 10^9 m^3$ and $13 \times 10^9 t$ during the 1993 to 2003 period (Table 16.2). Prior to the construction of the Kotri Barrage the average annual water and sediment contribution of Indus River to its delta was about $110 \times 10^9 m^3$ and $184 \times 10^9 t$, respectively (Table 16.3). Kotri Barrage and subsequently, Mangla and Terbela Dams, restricted the passage of freshwater and sediments to the deltaic area, causing significant ecosystem changes progressively compounded by increased freshwater removal (Table 16.3). For most part of the year, no flow travels down the river between Sajawal (about 90 km below Kotri Barrage) and the river mouth at Khobar Creek (Inam *et al.*, 2004). Fresh water now reaches the deltaic area infrequently during the south-west monsoon.

Sixteen major creeks make up the original Indus Delta but, following the reduction of flow downstream from the Kotri Barrage, only the area between Hajamro and Kharak Creeks now receives water from the Indus with one main outlet (Khobar Creek) to the sea. Compared with the other creeks of the Indus Delta, the bottom sediments of the Khobar Creek are significantly coarser and more compact. In general, the mean grain size suggests that the flow of the river is not capable of carrying coarse sediment downstream to the river mouth. The sediment that the Indus has carried to the delta is confined within the channel of the Khobar Creek until a flood event flushes out the unconsolidated sediment to the Arabian Sea (Inam *et al.*, 2004). No marine component, such as shell fragments, was found. The coarser sediments at the mouth of the channels are reworked by wave and tidal processes and the gentle slope favours sediment deposition. Such an environment facilitates the winnowing of the fines while the coarser sediment is deposited as lag material.

Currently the Indus River hardly contributes any sediment to the delta or the Arabian Sea. The active delta is reduced to only $1200 km^2$ in area from the $6200 km^2$ observed before the construction of the series of dams and barrages on the Indus (Asianics, 2000). Consequently, sea water has intruded upstream in the delta, extending up to 75 km locally in the coastal areas of Thatta, Hyderabad, and Badin districts. According to Sindh's irrigation and Power Department (IPD) seawater intrusion has resulted in tidal infringement over about $4850 km^2$ in delta. The near absence of riverine freshwater downstream of Kotri coupled with the strong seawater intrusion has destroyed large areas of prime agricultural land, including submersion of several villages on the coast (Figure 16.10). This in turn has caused desertification and displacement of a several hundred thousand local residents living there for

Figure 16.10 The Indus River flowing by the coastal village 'Sajanwari' in the Indus Delta. Seawater intrusion has destroyed one of the most fertile agricultural areas in the delta

Figure 16.11 (See also colour plates.) Satellite image of the Indus Delta in 2000 showing how the coast has changed since 1950. The coast in 1950 is shown as a red line, with yellow depicting sand bars developed near the mouth (unpublished, Stefan Constatinescu, University of Bucharest, Romania). (Image from NASA Visible Earth)

many generations. Furthermore, the Indus Delta is subject to the highest average wave energy of any major delta in the world (Wells and Coleman, 1984), mainly due to the intense monsoon winds that produce high energy waves. An extreme level of wave energy and little or no sediment contribution from the Indus River together are transforming the Indus Delta into a wave-dominated delta and sandy beaches and dunes are developing along the former deltaic coastline.

Comparison of recent satellite images with the topographic and bathymetric maps of the region published in 1950 provides evidence for widespread retreat of the coast and widening and deepening of tidal inlets (Figure 16.11). The subaerial morphology of the delta suggests wave and tide influences west of the active river channel, whereas it is tide-dominated to the east of the river mouth. Deltaic evolution in natural conditions between 1855 and 1954 was characterized by active sediment accumulation in two major depocentres: the nearshore zone along the entire delta coast and the western shelf between ~25 and 40 m water depth. Until 1954, the shoreline advanced or was stable along most of the delta coast. The progradation rate at the active mouth surpassed 100 m year^{-1}. The clinoform at the mouth has directly built into the head of a major submarine canyon that dissects the shelf. Deposition patterns on the shelf suggest that the Indus Delta has produced a compound clinoform on the western shelf, probably as a result of extremely active sediment transport under an energetic mixed wave-tide regime. Development of a nearshore clinoform simultaneously with an entirely submerged clinoform challenges the current sedimentation and facies models that emphasize single clinoform development as a delta progrades across the shelf. After the reduction in discharge in the late 1950s, the deltaic shoreline along most of the western coast started to recede at rates of ~50 m year^{-1}. Surprisingly, the eastern tide-dominated coast remained stable or even prograded. This differential shoreline behaviour suggests an active role for sediment transfer processes in the reworking of abandoned deltaic coasts (Giosan *et al.*, 2006). Active accretion of the coast is limited to the south-central part of the delta lobe where the river used to discharge until its recent westward shift to the Khobar Creek. Near the salt flats of the Rann of Kutch to the east, the coastline appears to be stable and has even advanced seaward since 1950. The tidal channels, however, are much wider closer to the sea than before, indicating active erosion. Loss of the coastal land is most acute between the Khobar Creek and Karachi (Giosan *et al.*, 2006).

16.11 CONCLUSION

Most of the upper drainage basin of the Indus River lies within the Karakoram with smaller parts within the Kohistan, Hindu Kush, and High Himalaya Mountains. The Indus has occupied a relatively stable course throughout its history due to its location within the Indus-Tsanpo Collision Suture and also because of the strike-slip alignment towards Afghanistan to the west. It has deposited a considerable amount of alluvium in the Himalayan foreland basin, and has built the huge alluvial plains of Punjab and Sindh. Over six millennia, the Indus River has been

the source of water that supported the economy of the region, nurturing old and modern civilizations. The flux from the river has enabled an extremely large irrigation system to be developed within its drainage basin. However, these engineering structures also had adverse impacts on the once fertile and richly vegetated deltaic area of the Indus.

The life of the delta is dependent on the availability of freshwater and sediment. The severe reduction of both as a result of dams, barrages and associated structures upstream has resulted in the pronounced erosion in parts of the delta and consequently in the reduction of the mangroves. The faunal and floral assemblages in the delta have shifted from estuarine to hypersaline types. Coastal erosion is increasing also due to unplanned coastal development in the area. The well-being of the delta requires a realistic assessment of the minimum volume of river water and sediment needed round the year to prevent the near-disappearance of the Indus Delta. The management of the delta should become part of an integrated coastal zone management in a holistic fashion. Not only the coastal environment should be managed integrally but environmental studies also need to be extended to the entire Indus ecosystem from the mountains to the Arabian Sea.

REFERENCES

Ahmad, N. (1993) *Water resources of Pakistan and their utilisation. Mirajuddin*, PUB. 61-B/2, Gulberg III, i-5, 19, Lahore.

Asianics Agro-Dev. International (Pvt) Ltd. (2000) *Tarbela Dam and related aspects of the Indus River Basin, Pakistan*. A World Commission on Dams case study prepared as an input to the World Commission on Dams, Cape Town, 212 pp.

Ayub, A. (1992) Channel-levee systems on the Indus Deep-Sea Fan. University of Wales, PhD thesis (unpublished), 385 pp.

Burbank, D.W., Leland, J., Fielding, E., Anderson, R.S., Brozovic, N., Reid, M.R. and Duncan, C. (1996) Bedrock incision, rock uplift and threshold hillslopes in the northwestern Himalayas. *Nature*, 379, 505–510.

Clift, P.D. (2002) A brief history of the Indus River, In: *The Tectonics and Climatic Evolution of the Arabian Sea Region* (P.D. Clift, D. Kroon, J. Craig and C. Gaedicke, Eds.). Geological Society of London Special Publication 195, pp. 237–258.

Clift, P.D. and Blusztajn, J. (2005) Reorganization of the western Himalayan river system after five million years ago. *Nature*, 438, 1001–1003, doi:10.1038/nature04379.

Clift, P.D., Shimizu, N., Layne, G., Gaedicke, C., Schlüter, H.U., Clark, M. and Amjad, S. (2001) Development of the Indus Fan and its significance for the erosional history of the Western Himalaya and Karakoram. *Geological Society of America Bulletin*, 113, 1039–1051.

Coumes, F. and Kolla, V. (1984) Indus Fan: seismic structure, channel migration and sediment thickness in the upper fan. In: *Marine Geology and Oceanography of Arabian Sea and Coastal Pakistan* (B.U. Haq and J.D. Milliman, Eds.). Van Nostrand Reinhold, New York, pp. 101–110.

Elston, D. and Young, R.A. (1991) Cretaceous-Eocene (Laramide) landscape development and Oligocene-Pliocene drainage reorganization of Transition Zone and Colorado Plateau. *Journal of Geophysical Research*, 96(B7), 12389–12406.

Fahlbusch, H., Schultz, B. and Thatte, C.D. (2004) *The Indus Basin: History of Irrigation, Drainage and Flood Management.* International Commission on Irrigation and Drainage, New Delhi.

Giosan, L., Constantinescu, S., Clift, P.D., Tabrez, A.R., Danish, M. and Inam, A. (2006) Recent morphodynamics of the Indus delta shelf and coast. *Continental Shelf Research*, 26(14), 1668–1684.

Hancock, G.S., Anderson, R.S. and Whipple, K.X. (1998) Beyond power: bedrock river incision process and form. In: *Rivers over Rock: Fluvial Processes in Bedrock Channels* (K.J. Tinkler and E.E. Wohl, Eds.). American Geophysical Union, Geophysical Monograph 107, Washington, DC, pp. 35–60.

Hoom, C., Guerrero, J., Sarmiento, G.A. and Lorente, M.A. (1995) Andean tectonics as a cause for changing drainage patterns in Miocene northern South America. *Geology*, 23, 237–240.

Iftikhar, U. (2002) Valuing the economic costs of environmental degradation due to sea intrusion in the Indus Delta. In: *Sea Intrusion in the Coastal and Riverine Tracts of the Indus Delta – a Case Study*. IUCN – The World Conservation Union, Pakistan Country Office, Karachi, p. 48.

Inam, A., Khan, A.T.M., Amjad, S., Danish, M. and Tabrez, A.R. (2004) Natural and man made stresses on the stability of Indus deltaic eco-region. Extended Abstract, The 5th International Conference on Asian Marine Geology, Bangkok, Thailand (IGCP475/APN).

Islam, S.R. (1959) The Indus submarine canyon. *Oriental Geography*, 3, 101–104.

Kazmi, A.H. (1984) Geology of the Indus Delta. In: *Marine Geology and Oceanography of Arabian Sea and Coastal Pakistan* (B.U. Haq and J.D. Milliman, Eds.). Van Nostrand Reinhold, New York, pp. 71–84.

Keerio, G.R. and Bhatti, M.A. (1999) Major factors of degradation of Indus Delta mangrove ecosystem. In: *Proceedings of the National Seminar on Mangrove Ecosystem Dynamics of the Indus Delta.* Sindh Forest & Wildlife Department, Karachi, pp. 91–101.

Kenyon, N.H., Amir, A. and Cramp, A. (1995) Geometry of the younger sediment bodies of the Indus Fan. In: *Atlas of Deep Water Environments: Architectural Style in Turbidite Systems* (K.T. Pickering, *et al.*, Eds.). Chapman and Hall, London, pp. 89–93.

Khan, A.A., Memon, M.G., Danish, M. and Inam, A. (1993) Distribution of surface sediments off Indus delta on the continental shelf of Pakistan. *Pakistan Journal of Marine Sciences*, 2(1), 33–39.

Malik, J.N., Merh, S.S. and Sridhar, V. (1999) Palaeo-delta complex of Vedic Sarasvati and other ancient rivers of northwestern India. *Memoir – Geological Society of India*, 42, 163–174.

Meadows, A. and Meadows, P.S. (Eds) 1999. The Indus River. In: *The Indus River: Biodiversity, Resources, Humankind.* Oxford University Press, Delhi, 441pp.

Meynell, P.J. and Qureshi, M.T. (1993) Sustainable management of the mangrove ecosystem in the Indus Delta. In: *Towards the Wise Use of Wetlands* (T.J. Davis, Ed.). Wise Use Project, Ramsar Convention Bureau, Gland, Switzerland.

Milliman, J.D., Quraishee, G.S. and Beg, M.A.A. (1984) Sediment discharge from the Indus River to the ocean: past, present and future. In: *Marine Geology and Oceanography of Arabian Sea and Coastal Pakistan* (B.U. Haq and J.D. Milliman, Eds.). Van Nostrand Reinhold, New York, pp. 66–70.

Naini, B.R. and Kolla, V. (1982) Acoustic character and thickness of sediments of the Indus Fan and the continental margin of western India. *Marine Geology*, 47, 181–185.

Nair, R.R., Hashimi, N.H. and Purnachandra Rao, V. (1982) On the possibility of high-velocity tidal streams as dynamic barriers to longshore sediment transport: evidence from the continental shelf off the Gulf of Kutch, India. *Marine Geology,* 47(1–2), 77–86.

Najman. Y., Garzanti, E., Pringle, M., Bickle, M., Stix, J. and Khan, I. (2003) Early-middle Miocene paleodrainage and tectonics in the Pakistan Himalaya. *Geological Society of America Bulletin*, 115, 1265–1277.

NIO Report. (2001) Feasibility study to restore and develop Bundal & Khiprianwala Island. A study carried out by National Institute of Oceanography, Karachi Pakistan, 256 pp (unpublished).

Pakistan Water Gateway. (2003) The gateway, hosted and managed by IUCN, addresses water as a resource in its many dimensions, serves to assess and disseminate shared experiences, publicize policies and guidelines and facilitate cooperation on water issues. http://www.waterinfo.net.pk.

Panhwar, M.H. (1999) Seepage of water of the River Indus and occurrence of fresh ground water in Sindh. In: *The Indus River: Biodiversity, Resources, Humankind* (A. Meadows and P. Meadows, Eds.). Oxford University Press, Delhi, pp. 180–197.

Possehl, G. (1997) Climate and the eclipse of the ancient cities of the Indus. In: *Third Millenium BC Climate Change and Old World Collapse* (H.N. Dalfes, G. Kukla and H. Weiss, Eds.), NATO ASI Series 1, vol. 49. Springer, New York, pp. 193–244.

Prins, M.A., Postma, G., Cramp, A.C. and Kenyon, N. (1995) Late Quaternary sedimentation on the Indus Fan. Abstract, Oral Presentation in the Workshop on the Arabian Sea. Texel.

Qayyum, M., Niem, A.R. and Lawrence, R.D. (2001) Detrital modes and provenance of the Paleogene Khojak Formation in Pakistan; implications for early Himalayan Orogeny and unroofing. *Geological Society of America Bulletin*, 113, 320–332.

Rajendran, C.P. and Rajendran, K. (2001) Characteristics of deformation and past seismicity associated with the 1819 Kutch earthquake, northwestern India. *Bulletin of the Seismological Society of America*, 91(3), 407–426.

Rasul, N. (1992) Late Quaternary to present day coarse-grained sedimentation of the Indus fluvial-marine system. University of Wales, PhD thesis (unpublished).

Rizvi, S.H.N., Ali, A., Naeem, S.A., Tahir, M., Baquer, J., Saleem, M. and Tabrez, S.M. (1988) Comparison of the physical properties of seawater offshore the Karachi coast between the northeast and southwest monsoons. In: *Marine Science of the Arabian Sea. Proceedings of an International Conference* (M. Thompson and N.M. Tirmizi, Eds.). American Institute of Biological Sciences, Washington, DC, pp. 519–569.

Said, R. (1981) *The Geological Evolution of the River Nile*. Springer-Verlag, Heidelberg.

Salman, A. (2002) Draft proposal for economic valuation of mangrove ecosystem in Pakistan. Prepared for South Asia Network for Development and Environmental Economics, Kathmandu.

Searle, M.P. and Owen, L.A. (1999) The evolution of the Indus River in relation to topographic uplift, climate and geology of western Tibet, the Trans-Himalayan and High-Himalayan Range. In: *The Indus River: Biodiversity, Resources, Humankind* (A. Meadows and P.S. Meadows, Eds.). Oxford University Press, Delhi, pp. 210–230.

Shah, G.R. (1999) Sociological conditions of Indus Delta Rehabilitation and Replanting of Mangrove Project (IDRRMP) community and the use of mangrove ecosystem. In: *Proceedings of the National Seminar on Mangrove Ecosystem Dynamics of the Indus Delta.* Sindh Forest & Wildlife Department, Karachi, pp. 112–123.

Shroder, J.F., Jr. (Ed.) (1993) Himalaya to the sea: geomorphology and the Quaternary of Pakistan in the regional context. In: *Himalaya to the Sea.* Routledge, London, pp. 1–42.

Shroder, J. F. and Bishop, M. P. (1999) Indus to the sea: evolution of the system and Himalayan geomorphology. In: *The Indus River: Biodiversity, Resources, Humankind* (A. Meadows and P.S. Meadows, Eds.). Oxford University Press, Delhi, pp. 231–248.

Stutz, M.L. and Pilkey, O.H. (2002) Global distribution and morphology of deltaic barrier island systems. *Journal of Coastal Research*, Special Issue 36, 694–707.

Tarar, R.N. (1982) Water resources investigation in Pakistan with the help of Landsat imagery snow surveys 1975–1978. In: *Hydrological Aspects of Alpine and High-Mountain Areas. International Commission on Snow and Ice (ICSI) Symposium, Exeter, UK, 19–30 July 1982. Proceedings* (J.W. Glen, Ed.). International Association of Hydrological Sciences, IAHS/AISH Publication no. 138, Boulder, CO, pp. 177–190.

von Rad, U. and Tahir, M. (1997) Late Quaternary sedimentation on the outer Indus shelf and slope (Pakistan); evidence from high-resolution seismic data and coring. *Marine Geology*, 138, 193–236.

World Bank. (1992) Reservoir Maintenance Facilities Project (PCR), Agriculture Operation Division, South Asia Region, Report 10725, Washington, DC.

Wells, J.T. and Coleman, J.M. (1984) Deltaic morphology and sedimentology, with special reference to the Indus River delta. In: *Marine Geology and Oceanography of Arabian Sea and Coastal Pakistan* (B.U. Haq and J.D. Milliman, Eds.). Van Nostrand Reinhold, New York, pp. 85–100.

17

The Ganga River

Indra B. Singh

Department of Geology, Lucknow University, Lucknow 226007, India

17.1 INTRODUCTION

From its source to the sea the river is intimately related to the civilization and culture of India. The 2525 km long Ganga (also known as the Ganges) drains a 1 060 000 km^2 basin that covers 26.2% of India's total surface area between the southern slopes of the Himalaya Mountains and the northern Indian Peninsula (Rao, 1975). About 80% of the basin lies in India, the rest in Nepal, China (Tibet), and Bangladesh. The collision tectonics of the Himalaya controls the Ganga system (Figure 17.1) and is responsible for the formation of Ganga Plain foreland basin (Lyon-Caen and Molnar, 1985; Singh, 1987, 1996). The huge discharge and sediment load of the river have formed an extensive alluvial plain, the large Ganga-Brahmaputra delta system, and the largest submarine fan in the world (the Bengal Fan). A large amount of sediment is derived from the fast-eroding Himalaya, a smaller portion from the Indian Peninsular Craton, and some is recycled from alluvial plain.

The Ganga begins as the Bhagirathi from the Gangotri Glacier at Gaumukh at an altitude of 3800 m. The combined flow, after the Bhagirathi meets the Alaknanda at Devprayag, is known as the Ganga. Both the Bhagirathi and the Alaknanda have well developed drainage networks in the Himalaya Mountains. About 300 km from Gaumukh, the river leaves the mountains to enter the alluvial plain at Haridwar at an elevation of about 290 m.

From Haridwar downstream, the Ganga flows in a well-defined valley. No significant tributary joins the Ganga for 410 km until Kannauj, where the Ramganga comes in from the north (Figure 17.2). After another 300 km downstream, the Yamuna (the largest tributary) joins the Ganga on its southern bank at Allahabad. Originating in the Himalaya, the Yamuna collects the discharges of several rivers of the Indian Peninsula from the south and contributes a large volume of water and sediment to the Ganga. About 58.5% of the total augmented flow of 130 billion m^3 at the confluence is from the Yamuna (Das Gupta, 1984). Between Allahabad and Patna, several important tributaries join the Ganga: the Gomati, Ghaghara, and Gandak from the north and the Tons and Son from the south. Beyond Patna, the Burhi Gandak and Kosi join the Ganga from the north, and smaller rivers, the Punpun and Phalgu, from the south.

The Ganga then passes through the volcanic Rajmahal trap rocks of Rajmahal Gap, enter the delta at Farakka, and splits into distributaries (Figures 17.2 and 17.3). The main distributary enters Bangladesh, where it is known as the Padma, to meet the Brahmaputra, locally known as the Jamuna. Their combined flow joins the Meghna, and this huge volume of water and sediment passes through the Meghna estuary into the Bay of Bengal. The other major distributary of the Ganga, the Bhagirathi, flows south through India, collecting drainage from a number of rivers off the north-eastern edge of the Indian Peninsula: the Ajay, Damodar, Rupnarayan, and Haldi. The Bhagirathi flows past Kolkata (Calcutta) to enter the Bay of Bengal as the Hugli.

17.2 HYDROLOGY

The Ganga is a seasonal river. The wet south-west monsoon brings 70–80% of annual rainfall between July

Large Rivers: Geomorphology and Management, Edited by A. Gupta

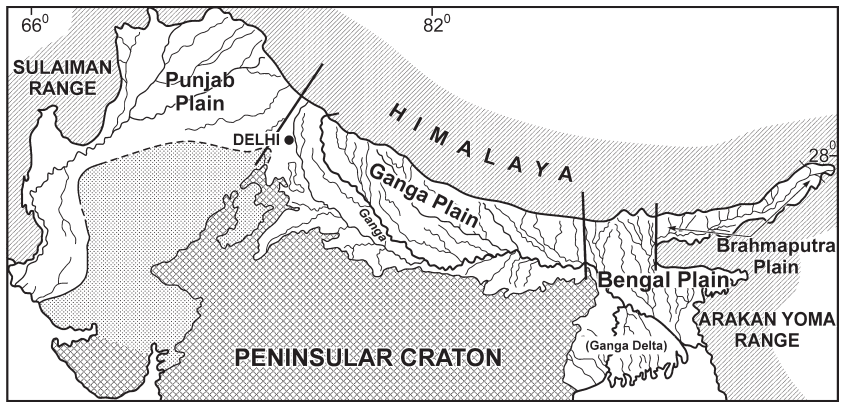

Figure 17.1 Schematic map showing the plains of north India and the alluvial basin between the Himalaya and Peninsular Craton

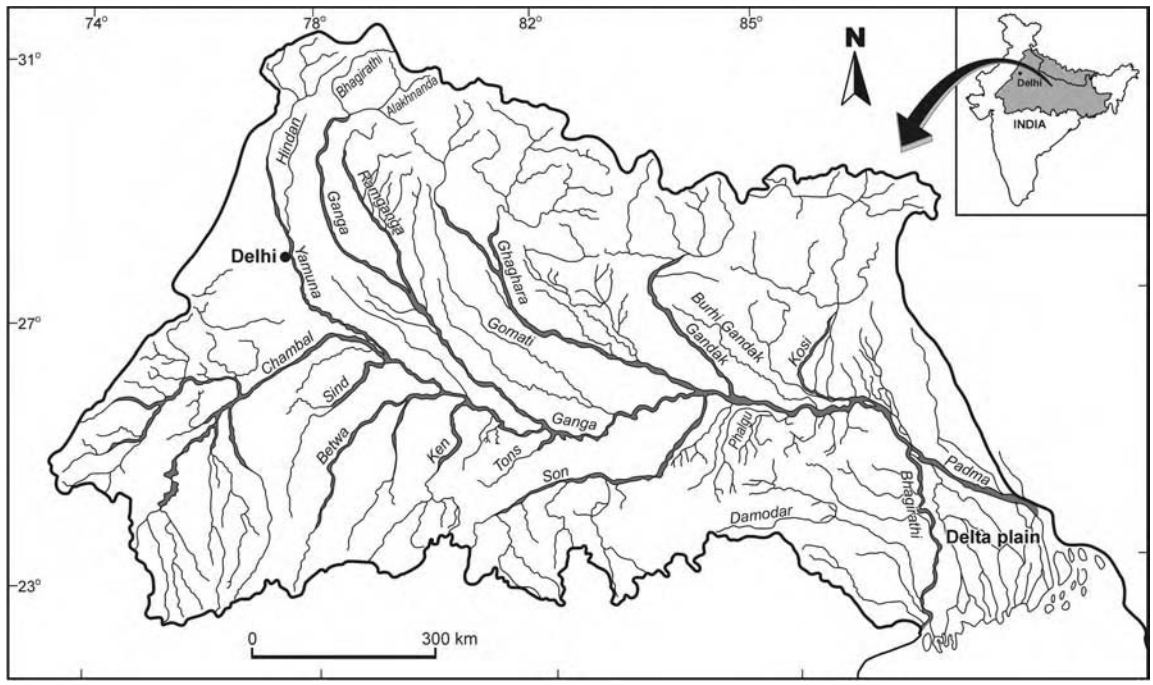

Figure 17.2 The Ganga Basin and the drainage net

and September over the basin. The percentage in certain locations rises to 90. The rain can be intense. For example, 150 mm in a single day has been reported. Normally, the south-west monsoon becomes active in Bengal by early June and extending westward covers the entire Ganga River basin by mid-July. The south-west monsoon continues to be effective until October. The average annual rainfall decreases gradually from east to west, from about 1600 mm in Bengal to about 500 mm in the western Uttar Pradesh and Haryana. Rainfall rises in the Himalaya to 1500–2300 mm. The south-western part of the basin has low rainfall of about 500–700 mm. The discharge of the Ganga varies not only seasonally, but also from day to day on certain occasions. Such a variation requires careful

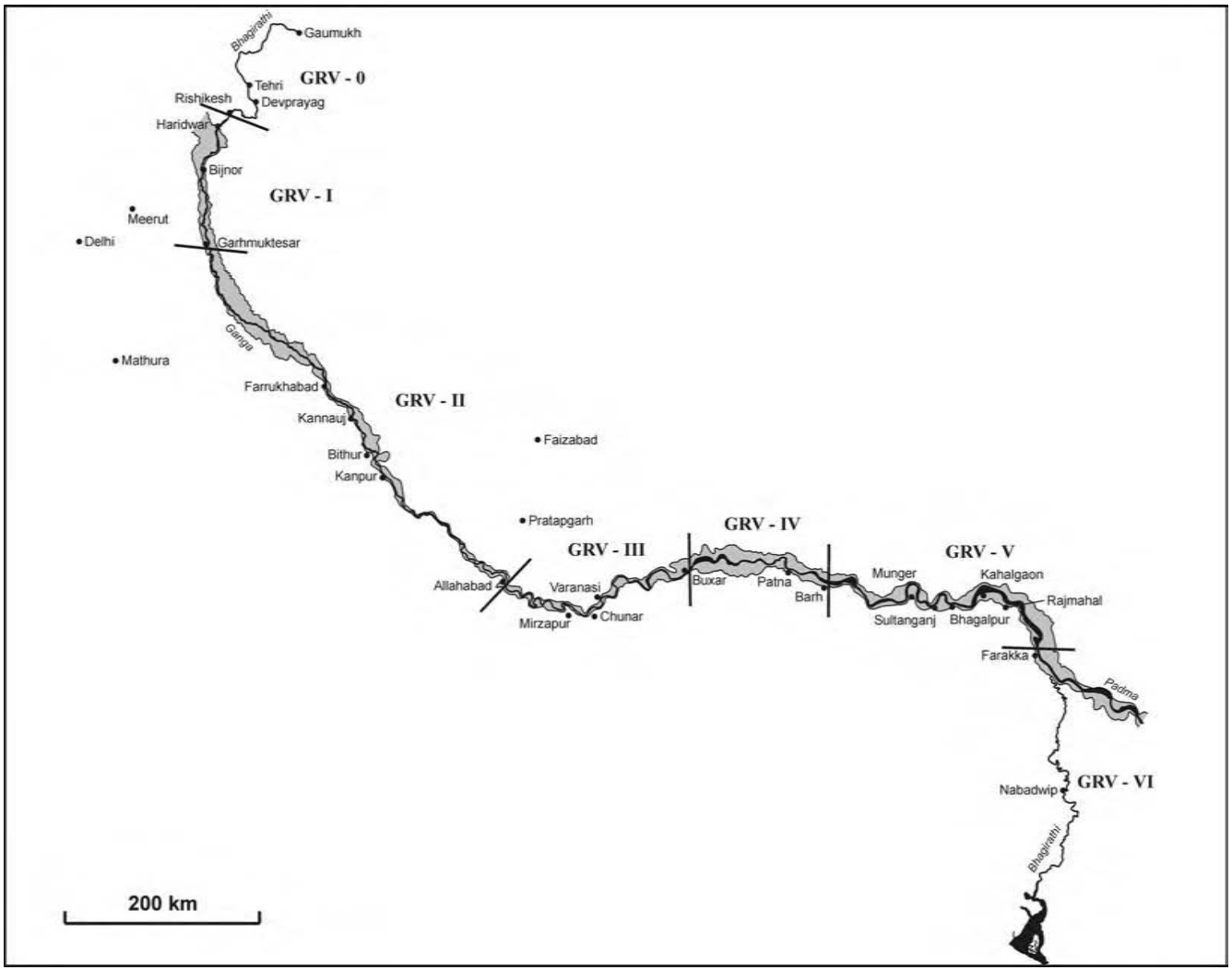

Figure 17.3 Schematic map showing Ganga River, its alluvial valley and segments (GRV-0 – GRV-VI) and principal towns

monitoring for pollution management and water utilization. The annual hydrograph at Farakka (Figure 17.4) indicates that the flow of the river remains low for most of the year. High flows occur during the wet monsoon season (July–October) including several peaks of very high discharge. The maximum and minimum discharges at different monitoring stations vary by a factor of 10–100. The seasonal variation is reflected in changes in channel pattern. The Ganga becomes a large single channel during the rainy season, reverting to a sandy braided course during the drier parts of the year. The Ganga River contributes about $460 \times 10^9\,m^3$ of water annually to the delta region. The total annual water discharge of the combined Ganga–Brahmaputra Rivers to the delta region is about $971 \times 10^9\,m^3$ (Milliman and Meade, 1983).

Rain and subsurface flows are the main sources of river discharge, with a limited contribution from the meltwater of the Gangotri Glacier at the source of the river. The discharge along the river demonstrates a stepwise increment due to the contribution of the major tributaries draining different parts of the basin. The large contributions are from the Yamuna, Ghaghara, Kosi, Gandak, Son and Gomati Rivers (Figure 17.5). The estimated discharge of Ganga River from Gangotri glacier is about $30–120\,m^3\,s^{-1}$.

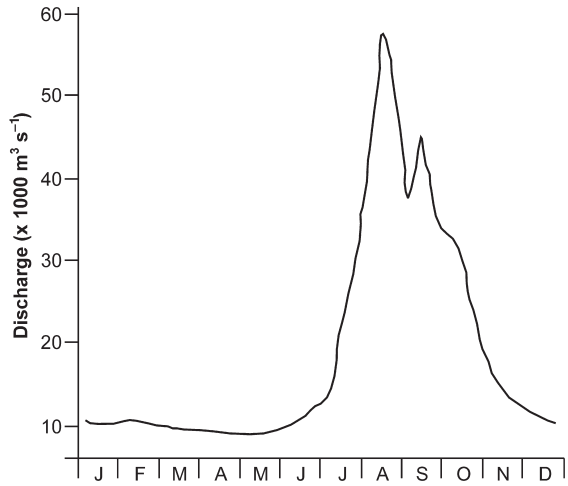

Figure 17.4 Hydrograph of the Ganga River at Farakka. High discharge during the months of south-western monsoon (July–October). (Modified after Rao, 1975)

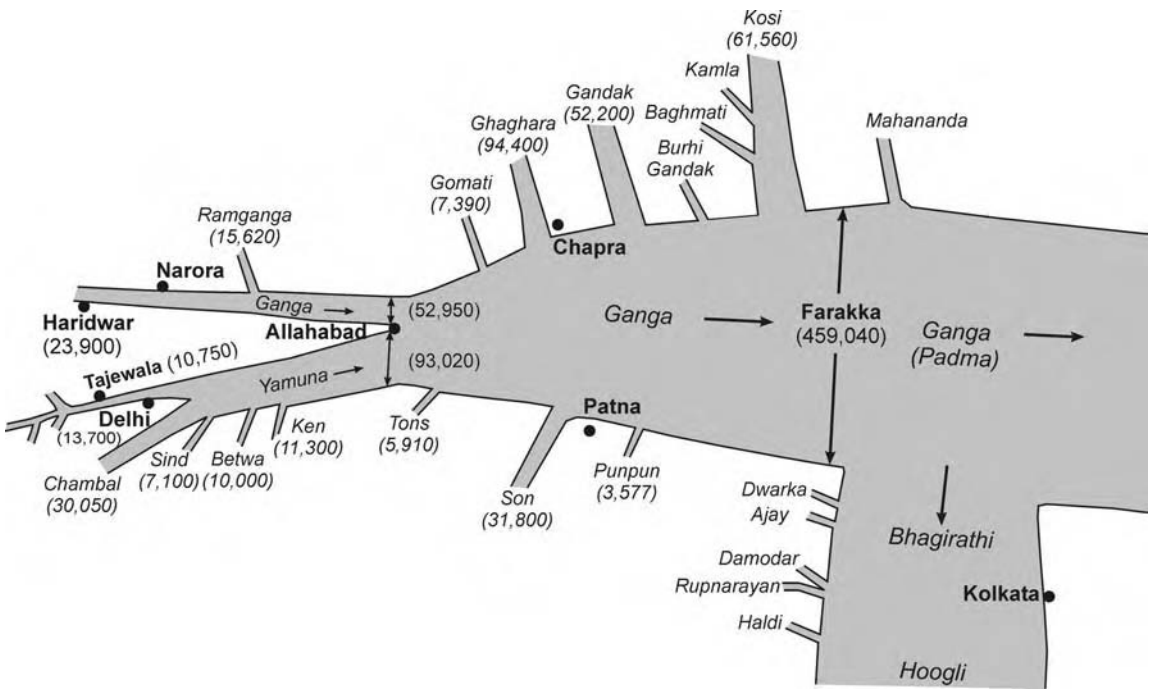

Figure 17.5 Schematic representation of contributions of different rivers in the Ganga basin and their annual discharge in $m^3\,year^{-1}$. (Modified after Rao, 1975)

At Devprayag, where the Alaknanda and Bhagirathi meet, the average peak flow is about 1775 $m^3 s^{-1}$, of which an estimated 28.7% is from glacial meltwater (Jain, 2002). Further downstream at Rishikesh, the monthly discharge is low from January to April, but increases in May possibly due to glacier melt. High discharges are from July to September. At Balawali, immediately downstream from Haridwar, the discharge is less than at upstream stations due to large-scale withdrawal of water through the Upper Ganga Canal System at Haridwar. Similar drop in discharge is seen at Fatehgarh, due to withdrawal of water at Narora (Naraura) for the Lower Ganga Canal System. Figure 17.6 and Table 17.1 summarize the seasonal variation of discharge along the Ganga. Details of the monsoon discharge of the Ganga River is given in Table 17.2. The discharge data of the Ganga River (Table 17.1) indicates (1) a small rise for more than 650 km from the source attributable to glacial meltwater in May, (2) contributions

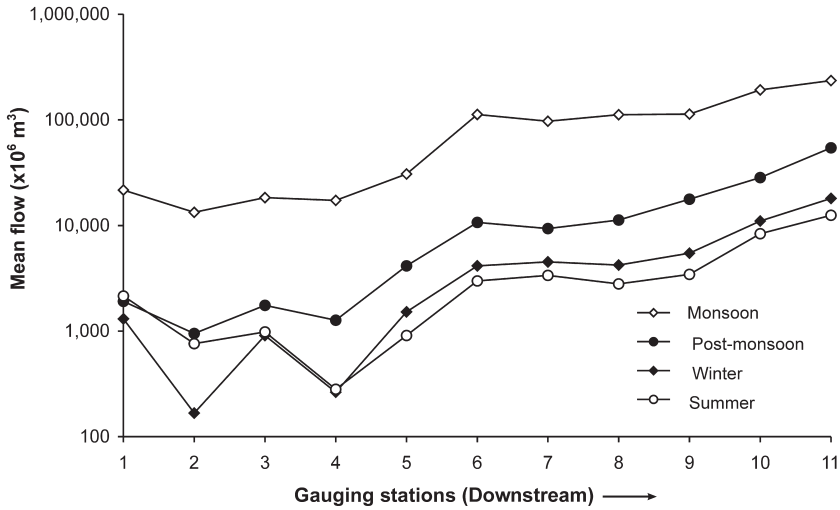

Figure 17.6 Seasonal flow at different gauging stations along the Ganga (based on Das Gupta, 1984). Monsoon (June–September); post-monsoon (October–November); winter (December–February); summer (March–May). Stations: 1, Rishikesh; 2, Balawali; 3, Garhmuktesar; 4, Fatehgarh; 5, Kanpur; 6, Allahabad; 7, Mirzapur; 8, Varanasi; 9, Buxar; 10, Patna; 11, Azamabad. Up to Fatehgarh summer discharge is more than winter discharge due to snowmelt contribution

Table 17.1 Seasonal variation in flow at various stations of the Ganga River (after Das Gupta, 1984)

Stations	Mean seasonal flow ($\times 10^6 m^3$)				
	Monsoon (June–Sept.)	Post-monsoon (Oct.–Dec.)	Winter (Jan.–March)	Summer (April–May)	Total flow ($\times 10^6 m^3$)
Rishikesh	21 631	1 912	1 305	2 150	26 998
Haridwar	15 952	2 447	1 507	1 467	21 393
Balawali	13 306	947	167	760	15 180
Garhmuktesar	18 392	1 756	908	982	22 038
Fatehgarh	17 300	1 266	264	281	19 111
Kanpur	30 763	4 139	1 518	910	37 330
Allahabad	112 278	10 703	4 148	2 987	130 116
Mirzapur	97 142	9 362	4 529	3 362	114 395
Varanasi	112 206	11 244	4 213	2 793	130 456
Buxar	113 247	17 741	5 463	3 438	139 889
Patna	192 625	28 488	11 044	8 341	240 498
Azamabad	235 357	54 494	18 055	12 474	320 380

from large tributaries such as the Yamuna at Allahabad and the Ghaghara, Gandak and Son near Patna, (3) loss of water due to withdrawal for irrigation at Rishikesh, Balawali, Narora, and Mirzapur, and (4) the passage of only a fraction of the Ganga water into the Bhagirathi after the bifurcation near Farakka. The mean peak discharge of the undivided river near Farakka is 70 547 $m^3 s^{-1}$ (Figure 17.5). About 60% of the discharge arrives from the Himalaya and the northern plains, the rest from the south (Das Gupta, 1984).

Table 17.2 Variation in monsoon discharge at various stations of the Ganga River (after Das Gupta, 1984 and other sources)

Stations	Mean monsoon flow ($m^3 s^{-1}$)	Maximum flow observed, $m^3 s^{-1}$ (year)	Mean annual flow ($m^3 s^{-1}$)
Devprayag	1 775	–	–
Haridwar	5 860	–	678
Balawali	3 898	–	481
Garhmuktesar	5 800	6 940 (1978)	699
Kanpur	6 317	14 071 (1961)	1 184
Allahabad	24 131	58 377 (1971)	4 126
Varanasi	21 262	46 186 (1971)	4 105
Patna	37 424	65 849 (1978)	7 626
Azamabad	49 968	83 047 (1971)	10 159
Farraka	55 776	–	–

On average, each square kilometre of the Ganga Basin receives a million m^3 of water annually as rainfall; 30% of this is lost through evaporation, 20% seeps to the subsurface, and the remaining 50% is available as surface runoff (Das Gupta, 1984). The deep channel of the river bounded by high banks facilitates the passage of groundwater as baseflow during the dry season.

Annual flooding is characteristic of all rivers in the Ganga Plain. Agarwal and Chak (1991) have discussed the flood problems of the Ganga plains and the Himalaya. The Ganga River rises during the wet monsoon but usually its high banks restrict the floodwater from spreading. Overtopping and lateral spreading occur only in certain areas. Water moves into the active floodplain also through gullies cut through the levees of the river. The floodplain is usually 0.5–2 km wide, sloping gently away from the levees and ending against a step, several metres high, leading to the next alluvial surface (T_1, see Section 17.7, Figure 17.7). This active flood plain surface is flooded almost on a yearly basis, the rise in stage varying between 2 and 8 m along the river. The next higher alluvial surface (T_1) is flooded only on a decadal scale. It is, however, usually waterlogged in the wet season due to the combined effect of (1) the expansion of shallow channels and other water bodies that occur on its surface, (2) rising shallow groundwater table, and (3) backwater effects on the yazoo-type streams when the Ganga is in flood. The next higher

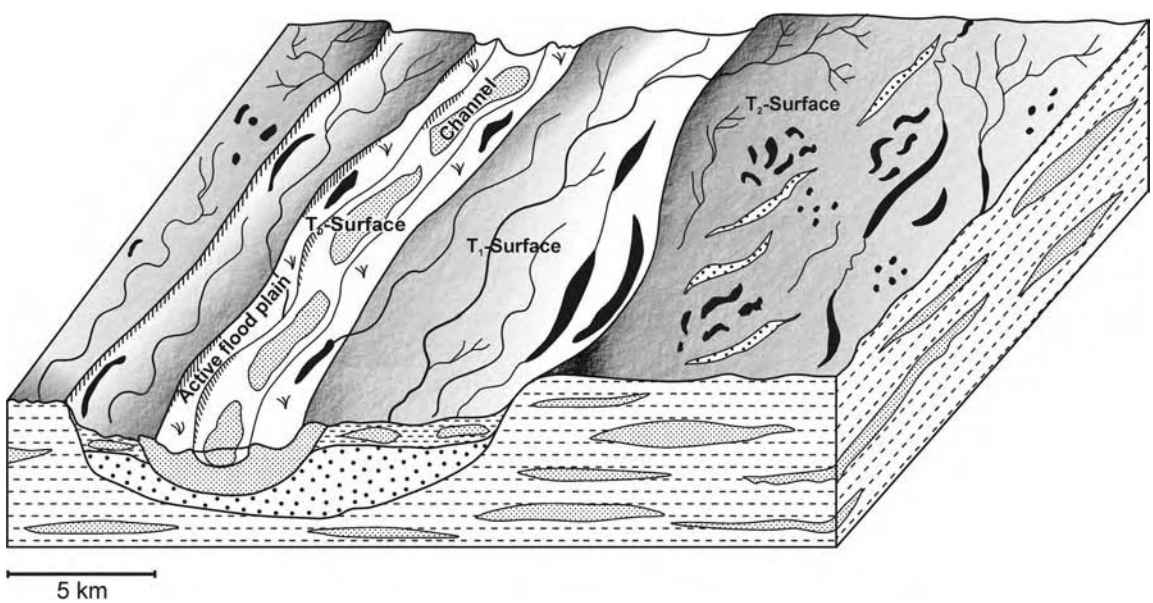

Figure 17.7 Schematic diagram of the T_0, T_1, and T_2 surfaces occupying different relative elevations. The subsurface of the river valley shows coarser sediments below the present Ganga River. The T_1 surface is covered by muddy sediments

surface in the Ganga Plain (T_2), tens of metres above the river channel, is not flooded by the river, although local waterlogging is common.

17.3 WATER QUALITY

Traditionally, the water of the Ganga is considered to be pure and with significant regeneration ability. The quality of its water, however, changes seasonally, and also downstream of certain locations and geologically different terrains. The hydrochemical parameters of the Ganga in the Himalayan area have been studied by Sarin *et al*. (1992), Bhatt and Saklani (1996), and Jain (2002). The geochemistry of the Ganga water in the alluvial plain has been discussed by Handa (1972), Abbas and Subramanian (1984), Raymahasay (1986) and Sarin *et al*. (1989). Mathur (1991) has discussed the physicochemical characteristics of the water of the Ganga. Sinha and Khan (2001) provide information on the water quality of Ganga River.

The average temperature of the river water in the Himalayan region varies between 2 and 8 °C depending on the season of the year. In the plains, the temperature ranges from 15 to 26 °C, at times rising to 32 °C in the lower Ganga channel. The river water is alkaline, with a pH generally over 7.5 and rising to more than 8 in the hot dry season. In the Lower Ganga, pH is commonly 7–7.5. In the Himalayan region, 60 % of the total dissolved solids (TDS) are bicarbonates with Na, K, Mg, and Ca as the major cations. In the source area of the Ganga, atmospheric contribution of Na and K can be as much as 20 % with Ca and Mg ~5 % (Sarin *et al*., 1992). Values of TDS and total suspended solids (TSS) are moderate. The amount of dissolved oxygen decreases between the upper and lower courses while conductivity increases in the lower reach and shows sharp seasonal changes.

The $^{87}Sr/^{86}Sr$ ratio and dissolved uranium of the river water is considerably higher than that of the global average runoff (Krishnaswami *et al*., 1992). Sarin *et al*. (1990) discuss significance of U, Th and Ra isotopes in the Ganga – Brahmaputra system. Stable hydrogen and oxygen isotope values of Himalayan Ganga water are those of average precipitation values, while in alluvial plain, the Ganga River indicates evaporation and ground water contribution (Navada and Rao, 1991; Ramesh and Sarin, 1992). High fluxes of radium and barium in the Ganga – Brahmaputra delta during low river discharges indicate groundwater as an important resource for these rivers (Moore, 1997). Preliminary studies of Ganga water give values of particulate nitrogen load (156×10^3 t year^{-1}) and dissolved nitrogen load (37.5×10^3 t year^{-1}) (Ittekot and Seifert, 1983). Dissolved organic carbon has been studied by Choudhury *et al*. (1982) and France-Lanord and Derry (1997) with values ranging between 9.4 and 1.4 mg l^{-1}. Geochemical cycling in the Hugli estuary is discussed by Somayajulu *et al*. (2002).

17.4 MATERIAL TRANSFER IN THE GANGA

17.4.1 Dissolved Load

Physical weathering is important in the Himalayan region but not chemical, and as a result dissolved load of the river is generally low; TDS values increase downstream as dissolved elements are added from groundwater seepage. It is likely that much dissolved load is added to the Ganga by groundwater discharge through silicate weathering in the Ganga Plain. The TDS values, however, show strong seasonal variations. They are low during the wet monsoon months due to the dilution by sudden increase in water discharge (Mathur, 1991). Near urban centres, metals and pesticide (BHC, DDT, and endosulfan) residues rise (Sinha, 1991). Concentration of heavy metals and pesticides, however, is much higher in the sediment than in the water.

The concentration of dissolved solids is 15 mg l^{-1} near Gaumukh, while at Haridwar it is 110 mg l^{-1}. Moving downstream across the plains the values are 280–350 (Kanpur), 260–1060 (Allahabad), and 370–490 mg l^{-1} (Varanasi). The values decrease downstream of Patna with an increase in water discharge due to the arrival of a number of large tributaries. It is 220 mg l^{-1} at Munger, 195 mg l^{-1} at Bhagalpur, and 165 mg l^{-1} at Rajmahal. The Ganga–Brahmaputra system transports about 180 million t of dissolved load annually to the Bay of Bengal (Sarin and Krishnaswami, 1984).

17.4.2 Suspended Load and Bed Load

The Ganga carries one of the highest volumes of sediment to the oceans. Milliman and Meade (1983) estimated the total annual sediment discharge of the Ganga–Brahmaputra system to be 1.7×10^9 t. Milliman and Syvitski (1992) estimated the suspended loads of the Ganga and the Brahmaputra in Bangladesh to be 520 and 540 million t year^{-1}, respectively. Several measurements of high suspended sediment concentrations are available along the river. At Devprayag it is 1405 mg l^{-1}, at Rishikesh it is 2002 mg l^{-1} (Jain, 2002), at Sultanganj it is 105–339 mg l^{-1} and at Bhagalpur it is 78–119 mg l^{-1} (Mathur, 1991). The annual sediment load measured in the Himalayan section is 33 million t at Rishikesh and 14 million t at Haridwar where the river emerges onto the plains. At Farakka near the head of the delta, Abbas and Subramanian (1984) have estimated an annual suspended sediment discharge of 729

million t, of which 328 million t is transported down the Hugli, the rest travelling down the main river into the active delta to join the Brahmaputra. The estimates vary but all the figures are high. About 90% of the sediment load of Ganga River moves into the delta region during monsoon months. The sediment load of the delta region is equally partitioned into floodplain – delta plain, continental shelf, and deep sea fan (Goodbred and Kuehl, 1999).

It is likely that a large amount of bed load is also transported by the Ganga River system into the delta region. It is estimated that the Ganga River moves 600×10^6–2500×10^6 t year^{-1} bed load to the delta area (Wasson, 2003). The estimated sediment yield of the Ganga River basin is 4.33 m^3 ha^{-1} year^{-1}. Wasson (2003) discusses the sediment budget of the Ganga – Brahmaputra system.

The basin area of the Ganga in the Himalaya is undergoing intense erosion which annually contributes a huge amount of sediment via the tributaries into the main river. A large part of this sediment is moved as bed load. A significant amount of bed load also arrives from the Peninsular Craton. A large volume of fine-grained sediment is added to the sediment load in the river from the plains after prior storage and chemical alteration. The Ganga plain acts as both the sink and source of the sediment in transport to the delta and submarine fan. The sediment undergoes two stages of chemical weathering and diminution, first in the Himalaya and later in the plains after deposition.

The sediment of the Ganga River is deposited as channel bars and gradually moved downstream. Availability of a large amount of bed load has strongly influenced the channel characteristics and geomorphic features of the Ganga. A large amount of suspended load is also transported during the wet season. Several centimetres thick muddy sediment is found deposited on top of channel bars after each flood, essentially representing the suspended load. Ganga River sediments show a strong overlap of grain size between bed load and suspended load deposits (Figure 17.8). The suspension load deposits are rich in silt fraction.

Grain size characteristics of the bed load has been studied along the river by analyzing the bar material at intervals (Singh and Singh, 1992; Singh, I.B., 1996; Singh, M., 1996). Coarse gravels, mostly centimetre to decimetre size pebbles but extending to metre-scale boulders, occur mixed with medium sand in the Himalayan section of the river. The texture of the sand has a mean value of 0–2 φ, its sorting moderate to poor, skewness negative, and the grain-size distribution mesokurtic. For about 400 km downstream from Haridwar, fine sand is predominant accompanied by medium and coarse sand and millimetre-

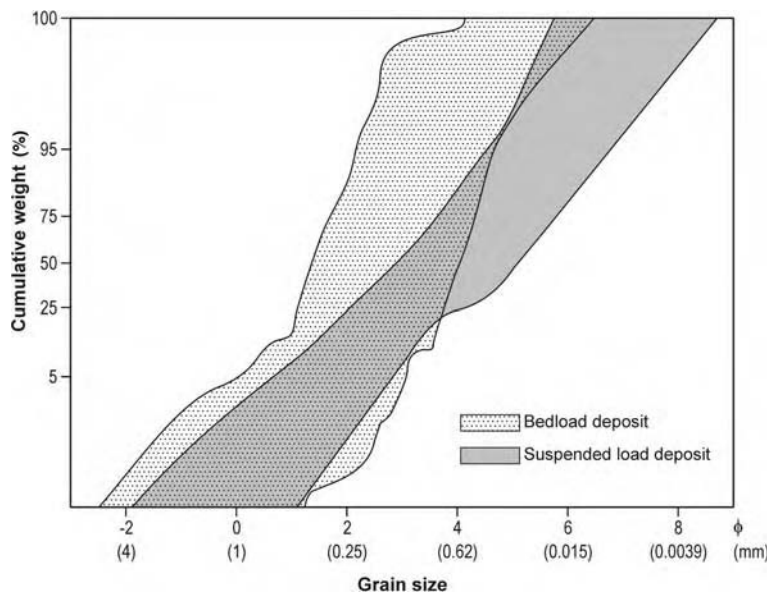

Figure 17.8 Distribution of grain size of the deposited bed load (n = 159) and suspended load (n = 27). Average figures for the Ganga in the alluvial plain. There is a strong overlap between the two in the coarse fraction but the suspended load deposits are also characterized by large proportion of silt

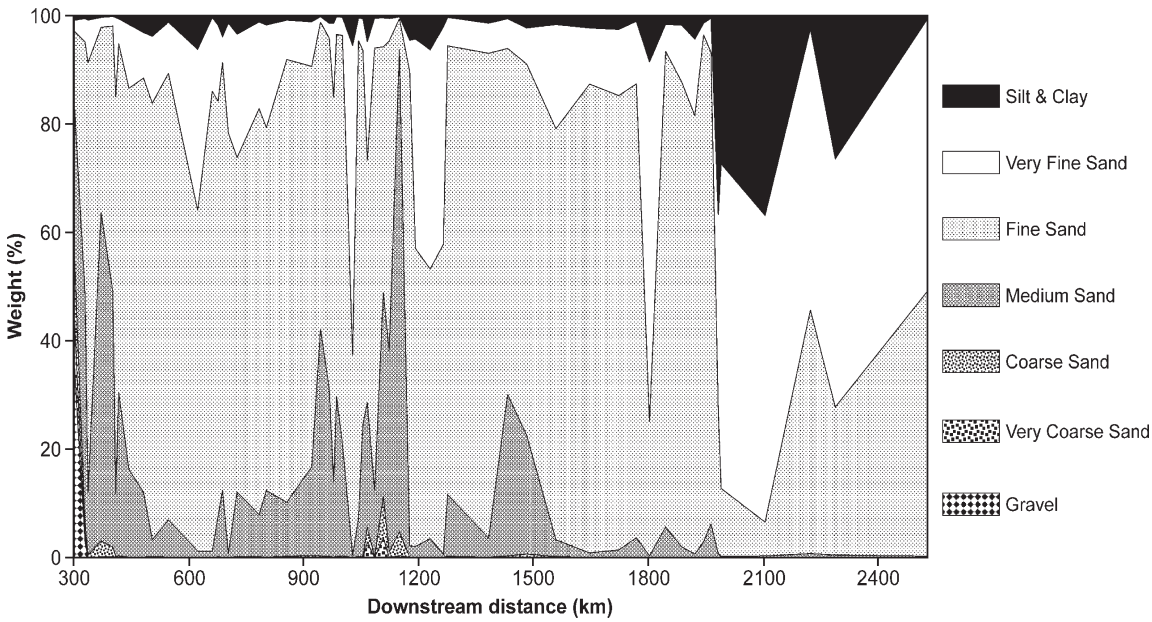

Figure 17.9 Changes in grain size of the bed load of the Ganga along its course in alluvial plain (between Haridwar and Ganga Sagar). Coarsening of the bed load in the middle reaches is due to the contribution from the southern rivers

size granules. Pebbles are transported only about 10 km downstream of Haridwar. Fine and very fine sand constitutes the bulk of the channel sediment further downstream with local coarsening to medium and coarse sand contributed by major tributaries (Figure 17.9). The mean grain size of the bed load therefore fluctuates within a narrow range of 1.5–3 φ. The Ganga River sand is moderately sorted with rather similar values at most of the stations. Skewness is essentially symmetrical exhibiting narrow range of fluctuation. Kurtosis changes from mesokurtic to leptokurtic. Strikingly, both bed and suspended load consists of mainly fine to very fine sand; the suspended load also includes a high proportion of silt and clay. Very fine sand and silt-clay fraction constitutes the sediment of the deltaic distributary of the Bhagirathi (Figure 17.9). Singh *et al*. (2007) discuss sediment characteristics and transportation dynamics of the Ganga River, emphasizing that nearly 80% of bed load is transported as graded suspension.

17.5 MINERALOGY AND GEOCHEMISTRY OF SEDIMENTS

The sand fraction of the Ganga is essentially composed of quartz with minor amounts of feldspars, micas and rock fragments. The coarser fractions are rich in mica. Sand in the upper river between Haridwar and Garhmuktesar consists of monocrystalline quartz, metamorphic quartz with a subordinate amount of mica, feldspar, and rock fragments. The common heavy minerals are tourmaline, garnet, zircon, sillimanite, chlorite, hornblende, and kyanite. The Himalayan tributaries as well as those of the northern alluvial plain contribute grey, micaceous sand, derived essentially from erosion of mica-rich metamorphic crystalline rocks of the Himalaya. For example, the sand of the Gomati, which originates in the northern plains, is mostly quartz (55%), rock fragments (19%), mica (17%), and feldspar (9%) (Kumar and Singh, 1978).

The tributaries from the Peninsular Craton contribute brown feldspathic sand. The sand is made of monocrystalline and polycrystalline quartz, potassium feldspar, rock fragments of granite-gneiss, reworked calcrete nodules and a little mica. However, the overall grey micaceous sand of the Ganga prevails throughout its course. Heavy mineral studies of the Ganga River in Bangladesh indicate epidote/garnet ratio of less than 1 (Heroy *et al*., 2003).

Illite and chlorite are the major clay minerals in the upper reaches, up to Kanpur, with a small proportion of kaolinite (Ansari, 1997). Smectite and kaolinite become important further downstream with some illite and chlorite (Sarin *et al*., 1989; Chakrapani *et al*., 1995; Heroy *et al*.,

2003). Illite and chlorite are essentially derived from the Himalaya, kaolinite and smectite from the reworking of the sediments of the plains (Kumar and Singh, 1978). The southern Ganga Plain draining the Peninsular Craton contributes mostly smectite.

Sediment brought down from the Himalaya and deposited in the Ganga Plains undergoes further chemical weathering within the alluvium, mobilizing a number of elements (Ansari *et al*., 2000). The movement of a large volume of water through the upper sediments flushes out many elements as dissolved load and others, considerably modified, are added to the bed load and suspended load of the river. The river sediments in upper reaches show low chemical index of alteration (CIA) values of 58–60, indicating low degree of silicate weathering in the source area. In contrast, the near surface sediments in the plains show higher CIA values of 65–73 and depletion in Na and Sr, Ca, K and Mg, indicating advanced chemical weathering of the alluvial sediments (Singh, 2004). Singh *et al*. (2005) discuss weathering in the Ganga Plain and demonstrate depletion in Na and Ca.

17.6 HEAVY METALS AND POLLUTANTS IN THE SEDIMENT

A number of studies discuss pollution and heavy metal concentration in the Ganga River (Prasad *et al*., 1986; Sharma and Ghosh, 1987; Subramanian *et al*., 1987; Mehrotra *et al*., 1991; Kumar, 1992; Singh, 1996; Ansari, 1997). The river carries a background concentration of heavy metals derived from the Himalaya in the Haridwar-Allahabad sector where the elements show a narrow range of downstream variation. Heavy metals in the sediment derived from the Peninsular Craton are also added between Allahabad and Farakka, although the Himalayan contributions still dominate. The elements show little downstream variations. Transportation by the Ganga has resulted in homogenization of sediment coming from different sources (Singh *et al*., 2003). The range of heavy metals include Cr, Mn, Co, Fe, Ni, Cu, Zn, Cd and Pb. The heavy metals tend to concentrate in the finer fractions of the river sediment. A study of the <20 µm fraction near the urban centres of Kanpur, Allahabad and Varanasi indicated a distinct enrichment in Cr, Cu, Zn, Pb and Cd. However, within several kilometres downstream of the urban centres, the heavy metal concentration drops to the background level, precipitating rapidly in the alkaline water of the river and bonding to clay particles and organic matter (Singh *et al*., 2002).

Ansari (1997) carried out a detailed study on the pattern of heavy metal pollution in the Kanpur area. Anthropogenically induced heavy metal enrichment is distinct for Cd, Cr, Sn, Cu, Zn, Co, Ni and Pb (Ansari *et al*., 1999). Concentration is high in both fine (<20 µm) and coarse (>125 µm) fractions. A comparison of pre- and post-monsoon samples indicates a slight decrease in concentration during the post-monsoon period due to the large-scale sediment movement during the wet monsoon times (Ansari *et al*., 2000). The river sediment also carries a considerable amount of pesticides, namely BHC, DDT, aldrin, edosulfan, malathion, ethion and methyl parathion between Kanpur and Allahabad (Sinha, 1991). Organic pollutants in sediments of Hugli estuary are described by Guzzella *et al*. (2005).

17.7 THE PLAIN AND THE RIVER

The Ganga Plain foreland basin (Figure 17.1) is tectonically active due to the compressional forces of the Himalayan collision tectonics. Compressional features dominate near the Himalaya Mountains whereas near the southern margin of the basin extensional features and orientation of basement tectonic lineaments are present (Agarwal *et al*., 2002). Three regions with characteristic tectonic features and orientations of tectonic lineaments occur in the basin: piedmont area, central basin, and the marginal area to the south (Singh, 1996; Singh *et al*., 1996). Furthermore, the basement rocks of the basin show a number of faults and basement highs of regional significance (Sastri *et al*., 1971; Rao, 1973) which appear to have influenced the morphology of the river (Singh, 2001, 2004).

Most of the basin of the Ganga (Figure 17.10) is a vast alluvial plain of low relief covering 250 000 km^2. The plain essentially represents a shallow asymmetrical depression with a gentle easterly slope. The elevation drops gradually eastward, from about 175 m near Mathura on the Yamuna to 25 m near Farakka. Within this plain, the channel of the Ganga is confined within a 10–25 km wide longitudinal alluvial lowland, often referred to as the Ganga River Valley, and bounded by several metres high alluvial cliffs. The valley includes the present active floodplain, a terrace, wetlands, meander scars, and braided channels. The higher plain adjacent to the valley is known as the *bangar* and the valley with the active channel is called the *khadar*. The plain is a combination of a variety of alluvial surfaces which have been identified on the basis of fieldwork, topographical maps, and satellite images (Singh, I.B., 1996, 2004). Their upper parts have been dated using luminescence methods. These surfaces (Figure 17.10) can be identified as:

1. active floodplain surface (T_0);
2. piedmont fan surface (PF);
3. river valley terrace surface (T_1);

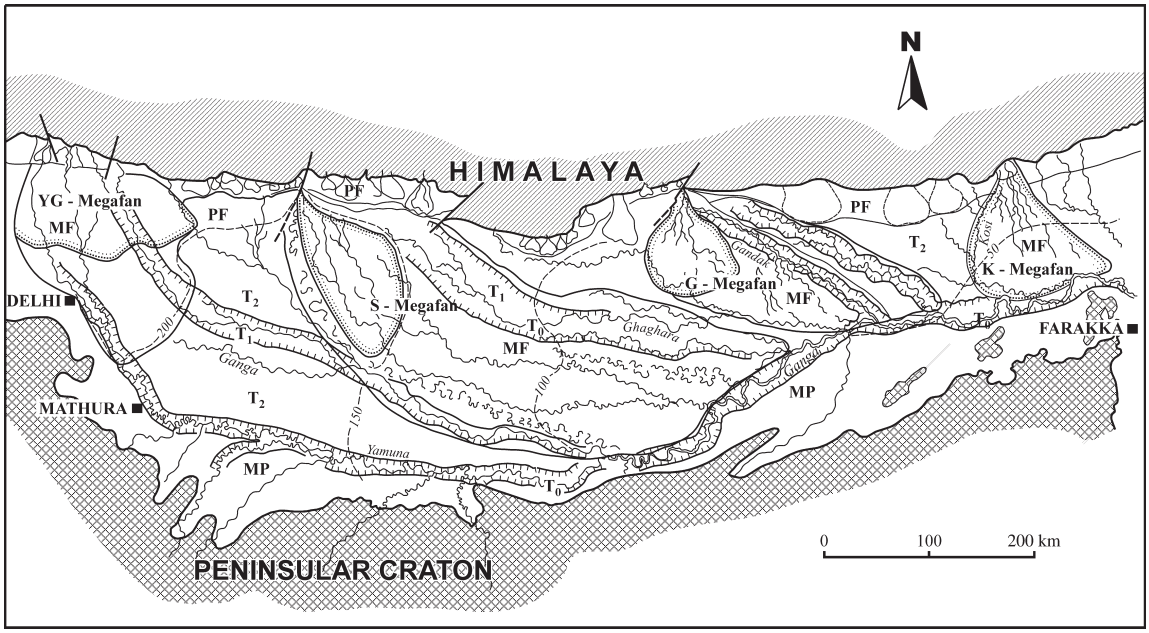

Figure 17.10 Regional geomorphic surface of the Ganga Plain. T_0, active floodplain surface; T_1, river valley terrace surface; T_2, upland interfluve surface; MF, megafan surface; MP, marginal plain upland surface; PF, piedmont fan surface. Megafans: YG, Yamuna-Ganga Megafan; S, Sarda (Ghaghara) Megafan; G, Gandak Megafan; K, Kosi Megafan. Contours at 50, 100, 150 and 200 m

4. megafan surface (MF);
5. marginal plain upland surface (MP);
6. upland interfluve surface (T_2).

The luminescence age of the upper parts of the upland interfluve surface is 51 000–57 000 years while that of the active floodplain is 200–500 years (Srivastava *et al*., 2003). All of these are depositional surfaces with a Holocene sediment cover. The materials of the first four surfaces (T_0 – MF) either lie over or are incised into the marginal plain upland surface or upland interfluve surface.

The Ganga River flows through the Himalaya in a narrow deep valley with poorly developed floodplain and terrace segments. Seeber and Gornitz (1983) have related its longitudinal profile with the Himalayan tectonics. The river cuts through a large alluvial fan (the Ganga Megafan) near Haridwar to descend from the mountains to the plain. The youngest deposits of the Ganga Megafan have been dated to 22 000 years whereas the Piedmont Fan deposits within the valley are 3000–8000 years in age (Srivastava *et al*., 2003). The Ganga River Valley, combining the river valley terrace surface and the active floodplain surface, is cut into the upland interfluve surface from Haridwar to Farakka. Inside the Valley, 10–20 m high cliffs mark the edge of the river valley terrace surface from the active floodplain and the channel. Such cliffs are sandy near Haridwar (Shukla *et al*., 2001), and gullies and minor ravines are common near the river. Further downstream, the cliff sections along the river display fine-grained clayey deposits. The nature of the cliff deposits varies in texture and colour along the main river downstream. Abandoned channel belts, meander cut-offs, small channels, wetlands and flat surfaces occur on top of the cliffs. The river valley terrace surface (T_1) exhibits linear water bodies, swamps and cutoff meanders along with yazoo-type channels. Within the river valley, however, a 20–30 m thick sand body, with a grain size coarser than carried by the present-day Ganga at a depth of 10–20 m can be identified (Figure 17.7), probably representing a different phase of sedimentation in the late Pleistocene (Singh *et al*., 1990). The valley itself is incised in regional upland surface (Figure 17.7). The southern valley margin often shows prominent cliffs of variable height, and evidences of neotectonic activity (Roy and Ghosh, 1981; Singh, 2001, 2004).

Together the Ganga channel and the active floodplain is between 0.5 and 3 km in width and entrenched below

the river valley terrace surface. The floodplain itself is 0.5–1 km wide, set 2–5 m below the terrace surface. The channel is braided over long reaches except where the valley narrows and a meandering pattern appears. The kilometre-long bars could be braid bars, lateral bars or point bars, depending on channel geometry. Several of the bars are vegetated and appear to be in place for decades. Shukla *et al*. (1999) have recognized changes in location, size and form of the braid bars near Kanpur on a decadal scale (Figure 17.11). Sinuous channels are seen between the braid bars at low discharge. At bankfull discharge a several kilometres wide channel inundates the bars. Where the valley narrows, a meandering pattern is seen and huge point bars (several km^2 in area) appear. The low flow depth between Haridwar and Allahabad is 1–3 m, increasing to 4–10 m downstream. Sediment transfer is confined to the channel at low flow and along both the channel and the floodplain in the wet season, with high floods partly

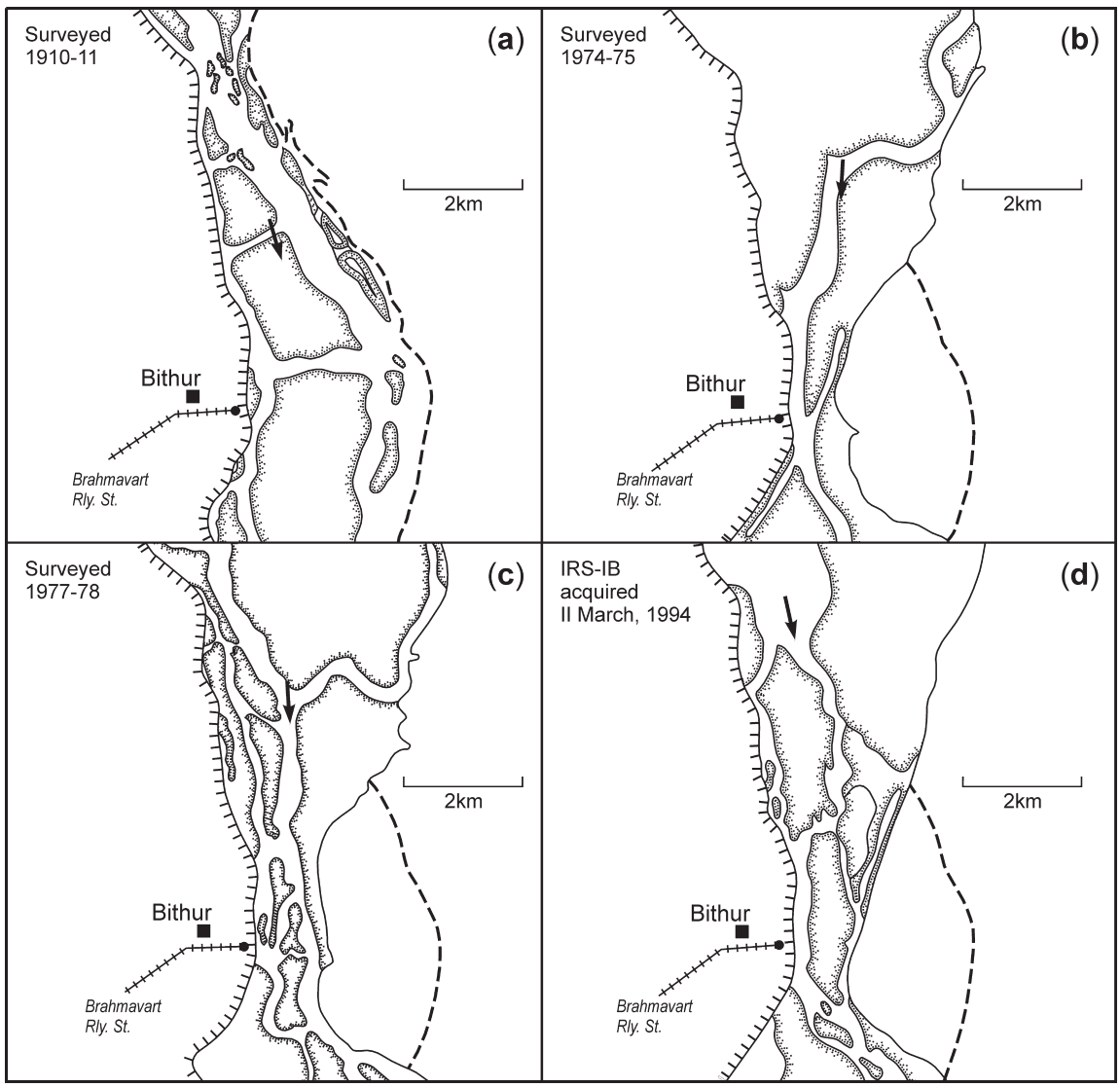

Figure 17.11 Changes in the bar morphology and the channel of the Ganga at Bithur near Kanpur. The broken lines in (b), (c) and (d) indicate the original location of the left bank

submerging also the river valley terrace surface. Some of the sediment is deposited on the floodplain and the terrace for temporary storage. At high flow, about 2–5 m of sediment is scoured from the bed and the river stage rises for 5–10 m above the low flow level.

The characteristics and downstream changes in the Ganga River valley and active Ganga River are essentially related to variation in sediment and water discharge, tectonic setting and geology along with Late Quaternary changes in climate, tectonics and base-level. The Ganga River valley is subdivided into distinct segments with their characteristic features (Singh, I.B., 1996, 2001; Singh, M., 1996) (Figure 17.3). Table 17.3 summarizses valley and channel forms along the Ganga.

As expected, the river shows a sharp change in gradient between the mountains and the plain. The mean slope in

Table 17.3 Ganga River segments and their geomorphic characteristics

River units	Valley segment (Figure 17.3)	Extent	Slope	Description
Himalayan	GRV-0	Gaumukh-Haridwar (300 km)	0.0128	Highly incised valley (Figure 17.12) in bedrock, meandering, broadening at the end with braided channel. Gorges and alluvium-filled segments with paired and unpaired terraces. Valley consists of channel and active flood plain, and gravel and sand bars (Figure 17.13) in the channel with some mud. Tributary mouth fans prominent (Khan *et al*., 1982; Rawat and Gariola, 1997; Bali *et al*., 2003).
Upper Alluvial Ganga River (Upper Ganga Plain)	GRV-I	Haridwar-Garhmuktesar (140 km)	0.00068	Broad straight river valley, trending southward with distinct margins and 10–30 m high cliffs. The margins of the northern part of the valley flat of the Ganga carry 1–3 km wide belt of badlands and ravines with 10–30 m banks, locally known as *khola* (Mukerji, 1963). The high banks have exposed sandy sediments of the Ganga Megafan (Shukla *et al*., 2001). Swamps, lakes and yazoo-type streams are common on the river valley terrace. The active river channel is 1–3 km wide at flood discharge. It is commonly of low sinuosity (1.18–1.27), and braided with 0.5–5 km long and 100–500 m wide sand bars. Such bars are about 2–3 m high above the low water level with 1–2 m deep channels separating them. The bars are generally submerged during floods and new bars form at different locations. A channel shift of about 6 km (Figure 17.14) has been identified between 1914 and 1964 from aerial photos (Das Gupta, 1975).
	GRV-II	Garhmuktesar-Allahabad (610 km)	0.00016	The river valley changes direction from southerly to south-easterly. In the beginning of this segment the river valley is mostly 10–30 km wide, the channel wanders from one margin of the valley to the other (Figure 17.15). The river channel exhibits huge braid and lateral bars. Swampy areas, linear water bodies, yazoo streams and meander scars are common on the river valley terrace surface (T_1). In the middle part of the segment the Ganga flows to the southern margin of the valley leaving wide valley flat on the northern part. The valley flat shows the meander scars as the one with 20 km wavelength near Bithur. Prominent cliff is developed along the southern valley margin along with a broad zone of badland and gullies dissected by small streams. The river is braided (Figure 17.16). The braid bars grow to become lateral bars (Shukla *et al*., 1999) (Figure 17.11). The distal part of this segment shows a 1–5 km wide narrow undulating reach, where the river wanders as a single channel from one edge of the valley to the other. Point bars and lateral bars are prominent. The T_1-surface carries swamps. The cliffs (10–20 m high) are present along both the valley margins, often cut deeply by minor creeks.

Table 17.3 *Continued*

River units	Valley segment (Figure 17.3)	Extent	Slope	Description
Lower Alluvial Ganga River (Middle Ganga Plain)	GRV-III	Allahabad-Buxar (300 km)	0.00011	At Allahabad Yamuna contributes a large amount of water and sediments (especially bed load) to the Ganga which flows close to the southern margin of the plain. Downstream of the Ganga-Yamuna confluence, a huge sand bar has developed. At Chunar, basement rocks are exposed on the southern banks of the river. At the beginning of this segment the Ganga flows east, then ENE. The river is influenced by peninsular lineaments and neotectonics. Cliffs are often present on both margins of the valley. The valley is narrow and sinuous (sinuosity~2), with the meandering channel shifting from one margin to the other. Meanders increase in dimensions downstream; those of the distal part of this segment are rectangular (Figure 17.17). Point bars are 5–10 km long and 0.5–1 km wide; braid bars are rarely seen. Meander scars and minor channels are displayed.
	GRV-IV	Buxar-Barh (200 km)	0.00005	This part exhibits a 20–30 km wide valley flat with several large tributaries from the Himalaya and Peninsula joining the Ganga within a short distance of 30 km. Valley flat is bounded by 2–5 m high rises broken by tributaries. The channel flows eastward showing kilometre-scale braid and lateral bars. The river enlarges in size enormously with contributions from the Ghaghara, Gandak and Son Rivers (Figure 17.18). The river changes downstream from sinuous to straight with huge braid bars. The T_1 surface shows meander scars, linear lakes, and small drainage channels. Some meander scars are huge, about 20–25 km. Large parts of the T_1 surface are inundated during floods.
	GRV-V	Barh-Farakka (305 km)	0.00006	The valley flat is 20–30 km wide with west to east orientation. The southern margin is straight with 10–20 m high cliffs and the northern margin is undulatory with 5–10 m high cliffs. The cliffs are eroded by tributaries joining the Ganga. The active channel is highly sinuous with large meander loops showing prominent northern curvature and distorted southern curvature and with both point and braid bars and multiple channels (Figure 17.19). The T_1 surface shows meander scars, small drainage channels and elongated lakes and its lower part is inundated when river is in high floods. The river channel is broad (Figure 17.20). The sand bars are 10–15 km long and 1–2 km wide, frequently changing their position (Figure 17.21). The river valley is only 20–30 m above sea level. Basement rocks are exposed along the river bank at Sultanganj (Figure 17.22), Kahalgaon indicating shallow depths of basement and influence of peninsular lineaments and neotectonics along the southern margin of the Ganga River. The Ganga turns south near Sahibganj to flow towards Farakka to enter the delta sector. Fluvial features are described by Godbole (1986) and Philip *et al*. (1991).
Delta Plain of the Ganga	GRV-VI	Farakka-sea (539 km)	0.00004	About 40 km downstream of Farakka, the delta of the Ganga begins and the river splits into distributaries. The Bhagirathi or the Hugli is the major distributary that flows through India; most of the water and sediment travels along the Padma into Bangladesh where the active part of the Ganga-Brahmaputra Delta is located. The levee-bounded meandering Bhagirathi (Basu, 1967a,b) collects water and sediment from a number of rivers draining the north-eastern edge of the Indian Peninsula. The river is tidal from Nabadwip, about 240 km from the sea.

Figure 17.12 The deep valley of the Ganga in the Himalaya. (Photograph: D.S. Singh)

Figure 17.13 Gravel bars in the Ganga River channel at Haridwar. (Photograph: M. Singh)

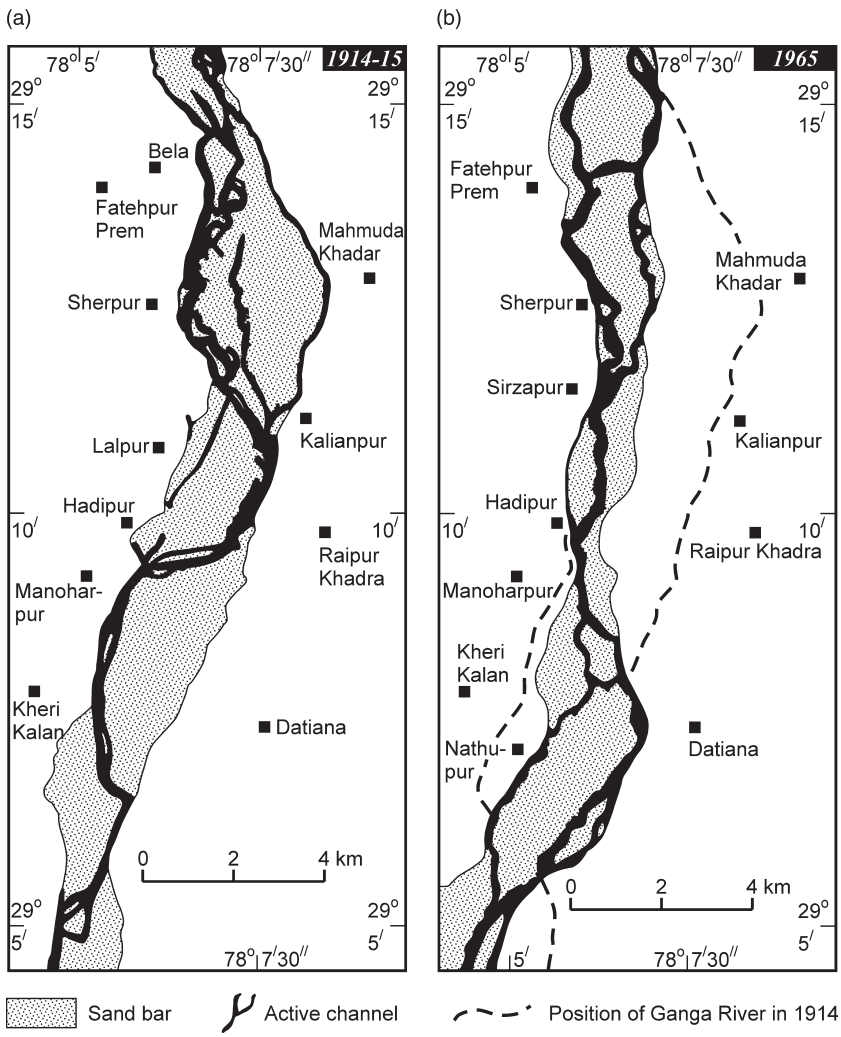

Figure 17.14 Comparison of the channel of the Ganga near Bijnore between (a) 1914 and (b) 1965 showing shift in channel and sediment bars by kilometres. (Simplified after Das Gupta, 1975)

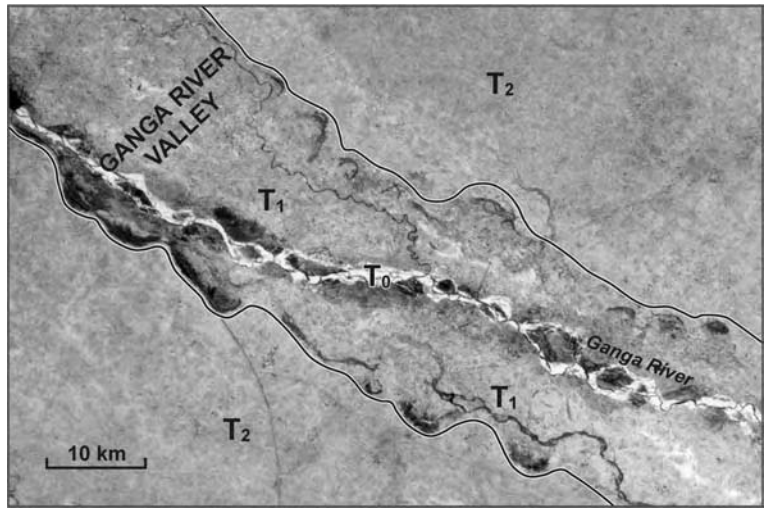

Figure 17.15 Satellite imagery showing the broad Ganga Valley south of Garhmuktesar. The river is braided with a narrow flood plain. Large meander cutoffs are common on valley flat. Based on Landsat 5, 14.11.84

Figure 17.16 Ganga River showing a complex system of bars at low discharge conditions near Kanpur (Photograph: I.B. Singh)

the Himalaya is 0.0128, a figure that drops to 0.000013 averaged over the 2500 km through the plains (Figure 17.23). The river gradient is extremely low for the last 1300 km, about 0.000005. Active subsurface structures and extensions of subsurface ridges from the peninsular highland, however, locally steepen and flatten the gradient (Figure 17.24).

17.8 THE DELTA

The delta is a contribution of three major rivers, the Ganga, Brahmaputra, and the Meghna, and the combined flow reaches the sea through the huge Meghna Estuary. The subaerial part of the delta covers 138 000 km^2 and a very large subaqueous part lies beyond. The northern part

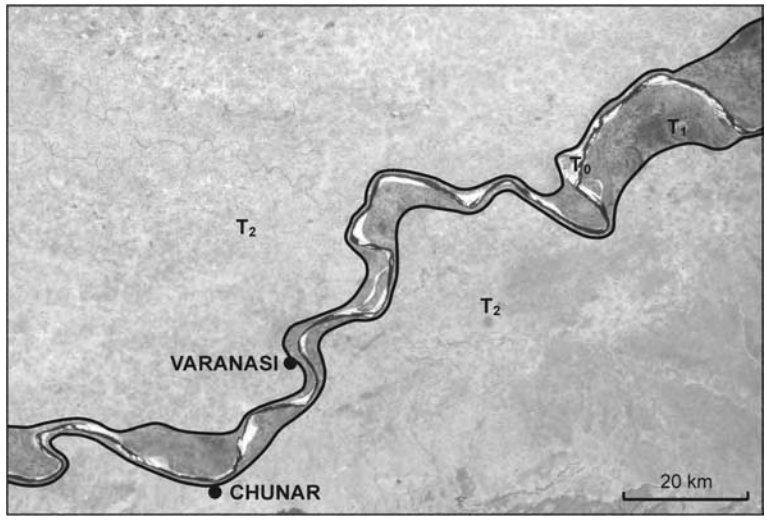

Figure 17.17 Highly sinuous Ganga River confined in a narrow valley near Varanasi. Based on Landsat 4, 17.11.84

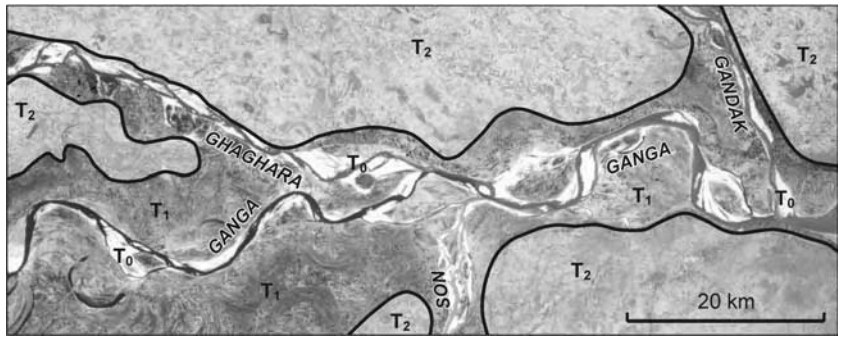

Figure 17.18 The Ganga River with confluences of Ghaghara, Gandak and Son Rivers showing complex channel-bar system and valley flat. Based on Landsat 4, 26.11.84

Figure 17.19 The Ganga River with huge distorted meanders and complex bar-channel system in Munger-Bhagalpur region. Based on ERTS, 7.12.75

Figure 17.20 Ganga River at Bhagalpur. On the left margin an alluvial cliff is present, followed by a sand bar and a huge channel. The left bank of the river is to the right side of the figure. (Photograph: I.B. Singh)

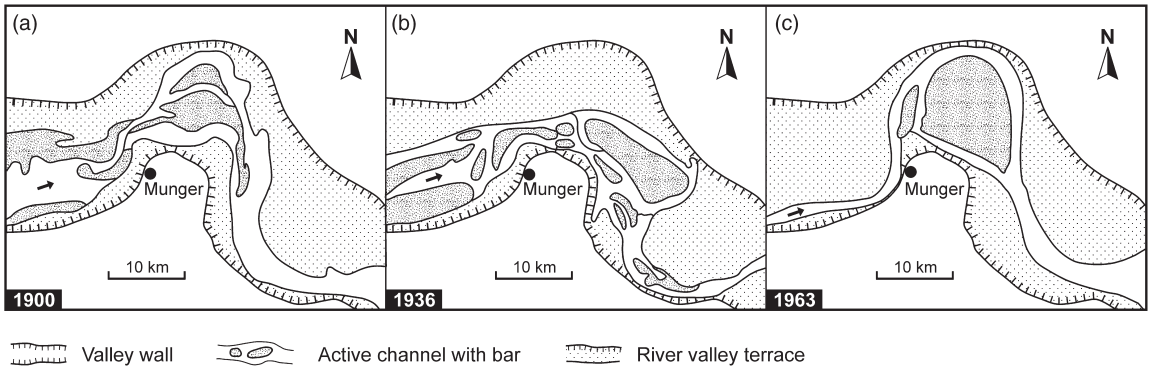

Figure 17.21 Comparison of channel and bar morphology of the Ganga River near Munger: (a) 1900; (b) 1936; (c) 1963. (Modified after Godbole, 1986)

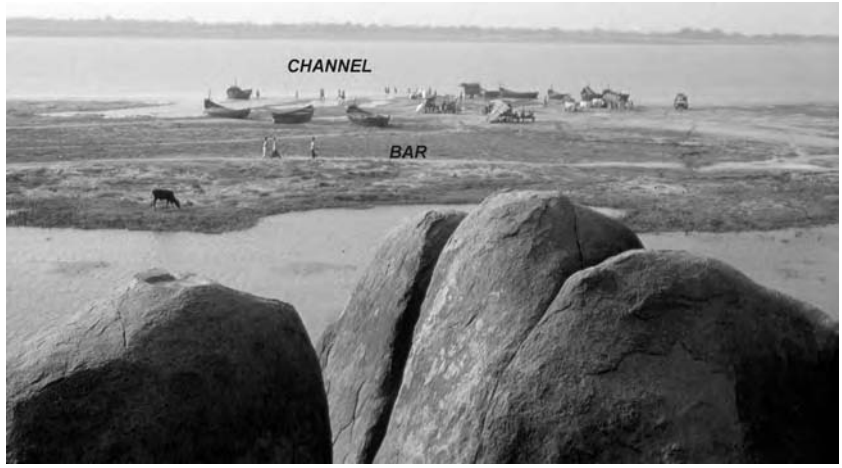

Figure 17.22 Ganga River at Sultanganj with a gneissic cliff in the foreground. (Photograph: I.B. Singh)

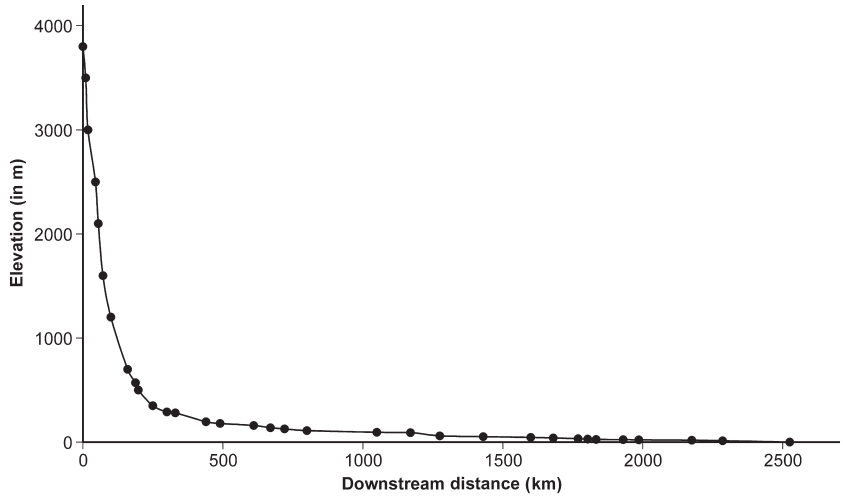

Figure 17.23 Longitudinal profile of the Ganga indicating the sharp break at the Himalaya-Plains contact. Compiled from various sources

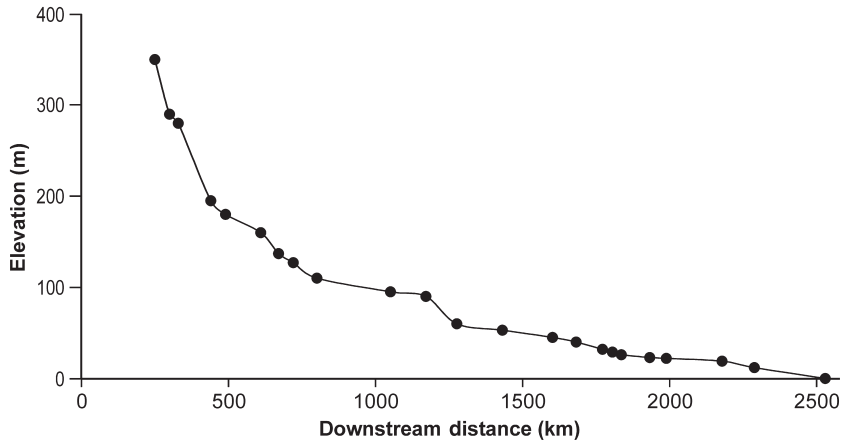

Figure 17.24 Longitudinal profile of the Ganga River within the alluvial plain showing local convexities and steepening of gradients due to neotectonic activities in basement rocks

is only 10–15 m above msl. A large number of distributaries, flowing south from the Ganga, become tidal creeks with interlocking pattern. Shallow water bodies, commonly accumulating freshwater peat deposits, occur on the delta surface. The upper delta is formed by fluvial processes and the lower part shows the strong influence of 4.5–6 m tides that prevail in this region. The stratigraphy of the delta region is partly controlled by tectonic activity. The Ganga Delta has been studied in detail by Morgan and McIntyre (1959), Umitsu (1993) and Michels *et al*. (1998). Goodbred and Kuehl (2000), Goodbred *et al*. (2003), Goodbred (2003) and Allison *et al*. (2003) discussed the stratigraphy and evolution of the Ganga-Brahmaputra Delta, as it is collectively known. Singh and Swamy (2006) describe the Ganga delta and its sedimentation model.

17.9 A SUMMARY OF CURRENT GEOMORPHIC PROCESSES

The Ganga River is entrenched within a cliff-bounded alluvial surface and its lateral shifting is limited to a scale of several kilometres (Figure 17.25). Within this

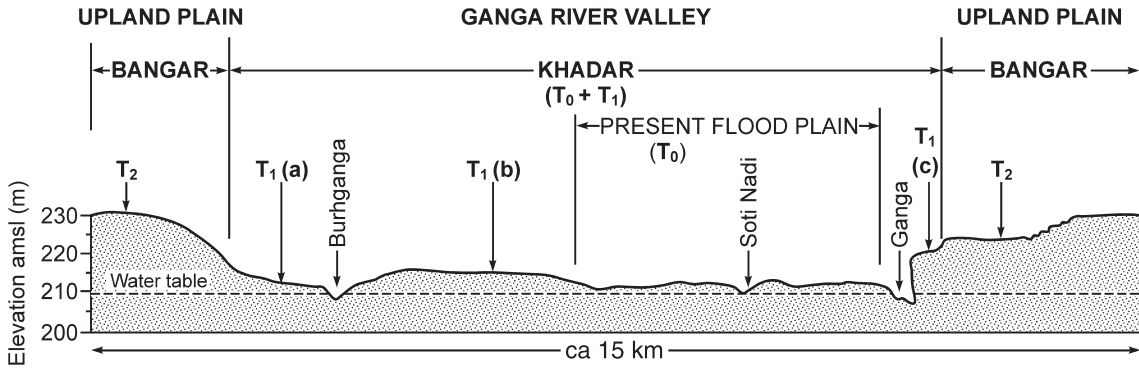

Figure 17.25 Schematic cross-section of the Ganga Valley at Hastinapur, near Delhi. The river is flowing along the margin of the valley. (Simplified after Das Gupta, 1975)

limitation it is a dynamic river system, transporting large volumes of water and sediment. The channel bars are readjusted annually after floods with changes in their shape, size and location. Frequently, minor channels that cut across the bar surfaces are silted up and new channels formed (Figures 17.11, 17.14 and 17.21). The relative proportion of active channels, sand bars and vegetated bars also changes within the entire river. There is an increase in area of bars over channel at most of places during time span of 1911–1975 (Singh, I.B., 1996; Singh, M., 1996; Singh *et al*., 1990). The changes perceived on a decadal scale can be summarized:

1. Lateral movement of the river leading to localized erosion of valley margin cliffs.
2. Conversion of braid bars into lateral bars attached to one of the banks and its subsequent erosion (Figure 17.11).
3. Changing relative proportions and position of the three major features in the river: channels, unvegetated bars, vegetated bars.
4. Probable aggradation in the channel.

17.10 QUATERNARY EVOLUTION OF THE GANGA

The river and its active floodplain (T_0 surface) is about 5–10 m below the river valley terrace surface (T_1), which in turn is located below the upland interfluve surface (T_2). The present active river tends to occupy only a part of the broad valley and the T_1 surface displays relict riverine features of different dimensions suggesting a possible river metamorphosis. Such features are common throughout the length of the river.

Ganga Megafan deposits (22–26 000 years in age) are made up of coarser sediments than that of the present-day Ganga (Shukla *et al.*, 2001; Srivastava *et al.*, 2003). A sand body of 10–50 m thickness occurs in the valley, resting with an irregular contact on a muddy surface. The lower part of the sand body is coarser grained (by 1–2 φ) than the sand of the present river. The present river has deposited a 5–10 m sand body on top of this older coarser sand deposit. A 5–10 m thick muddy deposit tends to occur on top of the T_1 surface that contains 1–2 m thick lenticular bodies of very fine sand (Figure 17.7). Below these muddy sediments, coarse sand, similar to that found below the T_0 surface may occur. Studies of the subsurface sediment near Kanpur has determined that the lower part of the sand body is 0.5–1.9 φ in grain size whereas the upper part and the present Ganga sand is 2.25–2.50 φ. Smaller channels found on top of the T_1 surface carries sand 3.25–4.00 φ in size (Bajpai, 1989; Singh *et al*., 1990). The topmost 10 m of the sediment of Ganga Plain is mid-late Holocene in age (Shukla *et al*., 2001).

The surface of the Ganga delta plain displays numerous active and abandoned channels, waterbodies, and swamps. The channels are bound by natural levees. These are part of an anastomosed network and exhibit avulsion on a scale of several hundred years. The top 5 m of the surface sediment is Late Holocene (2–5000 years in age) as indicated by the presence of freshwater peat deposits (Banerjee and Sen, 1987; Gupta, 1992). The subsurface, however, displays coarse sandy fluvial channel deposits, up to 50 m in thickness (Umitsu, 1993; Goodbred *et al*., 2003). Extensions of these channels are also seen in the subsurface of the continental shelf. These subsurface channel deposits represent active channel sediments associated with the low sea-level stands. The stratigraphy and the Late Quaternary evolution of the Ganga-Brahmaputra Delta have been discussed by Goodbred and Kuehl (2000) and Goodbred *et al*. (2003). They have indicated that the river went through an accelerated phase of sediment transportation and deltaic deposition between 7 and 11 000 years BP.

The present river valley was probably formed during a humid climate phase around 25–35 000 years ago. It was a meandering river with sediment coarser than the current Ganga. The river was incised into its own deposits during 25–15 000 years in response to lowering of base-level and reduced water discharge. Aggradation in the channel of the Ganga started around 8000 years ago in response to the rising sea level and the wetter climate of the Early Holocene and a large supply of sediment from the Himalaya. Increased aggradation and delta-building started in the lowest reach around 11 000 years ago (Goodbred and Kuehl, 2000; Goodbred *et al*., 2003). According to Goodbred and Kuehl (2000), the sediment discharge of the Ganga-Brahmaputra system during 7–11 000 years BP was twice that deposited in the following 7000 years. Singh (2001, 2002) and Srivastava *et al*. (2003) described the transfer of sediment from the alluvial plains of the Ganga to the delta area during the Holocene. Aggradation was very strong in active river channel (T_0). Stronger monsoons during the Early Holocene led to the accumulation of fine-grained sediment on the T_1 surface and formation of additional drainage channels and aggradation. This was followed by a drier period that led to abandonment of many small channels on the T_1 surface and a probable decrease in aggradation. New drainage channels and water bodies were filled and abandoned in response to climate change and tectonics in the Holocene on the higher T_2 surface (Srivastava *et al*., 2003; Singh, 2004).

17.11 UTILIZATION OF THE RIVER AND ASSOCIATED PROBLEMS

Every aspect of the life of people in the area (bathing, drinking, religious ceremonies, cremation, scattering of ashes after death) is associated with the river. About 242 million people live in the basin which gives it a population density of 297 persons per km^2. The density rises in the alluvial plains close to the river to almost 500 per km^2, and much of the population is living in poverty. Most live in villages and depend on agriculture that covers more than 62 % of the basin. Forests cover only 14 % at present. There are nearly 700 cities, of which 62 have a population of more than 100 000 (Das Gupta, 1984). Domestic and industrial waste water and solid wastes usually end up in the river or local water bodies without prior treatment. The natural drainage system in the plains has been extensively modified by anthropogenic activities such as construction of embankments, blocking of natural drainage, and encroachment of natural depressions, floodplains and wetlands. The quality of surface and groundwater is fast deteriorating. The biological, ecological and pollution details of the water of the Ganga are discussed by Krishna Murti *et al*. (1991). Singh and Singh (2007) provide a bibliography of papers related to natural characteristics and anthropogenic influences of the Ganga River.

The Ganga River receives industrial and urban pollutants from point sources and large amount of pesticides, fertilizers and organic pollutants from nonpoint ones throughout its course. Water management structures in the basin such as dams, reservoirs, and canals have strongly affected the hydraulic regime of the river influencing the dispersal of pollutants. This also affects the diverse flora and fauna of the river including a large variety of fish and the freshwater dolphin (*Platanista gangetica*) eponymous with the river. Bilgrami (1991) and Rao (2001) described the biological resources of the Ganga River. Environmental changes and their effects on fisheries are discussed by Sinha and Khan (2001).

A large amount of sediment is reaching the Ganga due to accelerated mass failures in the Himalaya and intense soil erosion by sheetflows and gullies that are common also along the river cliffs in the alluvial plains. In many places intense gully erosion occurs along a 50–500 m wide belt along the river cliffs. The channel is also affected by large-scale mining of sand from huge bars exposed during the dry season. No precise measurements are available but it appears likely that millions of tonnes of sand are mined from the river annually. During low water discharge periods (winter and summer months) *khadar* (T_1 – surface) and exposed sand bars, including *diara* of Bihar, are used for agriculture activity, when a large quantity of organic manure and chemicals are directly added to Ganga River sediments.

Religion and culture has determined that the river water is used extensively for bathing, both on a daily basis for locals and at 6- and 12-year intervals by millions of pilgrims travelling for hundreds of kilometres to reach the river. The important pilgrimage centres are Rishikesh, Haridwar, Garhmuktesar, Kannauj, Allahabad, Mirzapur and Varanasi. The intense use of the river for bathing, cremation, disposal of dead bodies, addition of untreated sewage and piles of garbage have increased the biological oxygen demand, bacterial contamination, faecal contamination and coliform count for the river (Srivastava *et al*., 1996; Bilgrami and Kumar, 1998). Faecal contamination is present even in Himalayan part of the Ganga River (Baghel *et al*., 2005). The quality of river water for long reaches could not be classified even as suitable for bathing (Das Gupta, 1984). Even then the water is extracted for drinking and other domestic uses and also for use in industry. The deteriorating quality of the water and its increasingly polluted nature led to the initiation of the Ganga Action Plan in 1985 by the Government of India. The second phase of this plan began in 1996. The environmentally sustainable

agricultural and industrial development would require the continuation of processes of cleaning the Ganga (Markandya and Murty, 2004).

Huge quantities of water are drawn for irrigation through the headworks and pumping stations along the river. A large quantity of water is diverted as early as Haridwar for irrigating the Ganga-Yamuna interfluve by the Upper Ganga Canal System. A small irrigation system operates at Bijnore where a barrage diverts water from the river into a canal. Another major canal system feeds the Lower Ganga Canal System at Narora, 240 km downstream of Haridwar. A large number of lift canals pump water out from the Ganga for irrigating agricultural fields.

Apart from water diversion as mentioned above, the river so far has not been impounded by large dams. At present, two dams are being constructed, mainly for power generation, on the Bhagirathi River, one of the headwaters of the Ganga, about 160 km from Gaumukh in the Himalaya. One of these is at Tehri (with a capacity of 2000 MW) and the other at Koteswar (400 MW). This is an extremely controversial project given the seismic nature of the region and the possible ecological consequences. The water of the Ganga is also used for cooling purposes at the nuclear power station built at Narora with a capacity of 440 MW.

In the lower part of the river, a barrage has been constructed near Farakka in the state of West Bengal to divert part of the water from the main distributary to the Hugli to maintain its navigational capability. Parua (1986) has discussed the associated degradation of the river bed and prominent bank erosion.

The river is navigable only downstream of Patna because of its low discharge for most of the year. The tidal part (Nabadwip to the sea) is used by a number of vessels. In contrast, the Upper Ganga, even in the plains, is not used for river transportation except by local boats. Wild water rafting, however, has become popular in the Himalayan Mountains with some campsites along the river. Besides that, recreation and water sports activities are rather limited on the river.

A number of important archaeological sites are located along the Ganga River, which go back in antiquity to about 3500 to 3000 years BP (Roy, 1983).

ACKNOWLEDGEMENTS

Much of the information and ideas presented in this paper were developed over the last two decades as a result of the ongoing research on the evolution of the Ganga Plain in which many students and colleagues have contributed. Special thanks are expressed to Munendra Singh for discussions and the use of unpublished data on the Ganga River. Thanks are expressed to U.K. Shukla, S. Sharma, M. Sharma, A.K. Tangri, P. Srivastava, D.S. Singh and D. Kapoor for their association with the study of the Ganga Plain. I am thankful to A.K. Tangri and V.N. Bajpai for stimulating discussion on the evolution of the Ganga River. A. Saxena, A. Srivastava and A.K. Kulshrestha helped with the preparation and finalisation of the manuscript and P. Joshi with the diagrams. M.P. Singh, Head, Department of Geology, University of Lucknow is thanked for providing departmental help.

REFERENCES

Abbas, N. and Subramanian, V. (1984) Erosion and sediment transport in the Ganges River basin, India, *Journal of Hydrology*, 69, 173–182.

Agarwal, A. and Chak, A. (Eds) (1991) *Floods, Floodplains and Environmental Myths*, Centre for Science and Environment, New Delhi, 167 p.

Agarwal, K.K., Singh, I.B., Sharma, M., Sharma, S. and Rajagopalan, G. (2002) Extensional tectonic activity in the cratonwards parts (peripheral bulge) of the Ganga plain foreland basin, India, *International Journal of Earth Sciences*, 19, 897–905.

Allison, M.A., Khan, S.R., Goodbred, Jr, S.L. and Kuehl, S.A. (2003) Stratigraphic evolution of the Late Holocene Ganges-Brahmaputra lower delta plain, *Sedimentary Geology*, 155, 317–342.

Ansari, A.A. (1997) Geochemical and Geomorphological Study of the Ganga Plain, Kanpur-Unnao Industrial Region, India, Doctorate Thesis, Universität Erlangen-Nürnberg, Germany, 188 p.

Ansari, A.A., Singh, I.B. and Tobschall, H.J. (1999) Status of anthropogenically induced metal pollution in the Kanpur-Unnao industrial region of the Ganga Plain, India, *Environmental Geology*, 38, 25–33.

Ansari, A.A., Singh, I.B. and Tobschall, H.J. (2000) Role of monsoon rain on concentrations and dispersion patterns of metal pollutants in sediments and soils of the Ganga Plain, India, *Environmental Geology*, 39, 221–237.

Baghel, V.S., Gopal, K., Dwivedi, S. and Tripathi, R.D. (2005) Bacterial indicators of faecal contamination of the Gangetic river system right at its source, *Ecological Indicators*, 5, 49–56.

Bajpai, V.N. (1989) Surface and sub-surface evidences of neotectonics and aquifer disposition in central alluvial terrain of Kanpur-Unnao region in Uttar Pradesh, India, *Photonirvachak, Journal of the Indian Society of Remote Sensing*, 17, 47–53.

Bali, R., Awasthi, D.D. and Tewari, N.K. (2003) Neotectonic control on the geomorphic evolution of the Gangotri glacier valley, Garhwal Himalaya, *Gondwana Research*, 6, 829–838.

Banerjee, M. and Sen, P.K. (1987) Palaeobiology in understanding the change of sea level and coastline in Bengal Basin during Holocene period, *Indian Journal of Earth Sciences*, 14, 307–320.

Basu, S.R. (1967a) Fundamental problems of meander formation with special reference to the Bhagirathi River, *Indian Journal of Power and River Valley Development*, February, 15–23.

Basu, S.R. (1967b) On some aspects of fluvial dynamics of river Bhagirathi with special reference to its physical and hydraulic characteristics, *Indian Journal of Power and River Valley Development*, June, 32–43.

Bhatt, K.P. and Saklani, S. (1996) Hydrogeochemistry of the Upper Ganges River, India, *Journal Geological Society of India*, 48, 171–182.

Bilgrami, K.S. (1991) Biological Profile of the Ganga: Bacteria and Bacteriophages. In: *The Ganga–A Scientific Study* (C.R. Krishna Murti, K.S. Bilgrami, T.M. Das and R.P. Mathur, Eds.), Northern Book Centre, New Delhi, 72–77.

Bilgrami, K.S. and Kumar, S. (1998) Bacterial contamination in water of the River Ganga and its risk to human health, *International Journal of Environmental Health Research*, 8, 5–13.

Chakrapani, G.J., Subramanian, V., Gibbs, R.J. and Jha, P.K. (1995) Size characteristics and mineralogy of suspended sediments of the Ganga River, India, *Environmental Geology*, 25, 192–196.

Choudhury, M.I., Safiullah, S., Iqbal Ali, S.M., Mofizuddin, M. and Enamul Kabir, S. (1982) Carbon transport in the Ganga and Brahmaputra, preliminary results, *Mitteilung Geologische Palaeontologische Institut Universität Hamburg*, *SCOPE/UNEP* Sonderband Heft 52 (I.T. Degens, Ed.), 457–468.

Das Gupta, S.P. (1975) *The Upper Gangetic Flood-Plain. A Regional Survey*, National Atlas Organization, India, Monograph 1, Calcutta 194 p.

Das Gupta, S.P. (1984) *The Ganga Basin, Part I*, Central Board for the Prevention and Control of Water Pollution, New Delhi, 204 p.

France-Lanord, C. and Derry, L. (1997) Organic carbon burial forcing of the carbon cycle from Himalayan erosion, *Nature*, 390, 65–67.

Godbole, M.L. (1986) Training of Ganga River from Mokameh to Mansi, *Seminar on morphology of Ganga River*, Ganga Flood Control Commission, New Delhi, 73–90.

Goodbred, Jr, S.L. (2003) Response of the Ganges dispersal system to climate change: a source-to-sink view since the last interstade, *Sedimentary Geology*, 162, 83–104.

Goodbred, Jr, S.L. and Kuehl, S.A. (1999) Holocene and modern sediment budgets for the Ganges-Brahmaputra river system: evidence for highstand dispersal to flood plain, shelf and deep-sea depocenters, *Geology*, 27, 559–562.

Goodbred, Jr, S.L. and Kuehl, S.A. (2000) Enormous Ganges-Brahmaputra sediment discharge during strengthened early Holocene monsoon, *Geology*, 28, 1083–1086.

Goodbred, Jr, S.L., Kuehl, S.A., Steckler, M.S. and Sarkar, M.H. (2003) Controls on facies distribution and stratigraphic preservation in the Ganges-Brahmaputra delta sequence, *Sedimentary Geology*, 155, 301–316.

Gupta, H.P. (1992) Palynology, man and environment in Ganga basin. In: *Gangetic Plain: Terra Incognita* (I.B. Singh, Ed.), Geology Department, Lucknow University, 67–72.

Guzzella, L., Roscioli, C., Viganó, L., Saha, M., Sarkar, S.K. and Bhattacharya, A. (2005) Evaluation of the concentration of HCH, DDT, HCB, PCB and PAH in the sediments along the lower stretch of Hugli estuary, West Bengal, northeast India, *Environmental International*, 31, 523–534.

Handa, B.K. (1972) Geochemistry of the Ganges River water, *Indian Geohydrology*, 8, 71–78.

Heroy, D.C., Kuehl, S.A. and Goodbred, Jr, S.L. (2003) Sand- and clay-size mineralogy of the Ganges and Brahmaputra rivers: records of river switching and Late Quaternary climate change, *Sedimentary Geology*, 155, 343–359.

Ittekot, V. and Seifert, R. (1983) Nitrogenous organic matter in world rivers. In: *Transport of Carbon and Minerals in Major World Rivers, Part 2*, Proceedings of SCOPE/UNEP Workshops (E.T. Degens, S. Kempe and H. Soliman, Eds.), University of Hamburg, 119–128.

Jain, C.K. (2002) A hydro-chemical study of a mountainous watershed: the Ganga, India, *Water Research*, 36, 1262–1274.

Khan, A.A., Dubey, U.S., Sehgal, M.N. and Awasthi, S.C. (1982) Terraces in the Himalayan tributaries of Ganges in Uttar Pradesh, *Journal of the Geological Society of India*, 23, 392–401.

Krishna Murti, C.R., Bilgrami, K.S., Das, T.M. and Mathur, R.P. (Eds) (1991) *The Ganga–A Scientific Study*, Northern Book Centre, New Delhi, 246 p.

Krishnaswami, S., Trivedi, J.R., Sarin, M.M., Ramesh, R. and Sharma, K.K. (1992) Strontium isotopes and rubidium in the Ganga-Brahmaputra river system: weathering of the Himalaya, fluxes to the Bay of Bengal and contributions to the evolution of oceanic $^{87}Sr/^{86}Sr$, *Earth and Planetary Science Letters*, 109, 243–253.

Kumar, S. (1992) Heavy metal pollution in Ganga River sediments, Uttar Pradesh: a preliminary report. In: *Gangetic Plain: Terra Incognita* (I.B. Singh, Ed.), Geology Department, Lucknow University, 59–66.

Kumar, S. and Singh, I.B. (1978) Sedimentological study of Gomti river sediment, Uttar Pradesh, India: example of a river in alluvial Plain. *Senckenbergiana Maritima*, 10, 145–221.

Lyon-Caen, H. and Molnar, P. (1985) Gravity anomalies, flexures of the Indian plate and the structure, support and evolution of the Himalaya and the Ganga basin, *Tectonics*, 4, 513–538.

Markandya, A. and Murty, M.N. (2004) Cost–benefit analysis of the cleaning of the Ganges: some emerging environment and development issues, *Environment and Development Economics*, 9, 61–81.

Mathur, R.P. (1991) Trend of physico-chemical characteristics of the Ganga water. In: *The Ganga – A Scientific Study* (C.R. Krishna Murti, K.S. Bilgrami, T.M. Das and R.P. Mathur, Eds.), Northern Book Centre, New Delhi, 27–38.

Mehrotra, M.N., Singh, S.N., Srivastava, A. and Singh, K.M. (1991) Lead in bulk sediments of Ganga and its role in water pollution, *Bulletin of the Indian Geological Association*, 24, 61–66.

Michels, K.H., Kudrass, H.R., Hübscher, C., Suckow, A. and Wiedicke, M. (1998) The submarine delta of the Ganges-Brahmaputra: cyclone dominated sedimentation patterns, *Marine Geology*, 149, 133–154.

Milliman, J.D. and Meade, R.H. (1983) World-wide delivery of river sediment to the oceans, *Journal of Geology*, 91, 1–21.

Milliman, J.D. and Syvitski, P.M. (1992) Geomorphic/tectonic control of sediment discharge to the ocean: the importance of small mountainous rivers, *Journal of Geology*, 100, 525–544.

Moore, W.S. (1997) High fluxes of radium and barium from the mouth of Ganges-Brahmaputra River during low-river discharge suggest a large ground water source, *Earth and Planetary Science Letters*, 150, 141–150.

Morgan, J.P. and McIntyre, W.G. (1959). Quaternary geology of the Bengal Basin, East Pakistan and India, *Geological Society of America Bulletin*, 70, 319–342.

Mukerji, A.B. (1963) Alluvial morphology of the Upper Ganga-Yamuna Doab, *The Deccan Geographer*, 2, 1–36.

Navada, S.V. and Rao, S.M. (1991) Study of Ganga River – groundwater interaction using environmental ^{18}O, *Isotopenpraxis*, 27, 380–384.

Parua, P.K. (1986) Resuscitation by Bhagirathi-Hugli River complex. In: Pre-session, *Proceedings, Seminar on Morphology of Ganga River*, 17–18 November 1986, Central Board of Irrigation and Power, New Delhi, 131–146.

Philip, G., Gupta, R.P. and Bhattacharya, A. (1991) LANDSAT image enhancement for mapping fluvial palaeo-features in parts of Middle Ganga Basin, Bihar, *Journal of the Geological Society of India*, 37, 63–74.

Prasad, G., Ulabhaji, A.V. and Mehrotra, M.N. (1986) Some aspects of pollution of the Ganga, near Rajghat, Varanasi (UP), *Journal of the Institute of Public Health Engineers, India*, 1, 51–127.

Ramesh, R. and Sarin, M.M. (1992) Stable isotope study of the Ganga (Ganges) river system, *Journal of Hydrology*, 139, 49–62.

Rao, K.L. (1975) *India's Water Wealth*, Orient Longman Limited, New Delhi, 475 p.

Rao, M.B.R. (1973) The subsurface geology of the Indo-Gangetic plain, *Journal of the Geological Society of India*, 14, 217–242.

Rao, R.J. (2001) Biological resources of the Ganga River, India, *Hydrobiologia*, 458, 159–168.

Rawat, P.V.S. and Gairola, B.M. (1997) Quaternary geological and geomorphological studies in parts of Bhagirathi valley, Uttarkashi District, *Geological Survey of India Records*, 131, 103–105.

Raymahasay, B.C. (1986) Geochemistry of bicarbonates in river water, *Journal of the Geological Society of India*, 27, 114–118.

Roy, R.K. and Ghosh, B.K. (1981) Quaternary morpho-stratigraphy and neo-tectonic framework of the southern Ganga Valley, Bihar, India. In: *Proceedings of the Neogene/Quaternary Boundary Field Conference*, Geological Survey of India, Calcutta, 153–158.

Roy, T.N. (1983) *The Ganges Civilization*, Ramanand Vidya Bhawan, New Delhi, 293 p.

Sarin, M.M. and Krishnaswami, S. (1984) Major ion geochemistry of the Ganges-Brahmaputra river system, India, *Nature*, 312, 538–541.

Sarin, M.M., Krishnaswami, S., Dilli, K., Somayajulu, B.L.K. and Moore, W.S. (1989) Major ion chemistry of the Ganga-Brahmaputra river systems; weathering processes and fluxes to the Bay of Bengal, *Geochemica et Cosmochemica Acta*, 53, 997–1009.

Sarin, M.M., Krishnaswami, S., Somayajulu, B.L.K. and Moore, W.S. (1990) Chemistry of U, Th and Ra isotopes in the Ganga-Brahmaputra river system: weathering processes and fluxes to the Bay of Bengal, *Geochemica et Cosmochemica Acta*, 54, 1387–1396.

Sarin, M.M., Krishnaswami, S., Trivedi, J.R. and Sharma, K.K. (1992) Major ion chemistry of the Ganga source waters: Weathering in the high altitude Himalaya. In: *Proceedings of the Indian Academy of Sciences, Earth and Planetary Sciences*, 101, 89–98.

Sastri, V.V., Bhandari, L.L., Raju, A.T.R. and Dutta, A.K. (1971) Tectonic framework and subsurface stratigraphy of the Ganga Basin, *Journal of the Geological Society of India*, 12, 222–233.

Seeber, L. and Gornitz, V. (1983) River profiles along the Himalayan arch as indicators of active tectonics. *Tectonophysics*, 92, 335–367.

Sharma, C.B. and Ghosh, N.C. (1987) Pollution of the River Ganga by municipal waste: a case study from Patna, *Journal of the Geological Society of India*, 30, 369–385.

Shukla, U.K. Singh, I.B. Srivastava, P. and Singh, D.S. (1999) Palaeocurrents pattern in braid-bar and point-bar deposits: examples from the Ganga River, India, *Journal of Sedimentary Research*, 69, 992–1002.

Shukla, U.K., Singh, I.B., Sharma, M. and Sharma, S. (2001) A model of alluvial magafan sedimentation: Ganga Megafan, *Sedimentary Geology*, 144, 243–262.

Singh, A.K. and Singh, M. (2007) Bibliography of environmental studies in natural characteristics and anthropogenic influences on the Ganga River, *Environmental Monitoring and Assessment*, 129, 421–432.

Singh, I.B. (1987) Sedimentological history of Quaternary deposits in Gangetic Plain, *Indian Journal of Earth Sciences*, 14, 272–282.

Singh, I.B. (1996) Geological evolution of Ganga plain – an overview, *Journal of the Palaeontological Society of India*, 41, 99–137.

Singh, I.B. (2001) Proxy records of neotectonics, climate changes and anthropogenic activity in late Quaternary of Ganga Plain. National Symposium Role of Earth Science: Integrated Development and Related Societal Issues, *Geological Survey of India Special Publication*, 65 (1), xxxiii–I.

Singh, I.B. (2002) Late Quaternary evolution of Ganga Plain and proxy records of climate change and anthropogenic activity, *Pragdhara*, 12, 1–25.

Singh, I.B. (2004) Late Quaternary history of the Ganga Plain, *Journal of the Geological Society of India*, 64, 431–454.

Singh, I.B. and Swamy, A.S.R. (2006) *Delta Sedimentation – East Coast of India*, Technology Publication, Dehradun, 392 p.

Singh, I.B., Bajpai, V.N., Kumar, A. and Singh, M. (1990) Changes in the channel characteristics of Ganga River during Late Pleistocene-Holocene, *Journal of the Geological Society of India*, 36, 676–673.

Singh, I.B., Ansari, A.A., Chandel, R.S. and Misra, A. (1996) Neotectonic control of drainage system in Gangetic Plain, Utttar Pradesh, *Journal of the Geological Society of India*, 47, 599–609.

Singh, M. (1996) *The Ganga River: Fluvial Geomorphology, Sedimentation Processes and Geochemical Studies*, Heidelberger Beiträge zur Umwelt-Geochemie, Band 8, Heidelberg, 133 p.

Singh, M. and Singh, I.B. (1992) *The Ganga River Valley: Alluvial Valley in an Active Foreland Basin*, 29th International Geological Conference, Kyoto, Japan, vol. 2, 30 (abstract).

Singh, M., Müller, G. and Singh, I.B. (2002) Heavy metals in freshly deposited stream sediments of rivers associated with urbanization of the Ganga Plain, India, *Water, Air and Soil Pollution*, 141, 35–54.

Singh, M., Müller, G. and Singh, I.B. (2003) Geogenic distribution and baseline concentration of heavy metals in sediments of the Ganga River, India, *Journal of Geochemical Exploration*, 80, 1–17.

Singh, M., Sharma, M. and Tobschall, H.J. (2005) Weathering of the Ganga alluvial plain, northern India; implication from fluvial geochemistry of the Gomati River, *Applied Geochemistry*, 20, 1–21.

Singh, M., Singh, I.B. and Muller, G. (2007) Sediment characteristics and transportation dynamics of the Ganga River, *Geomorphology*, 86, 144–175.

Sinha, A.K. (1991) River Ganga in the stretch between Kalakankar (Pratapgarh) and Phaphamau (Allahabad): a comprehensive study. In: *The Ganga – A Scientific Study* (Eds. Krishna Murti, C.R., Bilgrami, K.S., Das, T.M. and Mathur, R.P.), Northern Book Centre, New Delhi, 125–145.

Sinha, M. and Khan, M.A. (2001) Impact of environmental aberrations on fisheries of the Ganga (Ganges) River, *Aquatic Ecosystem Health and Management*, 4, 493–504.

Somayajulu, B.L.K., Rengarajan, R. and Jani, R.A. (2002) Geochemical cycling in the Hooghly estuary, India, *Marine Chemistry*, 79, 171–183.

Srivastava, R.K., Sinha, A.K., Pande, D.P., Singh, K.P. and Chandra, H. (1996) Water quality of River Ganga at Phaphamau (Allahabad) – effect of masss bathing during Mahakumbh, *Environmental Toxicology and Water Quality*, 11, 1–5.

Srivastava, P., Singh, I.B., Sharma, M. and Singhvi, A.K. (2003) Luminescence chronometry and late Quaternary geomorphic history of the Ganga Plain, India, *Palaeogeography, Palaeoclimatology, Palaeoecology*, 197, 15–41.

Subramanian, V., Van Grieken, R. and Van't Dack, L. (1987) Heavy metals distribution in the sediments of Ganges and Brahmaputra rivers, *Environmental Geology Water Science*, 9, 93–103.

Umitsu, M. (1993) Late Quaternary sedimentary environments and landforms in the Ganges delta, *Sedimentary Geology*, 83, 177–186.

Wasson, R.J. (2003) A sediment budget for the Ganga-Brahmaputra catchment, *Current Science*, 84, 1041–1047.

18

Erosion and Weathering in the Brahmaputra River System

Sunil K. Singh

Planetary Geosciences Division, Physical Research Laboratory, Navrangpura, Ahmedabad 380009, India

18.1 INTRODUCTION

The Brahmaputra is a major river system that flows through very distinct regions: the Tibetan Plateau, the Himalaya Mountains, the Assam Plains, and the delta in Bangladesh. Each of these has its own geology, climate, tectonics, and culture. Compared with other major river basins of Asia, the basin of the Brahmaputra, particularly its upper section, is pristine. Limited accessibility to a number of tributaries of the Brahmaputra, however, has led to a restricted number of studies on the system.

The Brahmaputra plays a significant role in the sediment and element budgets of the globe. It supplies 670 km^3 of water, 1000 million t of particulates, and 100 million t of dissolved material annually to the Bay of Bengal (Milliman and Mead, 1983; Sarin *et al*., 1989; Milliman and Syvitsky, 1992; Hay, 1998). Weathering and erosion rates in the basin are among the highest in the world. The weathered products are delivered to the ocean mostly between June and September when the south-west monsoon operates. The Brahmaputra is a fascinating river system regarding its morphology and operating processes. Floods are common in the river due to intense rainfall, the Assam plain almost invariably gets flooded during every south-west monsoon affecting millions of people. During these floods the Brahmaputra deposits a large volume of sediment along its course but it also removes material, mainly by bank erosion. The large sediment and solute flux transported by the Brahmaputra is a measure of the intense erosion and weathering of its basin, particularly from the mountain reaches. The high physical erosion and chemical erosion in the basin has both regional and global effects. It causes enhanced uplift in mountain ranges and consumption of a disproportionate amount of atmospheric CO_2 (Raymo and Ruddimann, 1992). Weathering in the Brahmaputra and the Ganga Basins contributes significantly to the evolution of seawater chemistry, particularly the Sr and Os isotope systematics and sediment budget (Krishnaswami *et al*., 1992; Pegram *et al*., 1992; Galy *et al*., 1999; Singh *et al*., 2005). Major efforts to investigate weathering and erosion of the Brahmaputra system have been initiated only recently (Singh and France-Lanord, 2002; Singh *et al*., 2003, 2005; Garzanti *et al*., 2004).

This review synthesises the available information on erosion and weathering in the Brahmaputra Basin. Isotopic and elemental data for the particulate and dissolved materials of the Brahmaputra have been taken from Singh and France-Lanord (2002) and Singh *et al*. (2005).

18.2 THE BRAHMAPUTRA RIVER SYSTEM

The source of the Brahmaputra was a matter of great speculation and discussion even a hundred years ago. The Tsangpo in Tibet and the Brahmaputra in India were recognized as the same river only in the late nineteenth century (Montgomerie, 1868). The Brahmaputra is known under different names along its course. Originating in the southern slopes of the snow-covered Kailash Mountain

Large Rivers: Geomorphology and Management, Edited by A. Gupta

(the Jimayangzhong Glacier) in the Trans-Himalaya, it flows eastward on a gentle slope (~0.001) for 1200 km along the Indus-Tsangpo Suture in Tibet known as the Yarlung Tsangpo, Tsangpo, Sangpo or Yaluzangbu. The Tsangpo takes a sudden U-turn (Figures 18.1 and 18.2) after Pai at 95 °E around the Namche Barwa Peak of the Eastern Syntaxis curving out a very deep gorge ~5075 m depth. The river then turns south and enters Arunachal Pradesh of India at Singing. This U-turn is also known as 'the Big Bend'. The river is known as the *Siang* or *Dihang* in Arunachal Pradesh, and characterized by a steep gradient (~0.03) and extremely turbulent and rapid flow. The Siang becomes the Brahmaputra in the Assam Plains where it merges with the Dibang and the Lohit (Figures 18.1 and 18.2). In the plains of Assam the Brahmaputra is a wide, deep and braided river that flows in the WWS direction. Turning south near Dhubri the Brahmaputra enters Bangladesh as the Jamuna to meet the Ganga at Arichaghat (see Chapter 19).

The total length of the Brahmaputra from its origin in the Kailash Mountain to Arichaghat is 2900 km. Of this 1600 km is in Tibet, 900 km in India, and the remaining 400 km in Bangladesh (Kumar, 1997). Along its length, the Brahmaputra receives many tributaries. The Lhasa He (Zangbo), Doilung and Nyang Qu (Figure 18.2) are its major tributaries in Tibet. The river also receives several other tributaries draining the northern slope of the Himalaya. The Parlung Zangbo, another tributary with a very high gradient merges with the Tsangpo near the deep gorge after Pai. Figure 18.3 summarizes the long profile and the cumulative discharge of the Brahmaputra.

Flowing through the Assam Plains the Brahmaputra receives many tributaries from the north, east and south. The Subansiri, Ranga Nadi, Jia Bhareli, Puthimari, Manas and Tipkai are some of the north bank tributaries from the Himalaya. The Dibang and Lohit are from the Mishmi Hills to the east, and the Burhi Dihing, Dhansiri and Kopili are from the south (Figure 18.2). The Brahmaputra receives the Tista, a large northern tributary draining the Himalaya, in Bangladesh.

The drainage basin of the Brahmaputra comprises different and contrasting geological and climatic zones. To illustrate, a significant fraction of its drainage is in the dry region of Tibet in the rain shadow of the Himalaya, whereas part of its eastern basin has extremely high rainfall, including Cherrapunji with the highest recorded rainfall (1270 cm year^{-1}) in the world. Average annual temperature varies among the different zones by as much as 40 °C. Lithologies also vary, from easily weathered evaporites to resistant silicates. Along the rivers of the

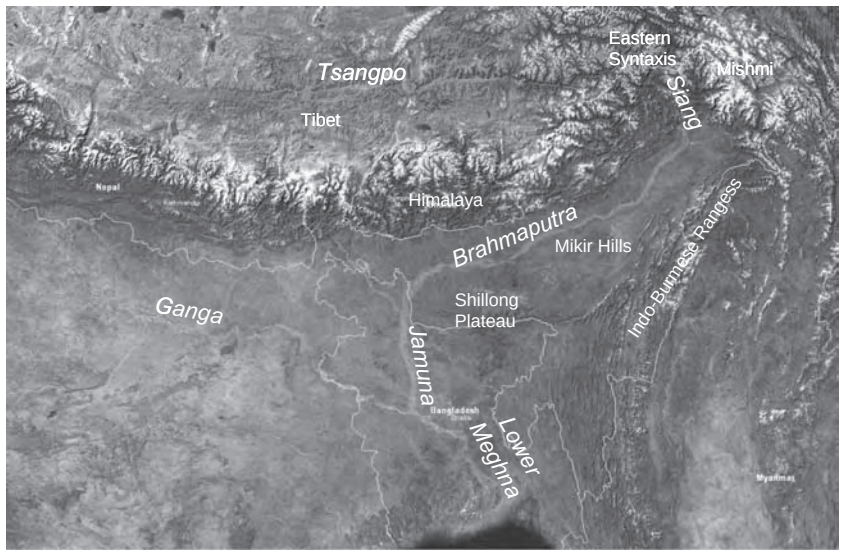

Figure 18.1 Annotated satellite (MODIS) image of the Brahmaputra Basin. The Brahmaputra originates from northern slope of the Himalaya and flows eastward in Tibet. It crosses the Himalaya after taking a U-turn near Namche Barwa. It flows westward in the Assam Plains, and turns south to enter Bangladesh as the Jamuna to join the Ganga. The narrow plain of Assam is bounded by the Himalaya, the Shillong Plateau and Mikir Hills, the Mishmi Hills and the Indo-Burmese (Indo-Myanmar) Ranges (MODIS, Nov. 2004)

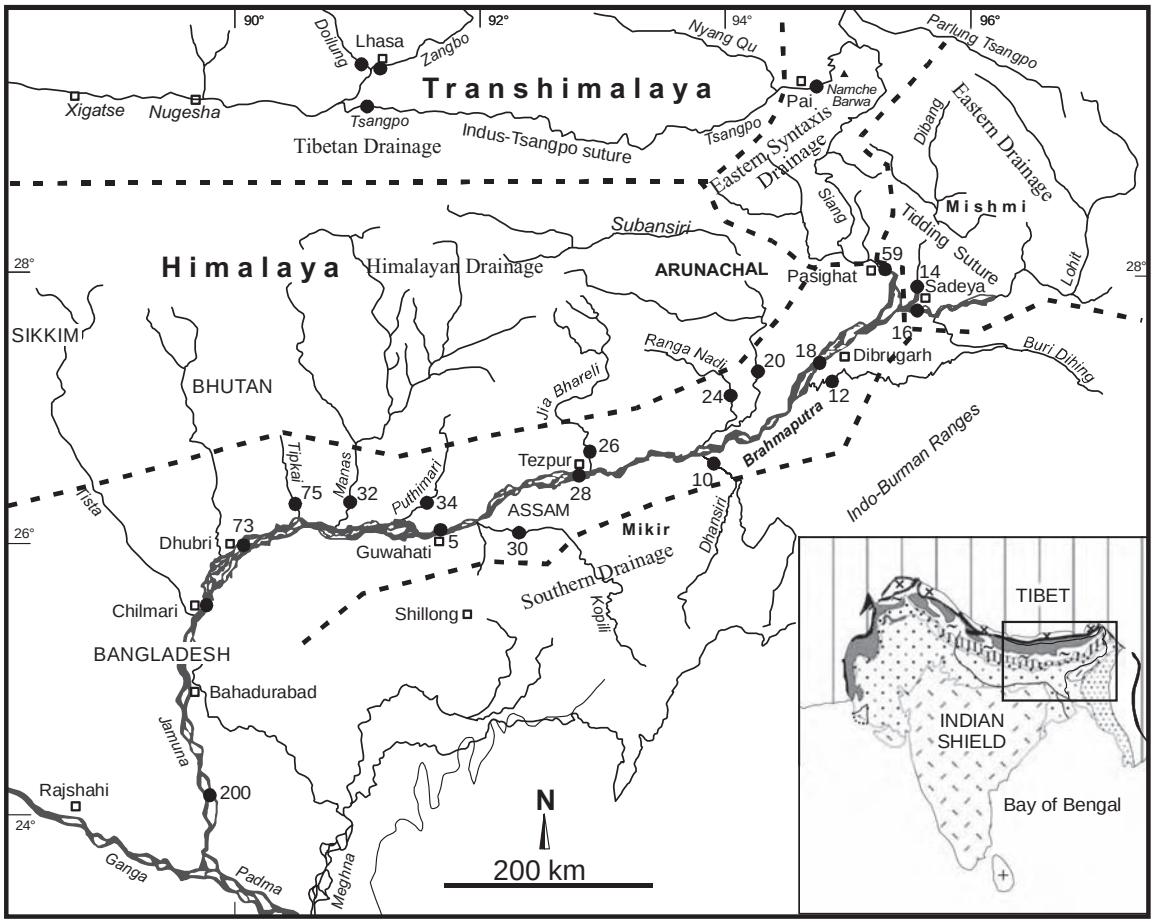

Figure 18.2 The Brahmaputra main stream and its major tributaries in Tibet and in the Assam Plains. Places mentioned in the text and the sampling locations are shown. Reprinted from Geochimica et Cosmochimica Acta, Vol. 69, Singh *et al*., Chemical erosion in the eastern Himalaya: major ion composition of the Brahmaputra and $\delta^{13}C$ of dissolved inorganic carbon, pp. 3573–3588, 2005, with permission from Elsevier

Brahmaputra system, there are sections characterized by some of the highest relief in the world, in contrast there are also sections which have very little relief.

The drainage basin of the Brahmaputra system, from the source to mouth, can be divided into six zones (Figure 18.2):

1. the high plateau of Tibet;
2. the Eastern Syntaxis;
3. the Mishmi Hills or the Eastern Drainage;
4. the Himalaya Mountains;
5. the Indo-Myanmar and Naga-Patkoi Ranges or the Southern Drainage;
6. the plains of Assam and Bangladesh.

18.3 GEOLOGY OF THE BASIN

The geology of the eastern Himalaya is still being studied, but it is possible to summarize the basic lithology of the different sections:

1. *The high plateau of Tibet.* The Tsangpo drains turbidites and ophiolites of the Indus-Tsangpo Suture Zone in its upper reaches in Tibet. The northern tributaries of the Tsangpo drain Trans-Himalayan gabbroic to granodioritic batholiths (Gangdese Belt). Part of the drainage consists of the Lhasa Block which includes Precambrian orthogneisses and metasediments. The Lhasa Block is the southernmost part of Tibet, which was accreted to Asia by a late Jurassic–early Creta-

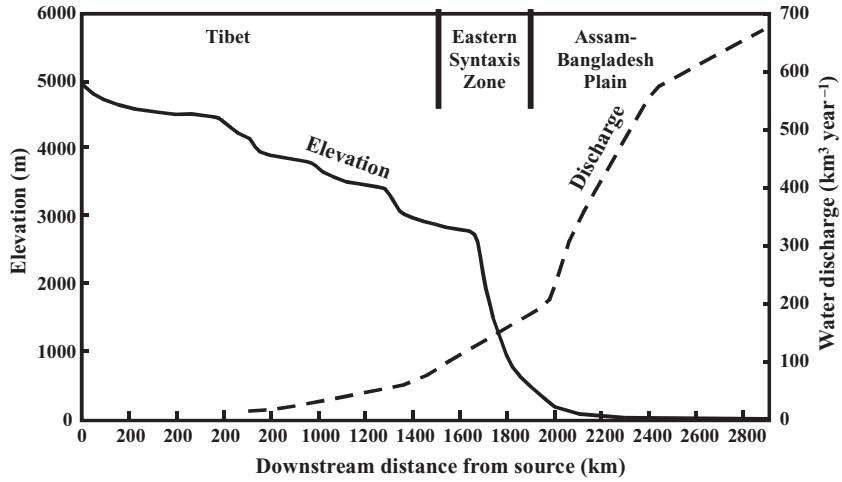

Figure 18.3 Long profile and water discharge of the Brahmaputra main stream. The gradient of the river is very high in the Eastern Syntaxis Zone and the river flows through a very deep gorge (~5000 m). Reprinted from Earth and Planetary Science Letters, Vol. 202, Singh S.K. and France-Lanord, C., Tracing the distribution of erosion in the Brahmaputra watershed from isotopic compositions of stream sediments, pp. 645–662, 2002, with permission from Elsevier

ceous collision after rifting from Gondwana (Booth *et al*., 2004). The tributaries joining the Tsangpo from the south drain the northern slope of the High Himalaya on gneiss and Palaeozoic to Eocene Tethyan sedimentary rocks. Many evaporite deposits and saline lakes are also present in the Tibetan part of the basin (Pascoe, 1963; Hu *et al*., 1982; Pande *et al*., 1994).

2. *The Eastern Syntaxis*. This is the zone where the Tsangpo River makes a U-turn around the Namche Barwa Peak. The rocks of the region are highly metamorphosed. The gneisses of the Indian Plate have been exhumed from below the Trans-Himalayan Plutonic Belt (TPB). These rocks have undergone metamorphism up to upper amphibolite to granulite facies (720–760 °C, 8–10 kb). Quartzites, phyllites and marbles surround the calc-alkaline plutons of the TPB in this zone. This zone is the continuation of the Indus-Tsangpo Suture as indicated by the presence of discrete lenses of metabasites and serpentinites (Burg *et al*., 1998). These are drained by the Siang, Dibang and Parlung Tsangpo.
3. *The Mishmi Hills or the Eastern Drainage*. The two eastern tributaries (the Lohit and Dibang) flow through the Mishmi Hills, the lithology of which includes calc-alkaline diorite-tonalite-granodiorite complexes and tholeiitic metavolcanic rocks of island-arc affinity (Kumar, 1997). It represents the eastern continuation of the TPB, continuing further in Myanmar. The Tidding Suture, the eastern extension of the Indus-Tsangpo Suture with chlorite-schists, amphibolites, and carbonates present in this area, marks the boundary between the TPB and the Himalaya.
4. *The Himalaya Mountains*. In the Brahmaputra Basin, the typical Himalayan formations terminate near the eastern syntaxis against the Tidding Suture. The Siang and other northern tributaries (the Subansiri, Ranga Nadi, Jia Bhareli, Puthimari and Manas) drain the Himalaya to join the Brahmaputra in the plains of Assam. A limited number including the Subansiri originate in the Tethys Himalayan sedimentary zone. The geology of the Himalaya in this section is similar to that of its central and western parts, which is drained by the headwaters of the Ganga. It comprises of the Higher and the Lesser Himalaya and the Siwaliks (Gansser, 1964; Thakur, 1986). The areal proportion of the Lesser Himalaya increases from east to west (Robinson *et al*., 2001; Singh and France-Lanord, 2002). The Higher Himalayan lithologies consist mainly of schists, gneisses, and marbles with amphiboles at some locations. Migmatites and Miocene leucogranites are also common in certain locations. The Manas and Tista drain through metamorphic rocks of the Higher Himalaya in Bhutan and Sikkim. The Lesser Himalaya in the Brahmaputra system is composed mainly of quartzites and schists. Precambrian limestones, dolostones, shales and quartzites along with orthogneiss bodies and dolerite sills are exposed in the Lesser Himalaya. Further south, the Siwalik Hills with thick sections of Neogene molas-

ses are discontinuous in the eastern section of the Himalaya. The Abor Volcanics is present in the Himalayan drainage of the Siang besides the common Himalayan rocks (Jain and Thakur, 1978).

5. *The Indo-Myanmar and Naga-Patkoi Ranges or the Southern Drainage*. These ranges consist mainly of Cretaceous–Eocene pelagic sediments overlain by thick Eocene–Oligocene turbidites associated with Naga ophiolites. These sediments were emplaced onto the eastern India shelf during mid-Tertiary collision with Asia. The southern tributaries (the Dhansiri and Kopili) drain these lithologies along with granite and gneisses of the Indian basement of the Shillong Plateau and the Mikir Hills (Kumar, 1997).
6. *The plains of Assam and Bangladesh*. Part of the plains of Assam and Bangladesh through which the Brahmaputra flows consist of the fluvial sediments brought by the Brahmaputra itself. However, the Indian basement is exposed in some regions in Assam. The floodplain of the Brahmaputra consists of alluvial features such as natural levees, pointbars, ox-bow lakes and channel bars (Goswami, 1998).

18.4 HYDROLOGY

The drainage basin of the Brahmaputra includes contrasting climatic and hydrologic zones. The Tibetan drainage is cold and arid in the rain shadow of the Himalaya. The climate of the rest of the basin is humid subtropical with the temperature varying significantly with altitude. The Assam Plains, the Indo-Myanmar Ranges and the Siwalik section of the Himalaya have hot and humid climate. The Lesser Himalaya and the Mishmi Hills are cooler and wet and the Higher Himalaya, the Tethyan Himalaya and the Eastern Syntaxis are Alpine (Kumar, 1997). Temperatures in Tibet vary from −5.0 to 20 °C (Guan and Chen, 1981). The Brahmaputra Basin outside Tibet has three seasons: summer, wet monsoon, winter. The summer is short, spanning about 2 months (April–May), but the temperature in the plains can rise up to 40 °C. The wet south-west monsoon is active from June to September, except in Tibet. The winter temperature in parts of the plains may drop as low as 0 °C, which is common in the mountains. The peaks of the Higher Himalaya are perennially snow clad.

The annual precipitation is about 300 mm in Tibet, a figure that rises to 5000 mm in the Eastern Syntaxis. Annual rainfall in the southern slopes of the Himalayan drainage of the Brahmaputra is between 1000 and 2000 mm, and over the Mishmi Hills it is about 3000 mm. Monthly precipitation for a period of 10 years (1994–2003) is shown in Figure 18.4 illustrating the seasonality in precipitation. Part of the Himalaya that falls in the rain shadow zone of the Shillong Plateau receives less rainfall. The Naga-Patkoi and Indo-Myanmar Ranges are exposed

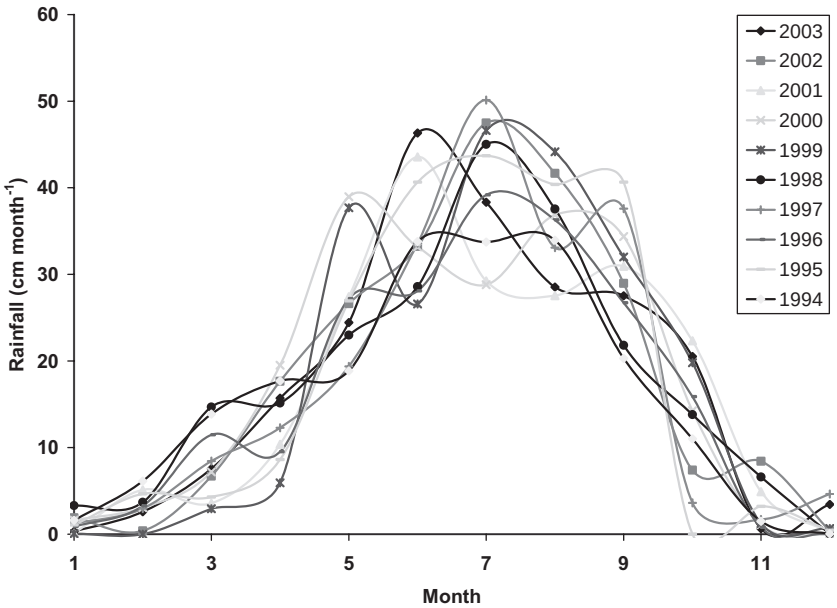

Figure 18.4 Monthly rainfall in north-east India in the Brahmaputra Basin (1994–2003) (from www.tropmet.res.in)

Table 18.1 Discharge and drainage of the Brahmaputra main stream and its tributaries

River	Station	Area (10^5 km^2)	Discharge (km^3 year^{-1})
Brahmaputra main stream			
Tsangpo	Nugesha	1.06	17
Tsangpo	Yangcun	1.53	29
Tsangpo	Nuxia	1.90	59
Tsangpo	Tsela D' Zang	1.91	63
Siang	Pasighat	2.46	200
Brahmaputra	Dibrugarh	2.98	323
Brahmaputra	Pandu	4.05	571
Brahmaputra	Bahadurabad	6.36	670
Tibetan tributaries			
Nyang He	Gyangze	0.06	0.7
Lhasa He	Lhasa	0.26	9.1
Assam Plain tributaries			
Dibang	Sadeya	0.13	63
Lohit	Sadeya	0.24	60
Subansiri	Nr confluence	0.33	54
Ranga Nadi	Nr confluence	0.02	5.8
Jia Bhareli	Nr confluence	0.12	26
Manas	Nr confluence	0.38	32
Puthimari	Nr confluence	0.02	4.4
Burhi Dihing	Nr confluence	0.08	14
Dhansiri	Nr confluence	0.12	20
Kopili	Nr confluence	0.16	28

Source: Rao, 1979; Guan and Chen, 1981; Goswami, 1998; www.grdc.sr.unh.edu.

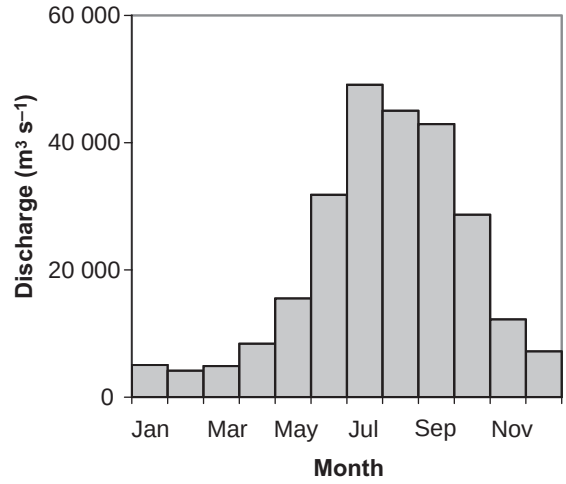

Figure 18.5 Monthly water discharge of the Brahmaputra at Bahadurabad (from www.grdc.sr.unh.edu). Rainfall during the south-west monsoon is the main contributor to annual discharge of the Brahmaputra

to heavy rainfall of 4000 mm year^{-1}. Cherrapunji, which receives the highest rainfall (~13 m year^{-1}) in the world, is located in this region.

Table 18.1 lists the discharge figures of the Brahmaputra main stream and many of its major tributaries and their drainage areas. The discharge of the Brahmaputra at Nugesha, Tibet is 17 km^3 year^{-1} which increases to 60 km^3 year^{-1} before the river enters the syntaxis region. At Bahadurabad in Bangladesh it increases to 670 km^3 year^{-1} (www.grdc.sr.unh.edu). Rainfall is the major source of water for the Brahmaputra, although contributions from meltwater and groundwater are also important during summer. The Tsangpo receives roughly equal contributions from meltwater, groundwater and rainfall (Guan and Chen, 1981). Between June and September, the south-west monsoon contributes 70–80% of the total discharge of the Brahmaputra. The monthly water discharge pattern of the Brahmaputra at Bahadurabad in Bangladesh reflects the impact of monsoon on the total discharge with significant temporal variation (Figure 18.5).

The total drainage area of the Brahmaputra system is about 630 000 km^2, of which about one-third is in Tibet at an average elevation of 5000 m. The Tibetan drainage contributes about 10% of the discharge of the Brahmaputra at its mouth. The plains of Assam and Bangladesh together have a drainage area of 200 000 km^2 and the southern slopes of the Himalaya cover an area of 120 000 km^2. About 50 000 km^2 in the Mishmi Hills is drained by the two eastern tributaries, the Lohit and Dibang. The rest of the drainage lies in the Indo-Myanmar and Naga-Patkoi Ranges.

18.5 FLOODS IN THE BRAHMAPUTRA

Floods are a very common annual feature of the Brahmaputra (Figure 18.6). Every year during the south-west monsoon the main stream and the tributaries of the Brahmaputra spill over their banks causing devastating floods in the Assam Plains associated with huge loss and damage to human lives, property, and infrastructure. Large floods with flows in the order of 70 000–100 000 m^3 s^{-1} have a return period of 100 years (Rangachari, 1994; Goswami, 1998). Floods with 25 years recurrence near Guwahati have a discharge of ~60 000 m^3 s^{-1}. In recent times, the highest flood discharge was recorded in 1962 near Guwahati as 73 000 m^3 s^{-1} (Figure 18.6). The average annual flood at Pandu near Guwahati has a magnitude of ~50 000 m^3 s^{-1} with a recurrence period of ~2.6 years (Bhattacharya and Bora, 1997). The bankfull discharge here is 35 000 m^3 s^{-1} which occurs every year on the Brahmaputra (Figure 18.6; Goswami, 1998). The flash floods

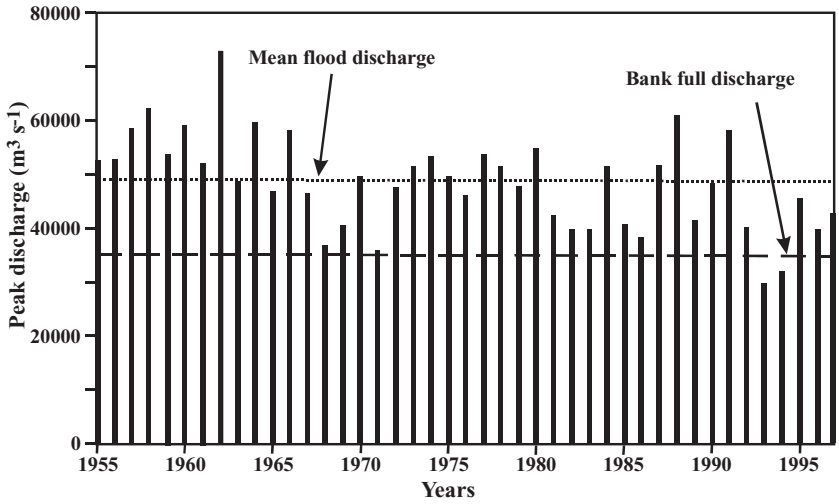

Figure 18.6 Annual peak discharge of the Brahmaputra at Pandu near Guwahati. Levels of bankfull discharge and the mean flood discharge are also shown. Overbank flooding is a yearly phenomenon in the Brahmaputra

of the Himalayan tributaries contribute huge peak discharges leading to flooding of the plains.

During the past 50 years, larger flood events occurred in 1954, 1962, 1966, 1972, 1973, 1977, 1978, 1983, 1984, 1987, 1988, 1991, 1993, 1995, 1996, 1998, 2000 and 2003 (Figures 18.6 and 18.7). More than 10 000 km^2 of land, which is 12.25 % of the geographical area of the state of Assam, is annually affected by floods. The flood of 1998, which inundated 38 000 km^2, about half of Assam, affected the lives and property of about 12.5 million people (Valdiya, 1999). Similarly, 46 500 km^2, including 13 350 km^2 of cropped land was damaged in 1988, affecting tens of millions of people in 10 000 villages (Figure 18.7).

The width of the Brahmaputra Plain in the Assam is about 80 km but the unit flood discharge is extremely high. The high discharge during the south-west monsoon, the restricted width of the valleyflat, and the low gradient in combination result in drainage congestion and floods. The width of the Assam Plains is affected by its northward and eastward underthrusting under the Arunachal Himalaya and the Indo-Myanmar Ranges, respectively (Valdiya, 1999). These tectonic activities cause the Shillong-Mikir Hills of the Peninsular Shield to move closer to the Himalaya, contributing to the narrowing of the plains in Assam. The active deformation of the Assam Plains is evident from the presence of many faults near the Shillong-Mikir Blocks. Most of these faults are seismically active. Valdiya (1999) has observed that the Mikir Block is uplifting rapidly at 31 mm year^{-1}, which is indicative of high seismic activity of this area. The uplift of the Shillong Plateau apparently obstructs the Brahmaputra River near Guwahati leading to a narrowing of the valleyflat (Figure 18.8). This along with the deposition of sediment upstream as islands and sandbars in the channel has reduced the carrying capacity of the Brahmaputra.

The Brahmaputra also has a history of flooding due to tectonic disturbances. The massive earthquake of 1897 of magnitude 8.7 partially blocked the flow of the Brahmaputra resulting in huge flooding of the riverine plain. Similarly the earthquake of 1950 (magnitude 8.7) stopped the flow of the Brahmaputra near Dibrugarh causing up to 3 m of siltation on the bed reducing the flow capacity and resulting in more floods in subsequent years (Valdiya, 1999). Anthropogenic activities also contribute to the frequent floods in the Assam Plains. Deforestation in the upper reaches has considerably reduced the resident time of the rainwater in the basin aggravating flood occurrences. The encroachment on the large number of the depressions on the floodplain has reduced the area of natural retention basins. The poorly planned road and railway embankments have also affected the drainage system. The presence of over 4000 km of embankments in the state of Assam, about a third of the total length of embankments in India, illustrates the dependence on structural measures for flood protection (Table 18.2). However, floods on a large river like the Brahmaputra are not very successfully controlled by building embankments. The active tectonics of the Brahmaputra Basin also does not encourage the construction of flood-control structures.

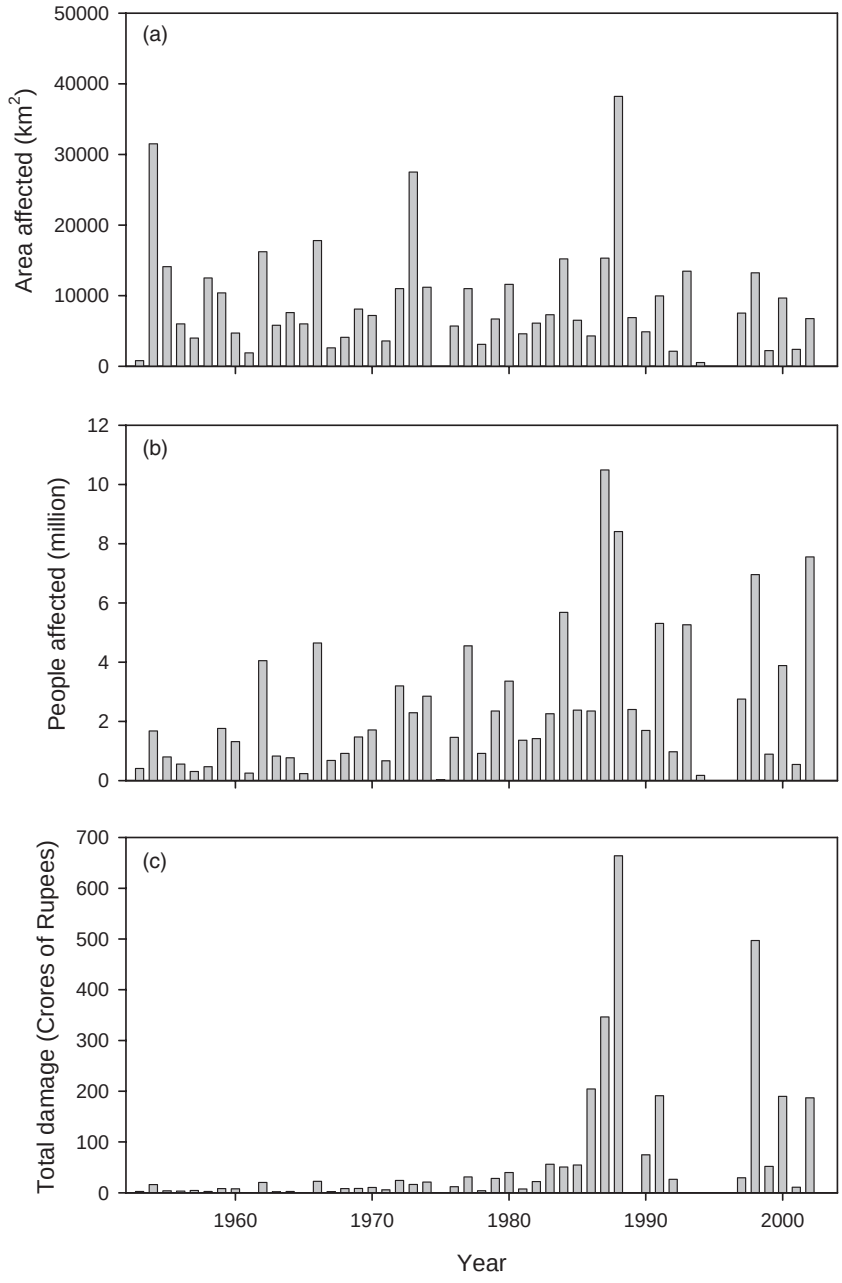

Figure 18.7 Flood effects: (a) area affected; (b) people affected; (c) damage of property (from Goswami, 1998 and Water Resources Department, Assam: www.assamgov.org/Ecosurvey/Flood.htm)

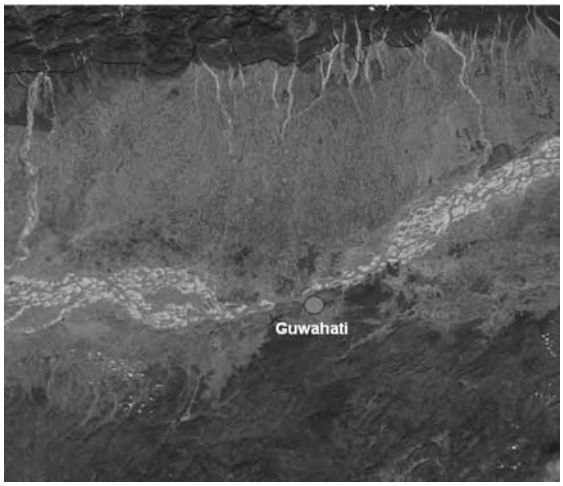

Figure 18.8 MODIS image of narrowed channel of the Brahmaputra mainstream near Guwahati. The continuous uplift and northward movement of the Shillong-Mikir Block has narrowed down the channel of the Brahmaputra near Guwahati, which impounds water flow

Table 18.2 Various flood control measures in Assam

Flood control measures	Dimension
Embankments	4460 km
Drainage channels	850 km
Protection and anti-erosion projects	685
Major sluices	85
Benefited area	16000 km^2

Source: Water Resources Department, Assam: www.assamgov.org/Ecosurvey/Flood.htm.

Building of upstream storage reservoirs has been considered as an effective flood control measure. The Brahmaputra Board, a statutory body under the Ministry of Water Resources, Government of India, drafted the Brahmaputra Basin Master Plan in 1986 with major emphasis on the construction of large storage reservoirs. The potential sites indicate proposed dams on the Siang, Subansiri and Manas with a total storage capacity of about 70 km^3. The proposals have undergone several modifications over the years. The current plan is to construct three dams each on the Siang and Subansiri. Dams on other rivers (the Pagladiya and the Tipaimukh) are also planned (Water Resources Department, Assam: www.assamgov.org/Ecosurvey/Flood.htm). The slow pace of implementation of these projects seems to indicate that it will take several years before the dams are completed. Besides tectonic activities, the other drawback of these big dams is heavy silting in these rivers. The Rastriya Barh Ayog (National Flood Commission of India) has suggested other structural measure such as the use of natural depressions for moderating the floods and taking anti-erosion measures to protect towns, industrial areas and vital installations.

Such floods are caused mainly by the heavy seasonal runoff, partially blocked by the tectonic configuration of the Assam Plains and reduction of the channel width near the Shillong-Mikir Block. One way to minimize this problem would be to channelize the flood discharge (50000 $m^3 s^{-1}$; Goswami, 1998) by providing extra passage to these waters through canals, aqueducts or tunnels in the region west of the Mikir Hills (Valdiya, 1999). The canals and river channels would have to be dredged and deepened periodically to take care of uplift and heavy silting. Structural measures, however, are not a complete solution for flood management on the Brahmaputra. There have been suggestions to strengthen the nonstructural methods, such as flood forecasting and warning, flood plain regulation, and disaster release.

18.6 CHARACTERISTICS OF THE BRAHMAPUTRA CHANNEL

The Brahmaputra displays a wide range of morphological variations ranging between steep gorges and wide channels with gentle slopes, probably due to its tectonics-driven gradient changes. The variation in the river slope is shown in Figure 18.3**.** The gradient of the river in Tibet is variable but, in general, it tends to be low. According to Zhang (2001), the alteration of gentle and steep slopes in Tibet is due to the presence of knickpoints at intervals, which leads to a downstream sequence of sediment accumulation–knickpoint–rapid erosion. Beyond Tibet, the Brahmaputra has cut an ~5000 m deep gorge in the mountains of the Eastern Syntaxis. Its origin has been attributed to rapid erosion, followed by uplift and knickpoint formation (Zeitler *et al*., 2001). The gradient of the Brahmaputra is as steep as 0.03 in the deep gorge but drops to 0.0001 near the Guwahati in the Assam Plains, about 900 km away. In Assam, the average width of the Brahmaputra channel is about 8 km but it does vary. For example, it is only 1 km near Guwahati where hills approach the river. The Brahmaputra acquires a maximum width of 20 km at several locations in the Assam Plains.

The pattern of the channel also varies: meandering, braided, single near-straight. The upper Tsangpo has a freely meandering channel that changes into a braiding pattern downstream. In the middle part of the Tibetan drainage, a single straight channel is common. In the

lower part of the river in Tibet, deeply trenched meandering channels flow in gorges. A single meandering channel cuts through the mountain barrier from Pai to Pasighat. Downstream of Pasighat, in the plains of Assam and Bangladesh, the Brahmaputra has a highly braided channel marked by the presence of numerous sandbars and islands (Goswami, 1985). In the Assam Plains the Brahmaputra is characterized by mid-channel bars, sidebars, and tributary mouth bars. Palaeochannels on the interfluves indicate the role of neo-tectonic activities. The plains in Assam and the adjoining hill ranges are seismically very active. Massive earthquakes have occurred in this area, which have changed the course of many rivers of the Brahmaputra system including the main stream (Goswami, 1985). Earthquakes of small magnitudes are a common feature in this area. The channel of the Brahmaputra River has been migrating because of channel widening and avulsion. The Majuli Island in Assam has an area of 600 km^2 between two channels of the Brahmaputra, the largest river island in the world (Kotoky *et al*., 2003). Rapid channel shifts and bank-line recession are characteristic features of the Brahmaputra in the plains.

18.7 EROSION AND WEATHERING

The Brahmaputra supplies large quantities of sediment and solutes to the ocean that amounts to 1000 million t of clastic sediment and 100 million t of dissolved matter annually (Milliman and Meade, 1983; Sarin *et al*., 1989; Milliman and Syvitski, 1992; Hay, 1998; Galy and France-Lanord, 1999; Singh *et al*. 2005). The large quantities of particulate and dissolved matter are derived from a total area of 6 300 000 km^2 (Rao, 1979; Goswami, 1985). The sampling of this river during high flows, especially during floods, is extremely difficult. As sediment transport is expected to peak close to the maximum flow, the paucity of sampling during this period introduces a major uncertainty in ascertaining sediment flux. Sediment budget is commonly based on suspended matter concentration measurements; bedload is hardly ever taken into account. Some of the recent studies (Galy and France-Lanord, 2001) have shown that bedload flux could be a significant part of the total sediment flux in a highly turbulent river such as the Brahmaputra.

Given the high runoff and lithology of the Eastern Himalaya, both physical and chemical erosion rates for the Brahmaputra Basin are higher than those for the Ganga, and much higher than the world average (Sarin *et al*., 1989; Galy and France-Lanord, 2001). Total erosion in the Brahmaputra is about 1.5 to 2 times higher than that of the Ganga (Galy and France-Lanord, 2001). Singh and France-Lanord (2002) and Singh *et al*. (2005) investigated the sources of the clastic sediment and dissolved matter in the Brahmaputra Basin. The erosion rates for the individual zones listed earlier are presented in the following section. The role of various parameters affecting the physical and chemical erosion in the Brahmaputra Basin also has been assessed.

Tracing the sediment in the Brahmaputra Basin is based on the premise that Sr and Nd isotope compositions of the sediments parallel that of their source rocks. The assumption is very likely to be valid for the Himalayan rivers as weathering intensity in these sediments are low (Singh *et al*., 2005). The high water discharge and low residence time of the sediments in the Brahmaputra Basin indicate that weathering in the basin is transport limited (Stallard, 1995) and alteration of the composition of the sediment is low. This is supported by the low proportion of clay in the sediment and the composition of this clay (Singh *et al*., 2005). This suggests that the isotopic composition of the sediments can be considered to be the same as that of the source rocks. To trace the source of sediments, both suspended load and bedload have been collected between Pasighat to Dhubri from the mainstream along with its major tributaries for two seasons: the south-western monsoon and post-monsoon. Samples have been collected from middle of the channel and from sandbars where possible. Care has been taken to collect the representative samples and also to avoid any contamination. The isotopic compositions of these sediments (Table 18.3) have been reported by Singh and France-Lanord (2002) and Singh *et al*. (2003). Figure 18.9 is a mixing plot of sediments based on a two isotope system, $^{87}Sr/^{86}Sr$ and ε_{Nd} (Singh and France-Lanord, 2002). Fields of various end-members present in the basins also have been shown. Sediments of the Brahmaputra main stream fall on the mixing curve between the Higher Himalaya (HH) and the Trans-Himalayan Plutonic Belt (TPB). Apparently about 70 % of the sediment of the Brahmaputra is derived from the HH. Contributions from the TPB and the Lesser Himalaya (LH) are 20 and 10 %, respectively. This confirms the earlier findings of France-Lanord *et al*. (1993) that three-fourths of the sediments of the Bay of Bengal, for which the Brahmaputra is a dominant contributor, carry HH affinity.

Sr, Nd and Os isotope compositions of the sediment of the Brahmaputra main channel are plotted along the river distance in Figure 18.10. It is evident from this plot that the isotopic compositions of these sediments are already determined by the time the river reaches Pasighat, and they hardly vary further downstream. This happens in spite of the Brahmaputra receiving many tributaries below Pasighat, delivering sediment with highly variable isotopic composition. The near-constancy of the isotopic composition of the sediment of the Brahmaputra main channel

Table 18.3 Rb, Sr, Sm, Nd, Re, Os concentrations and Sr, Nd, Os isotope compositions of the sediments of the Brahmaputra River system

Sample	Type	River/Place	Rb (ppm)	Sr (ppm)	$^{87}Sr/^{86}Sr$	Sm (ppm)	Nd (ppm)	ε_{Nd}	Os (ppt)	Re (ppt)	$^{187}Os/^{188}Os$
Brahmaputra main channel											
BR 19	Bank sed.	Dibrugarh	112	243	0.718655	5	28	−12.6	10	70	1.454
BR 19 Clay	Clay	Dibrugarh	224	109	0.72054	6	30	−12.4	–	–	–
BR 29	Bank sed.	Tezpur	116	160	0.728481	7	38	−14.0	13	52	0.969
BR 65SL	Susp. load	Tezpur	196	195	0.719199	7	38	−14.0	43	302	1.07
BR 66	Bank sed	Tezpur	114	157	0.725211	5	26	−13.6	17	57	0.926
BR-2	Susp. load	Guwahati	126	187	0.72105	6	32	−13.0	–	–	–
BR-3	Susp. load	Guwahati	146	175	0.722013	7	37	−13.4	56	275	0.766
BR-4	Susp. load	Guwahati	145	184	0.720567	6	31	−13.2	29	143	0.899
BR-6	Susp. load	Guwahati	147	170	0.720553	7	36	−12.5	57	270	0.834
BR-7	Susp. load	Guwahati	128	211	0.719331	7	37	−13.1	–	–	–
BR-8	Susp. load	Guwahati	129	198	0.719791	6	31	−14.7	–	–	–
BR 9	Bank sed.	Guwahati	83	208	0.717726	8	49	−13.4	15	60	0.835
BR 9 Clay	Clay	Guwahati	235	91	0.717923	8	41	−12.5	–	–	–
BR-52SL	Susp. load	Guwahati	126	232	0.719656	–	22	−13.3	38	359	0.678
BR-53SL	Susp. load	Guwahati	148	167	0.720589	3	–	–	22	419	1.091
BR-54SL	Susp. load	Guwahati	180	194	0.721623	5	–	–	–	–	–
BR-55SL	Susp. load	Guwahati	182	160	0.721859	4	17	−12.8	85	365	0.68
BR-56	Bank sed.	Guwahati	81	244	0.718249	12	66	−13.4	19	75	1.007
BR 73SL	Susp. load	Dhubri	224	148	0.734388	6	31	−14.0	38	210	1.161
BR 74	Bank sed.	Dhubri	100	196	0.721507	6	33	−14.4	17	32	0.64
BGP 14[a]	Bank sed.	Chilamari	126	148	0.734572	7	39	−16.9	12	161	1.596
BGP 82[a]	Bank sed.	Chilamari	74	183	0.721019	9	51	−13.6	18	803	0.815
BGP 18[a]	Susp. load	Chilamari	187	89	0.748838	7	34	−16.3	–	–	–
Eastern tributaries											
BR 15	Bank sed.	Dibang	44	363	0.705296	6	30	−6.9	92	295	0.286
BR 17	Bank sed.	Lohit	33	428	0.70881	9	52	−12.4	40	1040	1.215
Tsangpo											
BR-Ts[b]		Tsangpo	–	–	–	–	38	−10.0	44	230	0.501
T1[c]		Tsangpo	165	277	0.709597	–	–	–	–	–	–
T2[c]		Tsangpo	104	233	0.714306	–	–	–	–	–	–
T3[c]		Tsangpo	109	176	0.715917	–	–	–	–	–	–
T4[c]		Tsangpo	49	670	0.704593	–	–	–	–	–	–

Table 18.3 *Continued*

Sample	Type	River/Place	Rb (ppm)	Sr (ppm)	$^{87}Sr/^{86}Sr$	Sm (ppm)	Nd (ppm)	ε_{Nd}	Os (ppt)	Re (ppt)	$^{187}Os/^{188}Os$
Siang											
BR 59SL	Susp. load	Siang	175	202	0.725241	7	34	−14.6	32	331	1.443
BR 60	Bank sed.	Siang	94	214	0.720604	11	59	−12.0	18	397	2.294
Himalayan tributaries											
BR 21	Bank sed.	Subansiri	89	75	0.735633	7	40	−15.6	16	83	1.048
BR 61SL	Susp. load	Subansiri	127	117	0.730133	6	36	−12.7	36	164	0.9
BR 62	Bank sed.	Subansiri	88	71	0.741897	3	15	−14.1	11	55	1.431
BR 25	Bank sed.	Ranga Nadi	76	89	0.730654	3	20	−12.8	15	142	0.924
BR 58	Bank sed.	Ranga Nadi	106	70	0.738124	3	17	−12.3	11	98	1.07
BR 27	Bank sed.	Jia Bhareli	138	69	0.777051	4	23	−16.3	11	68	1.377
BR 63SL		Jia Bhareli	187	56	0.776816	8	42	−16.6	–	–	–
BR 64	Bank sed.	Jia Bhareli	182	53	0.777346	3	19	−16.4	14	106	1.486
BR 35	Bank sed.	Puthimari	208	61	0.758673	5	30	−17.9	19	180	1.8
BR 69SL		Puthimari	212	69	0.7703	6	36	−17.6	–	–	–
BR 70	Bank sed.	Puthimari	111	39	0.764176	2	10	−17.6	27	141	0.774
BR 33	Bank sed.	Manas	121	70	0.764398	8	45	−16.0	14	63	1.528
BR 71SL	Susp. load	Manas	256	102	0.760045	7	36	−17.2	26	167	1.151
BR 72	Bank sed.	Manas	147	67	0.762298	4	18	−16.4		44	1.21
BR 76	Bank sed.	Tipkai	104	38	0.784524	1	7	−20.2	3	7	1.571
BGP 11[a]		Tista	168	92	0.809621	9	46	−21.2	8	1154	2.859
BGP 76[a]		Tista	226	89	0.824959	8	41	−20.6	–	–	–
Southern tributaries											
BR 31	Bank sed.	Kopili	94	58	0.733421	7	36	−12.7	22	76	0.845
BR 67SL	Susp. load	Kopili	217	85	0.732516	10	55	−15.1	–	–	–
BR 68	Bank sed.	Kopili	37	32	0.736137	17	97	−20.5	10	37	1.003
BR 11	Bank sed.	Dhansiri	77	80	0.718137	6	32	−8.4	49	191	0.471
BR 13	Bank sed.	Buri Dihing	80	129	0.727418	5	29	−18.7	173	35	0.178
BR78	Bank sed.	Basistha Dhara	49	47	0.750154	2	7	−12.6	8	25	6.8
BR 36	Gneiss	Guwahati	115	40	1.076	4	16	−9.5	–	–	–

Source: [a]Galy, 1999; [b]Pierson-Wickman *et al.*, 2000; [c]Harris *et al.*, 1998.

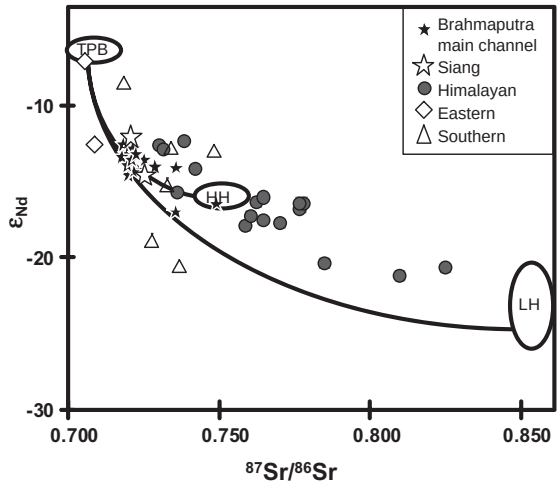

Figure 18.9 Two isotope mixing diagram of the sediments of the Brahmaputra. Also plotted are the fields of the important sources of sediments. The sediment of the Brahmaputra River system is mostly derived from the Higher Himalaya (HH) with a small contribution from the Trans-Himalayan Plutonic Belt (TPB). LH, Lesser Himalaya. Reprinted from Earth and Planetary Science Letters, Vol. 202, Singh S.K. and Fracne-Lanord, C., Tracing the distribution of erosion in the Brahmaputra watershed from isotopic compositions of stream sediments, pp. 645–662, 2002, with permission from Elsevier

from Pasighat to Dhubri at the India–Bangladesh border indicates that sediment derived from upstream of Pasighat determines the sediment characteristics of the Brahmaputra. The proportions of sediment contributed by the various zones in the basin were calculated according to the two end-member mixing model. The results showed that about half of the volume of sediment of the Brahmaputra is derived from upstream of Pasighat (Singh and France-Lanord, 2002). The isotope data and sediment abundance also indicate that the Eastern Syntaxis Zone is the primary contributor of sediment of the river. The contribution from Tibet is low due to factors such as low runoff, gentle slope, and presence of knickpoints on the Tsangpo prior to its entry into the gorge that cuts through the Eastern Syntaxis (Zeitler *et al*., 2001). Material balance calculations based on the isotopic compositions of these sediments show that sediment contribution from Tibet, Eastern Syntaxis, Eastern drainage/Mishmi Hills and the Himalayan basins to the Brahmaputra system are 5, 45, 10 and 40%, respectively (Singh and France-Lanord, 2002). The disproportionately high contribution of sediment from the Eastern Syntaxis Zone to the Brahmaputra system (45%) is striking as it occupies only about 4% of the drainage area.

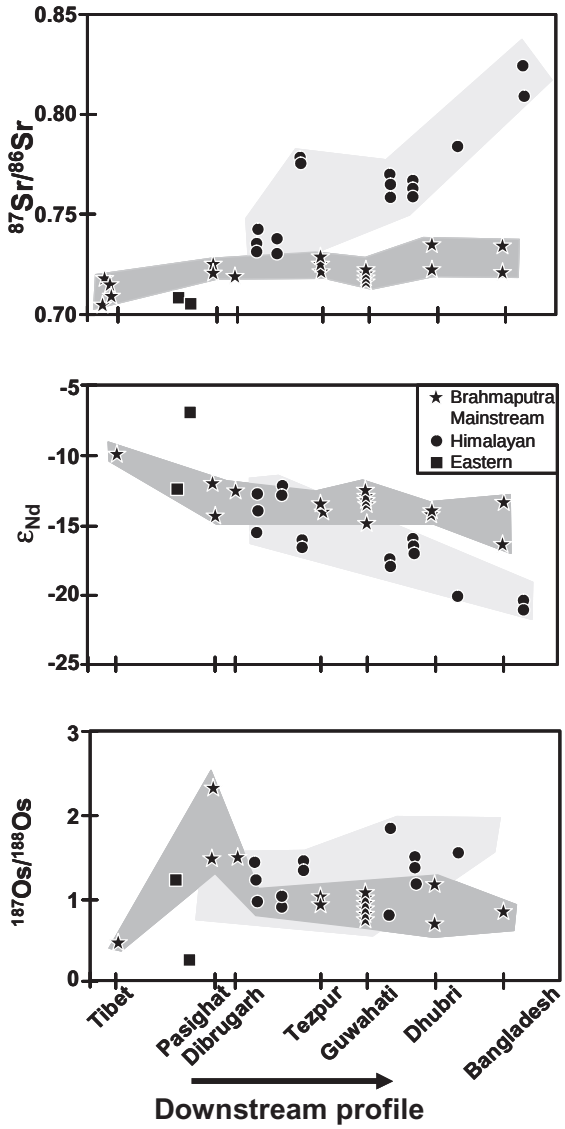

Figure 18.10 Downstream variation of Sr, Nd and Os isotope composition of the Brahmaputra River system. Near constancy of the isotope composition downstream of Pasighat indicates that above-Pasighat sediments are the major contributor to the sedimentary budget of the Brahmaputra system. Reprinted from Earth and Planetary Science Letters, Vol. 202, Singh S.K. and Fracne-Lanord, C., Tracing the distribution of erosion in the Brahmaputra watershed from isotopic compositions of stream sediments, pp. 645–662, 2002, with permission from Elsevier

Various parts of the Brahmaputra Basin have different erosion rates. Sediment yield or the physical erosion rate is the highest in the Eastern Syntaxis Zone and the lowest in Tibet.

18.8 SEDIMENT YIELD OR EROSION RATES IN THE VARIOUS ZONES

The estimates of suspended load flux from the Brahmaputra at Bahadurabad varies from 500 to 1600 million t year^{-1} (Hay, 1998). Studies by Galy and France-Lanord (2001) have shown that due to high energy condition and turbulent flow the fluxes of suspended and bed load are equal in the Ganga and the Brahmaputra Rivers. Considering this, the total annual sediment flux would double to 1000 to 3000 million t. A mean annual sediment flux of 2000 million t has been assumed for the Brahmaputra in order to calculate erosion rates. This flux in conjunction with estimates of sediment proportions from the different zones has been used to derive individual zonal erosion rates (Figure 18.11, Table 18.4). The erosion rates vary from 0.2 mm year^{-1} in Tibet to as high as 14 mm year^{-1} in the Eastern Syntaxis Zone (Singh, 2006). The erosion rate in the Eastern Syntaxis Zone is among the highest in the world (Milliman and Meade, 1983). The Himalayan and the Eastern drainages/Mishmi Hills are eroding at a rate of about 2 mm year^{-1}.

The estimated erosion rates compare well with the available long term erosion or exhumation rates of the Himalayan-Tibetan regions (Table 18.4) For example, the contemporary erosion rate, ~14 mm year^{-1} for the Eastern Syntaxis Zone, is similar to the exhumation rate of 10 mm year^{-1} (Burg *et al*., 1998) in this region for the last 3–4 Ma, and the erosion rate of 9–12 mm year^{-1} reported from the Western Syntaxis using cosmogenic isotopes (Leland *et al*., 1998).

Erosion at a high rate in the Eastern Syntaxis Zone not only supplies a large amount of sediment to the Bay of Bengal but also influences tectonic activity and geomorphology of the region. The intense and focused erosion in the Eastern Syntaxis Zone has contributed to higher uplift of the region because of isostatic rebound which in turn is responsible for the very high peaks of Namche Barwa (7750 m) and Gyala Peri (7150 m). Zeitler *et al*. (2001) is of the opinion that the generation of knickpoints in the river bed of the Tsangpo just before the gorge resulted from the uplift that followed the rapid erosion in this section. The stationary character of the knickpoint despite rapid erosion downstream suggests that the uplift due to the rapid erosion has been sustained for the last 3–4 Ma.

18.9 CHEMICAL WEATHERING AND EROSION

The Brahmaputra River brings, along with particulate matter, large quantities of dissolved solids to the Bay of Bengal (Sarin *et al*., 1989; Singh *et al*., 2005). Studies on the chemistry of river waters have provided a detailed understanding of the sources of dissolved matter in terms

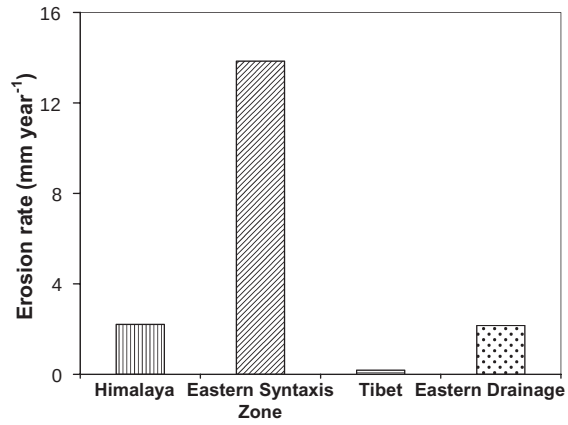

Figure 18.11 Erosion rates of the different parts of the Brahmaputra Basin. Reprinted from Current Science, Vol. 90, Singh, S.K., Copyright 2006, with permission form Current Science

Table 18.4 Erosion and exhumation rates of various regions of the Himalaya

Sub-basins	Erosion rate (mm year^{-1})		Exhumation rate[b] (mm year^{-1})
	Isotope study[a]	Other studies[b]	
Tibet-Tsangpo	0.2	0.01–1.0	–
Higher Himalaya		2.7	1.6–3.0
Lesser Himalaya	2.2	0.8	0.6–1.3
Eastern Syntaxis	14	–	10
Eastern Drainage	2.1	–	–
Nanga Parbat-Indus	–	9–12	4–12

Source: [a] Singh, 2006; [b] data from Burg *et al.*, 1998; Leland *et al.*, 1998; Lal *et al.*, 2003; Vance *et al.*, 2003.
Erosion rates are based on cosmogenic isotopes.

of the source area and lithology (Singh *et al*., 2005). These studies have helped also to quantify the weathering rates of silicates, carbonates, and minor lithologies of the basin and the CO_2 consumption due to silicate weathering.

18.9.1 Water Chemistry

The dissolved chemical constituents of river water are derived from the weathering of silicates and carbonates, dissolution of evaporites of the basin, and precipitation. Generally, for the major elements (excluding Cl and Na) the supply from the atmosphere is unlikely to be significant relative to input from chemical weathering of the basin. Even for Na, the significance of rain is likely to be restricted to regions near the sea. In the Brahmaputra system the contribution from precipitation would be negligible, particularly in its headwaters (Galy and France-Lanord, 1999). The total dissolved solids in the waters of the Brahmaputra system ranges between 50 and 182 mg ℓ^{-1} (Table 18.5; Singh *et al*., 2005).

Table 18.5 Major ion composition of waters of the Brahmaputra River system

Sample code	River (location)	Na^+	Na*	K^+	Mg^{2+}	Ca^{2+}	Cl^-	NO_3^-	SO_4^{2-}	HCO_3^-	SiO_2	TDS (mg ℓ^{-1})
		(μmol ℓ^{-1})										
Brahmaputra mainstream												
	Tsangpo (South Lhasa)[a]	396	240	32	209	752	156	–	255	1670	127	185
	Tsangpo (South Lhasa)[a]	446	248	37	191	717	198	–	223	1740	125	187
	Siang (Pai)[b]	387	244	28	103	500	143	–	188	984	125	150
BR-59	Siang or Dihang (Pasighat)	78	61	37	100	424	17	14	119	854	126	95
BR-18	Brahmaputra (Dibrugarh)	106	72	48	144	540	34	–	158	1197	152	128
BR-28	Brahmaputra (Tezpur bg.)	110	86	50	140	458	24	–	110	1154	189	119
BR-65	Brahmaputra (Tezpur bg.)	78	64	49	101	378	14	9	86	845	146	91
	Brahmaputra (Guwahati[1])	159	52	79	119	425	107	–	100	884	123	101
BR-5	Brahmaputra (Guwahati)	86	58	50	115	395	28	–	87	1005	137	102
BR-51	Brahmaputra (Guwahati)	90	69	67	111	475	21	17	114	1051	140	112
BR-73	Brahmaputra (Dhubri)	107	88	50	153	396	19	11	73	1018	200	106
	Brahmaputra (Chilmari)[c]	104	79	52	168	393	25	–	55	1114	155	105
BR 200	Brahmaputra (Jamuna bridge)	77	53	62	120	433	24	–	78	1060	127	105
Tibetan tributaries to Tsangpo												
	Zangbo at Lhasa[a]	380	180	36	39	270	200	–	75	751	134	90
	Doilung at Lhasa[a]	300	38	48	35	224	262	–	60	558	88	73
Eastern tributaries												
BR-14	Dibang	47	33	42	49	353	14	–	82	780	141	82
BR-16	Lohit	59	41	50	78	440	18	–	91	996	139	101
Himalayan tributaries												
BR-20	Subansiri	79	59	24	136	323	20	–	104	849	169	92
BR-61	Subansiri	71	62	26	108	303	9	15	95	667	148	77
BR-24	Ranga Nadi	137	120	33	45	158	17	–	38	550	294	67
BR-57	Ranga Nadi	105	94	28	37	126	11	20	34	373	218	50
BR-26	Jia Bhareli	101	86	32	70	235	15	–	59	682	206	75
BR-63	Jia Bhareli	90	80	32	60	191	10	12	33	537	185	60
BR-75	Tipkai	124	106	27	195	284	18	7	28	994	258	100
BR-32	Manas Biki	97	78	31	148	470	19	–	148	1096	158	117
BR-71	Manas Biki	59	49	27	101	416	10	8	102	844	105	90
BR-34	Puthimari	133	109	43	291	698	24	–	143	1877	218	182
BR-69	Puthimari	99	80	36	219	551	19	19	112	1336	166	135
Southern tributaries												
BR-10	Dhansiri	288	205	63	226	230	83	–	129	881	225	106
BR-12	Buri Dihing	189	147	31	293	228	42	–	85	1084	310	116
BR-30	Kopili	137	104	40	99	158	33	–	65	591	217	70
BR-67	Kopili	118	88	35	78	148	30	3	64	425	208	58

Source: [a]Hu *et al*., 1982; [b]Chen and Guan, 1981; [c]Galy and France-Lanord, 1999.
$Na^* = (Na_{riv} - Cl_{riv})$.

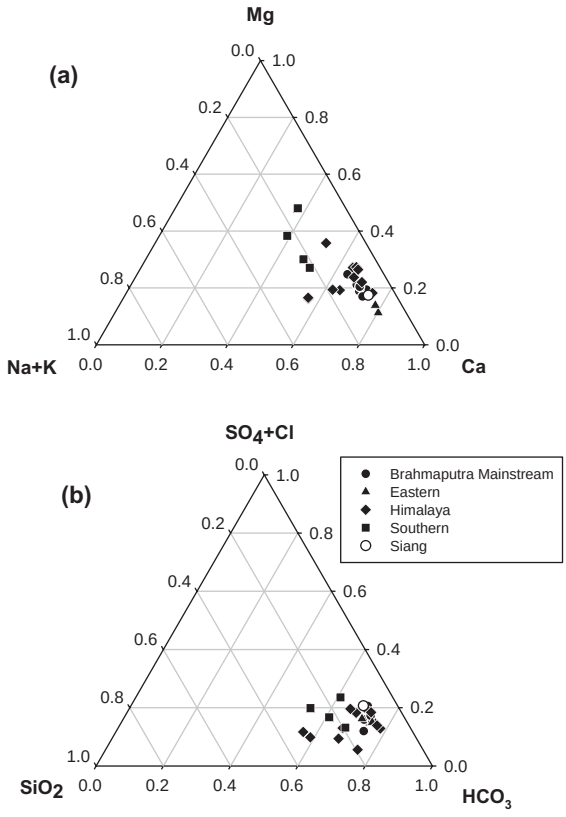

Figure 18.12 Ternary plots of (a) cations and (b) anions of the waters of the Brahmaputra River system showing the dominance of Ca and alkalinity in cations and anions budgets, respectively. Reprinted from Geochimica et Cosmochimica Acta, Vol. 69, Singh *et al*., Chemical erosion in the eastern Himalaya: major ion composition of the Brahmaputra and $\delta^{13}C$ of dissolved inorganic carbon, pp. 3573–3588, 2005, with permission from Elsevier

Figure 18.12 displays ternary plots of cations and anions in the Brahmaputra waters. Most of the samples fall towards the Ca apex indicating the dominance of Ca in the cation budget of the Brahmaputra. On the anion plot the samples cluster towards HCO_3^- with several of them tending towards the apex with SO_4^{2-}. A preliminary inference from these distributions is that a major source of dissolved cations to the water is carbonate weathering. On a global scale, carbonate weathering contributes about half of the dissolved solids in rivers (Meybeck, 1987).

18.9.2 Silicate Weathering

Weathering of silicate rocks of the drainage basin is another important source of major ions to rivers. Silicate weathering is studied for many reasons, including its role in drawing-down of atmospheric CO_2. Both carbonate and silicate weathering consume CO_2, however, on the million year timescale, CO_2 consumed by carbonate weathering will be released back to the atmosphere during carbonate deposition and hence silicate weathering is the net sink of atmospheric CO_2. Raymo and Ruddimann (1992) hypothesised that the origin and evolution of the Himalaya since the beginning of the Cenozoic has contributed to enhanced silicate weathering rates and hence to increased CO_2 drawdown from the atmosphere. Enhanced uplift coupled with monsoon climate has increased the silicate weathering in the Himalaya which has consumed an increased amount of CO_2 from the atmosphere. As CO_2 is a greenhouse gas, its reduction in atmospheric level has caused global cooling during the Cenozoic. Contemporary silicate weathering and CO_2 consumption rates can be computed from the water chemistry of rivers. This has been done for the Brahmaputra system to assess the significance of this basin compared with other global major river systems. The approach is to derive cation fluxes from silicates from the water chemistry using simple assumptions and use them to calculate CO_2 consumed from the atmosphere. Silicate weathering flux comprises Na, K, Ca, Mg, and SiO_2 derived from the silicate rocks of the basin. What is being measured in the water, however, is derived from multiple sources, and the silicate component has to be separated from the measured values using suitable models. Among the various major ions, SiO_2 and K in rivers are by and large derived from silicates. Na is derived from silicates, evaporites, and precipitation. Na from evaporites and precipitation exists mainly as NaCl, hence sodium from these sources will be accompanied by a similar concentration of chloride. Therefore sodium of silicate origin in rivers can be estimated as:

$$Na_{sil} = Na_r - Cl_r$$

where Na_{sil} is sodium from silicates, and Na_r and Cl_r are sodium and chloride concentrations in rivers, expressed in μE or μM.

Calculating Ca_{sil} and Mg_{sil} from water chemistry is not straightforward, as these cations can be derived from many sources such as silicates, carbonates, and evaporites. Therefore, the contribution of Ca and Mg is calculated assuming that Ca and Mg are released from rocks to rivers in the same proportion as their abundances in silicates or using data on monolithic (silicate basin) tributaries (Krishnaswami *et al*., 1999). Such calculations show that about 44% of the cations of the Brahmaputra River are of silicate origin (Singh *et al*., 2005). Based on silicate cations and SiO_2 ($mg\,l^{-1}$) and the specific discharge ($\ell\,km^{-2}$

year^{-1}) of the river, silicate weathering rates were calculated as:

$$\text{Silicate weathering rate} = Q \times (Na_{sil} + K_{sil} + Ca_{sil} + Mg_{sil} + SiO_2)$$

Contemporary silicate weathering rates for the various zones of the Brahmaputra are thus estimated. The rates range from 1 to 38 t km^{-2} year^{-1}, with the Tibetan drainage and the Eastern Syntaxis Zone having the lowest and highest rates respectively. From the silicate cation abundances, present day CO_2 consumption due to silicate weathering in the various zones can also be computed. It varies from 1.9 million mol km^{-2} year^{-1} in the Eastern Syntaxis Zone to 0.07 million mol km^{-2} year^{-1} in Tibet. For the entire Brahmaputra Basin the silicate weathering rate is ~12 t km^{-2} year^{-1} and CO_2 drawdown due to silicate weathering is about 0.6 million mol km^{-2} year^{-1}. Barring the Tibetan drainage, the silicate weathering rates and CO_2 consumption for the entire Brahmaputra and its various parts are significantly higher than the world average (Table 18.6, Figure 18.13). The Eastern Syntaxis Zone has the highest rates of total chemical weathering, silicate weathering, and CO_2 consumption.

18.10 BED LOAD AND WEATHERING INTENSITY

Weathering intensity in the Brahmaputra system can be gauged by the content and composition of the clay in the bed load and their chemical index of alteration (CIA). Low clay content (~2 %, except southern tributaries where it is ~20 %; Singh *et al*., 2005) of the bed loads of the Brahmaputra reflects the poor weathering of these sediments which is supported by the dominance of vermiculite in the clay of these sediments. Further the CIA of the sediments of the Brahmaputra range between 58 and 65 (Singh *et al*., 2005), similar to rocks of the Higher and the Lesser Himalaya. The lower value of CIA of sediments overlaps with those of their source rocks, which indicates that these sediments have undergone low intensity of weathering possibly due to their rapid transport. Sediments of the southern tributaries show higher intensity of weathering.

18.11 CONTROL OF PHYSICAL AND CHEMICAL EROSION IN THE BRAHMAPUTRA BASIN

Variability of an order of magnitude in physical and chemical erosion rates exists among the different zones of the Brahmaputra Basin. A similar variability is also seen when these rates are compared with erosion in major global river basins. A number of factors (climate, basin relief, stream gradient, tectonic activities, lithology, vegetation) have been suggested as controls over erosion rates and their variability (Velbel, 1993; Bluth and Kump, 1994; White and Blum, 1995; Berner and Berner, 1997; Edmond and Huh, 1997; Ludwig and Probst, 1998; Huh and Edmond, 1999; Dalai *et al*., 2002; Millot *et al*., 2002;

Table 18.6 Chemical erosion and CO_2 consumption rates in various zones of the Brahmaputra and selected basins of the world

Basin	TDS flux (t km^{-2} year^{-1})	Silicate cation flux (t km^{-2} year^{-1})	CO_2 consumption by silicate weathering (million mol km^{-2} year^{-1})
Brahmaputra			
Tibet	40	1.3	0.07
Eastern Syntaxis	304	38.0	1.9
Eastern	185	18.1	0.95
Himalaya	149	10.7	0.51
Southern	237	22	1.2
Brahmaputra River	120	11.8	0.6
Other Himalayan rivers			
Ganga	72	7.9	0.38
Indus	42	1.8	0.06
Mekong	72	6.2	0.24
Other Tibetan rivers			
Changjiang (Yangtze)	113	1.4	0.06
Huanghe (Yellow)	25	2.1	0.08
Global rivers			
Amazon	35	2.2	0.05
World average	36	2.0	0.09

Source: Sarin *et al*., 1989; Gaillardet *et al*., 1999; Singh *et al*., 2005.

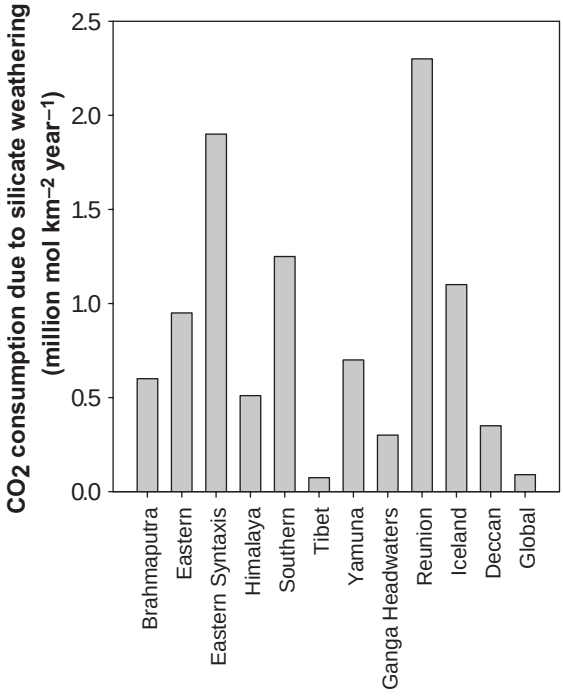

Figure 18.13 CO_2 consumption rates by silicate weathering in the various Himalayan zones as compared with a selection of drainage systems of the world (from Gislason *et al*., 1996; Louvat and Allegre, 1997; Gaillardet *et al*., 1999; Amiotte Suchet *et al*., 2003; Das *et al*., 2005; Singh *et al*., 2005). Reprinted from Geochimica et Cosmochimica Acta, Vol. 69, Singh *et al*., Chemical erosion in the eastern Himalaya: major ion composition of the Brahmaputra and $\delta^{13}C$ of dissolved inorganic carbon, pp. 3573–3588, 2005, with permission from Elsevier

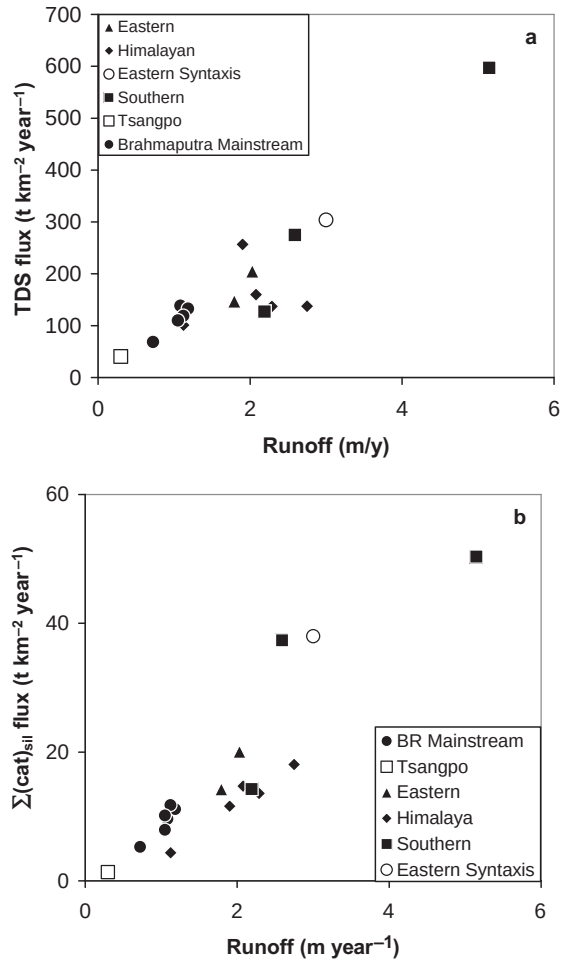

Figure 18.14 Variation of total and silicate erosion rates with runoff in the Brahmaputra River system. Good positive correlation among them shows that the runoff is an important factor controlling the chemical erosion. Reprinted from Geochimica et Cosmochimica Acta, Vol. 69, Singh *et al*., Chemical erosion in the eastern Himalaya: major ion composition of the Brahmaputra and $\delta^{13}C$ of dissolved inorganic carbon, pp. 3573–3588, 2005, with permission from Elsevier

France-Lanord *et al*., 2003). In general, erosion rates in the various parts of the Brahmaputra Basin correlate positively with runoff. However, the disproportionately high erosion rate in the Eastern Syntaxis Zone indicates that than runoff is not the only control over erosion. The river flows in the Eastern Syntaxis Zone over a gradient of 0.03 and an annual discharge of 100 km^3 (Figure 18.3). The stream power of the river is very high in this section. The model on Erosion Index based on stream power of the Brahmaputra (Finlayson *et al*., 2002) supports such an interpretation.

Figure 18.14 shows total chemical weathering and silicate weathering plotted against runoff. The good correlation suggests that chemical erosion in the Brahmaputra system is a function of runoff in the Brahmaputra main channel. The runoff rises by a factor of ten during the south-west monsoon but TDS changes marginally. Chemical and physical erosion of the different zones of the Brahmaputra Basin are plotted against each other in Figure 18.15. The chemical weathering in the different parts of the Brahmaputra is related to the physical erosion of these areas by a power law. In the Brahmaputra Basin, runoff and relief controls physical erosion which in turn controls the chemical erosion by increasing specific surface area for chemical reaction.

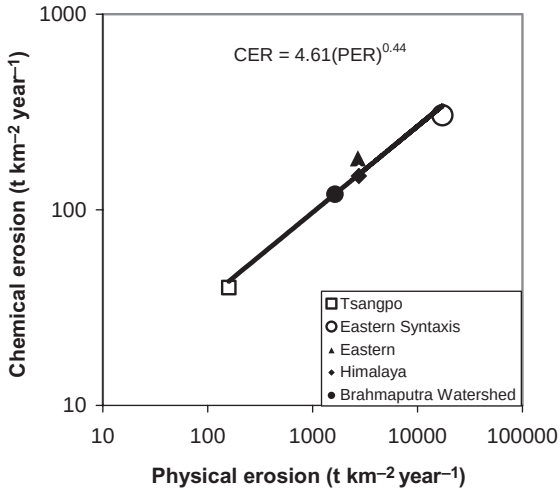

Figure 18.15 Plot of physical erosion rates against chemical erosion rates (CER). In the Brahmaputra system they are related by the power law shown in the figure. Physical erosion felicitates chemical erosion by providing more surfaces. Reprinted from Geochimica et Cosmochimica Acta, Vol. 69, Singh *et al*., Chemical erosion in the eastern Himalaya: major ion composition of the Brahmaputra and $\delta^{13}C$ of dissolved inorganic carbon, pp. 3573–3588, 2005, with permission from Elsevier

18.12 CONCLUSION

The Brahmaputra River system is characterized by high water discharge with high particulate and dissolved matter. Most of its discharge is concentrated in the 4 months of south-west monsoon. Its valley is undergoing uplift near the Shillong-Mikir Block causing narrowing of the valley and congestion to sediment-laden water and hence flooding. Embankments on the Brahmaputra main stream and its tributaries in the Assam Plains seem to be the major flood control measure taken by the government which has turned out to be of limited benefit.

Both physical and chemical erosion rates are high in the Brahmaputra Basin compared with the world average. The erosion rates are highly variable within the basin, with the Eastern Syntaxis Zone and Tibet representing the highest and lowest erosion rates. The Brahmaputra system is contributing significantly to the global CO_2 consumption due to silicate weathering. Erosion in the Brahmaputra seems to be governed by the runoff and the relief of the basin.

REFERENCES

Amiotte Suchet, P., Probst, J.-L. and Ludwig, W. (2003) Worldwide distribution of continental rock lithology: implications for the atmospheric/soil CO_2 uptake by continental weathering and alkalinity river transport to the oceans, *Global Biogeochem. Cycles* 17, 1038.

Berner, E.K. and Berner, R.A. (1997) Silicate weathering and climate. In: *Tectonic Uplift and Climate Change* (W.F. Ruddiman, Ed.), Plenum Press, New York, pp. 354–365.

Bhattacharyya, N.N. and Bora, A.K. (1997) Floods of the Brahmaputra River in India, *Water Int.* 22, 222–229.

Bluth, G.J.S. and Kump, L.R. (1994) Lithologic and climatologic controls of river chemistry, *Geochim. Cosmochim. Acta* 58, 2341–2359.

Booth A.L., Zeitler P.K., Kidd W.S.F., Wooden J., Liu Y., Idleman B., Hren M. and Chamberlain C.P. (2004) U-Pb zircon constraints on the tectonic evolution of southeastern Tibet, Namche Barwa area, *Am. J. Sci.* 304, 889–929.

Burg, J.-P., Nievergelt, P., Oberli, F., Seward, D., Davy, P., Maurin, J.-C., Diao, Z. and Meier, M. (1998) The Namche Barwa syntaxis: evidence for exhumation related to compressional crustal folding, *J. Asian Earth Sci.* 16, 239–252.

Chen, C. and Guan, Z. (1981) Hydrochemistry of rivers in Xizang. In: *Geological and Ecological Studies of Qinghai-Xizang Plateau*, Science Press, Beijing; Gordon and Breach Science Publishers, Inc., New York, pp. 1687–1982.

Dalai, T.K., Krishnaswami, S. and Sarin, M.M. (2002) Major ion chemistry in the headwaters of the Yamuna river system: chemical weathering, its temperature dependence and CO_2 consumption in the Himalaya, *Geochim. Cosmochim. Acta* 66, 3397–3416.

Das, A., Krishnaswami, S., Sarin, M.M. and Pande, K. (2005) Chemical weathering in the Krishna basin and Western Ghats of the Deccan Traps, India: rates of basalt weathering and their controls, *Geochim. Cosmochim. Acta* 69, 2067–2084.

Edmond, J.M. and Huh, Y. (1997) Chemical weathering yields and orogenic terrains in hot and cold climates. In: *Tectonic Uplift and Climate Change* (W.F. Ruddiman, Ed.), Plenum Press, New York, pp. 330–351.

Finlayson, D.P., Montgomery, D.R. and Hallet, B. (2002) Spatial coincidence of rapid inferred erosion with young metamorphic massifs in the Himalayas, *Geology* 30, 219–222.

France-Lanord, C., Derry, L. and Michard, A. (1993) Evolution of the Himalaya since Miocene time: isotopic and sedimentologic evidence from the Bengal Fan. In: *Himalayan Tectonics* (P.J. Treloar and M. Searle, Eds.), Geological Society of London Special Publication 74, Geological Society of London, London, pp. 603–621.

France-Lanord, C., Evans, M., Hurtrez, J.-E. and Riotte, J. (2003) Annual dissolved fluxes from Central Nepal rivers: budget of chemical erosion in the Himalayas, *Comptes Rendus Geosci.* 335, 1131–1140.

Gaillardet, J., Dupre, B. and Allegre, C.J. (1999) Global silicate weathering and CO_2 consumption rates deduced from chemistry of large rivers, *Chem. Geol.* 159, 3–30.

Galy, A. (1999) Etude Geochimique de l'erosion Actuelle de la Chaine Himalayenne, Thesis, Institut National Polytechnique de Lorraine, Nancy.

Galy, A. and France-Lanord, C. (1999) Weathering processes in the Ganges-Brahmaputra basin and the riverine alkalinity budget, *Chem. Geol.* 159, 31–60.

Galy, A. and France-Lanord, C. (2001) Higher erosion rates in the Himalaya: geochemical constraints on riverine fluxes, *Geology* 29, 23–26.

Galy, A., France-Lanord, C. and Derry, L.A. (1999) The Strontium isotopic budget of Himalayan rivers in Nepal and Bangladesh, *Geochim. Cosmochim. Acta* 63, 1905–1925.

Gansser, A. (1964) *Geology of the Himalaya*, Interscience Publishers, London.

Garzanti, E., Vezzoli, G., Andò, S., France-Lanord, C., Singh, S.K. and Foster, G. (2004) Sand petrology and focused erosion in collision orogens: the Brahmaputra, *Earth Planet. Sci. Lett.* 220, 157–174.

Gislason, S.R., Amorsson, S. and Armannsson, H. (1996) Chemical weathering of basalt as deduced from the composition of precipitation, rivers, and rocks in SW Iceland, *Am. J. Sci.* 296, 837–907.

Goswami, D.C. (1985) Brahmaputra River, Assam, India: physiography, basin denudation, and channel aggradation, *Water Resources Res.* 21, 959–978.

Goswami, D.C. (1998) Fluvial regime and flood hydrology of the Brahmaputra River, Assam. In: *Flood Studies in India* (V.S. Kale, Ed.), Geological Society of India, Bangalore, pp. 51–75.

Guan Z. and Chen, C. (1981) Hydrographical features of the Yarlung Zangbo River. In: *Geological and Ecological Studies of Qinghai-Xizang Plateau*, Science Press, Beijing; Gordon and Breach Science Publishers, Inc., New York, pp. 1693–1703.

Harris, N., Bickle, M., Chapman, H., Fairchild, I. and Bunbury, J. (1998) The significance of the Himalayan rivers for silicate weathering rates: evidence from the Bhote Kosi tributary, *Chem. Geol.* 144, 205–220.

Hay, W.W. (1998) Detrital sediment fluxes from continents to oceans, *Chem. Geol.* 145, 287–323.

Hu, M., Stallard, R.F. and Edmond, J. (1982) Major ion chemistry of some large Chinese Rivers, *Nature* 298, 550–553.

Huh, Y. and Edmond, J. (1999) The fluvial geochemistry of rivers of Eastern Siberia: III. Tributaries of the Lena and Anbar draining the basement terrain of the Siberian Craton and the Trans-Baikal Highlands, *Geochim. Cosmochim. Acta* 63, 967–987.

Huh, Y, Tsoi, M.-Y., Zaitsev, A. and Edmond, J. (1998) The fluvial geochemistry of the rivers of Eastern Siberia: I. Tributaries of the Lena River draining the sedimentary platform of the Siberian Craton, *Geochim. Cosmochim. Acta* 62, 1657–1676.

Jain, A.K. and Thakur, V.C. (1978) Abor volcanics of the Arunachal Himalaya, *J. Geol. Soc. India* 19, 335–349.

Kotoky, P., Bezbaruah, D., Baruah, J. and Sarma, J.N. (2003) Erosion activity on Majuli – the largest river island of the world, *Current Sci.* 84, 929–932.

Krishnaswami, S., Trivedi, J.R., Sarin, M.M., Ramesh, R. and Sharma, K.K. (1992) Strontium isotopes and rubidium in the Ganga-Brahmaputra river system: Weathering in the Himalaya, fluxes to the Bay of Bengal and contribitions to the evolution of oceanic $^{87}Sr/^{86}Sr$, *Earth Planet. Sci. Lett.* 109, 243–253.

Krishnaswami, S., Singh, S.K. and Dalai, T. (1999) Silicate weathering in the Himalaya: role in contributing to major ions and radiogenic Sr to the Bay of Bengal. In: *Ocean Science, Trends and Future Directions* (B.L.K. Somalyajulu, Ed.), Indian National Science Academy and Akademia International, New Delhi, pp. 23–51.

Kumar, G. (1997) *Geology of the Arunachal Pradesh*, Geological Society of India, Bangalore.

Lal, D., Harris, N.B.W., Sharma, K.K., Gud, Z., Ding, L., Liu, T., Dong, W., Caffee, M.W. and Jull, A.J.T. (2003) Erosion history of the Tibetan Plateau since the last interglacial: constraints from the first studies of cosmogenic ^{10}Be from Tibetan bedrock. *Earth Planet. Sci. Lett.* 217, 33–42.

Leland, J., Reid, M.R., Burbank, D.W., Finkel, R. And Caffee, M. (1998) Incision and differential bedrock uplift along the Indus River near Nanga Parbat, Pakistan Himalaya, from Be and Al exposure age dating of bed rock straths, *Earth Planet. Sci. Lett.* 157, 93–107.

Louvat, P. and Allegre, C.J. (1997) Present denudation rates on the island of Reunion determined by river chemistry: basalt weathering and mass budget between chemical and mechanical erosions, *Geochim. Cosmochim. Acta* 61, 3645–3699.

Ludwig, W. and Probst, J.-L. (1998) River sediment discharge to the oceans: present-day controls and global budgets, *Am. J. Sci.* 298, 265–295.

Meybeck, M. (1987) Global chemical weathering of surficial rocks estimated from river dissolved loads, *Am. J. Sci.* 287, 401–428.

Milliman, J.D. and Meade, R.H. (1983) World Delivery of River Sediment to the Oceans, *J. Geol.* 91, 1–21.

Milliman, J.D. and Syvitski, P.M. (1992) Geomorphic/tectonic control of sediment discharge to the ocean: the importance of small mountainous rivers, *J. Geol.* 100, 525–544.

Millot, R., Gaillardet, J., Dupré, B. and Allègre, C.J. (2002) The global control of silicate weathering rates and the coupling with physical erosion: new insights from rivers of the Canadian Shield, *Earth Planet. Sci. Lett.* 196, 83–98.

Montgomerie, T.G. (1868) Report of a route survey made by pundit, from Nepal to Lhasa, and thence through the upper valley of the Brahmaputra to its source, *J. R. Geograph. Soc. London* 38, 129–219.

Pande, K., Sarin, M.M., Trivedi, J.R., Krishnaswami, S. and Sharma, K.K. (1994) The Indus river system (India-Pakistan): major-ion chemistry, uralium and strontium isotopes, *Chem. Geol.* 116, 245–259.

Pascoe, E.H. (1963) *A Manual of the Geology of India and Burma*, Vol. 3, Government of India Press, Calcutta, pp. 2073–2079.

Pegram, W.J., Krishnaswami, S., Ravizza, G.E. and Turekian, K.K. (1992) The record of sea water $^{187}Os/^{186}Os$ variation through the Cenozoic, *Earth Planet. Sci. Lett.* 113, 569–576.

Pierson-Wickman, A.-C., Reisberg, L. and France-Lanord, C. (2000) The Os isotopic composition of Himalayan river bedloads and bedrocks: importance of black shales, *Earth Planet. Sci. Lett.* 176, 203–218.

Rangachari, R. (1994) Flood management. In: *Harnessing the Eastern Himalayan Rivers Regional Cooperation in South Asia* (Editors B.G. Vergese and R. Ramaswamy Iyer), Konark Publishers Pvt Ltd, Delhi, pp. 86–98.

Rao, K.L. (1979) *India's Water Wealth*, Orient Longman Limited, New Delhi.

Raymo, M.E. and Ruddiman, W.F. (1992) Tectonic forcing of late Cenozoic climate, *Nature* 359, 117–122.

Robinson, D.M., DeCelles, P.G., Patchett, P.J. and Garzione, C.N. (2001) The kinematic evolution of the Nepalese Himalaya interpreted from Nd isotopes, *Earth Planet. Sci. Lett.* 192, 507–521.

Sarin, M.M., Krishnaswami, S., Dilli, K., Somayajulu, B.L.K.and Moore, W.S. (1989) Major ion chemistry of the Ganga-Brahmaputra river system: weathering processes and fluxes to the Bay of Bengal, *Geochim. Cosmochim. Acta* 53, 997–1009.

Singh, S.K., (2006) Spatial variability in erosion in the Brahmaputra basin: causes and impacts, *Curr. Sci.* 90, 1272–1276.

Singh, S.K. and France-Lanord, C. (2002) Tracing the distribution of erosion in the Brahmaputra watershed from isotopic compositions of stream sediments, *Earth Planet. Sci. Lett.* 202, 645–662.

Singh, S.K., Reisberg, L. and France-Lanord, C. (2003) Re-Os isotope systematics of sediments of the Brahmaputra River system, *Geochim. Cosmochim. Acta* 67, 4101–4111.

Singh, S.K., Sarin, M.M. and France-Lanord, C. (2005) Chemical erosion in the eastern Himalaya: major ion composition of the Brahmaputra and $\delta^{13}C$ of dissolved inorganic carbon, *Geochim. Cosmochim. Acta* 69, 3573–3588.

Stallard, R.F. (1995) Tectonic, environmental, and human aspects of weathering and erosion: a global review using a steady-state perspective. *Ann. Rev. Earth Planet. Sci.* 23, 11–39.

Thakur, V.C. (1986) Tectonic zonation and regional framework of eastern Himalaya, *Science Terre* 47, 347–360.

Valdiya, K.S. (1999) Why does river Brahmaputra remain untamed?, *Curr. Sci.* 76, 1301–1304.

Vance, D., Bickle M., Ivy-Ochs, S. and Kubik, P.W. (2003) Erosion and exhumation in the Himalaya from cosmogenic isotope inventories of river sediments, *Earth Planet. Sci. Lett.* 206, 273–288.

Velbel, M.A. (1993) Temperature dependence of silicate weathering in nature: how strong of a negative feedback on long term accumulation of atmospheric CO_2 and global greenhouse warming?, *Geology* 21, 1059–1062.

White, A.F. and Blum, A.E. (1995) Effects of climate on chemical weathering in watersheds. *Geochimica et Cosmochimica Acta* 59, 1729–1747.

www.grdc.sr.unh.edu

www.tropmet.res.in

Zeitler, P.K., Meltzer, A.S., Koons, P.O., Craw, D., Hallet, B., Chamberlain, C.P., Kidd, W.S.F., Park, S.K., Seeber, L., Bishop, M. and Shroder, J. (2001) Erosion, Himalayan geodynamics, and the geomorphology of metamorphism, *GSA Today*, 4–9.

Zhang, D.D. (2001) Tectonically controlled fluvial landforms on the Yaluzangbu River and their implications for the evolution of the river, *Mountain Res. Dev.* 21, 61–68.

19

The Brahmaputra-Jamuna River, Bangladesh

James L. Best[1‡], Philip J. Ashworth[2], Maminul H. Sarker[3] and Julie E. Roden[4]

[1]*Earth and Biosphere Institute, School of Earth and Environment, University of Leeds, Leeds LS2 9JT, UK*
[2]*Division of Geography, School of the Environment, University of Brighton, Cockcroft Building, Lewes Road, Brighton BN2 4GJ, UK*
[3]*Center for Environmental and Geographic Information Services (CEGIS), House No. 6, Road No. 23/C, Gulshan-1, Dhaka-1212, Bangladesh*
[4]*BG Group, 100 Thames Valley Park Drive, Reading RG6 1PT, UK*

19.1 BACKGROUND

19.1.1 The River

Bangladesh is dominated by three great rivers – the Brahmaputra-Jamuna, Ganga and Meghna – that combine to feed sediment into one of the World's largest deltas in the Bay of Bengal (Figure 19.1). Bangladesh has been shaped by, and is dependent upon, its rivers, which provide fertile soils and a diverse flora and aquaculture but also bring significant flood hazard and risk to infrastructure for a large and growing population. The people of Bangladesh have adapted their lifestyle for centuries to live with river flooding – frequently moving their temporary bankside homes, planting on newly emergent river bars, and sometimes raising their homesteads above water level in flood periods (Paul, 1997). However, a growing population, coupled with the expansion of infrastructure and economic development, has resulted in an increase in the intensity of flood damage (FPCO, 1995; Paul, 1997; CPD, 2004). The lives of many millions of Bangladeshi citizens are reliant on these rivers, with up to 600 000 people living on the riverine islands alone (Sarker *et al*., 2003). Bangladesh's rural economy relies upon annual 'normal' floods to bring moisture and fresh sediments to the floodplain soils (Paul, 1997): for instance, two of the three seasonal rice varieties (*aus* and *aman*) cannot survive without floodwater and the fish caught both on the floodplain during flood season and from the many floodplain ponds (*'beels'*) provide the main source of protein for many rural populations (Chowdhury, 1994; Paul, 1997; de Graff, 2003; Shankar *et al.*, 2004). However, the effect of 'abnormal' floods can be devastating and result in appreciable damage to crops and houses, severe bank erosion with consequent loss of homesteads, schools and land, and loss of human lives, livestock and fisheries (BDER, 2004; Shankar *et al*., 2004). For example, in the 1998 flood, over 70 % of the land area of Bangladesh was inundated, affecting 31 million people and 1 million homesteads (Chowdhury, 2000). The 1998 flood, which had an unusually long duration from July to September, claimed 918 human lives and was responsible for damaging 16 000 and 6000 km of roads and embankments, respectively, and affecting 6000 km^2 of standing crops (Chowdhury, 2000). In the 2004 floods, over 25 % of the population of Bangladesh, or 36 million people, was affected by the floods; 800 lives were lost; 952 000 houses were destroyed and 1.4 million badly damaged; 24 000 educational institutions were affected, including the destruction of 1200 primary schools; 2 million government and private tubewells were affected, and over 3 million latrines were damaged or

‡Current address: Departments of Geology and Geography and Ven Te Chow Hydrosystems Laboratory, University of Illinois at Urbana-Champaign, 1301 W. Green St., Urbana, IL 61801, USA.

Large Rivers: Geomorphology and Management, Edited by A. Gupta

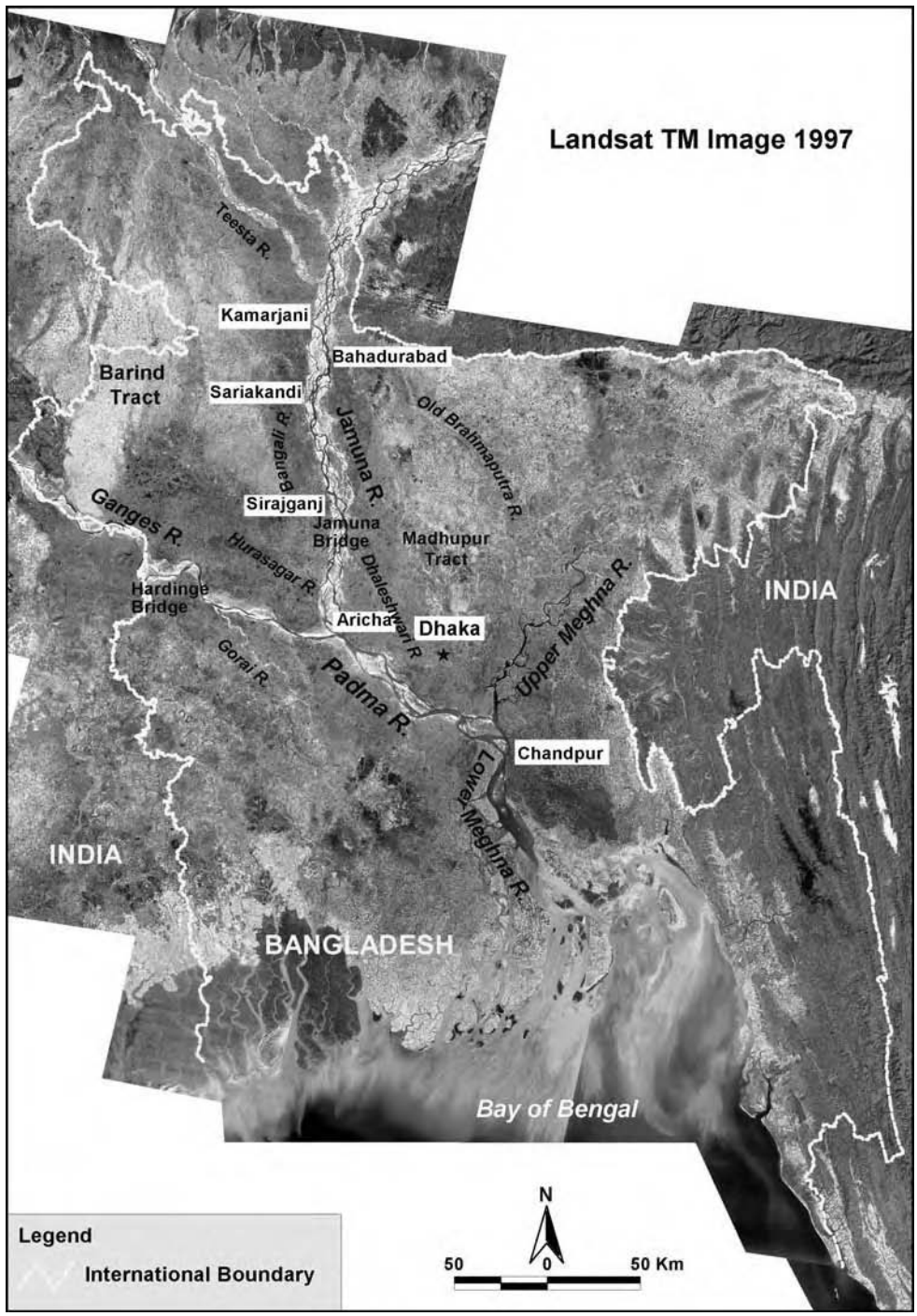

Figure 19.1 (See also colour plates.) Landsat image of Bangladesh, showing the Brahmaputra-Jamuna, Ganga (Ganges) and Meghna Rivers, together with the major features and towns referred to in this chapter

washed away, this increasing the risks of diarrhoea, cholera and other waterborne diseases. Also, 1.1 M ha of rice crop was submerged and lost before it could be harvested, with 7% of the yearly *aus* (early season) rice crop lost; 270 000 ha of grazing land was affected, 5600 livestock perished together with 254 000 poultry and 63 MT of lost fish production (BDER, 2004; CPD, 2004). In the districts that are dominated by the Brahmaputra-Jamuna River, the 2004 flood damage to infrastructure (homes, roads, culverts), tubewells and latrines, with ensuing unemployment of many of the population, were some of the areas of critical impact. The total cost of the damage caused by the 2004 flood is estimated at $7 billion (CPD, 2004).

Hence, due to the nature of these devastating floods, and their recent occurrence in 1987, 1988, 1998, 2004 and 2007, the possible influences on catastrophic flooding, such as the role of Himalayan deforestation (Kattelman, 1990; Mirza *et al*., 2001), the type of intervention and infrastructural response to flooding [e.g. the Brahmaputra Right Embankment (BRE) from the Teesta to Hurasagar confluences; Figure 19.1] and the nature, scope and need for the Flood Action Plan (Haggart *et al*., 1994; Paul, 1997) have thus received much attention and debate over recent years (Boyce, 1990; Hossain, 1993, Haggart *et al*., 1994; Reavill and Rahman, 1995; Paul, 1997; Islam, 2001). Additionally, political debates concerning water usage and construction of dams have become a major issue for Bangladesh (Patel, 1996; Wood, 1999; Mirza, 2004), since over 90% of the catchments of these three great rivers lies outside the boundaries of the country.

The Brahmaputra-Jamuna and Ganga Rivers combine to form the Padma, which carries the third greatest water discharge of all the World's rivers but is often ranked the highest in terms of sediment discharge (Schumm and Winkley, 1994), although a range of values exist for these estimates. The Jamuna is the local name given to the river for its entire length in Bangladesh to the Ganga junction (Figure 19.1; hereafter the river is referred to as the Jamuna). The Jamuna has one principal tributary input, the Teesta River in the north-west, and two major offtakes on the left bank that are the Old Brahmaputra (see below) and the Dhaleswari (Figure 19.1). The Jamuna River contributes ~51% of the water discharge and 38% of the sediment yield to the Padma according to Schumm and Winkley (1994), although FAP24 estimate these percentage contributions to the Padma at 66 and 65% for water and sediment discharge, respectively (FAP24, 1996a), with the sediment yield being estimated at 590 Mt year^{-1} and the sand fraction contributing 34% of this total (Sarker, 1996). The Jamuna can have a braidplain width up to 15 km in flood and scour depths of up to 40 m have been recorded (Klaassen and Vermeer, 1988). Thus, by any definition, the Jamuna is one of the World's truly great rivers, and has a direct and daily influence on the prosperity of its population and the country's economic growth and political stability.

Since the seminal work of Coleman (1969), much research has been conducted on these rivers, especially in the last 15 years as part of the Bangladesh Flood Action Plan (e.g. Haggart *et al*., 1994; Thorne and Thiagarajah, 1994; FAP24, 1996a–h; Paul, 1997), together with work from organizations such as the Center for Environmental and Geographic Information Services (CEGIS) and Water Resources Planning Organization (WARPO) in Bangladesh, and this has allowed a dramatic increase in our knowledge of the behaviour of the Jamuna River. This work, aided by major advances in monitoring techniques, such as frequent, all-year satellite imagery and whole-flow depth monitoring within the main channels at even the highest discharges, has resulted in the river being characterized in more detail than ever before (Takagi *et al*., 2007). The recent book by Hofer and Messerli (2006) provides a detailed account on the history of flooding and hydrology of the Brahmaputra-Jamuna River, as well as highland–lowland linkages and case studies of various flood years. Recent attempts to predict morphological change have also met with some success (EGIS, 2002; CEGIS, 2003; Mosselman, 2006), and together with numerical modelling (Jagers, 2003) offer some hope to both understand and predict river channel movement, and establish management plans for such change. Additionally, development of large-scale infrastructure within Bangladesh, such as construction of the Bangabandhu Multipurpose Bridge across the Jamuna, and numerous bank-protection works (Mosselman, 2006), has demanded an increased quantification of the alluvial channel processes and prediction of future channel change. This chapter seeks to provide a synthesis on aspects of the geomorphology and sedimentology of the Jamuna River within Bangladesh, between the northern Bangladesh border and its junction with the Ganga some 240 km to the south (Figure 19.1), and examines issues of applied geomorphology in response to the flooding and migration of this huge and largely untamed river. Details of the Brahmaputra River upstream of the Bangladesh border are given by Singh (see Chapter 18), and a recent synthesis on the water resources of the Brahmaputra Basin in India is provided by Singh *et al*. (2004), including a chapter on fluvial geomorphology by Bora (2004).

19.1.2 Basinal Setting and Controls on Sedimentation

The Jamuna River has developed in a region of significant tectonic activity associated with Himalayan uplift and

development of the Bengal foredeep (Alam *et al*., 1990; Barua, 1994; Goodbred *et al*., 2003), and the underlying structural control on the location of the major river systems of Bangladesh has been hypothesized by several researchers (Morgan and McIntire, 1959; Umitsu, 1993; Barua, 1994). Morgan and McIntire (1959) suggested there is a zone of 'structural weakness' along the present course of the Ganga–Jamuna–Padma Rivers due to either a subsiding trough or a fault at depth. However, much of the evidence on which this suggestion was based was indirect and awaits fuller seismic investigation to ascertain the exact subsurface controls on river channel migration and long-term evolution. The region is known to have suffered major seismic activity in the past 100 years (FAP24, 1996a), experiencing 20 earthquakes of Richter magnitude >7 in and around the Bengal Basin in the past 100 years, with the great 1950 Assam earthquake measuring Richter magnitude 8.6 and affecting up to 52 000 km^2 of territory in Assam (Sarker and Thorne, 2006). Seijmonsbergen (1999) reports on an analysis of Landsat MSS imagery and concludes that many structural lineaments, running broadly NW–SE and WSW–ENE, can be recognized from physical features on the floodplain, and concludes these are small faults that can influence local migration of the channels. Seijmonsbergen (1999) further contends that width changes in the Jamuna may respond to these faults and they may also cause increased sedimentation upstream of the fault. For example, Seijmonsbergen (1999; Figures 4 and 7) presents images to argue that a fault downstream of the Bangabandhu Multipurpose Bridge has affected channel migration, although the channel behaviour in the past 5 years does not now seem to support this contention (see Section 19.7). The importance of local structural controls on channel sedimentation must await further coring of the sediments, coupled with ground examination of the purported lineaments, in order to ascertain if they are real and the effect that they may exert on river planform changes (Seijmonsbergen, 1999: p. 135).

Deepening of the Bengal Basin has also produced huge accumulations of sediment that have been fed from Himalayan erosion, with the thickness of sediment above the Precambrian basement increasing from a few hundred metres in the shelf region to over 18 km in the Bengal foredeep to the south (EGIS, 1997). Ongoing subsidence in the Bengal Basin, combined with high rates of Himalayan uplift, thus set the tectonic and climatic context for the large water and sediment discharges in the rivers of Bangladesh (Goodbred and Kuehl, 2000a,b). There is also evidence for a significant Late Quaternary climate signal superimposed on the structural control on sediment supply and channel belt migration (Heroy *et al*., 2003).

The control of uplift and subsidence is, however, clear and Allison (1998), in a review of the geologic and environmental framework of the Ganga-Brahmaputra Delta, highlights the uplifted Pleistocene terraces of the Barind and Madhupur tracts (Figure 19.1) as being first-order controls on the courses of the Jamuna and Ganga Rivers. Barua (1994) also presents a synthesis of the major environmental controls on Bangladesh's river systems and, together with the major controlling factors of regional tectonics, geology, climate, sea-level rise and vegetation, highlights the controls by the 'fluvial loading' that is dictated by water and sediment discharge and sediment calibre. The nature of sea-level rise, together with other anthropogenic effects on Bangladesh's rivers such as flood control and water usage, will clearly take on great importance in the twenty-first century (Begum and Fleming, 1997a,b; Choudhury *et al*., 1997; Mirza *et al.*, 2001; Mirza, 2002).

19.1.3 Hydrology, Sediment Yield and Channel Size

The Ganga and Jamuna Rivers are sourced in the Himalayan range, whilst the Meghna rises in the Sylhet Trough. The Jamuna has a catchment area of ~560 000 km^2 that receives an average of 1.9 m rainfall year^{-1} (FAP24, 1996a; Sarker and Thorne, 2006), with approximately 8.1 % of the drainage basin area being within Bangladesh (Ojha and Singh, 2004). The rise in the hydrograph of the Jamuna begins due to Himalayan snowmelt in May, but the hydrograph is dominated by monsoon rainfall, and shows a broad peak between July and September (Figure 19.2). At Bahadurabad (Figure 19.1), the mean annual discharge is 20 200 m^3 s^{-1}, varying from a minimum dry season flow of ~2860 m^3 s^{-1} to ~100 000 m^3 s^{-1} in the disastrous 1988 flood (EGIS, 1997), and a record 102 500 m^3 s^{-1} in the 1998 flood (Chowdhury, 2000). Bankfull discharge is difficult to estimate because the channel bank edge and overbank level are ill-defined, but estimates range from 45 000 to 60 000 m^3 s^{-1} (FAP24, 1996e; Thorne *et al.*, 1993).The annual hydrograph shows a yearly change in water stage of ~6 m (FAP24, 1996a). The average water slope of the Jamuna is 0.000076 over the first 130 km and 0.000065 further downstream (FAP24, 1996b). Flow velocities within the main channels are of concern in design considerations and depth-averaged velocities may reach over 3.5 m s^{-1} (FAP24, 1996c).

The Jamuna is predominantly a braided river, with some anastomosed regions (cf. Sarker and Thorne, 2006, Figure 13) and possesses an average braidplain width of 11 km, flow depth of ~5 m and a Brice braiding index of 4–6 (FAP24, 1996a). Sarker and Thorne (2006) show that when slope is plotted against discharge on the classic

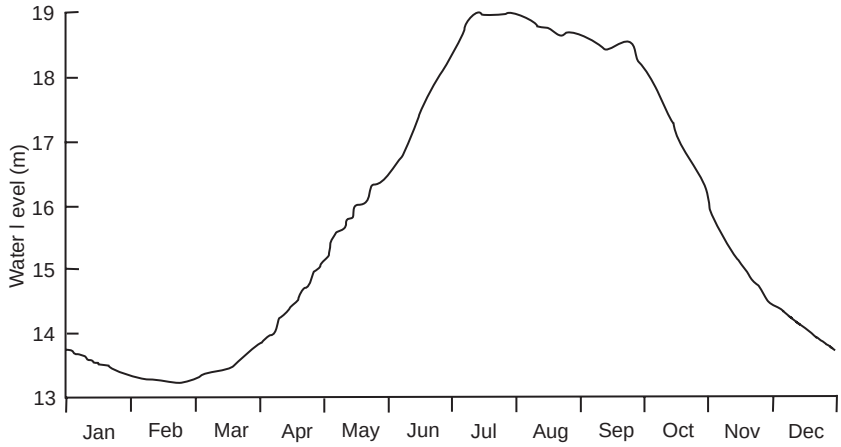

Figure 19.2 The stage-hydrograph of the Jamuna River at Bahadurabad (see Figure 19.1 for location), averaged over a 30-year period. Level is expressed relative to a standard low-water datum derived from long-term records. Reprinted from Braided Rivers: Process, Deposits, Ecology and Management, Eds Sambrook Smith *et al*., Special Pub. Int. Ass. Sedimentologists, Sarker, M.H. and Thorne, C.R., Morphological response of the Brahmaputra-Padma-Lower Meghna River system to the Assam earthquake of 1950, 2006, with permission of Blackwell Publishing

channel pattern discrimination diagram proposed by Leopold and Wolman (1957), the Jamuna, Padma and Meghna plot in the meandering field, highlighting the controls on channel planform are more complex than solely slope and discharge. The number of major channels in the braidbelt varies between three in the upper reaches and two in the lower reaches, with the planform being dominated by a range of vegetated and nonvegetated bars that divide the channel into a hierarchy of channel sizes (Bristow, 1987). The grain size of the Jamuna River shows a slight fining from north to south, with the median bed material grain size being 260 µm near the Indian border and 165 µm near Aricha (FAP24, 1996a), with an average of 220 µm (Barua, 1994; Sarker and Thorne, 2006). The majority of the sediment is fine sand and silt with less than 1% clay (FAP24, 1996h). The fine and abundant sediment supply result in sediment transport occurring throughout the year and this, together with high water discharges, gives rise to the massive sediment yields from the Jamuna River, with estimates being of 590 Mt year^{-1} (FAP24, 1996a) to 792 Mt year^{-1} (Islam *et al.*, 1999). Various estimates of the percentage of the total load transported as bedload have been proposed, with values between 10% (Islam *et al.*, 1999) and ~30% of the total sediment load as bed material (Sarker *et al.*, 2003). Various estimates of the total suspended load have also been given, with a wide range of between 541 and 1147 Mt year^{-1} (Islam *et al.*, 1999).

19.2 CHANNEL SCALE MORPHOLOGY AND HISTORICAL CHANGES IN THE COURSE OF THE BRAHMAPUTRA-JAMUNA RIVER

The course of the Brahmaputra-Jamuna River has changed dramatically over the past 250 years, with evidence of both large-scale avulsion in the period 1776–1850 and a more general westward migration of the Jamuna channel belt since this date (Figure 19.3). The avulsion of the Jamuna has been described by several authors, with Bristow (1999) presenting the most recent summary of theories for the trigger of the change in channel belt location. Prior to 1843, the Brahmaputra flowed within the channel now termed the 'old Brahmaputra' (Figures 19.1 and 19.3a), east of the Madhupur Tract, and joined the Meghna River. Sometime between 1830 and 1860, Bristow (1999) contends that avulsion of the river occurred, and caused a maximum of ~80 km of lateral shifting of the river course from the east to the west of the Madhupur Tract (Figures 19.3a and 19.4). Several studies have discussed the avulsion of the channel into its present course, and suggested a number of reasons including tectonic activity (Winkley *et al*., 1994), switches in the upstream course of the Teesta River (Morgan and McIntire, 1959), the influence of increased discharge (Coleman, 1969), catastrophic floods (La Touche, 1910) and river capture into an old river course (Bristow, 1999). From an analysis of maps between 1776 and 1843, Bristow (1999)

(a)

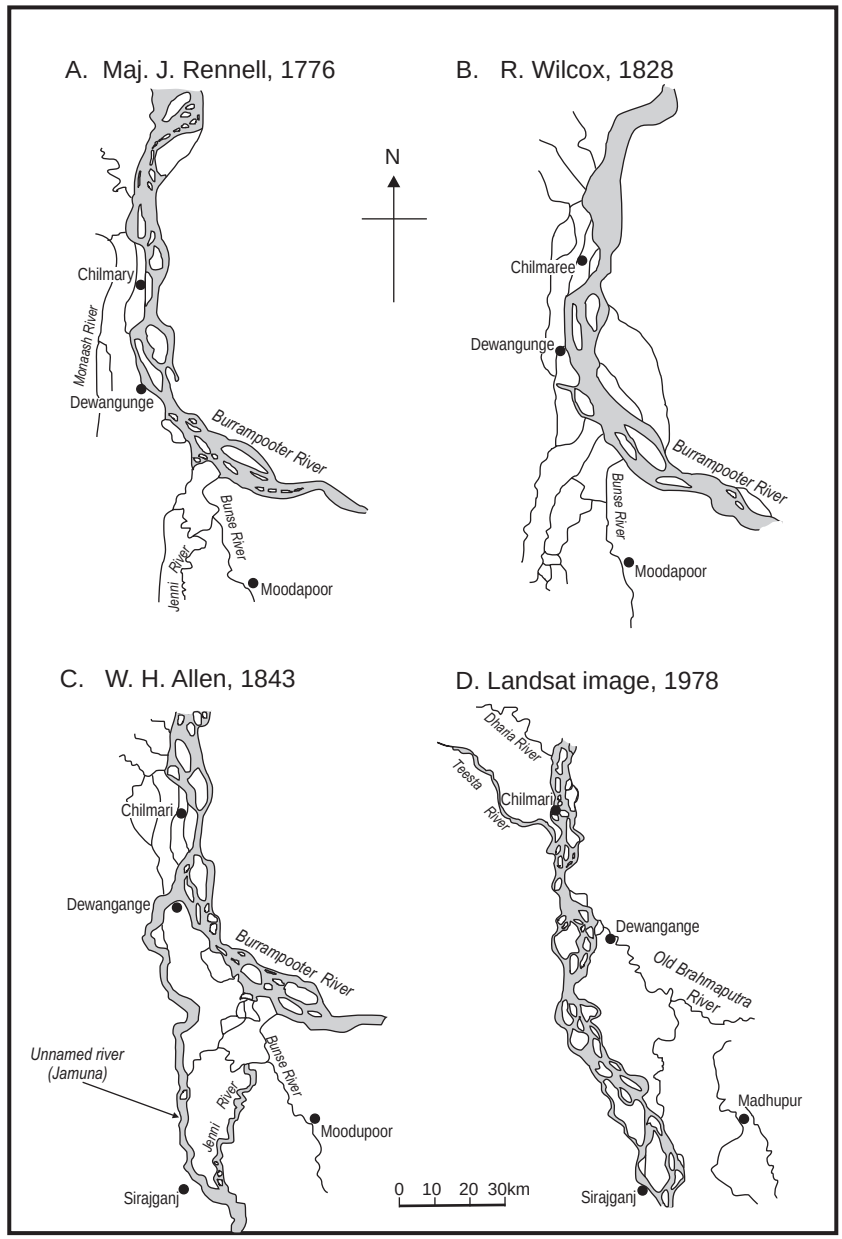

Figure 19.3 (a) Maps illustrating the position of the Jamuna River from 1776 to 1978: (A) 1776; (B) 1828; (C) 1843; (D) 1978. Reprinted from Fluvial Sedimentology 6, Eds Smith, N.D. and Rogers, J., Special Pub. Int. Ass. Sedimentologists, Bristow, C.S., Avulsion, river metamorphosis and reworking by underfit streams: a modern example from the Brahmaputra River in Bangladesh and a possible ancient example in the Spanish Pyrenees, 1999, with permission from Blackwell Publishing. (b) Historical changes in the position of the bankline of the Jamuna River. Reprinted from EGIS, Morphological dynamics of the Brahmaputra-Jamuna River, 1997, with permission from CEGIS

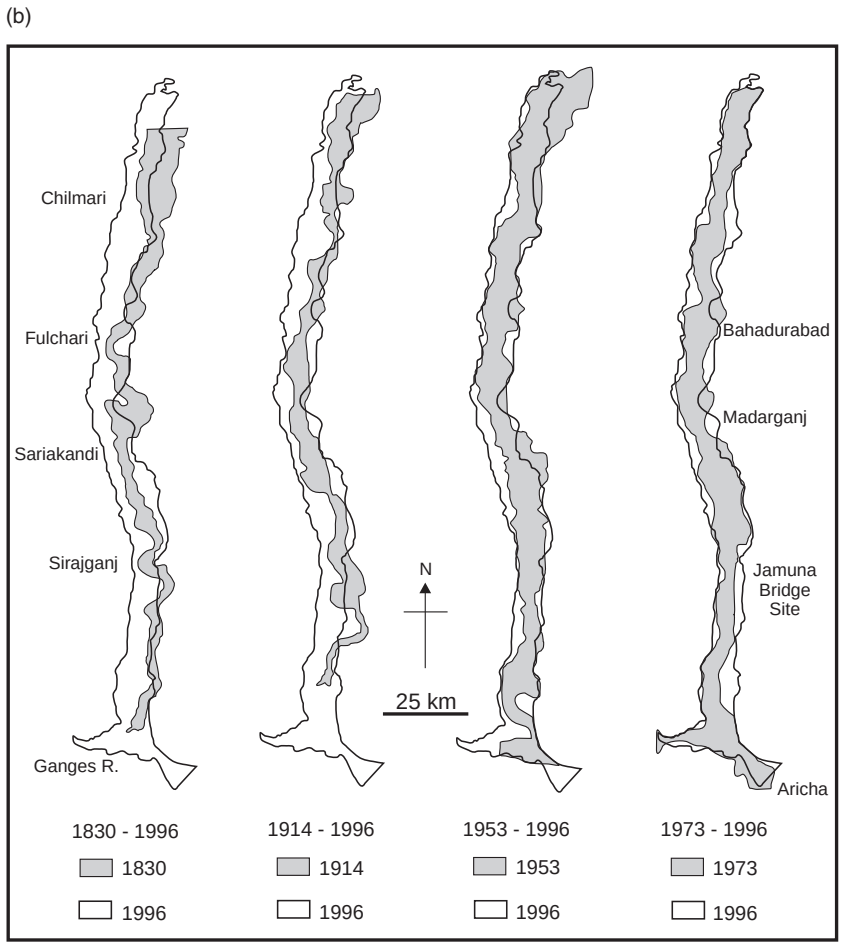

Figure 19.3 *Continued*

concludes that the river avulsion was more likely gradual than catastrophic, and may have been generated by bank erosion, perhaps around a large mid-channel bar, causing diversion of the channel into an existing floodplain channel. The map of Rennell (1776) clearly shows a sequence of large bars near the offtake of what is now the Jamuna (Figure 19.4a,b, label x) suggesting local sediment overload and diversion of flow against the banks. Significant flow may have previously been diverted down the Jamuna offtake, since the right bank at this point shows two large embayments that would funnel water down the offtake (Figure 19.4b, label x).

Several authors have also described the gradual westward migration of the Jamuna braidbelt (Coleman, 1969; Sarker, 1996; Khan and Islam, 2003) and noted that the braidbelt has widened since the early twentieth century (FAP24, 1996c; Sarker, 1996; EGIS, 1997, Figures 3 and 5). Even given the inherent uncertainties when using old maps to provide quantitative estimates of channel size, the trends in both mean, minimum and maximum braidplain width for the Jamuna (Figure 19.5) show a significant increase, although the rate of widening has decreased more recently (from 150 m year^{-1} between 1973 and 1992 to 30 m year^{-1} between 1992 and 2000; EGIS, 1997; Sarker and Thorne, 2006). The rate of widening averaged ~50 m year^{-1} over the period 1834–1992 (FAP24, 1996a), but with significant fluctuations in average rate up to ~170 m year^{-1} (FAP24, 1996a; Khan and Islam, 2003), and with *local* erosion rates reaching up to 1 km year^{-1}. ISPAN (1993) estimated that the length-averaged width of the

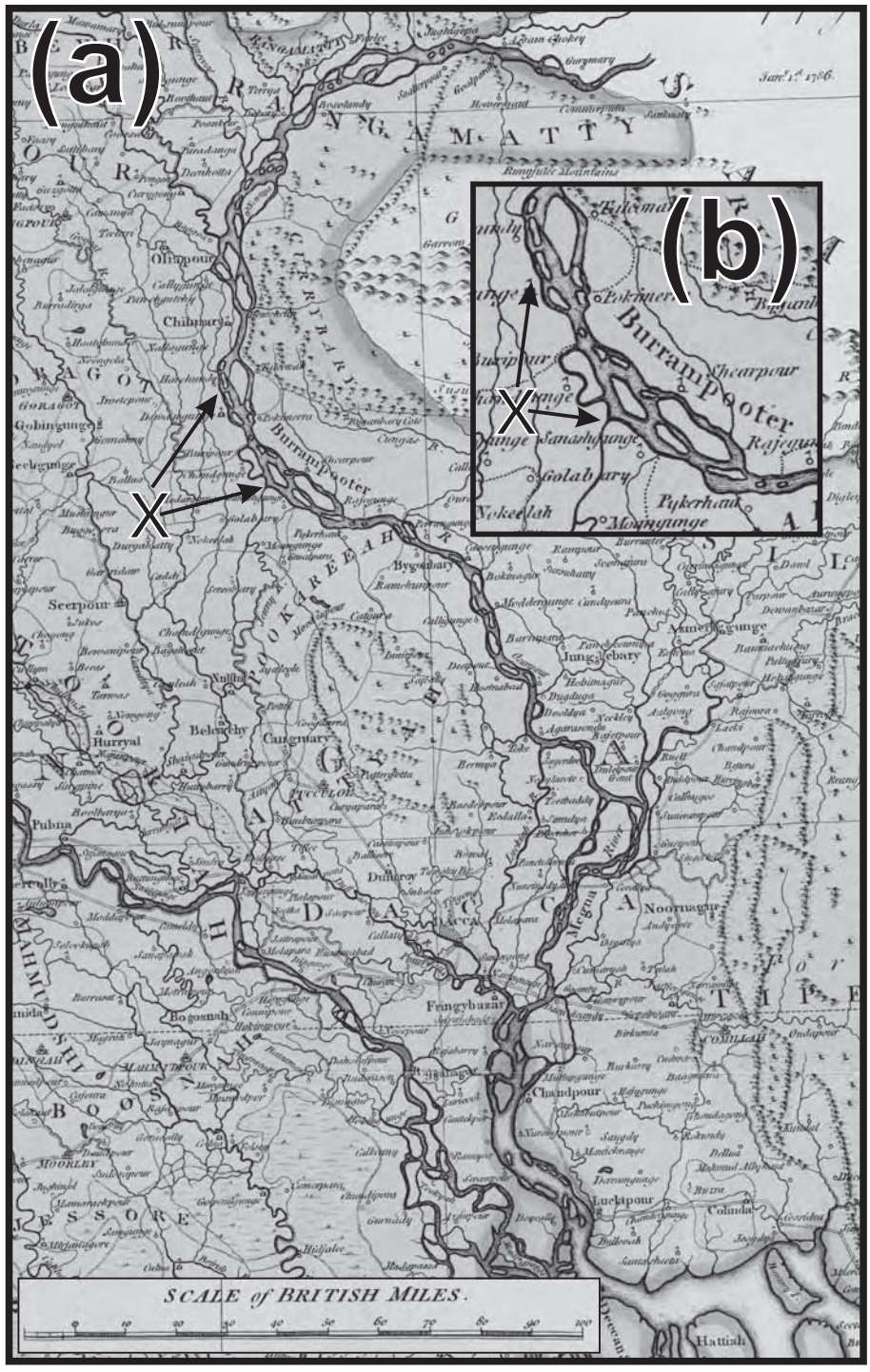

Figure 19.4 (a) Reproduction of part of Rennell's 1776 map illustrating the course of the Old Brahmaputra (Burrampooter) and the course the Jamuna was to adopt after its avulsion. Reprinted with permission from the David Rumsey Map Collection, www.davidrumsey.com. (b) Close up of the point of avulsion (labelled x in a and b). Note the large bars formed at the avulsion point and the bank erosion that appears in this region. Also compare this map with the image shown in Figure 19.1, and how the course of the Ganges changed after avulsion of the Jamuna. Today the Ganges/Jamuna combine to form the Padma, which then joins the Meghna to form one major channel exiting into the Ganges delta (Figure 19.1). In the map of Rennell (1776), the Ganges and Brahmaputra/Meghna Rivers form two separate channels flowing through the Ganges delta. Map reproduced courtesy of the David Rumsey Map Collection

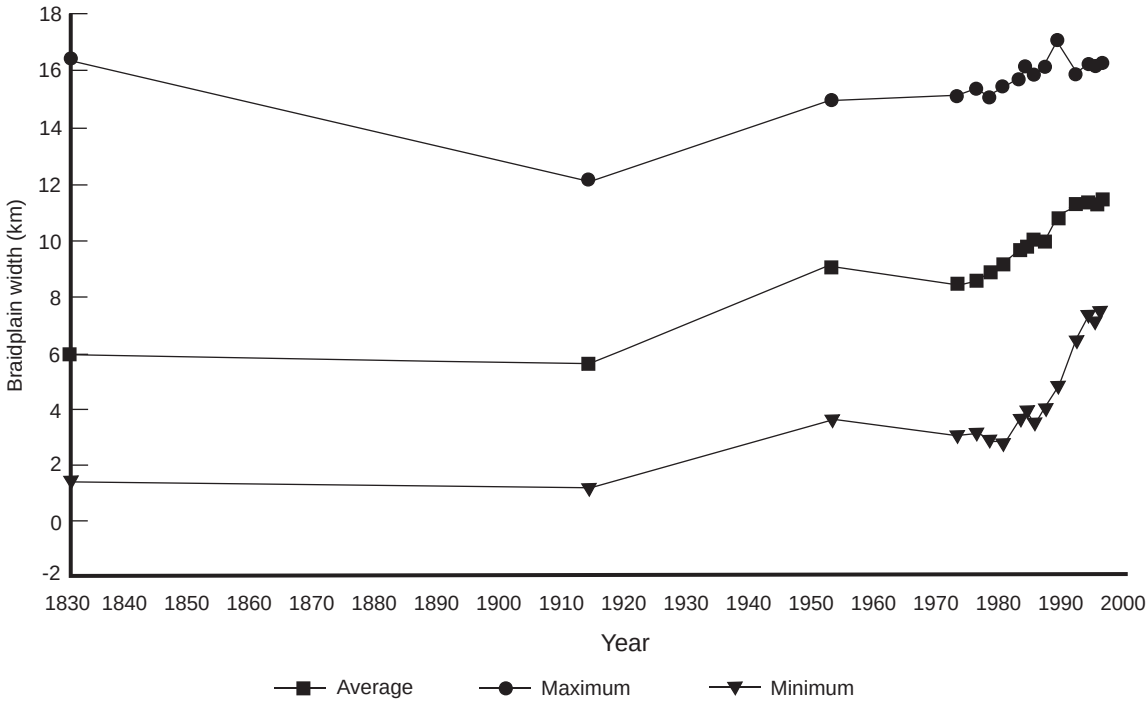

Figure 19.5 Trends in the mean, maximum and minimum width of the Jamuna braidplain 1830–1996. Reprinted from EGIS, Trends in the mean, maximum and minimum width of the Jamuna braidplain 1830–1996, 1997, with permission from CEGIS

Jamuna River in 1914 was 5.5 km, which is close to that found in the 1830 map. Later, the width of the river in the 1940s (Coleman, 1969) was found to be much higher, with the length-averaged width being ~9 km in 1952 (ISPAN, 1993) and, except for the lower reach, braiding was the predominant planform along almost the entire Jamuna River. The development of a braided channel was especially rapid in the period between the maps of 1914 and 1953, with the period between 1830 and 1914 being marked by a reduction in meander amplitude but a westward migration of the river (FAP24, 1996c). It is worthy of note that in the last three decades, the Jamuna River has eroded ~82 000 ha of floodplain, whereas only 12 000 ha of floodplain has been created through accretion. This net erosion has caused 0.7 million people to become homeless and landless (Sarker *et al*., 2003).

Coleman (1969) related the westward channel migration to uplift of the Madhupur Tract Pleistocene sediment, an argument that has found support from ISPAN (1993) Thorne *et al*. (1993), and Sarker (1996), although Burger *et al*. (1988) have rejected this contention. The debate concerning the westward migration of the Jamuna River emerged from the outward movement of both banks of the Jamuna River since the 1970s. During 1973–1992, the rate of eastward migration of the left bank was 79 m year^{-1} whilst the westward migration of the right bank was 68 m year^{-1}. This persistent high outward migration rate of both banks caused the apparent eastward migration of the centreline during these two decades, and probably led to the debate concerning the westward migration of the river. However, since the beginning of the 1990s, the eastward migration of the left bank has been greatly reduced to 16 m year^{-1} and the westward migration of the right bank has been slightly reduced to 44 m year^{-1}, thus causing the centreline of the Jamuna River to migrate westward (EGIS, 1997). These observations indicate that apparently the 'nil or eastward' migration of the centreline of the Jamuna River during 1973–1992 was probably for a short period and related to the very high widening phase of the river. Such westerly migration may be a product of braidplain widening as the channel adapts to its new post-avulsion course, and/or a response to underlying tectonic control (Morgan and McIntire, 1959). Thorne *et al*. (1993) also linked the location of erosion to the development of bankline curvature in the large-scale planform of the Jamuna and suggested this erosion on the outside of 'large

scale meanders' in the braidplain may be used to predict future sites and rates of bank erosion.

The planform analysis of the Jamuna River performed by EGIS (1997, 2000), using time-series satellite images, shows the width (Figure 19.3b) and braiding intensity of the Jamuna River to be changing spatially and temporally. Changes in the braiding intensity of the Jamuna River were also noted by Klaassen and Vermeer (1988), and Sarker and Thorne (2006) have related these changes in planform parameters, including the braiding intensity in the Jamuna, Padma and Lower Meghna Rivers, to the propagation of a sediment pulse generated from the 1950 Assam earthquake. Sarker and Thorne (2006) divided the Jamuna River into two halves and presented changes in width and braiding intensity for the upstream and downstream reaches (Sarker and Thorne, 2006, Figures 6 and 8a). Three points are worthy of note from these studies concerning the braiding intensity of the Jamuna River:

1. The braiding intensity is less in the downstream reaches of the Jamuna River than in the upstream reaches, possibly in response to a downstream decrease in slope (Klaassen and Vermeer, 1988).
2. The braiding intensity in the upstream reaches of the Jamuna River increased after 1973, but has started to decrease from the early 1990s.
3. In the downstream reaches of the Jamuna River, the braiding intensity decreased in the 1970s, but then increased through the 1980s up to the first half of 1990s. The braiding intensity has started to decrease in the downstream reaches of the Jamuna since the mid-1990s.

Using satellite images from 1967–2002, Takagi *et al*. (2007) showed that this temporal change in river activity and dynamics may fall into four distinct phases associated with alternating periods of quasi-dynamic equilibrium and more complex conditions. The transition between phases may have been triggered by significant and frequent flooding events.

Sarker (1996) and Bristow (1999) note that the initial planform of the Jamuna after the 1770–1830 avulsion was meandering with a dominantly braided planform in its upstream reaches, and that a fully braided planform has only developed since then. Coleman (1969) surmised that, with the increase in discharge generated by the joining of the Teesta River, the Jamuna started to braid. The date at which, and if, the Teesta River joined the Jamuna is unclear, with Morgan and McIntire (1959) stating this was contemporary with the avulsion of the Brahmaputra River. However, the absence of the Teesta River in the 1828 map of Wilcox makes this uncertain (Figure 19.3a), and only in the map of 1860 is the Teesta River found as a tributary of the Jamuna River. However, maps of 1860 and 1914 show that the planform of the Jamuna River was predominantly meandering, with the presence of a braided planform in some upstream reaches. Coleman (1969) recognized three nodal points along the banks of the Jamuna River, one downstream of Bahadurabad, another near Sirajganj, and the third upstream of Aricha (Figure 19.1). In these areas, which have remained fixed for long periods of time, the river is relatively narrow and deep, and it has been proposed that cohesive clays, together with the slightly more resistant natural levee, do not allow the river to migrate freely here as in other areas (Coleman, 1969). Klaassen and Masselink (1992), however, rejected the existence of such nodal points. Thorne *et al*. (1993) also considered the composition of the bank materials along the Jamuna River to be uniform and that the banks are formed in weakly cohesive silty-sand, which is highly susceptible to erosion. However, they also state that clay deposits exist along the right bank at Sariakandi, 40 km upstream of Sirajganj (Figure 19.1), and in the left bank at Bhuapur opposite Sirajganj, although these locations are not the same as mentioned by Coleman (1969). An analysis of the banklines derived from satellite images over the past three decades does suggest the existence of nonerodible bank materials in the left bank around Aricha, which corresponds with the location of the most downstream nodal point identified by Coleman (1969). Except for this location, the characteristics of the bank materials along the Jamuna River appear largely invariant.

A slight deviation from this homogeneity in bank erodibility was noticed by EGIS (2002), who report that the erosion rate was higher along bends on the left bank than along right bank bends with similar geometrical characteristics. This feature was attributed to the westward migration of the Jamuna River, which leaves relatively unconsolidated bank materials along its left bank. Analysis of high-resolution satellite images and aerial photographs shows the scars of recent channels on the eastern bank of the Jamuna River, the size of which is comparable with the active channels along this bank. However, such scars are not visible along the western right bank, thus supporting the contention that the river has migrated westwards. At present, the floodplains being eroded by the Jamuna River along its left (eastern) bank are newly formed, unconsolidated sediments, whilst those being eroded along its western, right bank comprise relatively old and consolidated floodplains. These consolidated floodplains are more resistant to erosion, and are also more fertile and productive than the unconsolidated and newly accreted floodplains along the left bank.

19.3 BEDFORM TYPES AND DYNAMICS

Sediment within the Jamuna is carried as bed, suspended and wash load, with the majority of the sediment being carried within the water column (Klaassen *et al*., 1988). However, the bed load, although only ~10 % of the total sediment load, is critical in generating a wide array of bedforms of different scale that drive channel change and migration. Bed material transport occurs at all flow stages in the Jamuna and the role of high-stage flood flow and subsequent reworking, or modification, of the high-stage deposits becomes significant on the falling limb of the flood hydrograph. The synthesis presented herein splits bedforms into two scales: (1) smaller-scale bedforms that are a small fraction of the flow depth (ripples, upper-stage plane beds) or generally scale with flow depth [dunes, this also including the 'megaripples' of Coleman (1969)] and (2) bedforms that scale with the channel width and are usually a significant fraction of the flow depth (various types of bars). Figure 19.6 shows some examples of these bedforms and their sedimentary structures.

19.3.1 Small-Scale Bedforms (ripples, dunes and upper-stage plane beds)

Recent work has shown that sand dunes are the predominant smaller-scale bedform within the Jamuna at all flow stages and in all parts of the channel (FAP24, 1996g; Roden, 1998): they thus form the nucleus of many larger scale bars (see below) and are a key component of the sedimentary facies (Best *et al*., 2003). Surveys over a 2-year period at Bahadurabad and Sirajganj (Figure 19.7) show that over 40 % of the bed is occupied by dunes at any flow stage, and this figure may rise to nearly 100 % (Roden, 1998). Ripples and smaller dunes are commonly superimposed on larger dunes, but upper-stage plane beds are rare and largely restricted to fast, shallow flows on bar-tops. Dune height and wavelength, plotted from a database of 1400 measurements at three sites (Figure 19.8a,b), range from 0.10 to 6 m (Figure 19.6a,b,c) and 2 to 331 m respectively. Both distributions are log-normal and the form index of the dunes (height/wavelength) ranges from 0.0005 to 0.27 (Figure 19.8c). The leeside slope angle of these dunes (Figure 19.8d) shows a wide spread from 1 to 58° (steeper than the angle-of-repose probably due to intense eddying in the leeside), with a mean of 8.4°. This demonstrates that many dunes do not possess an angle-of-repose leeside and may be of a form that does not generate permanent flow separation in the leeside, as has been demonstrated in other large rivers (Smith and McLean, 1977; Kostaschuk and Villard, 1996; ten Brinke *et al*., 1999; Best *et al*., 2001; Best and Kostaschuk, 2002). This finding is of considerable importance in considerations of dune form factor and estimates of flow resistance in alluvial channels, since previous work (Ogink, 1988) has demonstrated that a considerable reduction in roughness height is present for low-angle dunes due to the lesser effects, or even absence, of permanent flow separation in the dune leeside (Best and Kostaschuk, 2002). Plots of the form index of dunes (Figure 19.9) as a function of leeside slope shows the form index is lower at lower leeside slopes: for the average slope of 8.4°, the contribution to the form roughness would decrease to ~45 % of the value for an angle-of-repose dune, whereas for a leeside slope of 4.5° this decrease would be to ~10 % (see Figure 4.1 in FAP24, 1996c). These figures thus demonstrate that the contribution of dune-related roughness to total roughness may be much smaller than considerations based solely on dune height (FAP24, 1996c), a conclusion also reached by Klaassen *et al*. (1988). Additionally, these data suggest that the shape of the dune must be quantified accurately if bedform tracking is to be used as a method for estimating bedload transport (FAP24, 1996g). Ideally this should include quantification of both the dune profile and three-dimensional planform morphology, as available from side-scan sonar (Figure 19.10) or more recent developments in multibeam echo sounding (Parsons *et al*., 2005).

Plots of dune height and wavelength against flow depth (Figure 19.11) show a wide scatter but illustrate that maximum dune height approximates 0.25–0.33 of the flow depth, and that dune wavelength is generally less than seven times the flow depth (Julien and Klaassen, 1995). The scaling of maximum dune height with flow depth fits well with past work (Jackson, 1976; Best, 1996), with the smaller dunes either being present under nonequilibrium conditions or growing in response to the boundary layer thickness developed by larger dunes or bars. The planform of the dunes is often both two- and three-dimensional (Figure 19.10). Dune superimposition is ubiquitous, with the height of the secondary dunes generally becoming larger with the size of the primary dune (Figure 19.12) and showing superimposition on the stoss side, shoulder and leeside of the primary dunes, again confirming the absence of permanent large-scale flow separation in some leesides. This also highlights the likelihood of downstream dipping accretion surfaces, with superimposed smaller cross-stratification, being preserved in the depositional record. Analysis of dune dimensions through the flood hydrograph (Figure 19.13) shows that generally both dune height and wavelength increase with flow velocity, although both positive and negative hysteresis loops are present. However, the form factor of the dunes shows little change and there is little tendency for dunes to flatten as velocity rises: this again demonstrates that the

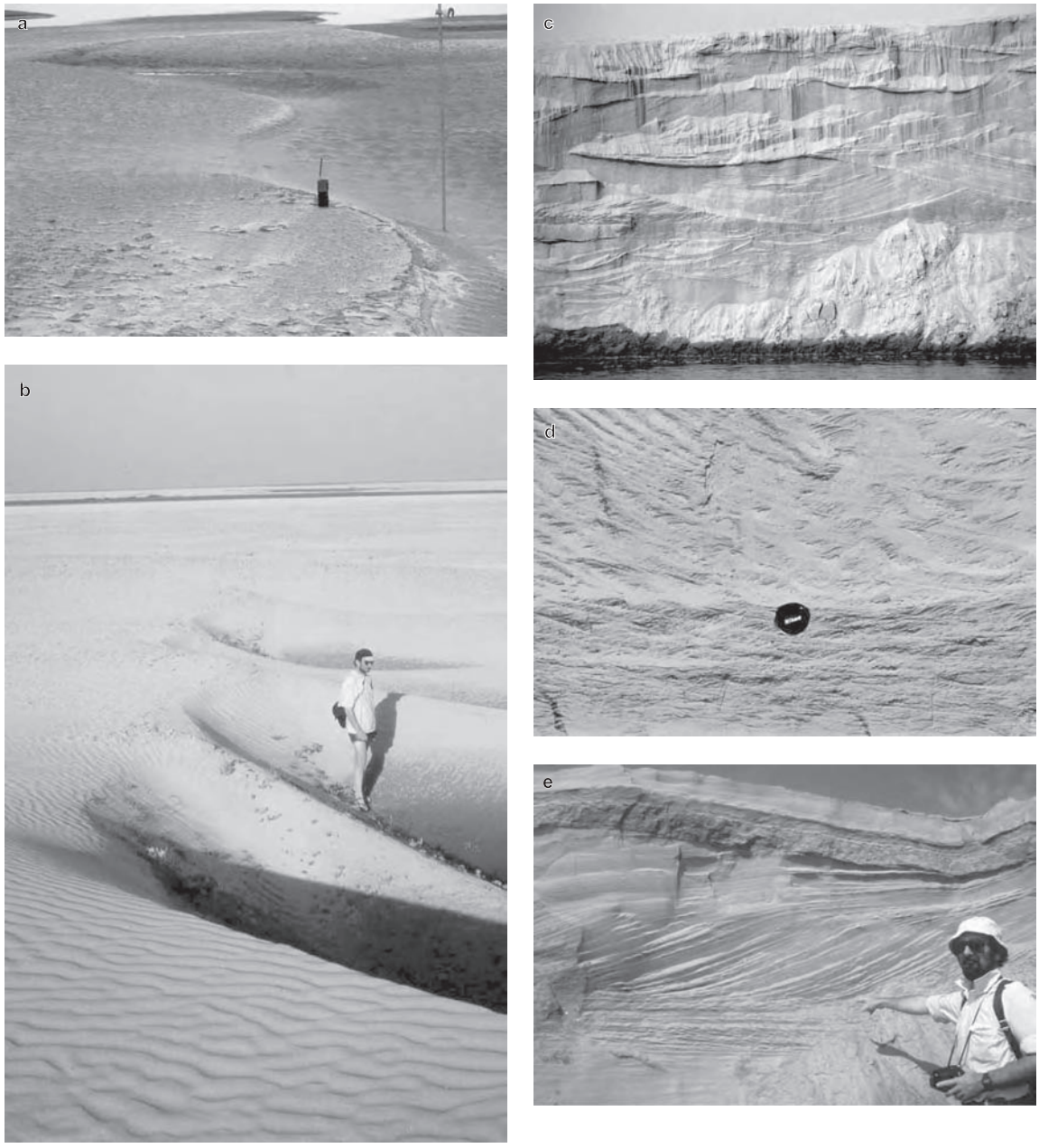

Figure 19.6 Examples of different bedforms and sedimentary structures found within the Jamuna River. (a) Small-scale (up to 0.3 m high) three-dimensional dunes; (b) large-scale (up to 3 m high) dunes; (c) dune cross-stratification in a 4 m high cutbank; (d) climbing ripples; (e) topset, bottomset and foresets preserved in a sand dune in the transitional regime to upper-stage plane beds; the topsets consist of upper stage plane-beds, whilst the toesets contain counter-current ripples, with current ripples below overlying upper-stage plane bed laminae. Reprinted from Braided Rivers, Eds Best, J.L. and Bristow, C.S., Bristow, C.S.; Sedimentary structures in bar tops in the Brahmaputra River, Bangladesh, pp. 277–289, 1993, with permission from the Geological Society of London

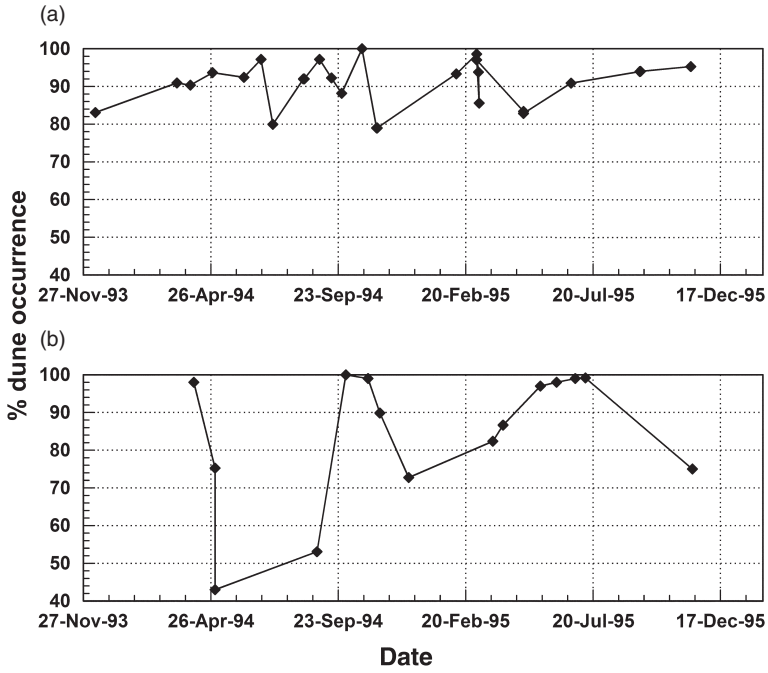

Figure 19.7 Percentage occurrence of dunes in the main channels of the Jamuna River at (a) Bahadurabad and (b) Siraganj, November 1993–December 1995 (from FAP24, 1996g)

majority of flows within the Jamuna generate bedforms within the dune stability field and not in the transitional regime to upper-stage plane beds, except in shallow flows on bar-tops (Bristow, 1993a; Julien and Klaassen, 1995; FAP24, 1996a,g; Figure 19.6e). Dune migration rates range from 1.1 to 16.8 m h^{-1} for dunes that range in height from 1 to 6 m (FAP24, 1996c), although from this limited database there is no indication of any strong link between dune height and migration rate.

The large dunes present in the Jamuna have also been described in relation to their mean flow field (FAP24, 1996g; Roden, 1998) and macroturbulence, the latter often seen as eruptions or 'boils' on the water surface (Figure 19.14; Coleman, 1969; Roden, 1998; Best, 2005). Such large-scale turbulence is related to upwellings of fluid over the dune troughs (Figure 19.6b) and has been linked to (1) eddy shedding of Kelvin–Helmholtz instabilities generated along the separation zone shear layer of steep leeside angle dunes, and (2) temporary shear layer development, and possible temporary flow separation (Best and Kostaschuk, 2002) in the lee of low-angle dunes, or in response to temporary dune oversteepening, possibly as a result of the migration and amalgamation of superimposed dunes (FAP24, 1996g).

Besides dunes, two other small-scale bedforms are present in the Jamuna: ripples (Figure 19.6d) and upper-stage plane beds (Figure 19.6e). Ripples are also ubiquitous and found both superimposed on dunes and also commonly on the bar-tops. The ripples on bar-tops may often be preserved as climbing ripples (Figure 19.6d) with high angles-of-climb, demonstrating the occurrence of high sedimentation rates (Bristow, 1993a). Aeolian erosion and sand transport, as ripples and small barchanoid dunes, may rework the top 0.1–0.5 m of bar surfaces during periods of exposure.

19.3.2 Large-Scale Bedforms (bars and bar complexes)

The Jamuna contains two different scales of larger bedforms that may be termed 'bars' and 'islands' (Thorne *et al*., 1993). Bars have lengths of the same order or greater than the channel width and heights that are comparable with the mean depth of the generating flow (ASCE, 1966). Islands are vegetated, relatively stable, large bar complexes (known locally as 'chars'), up to 15 km in length and with heights up to the adjacent floodplain level. Bars are frequently found attached to these islands but more

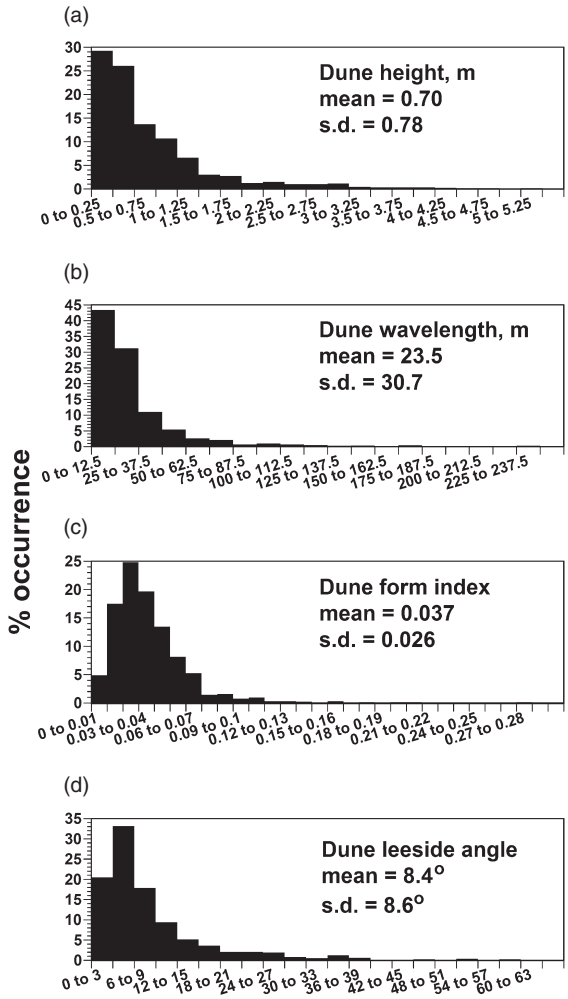

Figure 19.8 Histograms of (a) dune height, (b) dune wavelength, (c) dune form index (height/wavelength) and (d) dune leeside angle, from three study sites in the Jamuna River (from FAP24, 1996g and Roden, 1998). Sample size = 1400 dunes

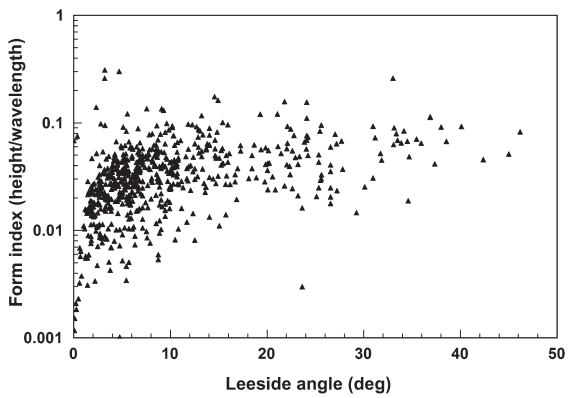

Figure 19.9 Form index of dunes in the Jamuna River as a function of leeside angle (from Roden, 1998)

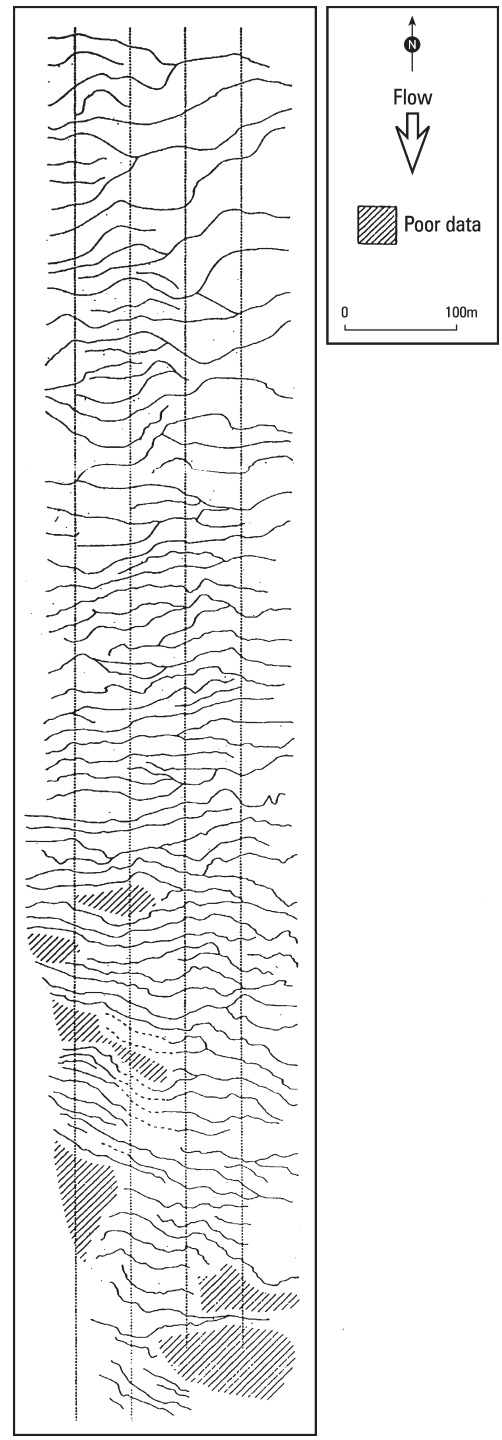

Figure 19.10 Composite tracing of dune crestline planform morphology as derived from sidescan sonar data collected in March 1995 near Bahadurabad (from FAP24, 1996g and Roden, 1998)

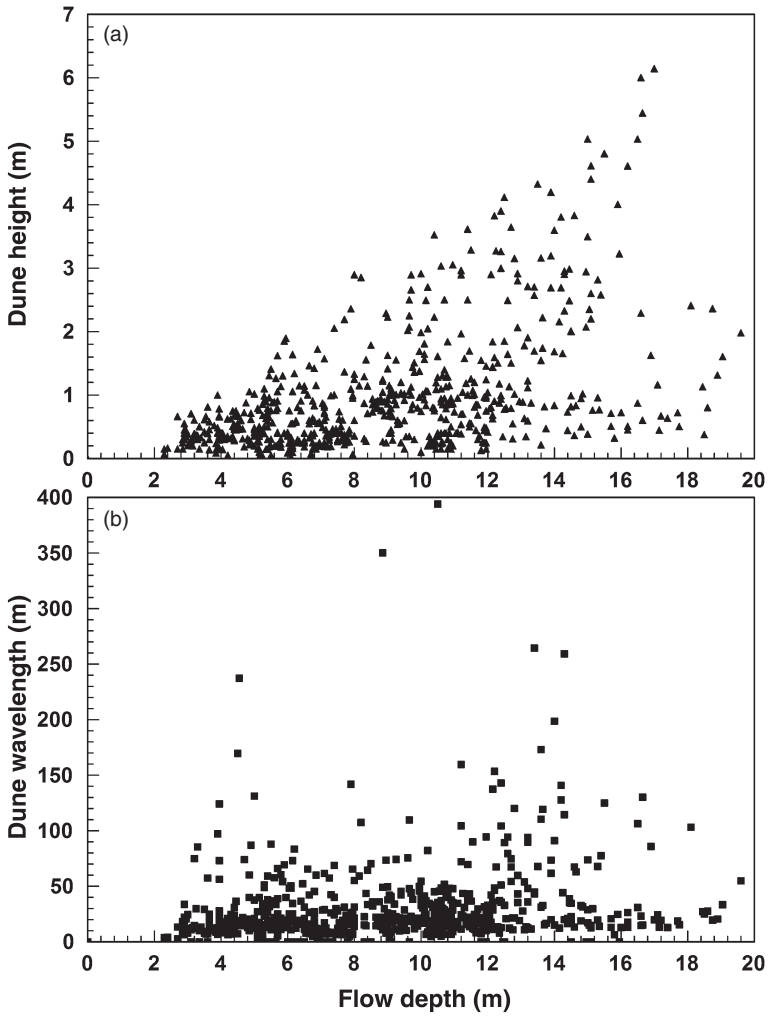

Figure 19.11 Plots of (a) dune height and (b) dune wavelength as a function of flow depth (from FAP24, 1996g)

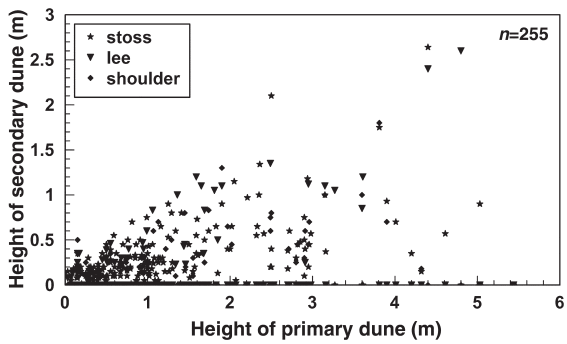

Figure 19.12 Plot of primary dune height against height of secondary dunes that are superimposed on the primary dune. The symbols denote the position on the primary dune where the secondary dunes are superimposed (stoss side, leeside and on crestal shoulder; from FAP24, 1996g)

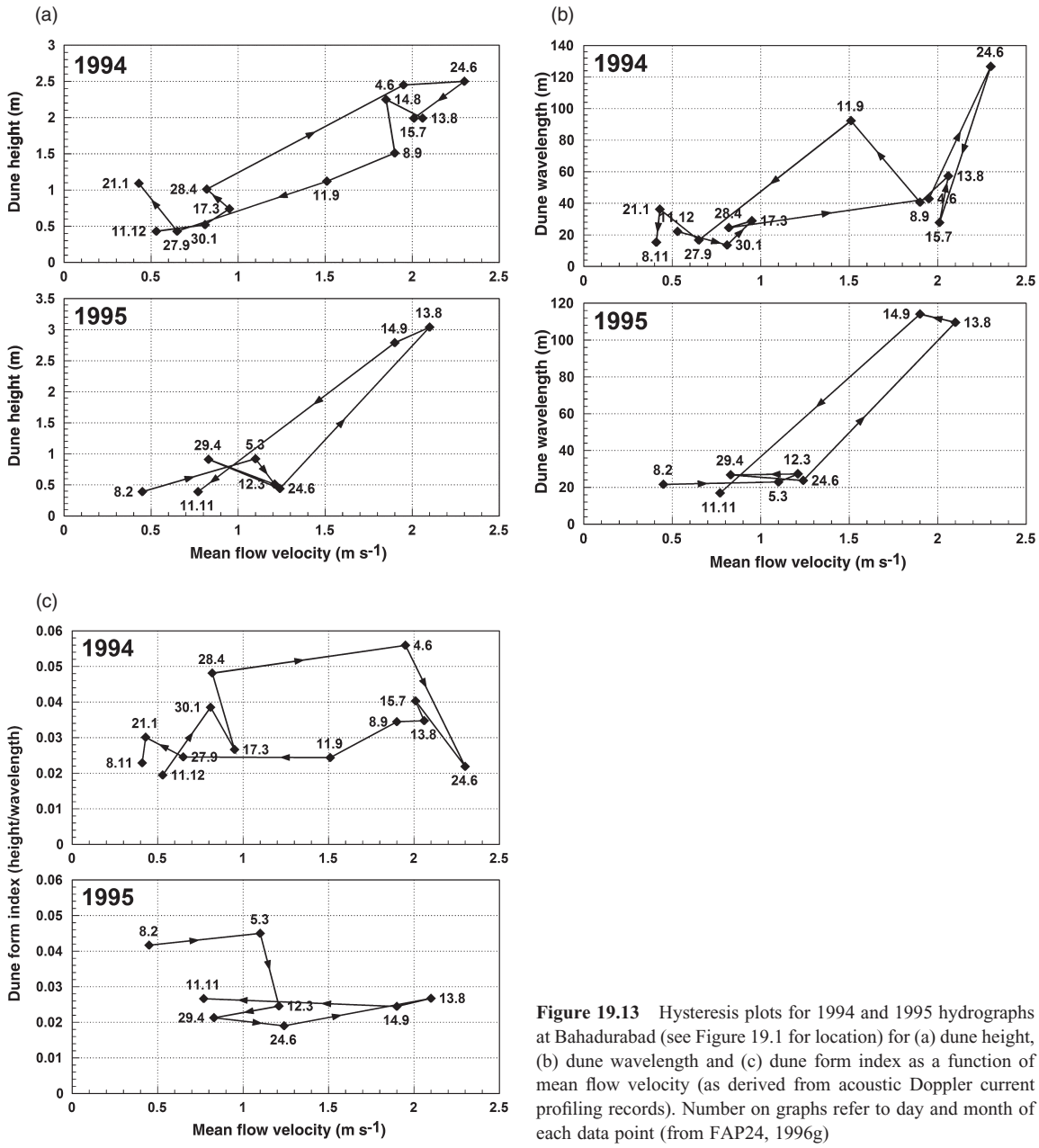

Figure 19.13 Hysteresis plots for 1994 and 1995 hydrographs at Bahadurabad (see Figure 19.1 for location) for (a) dune height, (b) dune wavelength and (c) dune form index as a function of mean flow velocity (as derived from acoustic Doppler current profiling records). Number on graphs refer to day and month of each data point (from FAP24, 1996g)

commonly within the anabranches that bifurcate around the node–island–node configuration that appears to dominate the downstream configuration of the active Jamuna channel belt (Figure 19.1). The Jamuna contains all sizes of sand bars ranging from tens of metres to several kilometres in length. Recent work has suggested the surface geometry of bars in the Jamuna (expressed as the ratio of long-to-intermediate bar axis) and some aspects of the subsurface facies associated with these bars may be scale independent and share many of the morphological and sedimentological characteristics of other sandy braided rivers (Best *et al*., 2003; Sambrook Smith *et al*., 2005).

The most common bar types are the scroll (or point) bar and mid-channel (compound braid) bar (Bristow, 1987;

Figure 19.14 Macroturbulence erupting on the water surface of the Jamuna River near Bahadurabad: this locality was above a field of 3–4 m high dunes at the time of survey (Best, 2005). Flow left to right, and flow depth ~15 m

Ashworth *et al*., 2000). Bridge and Lunt (2006) suggest that mid-channel bars in the Jamuna develop from double-row alternate bars (Fujita, 1989; Yalin, 1992) which create a 'unit bar' (Bridge, 1993, Figure 1), although no data are presented to substantiate this hypothesis. Ashworth *et al*. (2000) tracked the development of a 1.5 km long, 0.5 km wide, 12 m high, symmetrical mid-channel bar over a 28-month period in a major anabranch of the Jamuna near Bahadurabad (Figures 19.1 and 19.15) and noted that the bar was probably initiated by the stalling and amalgamation of dunes in the main channel thalweg. Supporting evidence for this mode of bar initiation was displayed in Best *et al*. (2003) using Ground Penetrating Radar (GPR) that imaged the subsurface of the same bar down to 12 m and revealed stacked two- and three-dimensional dunes at the base of the bar. Many mid-channel bars in the Jamuna enlarge (both up-, down- and across-stream) by the addition of smaller unit bars. Bristow (1987) calculated that up to 57% of the total area of bar deposition in the Jamuna may be through lateral accretion by the successive addition of individual unit or scroll bars to the bar nucleus. Unit bars are dominated by dunes whose crestlines are often oblique to the local anabranch direction (Bridge, 1993). Mid-channel bars in the Jamuna often develop downstream extensions to the bartails that have been termed 'horns' (Cant and Walker, 1978), 'limbs' (Ashworth, 1996) or 'wings' (EGIS, 2002) that may extend for up to 50% of the bar length.

Surprisingly, the Jamuna does not display many examples of the 'cross-channel bar' that features strongly in the 'classic' sand braid bar depositional model of Cant and Walker (1978). Many of the kilometre-wide anabranches are devoid of near-emergent lobate unit bars (Figure 19.16a–c) which is very different from observations of many other sand-bed braided rivers (e.g. Platte, South Saskatchewan; cf. Sambrook Smith *et al*., 2006). Width-depth ratios of the main anabranch channels are predominantly over 100 (up to 700, cf. Thorne *et al*., 1993) and can result in a simple flow convergence and divergence around and over bartops, rather than the development of single- and double-cell secondary flow circulation in the anabranches around bars (cf. Richardson and Thorne, 1998; McLelland *et al*., 1999; see Section 19.4).

Figure 19.15 shows a model for sand braid-bar growth in the Jamuna from Ashworth *et al*. (2000) based on 12 ship and land surveys, taken in the period 1993–1996, in a 9 × 2.5 km area immediately north of Bahadurabad (location in Figure 19.1). The model shows the creation of a central, symmetrical mid-channel bar from dune stacking in the channel thalweg (stages 2–3, Figure 19.15), followed by the enhanced development of one anabranch around the bar (stages 4–5, Figure 19.15), which then creates a lobate depositional front (stage 6, Figure 19.15) and an overall planform that resembles an alternate bar rather than a central unit braid bar. The availability of annual low-flow Landsat imagery since 1996 (represented by stage 6 in Figure 19.15) has allowed us to evaluate the longer-term stability and development of this particular kilometre-scale bar.

Figure 19.16a shows the morphology for the study reach at the end of the monitoring period described in Ashworth *et al*. (2000, Figure 5f: p. 540). The emergent mid-channel bar (labelled 1) had a 1 km long bartail and a discontinuous lobate bar front (labelled 2), but there was also deposition of a 3 km long mid-channel bar 2.5 km upstream (labelled 3) and side bars (labelled 4). Figure 19.16b shows that at low flow in 1997 the mid-channel bar under surveillance (labelled 1) appears to have migrated downstream by 3 km but maintained the same overall size and morphology. The lobate bar front (labelled 2) remained in place and became emergent, showing it was not an integral part of the mid-channel bar morphology as suggested in Ashworth *et al*. (2000). The study reach experienced downstream and lateral accretion of both bars 3 and 4. By 1998 (Figure 19.16c), the mid-channel bar had either been completely reworked or migrated downstream to accrete onto a bar complex (labelled 5). Bars 3 and 4 continued to grow but the 2 km wide main anabranch was essentially devoid of any partially emergent or newly developing mid-channel bars. Together with the survey data presented in Ashworth *et al*. (2000), this example of channel evolution near Bahadurabad illustrates that kilometre-scale bars may have a life-cycle of about 5 years (i.e. more than one flood season but then of limited duration). Mid-channel bars may maintain their basic morphological shape during development even when they migrate kilometres downstream. The annual record of bar evolution shown in

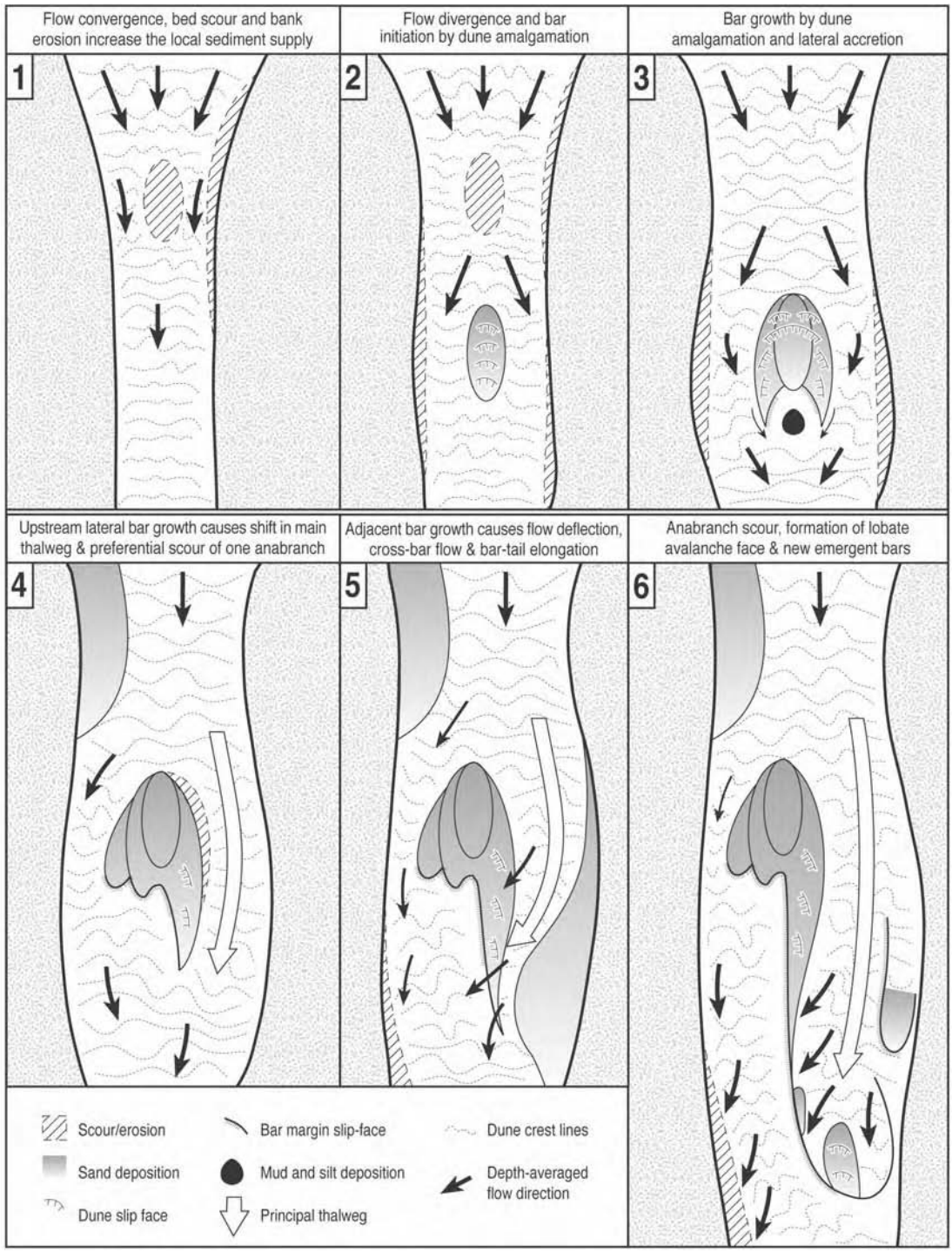

Figure 19.15 Summary model of the key stages in the evolution of a kilometre-scale mid-channel sand bar. Dune orientations and flow directions at the bed are inferred from the data presented in Roden (1998) and McLelland *et al.* (1999). Reprinted from Sedimentology, Vol. 47, Ashworth *et al*. Morphological evolution and dynamics of a large sand braid-bar, Jamuna River, Bangladesh, pp. 533–555, 2000, with permission from Blackwell Publishing

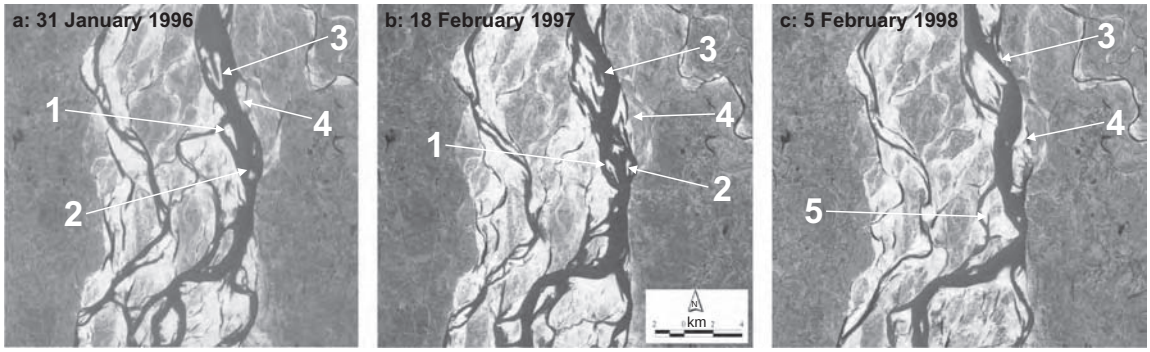

Figure 19.16 (See also colour plates.) Morphological evolution of the reach studied by Ashworth *et al*. (2000) at Bahadurabad: (a) January 1996 (which represents stage 6 in Figure 19.15); (b) February 1997; (c) February 1998

Figure 19.16a–c illustrates that in a river the size of the Jamuna, even kilometre-scale bars are extremely mobile and may be transient features in the braidplain depositional record.

19.4 BIFURCATIONS, OFFTAKES AND CONFLUENCES

Within the Jamuna River, the ubiquitous occurrence of bifurcations and confluences is a key aspect of the river channel pattern and dynamics, and these features form important nodes in the braidbelt. The braided nature of the river means that these nodes are present at a range of scales and orders of channel, and are central in dictating local and channel-wide erosion, deposition and morphological change.

Bifurcations occur as flow divides around the numerous braid bars and there has been much debate concerning the nature of flow within the distributaries, with Richardson *et al*. (1996) and Richardson and Thorne (2001) favouring a model that considers the flow similar to two back-to-back meander bends with helical flow developing at the bar-head. However, McLelland *et al*. (1999) argue that the main features of flow at the barhead bifurcation are convective acceleration as the flow shallows and modification of the primary flow caused by bedforms; they reason that these features, together with the high width : depth ratio of the channels and high relative roughness of dunes, cause a simpler flow pattern to that proposed by Richardson and Thorne (1998, 2001), with simple flow divergence around the barhead bifurcation.

EGIS (2002) report that of the 121 bifurcations considered in their study, 49 % were symmetrical in planform whilst 51 % were asymmetrical, and that the magnitude and direction of bifurcation migration were independent

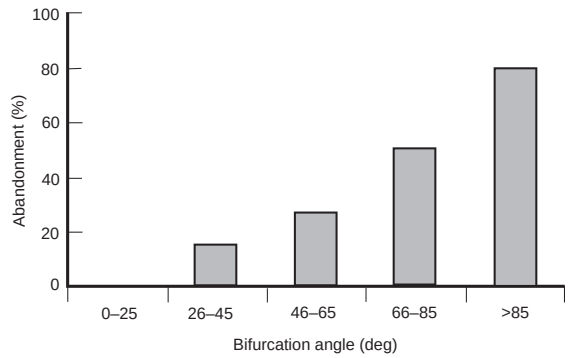

Figure 19.17 Distribution of channel abandonment as a function of bifurcation angle for bifurcations without appreciable barforms. Reprinted from EGIS, Developing and updating the empirical methods for predicting the morphological changes in the Jamuna River, 2002, with permission from CEGIS

of angle asymmetry. EGIS (2002) further detail that 17 % of the bifurcations migrated upstream whilst 83 % either remained static in position or migrated downstream. The rate of migration of bifurcations in the Jamuna ranges from −2200 to 3000 m year^{-1} (EGIS, 2002), whilst the length of the bifurcation, defined as the distance from bifurcation to confluence, varies between 2 and 40 km (EGIS, 2002). An important consideration in the evolution of bifurcations is the probability of channel abandonment of one of the distributaries, a process that is common in development of asymmetrical braid bars (Ashworth *et al*., 2000). It has been found (EGIS, 2002) that higher angle bifurcations are associated with higher rates of channel abandonment (Figure 19.17), with bifurcation angles <20° being very stable.

Besides bifurcations around braid bars, channel offtakes, which are more permanent divisions of flow, are key elements of the river morphology in Bangladesh. The dynamics of such offtakes have undoubtedly been of great significance during channel avulsions, such as: (1) the occupation of the current Jamuna channel and abandonment of the Old Brahmaputra (Figures 19.3 and 19.4), (2) the division of flow from the Jamuna into the Dhaleswari that is near the construction site of the Jamuna (Bangabandhu) Bridge (Figure 19.1; FAP24, 1996a), and (3) the current concern regarding the flow reduction and infilling of the Gorai channel which is an offtake from the Ganga just upstream of the Jamuna-Ganga confluence (Figure 19.1). The reduction in flow discharge down the Gorai River over the past decade has meant that during low flow the south-western region of Bangladesh receives much less fresh water, and therefore there is greater intrusion of the saline wedge from the Bay of Bengal into the distributary channels – a factor that has changed the livelihood of largely rural subsistence farmers (Alam, 1984). Study of the Gorai offtake (FAP24, 1996f) using historical data, satellite images and two-dimensional morphological modelling, highlights the influence of curvature in the upstream Ganga channel in affecting flow at the offtake and also the significant influence of flow stage in determining the division of flow. Rising flow stages appear to favour shallowing and widening of the channel at the offtake and during falling stage the channel becomes narrower and deeper. However, the influence of large, severe floods is significant and sediment accumulation in a bar at the mouth of the offtake generated during a very high flow can remain during subsequent years of normal floods (FAP24, 1996f).

Channel confluences are also key sites within the Jamuna, and have been documented as important sites of bed scour (Klaassen and Vermeer, 1988; FAP24, 1996a; Best and Ashworth, 1997; EGIS, 2002). The depth of the central confluence scour shows some dependence on the junction angle (Figure 19.18), with higher confluence angles possessing scour depths up to six times that of the confluent channels. Local factors, such as hydrograph shape, upstream channel curvature and low-stage modification may make this junction angle–scour depth relationship more complex, but the predictive equation of Klaassen and Vermeer (1988) is a reasonable estimate of scour depth (Sarker, 1996), and is given by:

$$h_{cs}/h = 1.292 + 0.037\theta$$

where h_{cs} is the confluence scour depth, h is the mean flow depth of the upstream channels and θ is the junction angle. Additionally, recent work comparing Jamuna scour data with other rivers in the World (Sambrook Smith *et al*., 2005) has suggested that scour depth relative to mean channel depth may be scale invariant over a threefold order of channel depths. Detailed bathymetric maps of the Jamuna-Ganga junction have shown the scale and rapidity of bed morphological change (Best and Ashworth, 1997), with the 30 m deep confluence scour migrating 2 km in two flood seasons (Figure 19.19).

19.5 FLOODPLAIN SEDIMENTATION

ISPAN (1995) provide a recent summary of sedimentation on the Jamuna floodplain, where most land is seasonally flooded, and which is characterized by an irregular relief. The nature of floodplain sedimentation and inundation is vital in planning annual crop growth and may adopt great significance in the ongoing debate on the sources, causes and accumulation of arsenic in the groundwaters of Bangladesh [see Ahmed *et al*. (2004) for a review]. ISPAN (1995) define several principal types of relief within the Jamuna floodplain (Figure 19.20):

1. Bars, scroll bars and sand dunes: generated by flood waters at the edge of the floodplain, often on the margins of the main or cross-floodplain channels. The difference in elevation between the top and bottom of this channel topography is rarely more than 1–2 m.
2. River levees: found along the edges of the active channels and formed by deposition from overbank flow, with grain size and deposition rate decreasing exponentially with distance from the channel. The height difference between the levee top and surrounding floodplain can be ~1 m over a distance of 100 m along small channels, but 2–3 m over 500 m or more alongside the major channels.
3. Crevasse splays: initiated due to a breach in the levee that forms a lobe of sediment which progrades onto the adjacent floodplain. The grain size of this crevasse splay decreases with distance from the initial breach.
4. Flood basin: nearly enclosed depressions between the levees of adjacent rivers that usually drain out through small channels on their downstream side. Subsidiary levees can form along these smaller channels and the flood basins may contain silts and clays that settle out in quiet water, whilst more permanently flooded areas in older floodbasins contain peat accumulations.

The older parts of the floodplain thus become more complex in topography (ISPAN, 1995), with the initial topography being smoothed out but with clay deposits up to 1 m thick. Elevation differences are generally 2–3 m over a lateral distance of 0.5–1 km. Soils within the

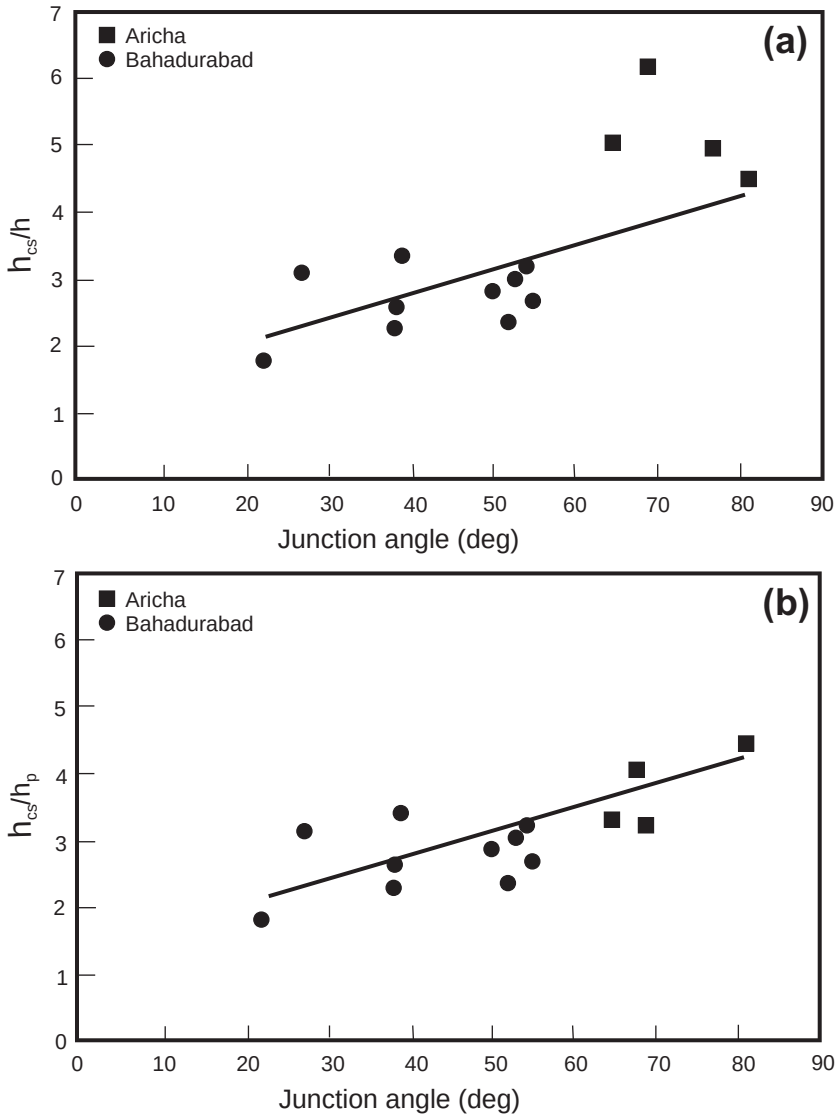

Figure 19.18 Confluence scour depth as a function of junction angle for data collected on the Jamuna river at Bahadurabad and Aricha: (a) with scour depth, h_{cs}, expressed in relation to flow depth at the time of measurement, h; (b) with scour depth, h_{cs}, expressed in relation to average flow depth in the upstream channels during the flood season, h_p. (b) shows a better relationship between junction angle and flow depth (from FAP, 1996d)

Jamuna floodplain change from east to west, from stratified alluvium on the active Jamuna floodplain to soils with well-developed profiles on the older floodplain and Old Brahmaputra. The main changes in soil-forming processes across this transect from east to west (Figure 19.21) involve increasing acidification, destruction of clays and accumulation of organic matter, with the soils increasingly displaying greater biotic mixing, mottling, coatings around peds and developing soil structure.

The depth of floodplain inundation is critical to farmers as this determines the annual cropping pattern and which type of rice will be grown. A classification of inundation on the floodplain (Table 19.1) shows the normal water depths in various categories of floodplain, although the

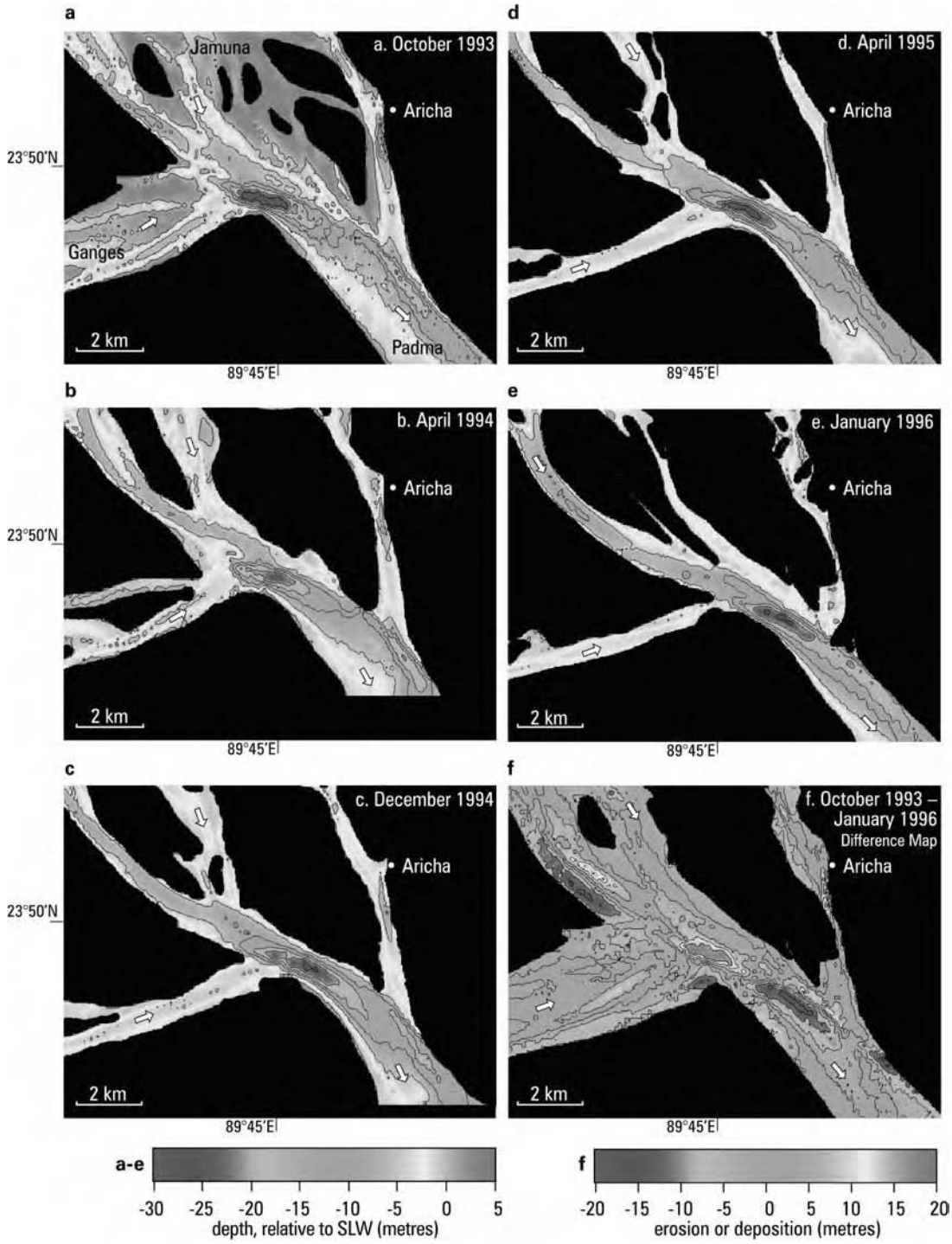

Figure 19.19 (See also colour plates.) Plots of bed morphology and channel change at the junction of the Jamuna and Ganga Rivers. SLW refers to Standard Low Water level. Reprinted by permission from Macmillian Publishers Ltd: Nature, Vol. 387, Best, J.L. and Ashworth, P.J., Scour in large braided rivers and the recognition of sequence stratigraphic boundaries, pp. 275–277, 1997

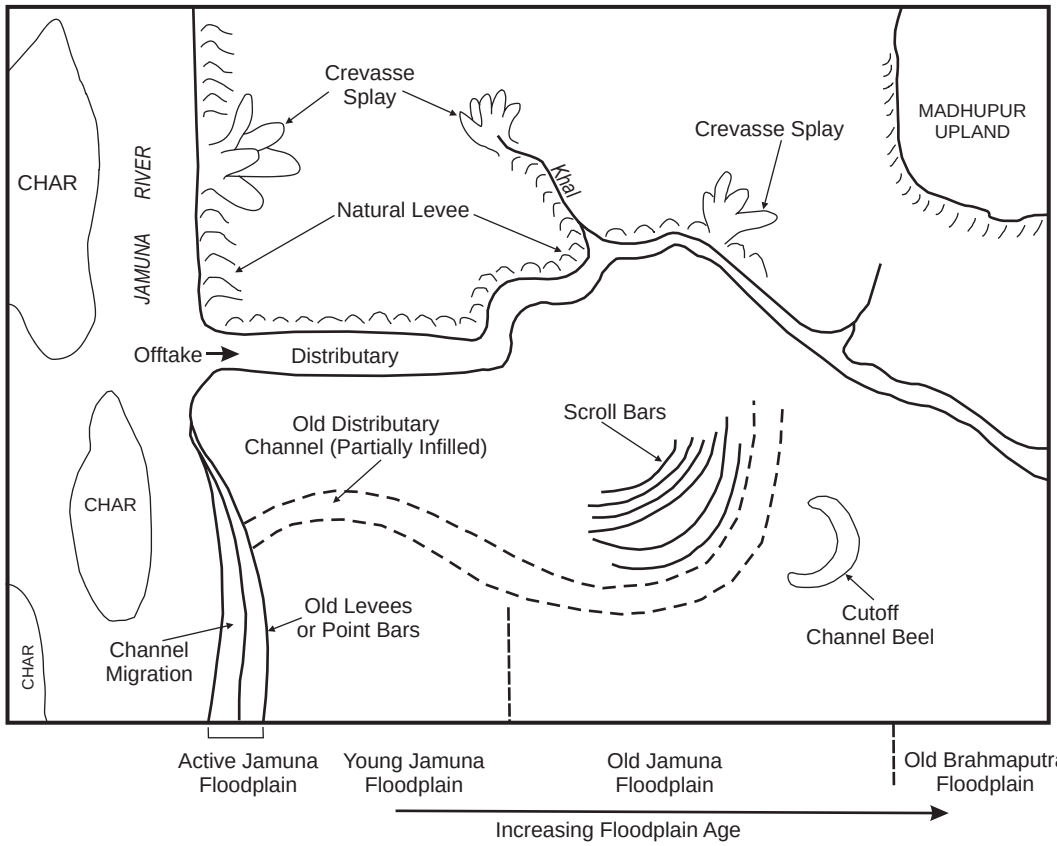

Figure 19.20 Representative landforms of the Jamuna floodplain. Reprinted from ISPAN, A study of sedimentation in the Brahmaputra-Jamuna floodplain, 1995, with permission from CEGIS

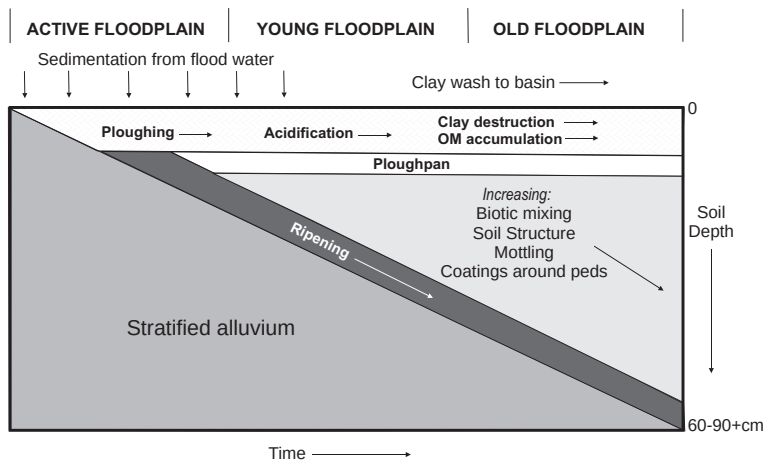

Figure 19.21 Stages of floodplain soil development in Bangladesh (after ISPAN, 1995). See text for discussion of lateral changes in soil characteristics. Reprinted from ISPAN, A study of sedimentation in the Brahmaputra-Jamuna floodplain, 1995, with permission from CEGIS

Table 19.1 Classification of floodplain water depths (after ISPAN, 1995)

Agro-ecological zone	Normal maximum water depth during flood (cm)
Highland	0
Medium highland-1	0–30
Medium highland-2	30–90
Medium lowland	90–180
Lowland	180–300
Very low lowland	>300
Bottomland	Mainly >300, but includes perennially wetland in other depth classes

effects of local ground subsidence (for instance earthquakes) and flood protection schemes, such as localized embankments that may increase flood inundation levels outside the embankments, may change the local floodplain water depths. ISPAN (1995) report average annual sedimentation rates of 7.6 mm $year^{-1}$ obtained from a GIS study, with a range from 0 to 76 mm $year^{-1}$. Allison *et al*. (1998) also report accumulation rates of ~40 mm $year^{-1}$ on the levees to <10 mm $year^{-1}$ within a few tens of kilometres into the floodplain flood basin. Allison *et al*. (1998) state that the important controls on local sedimentation rate are proximity to distributary channels, local topography and interannual variability of the flood pulse. Model results suggest that between 31 and 71 % of the total alluvial sediment budget may be trapped landward of the Ganga-Brahmaputra mouth, and highlight the key role of floodplain storage in controlling the sediment yield to the oceans (Allison *et al*., 1998). Islam *et al.* (1999) estimate that ~49 % of the total load is deposited before the coastal region, with 28 % being deposited on the floodplain and 21 % within the active channels. Islam *et al.* (1999*)* contend this deposition thus leads to significant aggradation within the channels as well as on the floodplain.

The nature of the annual flood hydrograph exerts a strong control on the grain size of floodplain sedimentation, and hence the contribution to soil fertility and subsequent crop success. For example, the large floods of 1998 and 2004 were very different, with overbank flows experienced for 65 and 45 days respectively (CPD, 2004). The nutrient-rich silt deposited during the longer duration 1998 flood led to a record *boro* rice crop the next year (BDER, 2004). However, the relatively fast-rising and receding monsoon flood in 2004 resulted in more overbank sand than silt deposition, and there was concern as to the impact this would have on the 2005 rice yields (BDER, 2004).

19.6 SEDIMENTOLOGY OF THE JAMUNA RIVER

The surface geomorphology of the braided Jamuna River, together with descriptions of the numerous cutbanks and more recent use of ground-penetrating radar, allows an insight into the depositional facies of the Jamuna. The principal papers concerning the sedimentology of the Jamuna are those of Coleman (1969), Bristow (1993a) and Best *et al*. (2003) and these are used below to highlight the depositional form of a braid bar within the Jamuna River. The Jamuna River has also been used as an analogue for deposition in other large ancient braided channels (e.g. see Bristow, 1993b; Miall and Jones, 2003) and thus description of a facies model is important for reconstructions of ancient alluvial architecture. Best *et al*. (2003), using a combination of detailed ground penetrating radar (Figure 19.22) and trench/core logging tied into surveys over an evolving, newly formed mid-channel braid bar (Ashworth *et al*., 2000), document four principal depositional facies: (1) large bar-margin slipfaces, up to 8 m high, that are generated as steep avalanche faces at the downstream end of actively migrating braid bars and are often associated with oblique flow over the braid bar; (2) medium-scale dune cross-stratification, 1–4 m high, generated by large-scale dunes within the active channels, or possibly as unit bars; (3) small-scale dune cross-stratification, 0.5–1 m high, generated by sinuous-crested sand dunes; and (4) mud drapes formed in quiet water regions, such as in the lee of mid-channel bars. These four facies were found to generate seven styles of deposition (Figure 19.23):

1. Bar-margin slipface: a dominant style of deposition within mid-channel bars that is created by oblique downstream growth and cross-channel bar-margin accretion. This deposition often occurs through amalgamation of complex sets of dune-scale cross-stratification and bar-margin slipface accretion with both large, low-angle and angle-of-repose foresets. Large bar-margin slipfaces may become progressively steeper until reaching the angle-of-repose.
2. Vertical accretion in channel: sets of trough cross-stratification, produced by sand dunes within the channels and decreasing in size towards the bar-top, are found in all areas of the bar and formed a significant proportion of the sedimentary facies.
3. Vertical accretion on bar-top: sets of trough cross-stratification are found on the bar-head, bar-tail and along the bar-margin, and are formed from deposition by small (<1.5 m high) three-dimensional dunes.
4. Upstream accretion: restricted to the upper 2–3 m of sediments in the mid-bar region and probably formed

(a)

Radar Facies No.	Radar Characteristics	Vertical & Lateral Extent	Sedimentary Characteristics & Interpretation
1	**1a.** Steeply dipping (angle-of-repose) planar or subplanar reflections and low-angle (10 – 15°) planar or subplanar reflections dipping into anabranch channel on western edge of bar.	up to 8 m high and extend laterally for >100 m	1a. Large-scale cross-stratification either at angle-of-repose, with large sets (a) dipping from bar margin into thalweg, or lower angle sets (b) that occur in deeper part of radar profile and on western side of bar, sloping into anabranch channels. May contain internal reactivation surfaces.
	1b. Planar and asymptotic dipping reflections in lens-shaped packages. Sometimes bounded by erosion surface at base or top.	up to 4 m high and extend laterally and downstream up to 100 m	1b. Large-scale cross-stratification (c) caused by deposition at the margins of the barhead by diverging flow.
2	**2a.** Strong, trough-shaped reflections that are laterally discontinuous, often with steeply dipping or low-angle internal reflections.	1 – 3 m high; 5 – 300 m lateral continuity	2a. Medium-scale trough (d) cross-stratification associated with preservation of large dunes.
	2b. Weak undulating reflections at depth often lacking internal dipping reflections (because foresets are beneath radar resolution).		2b. Medium-scale cross-stratification produced by large dunes in the deeper parts of radar profiles are identified from basal erosion surfaces (e) and the lack of discernible foresets.
	2c. Discontinuous sigmoidal packages of concave/convex dipping reflections.	2 – 4 m high; 20 – 200 m lateral continuity	2c. Complex sets of medium-scale cross-stratification (f) due to oblique migration of large dunes and superimposed dunes descending the bar margin. Sets may contain internal reactivation surfaces (g) and variable dip angles.
3	Small discontinuous reflections with weak concavity from trough shaped structures at the limits of radar resolution.	0.5 – 2 m high; 5 – 30 m wide	Small-scale trough cross-stratification (h) produced by dune deposition on the bar flanks. Set size increases with depth, larger sets are found on the bar western side and smaller sets on the eastern side.
4	High-amptitude, continuous, undulating reflections	~ 0.5 m high; ~ 40 m wide	Mud drape (i)

Figure 19.22 (a) The four principal ground-penetrating-radar facies documented from the GPR survey lines presented in Best *et al*. (2003), with (b) representative GPR examples and sedimentary interpretation. Vertical exaggeration = 1.58. Reprinted from Journal of Sedimentary Research, Vol. 73, Best *et al*. Three-dimensional sedimentary architecture of a large mid-channel sand braid bar, Jamuna River, Bangladesh, pp. 516–530, 2003, with permission from SEPM (Society for Sedimentary Geology)

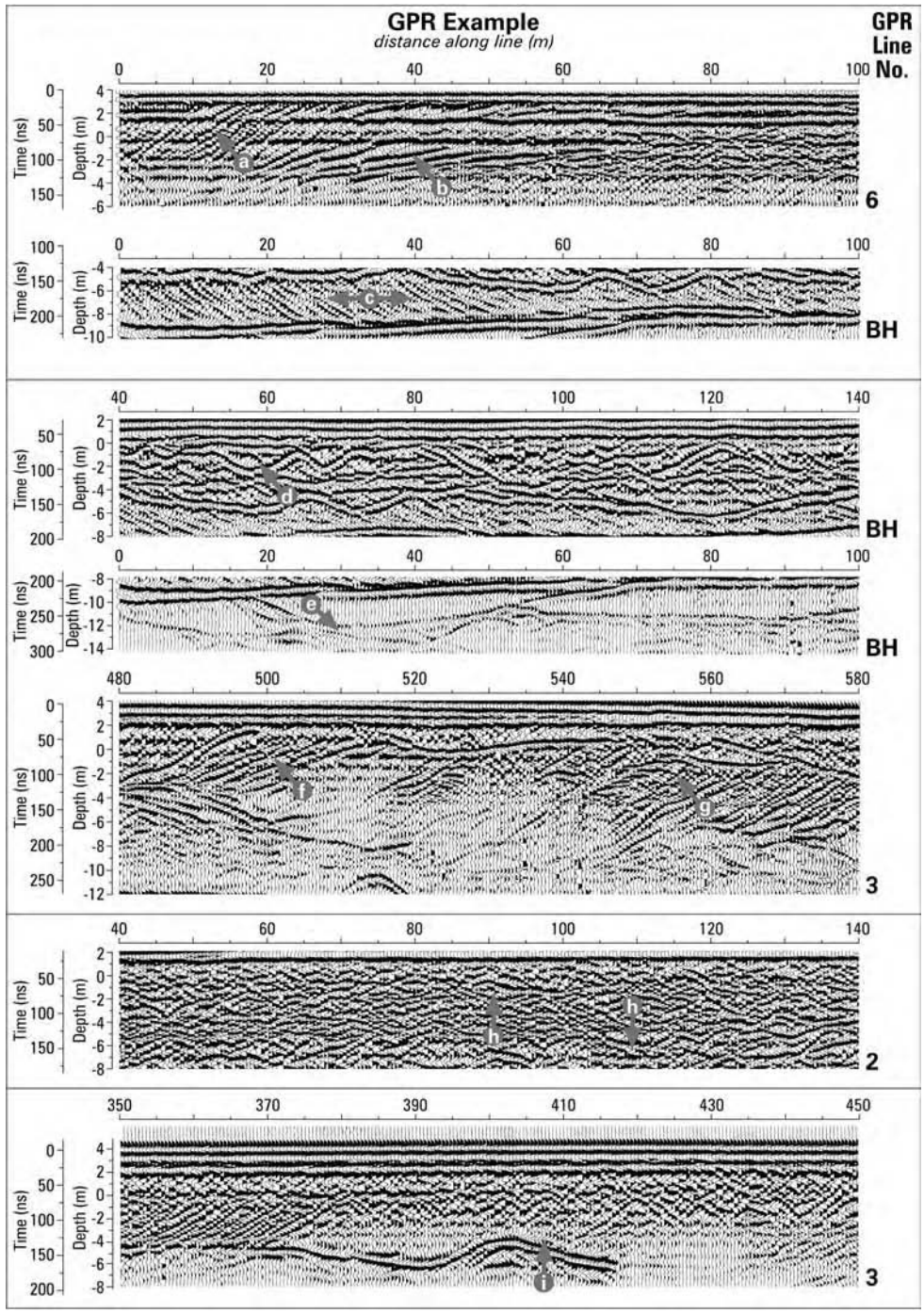

Figure 19.22 *Continued*

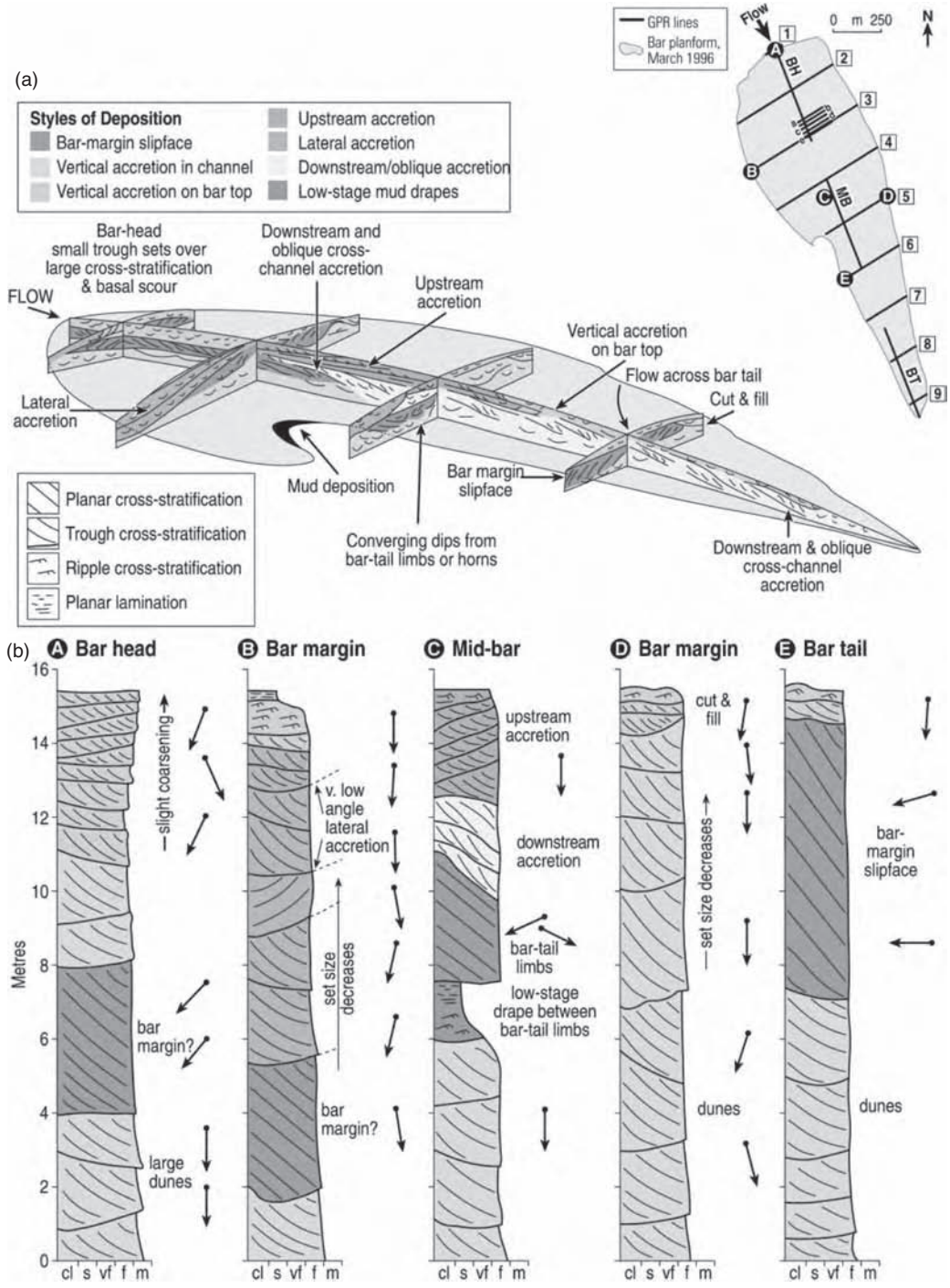

Figure 19.23 (See also colour plates.) Styles of deposition and vertical facies profiles for a mid-channel bar in the Jamuna River. (a) Three-dimensional diagram of the principal styles of deposition quantified within the Jamuna braid-bar (see text for details). The scale of the bar is 3 km long, 1 km wide and 12–15 m high. The different styles of deposition are coloured and the main sedimentary structures are labelled. (b) Schematic sedimentary logs at five localities within the large braid bar (see inset for location), illustrating the characteristic sedimentary structures, large-scale bedding surfaces, and styles of deposition (see a). Arrows depict the approximate flow directions for sedimentary structures at various heights in each profile, with flow down the page (e.g., profile A, bar head at 2 m) indicating flow parallel to the mean flow direction (see arrow on inset location map). Deviations in flow from this direction are shown, such as the oblique, cross-channel movement of the bar-margin slipface (e.g. profile E, bar-tail at 8.5 m). Reprinted from Journal of Sedimentary Research, Vol. 73, Best *et al*. Three-dimensional sedimentary architecture of a large mid-channel sand braid bar, Jamuna River, Bangladesh, pp. 516–530, 2003, with permission from SEPM (Society for Sedimentary Geology)

in response to dune stacking over the bar-top in shallow flows. The upstream accretion surfaces were separated by small-scale sets of trough cross-stratification, and mirror the observations of bar-top deposition by Bristow (1993a) (Figures 19.23 and 19.24).

5. Lateral accretion: this was documented on one side at the upstream end of the bar studied by Best *et al*. (2003) and attributed to deposition during the falling stage of the hydrograph as flow was diverted around the bar-head. Lateral accretion surfaces were separated by trough cross-stratification generated by small, three-dimensional dunes.
6. Downstream/oblique accretion: occurred on the central and downstream regions of the bar, representing downstream and oblique accretion of dunes across the bar, forming complex downstream-dipping surfaces.
7. Mud drapes: present as low-stage, fine-grained drapes that develop in the bar lee where fine-grained silt and clay are deposited from suspension.

Apart from this model of deposition within the entire braid bar, Bristow (1993a) presents a model of bar-top sedimentation in the Jamuna (Figure 19.24) which matches well with the later GPR surveys of Best *et al*. (2003) and is characterized by: (1) upstream accretion on the upstream part of the bar-top, that is formed from trough cross-stratification and rare upper-stage plane beds. The upstream part of the bar-top was found to sometimes be erosional with cantilever bank failures; and (2) the central section of the bar-top was characterized by both vertical and lateral accretion, containing dune-scale trough cross-stratification, upper-stage plane beds, and ripple cross-lamination. Bristow (1993a) proposed a characteristic vertical sequence of upper stage plane beds to trough cross-stratification and then ripple lamination, which reflects declining flow velocities and increasing aggradation rates within these bar-top sediments. The downstream ends of the bar-top were found to be more variable in composition, with dunes and scroll-bars (unit bars) migrating around the downstream bar margin (see also model of braid bar growth, Figure 19.15). Bristow (1993a) found that the downstream bar margins may become steepened to form avalanche faces and that flow separation/reduced velocities in the bar-lee can lead to deposition of current ripples and fine-grained drapes. Bristow (1993a) also highlights the role of falling-stage modification in forming

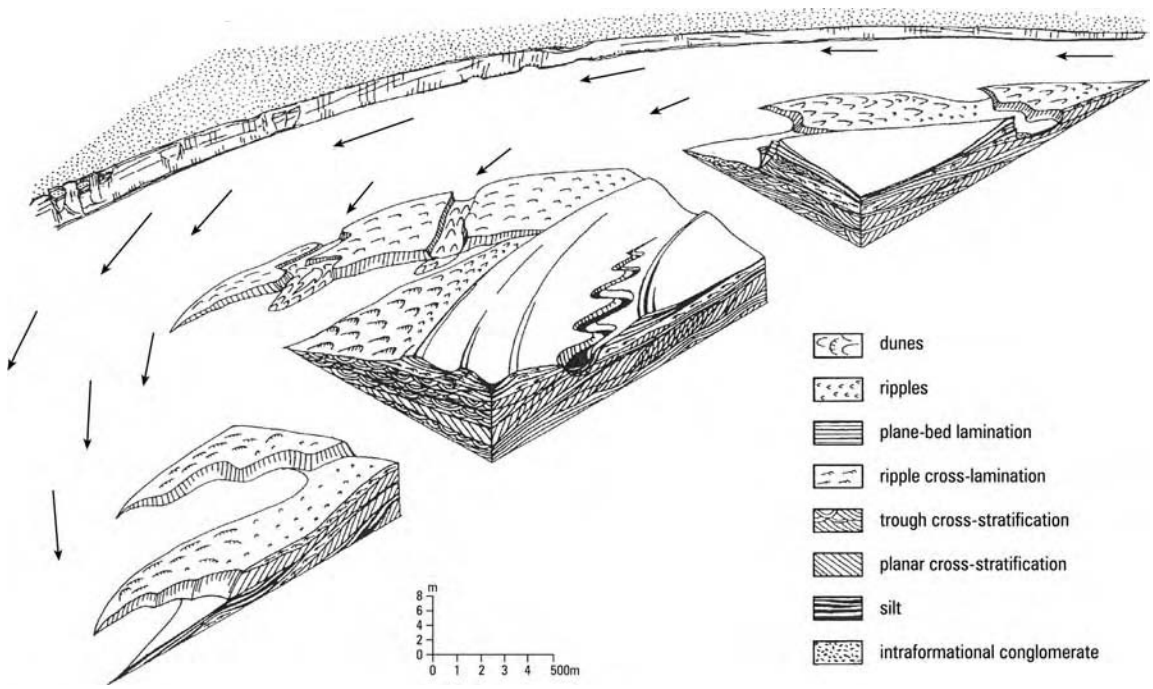

Figure 19.24 Facies model for bar-top deposition in the Jamuna River. Reprinted from Braided Rivers, Eds Best, J.L. and Bristow, C.S., Bristow, C.S. Sedimentary Structures in Bar Tops in the Brahmaputra River, Bangladesh, pp. 277–289, 1993, with permission from Geological Society of London

bar-top channels, with low-stage flow being unable to rework the bar-surface.

Recently, Sambrook-Smith *et al*. (2005) have considered the morphology and depositional facies of a range of braided rivers, including the Jamuna River, and have found that the surface planform morphology of braid bars, and the maximum relative depth of confluence scour, displayed a scale invariance over many different types and sizes of braided river. They also concluded that the subsurface sedimentary facies of three sandy braided rivers, which covered a twofold order of magnitude in channel width, exhibited a degree of scale invariance with the ubiquitous occurrence of trough cross-stratification associated with migrating dunes. However, the occurrence of bar-margin, high-angle planar cross-stratification and low-angle stratification was variable both between rivers and between bars within the same river. Sambrook-Smith *et al*. (2005) concluded that the relative presence of these two facies within the stratigraphy is related to a wide range of factors, including the discharge regime, local bar/channel topography, the channel width : depth ratio and the presence and abundance of vegetation. Hence, although the models described above for the Jamuna may share common characteristics with many other braided rivers, much work remains to be conducted to document and quantify the full range of depositional facies within large sandy braided rivers, especially in bars that are a complex product of successive periods of erosion and deposition.

Figure 19.25 Large-scale slab failure by bank undercutting near Shailabari (~4 km upstream of Sirajganj). Photograph taken at low flow. During seasonal floods the water level would be up to bankfull

19.7 APPLIED GEOMORPHOLOGY AND ENGINEERING IN THE JAMUNA RIVER

The Jamuna is one of the most dynamic rivers in the World with little to stop sustained channel migration, bank erosion, bar creation and destruction. The banks of the Jamuna have limited deep-rooted, permanent vegetation to bind together the weakly cohesive sand and silts, and there is commonly less than 1% clay (FAP24, 1996h). Bank erosion is usually through large-scale slab failure due to toe scouring (Figure 19.25), and blocks may disintegrate rapidly into their primary particles after failure so there is no potential for temporary stabilization of the bank through the accumulation of bank failure debris at the toe (Thorne *et al*., 1993). With the potential for up to 3 months of bankfull discharge each year, it is often difficult to conceptualize how any 'soft' or 'hard' engineering works can stop significant scour and bank erosion occurring on the Jamuna. Indeed, a report for the Bangladesh Government on the impact of the 2004 flood stated 'a number of the protection systems built over the six years since the last major floods have just failed' (BDER, 2004). However, there have been notable engineering successes in preventing bank erosion and flooding occurring at certain important strategic sites on the Jamuna.

An ambitious and relatively successful engineering scheme has been construction of the Brahmaputra Right Embankment (BRE) from the Teesta to Hurasagar confluences (Figure 19.1) that was built in the 1960s. Although the BRE has been breached on several occasions and has had to be 'retired' (replaced with a new section of embankment set back from the river edge) in at least 14 locations on the Jamuna (Thorne *et al*., 1993, Figure 12: p. 273), the original embankment or original alignment of the BRE is still in place.

Another example is the construction of the first, and at present only, bridge to span the Jamuna, the Bangabandhu Bridge (Figure 19.26a), 5 km south of Sirajganj (see Figures 19.1 and 19.26). The bridge cost about US$550 million to build and was completed in June 1998. It is 4.8 km long

with 49 spans and used 80 m long piles driven 60 m into the river bed. The deck is 18.5 m wide with four road lanes and has a wide-gauge railway track and also a 600 mm diameter gas pipeline attached underneath. Concrete pylons above carry power and telecommunication lines. The Bangabandhu Bridge is located at a position where the Jamuna braidbelt narrows (Figure 19.26b). Construction of arcuate embankments on the east bank and on a large mid-channel island, termed 'guide bunds' (labelled E1 and E2, Figure 19.26b), has been used to ensure the majority of the discharge is constricted within a narrow zone of the braidbelt as well as protecting the bridge from being outflanked by flood waters. Whilst the bridge has successfully withstood several years of high flows, including the largest flood of the twentieth century in 1998, the bridge site requires continual and sustained river engineering management. The annual sequence of satellite images up to 2007 for the bridge site shows sustained erosion of the floodplain in front of the eastern bund that protects the bridge and approach road (Figures 19.26c–h). The main channel has been right up against this bund since 2002 (Figure 19.26c) and a menacing bend developed 1 km upstream and caused erosion upstream of the nose of the eastern bund, which without engineering works could result in the outflanking of the bridge. Likewise, channel changes since 2002 have led to development of an aggressive main channel upstream of the western bund, and have formed a bar with lateral accretion (labelled a in Figure 19.26g,h) that is promoting severe outer bend erosion adjacent to, and upstream from, the western guide bund (labelled e in Figure 19.26g,h). Again, without upstream engineering works there is a danger that the western bund will be outflanked and the western approach road threatened. Although the design of the western guide bund considered the hard point at Sirajganj (see below) as capable of preventing west bank erosion, close monitoring of the morphological development of the channels in the vicinity of the Bangabandhu Bridge is clearly essential in the forthcoming years.

Certain sites of strategic interest on the Jamuna have been protected by construction of concrete revetments and groynes [e.g. Kamarjani, Bahadurabad (FAP21 site), Kalitola/Sariakandi/Mathurapara (known collectively as B1)]. One of the largest fixed, hard engineering structures on the Jamuna is at Siraganj (location in Figure 19.1; see also Figure 19.26b–h) where a 2 km long embankment was constructed at an approximate cost of US$65 million to protect the large ferry terminal and market town. Estimates suggested that without protection, one third of Sirajganj would disappear in 5 years and the entire settlement by 10 years. The embankment, termed the 'B2 hardpoint' (labelled B2 in Figure 19.26b), was constructed of a ridge of locally dredged river sand and silt covered by a plastic and geotextile membrane, then superimposed by broken bricks and topped with 0.45 m^3 or 0.65 m^3 concrete blocks (Figure 19.27a,b). Although largely successful, the B2 hardpoint suffered a major failure during the 1998 flood season when construction was 94% complete. A 32 m deep scour hole developed immediately downstream of the hardpoint 'nose' and caused collapse of at least four sections of the embankment. Repair costs were estimated in excess of US$10 million. Although now repaired and functioning well, the scale and cost of the damage that was inflicted on the B2 hardpoint illustrates the power of the Jamuna and the magnitude of the problem faced by river engineers and geomorphologists working in such a dynamic alluvial environment. The damage was caused by migration of the channel upstream of the hardpoint that changed the angle at which the channel approached the structure: this altered the flow dynamics at the nose of the hardpoint, triggering large-scale flow separation at the nose, and generated greatly enhanced scour. The 2004 satellite image for the Sirajganj area (Figure 19.26e) shows the B2 structure was threatened by an aggressively

Figure 19.26 (See also colour plates.) (a) Westward view across the only bridge that spans the Jamuna – the Bangabandhu Bridge; (b)–(f) The Bangabandhu Bridge site at (b) low flow 1999 after bridge completion; (c–f) development of the channel morphology during 2000–2005. In (b), labels E1 and E2 refer to the arcuate embankments, termed 'guide bunds', upstream of the Bangabandhu Bridge, and label B2 indicates the nose of the B2 hardpoint at Sirajganj. Label x in (e) points to the groyne at Shailabari that was eroded during the 2004 flood, and subsequently led to extensive erosion of the west bank in this vicinity (see label y in f). Label a in (g) and (h) indicates lateral accretion and bar growth that is causing erosion (labelled e) of the western channel bank. In (g) and (h), label z points to the mid-channel bar growth and lateral accretion upstream of the B2 structure that is causing bank erosion (labelled r)

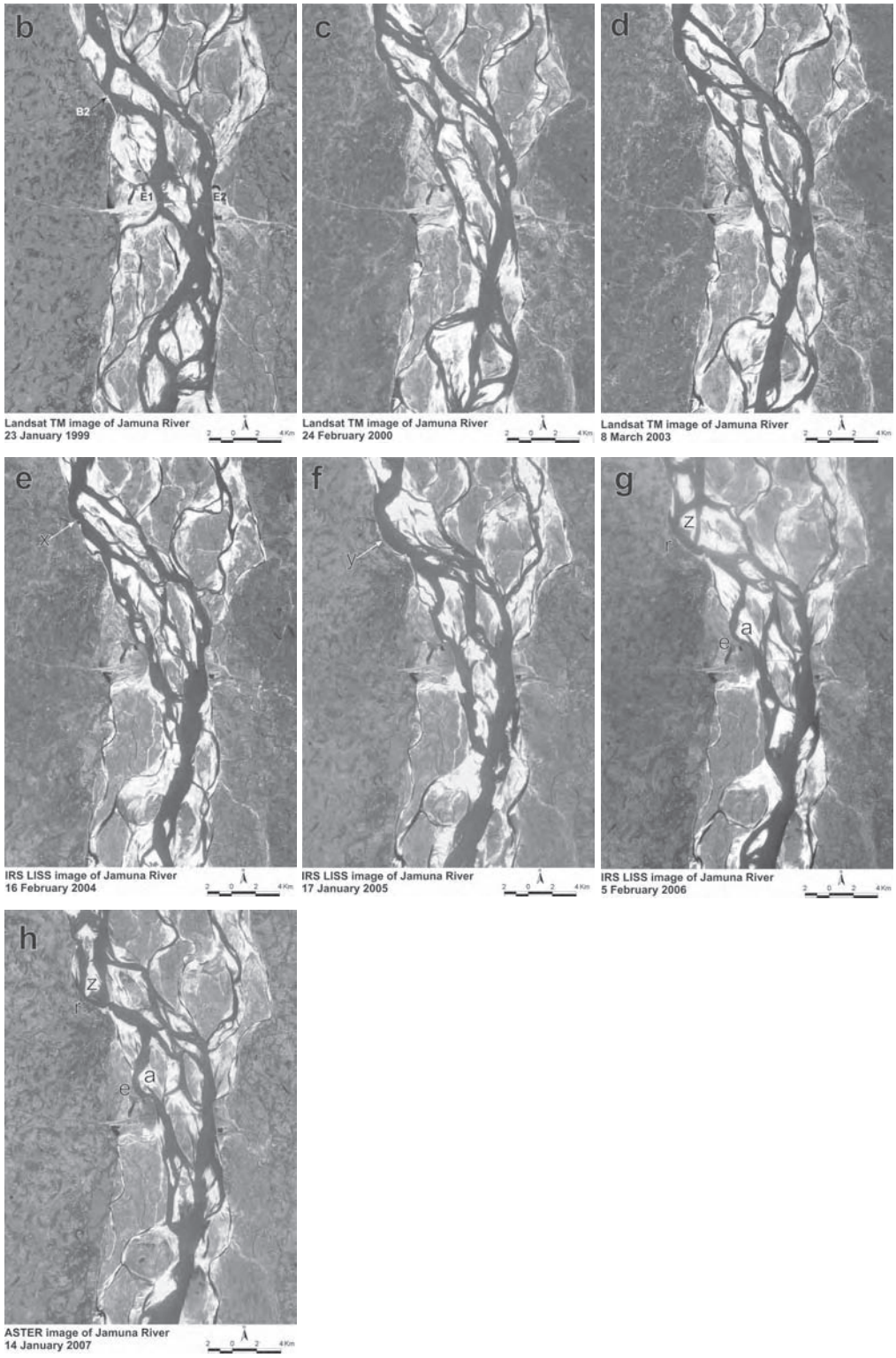

Figure 19.26 *Continued*

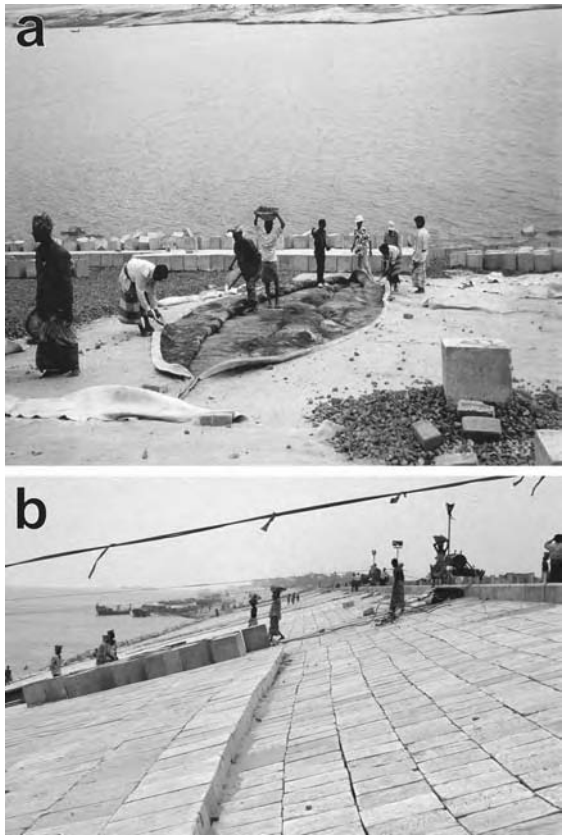

Figure 19.27 Construction of the B2 hardpoint at Sirajganj showing (a) dredged river silt covered with geotextile membrane filter, then covered by broken brick and concrete cubes (photograph courtesy of Mr Bob Courtier, W.S. Atkins Ltd) and (b) 0.45 m^3 concrete blocks in place, view looking downstream from the hardpoint 'nose'

eroding bend that was migrating down the west bank of the Jamuna braidplain. In 2004, this bend was about 2 km upstream of the B2 embankment, and eroding the protruding groyne at Shailabari (labelled x in Figure 19.26e). This groyne was built in the late 1970s but failed and was washed away on 19 May 2004 (see 2005 image; Figure 19.26f). Aggressive erosion of the west bank subsequently occurred during the 2004 flood season, with up to 750 m of bank retreat (labelled y in Figure 19.26f), and erosion in this region now threatens the B2 structure. Lateral growth and migration of the mid-channel bar on its western edge (labelled z in Figure 19.26g,h) in 2006 and 2007 has caused further erosion of the western bankline of the channel upstream of the B2 structure (Figure 19.26g,h), with erosion now occurring along the bankline to the west of the B2 hardpoint (labelled r), that in 1999 (Figure 19.26b) was 1.1 km from the major channel. The problems experienced at the B2 embankment highlight that it is essential to document both modern process and longer-term planform behaviour/evolution of the river channels when planning the construction of major, permanent structures on the Jamuna.

As well as fixed engineering structures, a complementary form of river management now being employed on the Jamuna is to predict how the channel may evolve and migrate and then attempt to mitigate any potential damage and plan for a change in local infrastructure and environment (e.g. irrigation, housing, transport). Building on the work first developed under FAP21/22, EGIS (2002) have produced a series of empirical 'laws' or 'rules' for channel planform prediction based on over a decade of observations from dry season satellite images. Three sets of empirical relationships have been derived that predict the probability of: (1) channel abandonment of curved channels, (2) the migration rate of bifurcations around bars and islands, and (3) the annual rate of bank erosion along the outer channels of the Jamuna that are adjacent to the floodplain. These empirical predictions presented by EGIS (2002) are reliant on the identification of a series of key 'sedimentary features' or barforms that are seen as fundamental to the morphological development of the Jamuna planform – EGIS (2002) term these contraction bars, sharpened bars, sand wings, sand tongues and bankside bars. Figure 19.28 shows an example flow chart that may be used to predict the rate of bank erosion on the outer banks of the Jamuna. The empirical prediction depends strongly on the presence/absence of a bar ('sedimentary feature') downstream of the channel and the radius of curvature of the channel (ratio of the radius of the outer bank of the curved channel to the low flow width of the channel). Data on channel radius of curvature, channel width, and rate of annual bank erosion were derived from Landsat images for the period 1992–2000 to build upon earlier data reported by Klaassen and Masselink (1992) and Klaassen *et al*. (1993).

Recently, EGIS were subcontracted by Sir William Halcrow and Partners to predict movements of the Jamuna River and associated braid bars adjacent to the strategically important Pabna Irrigation and Rural Development Project (PIRDP) that is 20 km upstream of the Jamuna-Ganga confluence on the western bank. In February 2002, the Jamuna had an anabranch that was attacking the west-bank immediately downstream of the Hurasagar tributary mouth and was around 200 m away from the embankment that protects the irrigation channels and the nearby Kaitola Pump House (Figure 19.29). Using the empirical relations for forecasting morphological

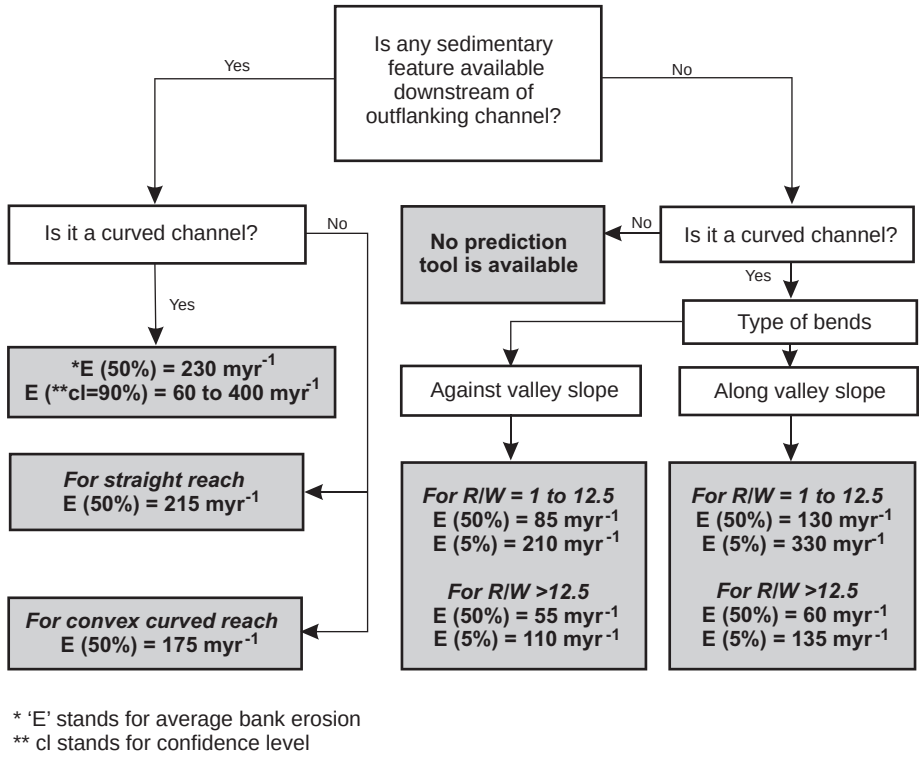

Figure 19.28 Flow diagram for predicting bank erosion along the outflanking channels of the Jamuna River. Data were obtained from 213 bends from sequential dry-season satellite images from 1992 to 2000. R and W are the radius of curvature to the outer bank line and the channel wetted width at low flow, respectively. Reprinted from EGIS, Developing and updating the empirical methods for predicting the morphological changes in the Jamuna River, 2002, with permission from CEGIS

development of the Jamuna outlined above (EGIS, 2002), CEGIS produced a series of predictions over the 2002 flood season for channel and bar development upstream and adjacent to the PIRDP (Table 19.2). A Landsat image taken at low flow in March 2003 (Figure 19.29) gives an indication of the success of the predictions of channel change. Every feature of morphological change predicted in February 2002 occurred in March 2003. Only the magnitude of bank erosion up and downstream of the Hurasagar tributary was outside the confidence limit of the empirical predictions (Table 19.2). The early success of this project illustrates both the great value of developing a large, historical database of morphological change on the Jamuna, and how it may be possible to predict channel change in even the largest and most mobile of sand-bed braided rivers. Such studies, when combined with more detailed understanding and modelling of the controlling flow processes, hold great potential for helping to maintain bank protection structures and select suitable sites for further construction in key areas along the river.

19.8 SUMMARY

The Brahmaputra-Jamuna is one of the World's truly great rivers and forms a dynamic and highly variable alluvial environment that has a huge impact on the daily lives of the growing population of Bangladesh. The past decade has seen a massive increase in our knowledge of the behaviour of this dynamic river, and a growing realization that a holistic management approach is required to plan for, cope with, and benefit from floods. The early and naïve plans for large-scale engineering works along the Jamuna (see reviews in Hossain, 1994; Yakub, 1994) have been shown to be inappropriate from a community and environmental perspective, let alone considerations of costs, but have set the agenda for some key schemes and approaches that have borne great benefits. Although the Flood Action Plan has had many critics and the nature of FAP has changed greatly over the years (see papers in Haggart *et al*., 1994), hindsight now shows many highly valuable products of the FAP projects, including both a

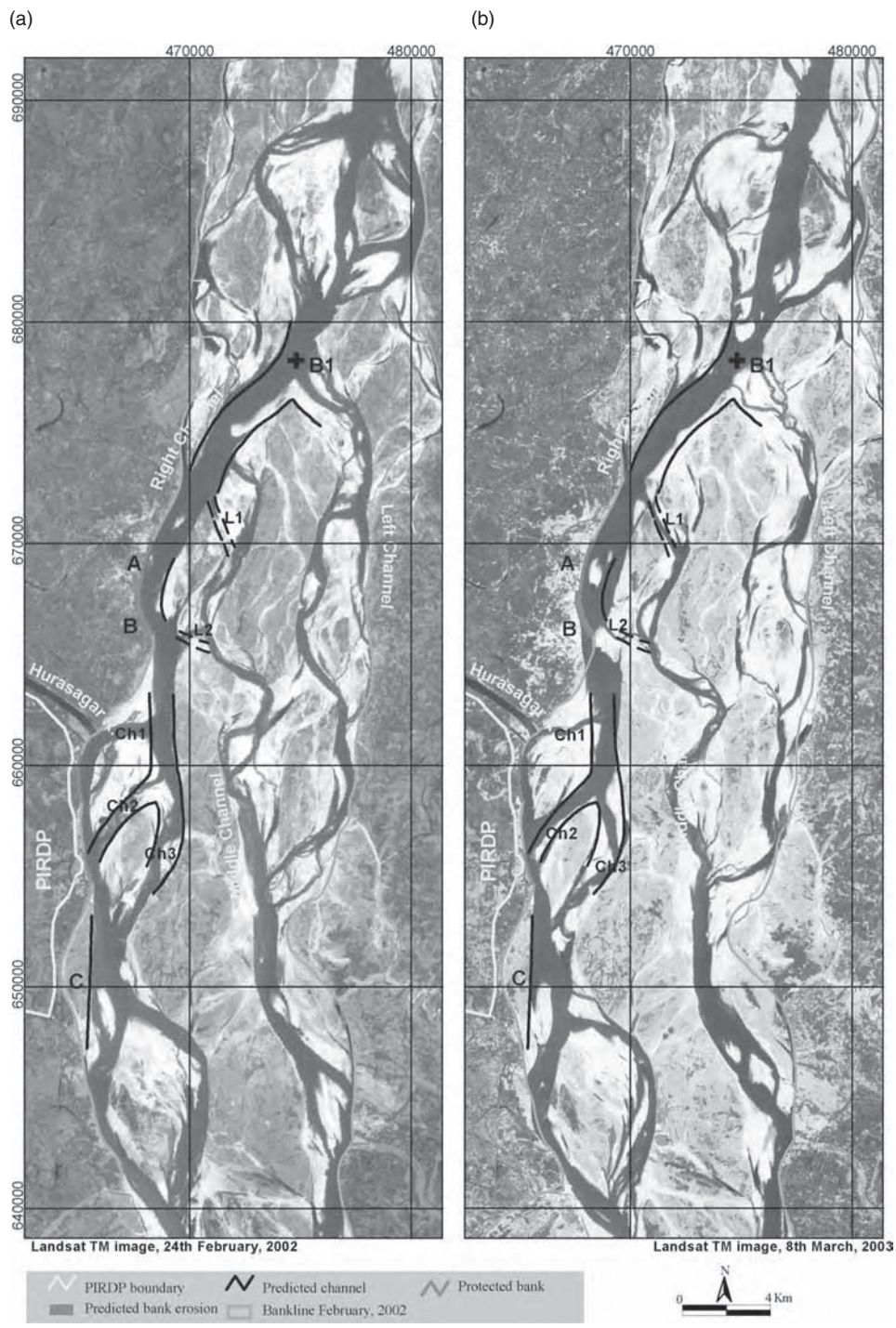

Figure 19.29 (See also colour plates.) Satellite images of the Jamuna River at the PIRDP site near the confluence with the Hurasagar River taken in (a) February 2002 and (b) March 2003, showing the predicted channel and bankline changes (a) and the resultant changes after the flood season (b) (see also Table 19.2). Reprinted from EGIS, Morphological analyses and prediction for the Jamuna River around the PIRDP site, 2003, with permission from CEGIS

Table 19.2 Predicted morphological changes in the region of the Hurasagar River junction and observations after the 2002 monsoon flood (adapted from CEGIS, 2003)

Key points of prediction made in February 2002	Observations in March 2003
The left channel will continue to decline and the high rate of bank erosion (>100 year^{-1}), along the left bank upstream of bifurcation B1, will enhance this process	The outflanking channel upstream of the bifurcation B1 eroded the floodplain more than 200 m and the decline in the left channel continued
The offtake of the middle channel will be abandoned. Consequently, either both, or any one, of the link channels L1 and L2 will be developed	The offtake was abandoned and the link channel L1 has developed
Severe bank erosion along bend B will continue	The maximum bank erosion was 500 m and bend-averaged erosion was 250 m, which was higher than the predicted erosion
Channel 1 will be abandoned, but before that a substantial amount of bank erosion within the range of 100 m is expected to occur in the area immediately downstream of the Hurasagar River junction, which will pose a threat to the embankment of the PIRDP	Channel 1 is nearly abandoned, and before infilling the channel eroded ~50 m in the immediate area downstream of the confluence of the Hurasagar River
Continuation of Channel 2 is likely. Attack of the flow may concentrate close to the Kaitola Pump House, threatening bank protection measures as well as the embankment	Channel 2 is continuing and the channel size increased (see Figure 19.29b). The attack of the flow was concentrated close to the Kaitola Pump House

far improved understanding of the processes and dynamics of the rivers of Bangladesh (Jagers, 2003), and establishment of long-lived remote sensing and field survey that has led to better predictive tools for assessing channel change (EGIS, 2002). This will be increasingly important in key infrastructural protection works, such as the Bangabandhu Bridge and the proposed bridges across the Dhaleswari and Padma, and also in allowing better assessment of the impact of future river planform change, such as the potential movement of the Jamuna into the channel of the Bangali River, near Sariakandi and Mathurapara (Figure 19.1). On a larger spatial and temporal scale, Bangladesh faces many challenges in coping with changing water resources dictated by decisions taken outside its borders, and the potential effects of climatic change on the monsoon and sea-level. The past decade has shown the immense benefits of using a multidisciplinary approach to studying these large rivers in Bangladesh. With the successful and continued development of infrastructure and expertise in Bangladesh [e.g. CEGIS, Institute of Water Modelling (IWM)], working in close collaboration with Government policy (i.e. WARPO), the future for assessing, predicting and managing river channel change should become more sustainable and environmentally acceptable.

ACKNOWLEDGEMENTS

We are very grateful to a wide range of organizations and individuals who have fostered, aided and enthused our interests and research in Bangladesh over the past decade. We are pleased to acknowledge the logistical and financial support of Delft Hydraulics and the Danish Hydraulics Institute as main contractors of the Flood Action Plan 24, the Flood Plan Coordinating Organization (FPCO) as client and the European Union as funding agency for FAP24. We are indebted to Gerrit Klaassen, Johan Grijsen, Maarten van der Wal, Hans Høyer, Dilip J. Barua, Zahirul Khan and Kim Kyle for their considerable advice and support in the FAP24 River Survey Project, together with Captain Monjoor and the crew of DH survey vessel-A, whose skill and dedication in the field were central to the success of our projects. Part of the work conducted by JLB, PJA and JR was funded by the UK Natural Environment Research Council through grant GR9/02034 and a NERC studentship to Roden, for which we are extremely grateful. We would also like to acknowledge and sincerely thank the Center for Environmental and Geographic Information Services (CEGIS) for their assistance and provision of several of the Landsat images used in this paper. The David Rumsey map collection is thanked for permission to reproduce Rennell's beautiful 1776 map (access to a wide range of historical maps can be found at www.davidrumsey.com). Full colour diagrams and further details of the ground-penetrating radar studies are available at http://www.sepm.org/jsr/data_files/2003_data/2003_data.asp. JLB gratefully acknowledges award of a Leverhulme Trust Research Fellowship that provided the time for this paper to be written and

completed, and Marcelo García at the Ven Te Chow Hydrosystems Laboratory, University of Illinois at Urbana-Champaign, for generous provision of facilities during this fellowship. We are grateful to David Appleyard and Alison Manson for their preparation of some of the figures and we would like to thank Chris Fielding for his thorough review of the manuscript. Finally, we are very grateful to Avijit Gupta for his invitation to write this chapter, his review comments, and his continuing enthusiasm and encouragement to complete it, which have allowed us the opportunity to synthesize some of the more recent work on this most beautiful and inspirational river.

REFERENCES

Ahmed, K.M., Bhattacharya, P. Hasan, M.A., Akhter, S.H., Alam, S.M.M., Bhuyian, M.A.H., Imam, M.B., Khan, A.A. and Sracek, O. (2004) Arsenic enrichment in groundwater of the alluvial aquifers in Bangladesh: an overview, *Applied Geochemistry*, 19, 181–200.

Alam, M. (1984) Other natural hazards. In: *Rivers of Life* (Eds Haggart, K., Huq, S., Rahman, A.A., Haq, E., Majumder, M.K. and Miranda, C.), Bangladesh Centre for Advanced Studies, Dhaka and Panos, 151–170.

Alam, M.K., Hasan, A.K.M.S., Khan, M.R. and Whitney, J.W. (1990) *Geological Map of Bangladesh*, Geological Survey of Bangladesh.

Allison, M.A. (1998) Geologic framework and environmental status of the Ganges-Brahmaputra River, *Journal of Coastal Research*, 14, 826–836.

Allison, M.A., Kuehl, S.A., Martin, T.C. and Hassan, A. (1998) The importance of floodplain sedimentation for river sediment budgets and terrigenous input to the oceans: insights from the Brahmaputra-Jamuna Rivers, *Geology*, 26, 175–178.

ASCE (1966) Nomenclature for bed forms in alluvial channels. Task Force on Bedforms in Alluvial Channels, *Proceedings of the American Society of Civil Engineers, Journal of the Hydraulics Division*, 92, 51–64.

Ashworth, P.J. (1996) Mid-channel bar growth and its relationship to local flow strength and direction. *Earth Surface Processes and Landforms*, 21, 103–123.

Ashworth, P.J., Best, J.L., Roden, J.E., Bristow, C.S. and Klaassen, G.J. (2000) Morphological evolution and dynamics of a large, sand braid-bar, Jamuna River, Bangladesh. *Sedimentology*, 47, 533–555.

Bangladesh Disaster and Emergency Sub-Group (BDER) (2004) *Monsoon Floods 2004: Post Flood Needs Assessment Summary Report*, 36 pp, Dhaka, Bangladesh (see http://www.reliefweb.int/w/rwb.nsf/0/0601496727bb568ac1256f230033fbc5 and http://www.reliefweb.int/library/documents/2004/lcg-bang-6oct.pdf).

Barua, D.K. (1994) On the environmental controls of Bangladesh river systems, *Asia Pacific Journal on Environment and Development*, 1, 81–98.

Begum, S. and Fleming, G. (1997a) Climate change and sea level rise in Bangladesh, Part I: numerical simulation, *Marine Geodesy*, 20, 33–53.

Begum, S. and Fleming, G. (1997b) Climate change and sea level rise in Bangladesh, Part II: effects, *Marine Geodesy*, 20, 55–68.

Best, J.L. (1996) The fluid dynamics of small-scale alluvial bedforms. In: *Advances in Fluvial Dynamics and Stratigraphy* (Eds Carling, P.A. and Dawson, M.R., John Wiley & Sons, Ltd, Chichester, 67–125.

Best, J.L. (2005) The kinematics, topology and significance of dune-related macroturbulence: some observations from the laboratory and field. In: *Fluvial Sedimentology VII* (Eds Blum, M.D., Marriott, S.B. and Leclair, S.), Special Publication of the International Association of Sedimentologists, No. 35, Blackwell, Oxford.

Best, J.L. and Ashworth, P.J. (1997) Scour in large braided rivers and the recognition of sequence stratigraphic boundaries, *Nature*, 387, 275–277.

Best, J.L. and Kostaschuk, R.A. (2002) An experimental study of turbulent flow over a low-angle dune, *Journal of Geophysical Research*, 107, 3135–3153.

Best, J.L., Kostaschuk, R.A. and Villard, P.V. (2001) Quantitative visualization of flow fields associated with alluvial sand dunes: results from the laboratory and field using ultrasonic and acoustic Doppler anemometry, *Journal of Vizualization*, 4, 373–381.

Best, J.L., Ashworth, P.J., Bristow, C.S. and Roden, J.E. (2003) Three-dimensional sedimentary architecture of a large, mid-channel sand braid bar, Jamuna River, Bangladesh, *Journal of Sedimentary Research*, 73, 516–530.

Bora, A.K. (2004) Fluvial geomorphology. In: *The Brahmaputra Basin Water Resources* (Eds Singh, V.P., Sharma, N. and Ojha, C.S.P.), Kluwer Academic Publishers, Dordrecht, 88–112.

Boyce, J.K. (1990) Birth of a megaproject: political economy of flood control in Bangladesh, *Environmental Management*, 14, 419–428.

Bridge, J.S. (1993) The interaction between channel geometry, water flow, sediment transport and deposition in braided rivers. In: *Braided Rivers* (Eds Best, J.L. and Bristow, C.S.), Special Publication of the Geological Society of London, No. 75, London, 13–71.

Bridge, J.S. and Lunt, I. (2006) Depositional models of braided rivers. In: *Braided Rivers: Process, Deposits, Ecology and Management* (Eds Sambrook Smith, G.H., Best, J.L., Bristow, C.S. and Petts, G.), Special Publication of the International Association of Sedimentologists, No. 36, Blackwell, Oxford, 11–50.

Bristow, C.S. (1987) Brahmaputra River: channel migration and deposition. In: *Recent Developments in Fluvial Sedimentology* (Eds Ethridge, F.G., Flores, R.M. and Harvey, M.D.), Special Publication of the Society of Economic Palaeontologists and Mineralogists, No. 39, Tulsa, OK, 63–74.

Bristow, C.S. (1993a) Sedimentary structures in bar tops in the Brahmaputra River, Bangladesh. In: *Braided Rivers* (Eds Best, J.L. and Bristow, C.S.), Special Publication of the Geological Society of London, No. 75, London, 277–289.

Bristow, C.S. (1993b) Sedimentology of the rough rock: a Carboniferous braided river sheet sandstone in northern England. In: *Braided Rivers* (Eds Best, J.L. and Bristow, C.S.), Special Publication of the Geological Society, No. 75, 291–304.

Bristow, C.S. (1999) Avulsion, river metamorphosis and reworking by underfit streams: a modern example from the Brahmaputra River in Bangladesh and a possible ancient example in the Spanish Pyrenees. In: *Fluvial Sedimentology 6* (Eds Smith, N.D. and Rogers, J.), Special Publication of the International Association of Sedimentologists, No. 28, 221–230.

Burger, J.W., Klaassen, G.J. and Prins, A. (1988) Bank erosion and channel processes in the Jamuna River, Bangladesh, *Proceedings of the International Symposium on the Impact of River Bank Erosion, Flood Hazard and the Problem of Population Displacement*, Dhaka, Bangladesh, 1–17.

Cant, D.J. and Walker, R.G. (1978) Fluvial processes and facies sequences in the sandy braided South Saskatchewan River, Canada. *Sedimentology*, 25, 625–648.

Center for Environmental and GIS Support Project for Water Sector Planning (CEGIS) (2003) *Morphological Analyses and Prediction for the Jamuna River around the PIRDP Site*, Prepared for Jamuna-Meghna River erosion Mitigation Project, BWDB, Dhaka, Bangladesh.

Centre for Policy Dialogue (CPD) (2004) *Rapid Assessment of Flood 2004: Interim Report*, August 12 2004, Dhaka, 47 pp. (see http://www.cpd-bangladesh.org/flood.pdf and http://www.cpd-bangladesh.org).

Choudhury, A.M., Haque, M.A. and Quadir, D.A. (1997) Consequences of global warming and sea level rise in Bangladesh, *Marine Geodesy*, 20, 13–31.

Chowdhury, M. (1994) Fisheries. In: *Rivers of Life* (Eds Haggart, K., Huq, S., Rahman, A.A., Haq, E., Majumder, M.K. and Miranda, C.), Bangladesh Centre for Advanced Studies, Dhaka and Panos, 95–120.

Chowdhury, M.R. (2000) An assessment of flood forecasting in Bangladesh: the experience of the 1998 flood, *Natural Hazards*, 22, 139–169.

Coleman, J.M. (1969) Brahmaputra River: channel processes and sedimentation, *Sedimentary Geology*, 3, 129–239.

de Graaf, G. (2003) The flood pulse and growth of floodplain fish in Bangladesh, *Fisheries Management and Ecology*, 10, 241–247.

Environmental and GIS Support Project for Water Sector Planning (EGIS) (1997) *Morphological Dynamics of the Brahmaputra-Jamuna River*. Prepared for Water Resources Planning Organization, Dhaka, Bangladesh, 76 pp.

Environmental and GIS Support Project for Water Sector Planning (EGIS) (2000) *Remote Sensing, GIS and Morphological Analyses of the Jamuna River, 2000, Part II*, Dhaka, Bangladesh.

Environmental and GIS Support Project for Water Sector Planning (EGIS) (2002) *Developing and Updating the Empirical Methods for Predicting the Morphological Changes in the Jamuna River*, EGIS Technical Note Series 29, Dhaka, Bangladesh.

Flood Action Plan 24; Delft Hydraulics and DHI (1996a) *FAP24 River Survey Project, Final Report, Main Volume* (prepared for FPCO), Dhaka, Bangladesh, 280 pp.

Flood Action Plan 24; Delft Hydraulics and DHI (1996b) *FAP24 River Survey Project, Final Report – Annex 3: Hydrology* (prepared for FPCO), Dhaka, Bangladesh.

Flood Action Plan 24; Delft Hydraulics and DHI (1996c) *FAP24 River Survey Project, Final Report – Annex 4: Sedimentology*, (prepared for FPCO), Dhaka, Bangladesh.

Flood Action Plan 24; Delft Hydraulics and DHI (1996d) *FAP24 River Survey Project, Final Report – Annex 5: Morphological Characteristics* (prepared for FPCO), Dhaka, Bangladesh.

Flood Action Plan 24; Delft Hydraulics and DHI (1996e) *FAP24 River Survey Project, Special Report 6, Floodplain levels and bankfull discharge* (prepared for FPCO), Dhaka, Bangladesh.

Flood Action Plan 24; Delft Hydraulics and DHI (1996f) *FAP24 River Survey Project, Special Report 10, Morphology of the Gorai Offtake* (prepared for FPCO), Dhaka, Bangladesh, 158 pp and Appendices.

Flood Action Plan 24; Delft Hydraulics, DHI and Leeds University (1996g) *FAP24 River Survey Project, Special Report 9, Bedform and bar dynamics in the main rivers of Bangladesh* (prepared for FPCO), Dhaka, Bangladesh, 107 pp.

Flood Action Plan 24; Delft Hydraulics and DHI (1996h) *FAP24 River Survey Project, Special Report 14, Physical properties of river sediments* (prepared for FPCO), Dhaka, Bangladesh, 36 pp.

Flood Plan Coordinating Organisation (FPCO) (1995) *Bangladesh Water and Flood Management Strategy*, FPCO, Dhaka, Bangladesh, 22 pp.

Fujita, Y. (1989) Bar and channel formation in braided streams. In: *River Meandering* (Eds Ikeda, S. and Parker, G.), Water Research Monograph, No. 12, American Geophysical Union, Washington, DC, 417–462.

Goodbred Jr, S.L. and Kuehl, S.A. (2000a) The significance of large sediment supply, active tectonism, and eustasy on sequence development: Late Quaternary stratigraphy and evolution of the Ganges-Brahmaputra delta, *Sedimentary Geology*, 133, 227–248.

Goodbred Jr, S.L. and Kuehl, S.A. (2000b) Enormous Ganges-Brahmaputra sediment load during strengthened early Holocene monsoon, *Geology*, 27, 559–562.

Goodbred Jr, S.L., Kuehl, S.A., Steckler, M.S. and Sarker, M.H. (2003) Controls on facies distribution and stratigraphic preservation in the Ganges-Brahmaputra delta sequence, *Sedimentary Geology*, 155, 301–316.

Haggart, K., Huq, S., Rahman, A.A., Haq, E., Majumder, M.K. and Miranda, C. (Eds) (1994) *Rivers of Life*, Bangladesh Centre for Advanced Studies, Dhaka, and Panos, 244 pp.

Heroy, D.C., Kuehl, S.A. and Goodbred Jr, S.L. (2003) Mineralogy of the Ganges and Brahmaputra rivers: implications for river switching and Late Quaternary climate change, *Sedimentary Geology*, 155, 343–359.

Hofer, T. and Messerli, B. (2006) *Floods in Bangladesh: History, Dynamics and Rethinking the Role of the Himalayas*, United Nations University Press, Tokyo, 468 pp.

Hossain, M.M. (1993) Economic effects of riverbank erosion: some evidence from Bangladesh, *Disasters*, 17, 25–32.

Hossain, M. (1994) Existing embankments. In: *Rivers of Life* (Eds Haggart, K., Huq, S., Rahman, A.A., Haq, E., Majumder, M. K. and Miranda, C.), Bangladesh Centre for Advanced Studies, Dhaka and Panos, 51–76.

Islam, M.R., Begum, S.F., Yamaguchi, Y. and Ogawa, K. (1999) The Ganges and Brahmaputra rivers in Bangladesh: basin denundation and sedimentation, *Hydrological Processes*, 13, 2907–2923.

Islam, N. (2001) The open approach to flood control: the way to the future in Bangladesh, *Futures*, 33, 783–802.

ISPAN (FAP 16 and FAP 19), (1993) *The Dynamic Physical and Human Environment of Riverine Charlands: Jamuna*, Dhaka, Bangladesh.

ISPAN (FAP 16 and FAP 19) (1995) *A Study of Sedimentation in the Brahmaputra-Jamuna Floodplain*, Dhaka, Bangladesh.

Jackson, R.G. (1976) Sedimentological and fluid-dynamic implications of the turbulence bursting phenomenon in geophysical flows, *Journal of Fluid Mechanics*, 77, 531–560.

Jagers, H.R.A. (2003) *Modelling planform changes of braided rivers*, PhD thesis, University of Twente, The Netherlands, 313 pp.

Julien, P.Y. and Klaassen, G.J. (1995) Sand-dune geometry of large rivers during flood, *Journal of Hydraulic Engineering*, 121, 657–663.

Kattelman, R. (1990) Conflicts and cooperation over floods in the Himalaya-Ganges region, *Water International*, 15, 189–194.

Khan, N.I. and Islam, A. (2003) Quantification of erosion patterns in the Brahmaputra-Jamuna River using geographical information system and remote sensing techniques, *Hydrological Processes*, 17, 959–966.

Klaassen, G.J. and Vermeer, K. (1988) Confluence scour in a large braided river with fine bed material. *Proceedings of the International Conference on Fluvial Hydraulics*, Budapest, Hungary, International Association of Hudraulic Research, Budapest, 395–408.

Klaassen, G.J and Masselink, G. (1992) Planform changes of a braided river with fine sand as bed and bank material, *Proceedings of the 5th International Symposium on River Sedimentation* (Eds Larson, P. and Eisenhauer, N.E.), Karlsruhe, Germany, 459–471.

Klaassen, G.J., Vermeer, K. and Uddin, N. (1988) Sedimentological processes in the Jamuna (Lower Brahmaputra) river, Bangladesh. *Proceedings of the International Conference on Fluvial Hydraulics*, Budapest, Hungary, 381–394.

Klaassen, G.J., Mosselman, E. and Brühl, H. (1993) On the prediction of planform changes of braided sand-bed rivers. In: *Advances in Hydroscience and Engineering* (Ed. Wang, S.S.Y.), University of Mississippi, Washington, DC, 134–146.

Kostaschuk, R. and Villard, P. (1996) Flow and sediment transport over large subaqueous dunes: Fraser River, Canada, *Sedimentology*, 43, 849–863.

La Touche, T.H.D. (1910) Relics of the great Ice Age in the plains of northern India, reprinted (1919). In: *Report on the Hooghly River and its Head waters*, The Bengal Secretariat Book Depot, Calcutta, v. I, 21–22.

Leopold, L.B. and Wolman, M.G. (1957) River channel patterns: braided, meandering and straight, *Professional Paper United States Geological Survey*, 262-B, 51 pp.

McLelland, S.J., Ashworth, P.J., Best, J.L., Roden, J.E. and Klaassen, G.J. (1999) Flow structure and transport of sand-grade suspended sediment around an evolving braid-bar, Jamuna River, Bangladesh. In: *Fluvial Sedimentology 6* (Eds Smith, N.D. and Rogers, J.), Special Publication of the International Association of Sedimentologists, No. 28, 43–57.

Miall, A.D. and Jones, B.G. (2003) Fluvial architecture of the Hawkesbury Sandstone (Triassic), near Sydney, Australia. *Journal of Sedimentary Research*, 73, 531–545.

Mirza, M.M.Q. (2002) Global warming and changes in the probability of occurrence of floods in Bangladesh and implications, *Global Environmental Change*, 12, 127–138.

Mirza, M.M.Q. (Ed.) (2004) *The Ganges Water Diversion: Environmental Effects and Implications*, Kluwer Academic Publishers, Dordrecht, 367 pp.

Mirza, M.M.Q., Warrick, R.A., Ericksen, N.J. and Kenny, G.J. (2001) Are floods getting worse in the Ganges, Brahmaputra and Meghna basins?, *Environmental Hazards*, 3, 37–48.

Morgan, J.P. and McIntire, W.G. (1959) Quaternary geology of the Bengal Basin, East Pakistan and India, *Bulletin of the Geological Society of America*, 70, 319–342.

Mosselman, E. (2006) Bank protection and river training along the braided Brahmaputra-Jamuna River, Bangladesh. In: *Braided Rivers: Process, Deposits, Ecology and Management* (Eds Sambrook Smith, G.H., Best, J.L., Bristow, C.S. and Petts, G.), *Special Publication of the International Association of Sedimentologists*, 277–288, No. 36, Blackwell, Oxford.

Ogink, H.J.M. (1988) *Hydraulic roughness of bedforms*, Delft Hydraulics Report M2017.

Ojha, C.S.P. and Singh, V.P. (2004) Introduction. In: *The Brahmaputra Basin Water Resources*, (Eds Singh, V.P., Sharma, N. and Ojha, C.S.P.), Kluwer Academic Publishers, Dordrecht, 1–16.

Parsons, D.R., Best, J.L. Lane, S.N., Kostaschuk, R., Orfeo, O. and Hardy, R.J. (2005) The morphology and flow fields of 3D dunes, Rio Paraná, Argentina: results from simultaneous multibeam echo sounding and acoustic Doppler profiling, *Journal of Geophysical Research, Earth Surface*, 110, F04503, doi: 10.1029/2004JF00231.

Patel, T. (1996) Bridge over troubled water, *New Scientist*, November, 12–13.

Paul, B.K. (1997) Flood research in Bangladesh in retrospect and prospect: a review, *Geoforum*, 2, 121–131.

Reavill, L.R.P. and Rahman, T.G. (1995) A systems-science-based analysis of the factors that influence and aggravate the effects of flooding in Bangladesh, *Technological Forecasting and Social Change*, 49, 89–101.

Rennell, J.J. (1776) *An actual survey of the provinces of Bengal, Bahar etc. by Major General James Rennell, Surveyor to the Honourable East India Company* (as referenced in Bristow, 1999).

Richardson, W.R.R. and Thorne, C.R. (1998) Secondary currents around braid bar in Brahmaputra River, Bangladesh, *Journal Hydraulic Engineering*, 124, 325–328.

Richardson, W.R.R. and Thorne, C.R. (2001) Multiple thread flow and channel bifurcation in a braided river: Brahmaputra-Jamuna River, Bangladesh, *Geomorphology*, 38, 185–196.

Richardson, W.R.R., Thorne, C.R. and Mahmood, S. (1996) Secondary flow and channel changes around a bar in the Brahmaputra River, Bangladesh. In: *Coherent Flow Structures in Open Channels* (Eds Ashworth, P.J., Bennett, S.J., Best, J.L. and McLelland, S.J.), John Wiley & Sons, Ltd, Chichester, 520–543.

Roden, J.E. (1998) *Sedimentology and dynamics of mega-sand dunes, Jamuna River, Bangladesh, PhD thesis*, University of Leeds, 310 pp.

Sambrook Smith, G.H., Ashworth, P.J., Best, J.L., Woodward, J. and Simpson, C.J. (2005) The morphology and facies of sandy braided rivers: some considerations of scale invariance. In: *Fluvial Sedimentology VII* (Eds Blum, M.D., Marriott, S.B. and Leclair, S.), International Association of Sedimentologists, Blackwell, Oxford, 145–158.

Sambrook Smith, G.H., Ashworth, P.J., Best, J.L., Woodward, J. and Simpson, C.J. (2006) Alluvial architecture and sedimentology of the sandy braided South Saskatchewan River, Canada, *Sedimentology*, 53, doi: 10.1111/j.1365–3091.2005.00769.x.

Sarker, M.H. (1996) *Morphological processes in the Jamuna River, MSc thesis*, International Institute for Hydraulic and Environmental Engineering, Delft, The Netherlands, 175 pp.

Sarker, M.H. and Thorne, C.R. (2006) Morphological response of the Brahmaputra-Padma-Lower Meghna River system to the Assam earthquake of 1950. In: *Braided Rivers: Process, Deposits, Ecology and Management* (Eds Sambrook Smith, G.H., Best, J.L., Bristow, C.S. and Petts, G.), Special Publication of the International Association of Sedimentologists, No. 36, Blackwell, Oxford, 289–310.

Sarker, M.H., Huque, I., Alam, M. and Koudstaal, R. (2003) Rivers, chars, and char dwellers of Bangladesh, *International Journal of River Basin Management*, 1, 61–80.

Schumm, S.A. and Winkley, B.R. (1994) The character of large alluvial rivers. In: *The Variability of Large Alluvial Rivers* (Eds Schumm, S.A. and Winkley, B.R.), American Society of Civil Engineers, New York, 1–13.

Seijmonsbergen, A.C. (1999) The influence of neo-tectonics on river patterns in Bangladesh; a preliminary study based on Landsat MSS imagery, *Geologie en Mijnbouw*, 77, 129–135.

Shankar, B., Halls, A. and Barr, J. (2004) Rice versus fish revisited: on the integrated management of floodplain resources in Bangladesh, *Natural Resources Forum*, 28, 91–101.

Singh, S.K. (2007) Erosion and weathering in the Brahmaputra River system. In: *Large Rivers: Geomorphology and Management* (Ed. A. Gupta), John Wiley & Sons, Ltd, Chichester, 373–393.

Singh, V.P., Sharma, N. and Ojha, C.S.P. (Eds) (2004) *The Brahmaputra Basin Water Resources*, Kluwer Academic Publishers, Dordrecht, 632 pp.

Smith, J.D. and McLean, S.R. (1977) Spatially-averaged flow over a wavy surface, *Journal of Geophysical Research*, 82, 1735–1746.

Takagi, T., Oguchi, T., Matsumoto, J., Grossman, M.J., Sarker, M.H. and Matin, M.A. (2007) Channel braiding and stability of the Brahmaputra River, Bangladesh, since 1967: GIS and remote sensing analyses, *Geomorphology*, 85, 294–305.

ten Brinke, W.B.M., Wilbers, A.W.E. and Wesseling, C. (1999) Dune growth, decay and migration rates during a large-magnitude flood at a sand and mixed sand-gravel bed in the Dutch Rhine river system. In: *Fluvial Sedimentology VI* (Eds Smith, N.D. and Rogers, J.), Special Publication of the International Association of Sedimentologists, No. 28, 15–32.

Thorne, C.R. and Thiagarajah, R.I. (1994) Discussion of 'Twelth Hunter Rouse Hydraulic Engineering Lecture: Future Trends and Needs in Hydraulics', *Journal of Hydraulic Engineering*, 120, 672–676.

Thorne, C.R., Russell, A.P.G., Alam, M.K. (1993) Planform pattern and channel evolution of the Brahmaputra River, Bangladesh. In: *Braided Rivers* (Eds Best, J.L. and Bristow, C.S.), Special Publication of the Geological Society of London, No. 75, 257–276.

Umitsu, M. (1993) Late Quaternary sedimentary environments and landforms in the Ganges delta. *Sedimentary Geology*, 83, 177–186.

Winkley, B.R., Lesleighter, E.J. and Cooney, J.R. (1994) Instability problems of the Arial Khan River Bangladesh. In: *The Variability of Large Alluvial Rivers* (Eds Schumm, S.A. and Winkley, B.R.), ASCE Press, New York, 269–284.

Wood, G. (1999) Contesting water in Bangladesh: knowledge, rights and governance, *Journal of International Development*, 11, 731–754.

Yakub, N.N. (1994) Overview. In: *Rivers of Life* (Eds Haggart, K., Huq, S., Rahman, A.A., Haq, E., Majumder, M.K. and Miranda, C.), Bangladesh Centre for Advanced Studies, Dhaka and Panos, 1–30.

Yalin, M.S. (1992) *River Mechanics.* Pergamon Press, Oxford, 219 pp.

20

The Mekong River: Morphology, Evolution, Management

Avijit Gupta

School of Geography, University of Leeds, Leeds LS2 9JT, UK and Centre for Remote Imaging, Sensing and Processing, National University of Singapore, Singapore 119260

20.1 INTRODUCTION

The 4880 km long Mekong flows in a northwest–southeast trending pan-shaped basin that drains into the South China Sea (Figure 20.1). The handle of the pan extends into China, where the river rises at an elevation of nearly 5000 m in Qinghai to flow through the highlands of eastern Tibet and Yunnan. Downstream of China, the rest of the basin covers parts of Myanmar, Thailand, Lao People's Democratic Republic, Cambodia, and Vietnam. A summary of the dimensions of the basin and river is given in Table 20.1.

For approximately 3000 km the Mekong runs on rock through narrow valleys in mountainous regions. The next 1000 km is on both rocks and alluvium and steep mountainous slopes are never far away. Only for the last 600 km of river length, this large river runs freely on alluvium in a 500 km wide lowland that converges to a large delta.

In the past a series of kingdoms and states have functioned in the basin. The existence of a first century CE seaport that traded with Roman coins and objects that originated in West Asia and the Indian subcontinent was revealed by archaeological excavations at Oc Eo on the edge of the delta west of the Bassac distributary. Chinese records described a state called Funan in the Mekong Delta that functioned between the second and the sixth centuries. Subsequent Chinese records described a two-part state, Chenla, probably covering the present Cambodia and the region around Wat Phu in southern Lao PDR. The Khmer Empire, which built the fabulous Angkor group of temples during the ninth to fifteenth centuries, existed for almost a thousand years. A series of stupendous structures were built during this period along with an irrigation system capable of supporting agriculture that carried an empire with large settlements. A population of more than 1 million has been estimated for the city of Angkor when London had less than 35 000 (Osborne, 2000). The capital at Angkor was abandoned under repeated attacks from the west by the Siamese army in the mid-fifteenth century for the new city of Phnom Penh (the current capital of Cambodia) on the west bank of the Mekong.

Governance in the basin lapsed into a number of smaller states, usually under some kind of hegemony of the bigger regional powers: Burma, China, and Siam. This was also the time of arrival of European traders and travellers in large numbers. Ultimately, almost the entire lower Mekong Basin was occupied by France and constituted part of French Indochina. The river with an inner channel cut in rock, transverse rock ribs, and a series of waterfalls near the present Lao PDR–Cambodia border never became an integrated waterway serving the basin. An illustrated and detailed account of the river has been left by a French expedition that travelled upriver from the delta to Yunnan between 1866 and 1868 (Osborne, 1975; Delaporte and Garnier, 1998). The final discovery of the river's source, however, was not achieved until 1994 (Peissel, 1997). The present-day Vietnam, Cambodia, and Lao PDR came into

Large Rivers: Geomorphology and Management, Edited by A. Gupta

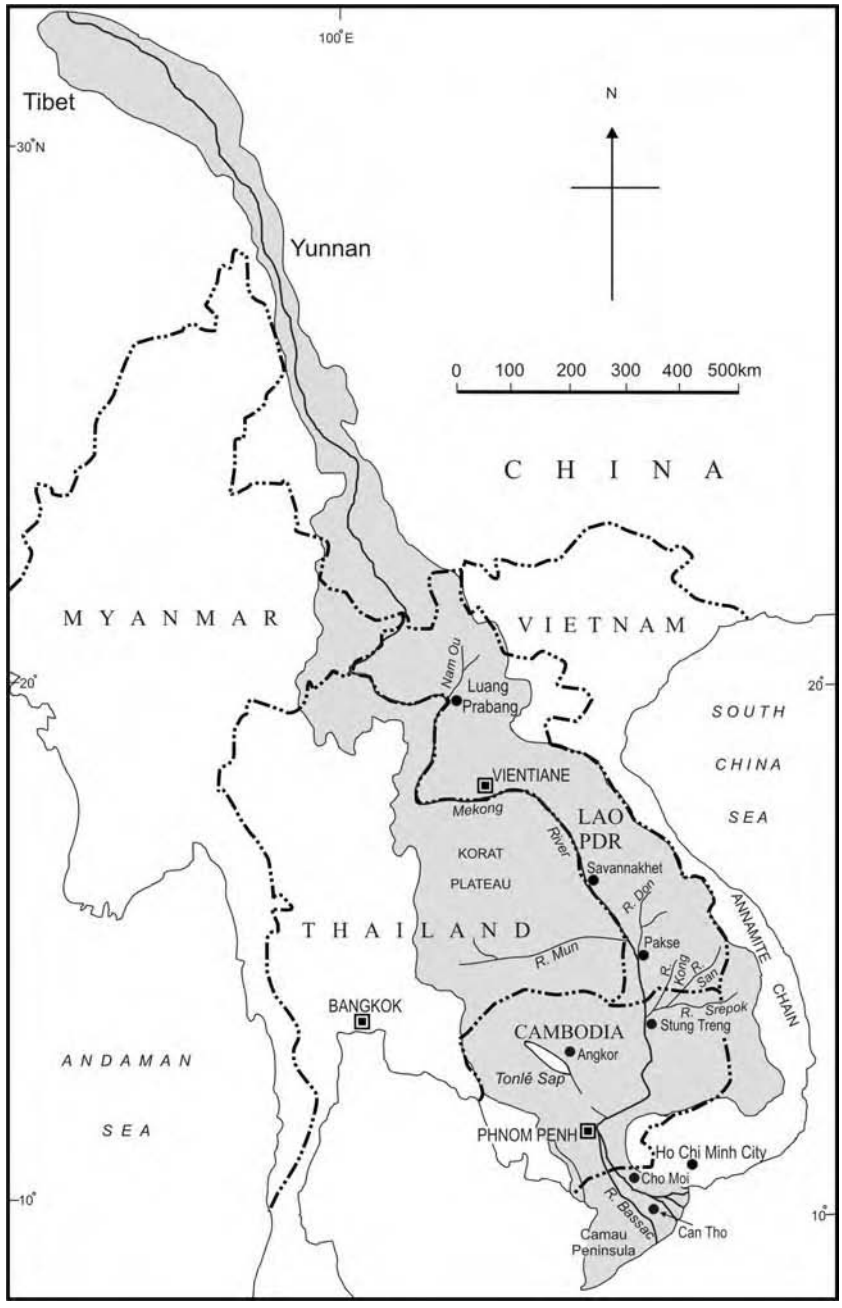

Figure 20.1 Location map

Table 20.1 Dimensions of the Mekong

Characteristics	Measurement	World rank
Basin area	795 000 km^2	21
Channel length	4 880 km	12
Volume of mean annual discharge at mouth	475×10^9 m^3	9
Mean discharge	15 000 m^{3}s^{-1}	8
Average annual suspended sediment discharge	160×10^6 t	10

Sources: Meade, 1996; Mekong River Commission, various publications.

existence after a series of post World War II hostilities. The basin has continued to be predominantly rural, being densely populated only in certain areas, such as the Mekong Delta. The Mekong Committee was convened in 1957 under the aegis of the United Nations to plan the development of the river in a multi-state basin. In 1995, this organization was reconstituted as the Mekong River Commission.

The Mekong has a number of striking characteristics. For a river of its size, it is remarkably structure-guided and flows on rock in a narrow valley for nearly 80% of its length. It has formed a large delta. The flow of the river is strongly seasonal in character. The basin is predominantly rural with a generally low population density. The first bridge over the lower Mekong was constructed only in 1994. It is a multi-state basin, but by consent of the riparian states, its development is planned in a structured fashion by an international agency (see Chapter 27). As demand for development grows and engineered barriers and improved navigation are planned for the river, the role of such an organization may turn out to be more and more essential.

20.2 THE MEKONG BASIN

20.2.1 Geology

The geology of the Mekong Basin is patchily known in the public domain and locally complicated (Figure 20.2). The valley probably opened up due to extrusion tectonics associated with the collision of the Indian Plate with the Eurasian one leading to the uplift of the Himalaya Mountains (Tapponier *et al*., 1982; Tapponier *et al*., 1986; Peltzer and Tapponier, 1988). The upper basin in China is a narrow valley, several kilometres wide, cut into granitic and sedimentary rocks of Palaeozoic and Mesozoic age. From the Chinese border almost up to Vientiane in Lao PDR, basin lithology consists of granitic rocks, folded Palaeozoic sedimentary and metamorphic rocks (sandstone, slate, schist, chert, limestone), Mesozoic sedimentary deposits (sandstone, limestone, evaporites), and local volcanic exposures. Basic and ultrabasic rocks, associated with an ancient suture zone, also occur in the area. A deposit of Quaternary alluvium stretches across the river over older rocks in the Vientiane area. Immediately downstream of this alluvium, mainly Mesozoic sandstones and evaporites are found. These rocks emerge from below a thin layer of alluvium to form numerous rock ribs in the channel of the Mekong. Downstream, volcanic rocks are exposed near the Lao PDR–Cambodia border (Choubert and Faure-Muret, 1976; ESCAP, 1990). In Cambodia the river flows over an alluvium of variable thickness, with local exposures of Triassic sedimentary rocks and Neogene basalts near the river, rocks that occur on the highlands that form the divides. In its lowermost reach, the Mekong flows on thick alluvium.

Such geology explains the deep valley of the Mekong in China and Lao PDR, with long reaches along structural lines and short ones cutting across such lineations. For part of its course in the mountains of China and Lao PDR, the Mekong runs parallel to and along several large faults. The alluvial fill of the lower Mekong lowland in Cambodia and Vietnam probably covers the pre-existing structure of the Tonlé Sap Graben (Hutchison, 1989). Grabens and half-grabens have been recognized in Thailand giving rise to Tertiary basins (Lorenzetti *et al*., 1994). It is likely that the Mekong had to adjust to such basins across its drainage area. The present delta postdates the wide shifting of the coastline during the Pleistocene. Details of the evolutionary history of the Mekong still remain an unknown and fascinating story.

20.2.2 Relief

In Yunnan (China) the Mekong flows in a narrow valley with steep side slopes. The gradient is steep, the river is in rock, and the satellite images show a channel partly filled with sediment. The accelerated sediment accumulation is probably associated with the destruction of natural vegetation and prevalence of landslides on the slopes. Further south, the mountainous Mekong Basin in Lao PDR and north Thailand is a collection of dissected, narrow-crested, near-parallel ridges separated by deep valleys (Figure 20.3). The peaks may rise to 1500–2000 m and the valley bottoms, within several kilometres, drop to around 1000 m. The hillslopes are steep, locally exceeding 25°, and eroded by mass movements. The V-shaped tributary valleys are in places transformed into narrow gorges. Dissected steep cliffs of limestone locally overlook the Mekong and its major tributaries. The Annamite Chain of mountains forms the steep eastern divide between Vietnam

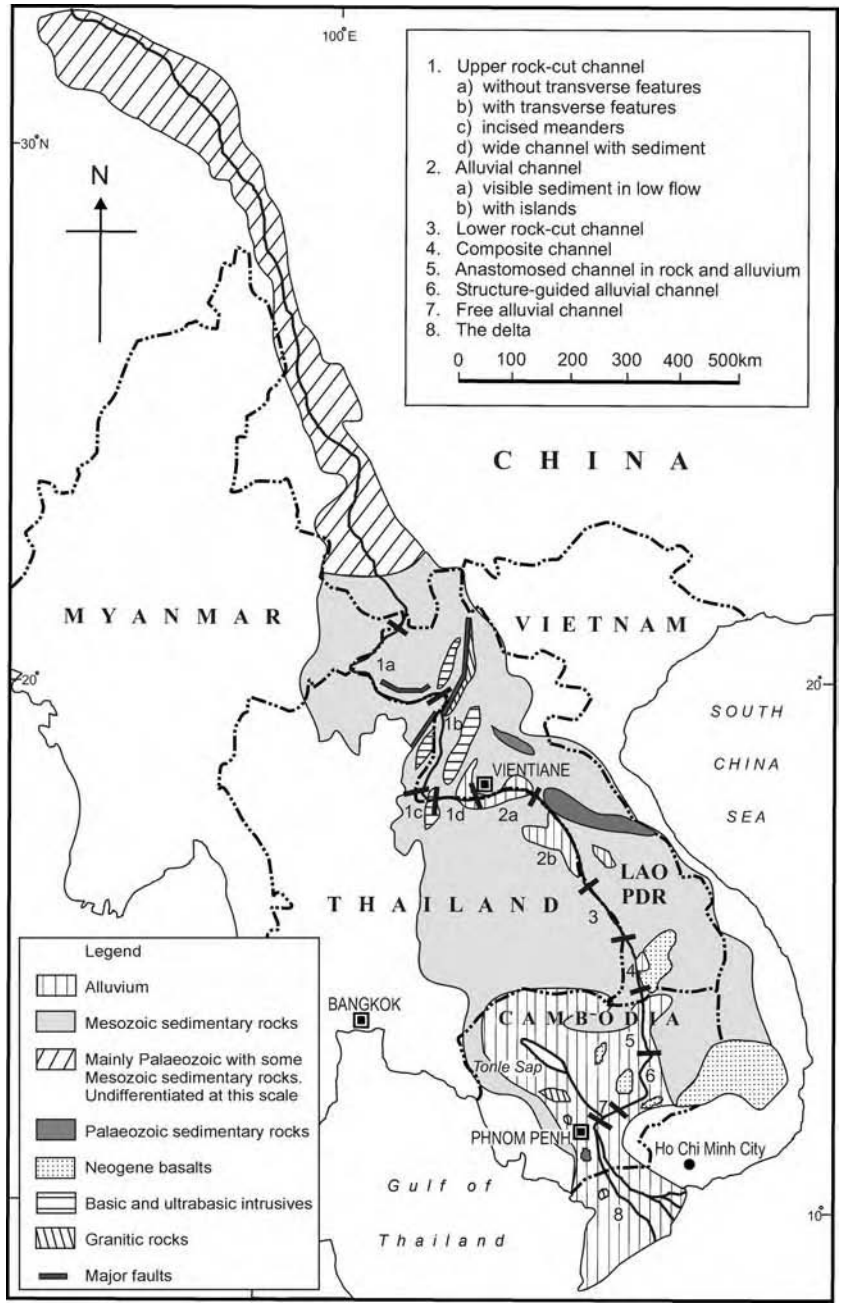

Figure 20.2 Map showing generalized basin geology and the river units

Figure 20.3 The Mekong, flowing through a narrow valley at Luang Prabang, with very little accommodation pace for sediment outside the channel. Photograph Avijit Gupta

and Lao PDR or Cambodia, with peaks rising to 2000 m along almost its entire length. Large streams (Don, Kong, San, Srepok) have eroded the Annamite Chain and built alluvial fans where they emerge onto the plains. In contrast, much of the western divide is gentle, marked by low ridges on top of the 200–500 m high Korat Plateau of Thailand. This is the area drained on gentle gradients by the Mun River and its tributaries. South of the Korat Plateau, the western divide continues as the small but steep Cardamom and Elephant Hills of Cambodia, which come abruptly to the sea at the northwestern corner of the Mekong Delta.

In the middle of mountainous northern Lao PDR, the narrow steep valley of the Mekong widens and flattens near Vientiane to form an area of low relief roughly coinciding with the two regions of alluvium deposition shown in Figure 20.2. The valley floor elevation is already below 200 m, about 1500 km from the sea. The valley narrows and steepens downstream beyond the alluvium and alternates between narrow valleyflats sharply demarcated between two ranges of hills and wider flat stretches where tributaries join the Mekong. Only where the river is about 600 km from the sea, the plain next to the Mekong channel abruptly widens to 500 km between the two divides, with isolated low rocky hills emerging from below this wide alluvial cover. An extension of this plain up to the Elephant Hills forms a westward embayment south of the Korat Plateau. Drainage from this embayment collects in the large lake of Tonlé Sap. The area of the lake changes seasonally. It is connected to the Mekong by the Tonlé Sap River, which reverses its flow depending on the season and the stage height of the Mekong. The Tonlé Sap River joins the Mekong near Phnom Penh, close to where, about 330 km from the sea, the first deltaic distributary, the Bassac, separates from the main river. Downstream from Phnom Penh, the delta stretches south from Cambodia to Vietnam.

20.2.3 Hydrology

The average precipitation over the part of the basin south of China has been calculated to be 1672 mm (MRC, 1997). The amount drops below 1000 mm over China to the north and the Korat Plateau to the west. In contrast, annual rainfall is high over the northern and eastern basin (2000–4000 mm), especially over parts of the Annamite Chain. The rain is strongly seasonal and associated with the southwest monsoon, 85–90 % falling between June and October.

The hydrologic data used in this paper are from the *Lower Mekong Hydrologic Yearbooks* of the Mekong River Commission, which are published each year. The Commission currently operates 125 gauging stations in the Mekong Basin downstream of the Chinese border, including 33 gauges along the river. Discharge is measured at 10 of the 33 stations. The rest maintain stage records. The length of record is quite long for several stations. For example, the daily discharge record for the Mekong at Vientiane goes back to January 1913. Stage heights with some gaps are available for another two decades.

The annual flow of the Mekong reflects the seasonality in precipitation. The river rises a little in May following the arrival of summer snowmelt from the Tibetan Plateau, but 80 % of the annual discharge occurs between June and November (Figure 20.4), 20–30 % may arrive in a single month. Large floods tend to occur late in the wet season, tailing off very slowly. The arrival time of the flood peak changes in the downstream direction. In Thailand and northern Lao PDR the bigger annual floods tend to arrive in August. This becomes September in Cambodia, and is likely to be October in the delta in Vietnam (MRC, 1997). Large floods, inundating thousands of square kilometres across the lower basin (Figure 20.5) and occurring late in the wet season, are often triggered by the arrival of tropical storms over the Annamite Mountains when the Mekong is already high. The tributaries, especially the smaller ones, are extremely seasonal, with steep short-term discharge peaks in the wet season and a prolonged low stage at other times (Figure 20.6). Their upper basins (except on the Korat Plateau) tend to be hilly and steep, the streams are entirely rainfed, and rise faster than the Mekong. The upper basin tributaries peak in July rather than in late August or September. The contribution of the tributaries also tends to be uneven along the Mekong (Figure 20.7). A disproportionately high amount of water

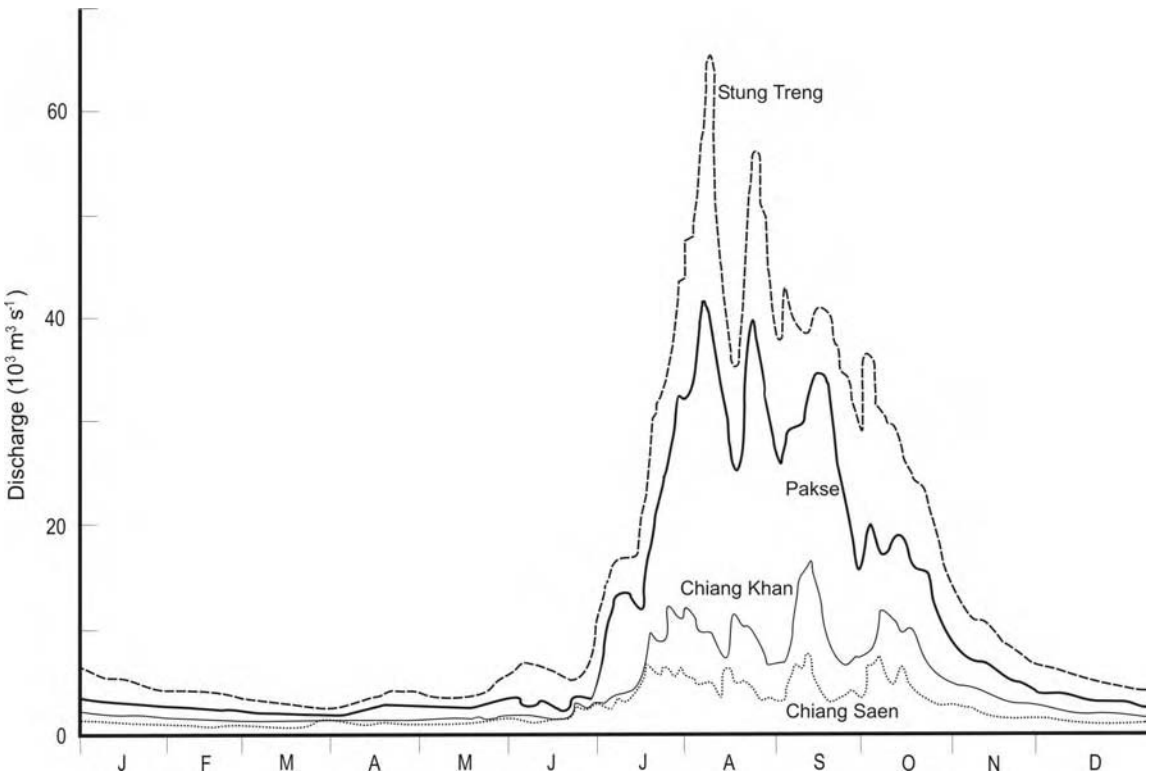

Figure 20.4 Annual hydrographs (1997) of the Mekong at Chiang Saen, Thailand (14% of the basin area), Chiang Khan, Thailand (36%), Pakse, Lao PDR (69%), and Stung Treng, Cambodia (80%). Data from Mekong River Commission, *Lower Mekong Hydrologic Yearbook*

arrives from (1) the steep northern hills of Lao PDR and the northern Annamite Chain via the Nam Ngum and Nam Theun systems and (2) the southern Annamite slopes via the large tributaries of Kong, San and Srepok (MRC, various dates). Before dams were built on the Mekong in Yunnan (China), 18.2% of the annual discharge of the Mekong used to arrive from the upper basin at Chiang Saen in Thailand (MRC, various dates), the proportion used to rise by several percentage points during the dry season. This contribution becomes less important when the southwest monsoon arrives and the lower tributaries contribute large volumes of flow to the Mekong.

20.2.4 Land Use

As expected, use of the land varies across the basin. In the highlands, the slopes are either in forest (including a substantive percentage in the degraded state) or under shifting cultivation (mostly hill rice with vegetables). Wet rice is grown in narrow alluvial plains next to the Mekong. Planting of wet rice is widespread in the widened alluvial plain of southern Cambodia, but the delta is the most fertile region. A series of canals for irrigation and drainage criss-cross the delta, supporting the common and well-organized practice of growing multiple rice crops in a year. Plantations of coffee and fruit crops share the slopes of the Annamite Chain with forests and shifting cultivation plots. The basin population in 1998 was estimated to be about 65 million with a 2% growth rate. The 2005 population is projected to be about 80 million. The basin south of the China border carries 84% of the population over 77% of the area. The rural population density is low, ranging from less than 10 per square kilometre in the highlands to nearly 600 in the delta, and up to about 3500 in urban areas. A number of urban settlements occur along the river (Luang Prabang, Vientiane, Savannakhet, Pakse, Phnom Penh), and a few more in the delta (Can Tho, My Tho, Ca Mau). A considerable disparity exists in the level of economic development across the basin (MRC, 1998).

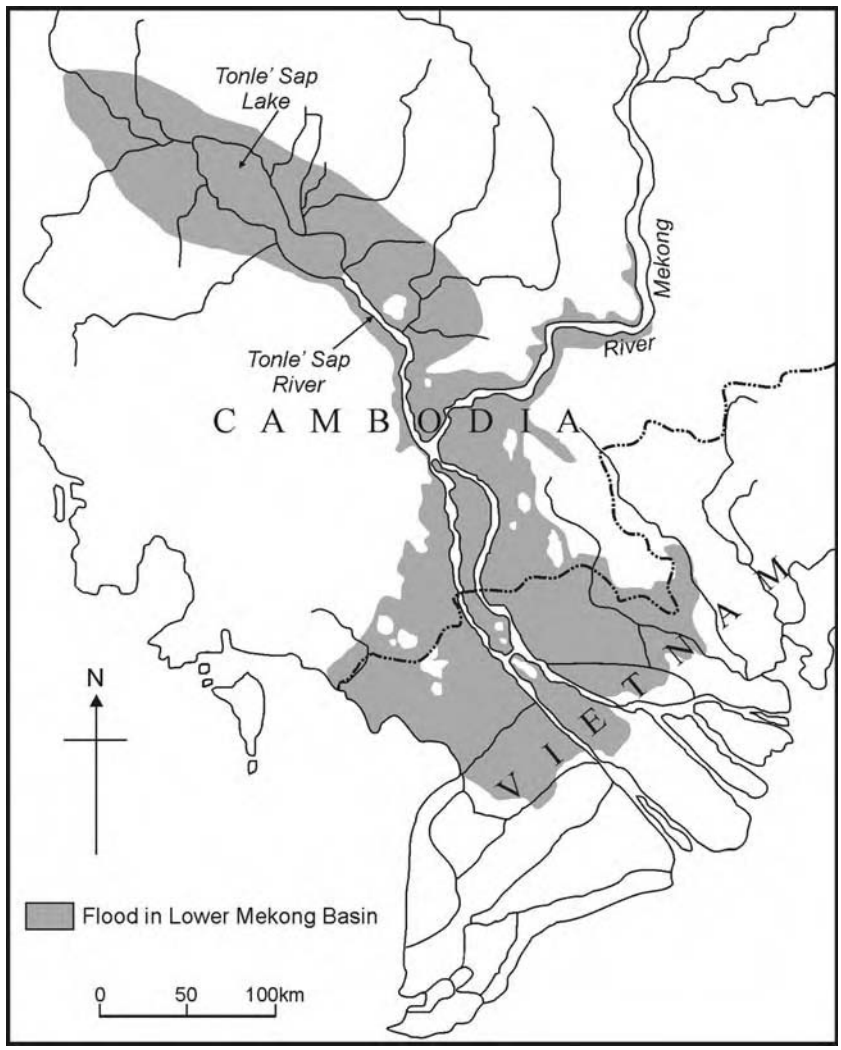

Figure 20.5 Mekong flood of 2000, Cambodia and Vietnam. Map prepared from SPOT imagery by Centre for Remote Imaging, Sensing and Processing, Singapore

In 1957, The Committee for Coordination of Investigations of the Lower Mekong Basin was established under the auspices of the United Nations Economic Commission for Asia and the Far East with the four member states of Cambodia, Lao PDR, Thailand, and Vietnam. In 1995, the same four states signed a new instrument, 'The Agreement on the Cooperation for the Sustainable Development of the Mekong Region.' The name of the investigating body was changed to the Mekong River Commission. The agreed 'vision' of the Commission was listed as 'An economically prosperous, socially just and environmentally sound Mekong River Basin' (MRC, 1998). The Agreement also highlighted the need for a timely and appropriately planned development of water resources in the basin and recognized the potential for conflicts. It also committed the countries concerned to maintain the quantity and quality of the flow in the Mekong River (MRC, 1998). These are useful arrangements, given the commonly recognized high potential for hydropower generation in the basin. Apart from planning the development of the river and its basin, the Commission also acts as a collector of information and as a database. Thus the development

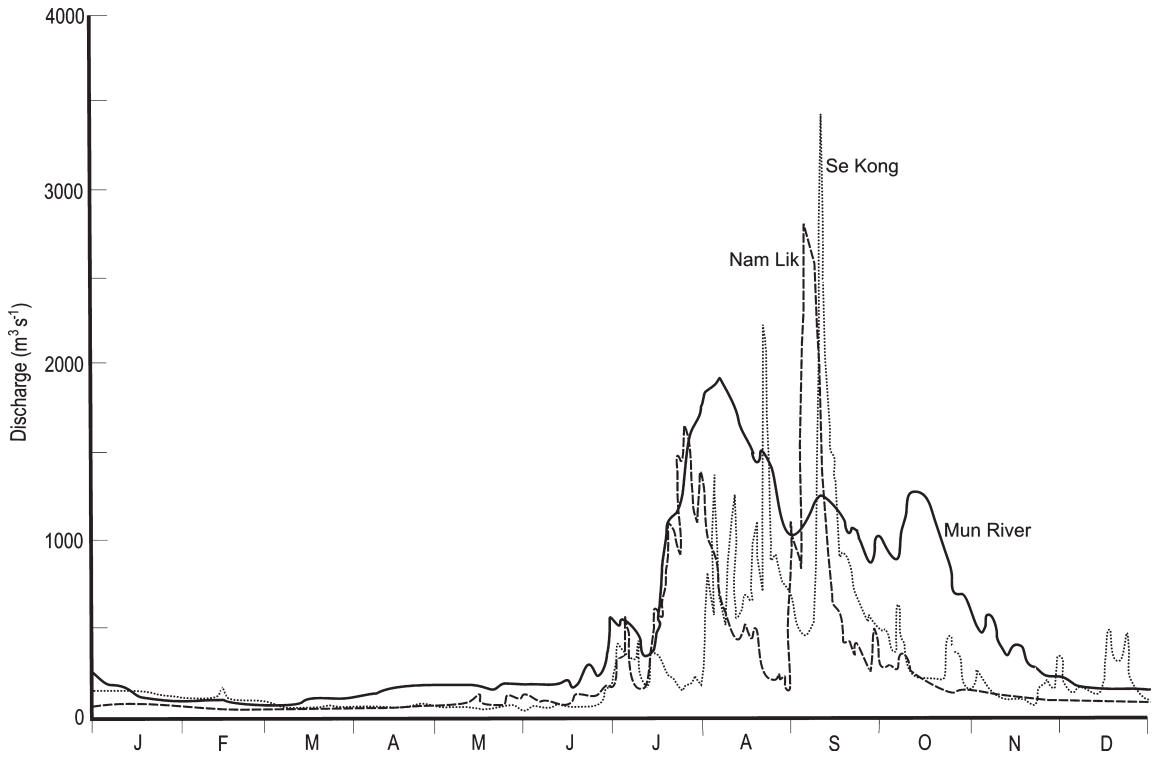

Figure 20.6 Annual hydrographs of the Mekong tributaries: Nam Lik at Muong Kasi, Lao PDR (basin area 374 km^2 in northern Lao PDR mountains), Mun River at Ubon, Thailand (104 000 km^2 on the Korat Plateau), Se Kong at Attopeu (10 500 km^2, Annamite Mountains). Except Se Kong at Attopeu, the rest of the hydrographs are for 1997; the Se Kong hydrograph is for 1993 as the 1997 data are not available. Notice the relatively large volume of discharge on rivers draining smaller areas in the northern Lao and southern Annamite Mountains. All data from Mekong River Commission, *Lower Mekong Hydrologic Yearbooks*

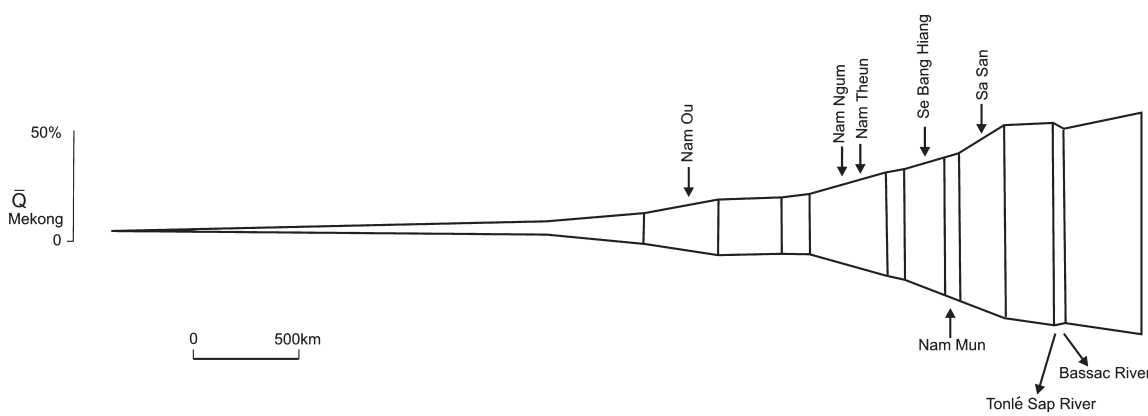

Figure 20.7 Cumulative discharge along the Mekong River. Reprinted from Geomorphology, doi:10.1016/j.geomorph.2006.03.036. Avijit Gupta, S.C. Liew, The Mekong from Satellite Imagery, Copyright (2007), with permission from Elsevier

of the Mekong Basin has been planned in a structured fashion over years. The other two states that occupy part of the basin, China and Myanmar, have been in dialogue with the original four riparian states. Concern for the environment is now growing due to certain types of development in the basin, especially the building of a series of dams on the Mekong in China. Controversies continue regarding the utilization of the water of the Mekong for power generation and the channel for navigation. These are potential issues for conflict between the states as these carry the likelihood of environmental disasters impacting the river and its people.

20.3 THE RIVER

The Mekong has been studied in detail south of China. The river is called Dza Chu (River of Rocks) in Tibet and Lancang Jiang (Turbulent River) in Yunnan, both names aptly describing the physical condition of the river. In China, it is generally an extremely steep, structure-guided river on rock, in places flowing fast through rugged high gorges, with straight sections joined together with short sharp bends and offset channels. It drops over 4500 m in the first 2500 km of its course, an overall gradient of nearly 0.002. Short tributaries join the river at a very high angle draining very steep small sub-basins. The valley of the main stream is the only relatively wide valley in the upper basin. In southern Yunnan, the relief between the ridge crests and valley bottoms reaches 600 m in many places with hillsides that frequently slope 25° or more. Further upstream, both measures increase. Slope failures that seem to be associated with both structural variations and vegetation destruction are visible in the tributary basins on SPOT satellite images with 20 m resolution. Satellite imagery also indicates the entry of coarse material via short tributaries at innumerable points along the river. A braided pattern has developed wherever the valley and channel of the Mekong widen. The common channel pattern, however, is steep, straight, and laden with coarse sediment.

More information is available on the Mekong downstream of the China border, including data acquired over years by the Mekong River Commission. It is therefore possible to construct a structured description for the lower 2000 km of this river. Sediment discharge data lag behind hydrologic observations and need to be extended by local field data on texture, structure, and volume of stored sediment. Channel morphology therefore can be described with greater confidence than river behaviour.

Gupta and Liew (2007**)** have divided the river from the China border to the sea in eight river units (Table 20.2). This classification (Figure 20.2) is based on satellite imagery, topographical maps, charts of the Mekong River Commission's hydrographic atlas, water data from the *Lower Mekong Hydrologic Yearbooks* of the Mekong River Commission, and field visits. Details of the classification technique are in Gupta and Liew (2007) from which the following description has been summarized.

Unit 1. For about 900 km from the China border to near Vientiane in Lao PDR, the Mekong runs on rock. The nature of the river, however, changes several times throughout this length. For the first 500 km almost up to Luang Prabang, the Mekong is a rocky conduit (unit 1a) that progressively increases in width through a set of

Table 20.2 The Mekong: characteristics of the river units, south of China border

Unit	Bed material	Bank material	Average slope	Length (km)	Width (km)	Low flow depth (m)	Seasonal stage change (m)
1a	rock	rock	0.0003	500	200–700	~5	10
1b	rock	alluvium on rock	0.0003	250	200–2 000	±10	15–20
1c	rock	alluvium on rock	0.0003	30	500–600	7	15
1d	rock	alluvium on rock	0.0003	130	200–1 400	<5	10–12
2a	alluvium	alluvium	0.0001	100	800–1 300	~3	13
2b	alluvium	alluvium	0.00006	400	2 000	≤5	12–14
3	rock	alluvium on rock	0.0002	200	400–2 000	variable	20
4	rock	alluvium	0.00006	150	750–5 000	variable	~15
5	rock	alluvium on rock	0.0005	200	15 000	8	9
6	alluvium	alluvium	0.00005	225	3 000	~5	14–18
7	alluvium	alluvium	0.000005	50			
8	alluvium	alluvium	0.000005	330			

Note: All measurements are approximate. *Variable* implies difficulty in averaging because of too many scour holes. For unit 7, width is several kilometres and increasing. Unit 8 consists of several deltaic distributaries and is tidal. Seasonal stage changes for units 7 and 8 are difficult to measure accurately.
Source: Gupta and Liew, 2007.

near-straight reaches joined by sharp bends. There is very little option for the river to shift its course in the narrow deep valley. A number of these straight reaches coincide roughly with faults shown on the small-scale geological map of ESCAP (1990). Fenton *et al*. (2003) have described the effect on the river by the Mae Chan Fault east of Chiang Saen in Thailand. Here the river has been locally deflected and flows through a marshy depression in a tectonic sag basin. Such changes occur in several places in Unit 1 but lack of detailed field investigation prevents further understanding of the features.

In cross-section the channel is either trapezoidal or has a 100 m wide deep inner channel bounded by rock benches. Scour pools and rock protrusions occur on top of the rock benches above the inner channel and also inside that channel. The inner channel is generally about 10 m deep, which locally increases to more than 30 m. The river apparently is capable of transporting coarse gravel-size material in high flow. The local relief inside the channel controls sediment accumulation, and sediment is visible during low flow as bars on rock benches. The wide U-shaped bend at the confluence with the Nam Ou, about 25 km north of Luang Prabang, marks the end of this unit. Lacassin *et al*. (1998) have linked an upstream U-bend in the river where the Mekong crosses the active Nam Ma Fault to Late Cenozoic strike-slip inversion. Between 20 and 5 million years ago, the Nam Ma Fault changed from a right-lateral to a left-lateral slip. Such U-bends occur in the Mekong in several places, and although usually they are diagnostic of river capture, these bends in the Mekong could also be due to tectonic changes.

The river continues on rock with inset banks in silt and sand for the next 250 km (Unit 1b). A profusion of tens of metre high cross-channel rock ribs, isolated transverse rock piles, and lines of rapids distinguish this reach from the previous one (Figure 20.8). The trapezoidal cross-section and the one with an inner channel are present, but a third type, a wide scabland-like section with rock ribs and piles, is also seen in the river (Figure 20.9). The river width ranges from the low figure of 200 m between bedrock hills to a maximum of 2 km. The NNE–SSW run of the river follows a fault (Choubert and Faure-Muret, 1976). The three sharp elbow bends in this reach could be due to either river capture or fault offsets. A number of elongated pools are scoured on the rock shoulders above the inner channel and parallel to it. These tend to follow the general fault direction. The maximum depth in the inner channel varies between 30 and 50 m. Figure 3 of Fenton *et al*. (2003) maps this unit (Unit 1b) of the Mekong River almost directly on top of the Loei Fold Belt. The river goes through an U-bend and a sharp change in direction between sub-units 1a and 1b and flows almost north–south until it changes direction and morphology again to form sub-unit 1c. Sub-unit 1b therefore is probably associated with a specific tectonic belt.

Figure 20.8 Rock ribs and flood marker in the Mekong channel, unit 1b, upstream of Luang Prabang. Photograph Avijit Gupta

The Mekong changes stage between 15 and 30 m (locally more) between the wet and dry seasons leading to a wide difference in shear stress, unit stream power, channel erosion, and sediment transport between seasons. With the falling stage, sand and gravel accumulate round cross-channel rock protrusions to form bars, to fill depressions between high spots on the channel floor and rock shoulders, and to form insets against the vertical rocky banks either as massive episodic beds or as plastered over the rock in small quantity. Material ranging up to boulders, exposed at low flow on the sand bars, indicates the high competence of the Mekong in flood.

At the end of unit 1b, the Mekong, without any apparent reason, sharply changes from a south-flowing river to an east-flowing one and within a length of 30 km crosses several low hills in a set of six meanders (sub-unit 1c). The meanders are all incised and near-symmetrical, except one of these is much larger in amplitude. The river, flanked by steep hills that rise to 150–300 m above the channel, maintains a width between 500 and 600 m. The average gradient of the river astonishingly stays the same, although the depth decreases, and the channel appears to be almost sediment-free until the next unit is reached (Figure 20.10a).

The final sub-unit (1d), which stretches for another 130 km almost to Vientiane, is on rock but differs in form and behaviour. The Mekong runs in 10–20 km long, near-straight reaches, separated from each other by sharp bends. Its width varies between 200 and 1400 m. The lowest value is reached at the eastern end of the sub-unit 1d where, about 5 km before Vientiane, the river after depositing considerable of sediment in bars cuts a gorge-like

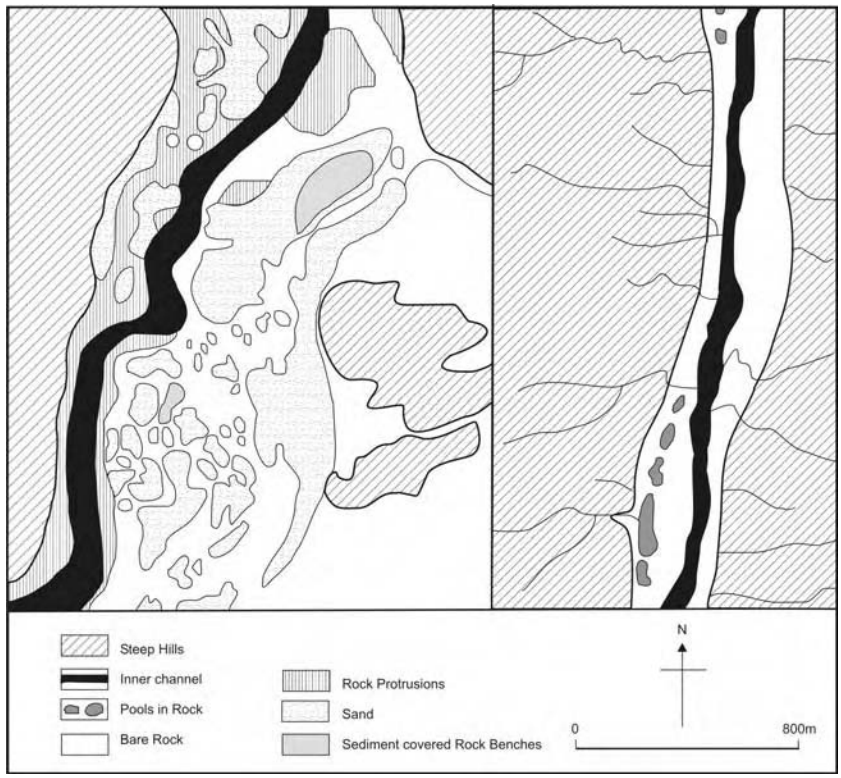

Figure 20.9 The Mekong channel (unit 1b), examples of scabland channel and narrower reach with inner channel. Depths generalized from Mekong River Commission (1996–99), *Hydrographic Atlas*, Mekong River Commission, Bangkok. Reprinted from *Journal of the Geological Society of India*, v. 64, no. 4, A. Gupta, Copyright (2004), with permission from the Geological Society of India

passage through a cuesta. While crossing this cuesta the river gradient increases to 0.125 and the depth increases from 5 to 30 m over a distance of 2 km. Unlike the previous sub-unit (1c), the channel is full of sediment that accumulates in various forms: rock-cored midchannel bars, bank insets, shallow channel fills.

Unit 2. For the next 500 km, the Mekong runs on alluvium. Emerging from the cuesta mentioned above, the river crosses an area of Quaternary alluvium in the first 100 km (sub-unit 2a) and the average river gradient drops to below 0.0001. Although the river is about 1 km wide, the seasonal fluctuation of its stage is still about 13 m. The wide, shallow, meandering channel is filled with sediment. In the dry season, the reduced flow produces a set of low sandy cross-channel bars (Figure 20.11) resembling the transverse braid bars described for the South Platt by Smith (1970) and the Auranga by Gupta and Dutt (1989). Downstream of this sub-unit, the river flows for another 400 km through alluvium that appears to thin in places (sub-unit 2b). The river in sub-unit 2b consists of 50–60 km near-straight courses joined by sharp bends on a very low gradient (0.00006). The dry season braiding also disappears. The major sedimentation form is a pointed-end, lozenge-shaped bar or islands skewed to one side of the channel. These are big depositional forms, measuring 1–3 km along their main axes and 200–400 m across. Gupta and Liew (2007) suggest that the bars are formed at locations determined by topographical highs or boulder piles on channel beds but not due to channel geometry. The Mekong almost reaches the mountains of northern Lao PDR before turning first south and then southeast to flow close and parallel to the Annamite Mountains, about 20 km from it.

Unit 3. Downstream, the Mekong flows on the Mesozoic sedimentary rocks of southern Lao PDR for another 200 km. In the first part of this unit, lozenge-shaped rock-cored islands up to 5 km long, occur in a 1.5–3 km wide channel. In the second part of this unit, the gradient steep-

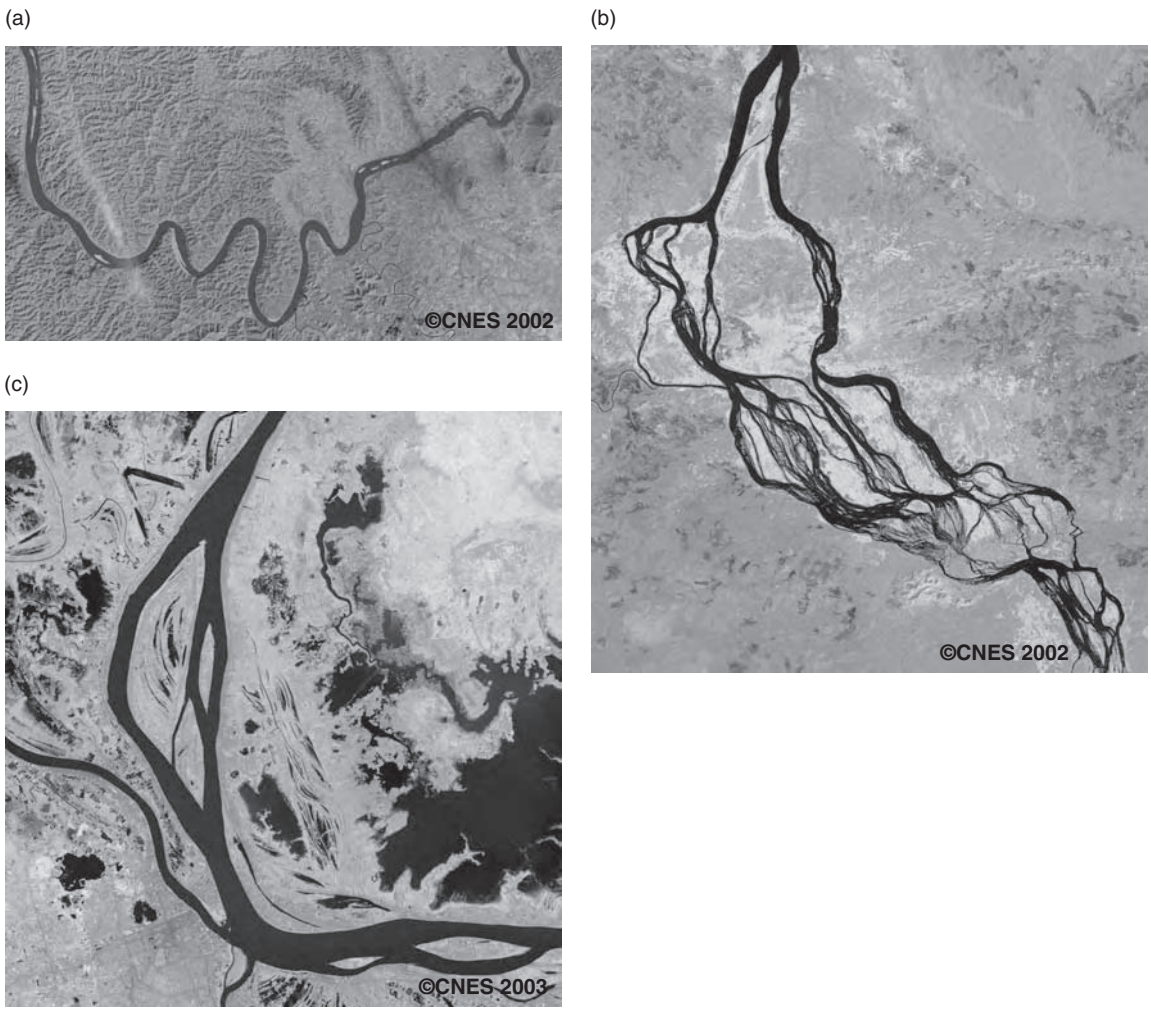

Figure 20.10 (See also colour plates.) Illustrations of selected river units. (a), (b) and (c) from SPOT images ©CNES and reproduced by CRISP (Singapore) under license from SPOT IMAGE ®. (a) Units 1b(left), 1c (middle) and 1d (right). Reprinted from Geomorphology, doi:10.1016/j.geomorph.2006.03.036, Avijit Gupta, S.C. Liew, 'The Mekong from satellite imagery', Copyright (2007), with permission from Elsevier. (b) Anastomosed channel in basalt, the 4000 islands, unit 5. Reprinted from Geomorphology, doi:10.1016/j.geomorph.2006.03.036, Avijit Gupta, S.C. Liew, 'The Mekong from satellite imagery', Copyright (2007), with permission from Elsevier. (c) Free-moving Mekong in unit 7. Reprinted from Geomorphology, doi:10.1016/j.geomorph.2006.03.036, Avijit Gupta, S.C. Liew, 'The Mekong from satellite imagery', Copyright (2007), with permission from Elsevier

ens, islands disappear, the channel narrows to hundreds of metres, and cross-channel rock exposures and an inner channel mark the river. The Mekong here has cut into the sedimentary rocks below a shallow layer of alluvium. Even the relatively large tributaries are on rock, at least locally. The Mekong flows through a couple of U-bends with rapids, rock exposures, deep inner gorges, scour pools, and strongly developed eddies on the surface (Figure 20.12). In one extreme case, a scour pool at a bend is 1250 m long, 150 m across, and up to 60 m deep below the low water level. At its narrowest part, the Mekong is less than 400 m wide between rocky hills with inner channels deepened up to 90 m below the low water level. Obviously there is some kind of structural control here.

The banks are in rock, locally plastered with sediment. At the end of this Unit, one of the main tributaries, the Mun, comes in from the west draining the surface of the Korat Plateau, and building a small fan at the confluence with the Mekong.

Unit 4. The Mekong flows over rocks for the next 150 km but with high alluvial banks. The channel is trapezoidal and its width varies between 750 m (close to the hills) and up to 5 km (where large elongated rock-cored islands, shown in Figure 20.13, appear again in the channel and the river flows in a wider valley). The gradient is gentle (0.00006) and widely spaced scour pools replace the continuous inner channel of the previous unit.

Unit 5. The next unit is a puzzling 200 km stretch of the Mekong where it alternates between near-straight and anastomosed channels. The most impressive example of the anastomosed channel occurs at the northern end of this unit, immediately to the north of the Lao PDR border. This is the so-called '4000 Islands', although the islands are definitely fewer in number. It is a 50 km long reach where the Mekong flows across a belt of Mesozoic basalt resulting in a series of rock-cored low islands and multiple channels (Figure 20.10b). The total river width (including multiple channels and islands) varies but the maximum figure is about 15 km. The river flows over a zone of waterfalls and rapids (including the well-known Phapheng Falls) at the downstream end of the 4000 Islands to the large alluvial plain of Cambodia where the combined water and sediment discharge of the Kong, San, and Srepok Rivers draining the Annamite Mountains to the east join the Mekong near Stung Treng. The Mekong near Stung Treng displays two or three secondary channels flowing parallel to the main channel with tens of kilometre long alluvial islands separating them.

Figure 20.11 Braid bars at low flow, Vientiane. Photograph Avijit Gupta

Unit 6. In spite of having reached the near 500 km wide Cambodian plain, the Mekong is still rock-controlled. The next 225 km consists of four 45–50 km long straight reaches. Alternate south-flowing reaches of the river are joined by right-angled bends to west-flowing ones. Triassic sedimentary rocks and Neogene basalts occur next to the Mekong, and it is possible that the sharp changes in the channel direction are related to local geology. Channel shifting over limited distance is demonstrated by abandoned courses very close to the river and welding of former bars to the banks.

Unit 7. Over the next 50 km the meandering Mekong moves freely across a wide floodplain (Figure 20.10c). Old

(a)

Figure 20.12 (See also colour plates.) (a) IKONOS image of a large U-bend in the Mekong (unit 3). Reprinted from Geomorphology, doi:10.1016/j.geomorph.2006.03.36. Avijit Gupta, S.C. Liew, The Satellite imagery, Copyright (2007), with permission from Elsevier and CRISP. (b) Map of the Mekong channel bend in unit 3 (from Gupta, 2004). Depths generalized from Mekong River Commission (1996–99), *Hydrographic Atlas*, Mekong River Commission, Bangkok

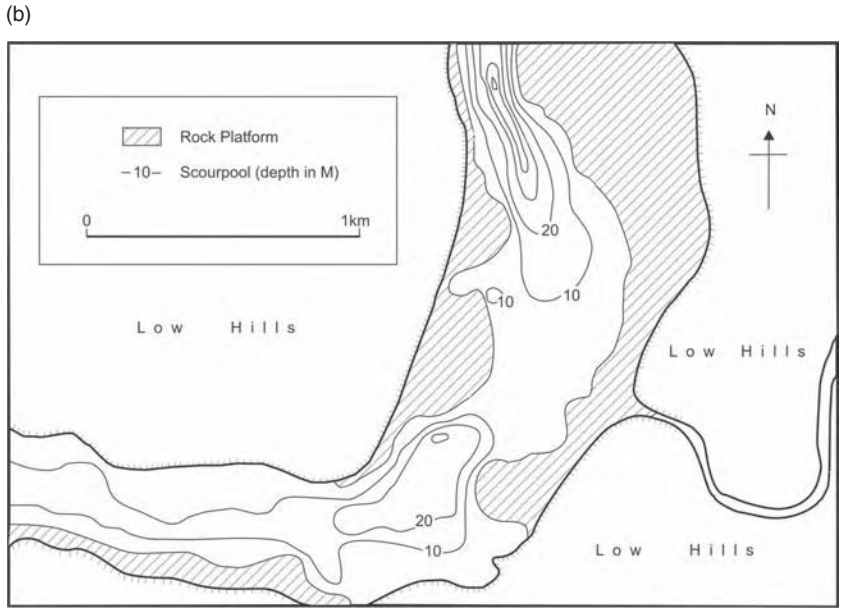

Figure 20.12 *Continued*

Figure 20.13 Rock-cored island downstream of Pakse (from Gupta, 2004). Reprinted from Geomorphology, doi:10.1016/j.geomorph.2006.03.036, Avijit Gupta, S.C. Liew, 'The Mekong from satellite imagery', Copyright (2007), with permission from Elsevier. Photograph Avijit Gupta

channels and scroll marks are common both overbank and on top of the midchannel islands. Overbank flooding occurs in the rainy season (Figure 20.5) and inundation of backswamps beyond the levee of the Mekong is common. During high flows of the wet season flow reversal happens in the Tonlé Sap River and water moves up its channel to fill the lake. This part of the Mekong Basin is a large wetland with several low granitic hills, part of the wetland has been converted to paddy fields.

Unit 8. The delta starts near Phnom Penh, where the first distributary, the Bassac, leaves the main channel 330 km from the sea. It runs parallel to the Mekong for the first 200 km without any other distributary or interconnecting channel between the two. The first such interconnecting channel appears at Cho Moi in Vietnam, 120 km from the sea. The delta is commonly defined as the triangular piece of land between Phnom Penh to the north, the mouth of the Saigon River to the east, and the southwestern cape of the Ca Mau Peninsula to the west (Ta *et al*., 2002).

The Mekong Delta is one of the largest in the world. Apart from the Bassac, three other main channels of the Mekong reach the sea. Their positions have not changed much over the last 200–300 years (Ta *et al*., 2002, 2005). The subaerial delta can be divided into an upper and a lower part that are dominated by fluvial and marine agencies respectively. The upper delta consists of levee-bound tidal channels and backswamps where floodwater accumulates during the wet southwest monsoon. A large swamp to the northeast is known as the Plain of Reeds. The lower delta carries a series of NE–SW trending well-developed beach ridges and inter-ridge swamps and flat plains. Subsurface cores indicate that the Mekong Delta was formed in the last 6000–7000 years (mostly after the mid-Holocene sea level high) extending the shoreline for about

200 km (Nguyen *et al*., 2000). The drainage in the delta has been modified by a set of canals, constructed over the last 300 years. Floods inundate the lowland in Cambodia but only the upper part of the delta. The floodwater flows to the sea to the south through the distributaries and canals or overland westward across the upper delta to the sea north of Ca Mau Peninsula (Figure 20.5).

20.4 THE MEKONG OVER TIME: THE GEOMORPHIC HISTORY

We know little about the geomorphic history of the Mekong. Hutchison (1989) mentioned a proto-Mekong considerably different from the current one. The current river and its basin, even if it existed earlier in a different form, owe its present location and geometry to the collision of the Indian Plate with the Eurasian one and the subsequent rise of the Himalaya Mountains (Tapponier *et al*., 1982, 1986). This probably explains the narrow upper basin, the association with the regional pattern of folds and faults, the straight segments interrupted by sharp turns including the U-bends, the inner channel and rock scabland, and the restriction on lateral channel movement for about 95 % of the river length. Other regional big rivers such as the Upper Yangtze (Changjiang), Red (Sông Hóng), and Salween also exhibit similar features.

The two other relevant factors are (1) the strengthening of the monsoon system in the Early Holocene and (2) the shifting of the coastline across the shallow South China Sea during the Quaternary. The Early Holocene with a stronger monsoon and associated storminess was probably a period of intense erosion and sediment transfer, especially for rivers with headwaters in the newly formed steep mountains (Goodbred and Kuehl, 2000; Goodbred, 2003; Kale *et al*., 2003). It is tempting to conjecture that the deeply cut channel of the Mekong in rock became possible due to both geological and climatic causes. The computed power of the present Mekong, even in floods, does not appear to be capable of eroding an inner channel in rock over such a long distance. The origin of the Mekong Delta is well documented with data from a number of boreholes (Nguyen *et al*., 2000; Ta *et al*., 2002), but the passage of the Mekong from a narrow rock-bound valley to a wide alluvial lowland across Cambodia is still an anomaly. As Hutchison (1989) has indicated, the Mekong lowland in Cambodia and Vietnam is probably the upper surface of an alluvial fill in a structural depression. Such a hypothesis also accounts for the location and hydrologic behaviour of the Tonlé Sap Lake and the emergence of low small rocky hills from underneath the alluvial cover.

A detailed evolutionary account of the Mekong is yet to be constructed. A number of curious features, however, can be listed that are probably related to the evolution of this major river and its basin. These have been discussed in Gupta (2004) and Gupta and Liew (2007).

1. The Mekong is a juxtaposition of several units of variable morphology and behaviour.
2. Transitions between the units are sharp, not gradual, and the river exhibits a number of sudden changes in direction and form as between units 1b and 1c or between 1c and 1d.
3. The Mekong in rock of units 1, 3, and 4 display three different types of channel morphology, best seen in unit 1b. These are (a) a smooth trapezoidal section, asymmetrical at meander bends, (b) a narrow and commonly straight course with a deep inner channel flanked by rock shoulders topped by rock protrusions and scour pools parallel to the inner channel, and (c) a wide scabland-type channel with cross-channel rock protrusions surrounded by coarse sediment forming bars, rapids, and scour pools.
4. The river flows through a number of U-bends and near right-angled turns. The U-bends tend to have a tributary joining the main channel on the convex side of the bend. Strong channel dynamics occur at these bends; scour holes occur in the bed and rapids and eddies on the surface.
5. Islands in the Mekong from unit 2b downstream are elongated, located in mid-channel, unrelated to channel geometry, and rock-cored.
6. The channel alternates between near-straight reaches and anastomosed channels cut in rock and alluvium in unit 5.
7. A combination of lithology and structure restricts lateral channel movement of the Mekong for about 4000 km until unit 7 is reached where the Mekong becomes a freely moving river in a wide floodplain.
8. A seasonal reversal of drainage happens between the Mekong and the Tonlé Sap Lake via the Tonlé Sap River.
9. Evolution of the alluvial Mekong in Cambodia and Vietnam is related to sea-level changes across the shallow wide Sunda Shelf; the present delta is Early Holocene in age.

These observations indicate a structure-guided river, whose channel configuration is probably post-Himalayan in age, whose location was determined by extrusion tectonics that opened up depressed lowlands in Southeast Asia as well as the South China Sea, the base level for the Mekong. A number of its sharp bends can be explained following Lacassin *et al*. (1998) as reversal of fault slip direction. Once in a fault-controlled gorge, that part of the

Mekong became anchored. The slip reversal may also explain why tributaries tend to join the Mekong from the opposite direction at the top of large bends. If the explanation forwarded by Lacassin *et al*. is accepted, then part of the channel is at least several million years old. The delta was formed in the last 6000–7000 years after the mid-Holocene sea level high (Nguyen *et al*., 2000). Ta *et al*. (2002) have indicated that the major distributary channels of the Mekong Delta have not shifted significantly over the last 2000–3000 years.

We therefore can fix two time limits for the evolution of the Mekong River. In between these time constraints, the present river came into existence amalgamating past river courses, probably capturing parts of older drainage systems, and occupying new locations. This hypothesis certainly requires further testing, especially in the field, but it does explain the various units of the Mekong and its unusual channel morphology, cross-channel rock barriers, and sharp bends.

The erosional features of the Mekong in rock cannot be produced without much enhanced stream power. The power of the present Mekong, even in a 100-year flood, falls far short of producing such erosional forms as seen in its channels (Gupta, 2004). It seems reasonable to presume that the Mekong at one time had larger floods with enough power to cut through lineations in rock to form the present channel. Palaeohydrological research on the Mekong is rather limited but research on rivers in India and climate proxies across South, Southeast, and East Asia indicate a pattern of much wetter and possibly floodprone Early Holocene with stronger monsoons (Williams and Clarke, 1984; Goodbred, 2003; see Kale *et al*., 2003 for a list of climate proxy references).

It is therefore likely that a combination of geological controls and large palaeofloods of the Early Holocene created the present Mekong, although part of it probably was inherited from an earlier drainage system. Once formed, the channel morphology has controlled river behaviour. Brookfield (1998) and Clark *et al*. (2004) have reviewed the possible evolution of the upper Mekong due to Himalayan tectonics and progressive river capture. Clift *et al*. (2003) have shown that offshore sedimentation rates increased during Early to Middle Miocene (15–20 Ma), indicating rapid erosion and sediment removal by the Mekong after the Himalayan orogeny and a functional drainage net in existence.

20.5 EROSION AND SEDIMENT TRANSFER

Sediment stored in the channel and the valleyflat of the Mekong tends to move downstream during high flows. The sources of the sediment include: (1) material from mass movements on steep valley slopes in China and northern Lao PDR that directly fall into the channel; (2) sediment contributed by short tributaries draining steep side slopes, usually deposited as small, steep fans of gravel and sand at confluence with the Mekong; (3) sediment contributed by larger rivers such as Nam Ou draining the Northern Lao hills, the Mun draining the Korat Highlands, and the Kong, San, and Srepok draining the Annamite Mountains; and (4) accelerated erosion on the slopes associated with current anthropogenic activities such as deforestation and shifting agriculture.

Sediment accommodation space outside the channel is limited for long stretches along the Mekong where sediment is stored primarily within the channel as insets against banks, material piled up against rock ribs arising out of the channel floor forming bars and islands, a mobile belt on bed, and plastered on rock shoulders of the inner channel.

Although the predominant texture of the Mekong sediment is sand, material up to the size of small boulders is visible on bars, on channel bed at very low flow, at the bottom of the scour pools in the inner channel, and on the rock shoulders of the inner channel. For the first 3000 km (from its source to the end of unit 1 upstream of Vientiane) the Mekong flows through a narrow steep-sided valley and sediment accommodation space outside is limited and localized. Sedimentation for thousands of kilometres along the Mekong is controlled not by channel geometry but by channel relief, and most of it is confined within the channel as a quasi-mobile belt of sand and gravel resting on or against bedrock. In unit 2, the Mekong builds elongated islands and bars skewed to one side of the channel, which results in small lateral channel shifts. In units 3 and 4, sediment is stored mostly as bed material or as rock-cored bars and islands. Outside sediment accommodation space is limited. The anastomosed channel of unit 5 allows deposition of sediment inside the channel forming islands and bars. The channel shows narrow lateral shifts between rocky hills in unit 6, the shifts being driven by welding of elongated islands to banks. Further downstream, sediment is transferred in the high flows of the wet monsoon and floods to the lowlands of Cambodia and Vietnam each year (Gupta and Liew, 2007).

Sediment transfer is seasonal and episodic in the Mekong. Rapid sediment transfer happens during high flows in the channel where sediment stored around rock barriers are entrained and carried downstream. Given the number of cross channel rock protrusions, bed load is likely to travel in stages. The zone of cataracts and waterfalls that includes the Phapheng Falls and the pools immediately downstream at the Lao–Cambodia border may very well act as a sediment trap. Lateral flux is limited until unit 6 is reached, where the Mekong is free to move and overbank flooding is expected in the wet season. Thus

overbank sedimentation is conspicuous only in the last 600 km of the Mekong. There, except in the lower delta, the Mekong overflows its banks and spreads out across flat wide flood basins behind the levees. These flood basins stay under water for weeks; for a couple of months in large floods like the one in 2000 (Figure 20.5). Flood basin sedimentation may happen only in the earlier part of this long inundation period, as shown by the changing colour of the standing water over time. Part of the sediment transferred from upstream may also travel to the Tonlé Sap and be trapped in and around the lake.

The banks of the Mekong are in rock, in places topped with reddish sandy silt and tens of centimetre thick beds of massive yellow sand with some silt inset against the rock suggesting episodic deposition in high flow. Wood, *et al.* (in press) have described stratigraphic bank sections near Chiang Saen (Thailand) which is representative for the rock-cut Mekong. They found sandy imbricated cobble gravel of unknown thickness overlain by 5–10 m of floodplain-and-levee type sandy silt. The latter is found typically in layers 1–2 m thick (Figure 20.14). They also list a radiocarbon date on a lens of charcoal and burnt bone under 5 m of silt as 1475 ± 38 calibrated years. They have also calculated sedimentation rates taking into account both the height of the bank sediment above datable material and the silty-sandy layers. The average annual sedimentation rate over nearly the last hundred years is 6.7 cm, but the sediment was probably deposited episodically in large events and a uniform rate may not be representative (Wood *et al*., in press). They also quote a maximum concentration of 1600 mg l^{-1} for a peak flow of 11 000 $m^3 s^{-1}$, but sediment transport data tend to be very uneven on the Mekong.

A fresh yellow fine sand is also seen as bank material, mostly as insets, especially in northern Lao PDR (Figure 20.14). Large storage of fresh sand in the channel is revealed during low flows every year (Gupta *et al*., 2002). It is probably derived from the current increase in slope-wash and gully erosion following deforestation and agriculture on steep slopes. It is possible that such sand and finer material arrive in the channel mostly during the first 6–8 weeks of the wet season (Gupta and Chen, 2002). In spite of this anthropogenic addition, the Mekong does not carry huge amounts of sediment unlike the Ganga or the Yangtze, and currently, the river plots almost on the regional average line for sediment yield against drainage area for South and Southeast Asian rivers (Gupta and Krishnan, 1994). The situation, however, may change as discussed in the next section.

Figure 20.14 Sand accumulation as bank inset. Photograph Avijit Gupta

20.6 THE MEKONG AND ITS BASIN: RESOURCE AND MANAGEMENT

The basin of the Mekong is primarily rural and the river is little utilized for navigation, irrigation or power generation. As such, the Mekong environmentally is in a better shape than many rivers of Asia at present. The conditions, however, may decline in future if various development plans that are periodically considered for the basin and the river are put into operation without proper environmental impact assessment. The performance of the Mekong River Commission as an international organization responsible for planning of the river and the basin in a holistic fashion and on a sustainable basis with collective consent from the riparian states therefore is extremely crucial. This is reflected in a number of changes, such as the improved river and road transport in the lower basin.

Three major areas of possible environmental impact due to currently ongoing or possible future changes can be identified:

- proposed and constructed dams and navigation projects on the river;
- increased erosion and accelerated sediment production on the basin slopes;
- degradation of the aquatic life.

Other problems undoubtedly exist at present, and will emerge in future, but these three should be considered as serious barriers towards keeping the Mekong Basin economically prosperous, socially just, and environmentally sound.

A series of dams and reservoirs, collectively described as the Mekong Cascade, were originally proposed on the Mekong River (Interim Committee for Coordination of Investigations of the Lower Mekong Basin, 1988). In spite of a later modification to run-of-the-river structures replacing conventional dams the plan has never been carried out. Several dams, however, had been constructed on several tributaries of the Mekong in the 1960s, mainly in Thailand. In 1968, the 150 MW Nam Ngum Dam in Lao PDR began to export hydroelectricity to Thailand. Generation of clean

power and hydroelectricity as an exportable resource became important issues for Lao PDR. At present, several dams on various tributary rivers of the Mekong are in operation in Lao PDR, Thailand, Cambodia and Vietnam. China has planned a series of eight dams (the Lancang Cascade) on the Mekong in Yunnan. The scheduled date for completing all eight is 2020 with a planned storage of 40 m^3 of water. Of these, two small ones are currently completed (Manwan, 1500 MW and Dachaoshan, 1350 MW), and three more are in the construction stage, the much bigger Xiaowan (4200 MW) and the smaller Jinghong and Nuozhadu (Kummu and Varis, 2007). The Xiaowan, which is 300 m high with an active storage of 990 million m^3, is planned as the second largest dam in China, next only to the Three Gorges.

Construction of dams and reservoirs results in a standard set of environmental impacts. These include sedimentation in the reservoir upstream of the dam along with sediment starvation, channel incision, channel narrowing, bed armouring, and modification of the riparian vegetation and fauna in the channel downstream of the dam (Williams and Wolman, 1984; Meade *et al*., 1990; Collier *et al*., 1996). Such changes may happen in the upper Mekong, but given the nature of the river, serious additional implications may be expected. It has been suggested that the effect of large dams constructed on the Mekong will extend up to the delta where water and sediment discharges, soil rejuvenation, nutrient flow, and fish productivity will be reduced, threatening prosperous local agriculture and fisheries (Douglas, 2005).

The discharge from the upper basin in China is only 18 % of the annual flow. This percentage, however, rises during the dry season and the steady release of water from the reservoirs may dampen the seasonality in Mekong's flow impacting local ecology. Given the nature of the Mekong's morphology and behaviour, the potentially disastrous impact of the dams is likely to involve the channel sediment stored loosely on rock. The data on sediment is not as extensive or in-depth as that on water discharge but it is generally assumed that about half of Mekong's sediment comes from the upper basin in China and is primarily coarse-grained. Kummu and Varis (2007) have concluded, using data from various sources, that the measured annual sediment flux has dropped from around 70×10^9 kg to 32×10^9 kg at Chiang Saen, about 660 km downstream of the Manwan Dam; and such figures have changed from 133×10^9 kg to 111×10^9 kg at Pakse in southern Lao PDR. The effect at Pakse could of course be due to multiple factors because of the river distance involved, the presence of several dams on the tributaries of the Mekong, and current land use changes. The wet season flooding of the Mekong generally is caused by heavy rainfall over the mountains of northern Lao PDR and the Annamite Chain, well downstream of the Lancang Cascade dams. In combination, floods, shortage of upstream coarse sediment, and loose sand and gravel on rock would lead to stripping of most of the sediment resting in Mekong's channel within years, effectively transforming the Mekong up to the zone of waterfalls at the Lao PDR–Cambodia border to a rock-cut canal. Bed armouring may slow the process but such armour, if present, is likely to be eroded in the next large flood and sediment stripping may happen in discrete stages transported by large floods rather than in every wet season.

This leads to the next environmental query. Where will the stripped channel sediment be deposited? Would it build up the floodplain and floodbasins in Cambodia and would part of it travel into the Tonlé Sap to partially fill the lake with serious consequences for local ecology and economic well-being as the lake and the regional Mekong lowland are the primary sources for rice and fish in the country? Subsequently, after the stripping and redistribution of the sediment, the delta face may undergo rapid erosion due to a combination of reduced sediment supply from upstream and a rise in sea level and storminess associated with global warming. All such conjectures, however, require detailed investigation but it can certainly be stated that any engineering structure on the Mekong requires careful and detailed pre-construction environmental impact analysis and post-construction monitoring. If all eight proposed dams and reservoirs are constructed, it may lead to very serious consequences downstream, complicated by the Mekong being an international river flowing through several countries.

Sediment transport to the Mekong Delta has not changed significantly over the last 3000 years (Ta *et al*., 2002). Their calculations, based on the rate of delta progradation from borehole data, yielded an annual rate of $144 \pm 36 \times 10^6$ t against 160×10^6 t for the current Mekong (Meade, 1996). The difference is well inside an acceptable range of error. This is different from the accelerated sediment yield measured for other regional rivers due to significant anthropogenic impact on their drainage basins (Saito *et al*., 2001). Gupta and Krishnan (1994) showed that the sediment yield of the Mekong Basin falls a little below the regional average. A lowering of sediment transfer to the delta face and a rise in sea level therefore would be a disastrous combination for this fertile and populated part of the Mekong Basin.

Parts of the basin are affected by deforestation and shifting cultivation on the slopes. Although shifting cultivation does not necessarily produce a large amount of sediment while the population density remains low (Gupta and Chen, 2002), a rise in density certainly does so. The

steep slopes of the upper basin are particularly vulnerable. Given the steep slopes and high intensity seasonal rainfall of the basin, the impact of deforestation during the long Indochina Wars has been extensive. Deforestation currently continues on both individual and organized basis and a significant part of the forest is probably secondary. The fresh yellow sand seen in the river could be a marker of bad land use practices. This phenomenon requires proper land management, especially of steep slopes. Currently, the vegetation cover is being removed along small valleys that follow geological lineations with a local relief of several hundred metres and with slopes exceeding 25° (Gupta *et al*., 2002). Field measurements of sediment loss are, however, few and far between. The Mekong River Commission (1997) indicated that Mekong tributaries in Lao PDR may carry 170 000 t day^{-1} in high flows, the figure dropping to 50–100 in the dry season. This source of sediment may partially compensate sediment loss from the Lancang, but at the cost of devastated hill slopes and degraded streams of the Mekong Basin.

The Mekong River system, especially the wetlands that include the Tonlé Sap and the delta is a very important source for fish and shrimps for the local population. As most of the catch is locally caught and consumed, reliable estimates are difficult to ascertain. Campbell in his chapter in this book (Chapter 27) mentions annual estimates of 2 million t of wild fish, and 400 000 t of catch in Cambodia. The Mekong River Commission has estimated the annual value of wild fish catch at about US$ 1 billion. The tributaries of the Mekong in northeast Thailand and Lao PDR and the wetlands of Cambodia are important breeding grounds for many species. Fish are caught in the main river, the mature individuals consumed and the fingerlings cultured in ponds (MRC, 1998). Prawn culture has become important in the wetland and the delta. The question of environmental degradation and its effect on the fish of the Mekong Basin and finally on the people is frequently raised. Projected degradation is anticipated from excessive sedimentation in the river from local sources, pollution from urban discharges and fertilizers, and the engineering control of the river upstream that would allow saline water to move further into the system. These undesirable factors undoubtedly affect some of the 1200 species identified so far, especially the endangered species. These include the giant freshwater catfish of the Mekong (*Pangasianodon gigas*) and the freshwater dolphins that are found below the Phapheng Falls at the Lao PDR–Cambodia border. A number of the dolphins were shot during the Pol Pot regime, reducing their number to a critical level. The Tonlé Sap area is especially threatened with excessive sedimentation and loss of aquatic species in the future. In the delta, apart from the problems listed above, forests of *Melaleuca* and mangroves are rapidly disappearing. The mangrove forests are being destroyed for uncontrolled wood extraction, paddy expansion, and extension of prawn farms. This may accelerate the erosion at delta face associated with loss of upstream sediment and sea-level rise. The total environmental degradation may also vary between the different river units of the Mekong thereby further complicating the task of river management.

20.7 CONCLUSION

The Mekong is an unusual river due to its morphology and behaviour. It has a fascinating evolutionary history which, like many other aspects of the river, has not been properly examined. Present changes in land use have started to impact negatively on the river and its basin. The dams already constructed on the Upper Mekong are likely to accelerate environmental degradation of the channel, and the level of deterioration will rise if all eight proposed dams are constructed. Although good hydrologic data exist for the Mekong, the shortage of data on sediment and the limited amount of scientific research on the river are barriers to investigations on such impacts. The basin is still mostly under vegetation and rural land use, and the responsibility for planning the development of the lower part of this multi-state basin lies with the Mekong River Commission.

ACKNOWLEDGEMENTS

The material in this chapter has evolved over a number of years following image interpretation, field visits, and various discussions with a number of colleagues. I should especially thank Brian Finlayson, S.C. Liew, and Matti Kummu. The Mekong River Commission graciously allowed visits to their library and access to the hydrological yearbooks and the hydrographic atlas. The satellite images were consulted in the Centre of Remote Imaging, Sensing and Processing, National University of Singapore. Spencer H. Wood very kindly sent me preprints of the various papers on tectonics and alluvial stratigraphy in northern Thailand prepared by him and his colleagues.

REFERENCES

Brookfield, M.E. (1998) The evolution of the great river systems of southern Asia, during the Cenozoic India-Asia collision: rivers draining southwards, *Geomorphology*, 22, 285–312.

Choubert, G. and Faure-Muret, A. (General co-ordinators) (1976) *Geological World Atlas (1/10 000 000)*, Unesco, Paris.

Clark, M.K., L.M. Schoenbohm, L.H. Royden, K.X. Whipple, B.C. Burchfiel, X. Zhang, W. Tang, E. Wang and L. Chen. (2004) Surface uplift, tectonics, and erosion of eastern Tibet from large-scale drainage patterns, Tectonics, 23, TC1006, doi: 10.1029/2002TC001402.

Clift, P.D., M.K. Clark and L.H. Royden. (2003) An erosional record of Tibetan Plateau uplift and monsoon strengthening in the Asian marginal seas, *Geophysical Research Abstracts*, 5, 04300.

Collier, M., Webb, R.H. and Schmidt, J.C. (1996) Dams and rivers: primer on the downstream effects of dams, *US Geological Survey Circular* 1126, Washington, DC.

Delaporte, L. and Garnier, F. (1998) *A Pictorial Journey on the Old Mekong; Cambodia, Laos and Yunnan: The Mekong Exploration Commission Report (1866–1868), Vol. 3,* translated by W.E.J. Tips, White Lotus Press, Bangkok.

Douglas, I. (2005) The Mekong River Basin, In: *The Physical Geography of Southeast Asia* (A. Gupta, Ed.), Oxford: Oxford University Press, 193–218.

Economic and Social Commission for Asia and the Pacific (ESCAP) (1990) Lao People's Democratic Republic, Explanatory Brochure, *Atlas of Mineral Resources of the ESCAP Region 7*, New York: United Nations, 19 pp.

Fenton, C.H., Charusiri, P. and Wood, S.H. (2003) Recent paleoseismic investigations in Northern and western Thailand, *Annals of Geophysics*, 46, 957–981.

Goodbred, S.L., Jr. (2003) Response of the Ganges dispersal system to climate change: a source-to-sink view since the last interstade, *Sedimentary Geology*, 162, 83–104.

Goodbred, S.L., Jr and Kuehl, S.A. (2000) Enormous Ganges-Brahmaputra sediment discharge during strengthened early Holocene monsoon, *Geology*, 28, 1093–1086.

Gupta, A. (2004) The Mekong River: morphology, evolution and palaeoenvironment, *Journal of Geological Society of India*, Special issue on Progress in Palaeohydrology: Focus on Monsoonal Areas (V.S. Kale, K.J. Gregory and V.U. Joshi, Eds), 64, 525–533.

Gupta, A. and Chen, P. (2002) Sediment movement on steep slopes to the Mekong River: an application of remote sensing, In: *The Structure, Function and Management Implications of Fluvial Sedimentary Systems* (F.J. Dyer, M.C. Thom and J.M. Olley, Eds), Wallingford: IAHS Publication 276, 399–406.

Gupta, A. and Dutt, A. (1989) The Auranga: description of a tropical monsoon river, *Zeitschrift für Geomorphologie*, 33, 73–92.

Gupta, A. and Krishnan, P. (1994) Spatial distribution of sediment discharge to the coastal water of South and Southeast Asia, In: *Variability in Stream Erosion and Sediment Transport* (L.J. Olive, R.J. Loughran and J.A. Kesby, Eds), Wallingford: IAHS Publication 224, 457–463.

Gupta, A. and Liew, S.C. (2007) The Mekong from satellite imagery: a quick look at a large river, *Geomorphology*, 85, 259–274.

Gupta, A., Lim, H., Huang, X. and Chen, P. (2002) Evaluation of part of the Mekong River using satellite imagery, *Geomorphology*, 44, 221–239.

Hutchison, C.S. (1989) *Geological Evolution of South-East Asia*, Oxford: Clarendon Press, 369 pp.

Interim Committee for Coordination of Investigations of the Lower Mekong Basin (1988) *Perspectives for Mekong Development*, Bangkok: Mekong Secretariat, 2 vols.

Kale, V.S., Gupta, A. and Singhvi, A. (2003) Late Pleistocene-Holocene Palaeohydrology of Monsoon Asia, In: *Palaeohydrology: Understanding Global Change* (K.J. Gregory and G. Benito, Eds), John Wiley & Sons, Ltd, Chichester, 213–232.

Kummu, M. and Varis, O. (2007) Sediment-related impacts due to upstream reservoir trapping, the Lower Mekong River, *Geomorphology*, 85, 275–293.

Lacassin, R., Replumaz, A. and LeLoup, P.H. (1998) Hairpin river loops and slip-sense inversion on Southeast Asian strike-slip faults, *Geology*, 26, 703–706.

Lorenzetti, E.A., Brennan, P.A. and Hook, S.C. (1994) Structural styles in rift basins; interpretation methodology and examples from Southeast Asia, *Bulletin, American Association of Petroleum Geologists,* 78, 1152.

Meade, R.H. (1996) River-sediment inputs to major deltas, In: *Sea-Level Rise and Coastal Subsidence: Causes, Consequences and Strategies* (J.D. Milliman and B.U. Haq, Eds), Dordrecht: Kluwer Academic Publications, 63–85.

Meade, R.H., Yuzyk, T.R. and Day, T.J. (1990) Movement and storage of sediment in rivers of the United States and Canada, In: *Surface Water Hydrology* (M.G. Wolman and H.C. Riggs, Eds), The Geology of North America, vol. 0-1, Boulder: Geological Society of America, 255–280.

Mekong River Commission (MRC) (various dates) *Lower Mekong Hydrologic Yearbook*, Bangkok and Phnom Penh: Mekong River Commission, published yearly.

Mekong River Commission (MRC) (1997) *Mekong River Basin Diagnostic Study: Final Report*. Bangkok: Mekong River Commission.

Mekong River Commission (MRC) (1998) *Water Utilization Program Preparation Project: Final Report*. Bangkok: Mekong River Commission, MKG/R.98/013.

Nguyen, V.L., Ta, T.K.O. and Tatheishi, M. (2000) Late Holocene depositional environments and coastal evolution of the Mekong River Delta, Southern Vietnam, *Journal of Asian Earth Science*, 18, 427–439.

Osborne, M. (1975) *River Road to China: the Mekong River expedition 1866–1873,* London: George Allen and Unwin Ltd., 249 p.

Osborne, M. (2000) *The Mekong: Turbulent Past, Uncertain Future*, New York: Atlantic Monthly Press, 295 p.

Peissel, M. (1997) *The Last Barbarians: The Discovery of the Source of the Mekong in Tibet*, New York: H. Holt, 253 p.

Peltzer, G. and Tapponier, P. (1988) Formation and evolution of strike-slip faults, rifts and basins during the India-Asia Collision: an experimental approach, *Journal of Geophysical Research,* 93, 15 085–15 117.

Saito, T., Yang, Z. and Hori, K. (2001) The Huanghe (Yellow River) and Changjiang (Yangtze River) deltas; a review on their characteristics, evolution and sediment discharge during the Holocene, *Geomorphology*, 41, 219–231.

Smith, N.D. (1970) Braided stream depositional environment – comparison of the Platte River with some Silurian clastic rocks, north-central Appalachians, *Geological Society of America*, *Bulletin*, 81, 2993–3013.

Ta, T.K.O., Nguyen, V.L., Tatheishi, M., Kobayashi, I., Tanabe, S. and Saito Y. (2002) Holocene delta evolution and sediment discharge of the Mekong River, southern Vietnam, *Quaternary Science Reviews*, 21, 1807–1819.

Ta, T.K.O., V.L. Nguyen, M. Tateishi, I. Kobayashi and Y. Saito. (2005) Holocene delta evolution and depositional models of the Mekong River Delta, southern Vietnam. In: *River Deltas – Concepts, Models, and Examples* (L. Giosan and J.P. Bhattacharya, eds.) SEPM Special Publication 83, Tulsa, Oklahoma, 453–466.

Tapponier, P., Peltzer, G., Le Dain, A.Y., Armijo, R. and Cobbold, P. (1982) Propagating extrusion tectonics in Asia, new insights from simple experiments with plasticene, *Geology*, 10, 611–616.

Tapponier, P., Peltzer, G. and Armijo, R. (1986) On the mechanics of the collision between India and Asia, In: *Collision Tectonics* (M.P. Coward and A.C. Ries, Eds), Geological Survey of London Special Publication, 19, 115–157.

Williams, M.A.J. and Clarke, M.F. (1984) Late Quaternary environments in North-central India, *Nature*, 308 (5960), 633–635.

Williams, G.P. and Wolman, M.G. (1984) Downstream effects of dams on alluvial rivers, *US Geological Survey Professional Paper* 1286.

Wood, S.H., Ziegler, A.D. and Bundarnsin, T. (in press) Floodplain deposits, channel changes and riverbank stratigraphy of the Mekong River area at the 14th century city of Chiang Saen, Northern Thailand, Geomorphology.

21

Dynamic Hydrology and Geomorphology of the Yangtze River

Zhongyuan Chen[1], Kaiqin Xu[2] and Masataka Watanabe[3]

[1]*State Key Laboratory for Estuarine and Coastal Research, East China Normal University, Shanghai 200062, People's Republic of China*
[2]*National Institute for Environmental Studies, Tsukuba 305-8506, Japan*
[3]*Faculty of Environment and Information Studies, Keio University, Kanagawa 252-8520, Japan*

21.1 BASIN GEOLOGY AND LANDFORMS

The Yangtze River originates from the Tuotuo on the southwestern slopes of the snow-draped Geladandong Mountains on the Tibetan Plateau at about 6000 m elevation (Figure 21.1). The river flows west to east across three major morphological surfaces in China into the East China Sea past the metropolitan city of Shanghai. This 6300 km long river drains a basin of about 1.80 million km^2 (Changjiang Water Conservancy Commission, 1999; Chen *et al*., 2001).

The 4500 km on the river from the source to Yichang is conventionally considered as the Upper Yangtze that drains an area of about 1 million km^2. The Upper Yangtze runs primarily through a mountainous region and flows out through the Three Gorges (Figure 21.1). The 938 km Middle Yangtze from Yichang to Hukou drains an area of 680 000 km^2. It meanders through the Jianghan and the Dongting Lake basins on a low-gradient plain where industry and agriculture are heavily concentrated. From Hukou to the estuary is the Lower Yangtze, with a length of 900 km and a drainage area of 130 000 km^2. This is an area of anabranching rivers with constricted floodplains and Early to Late Pleistocene terraces along the valley (Chen *et al*., 2001).

The Yangtze Basin includes a complex variety of geological units, primarily sedimentary rocks of different ages. The geological transect A-A′ (Figure 21.1) from the Upper to Lower Yangtze summarizes the geological characteristics of the basin. Limestone and terrigenous sedimentary rocks of Palaeozoic age with granite constitute the Upper Yangtze drainage basin. The sedimentary strata have been highly fractured due to the Himalayan uplift and erode easily. Cretaceous to Jurassic sandstone forms the Sichuan Basin, connecting the upstream Yangtze Plateau with the downstream Three Gorges Valley (Figure 21.1). The Sichuan Basin is surrounded by a complex of mountains framed by distinctive tectonic units (Tang and Xie, 1994). The alignment of highlands in the western and eastern basin are controlled by sets of major faults trending approximately NW–SE, and those in the northern and southern basin by faults running southwest (Tang and Xie, 1994). A set of linear faults running NW–SE across the east-central basin highlight the alternate anticlines and synclines of Permian and Triassic age (National Remote Sensing Center and Applied Institution of Remote-sensing Center, Chinese Academy of Sciences, 1984). The Yangtze River cuts through these geological structures to enter the Three Gorges.

Figure 21.2 illustrates the scale of landforms on the eastern flank of the Tibetan Plateau at 3000–4000 m. The photographs are from the Upper Minjiang Valley, one of the major tributaries of the Upper Yangtze. Sediment contribution to the valley is periodically accelerated by seismic

Large Rivers: Geomorphology and Management, Edited by A. Gupta

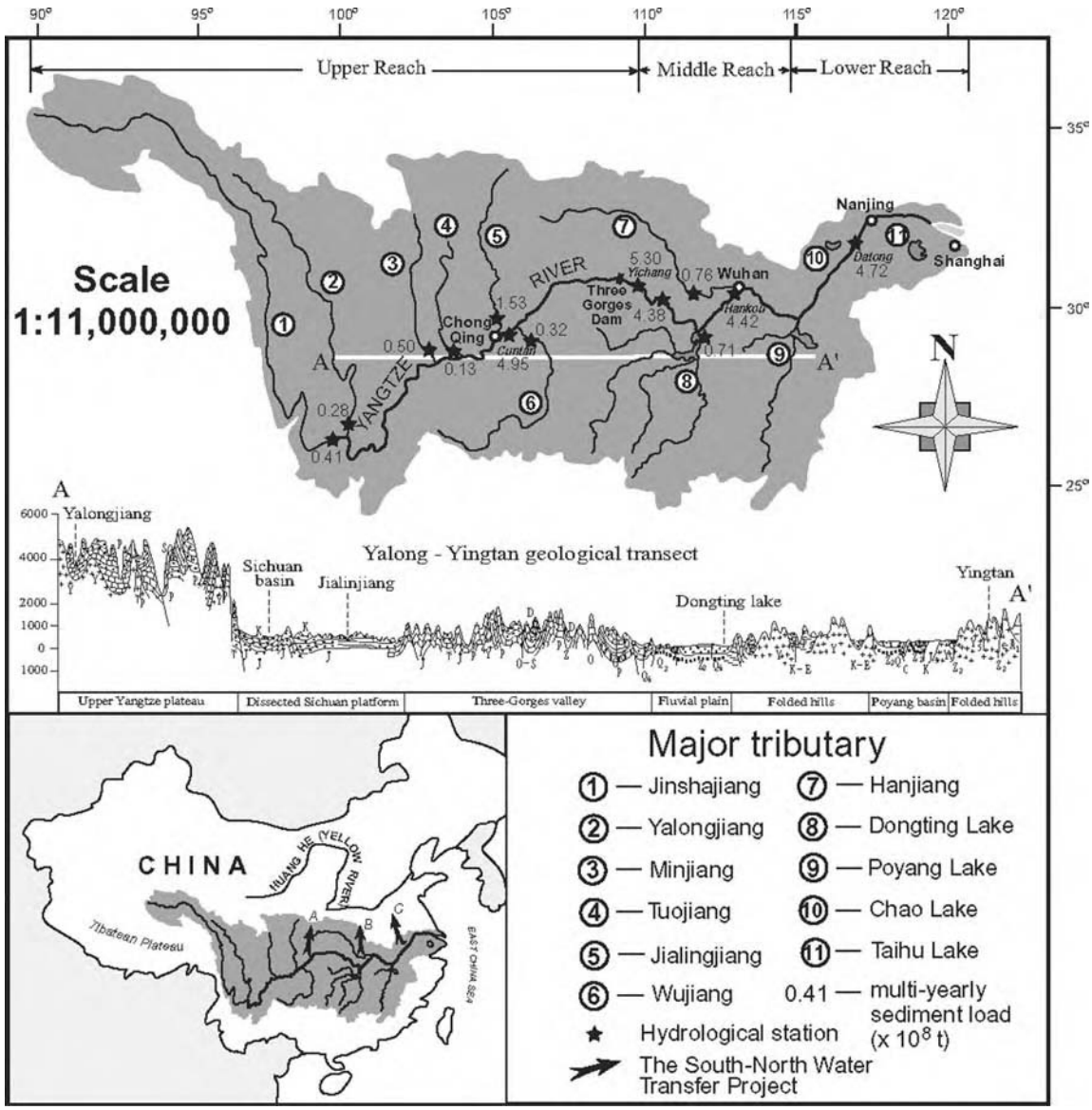

Figure 21.1 Drainage basin of the Yangtze River and multi-yearly sediment load. Reprinted from *Geomorphology*, 41, 2–3, Chen *et al.*, Yangtze River of China, pp. 77–91, Copyright (2001), with permission from Elsevier. Section AA' is modified after Changjiang Water Conservancy Committee, 1999

events such as the earthquake of 7.5 magnitude that occurred on 25 August 1933 in the area Die-Xi-Hai-Zi causing a landslide-blocked lake to form in the valley that subsequently collected sediment from the Upper Min.

The Three Gorges run for about 660 km from Chongqing to Yichang (Figure 21.1). Major faults run W-E through the mountain blocks to the south and north of the river. Between them occur several anticlines with short-axes roughly trending S–N. The western valley consists primarily of the red sandstone of Jurassic age, and the eastern valley of limestone thinly interbedded with red sandstone and peaty sediment of Triassic to Jurassic age (Three-Gorges Eco-Environmental Project Leader Group, 1987; Changjiang Water Conservancy Committee, 2001). Granite occurs locally. Sediment contributed by the tributaries commonly form fans at the confluences with the Yangtze (Figure 21.3).

Figure 21.2 Landforms of the eastern Tibetan Plateau at 3000–4000 m: (a,b) Upper Minjiang Valley; (c,d) earthquake-generated landslide blocked lake on the Minjiang

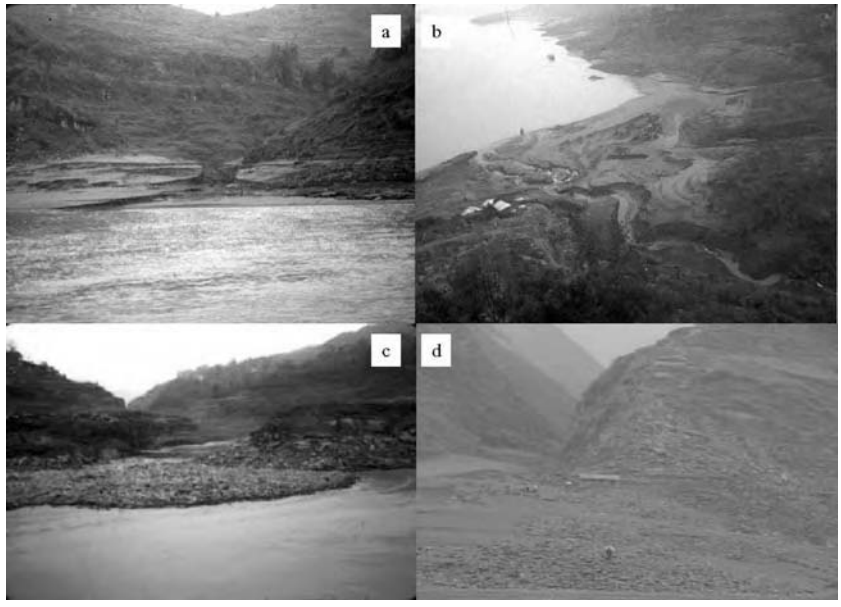

Figure 21.3 Coarse sediment load contributed by small tributaries forming alluvial fans at their confluences with the Yangtze River

Downstream of the gorges, the geological framework of the Middle Yangtze Basin is primarily delineated by the two large tectonics controlled subsidence basins: Jianghan and Dongting (Figure 21.1). The basins sagged since the Late Cretaceous to early Tertiary (Huang *et al*., 1965). The Huarong Rise separates the two basins. An earlier Yangtze channel flowed across the Jianghan Basin to the north when the subsidence rate was higher there than in the Dongting Basin (Yang and Tang, 1999). The river channel migrated southward to Dongting Basin following a subsequent shift in the location of rapid subsidence.

Granite and carbonates of Palaeozoic to Mesozoic age prevail in the lower basin of the Yangtze, marked by a series of 300–500 m hills. Quaternary alluvial sediments of 20–100 m thickness have accumulated in the Lower Yangtze reaches.

21.2 RIVER MORPHOLOGY

The major headwater of the Upper Yangtze, the Jingshajiang, is joined by five major tributaries: Yalongjiang, Mingjiang, Tuojiang, Jialingjiang and Wujiang in the Sichuan Basin (Figure 21.1). These rivers originate on the Tibetan Plateau at elevations above 4000 m. Rivers are deeply incised into rocky canyons with more than 1000 m difference in elevation between their beds and the mountain peaks. The 0.5–1.5 km wide, 5–20 m deep channels vary in slope between 0.0001 and 0.0004, although locally the gradient may steepen to >0.004.

Inputs from three different sources augment the Middle Yangtze: the Han River and the drainage from Dongting and Poyang Lake Basins (Figure 21.1). The channel slope decreases sharply to 0.00002–0.00003. The bed of the Yangtze indicates a slope reversal near the Dongting and Poyang Lakes. The channel of the Middle Yangtze is between 1 and 2 km wide and 10 and 15 m deep. Meandering with many cutoffs is the typical channel pattern. The well-known Jingjiang (local name of the upper section of the Middle Yangtze) dyke, constructed for flood protection, runs along the river. The dyke is 12–15 m above the ground surface in places. This area next to the Upper Middle Yangtze is extremely vulnerable to annual floods (Changjiang Water Conservancy Commission, 1999; Li *et al*., 2001). One of the objectives of the Three Gorges Dam (to be completed in 2009 at Yichang) is flood control. Several major meandering cutoffs on the Jingjiang Plain occurred during the early to mid-twentieth century. In the 1960s and 1970s, a set of cutoffs that shortened the river by 78 km, were designed to stabilize migration of the river. Channel straightening on the Jingjiang Plain has resulted in tremendous siltation in parts of the channel, bypasses, and interior lakes downstream (Geographic Institute of Chinese Academy of Sciences, 1985). As a result, beds of the river and the lakes rose to a higher level, increasing flood hazards (Yin and Li, 2001).

The Lower Yangtze is connected to several large inland lakes, such as the Chaohu and Taihu (Figure 21.1). The Yangtze here wanders among Holocene fluvial plains and Pleistocene terraces. The edge of the latter is marked with high stage water level at about 8 m above the mean sea level (Chen *et al*., 2001). The river gradient decreases to 0.000005–0.00001. The channel widens to 2–4 km and deepens to 10–20 m. At its mouth the Yangtze forms an estuary, wider than >30 km but only about 8 m deep due to estuarine turbidity-related sedimentation.

21.3 STORAGE AND TRANSFER OF WATER AND SEDIMENT

21.3.1 Discharge and Flood Patterns

A number of rainfall and gauging stations have recorded the variations in monsoon-driven precipitation and runoff in the Yangtze Basin for a period of 50–100 years (Changjiang Water Conservancy Committee, 1885–1985). A large amount of precipitation in the region is due to the monsoon, the strong atmospheric exchange between the warm air mass transferred from the lower Pacific and Indian Oceans and the cold air mass from Siberia. This exchange occurs strongly along the Yangtze Valley, generally between June and October. Rainfall starts and ends earlier in the Lower Yangtze Valley than upstream.

Annual precipitation in the basin generally ranges between 800 and 1200 mm (Figure 21.4). Two regions in the Yangtze Valley, however, have significantly higher precipitation. These are the Yalongjiang and Minjiang Basins of the Upper Yangtze Plateau with about 1600–2000 mm annual rainfall and the south-central Yangtze Basin including the Dongting and Poyang Lake systems. The lakes are linked to the Yangtze via tributary streams. The average annual precipitation near the lakes exceeds 1600 mm. About 50 % of the runoff of the Yangtze Basin is derived from the upper tributaries. The other half arrives primarily from the catchment of the two large lakes in the Middle Yangtze. The runoff from the Dongting and Poyang Lake basins approximate a third of the total Yangtze volume. The Dongting Basin virtually accounts for about 20 % of the total.

The high rainfall over the lakes usually occurs almost a month earlier than its arrival in the Upper Yangtze Valley, due to the migration of summer monsoon from the east coast towards the western highlands. This is a critical hydrological phenomenon, as the lake catchments are located about 400 km below the Three Gorges Dam

(Figure 21.1). The heavy floods generated from the lake region can threaten the Middle and Lower Yangtze Valley, as in 1998 when a flood with a return period of more than 60 years occurred. Stationary high rainfall over the lake region resulted in a discharge of >70 000 $m^3 s^{-1}$ downstream on the Yangtze. High flood peaks occurred from 28 June to 2 July at Dongting Lake in the Middle Yangtze Basin (Figure 21.5). No flood discharge, however, arrived from the Upper Yangtze Plateau. A series of major floods occurred after 2 July in the Middle and Lower Yangtze Basin when the zone with high rainfall shifted from the lakes to the Upper Yangtze Valley and remained there for

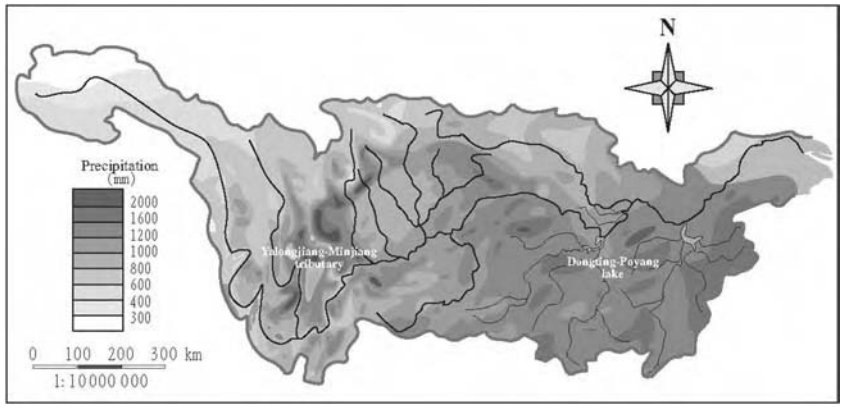

Figure 21.4 Rainfall distribution in the Yangtze drainage basin, heavy precipitation in the Yalong-Minjiang tributary basins and in the area around Dongting and Poyang lakes

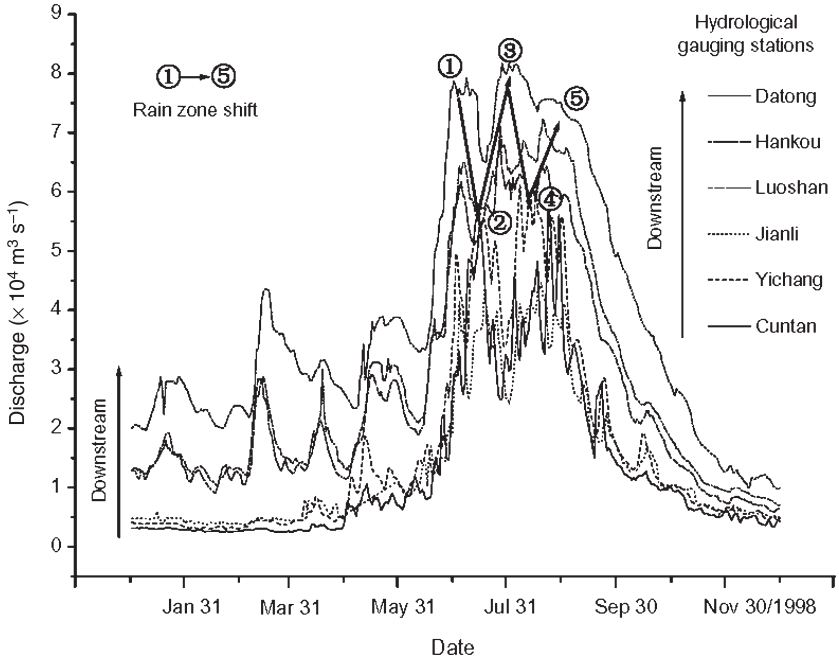

Figure 21.5 Discharge hydrographs of 1998 along the Yangtze River

almost 2 months (Figure 21.5). Similar conditions have occurred in the past (Changjiang Water Conservancy Committee, 1999, 2001). This increases the difficulty in flood mitigation and prevention (Ni and Zhang, 1999; Su *et al*., 2001; Yu, 2002).

21.3.2 Sediment Flux in the Yangtze: a Decreasing Trend over the Last 40 Years

The multi-year database of the Yangtze describes the storage and transfer of sediment load throughout the basin (Changjiang Water Conservancy Committee, 1999). The Jialingjiang tributary is the biggest contributor of sediment (annually, 1.53×10^8 t; Figure 21.1). The other major sediment contributors are the Minjiang (annual load 0.50×10^8 t) and Jingshajiang (0.41×10^8 t). The total annual sediment load from the tributaries of the upper plateau can reach 4.95×10^8 t, as recorded at the Cuntan hydrological gauging station near Chongqing (Figure 21.1), immediately upstream of the beginning of the Three Gorges.

The Yichang hydrological gauging station where the Yangtze leaves the Three Gorges is extremely important for evaluating variations in sediment budget of the Upper Yangtze Basin. The annual sediment load at Yichang is 5.30×10^8 t on the basis of 40 years of data. Between the upstream Cuntan and the downstream Yichang stations, about 0.70×10^8 t sediment load arrives annually from the Three Gorges. This volume is largely due to recent human activities, as detailed later.

Further downstream, the Hankou station near Wuhan records variations in sediment from three major sources: the Upper Yangtze, the Dongting Lake Basin, and the Hanjiang tributary (Figure 21.1). The annual sediment load from Dongting is 0.71×10^8 t, from Hanjiang it is 0.76×10^8 t, and at Hankou on the Yangtze 4.42×10^8 t. The amount at Hankou is less than that at upstream Yichang. Obviously, siltation occurs between Yichang and Hankou (Yin *et al.*, 2004).

The Datong station, about 600 km from the coast and established in 1950, is the lowermost one on the Yangtze above significant tidal limits. The data recorded help to understand sediment flux to the coast and eventually to the sea. The amount of annual sediment load recorded at Datong station is 4.72×10^8 t.

This is a summary of sediment distribution recorded over the last 40 years. However, the annual figure for Datong (Figure 21.6) shows a decrease in sediment load between 1960 and 2000 (Changjiang Water Conservancy Committee, 1885–1985): 5.12×10^8 t in the 1960s, 4.15×10^8 t in the 1970s, 4.11×10^8 t in the 1980s and 3.55×10^8 t in the 1990s (Yang *et al*., 2003).

The decrease in sediment load could be attributed to more than 35 000 dams constructed in the Upper Yangtze during the 1960s to 1980s (Changjiang Water Conservancy Committee, 1999). Sediment can be temporarily stored behind dams, but it is often flushed downstream during flood events. In the major flood year of 1998, the annual sediment load transported to the river mouth area was almost double that of the multiyear average (Xu *et al*., 2005). The deceasing trend can also be linked to the siltation of Dongting Lake in which about $0.8–1.0 \times 10^8$ t sediment accumulates annually (Yin *et al*., 2004).

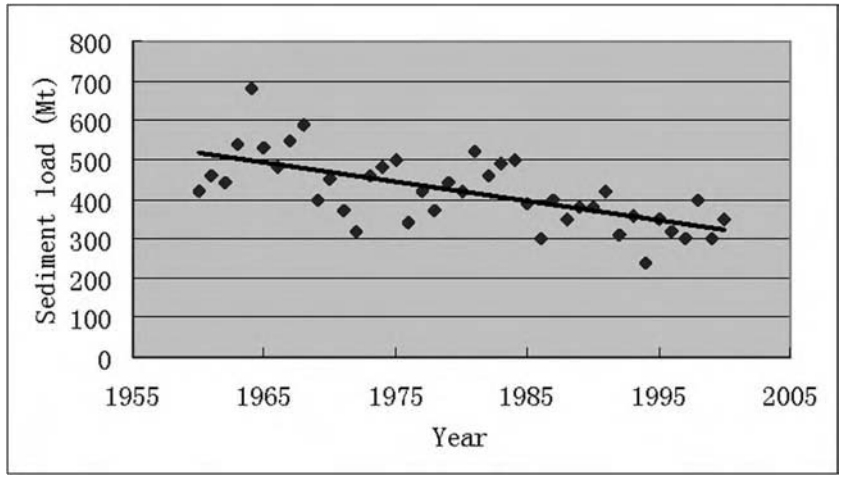

Figure 21.6 Decreasing sediment load at Datong hydrological gauging station over the last 40 years

21.3.3 Three Gorges Area: a New Sediment Provenance and a Depleted Valley

Almost 50 years ago, the Three Gorges barely yielded sediment for transfer downstream as evidenced from the long-term records at the hydrological gauging stations (Changjiang Water Conservancy Committee, 1885–1985). In the 1950s, about 5.70×10^8 t of sediment was measured annually at Cuntan and about 5.76×10^8 t at Yichang. The very small increase implied a low increment from a vegetation-covered steep landscape mostly on limestone and granite of Mesozoic age. However, as discussed above, the data of the last 40 years show a sediment load of about 0.7×10^8 t annually from the Three Gorges area. Part of this comes from the Wujiang between Chongqing and Yichang (Figure 21.1). This increase in sediment budget apparently is due to intense anthropogenic activities including relocation of urban centres from valley bottoms to upper slopes, farming on slopes, and changes in land use involving industry and agriculture. Figure 21.7 shows such anthropogenic sediment on the slopes of the Three Gorges. About 2.5×10^8 t of sediment was derived from the Three Gorges section during the big flood of 1998 (Xu *et al*., 2005).

In May 2002, we measured the stream velocity in the Three Gorges by ADP (Acoustic Doppler Profiler) guided by GPS. The average velocity was 3–4 m s^{-1} and the maximum exceeded 6 m s^{-1} recorded at the lower water column (1–3 m above the river bed). Little sediment will be deposited at such a high flow. Deposition of sediment was restricted to numerous small fans (approximately 20–50 m × 100–300 m) consisting largely of gravelly medium to coarse sand mixed with gravels that develop at the confluence of local small tributaries with the Yangtze in the gorges (Figure 21.3). These fans are formed in association with local sub-basins or canyons, and fine materials can be deposited only during the previous high water stage in the Yangtze.

21.3.4 Middle Yangtze: Sediment Sources and Sinks

Exiting from the Three Gorges, the river meanders into a vast flat plain (Figure 21.1). A great amount of sediment has been deposited below the gorges due to the sharp fall in river velocity to 1–2 m s^{-1}. Previous work (Chen and Zhao, 2001) on multiyear sediment budgets indicated heavy siltation in the region from almost a third of the total sediment load (~0.6×10^8 t) during the annual flood season (July and August; Figure 21.8). Yin *et al*. (2004) suggested long-term channel siltation from Shishou to Huangshi (about 600 km), 230 km below Yichang. This results in rapid aggradation of the riverbed, raising it to 12–15 m higher than that of the adjacent floodplain and an annual accumulation rate of 1.28 cm averaged over the last 900 years in the Jingjiang section below Yichang (Figure 21.9). Aggradation of the riverbed has resulted in a close correlation to the increase in water levels and dykes with time.

We measured sediment grain size along the main channel of the Yangtze in May 2002. Eight-seven suspended sediment samples were taken from the water surface at every

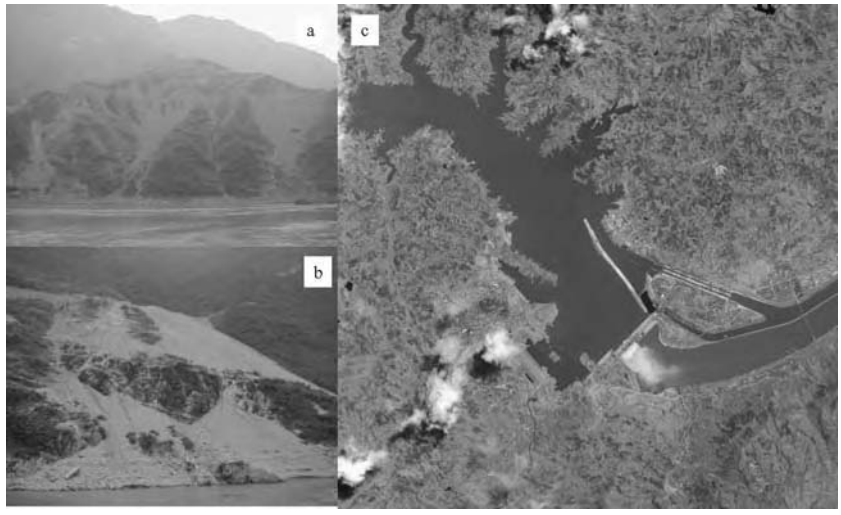

Figure 21.7 Anthropogenic supply of sediment to the gorges (a,b) and the Three Gorges Dam (c)

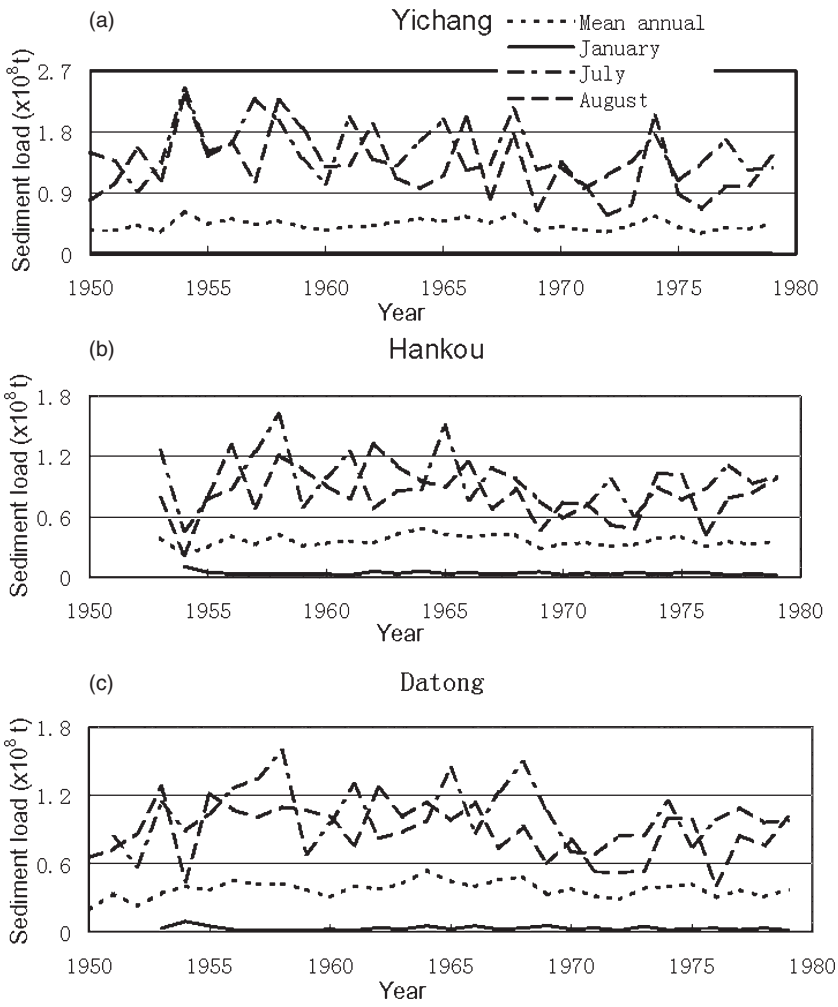

Figure 21.8 Changes of sediment load with time at (a) Yichang, (b) Hankou and (c) Datong. One-third of the sediment load is deposited in a channel between Yichang and Hankou during high flows of July and August. Reproduced from Geomorphology, 41, 2–3, Chen *et al.*, Yangtze River of China, pp. 77–91, Copyright (2001), with permission from Elsevier

25 km from Chongqing to the river mouth. Discharges measured during this sampling exercise were about 15 000 $m^3 s^{-1}$ in the Three Gorges and about 30 000–40 000 $m^3 s^{-1}$ in the Middle and Lower Yangtze. A particle size analyzer (LS13 320, Beckman Coulter Inc.) was used. The median size of the suspended sediment carried by the Yangtze in the Three Gorges ranged from 5 to 7 mm (Figure 21.10). However, the sediment in the channel of the Middle Yangtze is much coarser, the median size being between 20 and 24 mm at many stations, although a fine texture of 5–8 mm also occurs at many river channel sections.

The Dongting Lake sited in the Middle Yangtze used to be the largest interior lake in China. Its size, however, has shrunk by nearly 50 % over the last century (Du *et al.*, 2001). In the early 20th century, the water surface area measured 5400 km^2 which was reduced rapidly to 2600 km^2 by the end of the century (Changjiang Water Conservancy Committee, 2001). The storage capacity of the lake has been reduced nearly to half of what it was 80 years ago due to heavy siltation derived primarily from the Yangtze. More than 0.8×10^8 t of sediment has been entrapped in the Dongting Lake annually since the early twentieth century (Changjiang Water Conservancy Committee, 2001; Xu *et al.*, 2005).

Deposition of the upstream sediment in the Middle Yangtze Channel has resulted in considerable aggradation

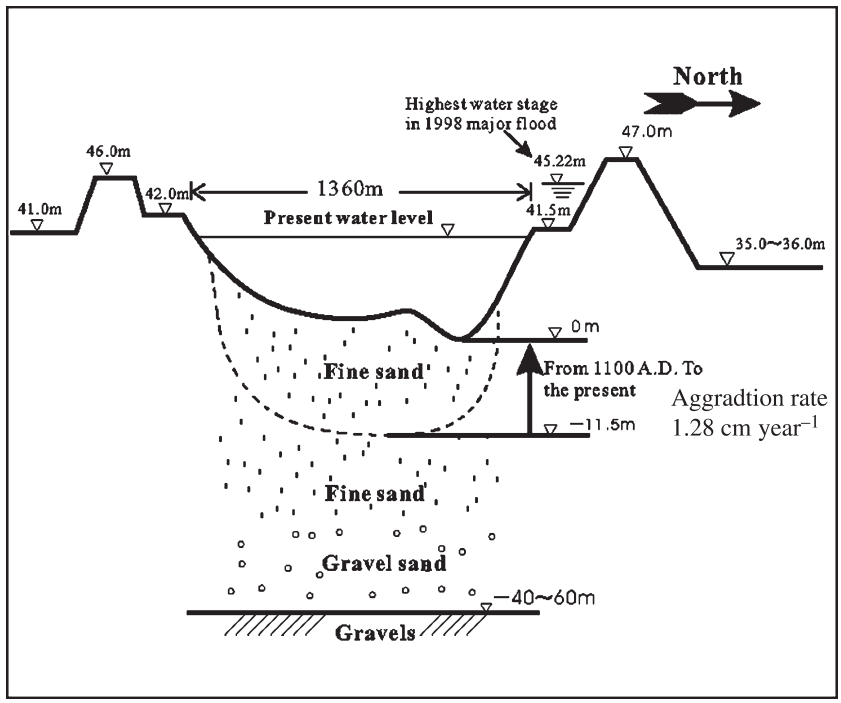

Figure 21.9 Schematic section showing riverbed aggradation at the Jingjiang reach below the Three Gorges. (Senior hydro-engineer Wang, personal communication, 1999)

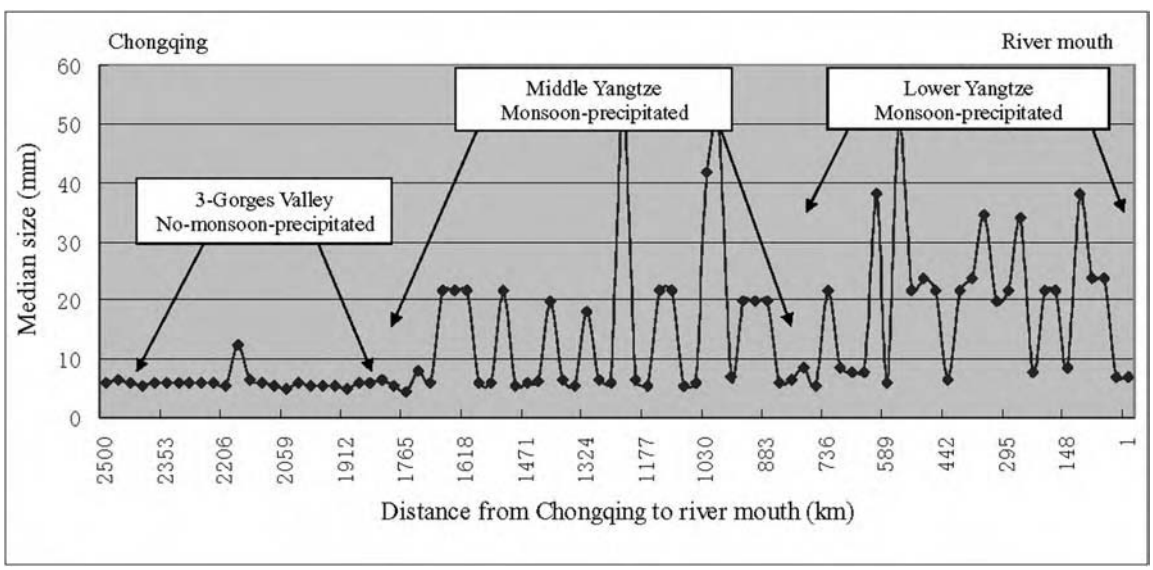

Figure 21.10 Suspended grain-size distribution in the Yangtze River channel during May 2002 illustrating the relationship between the upstream-travelling monsoon system and coarsening of the sediment

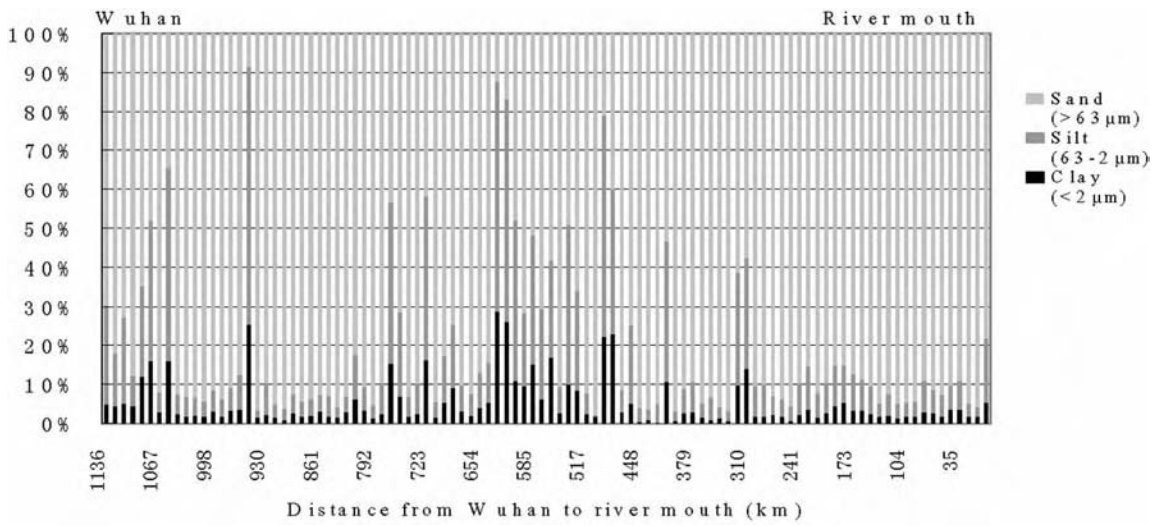

Figure 21.11 Sediment on river bed, the Middle and Lower Yangtze channel

and reduction of wetlands. Sediment is also added to the river during the wet period of April–June (Figure 21.10). The long-run sediment budget recorded both in the dry and wet seasons for the Middle Yangtze suggests that about 15% of the annual sediment flux in the river mouth area is derived from the Middle Yangtze sink, accounting for at least $0.6–0.8 \times 10^8$ t, given 4.7×10^8 t as annual sediment budget for the Lower Yangtze and the river mouth area (Chen *et al*., 2001).

21.3.5 The Lower Yangtze: Transfer of Sediment

An anabranching channel pattern typifies the Lower Yangtze River flowing between a series of low hills and Pleistocene river terraces (Wu, 1998). Comparison between long-term sediment budget recorded at upstream Hankou and downstream Datong stations demonstrates a slight increase: 4.42×10^8 t to 4.72×10^8 t (Figure 21.1). A number of small tributaries that flow into the Yangtze in this section are responsible for this increment. The Lower Yangtze River, bounded by high levees and engineered dykes, behaves as a passage for sediment, carrying almost all material entering into the Lower Yangtze to the river mouth and the continental shelf beyond.

We have found coarser sediment particles in the Lower Yangtze River channel during the nonflood season as in the Middle Yangtze (Figure 21.10). However, as the Lower Yangtze is primarily a transferring conduit, the coarser grains are possibly due to bank erosion in contrast to the smaller tributary-derived fine grains.

More than 300 riverbed samples taken by authors from the Lower Yangtze main channel at 10 km intervals indicate the widespread occurrence of medium and medium fine sands (>70% in most cases, Figure 21.11). The silt component is between 10 and 20%, and clay is less than 3–5% in general (Zhao and Chen, 2003).

21.3.6 The Yangtze Estuary: a Major Sediment Sink

The Yangtze is about 30 km wide and 8–10 m deep at its mouth. The tidal range is 2.7 m on average, but it can be >5 m occasionally during the astronomical spring tide (Chen *et al*., 1988). Tides can move upstream >200 km from the river mouth. The tidal velocity within the channel is generally about $1\,m\,s^{-1}$ but increases to $>1.5–2.0\,m\,s^{-1}$ off the river mouth. The ebb-tide velocity is faster than that of the flood tide. Due to being largely confined by the V-shaped estuarine morphology, tidal currents in the river mouth not only travel up and downstream but also rotate anticlockwise while moving towards the outer river mouth due to the funnel shape of the estuary. During July and August, when storms normally occur, strong littoral currents triggered by $>50\,km\,h^{-1}$ winds reform the sedimentary profile in the coastal zone, resulting in alternate erosion and siltation in the muddy tidal flat along the Yangtze coast.

The Yangtze Estuary serves as the major depositional sink for sediment transported from the drainage basin. A huge amount of fluvial sediment has accumulated in the river mouth due to 4.7×10^8 t being delivered to the estuary

per year. About 50% of this sediment, mostly fine sand and silt, is trapped in the estuary, and another half of the suspended sediment is dispersed seawards (Chen *et al*., 1988). Given that the Holocene Yangtze delta was initiated about 7000 years BP (Stanley and Warne, 1994), 1.7×10^{12} t sediment has since then been deposited in the river mouth area.

Tidal flats cover a wide area of this coast. The delta plain was constructed primarily as seaward prograding tidal flats against the rising sea level during the Early Holocene. The rise in sea level began to decelerate about 7000 years ago (Stanley and Warne, 1994). The estimated present progradation rate at the southern delta coast reaches 40–100 m year^{-1} (Yan and Xu, 1987). This, aided by human reclamation, has led to about 800 km^2 of additional coastal land over the last 50 years (Chen and Zhao, 2001). The (30×100 km) Chongming island, the biggest in the estuary, has increased its size by almost 40% since the mid-twentieth century (Chen and Zhao, 2001). Clusters of small submerged sandy shoals are being coalesced to form new estuarine islands seaward of existing ones.

The Yangtze estuary is dominated by fine-grained particles, >95% of sediment being sandy silt and silty clay (Chen *et al*., 2000). Suspended sediment disperses further seaward as freshwater plumes over the salt wedge that seeps inland, >150–200 km from the present coast, the distance varying seasonally. Investigations during May 2001 in the river mouth area revealed variations in salinity ranging from 11‰ near the river mouth to 34‰ offshore. During the winter, seawater travels further inland, as recorded by 1–2‰ salinity along the inner river mouth channel (Chen *et al*., 1988).

21.4 LARGE-SCALE RIVER MANAGEMENT – THREE GORGES DAM AND THE PLANNED WATER TRANSFER

This section examines the relationship between sediment transport and environmental challenge from recent intensifying human modification, chiefly represented by the on-going Three Gorges project and South–North Water Transfer project.

The sediment-depleted Three Gorges will change to a sediment reservoir soon after the closure of the dam in 2009. The current high-flow velocity (4–6 m s^{-1}) in the gorge will change to an impounded flow, presumably with a velocity below 1 m s^{-1} during most of the nonflood season. The changed flow setting is likely to cause heavy siltation in the gorges, taking into consideration many new settlements relocated on the upper slopes of the hills.

Flood events are standard hazards in the Middle Yangtze Basin (Changjiang Water Conservancy Committee, 1999). Annual maintenance of the high dykes built on flood levees is necessary. But, the potential risk from high water stage has been raised due to the confinement of the river channel between high dykes (Figure 21.9). Historical documents clearly indicate a rise in water stage with time and also the number of years with a high river level (Table 21.1).

The Dongting Lake region functions as the second most important source of water to the Middle and Lower Yangtze. The lake, however, has attenuated the flood arriving from the Upper Yangtze Basin for a long period. The abundant precipitation in the lake region also evens out the lower precipitation events in some years on the Upper Yangtze. However, the Dongting Lake did generate a large flood (Figure 21.5) in 1998 (Ni and Zhang, 1999; Li *et al*., 2001). The westward movement of the monsoon up the Yangtze Valley results in floods from the lake region below the Three Gorges Dam site peaking earlier than those from the western plateau through which the Upper Yangtze flows.

Reclamation of the lake and its surrounding floodplain has led to shrinking of the Dongting wetlands, largely weakening its ability for flood alleviation during the annual wet season. The aggraded riverbed of the Middle Yangtze also accelerates floods. This may change after the closure of Three Gorges Dam, as runoff carrying little sediment downstream of the dam may increase channel erosion. The Middle Yangtze channel, where large volumes of sediment have accumulated over years will become the major sediment source for the downstream channel and the coastal zone. It has been predicated that

Table 21.1 Historical record on highest water stage in Duochang Hydrological Gauging Station on the Middle Yangtze, and frequency of selected high water level (Changjiang Water Conservancy Committee, 2001)

	1950s	1960s	1970s	1980s	1990s
Multi-year averaged maximum water level (m)	18.51	18.38	18.93	19.10	20.19
Number of years in the decade with water level >19 m	2	4	6	5	8
Number of years in the decade with water level >20 m	1	2	2	2	4
Number of years in the decade with water level >21 m	1	0	0	1	2

the channel of the Middle Yangtze could deepen by 3–5 m after damming (Changjiang Water Conservancy Committee, 1999, 2001). Consequently, the river channel below the dam site will probably become unstable, eventually leading to erosion of riverbanks, mostly in recent loose sediments (Yang and Tang, 1999). In contrast, the bed of the Lower Yangtze could be raised due to the arrival of sediment from the middle section of the river. However, the entire river may subsequently undergo erosion. This could happen within decades after damming (Han and He, 1997). Active river monitoring in association with appropriate planning is the long-run strategy for better management of both the human needs and river behaviour.

The South–North Water Transfer project is planned with three routes connected to the Upper, Middle and Lower Yangtze (Figure 21.1). Presumably it would have little impact on the lower estuarine region, if a small amount of discharge (1000–2000 $m^3 s^{-1}$) is diverted, especially during the wet season. However, the seasonal hydrologic variations due to the monsoon regime result in both floods and droughts (Meteorological Institute, Chinese Academy of Sciences, 1981). The diversion of the Yangtze water to northern China should be carefully designed to prevent saltwater intrusion into the Yangtze Estuary, a topic of major concern. In the 1990s, an increase in river mouth salinity to 2–3 ‰ during a drought influenced industrial output on the Yangtze coast (Chen *et al*., 1988). Monitoring both water transfer and saltwater invasion is crucial in order to ensure the long-term feasibility of utilization of natural resources and societal development.

ACKNOWLEDGEMENTS

This project is supported by China National Natural Science Foundation (Grant No. 40341009), APN/START (Asia-Pacific Network for Global Change/Global Change of SysTem Analysis Research and Training) (Grant No. 2003-12), and Global Environment Research Fund of the Environment Agency of Japan.

REFERENCES

Changjiang Water Conservancy Committee (1885–1985) Hydrological Record of Changjiang Drainage Basin, 1885–1985 (internal report).

Changjiang Water Conservancy Committee (1999) *Atlas of Changjiang Drainage Basin*. China Mapping House, Beijing, 285 pp.

Changjiang Water Conservancy Committee (2001) *Atlas of Changjiang Flood Prevention*. China Sciences Publishing House, Beijing, 149.

Chen, J.Y., Shen, H.T. and Yu, C.X. (1988) *Processes of Dynamics and Geomorphology of the Changjiang Estuary*, Shanghai Scientific and Technological Publisher, Shanghai, 454 pp.

Chen, Z. and Zhao Y.W. (2001) Impact on the Yangtze (Changjiang) Estuary from its drainage basin: sediment load and discharge. *Chinese Science Bulletin*, 46, supp., 73–80.

Chen, Z., Song, B.P., Wang, Z.H. and Cai, Y.L. (2000) Late Quaternary evolution of the subaqueous Yangtze Delta: stratigraphy, sedimentation, palynology and deformation. *Marine Geology*, 162, 423–441.

Chen, Z., Yu, L.Z. and Gupta, A. (eds) (2001) Yangtze River, China: introduction. *Geomorphology*, 41, 73–75.

Du, Y., Cai, S., Zhang, X. and Zhao, Y. (2001) Interpretation of the environmental change of Dongting Lake, middle reach of Yangtze River, China, by ^{210}Pb measurement and satellite image analysis. *Geomorphology*, 41, 171–181.

Geographic Institute of Chinese Academy of Sciences (1985) *The Evolution of Yangtze River Channel*. Science Press, Beijing.

Han, Q.W. and He, M.M. (1997) Tendency of river channel evolution in Yangtze River's Middle and Lower reaches after Three Gorges project being completed. *Journal of Yangtze River Scientific Research Institute*, 14, 12–15 (in Chinese, with English Summary).

Huang, D.F., Yang, S.Z., Liu, Z.Q. and Mei, Z.Y. (1965) Geological studies of the formation and development of the three large freshwater lakes in the Lower Yangtze Valley. *Oceanologic et Limnology Sinica*, 7(4), 396–423.

Li, J.B., Yang, Y. and Xu, S.H. (2001) Study on formation of major flood hazards in the Dongting Lake region, 1991–2000 year. *Journal of Natural Science, Hunan Normal University*, 24, 90–94 (in Chinese).

Meteorological Institute, Chinese Academy of Sciences (1981) *Atlas of China Flood and Drought in the Recent 500 Years*. China Map Press, Beijing, 332.

National Remote Sensing Center and Applied Institution of Remote-sensing Center, Chinese Academy of Sciences (1984) *Images of Land Satellite – Atlas of Chinese Land Analysis*. Science Press, Beijing 223 pp.

Ni, F.R. and Zhang, Z.Q. (1999) Realization on 1999 major flood of the Dongting Lake. *Hunan Water and Electricity*, 5, 23–26 (in Chinese).

Stanley, D.J. and Warne, A.G. (1994) Nile Delta: recent geological evolution and human impact. *Science*, 260, 628–634.

Su, C., Mo, D.W. and Wang, H. (2001) Evolution of Lake Dongting and its flood disasters. *Research of Soil and Water Conservation*, 8(2): 52–55 (in Chinese, with English summary).

Tang, X.C. and Xie, S.Y. (1994) The exploration on the causes of geotectonic to form the regularity of distribution of the mountain calamity landforms surrounding Sichuan Basin. *Journal of Soil and Water Conservation*, 8, 76–84 (in Chinese, with English summary).

Three-Gorges Eco-Environmental Project Leader Group (1987) *Impact of Three-Gorges Project on Ecology and Environment and its Countermeasures.* Science Press, Beijing, 1126 pp. (in Chinese).

Wu, W.H. (1998) *Change of the Lower Yangtze River Channel*. River and Ocean Press, Nanjing, 97 pp. (in Chinese).

Xu, K., Chen, Z., Zhang, J. Hayashi, S. and Watanabe, M. (2005) Simulated sediment flux during the major 1998 big flood of the Yangtze (Changjiang) River, China. *Journal of Hydrology*, 20, 1–13.

Yan, Q. and Xu, S.Y. (1987) *The Recent Yangtze Delta Deposits*. Shanghai: East China Normal University Publisher, Shanghai, 437 pp. (in Chinese, with English summary).

Yang, H.R. and Tang, R.C. (eds) (1999) *Study on the Migration of Jingjiang of the Middle Yangtze River*. China Hydrologic and Electric Publisher, Beijing, 245 pp. (in Chinese, with English summary).

Yang, S.L., Bellkin, I.U., Belkina, A.I., Zhao, Q.Y., Zhu, J. and Ding, P.X. (2003) Delta response to decline in sediment supply from the Yangtze River: evidence of the recent four decades and expectation for the next half-century. *Estuarine Coastal and Shelf Science*, 56, 1–11.

Yin, H.F. and Li, C.A. (2001) Human impact on floods and flood disasters on the Yangtze River. *Geomorphology*, 41, 105–109.

Yin, H.F., Chen, G.J., Li, C.A. and Wei, Y. (2004) Siltation problem in the Middle Changjinag River. *Science in China*, 34(3), 195–209 (in Chinese).

Yu, M.P. (2002) Interconnection between Kuro-Shio and the precipitation over the Dongting area in summer. *Atmosphere*, 25, 21–23 (in Chinese, with English summary).

Zhao, Y.W. and Chen, Z.Y. (2003) Sediment characteristic and distribution in the Lower Yangtze River channel. *Acta Geographica*, 58, 223–230 (in Chinese, with English summary).

22

The Nile River: Geology, Hydrology, Hydraulic Society

M. Gordon Wolman[1] and Robert F. Giegengack[2]

[1]*Department of Geography and Environmental Engineering, Johns Hopkins University, Baltimore, MD 21218, USA*
[2]*Department of Earth and Environmental Science, University of Pennsylvania, Philadelphia, PA 19104, USA*

22.1 INTRODUCTION

The Nile fascinates us not simply because it is one of the largest rivers in the world, but because of its remarkable ancient history; the complex physiography of its drainage basin; its unique climatic setting, from the tropical equatorial region to the adjacent Sahara; its remarkably long hydrologic record; and the insight its history provides on the interaction of society and nature. In this account we attempt to touch briefly upon only several of these striking features, while recognizing that a vast and fascinating literature about the Nile reflects centuries of inquiry into the geography and natural and social history of the river and its basin. The three themes we have chosen are historical narratives, both physically and temporally related to one another. The geologic evolution and resulting landscape of the Nile drainage basin, in concert with the global atmospheric circulation, determines the unique and varied climate, and, in turn, the hydrology of the Nile. The hydrologic behavior of the river provided the stage for the evolution of a remarkable civilization whose historical records include a 1000-year record of Nile floods and the detailed social and cultural history of Egyptian civilization. This assemblage provides the basis for analyses of the complex inter-relationship of environment and society. Unique is emphasized here to convey the dictionary definition, one and only, not the common degraded sense of rare.

The Nile today is a poorly interconnected network of segments of several older river systems that are being integrated by contemporary erosion, even as the geometry of that network continues to be transformed by tectonic events.

The present configuration of the watershed, as is the case for any river system, is a snapshot of a moment in a continuing process of change, both geometric and hydrologic.

Crossing as it does a number of climatic zones and profoundly different physiographic provinces, the Nile has served as a corridor for the migration of organisms and, in recent years, for the transfer of human culture, among those disparate regions.

22.2 PHYSIOGRAPHY

The modern Nile is the longest river in the world, running some 6400 km from its most distant source in Rwanda-Burundi to its delta at the Mediterranean in Egypt. While its total length is great, it is not the largest watershed in the world, nor does it carry the greatest flow. Indeed, at least 30 rivers carry more water than the Nile, and the Congo, the Mississippi, and the Amazon drain larger watersheds (Leopold, 1962). The Nile today consists of a fortuitous convergence of at least five distinct segments. It seems likely that the linear geometry of the present Nile cannot long resist the tendency of headwater-flowing streams that drain to the Indian Ocean to capture components of the present Nile and fragment it.

Large Rivers: Geomorphology and Management, Edited by A. Gupta

It has been convenient for several generations of students of the Nile watershed (Ball, 1939 [1952]; Said, (1962) 1975, (1981) 1992; Giegengack, 1968) to divide the basin into five sub-basins (Figures 22.1 and 22.2):

1. The source of the White Nile: the Lake District surrounding Lake Victoria.
2. The lowlands of southern Sudan, including the vast wetlands of the Sudd.
3. The volcanic tablelands of Ethiopia, the source of both the Blue Nile and the Atbara.
4. The Cataract stretch below the confluence of the White and Blue Niles at Khartoum.
5. The low-gradient Nile Valley between the First Cataract at Aswan and the Nile delta.

22.2.1 The Lake District

The White Nile rises in the confusion of tectonically controlled topography where the African Rift System divides to form the Eastern and Western Rifts. Lake Victoria occupies a broad shallow depression between those two arms of the rift; the lake is contained between the recent uplifts of the western shoulder of the Eastern Rift and the eastern shoulder of the Western Rift. Overflow from Lake Victoria cascades over Owens Falls (now submerged under water impounded behind the Owens Falls Dam) and flows a short distance into one of the arms of Lake Kyoga, previously a westward-draining dendritic stream system in which drainage was reversed by the rise of the rift shoulder. The map configuration of the lake is reminiscent of that of any reservoir in the Great Plains of the United States. The divide between lakes Kyoga and Victoria is very low, and the southern arms of Lake Kyoga come very close to the northern margin of Lake Victoria. In the absence of continued lowering of the Owens Falls outlet of Lake Victoria, it seems inevitable that Lake Victoria will soon (in geologic terms) be captured by headward growth of one of the small streams feeding another arm of Lake Kyoga.

Overflow from Lake Kyoga cascades down the eastern wall of the Western Rift via Murchison Falls to enter the north end of Lake Albert, a lake that occupies the floor of the Western Rift, a foundered graben whose bedrock floor lies far below sea level. Outflow from Lake Edward, south of Lake Albert along the Western Rift, enters Lake Albert at its south end. From the outlet of Lake Albert, the Nile flows north to the lowlands of southern Sudan.

Much geomorphic and stratigraphic evidence of recent fault displacement can be observed throughout the Lake District; many shallow earthquakes, most of them indicative of contemporary extension, occur in this region today (Langston *et al*., 1998; USGS, 2004; Brazier *et al*., 2005).

In addition to extant lakes, the complex topography of the Lake District preserves many bodies of lake sediment (the best known of these sedimentary masses is the section now dissected by Olduvai Gorge) that may in the recent geologic past have been integrated into the Nile system.

The geometry of the Nile system within the Lake District is controlled by recent tectonic events; it seems likely that these events are frequent enough to overwhelm processes of erosional integration of elements of the system over geologic time.

22.2.2 The Lowlands of Southern Sudan

The White Nile leaves Lake Albert and flows into southern Sudan, soon to find its channel dissipated over the vast lowland of the Sudd, the largest swamp in the world. In the Sudd, the Nile loses ~45% of its flow to evaporation and transpiration by the rich growth of aquatic vegetation that chokes the channel and blocks the passage of river boats by huge, constantly shifting islands of floating vegetation that, until the interminable Sudanese civil war of the second half of the twentieth century, supported large populations of nomadic tribespeople. The earliest schemes to control the Nile included proposals either to drain the Sudd or to divert the White Nile around it.

Flow to the Sudd is augmented in the lower reach by the contributions of the Bahr el Ghazal, a stream that collects seasonal rainfall from the western Sudan and delivers it to the western reaches of the Sudd, and the Sobat, which enters the lower reach of the Sudd. Discharge from these rivers joins the diminished flow of the White Nile at the northern edge of the Sudd and from there flows north to be joined by the Blue Nile at Khartoum. The gradient of the Nile between the southern boundary of the Sudan and Khartoum is extremely low, 0.00001. In years of extreme flow in the Blue Nile, the White Nile backs up all the way from Khartoum to the northern margin of the Sudd.

22.2.3 The Ethiopian Tableland

The Blue Nile rises in Lake Tana, a volcanic caldera at 2400 m above sea level in the highest part of the volcanic pile that makes up most of Ethiopia and represents the topographic barrier that intercepts the orographic rainfall of the Indian Ocean monsoon. Lake Tana overflows to the east as the Blue Nile; the river describes a dogleg as it reverses direction to flow west across the volcanic highland and, through one of the most dramatic gorges in Africa, down the western slope of the Ethiopian Plateau to the lowlands of eastern Sudan. It seems inevitable that the upper Blue Nile will soon be captured to the Indian

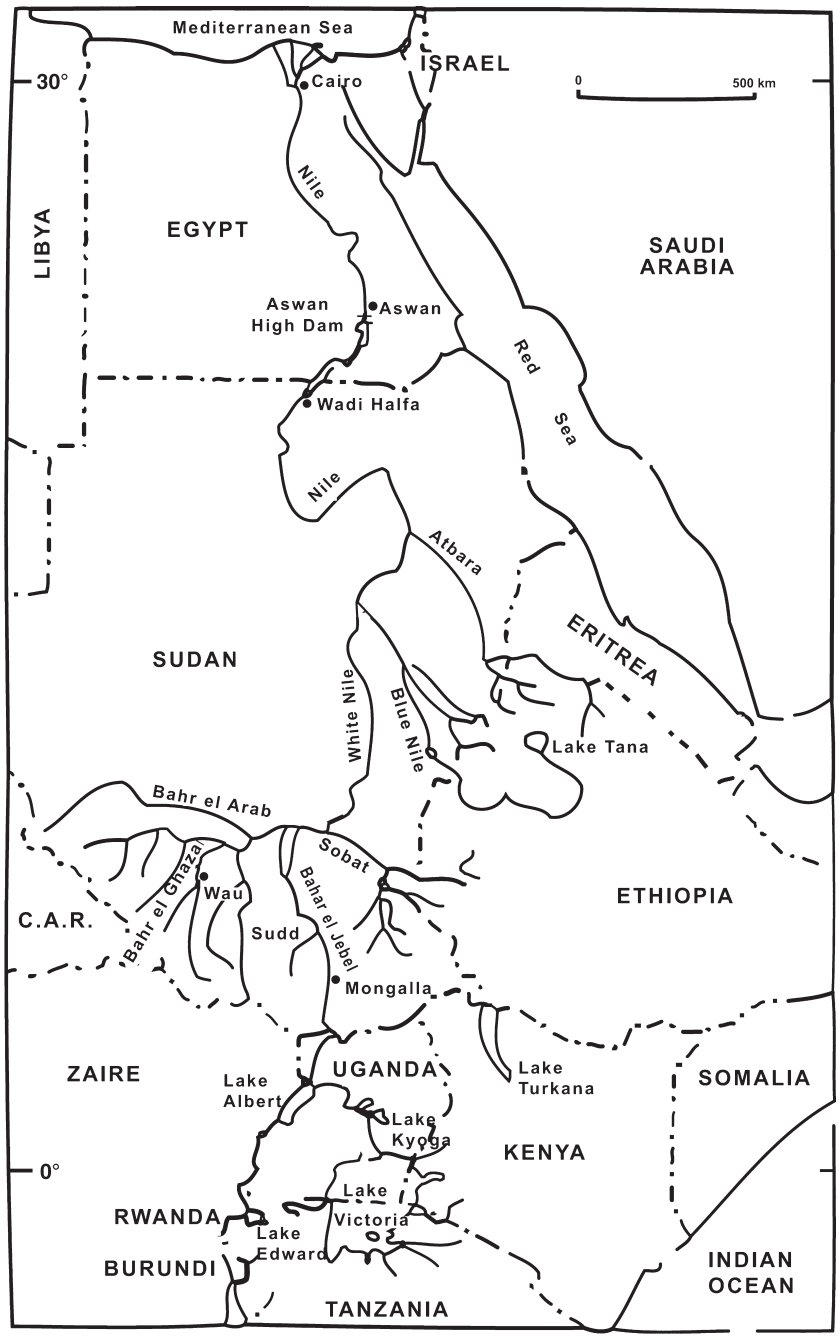

Figure 22.1 Map of the drainage basin of the Nile River. Reprinted from IAHS Special Publication no. 5, Sutcliffe, J.V. and Parks, Y.P., *The Hydrology of the Nile*, 1999, with permission from IAHS Press

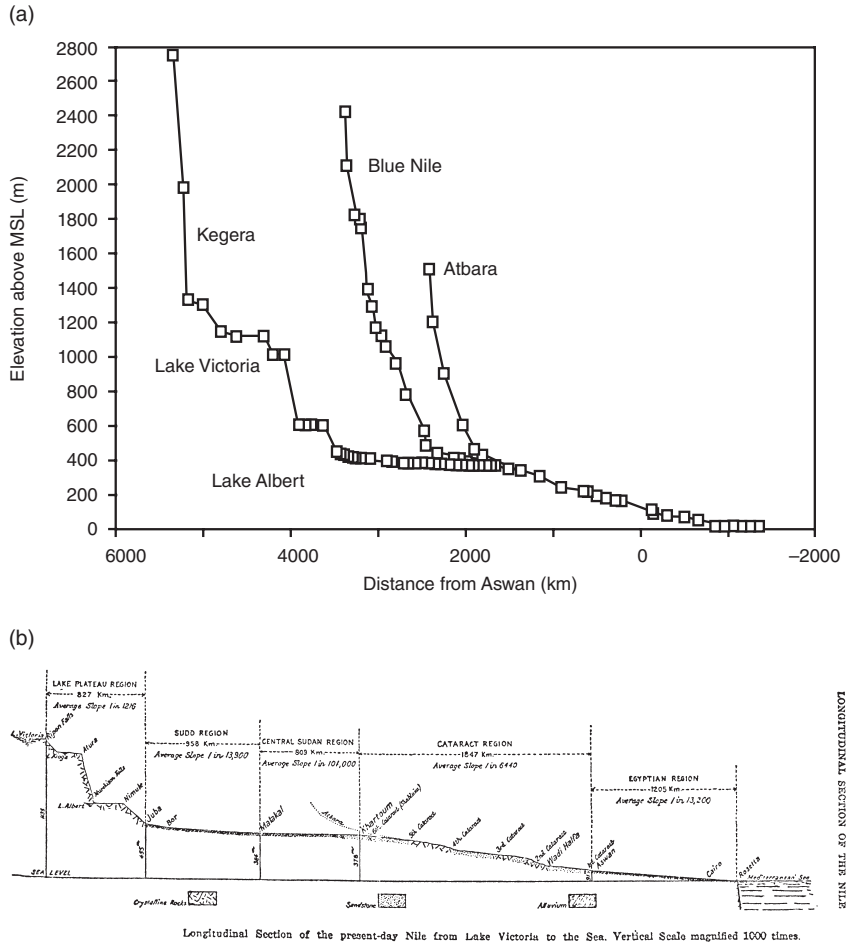

Figure 22.2 Longitudinal profiles of the Nile, White, and Blue Nile. Note very flat gradient at km 2000. Figure (a) modified from IAHS Special Publication no. 5, Sutcliffe, J.V. and Parks, Y.P., *The Hydrology of the Nile*, 1999, with permission from IAHS Press; (b) redrawn from Ball, 1939

Ocean by a stream draining the eastern slope of the Ethiopian Plateau.

The Blue Nile joins the White Nile at Khartoum; from the confluence to the Mediterranean, 3000 km north, the only significant additional water that enters the Nile system comes down the Atbara, another stream that rises on the north edge of the Ethiopian Plateau. In some years the Atbara makes a substantial contribution to Nile flow; in other years the Atbara Valley remains wholly dry.

22.2.4 The Cataract Reach

North of Khartoum the combined Nile flows across a low plateau underlain by late Palaeozoic and Mesozoic sedimentary rocks, beginning with the stratigraphically controversial Nubia Formation (Issawi, (1971) 1973; Issawi *et al*., 1999), to many still the Nubian Sandstone. The Nubia Formation lies unconformably over a deeply weathered igneous-metamorphic complex that is visible in the mountains of Sinai, in the core of the Red Sea Mountains along the western margin of the Red Sea, in upthrown basement masses in the western desert of Egypt, and in the small prominences of basement rock that rise to the ground surface along the course of the Nile in northern Sudan and southern Egypt, forming the six cataracts of the Nile (numbered sequentially from north to south).

Given that the sedimentary cover lies largely undisturbed over the six cataracts, it seems likely that the bedrock

islands of the cataracts are fault-bounded horsts across which the Nile was superposed during its recent erosional history. Some of those faults are mapped, but elsewhere the lithologic uniformity of thick sections of Nubia Formation make such structures difficult to identify.

22.2.5 The Alluvial Nile

Downstream from Aswan, the Nile flows over a progressively thicker section of sediment deposited by the Nile (or its ancestor) in the deep gulf excavated in Miocene-Pliocene time while the Mediterranean was briefly almost dry. The section in that gulf includes Miocene, Pliocene, and Pleistocene sediments; the column of sediments was partially excavated during each low-stand of sea level through the cycles of Pleistocene glaciation, and was most recently filled as the sea rose to its present level as the last continental ice sheet melted. Thus, the Nile below the First Cataract at Aswan flows across a column of alluvial sediment.

The deeper gulf actually extends some distance above the bedrock barrier of the First Cataract at Aswan. When the Aswan High Dam was under construction through the early 1960s, exploratory borings in the bed of the river, 30 km upstream from the Low Dam, built on the granite of the First Cataract, discovered a column of 240 m of Pliocene/Pleistocene sediment in the bed of the Nile (Chumakov, (1967) 1968; Butzer and Hansen, 1968; Giegengack, 1968). That column of sediment is connected to the filled valley downstream of the First Cataract via a deep valley, now dry and largely filled, that diverges from the present Nile course at Shellal, above the Cataract, follows a ~6 km arcuate course around the First Cataract, and joins the valley of the modern Nile below Aswan. The mesa that stands between this abandoned channel and the First Cataract is partly covered by a thin veneer of coarse, well-rounded gravel in a bright red silty matrix, the Early Nile Gravel of Giegengack (1968). Farther upstream, opposite Abu Simbel, sediment assigned to the same unit has yielded a dense concentration of Acheulean artifacts (Giegengack, 1968). Thus, it seems likely that the First Cataract, at least, is no more than a few hundred thousand years old.

Indeed, the lowermost 2000 km of the Nile represents a reach that receives no new water, and flows north across the eastern Sahara in close proximity to the opening rift system of the Red Sea. The Nile has not been captured by a stream flowing to the Red Sea, both because the western side of the Red Sea Rift continues to be uplifted and tilted to the west by the continuing process of rift-shoulder uplift, and because the hyperarid conditions that prevail in the Sahara have not provided enough surface runoff to enable streams draining the eastern Sahara to keep ahead of that uplift. However, it seems likely that the Nile must soon be fragmented by capture by a stream draining into the Afar triangle and/or by a stream that will intersect the headwaters of the Wadi Qena and abscond the Nile along a reversed Wadi Qena into the Red Sea.

22.3 GEOLOGIC HISTORY

> 'The Nile basin is [thus] a palimpsest of episodically reactivated geological structures (mylonites, shear zones, fractures) generated at least 550 Ma ago. These ancient structures account for the complexity and variable alignments of the world's longest river, and of all major depocentres within the Nile basin' (Adamson *et al*., 1992). Geology provides a sequential history of this complex physiography.

The physiography of northeast Africa and what eventually became the Nile basin owes its origin to the northward movement of the African continent and its subduction under southern Europe, and to tectonic events that created the rift valley of the Red Sea, the Gulf of Aden, and the grabens of the divided African Rift farther south. Tectonic uplifts and sea-level changes began with the retreat of the Tethys Sea in late Eocene time (40 Ma) (Issawi and McCauley, 1992). As the quotation from Adamson *et al*. (1992) suggests, major structural features stretch even farther back. In contrast, the integrated modern Nile is much younger, although students of its history hold varying opinions on when in Plio-Pleistocene time the river achieved its present configuration.

22.3.1 White Nile: Uganda, Kenya, Sudan

The most southerly boundary of the present Nile drainage basin lies just south of the margin of Lake Victoria, roughly 2° south of the Equator. Prior to uplift and inception of the Albert Rift, drainage was to the west. Uplift beginning in early to mid Tertiary produced ponding and alluviation, and initiated east-flowing streams and a *proto* Lake Victoria (Williams and Williams, 1980). Deposits on the floor of Lake Albert are of Miocene age; repeated faulting was accompanied by thick lacustrine deposition during Pliocene time, a process that continued into middle and late Pleistocene. Eventually, drainage from the early Lake Victoria flowed into Lake Albert and thence into southern Sudan. Overflow from Lake Victoria to the White Nile is thought to have resumed (Williams *et al*., 2003) in the late Pleistocene about 15 000 years ago. Recent discovery of a palaeolake extending over 500 km along the Nile from near Khartoum to above the junction

of the Sobat (the downstream limit of the Sudd) indicates that the White Nile was 'already active during the middle Pleistocene, more than 250 k.y. ago' (Williams *et al*., 2003: 1001). Not only is this finding of historical significance, but the existence of the palaeolake bed accounts for the extraordinary flat gradient of this portion of the longitudinal profile of the White Nile. Mio-Pliocene drainage from Lake Albert and Uganda to the Sudan has been dated as late Cenozoic. Uplift in Ethiopia and in the Uganda–Kenya region was accompanied by downwarping and faulting in the Sudan. Subsidence of major sedimentary basins allowed accumulation of thick sedimentary volumes beneath the areas over which the present White and Blue Nile flow, including 10–11 km beneath the Sudd (Williams and Williams, 1980). Major tributaries from the west follow major tectonic trends in the Sudan. Indeed, study of the complex structural and tectonic features of the Nile Basin indicates these to be fundamental controls of the drainage throughout the geologic past continuing until today (Adamson and Williams, 1980).

22.3.2 Egypt

In the north in Egypt toward the end of Eocene time (ca. 40 Ma), with the retreat of the Tethys Sea and uplift in the west, some streams flowed north across the emerging region, while others flowed toward southwest Egypt, as the western desert was denuded and limestone scarps retreated toward the west. Infrared satellite images have shown enhanced evidence of these streams underlying the late Quaternary surficial veneer that covers much of the Western Desert. The following account is drawn primarily from Issawi and McCauley (1992). On the east, streams flowed down the slopes of uplands flanking the Red Sea region. Uplift from doming in the region preceded rifting of the continents in Miocene time. Gravel sediments from erosion of the flanking Red Sea region are seen to the west in deposits overlying the limestone plateau, the region created by denudation of the emerging landscape. Remnants of these gravel deposits are the principal remains of the early drainage systems in this region. In the Fayum Depression, outcrops of fluvial sediment, derived from rocks in eastern Egypt, are of early Oligocene age. Climate during most of the Tertiary was hot and humid implying sufficient runoff for active erosion and sediment transport.

'During the Early Miocene (ca. 24 Ma) the Red Sea area underwent accelerated uplift associated with continental rifting' (Issawi and McCauley, 1992: 127). These authors outline the development of a major south-flowing river along the course of the present Wadi Qena, flowing parallel to the Red Sea uplift to the east and high limestone scarps on the west. The southward gradient of the Wadi Qena was controlled by uplift in the north. The prior south-flowing reach is roughly 150 km long, from the latitude of Qena south to the vicinity of Aswan. In the region to the south in southeastern Egypt and northeastern Sudan, structural uplift and depression created a northwest-trending low. The new 'Qena system' drained to the southwest, and its tributaries denuded a new erosion surface, leaving only remnants of the 'original' west-flowing streams on the rising Limestone Plateau. Intermittent uplift and erosion on the flanks of the Red Sea produced erosion of successive pediplains of southeastern Egypt. 'Southeastern Egypt remained south draining during much of Miocene time. The main channel of the Qena system to the south where the scarps pinch out flowed toward Wadi Halfa and Sudan roughly "coincident" with the valley of the present Nile' (Issawi and McCauley, 1992: 130).

The Blue Nile and other Ethiopian tributaries flowed north as the rivers in Egypt flowed south. Some evidence suggests an outflow channel to the west along what is now Wadi Howar (Pachur and Kröpelin, 1987). A later, shorter course to the Chad Basin may have been through a gap farther north. As base level dropped along the north shore of Egypt by Middle Miocene time, deltaic deposits accumulated as sediments were transported by north-flowing streams. Provenance of clasts in these deposits indicates sources from the Nubia Formation of Mesozoic age, but not from the crystalline rocks of the Nile Valley.

Continental movements closed the Mediterranean by the late Miocene time (ca. 6 Ma). With evaporation of the closed basin, base level dropped about 1000 m or more initiating downcutting and headward erosion of streams that drained to the Mediterranean Basin. A succession of rising and falling base levels followed.

Downcutting in the first of these produced entrenched streams that cut their valleys headward along zones of structural weakness through a limestone barrier that separated the downstream (Cairo) stretch of the Nile from the Qena region. With a gradient estimated at 20 times that of the present Nile, the headward-cutting north-flowing river captured the flow of the Qena system, along with major tributaries in the south. New tributaries were formed, others enlarged, and for the first time a north-flowing system extended from southern Egypt to the Mediterranean (Issawi and McCauley, 1992).

With the reopening of Gibraltar in early Pliocene time, sea level rose at least 125 m accompanied by a marine invasion of 900 km to Aswan accompanied by aggradation in tributaries. Following regression of this sea in late Pliocene time, a renewed north-flowing river transported sediments to accumulate in the Mediterranean Basin as a Pliocene delta. Most of the sediments of the early Pleistocene were derived from within Egypt and from the Red Sea range, and include clasts derived from Precambrian, Palaeozoic, and Mesozoic rocks. Issawi and McCauley

(1992: 133) suggest that the highest gravels (above 180 m) along the Nile are reworked from earlier Tertiary deposits. The oldest known Nile sediments with provenance in Equatorial Africa are those of the Dandara Formation in the vicinity of Qena. Integration of the modern Nile drainage is marked by these deposits. The river was transformed from one carrying much coarse bedload to one dominated by suspended load as the climate became increasingly arid. A minimum age for the Dandara Formation from uranium-series analysis of a calcareous root cast dating is 213 ± 14 ka.

22.3.3 The Blue Nile and the Atbara: Ethiopia

The major source of water and sediment in the modern Nile is the highlands of Ethiopia. Again, the geologic history of the region is complex, as is the history of the lower Nile in Egypt, with major tectonic and volcanic forces during the Cenozoic, setting the stage for the now dominant physiographic features.

Before rifting, uplift, and volcanism began in the Ethiopian region during the Cretaceous time (Williams and Williams, 1980), the region consisted of Precambrian metasediments and granites overlain by Mesozoic sandstones and limestones. Major uplift in the late Eocene (41–34 Ma) was contemporaneous with rifting in the Red Sea region. What became the eastern scarp of the Ethiopian highlands began as an early rift during the late Miocene. Faulting of the rift margin began in early Pliocene time and continued intermittently during the Pleistocene, accompanied by major volcanic eruptions. Parts of the rift valleys contained lakes; and the diatom fauna in the sediments indicates a wetter and fluctuating climate in Cenozoic and Pliocene time.

The Blue Nile and Atbara Rivers are younger than the lavas (flood basalts) of Oligocene to early Miocene age into which they are entrenched. Major shield volcanoes superimposed on the flood basalts are represented in the present landscape by the Semien and Choke-Mengistu Mountains (Adamson and Williams, 1980), and by significant bends in the Blue Nile and Atbara passing around them. Williams and Williams (1980: 212) characterize the history of Tertiary rivers in the Ethiopian region as 'chequered'. Between Lake Tana and the Sudan border, 'the Blue Nile has cut a gorge 1400 m deep and 20 km wide and is incised into a plateau at an elevation of 2600 m' (Williams and Williams, 1980: 213, citing McDougall *et al.* 1975). The calculated rate of lowering, 0.015 mm/year^{-1}, from determination of the volume of rock removed over the river basin areas, is low for a tectonically active region, suggesting intermittent periods of uplift and quiescence. Much of the path of the river system appears to be structurally controlled, a large lineament marking 'the boundary of volcanic rocks to the west and Precambrian rocks to the East in Ethiopia . . . Parallel courses of the Atbara and a reach of the Nile containing the Fifth Cataract are co-linear and parallel in the Sudan, suggesting structural control of both' (Adamson and Williams, 1980: 249).

Major sedimentary basins in south-central Sudan maintained by tectonic activity became the repositories of sediments periodically eroded from regions of uplift in Ethiopia and in Kenya–Uganda. Cenozoic alluvial fans, rejuvenated multiple times, comprise most of the fill, which includes the Gezira Formation deposited over the Nubia Formation, itself a fan deposit on older rocks. Considerable deposition also took place in the Turkana Lake basin in the Ethiopian Rift, now east of the boundary of the present Nile watershed boundary (Adamson and Williams, (1980) Figure 10.1: 227).

22.4 CLIMATE AND CLIMATE CHANGE

22.4.1 Introduction

The Nile today crosses a number of quite different climatic regimes on its way from the highlands of Central and East Africa to its mouth in the Mediterranean (Thompson, 1965; Griffiths, 1972; Buckel, 1996; Leroux, 2001). Precipitation is concentrated in two regions, the Lake District in the south and the Ethiopian highlands (Figure 22.3). The Lake District in the upper White Nile Basin experiences two wet and two dry seasons annually, the expression of the cyclical migration of the Intertropical Convergence Zone (ITCZ). The northward limit of that migration today lies across Central Sudan; thus, terrain between the Sudd and Khartoum experiences only a single wet season, associated with the months before and after the June Solstice. The intensity of that wet season diminishes to the North, so that downstream of Khartoum no discharge from local rainfall enters the Nile system.

The elevation of the Ethiopian Plateau accentuates orographic rainfall associated with the Indian Ocean Monsoon, so that the headwaters of the Blue Nile receive heavy precipitation off the Indian Ocean at the same time that ITCZ-driven precipitation reaches its most northward position. The combined contribution of the Blue Nile and the Atbara, in years when monsoonal rainfall reaches the Atbara watershed on the northwestern margin of the Ethiopian Plateau, has typically represented from 65 to 85% of the total Nile flow.

Below the confluence of the White and Blue Niles at Khartoum, the Nile receives further runoff only from the Atbara, where it joins the main Nile stream 300 km downstream from Khartoum. Below the Atbara, the Nile flows 2250 km across the hyperarid Sahara, where it loses flow both to intense evaporation (~2.5 m/year^{-1}) and to infiltra-

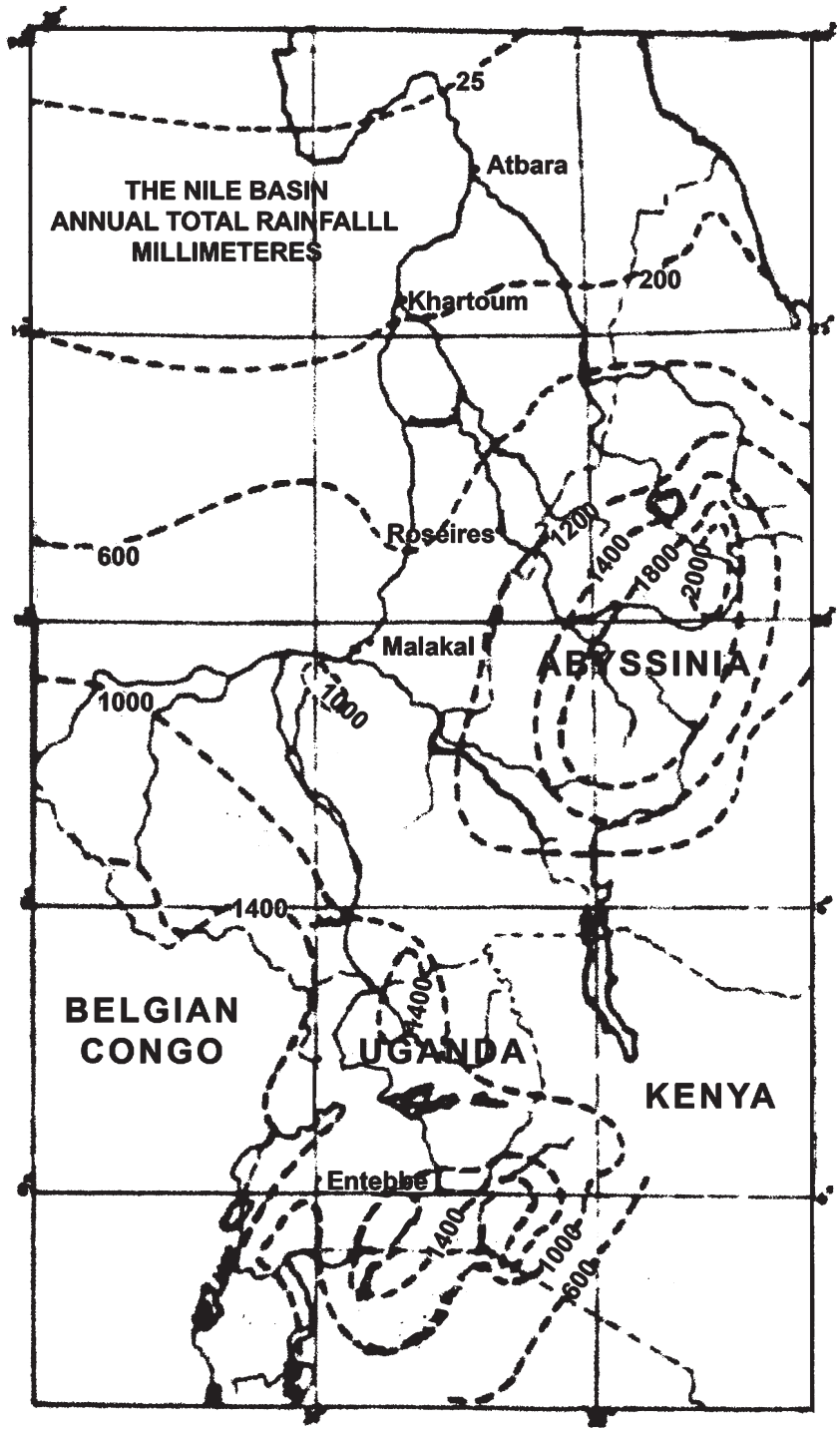

Figure 22.3 Map showing distribution of precipitation in the Nile drainage basin. Reprinted from *The Nile*, Hurst, H.E., 1952, published by Constable. Copyright, the Illustrator – every effort has been made to find the copyright holder

tion to unconfined aquifers in and adjacent to the Nile Valley. The higher flow shown in Figure 22.4 results from some artificial storage in the reach. From Cairo downstream, the Nile flows across the stretch of Saharan margin that receives meager winter precipitation, but, in typical years, none of that is ceded to the Nile flow.

The pattern of regional climates through which the Nile flows is a consequence of the global atmospheric circulation system superimposed on the topographic configuration of the African continent, on which only the Ethiopian Plateau represents a highland of major extent. Reconstruction of past climates over different parts of the Nile Basin is most simply achieved by postulating past variation of the circulation pattern that controls climate in the Basin today.

As the preceding description of the physiography and geologic history of the Nile and Saharan regions indicated, climate during the Cenozoic and well into the Pliocene was humid, much wetter than the present. The Saharan region and North Africa became arid during late Pleistocene time. Climate oscillated between wetter and drier conditions throughout late Pleistocene and into Holocene time. From latitude 2° S at the headwaters of the Nile south of Lake Victoria to 31° N at the delta, over 6000 km, the Nile traverses a range of climatic zones. This, coupled with the topographic diversity, the large lakes of the White Nile, and the precipitous topography of the Ethiopian highlands, combine to make simple correlations between regional climatic changes and the hydrologic regimen of the Nile in Egypt very difficult. Evidence for regional climatic variations is presented here along with the results of some studies correlating Nile flow and regional climate change.

22.4.2 The Region

Based on weathering, palaeobotany, freshwater lacustrine fauna, and a through-flowing drainage from the western Libya and Chad regions in the Sahara, many investigators have concluded that northwest Africa was wetter, perhaps tropical, during the Cenozoic and into Pliocene time (Issawi and McCauley, 1992). Through-flowing drainage indicates perennial streams transporting gravel, and vegetation indicative of a savanna landscape.

Wendorf *et al*. (1976) proposed a climatic chronology, based on records from oases in what is now the Egyptian Sahara, for the region of alternating drier and wetter periods dating back to a very tentative possible correlation with the cyclicity of several European glacial episodes. The history of climate was inferred from the presence of carbonate deposits, presumably associated with springs; vegetation remains; and lakes, alternating with aeolian deflation and dune sands. The region is now dominated by major dune fields, bare rock surfaces, and sheets of fluvial gravel. Extensive surficial veneers of archaeological lithic materials demonstrate continuous human occupation in earlier times. Using a wide variety of stratigraphic indicators, including plant remains and cave, lake, and groundwater deposits, subsequent investigators have demonstrated the occurrence of many wet periods during late Quaternary time that correlate with marine oxygen-isotope stages, suggesting that the wet episodes resulted from migrations of the tropical monsoonal belt (Osmond and Dabous, 2003). The wettest phases of this climatic oscillation do not coincide with periods of glaciation in Europe. Rather, they relate to northern and southern migrations of the ITCZ to latitudes that would seem anomalous today.

In today's extremely arid northern Sudan (25 mm of rain $year^{-1}$), Pachur and Kröpelin (1987) propose an east-flowing Wadi Howar linked to the Nile 9500 to 4500 years BP in an environment of a higher water table, active springs, and shallow channel pools in which sediments, including fossils of hippopotami, were deposited. The former channel and bottomland of Wadi Howar are now the site of extensive dune fields. Consistent with these observations in the eastern Sahara, Pachur and Hoelzmann (2000), from evidence of freshwater lakes and swamps and a high water table, suggest a wet period from 9000 years BP that faded by 5700–4500 years BP in the north and by 4500–3500 years BP in the south. Although these conditions lingered as a stable ecosystem, indicated by palaeolakes and swamps, by 3000 years BP desiccation was complete, as indicated by deflation of sediments throughout the region.

Radiocarbon dating and plant microfossils indicate a 'generally wetter' climate than today in the tropics during early Holocene time (11 000–7000 years BP), in contrast to the cool, dry, and windy climate of the last glacial maximum, 18 000 ± 2000 years BP. Drying began again about 4500 years BP. In contrast, to the east in northeastern Sudan, freshwater molluscs along now dry or ephemeral streams flowing westward from the Red Sea Hills from an elevation of 1200 m indicate a wetter climate and perennial steams about 2000 years BP. Mawson and Williams (1984) suggest that the wetter climate was regional, based upon lake remains in other presently dry areas in the region, fuel requirements of iron-smelting at Meroe along the Nile below Khartoum, and historic reports of swampy regions, both in the Nile Valley and in the Red Sea Hills, that are no longer present.

A 7000-year record from a sediment core in the Nile delta records changes in the hydrology of the basin, including the changing provenance of water and sediment. Provenance is discernible because the $^{87}Sr/^{86}Sr$ ratio of

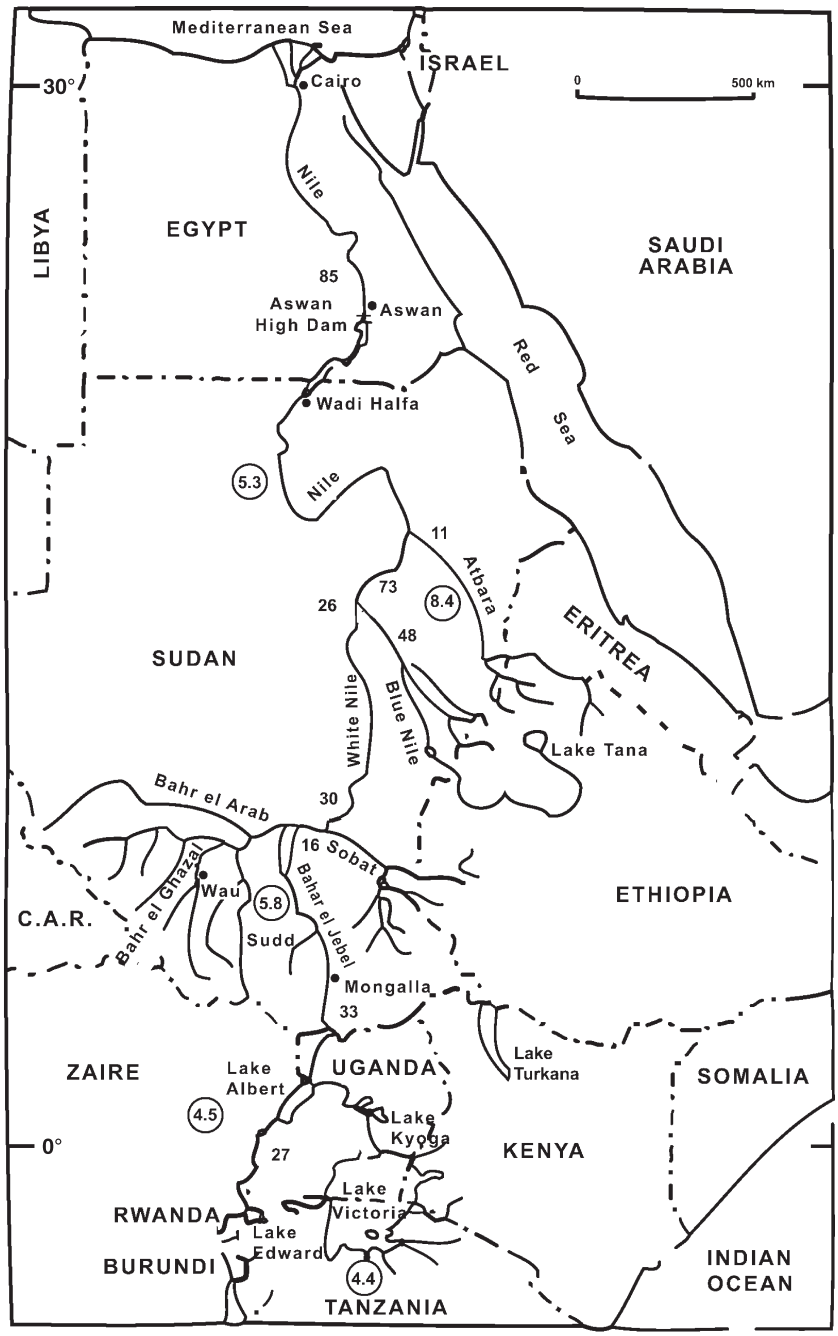

Figure 22.4 Map showing discharge and open water evaporation of the Nile River at selected locations. Note halving of flow through the great swamp, the Sudd. Numerals alone, annual flow ($\times 10^9 m^3$). Numerals in circles, daily evaporation (mm). Reprinted from IAHS Special Publication no. 5, Sutcliffe, J.V. and Parks, Y.P., *The Hydrology of the Nile*, 1999, with permission from IAHS Press

crystalline rocks from the White Nile differs from that of the Tertiary volcanic rocks in the Ethiopian Highlands, the source of the Blue Nile and Atbara. Greater volume of river flow was associated with 'decreased input of Blue Nile-derived and total sediment', as increased density of vegetative cover in the Blue Nile Highlands damped erosion and, hence, sediment supply. Periodic deposition in the Mediterranean Basin of organic-rich sediments (sapropels), associated with reduced inputs of sediment from the Blue Nile, occurred throughout the Neogene and Quaternary. Krom *et al*. (2002: 71) suggest that extended periods of 'catastrophic low floods' on the lower Nile in the period 4200–4500 years BP might have contributed to the demise of the Old Kingdom.

As noted earlier, recent research has confirmed early speculation that the very flat gradient (~0.00001) of the White Nile in the reach extending from the Sudd to Khartoum represents the extension of the north-flowing Nile across the bed of a large lake, >500 km long and 70 km wide, which formed initially over 250 ka ago. Thus, contrary to the assumption that overflow from Lakes Victoria and Albert to the White Nile did not resume until about 15 ka, the existence of the lake demonstrates overflow during Middle Pleistocene time (Williams *et al*., 2003). Stratigraphic analysis of lake sediments documented by radiocarbon and optically stimulated luminescence dating indicates 'resumption of flow from the equatorial headwaters to the White Nile' (Williams *et al*. 2003: 1004) about 15–14 ka, a period of very high Nile floods and enhanced summer rains associated with the youngest sapropel layer on the floor of the eastern Mediterranean. Slow rates of sedimentation in the palaeolake clay, coupled with deposits dated as older than 240 ka, suggest a very long interglacial period for which the authors' 'preferred correlate' is marine stage 11 (420–360 ka) (Williams *et al*., 2003: 1004).

At a site east of Lake Victoria, Barker *et al*. (2001), from a study of the moisture balance, oxygen 16/18 ratios, and diatoms in a tarn lake, define four periods of heavy precipitation at Mt Kenya during Holocene time while Rietti-Shati *et al*. (1998) suggest a warmer lake on the mountain from 2300 to 1500 years BP.

Table 22.1 includes selected data showing variations of climate in northeastern Africa, the complex region affecting the flow regimen of the Nile River. The most consistent feature of the history summarized in the table is the Holocene wet period (9500–4500 years BP) followed by desiccation. While the global circulation of the atmosphere, including seasonal geographic migration of the intertropical convergence zone, drives the climate over broad regions contributing to Nile flows, these are not detailed here. The following section reviewing features of the record of flows recorded by early Nile civilizations touches upon the relationship of flows of the Nile at Cairo to regional climate.

22.5 HYDROLOGY

22.5.1 Introduction

As the map (Figure 22.3) shows, the average monthly rainfall over the sources of the Nile reaches about 1200 mm

Table 22.1 Climatic conditions: selected locations, Nile River region (Pleistocene to present)

Location	Past climate measure	Age (ka BP)	Reference
Lake Victoria	Overflow	13.0	Beuning *et al.*, 2002
1° S 33° E	Decline biogenic silica		
Mt Kenya	Heavy precipitation	11.1–8.6	Barker *et al.*, 2001
0°9′S 37° 19′E	Diatoms, ^{18}O	6.7–5.6	
		2.9–1.9	
Mt Kenya	Warm lake temperature	2.3–1.5	Rietti-Shati *et al.*, 1998
	Biogenic opal		
Red Sea Hills	Wetter	2.0	Mawson and Williams, 1984
NE Sudan	Freshwater molluscs		
17° N 34° E			
Northern	Rivers	9.5–4.5	Pachur and Kröpelin, 1987
Sudan	Lakes		
17.5° N 28.5° E			
Egyptian Sahara	Pluvial	220.0	Osmond and Dabous, 2003
26° N 31° E	Groundwater	160.0	
	Ore deposits	100.0	
		80.0	
Kilimanjaro	Warmer/wetter	11.0–4.0	Thompson *et al.*, 2002
3° S 37.3° E	Cooler/drier	4.0–present	

in the Lake Victoria region and is as high as 2400 mm in Ethiopia. These rains produce significant runoff that increases downstream with progressive contributions from tributaries. Mean annual discharge at successive downstream locations is shown in Figure 22.4. Flowing north, the river traverses increasingly arid regions, in which evaporation rises. The most dramatic illustration of these counteracting influences can be seen above and below the extensive wetland of the Sudd. At Mongalla, the upstream limit of the Sudd, the mean flow is $1070\,m^3\,s^{-1}$, whereas at the outlet the flow is $490\,m^3\,s^{-1}$; roughly half of the flow is lost to evapotranspiration from water and wetland vegetation. While flow increases with the contribution of the Sobat to the White Nile below the confluence of the White and Blue Niles at Khartoum, with the exception of seasonal or ephemeral inflow from the Atbara, the natural flow of the Main Nile declines as a result of evaporation and infiltration to the groundwater system until the river reaches the vicinity of the Mediterranean. Modern manipulation of flows results in the higher flows at Aswan shown in Figure 22.4. The annual hydrograph of the White, Blue, and Main Nile at and below Khartoum is shown in Figure 22.5.

The Hydrology of the Nile, a remarkable volume by Sutcliffe and Parks (1999), provided the basis for the narrative of the hydrology given below.

22.5.2 The White Nile

The headwaters of the Nile, the longest river in the world at about 6400 km lie at 4° S latitude at the headwaters of the Kagera River in Uganda (Figure 22.1). Lake Victoria, into which the Kagera flows, has a surface area of about $67\,000\,km^2$. In this tropical region the river flows in a succession of lakes and river reaches, as described above, to Bahr el Jebel at Mongalla in the south where the Nile becomes the Sudd. Each of the river segments is characterized by alternating flat wetland reaches separated by steep and sometimes high falls, such as Murchison Falls, with a drop of 36 m.

Development of the complex water budget of the White Nile required many years of observation and analysis due to the scale of the region, and to the demanding task of measuring rainfall, runoff, and evaporation from vast lakes and wetlands fluctuating in both depth and surface area. Lake Victoria and the Sudd provide excellent examples. Rainfall over the lake itself provides about 85 % of the inflow; the remainder is contributed by tributaries. Much of the direct precipitation evaporates. Quoting Flohn and Burkhardt (1985), Sutcliffe and Parks (1999: 18) state, '. . . the nocturnal cloud above the lake itself . . . provides most of the water supply to the lake.' For many years, the level of the lake fluctuated over a

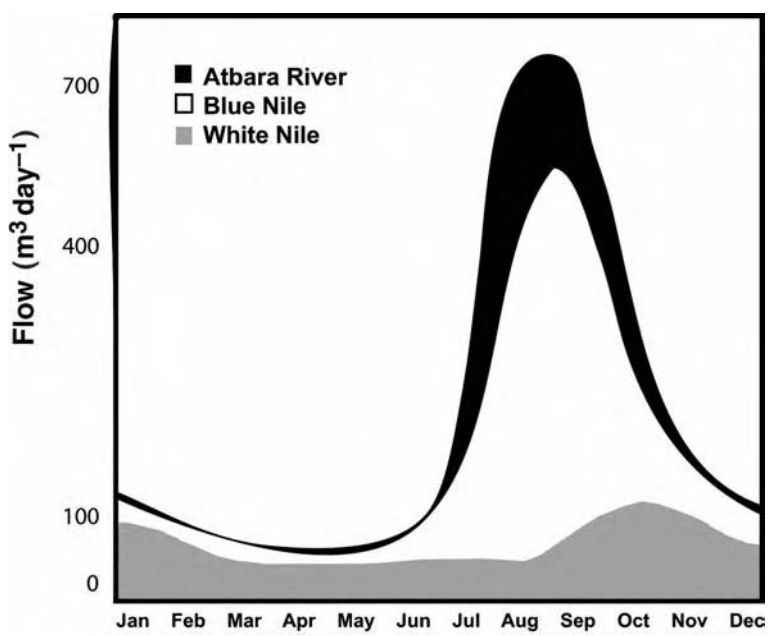

Figure 22.5 Annual hydrographs of White, Blue and Main Nile at and below the confluence at Khartoum (University of Michigan, 1980)

relatively narrow range of about 1–1.5 m but rose sharply, more than 2.5 m, from 1961 to 1965. After much investigation it was determined that the abrupt rise was due to an increase in precipitation beginning in 1961–1962, an increase reflected in flows of the main Nile as well. Flows have subsequently declined. The outflow record from 1895 to 1995, the longest flow record in the White Nile Basin, mirrors the lake levels.

The Sudd covers a surface area of about 6.5×10^3 km^2. Often referred to as the swamps, the area supports a variety of wetland vegetation sensitive to fluctuations and differences in water depth among a labyrinth of channels subject to overflow and backflow as discharge changes with tributary inflows and season. Vegetation growth and grazing has been an important part of the economy of the region. Our prose cannot capture the dynamic hydrologic scene nor the profusion of wildlife and vegetation of the 'swamp'. Seasonally flooded land is used by the Nuer and Dinka, who migrate with their herds from 'higher' lands receiving water during the rainy season to the river floodplains during the dry season. The rise of Lake Victoria in 1961–1964 led to doubled inflows to the Sudd. In recognition of the huge evaporation losses, the Jonglei Canal was proposed to bypass the Sudd as part of a more comprehensive plan, including Lake Albert as a reservoir and other structures upstream to regulate the flow. While canal construction was begun in 1978, work was suspended in 1983. The effect of the canal on grazing potential would depend heavily upon the operating rules for the diversion. Sutcliffe and Parks (1999) provide an extensive discussion of the hydrology, vegetation, and topography of this remarkable region.

22.5.3 The Blue Nile

The Blue Nile provides about 65 % of the main Nile flow. Rising on the highlands of Ethiopia at elevations of 2000–3000 m, the river and tributaries have cut deep ravines and gorges in steep reaches with perennial seasonal flows. The steep terrain gives way to the Sudan plains, marked by isolated hills. Vegetation reflects the altitude, from thin woodlands on the upland to savanna vegetation on the plains at an elevation of about 700 m. The Blue Nile, originating in headwaters above Lake Tana, traverses a series of cataracts. Flow is augmented by steep tributaries. Some regulation is achieved by a weir providing hydropower and controlling the stage of Lake Tana, while the main reservoir storage is at the Roseires Dam, where irrigation water is diverted for the Sudan. Two smaller reservoirs are developed downstream at the Sennar dams.

Annual precipitation ranges from about 1000 mm at the Sudan border to more than 2400 mm at Gore on the highland of the upper Baro river basin in the south. Reflecting the distribution of precipitation, runoff of the tributaries and the Blue Nile is seasonal, concentrated in the period July–October. Annual runoff, 17 % of the annual rainfall of 1590 mm, from the Blue Nile above its confluence with the White Nile for the period 1951–1987 was estimated to be 47.37 km^3 (269 mm) from a drainage area of 176 000 km^2. A combination of withdrawals for irrigation and some urban supply, which increased steadily from near zero in 1920 to a plateau of about 10 km^3 year^{-1} from 1975 to 1995, and uncertain calculated channel losses of about 2 km^3 annually, reduce flows in the reach between Roseires and Khartoum.

The Blue Nile joins the White Nile downstream from the junction of the Sobat. The large triangle of land between the two above the confluence, the Gezira, the generic name for such a topographic feature, includes over 2.4×10^3 km^2 of irrigated agriculture. Over the last century, the relative contribution of the Blue Nile to the main Nile has decreased from about 65 to 55 %, due to the rise in Lake Victoria after 1961 and recent declines in flow of the Blue Nile.

Based on a record for the period from 1902 to 1992, an annual flood at Khartoum with a return period of 2 years has a discharge of about 7500 m^3 s^{-1}, while the 100-year flood is approximately 11 000 m^3 s^{-1}. The relatively narrow range of peak discharges reflects the regularity of the seasonal precipitation and runoff (Sutcliffe and Parks, 1999).

In contrast to the low sediment load of the White Nile where tributary sediment inflow is trapped in the succession of lakes and wetlands, the suspended load of the Blue Nile is estimated at 140 million tonnes year^{-1}, with peak concentration about 6000 ppm below the Sennar Dam (Sutcliffe and Parks, 1999). The Atbara supplies about 82×10^6 year^{-1} (Garcanti *et al*., 2006). Throughout late Pleistocene time, the Blue Nile and the Atbara have contributed sediment to the formation of the modern Nile Delta in the Mediterranean.

22.5.4 The Nile below Khartoum

The longitudinal profile of the Nile from Khartoum to Aswan, a distance of 1900 km, includes the six major cataracts. The Atbara, with a drainage area of about 68 800 km^2, enters the Nile above the Fifth Cataract. The reach below the Fifth Cataract contains many lesser rapids. Generally flowing through an arid plain, rapids and narrows occur where the river cuts through rocks of the basement complex. The river here is about 600 m wide. The seasonal (July–September) contribution of the Atbara is approximately 11 km^3 while mean annual flow on

the Main Nile for the period 1911–1995 was 76 km^3 at Tamaniat below Khartoum and 84 km^3 from 1890 to 1995 at Wadi Halfa, near the upstream end of Lake Nasser above the Egypt–Sudan border.

22.5.5 The Nile Flows in Egypt

The Nile in Egypt now consists of the reach beginning at the head of Lake Nasser near the Sudan–Egyptian border through the 480 km length of the reservoir and a downstream reach of 1500 km to the Mediterranean Sea. The Aswan High Dam, behind which Lake Nasser is impounded, lies several kilometers upstream from the original Aswan Dam, constructed at the First Cataract in 1902 and subsequently raised in 1912 and 1933. Storage behind the Dam is approximately 163 km^3, and average annual evaporation has been ~10 km^3. Virtually continuous observations of stage and river flow made at the Roda gauge at Cairo for over 1000 years, record annual maximum and minimum river levels for the period 622 AD to 1921 AD. The Palermo Stone, a tablet recording chronology and events in Egyptian antiquity, records 60 flood levels extending as far back as 3000 BCE (Sutcliffe and Parks, (1999) quoting Said, 1993). Correlation of 'maximum Roda levels with annual maximum 10-day flows at Aswan for the common period 1869–1921' is deemed 'reasonable', and the record indicates that maximum stages in selected years correlate with high levels of Lake Victoria and, on other occasions, with recorded flows in the Bahr el Jebel, and jointly with events on both the Blue and White Niles (Sutcliffe and Parks, 1999: 159). One study (Flohn and Burquardt, (1985) cited by Sutcliffe and Parks, 1999: 160) indicated that about half the variance in the correlation between low flows at Aswan and contributions from Ethiopia and Lake Victoria could be attributed to each. Changes in the location of the gauge, gaps in the record, as well as evidence of slow aggradation of the river bed have made precise reconstruction of past river discharges somewhat uncertain. Thus, Sutcliffe and Parks (1999) in their exhaustive study note that, in the modern era, river flows at Aswan have been published since 1869, and a variety of estimates, based on water-balance studies, have also been made. They conclude that the 'most useful' (p. 152) record is of water arriving at Aswan from 1870 to 1990.

Construction of the Aswan High Dam has completely altered downstream flows on the river, reducing peaks and virtually eliminating the sediment supply downstream, as most of the sediment carried by the Nile is now deposited in Lake Nasser. The reduction of sediment supply has resulted in modest degradation and erosion downstream, accompanied by wave and current erosion in the Mediterranean and retreat of the distal margin of the delta aided by subsidence. Similarly, reduction of nutrients associated with both reduced sediment load and reduced discharge has virtually eliminated the sardine fishery in the eastern Mediterranean which, in years before construction of the High Dam, amounted to an annual catch of ~18 000 tonnes. More recent data suggest a revival of fish populations, perhaps as sewage waste introduced into the lower river compensates for loss of natural nutrients that now remain in Lake Nasser (Nixon, 2004). At the same time, production of other species of fish in Lake Nasser now greatly exceeds the quantity of fish previously harvested in the river, reaching an annual total of about 34 000 tonnes. Stored water has sustained agriculture in periods of drought, and storage of floodwater has prevented potentially devastating flooding of Cairo. Hydroelectric power from the dam now supplies the bulk of the demand for electric power in Egypt. Not surprisingly, about one-third of the annual regulated flow is lost to evaporation in a region where evaporation is about 2.7 m $year^{-1}$ over a lake area roughly 500 km long and 5–8 km wide.

22.6 A UNIQUE RECORD

During the course of an investigation to determine the volume of storage needed to guarantee a supply equal to the mean inflow over 100 years by a reservoir at Aswan, Hurst (1951), in a pioneering analysis of the Nile record determined that the range of Nile River flows did not follow the expected range based upon a random distribution of annual flows. Figure 22.6 (Hurst, 1952) shows the symmetrical distribution of flows around the mean when the distribution of floods in all years is determined simply by magnitude without regard to time. The equation for the range R is: $R = 1.65\ \sigma\ N^K$, where N is the number of years, σ is the standard deviation of the series, and K is a coefficient equal to 0.5 for a random distribution. Hurst (1951) determined that, for the Nile River flows, K equaled about 0.75, a value similar to that characterizing series of many natural phenomena (Table 22.2). Rather than random in time, there are sequences of high and low flows. The result came to be known as the 'Joseph effect' in accord with Joseph's interpretation of the Pharaoh's dream described in Genesis 1.

> 'And Joseph said to Pharaoh, "Pharaoh's dreams are one and the same: God has told Pharaoh what He is about to do. The seven healthy cows are seven years, and the seven healthy ears are seven years; it is the same dream. The seven lean and ugly cows that followed are seven years, as are also the seven empty

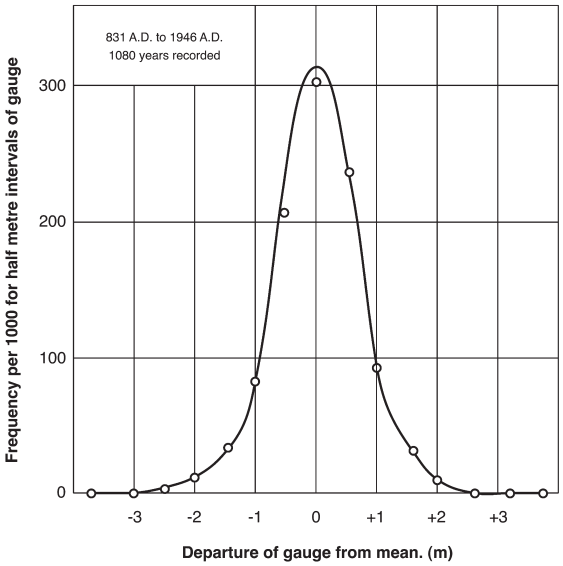

Figure 22.6 Frequency distribution of annual floods of the Nile River at the Roda gauge at Cairo. Record from 641 to 1945. Reprinted from *The Nile*, Hurst, H.E., 1952, published by Constable. Copyright, the Illustrator – every effort has been made to find the copyright holder

Table 22.2 Distribution of coefficient K in equation for the range R where $R = 1.65\ \sigma\ N^K$ (see text for definition of terms) of time series of natural data. Reprinted from Trans. Am. Soc. Civ. Engr. Vol 116, Hurst, H.E., Long-term storage capacity of veserroirs, pp. 788, 1951, with permission from ASCE

Source	K value
River discharge (Roda gauge, Nile 1000-year record)	0.75
Rainfall	0.70
Temperature and pressure	0.70
Tree ring width	0.80
Varves, thickness (Lake Saki, Crimea 2000 years)	0.69
Varves, thickness (Canada and Norway)	0.77
Sunspots	0.69
Wheat prices	0.69
Mean value adopted by Hurst for large number of cases	0.72
For random distribution	0.50

ears scorched by the east wind; they are seven years of famine"'

(Union of American Hebrew Congregations, 1981: 265)

The principle of storage in plentiful years to ameliorate shortage in the future became known as the 'ever normal granary' in the field of agriculture. It is however, of broad applicability to variable supply and storage problems. The phenomenon became known as the 'Hurst effect', a fundamental concept in hydrology and in many aspects of time series in nature. Based on the very long record of stages of the Nile, rough frequencies of high and low floods and their consequences, as reflected in the written records, are shown in Table 22.3.

Table 22.3 Frequency and characterization of Nile floods from long historical record (data from Lyons, 1906)

Frequency	Stage (above mean) (m)	Resultant effects
290/1000	+0.3	Some damage
	+1.0	'Flood'
80/1000	+1.2	Flood torrent
150/1000	0.75	Pinched year
	−1.0	Irrigation difficult
20/1000	−1.5	Famine

Much analysis has been undertaken of the hydrologic record of the Nile in attempts to tie the record to climatic variations, to relate flows at Cairo to lake levels in the headwaters, and to account for the Hurst effect. The effect has been simulated in autocorrelation studies with reasonable results. To date there is not firm agreement on a geophysical explanation of the Hurst effect, although a number of studies have indicated that the sequences of high and low flows are related to variations in the global circulation, including the El Niño cycles in the Pacific (Eltahir, 1996). The logic ties these phenomena together with oscillations in the latitudinal position of the ITCZ that controls the supply of water to the Upper Nile Basin.

22.7 THE NILE AND HYDRAULIC CIVILIZATIONS

The concept of 'hydraulic societies' or 'hydraulic civilizations' has been applied to many societies where command or control of water primarily for irrigation appears to be essential to sustaining the population of a community or state. The term has been used to describe small systems, such as those employing floodwater farming on terraced waterways in ephemeral channels, as well as very large systems, such as those found in Mesopotamia along the Tigris and Euphrates, in China on the Yellow and Yangtze, and in Egypt on the Nile. Water management has served as a basis for inquiry into the comparative social and cultural features that may evolve in association with the development of complex civilizations in an effort to develop cross-cultural themes or general principles of cultural development (Steward, 1955).

The following quotation from an essay by Karl A. Wittfogel (1955: 44), a leading scholar expositor of the subject, captures the major features of the concept:

> 'I suggest that the term "hydraulic agriculture" be applied to a system of farming which depends on large-scale and government-directed water control. I suggest that the term "hydraulic society" be applied to agrarian societies in which agro-hydraulic works and other large hydraulic constructions, that tend to develop with them, are managed by an inordinately strong government. I suggest that the term "state" be applied to a government that, on the basis of sufficient surplus, is operated by a substantial number of full-time specialists: civil and military officials. I suggest that the term "hydraulic society" be used interchangeably with "Oriental society" in recognition of the geo-historical fact that the societal order under discussion appeared most significantly and lastingly to the east of those European countries, in which social scientists first tried to define these phenomena. To the best of my knowledge, John Stuart Mill was the first to use the formula "Oriental society" (Mill, 1909: 20).'

In his classic study, *Oriental Despotism: a Comparative Study of Total Power* (1957), Wittfogel delineated an evolutionary or developmental history of hydraulic societies. As noted, Oriental, non-European, is offered as synonymous with the system itself, deriving from Wittfogel's analysis of historical development in China. Recognizing a diversity of agricultural societies as well as many modes of development, Wittfogel, in a shorter paper (1956: 44), distinguished 'hydraulic agriculture' from rainfall farming and hydroagriculture, stating: 'the term "hydraulic agriculture" may be applied to a situation in which the dimension of the available water supply leads to the creation of large productive and protective waterworks that are managed by the government' (1956: 153). Construction of large waterworks, and the management and operation of both hydraulic works and related activities, weakened private property, and led to a 'monopoly bureaucracy' to carry out these functions, supported by a controlled labor force (1955: 45). Such a powerful despotic centralized state controlled all aspects of the cultural, economic, and social life of the society. Hydraulic civilizations often supported large populations through high agricultural productivity, but were subject to rebellious internal forces, external pressures such as war and conquest, and the vicissitudes of a changing environment.

While we acknowledge both the complexity and variety of cultural development as well as the diversity of hydraulic societies and stages of their development, the dependence on climate and gravity-driven hydrology in semi-arid regions of the major hydraulic civilizations gives a strong environmental deterministic flavor to explanations of their existence. Some commentators read an inevitability into the concept of hydraulic civilization, an inevitability that is implied in the sequence from behaviour of the environment, the hydrology; to the need for and requisite of water management; to the need for system managers, a bureaucracy; to an autocratic, despotic, state elite that exercises complete control. Any 'successful' society in an environment constrained by the behaviour of the water resource it is argued will develop similar technologic, social, and governmental structures. Comparisons of smaller systems of water management, for example, floodwater farming or qanats in many settings, do reveal many similarities in physical features and techniques of operation, but wide divergences in social control (Mabry, 1996). Perhaps these are best described as hydro-agriculture, not hydraulic societies. If the analysis first offered by Wittfogel is valid, however, historical periods of a thriving economy and expanding development should coincide with resource availability and despotic control. Detailed historical analyses of economic development, resource use, and social structure in China and Egypt do not, however, show a consistent coincidence of despotic control and hydraulic development (Byrne, personal communication; Butzer, 1980).

In light of the complexity of the issue and the recent revival of interest in the impact of environment on society, the history of Nile development is of special interest, as it sheds light not only on the concept of environmental determinism but on the rise and fall of civilizations themselves. Much debate, however, characterizes the voluminous scholarly literature on the origin and evolution of civilizations. At the same time, virtually all studies recognize the three river civilizations, the Nile, Tigris-Euphrates, and the Indus as the oldest and among the greatest. While recognizing the complexity of the subject, we draw upon Butzer's (1980) analysis because of the direct association of the behaviour of a dominant environmental force, the Nile flows, and the vicissitudes of society.

Butzer (1980) introduces a study of civilizations noting that distinguished scholars have likened civilizations to organisms characterized by a life cycle of youth, maturity and old age. In proposing an alternative to an organic model, he examines the history of societies in the Nile to illustrate the concept of civilizations as adaptive systems responding with varying degrees of success or failure to endogenous and exogenous forces. The rich history of the Nile, including a direct measurement of the quality of the environment, the record of Nile floods, provides the

empirical evidence for his thesis. Moreover, the data and the analysis suggest caution in too facile acceptance of environment as the predominant factor in the development and 'success' of human societies. The discussion here is limited to a brief outline of Butzer's (1980) illustration of an 'ecosystemic' view of the history of society in the Nile.

Butzer separates periods of growth, stability, and decline. 'Episodes of growth in Egypt were made possible by such innovations as improved irrigation organization, devices for controlled water distribution during bad flood years, lift mechanisms to allow cultivation of marginal areas or several crops per year, as well as new cultigens better suited for poorer or drier soils and for summer cultivation–in an agricultural system originally geared only to postflood, winter crops' (Butzer, 1980: 518). He identifies five periods of growth, each associated with technological, social, and environmental changes. These intervals and the attributes associated with them are given in Table 22.4.

In contrast to periods of growth, the historical record documents various periods of instability associated with a myriad of features:

> 'The common denominator of each period of decline was rural depopulation and decreasing economic productivity. The responsible processes were complex and involved at least two of three major factors: excessive demands on the productive population; a high incidence of poor or destructively high Nile floods; and insecurity due to political instability, foreign rule, or invasion. Each retrograde phase coincided with negative social developments within, as well as negative environmental or social interventions from without'
>
> (Butzer, 1980: 521).

Table 22.4 Periods of growth in societies in Egypt and associated factors (after Butzer, 1980)

1. First dynasty 3000–2780 BCE controlled irrigation began, final unification of Egypt
2. Early Old Kingdom 2780–2560 BCE strengthening bureaucratic structure, development of central delta, diversified agriculture
3. Middle Kingdom 2160–2000 BCE post Nile failures, improved food distribution, Fayum Depression drained, colonization
4. New Kingdom 1580–1090 BCE shaduf (bucket) water lever lifts water, market gardens, demographic shift from valley to delta
5. Northern Delta Colonization 650–525 BCE Maryut depression, 300 BCE Ptolemies in power, efficient administration, resource use, Fayum drainage completed including canals from Nile, saqiya waterwheel, 2 crops year^{-1}

Butzer (1980: 521) identifies four 'systemic variables':

1. progressive social pathology characterized by exploitation of the masses by a small elite, as suggested by Wittfogel;
2. leadership, best exemplified by strong leadership such as that of Rameses III (1182–1151 BCE), who repelled foreign invaders and maintained order during grain shortages and whose reign was followed by chaos;
3. foreign intervention, illustrated by the destabilizing Hyksos and subsequent Assyrian (664 BCE) invasions;
4. 'ecological stress' as exemplified by the behaviour of the Nile, characterized as '. . . the most prominent agent overall', noting, however, that, 'This does not attribute the role of a determinant to Nile behaviour' (Butzer, 1980: 522).

While observing that many variables may enter into the dynamic system, Butzer illustrates the potential interaction of several factors oscillating over time, producing periods of positive and/or negative reinforcement, leading to favourable or unfavourable conditions in society. While environment may be the most important, as the quotation above indicates, it is only one among a number of important factors contributing to well being and social stability or instability, not the sole 'determinant'.

Both the environment and the idea of hydraulic societies are much in evidence today in explanations of both the asccendancy and the decline or demise of societies and in characterizing the organization and control of large irrigated agricultural systems. Thus climate change, a current passion, is cited as the 'cause' of the demise of the Akkadian empire in northern Mesopotamia in 3000 BCE (Weiss *et al*. 1993; Kerr, 1998). The extreme aridification of the Sahara, noted earlier, did of course preclude agricultural settlements in most of the desert. The physical archaeological evidence of climate change, particularly in such dry regions, and societal response is strong, but in many reports less attention is given to potential concurrent social and political factors, and *prominent* becomes *determinant*.

Emphasizing not climate but society, Worster (1982), in an article entitled 'Hydraulic society in California: an ecological interpretation', observes a parallel between the present control of massive irrigation systems in California by a few huge commercial corporations or individuals employing thousands of poorly paid laborers and the oriental despotism of Wittfogel. While drawing the parallel,

Worster suggests an 'important difference' between our own modern irrigation society and its ancient counterparts: the first operates under relenting world and national capitalist pressures, which are impersonal, anonymous, and identified with 'iron laws of economic necessity'; while the second were self-contained, bureaucratic command economies that took the personal word of the emperor as the word of God (Worster, 1982: 513). The distinction appears to do little damage to the analogy, particularly as the author characterizes the history of this mode of agricultural production in California as a 'story of the establishment of concentrated hegemony, at once economic and ideological over developed engineering works' (Worster, 1982: 513–514).

Ultimately concerned with the relation of man to nature in arid California and the West, Worster (1982: 515) observes, '. . . we are able to see etched in sharpest detail the interplay between humans and nature and to track the social consequences it has produced – to discover the process by which, in the remaking of nature, we remake ourselves'.

Tarlock (1987), in a careful review of Worster's more comprehensive study, *Rivers of Empire: Water, Aridity and the American West*, contests the view that reclamation and irrigation development in the western United States represents a series of steps promoting totalitarian control of water and concomitant domination by bureaucratic and commercial enterprises over the economy and society in the region. Contesting the applicability of the framework of hydraulic societies to water development and water allocation in the western United States, Tarlock points out that, in reality, the doctrine of prior appropriation and the resultant allocation of water to a broad class of users has not been tyrannical in execution nor inequitable in result. Even the social and political dominance of large agricultural corporations and farms in California has a complex history not amenable to the deterministic concept of development of hydraulic societies.

Several significant features also distinguish the large ancient systems from the California scene. The former were each confined to a single watershed, and within each watershed all those who contributed labour to the management of the gravity-driven water resource were immediate beneficiaries of their own labour: they raised food to eat. The ancient systems depended on water delivered down a gravitational gradient, supplemented more or less by human and domestic-animal power, while the California example depends on wholesale interbasin transfer of water, enabled by massive inputs of fossil-fuel energy.

While these differences do not negate the analogy, the California example necessarily engages contributions to recipients of California water by participants in the US economy who are not in a position to benefit directly from the water transfer and, in most cases, are not even aware of the extent to which their tax dollars have subsidized an unsustainable system that enriches politically well connected agribusiness entrepreneurs in a distant state. The California example is far more an exercise in power politics over a broad domain than it is an example of the operation of a resource-driven economy.

Nonetheless, the writings of Worster and others (Reisner, 1987) have drawn deserved attention to changing social and economic values of water, reflecting the current interest of American society in environment, ecology, urbanization, and reclamation. Of interest here is the use and misuse of the Egyptian experience and the staying power of the concept of hydraulic societies as part of the current argument over the importance of water management, as well as the significance of environment in human affairs. The multifactor character of Butzer's analysis using the remarkable record of the Nile and Egyptian history represents a fascinating contribution to the discussion of both of these ideas, in particular, the significance of water and water management in society, and, more broadly, the role of environment in development of society.

The Nile, Tigris-Euphrates, and Indus civilizations all depended upon the sophisticated management of rivers. While the economy, society, and political structure of each varied (Hillel, 1994), from place to place and over time, the fundamental elements of management were of necessity the same in antiquity as they are today. Construction and operation of the hydraulic works – dams, barrages, and canals – required labourers and competent engineers, allocation of the available water to irrigators and other users and protection of people and property against flooding require administrators, and financing of construction and maintenance requires producers, tax collectors, and management by government in one form or another. Given a variety of users and a limited supply of water in both time and place demands consideration of equity as well as efficiency in allocation of the water. Dealing with these issues, Egyptian history reveals management at a range of scales from region to kingdom and rights in land from private property to royal ownership.

Modern management includes all of these requisites, often made more complicated by the large scale of the river basins involved and the conflicting values of many nations dependent upon the same river flow. Further complicating the task is the fact that, on many rivers, major developments initially took place along the downstream reaches of the rivers. The Nile is a classic case, but one matched by many others such as the Ganga, the Yellow, the Yangtze, the Colorado, and the Mekong. To meet

growing demands for development in upstream regions and nations requires not only technology but also management structures embodying equity and built upon trust. Dealing with these issues began at least 1000 years ago on the Nile, but resolution here and elsewhere is, at best, slow and uncertain as suggested by the discussion in other chapters in this volume.

ACKNOWLEDGEMENTS

The authors are indebted to Natalie Nahill for preparation of the figures and to Gregory Baecher for review of the manuscript.

REFERENCES

Adamson, D. and Williams, F., (1980) Structural geology, tectonics and the control of drainage in the Nile basin. In: *The Sahara and the Nile: Quaternary Environments and Pre-historic Occupation in Northern Africa* (M.A.J. Williams and F. Hugues, Eds.), Balkema, Rotterdam, pp. 225–252.

Adamson, D., McEvedy, R. and Williams, M.A.J., (1992) Tectonic inheritance in the Nile basin and adjacent areas, *Israel J. Earth Sci*., 41, 75–85.

Ball, J., (1939) [reprinted 1952], *Contributions to the Geography of Egypt*, Survey and Mines Department, Egypt, 308 p.

Barker, P.A., Street-Perrott, F.R., Leng, M.J., Greenwood, P.B., Swain, D.L., Perrott, R.A., Telford, R.J. and Ficken, K.J., (2001) A 14 000-year oxygen isotope record from diatom silica in two Alpine lakes on Mt. Kenya, *Science,* 92, 2307–2310.

Beuning, K.R.M., Kelts, K., Russell, J. and Wolfe, B.B., (2002) Reassessment of Lake Victoria-Upper Nile River paleohydrology from oxygen isotope records of lake-sediment cellulose, *Geology*, 30, 559–562.

Brazier, R.A., Nyblade, A.A. and Florentin, J., (2005) Focal mechanisms and the stress regime in NE and SW Tanzania, East Africa, *Geophys. Res. Lett.*, 32, L14315.

Buckel, C., (1996) *Weather and Climate in Africa*, Addison Wesley Longman, Ltd, Harlow, 312 p.

Butzer, K.W., (1980) Civilizations: Organisms or systems? *Am. Sci.*, 68, 517–522.

Butzer, K.W. and Hansen, C.L., (1968) *Desert and River in Nubia*, University of Wisconsin Press, Madison, 562 p.

Chumakov, I.S., (1967) Pliocene and Pleistocene deposits of the Nile Valley in Nubia and Upper Egypt, *Trans. Geol. Inst. Acad. Sci. USSR*, 170, 1–110.

Chumakov, I.S., (1968) Pliocene ingression into the Nile Valley according to new data. In: *Desert and River in Nubia* (K.W. Butzer and C.L. Hansen, Eds.), University of Wisconsin Press, Madison, pp. 521–522.

Eltahir, E.A.B., (1996) El Niño and the natural variability in the flow of the Nile river, *Water Res. Res*., 32, 131–137.

Flohn, H. and Burkhardt, Th. (1985) Nile runoff at Aswan and Lake Victoria: a case of discontinuous climate time series, *Zeitschr. Gletscherkunde Glazialgeo*l., 21, 125–130.

Garzanti, E., Ando, S., Vezzoli, G., All Abdel Megid, A. and El Kammar, A., (2006) Petrology of Nile River sands (Ethiopia and Sudan): sediment budgets and erosion patterns. *Earth Planet. Sci. Lett.*, 252, 327–341.

Giegengack, R., (1968) Late Pleistocene History of the Nile Valley in Egyptian Nubia, PhD thesis, Yale University, 181 p.

Griffiths, J.F. (ed.), (1972) *Climates of Africa*, World survey of climatology, vol. 10, Elsevier, Amsterdam.

Hillel, D., (1994) *Rivers of Eden*: *The Struggle for Water and the Quest for Peace in the Middle East*, Oxford, New York, 355 p.

Hurst, H.E., (1951) Long-term storage capacity of reservoirs, *Trans. Am. Soc. Civ. Engr*., 116, 770–808.

Hurst, H.E., (1952) *The Nile*, Constable, London, 326 p.

Issawi, B., (1971) On the Nubia Sandstone, *AAPG*, 55, 891–893.

Issawi, B., (1973) Nubia Sandstone: type section, *AAPG*, 57, 741–745.

Issawi, B. and McCauley, J.F., (1992) The Cenozoic rivers of Egypt: The Nile problem. In: *The Followers of Horus* (R. Friedman and B. Adams, Eds.), Egyptian Studies Association Publication No. 2, Oxbow Monograph 20, Oxford Books, Oxford, pp. 121–138.

Issawi, B., El Hinnawi, M., Francis, M. and Mazhar, A., (1999) *The Phanerozoic Geology of Egypt: a geodynamic approach*: Special Publication No. 76, The Egyptian Geological Survey, 464 p.

Kerr, R.A., (1998) Sea-floor dust shows drought felled Akkadian empire, *Science*, 279, 325–326.

Krom, M.D., Stanley, J.D., Cliff, R.A. and Woodward, J.C., (2002) Nile River sediment fluctuations over the past 7,000 yr and their key role in sapropel development, *Geology*, 30, 71–74.

Langston, C.A., Brazier, R., Nyblade, A.A. and Owens, T.J., (1998) Local magnitude scale and seismicity rate for Tanzania, East Africa, *Bull. Seis. Soc. Am.*, 88, 712–721.

Leopold, L.B., (1962) Rivers, *Am. Sci.*, 50, 511–537.

Leroux, M., (2001) *The Meteorology and Climate of Tropical Africa*, Springer-Praxis Books in Environmental Science, Springer-Verlag, New York, 548 p.

Lyons, H.G., (1906) *The Physiography of the River Nile and its Basin*, Survey Department Egypt, Cairo, 411 pp.

Mabry, J.B. (ed.), (1996) *Canals and Communities: Small Scale Irrigation Systems*, University of Arizona. Press, Tucsan, 273 p.

Mawson, R. and Williams, M.A.J., (1984) A wetter climate in eastern Sudan 2000 years ago? *Nature*, 309, 49–51.

McDougall, I., Morton, W.H. and Williams, M.A.J., (1975) Age and rates of denudation of Trap Series basalts at Blue Nile gorge, Ethiopia, *Nature*, 254, 207–209.

Mill, J.S., (1909) *Principles of Political Economy*, Longmans, Green and Company, London.

Nixon, S.W., (2004) the artificial Nile: the Aswan high dam blocked and diverted nutrients and destroyed a Mediterranean fishery, but human activities may have revived it, *Am. Sci.*, 92, 158–163.

Osmond, J.K. and Dabous, A.A., (2003) Timing and intensity of groundwater movement during Egyptian Sahara pluvial periods

by U-series analysis of secondary U ores and carbonates, *Quat. Res*., 61, 85–94.

Pachur, H.-J. and Krőpelin, S., (1987) Wadi Howar: paleoclimatic evidence from an extinct river system in the southeastern Sahara, *Science*, 237, 298–300.

Pachur, H.-J., and Hoelzmann, (2000) Late Quaternary paleoecology and paleoclimates of the eastern Sahara, *J. African Earth Sci*., 30, 929–938.

Reisner, M., (1987) *Cadillac Desert: The American West and its Disappearing Water*, Penguin, New York, 582 p.

Rietti-Shati, Shemesh. A. and Karlen, W., (1998) A 3000-year climatic record from biogenic silica oxygen isotopes in an equatorial high-altitude lake, *Science*, 281, 980–982.

Said, R., (1962) *The Geology of Egypt*, Elsevier, Amsterdam, 377 p.

Said, R., (1975) The geological evolution of the River Nile. In: *Problems in Prehistory: Northern Africa and the Levant* (F. Wendorf and A.E. Marks, Eds.), Southern Methodist University Press, Dallas, pp. 1–44.

Said, R., (1981) *The Geological Evolution of the River Nile*, Springer-Verlag, New York, 151 p.

Said, R. (ed.), (1992**)** *The Geology of Egyp*t, Balkema, Rotterdam, 734 p.

Said, R., (1993) *The River Nile: Geology, Hydrology and Utilizatio*n, Pergamon Press, Oxford.

Steward, J.H., (1955) Introduction: the irrigation civilizations, a symposium on method and result in cross-cultural regularities. In: *Irrigation Civilizations: a Comparative Study*, Society of Science Monograph I, Pan American Union, Washington, DC, pp. 1–6.

Sutcliffe, J.V. and Parks, Y.P., (1999) *The Hydrology of the Nile*, International Association of Hydrological Sciences, Special Publication No. 5, IAHS Press, Wallingford, p. 179.

Tarlock, A.D., (1987) Damning the dams and ditches: a review of D. Worster, Rivers of Empire: Water, Aridity and the American West (Pantheon, NY), Natural Res. J., 27, 477–490.

Thompson, B.W., (1965) *The Climate of Africa*, Oxford University Press, Oxford.

Thompson, L.G., Mosley-Thompson, E., Davis, M.E., Henderson, K.A., Brecher, H.H., Zagorodnov, V.S., Mashiotta, T.A., Lin, P.-N., Mikhalenko, V.N., Hardy, D.R. and Beer, J., (2002) Kilimanjaro ice core records: evidence of Holocene climate change in tropical Africa, *Science*, 298, 589–593.

Union of American Hebrew Congregations, (1981) *The Torah*, New York, 1787 p.

University of Michigan, (1980) Aswan and after: the taming and transformation of the River Nile, *The Research News*, 31, 4–29.

US Geological Survey (USGS), (2004) Seismicity of Africa: 1977–1997, http://neic.usgs.gov/neis/general/seismicity/africa.html.

Weiss, H., Courty, M.A., Wetterstrom, W., Guichard, F., Senior, L., Meadow, R. and Curnow, A., (1993) The genesis and collapse of third millennium north Mesopotamian Civilization, *Science,* 262, 995–999.

Wendorf, F., Schlid, R., Said, R., Haynes, C.V., Gauthier, A. and Kobusiewicz, M., (1976) The prehistory of the Egyptian Sahara, *Science,* 193, 103–114.

Williams, M.A.J. and Williams, F.M., (1980) Evolution of the Nile basin. In: *The Sahara and the Nile: Quaternary Environments and Pre-historic Occupation in Northern Africa* (M.A.J. Williams and F. Hughes, Eds.), Balkema, Rotterdam, pp. 207–224.

Williams, M.A.J., Adamson, D., Prescott, J.R. and Williams, F.M., (2003) New light on the age of the White Nile, *Geology*, 31, 1001–1004.

Wittfogel, K.A., (1955) Developmental aspects of hydraulic societies, In: *Irrigation Civilizations: A Comparative Study*, Society of Science Monograph I, Pan American Union, Washington, DC, pp. 43–52.

Wittfogel, K.A., (1956) The hydraulic civilizations. In: *Man's Role in Changing the Face of the Earth* (W.L. Thomas, Jr, Ed.), University of Chicago Press, Chicago, pp. 152–163.

Wittfogel, K.A., (1957) *Oriental Despotism: a Comparative Study of Total Power*, Yale University Press, New Haven, 556 p.

Worster, D., (1982) Hydraulic society in California: an ecological interpretation, *Agri. Hist*, 56, 503–515.

23

Patterns and Controls on Historical Channel Change in the Willamette River, Oregon, USA

Jennifer Rose Wallick[1], Gordon E. Grant[2], Stephen T. Lancaster[3], John P. Bolte[4] and Roger P. Denlinger[5]

[1]*DHI, Inc., 319 SW Washington St Suite 614, Portland, OR 97204, USA*
[2]*Pacific Northwest Research Station, USDA Forest Service, Corvallis, OR 97331, USA*
[3]*Department of Geosciences, Oregon State University, Corvallis, OR 97331 USA*
[4]*Department of Bioengineering, Oregon State University, Corvallis, OR 97331, USA*
[5]*Cascade Volcano Observatory, Vancouver, WA 98683, USA*

23.1 INTRODUCTION

Distinguishing human impacts on channel morphology from the natural behaviour of fluvial systems is problematic for large river basins. Large river basins, by virtue of their size, typically encompass wide ranges of geology and landforms resulting in diverse controls on channel form. They also inevitably incorporate long and complex histories of overlapping human and natural disturbances. Wide valleys were historically prime locations for human settlement, as immigrants were attracted to relatively flat and fertile floodplain soils and rivers served as conduits of travel and commerce. Over the span of multiple centuries, humans typically modified many aspects of a river's hydraulic and hydrologic behaviour, including streamflow regimes, bank erodibility, and sediment supply. Distinguishing anthropogenic impacts from natural influences in large river basins is therefore difficult because there are so many potential drivers of channel change, and human interventions have occurred over long timescales.

Even where human impacts are minimal, the intrinsic temporal and spatial variability of the flow regime, sediment supply, bank materials, channel planform, and riparian vegetation interact to create diverse channel morphologies that vary longitudinally. Human activities and interventions are both inset within these natural determinants of channel form, and can affect nearly all of them. Although these interactions are present in all rivers, the broad spatial scale of large rivers provides many opportunities for complex interactions, confounding interpretation of natural from anthropogenic impacts on channel morphology.

Yet distinguishing human impacts from the intrinsic evolution and change of large rivers remains a critical need. Human pressure on large rivers, their valleys and resources is increasing worldwide, while efforts to restore, renaturalize, and re-engineer rivers to meet changing social and ecologic objectives and expectations is also a global enterprise. Efforts to either mitigate human impacts or restore natural functions to rivers requires a clear understanding of how much of the behaviour of rivers is fundamental to their position in the landscape or evolutionary trajectory in time – and therefore difficult to modify – as opposed to the result of one or more human impacts, which may or may not be reversible.

Large Rivers: Geomorphology and Management, Edited by A. Gupta

We propose a general framework for distinguishing the relative importance of natural and anthropogenic controls on channel change in large rivers. Our conceptual model describes how channels evolve in complex natural settings amid overlapping anthropogenic activities. We illustrate this framework by interpreting patterns of historical channel change along the Willamette River, a large alluvial river occupying a 28 800 km^2 basin in western Oregon, USA (Figure 23.1). The Willamette is well-suited to this type of analysis because it has a relatively recent Euro-American history (settlement began in the mid-nineteenth century), and most geomorphically relevant historical events are well documented. Settlement of the Willamette Valley took place in stages, causing anthropogenic impacts to generally follow a well-defined temporal sequence. This timeline of human interaction with the Willamette allows us to better link channel changes with their causes. Our analysis of the Willamette reveals a number of lessons that can be generalized to other larger rivers. In particular, it suggests that although river channels respond to a diverse range of anthropogenic and natural influences, channel change is typically dominated by a few controlling variables and events.

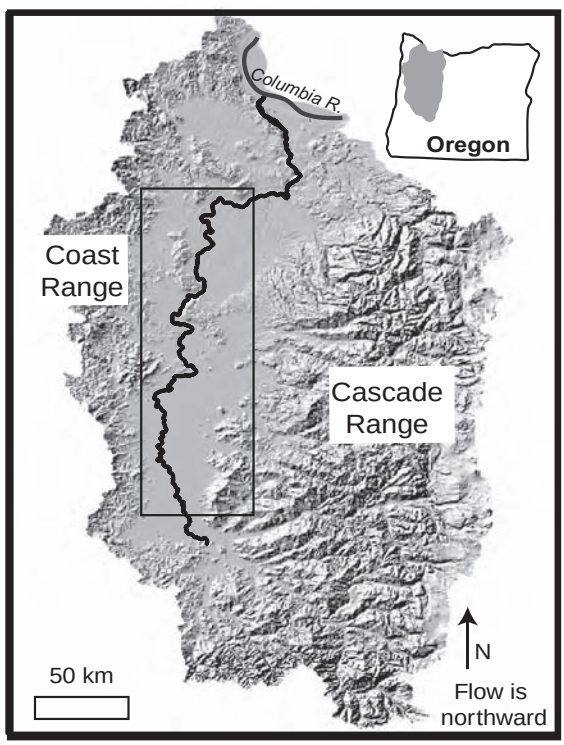

Figure 23.1 Willamette River Basin in northwestern Oregon. Box indicates 200 km study area shown in Figure 23.2

The Willamette is the thirteenth largest river (by volume) in the conterminous US, similar in size to other well-studied rivers such as the Sacramento in California (Singer and Dunne, 2001, 2004) or the Ain in southern France (Marston *et al*., 1995). Like other large rivers, the Willamette is composed of a series of geomorphically distinct reaches each of which have evolved uniquely in the century following Euro-American settlement. More than two-thirds of Oregon's population of 3.4 million lives in the Willamette Valley, with most people living in major metropolitan centres situated along the river (e.g. Portland, Eugene), leaving the majority of the Valley in agricultural and forest lands (Hulse *et al*., 2002). Historical channel change along the Willamette has occurred in response to a range of natural and anthropogenic events, including floods, riparian and valley logging, agricultural development, erosion control and other engineering works, and modification of sediment and flow regimes by dams. Prior to Euro-American settlement, much of the Willamette was a dynamic anastomosing stream flowing through dense riparian forests. Today the modern Willamette is predominantly a single-thread river bordered by agricultural fields and revetments.

The Willamette Valley also faces many challenges common to other large rivers, as there is increasing demand to balance agricultural, urban and industrial demands while protecting endangered species, drinking water, and recreation. As a result, several large-scale restoration projects have been proposed for the Willamette River floodplain and there is large public interest in increasing riparian habitat along the river corridor (Jerrick, 2001). Lessons learned from attempts to interpret and restore the Willamette may therefore have much wider applicability to other larger rivers.

Previous work on the Willamette has emphasized the role of humans on channel change (Benner and Sedell, 1997; Dykaar and Wigington, 2000; Gutowsky, 2000). These earlier studies generally conclude that channel stability has increased following Euro-American settlement, and that this change is largely due to anthropogenic activities, particularly riparian logging, bank stabilization and flow regulation (i.e., Hulse *et al*., 2002). We believe that this view underemphasizes the role played by floods, bank materials and the overall geologic setting as factors influencing channel change. Here, we seek to develop a more comprehensive model of channel evolution in which we examine the physical setting of the Willamette floodplain, its flood history and the full spectrum of human activities that have influenced channel change.

23.2 AN APPROACH FOR INTERPRETING MULTIPLE IMPACTS ON LARGE RIVERS

We aim to interpret the causes of long-term and geographically distributed changes in the form of large rivers. As noted, causal relationships between geomorphic and anthropogenic drivers and channel change can be problematic due to the multiplicity of factors contributing to change, intrinsic river variation in form and processes, long time and large spatial scales over which both drivers and change occur, and the fact that the signature of change may not be unique for specific causal mechanisms. Faced with such difficulties, which are not unique to the Willamette but characteristic of all large rivers, our overarching approach is to build a compelling narrative of change that links plausible drivers with anticipated response patterns in time and space, all subject to the overriding effect of intrinsic geologic controls. This is in contrast to a strict cause-effect approach more suitable to smaller rivers with more limited driving mechanisms. By narrative, we mean a reasonable and logical characterization of driving causal factors and consequent responses, distinguished by their chronology and ranked according to their relative importance.

We first distinguish factors that drive channel change from the response of the channel itself. Drivers of channel change include both natural changes in discharge and sediment regimes, and anthropogenic changes such as bank stabilization and flow regulation. The river's geomorphic response to these drivers is manifested as changes in channel geometry and planform. Disentangling these cause–effect relations is the initial step in identifying whether the dominant impacts in a particular time period is natural or anthropogenic (Table 23.1).

Drivers of channel change are extensive and well known, and involve changes to the discharge regime, bank erodibility, or sediment supply (Schumm and Lichty, 1965; Lane and Richards, 1997). Along the Willamette, for example, natural drivers of geomorphic change include changing flow and sediment regimes in response to changing climate, particularly glaciation of the headwater basins during the Pleistocene and deglaciation during the Holocene. In addition, singular events such as broad regional floods contribute high volumes of sediment and large wood that, together with high streamflows, act as tools to reshape channels. Human drivers of channel change include navigation improvements by wood snagging, bank protection schemes, flood control dams, and land clearance and conversion.

We define channel response as a change in the physical form of a river channel due to the action of a geomorphic or anthropogenic driver. Channel responses range from one-dimensional changes in channel geometry to transformations in river planform, all of which may occur at different rates. One-dimensional change includes adjustments in width, depth or centreline length. Planform adjustments refer to two-dimensional changes in river morphology; examples include anastomosing channels that become single-thread, or meandering channels that become straight. Each type of river planform displays unique styles of change, and we measure rate of change using metrics best suited for that planform as discussed below. For example we measure migration rates for meandering reaches and avulsion frequency for anastomosing reaches. Because of reach-to-reach variation in channel or floodplain properties, the style and rate of response can vary dramatically along the length of large rivers.

Table 23.1 Predicted channel response to natural and anthropogenic disturbance processes that act as drivers of channel change on the Willamette River

Drivers of channel change		Predicted channel response			
		Channel width	Migration rate	Avulsion rate	Channel length
Natural	Large floods	Increase	Increase	Increase	Decrease due to avulsions
	Moderate floods (bankful)	Increase	Increase	Increase	Increase through migration
Anthropogenic	Loss of riparian vegetation	Increase	Increase	Indeterminate	Increase
	Snag removal	Decrease	Decrease	Decrease	Increase or decrease
	Revetment construction	Decrease	Decrease	Decrease	Stabilize
	Dam construction	Decrease	Decrease	Decrease	Stabilize
	Channel modifications (wing dams, cut-off dykes etc.)	Decrease	Decrease	Decrease	Stabilize

We can draw on the geomorphic literature to make first-order predictions on the likely direction of change in key metrics as a result of specific drivers (Table 23.1). Such predictions constitute hypotheses linking geomorphic and anthropogenic drivers with plausible responses, and provide a reasonable means of interpreting historical patterns of channel change. For example, riparian deforestation generally increases bank erodibility through loss of root strength, leading to increased channel widening and migration (Zimmerman *et al*., 1967; Rowntree and Dollar, 1999; Murray and Paola, 2003). Large mobile wood accumulations generally redirect flows and obstruct channels, leading to avulsions and multi-thread channels (Tooth and Nanson, 2000; O'Connor *et al*., 2003). Removal of large wood (through snagging) might therefore be expected to reduce avulsions and promote a wider, single-thread planform (Abbe and Montgomery, 1996, 2002). Bank stabilization structures and flood-control dams decrease bank erodibility and flow erosivity respectively, thus decreasing migration rates and avulsion frequency (Larsen and Greco, 2002). As the channel becomes more stable, relict gravel bars and other formerly active channel surfaces are typically colonized with vegetation and channel width decreases (Nadler and Schumm, 1981). These relationships can be summarized by linking various natural and anthropogenic impacts with their anticipated effects on the channel, hence metrics of channel change.

Table 23.1 summarizes the anticipated effects of different drivers of channel change, and provides a useful framework for linking rates and styles of channel change observed during a particular time period with specific impacts. A key point, however, is that predicted channel responses are not unique to specific drivers, but display equifinality, wherein the same result can be due to multiple causes. To construct a reasonable narrative of causal linkages of channel change, interpretation of change must be constrained by other factors.

The most obvious factors that influence the interpretation of channel are the timescales and locations of change relative to the timing and location of drivers. For example, an action or event that directly modifies the channel (e.g. bank protection or dredging) has a higher likelihood of directly effecting channel change than activities occurring on the adjacent floodplain. Furthermore, human actions that directly impact discharge or sediment transport (such as dams) would have a greater influence than activities that indirectly influence runoff and sediment generation (such as timber harvest and other land uses conducted away from the channel). The scale of any activity is also critical, as large flood control dams, lengthy revetments or widespread riparian deforestation would clearly have a greater effect than smaller-scale versions of similar impacts. Another important constraint for interpreting complex patterns of channel change is imposed by the geological setting of the channel itself. Variations in intrinsic erodibility of bed and bank materials, including location of erosion-resistant valley walls and bedrock, can be used to interpret spatial variations in response due to other drivers.

Floods play a unique role as mechanisms for initiating and promoting accelerated channel changes that may or may not have other primary causes or for shifting trajectories of channel adjustment. In particular, floods can catalyze or galvanize impacts that have been latent or hidden up to that point, as thresholds are exceeded (Grant *et al*., 1984). Through lateral migration, for example, small to moderate-sized floods (e.g. 2- to 10-year events) can set the stage for abrupt planform shifts during large floods due to avulsions and scour of secondary channels. Floods typically elicit planform changes and can thereby cause the river to adopt a dramatically different style of evolution. For instance, a highly sinuous, meandering channel may experience a series of avulsions and meander cutoffs, causing the channel to adopt a low-sinuosity planform with higher gradient. Depending on sediment supply, bank erodibility and the ensuing discharge regime, such planform changes could initiate further channel changes, such as incision. Floods can therefore be seen as the triggers to disturbance cascades (*sensu* Nakamura *et al*., 2000) wherein one impact can trigger a series of subsequent adjustments. Within a cascade, the magnitude and style of sequential adjustments steers the overall direction of channel change in some direction until another large impact resets the trajectory of channel change. These adjustments and their net outcome are highly contingent upon the pre-existing channel planform, distribution of resistant bank materials, floodplain physiography and other floodplain characteristics.

On the Willamette and other large rivers, the channel that we observe today is inevitably a function of the order in which various impacts occurred. Large river basins are contingent systems whereby the channel response to a particular impact in a given time period is contingent upon all previous events. This contingency inevitably limits reliance on precise cause-and-effect models to explain observed phenomena, but lends itself to a plausible and quantitatively supported historical narrative that accounts for the sequence of events as well as the events themselves. In this sense, river evolution mimics biological evolution (Gould, 1989),

In the following sections, we use these concepts of plausible hypotheses, disturbance cascades and a quantitatively supported narrative to examine natural and anthropogenic impacts on the Willamette River. We do this by

relating channel planform and trajectories of change to both geological controls and impacts to the channel and floodplain. We set the stage for our analysis by briefly describing the physical setting and human history of the Willamette Valley, and illustrate inherent controls on channel change by focusing on how the geological history of the Willamette Valley helps define floodplain physiography, bank materials, sediment supply and other aspects. What emerges is a reasonably compelling and heretofore unreported narrative ordering the relative importance of natural and anthropogenic impacts on the last 150 years of channel evolution. We conclude with considerations of how this type of analysis can be generalized to other large rivers.

23.3 GEOLOGIC SETTING, HUMAN AND FLOOD HISTORY OF THE WILLAMETTE

Some geographic and historical context for the Willamette River is required in order to properly interpret both our study and the patterns of channel evolution. Here we consider some of the most important physical factors that set the geomorphic constraints on channel pattern, describe our reach-scale delineations with respect to those factors, briefly discuss the history of human settlement of the Willamette Valley and its consequences for the channel, and summarize what is known about the flood history over the past 150 years.

23.3.1 Watershed Physiography and Climate

The Willamette Valley is situated between two rugged and deeply dissected mountain landscapes, the volcanic Cascade Range to the east and the uplifted marine sandstones of the Coast Range to the west (Figure 23.1). Although heading in the mountains, the Willamette River itself is a relatively low-gradient river, with an average slope of 0.0005 over its lowermost 250 km, and a planform that ranges from braided and anastomosing in its upper reaches to wandering and meandering in its lower reaches, all within a broad valley floor ranging in width from 10 to 50 km. The mainstem Willamette begins at the confluence of the Coast and Middle Forks of the Willamette in the southern valley, and flows northward through alluvium and lacustrine deposits for more than 200 km. In the northern valley, the Willamette River incises a gorge through Tertiary basalt flows and passes over the 15 m high Willamette Falls. Below Willamette Falls, the river is tidally influenced for 20 km to its confluence with the Columbia River near Portland.

The Willamette Valley is characterized by a Mediterranean climate with cool, wet winters and warm, dry summers. Average precipitation in the valley floor is approximately 1200 mm $year^{-1}$, which falls mainly as rainfall during the winter. Headwater reaches receive as much as 2500 mm, which falls as both rain and snow (Oregon Climate Service, 2006). Major Willamette floods typically result from basin-wide rain-on-snow events (Harr, 1981).

23.3.2 Geological Setting of the Willamette in Relation to Channel Stability

The floodplain physiography that we observe today in the Willamette Valley results from a geological history of constructional volcanism, uplift and deformation, incision, and an unusual depositional sequence from catastrophic Pleistocene outbreak floods on the Columbia that resulted in backwater flooding of the Willamette River. The Willamette Valley is a fore-arc basin that formed in response to subduction of the Pacific Plate beneath the North American Plate. Tertiary marine sandstones (unit Tm, Figure 23.2) form the basement of the Willamette Valley, which was separated from the Pacific Ocean approximately 20–16 Ma when submarine volcanic rocks were uplifted, forming the Coast Range. About 15 Ma, subareal flood basalts of the Columbia River Basalt Group (CRBG) flowed westward from eastern Oregon, covering large portions of the northern Willamette Valley (Hooper, 1997). Structural deformation has created local uplands of CRBG flows in the middle Willamette Valley that locally restrict valley width while the lower 25 km of the Willamette is incised through CRBG flows (Yeats *et al*., 1996; O'Connor *et al*., 2001).

During the Pleistocene, volcanic construction of the High Cascades on the eastern boundary of the Willamette Valley coincided with a cooler, moister climate to cause enhanced sediment production. Sands and gravels generated by glacial and periglacial processes fed a vast network of braided rivers that extended across the valley floor, depositing valley fill sediments and alluvial fans primarily along the eastern margin of the basin (Qg2 unit, Figure 23.2), and displacing the river to the west (O'Connor *et al*., 2001). Between 15 and 12.7 Ka, dozens of catastrophic glacial dam outbreak floods originating in Glacial Lake Missoula swept across southeastern Washington and flowed down the Columbia River (Waite, 1985; Benito and O'Connor, 2003). The Missoula Floods back-filled the Willamette Valley from its confluence with the Columbia and blanketed the valley with fine-grained silts and clays. These Missoula Flood deposits (unit Qff, Figure 23.2) form the surface of the main valley floor and range in thickness from 35 m in the northern valley to less than 5 m in the southern valley (O'Connor *et al*., 2001).

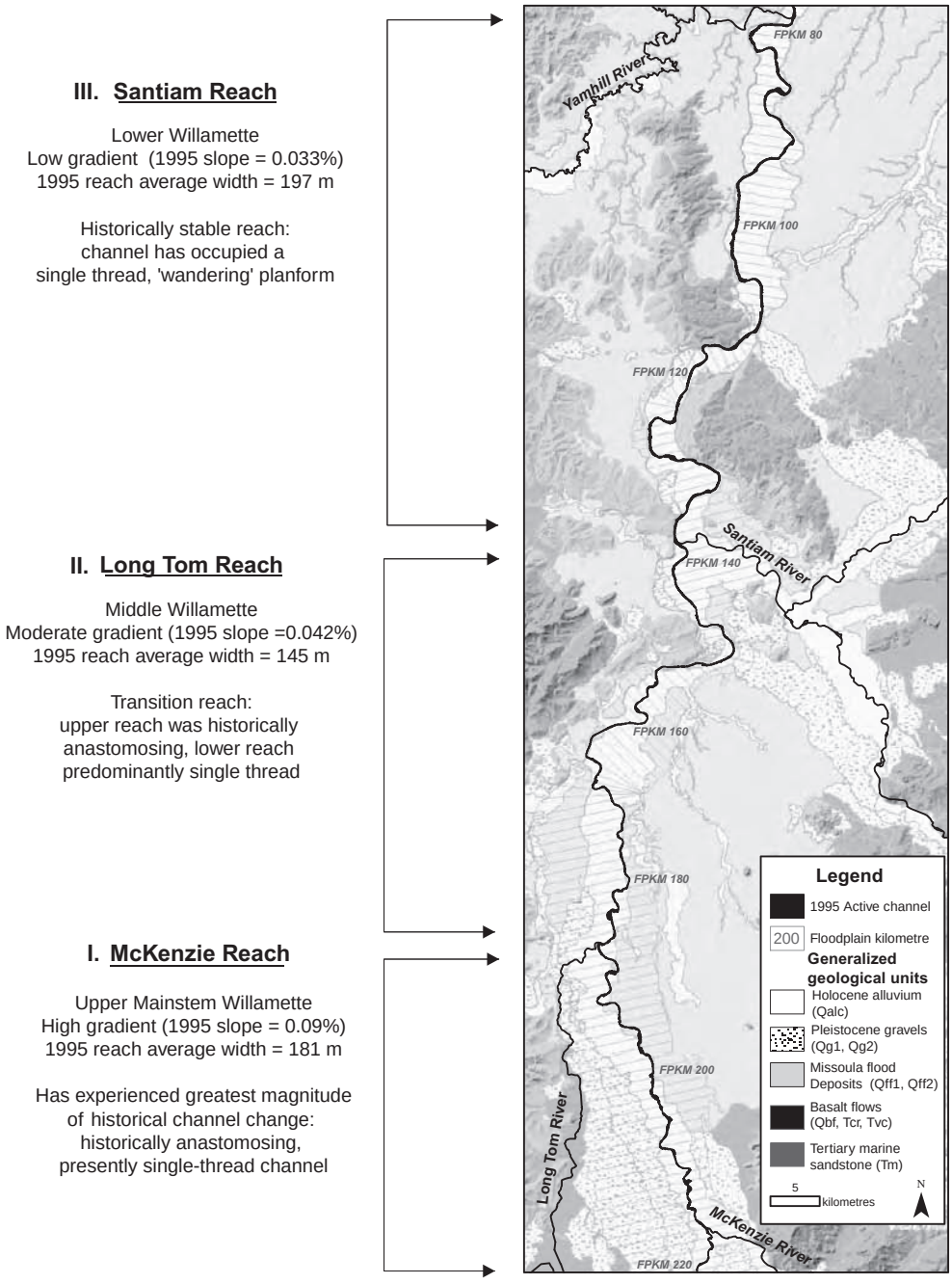

Figure 23.2 Geologic and physiographic setting of Willamette River study area. The 220 km long study area was divided into three reaches on the basis of planform, discharge and tributary influence. (Geological map from O'Connor *et al*., 2001. Willamette River active channel and floodplain transect maps from Hulse *et al*., 2002)

The warmer, drier Holocene climate triggered a wave of regional incision, and Pleistocene braid plains were replaced by the inset anastomosing planform of the modern Willamette. In historical documents, the Holocene floodplain is frequently termed the valley bottom as it is situated 3–35 m below the surfaces of the terraces comprising the main valley floor (Figure 23.3). Holocene floodplain surfaces (unit Qalc, Figure 23.2) range from recent point-bar and active-channel deposits to forested floodplains, and form a 1–2 km wide swath of silts, sands and gravels, deposited less than 12 000 years ago.

The location of the Willamette River with respect to the Holocene floodplain and adjacent older terraces has implications for bank stability and channel change. Along much of its length, the river is flanked on both sides by Holocene alluvium, whereas in other areas, the Willamette flows against older, more indurated bank materials along the floodplain margins (Figure 23.2). The most extensive of these more resistant bank materials include partially cemented Pleistocene gravels (Qg2) that underlay Missoula Flood sediments. Other resistant geological units are locally important and include Tertiary marine sandstones (Tm) that crop out near Albany at floodplain km 110 (FPKM 110) and Tertiary volcanic deposits (Tvc and Tcr) that border the channel near Salem (FPKM 70). Although not strictly speaking a geological control, the Army Corps of Engineers have stabilized large portions of the Willamette River with large, angular boulders (revetments) that form a resistant bank material.

Geological factors also control bank height along the Willamette. Bank height steadily increases downstream as the river becomes increasingly entrenched within both Holocene and Pleistocene surfaces. In the southern valley, elevations of terrace surfaces typically rise 2–5 m above low-water stage, whereas surfaces in the northern valley are up to 15 m higher than low-water stage (O'Connor *et al*., 2001). Banks are highest where the river flows against Pleistocene terraces composed of indurated Qg2 gravels and overlying Missoula Flood deposits. Along the upper reaches, Qg2 gravels typically comprise the lower 1–2 m of banks, while along the lower river these same gravels comprise the lower 5–10 m (O'Connor *et al*., 2001).

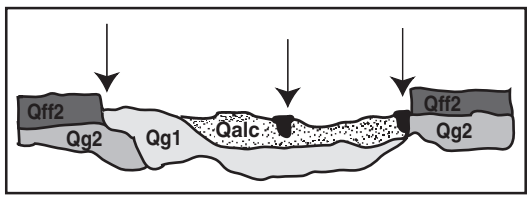

Figure 23.3 Generalized cross-section of Willamette floodplain. Geological units are same as those shown in Figure 23.2. Arrows indicate typical locations of Willamette River within Holocence floodplain. (Geological units are from O'Connor *et al*., 2001)

23.3.3 Study Length Delineation

The changing geological setting of the river as it proceeds northward requires that different units be delineated within the study length in order to compare channel responses to various geomorphic drivers. These reaches provide the spatial template for our analysis. The Willamette can be broadly delineated into three alluvial reaches on the basis of valley slope, planform, bankful discharge and location of major tributary junctions (Figure 23.2). The uppermost reach (McKenzie Reach) spans the relatively steep and historically anastomosing Willamette River between the confluences of the McKenzie and Long Tom Rivers. The Long Tom Reach includes portions of both the upper and middle Willamette Valley between the confluences of the Long Tom and Santiam Rivers with the Willamette. The Santiam Reach is the lowest-gradient reach, as it begins at the Willamette's confluence with the Santiam River and continues to the Yamhill River confluence in the northern valley.

Much of the McKenzie Reach was historically bordered by erodible Holocene alluvium and flow in the main channel was divided by large (2–4 km) semi-stable forested islands. Voluminous inputs of large wood and sediment combined with floods led to frequent avulsions and high rates of bank erosion. An extensive network of side channels bordered the main channel and were frequently abandoned, eroded or re-occupied following avulsions and channel migration. This dynamic channel system provided many obstacles to early navigation and nineteenth century channel improvement efforts were focused on maintaining a stable, single-channel on the upper Willamette (including the upstream portion of the Long Tom Reach).

In the Long Tom Reach (Reach II), the channel transitions from an anastomosing planform to a single-thread, wandering planform. Like the McKenzie Reach, the flow in the upper Long Tom Reach was historically divided among multiple channels separated by large islands. Beginning near Corvallis at FPKM 165, the channel adopts a single-channel planform with fewer islands and side channels. While the multi-threaded sections of the Long Tom Reach historically experienced frequent channel shifting, the single-thread areas have been more stable.

The Willamette along the Santiam Reach is generally contained within a single-channel that wanders between

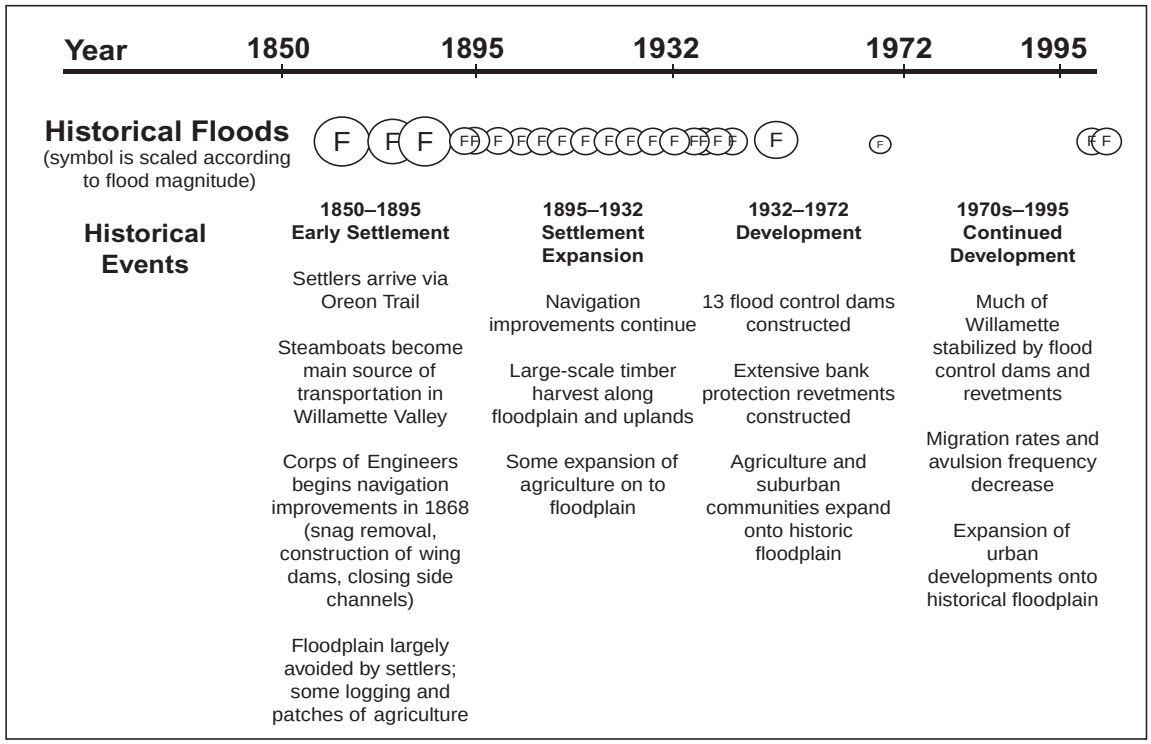

Figure 23.4 Timeline of geomorphically relevant historical events in Willamette Valley. Prior to Euro-American settlement in the late 1840s, the Willamette River and its floodplain were largely unaffected by human activities. The first Euro-Americans to enter the Willamette Valley were Lewis and Clark in 1805, and the region remained largely unsettled untill the late 1840s following the development of the Oregon Trail

paired terraces formed of Pleistocene and Holocene alluvium and bedrock. Along the floodplain margins, the Willamette forms 3–5 km long bends which impinge upon Qg2 gravels. Low-sinuosity bends alternate with fairly straight reaches creating a 'wandering' planform (*sensu* Church, 1983). The low gradient Santiam Reach ends at the Newburg Pool, a 40 km long backwater area created by ponding above Willamette Falls.

23.3.4 Timeline and Consequences of Euro-American Interaction with Willamette River

Humans have lived in the Willamette Valley for 9000 years (Cheatham, 1988), but the Willamette River and its floodplain were largely unaffected by anthropogenic activities until the mid-nineteenth century following the arrival of Euro-Americans. Although Lewis and Clark were the first Euro-Americans to enter the Willamette Valley in 1805, settlement of the Willamette Valley did not fully begin until the late 1840s following the development of the Oregon Trail. We therefore focus our attention on major human modifications since 1850 that may have directly impacted channel planform, style of adjustment, or overall channel behaviour (Figure 23.4).

Early Settlement 1850–1895

Early settlers to the Willamette Valley generally avoided the floodplain, preferring to homestead along the outer margins of the main valley floor, a location which provided safety from floods, while granting access to both prairie and upland timber (Bowen, 1978; Towle, 1982). General Land Office (GLO) maps of the Willamette floodplain from 1851 to 1853 show that much of the floodplain was densely forested and depict the lower reaches of the Willamette as primarily confined to a single channel, while the upper Willamette was divided among multiple channels containing numerous gravel bars, and large wood rafts. GLO maps also show that in each township (9324 ha in area), only a few claims, fields or houses appear to have

been situated on the floodplain. In the following decades floodplain lands were increasingly utilized for agriculture while riparian logging spread through the Willamette Valley (Nash, 1904; Towle, 1982). By 1895, approximately 23 % of the middle and lower Willamette and only 11 % of the upper Willamette was bordered by agriculture, leaving the remaining floodplain lands in either original riparian forest or logged areas (Gregory *et al*., 2002a).

Steamboats became the main form of transportation along the Willamette Valley in the mid-1850s, which required that a navigable channel be maintained between agricultural towns along the upper Willamette and trading centres downstream (Anderson, 1974). In 1868, the Corps of Engineers began removing downed trees (snags) from the Willamette (Sedell and Froggatt, 1984). Yearly snagging records show that about 1000 downed and streamside trees were removed annually from the mainstem Willamette between 1868 and 1935 (Figure 23.5) (USACE, 1867–1892; Sedell and Froggatt, 1984). In the 1870s the Corps began channelizing the Willamette (Figure 23.4) by eliminating side channels and narrowing the main channel (Benner and Sedell, 1997). The 1895 navigational survey conducted by the Corps shows that approximately 18 km of man-made structures (including wing dams, check dams, retaining walls, bridges and revetments) bordered the Willamette (USACE, 1895). In addition to the structures, the Corps filled secondary channels with downed trees, blocked the heads of side channels with logs, and deepened the main channel by scraping shoal bars (USACE 1875: 765; Benner and Sedell, 1997). Whereas most of the channelization occurred along lower reaches where the river was largely confined to a single channel, snagging predominantly occurred on the upper Willamette where large wood rafts were more common.

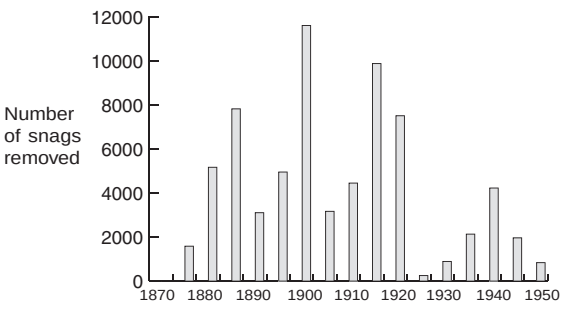

Figure 23.5 Snag removal 1870–1950 along upper Willamette. Plot shows total number of snags removed per 5-year interval between Albany and Eugene (FPKMs 150–220). Logs removed include harvested streamside trees and downed trees (snags). (Adapted from data provided by Sedell and Frogatt, 1984)

First-hand accounts by the Corps of Engineers in the Annual Reports to the Chief of Engineers provide telling statements on the efficacy of channel improvements in the late nineteenth century. In 1875 after 7 years of channel improvements, the Corps claimed that the upper Willamette underwent such frequent changes that 'it would be impossible to confine its waters into one main and permanent bed' (USACE 1875: 765). In 1881 another author wrote that, the upper Willamette remained 'exceedingly troublesome' while the middle and lower reaches of the Willamette were 'free from material obstructions' (USACE, 1882: 2655–2659). In the early 1890s, one author described a particularly laborious season of channel maintenance then concluded his passage by writing, 'this work, however is but temporary, and in the nature of things much of it may have to be done over again' (USACE, 1892: 2836). Such statements suggest that even after several decades of channel improvements, the upper Willamette remained prone to frequent channel change, whereas the lower reaches were more easily coaxed into a stable planform.

Agricultural development 1895–1932

The period 1895–1932 was marked by increased development of the Willamette River floodplain, as channel improvements, riparian logging, and expansion of floodplain agriculture continued. Dredging was authorized by Congress in the 1896 River and Harbor Dredging Act, and from 1908 to 1929, approximately 78 000 m^3 of material were removed annually from the middle and lower Willamette (USACE, 1969b; Willingham, 1983; Benner and Sedell, 1997). The Corps also continued to improve navigation through snag removal and construction of various structures so that by 1932, approximately 16 km of wing-dams and other structures (bridges, dikes, retaining walls, revetments, etc.) bordered the Willamette (USACE, 1932).

Logging of riparian forests for paper production and timber export increased greatly during the early twentieth century and caused the percentage of forested lands bordering the river to decrease by more than 50 % along much of the Willamette (Gregory *et al*., 2002a). Although logging led to increases in cleared floodplain lands, much of the floodplain was still avoided because bottomlands were plagued by frequent floods, high erosion rates, and poor drainage (Anderson, 1974). Despite these problems, floodplain agriculture continued to increase so that by 1932, 40–50 % of the Willamette was bordered by agriculture, with the most substantial increases occurring along the upper Willamette, where there was a four-fold increase in the length of channel bordered by cultivated crops (Gregory *et al*., 2002a).

Urbanization, development, and dam construction 1932–1972

The interval 1932–1972 was marked by rapid development of the Willamette River floodplain. Within the span of several decades, dams, revetments, and drainage-control and irrigation projects were constructed that enabled agriculture and suburban development to expand onto the historic floodplain.

Although bank protection had begun in the late nineteenth century, the extent and rate of bank stabilization efforts increased dramatically in the mid-1930s (Figure 23.6). Revetment construction by the Corps and private individuals continued through the late twentieth century (Fig. 23.6), and by the 1970s, 90% of all present-day revetments were constructed (Gregory *et al*., 2002c).

Dam building quickly followed authorization of the Willamette Valley Project in 1938, which entailed the construction of a series of multiple-purpose projects (Oregon State Planning Board, 1938; USACE, 1969a). By 1970, every major tributary of the Willamette had at least one flood control project, so that the entire Willamette Basin was regulated by a total of 13 reservoirs. Of these reservoirs, 11 are major flood control projects and two are primarily re-regulating reservoirs (Willingham, 1983). The multiple-purpose projects reduce flood peaks, support higher summer flows, and in some cases, provide hydropower (USACE, 1969a).

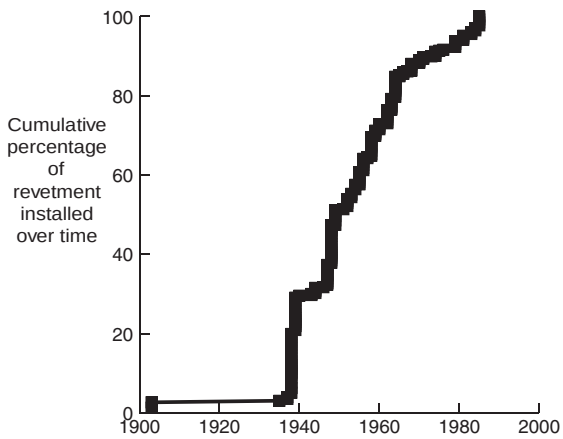

Figure 23.6 Cumulative percentage of revetment constructed along Willamette River, 1900–1985. Percentage is computed from lengths of revetment that have a known construction date (about 45% of total revetments). (Adapted from data provided by Gregory *et al*., 2002c)

Post-development and continued change 1972–1995

Development of floodplain lands slowed in the late twentieth century as many farms were converted to rural residences (Towle, 1982). Although the majority of revetment had been constructed by the early 1970s, the Corps of Engineers and private agencies continued to maintain and extend existing bank stabilization projects (Gregory *et al*., 2002c). Major actions undertaken during the period 1972–1995 that affected channel change involved dredging, gravel mining and management of riparian lands. In addition, several large cities have developed their waterfronts, requiring extensive bank stabilization to protect nearby developments. Channel improvements for navigation were limited to the lowermost reaches of the Willamette River (primarily downstream of Willamette Falls, near the confluence with the Columbia) whereas instream gravel mining occurs at many locations along the mainstem channel.

23.3.5 Flood History of the Willamette River

The Willamette River has historically experienced a wide range of floods of different magnitudes (Figures 23.4 and 23.7). Peak flows generally occur in the rainy season between November and March, and are typically associated with rain-on-snow events involving warm, moist subtropical air masses. Infrequent, extreme events (which we refer to as 'large floods') arise when these extra-tropical excursions result in intense rainfall accompanied by warm air temperatures over a period of several days, rapidly melting pre-existing deep and extensive snow packs in the Cascade Mountains and foothills. Such conditions led to the largest historic floods, which occurred in 1861, 1881, and 1890, though several other large floods may have also occurred earlier in the nineteenth century before the advent of gauged records (Figure 23.7). Many communities were wholly or partly destroyed in the 1861 flood (approximately 14 160 $m^3 s^{-1}$ at Salem) as floodwaters filled the Holocene floodplain and in some areas, overtopped the Pleistocene terraces (Miller, 1999; Gregory *et al*., 2002b). The large floods of 1881 (12 120 $m^3 s^{-1}$ at Salem) and 1890 (12 690 $m^3 s^{-1}$) also heavily damaged several towns and caused extensive erosion (USACE, 1881; Brands, 1947; Anderson, 1974).

Prior to construction of flood-control dams in the 1940s, the Willamette also experienced many moderate magnitude floods that were two to three times greater than modern bankful flow (Figure 23.7). Corps of Engineer reports from the late nineteenth century state that, even during these more common 'freshets', the floodplain was inundated to a depth of several metres and logs would fill the Willamette and adjacent sloughs (USACE, 1875).

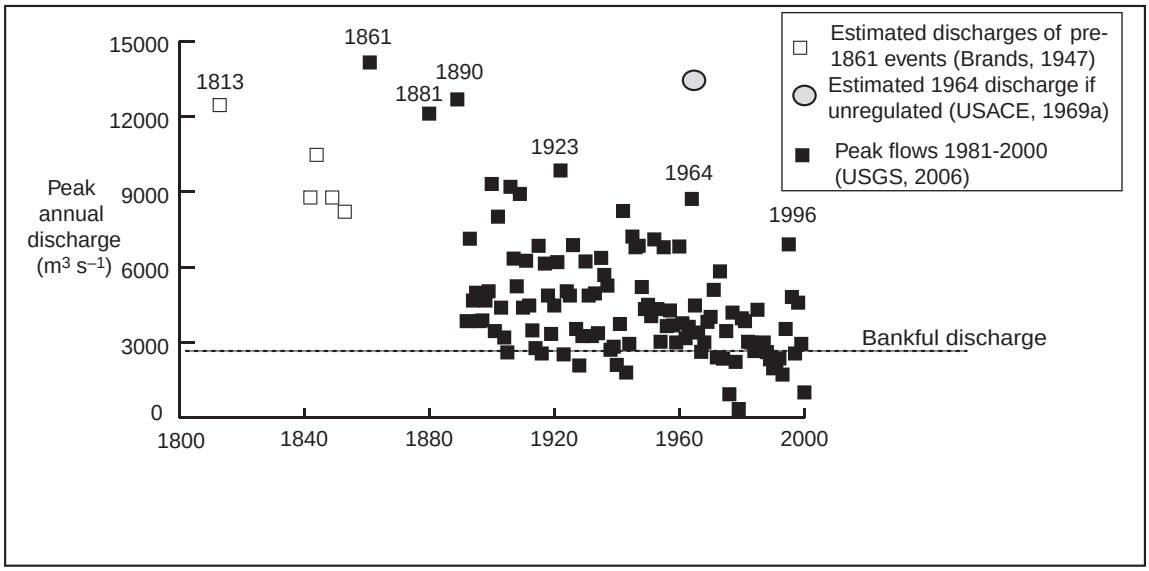

Figure 23.7 Peak discharge 1813–2000 for Willamette River at Salem. Peak flows have decreased steadily following construction of 11 major flood control reservoirs. Discharge for pre-1861 events was estimated from historic highwater marks (Brands, 1947)

During the moderate floods of 1951 and 1955, soil was stripped from fields situated atop Holocene alluvium, and erosion isolated several fields on newly created islands (Anderson, 1974).

Flood magnitudes began to decrease in the 1950s as increasing numbers of flood control dams were completed (Figure 23.4). The largest flood of the regulated era occurred on Christmas Eve of 1964 (peak discharge at Salem of $8700\,m^3\,s^{-1}$) and that flood may have been similar in magnitude to the 1861 flood of record (Figure 23.7) if seven flood control dams had not reduced peak discharge (USACE, 1969a). The February 1996 flood was the largest post-dam event, though its discharge was similar in magnitude to 'moderate' floods experienced every few years prior to flow regulation ($6900\,m^3\,s^{-1}$ at Salem). Although many low-lying areas were inundated, channel change was relatively minor compared with previous floods.

23.4 DATA AND METHODS FOR MEASURING HISTORICAL CHANNEL CHANGE

23.4.1 Historical Channel Maps

We calculate rates and styles of channel change using digital maps of the Willamette River compiled from historical maps and aerial photographs from 1850, 1895, 1932, 1972 and 1995 (Table 23.2). For 1850, 1895 and 1932, we used maps of the active channel produced by the Pacific Northwest Ecosystem Research Consortium (PNWERC) from surveys conducted by the General Land Office in 1850 and USACE in 1895 and 1932 (Hulse *et al*., 2002). The PNWERC also produced the 1995 channel map from aerial photographs provided by the USACE (Hulse *et al*., 2002). For the Long Tom and Santiam Reaches, this set of maps allows us to measure channel change for three time periods: 1850–1895, 1895–1932 and 1932–1995.

Inspection of the 1932 and 1995 channel maps for the Long Tom and Santiam Reaches reveals that the lower and middle Willamette did not experience significant channel change over the 1932–1995 period (an interval marked by widespread revetment and dam construction). In contrast, the McKenzie Reach contained numerous bends that initially migrated rapidly in the 1930–1950s and were subsequently stabilized with revetment by 1972. Averaging migration over the interval 1932–1995 would therefore provide inaccurate results for areas that experienced channel shifting followed by several decades of stability. We thus exclude the period of rapid development (1932–1972) from our analysis of the McKenzie Reach and calculate channel change for the three periods: 1850–1895, 1895–1932 and 1972–1995. We digitized the 1972 channel along the McKenzie Reach from aerial photographs produced by the USACE (USACE, 1972).

Table 23.2 Channel maps used to quantify historical channel change

Map date	Original survey or photo source	Map description	Source for georeferencing and digitizing	Precision
1850	General Land Office (GLO) Cadastral Surveys	Cadastral survey of townships and sections. Most of study area surveyed 1851–1853	Hulse *et al.*, 2002[a]	±10 m
1895	Army Corps of Engineers (USACE)	Navigational blue-line survey. Study area surveyed October–November of 1894	Hulse *et al.*, 2002	Unknown
1932	USACE	Navigational survey of study area conducted 1931–1932	Hulse *et al.*, 2002	±5 m
1972	USACE	Main channel and active channel[b] digitized from mosaic of orthophotographs in 1972 Willamette River and Tributaries Map Book. Photography flown May 2, 1972 at ~300 $m^3 s^{-1}$	These authors	±10 m
1995	USACE	Main channel and active channel digitized from orthophotographs flown August 1994 and September 1995 (~150–200 $m^3 s^{-1}$)	Spencer Gross Photography, PNWERC	±5 m

[a] Pacific Northwest Ecosystem Research Consortium (PNWERC) presented in Hulse *et al.* (2002).
[b] For 1972 we digitized the active channel from aerial photographs. Although discharge at the time the 1972 photos were taken is about twice that of flow during the 1995 photos, there is only about 1 m difference in stage, and reach-averaged channel width for the low-water channel varies by less than 2% between the photo series.

For the historic maps and the aerial photos, the active channel was defined as the area within the boundaries of the annual high water (1–2 year flow) mark, although definition of these boundaries was sometimes subjective. Gravel bars, small side channels, and surfaces vegetated with annual species (e.g. small shrubs, grasses, and willows) were included within the active channel, and channel-adjacent areas and islands containing larger woody vegetation were excluded (Hulse *et al*., 2002). Where present, steep banks clearly demarcated active channel boundaries.

23.4.2 Measuring Rates and Styles of Channel Change

We focused our analysis on several metrics that best describe adjustments in planform, erosion style and erosion rates. Channel width was measured by digitizing transects orthogonal to the channel centreline for each time interval. Transects were drawn at the intersection of the active channel with each floodplain kilometre boundary for kilometres 18–223. We digitized channel centrelines at a scale of 1 : 5000 to compute centreline length and sinuosity for each time period. In areas with multiple channels, the centreline was drawn for the largest channel, and in instances where wide bends (e.g. width >500 m) appeared to contain backwater areas, the centreline was drawn to reflect the assumed position of the thalweg. We determined the length of channel bordered by resistant banks by overlaying the channel maps and digitized centrelines from each time period with the surficial geology map of O'Connor *et al*. (2001). For each time period, the centrelines are divided into bend-sized sections, and each section is classified according to the type of bank material being eroded. Resistant banks include areas stabilized with revetments or any geological unit more indurated (and older) than Holocene alluvium including Pleistocene gravels, Tertiary marine sandstones and Tertiary volcanics.

To measure the rate and style of channel change between two time periods, we calculated migration rates, avulsion frequency and several other metrics to describe the relative dominance of each process. Digitized channel centrelines from sequential time periods were overlain, and we calculated the change in area of channel polygons. Stable areas are characterized by nearly congruent centrelines or very thin flow-parallel polygons; larger channel change polygons indicate areas where the channel either migrated or avulsed away from its original position. Each polygon was then classified according to the style of erosion (lateral migration versus avulsion). Lateral-migration polygons were further classified according to whether the centreline shifted towards the inside of the bend (straightening) or whether the centreline shifted towards the outside of the bend (normal migration). Because meander migration frequently involves both straightening and normal migration as bends elongate and migrate downstream, we restricted our classification of straighten-

ing to polygons where the centreline clearly moved to the inside of the bend, resulting in significant (e.g. >15 m) erosion.

Channel migration was measured as distance travelled orthogonal to the centreline for a particular time interval. Following the methodology of Micheli and Kirchner (2002), polygon width serves as a proxy for average distance travelled orthogonal to the centreline and was calculated by dividing polygon area by one-half of the polygon perimeter. Migration rates for each polygon were then calculated by dividing polygon width by the number of years in the time interval. We calculated reach-average migration rates for three styles of erosion: normal migration, straightening, and lateral migration (an average of both normal migration and straightening). Avulsion frequency was easily computed by summing the number of avulsion-related polygons in each reach, for each time period.

The relative dominance of each type of erosion was assessed by computing the percentage of centreline length subject to avulsion, straightening, and lateral migration. We also computed the annual area eroded per length of channel for lateral migration and avulsion. This latter analysis avoids the bias introduced by averaging migration rates derived from various-sized polygons, and provides a better indication of the area of floodplain reworked by different styles of erosion.

23.4.3 Development of a Two-Dimensional Flood Model for Willamette River

In order to better understand how different magnitude floods influenced avulsions, migration rates and widening, we relied upon the two-dimensional flood models of Denlinger (2002) and DHI (2005) to examine stream power generated during different-sized floods. We used these models to compute the magnitude and distribution of stream power for the 1861 and November 1996 flood along 10 km of the upper Willamette near FPKM 206. This allows us to compare patterns of erosion and deposition from large-scale versus moderate floods.

The flow models are both two-dimensional, finite difference models that solve the shallow-water flow equations on a two-dimensional grid of any surface. We built the grid from a digital elevation model giving spatial coordinates of the ground surface for the upper Willamette, and forming a rectangular mesh with square cells 10 m on each side. The inflow hydrograph for the 1996 flood is constructed from stage and discharge records at Harrisburg (USGS Station 1416600). Because time-series data for the 1861 flood are not available, the 1861 hydrograph is estimated by scaling the 1996 hydrograph according to estimated stage at the Harrisburg. A single value for bed friction is used to parameterize velocity gradient with depth, and this resistance combined with the forcing of the topography determines the three-dimensional variation of stage throughout the reach.

By comparing modelled stage with observed high-water marks over the three-dimensional terrain we can constrain both the average value for bed friction and discharge. Along the upper Willamette, there are few well-defined highwater marks for the 1861 and 1996 floods and we therefore rely upon digital inundation maps compiled by the PNWERC to constrain our modelled stage (Gregory *et al*., 2002b). The variation of stream power, which is the product of bed friction and depth-averaged velocity then provides a means to compare where erosion and deposition will occur for a flood with the modelled discharge.

23.5 RESULTS: PATTERNS AND CONTROLS ON HISTORICAL CHANNEL CHANGES

Each of our three reaches changed in the century following Euro-American settlement. For each reach, we summarize both the net changes that occurred during 1850–1995 and the dominant styles of adjustment that occurred in each time period.

23.5.1 McKenzie Reach, 1850–1995

In 1850, the Willamette River along the McKenzie Reach was a narrow, sinuous anastomosing channel dominated by avulsions and rapid migration. By 1995, the channel width had increased by 13% and flow was primarily contained within a single channel that evolved primarily through lateral migration (Figure 23.8). This transition occurred in three stages. Between 1850 and 1895, the McKenzie Reach experienced 46% increase in channel width and 11 large avulsions while lateral migration was limited to less than half of the channel length. Many of the avulsions involved the re-occupation of 1–4-km-long side-channels spanning large-amplitude bends (Figures 23.8 and 23.9) and resulted in a 20% decrease in centreline length between 1850 and 1895.

After experiencing a general widening and straightening during 1850–1895, the McKenzie reach narrowed by 15% as lateral migration became dominant during 1895–1932 (Figures 23.8 and 23.10). Although migration rates more than doubled and the length of channel subject to migration increased by 20%, centreline length only increased slightly. The overall style of migration was quite dynamic as several low-sinuosity portions of the 1895 channel developed into bends that subsequently migrated downstream (Figure 23.10).

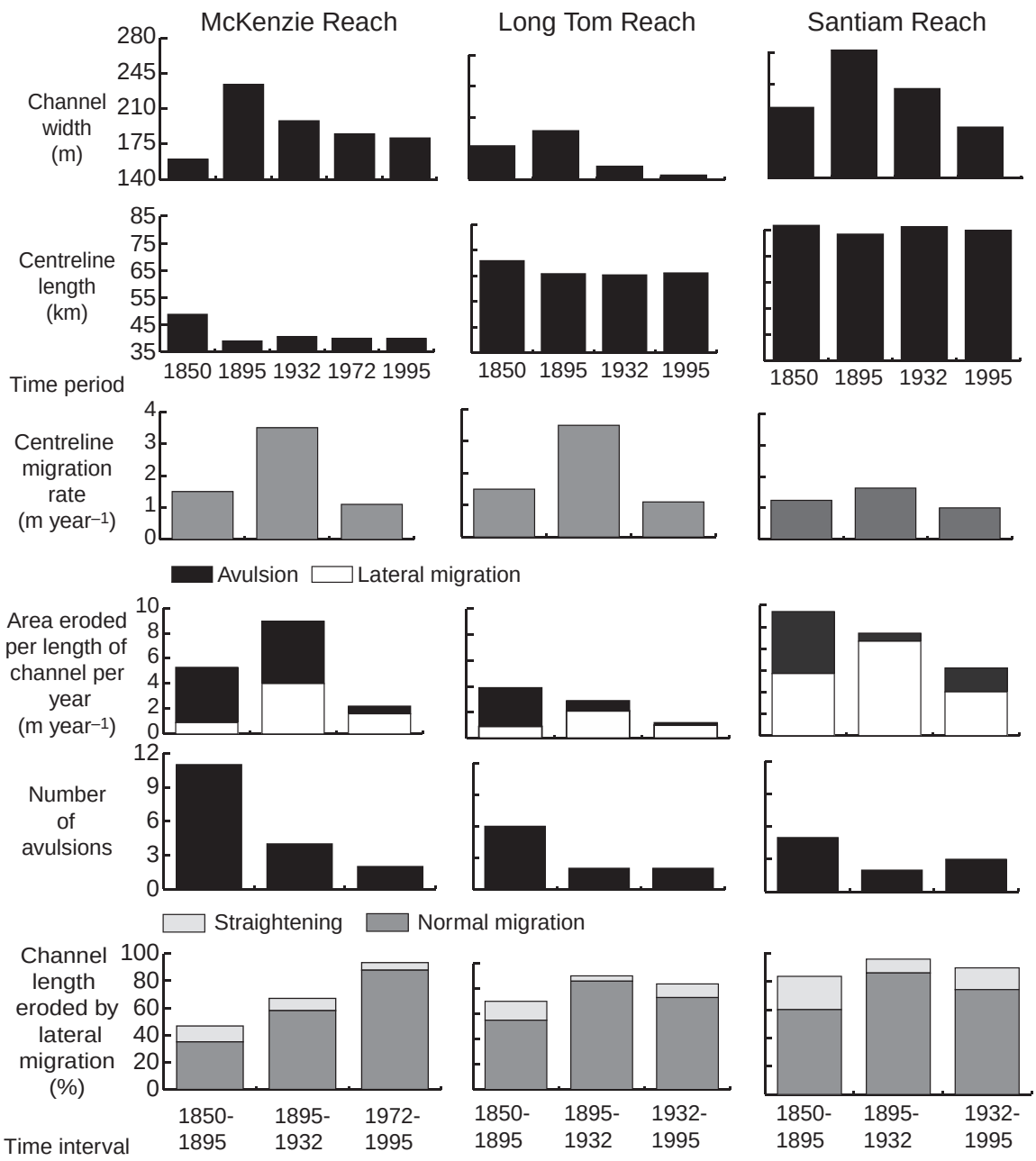

Figure 23.8 Patterns of channel change for mainstem Willamette River, 1850–1995

Figure 23.9 Example of avulsions 1850–1895 along upper Willamette River. Similar large-scale avulsions occurred along the entire Willamette River during this time period. In many cases, the 1895 channel avulsed into former side channels (e.g. FPKM 165–170) or carved cut-off channels (e.g. FPKM 169). (Geological map from O'Connor *et al*., 2001. Historical Willamette River channel maps and floodplain transect maps from Hulse *et al*., 2002)

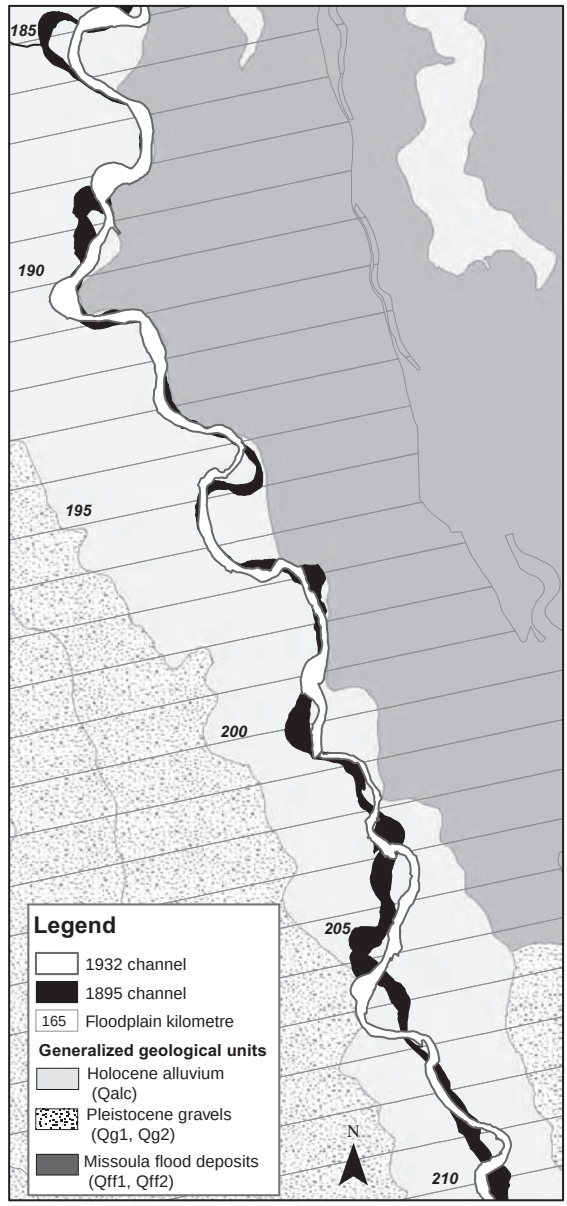

Figure 23.10 Example of rapid meander migration 1985–1932 along upper Willamette River. Along much of the Willamette River, small initial bends in the 1895 channel developed into larger bends which subsequently migrated downstream by 1932 (e.g. FPKM 200–205). As sinuousity increased, channel width also narrowed during the 1895–1932 time period. (Geological map from O'Connor *et al*., 2001. Historical Willamette River channel maps and floodplain transect maps from Hulse *et al*., 2002)

Channel change during 1972–1995 was more subtle than during earlier periods as migration and avulsions were limited to areas of the floodplain where revetments did not restrict channel movement (Figure 23.8). Migration rates decreased by 60% from those experienced during 1895–1932, avulsion frequency decreased and the channel narrowed slightly. Although much of the centreline experienced some movement during the late twentieth century, in many areas of floodplain, channel narrowing caused the centreline to appear to shift laterally though actual bank erosion was minimal.

23.5.2 Long Tom Reach, 1850–1995

Historical channel change along the Long Tom Reach reflects its position as a transition zone as the upstream portion of the reach has transformed from a dynamic, anastomosing channel towards a more stable channel, whereas the lower reach has maintained its more stable single-thread planform. Over our 150-year study period from 1850 to 1995, the Long Tom Reach experienced an 18% net decrease in channel width and a 7% decrease in channel length (Figure 23.8). Whereas the McKenzie and Santiam Reaches experienced large increases in width during 1850–1895, the Long Tom only widened by about 10% and appears more prone to narrowing, as channel width decreased by 20% between 1895 and 1932 and an additional 6% from 1932 to 1995. Like the McKenzie Reach, much of the net decrease in sinuosity was accomplished during 1850–1895 by avulsions along the upper sections of the Long Tom Reach that were historically anastomosing (Figure 23.8).

The Long Tom Reach is unique in that while avulsions between 1850 and 1895 influenced a large portion of the floodplain, lateral migration has influenced a greater portion of the total channel length during all time periods. Migration rates were greatest during the interval 1895–1932 when several low-sinuosity sections of the upper Long Tom Reach developed small initial bends while other existing bends migrated downstream (similar to the example shown in Figure 23.10 for the McKenzie Reach).

Although reach-average channel change trends for 1932–1995 indicate that erosion due to avulsions and meander migration decreased during the twentieth century, the entire Long Tom Reach did not immediately become more stable. Aerial photographs of the upper Long Tom Reach show that several bends migrated rapidly from 1932 to 1972 so that local migration rates exceeded 10 m annually in some areas. Nearly all of these rapidly eroding bends were stabilized with revetments by 1972 and bank erosion from 1972 to 1995 was generally limited to areas unprotected by revetments. In contrast, the channel downstream of Corvallis (FPKM 165) experienced little net change over the entire 1932–1995 interval.

23.5.3 Santiam Reach, 1850–1995

Although the Santiam Reach has generally been much more stable than the upper reaches, this lower study reach has followed similar trends to the others. Similar to the Long Tom Reach, the Santiam Reach experienced a net decrease in channel width and slight decreases in channel length over the entire study interval of 1850–1995 (Figure 23.8). Much of the loss in centreline length was accomplished through several large avulsions during 1850–1895 though subsequent migrations during 1895–1932 nearly recovered much of the 1850 sinuosity. Like the McKenzie Reach, the Santiam Reach initially experienced large (~30%) increases in channel width between 1850 and 1895. However, during the intervals 1895–1932 and 1932–1995, channel width decreased by 15% and 18%, resulting in a 10% net decrease in reach-average width by 1995.

In all time periods, the Santiam Reach has been dominated by lateral migration. The overall annual rate of migration has fluctuated slightly (1–1.6 m) and most lateral migration has occurred in Holocene alluvium along the lower portion of the reach downstream of Salem (FPKM 110). Bends situated adjacent to Qg2 gravels appear to remain locked in place and have only migrated slowly outward against the terrace. Like the other reaches, during the period 1895–1932 the river experienced the greatest lateral migration rates, but along the Santiam Reach, migration was dominated by lateral shifting of large (>5 km) bends, rather than the development and subsequent downstream migration of small bends as seen on upper reaches.

Twentieth century channel change along the Santiam Reach was marked by channel narrowing and an overall decrease in floodplain erosion (Figure 23.8). Although three avulsions occurred, they generally bypassed smaller portions of the floodplain compared with larger, historic avulsions. Migration rates were similar to rates experienced during the mid–late nineteenth century, but the area affected by migration is much less than for historic periods. Decreased migration, fewer avulsions and continued channel narrowing cause much of the 1995 channel to be positioned within the boundaries of the 1932 channel.

23.5.4 Summary of Willamette River Channel Change, 1850–1995

Our results revealed that, between 1850 and 1895, all reaches experienced numerous avulsions, increases in

channel width, and decreases in centreline length. Between 1895 and 1932, migration rates increased by 50–300%, which led to increases in sinuosity while channel width decreased. During the period 1932–1995, the Long Tom and Santiam Reaches displayed similar migration rates as during 1850–1895, yet channel width continued to narrow. Along the McKenzie Reach, channel change from 1972 to 1995 was primarily limited to lateral migration along areas unrestricted by revetments and occurred at rates similar to 1850–1895 levels. While sinuosity decreased along all reaches between 1850 and 1995, the Long Tom and Santiam Reaches experienced an overall decrease in channel width whereas the McKenzie Reach experienced net widening.

Along all reaches, the percentage of channel bordered by resistant banks has increased substantially over the 150-year study interval (Figure 23.11). Moreover, we see that some bends situated adjacent to naturally resistant bank materials (e.g. the Qg2 located along floodplain margins) were historically able to migrate or avulse away from resistant banks, causing the percentage of channel bordered by resistant banks to fluctuate slightly over time (Figure 23.11). However, bank stabilization in the mid-twentieth century apparently causes many of these bends

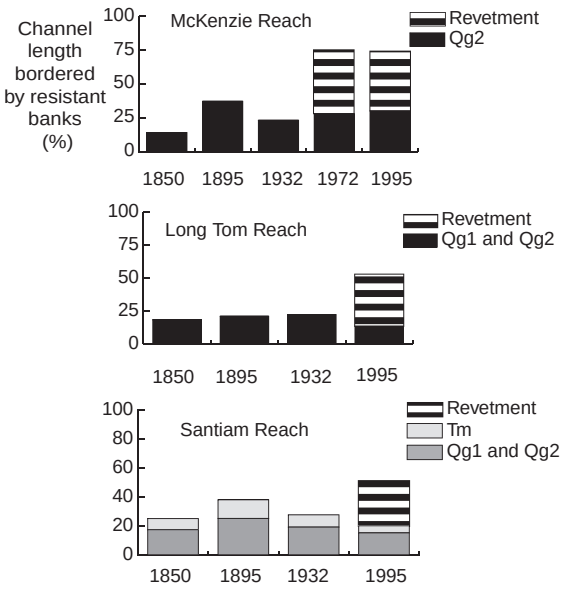

Figure 23.11 Length of channel bordered by resistant bank materials. Revetment installed in the 1930s–1970 stabilizes large areas of the Willamette River, while naturally resistant banks have historically bordered an additional 13–40% of each reach. (Geological units from O'Connor *et al*., 2001)

to remain locked in place, as key sections of revetment prevent the channel from avulsing or migrating back towards the Holocene floodplain.

23.5.5 Flood Model Results

On the upper Willamette, large-magnitude floods such as the 1861 event (~7930 $m^3 s^{-1}$ at Harrisburg) inundate the entire Holocene floodplain and generate erosive overbank flows (Figure 23.12a). In many areas, flow follows the regional (floodplain) topography rather than the river, causing streampower to be concentrated in areas outside the main channel. Power is typically highest along inside, rather than the outside, of meander bends. Such patterns of erosive flows could have led to scouring of point bars, and may have caused widening of the channel or migration towards inside of bend (straightening). Streampower is also high at the downstream end of bends, but on the outside of the channel where chute formation and avulsions are likely to occur. Overbank flows in areas not adjacent to the channel could have carved new side-channels, or triggered migration and avulsions along existing secondary channels.

Moderate sized floods such as the 1996 event (~2100 $m^3 s^{-1}$ at Harrisburg) and those experienced every few years in the early twentieth century may inundate the floodplain but do not produce erosive overbank flows (Figure 23.12b). Stream power from modern, post-dam floods is generally greatest in the channel and more likely leads to within-channel scouring and local bank erosion rather than chute formation. Overbank stream power for moderate-sized floods is much lower than power generated by large-scale floods (typically $<10\ W\ m^{-2}$ versus $>40\ W\ m^{-2}$ for large floods). These streampower patterns indicate that avulsions may have only been possible in areas with high erodibility, e.g. sparsely vegetated point bars or along multi-thread reaches. Model results are consistent with post-1996 channel changes, which indicate bank erosion was greatest in areas where the active channel is relatively wide and characterized by gravel bars and side channels.

23.6 DISCUSSION, NARRATIVE OF HISTORICAL CHANNEL CHANGE

Our results reveal the inherent complexities in interpreting causative mechanisms for channel changes in large rivers. Against an ever-changing backdrop of flood history, evolving land uses, flow regulation, and engineering interventions in the channel itself, patterns and rates of channel change vary by both reach and time period. Interpretation of factors forcing or controlling river evolution at the scale

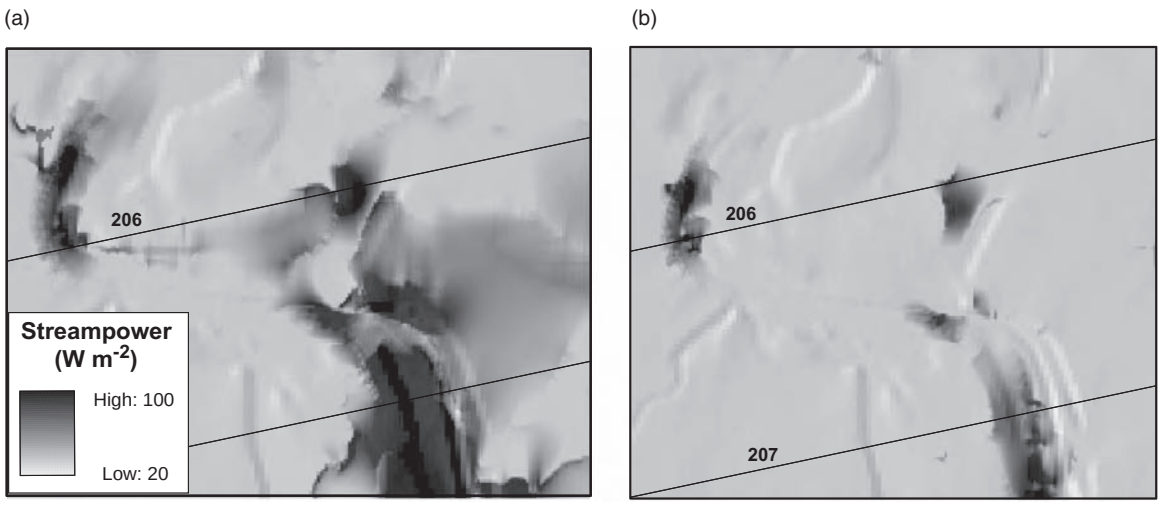

Figure 23.12 Comparison of streampower for large floods and moderate floods. Streampower was calculated as the product of shear stress and velocity using MIKE 21, a two-dimensional hydrodynamic model. Area shown spans FPKM 205–208 along the upper Willamette upstream of Harrisburg. (a) Streampower at 7930 $m^3 s^{-1}$, estimated peak discharge for the 1861 flood of record at Harrisburg. (b) Streampower at 2100 $m^3 s^{-1}$, approximate peak discharge for the 1996 flood at Harrisburg. The 1996 flood was similar in magnitude to the 'moderate' floods that occurred frequently in the early twentieth century

of the entire river must therefore rely more on a plausible narrative supported by multiple lines of evidence rather than simple cause-and-effect type models. Here we discuss some salient aspects of that narrative for the Willamette, interpret the history of channel changes, and consider how this one case study informs interpretation of processes of channel change in other large rivers.

23.6.1 Interpreting Historical Channel Change, 1850–1995

In order to determine why the Willamette has displayed varying rates and styles of channel change over the 150-year study interval, we compared our results against the list of natural and anthropogenic impacts in Table 23.1 that may have triggered the observed patterns of channel change. This analysis suggests that large floods, smaller floods and the full spectrum of human modifications to the channel and floodplain each have had distinct effects on channel planform and behaviour, but that the impact of these different causative factors varies in magnitude and timing.

Large magnitude floods appear to have had a profound impact on the entire Willamette River system in the mid–late nineteenth century, in particular the avulsions, channel widening and decreased sinuosity that occurred during 1850–1895. This interpretation is consistent with: (1) gauge records indicating that the three largest historical floods in 1861, 1880 and 1891 occurred during this time period (Figure 23.7); (2) flood model results showing stream power during the largest floods is concentrated in overbank areas and therefore more likely than smaller floods to cause channel widening and avulsions (Fig. 23.12); (3) the observation that the 1850–1895 period was marked by numerous avulsions whereas subsequent time periods with fewer large floods had substantially fewer avulsions (Figure 23.8); (4) historical records during this early period (e.g. Brands, 1947) that describe large, channel-spanning, wood rafts that, once mobilized during exceptional floods, could readily have served as tools for stripping surfaces and eroding banks, thereby facilitating channel widening (Johnson *et al*., 2000); (5) aerial photographs of the Willamette floodplain that reveal many examples of large-amplitude bends having been abandoned through avulsions, with few examples of meander bends that have evolved entirely through lateral migration (Figure 23.13).

Periods of frequent, more moderate magnitude floods appear to result in accelerated lateral migration as opposed to avulsive 'hopping', as evidenced by channel changes during the period 1895–1932 (Figure 23.10). Over this time, at least 25 flood events (Figure 23.7) occurred that were twice or greater the magnitude of the modern bankful flood (USGS, 2006). This coincided with an increase in

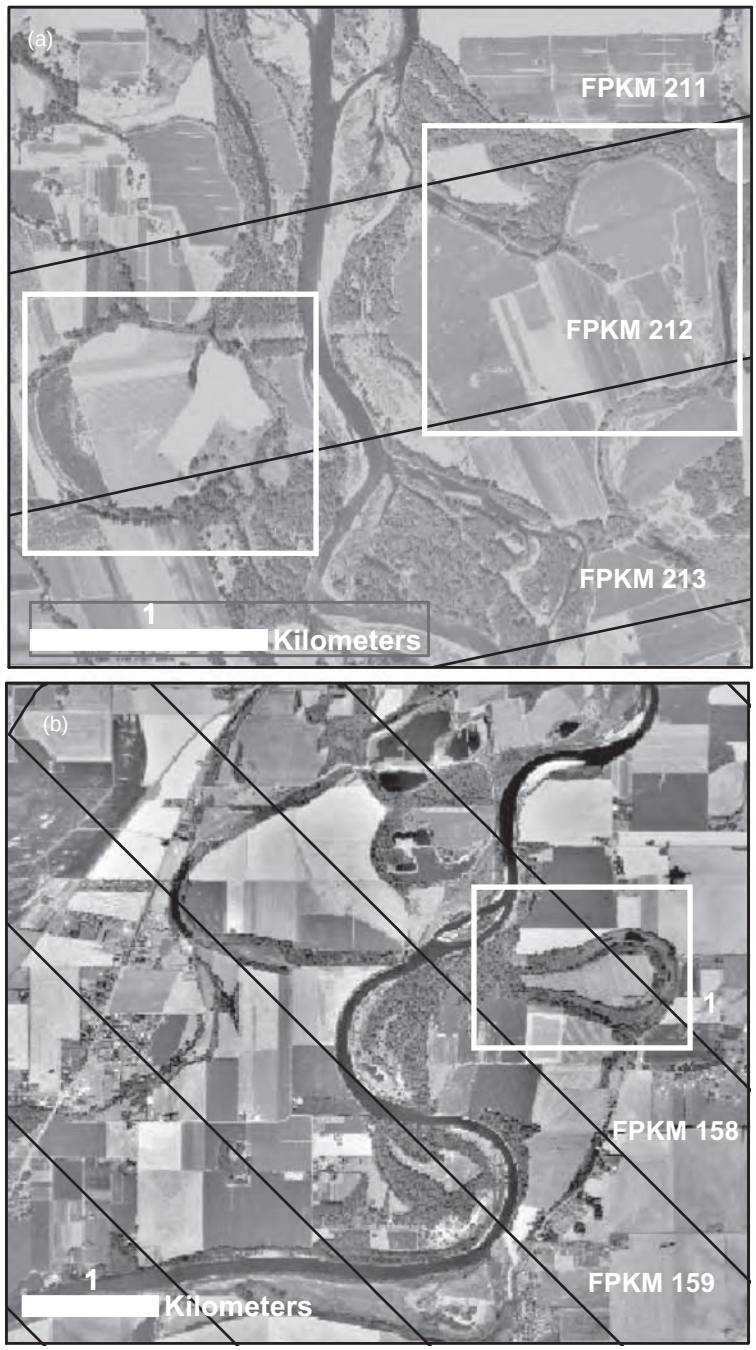

Figure 23.13 Examples of avulsions and meander migration recorded in remnant floodplain features. (a) Examples of abandoned large-amplitude bends as recorded in aerial photographs of Willamette River floodplain. These bends were probably active in the nineteenth century. Similar features are found in many other areas of the southern Willamette Valley. (b) Example of meander bend that evolved entirely through lateral migration. Such bends are rare in the Willamette Valley floodplain. This bend is located between Corvallis and Albany and probably formed along a side channel in the early twentieth century

migration rates of 50–300% and greater sinuosity. Our stream power modelling demonstrates that during moderate-sized floods (such as the 1996 flood and those experienced every few years prior to flood control), stream power is concentrated in the channel rather than on the floodplain, thereby promoting lateral migration (Hickin and Nanson, 1984). Aerial photographs from 1995 to 2000, for example, show that annual local migration rates in areas of the McKenzie Reach without artificial revetments (e.g. FPKM 210–212) exceeded 20 m, a rate that is much higher than reach-averaged migration rates for the interval 1972–1995. Such rapid channel change is likely due to moderate magnitude floods that occurred within a year of each other in February and November 1996. Floodplain inundation during such moderate floods is typically not deep or swift enough to carve cut-off channels or trigger avulsions except in highly erodibile areas or former low-lying channels.

In addition to the frequency of moderate floods, another factor promoting the rapid migration rates observed from 1895 to 1932 was the prevalence of erodible banks. At the beginning of the twentieth century and prior to the erosion-control engineering that took place mid-century, most of the Willamette River was bordered by erodible Holocene alluvium (Figure 23.11) (Wallick *et al*., 2006). Again using the 1996 floods as an example of the style of channel changes that were common early in the last century, most lateral erosion that occurred during those floods was concentrated in areas where the active channel was fairly wide and both banks were flanked by Holocene alluvium.

Human activities do not appear to have had a major influence on rates and styles of channel change until the mid–late twentieth century. Although some previous work has suggested that the Willamette became increasingly stable following Euro-American settlement in the mid-nineteenth century (i.e. Benner and Sedell, 1997; Hulse *et al*., 2002), our results clearly demonstrate that the Willamette was an active and dynamic river subject to avulsions and rapid migration well into the first third of the twentieth century. The timing of human settlement of the valley (Figure 23.4) does correspond to the previously discussed shift from avulsion to lateral migration, but we interpret this shift as being more due to flood history than direct human impacts on the river and its environs, which were modest until the mid-1900s. Navigation improvements by the Corps of Engineers in the nineteenth century targeted only a small percentage of the entire channel (<10% of total river length), and historical records indicate that many of the wing-dams and other structures were swept away or disrupted by channel shifting following floods (USACE, 1875, 1882, 1891). Land conversion and riparian deforestation may have accelerated bank erosion locally, but we do not believe this was a major driver of channel change because very few settlements were located along the Willamette floodplain in the nineteenth and early twentieth centuries (General Land Office, 1851–1853; USACE, 1895; Bowen, 1978; Towle, 1982). Even by 1932, less than half of the entire mainstem Willamette was bordered by farm lands, and most agriculture occurred along the more stable lower reaches. The upper Willamette, which had the highest migration rates, experienced very little floodplain agriculture until the mid–late twentieth century (Anderson, 1974; Gregory *et al*., 2002a).

Similarly wood snagging, which has been interpreted as a major factor contributing to reduced channel migration (e.g. Sedell and Froggatt, 1984), removed only a small portion of the total volume of large wood available in the historical Willamette floodplain. Many historical records indicate that sloughs and side channels were frequently filled with downed trees following 'freshets' throughout the late 1800s (USACE, 1875: 763). On average, approximately 1000 snags were removed annually from the upper Willamette roughly between 1870 and 1920 (Sedell and Froggatt, 1984). Assuming that these logs were taken from a 50 km area extending upstream of Corvallis (FPKM 165), this resulted in approximately 20 logs removed per kilometre of floodplain per year. Without minimizing the cumulative impact of large wood removal, it is important to recognize that the upper Willamette floodplain extended laterally for several kilometres and was still densely forested in many areas until the 1930s. We therefore suggest that snagging by itself did not have a significant impact on channel change. Rather, it was snagging in combination with the widespread conversion of floodplain forests to agriculture (which diminished local availability, hence recruitment of large wood) and dam construction (which limited the transport of wood from tributary channels to the mainstem Willamette) that reduced the in-channel abundance of wood. With both wood supply and flood peaks reduced, the channel was less prone to avulsions due to wood clogging of channels. Clearly disentangling the specific effects of woody debris removal on channel morphology from other concurrent changes to the channel regime is difficult, but on balance we suggest that it played a secondary role to flow regime changes.

Another interpretation of decreased migration rates and channel narrowing that occurred from the 1930s onward is that they are broadly consistent with predicted patterns of increased channel stability and incision following dam construction and bank stabilization (Williams and Wolman, 1984; Shields and Cooper *et al*., 2000). Migration rates decreased by 40–70% along the entire Willamette during this period, while avulsion frequency

diminished by 50% on the upper Willamette. From 1932 to 1995, channel width decreased slightly on the upper and lower reaches of the Willamette, while the Santiam reach narrowed by nearly 20%. At the same time, aerial photographs from 1939 to 1996 show maturation of riparian vegetation and decreases in the number of bare gravel bars adjacent to the main channel (Gutowsky, 2000). Distinguishing between dam construction versus bank stabilization as driving these changes is problematic, however, since both activities occurred concurrently. The rapid development of bank stabilization measures from the 1930s onward, however, has to be seen as having a primary control on channel migration rates (Figure 23.6), as it represents a direct intervention in the channel designed specifically for the purpose of reducing bank erosion, hence lateral migration. By 1995, nearly 50–75% of the Willamette was bordered by either naturally resistant bank materials (e.g. cemented Pleistocene gravels, Tertiary marine sandstones, or basalts) or revetments (Figure 23.9). Many areas that were not stabilized with revetments or had intrinsically resistant banks were nonetheless 'inherently stable' (and predominantly straight) reaches that had experienced little net change over the 150-year study period. The modern Willamette River is highly constrained, with lateral adjustments possible on only a few reaches.

Dam construction from the 1930s onward was highly effective in limiting the sizes of most winter floods. By 1970, 13 major flood control reservoirs had been constructed, and the largest peak flow of the post-dam era was the 1996 flood, which as noted above, was similar in magnitude to the 'moderate' sized floods that occurred every few years in the early twentieth century (Figure 23.7). Reduced peak flows limited opportunities for lateral change, although the tendency for the channel to incise would also have been limited by reduced stream power (Grant *et al*., 2003). Reduction in sediment supply due to upstream dams was probably not much of a factor driving channel changes in the Willamette, since other studies have shown no change in sediment rating curves following dam construction (Klingeman, unpublished data; Laenen, 1995). Abundant sediment supply in tributaries below dams and on the valley floor apparently compensates for sediment deposited in reservoirs upstream of dams.

Our estimates of rates of channel change are limited by the long time intervals between sequential aerial photos and maps. A more accurate picture of the timescales of changes relative to specific flood events and human activities might have emerged had the inter-photo intervals been less. For example, on the McKenzie Reach, we were able to discriminate channel changes that occurred in the post-dam and revetment era of 1972–1995 from changes that occurred during 1932–1972. Because rates of channel change during the 1972–1995 period are significantly lower than for previous time periods, we hypothesize that migration rates calculated for the period 1932–1995 along the Long Tom and Santiam Reaches may underestimate rates of channel change from 1932 to 1972 while overestimating channel changes from 1972 to 1995. Along all reaches, our use of centreline migration rates probably overestimates actual bank erosion during the twentieth century, because during periods of channel narrowing, the centreline may appear to shift laterally though actual bank erosion is negligible (Wallick, 2004). Thus, while our calculated migration rates for all reaches during the twentieth century were lower than for previous intervals, we suspect that actual bank erosion may be even lower than our the migration rates reported here.

23.6.2 Extending Lessons learned on the Willamette to Other Large Rivers

What can we learn from this detailed examination of historical channel changes on the Willamette that is applicable to other large rivers? Several key lessons emerge from this analysis that provide insight into factors controlling the intrinsic evolution of large rivers and disentangling how human activities modify and shape channel behaviour. In particular, this study gives some confidence that the complex history of large rivers can be deciphered using historical records, and a general explanatory narrative can be developed.

For rivers where the human history is relatively recent (i.e. last one to two centuries), it is still possible to interpret patterns and controls on intrinsic channel behaviour prior to any human interventions or modifications. What emerges from our examination of the Willamette is that there exists a hierarchy of factors controlling the pattern and evolution of the river. This is not a new concept (Schumm and Lichty, 1965), and we need to be cautious in extending conclusions from our particular case study to other rivers. Nevertheless, the patterns, timing and longitudinal trends of channel changes experienced by the Willamette from 1850 to 1900 suggest that in the absence of human impacts, channel evolution is inevitably steered by spatial variations in channel morphology and temporal variations in basin disturbances such as floods.

In particular, spatial variation in channel gradient, valley geometry, and bed and bank erodibility provide first-order controls on channel form, particularly planform and determine the sensitivity with which a given reach will respond to drivers of channel change. Of these, channel gradient and valley geometry appear to be overarching

controls on channel form, with variation in erodibility introducing a factor that can locally trump these broader scale controls. We find it noteworthy that the overall style of channel change in a given time period was remarkably similar across the entire study area, but the magnitude of change (e.g. the increase in migration rates or magnitude of channel widening) varied widely according to study reach. For example, the higher-gradient McKenzie Reach responded quite sensitively to the flood-rich period 1895–1932 through rapid migration of numerous bends, whereas the lower gradient Santiam Reach experienced a more dampened version of 'rapid migration' regarding both observed erosion rates and the number of bends that experienced this style of change.

This finding is consistent with the general longitudinal transition of the Willamette from an anastomosing to a more meandering or wandering system, and accords with other findings on both mountain (Ferguson and Ashworth, 1991; Grant and Swanson, 1995) and lowland rivers (Leopold and Wolman, 1957; Knighton and Nanson, 1993).

Along with the physical setting of the channel, a key factor influencing the channel condition at any particular time is the magnitude, recency and sequence of flood flows. Large scale differences in Willamette River morphology and processes – for example, the predominance of avulsions versus lateral migration as a mechanism of channel change – appear to result from whether particular periods of time include large or more moderate floods. During flood-rich periods, more of the valley bottom is maintained as active channels whereas during flood-poor periods, the channel tends to wander laterally. The time period between flows doing significant geomorphic work has been identified as an important factor on par with the magnitudes of floods themselves in terms of shaping the channel (Wolman and Gerson, 1978). Not only the interval between floods, but also the sequence of flows may also play a role in determining channel condition at any given point in time, particularly where vegetation and woody debris are present (Tal *et al*., 2004). Vegetation in particular, and the cohesion it provides for bank sediments, is emerging as a first-order control on channel pattern, and its presence or absence can determine whether the channel is braided or meandering (Gran and Paola, 2001; Murray and Paola, 2003). With floods acting as vegetation-resetting events, an important time-scaling factor for interpreting channel behaviour is the magnitude and frequency of floods relative to the timescale of recolonization and growth of vegetation.

Turning now to what the Willamette study reveals about the role of human activities on geomorphic evolution of large rivers, we observe that human impacts are invariably overlain onto a river system with certain intrinsic controls, as discussed above. This suggests that any attempt to interpret human impacts requires that those intrinsic controls be accounted for first, a daunting task where human modifications to the channel span multiple centuries. Because of the recency of human modifications to the channel, rivers such as the Willamette can provide a useful reference point for more disturbed rivers elsewhere. But even where the human history is relatively short and decipherable, interpreting the river's response is quite complex, particularly since human actions occur in concert with each other and with external drivers such as floods.

The Willamette study highlights that both the sequence and timing of human interventions in rivers has important implications for interpreting long-term channel behaviour. Sequence involves the order in which interventions occur, while timing reflects when they occur in relation to other channel-shaping events, particularly floods. Our results suggest that the sequential order of disturbances can have important effects on rates and styles of channel change in subsequent time periods. On the Willamette, periods of moderate floods enhance lateral migration which causes the channel to develop a more sinuous planform. Bends created by migration are then susceptible to avulsions and straightening by large-magnitude floods. In the absence of anthropogenic activities, flooding patterns along the densely forested historic floodplain probably caused the Willamette to alternate between a narrow, sinuous planform (e.g. the 1850 planform) and a wider, straighter planform (e.g. the 1895 planform) over the scale of multiple decades. However, it seems that the upper Willamette never recovered its pre-large flood planform because closure of side channels, bank stabilization and other Euro-American activities forced greater amounts of flow into a larger, single channel while also suppressing lateral migration. Thus, a century after the large-magnitude floods of the 1800s, the upper Willamette still maintains a wider, straighter planform than was observed in 1850.

It is interesting to speculate whether the channel planform evolution would have been markedly different had the first half of the twentieth century included more large floods similar to the 1861 event. Would the loss of riparian forests and concomitant reduction in large wood stored within the channel as agricultural use of the valley bottom expanded have increased (because of reduced vegetation and bank cohesion) or decreased (because of lower concentrations of potentially mobile wood) the erosive power of a large flood? These kinds of speculations underscore the contingent nature of channel response. Although he was writing about biological evolution, Gould (1989: 283) could have been describing channel evolution:

> 'I am not speaking of randomness, but of the central principle of all history – contingency. A historical explanation does not rest on direct deductions from laws of nature, but on an unpredictable sequence of antecedent states, where any major change in any step of the sequence would have altered the final result. This final result is therefore dependent, or contingent, upon everything that came before – the unerasable and determining signature of history.'

Although clearly obeying physical laws and constrained by both physical setting and process dynamics, channel evolution in large (and, to a lesser extent, smaller) rivers is inevitably contingent – it cannot be interpreted solely on the basis of physics. The history of channel changes, whether due to natural or anthropogenic actors, sets the river's evolutionary course and predisposes it to respond to subsequent actors or events in a way different than had those initial changes not transpired. Simple cause-and-effect models can be used to explain some aspects of this behaviour, for example why a particular bank failed under a particular flow regime. The overall trajectory of changes requires that these direct causal linkages be supplemented by a broader narrative that weaves the sequence and timing of factors driving change and consequent responses. This narrative can be developed using historical information and relatively simple metrics, and while it does not constitute proof of why certain changes occurred when they did, it can provide a plausible and rational explanation for complex fluvial phenomena.

23.7 CONCLUSION

Our study of the Willamette River reveals that geologic controls, flooding and human activities have all exerted large influences on channel change, but that the relative importance of these variables has shifted over time. Prior to flow regulation and bank stabilization, the Willamette was an anastomosing river flowing through a densely forested floodplain. During periods of moderate floods, meander migration led to the development of bends along both the mainstem Willamette and side channels. Large-scale floods led to avulsions and extensive increases in channel width and decreases in sinuosity. In the periods following these large floods, meander migration probably led to the redevelopment of bends with migration occurring rapidly along reaches flanked by Holocene alluvium. Anthropogenic activities had no clear effect on planform or erosion rates until the 1930s when widespread bank stabilization and dam construction resulted in diminished migration rates, fewer avulsions and channel narrowing. By the late twentieth century, more than 30% of the Willamette was stabilized with revetments, while naturally resistant bank materials bordered an additional 13–30% of the three study reaches. Large-scale geological controls in combination with bank materials determine the magnitude of channel response to anthropogenic and natural impacts: more intrinsically stable reaches (e.g. the lower Willamette and those bordered by resistant banks) required little to no effort to maintain a navigable channel. In contrast, steeper reaches along the upper Willamette required substantial maintenance and were not fully stabilized until flood control dams and extensive revetments were constructed.

The approach we employed here was successful in providing a framework for understanding how large rivers evolve over time amid overlapping drivers of channel change. This framework leads to a narrative of historical channel changes that provides some basis for assessing how large rivers may respond to future anthropogenic or natural impacts.

Channel change along the historically dynamic Willamette River is presently limited to lateral migration along reaches unconfined by revetments or naturally resistant banks. Avulsions are infrequent but may occur during moderate sized floods particularly along side-channel areas. Restoration efforts aiming to increase lateral migration, side-channel connectivity and avulsions will likely be most successful along historically dynamic reaches bordered by Holocene alluvium. These reaches tend to have erodible banks and relict side channels, and have historically responded more sensitively to flooding and other disturbances.

The analyses applied here are applicable to other large rivers because nearly all large rivers are influenced by a myriad of spatially and temporally varying impacts. However, assembling a narrative of historical channel change is an ambitious task because it requires a wide range of historical, geomorphic, geologic and hydraulic analyses. The datasets that support these analyses are necessarily extensive and must encompass broad spatial and temporal timeframes. On the Willamette, historical channel maps, and geological maps are readily available while records of landuse and human activities required more in-depth analyses of historical documents. In addition, our approach relied heavily on previous work, especially the data collection and compilation efforts by the PNWERC (Hulse *et al*., 2002).

Despite the extensive analytical effort required for such a large-scale study, such an approach is important because it avoids the bias introduced by smaller-scale studies wherein only a single driver of channel change is analyzed. For example, had we limited our analyses to the impact of large floods on channel morphology, the various

roles geology plays in dampening flood-related channel change might have been neglected. Moreover, by studying large rivers over broad spatial and temporal timescales in light of a full range of natural and anthropogenic impacts, a much more comprehensive picture of channel evolution in large rivers emerges.

ACKNOWLEDGEMENTS

We wish to thank Stan Gregory, Linda Ashkenas, Randy Wildman and other members of the Pacific Northwest Ecosystem Research Consortium for providing many of the datasets, and background material used in this study. This work was largely based on the exhaustive efforts of the PNWERC and we are grateful for their collaboration and assistance. Jim O'Connor provided field equipment, guidance and insight into the Willamette's Quaternary history. We thank Søren Tjerry for his modelling expertise. Reviews and comments by Sarah Lewis greatly improved this chapter. This work was supported by the National Science Foundation (Biocomplexity Grant 0120022).

REFERENCES

Abbe, T.B. and Montgomery, D.R. (1996) Large woody debris jams, channel hydraulics and habitat formation in large rivers, *Regulated Rivers: Research and Management* 12, 201–221.

Abbe, T.B. and Montgomery, D.R. (2003) Patterns and processes of wood debris accumulation in the Queets River Basin, Washington, *Geomorphology* 51, 81–107.

Anderson, R.V. (1974) Flooding and settlement in the Upper Willamette Valley. MA thesis, University of Oregon, Eugene, 69 pp.

Benito, G. and O'Connor, J.E. (2003) Number and size of last-glacial Missoula floods in the Columbia River valley between the Pasco Basin, Washington, and Portland, Oregon, *Geological Society of America Bulletin* 115(5), 624–638.

Benner, P.A. and Sedell, J.R. (1997) Upper Willamette River landscape: a historic perspective, In: *River Quality: Dynamics and Restoration* (A. Laenen and D.A. Dunnette, Eds.), pp. 23–47, CRC Press, Inc., Salem, MA.

Bowen, W.A. (1978) *The Willamette Valley, Migration and Settlement on the Oregon Frontier*. University of Washington Press, Seattle, 119 pp.

Brands, M.D. (1947) Flood runoff in the Willamette Valley, Oregon. *US Geological Survey Water Supply Paper* No. 968-A. Washington, DC, 57 pp.

Cheatham, R. (1988) Late archaic settlement pattern in the Long Tom sub-basin, Upper Willamette Valley, Oregon. University of Oregon Anthropological Paper No. 39. Department of Anthropology, University of Oregon, Eugene, 303 pp.

Church, M. (1983) Pattern of instability in a wandering gravel bed channel, In: *Modern and Ancient Fluvial Systems, Special Publication 6* (J.D. Collinson and J. Lewin, Eds.), pp. 169–180. International Association of Sedimentologists, Oxford.

Denlinger, R.P. (2002) Robust determination of stage and discharge: an example from an extreme flood on the Verde River, Arizona, In: *Ancient Floods, Modern Hazards: Principles and Applications of Paleoflood Hydrology, Water Resources Monograph 5* (P. Kyle House *et al*., Eds.), pp. 127–146. American Geophysical Union, Washington, DC.

DHI (2005) *MIKE 21 Flow Model, Hydrodynamic Module Scientific Documentation*. Hørsholm, DHI Software, 58 pp.

Dykaar, B.B. and Wigington, P.J. (2000) Floodplain formation and cottonwood colonization patterns on the Willamette River, Oregon, USA, *Environmental Management* 25(1), 87–104.

Ferguson R. and Ashworth, P. (1991) Slope-induced changes in channel character along a gravel-bed stream: the Allt Dubhaig, Scotland, *Earth Surface Processes and Landforms* 16, 65–82.

General Land Office (1851–1853) *Township Survey Plats, Willamette Valley Oregon*. General Land Office, Washington, DC.

Gould, S.J. (1989) *Wonderful Life: the Burgess Shale and the Nature of History*. W. W. Norton & Co., New York, 347 pp.

Gran, K. and Paola, C. (2001) Riparian vegetation controls on braided stream dynamics, *Water Resources Research* 37(12), 3275–3283.

Grant, G.E. and Swanson, F.J. (1995) Morphology and processes of valley floors in mountain streams, western Cascades, Oregon, In: *Natural and Anthropogenic Influences in Fluvial Geomorphology: the Wolman Volume, Geophysical Monograph No. 89* (J.E. Costa, A.J. Miller, K.W. Potter and P.R. Wilcock, Eds.), pp. 83–101. American Geophysical Union, Washington, DC.

Grant, G.E., Crozier, M.J. and Swanson, F.J. (1984) An approach to evaluating off-site effects of timber harvest activities on channel morphology, In: *Proceedings, Symposium on the Effects of Forest Land-use on Erosion and Slope Stability*, pp. 177–186. University of Hawaii, Honolulu.

Grant, G.E., Schmidt, J.C. and Lewis, S.L. (2003) A geological framework for interpreting downstream effects of dams on rivers, In: *A Peculiar River* (J.E. O'Connor and G.E. Grant, Eds.), pp. 209–225. American Geophysical Union; Washington, DC.

Gregory, S., Ashkenas, L., Haggerty, P., Oetter, D. Wildman, K., Hulse, D., Branscomb, A. and Van Sickle, J. (2002a) Riparian vegetation, In: *Willamette River Basin Planning Atlas* (D. Hulse, S. Gregory and J. Baker, Eds.), pp. 40–43. Oregon State University Press, Corvallis.

Gregory, S., Ashkenas, L.R., Jett, S.M. and Wildman, R.C. (2002b) Flood inundations/FEMA floodplains, In: *Willamette River Basin Planning Atlas* (D. Hulse, S. Gregory and J. Baker, Eds.), pp. 28–29. Oregon State University Press, Corvallis.

Gregory, S., Ashkenas, L., Oetter, D., Wildman, R., Minear, P., Jett, S. and Wildman, K. (2002c) Revetments, In: *Willamette River Basin Planning Atlas* (D. Hulse, S. Gregory and J. Baker, Eds.), pp. 32–33, Oregon State University Press, Corvallis.

Gutowsky, S. (2000) Riparian cover changes associated with flow regulation and bank stabilization along the Upper Willamette

River in Oregon between 1939–1996. MS thesis, Oregon State University, Corvallis, 92 pp.

Harr, R.D. (1981) Some characteristics and consequences of snowmelt during rainfall in western Oregon, *Journal of Hydrology* 53, 277–304.

Hickin, E.J. and Nanson, G.C. (1984) Lateral migration rates of river bends, *Journal of Hydraulic Engineering* 110(11), 1557–1567.

Hooper, P. (1997) The Columbia River flood basalt province: current status, In: *Large Igenous Provinces* (J. Mahoney and M. Coffin, Eds.). p. 438. American Geophysical Union, Washington DC.

Hulse, D., Gregory, S. and Baker, J. (Eds) (2002) *Willamette River Basin Planning Atlas.* Oregon State University Press, Corvallis, 178 pp.

Jerrick, N. (2001) *Restoring a river of life: the Willamette Restoration Strategy Overview.* Willamette Restoration Initiative, Portland.

Johnson, S.L., Swanson, F.J., Grant, G.E. and Wondzell, S.M. (2000) Riparian forest disturbances by a mountain flood – the influence of floated wood, *Hydrological Processes* 14, 3031–3050.

Knighton, A.D. and Nanson, G.C. (1993) Anastomosis and the continuum of channel pattern, *Earth Surface Processes and Landforms* 18, 613–625.

Laenen, A. (1995) Willamette River water quality study – sediment transport in the main stem and major tributaries Oregon Water Resources Institute Fact Sheet. Oregon Water Resources Institute, Corvallis, 4 pp.

Lane, S.N. and Richards, K.S. (1997) Linking river channel form and process: time, space and causality revisited, *Earth Surface Processes and Landforms* 22, 249–260.

Larsen, E.W. and Greco, S.E. (2002) Modeling channel management impacts on river migration: a case study of Woodson Bridge State Recreation Area, Sacramento River, California, USA, *Environmental Management* 2(30), 209–224; DOI 10.1007/s00267-002-2663-1.

Leopold, L.B. and Wolman, M.G. (1957) River channel patterns: braided, meandering and straight. *US Geological Survey Professional Paper 282-B*, Reston, 51 pp.

Marston, R.A., Gurel, J., Pautou, G., Plegay, H., Bravard, J.-P. and Arneson, C. (1995) Channel metamorphosis, floodplain disturbance, and vegetation development: Ain River, France, *Geomorphology* 13, 121–131.

Micheli, E. and Kirchner, J. (2002) Effects of wet meadow riparian vegetation on streambank erosion. 1. Remote sensing measurements of streambank migration and erodibility, *Earth Surface Processes and Landforms* 27, 627–639.

Miller, G.R. (1999) The Great Willamette River Flood of 1861, *Oregon Historical Quarterly* 100(2), 182–207.

Murray, A.B. and Paola, C. (2003) Modeling the effect of vegetation on channel pattern in bedload rivers, *Earth Surface Processes and Landforms* 28, 131–143.

Nadler, C.T. and Schumm, S.A. (1981) Metamorphosis of the South Platte and Arkansas Rivers, eastern Colorado, *Physical Geography* 2(2), 95–115.

Nakamura, F., Swanson, F.J. and Wondzell, S.M. (2000) Disturbance regimes of stream and riparian systems – a disturbance-cascade perspective, *Hydrological Processes* 14, 2849–2860.

Nash, W. (1904) *The Settler's Handbook to Oregon*. J.K. Gill Company, Portland, 190 pp.

O'Connor, J.E., Sarna-Wojcicki, A., Wozniak, K.C., Polette, D.J. and Fleck. R.J. (2001) Origin, extent, and thickness of Quaternary geologic units in Willamette Valley, Oregon. *US Geological Survey Professional Paper* 1620, Reston, 52 pp.

O'Connor, J.E., Jones, M.A. and Haluska, T.L. (2003) Flood plain and channel dynamics of the Quinault and Queets Rivers, Washington, USA, *Geomorphology* 51, 31–59.

Oregon Climate Service (2006) *The Climate of Oregon*. Oregon Climate Service (Accessed July 15, 2006). http://www.ocs.oregonstate.edu/page_links/climate_data_zones/climate_oregon.html

Oregon State Planning Board (1938) Present and potential land development in Oregon through flood control, drainage and irrigation. Salem, 221 pp.

Rowntree, K.N. and Dollar, E.S.J. (1999) Vegetation controls on channel stability in the Bell River, Eastern Cape, South Africa, *Earth Surface Processes and Landforms* 24(2), 127–134.

Schumm, S.A. and Lichty, R.W. (1965) Time, space and causality in geomorphology, *American Journal of Science* 263, 110–119.

Sedell, J.R. and Froggatt, J.L. (1984) Importance of streamside forests to large rivers: The isolation of the Willamette River, Oregon, USA, from its floodplain by snagging and streamside forest removal, *Internationale Veriningung fur Theoretische and Angewandte Limnologie Verhandlungen (International Association for Theoretical and Applied Limnology)* 22, 1828–1834.

Shields, F.D., Jr and Cooper, C.M. (2000) Woody vegetation and debris for in-channel sediment control, *International Journal of Sediment Research* 15, 83–92.

Singer, M.B. and Dunne, T. (2001) Identifying eroding and depositional reaches of valley by analysis of suspended-sediment transport in the Sacramento River, California, *Water Resources Research* 37(12), 3371–3381.

Singer, M.B. and Dunne, T. (2004) Modelling decadal bed material sediment flux based on stochastic hydrology, *Water Resources Research* 40, W03302; doi 10.1029/2003WR002723.

Tal, M., Gran, K., Murray, A.B., Paola, C. and Hicks, D.M. (2004) Riparian vegetation as a primary control on channel characteristics in multi-thread rivers, In: *Riparian Vegetation and Fluvial Geomorphology: Hydraulic, Hydrologic, and Geotechnical Interactions* (S.J. Bennett and A. Simon, Eds.). American Geophysical Union, Washington, DC, 43–58.

Tooth, S. and Nanson, G.C. (2000) The role of vegetation in the formation of anabranching channels in an ephemeral river, Northern plains, arid central Australia, *Hydrological Process* 14(16–17), 3099–3117.

Towle, J.C. (1982) Changing geography of Willamette Valley woodlands, *Oregon Historical Quarterly* 83, 66–87.

USACE (1867–1892) Annual Reports of Chief of Engineers. United States Army Corps of Engineers, Washington, DC.

USACE (1895) Upper Willamette Navigational Surveys 1884–1895. United States Army Corps of Engineers, Washington, DC. 15 sheets.

USACE (1932) Willamette River Portland-Eugene Navigational Surveys 1931–1932. United States Army Corps of Engineers, Washington, DC. 52 sheets.

USACE (1969a) Willamette Basin Comprehensive Study, Appendix E. Flood Control, Willamette Basin Task Force-Pacific Northwest River Basins Commission, 136 pp.

USACE (1969b) Willamette Basin Comprehensive Study, Appendix B. Hydrology, Willamette Basin Task Force-Pacific Northwest River Basins Commission, 162 pp.

USACE (1972) Willamette River and Tributaries 1972. United States Army Corps of Engineers, Portland. 57 sheets.

USGS (2006) Peak streamflow for Willamette River at Salem. United States Geological Survey (Accessed July 15, 2006). http://nwis.waterdata.usgs.gov/or/nwis/peak/?site_no=14191000&agency_cd=USGS

Wallick, J.R. (2004) Geology, flooding and human activities: establishing a hierarchy of influence for controls on historic channel change, Willamette River, Oregon. MS thesis, Oregon State University, Corvallis, 171 pp.

Wallick, J.R., Lancaster, S.T. and Bolte, J.P. (2006) Determination of bank erodibility for natural and anthropogenic bank materials using a model of lateral migration and observed erosion along the Willamette River, Oregon, USA, *River Research and Applications,* 22(6), 631–649.

Waite, R.B., Jr. (1985) Case for periodic, colossal jökulhlaups from Pleistocene glacial Lake Missoula, *Geological Society of America Bulletin* 96, 1271–1286.

Williams, G.P. and Wolman, M.G. (1984) Downstream effects of dams on alluvial rivers. *US Geological Survey Professional Paper* 1286, US Government Printing Office, Washington, DC.

Willingham, W.F. (1983) *Army Engineers and the Development of Oregon*. United States Army Corps of Engineers, Portland, 259 pp.

Wolman, M.G. and Gerson, R. (1978) Relative scales of time and effectiveness of climate in watershed geomorphology, *Earth Surface Processes* 3, 189–208.

Yeats, R., Graven, E., Werner, K., Goldfinger, C. and Popowski, T. (1996) *Tectonics of the Willamette Valley, Oregon. Assessing Earthquake Hazards and Reducing Risk in the Pacific Northwest*. US Geological Survey, Washington, DC, pp. 183–222.

Zimmerman, R.C., Goodlett, J.C. and Comer, G.H. (1967) The influence of vegetation on channel form of small streams, In: *Symposium on River Morphology, Publication* 75, pp. 255–275. International Association of Scientific Hydrology, Bern.

24

Rivers and Humans – Unintended Consequences

Stanley A. Schumm

Mussetter Engineering, Inc., Fort Collins, CO 80525, USA

24.1 INTRODUCTION

In the United States, the westward migration into drier regions led to the development of initially small, but later, large irrigation projects. Construction of dams and diversions for irrigation led to significant impacts on wildlife as did major channel modifications for flood control and navigation. In the late nineteenth and early twentieth centuries, little concern was expressed for the impact of these projects on wildlife habitat or on the human condition. More recently, attempts at rehabilitation of river character and restoration of habitat for endangered species have had mixed results. The purpose of this chapter is to present examples of how projects aimed at flood control, irrigation, and navigation have often had surprising and unanticipated consequences.

For example, small quantities of gravel in the bed of the Missouri, Mississippi, and Nile Rivers significantly influence river response to human impacts, and changes of the hydrologic character of the Platte, Missouri, and Middle Mississippi Rivers result in pattern change, aggradation, and increased flood peaks. These consequences were costly and could only be anticipated if more comprehensive studies of the rivers were undertaken.

Part of the chapter reproduced from *River Complexity and Variability*, Stan Schumm, Copyright (2005) with kind permission from Cambridge University Press.

24.2 ARMOUR

Students of gravel-bed rivers are well aware of the protective qualities of gravel armour. In the simplest case the armour prevents degradation. It is perhaps less well recognized that small amounts of gravel in sand-bed rivers can have significant sediment-transport and morphological effects. The Missouri, Nile, and Mississippi Rivers will be used to illustrate the impacts of small amounts of gravel on the morphology and response of sand-bed rivers.

24.2.1 Missouri River

The Missouri River provides an example of how a small amount of gravel in the sediment forming the channel confounded the best plans of river engineers. The Missouri River basin has numerous dams and reservoirs that are designed to retain water for irrigation and flood control. Six large dams were constructed on the mainstem of the Missouri River, primarily for flood control between 1937 and 1963. Storage began behind the Fort Randall Dam upstream of the Niobrara River in southern South Dakota in 1953 (Figure 24.1).

In preparation for construction of the Fort Randall Dam, estimates were made of the depth of scour that was anticipated below the dam. The estimate depended to a large extent upon the size of sediment in the alluvium. Coring and bed samples contained sediment with a median size of 0.20 mm. Based upon this information, it was calculated that there would be 4.57 m of degradation below the dam

Large Rivers: Geomorphology and Management, Edited by A. Gupta

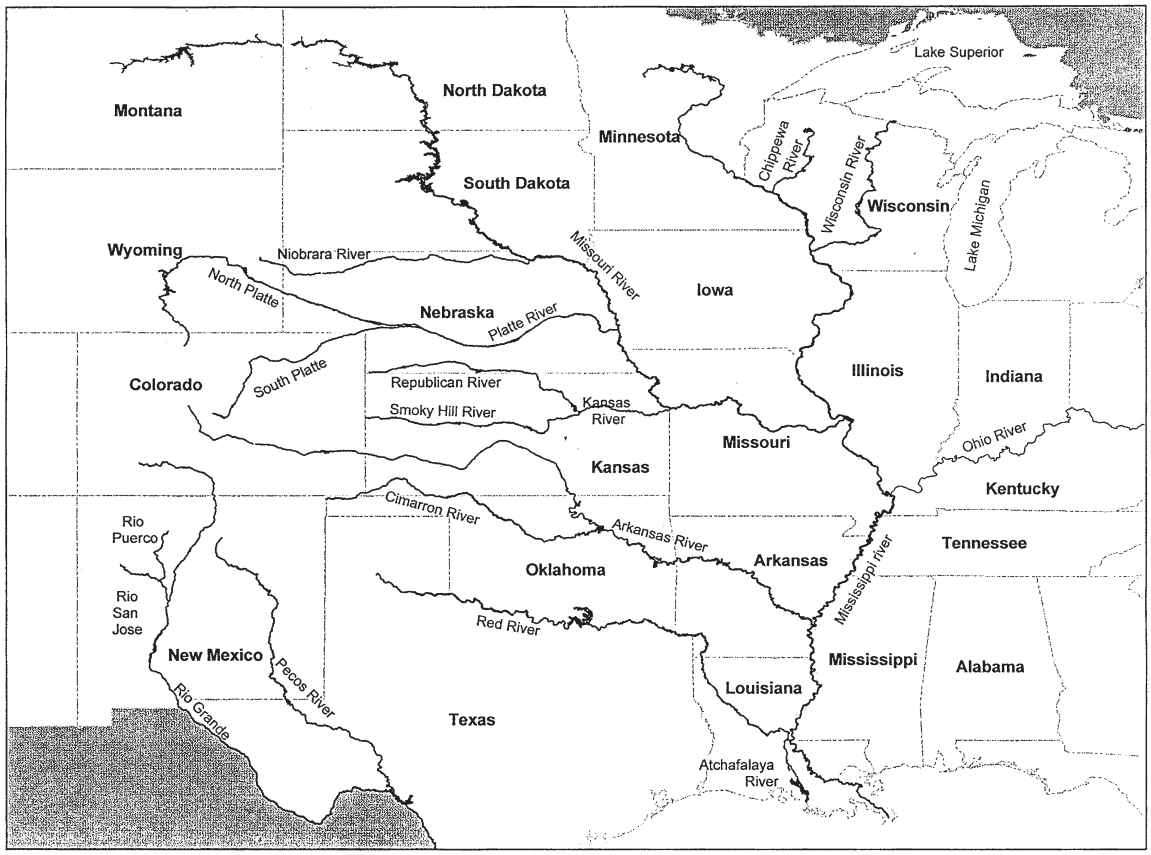

Figure 24.1 Map showing location of many rivers discussed

(Livesey, 1963). For the first 2 years after closure of the dam, water levels declined at a rate of one foot (30 cm) per year, but after 1954, the rate decreased to about one-tenth of that value (Figure 24.2). The reason for this decrease was revealed in 1962 when the bed of the river was exposed during a period of no water release from the reservoir. The bed had armoured. A very small amount of gravel in the alluvium was concentrated on the bed during degradation, which greatly reduced the depth of erosion. The small amount of gravel in the alluvium was not detected during sampling, but this gravel had a major impact on the river and dam operations. Immediately below the dam d_{90} increased from 0.35 to 10 mm. High-discharge releases from the dam apparently have been able to breach the armour, and 32 years after dam closure, degradation has reached 1.95 m. Breaching of the armour apparently occurred at 20 and 27 years after dam closure (Figure 24.3), and therefore, high releases from Fort Randall Dam will cause future degradation.

In summary, a small amount of gravel that was undetected during sampling formed an armour that significantly inhibited degradation. It is also possible that the armour determined where degradation took place during high flows, and it may have shifted the tendency to erode from the bed to the banks of the river. Initially, most of the erosion was concentrated on islands and sandbars. The river then eroded both banks on the inner and outer sides of meanders and both banks at crossings (Rahn, 1977). The river was replacing its sediment load by bank erosion, thereby changing the character of the river (Figure 24.4). The response to this unintended consequence was expensive bank stabilization works.

24.2.2 River Nile

The Nile is a relatively straight and stable river (Schumm and Galay, 1994). Morphologic variability can be attributed to changes of valley slope, which causes adjust-

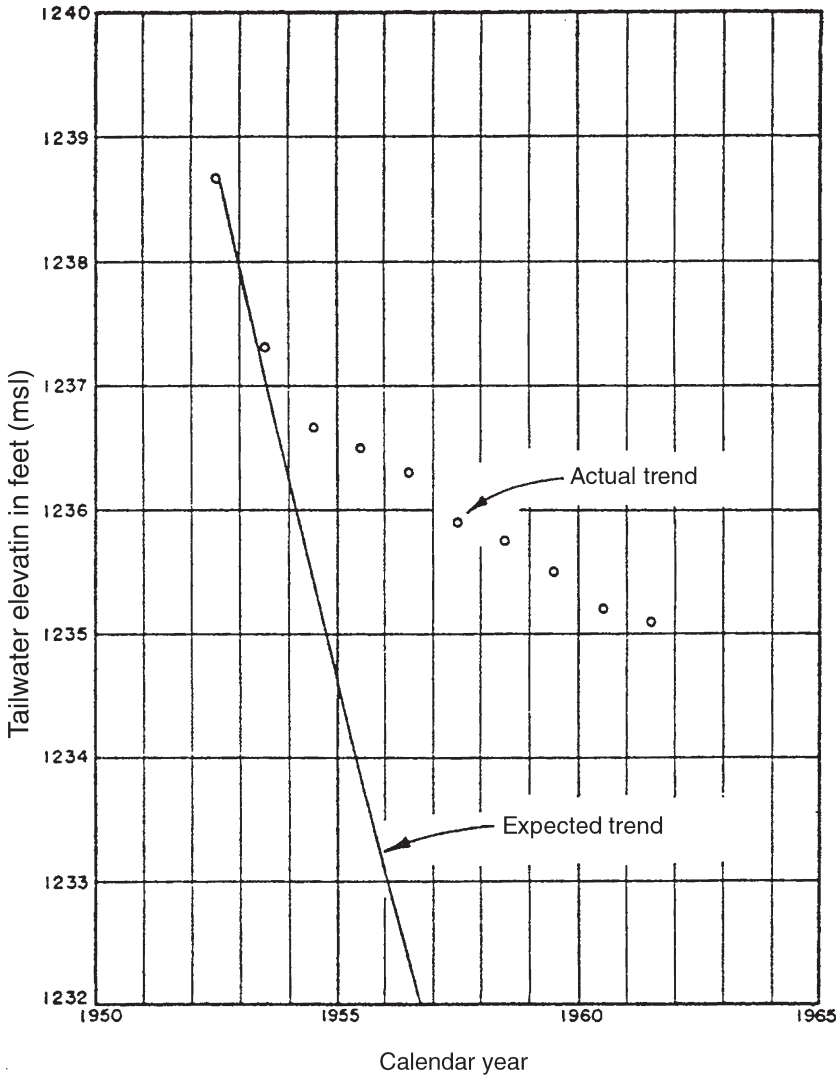

Figure 24.2 Decrease of water-surface elevation downstream of Fort Randall Dam, as compared with the expected decrease (from Livesey, 1963)

ments of sinuosity and width. The valley slope changes reflect wadi contributions and faults (Schumm and Galay, 1994). As in the Missouri River valley, the anticipated impact of the Aswan High Dam on hydrology and sediment loads was a matter of great concern for engineers involved with making estimates of bank stability and potential channel degradation. Perhaps of greatest concern was the potential for major degradation of the Nile following construction of the dam. Potential degradation was estimated by many researchers prior to (Fathy, 1956; Mostafa, 1957) and after construction of the Aswan High Dam (Hammad, 1972; Shalash, 1980, 1983). The construction of the dam commenced in 1963 and continued to 1968, and some degradation was expected from the damsite to the Esna Barrage (Figure 24.5). Measurements of water levels during the construction years downstream from each barrage showed some water-level lowering as far downstream as 600 km at the Assiut Barrage (Figure 24.5). Pre-dam estimates of degradation ranged from 2.0 to 8.5 m, but 18 years after the dam was in operation

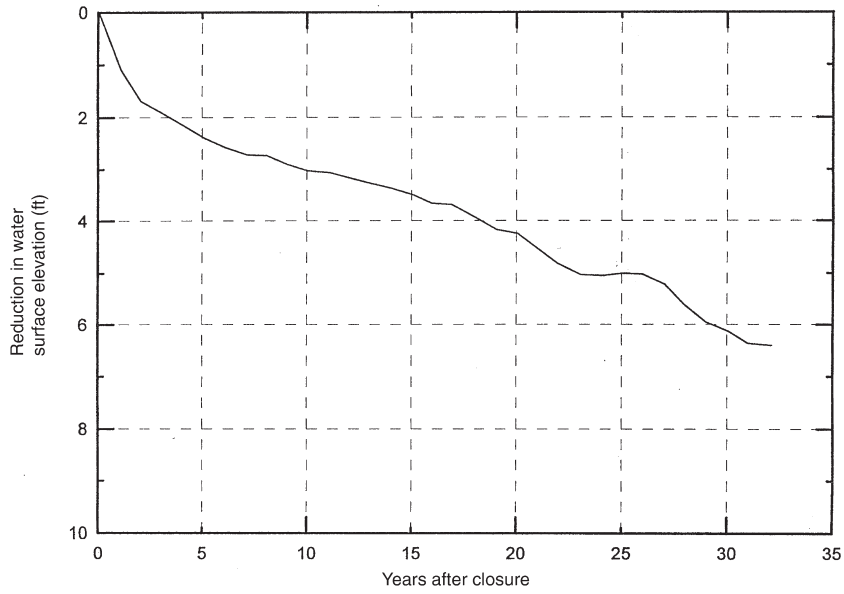

Figure 24.3 Decrease of water-surface elevation downstream of Fort Randall Dam after closure (from Livesey, 1963)

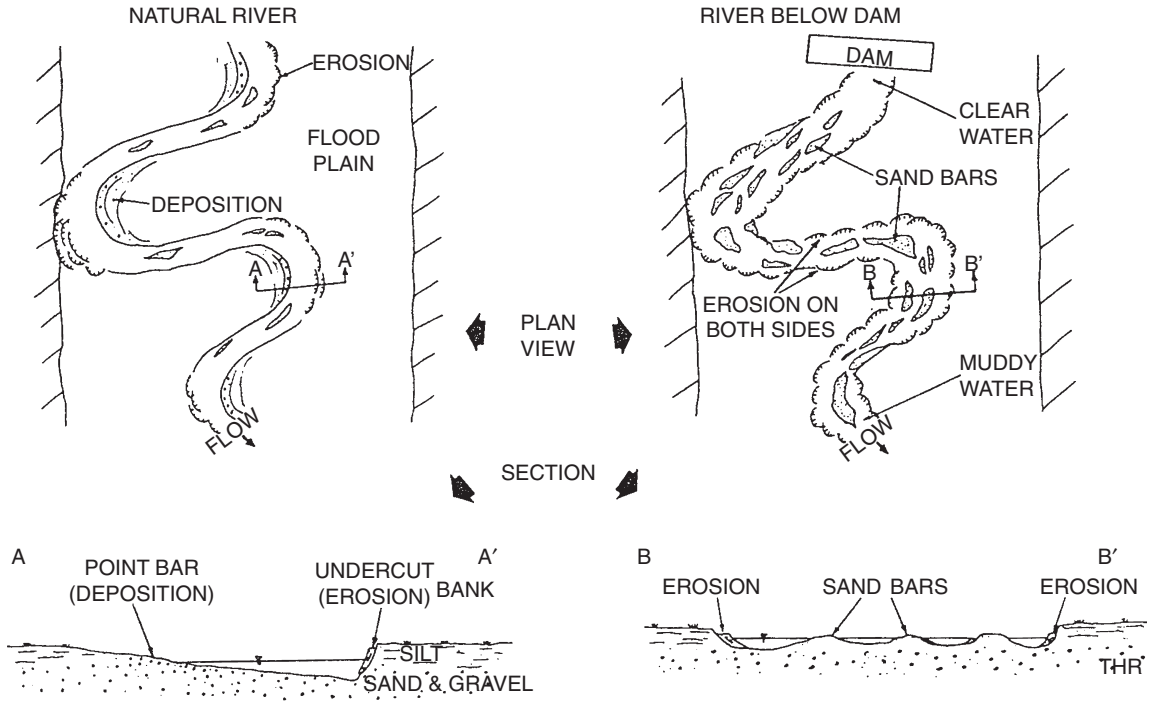

Figure 24.4 Impact of dam on downstream channel. Reproduced from Rahn, P.H., Erosion below mainstem dams on the Missouri River, Bull. Assoc. Eng. Geologists, Copyright (1977) with permission from AEG

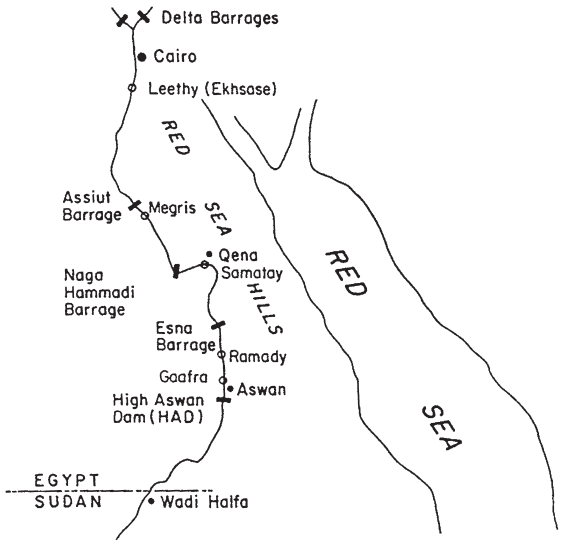

Figure 24.5 Map of River Nile course in Egypt. Distance from Aswan to Cairo is about 1380 km

maximum degradation below the barrages was only 0.70 m.

Several factors may account for the fact that degradation has been minimal after closure of the Aswan High Dam, but it is important to recognize that during past humid periods in Egypt, tributary wadis delivered coarse sediments to the valley, which could act as a control of degradation today. The most recent such period was between 11 000 and 6000 years ago (Paulissen and Vermeersch, 1987), but even today, wadi flooding introduces coarse sediment into the river. For example, there is an abundant supply of sand, pebble, and cobbles in Wadi Qena, which drains a large area to the north of Qena (Figure 24.5). The bed of the large Wadi el Matuh, which enters the valley south of Qena, appears very sandy, but gravel and some cobbles occur on the alluvial surface. A deep trench was excavated in a small wadi that enters the Nile valley at Khuzam about 30 km upstream from Qena. Boulders and cobble are abundant in the trench, and such sediments undoubtedly were and are moved into the Nile during wetter periods and during major floods. All of the wadis contain much stored sediment of pebble, cobble, and boulder size. Archaeologists and other investigators describe cobbles and gravel at wadi mouths (Wendorf *et al*., 1970) and in older terrace deposits (Butzer, 1959).

Based upon an analysis of borings in the Nile valley, Attia (1954) concluded that within the valley, 'Coarse deposits composed of coarse sand, sand and gravel, or gravel which lie beneath the fine alluvial deposits, have an irregular upper surface. The depth from ground-surface to the top of these gravels, etc. varies from 8 to 26 m.' This suggests that at many locations, the bed of the Nile could be in contact with sediment that is coarser than sand. Additional support for this hypothesis is provided by gravels encountered in the bores at Esna and Naga Hammadi Barrages (Figure 24.5). At Naga Hammadi, there was 25 % gravel at a depth of 1 m in two bores. At Esna, there was 9 % gravel at the depth of 1 m in one bore. At other barrages, gravels were encountered in the bores, but at greater depths. As shown by the Missouri River example, armour can develop from only a small percentage of coarse bed material.

There is a distinct change in both valley slope and river slope downstream of Qena. Coarse sediments introduced by Wadi Qena resist erosion by the Nile, and they appear to act as a partial control of river slope. Although the bed sediment of the Nile ranges from 0.25 to 0.43 mm (Schumm and Galay, 1994), the coarse gravel and cobbles introduced by wadi discharges of the past and present, probably produce gravel and cobble hard points in the bed of the river that only emerge from beneath the sand cover during floods when they prevent degradation.

The Missouri River and River Nile examples suggest that to understand river sedimentology and behaviour, a different sediment sampling procedure may be required. Perhaps sampling needs to be done at high water when the fine sand is moving largely in suspension. Large boats and large samplers would be needed in order to sample both the surface and subsurface sediment.

24.2.3 Mississippi River

Unlike the previous examples, the lower Mississippi River between the junction of the Ohio River (Figure 24.1) at Cairo, Illinois, and the Gulf of Mexico is not dammed, but it has been subject to cutoffs, dykes, bank stabilization, and gravel mining. The median grain size ranges from about 0.3 to 2.6 mm, and the river is considered to be a sand-bed river. Nevertheless, sampling of the bed in 1932 along the 1070 miles (1721 km) of river downstream of Cairo produced the relation between grain size and distance of Figure 24.6. Gravel (sediment larger than 2 mm) made up 25 % of the bed sediment for the first 100 miles (161 km) below Cairo, and then rapidly decreased. Between 1932 and the present, the river has been greatly modified, especially by the meander cutoff program, which shortened the river by about 150 miles (240 km). The shortening and constriction of the channel by dykes and dredging to maintain navigation led to the assumption that the bed sediment would have coarsened since 1932. In 1989, a repeat of the 1932 sampling was begun, and 504 samples were collected

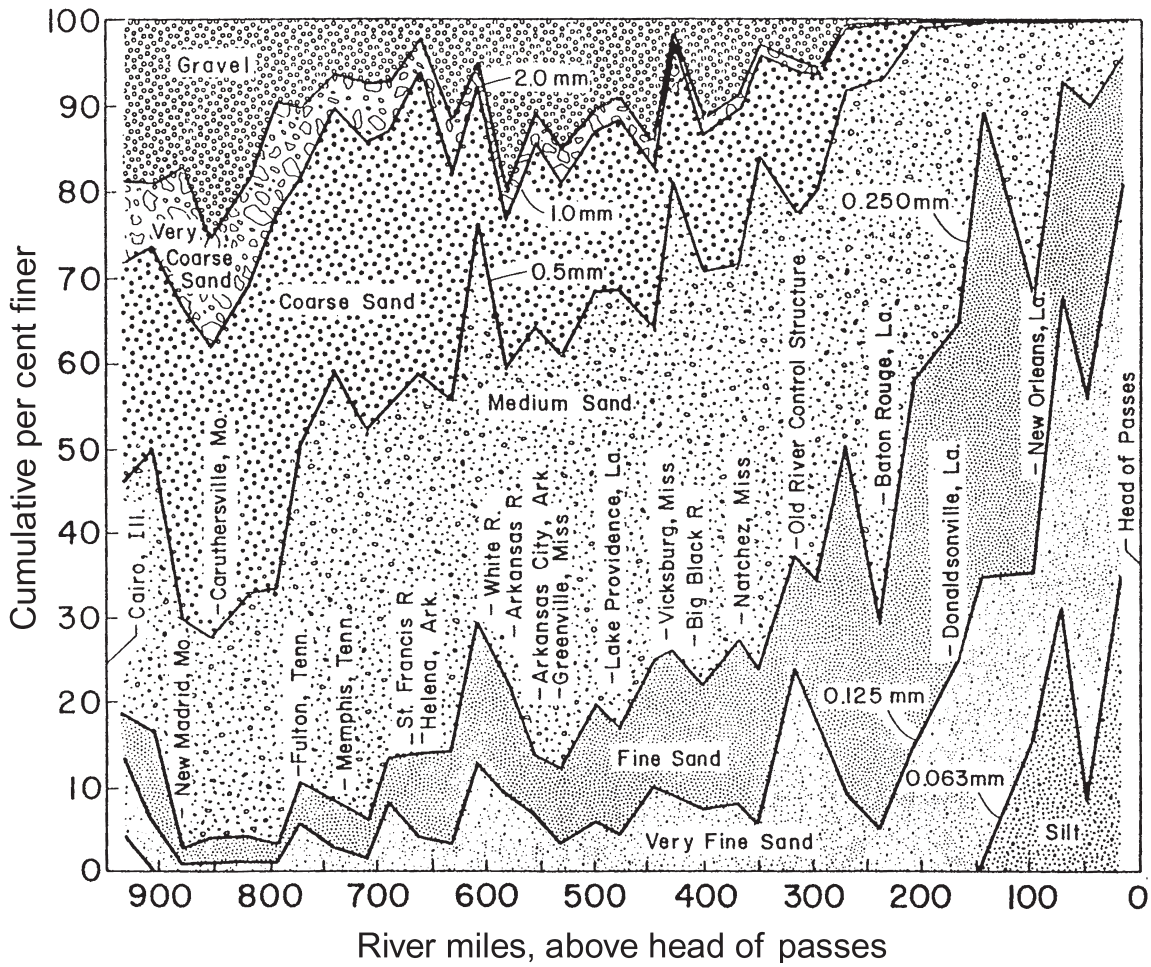

Figure 24.6 Composition of Mississippi River bed sediment sampled in 1932 (from Queen, 1994)

between Cairo and Head of Passes. The results of the sampling programme are presented in Figure 24.7, which shows a significant decrease of gravel and a decrease of median grain size. This is contrary to what was expected. A possible explanation for the smaller percentage of gravel in the bed in 1989 is gravel dredging, but the discharge during sampling in 1989 was 2000 cfs ($57\,m^3\,s^{-1}$) less than in 1932. This difference appears negligible when the peak discharge in both years was about 1.2 million cfs ($34\,000\,m^3\,s^{-1}$), but at low discharges, the bed of the river is covered with sand; whereas, at high discharges, coarser sediment may be exposed. For example, a dredge operator stated that coarse gravel and cobbles were dredged from the thalweg at high discharges. However, at the low discharge of 100 000 cfs ($2830\,m^3\,s^{-1}$) during the 1989 sampling, he predicted that only sand would be captured, and indeed, sand was sampled at this location in 1989. This reinforces the earlier suggestion that sand on the bed of the Nile covers the coarser wadi gravels.

During the 1989 sampling programme, gravel was exposed at numerous locations at the head of bars and islands and on the outer margin of point bars, although there was less gravel on the bed. According to Winkley (1994), gravel stabilizes the bed, banks, and bars of the Mississippi River, and prevents excessive sediment movement. Gravel-armoured sand bars served as semi-permanent channel controls between major floods, but removal of the gravel armour from the bars and islands by

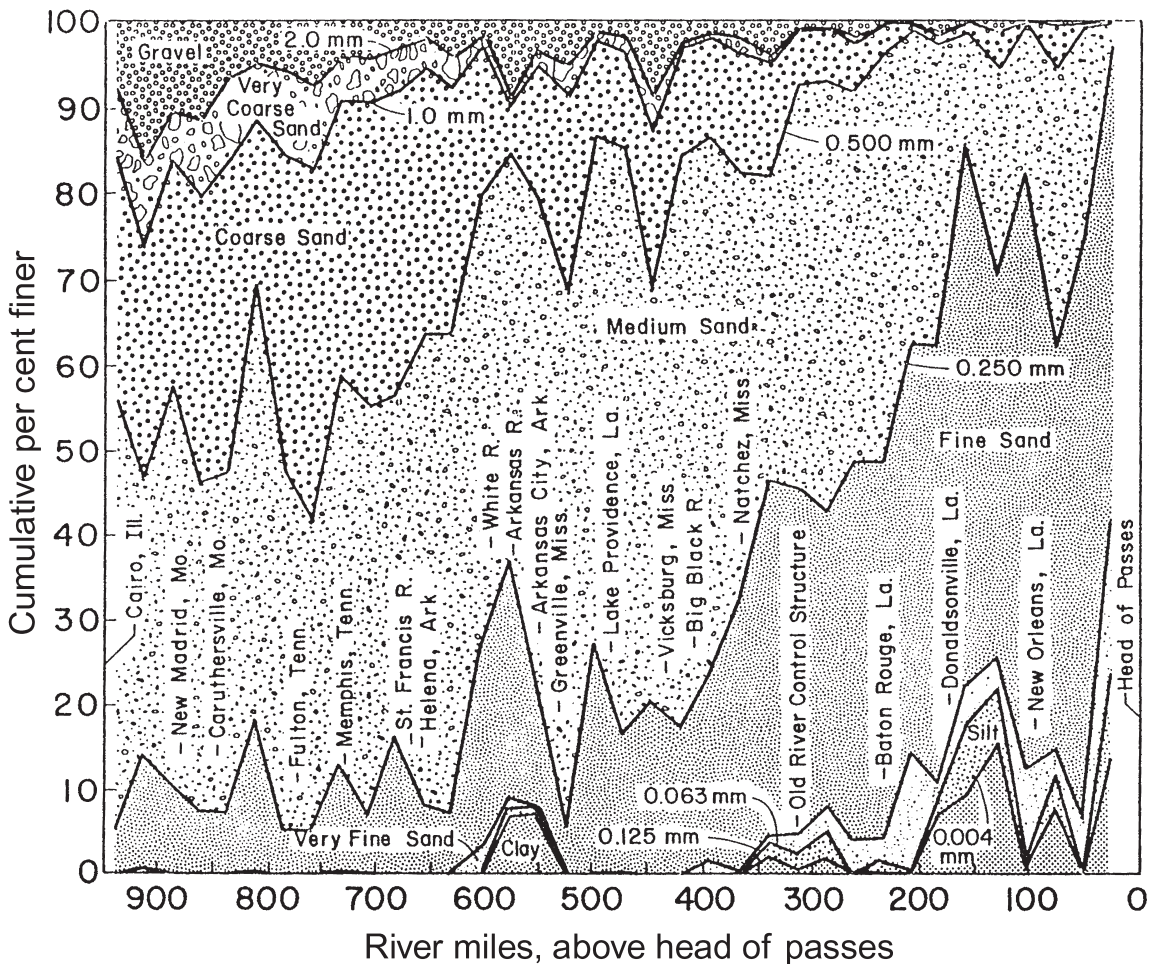

Figure 24.7 Composition of Mississippi River bed sediment sampled in 1989 (from Queen, 1994)

gravel mining can lead to erosion and loss of this control. As a result, meandering reaches may tend toward a braided character (Figure 24.4), and bed sediment transport may increase. Also, removal of gravel makes it easier for the river to cut chute channels across point bars. Although the removal of a veneer of gravel from bars and islands appears to be a minor change, it can seriously destabilize a channel.

The availability of a small percentage of gravel in the bed provides armouring material that may help to limit the depth and areal extent of scour around river contraction works such as spur dykes, and to limit degradation downstream from all types of hydraulic structures. These effects have a significant economic benefit in that the presence of gravel results in better protected river training works and structures. Thus, the uncontrolled removal of gravel can change the river including its form, slope, velocity, transport capacity, stability, and environmental characteristics (Winkley, 1994). Viewing the conclusions on the impact of gravel removal another way, it is clear that small amounts of gravel in alluvium can have a very significant role in river stability and channel morphology. Also, sediment sampling of the bed during low flows may create a false impression of river sedimentology. A veneer of sand may obscure the important coarser bed sediment. Sampling should be done at least at a medium discharge, and a robust sampler capable of collecting cobbles should be employed.

24.3 HYDROLOGY

Unintended consequences of hydrologic changes, as a result of dams and irrigation diversions are invasion of woody vegetation into the channel, dramatic channel narrowing, degradation, and aggradation. The Platte and Niobrara Rivers of Nebraska (Figure 24.1) provide examples of such changes, and the Middle Mississippi River downstream of St Louis has experienced major increases of flood peaks as a result of attempts to stabilize the river.

24.3.1 Platte River

The Platte River system (North Platte, South Platte, and Platte Rivers) (Figure 24.1) occupies large areas in the three states of Wyoming, Colorado, and Nebraska (Figure 24.8). The Platte River valley was the route of pioneers travelling to Oregon and California in the mid-nineteenth century. The Oregon Trail followed the south bank of the river and the Mormon Trail occupied the north side. The pioneers travelling along the river were astonished by its morphologic and hydrologic character, which was so different from rivers east of the Missouri and Mississippi Rivers. In fact, the rivers of the Platte River system were classic examples of braided rivers, and were cited as such in geomorphology texts. In addition, the Platte River provided food and a resting place for the spring and autumn migrations of huge flocks of sandhill cranes and smaller groups of whooping cranes in the Big Bend reach of the river (Figure 24.8).

Historically, the North Platte and Platte Rivers were characterized by wide channels with some large islands and an annual discharge, which receded rapidly from large peak spring flows in late May and June to relatively low flows in July and August (Williams, 1978; Kircher and Karlinger, 1983). Habitat modification began in the mid-1800s when settlers began irrigating land using water from the North Platte and Platte. Subsequent diversions and storage projects since settlement have contributed to changes in the pre-settlement hydrology, and consequently, to alteration of the Platte River that was not only dramatic but largely unanticipated.

The current hydrological conditions along the Platte and North Platte Rivers are different from those prior to settlement (Eschner *et al*., 1981). In the late 1800s, the Platte River was uncontrolled, from headwaters in Colorado to its confluence with the Missouri River in Nebraska. The river carried snowmelt from the mountains across the

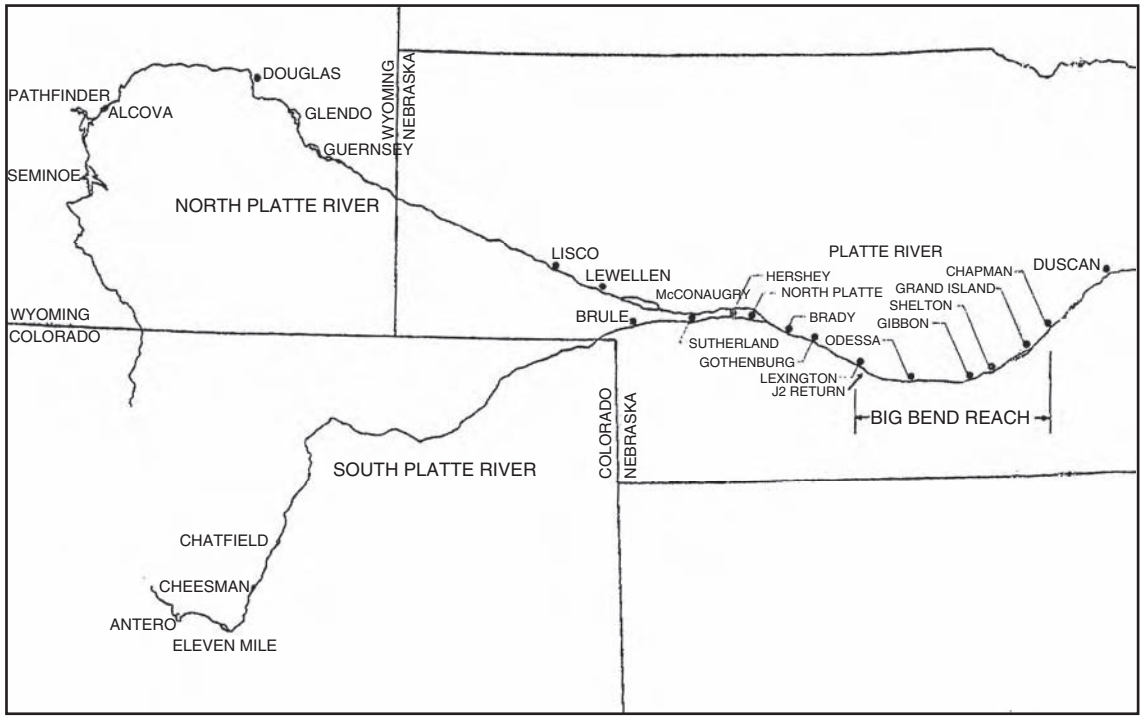

Figure 24.8 Map of Platte River system. Distance from Brady to Grand Island (Figure 24.9) is 120 river miles (193 km)

plains with flow that peaked in late spring and diminished to limited flows in late summer. This natural condition of water conveyance from the mountains across the plains maintained the natural habitats along the Platte River, but this was not conducive to irrigated agriculture. The current hydrological conditions along the North Platte and Platte Rivers are dictated by the operation of large dams and reservoirs located in Wyoming and Nebraska. These facilities, developed between 1909 and 1957, served to control the peak snowmelt pulses, and extend the water release period into late summer. The result of these hydrological changes was that the areal extent of active channels of the Platte and North Platte Rivers decreased dramatically (Williams, 1978), as woody vegetation rapidly expanded into the channel (Johnson, 1994).

In order to document vegetation encroachment into the Platte River channel, the Remote Sensing Applications Laboratory of the University of Nebraska at Omaha used 1860 maps and 1938, 1957, and 1983 aerial photographs to determine channel change (Peake *et al*., 1985). Using data from that report, the related maps, and 1995 aerial photography, it was possible to calculate an average channel width for each of the US Geological Survey quadrangles (topographic maps) between Brady and Grand Island, Nebraska (Figure 24.9). The 1860 width is probably too large because numerous small vegetated islands were not mapped by the surveyors (Johnson, 1994: 58; Eschner *et al*., 1983: 14). The greatest changes of width along the Platte River occurred between 1860 and 1938 and between 1938 and 1957 (Figure 24.9). Since 1860, the Platte River has adjusted to altered hydrologic conditions throughout the Brady–Phillips reach.

The trend of average channel width downstream of Brady in 1860 is unusual. Average width generally increased in a downstream direction from the Brady quadrangle to the Kearney quadrangle, as expected (Figure 24.9). However, between the Kearney and Doniphan quadrangles, average width decreased dramatically. In this reach, the river was not braided, but anastomosing. That is, the single-braided channel (Figure 24.10a) became a multiple channel complex (Figure 24.11a). The total width of the multiple anastomosing channels was less than the width of the upstream braided channel (Figure 24.9). If the same volume of water moved through the braided channel at Kearney, as through the anastomosing channels downstream, then each anabranch must have been deeper than the braided channel. An explanation for this pattern change may be because the gradient was about

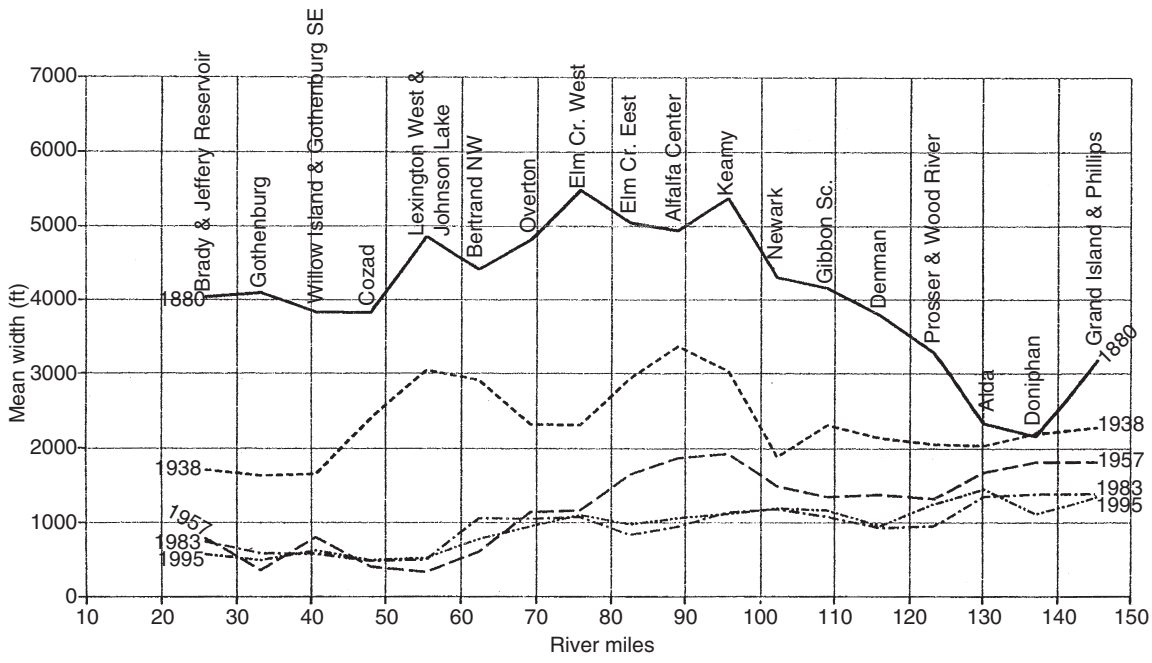

Figure 24.9 Mean width of the Platte River for each US Geological Survey quadrangle (topographic map) between Brady and Phillips, Nebraska. Mean widths for the years 1860, 1938, 1957, and 1983 were obtained from Peake *et al*. (1985). Mean widths for 1995 were determined from measurements made on 1995 aerial photographs

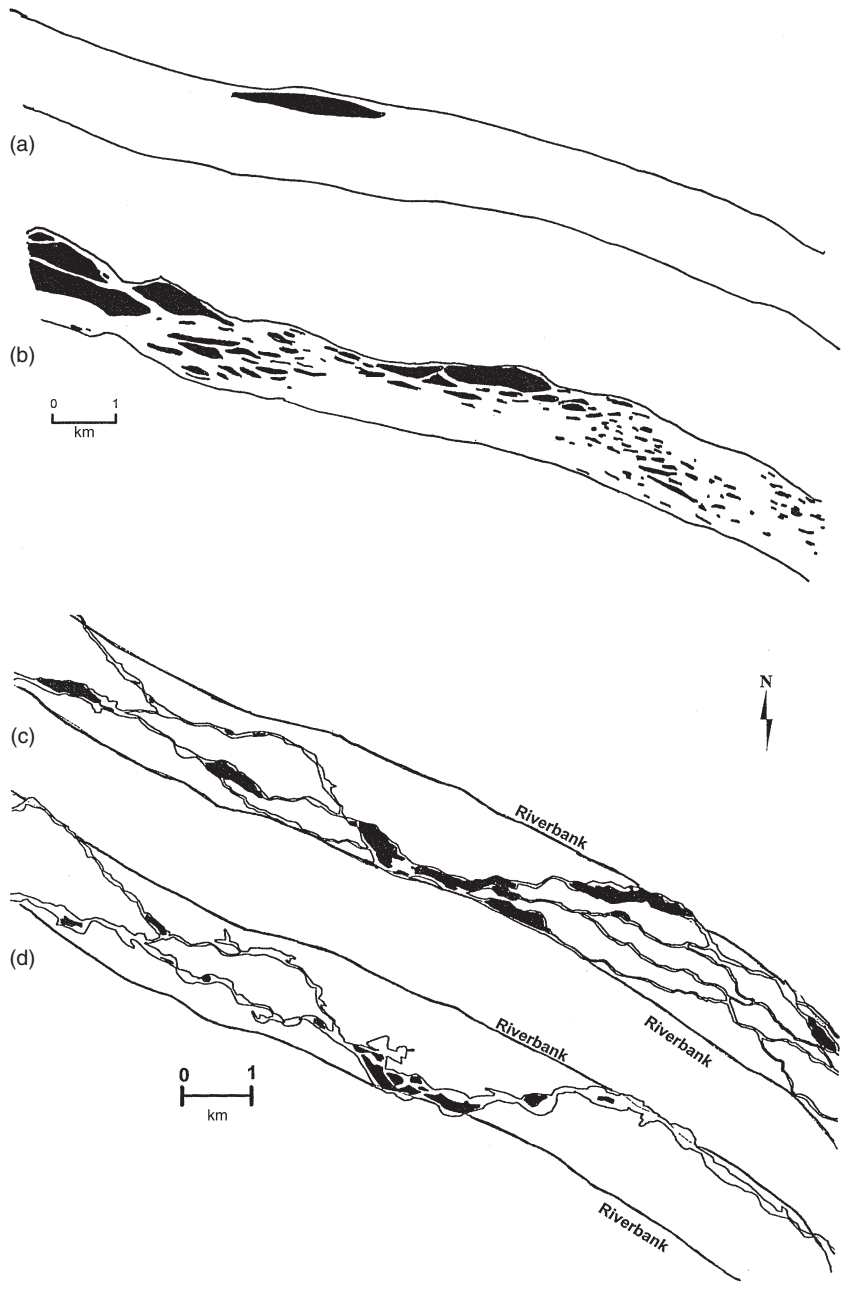

Figure 24.10 Platte River on Cozad quadrangle: (a) 1860; (b) 1938; (c) 1957; (d) 1983 (from Peake *et al*., 1985). Dark areas are islands. Thin lines show 1860 riverbank. Flow is from left to right

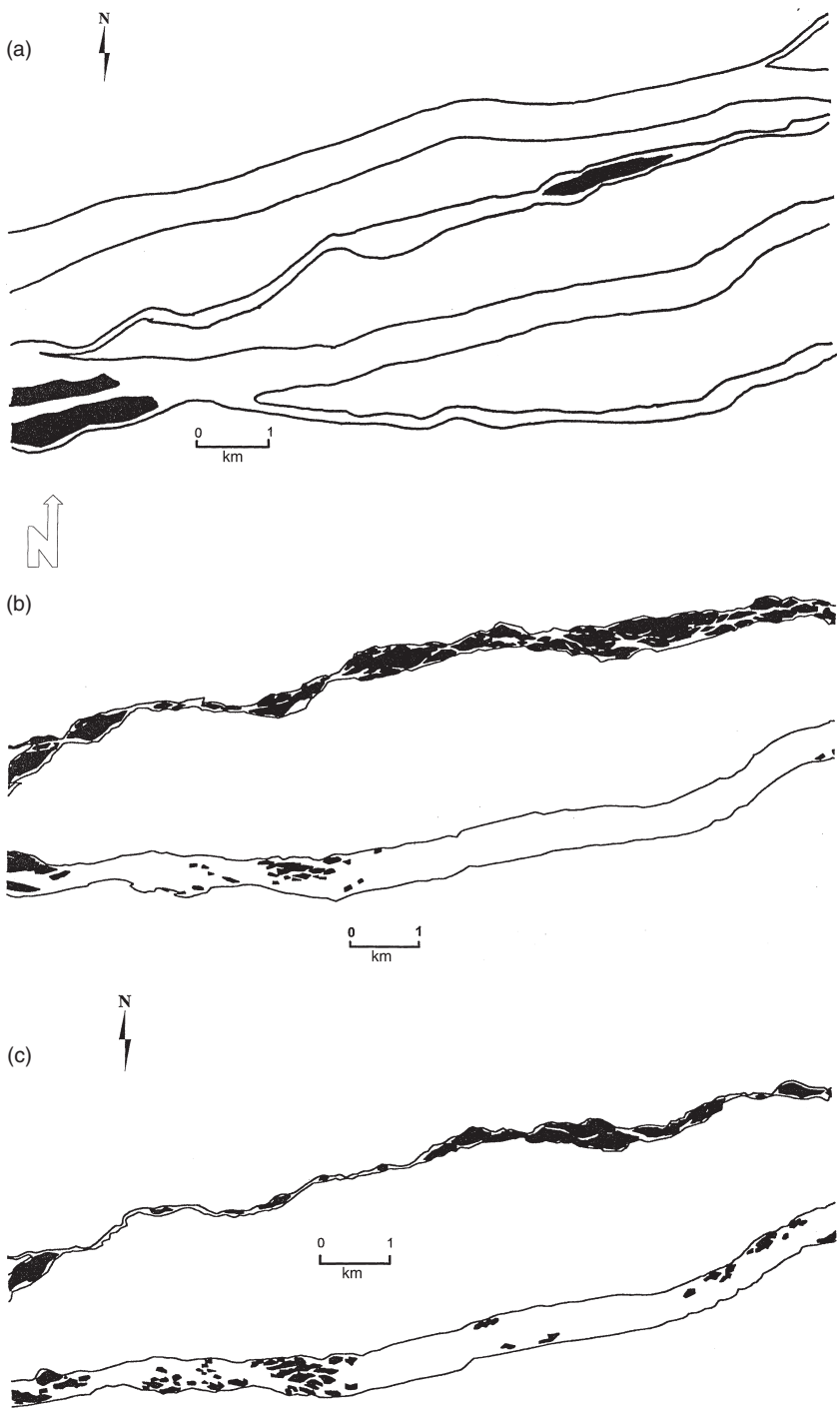

Figure 24.11 Platte River on Newark quadrangle: (a) 1860; (b) 1938; (c) 1957; (d) 1983 (from Peake *et al*., 1985). Dark areas are islands in the active channel. Flow is from left to right

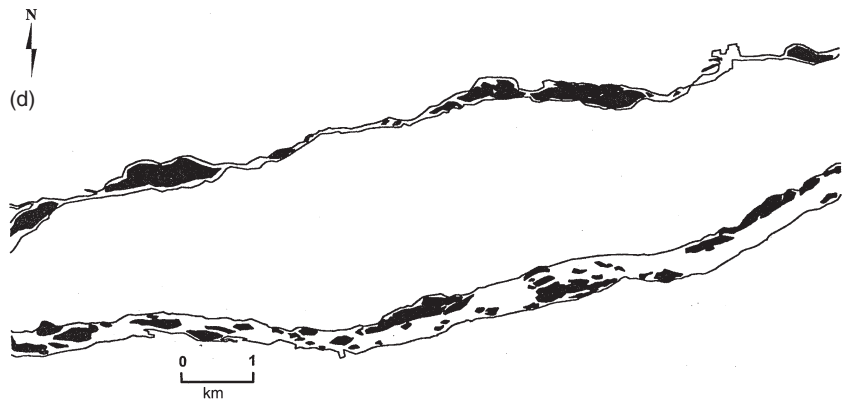

Figure 24.11 *Continued*

5% less in the anastomosing reach. Near Grand Island (Doniphan quadrangle) in 1860, the river reverted to a braided pattern, which is the present condition.

The two different channel patterns of the Platte River in 1860 responded differently to the hydrologic changes that caused width reductions between 1860 and 1995. The Platte River between Brady and Grand Island provides an excellent example of river variability through time. For example, the upstream braided reach in 1938 contained many more vegetated islands, and it had become an island-braided river (Figure 24.10b).

As these islands coalesced and increased in size, the single-channel braided stream became a smaller multiple-channel anastomosing river (Figure 24.10c), which with time and abandonment of secondary channels, was becoming a much narrower, single-braided channel (Figure 24.10d), although this condition was not achieved everywhere. In contrast, in the anastomosing reach near Newark, two secondary anabranches were abandoned between 1860 and 1938 (Figures 24.11a, b). Two channels remained; the northern anastomosing channel was much reduced in size, and the southern channel became the dominant braided channel (Figure 24.11b). By 1957, the northern channel was becoming a narrow single channel, and the southern channel remained essentially as it was in 1860 (Figure 24.11c). In 1983, the northern channel was still approaching a single-channel morphology, and the southern channel remained island-braided (Figure 24.11d).

Although the Platte River became narrower between 1860 and 1995 (Figure 24.9), the adjustment differed between the braided (upstream of Kearney) and anastomosing reaches (Kearney to Grand Island). Figure 24.12 presents an idealized evolutionary sequence of channel changes through time for both types of channel. There does not appear to have been a progressive downstream effect of upstream dams and diversions. Rather, the Platte River from Brady to Grand Island adjusted, but the nature of the channel adjustment was different between the braided and the anastomosing reaches (Figure 24.12).

The dramatic changes of channel width (Figure 24.9) through time require an explanation. One can assume that the river in 1860 was essentially unchanged from natural conditions, although some diversions undoubtedly had commenced. Nevertheless, it should be noted that the Platte River during the 1860 surveys was hydrologically different from the present river. It was intermittent, as described by Ware (1911) in 1863:

> 'From Fort Kearney, for many miles up, there was not water in the river. The water seemed to be in the under-flow. We not infrequently rode down to the river and with shovels dug watering-places in the sand of the bed. We always found permanent water within eighteen inches of the top, no matter how dry the sand on top appeared to be. We were told that 75 miles of the river were then dry, and that generally about 125 miles of it were dry in the driest season.'

The large number of no-flow days was a characteristic of some reaches of the river until about 1942 (Table 24.1), when the impact of Kingsley Dam and Lake McConaughy (the project) on the Platte River became significant. Hydrologic data show that before 1942 (pre-project), the average annual number of no-flow days at Overton (24 km upstream from Odessa) was 78, but there were zero no-flow days at this gauge after 1941 (post-project). At the Odessa gauge, there were on average 150 no-flow days before 1942, but only 19 no-flow days per year after 1941, and there were zero no-flow days after 1957. At the Grand

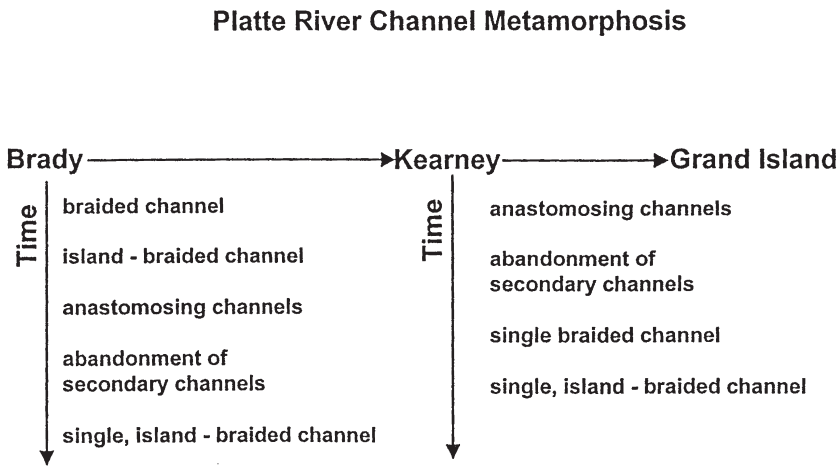

Figure 24.12 Chart listing stages of channel change for the braided and anastomosing reaches of the Platte River

Table 24.1 No-flow days at Platte River gauges

Station	Period of record	Total number of no-flow days	Mean annual days of no-flow
Overton			
Pre-project	1931–1941	863	78
Post-project	1942–1994	0	0
	1931–1938	657	82
	1939–1957	207	11
	1958–1995	0	0
Odessa			
Pre-project	1939–1941	450	150
Post-project	1942–1957	309	19
Post-project	1957–1991	0	0
	1939–1957	760	40
	1958–1983	3	0
	1984–1995	0	0
Grand Island			
Pre-project	1934–1941	1200	150
Post-project	1942–1978	852	23
Post-project	1978–1995	0	0
	1934–1938	699	140
	1939–1957	1114	59
	1958–1983	253	10
	1984–1995	0	0

Island gauge, there were an average of 150 no-flow days per year before 1942, but only 23 for the 1942 to 1978 period. There were zero no-flow days at Grand Island after 1978. Clearly, the hydrologic character of the river had changed from intermittent to perennial, which had a major effect on channel width.

Johnson (1994) attributed width reduction during the drought years to low flows which expose large areas of the channel bed to colonization by vegetation (woodland expansion). The low flows maintain the water table whereas, long periods of no-flow days cause lowering of the water table and a high mortality of seedlings. Therefore, conversion of the Platte River from an intermittent river with many no-flow days to a perennial river allowed colonization of the exposed channel bed by vegetation.

Johnson's (1994) conclusions and the record of the hydrologic changes in the Platte River permit the development of explanations of the width changes between 1860 and 1995 (Figure 24.9, Table 24.1). The marked decrease of width between 1860 and 1938 (Figure 24.9) can logically be attributed to effects of diversions, dam construction (Pathfinder and Guernsey), and the low-flow years of the 1930s. The limited hydrologic data for this period show that the number of no-flow days at Overton and Grand Islands were numerous (Table 24.1). For example, at Overton, during the period 1931 through 1938, there were on average 82 no-flow days per year. There were 140 no-flows days per year at Grand Island for the period 1934 through 1938. The large number of no-flow days probably inhibited vegetation growth in the channel. Nevertheless, width reduction probably occurred during the 1930s as a result of reduced peak and annual discharge.

For the period 1939 through 1957, an additional significant decrease of width occurred between Brady and Grand Island (Figure 24.9). The average annual number of no-flow days for this period at Overton was 11 per year; whereas, at Grand Island, the average was 59 per year (Table 24.1). At Overton, there were zero no-flow days

after 1951, and the channel adjusted to discharges released from Kingsley Dam and irrigation return flow.

By 1957, width upstream of the Elm Creek West quadrangle (Figure 24.9) appears to have stabilized, and there were only minor width changes between 1957 and 1995. However, downstream of the Elm Creek West quadrangle, the decrease of width continued through 1983, because it was not until 1957 and 1978 that there were zero no-flow days at Odessa and Grand Island, respectively. The absence of no-flow days permitted adjustment of this part of the channel to a relatively stable condition during the period 1984–1995.

These relations suggest that in addition to decreases of mean annual and peak discharges, no-flow days also significantly influenced vegetational colonization of the channel. The cause of the decrease of no-flow days during the period 1939–1983 can be attributed largely to the construction of Kingsley Dam and to the storage and release of water from Lake McConaughy (Figure 24.8). The reduction of flow variation by this project is demonstrated by the absence or low frequency of no-flow days after 1941 (Table 24.1).

In summary, at Overton, Odessa, and Grand Island, river width decreased as irrigation return flows eliminated no-flow days. The establishment of perennial flow and a raised water table promoted vegetation establishment in the channel. A similar conclusion was reached by Nadler (1978) and Nadler and Schumm (1981) for the South Platte River. In contrast, a series of no-flow days in the wide sandy channel created a harsh environment for plant growth. The bare sand surface and the decline of the water table prevented survival of plants, that were established in the channel during previous wetter months.

When the dams and irrigation projects were constructed, there was no concern about wildlife habitat and the channel changes were of little consequence. Now there are proposals to release pulsed flows to maintain channel width, and vegetation is being removed by bulldozers from islands and floodplain areas to increase whooping crane habitat. Although degradation downstream of dams is usually anticipated, neither the great reduction of channel within the Platte River system nor the different responses (Figure 24.12) of the braided and anastomosing reaches were anticipated.

24.3.2 Niobrara River

Another unintended consequence of the construction of Fort Randall Dam is major sediment deposition in the Niobrara River (Figure 24.1), a tributary of the Missouri River. The Niobrara River is a braided sand-bed river that joins the Missouri downstream of the Fort Randall Dam.

The Niobrara River delivers a load of well-sorted sand with a median diameter of 0.012 mm to the Missouri River. At the confluence with the Missouri, the Niobrara has formed a delta following construction of dams on the Missouri (Livesey, 1963), which resulted in reduced mean and peak discharges. The competence of the Missouri River to transport sediment has been greatly reduced (Livesey, 1963). As a result of these conditions, aggradation of up to 2.9 m has occurred in the Missouri River at the mouth of the Niobrara River. Surveys of the Niobrara River channel cross sections, indicate that channel-bed elevations have increased over 2 m between 1956 and 1983.

The town of Niobrara, Nebraska was sited on the low terrace above the Missouri River. As a result of rising ground water table and frequent flooding, the town was relocated on a bench well above the Missouri and Niobrara Rivers at considerable cost. In addition, the facilities of Niobrara State Park were subject to increased flooding and partial burial by the aggrading Niobrara River. Because of Niobrara River aggradation, a railroad bridge was abandoned and a highway bridge was relocated, and it has been raised twice.

Aggradation downstream of a dam is unexpected, but high sediment delivery from downstream tributaries, such as the Niobrara River, can cause unexpected results. For example, in the Yazoo basin of Mississippi, the Tallahatchie River, downstream of Sardis Dam, is dredged to keep the channel open because of coarse sediment delivery from a tributary downstream of Sardis Dam (Biedenharn, 1984).

24.3.3 Middle Mississippi River

In addition to hydrologic changes affecting channel morphology, changing channel morphology will significantly affect hydrologic conditions. People living along the Mississippi River in the nineteenth century were not, as a whole, happy with its behaviour. Navigation was extremely hazardous and people living within the floodplain were subject to frequent floods; therefore, they petitioned the Federal government to provide a more navigable waterway and flood-protection works.

The first effort to improve conditions on the Middle Mississippi River between the confluences of the Missouri and Ohio Rivers (Figure 24.1) was to remove snags (sunken debris such as trees), which were hazardous to navigation between New Orleans and the Missouri River. On 31 March 1881, a comprehensive plan for regulation of the Middle Mississippi River was approved by Congress. The plan called for the continuous improvement of the navigation channel by reducing the width of the river

to 2500 feet (760 m). The US Army Corps of Engineers started the work at St Louis and continued downstream with construction of revetments and permeable dykes. One hundred and twenty-two miles (196 km) of bankline revetment prevent the river from eroding into floodplain properties (Degenhardt, 1973). Over 800 dykes with a total length of 91 miles (146 km) have been constructed from the riverbanks into the river channel.

The Middle Mississippi River has been deepened for navigation by decreasing the width with rock and pile dykes. An example of the change of cross-sectional geometry is shown in Figure 24.13. In 1837, the river section at St Louis was 3700 feet (1130 m) wide and had an average depth of 30 feet (9 m) at bankfull stage. The dykes decreased the width to 2100 feet (640 m).

Because the floodplain was not protected by levees in 1844, the peak discharge of 1 300 000 cfs (36 800 $m^3 s^{-1}$) passed St Louis at a 41.3 foot (12.6 m) stage. Now the same discharge will pass St Louis at approximately a 52.0 foot (15.8 m) stage (Figure 24.13). While the peak discharge stage is now some 10 feet (3 m) higher, as opposed to natural conditions, rural and urbanized areas suffer less flood damage due to the flood protection provided by levees (Stevens *et al*., 1975).

The effects of 100 years of development in the Middle Mississippi River on river stage were illustrated during the 1973 floods. The 1973 peak flood discharge at St Louis was 852 000 cfs (24 122 $m^3 s^{-1}$), which resulted in a maximum high-water stage of 43.3 feet (13.2 m), which is higher than the 1844 record discharge of 1 300 000 cfs (36 800 $m^3 s^{-1}$).

The largest flood discharges for the period 1843 to 1973 at St Louis are listed in Table 24.2. The 1973 flood ranks No. 10. The record high stages are listed in Table 24.3. The 1973 flood stage ranks No. 1.

The reason for the changes in water stage at St Louis in the last century is due to the dykes and the levees. Construction of rock and pile dykes caused deposition in the dyke fields and trees and willow grew on the deposits and stabilized them. The tree and willow growth encourages additional deposition whenever the area is flooded. In most cases, the ultimate effect of the dyke field is to cause the river to develop a new bankline at the extremity of the dyke field resulting in reduced channel width and a lowering of the riverbed level. The levee has isolated the major portion of the floodplain from the river channel so that all floodwaters are now confined to the river channel

Table 24.2 Top ten flood discharges at St Louis

Rank	Peak discharge (cfs)	Year
1	1 300 000 (36 800)	1844
2	1 054 000 (29 860)	1858
3	1 050 000 (29 750)	1855
4	1 040 000 (29 460)	1903
5	1 022 000 (28 950)	1851
6	926 000 (26 230)	1892
7	889 000 (25 180)	1927
8	863 000 (24 450)	1883
9	861 000 (24 390)	1909
10	855 000 (24 220)	1973

Note: Figures within brackets in $m^3 s^{-1}$.

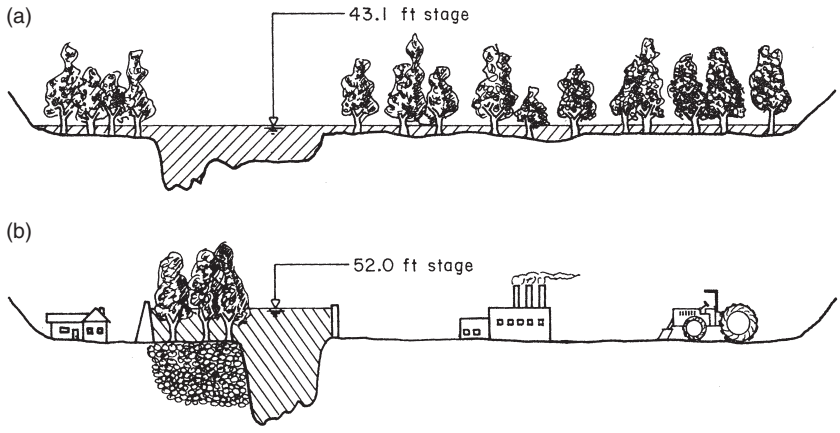

Figure 24.13 Cross-section of Middle Mississippi River downstream of St Louis at a discharge of 1 300 000 cfs (36 806 $m^3 s^{-1}$) in (a) 1844 and (b) 1973. From Man-induced changes in Middle Mississippi River, Stevens, M.A., Simons, D.B. and Schumm, S.A., Journal of Waterways, Harbours and Coastal Engineering, 1975. Reproduced by permission of ASCE

Table 24.3 Top ten flood discharges at St Louis

Rank	Maximum stage (ft)	Year
1	43.3 (13.20)	1973
2	41.3 (12.59)	1844
3	40.2 (12.26)	1947
4	40.2 (12.26)	1951
5	39.0 (11.89)	1944
6	38.9 (11.86)	1943
7	38.0 (11.58)	1903
8	37.2 (11.34)	1858
9	37.1 (11.31)	1855
10	36.6 (11.16)	1851

Note: Figures within brackets in m.

and that portion of the floodplain between the channel and the levees (Figure 24.13). It should also be noted that because the bed is lower in the narrowed river, the stages are lower than in the 1837 river most of the time. For a flow of 54 000 cfs (1529 $m^3 s^{-1}$), the stage was approximately 11 feet (3.4 m) lower in 1946 than in 1937. At a discharge of 90 000 cfs (2548 $m^3 s^{-1}$), the stage in 1837 and 1946 are equal, but at 500 000 cfs (14 156 $m^3 s^{-1}$), the 1946 stage is higher.

Although flood stages are now higher than those under natural conditions, levees prevent flood damage when the Middle Mississippi River exceeds bankfull stage. Under natural conditions, flood damage occurred whenever the river exceeded bankfull stage.

24.4 CONCLUSION

It is obvious that one cannot be too careful when modifying discharge and sediment load of rivers. The small amount of gravel that inhibited degradation in the Missouri River could have been detected with a more careful sampling programme, and the development of gravel controls in the Nile and the Lower Mississippi River could have been anticipated if bed sediment sampling could have been undertaken at high discharges. In addition, removal of gravel from a channel can destabilise it.

A reduction of peak flows can permit downstream tributaries to exert an unexpectedly large effect on the main channel as the Niobrara River did on the Missouri River and a small tributary did below Sardis Dam in Mississippi.

In semiarid regions, the conversion of an intermittent-flow channel into a perennial-flow channel permitted woody vegetation to greatly influence the morphology of the Platte River. Although the constriction of the Middle Mississippi River and its effect on flood stages should have been readily anticipated, it was not.

The problems described in each case discussed are the result of concentrating too little on the broader situation, which would include the effect of downstream tributaries (Niobrara River), the detection of gravel at depth (Missouri, Nile, and Mississippi Rivers), and hydrologic changes of other than peak and mean annual discharge (Platte River).

In order to prevent such problems, there are three concerns when undertaking practical work or, in fact, during any river investigation. These concerns are as follows:

(1) An investigation should always consider not only the site of interest, but upstream and downstream river reaches to determine if the reach of concern is representative of the river. That is, an investigator should back away from the specific problem site and view it in a broader context. For example, a meander bend upstream of a reach of concern could, through time, migrate downstream and significantly impact the reach. Even a brief reconnaissance upstream could identify the problem and plan for its mitigation.
(2) Rivers may range in sensitivity from very to not at all. An attempt should be made to evaluate river and reach sensitivity to determine if change is likely. For example, a series of tight meanders suggests that cutoffs are imminent and dramatic changes of channel morphology and hydraulics can be expected. However, if the channel is controlled by clay plugs or other resistant sediments, the channel may be fixed in position by these resistant materials.
(3) The multiple hypothesis approach should always be considered in an attempt to explain or anticipate river behaviour. That is, the most obvious conclusion may be incorrect. The complexity and variability of rivers yields many opportunities for error and the potential for undesirable unintended consequences. Experience and an open mind are critical for anyone dealing with rivers, large or small.

REFERENCES

Attia, M.I., (1954) *Deposits in the Nile valley and the delta*. Geological Survey of Egypt, Government Press, Cairo.

Biedenharn, D.S., (1984) Channel response on the Little Tallahatchie River downstream of Sardis Dam. In: *River Meandering* (C.M. Elliott, Ed.), American Society of Civil Engineers, New York, pp. 500–509.

Butzer, D.W., (1959) Contributions to the Pleistocene geology of the Nile valley. *Erdkunke*, 13, 46–67.

Degenhardt, E.A., (1973) Channel stabilization of the Middle Mississippi River. Unpublished MS thesis, Colorado State University, Fort Collins, CO, 99 p.

Eschner, T.R., Hadley, R.D. and Crowley, K.D., (1983) Hydrologic and morphologic changes in channels of the Platte River Basin in Colorado, Wyoming, and Nebraska: a historical perspective. *US Geological Survey Professional Paper* 1277A, 39 p.

Fathy, A., (1956) *Some consideration on the degradation problem in the Aswan High Dam scheme*. University of Alexandria, Egypt.

Hammad, H.Y., (1972) River bed degradation after closure of large dams. *Hydraulics Division of the American Society of Civil Engineers*, 98, HY 4.

Johnson, W.C., (1994) Woodland expansion in the Platte River, Nebraska: patterns and causes. *Ecological Monographs*, 64, 45–84.

Kircher, J.E. and Karlinger, M.R., (1983) Effective of water development on surface-water hydrology, Platte River Basin in Colorado, Wyoming, and Nebraska upstream from Duncan, Nebraska. *US Geological Survey Professional Paper* 1277B, 49 p.

Livesey, R.H., (1963) Channel armoring below Fort Randall Dam. *US Department of Agriculture, Miscellaneous Publication* 970, pp. 461–470.

Mostafa, G., (1957) River-bed degradation below large-capacity reservoirs. *Transactions of the American Society of Civil Engineers*, 122, 688–695.

Nadler, C.T., Jr, (1978) River metamorphosis of the South Platte and Arkansas Rivers, Colorado. Unpublished MS thesis, Colorado State University, Fort Collins, CO, 151 p.

Nadler, C.T. and Schumm, S.A., (1981) Metamorphosis of South Platte and Arkansas Rivers, eastern Colorado. *Physical Geography*, 2, 95–115.

Paulissen, E. and Vermeersch, P.M., (1987) Earth, man, and climate in the Egyptian Nile Valley during the Pleistocene. In: *Prehistory of Arid North Africa* (A.E. Close, Ed.), Southern Methodist University Press, Dallas, TX, 26–67.

Peake, J., Peterson, M. and Lavstrump, M., (1985) *Interpretation of vegetation encroachment and flow relationships in the Platte River by use of remote sensing techniques: remote-sensing applications laboratory*. Department of Geography and Geology, University of Nebraska at Omaha, 36 p. plus appendices.

Queen, B.S., (1994) Changes in bed material along the lower Mississippi River 1932 to 1989. Unpublished MS thesis, Colorado State University, Fort Collins, CO, 84 p.

Rahn, P.H., (1977) Erosion below mainstem dams on the Missouri River. *Association of Engineering Geology*, 14, 157–181.

Schumm, S.A. and Galay, V.J., (1994) The River Nile in Egypt. In: *The Variability of Large Alluvial Rivers* (S.A. Schumm and B.R. Winkley, Eds.), American Society of Civil Engineers Press, New York, pp. 75–100.

Shalash, S., (1980) The effects of the High Aswan Dam on the hydrological regime of the River Nile. Proceedings of Helsinki Symposium, *IAHS Publication* No. 130, 119–126.

Shalash, S., (1983) Degradation of the River Nile. *International Water Power and Dam Construction*, 35(8), 56–58.

Stevens, M.A., Simons, D.B. and Schumm, S.A., (1975) Man-induced changes in Middle Mississippi River, *American Society of Civil Engineers, Journal of Waterways, Harbors, and Coastal Engineering Division*, 101, 119–133.

Ware, E.F., (1911) *The Indian War of 1864*. Bison Books, University of Nebraska Press, Lincoln, NE, reprinted 1963, 483 p.

Wendorf, F., Said, R. and Schild, R., (1970) Egyptian prehistory: Some new concepts. *Science*, 169, 1161–1171.

Williams, G.P., (1978) The case of the shrinking channels: The North Platte and Platte Rivers, Nebraska, *US Geological Survey Circular* 781, 48 p.

Winkley, B.R., (1994) Response of the Lower Mississippi River to flood control and navigation improvements. In: *The Variability of Large Alluvial Rivers* (S.A. Schumm and B.R. Winkley, Eds.), American Society of Civil Engineers, New York, pp. 45–74.

25

Large Rivers from Space

Leal A.K. Mertes[†] and T. Tamuka Magadzire[‡]

Department of Geography, University of California, Santa Barbara, CA 93106, USA

25.1 INTRODUCTION

Large rivers by their nature are amenable to examination by a wide variety of remote sensing instruments. In the classic tradition of interpretation of image data wherein presence or absence is defined by 1–2 pixels, general characteristics are defined by 3–4 pixels, and 7–10 pixels are required in order to begin analysis, large rivers provide both water and floodplain landscapes of sufficient size such that relatively coarse (500–1000 m) resolution pixels may still provide information of value (Figure 25.1 and Table 25.1). Within this context it is appropriate to define terms that express the relationship between the object of interest (e.g. an oxbow lake) and the image characteristics that determine the ability of the user to interpret the object. Scale has numerous definitions, the one used here is as defined by Schneider (1994) as the resolution within the range of a measured quantity (Bult *et al.*, 1998). In a similar fashion, the dimensionless ratio of extent to resolution has been defined as the scope (Schneider, 2001) and is the comparable statistic for the interpretation rules described previously. For example, a floodplain that is 3 km across in extent examined with Landsat pixels with a spatial resolution of 30 m, would have a scope of 3000 m/30 m = 100. Scope in this riverscape would be reduced to 6 if the instrument were MODIS (Moderate Resolution Imaging Spectroradiometer) and pixels with 500 m resolution were being analyzed. In summary, a scope of 10 or greater provides sufficient information for analysis for many critical elements of the channel-floodplain systems of large rivers.

Complementary to the discussion on the scale of the pixel and its relationship to the object of interest, is a brief discussion of the 'footprint' required in order for the remote sensing instrument to be able to acquire sufficient data for analysis. As one type of example, for radar altimetry from satellites such as the TOPEX/POSEIDON instruments, the large (tens of kilometres) scale of the requisite footprint (Birkett, 1994) is such that extensive, homogeneous areas are essential in order for the data processing to be able to produce an accurate measurement at a precise location. The data sets from these type of instruments are therefore inherently different than those emanating from the gridded data sets typically associated with remote sensing, e.g. Landsat or SPOT.

The constraints on temporal resolution with respect to remote sensing of large rivers are less and less of a concern as the field of instruments has expanded rapidly in the past two decades (Figure 25.1). Basically, instruments are now capable of acquiring data at almost every time period of interest to riverine scientists. The difficulty of acquiring data, especially optical data, is most often a weather problem related to cloud cover (Asner, 2001). In a recent analysis of data quality for several large rivers based on 8-day composite images from the MODIS instrument we found that up to 20–30 quality images are available each year for sites along the Danube, Mekong, Amazon, Jubba (Somalia), Mississippi, and Zambezi. The successful

[†] Deceased.

[‡] Current address: USGS FEWS NET Regional Representative for Southern Africa, c/o SADC Regional Remote Sensing Unit, SADC Food, Agriculture and Natural Resources Directorate, SADC Secretariat, Gaborone, P. Bag 0095, Botswana.

Large Rivers: Geomorphology and Management, Edited by A. Gupta

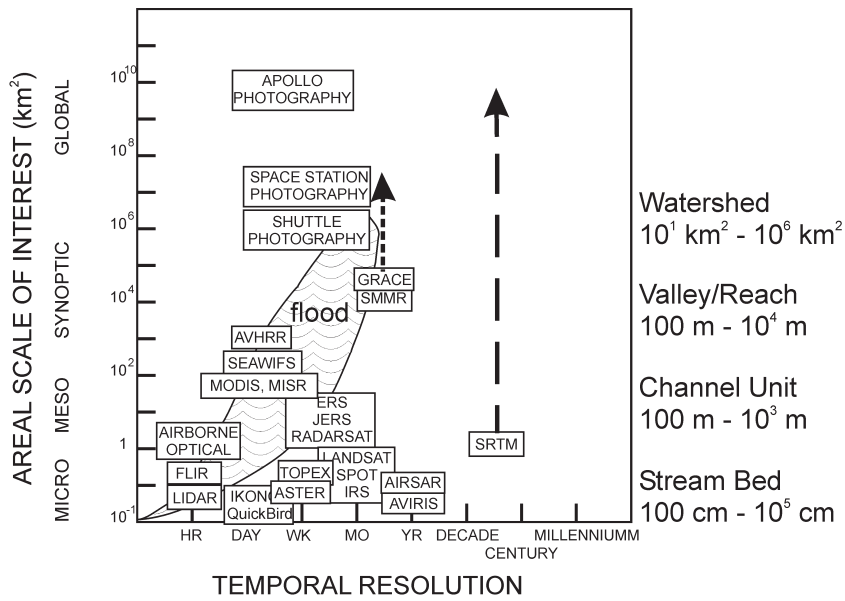

Figure 25.1 Spatial and temporal resolution of remote sensing instruments. The abscissa shows the temporal resolution, i.e. the frequency of acquisition, of image data at the finest resolution for the listed instruments (Table 25.1 lists acronyms and names). The scale of the watershed/river features is listed according to material presented by Poff (1997). The abscissa also represents the flood duration (as shown by Hirschboeck, 1988) for watersheds at the scales shown on the ordinate. The ordinate scale represents the finest spatial resolution of the picture element (pixel) for each of the named detectors. The arrows associated with GRACE (Ward, 2003) and SRTM (two of the newest data image data sets available) suggest that although data were collected at one resolution they are applicable over the range shown

acquisition of these quality data for large areas in these river basins is the result of the improvement in cloud detection techniques that allow selection of the clearest pixel over an 8-day period. The characteristics of many large rivers (flow, sediment concentration, and habitat characteristics) do not change rapidly. Hence, the 8-day time average still allows for significant analysis. Fewer limitations exist for active radar systems with respect to temporal resolution, because of their ability to penetrate through modest cloud cover (Smith, 1997 2002). Detailed reviews exist for techniques at all scales (Smith 1997 2002; Mertes *et al.*, 2004). The emphasis here will be on a representative suite of examples of the most effective measurements that are now routinely available for large rivers that have become crucial for study of these systems.

25.2 BASIN CHARACTERISTICS

Potter (1978) pointed out that continental-scale tectonic deformation controls the physiographic setting of large rivers, in that most large rivers are located in structural lows or continental rifts, and flow into oceans off trailing edges of continents. Figure 25.2 illustrates the general structural patterns depicted by Potter (1978) and each type is labelled with the rivers covered in this book by the Potter category that we have named P1 through P5 (see Table 25.2 for list by river).

With the advent of availability of digital elevation data for the world, it is now possible to characterize the boundaries of large river basins in a relatively consistent way, so that the hypotheses generated by Potter's work can be examined in greater detail. These basin shapes and extents are shown in Figure 25.3 for the rivers listed in Figure 25.2. The maps generated for Figure 25.3 were completed using the Hydro1K data set available from the USGS Eros Data Center and the data sets are based on the GTOPO30 digital elevation data set (Verdin and Verdin, 1999). For the Hydro1K data products, the GTOPO30 data set was cleaned up to insure that drainage networks were coherently connected from the headwaters to the mouth of each river. Often, digital data sets, such as the Shuttle Radar Topography Mission (Figure 25.1) still suffer from electronic noise and interference from canopy cover such that

Table 25.1 Alphabetical list of instrument acronyms and names (representative, but not comprehensive, list of available instruments)

Acronym	Name	ER region
AIRBORNE OPTICAL/ THERMAL	e.g. CASI/TABI[a], Hymap[a], AMS[a]	optical, IR, thermal
AIRSAR	Airborne Synthetic Aperture Radar	active microwave
ASTER	Advanced Spaceborne Thermal Emission and Reflection Radiometer	optical, IR, thermal
AVHRR	Advanced Very High Resolution Radiometer	optical, IR, thermal
AVIRIS	Airborne Visible/Infrared Imaging Spectrometer	optical, IR, thermal
ERS[b]	European Remote Sensing Satellite Synthetic Aperture Radar	active microwave
FLIR[a]	Airborne Forward-Looking Infrared	thermal
IRS LISS	Indian Remote Sensing Linear Imaging Self Scanning Camera	optical, IR
GRACE	Gravity Recovery and Climate Experiment	Earth gravity
IKONOS[a]	Derived from 'images' in Greek	optical, IR
JERS	Japanese Earth Remote Sensing Synthetic Aperture Radar	active microwave
LANDSAT[b]	Landsat Multi-Spectral Scanner (MSS), Thematic Mapper (TM), Enhanced Thematic Mapper (ETM)	optical, IR, thermal
LIDAR[b]	Laser Radar or Light Detection and Ranging	active microwave
MODIS, MISR	Moderate Resolution Imaging Spectroradiometer; Multiangle Imaging SpectroRadiometer	optical, IR, thermal
QuickBird[a]	Part of Ball Global Imaging System	optical; IR
RADARSAT[a]	Canadian Synthetic Aperture Radar	active microwave
SEAWIFS[b]	Sea-Viewing Wide-Field-of-View Sensor	optical, IR
SMMR	Scanning Multichannel Microwave Radiometer	passive microwave
SPOT HRV[a]	le Systéme pour l'Observation de la terre; High Resolution Visible Sensor System	optical, IR
SRTM	Shuttle Radar Topography Mission	active microwave
TOPEX	Topex/Poseidon	active microwave

The region of the electromagnetic spectrum (ER region) indicates the range of wavelengths covered by instrument. IR, infrared wavelengths. Superscripts are for commercial and commercial/government joint ventures. If no superscript then the funding source is governmental.
[a] Commercial.
[b] Commercial/government.

the consistent, computationally derived drainage networks are not yet available for large rivers.

25.3 VALLEY CONFIGURATION

The structural outline of the highlands constraining the river valley, which is the primary way in which Potter defines the different categories of structural settings, is not immediately obvious from the maps in Figure 25.3. Therefore, Figure 25.4 was generated to demonstrate these valley patterns within the context of the basin shape. If one views the Indus River on all three figures (P2 – marginal to folded mountains in Figure 25.2), the pattern of the main valley running along the eastern margin of the Sulaiman Range in Pakistan is clear, especially as the green, arcuate valley in Figure 25.4. In contrast, the remarkable west-to-east trend of the Brahmaputra (P4 – along strike of folded mountains) as it passes through the high mountain valleys in Tibet, changes dramatically when it emerges onto the plains of Bangladesh and turns south. Each of the rivers depicted in Figures 25.2–25.4 can be visually analyzed for an understanding of these structural characteristics within the framework of Potter's suggested structural settings.

Earlier the SRTM was not ready for delineation of basin boundaries, but it did allow more consistent comparisons at finer resolution along major river and valley corridors (Mertes and Mason, 2002) than was possible with the more inconsistent national data sets used to construct the GTOPO30. A simple technique for analyzing the extent of the active floodplain (várzea) of the Amazon (Amazonas) floodplain is shown in Figure 25.5. Until the SRTM data became available in 2001–2002, these type of data were simply not available for most of the Amazon River Basin. The generalized elevation map for this area with respect to mean sea level is Figure 25.5a. The course of the river is seen as a series of meander bends crossing the floodplain, with an oxbow lake in white just north of the largest meander bend. The valley boundary can be seen as a series of higher elevation terraces that were masked to distinguish just the active floodplain area in Figure 25.5b. For confirmation of these results, an overlay

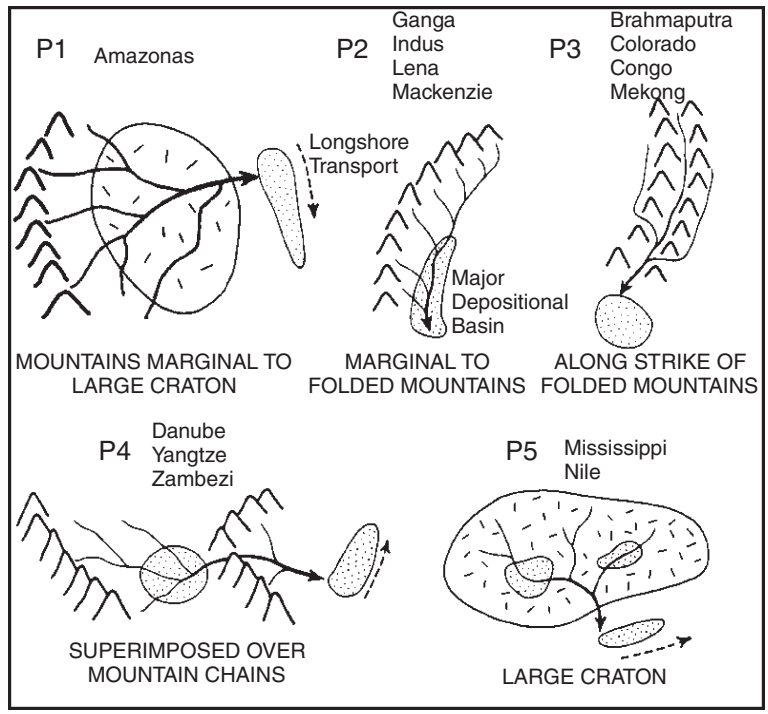

Figure 25.2 Schematic illustrations of continental settings for large rivers according to Potter (1978). The labels P1–P5 have been added for easier reference to the different settings for this chapter. Rivers mentioned in this chapter and in book are listed according to their most applicable physiographic setting. Reproduced by permission of the University of Chicago Press

Table 25.2 Summary statistics for 13 large rivers shown in Figures 25.2 and 25.3

River name	Continent	Area[a] (10^6 km^2)	Length[a] (km)	Basin shape[a] (S_b)	Elongation ratio[a]	Potter code[b]	Hayden code[c]
Amazon	SA	5.854	4327	1.79	0.63	P1	Tpz
Nile	AF	3.826	5909	3.02	0.37	P5	Tpu
Congo (Zaire)	AF	3.699	4339	2.26	0.50	P3	Tsz
Mississippi	NA	3.203	4185	2.34	0.48	P1	TsuCpSe
Lena	EU	2.418	4387	2.82	0.40	P2	CSs[d]
Zambezi	AF	1.989	2541	1.80	0.63	P4	Tsz
Yangtze (Changjiang)	AS	1.794	4734	3.53	0.32	P4	Tszo
Mackenzie	NA	1.713	3679	2.84	0.40	P2	CSs[d]
Ganga-Brahmaputra	AS	1.628	2221	1.74	0.65	P3	Tszo
Indus	AS	1.143	2382	2.20	0.51	P2	Tszo
Colorado	NA	0.808	1808	2.01	0.56	P3	Tsu
Danube	EU	0.788	2222	2.55	0.44	P4	CpSe
Mekong	AS	0.774	3977	4.52	0.25	P3	Tpz

[a] Mainstream length and basin area statistics extracted from Vörösmarty *et al.* (2000, Table 3: 36).
[b] Potter code assigned according to examples as shown in Figure 25.2 (Potter, 1978).
[c] Hydroclimatology codes as reported by Hayden (1988): T, barotropy; p, perennial; z, ITCZ; u, unorganized convection; s, seasonal snow cover; C, baroclinicity; S, snow cover; e, ephemeral snow cover; o, organized convection.
[d] Snow cover 50 cm or more.

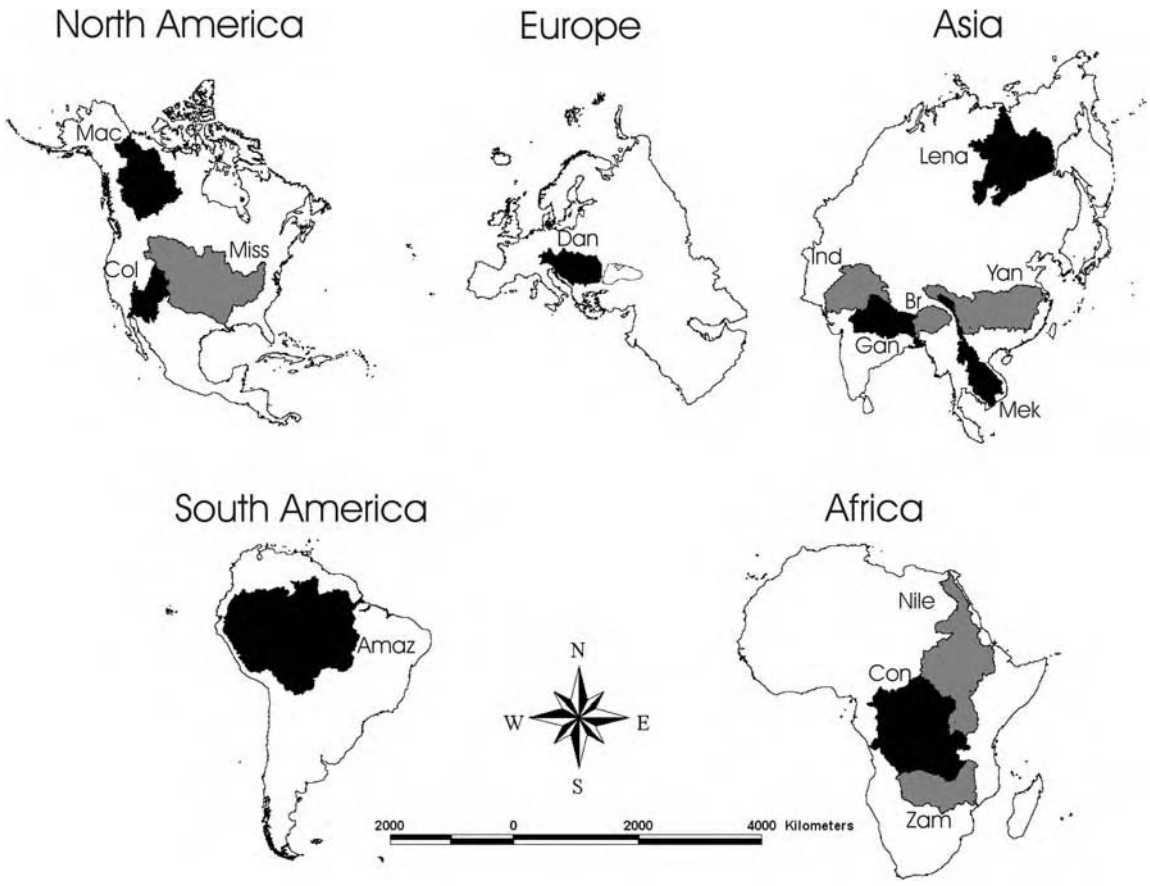

Figure 25.3 Watershed boundaries for 14 large rivers described in this chapter. Boundaries delineated from Hydro1K products as derived from GTOPO30 according to the techniques of Verdin and Verdin (1999). The names of the rivers are shortened and the colour scheme of grey and black is designed to allow all of the watersheds to be distinguished from each other. In North America: Mac, Mackenzie; Col, Colorado; Miss, Mississippi. In Europe: Dan, Danube. In Asia: Lena; Yan, Yangtze; Mek, Mekong; Br, Brahmaputra; Gan, Ganga; Ind, Indus. In South America: Amaz, Amazon. In Africa: Nile; Con, Congo; Zam, Zambezi

of the valley boundary derived from an analysis of land-cover data derived from Landsat images is shown to be nearly identical (Figure 25.5c – dark area with speckles) to the outline in Figure 25.5b. This type of simple analysis for the extent and areal cover of the floodplain on a large river is one of the many types of analyses that can now be completed on any large river floodplain.

Table 25.2 provides a summary of data related to the geometry of each of the rivers shown in Figures 25.3 and 25.4 using data from Vörösmarty *et al.* (2000). Of particular interest is the shape statistics for the different basins, $S_b = L/A^{0.5}$, where L is the mainstream length (km) and A is the drainage area (km^2) at the basin mouth. The global mean value of S_b is about 2.1 with a range from 1.0 to 5.0. The most elongate rivers would have the highest values (e.g. the Nile, P5, and Mekong, P3). Another way to measure the roundedness of the watershed is to examine it directly with Schumm's (1956) elongation ratio which ranges from one (a perfectly circular basin) to nearly 0 (an extremely linear configuration). As expected, the Nile and the Yangtze (P4) show elongate patterns, with the Mekong being the most extreme.

25.4 GEOMORPHOLOGY

The number and types of efforts incorporating remote sensing into geomorphic studies is based on the long tradition of the use of aerial photographic interpretation for

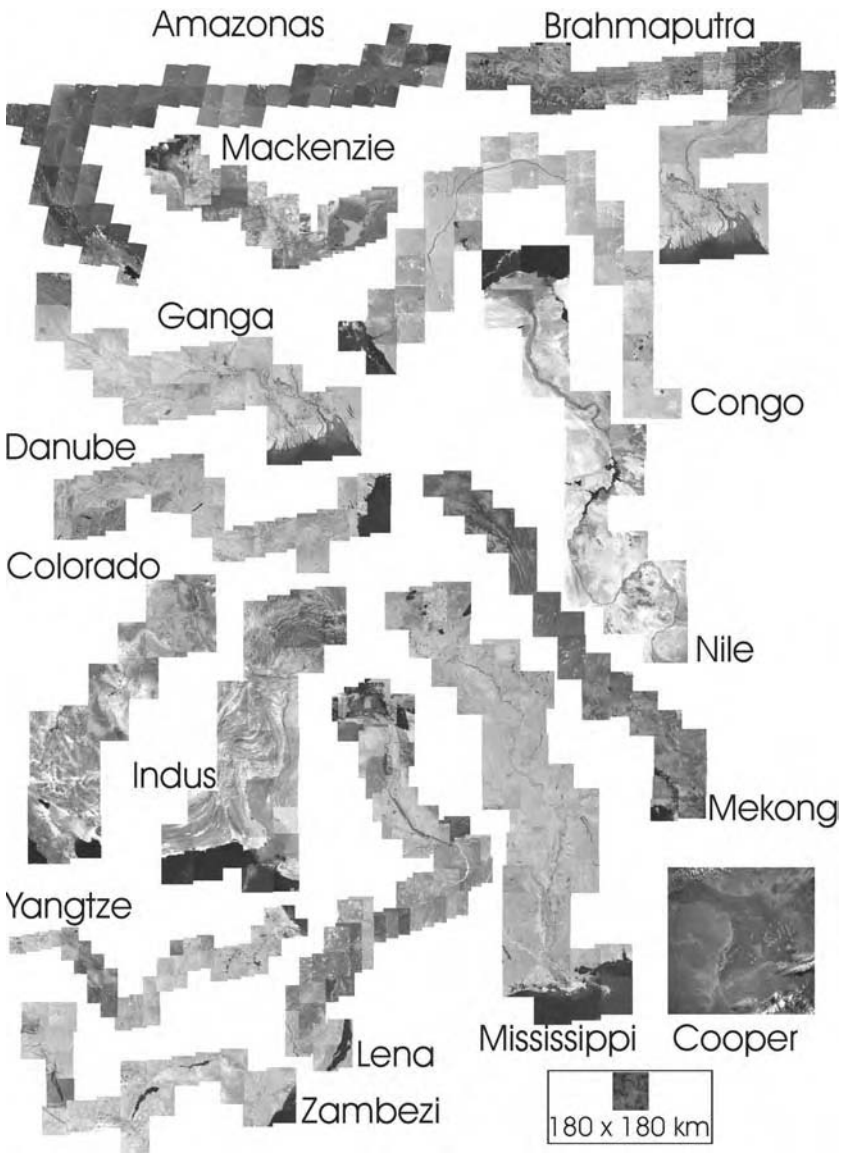

Figure 25.4 (See also colour plates.) Landsat mosaics of 14 rivers showing valley configuration along the course of the main river channels. Each of the rivers represented in Figure 25.3 is shown here assembled from Landsat image colour composites. Each of the individual Landsat scenes is approximately 180 × 180 km. The mosaics were assembled by undergraduate students at the University of California, Santa Barbara. The Cooper River image (Australia) is a NASA space shuttle image showing flooding during November 1989. (Image courtesy of NASA)

analysis of landscape elements and geomorphic landforms in riverine environments. The advantage of remote sensing data is its large-scale, synoptic view, while its greatest disadvantage is the scale of the spatial resolution, which until recently has been on the order of tens of metres (Figure 25.1). In this brief review it is not possible to describe in detail all of the types of geomorphic studies that have been undertaken using remote sensing data. However, one could categorize the types of efforts into four general categories:

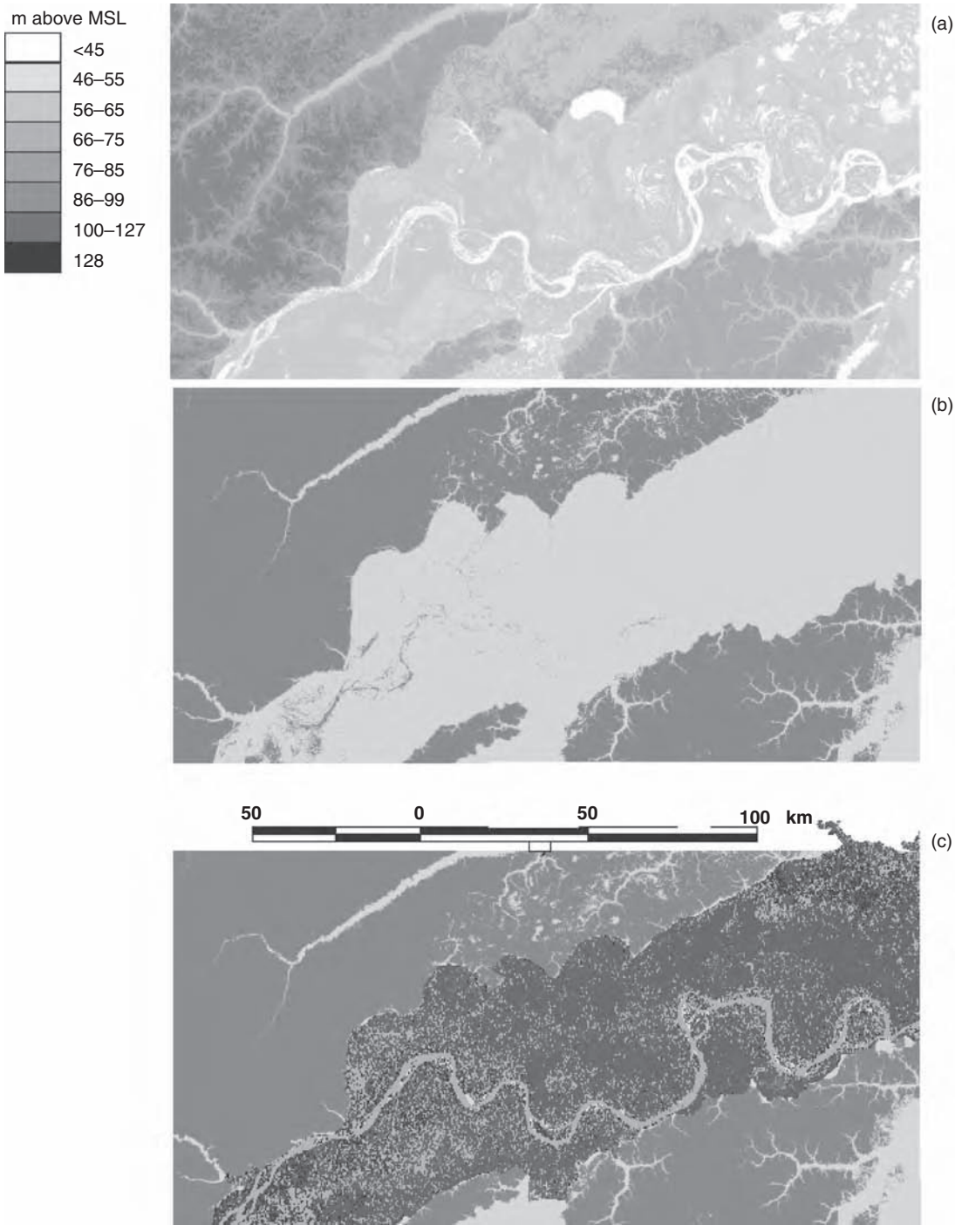

Figure 25.5 Examples of analyses of Shuttle Radar Topography Mission (SRTM) data for sinuous reach of Amazon River (see Chapter 8). Image centred at approximately 2.6° S and 67.1° W. (a) Elevation map is coded to highlight features on floodplain and to distinguish the valley boundary. (b) Map of river valleys (light grey) versus upland areas (*terra firme*). The boundary between the upland and valleys was determined using elevation thresholds that take into account the fact that the SRTM data measure the top of the tree canopy as well as the ground surface, depending on the density of the canopy cover. (c) Overlay of river valley as derived from a landcover classification using Landsat images (Shimabukuro *et al.* 2002). The consistency of the river valley edge shown by both SRTM and Landsat data helps to confirm the usefulness of the SRTM data despite the fact that the elevation measurements inconsistently represent ground and canopy surfaces. Reprinted from International Journal of Remote Sensing. Vol. 23:1, Shimabukuro *et al.*, Amazon River Mainstream Floodplain Landsat TM Digital Mosaic, pp. 57–69, 2002, with permission from Taylor & Francis Ltd. http://.www.tandf.co.uk/journals

- landform mapping (Tricart, 1977; Brivio *et al.*, 1988; Mouchot *et al.*, 1991; Sippel *et al.*, 1992; Wivell *et al.*, 1993; Mertes *et al.*, 1996; Florenzano, 1998; Thomson *et al.*, 1998; Yang *et al.*, 1999b; Forsberg *et al.*, 2000; Wright *et al.*, 2000; Townsend and Walsh, 2001; Gupta *et al.*, 2002; Hudson and Colditz, 2003; Hudson, 2004);
- channel and landscape change (Ramasamy *et al.*, 1991; Kalliola *et al.*, 1992; Stolum, 1998; Bryant and Gilvear, 1999; Yang *et al.*, 1999a; Gomez *et al.*, 2000; Townsend and Walsh, 2001);
- process interpretation (Mertes, 1994; Vörösmarty *et al.*, 1996; Bates *et al.*, 1997; Portmann, 1997; Souza *et al.*, 2002; Lane *et al.*, 2003);
- geologic studies (Jacobberger, 1988).

25.5 WATER-SURFACE ELEVATION, GRADIENT AND DISCHARGE

Study of large rivers will necessarily require data on water-surface elevation and gradient for hydraulics and discharge for hydrology. Table 25.2 lists hydroclimatological codes derived from Hayden (1988) for each of the rivers. These codes loosely define the characteristic climate elements that contribute most significantly to flooding on these rivers, thus, expressing the major controls on the seasonality of the hydrographs.

As the ground-based effort to acquire these measurements has suffered a significant reduction in funding over the past decade, many are looking to remote sensing analyses to retrieve these critical data sets. The instruments and data that show the most promise involve measuring the relative change of elevation or interferometric radar-based measurements (Alsdorf *et al.*, 2000; Smith, 2002). A different application is shown for altimetric measurements based on data from the TOPEX Poseidon missions as reported by Birkett *et al.* (2002) for several locations along the Amazon River (Figure 25.6). With the accuracy of these data confirmed by comparison with adequate ground-based gauge records, it is possible to extend analysis of their properties to such measurements as the seasonal change in the water-surface gradient as shown in Figure 25.6b. As described by Birkett *et al.* (2002), the irregular patterns of water surface gradient can be explained by the seasonal movement of the flood wave through the main channel of the Amazon.

25.6 WATER EXTENT AND INUNDATION MAPPING

One of the most exciting developments in the past two decades related to mapping floodplain environments on rivers of any size is the discovery that the wavelengths associated with Side-Looking Airborne Radar (SLAR) and Synthetic Aperture Radar (SAR), especially the C-band at 5.3 GHz, are responsive to the presence of water under vegetation to a high degree of accuracy (Hess *et al.*, 1990) due to the 'double-bounce' of the energy off the water surface and the faceted surfaces of tree trunks and other vegetation. Numerous studies have taken advantage of this effect to produce maps of inundation extent under different types of vegetation. Figure 25.7a shows a Band C image that was used to calculate the boundaries of open water (right line) and inundated vegetation (left line) overlaid onto a map of digital elevation derived from LIDAR elevation data (Horritt, 1999; Horritt *et al.*, 2003) with modelling techniques that are both efficient and accurate. The results have been compared successfully with both field measurements and hydrodynamic modelling results (Bates *et al.*, 1997) for inundation. Image processing techniques of varied types using radar data can be applied over vast areas as shown by the recent analysis of the floodplain boundary for parts of the floodplain of the Amazon River and its tributaries (Hess *et al.*, 2003).

25.7 MAPPING SEDIMENT CONCENTRATION

Time series data of hydrology and hydraulics and patterns of flood inundation are critical elements in studying large rivers. In addition, an understanding of the patterns of sediment transport, erosion, and deposition, provides insight into the evolution of the geomorphology of the channel-floodplain system, the biogeochemistry of the waters and substrate, and the conditions in the water column and substrate that are supportive or detrimental to biological activity. Therefore, examination of water quality with remote sensing has been a focus for remote sensing scientists since the deployment of the first Landsat Multi-Spectral Scanner (MSS) instrument in 1972 (Klemas *et al.*, 1973).

As reviewed recently (see details in Mertes *et al.*, 2004), given the nature of the wavelengths from the blue to infrared range it is possible to use a series of techniques for calibration of the nonlinear signals associated with turbidity, colour, and algal characteristics in the water. Using laboratory data surface reflectance for calibration to surface reflectance data from remote sensing instruments (most recently shown with MODIS data for the Mississippi River) we were able to derive an absolute sediment concentration in milligrams per litre for surface waters without relying completely on a calibration to field data. This technique is particularly applicable to large rivers, because in many instances the characteristics of the sediments in suspension in large rivers is that they are primarily comprised of clay- and silt-sized particles that are frequently coloured by organic acids adsorbed from

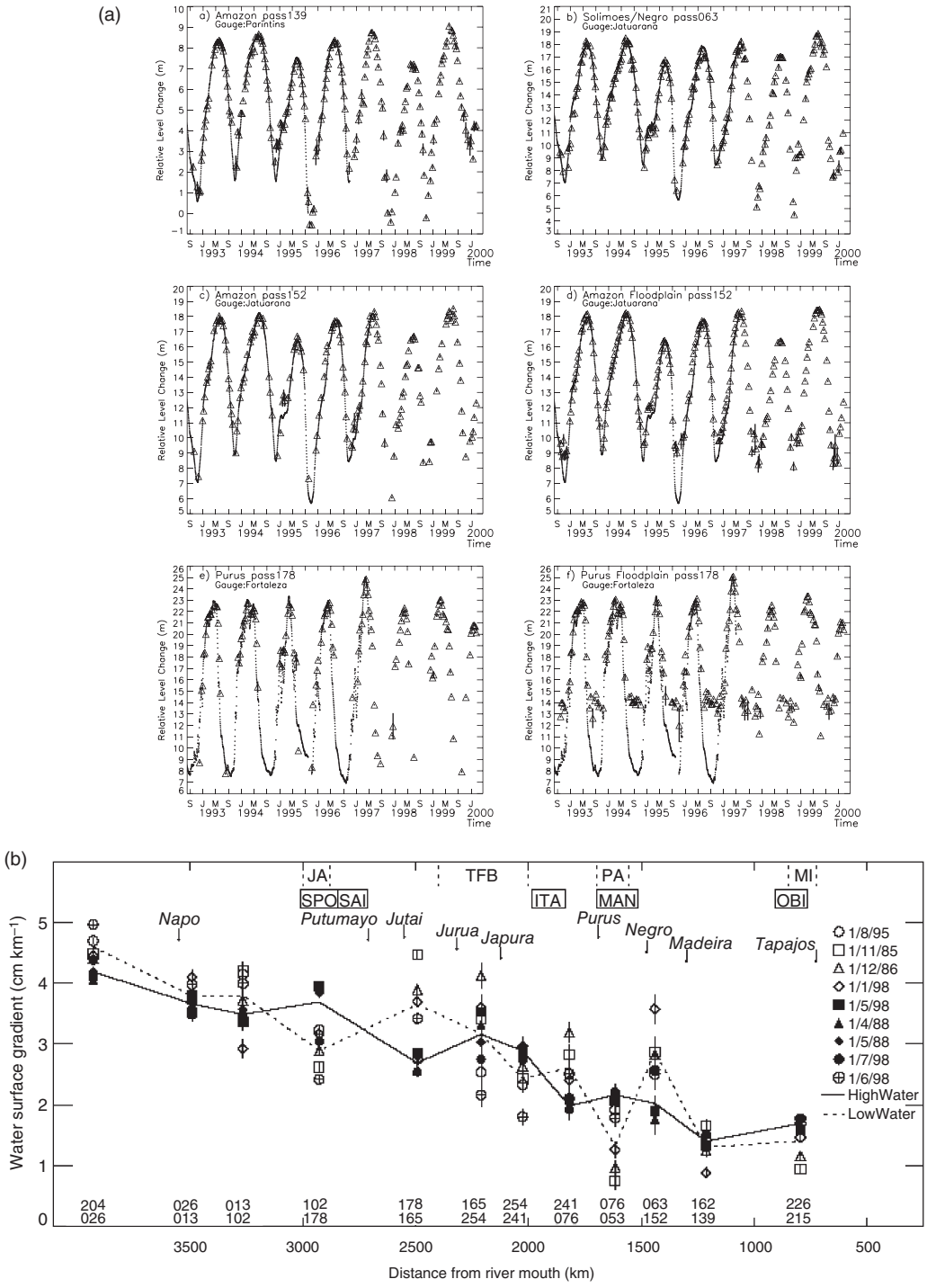

Figure 25.6 Examples of water-surface elevation, gradient, and discharge derived from satellite data. (a) Comparison of stage measurements to TOPEX/POSEIDON radar altimetry measurements of water surface for six river cross-sections in the Amazon Basin as reported by Birkett *et al.* (2002, Figure 2). Cross-sections are for the Amazon River and floodplain and across the Purús tributary. See Chapter 8 for more information on the Amazon River. (b) Calculated water-surface gradients along main channel of Amazon River for early January, 1995 using TOPEX/POSEIDON radar altimetry data (Birkett *et al.*, 2002, Figure 7). Additional data reported for the average values for high water (March–July) and low water (August–January), show hydraulic differences during these hydrologically distinct seasons. Names at the top indicate different tectonic elements of the river valley (see Dunne *et al.*, 1998; Mertes *et al.*, 1996, and Chapter 8). Names within boxes indicate locations of river gauge stations and names in italics indicate position of confluences with large tributaries

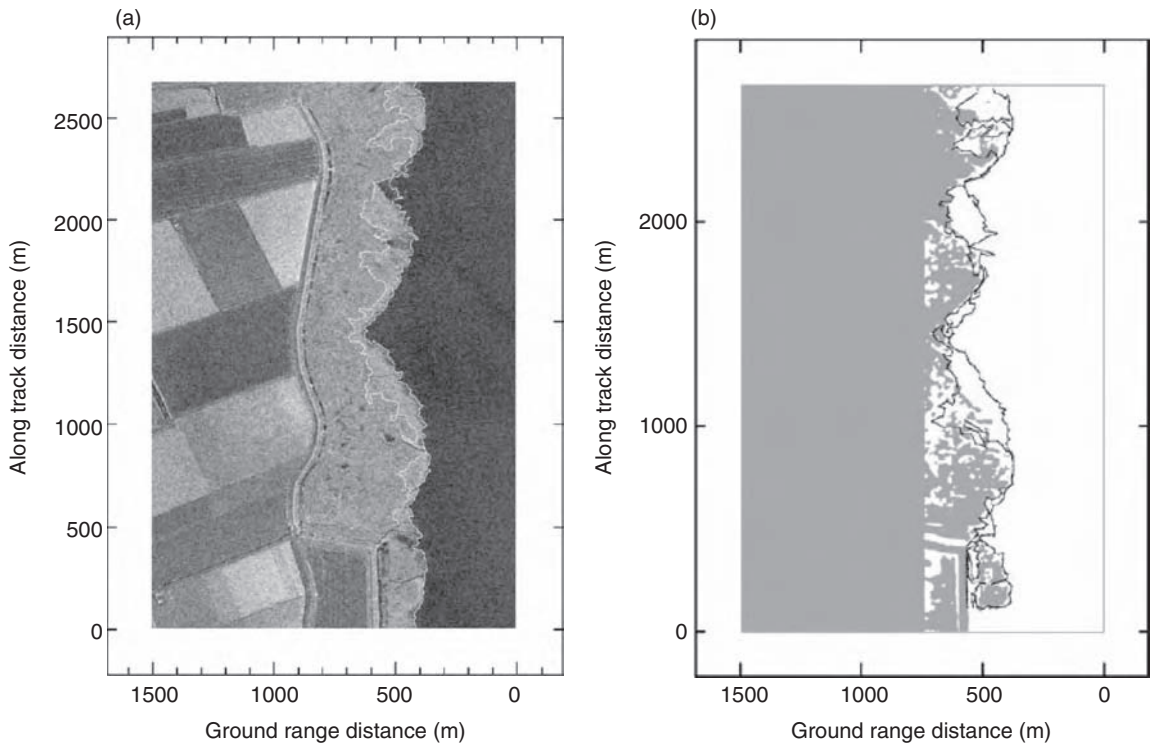

Figure 25.7 Examples of analyses of synthetic aperture radar (SAR) and (LIDAR) data for delineation of inundation boundaries and water extent. (a) Band C image with VV polarization showing the results of model calculations for delineating the open water boundary (line on right) and inundated vegetation boundary (line on left) based on active contour segmentation (Horritt, 1999; Horritt *et al.*, 2003). (b) Calculated open water (right) and inundated vegetation (left) boundaries overlaid onto LIDAR elevation data for area shown in (a). The inundated areas as mapped from just the elevation data are not shaded. (a, b) Reprinted from Remote Sensing of Environment, Vol. 85, Horritt *et al.*, Waterline mapping flooded vegetation from airborne SAR imagery, pp. 271–281, 2003, with permission from Elsevier

the water column. As suggested by Mertes *et al.* (1993), using laboratory results based on experiments with Mississippi River sediment samples (Witte *et al.*, 1981; 1982a,b) as a surrogate for analyses of spectral data for other large rivers is reasonable given the predicted similarity in optical properties because of the dominance of the organic acid coatings. Other techniques that rely on theoretical computations based on the radiometric properties of the spectral signals and material properties have also shown success (see details in Mertes *et al.*, 2004).

The success of the linear mixing technique (Mertes *et al.*, 1993) has now been proven for several different instruments (SeaWiFS, Landsat, SPOT, MODIS) with accuracies of the satellite derived surface suspended sediment concentrations predicted to be within 10–20 mg l^{-1} of ground measurements of surface suspended sediment concentration (Mertes, 1997; Mertes and Warrick, 2001; Warrick *et al.*, 2004). Examples are shown here for a time series analyses over the entire hydrograph for the year 2001 derived from the MODIS instrument for the Amazon River and a few of its major tributaries (Figure 25.8). The results show relatively consistently the rise and fall of the sediment concentration in suspension at the surface, with the highest concentrations observed during the period of rising water and the lowest concentrations observed during the flood season. Comparison of the satellite derived surface sediment concentrations (open circles) to the field measurements of depth-averaged sediment concentrations (solid triangles) shows that although, as expected, the magnitudes of the depth-averaged concentrations are higher, seasonal patterns corresponding to the rise and fall of the hydrograph are similar.

The temporal availability and reliability of these satellite-derived results for surface sediment concentrations for

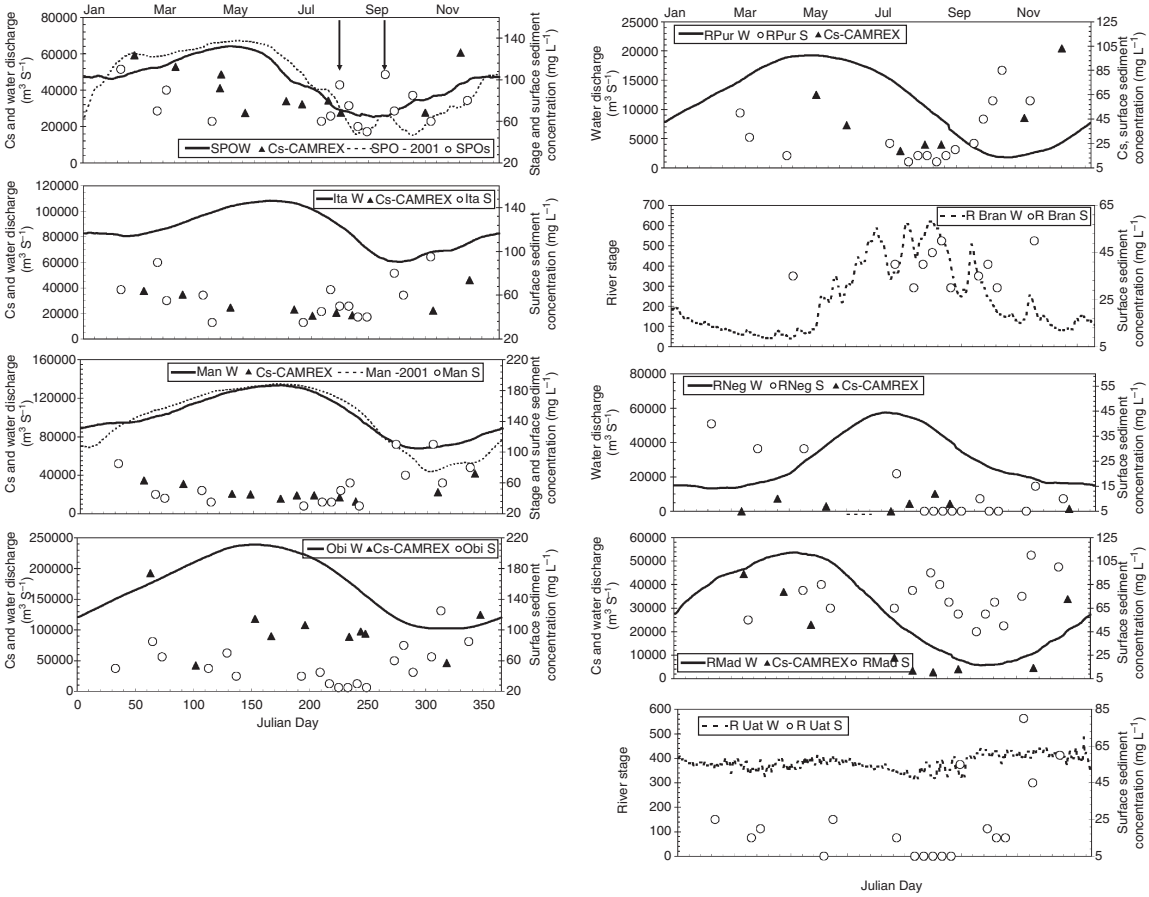

Figure 25.8 Satellite derived surface sediment concentrations from MODIS data for Amazon River (see Figure 25.1, Table 25.1 and Chapter 8). Comparison of hydrograph (W) by average discharge (1972–1989) and stage (2001) and sediment concentration from field sampling (Cs) (Meade, 1985) and MODIS (S) for sites along Amazon River main channel and on major tributaries. All data were not available for all sites. In order to effectively plot the field concentrations of depth-integrated suspended sediment, the values were multiplied by different factors (as noted). SPO is the furthest upstream gauge in Brazil for which there are sediment data available from the CAMREX project. Additionally, the 2001 gauge data were also available from the Brazilian Water Agency, ANA. The scale for the Cs-CAMREX (Meade, 1985) is the left axis and the value needs to be divided by 100 to correct for the scaling of the depth-integrated concentration. Ita is the middle gauging section for which the 2001 gauge data were not available from ANA. The scale for the Cs-CAMREX is the left axis and the value needs to be divided by 100 to correct for the scaling of the depth-integrated concentration. Man is the gauge nearest to the Rio Negro confluence and the 2001 data were available for this gauge. The scale for the Cs-CAMREX is the left axis and the value needs to be divided by 100 to correct for the scaling of the depth-integrated concentration. Óbi is the last primary gauge on the mainstem upstream of large-scale tidal influences. ANA data for 2001 were not available. The scale for the Cs-CAMREX is the left axis and the value needs to be divided by 500 to correct for the scaling of the depth-integrated concentration. A selection of tributary data are plotted in order of confluences from upstream to downstream with the exception of the Rio Branco, which is a tributary to the Rio Negro. Rio Purús (RPur) has a complete series of sediment measurements from the CAMREX project. Gauge data for 2001 are not available. The scale for the Cs-CAMREX is the right axis and the value is not multiplied by a scale factor. Rio Branco is the furthest northern tributary shown and it flows into the Rio Negro. No depth-integrated sediment data are available for comparison with the MODIS data, but 2001 gauge data are available. Rio Negro has a complete series of sediment measurements from the CAMREX project. Gauge data for 2001 are not available. The scale for the Cs-CAMREX is the right axis and the value is not multiplied by a scale factor. Rio Madeira has a complete series of sediment measurements from the CAMREX project. Gauge data for 2001 are not available. The scale for the Cs-CAMREX is the left axis and the value is multiplied by a factor of 50 to correct for the scaling of the depth-integrated concentration. Rio Uatuma is the only tributary shown that is controlled by reservoir discharge management. No depth-integrated sediment data are available for comparison to the MODIS data, but 2001 gauge data are available

many rivers shows that it may now be time to investigate more completely the theoretical relationships between the surface suspended sediment concentration in large rivers that is often dominated by wash load, to the depth-averaged field measurement (Aalto, 1995). With development of the proper theory, it would then be possible to build sediment-rating curves that combine the altimetry data as shown in Figure 25.6 with sediment data as shown in Figure 25.8 to yield remotely derived measurements of total sediment discharge at river cross-sections.

25.8 ZAMBEZI RIVER – WATER TYPE MAPPING ON FLOODPLAINS

As a corollary to the community's effort to map surface sediment concentrations for channels, there are also many efforts to map sediment concentrations in inundating waters during floods on large rivers. Figure 25.9b shows a Landsat image and the corresponding section of a MODIS image for the 2001 Zambezi River flood. Both images were acquired on 4 March 2001. Inspection of both images shows that the pattern of sediment concentrations is similar for both images, thus once again proving the reliability of the linear unmixing technique. With confidence in the results, it is reasonable to take the analysis a step further and view the spatial and temporal characteristics of the patterns of surface sediment concentration. The boxes outlined on the Landsat image in Figure 25.9b show the boundaries for the corresponding sub-images shown in Figure 25.9c. Here it is possible to see for each of the study sites the remarkable variability in the patterns for each of the river reaches.

Through analysis of the sediment concentrations in local tributaries, Magadzire (2002) determined the probable concentrations for water that would have as its source regional flow such as down the main channel or flow from local sources such as small tributaries entering the floodplain directly. Typically the local sources had lower sediment concentrations, and on occasion an identifiable mixing or perirheic zone (Mertes, 1997) could be measured. The water type graphs shown in Figure 25.9d summarize these measurements by showing the percentage of the different water types present for the each of the study sites for the times as marked. Of interest is that over time the percentages change as the dynamics of each flood are different. The most dramatic changes appear to occur at study sites 5 and 6, where local tributaries seem to contribute significantly to inundation during the 2001 flood.

25.9 THERMAL PROPERTIES

Significant advances have been made in the study of large rivers using the thermal properties of these systems as a data source (Mertes, 2002; Mertes *et al.*, 2004) The simple example shown in Figure 25.9a is designed to illustrate that readily available data from on-line remote sensing data storage sites (www.geog.ucsb.edu/~rivers), especially in the United States, can offer nearly free opportunities for time series analyses of various types. Two thumbnail images from the EROS Data Center were acquired as a download from the internet and analyzed to show the track of the thaw line as summer commenced in the central reaches of the Mackenzie River, Canada. The colour composite for June (Red, Green, Blue are Bands 5,3,4 for Landsat Enhanced Thematic Mapper) is especially amenable to analysis for ice and water properties. The light blue surfaces are ice-covered lakes and the darker blue surface shows the flowing river and thawed lakes to the south of the black 'ice' line.

Figure 25.9 (See also colour plates.) Examples of analyses of water properties using Landsat data. (a) Simple analysis of Landsat colour composites to show progression of thaw across riverine landscape of Mackenzie River. Image on left shows winter conditions while June image on right (colour composite of red, green, and blue applied to Landsat bands 5, 3, and 4 respectively) is used to show position of the ice line marked at the boundary between frozen lakes (light blue) and thawed lakes (dark blue). (b) Comparison of calculation of surface sediment concentration from Landsat and MODIS data for lower Zambezi River. Data shown for 4 March 2001 for both images and surface sediment concentrations are in milligrams per liter. The red box outlines the approximate extent of the Landsat image positioned at path/row 167/72. Numbered rectangles are locations of study sites for which data are shown in (c) and (d). Using the algorithm structure of spectral mixture analysis (Mertes *et al.*, 1993, 2004), these results show that with proper expression of laboratory data, sediment concentration results from different remote sensing instruments are identical. (c) Detail of areas shown in (b) for different dates as derived from Landsat images. Blue lines show the location of theoretical stream channels derived from a morphometric analysis of the GTOPO 30 DEM. (d) Water type graphs for three different flood periods for study sites 5–10 and 13 on Lower Zambezi River as derived from Landsat data. The range of concentrations are for the regional (>60 $mg\,l^{-1}$), perirheic (40–60 $mg\,l^{-1}$, only for 4 March 2001) and local water (0–60 $mg\,l^{-1}$ except for 4 March 2001 when 0–40 $mg\,l^{-1}$). The study site (LSS) that each bar corresponds to is denoted on the x-axis. The number above each bar indicates the inundated area that was detected within the LSS (in km^2). The LSSs are all rectangular boxes with areas of between 350 and 550 km^2

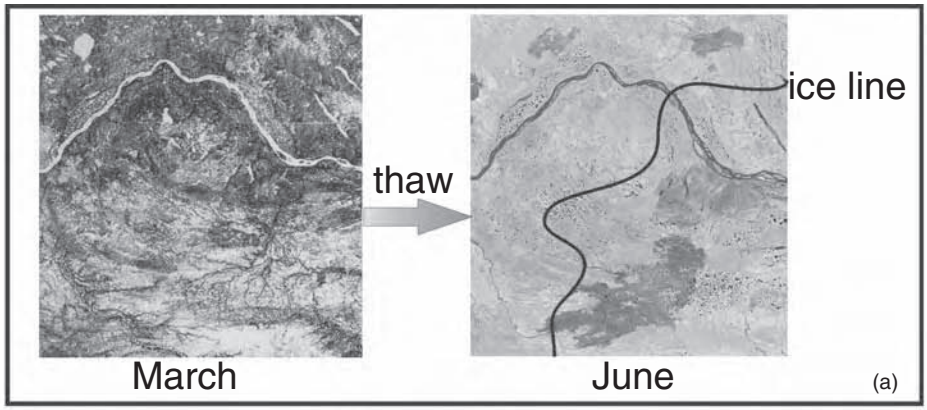
thaw
ice line
March
June
(a)

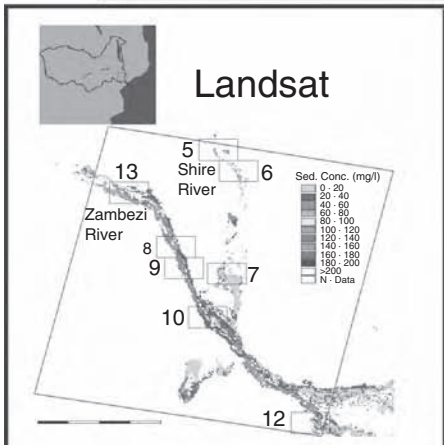
Landsat
5
13
Shire
River
6
Zambezi
River
8
9
7
10
12
Sed. Conc. (mg/l)
0 - 20
20 - 40
40 - 60
60 - 80
80 - 100
100 - 120
120 - 140
140 - 160
160 - 180
180 - 200
>200
N - Data

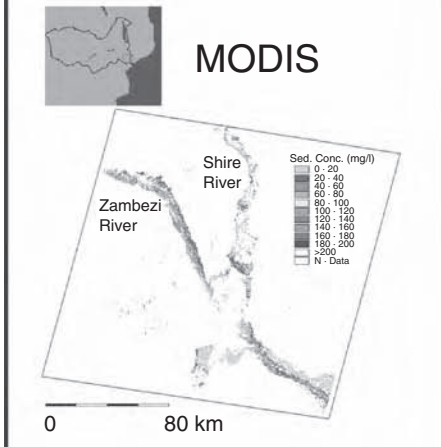
MODIS
Shire
River
Zambezi
River
Sed. Conc. (mg/l)
0 - 20
20 - 40
40 - 60
60 - 80
80 - 100
100 - 120
120 - 140
140 - 160
160 - 180
180 - 200
>200
N - Data
0
80 km
(b)

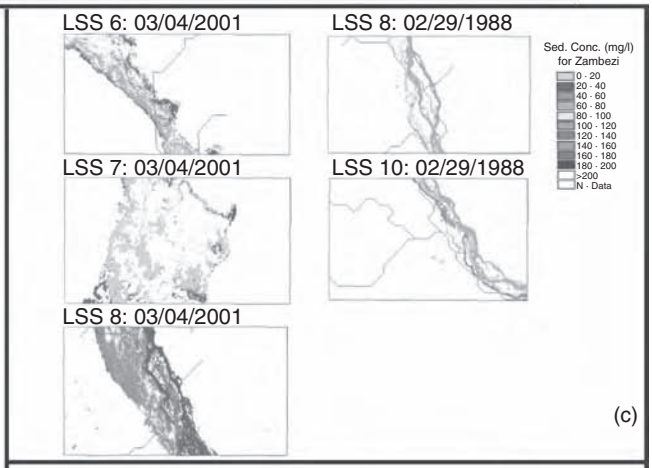
LSS 6: 03/04/2001
LSS 8: 02/29/1988
LSS 7: 03/04/2001
LSS 10: 02/29/1988
LSS 8: 03/04/2001
Sed. Conc. (mg/l)
for Zambezi
0 - 20
20 - 40
40 - 60
60 - 80
80 - 100
100 - 120
120 - 140
140 - 160
160 - 180
180 - 200
>200
N - Data
(c)

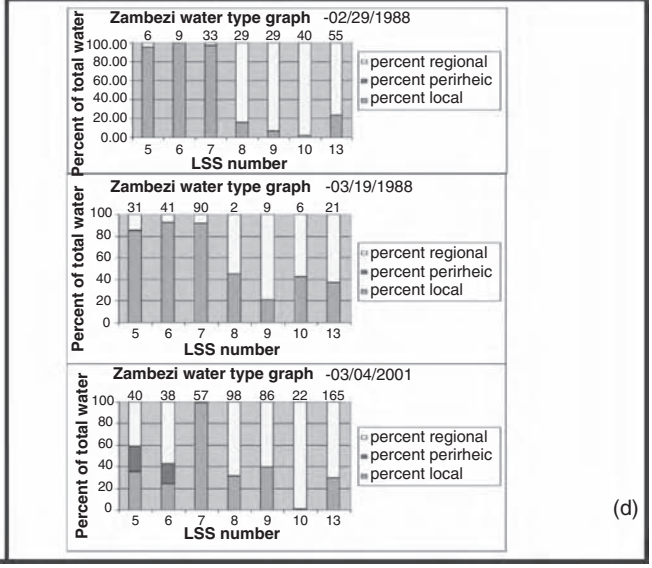
Zambezi water type graph -02/29/1988
6 9 33 29 29 40 55
Percent of total water
100.00
80.00
60.00
40.00
20.00
0.00
5 6 7 8 9 10 13
LSS number
percent regional
percent perirheic
percent local
Zambezi water type graph -03/19/1988
31 41 90 2 9 6 21
100
80
60
40
20
0
5 6 7 8 9 10 13
LSS number
percent regional
percent perirheic
percent local
Zambezi water type graph -03/04/2001
40 38 57 98 86 22 165
100
80
60
40
20
0
5 6 7 8 9 10 13
LSS number
percent regional
percent perirheic
percent local
(d)

25.10 CHANGE DETECTION

25.10.1 Mesopotamian Marshlands

The natural occurrence of floods in rivers is a certain way to alter a landscape. Humans also have had a tremendous influence on the evolution and form of most large rivers, their floodplains, and other large wetlands in the world. Although the Tigris and Euphrates Rivers are not covered separately in this book, the circumstances and severity of the human impact on the Mesopotamian Marshlands at

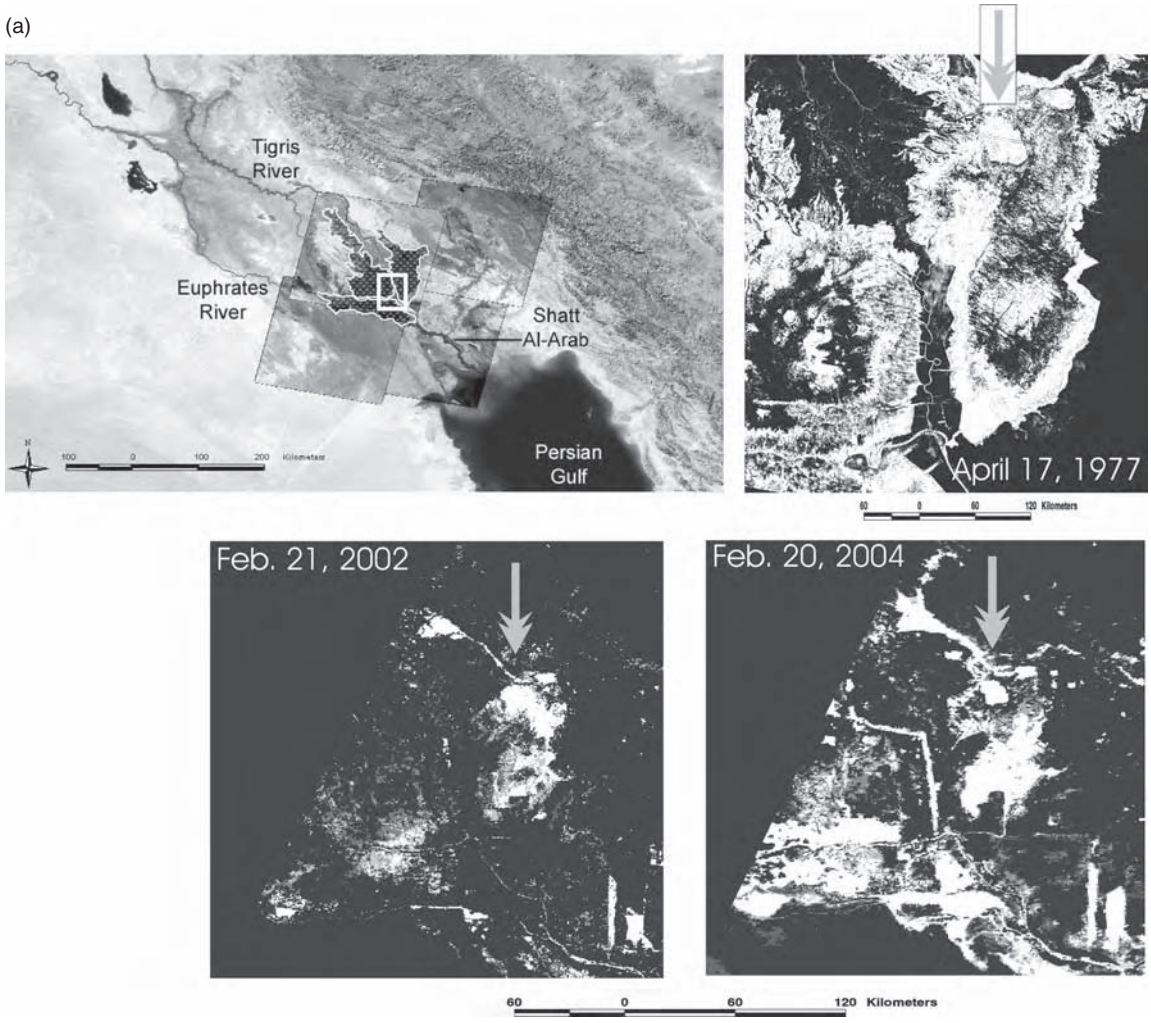

Figure 25.10 (a) Location map showing the Euphrates and Tigris Rivers and the Mesopotamian Marshlands at their confluence. The figure is an overlay of MODIS for the background image and four thumbnail images of Landsat data from the mid-1970s for covering the marsh region. The white box shows the area covered by the 17 April 1977 Landsat image. Slightly smaller areas are covered by the two MODIS images for 21 February 2002 and 20 February 2004. The arrow above the lake is shown for reference. The processing techniques used to achieve the classification of open water (white) and wetland vegetation (greys) are described by Mertes (2004). (Cartography of location map completed by G. Edgar and A. Celay.) (b) Areal cover for open water measured for six Landsat images (1976–1977) and 83 MODIS images (2002–2005). Desert conditions, with areal cover <500 km^2, dominated the landscape from 2002 to early 2003. At the onset of the First US–Iraq conflict in March 2003, water releases increased. The pattern of water releases tracked since mid-2003 shows as a sequence of increases and decreases in the presence of open water in the marshlands, with the maximum levels reached in February 2004 and March 2005

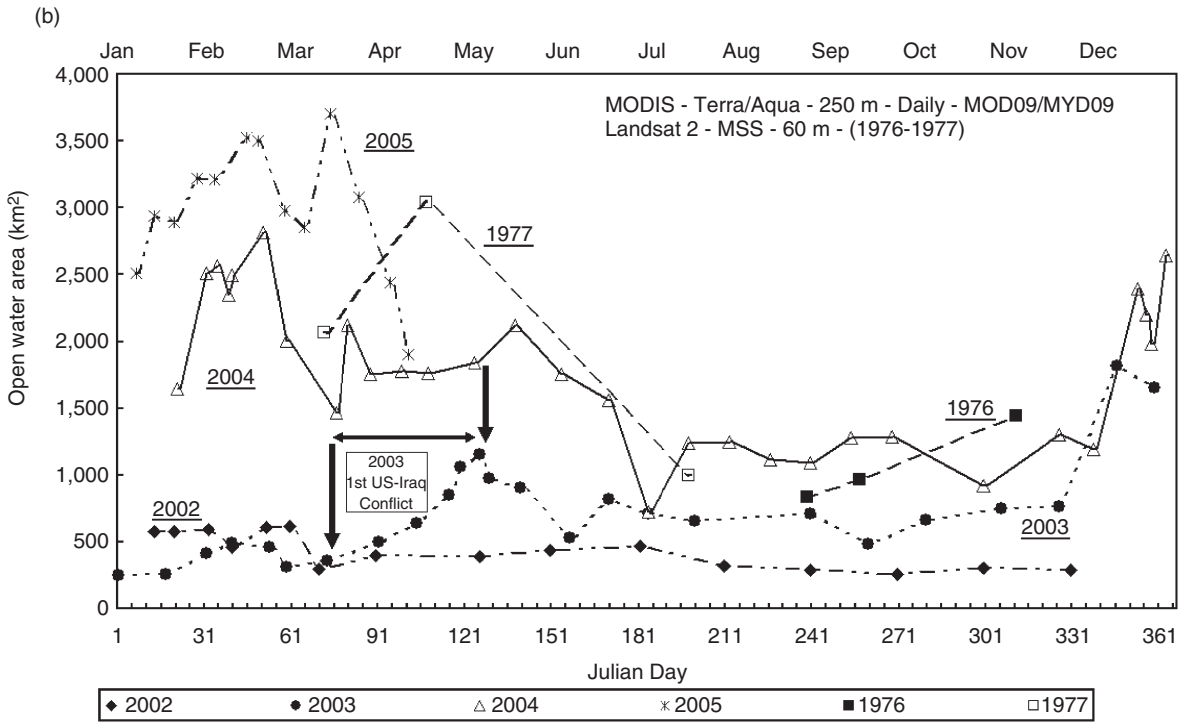

Figure 25.10 *Continued*

their confluence is such that including this as an example of monitoring change with remote sensing seemed appropriate.

One of the more dramatic recent examples of human impact on a floodplain system is the recent destruction of the nearly 10 000 km^2 of the Mesopotamian Marshes in the last two decades of the twentieth century. The marsh areas form at the confluence of the Tigris and Euphrates Rivers (Figure 25.10a). The cultural history of these marshes extends back to at least 3000 BC when the Sumerian culture flourished and gave us the first form of written language (Thesiger, 1964). As we follow the time line to the latter half of the twentieth century it is somewhat remarkable how well these marshes and the culture of the Marsh Arabs survived through multiple governmental changes and construction of dams (Gruen, 2000). Unfortunately – in the space of less than 20 years – some 85% of the marshes were destroyed, mainly due to the construction of dams upstream, and drainage schemes (Partow, 2001), leaving behind a desert landscape (Miller, 2003).

An unexpected consequence of the US–Iraqi conflict that commenced in the winter of 2003 is that increasing amounts of water were released into the marshes – first as a military tactic by the Iraqis (Dixon, 2003) and subsequently in response to an international effort to help restore the marshes (Mertes, 2004). Of particular interest to the work discussed here is our considerably enhanced ability to monitor these types of temporal changes with data from space. As illustrated in Figure 25.10 the three processed remote sensing images show extreme changes in the conditions over a 30-year period. The white areas on the three images for different dates show open water while the grey tones represent vegetation with a varying amount of water. In 1977 the arcuate and natural looking patterns of the marsh areas are relatively intact. Moving to the 2002 image (using the arrow and lake for reference) – we can see that there is essentially no open water during what would be the flood season. Finally, with the unexpected releases related to the Spring 2003 conflict, the open water areas are substantial and studies show some evidence of marsh recovery (Richardson *et al.*, 2005). Yet, the open-water areas are arranged differently with new canals and straightened waterways apparent in 2004. The pattern of relatively high water releases has continued through the winter of 2005. This one example alone shows how our ability to monitor the geomorphic template of

riverine landscapes and its rearrangement through human engineering has advanced rapidly due to the availability of remote sensing data.

REFERENCES

Aalto, R.E. (1995) Discordance between suspended sediment diffusion theory and observed sediment concentration profiles in rivers. MS thesis, University of Washington, 98 p.

Alsdorf, D.E., Melack, J.M., Dunne, T., Mertes, L.A.K., Hess, L.L. and Smith, L.C. (2000) Interferometric radar measurements of water level changes on the Amazon flood plain. *Nature*, 404, 174–177.

Asner, G.P. (2001) Cloud cover in Landsat observations of the Brazilian Amazon. *International Journal of Remote Sensing*, 22, 3855–3862.

Bates, P.D., Horritt, M.S., Smith, C.N. and Mason, D. (1997) Integrating remote sensing observations of flood hydrology and hydraulic modeling. *Hydrological Processes*, 11, 1777–1795.

Birkett, C., Mertes, L.A.K., Dunne, T., Costa, M.H. and Jasinski, M.J. (2002) Surface water dynamics in the Amazon Basin: application of satellite radar altimetry. *Journal of Geophysical Research – Atmospheres*, 107, D20.

Birkett, C.M. (1994) Radar altimetry: a new concept in monitoring global lake level changes. EOS, American Geophysical Union *Transactions – American Geophysical Union*, 75, 273–275.

Brivio, P.A., Dessena, M.A., Zilioli, E., Bolzan, G., Moriondo, S. and Tomasoni, R. (1988) The use of Landsat images over the inland delta of Niger River for the assessment of regional hydrology, in Proceedings of the 22nd International Symposium on Remote Sensing of Environment (ERIM), Abidjan, Cote d'Ivoire, pp. 665–675.

Bryant, R.G. and Gilvear, D.J. (1999) Quantifying geomorphic and riparian land cover changes either side of a large flood event using airborne remote sensing: River Tay, Scotland: *Geomorphology*, 29, 307–321.

Bult, T.P., Haedrich, R.L. and Schneider, D.C. (1998) New technique describing spatial scaling and habitat selection in riverine habitats. *Regulated Rivers–Research and Management*, 14 107–118.

Dixon, R. (2003) Back into the rhythm of the fisherman's life. *Los Angeles Times*, A6 (May 5).

Dunne, T., Mertes, L.A.K., Meade, R.H., Richey, J.E. and Forsberg, B.R. (1998) Exchanges of sediment between the flood plain and channel of the Amazon River in Brazil. *Geological Society of America Bulletin*, 110, 450–467.

Florenzano, T.G. (1998) Landsat-TM and SPOT-HRV image data applied to geomorphologic mapping in a section of Taquari river, Brazil. *Pesquisa Agropecuaria Brasileira*, 33, 1721–1727.

Forsberg, B.R., Hashimoto, Y., Rosenqvist, A. and de Miranda, F.P. (2000) Tectonic fault control of wetland distributions in the Central Amazon revealed by JERS-1 radar imagery. *Quaternary International*, 72, 61–66.

Gomez, B., Smith, L.C., Magilligan, F.J., Mertes, L.A.K. and Smith, N.D. (2000) Glacier outburst floods and outwash plain development: Skeiðarársandur, Iceland. *Terra Nova*, 12, 126–131.

Gruen, G.E. (2000) Turkish waters: source of regional conflict or catalyst for peace? *Water, Air, and Soil Pollution*, 123, 565–579.

Gupta, A., Lim, H., Huang, X. and Chen, P. (2002) Evaluation of part of the Mekong River using satellite imagery. *Geomorphology*, 44, 221–239.

Hayden, B.P. (1988) Flood climates, In: *Flood Geomorphology* (V.R. Baker, R.C. Kochel and P.C. Patton, Eds.). New York, John Wiley & Sons, Ltd, pp. 13–26.

Hess, L.L., Melack, J.M. and Simonett, D.S. (1990) Radar detection of flooding beneath the forest canopy – a review. *International Journal of Remote Sensing*, 11, 1313–1325.

Hess, L.L., Melack, J.M., Novo, E.M.L.M., Barbosa, C.C.F. and Gastil, M. (2003) Dual-season mapping of wetland inundation and vegetation for the central Amazon basin. *Remote Sensing of Environment*, 87, 404–428.

Hirschboeck, K.K. (1988) Flood hydroclimatology, In: *Flood Geomorphology* (V.R. Baker, R.C. Kochel and P.C. Patton, Eds.). New York, John Wiley & Sons, Ltd, pp. 27–49.

Horritt, M.S. (1999) A statistical active contour model for SAR image segmentation. *Image and Vision Computing*, 17, 213–224.

Horritt, M.S., Mason, D., Cobby, D.M., Davenport, I.J. and Bates, P.D. (2003) Waterline mapping in flooded vegetation from airborne SAR imagery. *Remote Sensing of Environment*, 85, 271–281.

Hudson, P.F. (2004) Geomorphic context of the prehistoric Huastec floodplain environments: lower Panuco basin, Mexico. *Journal of Archaeological Science*, 31, 653–668.

Hudson, P.F. and Colditz, R.R. (2003) Flood delineation in a large and complex alluvial valley, lower Panuco basin, Mexico. *Journal of Hydrology*, 280, 229–245.

Jacobberger, P.A. (1988) Mapping abandoned river channels in Mali through directional filtering of Thematic Mapper data. *Remote Sensing of Environment*, 26, 161–170.

Kalliola, R., Salo, J., Puhakka, M., Rajasilta, M., Hame, T., Neller, R.J., Rasanen, M.E. and Arias, W.A.D. (1992) Upper Amazon Channel migration – implications for vegetation perturbance and succession using bitemporal Landsat MSS images. *Naturwissenschaften*, 79, 75–79.

Klemas, V., Borchhardt, J.F. and Treasure, W.M. (1973) Suspended sediment observations from ERTS-1. *Remote Sensing of the Environment*, 2, 205–221.

Lane, S.N., Westaway, R.M. and Hicks, D.M. (2003) Estimation of erosion and deposition volumes in a large, gravel-bed, braided river using synoptic remote sensing. *Earth Surface Processes and Landforms*, 28, 249–271.

Magadzire, T.T. (2002) An investigation into the effect of different water sources on inundation hydrology for selected floodplain reaches of the Zambezi and Limpopo Rivers, Africa. MA thesis, University of California, 148 p.

Meade, R.H. (1985) Suspended sediment in the Amazon River and its tributaries in Brazil during 1982–1984. US Geological Survey Open-File Report, 85–492.

Mertes, L.A.K. (1994) Rates of flood-plain sedimentation on the central Amazon River. *Geology*, 22, 171–174.

Mertes, L.A.K. (1997) Documentation and significance of the perirheic zone on inundated floodplains. *Water Resources Research*, 33, 1749–1762.

Mertes, L.A.K. (2002) Remote sensing of riverine landscapes. *Freshwater Biology*, 47, 799–816.

Mertes, L.A.K. (2004) Synoptic monitoring of water's return to Mesopotamian marshlands. *EOS, American Geophysical Union Transactions*, 33, 309–310.

Mertes, L.A.K. and Mason, J.A. (2002) Floodplain hypsometry of large rivers (abstract), in American Association of Geographers Annual Meeting, Los Angeles.

Mertes, L.A.K. and Warrick, J.A. (2001) Measuring flood output from 110 coastal watersheds in California with field measurements and SeaWiFS. *Geology*, 29, 659–662.

Mertes, L.A.K., Smith, M.O. and Adams, J.B. (1993) Estimating suspended sediment concentrations in surface waters of the Amazon River wetlands from Landsat images. *Remote Sensing of Environment*, 43, 281–301.

Mertes, L.A.K., Dunne, T. and Martinelli, L.A. (1996) Channel-floodplain geomorphology along the Solimões-Amazon River, Brazil. *Geological Society of America Bulletin*, 108, 1089–1107.

Mertes, L.A.K., Dekker, A., Brakenridge, G.R., Birkett, C. and Létourneau, G. (2004) Rivers and lakes, In: *Remote Sensing for Natural Resource Management and Environmental Monitoring: Manual of Remote Sensing* (S.L. Ustin, Ed.). New York, John Wiley & Sons, Ltd, pp. 345–400.

Miller, C. (2003) Garden of Eden fading fast. *Frontiers in Ecology and the Environment*, 1, 173.

Mouchot, M.-C., Alföldi, T., de Lisle, D. and McCullough, G. (1991) Monitoring water bodies of the Mackenzie Delta by remote sensing methods. *Arctic*, 44, 21–28.

Partow, H. (2001) The Mesopotamian Marshlands: Demise of an Ecosystem. United Nations Environmental Program, UNEP/DEWA/TR.01–3 Rev. 1.

Poff, N.L. (1997) Landscape filters and species traits: towards mechanistic understanding and prediction in stream ecology. *Journal of North American Benthological Society*, 16, 391–409.

Portmann, F.T. (1997) Hydrological runoff modelling by the use of remote sensing data with reference to the 1993–1994 and 1995 floods in the River Rhine catchment. *Hydrological Processes*, 11, 1377–1392.

Potter, P.E. (1978) Significance and origin of big rivers. *Journal of Geology*, 86, 13–33.

Ramasamy, S.M., Bakliwal, P.C. and Verma, R.P. (1991) Remote sensing and river migration in Western India. *International Journal of Remote Sensing*, 12, 2597–2609.

Richardson, C.J., Reiss, P., Hussain, N.A., Alwash, A.J. and Pool, D.J. (2005) The restoration potential of the Mesopotamian Marshes of Iraq. *Science*, 307, 1307–1311.

Schneider, D.C. (1994) *Quantitative Ecology: Spatial and Temporal Scaling*. San Diego, CA, Academic Press, 395 p.

Schneider, D.C. (2001) The rise of the concept of scale in ecology. *Bioscience*, 51, 545–553.

Schumm, S.A. (1956) Evolution of drainage systems and slopes in badlands at Perth Amboy, New Jersey. *Geological Society of America Bulletin*, 67, 597–646.

Shimabukuro, Y.E., Novo, E.M. and Mertes, L.K. (2002) Amazon River mainstem floodplain Landsat TM digital mosaic. *International Journal of Remote Sensing*, 23, 57–69.

Sippel, S.J., Hamilton, S.K. and Melack, J.M. (1992) Inundation area and morphometry of lakes on the Amazon River floodplain, Brazil. *Archiv für Hydrobiologie*, 123, 385–400.

Smith, L.C. (1997) Satellite remote sensing of river inundation area, stage, and discharge: a review. *Hydrological Processes*, 11, 1427–1439.

Smith, L.C. (2002) Emerging applications of interferometric synthetic aperture radar (InSAR) in geomorphology and hydrology. *Annals of the Association of American Geographers*, 92, 385–398.

Souza, O.C.d., Araujo, M.R., Mertes, L.A.K. and Melack, J.M. (2002) Form and process along the Taquari River alluvial fan, Pantanal, Brazil. *Zeitschrift für Geomorphologie*, 129, 73–107.

Stolum, H.H. (1998) Planform geometry and dynamics of meandering rivers. *Geological Society of America Bulletin*, 110, 1485–1498.

Thesiger, W. (1964) *The Marsh Arabs*. New York, E.P. Dutton & Co. Inc., 242 p.

Thomson, A.G., Fuller, R.M. and Eastwood, J.A. (1998) Supervised versus unsupervised methods for classification of coasts and river corridors from airborne remote sensing. *International Journal of Remote Sensing*, 19, 3423–3431.

Townsend, P.A. and Walsh, S.J. (2001) Remote sensing of forested wetlands: application of multitemporal and multispectral satellite imagery to determine plant community composition and structure in southeastern USA. *Plant Ecology*, 157, 129–149A.

Tricart, J. (1977) Types de lits de fluviaux en Amazonie brésilienne. *Annales de Geographie*, 473, 1–54.

Verdin, K.L. and Verdin, J.P. (1999) A topological system for delineation and codification of the Earth's river basins. *Journal of Hydrology*, 218, 1–12.

Vörösmarty, C.J., Willmott, C.J., Choudhury, B.J., Schloss, A.L., Stearns, T.K., Robeson, S.M. and Dorman, T.J. (1996) Analyzing the discharge regime of a large tropical river through remote sensing, ground-based climatic data, and modeling. *Water Resources Research*, 32, 3137–3150.

Vörösmarty, C.J., Fekete, B.M., Meybeck, M. and Lammers, R.B. (2000) Geomorphometric attributes of the global system of rivers at 30-minute spatial resolution. *Journal of Hydrology*, 237, 17–39.

Ward, A. (2003) *Weighing Earth's Water from Space*. NASA, Earth Observatory.

Warrick, J.A., Mertes, L.A.K., Siegel, D.A. and McKenzie, C. (2004) Estimating suspended sediment concentrations in turbid coastal waters from multi-spectral SeaWiFS Imagery. *International Journal of Remote Sensing*, 25, 1995–2002.

Witte, E.G., Whitlock, C.H., Usrey, J.W., Morris, W.D. and Gurganus, E.A. (1981) Laboratory measurements of physical, chemical and optical characteristics of Lake Chicot sediment waters. Langley Research Center, 1941.

Witte, E.G., Whitlock, C.H., Harriss, R.C., Usry, J.W., Poole, L.R., Houghton, W.M., Morris, W.D. and Gurganus, E.A. (1982a) Influence of dissolved organic materials on turbid

water optical properties and remote sensing reflectance. *Journal of Geophysical Research*, 87, 441–446.

Witte, W.G., Whitlock, C.H., Morris, W.D. and Gurganus, E. (1982b) Laboratory upwelled radiance and reflectance spectra of Kerr Research Reservoir Sediment Waters. Langley Research Center, 1993.

Wivell, C.E., Olmsted, C., Steinwand, D.R. and Taylor, C. (1993) An earth remote sensing satellite. 1. Synthetic Aperture Radar Mosaic of the Tanana River Basin in Alaska. *Photogrammetric Engineering and Remote Sensing*, 59, 527–528.

Wright, A., Marcus, W.A. and Aspinall, R. (2000) Evaluation of multispectral, fine scale digital imagery as a tool for mapping stream morphology. *Geomorphology*, 33, 107–120.

Yang, X., Damen, M.C.J. and van Zuidam, R.A. (1999a) Satellite remote sensing and GIS for the analysis of channel migration changes in the active Yellow River Delta, China. *International Journal of Applied Earth Observation and Geoinformation*, 1, 146–157.

Yang, X.J., Damen, M.C.J. and Van Zuidam, R.A. (1999b) Use of thematic mapper imagery with a geographic information system for geomorphologic mapping in a large deltaic lowland environment. *International Journal of Remote Sensing*, 20, 659–681.

26

Channel Geometry Analysis Technique for the Lower Mississippi River

Philip J. Soar[1], Colin R. Thorne[2], Oliver P. Harmar[3], David S. Biedenharn[4] and C. Fred Pinkard[4]

[1]*JBA Consulting, Magna House, South Street, Atherstone CV9 1DF, UK and Industrial Research Fellow, School of Geography, University of Nottingham, Nottingham NG7 2RD, UK*
[2]*School of Geography, University of Nottingham, Nottingham NG7 2RD, UK*
[3]*Halcrow Group Ltd., Arndale House, Otley Road, Leeds, LS6 2UL and Industrial Research Fellow, School of Geography, University of Nottingham, Nottingham NG7 2RD, UK*
[4]*Coastal and Hydraulics Laboratory, US Army Engineer Research and Development Center, ERDC, Vicksburg, MS 39180, USA*

26.1 INTRODUCTION

The channel of the Lower Mississippi River is primarily the product of natural flows acting on the floodplain materials over centuries and millennia to form an alluvial stream. However, the modern channel has been modified by engineered channel improvements performed as part of the Mississippi River and Tributaries (MR & T) project. Channel improvement features include meander cutoffs, levees, diversion structures, bank stabilization and low training dykes, which have been constructed to enhance flood control, stabilize the channel and provide sufficient depth for navigation even at times of low water (Moore, 1972). The form of the modern channel has been further influenced by morphological responses to artificial stabilization and training. Historically, morphological adjustments included bank erosion, channel siltation and recovery of some of the sinuosity lost due to artificial cutoffs, though more recently bank erosion, channel migration and planform evolution have all but ceased as revetments now extend along a great proportion of the banklines.

Substantive legislation for the MR & T project, and the initiation of the construction programme, began following the catastrophic flood of 1927, and this event marked the beginning of a new era in terms of channel form and process in the Lower Mississippi River. Since that time, channel dimensions and geometries have evolved under the influence of natural flows, direct engineering interventions and dynamic adjustment driven by process-response feedback loops linking flow hydraulics and channel morphology.

Previous studies by the authors have documented the stage and slope adjustments on the Lower Mississippi River (Biedenharn and Watson, 1997; Biedenharn *et al*., 2000), but the associated changes in channel geometry are only now being fully investigated (Harmar, 2004).

Channel geometry analysis is possible for the Lower Mississippi River thanks to the existence of historical, comprehensive and annual hydrographic surveys of the river. The comprehensive hydrographic surveys, made at approximately decadal intervals since the late nineteenth century, provide valuable information with respect to long-term channel changes during the twentieth century (Harmar *et al*., 2005). However the comprehensive surveys only represent snapshots of channel form at the time when the survey was performed and local adjustments in channel geometry have been observed over much shorter, seasonal

Large Rivers: Geomorphology and Management, Edited by A. Gupta

timescales (Harmar, 2004). While both types of change are important, it is only the longer-term changes that represent the evolution of the river under the action of formative flows and in response to past and present engineering interventions. This evolution is now believed to be more complex than was indicated by analysis of water surface profiles alone (Biedenharn *et al*., 2000; Harmar *et al*., 2005). For this reason it is necessary to investigate changes in channel form based on analysis of the annual hydrographic surveys to elucidate the degree of spatial variability and the nature of short-term changes present in the river.

In this context, the research reported in this chapter concerns a pilot study performed in 2003 to ascertain the feasibility of using annual hydrographic survey data to investigate the channel geometry of the Lower Mississippi River. A test reach was selected between river miles 565 and 618 as the basis for detailed analysis of channel geometry and geometric changes that occurred during the 1990s. This reach was chosen as hydrographic survey data were readily available in electronic format. The aims were to develop a better appreciation of the inherent variability of channel geometry through time and space, and to provide improved geomorphological insights into dynamic adjustments that take place at the reach scale, over annual to decadal timescales. Only by combining knowledge of short-term variability with an understanding of longer-term process-response in the fluvial system will it be possible to separate local adjustments in channel geometry from wider-scale and longer-term channel evolution. Improved understanding of river forms and behaviour will provide a sound basis for future adaptive management and sustainable engineering of the river. As the research reported here was originally submitted to the US Army Engineer Research and Development Center, Vicksburg, the channel geometry analysis was undertaken using imperial units of measurements, although conversion to SI units has been made in the discussion below.

26.2 CONTEXT

26.2.1 Lower Mississippi River Channel Geometry

The Lower Mississippi River flows from the confluence of the Ohio River at Cairo, Illinois to the Gulf of Mexico, east of New Orleans, Louisiana (Figure 26.1). The river exhibits a meandering planform, first flowing through its alluvial valley and, farther downstream, across its deltaic plain. Prior to extensive engineering modification as part of the MR & T project, the Lower Mississippi River featured high rates of lateral channel mobility and was free to adjust its energy gradient through a combination of gradual evolution and avulsive changes to its cross-sectional form and planform geometry. Adjustments were achieved through changes to the width, depth and bar morphology at pools and crossings that were integral to incremental growth and periodic cutoff of meander bends (Schumm *et al*., 1994; Hudson and Kesel, 2000). Winkley (1977) reports that in its natural condition meander bend cutoffs developed quickly though not instantaneously along the river, and that, following a cutoff, the river took 30 to 80 years to regain its pre-cutoff width and bar sequencing. Moreover, cutoffs rarely occurred in multiples (with the exceptions of the occurrence of several cutoffs simultaneously following the New Madrid earthquake of 1811–12 and in response to riparian vegetation clearance along the Lower Mississippi River valley), but rather a long-term balance existed between reaches that were shortened by cutoffs and those being lengthened through meander growth.

During the twentieth century the geomorphology of the Lower Mississippi River was influenced by a series of engineering modifications to improve flood control and aid navigation. Channel slope was artificially steepened and sinuosity reduced by the construction of 14 artificial cutoffs in the reach between Memphis and the Old River distributary during the period 1932–1942 (Figure 26.1). Following the cutoff period, bank stabilization was undertaken along most of the length of the river using articulated concrete mattress and upper bank riprap (Moore, 1972). The effect has been to almost fix the relatively steep, low sinuosity, post-modification morphology of the river into a non-varying planform alignment. This is significant geomorphologically because the Lower Mississippi River can no longer adjust its energy slope through planform adjustments, but is, instead, restricted to making adjustments to its cross-sectional shape and longitudinal profile. MR & T work, as the name suggests, included measures on the tributaries as well as the Lower Mississippi itself. Improved land management practices in the catchment, together with construction of large reservoirs and channel improvement works on the Missouri and other large tributaries are believed by some researchers to have led to a dramatic reduction in suspended sediment load supplied to the Lower Mississippi River (Robbins, 1977). Reduction of upstream supply, coupled with the virtual elimination of sediment input from bank erosion, has been reported to have resulted in a marked reduction in the amount of sediment transported by the Lower Mississippi River (Keown *et al*., 1981; Kesel, 1989; Chapter 9).

Recognition is growing that the geomorphological drivers and behaviour of the Lower Mississippi River have changed as a result of these engineering modifications (Smith and Winkley, 1996; Harmar and Clifford,

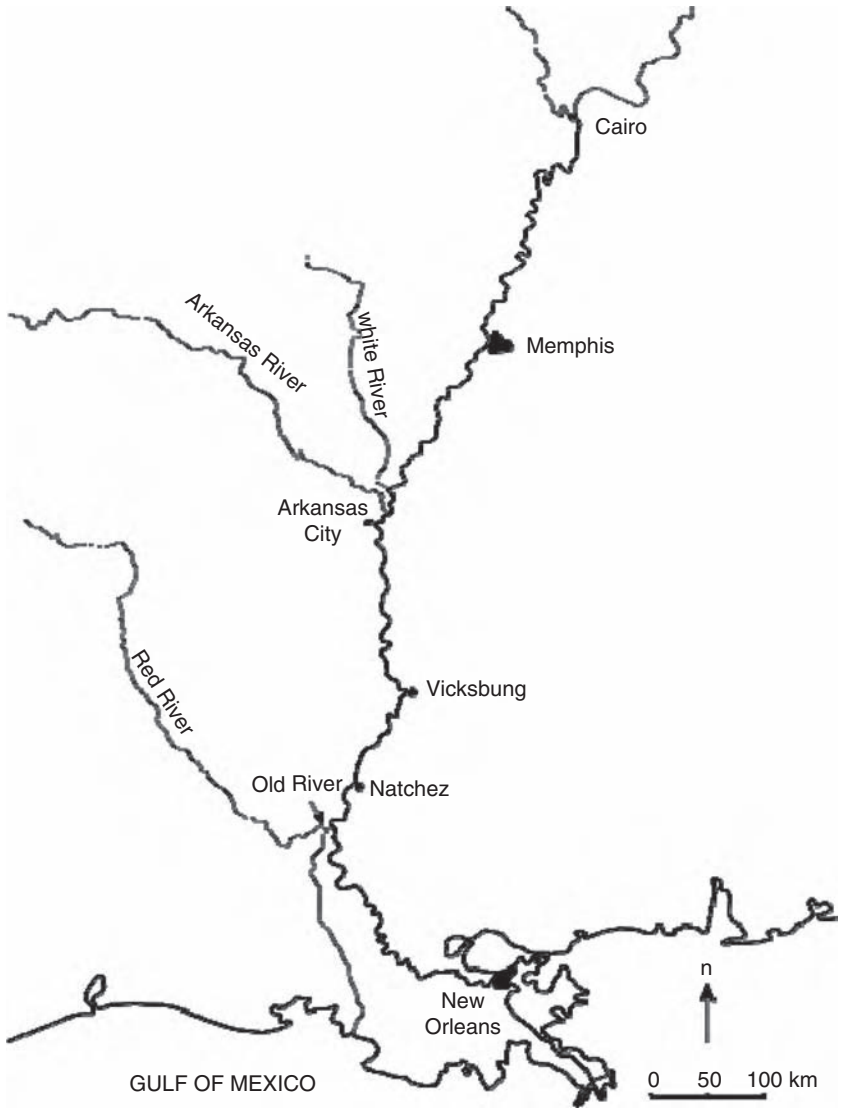

Figure 26.1 Location map showing the Lower Mississippi River, pilot study reach and gauging stations

2006). Accepting that geomorphological change (partly natural and partly in response to engineering interventions and catchment management) is occurring, inevitably leads to the conclusion that improved shorter-term and longer-term channel management strategies require an accurate understanding of how the river responded during the twentieth century and how it is likely to continue evolving during the twenty-first century.

Previously, morphological adjustments in the channel have been inferred from temporal variations in river stages for selected discharges recorded at gauging stations along the Lower Mississippi River (Winkley, 1977). The discharge chosen for basis of comparison was usually that associated with the bankfull stage because this stage has been shown to approximate the dominant or channel-forming flow (Wolman and Miller, 1960; Hey 1975). Winkley (1977) concluded from temporal patterns in bankfull stages at gauging stations that, in the pre-cutoff period, the Lower Mississippi River was a stable system between Cairo, IL and Natchez, MS. Biedenharn and

Watson (1997) subsequently analysed specific gauge records for stations between Cairo and the Old River distributary in the post-cutoff period between 1950 and 1994 to propose a pattern of response through adjustments to the long profile at the regional scale (Figure 26.2).

Upstream of Arkansas City, the specific gauge records analysed by Biedenharn and Watson (1997) suggest a degradational trend during the late twentieth century, while downstream of Vicksburg the records suggest an aggradational trend. The absence of a significant trend in the reach between Arkansas City and Vicksburg has been interpreted as indicating that a 'hinge zone' of relative stability existed there during the late twentieth century. Hence, this model presents evidence to suggest that at the reach scale, the river responded to the cutoffs in a manner broadly similar to the type of morphological response associated with a single cutoff (as outlined by Lane, 1947).

Biedenharn and Watson's model provides a useful overview of geomorphological response, but its utility for future planning of river management is limited for two reasons. First, while specific gauge records reveal spatial and temporal variations in the water surface, these do not necessarily represent changes at the channel bed because changes in flow resistance are unaccounted for. Second, the simplicity of the model inevitably masks important details of reach and sub-reach scale morphological behaviour. These issues are explored further using the decadal comprehensive hydrographic surveys by Harmar (2004) and Harmar *et al*. (2005). Schumm *et al*. (1994) have described the importance of neotectonic activity and geological factors in influencing pre-modification morphological behaviour at the reach and sub-reach scales. However, no study has investigated the continued importance of such influences on morphological behaviour during the post-modification period, and this is an urgent research need.

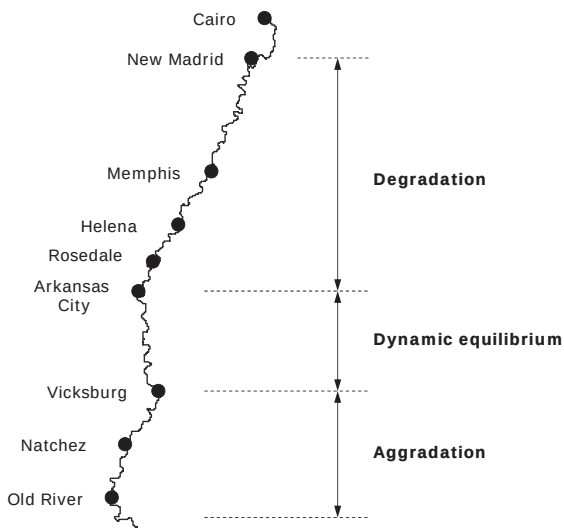

Figure 26.2 Regional scale adjustments to the longitudinal profile in the period 1950–1994, proposed by Biedenharn and Watson (1997) from analysis of specific gauge records

Hydrographic survey data collected during the late nineteenth and twentieth centuries can be used to improve understanding of long-term river behaviour because these data characterize morphological changes *directly* through examination of the bed topography, rather than indirectly through specific gauge records. Also, analysis of the survey data provides much finer spatial and temporal resolution than specific gauge records because surveyed sections are spaced a few tens or hundreds of metres apart while gauges are spaced at intervals of tens of kilometres along the channel.

26.3 DATA ACQUISITION AND PRE-PROCESSING

26.3.1 Pilot Study Reach

To explore the potential for channel geometry analysis using hydrographic survey data, a pilot study reach was selected between river miles 565 and 618 (Figure 26.1), for which data were readily available (river miles are counted upstream from the mouth of the Mississippi). The nearest gauging stations are Arkansas City at river mile 554.1, Rosedale at river mile 592.2 and Helena at river mile 663.1. The reach includes the confluences of the Arkansas and White Rivers with the Mississippi. Annual hydrographic surveys performed by the Vicksburg District, Corps of Engineers between 1992 and 2001 were obtained to represent channel variability and adjustment at a sub-decadal timescale. Cross-sections were surveyed at intervals of approximately 1000–1100 ft along the channel, with annual surveys repeated at the same fractional river miles. In general, the position of each cross-section varies by less than 100–150 ft, or 10% of the distance between successive cross-sections, which is considered to be an acceptable level of variability for this study.

26.3.2 Low Water Reference Plane

In extracting data to define the channel geometry from hydrographic surveys conducted on different dates, it is necessary to reference all elevations to a common datum.

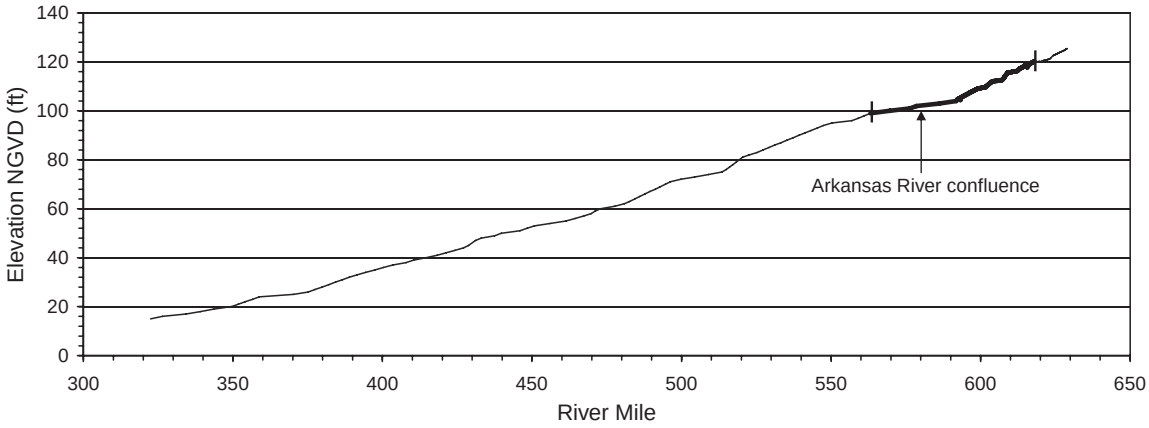

Figure 26.3 LWRP elevations in the Lower Mississippi computed by the Vicksburg District (including elevations computed by the Memphis District above RM 592). Thick line delimits the extent of the profile used in this study

In this study, the Low Water Reference Plane (LWRP) of the Mississippi River was used for this purpose. The LWRP was established by the US Army Corps of Engineers to set the crown elevations for dykes and other engineering works. It is also used by navigation interests as a guide to the depth of water available at critical locations in the river.

LWRP elevations along the Mississippi River are developed from stages computed at individual gauging stations based on the 97% exceedance flow for a specified period of record (typically from 1954 to the time of computation) being applied to a series of rating curves for a recent period (typically the past 10 years). This study used the most recent LWRP, which was computed in 1993 using the 1954 to 1991 flow period of record and 1982 to 1991 rating curves (Figure 26.3).

As this study has centred on an analysis of channel geometry above the LWRP, variability in the morphology of the bed due to bedforms, such as migrating dunes, cannot be discerned at this scale of analysis and is therefore not an objective of this study.

26.3.3 Separation of Bends and Crossings

A salient feature of most rivers, including the Lower Mississippi River, is local variability in the cross-sectional geometry of meander bends and crossings. It follows that useful additional information on the variability of channel geometry is obtained if cross-sections within bend reaches and crossing reaches are considered separately. Consequently, a channel planform curvature parameter was developed to discriminate between bends and crossings, with separate channel geometry analyses being performed for each, in addition to the full data set of all cross-sections in each annual survey.

The technique assumes that meander bend and crossing 'reaches' can be suitably distinguished based solely on changes in channel curvature between successive cross-sections (Figure 26.4). The process adopted involved:

(1) plotting the point in each cross-section with the lowest elevation, the thalweg (not the centreline, as there are marked discontinuities along the study reach where the length of cross-section changes markedly over a very short distance);
(2) smoothing the line using MapInfo GIS software (particularly within the crossing reaches where the deepest point in the channel is not always clearly defined);
(3) applying a macro to calculate the absolute (positive) change in channel direction between cross-sections;
(4) applying a smoothing algorithm using Tecplot data processing and visualization software to define similar reaches.

The approach revealed that bend and crossing sub-reaches tend to be distinguished by a threshold of about 5° of change in channel direction between consecutive cross-sections. The final classification scheme therefore defined bend reaches as having a change in direction greater than 6°, crossing reaches less than 4° change, and transitional reaches between 4° and 6° change (Figure 26.5).

26.3.4 Divided Channels

While the modern Lower Mississippi River predominantly has a single-thread, meandering channel, it does exhibit

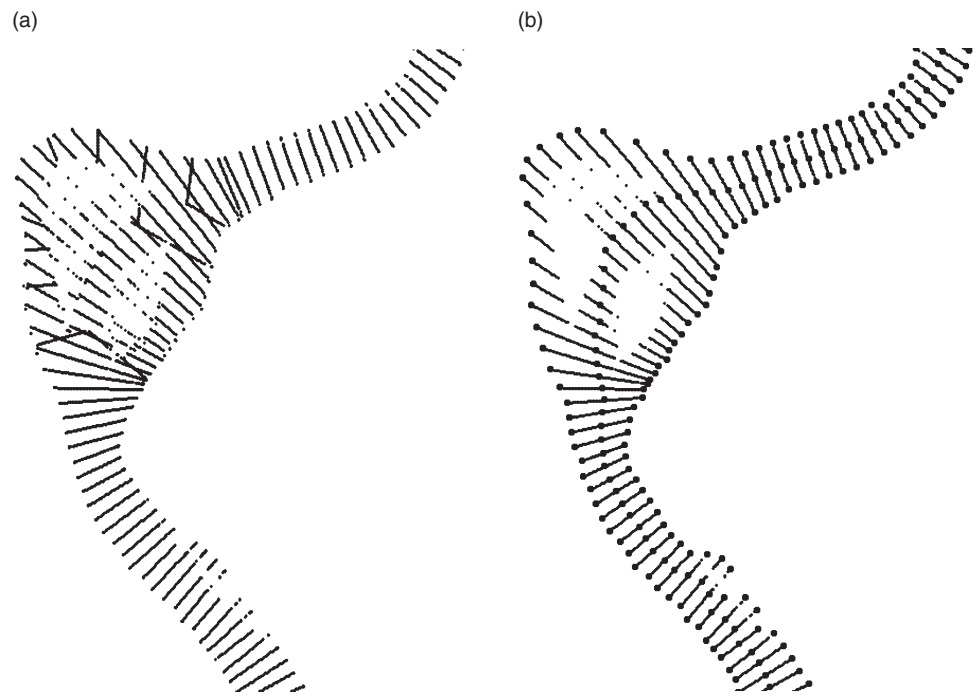

Figure 26.4 Example of initial data processing: (a) original cross-sections plotted in ESRI Arc View 3.3 GIS and (b) processed cross-sections following initial removal of 'problem' data and application of automated routines (Harmar, 2004)

some reaches with divided channels. These are often found in asymmetrical cross-sections with wide point bars and chute channels. Clearly, the cross-sectional geometry of divided reaches with secondary channels differs to that of single-thread reaches. Given the ecological importance of secondary channels, information on the geometry of such reaches is of interest. Care was therefore taken to identify cross-sections located within reaches with divided channels and treat them separately to explore the possibility of defining separate channel geometry analyses for these reaches.

To meet this objective, where secondary channels were present in a cross-section, the width, average depth, etc., were calculated for both the entire cross-section (all channels added together) at the specified elevation and then for just the primary channel, defined as that part of the cross-section containing the lowest elevation. The effect on the channel geometry analysis was, however, found to be minor when considering the reach as a whole and only very localized when comparing the geometry of individual cross-sections, because secondary channels are uncommon and, where they do exist, they tend to become included within the primary channel at elevations at or about LWRP.

26.3.5 Pre-Processing Procedure for Hydrographic Survey Files

Pre-processing of the hydrographic survey data was undertaken at the University of Nottingham as part of a doctoral research project (Harmar, 2004). The objective of pre-processing was to develop a series of automated routines for extracting survey data pertaining to individual cross-sections as stand alone text files from the full data set of each annual survey, originally compiled in GIS format.

Each annual hydrographic survey file for the period 1992–2001 was obtained in Microstation design file format (.dgn) from the USACE Vicksburg District Office, Vicksburg, MS. Four stages of data pre-processing were then applied:

(1) extraction of xyz hydrographic coordinates into a standard text file;
(2) identification of individual cross-sections;
(3) sorting of cross-sections into the downstream order;
(4) rectifying the cross-section points into straight lines.

Once pre-processing was complete, a final visual inspection was undertaken. This involved displaying the com-

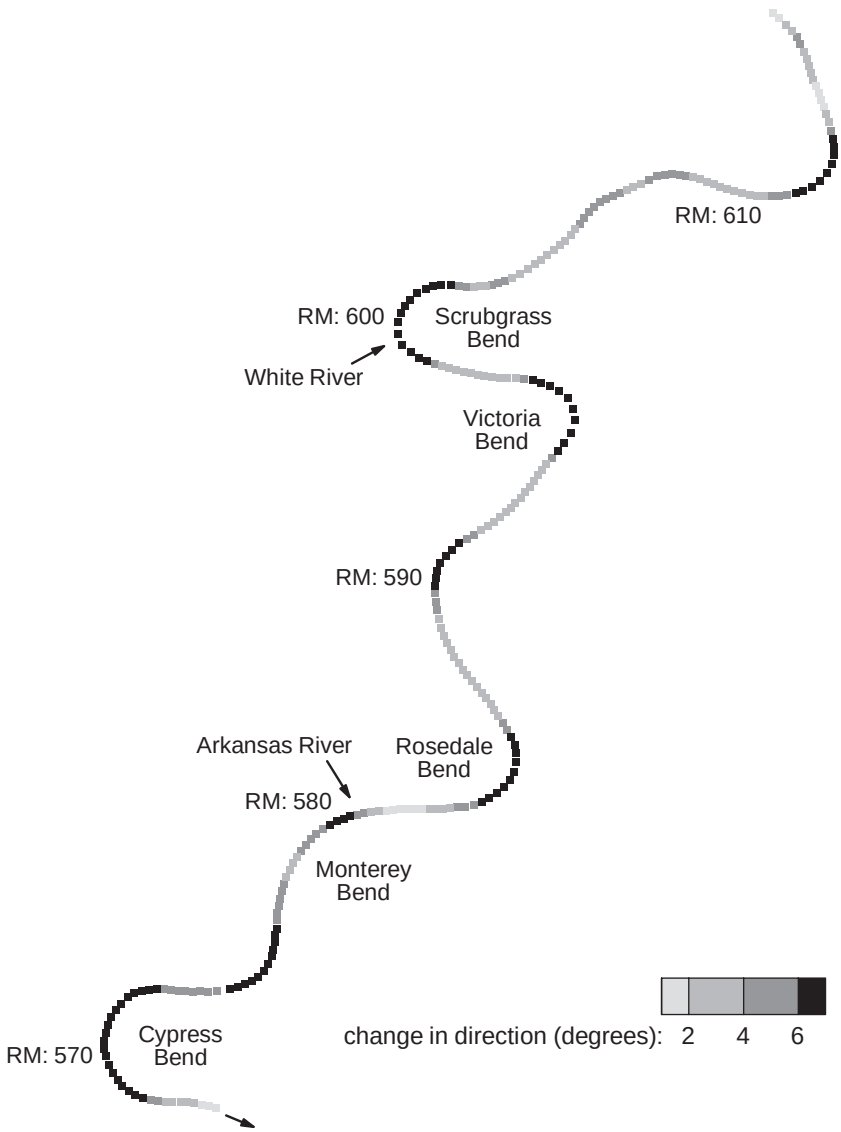

Figure 26.5 Change in channel direction (positive) between cross-sections

puted centre-point and associated left and right bank coordinates for each cross-section in a GIS layer (Figure 26.4).

26.3.6 Data Projection

Corpscon (Corps conversion) software, developed by the US Army Topographic Engineering Center (TEC), was used to convert all cross-section point coordinates to the regional standard, NAD 1983, Universal Transverse Mercator (UTM) Zone 15 system. All elevations are given in US customary units and are referenced to the National Geodetic Vertical Datum of 1929 (NGVD29).

26.3.7 Cross-Section Screening

The first task in processing the cross-sectional data was to 'screen' the cross-sections and determine how far above LWRP each one extends. This was essential to check the feasibility of analyzing channel geometry distributions for

Table 26.1 Results of initial screening of cross-sections

Year	<LWRP	>LWRP	>LWRP + 5 ft	>LWRP + 10 ft	>LWRP + 15 ft	>LWRP + 20 ft	>LWRP + 25 ft	>LWRP + 30 ft	Total
1992	188	68	51	34	19	10	0	0	256
1993	196	60	25	8	0	0	0	0	256
1994	126	153	119	62	6	1	0	0	279
1995	196	60	25	6	0	0	0	0	256
1996	36	220	185	5	5	0	0	0	256
1997	23	233	230	226	213	194	81	6	256
1999	127	132	79	48	5	0	0	0	259
2000	245	11	0	0	0	0	0	0	256
2001	50	205	184	163	131	100	87	64	255

Table 26.2 Revised screening of cross-sections, following limited extrapolation

Year	<LWRP	>LWRP	>LWRP + 5 ft	>LWRP + 10 ft	>LWRP + 15 ft	>LWRP + 20 ft	>LWRP + 25 ft	>LWRP + 30 ft	Total
1992	159	97	67	50	31	17	7	0	256
1993	158	98	63	27	6	0	0	0	256
1994	107	172	153	119	66	14	1	1	279
1995	141	115	77	35	5	0	0	0	256
1996	30	226	201	175	36	5	4	0	256
1997	14	242	233	230	224	203	190	115	256
1999	60	199	158	82	48	11	1	0	259
2000	126	130	35	0	0	0	0	0	256
2001	41	214	208	187	160	134	105	91	255

the separate years and the elevations proposed. The results (Table 26.1) indicate that the vertical extent of cross-sections varies widely between years. For example, the dataset for the year 2000 is of limited use as this was a very low flow year and the survey was only undertaken for the wetted perimeter. In contrast, cross-sections for high water years, such as 1992, 1994, 1997 and 2001, extend to higher elevations and cover a greater range of elevations above LWRP.

Initial screening adopted a strict approach whereby a cross-section was excluded if either of its end points fell below the specified elevation, even by a small amount. In this initial process, many cross-sections that fell just short were excluded by this criterion. A sensitivity analysis was performed to investigate whether limited linear extrapolation of cross-sections would improve matters significantly. The final scheme adopted was to allow extrapolation of the bank for a vertical distance of 3.05 m (10 ft) if the bank slope (vertical to horizontal) was greater than 0.2 (which corresponds to banks covered by revetments, where it may be assumed that the steep slope of the bank is likely to continue to a higher elevation) and extrapolation through a vertical distance of 1.52 m (5 ft) if the bank slope was between 0.025 and 0.2. Cross-sections with flatter side slopes were not extrapolated at all, due to uncertainty concerning the topography of low angle, shelving banks. The revised cross-section screening results are listed in Table 26.2.

The outcome of the extrapolation process varies between years, but overall it assisted in developing a substantially larger dataset for undertaking channel geometry analysis. At the LWRP elevation, extrapolation has had a negligible impact in 1996, 1997 and 2001 (the latter two years being high water years) but a large impact in 1995, 1999 and 2000. However, at higher elevations, the impact in the higher water years was marked, with, for example, an additional 170 cross-sections included in 1996 for 3.05 m (10 ft) above LWRP and an additional 109 cross-sections included in 1997 for both 7.62 m (25 ft) and 9.14 m (30 ft) above LWRP.

26.4 ANALYTICAL APPROACH AND METHODOLOGY

26.4.1 Channel Geometry Analysis

For each cross-section, the width, average depth, maximum depth, wetted perimeter, hydraulic radius and cross-section

area were calculated at the water surface elevation corresponding to LWRP and at 0.30 m (1 ft) increments above this, up to LWRP + 9.14 m (30 ft), which corresponds approximately to bankfull stage identified by Biedenharn and Thorne (1994), or once the elevation was greater than either of the cross-section end points. This involved two analytical stages:

First, a macro was used to prepare the data into a suitable format for calculating the above parameters. This macro included:

(1) extending the cross-section according to the criteria previously discussed;
(2) calculation of the distance between cross-section points;
(3) calculation of the elevation difference between the interpolated LWRP and both cross-section end points and then recording the lowest. This became the largest 'Elevation above LWRP' for which the channel geometry analysis was undertaken (and also facilitated the development of Tables 26.1 and 26.2);
(4) calculation of the Easting and Northing coordinates of the deepest point in each cross-section (used to calculate changes in channel direction for defining bend and crossing reaches).

The second stage involved calculation of the channel geometry parameters. A further macro was used to undertake the calculations and involved dividing each cross-section into vertical panels, calculating the top width, wetted perimeter (for channel boundaries only) and cross-section area of each panel and then summing these values to find the cross-section totals. The average depth was defined as the ratio of the cross-sectional area to the total width and the hydraulic radius as the ratio of the cross-section area to the wetted perimeter. The procedure was applied to the main channel only in cross-sections with a secondary channel (see discussion on divided reaches above).

26.4.2 Probability Analysis

Conventional hydraulic geometry analysis involves developing power-law relations to predict various channel geometry parameters. However, examination of the variation of width, average depth, etc., with elevation above LWRP did not reveal the type of close association that is normally required to define a best-fit regression line. Instead, for a given elevation above LWRP, it was apparent that there are wide-ranging values of width, depth, etc., and fitting any type of best-fit line would not only be questionable statistically, but would also obscure the inherent variability in channel geometry that is an important characteristic of the Lower Mississippi River. Clearly, an alternative technique was required to 'capture' this variability, display it and represent how it changes with elevation above LWRP, downstream location and between annual surveys, without any loss in information.

For each annual dataset, the approach adopted was to plot elevation above LWRP against channel geometry parameter for each cross-section on the same graph. Then, each data point on the graph was assigned a cumulative probability (from 0 to 1), which can be interpreted as the probability of the channel geometry parameter being less than or equal to that particular data value, at the chosen elevation above LWRP (Stage 1). These probabilities were then rectified to a regular grid by linear interpolation, first along the y-axis for each 0.30 m (1 ft) increment above LWRP (Stage 2) and then across the remainder of the grid (Stage 3). This procedure is illustrated for width in Figure 26.6, which also demonstrates the high degree of variability that has warranted this probabilistic approach. With each annual dataset, the probability analysis was repeated for each channel geometry parameter, firstly for all cross-sections in the study reach, secondly for those cross-sections located in pool sub-reaches and thirdly for those cross-sections located in crossing sub-reaches.

To avoid misleading representations of probability distribution associated with very small sample sizes, cumulative probabilities for each elevation above LWRP were calculated only if they contained at least 10 cross-sections that extended above that elevation. Thus, many of the final plots do not extend as far as 4.57 m (15 ft) above LWRP and very few go all the way up to 9.14 m (30 ft) above LWRP. Finally, the 50th percentile line was calculated and plotted on the cumulative graphs to illustrate how the median channel width varied with stage for that survey date. A series of Visual Basic macros and Tecplot processing and visualization routines were used to undertake these processes.

26.4.3 Spatial Analysis

Spatial analysis was undertaken to explore how channel geometry varied along the study reach at the time of each hydrographic survey. The approach involved plotting the location of each cross-section as a series of symbols on a map of the river in the study reach and colouring the symbols according to the value of width, average depth, etc.

As the precise locations of the cross-sections established in each of the hydrographic surveys vary only slightly, for visualization purposes (and to facilitate the temporal analysis described below) the 2001 survey was

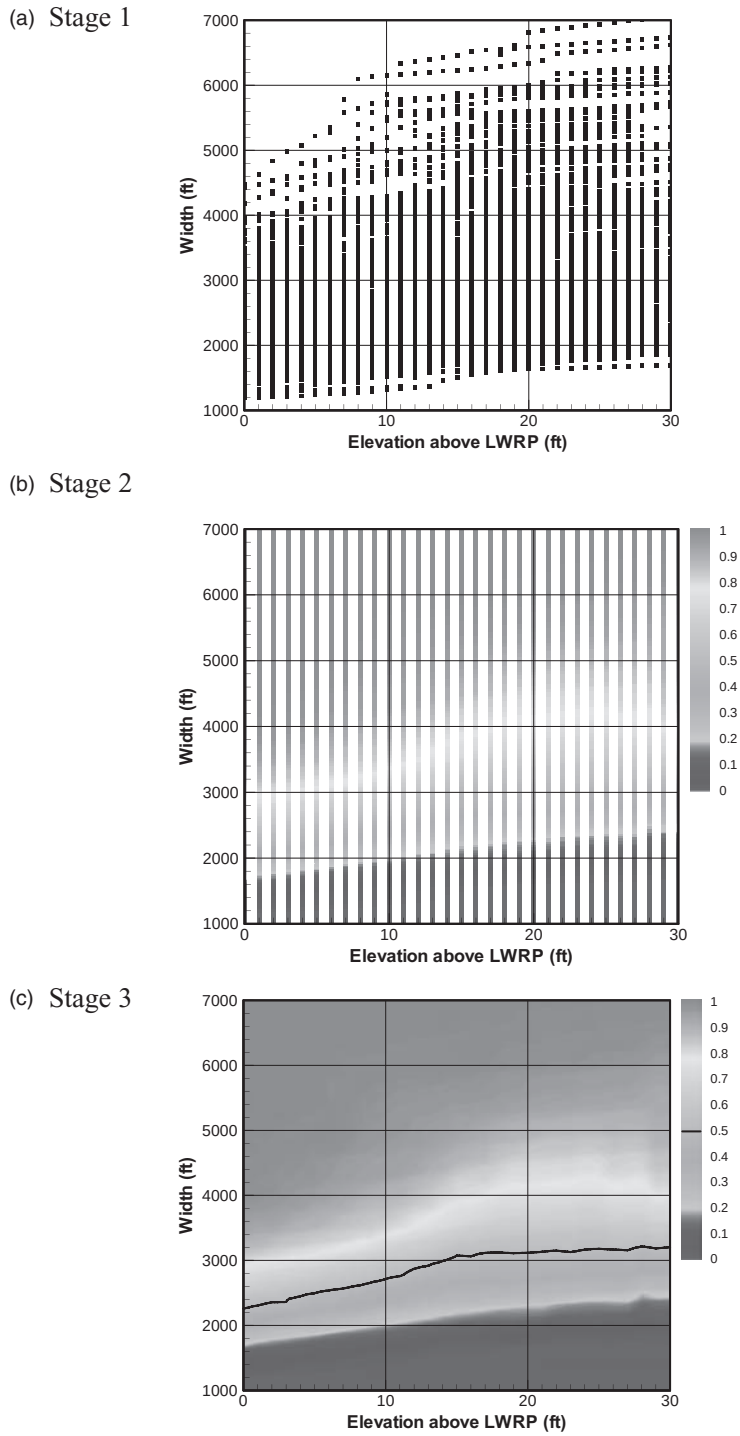

Figure 26.6 (See also colour plates.) Development of cumulative frequency plots of channel geometry variability with elevation above LWRP. (a) Stage 1: plotting data values for each cross-section. (b) Stage 2: assigning probability (0 to 1) and interpolation along the y-axis. (c) Stage 3: interpolation of probability across the remainder of the grid, showing the 50% probability line. The example shown is for width in the 1997 survey

used to represent the location of each cross-section for all years. Values for cross-sections that could not be calculated (because one or both end points did not extend above the specified elevation) were interpolated from neighbouring sections. If less than 10 cross-sections were available, then no values were shown in the final plots as results for the specified elevation above LWRP were unsuitable for spatial analysis due to the very small sample size.

26.4.4 Temporal Analysis

Temporal analysis was performed to reveal fluctuations and/or trends of change in channel geometry during the 1990s. The analysis used the same graphical format as the spatial analysis, but with the cross-section symbols coloured according to the direction and magnitude of change in average depth and change in cross-section area between annual surveys and over the period of observation, 1992–2001. As all parameters are referenced to a fixed datum (LWRP), changes in average depth are indicative of aggradation/degradation within the study reach, while changes in cross-section area highlight zones of scour and fill.

The temporal analysis was only undertaken for the LWRP elevation as the large number of interpolated values at higher elevations could generate misleading patterns of channel change.

26.5 RESULTS

26.5.1 At-a-station Channel Geometry

Archived results

The database and results generated by the probability, spatial and temporal analyses are not amenable to publication in printed format because there are, in total, 1305 plots (324 for the probability analysis, 945 for the spatial analysis, and 36 for the temporal analysis). Instead they can be obtained by contacting the first author at JBA Consulting or the second author at the University of Nottingham. The archive contains all the cross-sectional data, with Eastings and Northings referenced to the NAD 1983, Universal Transverse Mercator (UTM) Zone 15 coordinate system. Elevations are given in US customary units (feet and tenths) as these are the units in which the original observation were made, and are referenced to the National Geodetic Vertical Datum of 1929 (NGVD29). The main functionality of the data archive is its interactive browser facility which permits users to navigate through the plots and scroll through different years to examine central tendencies, variability and changes in channel geometry at will. Complete instructions for using the browser are provided.

Results for at-a-station channel geometry

Sample results from the probability analysis used to display at-a-station channel geometry are illustrated in Figure 26.7. Each plot in Figure 26.7 represents data from a single annual hydrographic survey and for a single channel geometry parameter. The first two plots represent channel geometry for cross-sections located firstly in bend reaches and secondly in crossing reaches. The full set of results is available in the interactive archive.

26.5.2 Spatial Variability and Adjustments

Sample results from the spatial analysis to examine how channel geometry parameters vary along the study reach are illustrated in Figure 26.8. The full set of results is available in the interactive archive.

26.5.3 Temporal Variability and Adjustments

Sample results from the temporal analysis, used to examine how average depth and cross-section area within the study reach change between years and over the period of record (1992–2001), are illustrated in Figures 26.9 and 26.10. The results are relative to LWRP, which provides a time-invariant reference plane. Aggradation and degradation can be inferred from the changes in average depth shown in Figure 26.9, while scour and fill can be inferred from changes in the cross-sectional area shown in Figure 26.10. The full set of results is available in the interactive archive.

26.6 INTERPRETATION AND COMMENTARY

26.6.1 Channel Geometry Analysis

With over 1300 plots in the results database, the following commentary summarizes the channel geometry characteristics for the 1992–2001 period as a collective dataset only and differences between annual surveys are reserved for the discussion on temporal variability.

Width

The results indicate that, in the study reach, channel width at LWRP fluctuates around a value of 670 m (2200 ft) ± 61 m (200 ft), with bends ranging 625–823 m (2050–2700 ft) being generally wider and more variable in width

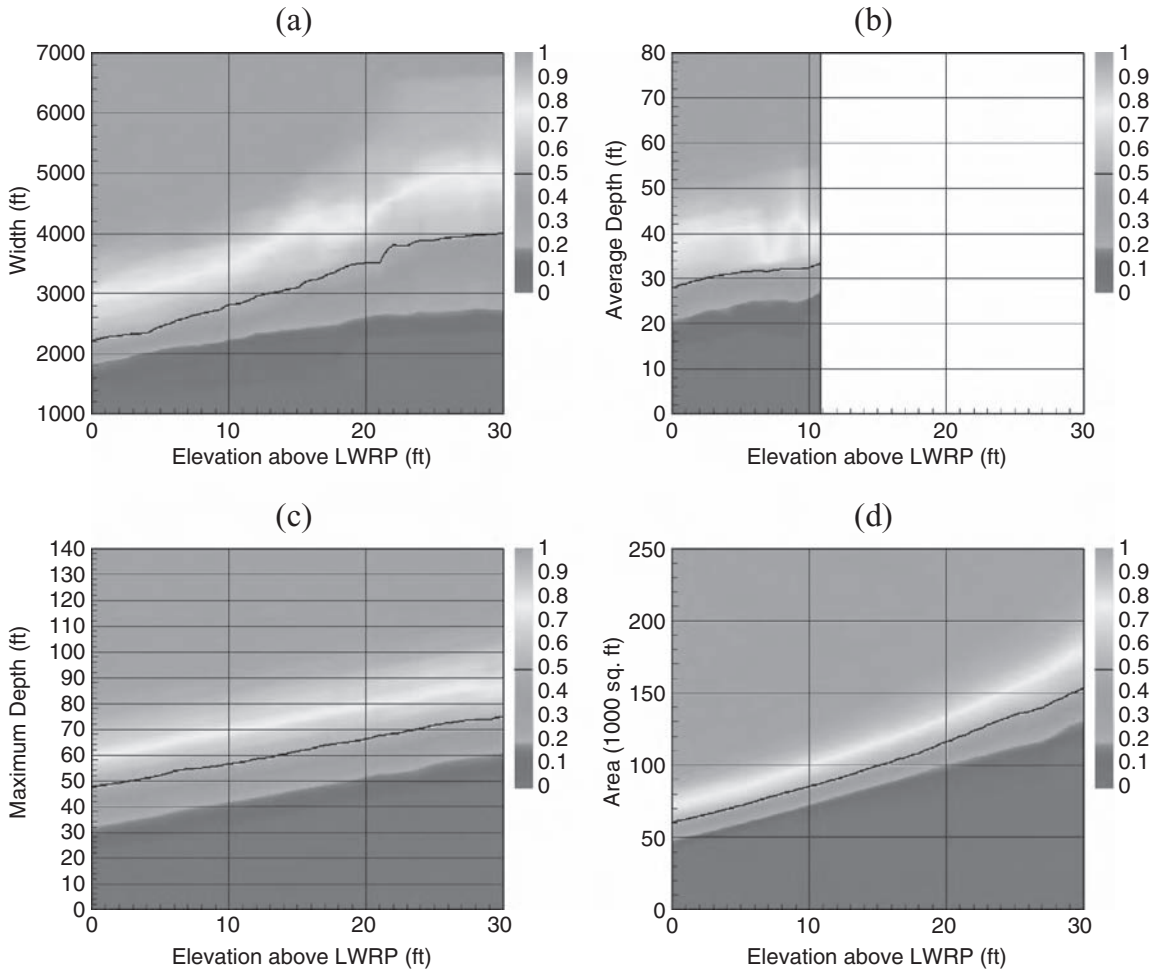

Figure 26.7 (See also colour plates.) Sample results from the probability analysis: (a) width in 2001 for bends; (b) average depth in 1995 for crossings; (c) maximum depth for all sections in 2001; (d) cross-sectional area in 1997 for all sections

than crossings ranging 533–670 m (1750–2200 ft). Channel width appears to increase with stage more rapidly at bends than at crossings. At high stages [based on LWRP + 6 m (20 ft)], channel widths in bends and crossings converge and are consistently around 945 m (3100 ft). Unfortunately, due to limitations in the hydrographic surveys, extrapolation to the bankfull stage is not possible.

Average depth

Channel average depth at LWRP fluctuates about 8.5 m (28 ft), ranging between 7.6 and 9.8 m (25 and 32 ft). Bend and crossing average depths are generally similar, although the inter-quartile range for crossing average depths is usually wider than that for bends. In high water years, average depths are approximately equal at bends and crossings. The high flow channel average depth [based on LWRP + 6.10 m (20 ft)] is usually 10 to 11 m (33 to 37 ft).

Maximum depth

The relationship between maximum depth and elevation above LWRP should be linear by definition. Deviations from linearity present in the results reflect data limitations. They occur because as stage increases, the number of cross-sections with data decreases, producing changes in the sampled data and nonlinearity in the median line.

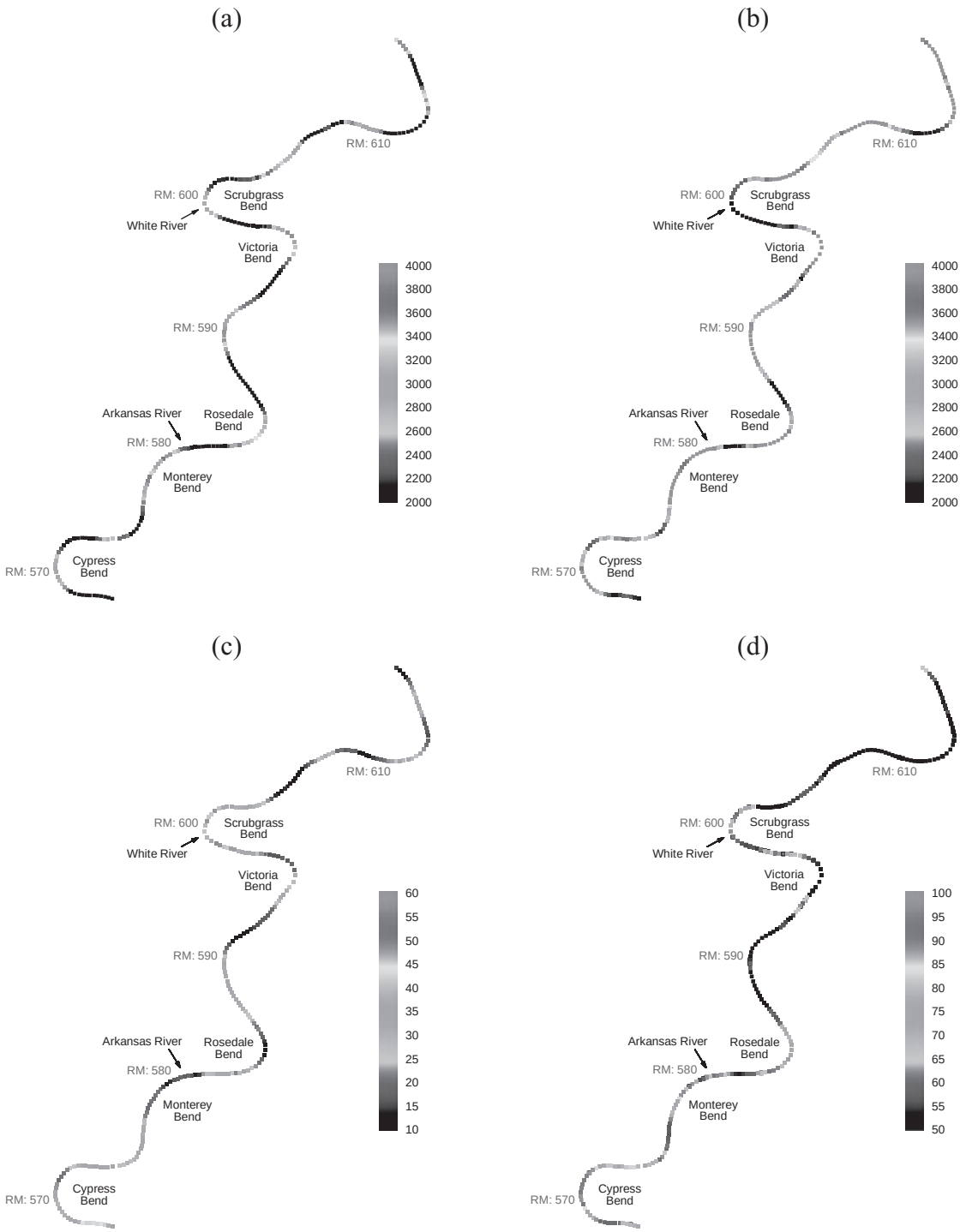

Figure 26.8 (See also colour plates.) Example results from the spatial analysis: (a) width (ft) in 1997 at LWRP; (b) width (ft) in 1997 at 20 ft above LWRP; (c) average depth (ft) in 2001 at LWRP; (d) area (1000 ft^2) in 1996 at LWRP (this plot also shows interpolated values in white)

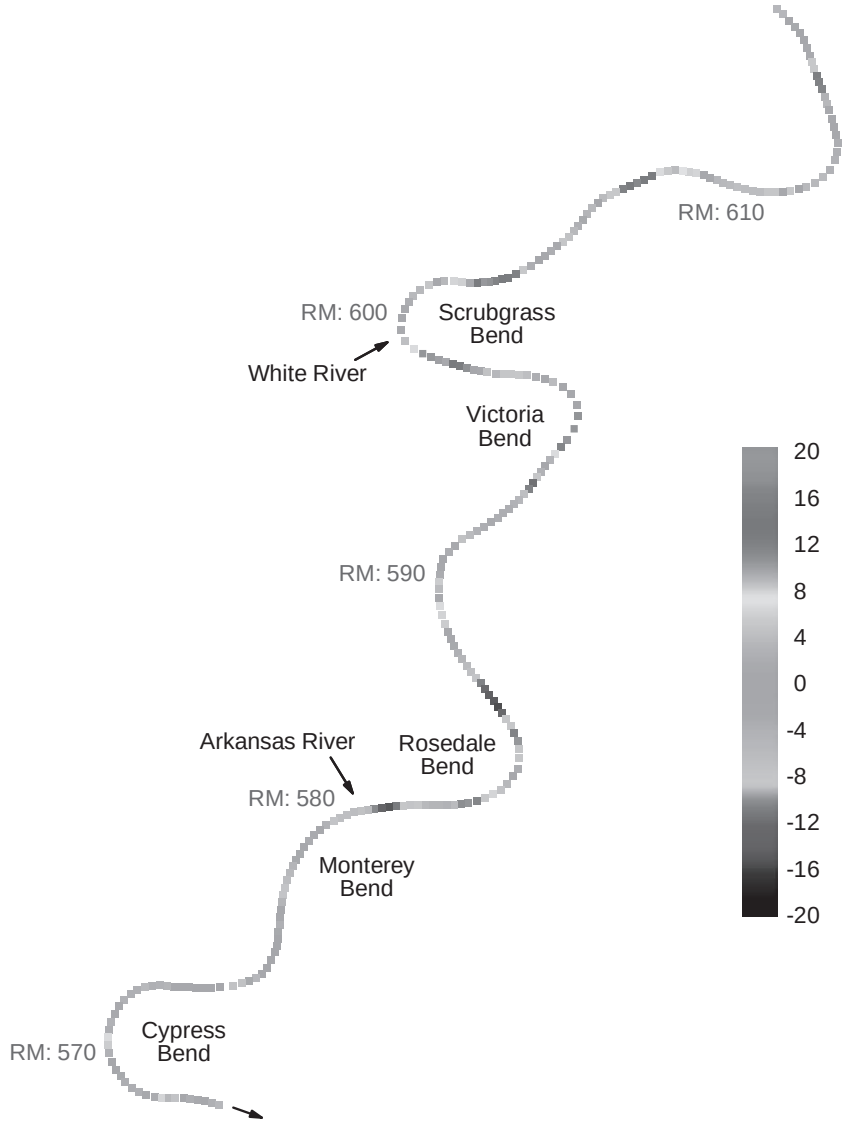

Figure 26.9 (See also colour plates.) Changes in average depth (ft) between 1992 and 2001, indicative of aggradation and degradation

Channel maximum depth at LWRP fluctuates about 15.9 m (52 ft), ranging between 14 and 16.4 m (46 and 54 ft). Bend and crossing maximum depths are generally similar, although bend maximum depths at LWRP are more variable. The lack of difference between bend and crossing maximum depths may be explained by the fact that what is plotted is the median maximum depth for several cross-sections and the fact that the deepest point in a bend pool may not actually lie within the planimetric bend, being located in the next crossing reach downstream. The high flow channel-averaged maximum depth [based on LWRP + 6.10 m (20 ft)] is around 20 to 21.9 m (66 to 72 ft).

Wetted perimeter and hydraulic radius

Wetted perimeter and hydraulic radius are indistinguishable from width and average depth respectively, due to

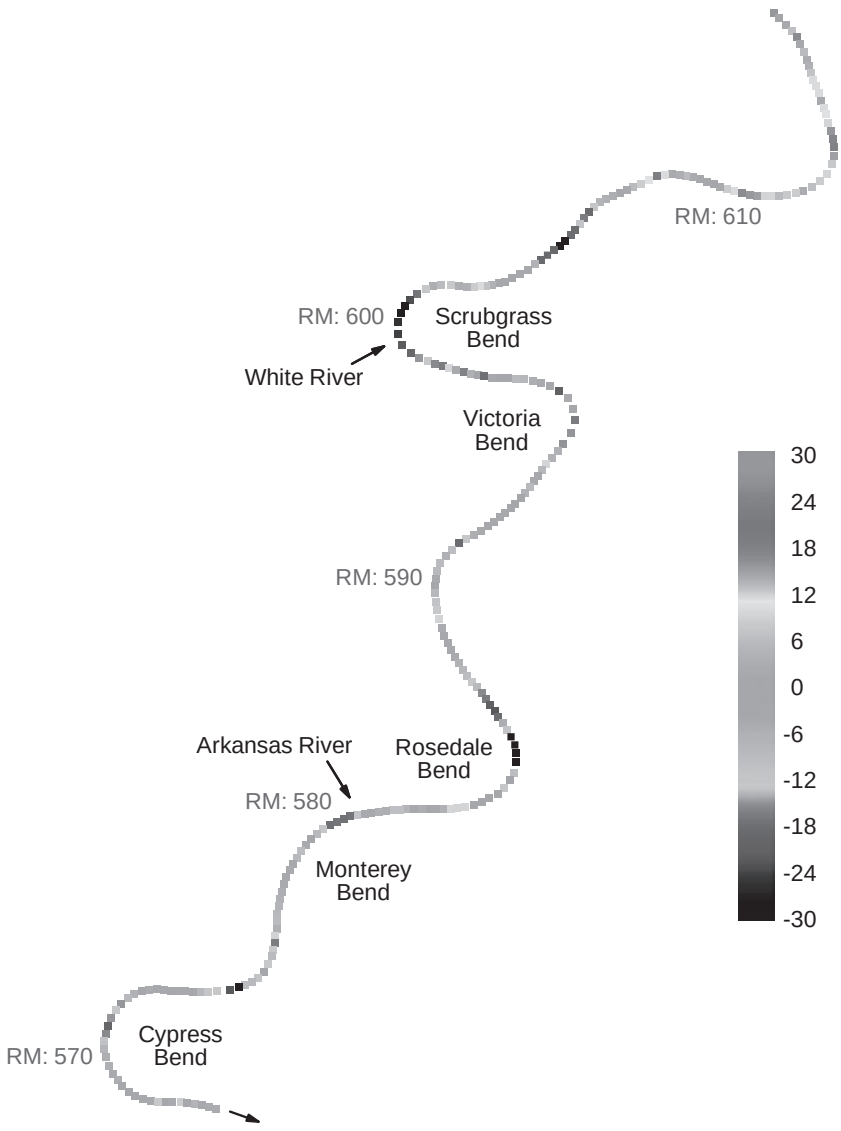

Figure 26.10 (See also colour plates.) Changes in area (1000 ft^2) between 1992 and 2001, indicative of scour and fill

the high width–depth ratio of the channel of the Lower Mississippi River.

Cross-sectional area

Channel cross-sectional area at LWRP fluctuates about 5574 m^2 (60 000 ft^2), ranging between 5110 and 6039 m^2 (55 000 and 65 000 ft^2). Bends tend to have larger and more variable areas than crossings. This difference may be explained by differences between cross-section shapes at bends and crossings. Compared with crossings, bend reaches tend to be less uniform, less trapezoidal and more variable in depth across their point bars.

At high flow [based on LWRP + 6.10 m (20 ft)], the channel area is around 10 219 to 11 613 m^2 (110 000 to 125 000 ft^2) again with bends ranging 11 148 to 11 613 m^2 (120 000 to 125 000 ft^2) having larger areas than crossings between 10 219 to 11 148 m^2 (110 000 to 120 000 ft^2). The

inter-quartile ranges for cross-sectional area at both bends and crossings are narrow.

26.6.2 Spatial Analysis

Width varies locally between bends and crossings, but there are no marked reach-scale differences. Average depths display no reach-scale trend. The greatest average depths are found at bend exits or in the upstream parts of crossing reaches (just downstream of bend exits). The cross-sections with the greatest maximum depths are located at bend exits or upstream of the inflection points in crossing reaches and no reach-scale spatial variation can be discerned.

26.6.3 Temporal Analysis

There may be a tendency for the channel at LWRP to widen between 1992 and 1997, but to be narrower in 2001 (especially at Scrubgrass Bend). At the reach-scale, average depth changes little between 1992 and 2001. About 75 % of changes are less than ±1.5 m (5 ft) in magnitude. Changes that are apparent indicate a tendency for bed scour at and downstream of bend exits. For example, average depth increases in excess of 3 m (10 ft) at Rosedale, Monterey and Cypress bends in 1993–1994, and aggradation on the crossings downstream.

Examination of changes on a year to year basis reveals only short-term adjustments that are not sustained over the longer period. Considerable activity occurs in the period 1993–1994, possibly related to the higher volume of runoff experienced in 1994 (high water year), compared with the lower volume in 1993 (as illustrated in Figure 26.11, based on flow data from the Vicksburg gauging station). In addition, there was over 6 m (20 ft) of bed scour at Victoria Bend between 1997 and 1999, which may be a local adjustment or could be a response to bendway weirs that were installed at that bend in 1995, and which did not initially operate as intended.

The absence of reach-scale changes in average depth indicates a lack of aggradation or degradation that is consistent with the reach being dynamically stable during the 1990s, as indicated by specific gauge analyses performed by Biedenharn and Watson (1997).

Examination of cross-sectional areas reveals that between 1992 and 2001 there were notable reductions in channel area around the Scrubgrass and Rosedale Bends. At both bends, the channel has filled by more than 2322 m^2 (25 000 ft^2). Crossings generally changed by less than ±743 m^2 (8000 ft^2) between 1992 and 2001.

In terms of year on year changes, there is little activity in 1992–1993, but in 1993–1994 there was more scour and fill. This did not, however, follow any systematic pattern related to bends and crossings. Scour and fill in 1994–1995 tended to reverse the changes that occurred during the previous period. There was little activity in 1995–1996, 1996–1997 and 1997–1999. Apparent activity at Victoria Bend in 1999–2000 and at other locations in 2000–2001 is probably due to lack of data in this area for 2000, which was a low runoff year.

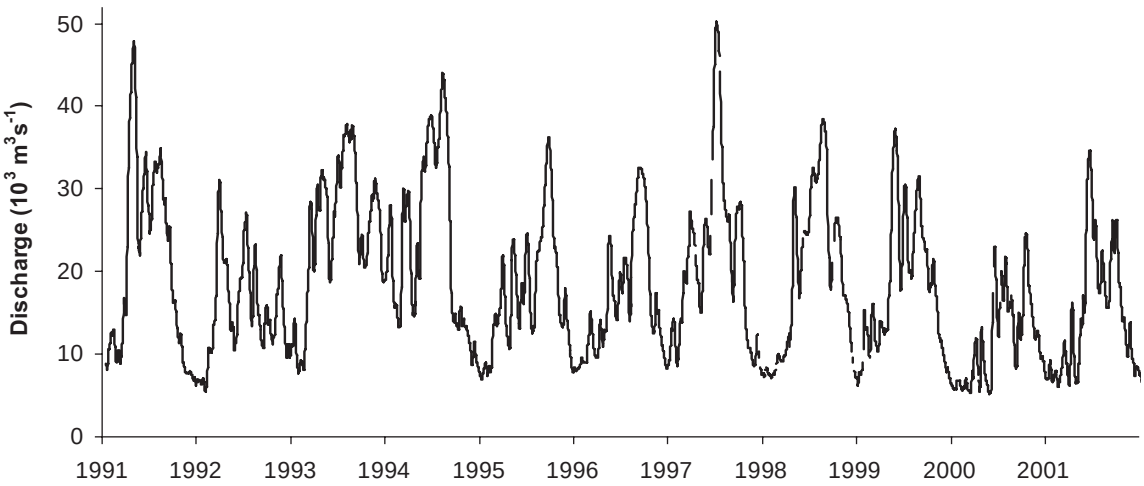

Figure 26.11 Discharge recorded at Vicksburg between 1991 and 2001

26.7 CONCLUSION

The channel geometry analysis performed in this project has showed the viability of extracting useful morphological information from historical, annual hydrographic surveys. The strength of the probabilistic technique developed to analyze and display the channel geometry data extracted from the hydrographic surveys lies in the fact that the results preserve all of the original data and demonstrate that the cross-sectional geometry of the Lower Mississippi River is highly variable in both time and space. Despite this, the fact that median values of key at-a-section parameters such as width, average depth, maximum depth, and cross-sectional area increase monotonically with increasing stage gives an insight into the cross-sectional morphology of this extensively engineered river.

Morphological diversity of the type evident in the Lower Mississippi River is a property inherent in natural channels that is often lost when river re-sectioning or training works are designed on the basis of regression equations describing the stable hydraulic geometry of regime channels. Application of engineering designs that use regime-style equations for dynamic stability as templates, while allowing for natural variability that mimics that displayed by the study reach, may provide more sustainable solutions to channel instability problems (Soar and Thorne, 2001).

Temporal changes in cross-sectional geometry demonstrate that the behaviour of this reach is highly dynamic. Examination of the full archived dataset shows that year-on-year changes observed in the study reach are larger than the net change observed over the decadal period of record, and there is some evidence that morphology responds to the magnitude of annual runoff. However, even a decade long period of record is short for a river as large as the Lower Mississippi and no firm conclusion concerning the adjustment status of this reach can be drawn from the analysis presented herein.

Establishing the historical and current status of morphological channel adjustment would be very useful in decision-making concerning engineering measures to deal with sediment and morphology-related problems in this sub-reach and this is the subject of parallel research by the authors that uses a multi-scaled approach to examine morphological changes at the sub-reach, reach, and system scales (Harmar *et al*., 2005).

The pilot analysis performed in this study covered a sub-reach that is only a fragment of the Lower Mississippi River. It would be highly informative to apply the channel geometry analysis technique to other selected reaches, within the context of channel stability analyses at the local, reach, and system scales, in order to better understand the response of the Lower Mississippi to past engineering interventions in the fluvial system.

ACKNOWLEDGEMENTS

The research reported here was performed jointly between the University of Nottingham and the US Army Engineer Research and Development Center, Vicksburg. The work was administered by the US Army Research Office (London) under grant number 9474-EN-01. Hydrographic and supporting data were supplied by staff from US Army Corps of Engineer offices in Vicksburg, Mississippi. In particular, at the Mississippi Valley Division, Steve Ellis, John Brooks, Terecia Price and the late Donald Williams provided the historic hydrographic survey datasets, while Glenda Hill and Jack Smith at the Vicksburg District supplied long-term discharge and flow stage records. The doctoral research reported here was undertaken while O. P. Harmar was in receipt of a University Studentship at the University of Nottingham under the supervision of C. R. Thorne and N. J. Clifford.

REFERENCES

Biedenharn, D.S. and Thorne, C.R. (1994). Magnitude frequency analysis of sediment transport in the Lower Mississippi River. *Regulated Rivers: Research and Management* 9: 237–251.

Biedenharn, D.S. and Watson, C.C. (1997). Stage adjustment in the Lower Mississippi River, USA. *Regulated Rivers: Research and Management* 13: 517–536.

Biedenharn, D.S., Thorne, C.R. and Watson, C.C. (2000). Recent morphological evolution of the Lower Mississippi River. *Geomorphology* 34: 227–250.

Harmar, O.P. (2004). Morphological and process dynamics of the Lower Mississippi River. *Unpublished PhD thesis*. University of Nottingham, UK.

Harmar, O.P. and Clifford, N.J. (2006). Planform dynamics of the Lower Mississippi River. *Farth Surface Processes and Landforms* 31: 825–843.

Harmar, O.P., Clifford, N.J., Thorne, C.R. and Biedenharn, D.S. (2005). Morphological changes of the Lower Mississippi River: geomorphological response to engineering intervention. *River Research and Applications* 21: 1107–1131.

Hey, R.D. (1975). Design discharge for natural channels. In: *Science, Technology and Environmental Management* (R.D. Hey and T.D. Davies, Eds.). Saxon House, Farnborough: 73–88.

Hudson, P.F. and R.H. Kesel (2000). Channel migration and meander-bend curvature in the Lower Mississippi River prior to major human modification. *Geology* 28: 531–534.

Keown, M.P., Dardeau, E.A. and Causey, E.M. (1981). Characterization of the suspended-sediment regime and bed-material gradation of the Mississippi River Basin. Potamology Programme (P-1) Report 1. US Army Corps of Engineers Waterways Experiment Station, Vicksburg, MS, 44 pp.

Kesel, R.H. (1989). The role of the Mississippi River in wetland loss in south-eastern Louisiana, USA. *Environmental Geology and Water Sciences* 13: 183–193.

Lane, E.W. (1947). The effect of cutting off bends in rivers. University of Iowa Studies in Engineering, *Proceedings of the Third Hydraulic Conference*, University of Iowa, Iowa City, IA.

Moore N.R. (1972). Improvement of the Lower Mississippi River and tributaries, 1931–1972. US Army Corps of Engineers Mississippi River Commission, Vicksburg, MS.

Robbins, L.G. (1977). Suspended sediment and bed material studies on the Lower Mississippi River. Potamology Investigation Report 300-1. US Army Engineer District, Vicksburg, MS, 29 pp. plus appendices.

Schumm, S.A., Rutherfurd, I.D. and Brooks, J. (1994). Pre-cutoff morphology of the Lower Mississippi River. In: *The Variability of Large Alluvial Rivers* (S.A. Schumm and B.R. Winkley, Eds.). American Society of Civil Engineers, New York: 13–44.

Smith, L.M. and Winkley, B.R. (1996). The response of the Lower Mississippi River to river engineering. *Engineering Geology* 45: 433–455.

Soar, P.J. and Thorne, C.R. (2001). Channel restoration design for meandering rivers. Final Report ERDC/CHL CR-01-1. US Army Engineer Research and Development Center, Vicksburg, MS, 416 pp. plus appendices.

Winkley, B.R. (1977). Man-made cutoffs on the Lower Mississippi River, conception, construction, and river response. Potamology Investigation Report 330-2. US Army Engineer District, Vicksburg, MS, 209 pp.

Wolman, M.G. and Miller, J.P. (1960). Magnitude and frequency of forces in geomorphic processes. *Journal of Geology* 68: 54–74.

27

The Management of Large Rivers: Technical and Political Challenges*

Ian C. Campbell‡

Mekong River Commission, 364, MV Preah Monivong, Phnom Penh, Cambodia

27.1 INTRODUCTION

Rivers and their catchments form necessary and sufficient units for many types of natural resource management. Growing awareness of this among politicians as well as natural resource managers has lead to an increasing emphasis on the need to develop coherent catchment management programmes even for very large rivers (e.g. see USEPA, 1996). The development and implementation of a coherent management strategy implies the establishment of some agency to coordinate the development of the strategy – a river basin management organization which may be limited to a coordinating role, or may also function as an implementing agency.

The model of river basin management organizations is being adopted at a wide range of spatial scales. At smaller scales, governments in many countries are establishing coordination and/or management committees at the subcatchment level. Examples abound for example in Australia, the United States, Thailand, Vietnam and elsewhere (e.g. see Schofield *et al*., 2000). At the scale of large rivers the model is increasingly being applied with varying levels of success. The model is being applied both within countries and across international borders as the examples which follow illustrate.

The Tennessee Valley Authority (TVA) in the United States provided the inspiration for the development of many of the river basin agencies elsewhere. Established in 1933 originally to manage a hydroplant and to convert two first world war munitions factories to peacetime uses, the TVA has grown and broadened its activities to basinwide river management. It is now the largest public electricity supply company in the United States (TVA, 2003) with 29 hydroelectric dams as well as other power generation plants. It has responsibility for flood control, navigation and electric power generation in the Tennessee Valley region.

Curiously the TVA model has not been adopted for several other major river basins in the United States. For the Mississippi as a whole for example, there has apparently not been any attempt to establish a more comprehensive river basin management agency to coordinate between the plethora of state and federal agencies with an interest in the basin. However, in other countries and on other continents the model of a basin management organization or development coordination organization has been taken up and adapted for local use. River basin management organizations (RBMOs) appeared earlier in developed regions and in national basins (e.g. the Rhine in Europe and the Murray-Darling in Australia) and more recently in developing countries and in more politically divided basins (e.g. the Mekong in Asia and the Danube in Europe).

In Australia the River Murray Commission was established in 1917 primarily to address issues of water provision for South Australia and construction of locks to support navigation on the river. As salinity became an

* The views in this chapter represent the views of the author and not the views of the Mekong River Commission.

‡Current address: School of Biological Sciences, Monash University, Victoria 3800, Australia

Large Rivers: Geomorphology and Management, Edited by A. Gupta

increasing issue in the 1960s, and other environmental concerns grew, the Commission was replaced by the Murray-Darling Basin Commission (MDBC) in 1987 following 2 years of detailed negotiations between three states and the Commonwealth government (MDBC, 2003). The 1987 Agreement was very broad and gave the Commission the power to consider any and all relevant water management objectives, including water quality, and the power to make recommendations to any government agency concerning any matter which may affect the quantity or quality of River Murray waters.

In Europe the first agreement on navigation on the Rhine River was included in the 1815 Congress of Vienna (CCNR, 2003), the present Central Commission for Navigation on the Rhine operates on the basis of the 1963 version of the 1868 Mannheim Act. However, international cooperation for environmental management is more recent. In 1885 the Salmon Treaty was signed and the International Salmon Commission set up to protect the salmon but environmental problems continued to grow (Weber, 2000). In 1950 the International Commission for the Protection of the Rhine (ICPR) was established and in 1963 the first draft agreement to clean up the Rhine was signed in Berne and the ICPR was given a permanent headquarters, first in Luxemburg and from 1964 in Koblenz. The ICPR has no executive or coercive power. Decisions by Environment Ministers and government officials taken at the ICPR meetings are followed by ensuing legal measures on implementation taken by relevant national and state jurisdictions. Costs of implementation are met by the jurisdictions passing the legislation, and the Commission's role is limited to monitoring the implementation and the condition of the river.

The earliest international agreements on the Danube River date back to at least 1862 (Wolf, 2002) but were primarily concerned with border demarcation. In 1948 a convention on navigation was agreed between 7 countries and in the 1950s several agreements were struck on water use and flooding between neighbouring riparian states (Wolf, 2002). However, a comprehensive international agreement for environmental management of the Danube came much more recently. The Danube River Protection Convention was signed by 11 riparian states in Sofia, Bulgaria, in 1994 and entered into force in May 1998 when it was ratified by the ninth member country.

The development of river basin management approaches for large rivers in developing countries has been more recent. In the Nile Basin, for example, there is a long history of, usually bilateral, international agreements on water sharing dating back to the colonial era (Waterbury, 2002) but attempts to bring a basinwide perspective began with the Hydromet project in 1967. The Hydromet project essentially attempted to provide a better hydrological understanding of the upper basin, and, in particular, the changes in water levels of some of the Equatorial lakes, especially Lake Victoria which had risen by 2.5 m between 1961 and 1964. In 1983 Egypt strongly supported the establishment of the Undigu group of Nile riparian countries to focus on issues of basinwide development, however Ethiopia was sceptical of Egyptian motives and other countries had internal political difficulties and the initiative died (Waterbury, 2002). In 1992 Tecconile – the Technical Cooperation Committee for the Promotion of Development and Environmental Protection of the Nile Basin – was established with support from Canada, FAO, UNDP and the World Bank.

The Nile Basin Initiative (NBI) was launched in 1999 to replace Tecconile, and now includes all 10 Nile basin countries within the Council of Ministers (Nile COM). The NBI also includes a Technical Advisory Committee and a secretariat based in Entebbe, Uganda. The NBI aims to achieve sustainable socio-economic development through the equitable utilization of, and benefit from, the common Nile Basin water resources (Foulds, 2002; Waterbury, 2002). Much of the work will be achieved through donor support, and an International Consortium for cooperation on the Nile was launched in 2001 in Geneva to coordinate donor funding for development projects within the Nile Basin (Africaonline, 2001).

In South America the Amazon Cooperation Treaty was executed in 1978 between the eight Amazon Basin countries (Botto, 1999). Like the other basin organizations it is headed by a council of government ministers, in this case Ministers of Foreign Affairs. The secretariat was initially established to rotate between the member countries, but has recently been permanently established in Brasilia. Under the treaty a number of special Commissions have been established to deal with issues such as the environment, native affairs, transportation, tourism, education and science and technology. For other large rivers in South America, such as the Paraná or La Plata, there are international agreements addressing sectoral interests such as hydropower, navigation or water sharing but few which address broad river basin management issues (Garcia, undated; Wolf, 2002).

Within Asia the Committee for the Coordination of Investigations of the Lower Mekong Basin was established under ECAFE (later to become ESCAP) in 1957 with Cambodia, Laos, Thailand and Vietnam as participating nations (MRC, 2002b). Because the committee was established within the United Nations framework, China, which was not at that time a member of the UN was ineli-

gible to participate, and Myanmar declined an invitation to join. The Committee was charged with facilitating the financing, construction, management and maintenance of projects on the Mekong River. In the late 1970s Cambodia withdrew from the Mekong Committee and the three remaining countries adopted a new statute constituting an Interim Mekong Committee designed to allow Cambodian membership to be reactivated at a future date. Cambodia requested reactivation in 1991 and this request led to a series of discussions which in turn led to the drafting of the 1995 Agreement on the Cooperation for the Sustainable Development of the Mekong River Basin, and the establishment of the present Mekong River Commission (MRC). The MRC as presently constituted has a far greater emphasis on assisting the member countries to achieve an equitable use of water and related resources and maintain environmental conditions in the basin than did the Mekong Committee.

Management agencies for large rivers and their catchments encounter all the difficulties facing managers of smaller catchments plus a set of quantitatively or qualitatively unique problems which arise from the size and nature of the large river systems (Stanley and Boulton, 2000). As the spatial scales of the basins increase their resistance to disturbance is probably greater and the response time slower (Lubinski, 1999), but the time taken for the consequences of corrective actions to become apparent is probably also greater. It takes a bigger push to make them fall over, they fall over more slowly when they fall but it takes a greater effort to stop them falling once they begin.

River management challenges can be broadly separated as either technical or political. Technical challenges arise from an imperfect scientific understanding of rivers and their basins, or imperfect engineering skills to manage in accordance with that understanding. Political challenges arise from the difficulty of achieving a consensus among catchment stakeholders about the goals of the management activities. Larger river basins are both technically and politically more difficult to manage than small basins. Usually they encompass a larger suite of management concerns, a larger suite of stakeholders and practical difficulties in data collection. Large river basins often encompass the territory of several different sovereign states, which exacerbates the political difficulties of management.

Management of large rivers also encompasses management of rivers in developing countries, because that is where many of the world's largest rivers are located. Six of the world's 10 longest rivers, and 7 of the 10 largest by discharge, are located in developing countries (Tables 27.1 and 27.2), and only one, the Mississippi, is located in a wealthy developed country. Rivers in developing countries usually are far more important for supporting the subsistence of local populations than rivers in developed countries. However, the knowledge base and capacity to improve the knowledge base about the river are both likely to be weaker than for rivers in developed countries. In developing countries there is understandably strong pressure for rapid development within the catchment, but the capacity of the local community to comprehend the environmental consequences of development proposals is often low.

Table 27.1 The 10 longest rivers in the world with their locations

River	Length (km)	Length ranking	Region or final country
Nile	6650	1	Egypt
Amazon	6400	2	Brazil
Yangtze	6300	3	China
Mississippi	5970	4	USA
Yenisei	5540	5	Russia
Huanghe	5460	6	China
Ob	5410	7	Russia
Paraná	4880	8	Argentina
Congo	4700	9	Congo
Amur	4440	10	Russia

Listing taken from van der Leeden *et al.* (1990) rounded to the nearest 10 km. River lengths are fractal dimensions and thus vary depending on the scale at which they are measured, the larger the scale the longer the river. van der Leeden *et al*. took these data from the *Encyclopaedia Britannica* and do not indicate whether all these rivers were measured at the same scale. The MRC cites the length of the Mekong River as 4800 km (MRC, 2003b).

Table 27.2 The 10 largest rivers in the world by discharge

River	Average discharge (thousand cumecs)	Discharge ranking	Region or final country
Amazon	210	1	Brazil
Congo	40	2	Congo
Yangtze	22	3	China
Brahmaputra	20	4	Bangladesh
Ganga	19	5	India
Yenisei	17	6	Russia
Mississippi	17	7	USA
Orinoco	17	8	Venezuela
Lena	16	9	Russia
Paraná	15	10	Argentina

Data from van der Leeden *et al.* (1990) converted and rounded to two significant figures. More recent data from the MRC (MRC, 2003b) would rank the Mekong above the Paraná in terms of discharge.

27.2 THE CHALLENGES OF RIVER MANAGEMENT

Approaches to the management of rivers and their basins have changed dramatically over the past 30 years. Changes have been brought about by rapid growth in our understanding of the way rivers work as ecological systems, and in the expectations of societies about both environmental management outcomes and public participation in decision making. I will distinguish the challenges associated with these two sets of changes as the technical and political challenges.

Various environmental impact assessment processes remain central tools for managing river basins, especially in developing countries. Environmental impact assessment for water resources projects faces the same technical and political challenges as river basin management in general but there are some additional specific issues. Cumulative environmental impacts are frequently poorly managed in environmental impact assessments, and unless they are included within a planning process which can take account of the cumulative impact they will do little to promote good long term environmental management.

It is essential that environmental impact processes in large river basins incorporate post-project monitoring. This allows testing of predictions about likely environmental impacts, detection of unforeseen impacts and an assessment of the effectiveness of mitigation activities (ESA, 2004). One of the most common weaknesses of environmental impact assessment procedures throughout the world has been the frequent absence of any sort of monitoring follow up (Buckley, 1989). A second problem, especially in developing countries, is that environmental studies including environmental impact assessments and environmental flows tend to be tacked on to the end of the project development work, with insufficient time allowed for adequate studies to be conducted. Environmental evaluations need to be conducted in parallel with the engineering investigations, rather than subsequent to them.

27.2.1 Technical Challenges

Understanding of river and catchment ecosystems has developed enormously since Hynes (1970) reviewed knowledge of river ecology. His book (1970) did not even consider the stream catchment interaction as a distinct topic, but 30 years on such an omission would seem unthinkable, partly due to the work of Hynes himself and his co-workers. There are four major technical areas that I would identify as having brought about, or are in the process of bringing about, fundamental changes in the way river managers think of the systems they manage.

The significance of the catchment

As an understanding of river management has grown, the focus has moved from the river alone to the importance of the catchment as a whole. Among river ecologists key steps in understanding were signposted by Noel Hynes (1975) in his paper 'The stream and its valley' and the work on the river continuum concept by Vannote and others (Vannote *et al*., 1980; Cummins, 2002). These papers emphasized the dependence of ecological processes within streams on processes which occur within the catchment. For example the riparian vegetation has a major influence on the biological communities in headwater streams influencing instream photosynthesis through shading while providing sources of food and habitat from terrestrial plant litter which falls in to the stream (Figure 27.1). In downstream reaches riparian vegetation becomes less influential, but imports of carbon from upstream, from groundwater and from the floodplain become more so.

There have been similar changes in perspective by water quality chemists. Early approaches to chemical water quality management focused on setting of water quality

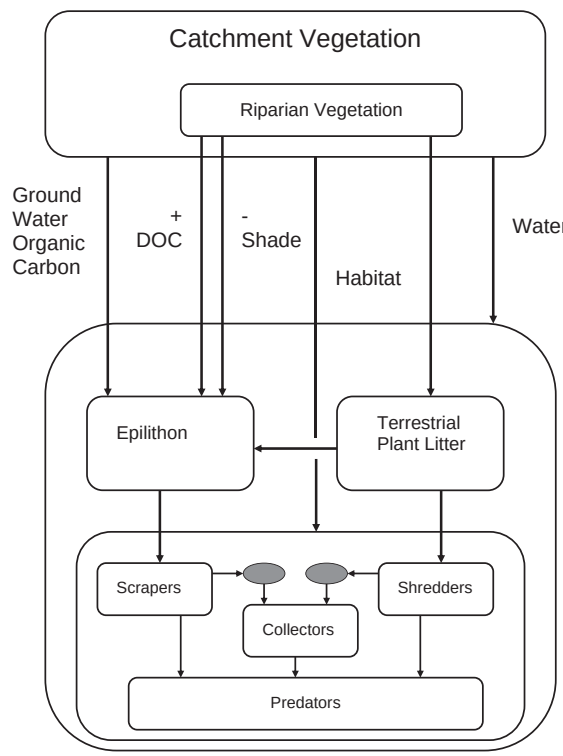

Figure 27.1 Diagram indicating the linkages between stream catchments and the instream biological community

criteria and water quality standards (e.g. USEPA, 1968 cited in USEPA, 1986) which could include limits for discharge quality and/or receiving waters. While this approach was quite successful where it was enforced for point source discharges such as industrial effluents or sewage discharges, it was not suitable for the control of nonpoint source water quality problems. These include degradation of water quality due to runoff from urban and agricultural areas. It was soon realized that managing diffuse pollution meant managing the catchment (Hart, 1982).

Thus increasingly water quality management has become synonymous with catchment management. The tools of water quality managers, originally focused on legislative approaches emphasizing effluent standards and compliance monitoring, are changing to adapt to the new understanding. Land use practices have such a large cumulative impact, although the impact from any given, small portion of the catchment is usually small. In large catchments land management or ownership often involves many participants so legislative enforcement approaches are of less value. Instead land managers need to understand their impacts, appreciate the benefits of ameliorating those impacts, and be committed to amelioration programmes. Programmes focus on improved land use practices, establishment and maintenance of buffer zones along waterways and restoration of degraded areas of catchment and channel. None of these will be feasible or successful without landholder support and participation. In large catchments this will often be a slow process, often most successful if commenced with selected small subcatchments which can serve as demonstration sites.

The ecological significance of the hydrological regime

Increasing understanding of the ways in which the stream biota responds to, and in many cases depends on, the flow regime also emphasized the link between the instream biota and the catchment. Hydrologists had long known that changing catchment land use alters the amount and timing of runoff and thus the hydrological environment in the stream. Fish ecologists, particularly those working on species from floodplain rivers, were among the first to identify the importance of hydrological changes in triggering key lifecycle changes in riverine species. Reproduction and migration are two of the most commonly identified examples (Welcomme, 2001). But many invertebrates, especially those which are passive filter feeders, are also sensitive to changes in flow patterns at a variety of spatial and temporal scales.

The flow regime of the river is also critical in maintaining the structure of the river channel (Rowntree, 2000). The structure of the channel and the channel capacity influences the flooding characteristics of the river which may directly impact terrestrial ecosystems, including people, living along the river. The channel forms the habitat for the biota of the river, so changes in geomorphology which result from flow changes will trigger alterations in the biota. Such changes may include the accumulation of fine sediments and organic material due to lowering of water velocity which fill habitat spaces or lower oxygen concentrations, changes in water depth which allow increased growth of emergent macrophytes, and so on.

The increasing awareness of the role of flow characteristics in maintaining the ecological health of rivers has changed perceptions of the impact of dams and flow regulation. Whereas relatively simple concepts such as maintaining the 'minimum flow' or a fixed proportion of the annual or seasonal flows (Tennant, 1976) were initially seen as appropriate to manage rivers, they are now seen as manifestly inadequate. Newer methods such as the 'Building Block Method' (King *et al*., 2000), DRIFT (King *et al*., 2003) and various expert panel methods have been developed to try to incorporate essential ecological and geophysical considerations into managed flow regimes. As yet this has not been attempted for any very large rivers, although expert panel methods have been employed for the Murray-Darling system in Australia, a river with an extensive catchment (Thoms *et al.*, 1996), and a method similar to DRIFT is now being attempted for the Lower Mekong River.

Significance of the floodplain

The third major change in scientific thinking about river management has been a growing appreciation of the special importance of the floodplain. This tends to be particularly significant in large rivers where the floodplain in the lower reaches may be very extensive. This has been well documented, for example, in rivers such as the Amazon (Sioli, 1984; Junk, 1997), the Mississippi (Lubinski, 1999) and the Mekong (MRC, 2003b). The importance of the floodplain is linked to the annual flood pulse on many of these rivers (Junk *et al*., 1989), which connects the river channel with floodplain water bodies, and also triggers a variety of other interactions between the river and the inundated terrestrial or semi-terrestrial systems.

When the river spreads across the floodplain it can trigger a number of responses both in the riverine biota and the floodplain biota. Many species from the river suddenly have access to a range of additional resources including both food and space. For the aquatic floodplain biota there may also be additional space and food resources. For terrestrial species silt deposition provides

nutrient renewal, and the water provides a medium for dispersal of propagules. The extent to which the floodplain is inundated will vary during the course of the flood, as it rises and falls, but also from year to year as the size of the flood varies. The spatial and temporal distribution of various species on the floodplain is strongly influenced by inundation duration and inundation frequency patterns. For example, in Australia the river redgum trees (*Eucalyptus camaldulensis*) which line the river in many areas and are characteristic of the floodplain of the Murray-Darling river system require flooding to trigger seed germination. Many species have life cycles adapted to this flood pulse. For example, a number of tree species around Tonlé Sap Great Lake in Cambodia bear fruit and seeds during the time of flooding apparently using the floodwaters as a dispersal mechanism (MRCS/UNDP, 1998).

River restoration projects in developed countries have paid increasing attention to re-establishing links between the river and the floodplain. In many cases these have been lost or reduced as a result of regulation by dams, construction of levees or channelization. Dams can reduce the frequency of floods, often eliminating small and mid-sized floods. Usually very large floods are too large to be affected by dams, but the elimination of the smaller floods means that inundation of the floodplain occurs far more rarely than in the past. Reservoir managers are increasingly realizing that some smaller floods must be allowed if the ecological values of downstream floodplains are to be maintained, but there may be problems if dam design has not taken this need into account.

Levees also reduce the frequency of floodplain inundation. Once again large floods may overtop the levee, but small and mid-sized floods are retained within the channel. Isolation of the floodplain from the river through the construction of levees is seen as one of the main impediments to improvement of ecological health in unimpounded reaches of the Upper Mississippi River and one of a number of impediments in the impounded sections of the river (Lubinski and Theiling, 1999).

In some cases, such as the Kissimmee River in Florida, channelization increased flow rates through the river basin thus reducing the frequency of floods. An important component of the restoration of the Kissimmee is the attempt to return the river to the original channel and returning parts of the floodplain to public ownership so that private property is less affected by annual flooding (Cummins and Dahm, 1995; Dahm *et al*., 1995).

Integrated water resource management

Integrated water resource management (IWRM) has become the textbook paradigm for managing river basins. It is defined as a 'process which promotes the coordinated development and management of water, land and related resources, in order to maximize the resultant economic and social welfare in an equitable manner without compromising the sustainability of vital ecosystems' (GWP TAC, 2000).

Jonch-Clausen and Fugl (2001) identify three basic goals implicit in the definition, economic, social and environmental:

1. Economic efficiency of water use is necessary because of the increasing scarcity of water relative to demands.
2. Social equity is a necessary recognition that all people have a right to access to adequate amounts of water of appropriate quality to sustain their well-being.
3. Environmental and ecological sustainability is necessary to ensure that potential resource use by future generations is not compromised.

The three basic goals date back to at least the early work on multi-objective planning for water resources development. They have now become incorporated into thinking about 'the triple bottom line' in reporting on sustainability and environmental reporting (e.g. GRI, 2002; Environment Australia, 2003). The difficulty has always been to balance the three objectives, and, in developing countries, to incorporate goals beyond the purely economic goals into the management process.

While IWRM in its various forms including integrated watershed management and integrated catchment management, has become the paradigm in textbooks and university courses (e.g. see Heathcote, 1998; Reimold, 1998) many of those in the water industry feel that there are as yet few examples where IWRM is actually being effectively implemented (Hooper and Margerum, 2000). The difficulties in implementation may spring from the historical administrative structures established by governments – with agriculture, forestry, water resources and water quality all often being managed by different government agencies. Establishing real understanding and cooperation between the different bailiwicks, staffed by professionals from different discipline backgrounds is a major impediment.

27.2.2 Political Challenges

The political challenges facing river managers in large basins include both the challenges which face managers in basins of any size as well as a suite of problems unique to large basins. The most significant challenges are to obtain stakeholder participation in decision making, and

achieving a stakeholder consensus on the desired outcome of river management.

Developing the vision for the river

River management, like any other aspect of environmental management requires the agreement on a vision for the river and its basin. A river cannot be effectively managed unless the managers are provided with a clear goal of what sort of river is desired. This, as with any environmental issue, requires an interface between technical issues and political and value judgements. Science and engineering can determine or even predict the extent of the impact of a hydropower proposal on the fish populations in a river. But science can say nothing about whether or how the project ought to be built. That depends on how much the community wants hydropower and how much it wants fish.

There are important technical roles in developing clever ways of minimizing impacts. For the examples above these could include finding ways to operate dams to maintain key features of natural flows to reduce downstream impacts, and finding ways of building dams and barrages so that the disruption to fish migration is reduced or eliminated. Science and engineering can also assist by finding alternative ways of generating electricity or developing technologies which can deliver benefits in energy efficient ways so that energy demand is reduced. But at the end of the day there will still be value judgements which will need to be made. It is not possible to have rivers in their pristine ecological condition and still have large-scale fisheries, hydropower, large-scale irrigation, and intensive navigation. Decisions must be made about what sort of river is desired, but who makes the decisions and how?

Value judgements in environmental decisions

Making the value judgement about what sort of river is wanted is the core of river management. Without it the river cannot be managed and the outcome is predictable – river degradation – but often unexpected by politicians. It is not possible to use a river and maintain it as an ecologically pristine river. Indeed with acid rain, global warming, and the spread of alien species it is not possible for any catchment on earth to be entirely unimpacted by the activities of humans. In this situation we are constrained to try to manage rivers and their catchments to maintain them in an *acceptable* ecological condition. What constitutes an acceptable ecological condition is a value judgement, and will have to be decided through some kind of political process.

A particular group of stakeholders may well make differing value judgements and define different acceptable conditions for different catchments over which they have influence. For example a different condition may be desired for a water supply stream where a largely undisturbed forest may be desired to ensure maintenance of water quality, than for an urban stream where the major concerns may be to allow the construction of infrastructure in areas that are not subject to frequent flooding, the provision of active recreation areas and management of water quality to prevent offensive odours and health risks and perhaps provide habitat for more robust fish and wildlife species.

Stakeholders may also make different value judgements at different times. Temporal differences may arise through a variety of different factors. One of these may be access to different technical information which may change community perceptions of the cost of particular choices or the risks associated with particular choices. However, changes in the community over time may also influence value judgements. As the economic situation of a community either improves or deteriorates the emphasis on the use of resources for direct productive use changes. People with insufficient to eat today are not likely to be concerned about the biodiversity heritage which may be available for their grandchildren.

Developing a shared vision of the river basin is always difficult. Inevitably the outcome will be a compromise between competing interests. If the river is to be used to any significant extent then the ecological condition of the river will be impacted to some extent. How much impact is acceptable? Within any diverse community there will be different legitimately held views ranging from those who want all species and populations maintained, to those who simply want the river to still look nice regardless of what species are still present, to those who would be prepared to sacrifice the entire river ecosystem if other goals can be achieved thereby.

In small river basins consensus may more easily be achieved. Land use is more likely to be less diverse, and potential land use more limited. Similarly there is likely to be less diversity, and a greater sense of community among the population. This makes it easier to reach consensus among the population about the goal of management, and easier for peer group pressure rather than regulation, to be used as a management mechanism. The Landcare programme in Australia is one example of landowners in small catchments combining together to restore streams though fencing and revegetation of riparian areas and soft engineering works to stabilize stream beds. The programme is supported by government funds to provide plant stock and fencing materials, but labour and

maintenance costs are met by the landowners (Campbell *et al*., 1998). Hopefully the restoration of many small catchments will provide a pathway which will lead to the restoration of larger catchments.

In large river basins it is far more difficult to achieve such consensus. A far greater range of activities is possible due, apart from anything else, to the greater amount of land and the variety of topography available. The diversity of people is also greater with larger basins controlled by a wider range of political entities up to the level of sovereign states.

The potential for conflicts across scales is one of the more difficult river management issues to address. In one manifestation it is the 'NIMBY' (Not In My Back Yard) effect where a government, or society identifies a need but no local community is prepared to host the particular use. A typical example would be a toxic waste dump. Even communities in which no further waste is being generated there are often still waste stocks in existence that must be stored or treated, and communities are understandably reluctant to host storage or treatment activities. This rapidly reduces to the argument about sacrifices for the greater good.

How do we deal with the conflict between a local farming community and a central government that wishes to resume community land as part of the inundation area for a hydropower dam, or to extend a national park? The farming community may be compensated through provision of land or money, but what of people who have no interest in compensation, who simply wish to be allowed to continue their lives in the style and location to which they are accustomed?

All of these situations reflect conflicts of values between small communities and the larger groups within which they may be embedded. How can the regional, national or provincial interests be reconciled with those of their embedded communities? In part the present solution seems to depend on public opinion and peer group pressure. If public opinion within a country strongly supports a small community in conflict with their national government then governments will usually back off. If a powerful upstream country proposes developments which would substantially deleteriously affect a downstream country it is international pressure, or concern about international pressure, which will encourage the more powerful to negotiate.

No society has yet developed an entirely satisfactory way of dealing with developing value judgement consensus. It is not simply an issue of democracy. Democratic governments who simply reflect the opinions of their people are frequently referred to disparagingly as 'populist'. Democratically elected governments will sometimes make decisions with which opinion polls indicate the majority of the voters disagree, often in the hope that voter opinion will change before the next election. In the recent war in Iraq both the British and Australian governments sent troops to participate even though polls indicated that there was not majority support for such an action amongst their constituencies. Those who agree with such decisions tend to praise the government for providing 'leadership', whilst those who disagree describe them as 'trampling on democracy'.

International politics in large river basins

In international river basins the highest level stakeholders are sovereign states, and the success of international river basin management agencies very much depends on the preparedness of states to sacrifice some of their own interests to accommodate those of their neighbours. Within states governments may use force as a (hopefully) last resort to enforce what are seen as common good solutions to management disputes, and the concern in international basins is that states may also resort to force in an attempt to secure favourable outcomes. There are as yet few examples in the case of river management, although there have been dire predictions, and three books published in the last few years with the title 'Water Wars' (Shiva, 2001; Ward, 2002; Rand, 2003).

International law provides little practical assistance on international river basin management. Two pertinent principles have been generally accepted in international law, and a third occasionally invoked (Beach *et al*., 2000; Yan and Radosevich, 2001). Generally accepted are the principle of prior appropriation and the principle of equitability of use while the principle of sovereign rights has occasionally been invoked.

The principle of prior appropriation confirms the right of those making use of the water or aquatic resources to continue that use. Thus a downstream user should not have his or her use stopped or curtailed by the demands of a later upstream user. Those proposing to use water from a river need to ensure that their use does not impinge on the activities of existing downstream users. Later users have the right to appropriate water that is in excess of the needs of earlier users, and additional users can be accommodated until all the water has been allocated. It is a simple procedure in principle but rather more difficult to apply given the variability in river discharge.

The principle of equitability affirms the rights of all users to a fair share of the water resource. Thus one particular user should not have the right to monopolize the resource to the exclusion of other users. This implies that a downstream user who may have a claim under prior

appropriation, would not have the right to prevent an upstream user making equitable use of the water.

The principle of sovereign rights, sometimes referred to as the Harmon Doctrine (Beach *et al.*, 2000) suggests that a sovereign state should have exclusive use and rights over resources within its own boundaries. Thus water falling within the national borders, and runoff generated thereby, should be the exclusive property of the particular state. This principle is now seen as extreme and is now rarely invoked except as an opening bargaining strategy (Beach *et al*., 2000).

All three principles have been invoked by various countries in discussions and establishment of management arrangements for large international river basins. In general downstream countries tend to argue for agreements based on prior appropriations since large river deltas were often the earliest parts of the river basin to be used. This is true for example in the Nile, the Mekong and the Ganga where there are, and have long been, extensive areas of agriculture and extensive fisheries dependant on the river and, especially, the flood. In the Nile Basin, for example, Egypt and Sudan have had a series of agreements based on the prior appropriation principle starting with the Nile Waters Agreement of 1929 and followed by the 1959 agreement prior to the construction of the Aswan High Dam (Chesworth, 1994). These Agreements caused great concern amongst other upstream countries because, were they to be accepted by the upstream countries, no water resources developments would be possible within their territories (Howell, 1994).

Upstream countries tend to use the principles of sovereign rights or, more frequently of equitable use to justify later water resources developments. For example Chinese academics have argued that China should not join the MRC because the 1995 Mekong agreement is not equitable to upstream countries (Yan and He, 2001). Amongst other things they are concerned that the agreement specifies that the participants will protect the river from pollution and other harmful effects. They suggest revising the agreement to include the terms substantial or significant as a qualifier to 'admit accepted changes to the water's natural status'.

Alternatively upstream countries simply deny that projects undertaken will have negative impacts on downstream users. In the Mekong for example comments by various Chinese experts have denied that there is potential for significant downstream impact from the construction and operation of the 292 m high Xiaowan Dam, which will be the second largest in China after Three Gorges. Ma Hongqi, chief engineer of the Yunnan Lancang River Hydropower Development Co Ltd, the major developer of these projects, is quoted as saying that a comprehensive analysis of the Xiaowan project's potential impacts on the lower reaches of the Mekong River by Chinese scientists before construction of the dam began concluded that the Xiaowan project will have limited impacts on the lower reaches of the river and would help with irrigation and navigation (Chen, 2002). Similarly Xu Rongkai, the Governor of Yunnan Province is quoted as saying that the ecosystem of the Mekong River will not be affected by the construction of hydropower stations along the Lancang River, the upstream section of the Mekong (Xinhua News Agency, 2002). He Daming, Director of the Asian International River Center, affiliated with Yunnan University is quoted as stating that 'The experience of building power stations in international rivers has proved that they exert no negative influences on the environment' (South China Morning Post, 2002).

The International Convention in the Law of the Non-navigational Uses of International Watercourses, 1997, includes articles encompassing two of the three principles. Article 5 addresses 'equitable and reasonable utilization and participation' while Article 27 addresses 'prevention and mitigation of harmful conditions'. As Beach *et al*. (2000) point out, Article 27 essentially encompasses prior appropriation since any upstream user taking water sufficient to impact a downstream prior user would be causing harm to another watercourse state. The principle of sovereign rights is not included in the convention, and is now rarely invoked, since Article 5 can be invoked usually to the same effect.

Effectiveness of large river basin organizations

A number of the organizations that have been established to facilitate management of large river basins were mentioned in the introduction. They encompass a range of river basin types, national and international, and a range of national economies from some of the wealthiest to some of the poorest. The effectiveness of any of these organizations depends on several factors. Principal amongst these are the resources they have available to carry out their assigned tasks, the capacity they have to carry out their work, and, most critically, the political environment within which they work. These issues are more problematic in developing countries where resources and capacity are more limited.

27.2.3 Resources

River basin management agencies require funds and facil–ities to operate effectively. For international basin organizations these may derive from the countries within the basin or through external donors, or through some mixture.

For example the Rhine and Danube Commissions are funded equally by their member countries. Most of the operating budget of the MRC comes from direct donor contributions with a smaller amount (<10% in 2002) (MRC, 2002a) being contributed by the member countries. Similarly the Nile and Niger Basin agencies depend on international donors.

For international river basin organizations dependant on donors there is often a concern that the agenda of the organization tends to be donor driven. Agencies from donor countries are accountable to their own governments and electorates and obviously the sorts of activities they are likely to provide support for are those likely to win approval from those audiences – similarly they are unlikely to support activities which are likely to be criticized at home. Most donor agencies also place a strong emphasis on recipient agencies becoming self sustaining – however unrealistic this may be in the short term.

Where a river basin agency is supported entirely by member countries, the level of support depends on the priority it receives in national budgets. The members of the Rhine Commission are responsible for funding the activities which occur within their national boundaries, and, while the other members may exert considerable pressure ultimately it is up to each state to decide to what extent it will support the management activities on its own stretch of river.

Resources are not necessarily limited to direct funding. International agencies may operate at one end of a spectrum by developing their own entirely independent infrastructure resources, such as laboratories and technical facilities. At the other end of the spectrum they may be restricted to a small secretariat with little independent physical infrastructure. The MRC, for example, like many other river basin organizations has no laboratories of its own – relying instead on national laboratories in each member country. Such an approach avoids duplicating costly facilities but makes the organization dependent on facilities for which it has limited ability to manage quality control. There may also be distrust by the member countries in results produced by laboratories in other countries.

27.2.4 Commitment and Political Influence

Most crucial to the functioning of international river basin organizations is their political context. Large river basin organizations in single states are subject to national governments who have the ability to influence the state of provincial authorities that usually play important roles within the organization. For international organizations their effectiveness depends on the extent to which member governments are committed to cooperation through the organization (Smith and Rast, 1998), the extent to which individual states are prepared to 'think basinwide', and the political level at which the organization is connected to the member countries. Concerns about levels of commitment to cooperation by member countries have been raised by several authors in relation to basins such as the Mekong (Rattner, 2003) and the Nile (Foulds, 2002).

If the member countries have little commitment to the goals of the organization it will achieve little, however, well it is resourced. National bureaucrats have the ability to slow down or even block the activities of the organization, and there are always a myriad of excuses which can be invoked. Lack of capacity, lack of support from the central secretariat and problems with contracts are all commonly used to explain failure to cooperate while still professing a desire to cooperate.

In the cooperative use of river basins all users will have some losses and some gains. States need senior bureaucrats with sufficient vision to see both the gains and the losses. An upstream country may not be able to get the full benefit of all the hydropower potential from its rivers, but if harnessing the full potential causes a human catastrophe because the subsistence fishery in a downstream neighbour collapses, the upstream country will also lose. Countries do better if their neighbours are doing well – there are fewer problems with illegal immigrants seeking a better life, more opportunities to trade, and less concern to maintain expensive guarded national boundaries. Western Europe provides a fine example. In a worst case scenario political friction between neighbours caused by transboundary resource disputes can lead to armed conflict. Government agencies need to see the river basin organization as a tool to achieve basinwide consensus. In some basins, such as the Mekong, the international river basin organization has been a significant influence in promoting greater cooperation between the member countries beyond river basin management.

Finally, the river basin organization needs to be connected at the right political levels in the member countries. Inter-government negotiations cannot succeed unless participants are senior enough to be able to make the decisions necessary. If that is not the case each contentious issue needs to be referred to a higher decision-making level which at the least slows down the negotiating process. Natural resource management decisions made in a transboundary river management context can impinge on a wide variety of national interests including national economic development strategies and goals, environmental impact procedures, and national health and social development programmes. As a consequence, agreements

with other riparian nations will often require cabinet level decisions.

27.3 MANAGEMENT OF RIVERS IN DEVELOPING COUNTRIES

Within the developing world there is an additional overlay of difficulties in river management. Several of these are interrelated. The three most critical may be the lack of resources/capacity to manage rivers, the need for rapid development to alleviate poverty, and the lack of inclusivity in governance. In addition to these issues of difficulty there is often a heavy subsistence dependency of the river by those in the catchment. In the lower Mekong River Basin for example about 80% of the population consists of rural subsistence farmers supplementing the crops they grow with wild caught fish and wild plants harvested from wetlands and forests (MRC, 2003a). These populations are particularly vulnerable to changes in the river which could affect the fish and riverine wetlands from which they derive critical parts of their livelihoods.

27.3.1 Capacity

The lack of capacity in developing countries manifests itself through the lack of financial resources to fund and maintain management infrastructure and the lack of adequate personnel to conduct the technical work necessary to provide basic data, to interpret data that are collected and to manage a river basin organization.

River management requires reliable data to evaluate and monitor the resource. This includes data on hydrology, water quality, climate (rainfall and evaporation), water use, etc. In large river basins the difficulty and expense of obtaining such data is great, simply because of the large number of sites which must be sampled or fitted with sampling equipment, and the large distances which must be travelled for sample or data collection, or over which samples must be shipped prior to analysis. In developing countries these problems may be exacerbated by the poor infrastructure of the country. Roads in poor condition may make travel times slow increasing labour time and adding to the problem of preserving samples so they arrive at the laboratory in good condition. Poor road systems also take a toll on field equipment with the battering during road transport reducing serviceable lifetimes. Telephone systems are also often limited making it difficult to transmit data from automated recording stations, etc.

Obtaining equipment is often more expensive in developing countries. Delivery is often slow and expensive, and there are rarely good local suppliers capable of repairing or recalibrating instruments obtained from suppliers in developed countries. This leads to reluctance in many cases to use modern field-based equipment.

Well equipped laboratories are rare in developing countries. Donors are often prepared to provide equipment but more reluctant to provide maintenance support, considering that this should be provided by the recipient country to indicate their commitment to the particular programme. As a result equipment is often not maintained, and expensive new replacements are bought when existing nonoperational equipment could be far more cheaply repaired. Where the staff operating the equipment have only low levels of training and understanding of the equipment they are using the rate at which equipment requires repair may be substantially greater than in laboratories with better trained staff.

The pool of trained people available with skills relevant to river basin management tends to be small in developing countries. A relatively small proportion of the population has tertiary education, and a very small number have training in sciences relevant to natural resource management. Wishart *et al.* (2000) have emphasized the weakness of freshwater ecology in developing countries as an impediment to river conservation while Campbell and Parnrong (2000) documented the weakness in freshwater ecology in Thailand and warned of the potential consequences for river management. The numbers of trained engineers are usually higher, but often the training seems to be very narrow with fields such as environmental engineering not prominent. As a result the collection of reliable data may be problematic.

Once data are collected they require interpretation before they can be used. Interpretation skills are far more difficult to develop than the relatively straightforward skills involved in operating analytical equipment or processing samples. Interpretation involves two steps, the first and simplest is data analysis – the statistical processing of data to determine trends and variability for example. The second, more difficult process, is understanding what the analyzed data is telling about the system. How is the system changing, how does it compare with other systems? This requires experience and knowledge of the way systems operate under a wide range of conditions. Some of the knowledge can be gained first hand, but much must come from reading the technical literature – difficult when the literature is not in the native language nor accessible due to lack of libraries and on-line resources. Interpretive skills are difficult to teach in university courses, and many university courses focus on content rather than skills. This is especially true in many developing countries.

An additional set of critical skills for any organization are management skills. Positions in international river basin organizations in developing countries are often

highly valued. They are mostly donor funded and may pay salaries substantially higher than the usual local salaries. This may result in them attracting highly competent qualified staff, or it may result in them becoming a focus for nepotism or worse. Social systems in many developing countries tend to be feudal rather than merit based, which may result in a small pool of competent, experienced managers on which international river basin organizations and others can draw.

27.3.2 Need for Rapid Development

The imperative for developing countries is rapid development with an aim to raise living standards. In the Mekong Basin, for example Cambodia has a per capita GDP of US$ 1361 and Lao PDR a per capita GDP of US$ 1471, and in a number of the provinces within the basin more than 50% of the population are living below the poverty line (MRC, 2003a). However, development and poverty alleviation are not synonymous. Developing countries are often characterized by a very wide gap between rich and poor, which has led to an increasing emphasis by donor agencies such as the World Bank on poverty reduction strategies (Morrow, 2001).

There is an active debate amongst the development community about the desirable trajectories for development. What sorts of development projects are appropriate? Is there too much emphasis on large-scale projects which may contribute to perceived national prestige ('mine is bigger than yours!') and even be popular politically within the country, but may, in the end, have little impact on the number of people living in poverty. The world GDP increased by more than 50% between 1987 and 1998 but the number of people living in poverty remained about the same – 1.23 billion (Morrow, 2001).

Developing countries have the opportunity to choose development paths different to those of the developed world. For example it is possible to leapfrog direct to new technologies in fields such as communications and manufacturing. Sonnenfeld (1998) argues that one advantage to late industrialization is the ability to incorporate advanced environmental technology in manufacturing. He suggests that Thailand has one of the cleanest paper manufacturing industries in the world because the plants are all new using new cleaner technologies.

The circumstances in present day developing countries often do not match the conditions that previously occurred in developed countries, so successful development strategies will necessarily be different to solve these unique development problems. In many cases, for example, populations are far less centralized in developing countries than they were in developed countries. In the Mekong Basin, for example, with a population of about 60 million people there is only a single city with a population of more than 1 million people. Most people live in small villages and towns. In such a situation do you provide services such as electricity and water by developing large scale infrastructure and distribution networks or is it preferable to develop small distributed infrastructure?

27.3.3 Lack of Inclusivity in Governance

For many developing countries governmental structures are poorly representative. This makes it difficult or impossible to establish a dialogue between stakeholders about the desired river condition. Local communities may have little access to information on which to base decisions about natural resource management issues and little or no opportunity to express their views. Typically it is the poorest who are both most dependant on the river and the most likely to be excluded from the decision-making process (Horowitz, 2001). They are the least literate, the least confident about expressing their views, and the least listened to when they do.

27.3.4 Subsistence Use

In many developing countries in large river basins there is substantial subsistence use of the river. Often the extent of subsistence use is poorly understood and not accurately documented. Recent work in the Lower Mekong River basin provides a valuable illustration of the problem, but seems to be typical of the situation in many large tropical river basins (Horowitz, 2001).

The Mekong River provides a substantial harvest of fish for the residents of the basin. However, as with other similar inland water subsistence fisheries, the extent of the resource and resource use had been extremely difficult to assess quantitatively. Probably a majority of the approximately 60 million people in the basin are involved in catching or processing fish at some time during each year. Almost none of the catch passes through large central fish markets – most being eaten by the family of the fisher, directly exchanged for other goods, or sold at a small local market. Hence, obtaining data on the catch is extremely difficult. Instead the MRC fishery programme conducted surveys on household fish consumption in various parts of the basin (Jensen, 2000). This knowledge combined with information on the amount of fish imported into the basin and data on fish from aquaculture allows an estimate of the total catch of wild fish in excess of 2 million tonnes (MRC, 2003b).

Estimates of the fish catch made in 1960–1963 put the amount in Cambodia at around 50 000 tonnes year^{-1}; based on more recent survey data it is now believed to be more

than 400 000 tonnes year^{-1} (Jensen, 2000). This illustrates the difficulty and the size of the possible errors in estimating the importance of subsistence use of river basins. Government statistics are often underestimates for a variety of reasons, and tend not to include those resources not associated with taxes or charges.

The enormous dependence of subsistence users on wild resources in large rivers is a key factor which must be incorporated into environmental decision making in these basins. For the Mekong, for example, the wild fish catch has an estimated annual value of about US$1 billion (MRC, 2003b). This value does not include the value of wild aquatic plant resources which are also extensively used within the basin. Hence, any proposed project which could alter the river in such a way as to place these resources at risk would have to return an annual net financial benefit greater than US$1 billion before it would be economically justified.

Compensation for subsistence users is very difficult in practice. Provision of sums of money may be difficult to manage in corruption-prone environments, and difficult for the recipients to handle if they are poor and lack access to financial advice. Subsistence users often lack the skills to adapt successfully to the new mix of resources available, and there is often not sufficient suitable available land to which they can be relocated. A significant source of conflict in water resource development projects in the developing world has been compensation for those disadvantaged by the project. Frequently there are allegations that compensation was too little, or not received at all, or that the process was corrupt in some way (Bangkok Post, 1998; WCD, 2000; Roy, 2001).

27.4 CONCLUSION

If the management difficulties of river basins could be quantified and plotted against basin size I doubt the relationship would be linear, I suspect it may be exponential. It has been said that managing river basins is not rocket science – it is more difficult than that. Most large rivers flow across national boundaries, and their basins in many cases lie in poor countries with few resources and little capacity to address the challenge. The Joint Action Programme to achieve sustainable management of the Danube River under the ICPDR proposes to implement projects costing 4.3 billion Euro between 2001 and 2005. This is about 80 times the budget likely to be available to the MRC over the same period and triple the amount that has been donated or pledged to the Nile Basin Initiative (Africaonline, 2001).

River basin organizations have been established to facilitate management of many of the world's large rivers but this is only a first step. The extent to which river management organizations lead to improved river management will depend on the commitment of the member countries, the capacity of the organizations and the national line agencies with which they work, and whether they have the appropriate political connections within the member countries.

The technical challenges are great, and those attempting to manage river basins have had to adjust their breadth of vision as the importance of catchment processes, complex hydrological patterns, the floodplain, and the need for integrated management all became apparent. In many basins, especially in the developing world, basin managers are still struggling to catch up with the new technical paradigms.

Even if technical understanding is perfect, river basin managers, and the governments and people they serve, are still challenged to develop a common vision for the river. The most difficult issue is to reach agreement on what sort of river do the people who use it, depend on it, share it, and live along it want? How can the competing claims between communities, sectoral groups, and even sovereign states be resolved? This is the greatest challenge for environmental management in general and for the management of large rivers in particular.

REFERENCES

Africaonline (2001). Donor community backs Nile Basin Initiative. http://www.africaonline.com/site/articles/1,3,3761.jsp. Accessed August 2001.

Bangkok Post (1998). Ministry moves to sort out compensation confusion, 11 November; MP charged with taking dam cash, 23 June.

Beach, H.L., Hamner, J., Hewitt, J.J., Kaufman, E., Kurki, A., Oppenheimer, J.A. and Wolf, A.T. (2000). *Transboundary Freshwater Dispute Resolution. Theory, Practice and Annotated References.* United Nations University Press, Tokyo, 324 pp.

Botto, M.P. (1999). The Amazon Cooperaton Treaty: a mechanism for cooperation and Sustainable development, pp. 68–100 In: *Management of Latin American River Basins: Amazon, Plata, and Sao Francisco* (A.K. Biswas, N.V. Cordeiro, B.P.F. Braga and C. Tortajada, Eds.). United Nations University Press, Tokyo, 325 pp.

Buckley, R. (1989). What's wrong with EIA? *Search* **20:** 146–147.

Campbell, I.C. and Parnrong, S. (2000). Limnology in Thailand: present status and future needs. *Verh. Int. Verein. Limnol.* **27:** 2135–2141.

Campbell, I.C., Boon, P.J., Madsen, B.L. and Cummins, K.W. (1998). Objectives and approaches in lotic and riparian restoration projects. *Verh. Int. Verein. Limnol.* **26:** 1295–1302.

CCNR (Central Commission for the Navigation on the Rhine) (2003). http://www.onu.admin.ch/sub_dipl/e/home/thema/transports/ZKR.html. Accessed September 2003.

Chen, L. (2002). Xiaowan Dam, a reservoir for progress. www.ipsnews.net/mekong/stories/xiaowan.htm. Accessed October 2003.

Chesworth, P.M. (1994). The history of water use in the Sudan and Egypt, pp. 65–79 in *The Nile: Sharing a Scarce Resource* (Howell, P.P. and Allan, J.A. (eds)). Cambridge University Press, Cambridge, 408 pp.

Cummins, K.W. (2002). Riparian-stream linkage paradigm. *Int. Verein Limnol*. **28:** 49–58.

Cummins, K.W. and Dahm, C.N. (1995). Introduction: restoring the Kissimmee. *J. Restor. Ecol*. **3:** 47–148.

Dahm, C.N., Cummins, K.W., Valett, H.M. and Coleman, R.L. (1995). An ecosystem view of the restoration of the Kissimmee River. *J. Restor. Ecol*. **3:** 181–194.

Environment Australia (2003). *Triple Bottom Line Reporting in Australia*. Commonwealth of Australia, Canberra, 68 pp.

ESA (2004). Ecological factors in environmental impact assessment. Position Statement by the Ecological Society of Australia. http://www.ecolsoc.org.au/Position_papers/EIA.htm, Accessed February 2004.

Foulds, K. (2002). The Nile Basin Initiative: challenges to implementation. Paper presented to conference 'Managing Shared Waters', Hamilton, Ontario, Canada. http://nilebasin.com/wwf/doc/kim1.htm. Accessed August 2003.

Garcia, L. (undated). Review of the role of river basin organizations in Latin America. Paper prepared for Thematic Review V.3: River basins – institutional frameworks and management options. Contributing paper to World Commission on Dams. http://www.dams.org. Accessed August 2003.

GRI (Global Reporting Initiative) (2002). *Sustainability Reporting Guidelines*. Boston, MA, 104 pp.

GWP TAC (Global Water Partnership Technical Advisory Committee) (2000). *Integrated Water Resources Management*. TAC Background Paper No. 4, Stockholm.

Hart B.T. (ed.) (1982). W*ater Quality Management: Monitoring Programmes and Diffuse Runoff.* Australian Society for Limnology / Water Studies Centre Chisholm Institute of Technology, Caulfield, 121 pp.

Heathcote, I.W. (1998). *Integrated Watershed Management. Principles and Practice*. John Wiley & Sons, Ltd, New York, 414 pp.

Hooper, B.P. and Margerum, R.D. (2000). Integrated watershed management for river conservation: perspectives from experiences in Australia and the United States, pp. 509–517 In: *Global Perspectives on River Conservation: Science, Policy and Practice* (P.J. Boon, B.R. Davies and G.E. Petts, Eds.). John Wiley & Sons, Ltd, New York, 548 pp.

Horowitz, M.M. (2001). For fewer downstream victims: an alternative approach to the management of dam-regulated tropical floodplain rivers, pp. 22–30 In: *Towards Cooperative Utilization and Coordinated Management of International Rivers* (He Daming, Zhang Guoyou and Hsiang-te Kung, Eds.). United Nations University and Science Press, New York, 307 pp.

Howell, P.P. (1994). East Africa's water requirements: the Equatorial Nile Project and the Nile Waters Agreement of 1929. A brief historical review, pp. 81–107 In: *The Nile: Sharing a Scarce Resource* (P.P. Howell and J.A. Allan, Eds.). Cambridge University Press, Cambridge, 408 pp.

Hynes, H.B.N. (1970). *The Ecology of Running Waters.* Liverpool University Press, Liverpool, 555 pp.

Hynes, H.B.N. (1975). The stream and its valley. *Ver. Int. Ver. Limnol.* **19:** 1–15.

Jensen, J.G. (2000). Can this really be true? *Catch Culture* **5**(3)**:** 1–2.

Jonch-Clausen, T. and Fugl, J. (2001). Firming up the conceptual basis of integrated water resources management. *Int. J. Water Resources Manag.* **17:** 501–510.

Junk, W.J. (ed.) (1997). *The Central Amazon Floodplain. Ecology of a Pulsing System*. Springer Verlag, Berlin, 525 pp.

Junk, W.J., Bayley, P.B. and Sparks, R.E. (1989). The flood-pulse concept in river-floodplain systems. Proceedings of the International Large Rivers Symposium. *Can. Spec. Publ. Fish. Aquat. Sci*. **106:** 110–127.

King, J.M., Tharme, R.E. and de Villiers, M.S. (eds) (2000). *Environmental Flow Assessments for Rivers: Manual for the Building Block Methodology*. Water Resource Commission of South Africa Report No. TT131/00, 339 pp.

King, J.M., Brown, C. and Sabet, H. (2003). A scenario-based holistic approach to environmental flow assessments for rivers. *Rivers Research and Management* **14:** 53–67.

Lubinski, K. S. (1999). Floodplain river ecology and the concept of river ecological health, In: *Ecological Status and Trends of the Upper Mississippi River System – 1998*. Environmental Management Technical Center, USGS, Onalaska, WI, 157 pp.

Lubinski, K. S. and Theiling C. (1999). Assessments and forecasts of the ecological health of the Upper Mississippi River system floodplain reaches In: *Ecological Status and Trends of the Upper Mississippi River System – 1998*. Environmental Management Technical Center, USGS, Onalaska, WI, 157 pp.

MDBC (2003). A brief history of the Murray-Darling Basin Agreement. http://www.mdbc.gov.au/about/governance/agreement_history.htm. Accessed August 2003.

Morrow, D. (2001). Poverty reduction strategy papers and sustainable development. Paper presented to The Workshop on Poverty and Sustainable Development, Ottawa, January 2001. www.iisd.org/pdf/pe_morrow_presentation.pdf. Accessed 12 June 2007.

MRC (2002a). Annual Report 2002. Phnom Penh, Cambodia, 34 pp.

MRC (2002b). The story of Mekong cooperation. Phnom Penh, Cambodia, 22 pp.

MRC (2003a). Social atlas of the Lower Mekong Basin. Phnom Penh, Cambodia, 154 pp.

MRC (2003b). State of the Basin Report 2003. Phnom Penh Cambodia, 300 pp.

MRCS/UNDP (1998). Environment in the Tonle Sap area, In: *Natural Resources-Based Development Strategy for the Tonle Sap Area, Cambodia*. Final Report. Volume 2, Part B. Sectoral Studies, 245 pp.

Rand, H. (2003) *Water Wars: A Story of People, Politics and Power*. Xlibris Press, Philadelpha, 284 pp.

Rattner, B.D. (2003). The politics of regional governance in the Mekong River basin. *Global Change* **15**(1)**:** 59–76.

Reimold, R.J. (ed.) (1998). *Watershed Management. Practice, Policies and Coordination.* McGraw-Hill, New York, 391 pp.

Rowntree, K. (2000). Geomorphology, pp. 169–194 In: *Environmental Flow Assessments for Rivers: Manual for the Building Block Methodology* (J.M. King, R.E. Tharme and M.S. de Villiers, Eds.). Water Resource Commission of South Africa Report No. TT131/00, 339 pp.

Roy, A. (2001). *Power Politics*. South End Press, Cambridge, MA, 182 pp.

Schofield, N.J., Collier, K.J., Quinn, J., Sheldon, F. and Thoms, M.C. (2000). River conservation in Australia and New Zealand, pp. 311–333 In: *Global Perspectives on River Conservation: Science, Policy and Practice* (P.J. Boon, B.R. Davies and G.E. Petts, Eds.). John Wiley & Sons, Ltd, New York, 548 pp.

Shiva, V. (2001). *Water Wars*. South End Press, Cambridge, MA, 188 pp.

Sioli, H. (ed.) (1984). *The Amazon: Limnology and Landscape Ecology*. Dr W. Junk Publishers, Dordrecht, 763 pp.

Smith, D. and Rast, W. (1998). Environmentally sustainable management and use of internationally shared freshwater resources, pp. 277–297 In: *Watershed Management. Practice, Policies and Coordination* (R.J. Reimold, Ed.). McGraw-Hill, New York, 391 pp.

Sonnenfeld, D.A. (1998). From brown to green? Late industrialization, social conflict and adoption of environmental technologies in Thailand's pulp industry. *Organiz. Environ.* **11**(1)**:** 59–87.

South China Morning Post (2002). Xiaowan hydropower project goes ahead despite objections, 21 January.

Stanley, E.H. and Boulton, A.J. (2000). River size as a factor in conservation, pp. 403–413 In: *Global Perspectives on River Conservation: Science, Policy and Practice* (P.J. Boon, B.R. Davies and G.E. Petts, Eds.). John Wiley & Sons, Ltd, New York, 548 pp.

Tennant, D.L (1976). Instream flow regimens for fish, wildlife, recreation and related environmental resources. *Fisheries* **1**(4)**:** 6–10.

Thoms, M.C., Sheldon, F., Roberts, J., Harris, J. and Hillman, T.J. (1996). *Scientific Panel Assessment of Environmental Flows for the Barwon-Darling River.* Report to the Technical Services Division of the New South Wales Department of Land and Water Conservation, NSW, Australia, 161 pp.

TVA (Tennessee Valley Authority) (2003). http://www.tva.gov. Accessed August 2003.

USEPA (1986). *Quality Criteria for Water 1986*. EPA 440/5-86-001. US Government Printing Office, Washington, DC, 477 pp.

USEPA (1996). A watershed approach framework. Reprinted as pp. 369–384 In: *Watershed Management. Practice, Policies and Coordination* (R.J. Reimold, Ed.). McGraw-Hill, New York, 391 pp.

van der Leeden, F., Troise, F.L. and Todd, D.K. (1990). *The Water Encyclopedia*. Lewis Publishers, CRC Press, Boca Raton, FL, 808 pp.

Vannote, R.L., Minshall, G.W., Cummins, K.W., Sedell, J.R. and Cushing, C.E. (1980). The river continuum concept. *Can. J. Fish. Aquat. Sci.* **37:** 130–137.

Ward, D.R. (2002). *Water Wars: Drought, Flood, Folly and the Politics of Thirst*. Putnam Publishing Group, New York, 288 pp.

Waterbury, J. (2002). *The Nile Basin: National Determinants of Collective Action*. Yale University Press, New Haven, 211 pp.

WCD (World Commission of Dams) (2000). *Dams and Development. A New Framework for Decision-making.* Earthscan Publications, London, 404 pp.

Weber, U. (2000). The 'miracle' on the Rhine. http://www.unesco.org/courier/2000_06/uk/planet.htm. Accessed August 2003.

Welcomme, R.L. (2001). *Inland Fisheries: Ecology and Management.* Fishing News Books, Blackwell Science, Oxford, 358 pp.

Wishart, M.J., Davies, B.R., Boon, P.J. and Pringle, C.M. (2000). Global disparities in river conservation: 'First world' values and 'third world' realities, pp. 353–369 In: *Global Perspectives on River Conservation: Science, Policy and Practice* (P.J. Boon, B.R. Davies and G.E. Petts, Eds.). John Wiley & Sons, Ltd, New York, 548 pp.

Wolf, A.T. (compiler) (2002). *Atlas of International Freshwater Agreements.* UNEP, Nairobi, 184 pp.

Xinhua News Agency (2002). Yunnan Governor claimed hydraulic works on Lancang River 'not detrimental', 7 September.

Yan, F. and He, D. (2001). An assessment of the 'Agreement on the cooperation for the Sustainable Development of the Mekong River Basin', pp. 177–183 In: *Towards Cooperative Utilization and Coordinated Management of International Rivers* (He Daming, Zhang Guoyou and Hsiang-te Kung, Eds.). United Nations University and Science Press, New York, 307 pp.

Yan, F. and Radosevich, G.E. (2001). Policies and strategies for the sustainable development of the Lancang River basin – international law and PRC/Yunnan water laws and regulations, pp. 164–176 In: *Towards Cooperative Utilization and Coordinated Management of International Rivers* (He Daming, Zhang Guoyou and Hsiang-te Kung, Eds.). United Nations University and Science Press, New York, 307 pp.

28

The Physical Diversity and Assessment of a Large River System: the Murray-Darling Basin, Australia

Martin C. Thoms[1], Scott C. Rayburg[1] and Melissa R. Neave[2]

[1]*Riverine Landscapes Research Laboratory, University of Canberra, ACT 2601, Australia*
[2]*Department of Geosciences, The University of Sydney, NSW 2006, Australia*

28.1 INTRODUCTION

A trend in river science over the last 15 years has been the increased emphasis on larger systems. This has been reflected in an expanding literature base describing the physical character and processes of large rivers. The 1989 special issue of *Canadian Journal of Fisheries and Aquatic Sciences* was one of the first publications to deal specifically with large river systems. Although papers from this symposium (Dodge, 1989) had a multidisciplinary focus, 11 of the 49 papers dealt with the form and process of large floodplain rivers. The geomorphological character of large lowland rivers was presented in *Lowland Floodplain Rivers: Geomorphological Perspectives* (Carling and Petts, 1992). Here the aim was to describe the holistic nature of the river valley, shifting attention away from the river bed per se to consider the understanding of channel–floodplain relationships over a range of spatial and temporal scales. More recently, selected papers from the International Conference on Sustaining the Ecological Integrity of Large Floodplain Rivers were presented in an issue of *River Research and Applications*. A common theme of these papers was the highly variable physical, chemical and biological nature of large river systems. Large rivers were portrayed as 'moving targets' or highly dynamic systems with a recommendation that research should focus on their collective status rather than at specific points in time and space. Two issues of the journal *Geomorphology* edited by Chen *et al*. (2001) and Gupta (2002) also highlight the physical complexity of large rivers thereby challenging the traditional approach of selecting representative reaches for detailed analysis followed by extrapolation to the entire system.

A positive relationship between scale and complexity is an accepted paradigm in the study of natural ecosystems (Wiens, 1989; Levin, 1992). Larger ecosystems can be characterized by an increase in the number of components; an increased number of different types of components; interconnections between components; the presence of both positive and negative feedback loops; and, the number of interactions between different levels of organization within a system compared with smaller ecosystems. Hence, larger river ecosystems can be assumed to be more complex than smaller river ecosystems. The scientific community has had a love–hate relationship with large rivers. In spite of the curiosity about their unique physical, chemical and biological patterns and functions (Davies and Walker, 1986) there has been frustration because they do not conform with contemporary, empirically derived, models of river function (Phillips, 1995; Sheldon and Thoms, 2006). Large rivers have been described as being in a nonequilibrium state (Chen *et al*., 2001; Gupta, 2002) and as a result, they have tended to be less popular to study than more manageable smaller systems.

Large Rivers: Geomorphology and Management, Edited by A. Gupta

With increasing pressures on the environment, there is a strong trend to manage rivers as ecosystems. This requires a holistic, interdisciplinary approach that simultaneously considers the physical, chemical and biological components of river ecosystems, as well as longitudinal (upstream–downstream), lateral (channel-floodplain) and vertical (channel-hyporheos) connectivity, and spatial and temporal scaling (Thoms and Parsons, 2002). This approach has been embraced in many areas (Rogers, 2003; Brierley and Fryirs, 2005; Thoms *et al*. 2005) and it has been accompanied with a focus on the management of landscapes. Natural resource management agencies are incorporating large-scale ideas, such as ecosystem management, landscape heterogeneity, gap analysis and metapopulation conservation (Bissonette and Storch, 2003) and putting these concepts into practice. The Kruger Experience in South Africa is an excellent example of contemporary river ecosystem management within a landscape context. Previous river research and management in the Kruger National Park focused on issues principally at a reach scale which generated much compartmentalized knowledge about, inter alia, channel hydraulics, sediment transport, river morphology and riparian vegetation (Bell, 1995). These research activities were driven by individual scientific disciplines but this reductionist approach limited the application of much of the science to the management of the rivers in the park or the management of the Kruger National Park ecosystem (Biggs, 2003), which also included management of terrestrial vegetation and animal communities. This situation has been echoed in many river research and management programmes (Boon *et al*., 1992; Kelman, 2005) where there is a disjunct between the scale at which most river research takes place and the need of natural resource managers (Rogers, 2006). The breakdown of scientific discipline boundaries combined with an ecosystem research focus, at appropriate scales, is a key attribute for the advancement of river science and its application to management (Du Toit *et al*., 2003).

This chapter is the outcome of a challenge by natural resource managers to river scientists to assess the physical condition of rivers within the Murray-Darling Basin, Australia. The essence of the management questions were; at the catchment scale what type of rivers do we have; what is their physical condition; and, what are the main drivers of this condition? In response, the approach taken highlights the importance of understanding the ecogeomorphology of river systems (Thoms and Parsons, 2002), integrating the disciplines of hydrology, geomorphology and ecology, and it makes a number of sequential points. First, natural resource managers required information on the condition of rivers at the catchment scale, thus providing a spatial domain or boundary, for data collection and its reporting. Second, the physical characterization of rivers, at the catchment scale, was deemed to be an important step in understanding the overall structure and behaviour of rivers within the basin for several reasons. The assessment of the physical condition of rivers was part of a larger audit on the sustainability of rivers in the Murray-Darling Basin, which also incorporates a series of chemical and biological components. The common link between the biological and physical components of a river system is the expression of physical habitat as a templet for biological communities (Southwood, 1977). From a biological perspective, physical habitat is considered as a templet upon which the ecological organization and dynamics of ecosystems are observed (Townsend and Hildrew, 1994). Audit protocols require a comparison of the physical, chemical and biological components from similar river types. In addition, physical diversity (a measure of the abundance and frequency of different river types) is also a useful indicator of the condition of river systems (Thoms *et al*., 2004). Third, many factors contribute to the physical condition of rivers and commonly a single index of condition is provided (Stevenson and Hauer, 2002). Whilst useful, interpretations would benefit from the addition of sub-indices that allow for more specific interpretation of environmental condition. In this study an aggregated index is provided along with four sub-indices that consider the influence of changes in habitat, hydrology, land use and sediment transport on the physical condition of rivers. In this chapter an overview of the geomorphology of the Murray-Darling Basin is provided, highlighting the influence of larger scale constraints on the contemporary character of river systems within the basin. The character of rivers is described followed by an assessment of their physical condition.

28.2 THE MURRAY-DARLING BASIN

A precise definition of large rivers is lacking despite the attempts of studies to provide detailed descriptions of their various physical and biological character and processes operating within them (Davies and Walker, 1986; Thoms and Walker, 1992; Thoms *et al*., 2006). Recently, Miall (2006) suggested that large rivers are those that have a catchment area greater than 50 000 km^2. While this may be an arbitrary classification, it is a starting point. Thus most of the rivers in the Murray-Darling Basin, Australia are large by this definition. As a collective, the Murray-Darling Basin has a catchment area of 1.07 m km^2 and the combined length of the Murray River and Darling River (5300 km), the two principle rivers in the basin, make it the fourth longest river system in the world, behind the Amazon, Mississippi-Missouri and Nile systems.

The Murray-Darling system drains the inland slopes of the South-eastern Highlands of Australia (Figure 28.1). The evolution of the drainage network of the Murray-Darling Basin and hence the diversity of contemporary river systems is strongly associated with the development of the landscape of South-eastern Australia. Major features of the headwater drainage in the basin were inherited before the break up of Gondwana. Rifting in the Late Cretaceous–early Cenozoic period (80–60 million years ago), associated with the formation of the Tasman Sea, resulted in a new continental margin east of the Australian landmass and the formation of The Great Dividing Range

Figure 28.1 The Murray-Darling Basin and its major tributaries

or South-eastern Highlands. During the Palaeocene, the Murray Basin began to subside, which contributed to the separation of the Murray and Darling sub-basins. Despite the uncertainty over the evolutionary details of the Canobolas Divide, which separates the two main sub-basins, it is thought that the current drainage network of the Darling system was present in the Tertiary (Thoms *et al.*, 2004).

The Darling Basin is 650 000 km^2 in area and characterized by low relief, with altitudes ranging from 1000 m above sea level in the South-eastern Highlands to 50 m in the south-west of New South Wales. Sixty per cent of the catchment has altitudes of less than 300 m. The Darling River, receives major contributions of runoff from the Border, Gwydir, Namoi and Macquarie Rivers with minor contributions from the Bogan and tributaries that flow from the west, namely the Culgoa, Paroo and Warrego Rivers (Figure 28.1). River valleys along the eastern rim of the Basin are old, shown in part by a coincidence with structural trends in the Palaeozoic basement and by the direction of the many headwater tributaries, such as in the Macquarie River. In some areas the headwater tributaries cut across the Palaeozoic structures, modifying the older drainage pattern. River patterns in the central region of the Darling Basin characterize an inland drainage system associated with a depositional area. Flattening of the landscape in this region of the basin has occurred primarily through infilling of a prior landscape by younger Cenozoic sediments. As a result drainage networks in this region are typical of low gradient meandering systems with bed slopes ranging between 10^{-4} and 10^{-5} that are bordered by extensive alluvial plains (Riley and Taylor, 1978; Thoms *et al*., 2004).

One of the many remarkable features of the Darling River – the principal river system in the basin – is the relatively straight path it takes across the landscape. For most of its length the Darling River is essentially controlled by structural contortions in the basement rocks. Faulting and other structures in the basement complex are simply expressed by patterns in the river planform at the surface. The basement geology of the Darling valley consists of a series of fault-bounded sub-basins or centres of deposition that form a chain along the Darling River. Each sub-basin is rhombic in shape, defined by block movements on two intersecting lineament (fault) sets. The boundary between each pair of individual fault compartments or sub-basins is a shared or common fault. Vertical displacements on the faults vary, so that the Cenozoic fill in some blocks is thicker than in others, while some substrates may be stepped, or tilted. The geometry of each compartment and individual lineament is complex in its expression, displaying a fractal configuration. The path of the Darling River follows elements of these lineament sets. Locally, the river channel switches from one set to another, producing a step-like pattern as the river flows across lineaments from one sub-compartment to the next.

The Murray Basin by comparison has an area of 420 000 km^2. Its headwaters are in the wet upland regions of the Southeastern Highlands at an elevation of 1430 m above sea level and the river flows in a north-west direction through a predominantly semi-arid region, before turning due south in South Australia to meet the sea. The South-eastern Highlands is also an area of maximum bedrock outcropping in the basin. It is a complex area of sedimentary, metamorphic and igneous rocks, parts of which form the Lachlan Geosyncline. The near-meridional disposition of rock types in the highlands controls dissection so that, in many cases, valleys run north–south, joining east–west streams. The highlands are characterized by steep slopes, limited mass movement of the slopes, and moderately large-scale sediment movement in channels. This area is likely to be a relatively high sediment yield zone in the River Murray catchment. Subsidence in the Murray Basin created a large saucer-shaped depression that gradually infilled with sediment. A complex sequence of Tertiary deposits occur in the basin, with sediments being dominated by marine deposits (The Murray Group) in the western section and fluvio-lacustrine deposits in the east (The Renmark Group). Sediments that infilled the basin were derived from two main sources: the South-eastern Highlands and marine incursions. The long depositional history within the basin is reflected in low gradient river systems. The River Murray has a channel slope of less than 0.0017 m km^{-1} for 89 % of its length downstream of Wentworth. Despite the overall stability of underlying basement rocks, there has been some movement of the basement blocks along ancient fault lines. The Cadell Fault is one of the most significant tectonic influences on the River Murray. Displacement along the fault occurred approximately 25 000 years ago, tilting the Cadell Block to the west and resulting in a rise of some 8–12 m to the east. Before this displacement, the Murray flowed across the top of the faulted block to join the Goulburn River north of Echuca. The block diverted the river around its northern end whilst the Goulburn River formed a large lake (Lake Kanyapella) at its southern end. Between 25 000 and 13 000 years ago this lake emptied and the Goulburn cut a new path around the block. Around 8000 years ago the River Murray abandoned its course to the north to rejoin the Goulburn near Echuca, establishing the present course of the Murray. The former course of the Murray to the north of the block is now occupied by the Edward River.

In summary, the complex evolution of the Murray-Darling Basin and its drainage network has the following

implications for the contemporary geomorphology of its river systems:

- sections of the drainage network are extremely old, especially those along the eastern margins of the basin;
- the composite drainage network of the Murray-Darling Basin is approximately 65 million years old, although those in the Darling sub-basin are probably much older;
- the northern flowing rivers within the Murray Basin (namely the Kiewa, Ovens, Campaspe) are probably the youngest river systems.

The Murray-Darling Basin spans 13° of latitude and longitude (24–37° S; 138–151° E) and regional climates vary accordingly. Four main climatic regions occur within the basin (Nix and Kalma, 1982). The northern region is subtropical; the eastern region of the Southeastern Highlands is cool-temperate; the southern region is temperate; and, extensive intervening inland area is semi-arid to arid. As such, the Murray-Darling Basin is characterized by extreme climatic variability. High summer temperatures are a feature, averaging more than 33 °C and with extremes well above 40 °C. Australia's second highest temperature of 52.8 °C was recorded at Bourke in 1877. Median annual rainfall varies from 3800 mm at Mt Kosciuszko to less than 200 mm at Broken Hill, and most of the catchment receives less than 600 mm. Rainfall tends to decrease westward across the catchment as the altitude decreases. Moreover, there is a seasonal pattern in rainfall that varies from winter dominance in the south, to a relatively even spread through the central parts, to summer dominance in the northern parts. There is also a parallel westward increase in evaporation rates, from a long-term median annual of 125 cm in the uplands to over 225 cm in the semi-arid western parts. Although low rainfall is a general feature of the catchment, some areas occasionally experience periods of intense rainfall. These are generally associated either with deep tropical depressions moving over the southern portion of the catchment or with the decay of tropical cyclones that have moved inland. Such rainfall has resulted in severe and widespread flooding. For example, in April 1990 flooding in the Darling Basin inundated an area larger than England and Wales combined. In contrast to these events, large sections of the Basin also experience prolonged periods with no rainfall. For example, less than 10 mm of rain has been recorded in a 12-month consecutive period at Bourke on the Darling River five times. Indeed, throughout most of the western areas of the catchment there is a 10 % chance of receiving less than 15 mm of rainfall in a year.

Hydrological variability is a feature of the rivers in the Murray-Darling Basin (Maheswari *et al*., 1995). Long-term variations in mean annual flow for selected stations range from 0.04 to 911 % (MDBMC, 1987). Puckridge *et al*. (1998), in a multivariate analysis of the hydrographs of 52 rivers with similar catchment character, showed a number of rivers in the Basin to be among the most hydrologically variable in the world. The average coefficient of variation (CV) for annual runoff for selected rivers in the Murray-Darling Basin is 0.72 – much higher than for the humid regions of North America (0.3), Europe (0.2) and Asia (0.2) (Finlayson and McMahon, 1988). Key hydrological features of rivers in the semi-arid to arid regions of the Basin include a nonlinear temporal response of runoff to rainfall and basin size, and highly variable seasonal flow (McMahon, 1979). This variability may be further amplified by climatic conditions such as El Niño–Southern Oscillation (ENSO) events, because the discharges of rivers in south-eastern Australia correlate significantly with the Southern Oscillation Index (SOI) (Simpson *et al*., 1993).

28.3 THE SCIENCE CHALLENGE FOR ASSESSING RIVERS IN THE MURRAY-DARLING BASIN

28.3.1 The Theory

Rivers are complex elements of the landscape with many interacting factors governing their physical character and the processes operating within them. Spatial controls on river morphology reflect not only discharge and sediment regime variations related to basin size, but also direct and indirect geological influences of the valley, climate and evolutionary traits of the basin.

The complexity of river systems challenges many traditional scientific methods. Their multi-causal, multiple-scale character limits the usefulness of the conventional reductionist falsification approach, except when applied at very small scales and within limited domains. Hierarchy theory provides an approach for interpreting river complexity (Dollar *et al*., 2007; Parsons and Thoms, 2007). A hierarchy is a graded organizational structure and a particular level (or holon) with a hierarchical system is a discrete unit of the level above it and an agglomeration of discrete units of the level below it. Any level within a hierarchy exerts some constraint on lower levels (O'Neill *et al*., 1986), especially the one immediately below; lower levels, conversely, can influence the structure and functioning of higher levels. In consideration of a particular level, the downward constraints and upward influences of all other levels are encapsulated by the characteristics and

properties of the levels immediately above and below only. The simultaneous operation of processes at different levels, within particular contextual constraints, gives rise to emergent properties. A level within the hierarchy can be characterized by a scale (O'Neill, 1989). Scale defines physical dimension, e.g. in terms of grain size and extent, where grain size describes the smallest interval in an observation set or the smallest scale of influence of an ecosystem or process driver (Rogers, 2003). Extent is the total area or duration over which observations are made; the largest scale at which a disturbance or process driver exerts influence on the system. Grain size and extent define the upper and lower limits of resolution of level within a hierarchy. Scale determines the units appropriate for the measurement of variables associated with each level of a hierarchy. For example, two river systems may both represent the same level of organization in a geomorphological hierarchy and can be characterized by the same variables (such as channel density, channel width and inter-channel spacing). If the spatial extent (scale) or scale of focus of the two river systems differs, however, appropriate units for measurement must also differ (Dollar *et al*., 2007).

River characterization requires the ordering of sets of observations into meaningful groups based on their similarities or differences. Implicit in this exercise is the assumption that relatively distinct boundaries exist and that these may be identified by a discrete set of variables. Although river systems are continuously evolving and often display complexity, the grouping of a set of elements with a definable structure can aid in relating broader physical factors. Most geomorphological characterization systems for rivers are hierarchical (Frissell *et al.*, 1986; van Niekerk *et al*., 1995; Montgomery and Buffington, 1998; Thoms *et al*., 2004). Schumm and Lichty (1965) were the first to use hierarchy to describe independent and dependent variables in river function but did not utilize the hierarchical arrangement for detailed river characterization exercises. In short, any characterization approach must be cognizant of scale and the scale of purpose for which the characterization will be employed. In this study, information on the physical character and assessment of the condition of rivers within the Murray-Darling Basin was at the catchment level.

A typical river characterization hierarchy is presented in Figure 28.2, illustrating interrelationships between different geomorphological levels: basin, river system, functional process zone, functional set, functional unit, and mesohabitat. The different levels of this fluvial geomorphological hierarchy are described in Table 28.1. Each level displays a characteristic pattern in response to a host of process variables. According to hierarchical principles, the physical character of river channels and their floodplains at any one level or scale in the hierarchy is constrained by larger scale processes and structures and is also influenced by processes and structures operating at smaller scales. Therefore, the division of a river system into component levels at different scales, is important as it provides a practical way of identifying the interrelationships between physical and geomorphological factors across a range of spatial and temporal scales.

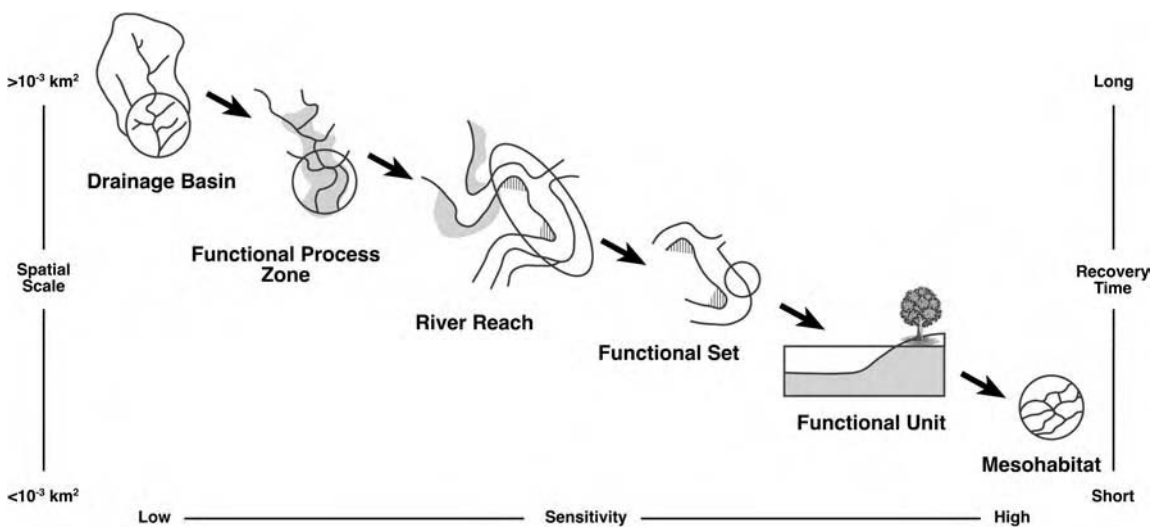

Figure 28.2 A hierarchical scheme for the characterization of rivers

Table 28.1 A physical characterization scheme applicable to rivers in the Murray-Darling Basin

Spatial scale	Description
The catchment	Area of the primary catchment
River system	The river channel and floodplain from its source to its mouth or a defined distance downstream
Functional process zone	Lengths of the river system that have similar discharge and sediment regimes; can be defined from major breaks in slope and from style of river channel or floodplain
River reach	Repeated lengths of river channel within a process zone that have similar channel style
Functional channel sets	Ecological units associated with specific landforms such as major cutoffs, aggrading floodplains, main channels
Functional units	Characterized by a typical aquatic community that is indicative of the habitat conditions present at a site
Mesohabitats	Areas sensitive to variations in control variables that may change from year to year reflecting the sequence of discharge and sediment loads; examples include sand bars, gravel patches, scour holes

28.3.2 Application

The main river systems within the Murray-Darling Basin have been characterized according to the schema described above. Because the scale of reporting for this study was predetermined at the catchment scale by natural resource managers, river characterization was focused at the functional process zone scale (Figure 28.2 and Table 28.1). The characterization exercise was undertaken through an analysis of remote sensing images, airborne video, geological surveys, topographic maps, sediment yield and discharge data and ground truthing exercises. Initial mapping was undertaken of the main river channels at the 1 : 100 000 scale in order to ensure continuity across the basin. Detailed descriptions of the methods used and their application are provided in Thoms *et al*. (2004) and Thorp *et al*. (2007).

Eight functional process zones were identified in the Murray-Darling Basin, a description of each is given in Table 28.2. Each functional process zone has a distinct valley floor trough–river association in terms of the degree of valley dimensions, gradient, stream power (or energy), boundary material or sediment yield, and river channel planform and cross-sectional character. The different assemblages of morphological units in the channel and on the floodplain influence the presence and structure of in-stream habitat and associated biological communities (Boys and Thoms, 2006; Thoms *et al*., 2004). The Anabranch Zone is the dominant functional process zone in the Murray-Darling (Figure 28.3) comprising 39% of the total length of rivers mapped (2.8 million km). This is followed by the Distributary, Confined, Mobile and Meandering Zones which account for 25, 11.5, 10 and 7.5% of the total river length respectively. The Pool Functional Process Zone was the rarest functional process zone, accounting for less than 1% of the total river length.

No sub-catchment contained all functional process zones (Figure 28.4a). The Murray, Goulburn, Lachlan, Macquarie and Murrumbidgee Rivers all contained seven of the eight functional process zones identified while the Bogan and Darling Rivers contain only two functional process zones. As a result, there is a great variation in the composition of functional process zones between the different sub-catchments of the Murray-Darling Basin. In the Darling for example, only two functional process zones (Anabranch and Distributary Zones) occur, and the Anabranch functional process zone accounts for 99% of its total river length. By comparison the Campaspe River in northern Victoria contains five functional process zones: Confined, Armoured, Mobile, Meandering, and Anabranch and these account for 18.1, 20.5, 26.7, 21.8 and 12.9% of the total length of this river, respectively. Differences in the physical diversity of the sub-catchments in terms of the length of various functional process zones are reflected in variations of the Simpson Diversity Index (D_{Si}); a diversity measure which utilizes the abundance and frequency of occurrence of functional process zones (Magurran, 2004). Diversity values range from 0.01 for the Barwon-Darling to 0.82 for the Macquarie River (Figure 28.4b). On average, those sub-catchments in the Murray Basin have a higher physical diversity of functional process zones compared with the Darling Basin. However, those rivers in the Murray Basin have a lower overall variation in physical diversity compared with the Darling at the basin scale. The mean and range of Simpson Diversity Index values for the Murray Basin are 0.676 and 0.500–0.780 respectively, compared with 0.586 and 0.199–0.820 for the Darling Basin. Overall, the physical diversity of rivers in the Murray-Darling Basin is high compared with other rivers: 0.560 for the Orange in South Africa, 0.412 for the Malibamastso in Lesotho and 0.522 for the Missouri in the US (Thorp *et al*., 2007).

Table 28.2 A description of the physical character of functional process zones found in the Murray-Darling Basin

Functional process zone	Valley gradient	Channel properties[a]	Dominant sediments	General description
Anabranch Zone	0.0003	P = 1.8 ω = Low RBS = 0.98–4.85	Sand, silt, clay (cohesive banks)	Channels in the Anabranch functional process zone consist of a series of effluent or anabranch channels that often flow across very broad floodplains or outwash surfaces. River channels in this zone can be 'underfit', i.e. smaller modern channels with high sinuosities that flow within older palaeo-channel systems having much larger meander wavelengths and channel dimensions. The main river channel in this zone is generally a wash load system with highly cohesive bank materials and steep banks
Armoured Zone	0.01 to 0.002	P = 1.4 ω = High RBS > 1	Cobble and gravel surface layer protecting poorly sorted finer sub-sediments	Armoured Zone channels typically exhibit meandering patterns superimposed on the larger valley pattern. Rivers in these zones display characteristics of a bed load/mixed load channel with relatively steep bed slopes, meander arcs and wavelengths. Armoured functional process zones are also characterized by a series of floodplains of different ages that are typically inset into high level terraces. Thus the river channel is relatively constrained, being controlled by the configuration of the valley with the presence and extent of floodplains determining the degree of control
Confined Zone	0.004	P = 1.2 ω = Very high RBS = 0.46	Bedrock, boulder, cobble	Confined (or gorge) functional process zones are dominated by steep bed slopes, often greater than 0.010, with bedrock chutes, accumulations of boulders or cobbles with scour pools or step-pool systems dominating the in-channel environment. Boulder materials are relatively immobile; however, flood flows can move cobble accumulations, producing well sorted deposits. These zones do not have adjacent floodplains, so sediments are added directly to the channel from adjacent valley slopes
Distributary Zone	0.0002	P = 1.8 ω = Low RBS > 1	Silt and clay	Bifurcating channels (channels that branch off from each other) are the main distinguishing features of distributary functional process zones. These secondary channels can persist relatively independently of the main channel and may flow for considerable distances across the floodplain before rejoining the main channel, joining with another secondary channel or terminating on the floodplain. In all channels (both main and secondary) there is a decrease in bankfull cross-sectional area or channel size downstream which is attributed to losses of water by evaporation, infiltration and in-channel storage. Most Distributary Zone channels are relatively narrow and featureless with occasional deep holes scattered along their length

Table 28.2 *Continued*

Functional process zone	Valley gradient	Channel properties[a]	Dominant sediments	General description
Lowland Confined Zone	0.0002	P = 1.5 ω = Low RBS > 1	Sand, silt, clay (cohesive banks)	The Lowland Confined functional process zone contains features similar to the meander zone but is relatively more confined because of geological structures or within palaeo-channels. Lateral movement of the main river channel is therefore restricted. These zones characterized have valley widths of 2–3 km
Meander Zone	0.0013	P = 1.6–1.8 ω = Moderate to low RBS < 1	Bimodal distribution of sand/gravel and finer particles (cohesive banks)	A distinguishing feature of the Meander functional process zone is the significant increase in the width of the valley floor (generally wider than 15 km) and associated floodplain surface. The river channel is relatively active and displays a typically meandering pattern. The presence of well-developed floodplain features, such as flood channels, former channels, avulsions, cutoffs and minor anabranching, testifies to the relatively active and unrestricted nature of the river–floodplain environment in this reach. The river in this zone is typical of a mixed to wash load channel with the cohesive bank sediments contributing to relatively steep banks
Mobile Zone	0.0013	P = 1.4–1.6 ω = Moderate RBS = 1–3	Bimodal distribution of gravel/pebble and finer particles	The Mobile functional process zone is an area characterized by a relatively active river channel with mobile bed sediments, large sediment storage areas and well developed inset floodplain features. The valley floor is moderately wide, allowing floodplain development to occur. The river channel is typically meandering with irregular planforms
Pool Zone	< 0.0001	P = 1.2 ω = Low RBS = 1–2.3	Bedrock, boulder with overlaying silts and clays in pools	Pool functional process zones are characterized by long pools separated by short channel constrictions. The pools form upstream of the channel constrictions and are the dominant morphological feature in the zones. Channel constrictions are generally associated with major bedrock bars that extend across the channel or substantial localized gravel deposits that act as riffle areas. Local riverbed slopes increase significantly at these constrictions; they therefore are small areas of relatively high energy, in contrast to the relatively low bed slopes and energies of the pool environment

[a] P, sinuosity; ω, stream power; RBS, relative bed stability index (values <1 indicate unstable, mobile beds).

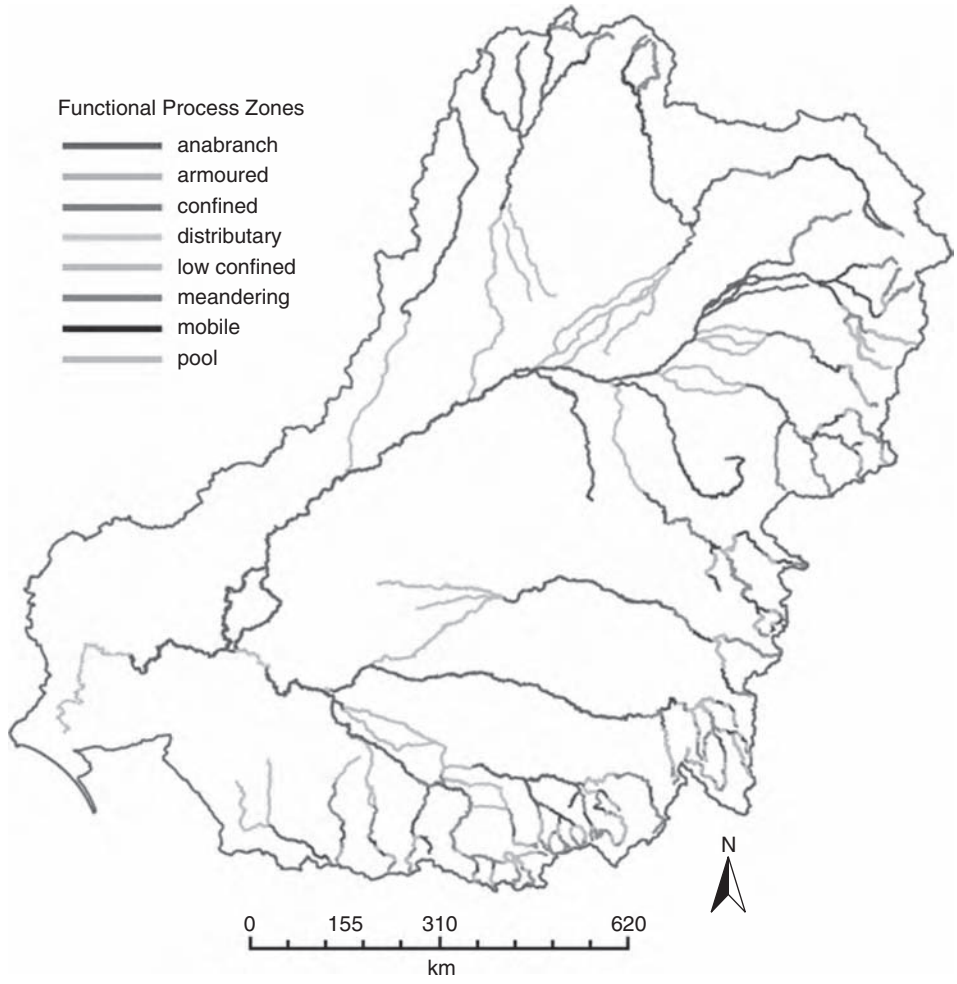

Figure 28.3 (See also colour plates.) The spatial arrangement of functional process zones within the Murray-Darling Basin

28.4 ASSESSING THE PHYSICAL CONDITION OF RIVERS AT THE CATCHMENT SCALE

In 2000 the National Land and Water Audit was commissioned to assess the condition of rivers within the intensive land zone of Australia. It provided an assessment of the environmental and biological condition of more than 14 000 river reaches (average length 14 km) within 193 catchments (average area 13 500 km^2) and covered most of the Australian Capital Territory, New South Wales, Queensland, Victoria and significant areas of South Australia, Western Australia and Northern Territory (ASRIS, 2001). There has been limited application of these data and here we aggregate the data for the functional process zones within the Murray-Darling Basin.

Details of the approach taken, development of methods, their application, analysis, and the preliminary interpretation of results are provided in Norris *et al*. (2001, 2007). The physical condition of the rivers are measured via an Aggregate Environment Index (ARC_e), which is made up of four unweighted sub-indices (catchment disturbance, *CDI*; habitat, *HI*; hydrological disturbance, *HDI*; suspended sediment and nutrient load, *SSNLI*). A description of each index is provided in Table 28.3. Each sub-index is scaled between zero and one, with a value of 1 corresponding to pristine conditions while 0 indicates the most degraded condition. The range of scores for the aggregate ARC_e was divided into four categories: (a) 1.0–0.75, largely unmodified; (b) 0.75–0.5, moderately modified; (c) 0.5–0.25, substantially modified; (d) 0.25–0, severely

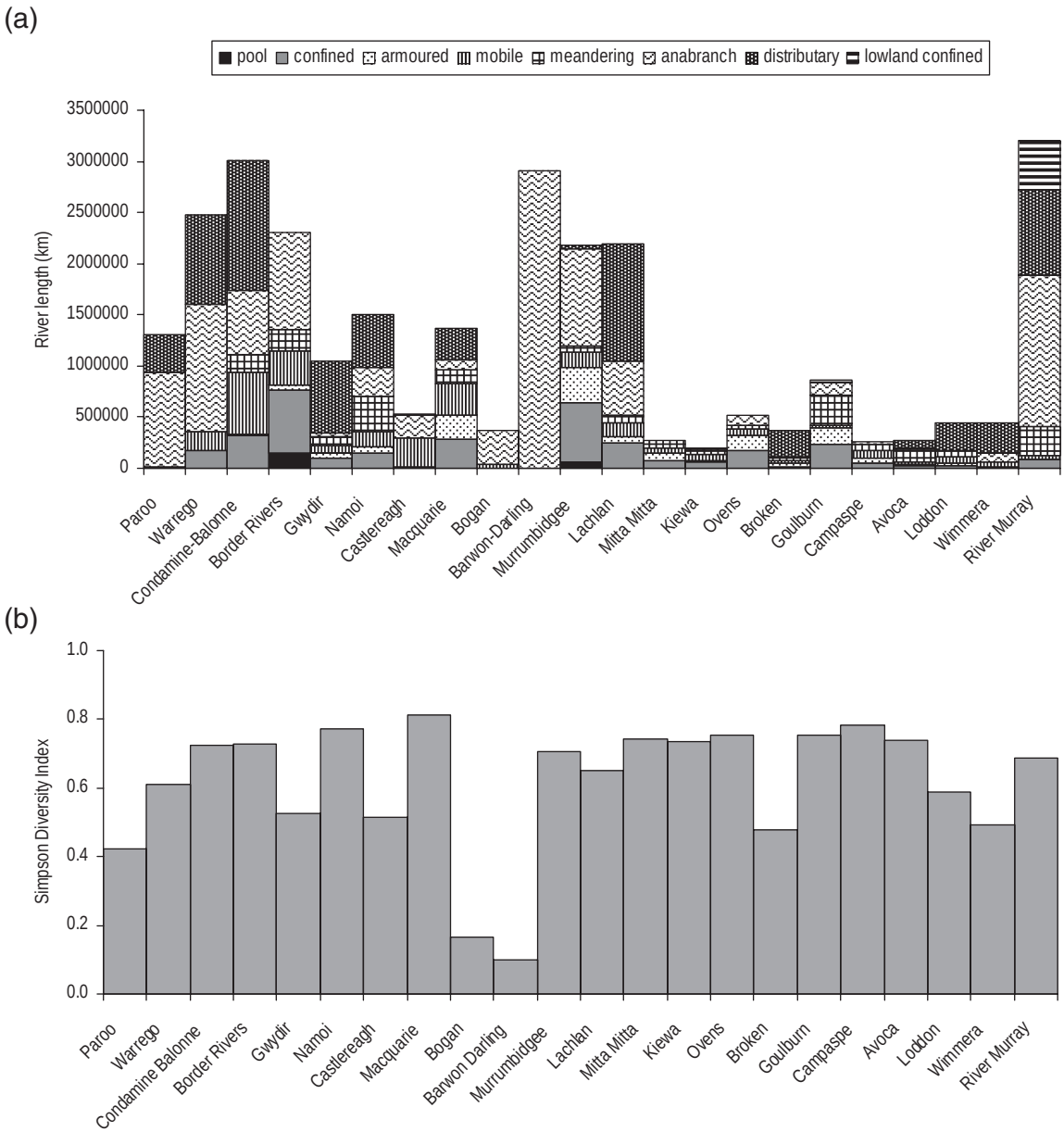

Figure 28.4 The functional process zones of sub-catchments within the Murray-Darling Basin. (a) The overall distribution; (b) the diversity of functional process zones

modified. The four sub-indices were combined, unweighted, using the standardized Euclidean distance procedure to calculate the ARC_e [Equation (28.1)]. The overall Environment Index was used for general assessment and the sub-indices for more specific interpretation of the physical condition.

$$ARC_e = 1 - \frac{\sqrt{(1-CDI)^2 + (1-HI)^2 + (1-HD)^2 + (1-SSNLI)^2}}{\sqrt{n}} \quad (28.1)$$

where n is the number of sub-indices.

Table 28.3 Metrics used to assess the physical condition of rivers in the Murray-Darling Basin

Indices	Variables used	Description
Environment Index (ARC_E)	Catchment disturbance (*CDI*) Habitat (*HI*) Hydrological disturbance (*HDI*) Suspended sediment and nutrients load (*SSNLI*)	ARC_E assesses the overall disturbance along channel reaches. An unweighted function of the four sub-indices *CDI, HI, HDI* and *SSNLI*
Catchment Disturbance Index (*CDI*)	Land use: includes impacts on nutrient enrichment, salinity, biocides, hydrological change, sediment supply, riparian change, toxicants Land cover: based on the proportion of land cleared in a reach catchment. (Note, is a measure of recent, rather than historic, land clearing) Infrastructure (e.g. railways, roads, pipelines): based on the area of each infrastructure category	*CDI* assesses the impacts of three broad scale nonpoint source disturbances. As these disturbances tend to be cumulative, *CDI* is defined as the sum of these three impacts
Habitat Index (*HI*)	Bed load: compares SEDNET modelling of sediment supply with sediment transport capacity over the last 150 years. Significant reductions in *HI* occur when >30 cm of sediment are deposited within a reach Riparian vegetation condition: % vegetation cover within 100 m on each side of the river (does not consider natives vs exotics) Connectivity (dams, weirs and levee banks): longitudinal connectivity considers the effects of cross-river structures that impede fish passage. Lateral connectivity is represented by the proportion of unleveed bank for a reach	*HI* is an integration of bed load, riparian vegetation condition and connectivity and assesses the state of local habitat and its likely ability to support aquatic life
Hydrological Disturbance Index (*HDI*)	Mean annual flow volumes: assesses changes in flow caused by diversions, abstractions and inter-catchment transfers Flow variability: assesses the deviation from the expected monthly flow duration curve Seasonality of flow: assesses changes in the seasonal timing of high and low flows using a seasonal periodicity measure Seasonal amplitude: assesses changes in the season magnitude of flows using a seasonal amplitude measure	*HDI* assess the impact of changes in flow regime to aquatic ecosystem function. An HDI is computed based on the cumulative deviation from an unimpacted condition for four hydrologic measures
Suspended Sediment and Nutrient Load Index (*SSNLI*)	Nutrients: assesses total nitrogen and total phosphorus based on the ratios of 'natural' (pre-disturbance) to current nutrient loads for a reach. The values for nutrient loads were obtained from NLWRA modelling (Norris *et al.*, 2007) Suspended solids: assesses suspended sediment load using an NLWRA model that predicts the amount of sediment arriving in rivers from hillslope, gully and riverbank erosion, under 'natural' (pre-disturbance) and current conditions	*SSNLI* assesses the impact of suspended sediments and/or nutrient loads on river health. The index is taken as the lowest value of the three standardized components based on the theory that if one measure is poor then overall reach condition is poor regardless of the state of the other two measures

28.5 THE PHYSICAL CONDITION OF RIVERS IN THE MURRAY-DARLING BASIN

The overall condition of rivers in the Murray-Darling Basin, as expressed by the Environment Index (ARC_e) is given in Figure 28.5 along with the individual index assessments. The majority assessed within the Basin recorded an ARC_e classification of moderately modified (66.4%), while 20% of the total length of rivers was classified as being substantially modified. In contrast, a relatively small proportion of the total length of rivers (5%) was classified as largely unmodified. Thus human activities have had a profound impact on rivers in the Murray-Darling Basin and very few river zones remain

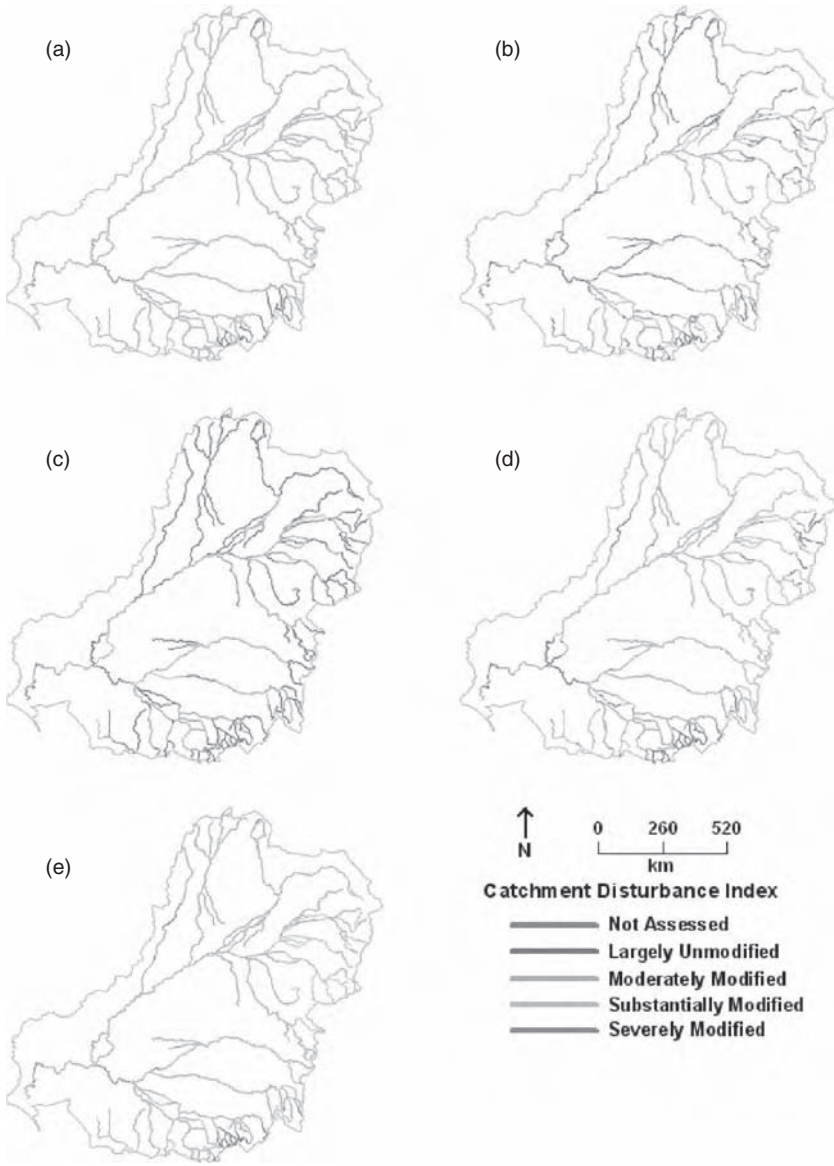

Figure 28.5 (See also colour plates.) The physical condition of rivers within the Murray-Darling Basin: (a) the overall Environmental Index (ARC_e); (b) Catchment Disturbance Index (*CDI*); (c) Habitat Index (*HI*); (d) Hydrological Disturbance Index (*HDI*); (e) Sediment Transport of Nutrient Load Index (*SSNLI*)

in a pristine condition. Moreover, although most river zones were classed as moderately modified, activities continue in many locations that could further degrade river systems thereby increasing the proportion of substantially modified lengths in the future.

Large lengths of river are impacted by catchment disturbance with 84.5% recording a moderately modified *CDI* (Figure 28.5). The remainder of the river lengths were largely unmodified (6.0%) or substantially modified (<2%). These results highlight the relatively small proportion of the Murray-Darling Basin that has been urbanized but may also illustrate one of the weaknesses of this index. The land cover parameter of the *CDI* only includes recent land clearing. The majority of the Murray-Darling Basin

was cleared in the 1920s, therefore this index under represents the impact of land clearing on fluvial and ecosystem processes in this system. Thus, the impacts on river condition indicated by the *CDI* are likely a response of the land use parameter that incorporates the current impacts of agriculture and other land uses rather than either the land cover or infrastructure parameters.

The *HI* which records in-channel disturbances shows relatively higher proportions of river lengths in the Murray-Darling Basin being more degraded than that recorded by the *CDI* (Figure 28.5). Here, 34.6% of the river lengths were classified as being moderately modified, with 27.3 and 3.6% substantially and severely modified respectively. This suggests that habitat disturbances are much more significant than catchment disturbances in deteriorating overall river condition. The values reported here include the substantial impacts dams and weirs have on longitudinal connectivity in the Murray-Darling, over 8000 structures inhibiting the movement of aquatic organisms within it. This index also highlights losses in riparian vegetation often associated with agricultural activities and/or reductions in flow levels, and incorporates the presence of sand slugs in the Basin, a common problem along many river reaches.

The *HDI* was not well represented in the overall assessment in the Murray-Darling Basin with only about 43% of the total river length being assessed. However, of the river lengths assessed, most displayed moderately modified conditions (25%), with 12% largely unmodified and about 5% substantially modified (Figure 28.5). As with the *CDI*, this index shows significant disturbance in some regions of the Murray-Darling Basin indicating that flow characteristics are considerably different today than they were pre-settlement. Water resource developments within the Murray-Darling Basin have significantly altered the flow regime of its rivers (Thoms and Sheldon, 2000). Flow regulation typically results in substantial changes to the volume, timing and variability in flows, all of which negatively impact on the *HDI*. However, the low percentage of the basin that was classified for this index may have resulted in the under- representation of hydrological disturbances within the Basin.

The final sub-index considered in this study is the *SSNLI*. The *SSNLI* values reported for the Murray-Darling Basin are similar to those for the *HI*, in that considerable disturbances are recorded in sediment and nutrients within the Basin (Figure 28.5). Only 8.3% of the river length were largely unmodified while 39% was either substantially (35%) or severely (4%) modified. The remaining 43% of assessed river length were moderately modified. These results indicate that suspended solids, total nitrogen and/or total phosphorous have increased substantially along many river lengths of the Murray-Darling Basin. These increases can have significant impacts on the health of aquatic ecosystems resulting in degraded river conditions.

28.5.1 Functional Process Zones

A detailed index by index analysis of disturbances in the various functional processes zones is presented below.

Catchment Disturbance Index

The *CDI* values vary with respect to functional process zones (Figure 28.6). In general, most functional process zones display moderately modified conditions and this category is the greatest for each of the eight functional process zones. Three functional process zones (the Armoured Zone, the Confined Zone and the Pool Zone) also have a significant proportion of largely unmodified reaches (17.0, 24.5, and 16.2% respectively) while only one functional process zone (the Meandering Zone) has more than 5% of its length being classified as substantially modified (5.4%). None of the functional process zones have lengths of river classified as severely modified *CDIs*. The three functional process zones with the highest proportions of largely unmodified reaches are those found mostly in the headwaters of the river system (Figure 28.6). This may be a function of the lack of floodplains in these functional processes zones which would limit the amount of land modification or infrastructure possible along these sections of rivers. All of the mid and lowland functional process zones had higher levels of disturbance, again likely resulting from the increased proportion of floodplain area along these sections of rivers.

Habitat Index

Five of the eight functional process zones exhibit comparable patterns of *HI*. The Anabranched, Armoured, Distributary, Low Confined and Mobile Zones have largely unmodified conditions for about 25% of their river length and moderately and substantially modified conditions for about 60% of their river length (Figure 28.6). The Confined functional process zones are the least disturbed in terms of their in-channel habitat with nearly 50% of their length being classified as being in a largely unmodified condition. In contrast, the Meandering and Pool functional process zones are largely unmodified for only 13.8 and 8.9% of their river lengths respectively. Only the Pool Zone had a significant proportion of its river length reaches (~19%) in a severely modified state with the remainder of the functional process zones having between 1 and 5% severely modified. Similar patterns in

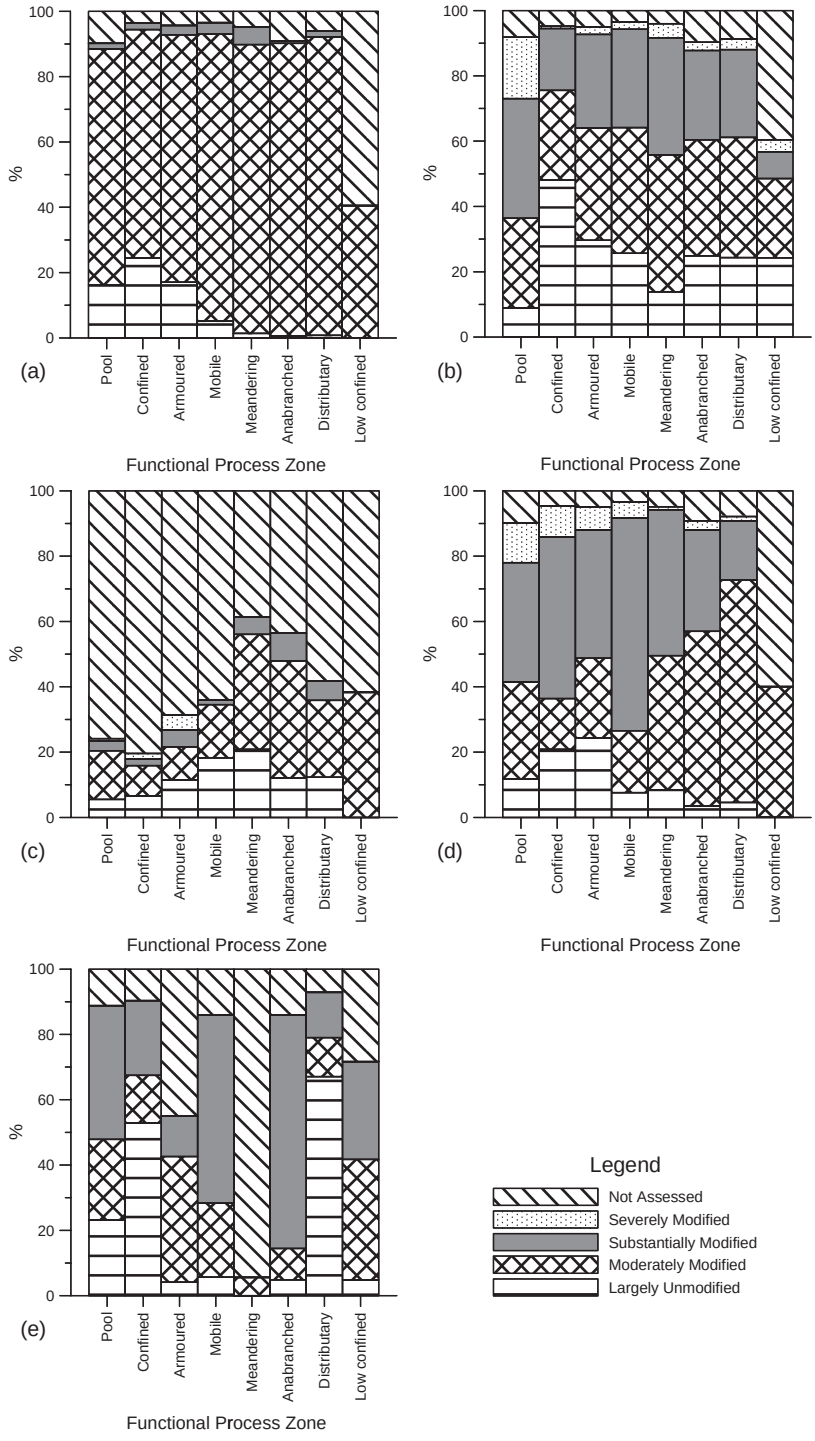

Figure 28.6 The physical condition of functional process zones throughout the Murray-Darling Basin: (a) the overall Environment Index (ARC_e); (b) Catchment Disturbance Index (*CDI*); (c) Habitat Index (*HI*); (d) Hydrological Disturbance Index (*HDI*); (e) Suspended Sediment and Nutrient Load Index (*SSNLI*)

HI classification for most functional process zones indicate that habitat disturbances are fairly uniform throughout the Murray-Darling Basin. For the most part, habitat disturbances are common and a significant proportion of functional process zones have highly modified habitats. This reflects the amount of riparian degradation, the number of flow control structures and the prevalence of sedimentation problems within the Murray-Darling Basin. Although poor conditions are common, the largest proportion of largely unmodified reaches are also observed for this index. Thus, many reaches are either very good or very poor with only about one-third of reaches in moderate condition.

Hydrological Disturbance Index

Assessments of hydrologic changes are difficult given the low percentage of river length classified with respect to this sub-index (Figure 28.6). Only the Anabranch and Meandering functional process zones had more than 50% of their river length classified according to the *HDI*, and both of these had moderately modified conditions for more than 35% of their length. Of the remaining functional process zones, most had an equal proportion of their assessed river length as being largely unmodified and moderately modified. No functional process zones had more than 10% of their length as being largely modified or worse. All of the functional process zones were again quite similar for the *HDI*, although this is mostly a function of the large proportion of reaches that were not assessed. Consequently, these data are difficult to interpret although it would appear that most functional process zones are in moderate or good condition. Several of the functional process zones, however, appear to have potentially significant disturbances in hydrology including the Anabranch, Armoured, Confined, Distributary, and Meandering Zones all of which would have greater than 10% of their river length substantially modified if the data were scaled up as a proportion of those reaches assessed.

Suspended Sediment and Nutrient Load Index

The *SSNLI* indicates modified conditions for most functional process zones (Figure 28.6). While the Armoured and Confined functional process zones are largely unmodified for 24.3 and 20.8% of their river lengths, respectively, the other six functional process zones have no more that 12% of their river lengths classified as largely unmodified. The Mobile functional process zone displays the highest level of *SSNLI* disturbance with over 65% of its river lengths being classified as substantially modified. However, the Anabranch, Confined, Meandering and Pool functional process zones also have large percentages of their channels (>30%) classified as substantially modified. In general, most functional process zones had significant levels of disturbance according to the *SSNLI*. This indicates that either suspended sediment, total nitrogen or total phosphorous (or some combination thereof) was considerably elevated above natural conditions. Although these parameters are often linked to agricultural activities, the results for the *SSNLI* are significantly different to those for the *CDI* indicating that other factors must also be contributing to sediment and nutrient loads in the Murray-Darling Basin. For example, in functional process zones with larger proportion of their length with largely unmodified *CDIs* (i.e. the Armoured Zone, the Confined Zone and the Pool Zone) more than 40% of the river length were either substantially or severely modified *SSNLIs*. For all functional process zones with the exception of the Distributary Zone and the Low Confined Zone (for which *HI* was the most disturbed), the *SSNLI* had the largest proportion of substantially or severely modified reaches. This suggests that, along with habitat disturbances, suspended sediments and nutrient loads are a key threat to the long term viability of aquatic ecosystems within the Murray-Darling Basin and should be targeted for management initiatives.

Environment Index

All of the functional process zones were dominated by a moderately modified classification of their river length (Figure 28.6). This is notable in the Anabranch, Confined, Distributary, Low Confined, Meandering and Mobile functional process zones all of which have greater than 50% of their river length classified as moderately modified. Only two functional process zones have a significant proportion of their length largely unmodified, and these being the Armoured Zone (~16%) and the Confined Zone (~17%). Many functional process zones, however, have large proportions of their reaches classified as substantially modified, most notably the Armoured Zone (~32%), the Confined Zone (~23%), the Meandering Zone (~25%), the Mobile Zone (~30%) and the Pool Zone (~42%). Both the Anabranch and Distributary Zones also have greater than 10% of their river length classified as substantially modified. Thus, in terms of their overall condition, most functional process zones have considerable reach lengths classified as either moderately modified or substantially modified.

Although four sub-indices are included in the computation for the Environment Index, the significant proportion of unassessed reaches for the *HDI* means that many

reaches included only three of the four sub-indices. This is especially true for the Pool and Confined Zones, given that each had fewer than 25% of their reaches assessed for hydrological disturbances. Similarly, the Low Confined Zone had at least 40% of its reaches unassessed for each of the four sub-indices and consequently nearly 60% of its reaches were not assigned a value for the Environment Index. Consequently, the results for the Environment Index largely reflect the very high proportion of reaches classified as moderately modified in the *CDI* and the relatively high proportions of reaches classified as substantially modified in the *HI* and *SSNLI*. This reinforces the previous conclusion that habitat, suspended sediment, and nutrient load disturbances are perhaps the most significant contributors to the deteriorating condition of the rivers in the Murray-Darling Basin.

28.6 THE GEOGRAPHY OF DISTURBANCE

Spatial patterns in disturbances are assessed by looking at two factors: (1) the location of disturbances within the Murray-Darling Basin; and (2) the connectivity of disturbances within the Murray-Darling Basin.

Catchment disturbances, as measured by the *CDI*, are fairly uniform throughout the Murray-Darling Basin with most lengths of river being classified as moderately modified. However, two areas, both in the River Murray section of the basin, show distinct groups of largely unmodified lengths of river to the east and substantially modified lengths of river to the west (Figure 28.5). Only a few scattered river lengths of either class are found outside these areas. This may be a result of recent land clearing in the case of the substantially modified reaches, and low levels of agricultural land use in the case of the largely unmodified reaches. In both cases, these discontinuous lengths of river occur along fingertip tributaries. Therefore, it would not be possible for aquatic organisms to migrate from one largely unmodified reach to another without passing through a moderately modified reach. The substantially modified lengths of river, on the other hand, typically occur in the middle of longer river reaches instead of along fingertip tributaries. Therefore, these reaches represent a barrier to the passage of aquatic organisms in that they typically occur between two moderately modified reaches.

Rivers in the Murray-Darling Basin exhibit highly fragmented habitat disturbance with interchangeable sections of moderately modified and substantially modified lengths of river (Figure 28.6). Severely modified lengths of river are also evident, but only in small patches in the headwater regions of many of the river systems. The northern areas of the Murray-Darling Basin have extensive regions of largely unmodified conditions, although these are disrupted by the presence of smaller lengths of river that are moderately or substantially modified. The Lachlan and Murrumbidgee Rivers also have relatively long lengths of river classified as largely unmodified, again interspersed with smaller moderately modified reaches. However, these unmodified lengths of river are located downstream of severely modified river lengths. The extremely disturbed nature of in-channel habitat in the Murray-Darling Basin indicates the untenable condition of the river with respect to this index. Riparian vegetation is degraded along major lengths of the rivers in the basin, reducing habitat availability, while the presence of numerous physical structures (dams and weirs) limits the ability of organisms to move freely along the rivers (longitudinal connectivity) and reduces the interchange of nutrients between river channels and floodplains (lateral connectivity). Fragmentation of unmodified lengths of river also reduces the longitudinal connectivity of the system, with disturbed sections (some of which are severely modified) acting as barriers for migrating organisms. Thus, the ability of many reaches within the Murray-Darling Basin to support in-channel aquatic life is degraded.

Spatial patterns of the *HDI* in the Murray-Darling Basin are difficult to assess because of the number of unassessed reaches. It is evident, however, that there are long lengths of river that are largely unmodified. In particular the Paroo River in the Darling Basin is classified as being largely unmodified for its entire length and is the last unregulated river in the Murray-Darling Basin. There are also considerable lengths of unmodified river in the headwaters of the Condamine-Balonne Basin and other headwater regions within the River Murray Basin that exhibit largely unmodified conditions. By comparison the majority of the substantially or severely modified lengths of river are in the River Murray catchment and, like the *CDI* disturbances, these reaches tend to be discontinuous, being separated by moderately modified reaches. Similarly, the largely unmodified lengths of river within the River Murray catchment are also separated by more highly disturbed lengths of river. Hydrological disturbances of the nature observed within the River Murray catchment have been associated with disruptions to aquatic ecosystems (Thoms *et al*., 2004). In particular, the flow regime in those sections of the Murray-Darling Basin that are moderately, substantially or severely modified are often no longer highly variable, rather they will be maintained at constant levels year round. Alternatively, large floods may occur in seasons that normally would have been dry while a dry period may occur during wet periods. In addition, perpetual inundation behind flow control

structures can also have significant impacts on aquatic ecosystems. Only the Paroo River is exempt from these sorts of impacts while the rest of the Murray-Darling Basin is experiencing relatively constant flow conditions dissimilar to those that would have occurred under pre-settlement conditions.

Several spatial patterns emerge with the *SSNLI*. The majority of headwater reaches are classified as either substantially modified or severely modified. The exception to this is a group of tributaries in the southern parts of the River Murray catchment that are classified as being largely unmodified. These lengths of river in upland regions are environments that have limited land clearing and vegetation change and, therefore are classified as being largely natural with respect to sediment and nutrient loads. The remaining headwater sections of these rivers are associated with catchments that have undergone substantial land clearing. The most significant implication of this is the location of substantially to severely modified lengths of river in the headwater regions of many of the river systems in the Murray-Darling Basin. Sediments and nutrients originating from these upstream sites can be transported throughout the entire system and have the potential to contribute to the degradation of reaches in the downstream direction. Downstream of these headwater regions, the majority of rivers within the Murray-Darling Basin are classified as having moderately modified sediment and nutrient load conditions. These lengths of river are predominantly associated with floodplain settings that have been extensively developed for agricultural activities that also contribute sediments and nutrients both directly (through the discharge and effluents into channels) and indirectly (through increased erosion from land clearing) to the adjacent channels. The only floodplain section classified as being largely unmodified with respect to its sediment and nutrient loads is the Paroo River.

Overall, the majority of rivers in the Murray-Darling Basin are moderately to substantially modified. The only significant sections of river with an ARC_e classification of largely unmodified are located in the south-eastern corner of the River Murray catchment and the Paroo River in the Darling Basin. The eastern portion of the Darling River Basin has the highest density of substantially modified lengths of river both as long continuously disturbed reaches or interspersed with moderately modified river lengths. The ARC_e classification suggests that the most degraded part of the Murray-Darling Basin is the headwaters of the Darling River with the Macintyre, Gwydir and Namoi Rivers in particularly poor condition. These rivers could be potential targets for new management initiatives that seek to redress these disturbances in order to return these systems to a more natural condition, thereby reducing their modification levels down to the moderately modified classification.

28.7 CONCLUSION

Science must form the basis for environmental or natural resource management (Cullen, 1990). The basic processes that govern any river system should be investigated and understood before they can be effectively and efficiently managed. The approach applied in this study of the Murray-Darling Basin provides a framework that has enabled managers to take an important step in the understanding of the character and dynamics of large river systems. Rivers are complex elements of the landscape and their character may change along their length and over time. Broad-scale differences occur in the character and function of rivers within the Murray-Darling Basin. Rivers in the different parts of the Basin have different characteristics and behaviours hence they have responded to disturbances, both natural and human induced, in varying ways. Some responses have been subtle and within the natural range of river system functions, while others are more obvious and result in major changes to the character and functioning of the river. These responses can impinge upon the health or condition of the river system. The river characterization exercise undertaken in this study underpins the current, more detailed auditing, of the condition of river systems in the Murray-Darling Basin. The Sustainable Rivers Audit is a programme to systematically assess the river health across the Murray-Darling Basin by collecting information in a consistent way across a range of indicators. The Audit reports on the condition of the rivers in the Basin at the catchment for which indicators are collected from functional process zones. Thus, the physical form of the rivers and floodplains constitute the basic template upon which the Audit is based.

The geographic distribution of disturbances in the Murray-Darling Basin highlights several ways in which management initiatives might be targeted. First, connectivity is an issue in many sub-catchments in the Basin. Sections of river that are assessed as being in a good physical condition are being fragmented from one another by highly disturbed or unhealthy sections. These disturbances provide barriers to the passage of aquatic organisms. Therefore, great gains could be made in the overall connectivity of the system by targeting management initiatives in those disturbed sections that fall between less disturbed reaches thereby producing relatively longer sections with minimal disturbance. This is true where only small substantially or severely modified sections of river

occur between two moderately modified or largely unmodified river sections. Second, many of the most highly disturbed reaches occur in headwaters of regions of the Murray-Darling Basin, which have impacted low *SSNLI* and *HI* values. Disturbances in headwater regions have the potential to translate downstream. Thus, another management initiative might be to target these regions where disturbances are substantial or severe thereby having the corollary benefit of improving the condition of those downstream sections. Finally, the high diversity of river types found within the Murray-Darling Basin is one of its principal environmental assets and is a key driver underpinning the ecological diversity. This physical diversity should be maintained wherever possible. However, several functional process zones, in particular the Pool Zone and to a lesser extent the Armoured, Mobile, Confined and Meandering Zones have a large proportion of their total length in highly degraded states. This condition could lead to a loss of viable sections of river of a particular type unless direct effort is made to conserve these sections of river. This problem is compounded in specific regions of the Murray-Darling Basin. In many of the subcatchments within the Darling Basin most of the functional process zones already exhibit substantially modified (or worse) conditions. The viability of these functional process zones to maintain healthy aquatic ecosystems maintenance is therefore considerably reduced and the loss of biological diversity in the Darling becomes more likely. Thus, a final management initiative for the Murray-Darling Basin is to target the establishment of only lightly modified reaches from each functional process zone in each major sub-catchment within the Basin to ensure the maximum diversity, both physical and biological, is maintained.

Often there can be difficulty in applying broad principles to proposed management activities. Many large rivers like those in the Murray-Darling Basin have had only limited studies made of them, and there are still insufficient data for making responsible decisions. Because of the highly unpredictable and variable nature of flows and sediment movement in these systems, it is recommended that an adequate data set be collected. It is the responsibility of government to ensure appropriate data are available on which to base responsible decisions. The widely accepted 'precautionary principle' advises that. For example, sand and gravel or water extractions should not take place until there is sufficient understanding to enable the river system's stakeholders to make reasonable predictions about their impacts.

Responsible decision making about natural resource issues requires a good understanding of both the physical character of these systems, because the intrinsic complexity of large river systems is an important ecosystem control. Although knowledge can be directly transferred from other regions, it is no substitute for sound information and knowledge of these ecosystems. Further detailed studies are required in the rivers of the Murray-Darling Basin. The results of this broad scale assessment underpin future activities of river assessment in the Murray-Darling Basin. Effective and efficient management of Australia's large river systems must be adaptive because of their natural complexity and variability.

ACKNOWLEDGEMENTS

Data for the assessment of the physical condition of rivers in the Murray-Darling Basin were kindly provided by Blair Woods of the National Land and Water Audit Office.

REFERENCES

ASRIS (Australian Soil Resource Information System) (2001) http://audit.ea.gov.au/ANRA/agriculture/docs/national/Agriculture_ASRIS.html.

Bell, R.H.V. (1995) A review of the programme of the Scientific Services Section, Kruger National Park. Warwick.

Biggs, H.C. (2003) Integration of science: successes, challenges, and the future. In: *The Kruger Experience: Ecology and Management of Savanna Heterogeneity* (J.T. Du Toit, K.H. Rogers and H.C. Biggs, Eds.). Island Press, Washington, 469–487.

Bissonette, J.A. and Storch, I. (2003) *Landscape Ecology and Resource Management*. Island Press, Washington.

Boon, P.J, Calow, P. and Petts, G.E. (eds) (1992) *River Conservation and Management*. John Wiley & Sons, Ltd, Chichester.

Boys, C.A. and Thoms, M.C. (2006) A hierarchical scale approach to the assessment of fish assemblages and their habitat associations in large dryland rivers. *Hydrobiologia*, 572: 11–31.

Brierley, G.J. and Fryirs, K.A. (2005) *Geomorphology and River Management; Application of the River Styles Framework*. Blackwell, Oxford.

Carling, P.A. and Petts, G.E. (1992) *Lowland Floodplain Rivers: Geomorphological Perspectives*. John Wiley & Sons, Ltd, Chichester.

Chen, Z., Yu, L. and Gupta, A. (eds) (2001) The Yangtze River. *Geomorphology*, 41.

Cullen, P. (1990) The turbulent boundary between science and water management. *Freshwater Biology*, 24: 201–209.

Davies, B.R. and Walker, K.F. (1986) *The Ecology of World Rivers*. Junk, Dordrecht.

Dodge, D.P. (ed.) (1989) *Proceedings of the International Large River Symposium*. Canadian Special Publication of Fisheries and Aquatic Sciences, 106.

Dollar, E.S.J., James, C.S., Rogers, K.H. and Thoms, M,C. (2007) A framework for interdisciplinary understanding of rivers as ecosystems. *Geomorphology* (in press).

Du Toit, J.T., Rogers, K.H. and Biggs, H.C. (eds) (2003) *The Kruger Experience: Ecology and Management of Savanna Heterogeneity*. Island Press, Washington, 519 pp.

Finlayson, B.L. and McMahon, T.A. (1988) Australia vs the world: a comparative analysis of streamflow characteristics. In: *Fluvial Geomorphology of Australia* (R.F. Warner, Ed.). Academic Press, Sydney, 17–40.

Frissell, C.A., Liss, L.J., Warren, C.E. and Hurley, M.D. (1986) A hierarchical framework for stream habitat classification: viewing streams in a watershed context. *Environmental Management*, 10: 199–214.

Gupta, A. (ed.) (2002) Large Rivers. *Geomorphology*, 44.

Kelman, A. (2005) *A river and its City. The Nature of Landscape in New Orleans.* University of California Press, Berkley, 283 pp.

Levin, S.A. (1992) The problem of pattern and scale in ecology. *Ecology*, 73: 1943–1967.

Magurran, A.E. (2004) *Measuring Biological Diversity*. Blackwell, Oxford, 256 pp.

Maheshwari, B.L., Walker, K.F. and McMahon, T.A. (1995) Effects of regulation on the flow regime of the River Murray, Australia. *Regulated Rivers: Research and Management*, 10: 15–38.

MDBMC (1987) *An Audit of Water Use in the Murray-Darling Basin.* Murray-Darling Basin Ministerial Council, Canberra, 40 pp.

Miall, A.D. (2006) How do we identify big rivers? And how big is big? *Sedimentary Geology*, 186: 39–50.

Montgomery, D. R. and Buffington, J. M. (1998) Channel-reach morphology in mountain drainage basins. *Geological Society of America Bulletin*, 109: 596–611.

Nix, H.A. and Kalma, J.D. (1982) *The Climate of the Murray-Darling Basin*. CSIRO Division of Land and Water Resources, Canberra.

Norris, R.H., Prosser I., Young B., Liston P., Bauer N., Davies N., Dyer F., Linke S. and Thoms M.C. (2001) *The Assessment of River Condition (ARC). An audit of the ecological condition of Australian Rivers*. Final report submitted to the National Land and Water Resources Audit Office, Canberra.

Norris, R.H., Linke, S., Prosser I., Young, W.J., Liston, P., Bauer, N., Sloane, N., Dyer F. and Thoms, M.C. (2007) Very-broad-scale assessment of human impacts on river condition. *Freshwater Biology*, 52: 959–976.

O'Neill, R.V. (1989) Perspectives in hierarchy and scale. In: *Perspectives in Ecological Theory* (J. Roughgarden, R.M. May and S.A. Levin, Eds.). Princeton University Press, New Jersey, pp. 140–156.

O'Neill, R.V., DeAngelis, D.L., Waide, J.B. and Allen, T.F.H. (1986) *A Hierarchical Concept of Ecosystems*. Princeton University Press, New Jersey.

Parsons, M.E. and Thoms, M.C. (2007) Hierarchical patterns of physical-biological associations in river ecosystems. *Geomorphology* (in press).

Phillips, J.D. (1995) Biogeomorphology and landscape evolution: the problem of scale. *Geomorphology*, 13: 337–347.

Puckridge, J.T., Sheldon, F., Walker, K.F. and Boulton, A.J. (1998) Flow variability and the ecology of large rivers. *Marine and Freshwater Research*, 49: 55–72.

Riley, S.J. and Taylor, G. (1978) The geomorphology of the Upper Darling River system with special reference to the present fluvial system. *Proceedings of the Royal Society of Victoria*, 90: 89–102.

Rogers, K.H. (2003) Adopting a heterogeneity paradigm; implications for management of protected savannas. In: *The Kruger Experience: Ecology and Management of Savanna Heterogeneity* (J.T. Du Toit, K.H. Rogers and H.C. Biggs, Eds.). Island Press, Washington, 41–58.

Rogers, K.H. (2006) The real management challenge: integrating scientists, stakeholders and service agencies. *River Research and Applications*, 22: 269–280.

Schumm, S.A. and Lichty, R.W. (1965) Time, space and causality in geomorphology. *American Journal of Science*, 263: 110–119.

Sheldon, F. and Thoms, M.C. (2006) Geomorphic In-channel Complexity: the key to organic matter retention in large dryland rivers? *Geomorphology*, 77: 275–285.

Simpson, H.J., Cane, M.A., Herczeg, A.L., Zebiak, S.E. and Simpson, J.H. (1993) Annual river discharges in southeastern Australia related to El Niño Southern Oscillation forecasts of sea surface temperatures. *Water Resources Research*, 29: 3671–3680.

Southwood, T.R.E. (1977) Habitat, the Templet for Ecological Strategies? *Journal of Animal Ecology*, 46: 337–365.

Stevenson, R.J. and Hauer, F.R. (2002) Integrating hydrogeomorphic and index of biotic integrity approaches for environmental assessment of wetlands. *Journal of the North American Benthological Society*, 21: 502–513.

Thoms, M.C. and Parsons, M. (2002) Ecogeomorphology: an interdisciplinary approach to river science. *International Association of Hydrological Sciences*, 27: 113–119.

Thoms, M.C. and Sheldon, F. (2000) Water resource development and hydrological change in a large dryland river system: the Barwon-Darling River, Australia. *Journal of Hydrology*, 228: 10–21.

Thoms, M.C. and Walker, K.F. (1992) Morphological changes along the River Murray, South Australia. In: *Lowland Floodplain Rivers: Geomorphological Perspectives* (P.A. Carling, and G.E. Petts, Eds.). John Wiley & Sons, Ltd, Chichester, 235–249.

Thoms, M.C., Hill, S.M., Spry, M.J., Chen, X.J., Mount, T.J. and Sheldon, F. (2004) The geomorphology of the Darling River. In: *The Darling* (R. Breckwodt, R. Boden and J. Andrews, Eds.). Murray Darling Basin Commission, Canberra, 68–105.

Thoms, M.C., Southwell, M.R. and McGinness, H.M. (2005) Water resource development and the fragmentation of floodplain river ecosystems. *Geomorphology*, 71: 126–138.

Thoms, M.C., Beyer, P. and Rogers, K.H. (2006) Variability, complexity and diversity – the geomorphology of river ecosystems in dryland regions. In: *The Ecology of Desert*

Rivers (R.T. Kingsford, Ed.). Cambridge University Press, Cambridge, 47–75.

Thorp, J.H., Thoms, M.C. and Delong, M.D. (2007) *The River Ecosystem Synthesis*. Elsevier (in press).

Townsend, C.R. and Hildrew, A.G. (1994) Species traits in relation to a habitat templet for river systems. *Freshwater Biology*, 31: 265–275.

Van Niekerk, A.W., Heritage, G.L. and Moon, B.P. (1995) River classification for management: the geomorphology of the Sabie River in the eastern Transvaal. *South African Geographical Journal*, 77: 68–76.

Wiens J.A. (1989) Spatial scaling in ecology. *Functional Ecology*, 3: 385–397.

29

Climatic and Anthropogenic Impacts on Water and Sediment Discharges from the Yangtze River (Changjiang), 1950–2005

Kehui Xu[1], John D. Milliman[1], Zuosheng Yang[2] and Hui Xu[3]

[1]*School of Marine Science, College of William & Mary, Gloucester Point, VA 23062, USA*
[2]*College of Marine Geosciences / Key Lab of Submarine Science and Exploration Technology, Ministry of Education, Ocean University of China, Qingdao 266003, People's Republic of China*
[3]*Institute of Atmospheric Physics, Chinese Academy of Sciences, Beijing 100029, People's Republic of China*

29.1 INTRODUCTION

Rivers form the major links between land and ocean through their transfer of water and sediment. Fluvial discharges to the oceans, however, are unevenly distributed in both space and time, in large part influenced by both climatic (e.g. precipitation) and anthropogenic (e.g. dam construction) forcings.

The global water system has been greatly impacted by humans (Vörösmarty *et al*., 2003), and more than half the world's large river systems are significantly affected by dams or water diversions (Nilsson *et al*., 2005; Syvitski *et al*., 2005). Considering projected climate change and growing demographic pressures, the availability and quality of freshwater have become increasing concerns (Gleick, 1993, 2000; Shiklomanov and Rodda, 2003). Nowhere are these concerns more acute than in southern Asia, where water withdrawal has increased about fourfold since 1950 (Shiklomanov, 1999). China and India alone account for more than 40% of the global freshwater used for irrigation (Gleick, 2000), and since 1950, China has built almost half the world's large dams higher than 15 m (Fuggle and Smith, 2000).

Historically, terrestrial erosion has accelerated in response to deforestation and land cultivation, but in recent years sediment delivery from many rivers has decreased following construction of large dams. Those on the Colorado and Nile Rivers, together with extensive downstream irrigation systems, have resulted in almost total elimination of riverine sediment discharges to the coastal regions. As a result, the deltas of these two rivers are actively receding (Stanley and Warne, 1998; Carriquiry *et al*., 2001). In the Yellow River, the impact from dam construction has been greatly amplified by decreased precipitation, leading to increased water consumption (Wang *et al*., 2006); water and sediment discharges now are <15% of the 1950–1960s levels, and its once-prograding delta is now being eroded (Chu *et al*., 2006).

The basin of the Yangtze River (Changjiang, Figure 29.1) is home to 400 million inhabitants and includes >50 000 dams within its boundaries, making it one of the most highly impacted rivers in the world (Nilsson *et al*., 2005; Yang, Z.S. *et al*., 2006). Recent climatic change in the Yangtze drainage basin has resulted in more melting of snow and ice at higher elevations (Wu, 2000; Chen, X. *et al*., 2001; Cyranoski, 2005), significant decline in regional annual precipitation over the northern tributaries, as well as more frequent and extreme flooding in recent years (Menon *et al*., 2002; Xu *et al*., 2005).

Large Rivers: Geomorphology and Management, Edited by A. Gupta

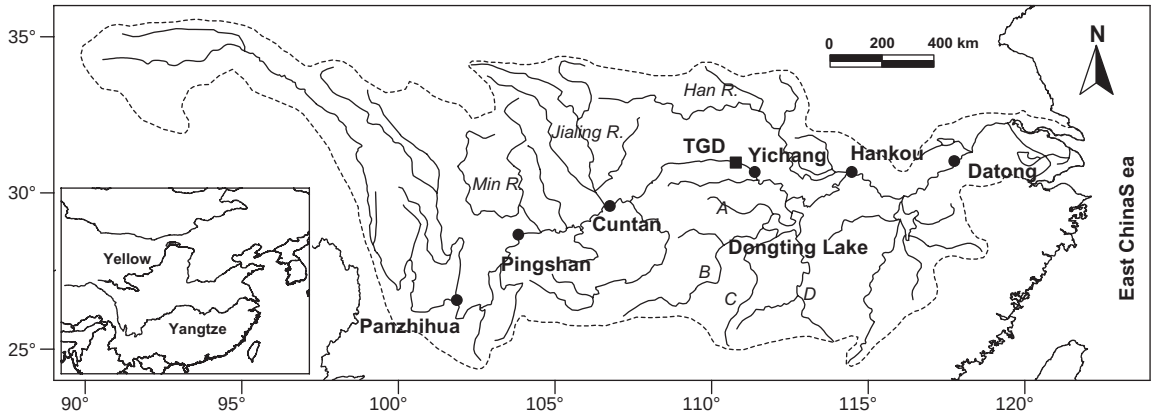

Figure 29.1 Yangtze River drainage basin. Dots represent six major gauging stations along the main stream. TGD, Three Gorges Dam. Four southern tributaries (A, Lishui River; B, Yuan River; C, Zishui River; D, Xiang River) flow into Dongting Lake and then enter the mainstem. Traditionally the Yangtze is divided into upper (above Yichang), middle (Yichang to Hankou) and lower (downstream of Hankou) reaches

Numerous anthropogenic activities also have increasingly impacted the Yangtze since the 1950s. Water withdrawal and consumption of the Yangtze have expanded about fourfold as the population has doubled and irrigation withdrawals have increased (Ren *et al*., 2002). Since 1988, sediment discharges in headwater streams have decreased greatly due to the Yangtze Water and Soil Conservation Project. Moreover, since June 2003, the Three Gorges Dam (TGD, the world's largest in terms of hydropower-generating capacity) also started to impound both water and sediment. With full operation of TGD to begin in 2009, its threatening impact to the channel downstream of the dam and the coastal ecosystems is a cause for acute concern (Xie *et al*., 2003; Shen and Xie, 2004). Plans for future large dams upstream of the TGD and the proposed south–north water diversions, almost certainly will accentuate existing anthropogenic impacts on the Yangtze.

In the past two decades, more than 100 papers have been published on water and sediment variations of the Yangtze River (Shi *et al*., 1985; Liu and Zhang, 1991; Zhang, 1995; Higgitt and Lu, 1996; Deng and Huang, 1997; Chen, Z. *et al*., 2001; Yang *et al*., 2002; Zhang and Wen, 2004; Yang, Z.S. *et al*., 2006), but few have been able to (a) address both spatial and temporal change of the whole Yangtze in a comprehensive way, (b) delineate and compare sub-basin variations, and (c) quantitatively separate climatic impacts from the human ones. In this chapter we discuss the spatial and temporal trends of both water and sediment fluxes of the Yangtze drainage basin from 1950 to 2005, and attempt to quantify the river's responses to various impacts. Specifically, we ask how have basin-wide and sub-basin water and sediment discharges responded to climatic (e.g. precipitation) as opposed to anthropogenic (e.g. dams) forcings? Given the recent changes within the basin, what can we expect in the future and how will the coastal regions respond to these changes?

29.2 PHYSICAL SETTING

Draining a basin of 1.8×10^6 km^2, the largest in southeastern Asia, the Yangtze River is one of the world's biggest rivers in terms of both water (5th; 900 km^{3}year^{-1}) and sediment discharges [4th; 480 million tons (mt) year^{-1}] (Milliman and Meade, 1983; Milliman and Syvitski, 1992; Meade, 1996). Originating in the Qinghai-Tibet Plateau (Saito *et al*., 2001), the Yangtze drains high mountains and flows through steep valleys in its upper reaches, meanders across low-gradient alluvial plains in its middle and lower courses, and merges with numerous northern and southern tributaries before debouching into the East China Sea (Figure 29.1). Mean annual precipitation rapidly increases in the downstream direction, from <400 mm in the northwest to >1600 mm in the southeast; with the basin-wide annual precipitation averaging 1050 mm (Figure 29.2). Rainfall in the Yangtze Basin follows a typical monsoonal regime (Shi *et al*., 1985), with more than 60% of annual precipitation falling during the wet season (March–August in the middle and lower sections; May–September farther upstream).

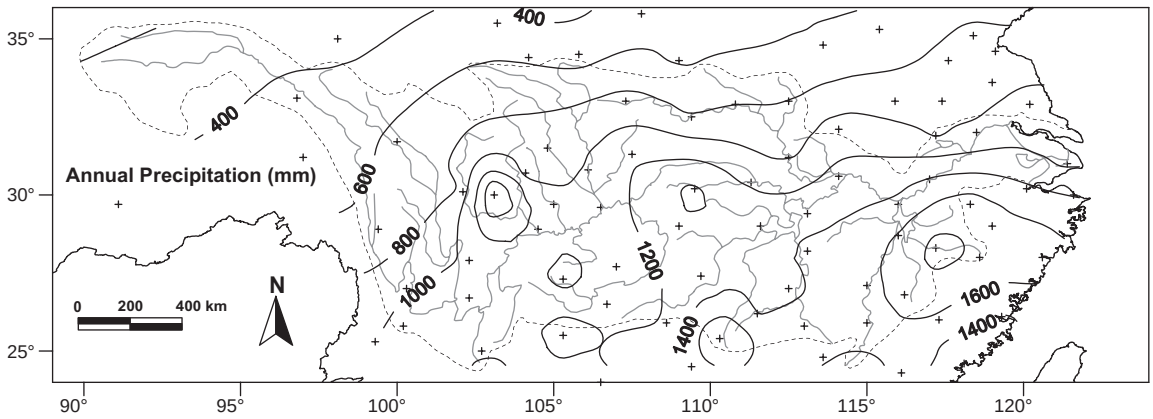

Figure 29.2 Mean annual precipitation (mm) in Yangtze drainage basin, 1951–2000. Crosses represent locations of meteorological stations

29.3 DATA AND METHODS

Monthly precipitation data (1951–2000) from 47 meteorological stations throughout the Yangtze Basin (shown as crosses in Figure 29.2) were extracted from a 160-station precipitation dataset released by the Ministry of Meteorology in China. Since these stations are not evenly distributed in space, basin-wide and sub-basin annual average precipitation were determined by interpolation and gridding in a Golden Surfer program after equal-area projection in ArcView GIS software.

Water and suspended-sediment discharges were obtained primarily from the Bulletin of Yangtze Sediment in 2000–2005, Changjiang Water Resources Commission, as well as from published papers (Shi *et al*., 1985; Higgitt and Lu, 1996; Deng and Huang, 1997; Pan, 1997; Lu and Higgitt, 1998; Chen, Z. *et al*., 2001; Shen, 2001; Yang *et al*., 2002; Zhang and Wen, 2004). Since bed load represents only 5% of total sediment discharge from the Yangtze River (Chen, Z. *et al*., 2001), it is not discussed here. Annual water and suspended-sediment discharges from 23 gauging stations were collected to delineate temporal and spatial trends between 1950 and 2005. Runoff was calculated by dividing water discharge by its corresponding drainage basin area upstream from the gauging station. Monthly data were collected from three mainstem stations (Yichang, Hankou and Datong, Figure 29.1). Sediment-yield data were compiled from Liu and Zhang (1991) and Dai and Tan (1996).

Trends for precipitation, runoff, sediment discharges as well as correlation coefficients (R^2) between precipitation and runoff were calculated by linear regression. Nonparametric Mann–Kendall analysis (Mann, 1945; Kendall, 1975) was used to analyze the trends for precipitation and runoff over the same period, its calculation procedure explained in Smith (2000).

29.4 SPATIAL VARIATIONS OF WATER AND SEDIMENT

The Yangtze drainage basin can be divided into four distinct sub-basins (Upper1, Upper2, North and South, Figure 29.3) based on patterns of runoff, sediment yield and sediment concentration. The drainage area upstream from the seaward-most Datong Station incorporates 94% of the entire basin area and represents the basin-wide values (the grey regions in Figure 29.3). A disproportionate amount of Yangtze water comes from the south-east whereas its sediment mostly comes from the upper and northern parts of the basin. Controlled by precipitation (Figure 29.2), the runoff is the lowest in the headwaters (sub-basin Upper1, 300 mm year^{-1}, Figure 29.3) and the highest in the south-eastern tributaries (sub-basin South, 800 mm year^{-1}). In contrast, sediment concentrations are greatest in the upper and northern basins (1.8 kg m^{-3} in sub-basin Upper1) where valleys are steep and soils are erodible, falling to about 0.2 kg m^{-3} toward the south-east (sub-basin South), where the regional tributaries of the Yangtze flow through low-relief alluvial plains.

This spatial pattern leads to matching water and sediment variations (Figure 29.4) noted at six gauging stations (see locations in Figure 29.1) along the Yangtze mainstem. The Yangtze water discharge gradually increases downstream following cumulative contribution from numerous tributaries, reaching a maximum at the seaward-most station at Datong (Figure 29.4). Sediment discharge, in

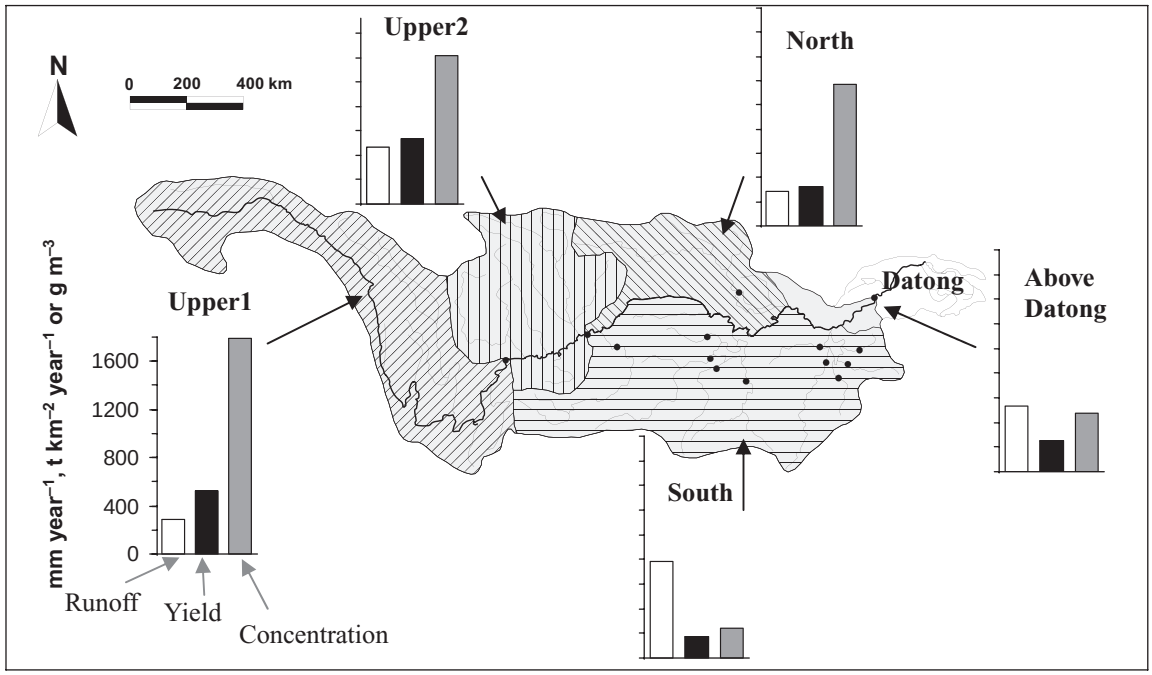

Figure 29.3 Runoff, sediment yield, and suspended-sediment concentrations in the Yangtze sub-basins. Black dots are hydrological stations used for the calculations of sub-basins: Pingshan for sub-basin Upper1, the difference between Cuntan and Pingshan for Upper2, Huangzhuang for the North, and 10 stations (Wulong, Xiangtan, Taojiang, Taoyuan, Shimen, Waizhou, Lijiadu, Meigang, Hushan, Wanjiabu, from west to east) for the South. Datong Station represents 94% the total Yangtze drainage basin. See Figure 29.1 for the locations of the mainstem stations

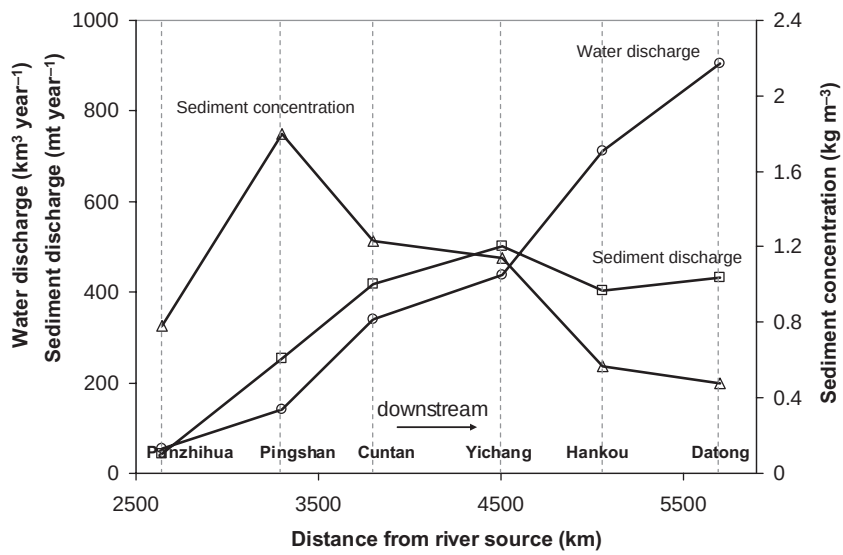

Figure 29.4 Spatial variation of water discharge, sediment discharge, and concentrations along the mainstem of the Yangtze River. These values are generally 1950–2000 means from the Bulletin of Yangtze Sediments (2000–2005). See Figure 29.1 for the locations of the six gauging stations

contrast, shows a maximum at upper reaches at Yichang, decreasing slightly in the middle (Hankou) and lower (Datong) reaches because the river loses sediment into the floodplain channels and lakes (Figure 29.4). Because water discharge increases downstream while sediment discharge decreases, average sediment concentration decreases from 1.8 kg m^{-3} in the upper reaches to about 0.5 at Datong.

The combination of steadily increasing water discharge and somewhat decreasing sediment discharge in the lower Yangtze is also typical of the lower reaches of other large alluvial rivers: Ob River of Siberia (Bobrovitskaya *et al*., 1996; Meade *et al*., 2000) and Amazon River of Brazil. Those downstream decreases in suspended sediment (both discharge and concentration) usually are attributable to deposition in the lakes and lowlands on the large floodplains of these rivers.

29.5 TEMPORAL VARIATIONS OF WATER AND SEDIMENT

Superimposed on these spatial variations, various temporal changes have occurred in the Yangtze drainage basin since 1950. Variations in both water and sediment discharges are discussed below at two timescales: annual and monthly.

29.5.1 Annual Variations

Water (precipitation and runoff)

During the five decades from 1951 to 2000, annual precipitation increased in the south-east (>100 mm, solid lines in Figure 29.5) while it decreased in the upper reaches (–200 mm, dashed lines in Figure 29.5), particularly in the Jialing and Min tributary basins (Figure 29.1). Sub-basins Upper1 and South showed slightly increased precipitation, whereas a striking decrease in precipitation occurred in Upper2 (–11.0 %) and a slight decline in North (Figure 29.6). Correspondingly, runoff (water discharge per unit area) also increased in the Upper1 and South but decreased in the Upper2 and North (Figure 29.6).

Because of limited runoff and precipitation data, precipitation was compared with runoff for the period 1951–2000 for sub-basins North and Above-Datong, but for 1956–2000 for sub-basins Upper1, Upper2 and South (Table 29.1). The statistically significant decrease of runoff (–25.7 %, –100 mm) in 1951–2000 in sub-basin North far exceeded the nonsignificant decrease (–2.5 %, <24 mm) in precipitation (Table 29.1). By contrast, the increase in runoff (18.6 %, 134 mm) over 1956–2000 in sub-basin South was larger than that of precipitation (7.8 %, 106 mm) although both trends were significant and the correlation was 0.82 (Figure 29.6; Table 29.1).

Despite these sub-basin changes, water discharges along the mainstem in upper (Pingshan and Yichang stations), middle (Hankou) and lower (Datong) reaches of the Yangtze (Figure 29.1) have varied little since 1950 (Figure 29.7a), reflecting increases in some sub-basins being offset by decreases in others. Basin-wide runoff measured at Datong correlated well with precipitation (R^2 = 0.83), but neither showed a significant change over time (Figure 29.6; Table 29.1).

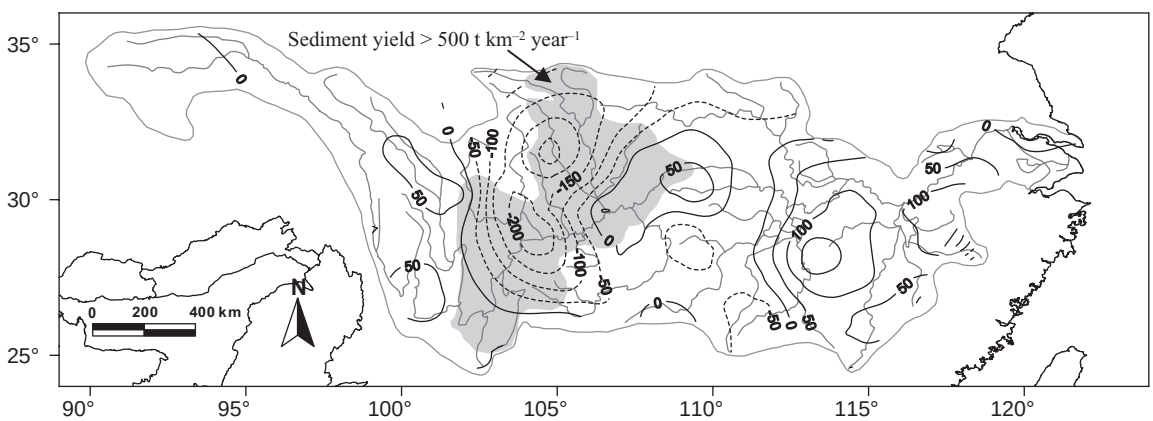

Figure 29.5 Precipitation change (mm) of the Yangtze drainage basin, 1951 to 2000. Solid and dashed lines correspond to increased or decreased precipitation, respectively. The grey area is the region with sediment yields greater than 500 t km^{-2} year^{-1} (modified after Liu and Zhang, 1991; Dai and Tang, 1996)

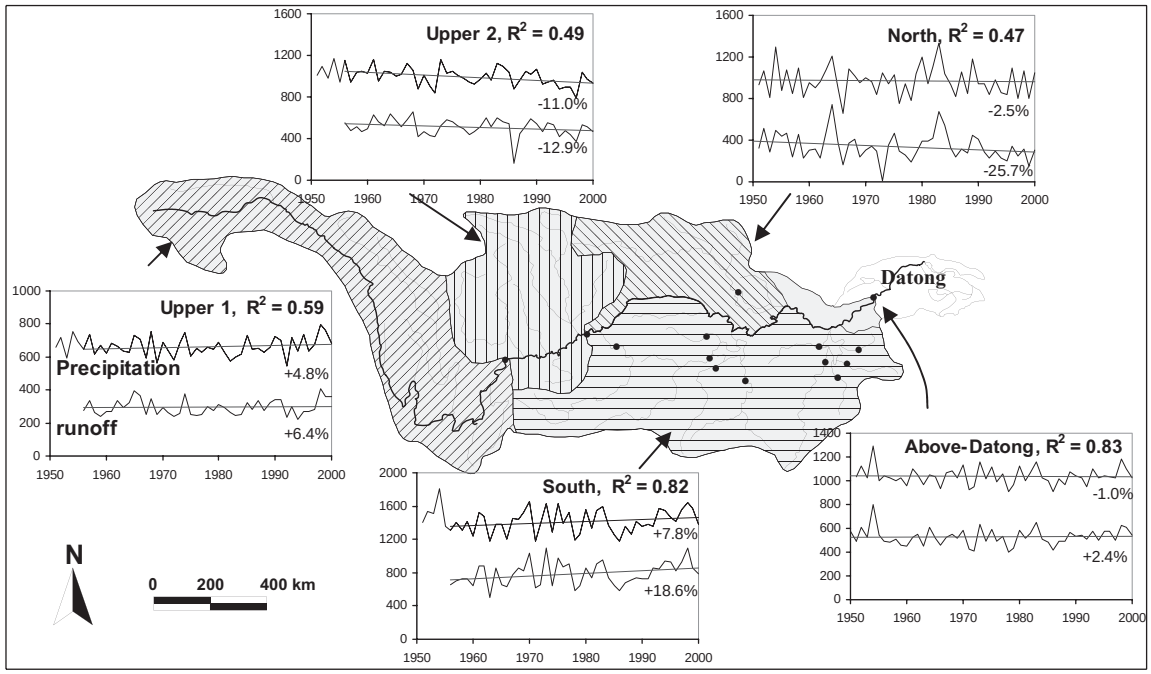

Figure 29.6 Spatial and temporal variations of precipitation and runoff in the Yangtze, 1950–2000. Upper and lower lines are average annual precipitation and runoff (in mm) for sub-basins along with their trends in percentages. Correlation coefficient (R^2) between precipitation and runoff is marked in each panel. Black dots are gauging stations used for the calculations of cumulative runoff. Datong Station covers 94% the total Yangtze drainage basin. See Figure 29.3 for station explanation and Table 29.1 for the results of Mann–Kendall analyses

Table 29.1 Mann–Kendall trend analyses of precipitation and runoff from the sub-basins of the Yangtze River

Sub-basins	Year data	Precipitation				Runoff				R^2
		Change (%)	Change (mm)	z-statistic	Confidence (%)	Change (%)	Change (mm)	z-statistic	Confidence (%)	
Upper1	1956–2000	4.8	31	1.03	NS	6.4	18	0.89	NS	0.59
Upper2	1956–2000	–11.0	–116	–2.59	99.5	–12.9	–70	–1.44	90	0.49
North	1951–2000	–2.5	–24	–0.35	NS	–25.7	–100	–1.86	95	0.47
South	1956–2000	7.8	106	1.54	90	18.6	134	1.95	95	0.82
Above-Datong	1951–2000	–1.0	–11	–0.03	NS	2.4	13	1.02	NS	0.83

R^2 is the correlation coefficient between precipitation and runoff. NS, not significant.

Sediment

Over the past 56 years, annual sediment discharges in all parts of the Yangtze Basin have been varied considerably more than water discharges, and have declined markedly since the 1980s (Figure 29.7b). As a result of several major declines (discussed below), annual discharges from upper (as measured at Yichang) and lower (as measured at Datong) reaches during the 2003–2005 period after the closure of TGD were 90 and 190 mt, respectively, only 17% and 38% of their 1950–1960s averages (Figure 29.7b).

Sediment discharges from all 23 stations, located on the mainstem or tributaries, have decreased except for some minor increases along a few south-eastern tributaries (Figure 29.8). Decreases have been most striking (>80%)

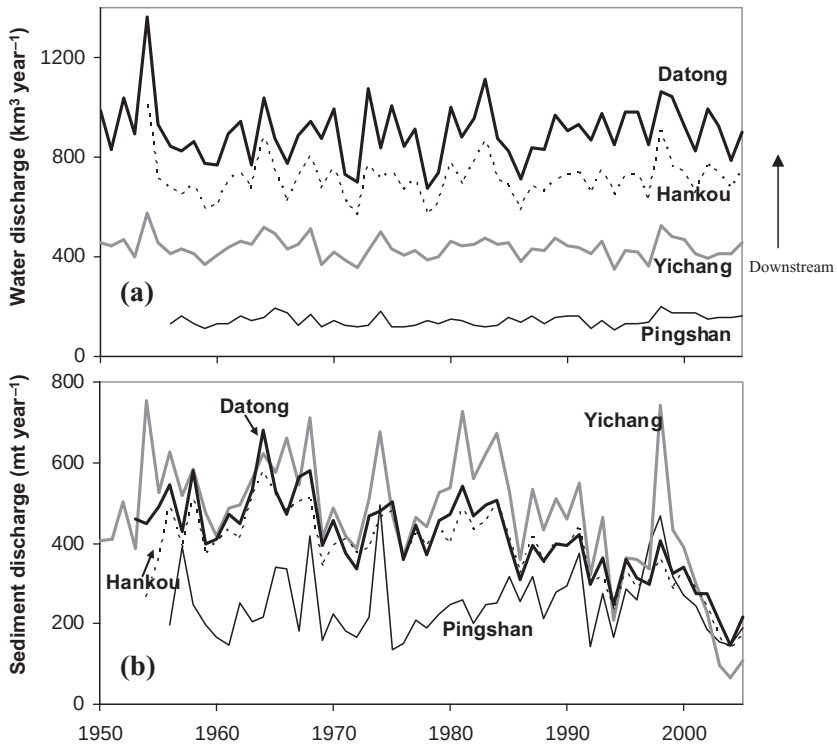

Figure 29.7 Temporal variations of water discharge (a) and sediment discharge (b) in upper (Pingshan and Yichang), middle (Hankou) and lower (Datong) reaches of the mainstem Yangtze River, 1950–2005

for the two northern tributaries (Jialing and Han) as well as the two passages between the Yangtze mainstem and Dongting Lake (Figure 29.1). Unlike the sharp decreases noted for the Jialing (in 1986) and Han (in 1968) tributaries, declines at the two passages have been more gradual (Figure 29.8). Sediment discharges along the tributaries have decreased in general along the mainstem of the Yangtze. An 80-mt sediment reduction in 1968 at the Han River in the north (Figure 29.8, marked 1) correlates well with (and partially led to) decreased discharge at Datong at that time. A 100-mt decrease in the sediment discharge of the Jialing in 1986 (Figure 29.8, marked 2) and the impoundment of TGD in 2003 (Figure 29.8, marked 3) both led to corresponding drops at Yichang and Datong.

29.5.2 Monthly Variations

The aforementioned variations can be shown in more detail at the monthly scale. Under a monsoon regime, the monthly water and sediment discharges in the Yangtze display a strong seasonal pattern, about 70% of water and 85% of sediment being discharged between May and October in upper (Yichang), middle (Hankou) and lower (Datong) reaches (Figure 29.9). Although both show unimodal patterns, variations in water discharge are less seasonal than those of sediment load; low water discharge in January generally is around 20% of the peak water discharge in July whereas January sediment discharge is <3% of that in July (Figure 29.9).

From 1950 to 2005, the annual pattern of monthly water discharge showed small changes from upper reaches to lower reaches (Figure 29.9a), similar to minor variations in annual values (Figure 29.7a). In order to delineate detailed changes in seasonality, we compared 5-year mean monthly water discharges for a period before many dams have been built (1955–1959) with the period 2001–2005 when >50 000 dams have been in operation in the basin. During this interval, the flood-season (July–August) water discharge decreased slightly at Yichang (presumably because of the TGD impoundment) but changed little downstream at Hankou or Datong (Figure 29.9a). The dry-season (January–February) monthly discharge, however, increased by about 40% at Datong, probably

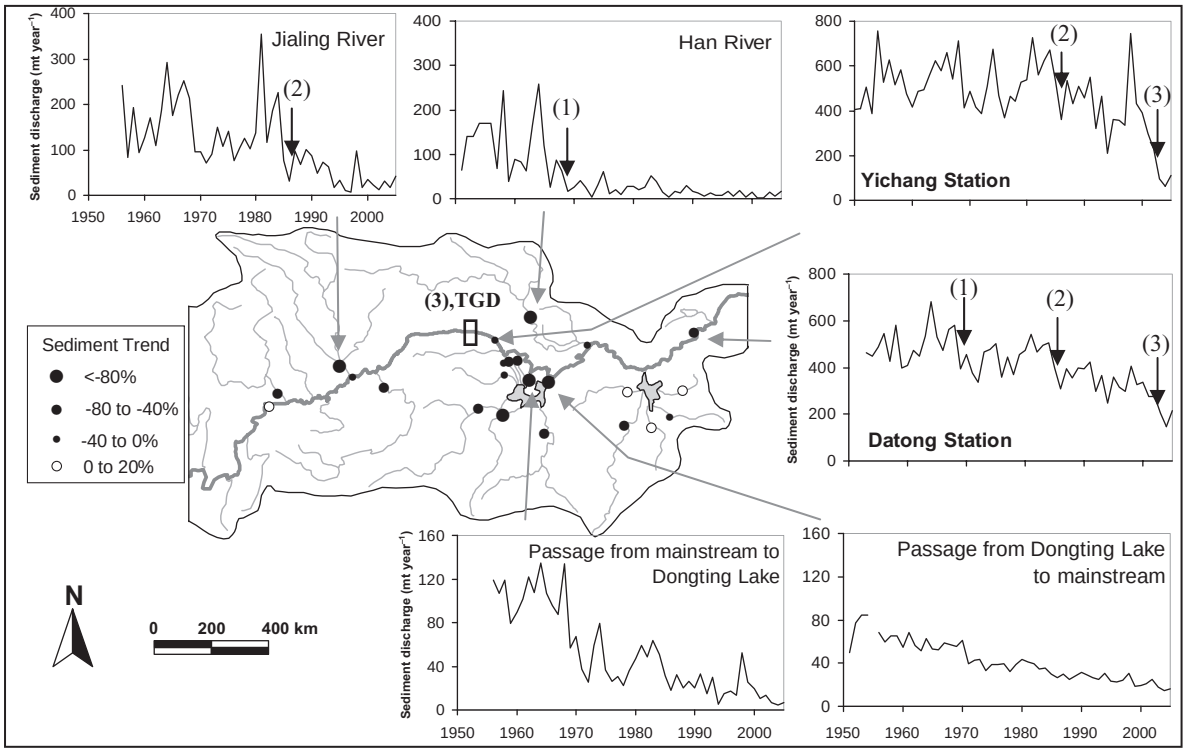

Figure 29.8 Temporal sediment variations at four stations in which sediment discharge decreased more than 80%. Also shown are variations at Yichang and Datong on the mainstem as well as sediment trends from 1950 to 2005 at 23 stations. Gauging stations for the Jialing and Han Rivers and two passages are Beibei, Huangzhuang, Ouchiguan and Chenglingji respectively. See Figure 29.11 for Dongting Lake details

reflecting a change in seasonal precipitation or winter release of water stored in the reservoirs upstream of dams.

Monthly sediment discharges have changed much more dramatically than water discharges. Except for minor decreases in August discharges, monthly sediment discharges remained more or less constant along the Yangtze from 1950 to 1985 (Figure 29.9b). Subsequently discharges declined moderately between 1986 and 2002, and dramatically after 2003 (Figure 29.9b). Peak sediment discharges during July–August in 2003–2005 at Yichang, Hankou and Datong were only 17%, 33% and 36% of their discharges in 1950–1967 respectively (Figure 29.9), thereby reflecting a damped downstream signal as well as channel erosion downstream of the TGD (Xu *et al*., 2006). About 100–150 mt of sediment have been trapped in the reservoir upstream of the TGD annually between 2003 and 2005, and more than 70% of that occurred between June and September (Bulletin of Yangtze Sediment, 2000–2005).

29.6 DISCUSSION – CLIMATIC AND ANTHROPOGENIC IMPACTS

Temporal variations in water and sediment discharges in the Yangtze Basin have been controlled by various forcings: climatic (precipitation and evapotranspiration) and anthropogenic (water diversions, dam construction and lake reclamation).

29.6.1 Climatic Impacts

As shown in Figures 29.5 and 29.6, local precipitation and runoff in the Yangtze drainage basin changed considerably between 1951 and 2000, although basin-wide values changed little. Increases in the south-east (sub-basin South) and decreases in the north (sub-basin North) have been especially striking. In a natural hydrological regime, runoff is the difference between precipitation and the sum of evapotranspiration and storage. In a heavily human-

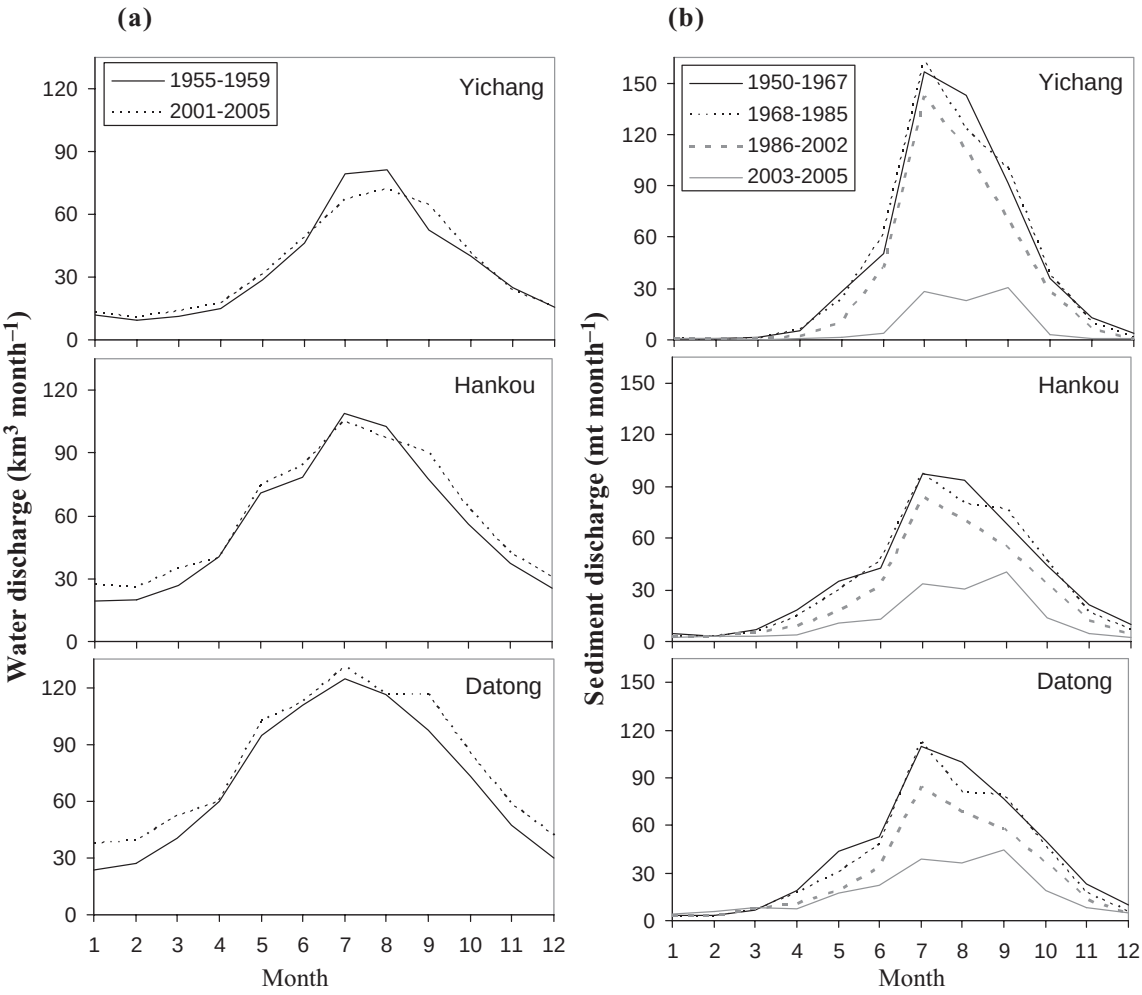

Figure 29.9 Changes in monthly water discharge (a) and sediment discharge (b) in upper (Yichang), middle (Hankou) and lower (Datong) reaches of the Yangtze River, 1950–2005. Note that Yichang and Hankou Stations lack the 2000 data and Datong that of 1970, 1971, 1974 and 1975

impacted basin like the Yangtze, water consumption, the withdrawn water directly lost to the basin, also must be taken into account. As water storages as groundwater and in reservoirs are small relative to precipitation and runoff throughout the watershed (Xu, 2006), the runoff of the Yangtze should mainly reflect the difference between precipitation and the sum of evapotranspiration and water consumption.

Runoff in the sub-basin South (Figure 29.6, Table 29.1) increased (18.6%, 134 mm, 95% confidence interval) more than precipitation (7.8%, 106 mm, 90% confidence interval). As there is no evidence of decreased water consumption (which actually may have increased) the increased runoff more likely reflects decreased evapotranspiration. This conclusion generally agrees with both measured pan evaporation (Liu *et al*., 2004) and calculated potential evapotranspiration (Thomas, 2000). From 1955 to 2000, pan evaporation decreased significantly in south-eastern China (near sub-basin South) mainly due to decreasing solar irradiance (Liu *et al*., 2004). From 1954 to 1993, potential evapotranspiration also decreased in southern China (south of 35° N) where sunshine appears to play a key role in evapotranspiration (Thomas, 2000). Therefore, decreased evapotranspiration in sub-basin South of the

Yangtze might be explained by decreased sunshine, increased atmospheric haze (Roderick and Farquhar, 2002), decreased plant transpiration owing to stomatal closure in response to increased atmospheric CO_2 levels (Gedney *et al*., 2006), or a combination of all three.

In the sub-basin North (Figure 29.6), however, runoff decrease (−25.7%, −100 mm) was about four times of the decline in precipitation (−2.5%, −24 mm). Since we find no proof of increased evapotranspiration, this decreased runoff in sub-basin North was probably caused by increased water consumption, similar to the situation in the basin of the Yellow River to the north (Wang *et al*., 2006).

Precipitation also plays a key role in eroding and transporting sediment within the Yangtze drainage basin, particularly in the upper reaches (Ma *et al*., 2002; Zhang and Wen, 2002). Lying in an area of high sediment yield (>500 t km^{-2} year^{-1}) drained by the Jialing and Min tributaries (Figure 29.5), sub-basin Upper2 experienced the greatest decrease in precipitation between 1951 and 2000 (−11.0%, Figure 29.6), to which both runoff (R^2 = 0.56, Figure 29.10a) and sediment discharges (until 1985; R^2 = 0.51, Figure 29.10b) responded accordingly. Although precipitation has remained relatively steady since 1986, the measured sediment discharge in sub-basin Upper2 has declined dramatically (bold black line, Figure 29.10c). Based on the 1956–1985 runoff-sediment correlation (Figure 29.10b), calculated post-1986 sediment discharges (bold grey line, Figure 29.10c) were significantly higher than those actually measured. Therefore, decreased pre-

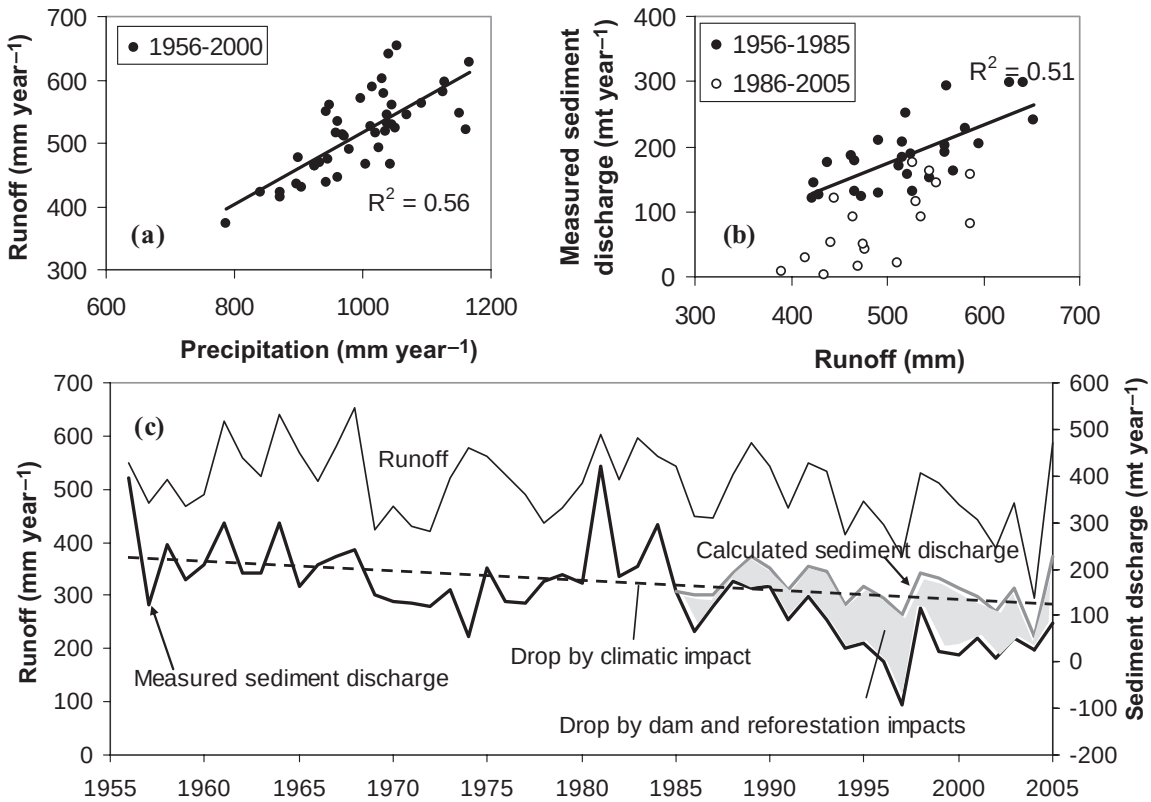

Figure 29.10 Precipitation, runoff and sediment discharge between Pingshan and Cuntan gauging stations (Sub-basin Upper2, Figure 29.6). Runoff and sediment discharge are determined by subtracting discharge of Pingshan from that of Cuntan. Correlation analysis of 1956–2000 in (a) excludes 1986 owing to extensive dam impoundments. In (b), the 1956–1985 runoff-sediment correlation excludes three abnormal years (1956, 1974 and 1981). In (c), the negative measured discharge of 1997 probably indicates channel siltation. The dashed trend line indicates the sediment drop due to decreased precipitation, and the difference (grey region) between measured and calculated sediment (derived from b) in 1986–2005 is mainly caused by anthropogenic activities, such as dam construction and reforestation

cipitation and runoff have caused about 80 mt decrease in sediment discharge from 1956 to 2005 (dashed line for 'climatic impact', Figure 29.10c). However, the difference between the calculated and measured discharges between 1986 and 2005 (grey region, Figure 29.10c) can be regarded as sediment decline due to human activities, such as reforestation and dam construction.

29.6.2 Anthropogenic Impacts

Because anthropogenic activities and climate change synchronize with respect to both space and time, it is difficult to separate their impacts on the Yangtze Basin quantitatively (Higgitt and Lu, 1996; Yang *et al*., 2002; Li *et al*., 2004; Zhang and Wen, 2004; Yang *et al*., 2005). In general, deforestation and agriculture increase the sediment discharge (Dai and Tan, 1996), but they can be counteracted by dam construction, water diversion, lake reclamation and reforestation. Three major types of anthropogenic activities are discussed below.

Dam construction

The number of dams in the Yangtze Basin has increased dramatically from only a few in the 1950s to more than 50 000 at present. Dams have played a key role in reducing sediment transport throughout the entire Yangtze drainage basin. On the Han River, Danjiangkou Dam decreased sediment sharply in 1968, as its reservoir had a trapping efficiency greater than 95% (Figure 29.8, 1). Sediment decrease in the Jialing (Figure 29.8, 2) in sub-basin Upper2, was initiated by a decrease in precipitation in 1986 (Figure 29.5), but more importantly, by construction of about 12 000 dams and extensive watershed reforestation in its basin. These activities have trapped about 100 mt year^{-1} since 1986 (EGRSTGP, 2002). Since the beginning of the impoundment upstream of the TGD in 2003, about 150 mt year^{-1} of sediment discharge has been reduced in both the upper (Yichang) and lower (Datong) reaches of the river (Figure 29.8, 3).

Water consumption

Withdrawal and consumption of water has occurred concurrently with dam construction in the Yangtze Basin. From 1949 to 2000, Yangtze water withdrawal increased rapidly in response to increased irrigation for agriculture and demand for an expanded population from about 180 to >400 million. Over the same period, water consumption also increased from 15 to 90 km^3 year^{-1} (Bulletin of Water Resources in China, 1997–2005; Heilig, 1999). The present pattern of Yangtze Dam impoundments and water diversion, however, appears to have had relatively small impact on annual and monthly water discharges (Figures 29.7a and 29.9a), even though the Yangtze is a highly impacted river in terms of fragmentation and flow regulation (Nilsson *et al*., 2005).

That the Yangtze's water discharge has not changed significantly over the past 56 years is explained mainly by the sheer magnitude of the basin area and the high volume of discharge – fifth largest in the world. Even with a sixfold increase in water consumption since 1950, a figure of 90 km^3 year^{-1} represents only 10% of its annual discharge. Although by 1995 more than 46 000 dams had been constructed in the basin and their total water-storage capacity had reached 142 km^3 (Yang *et al*., 2005), the volume of annual stored water in the reservoirs upstream of dams was less than 10 km^3, about 1% of the annual discharge (Bulletin of Water Resources in China, 1997–2005). Even the TGD impoundment in 2003 only trapped about 17 km^3 water, 2% of the annual discharge of the Yangtze. The total capacity of TGD will be 39 km^3 in 2009 when the TGD is in full operation, thereby impounding 5% of the annual discharge of the Yangtze to the coastal region. In 2003, this TGD impoundment caused moderate declines of discharge upstream at Yichang only in July and August, underscoring the modulating capacity of a high-discharge river like the Yangtze.

Lake reclamation

Many lakes occur in the Yangtze Basin, including Dongting Lake located in the middle reaches. This major lake receives discharges both from mainstem passages (labelled 1–5, Figure 29.11a) and southern tributaries (labelled 6–9), the water then flows back to the Yangtze mainstem at Chenglingji Station (Figure 29.11a). Historically Dongting Lake has supplied freshwater to tens of millions of inhabitants and buffered the impact of floods in the middle reaches.

Since the 1950s, however, extensive reclamation, together with siltation, have led to a rapidly declining lake area (Shi *et al*., 1985; Du *et al*., 2001), from 4350 km^2 in 1949 to 2623 km^2 in 1995 (Bulletin of Yangtze River Sediment, 2000–2005). Since 1956, both water and sediment flowing in and out of Dongting Lake have declined. The differences between the sediment discharges measured in the five passages draining from mainstem to Dongting Lake and those measured as the return flow at Chenglingji, indicate that less and less net sediment has escaped from the mainstem (Figure 29.11b). Similarly, an input–output sediment budget for Dongting Lake (1–9, Chenglingji) shows that net trapped sediment into the lake also has declined sharply (solid line, Figure 29.11b). In the 1950s,

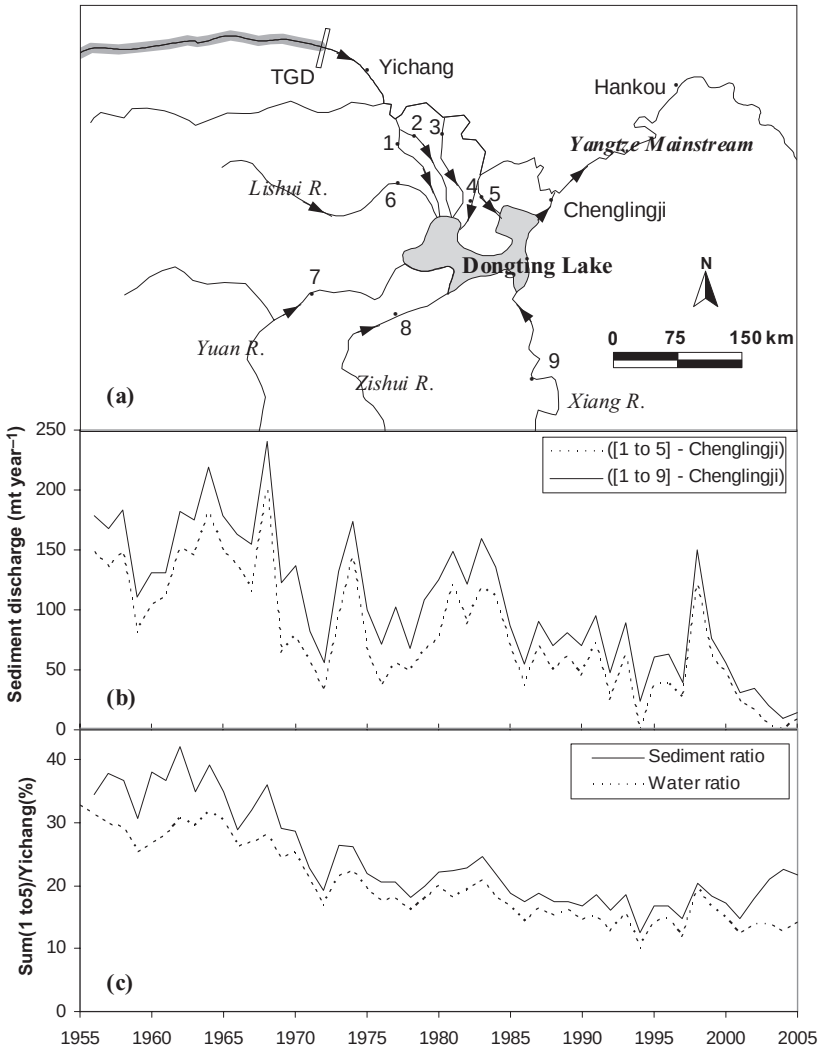

Figure 29.11 (a) The passages and tributaries connecting to Dongting Lake as well as their gauging stations: 1, Xinjiangkou; 2, Shadaoguan; 3, Taipingkou; 4, Ouchikang; 5, Ouchiguan; 6, Shimen; 7, Taoyuan; 8, Taojiang; 9, Xiangtan. The broad grey line upstream of the TGD (Three Gorges Dam) represents the impounded channel. (b) Sediment trapped in Dongting Lake. Dashed line is the difference between sediment discharged into the lake from Yangtze mainstem (as measured at stations 1–5) minus sediment discharged from the lake back into mainstem (as measured at Chenglingji). Solid line adds the inputs from four southern tributaries to Lake Budget. (c) Water and sediment passing into Dongting Lake from Yangtze mainstem, expressed as proportions of the total water and sediment passing Yichang

the five passages transported 35% of water and sediment passing Yichang Station, but in recent years they have carried only 15% of these from Yichang (Figure 29.11c), indicating Dongting's declining role in flood modulation. Since the construction of the TGD led to active channel erosion downstream of Yichang after 2003 (Xu *et al*., 2006), scouring has taken place in the mainstem channel, probably further decreasing discharge into the lake, as forecasted by Zhang (1995). Although the TGD can buffer the flood water arriving from the upper reaches, the four high-runoff southern tributaries (Figure 29.3) can discharge massive quantities of water directly into the shrinking Dongting Lake, thereby causing an unsolved serious flood problem for the middle Yangtze. The extended sur-

vival of the Dongting Lake, the major freshwater source in the middle reaches of the Yangtze, has become a serious problem.

29.7 FUTURE CHANGE AND COASTAL RESPONSES

29.7.1 Water Discharge

Over the past 56 years, water consumption within the Yangtze River basin has represented fairly small proportions of its total water discharge. The South–North Water Diversion Project of the future, however, is scheduled to transfer freshwater from the humid southern China, mainly from the Yangtze, to the dry northern China, including the Yellow River (Figure 29.1). This will take place through three passages termed East, Middle and West (Chen *et al*., 2003). The reservoir upstream of the Danjiangkou Dam on the Han tributary will be one of the major freshwater sources of the Middle Passage, delivering water directly to Beijing. This diversion will certainly diminish further both water and sediment discharges of the Han tributary in the northern Yangtze. Although only 5 % (45 $km^3\,year^{-1}$) of the Yangtze annual water discharge will be diverted (Chen, X. *et al*., 2001), this anthropogenic transfer may fundamentally change the Yangtze water cycle since most of the diverted water will be removed from the Yangtze drainage basin.

29.7.2 Sediment Discharge

Sediment discharge at Datong (the seaward-most station, 600 km from the river mouth) has declined to 140 mt from a mean level of 480 mt $year^{-1}$ in the 1950–1960s, since the TGD impoundment (Figure 29.7). Both Yang *et al*. (2002) and Yang, Z.S. *et al*. (2006) forecasted the volume of the future sediment passing Datong in the next half century. It is difficult, however, to extend their predictions to the amount of sediment that would enter the East China Sea owing to various ongoing and future impacts as detailed below.

First, we need to understand the impact of ongoing and proposed upstream dam construction. Except for the Gezhouba, no dams had been constructed on the mainstem of the Yangtze before the TGD in 2003. In the next two decades, however, China is going to build four large dams (Wudongde, Baihetan, Xiluodu and Xiangjiaba) on the Yangtze upstream of the TGD where sediment yield is extremely high (Figure 29.5). These four dams would add an additional 41 km^3 of total water-storage capacity, and their total installed hydropower capacity would be 38 500 MW, about double that of the TGD. One of the objectives of these four planned dams is to prolong the useful life of the TGD by trapping the sediment that otherwise would fill its reservoir. However, the impact of these dams has not been figured into the two predictions mentioned earlier (Yang *et al*., 2002; Yang, Z.S. *et al*., 2006).

Second, sediment trapping in Dongting Lake has decreased from 180 mt in the 1950s to nearly zero at present (solid line, Figure 29.11b). This decline has fundamentally changed the sediment correlation between Yichang and Datong, the major sites used for two predictions. Third, channel erosion downstream of dams may counteract the trapping of sediment by the reservoir to some extent. Channel erosion has already occurred downstream of the TGD (Xu *et al*., 2006), and will surely happen downstream of four planned dams. Last, little is known regarding the ungauged section from Datong 600 km downstream to the river mouth. Many uncertainties remain concerning the possible response (erosion and resuspension) of this last downstream reach to the cessation of sediment from the upper river.

29.7.3 Coastal Responses

The sediment threshold at Datong that is required to sustain the geometry of modern Yangtze Delta was estimated to be 263 mt $year^{-1}$ (Yang *et al*., 2005). The sediment discharge, however, has been below this level since 2000 (Figure 29.7). Given dam construction of the future, decreased erosion in response to ongoing conservancy in the basin, and diversions of water, sediment discharge of the Yangtze most likely will continue to decline, impacting the delta and coastal region.

Accretion in the Yangtze subaqueous delta has slowed down and erosion has occurred on the outer side of the Yangtze Delta front (Yang *et al*., 2002). Coastal wetland located in the eastern part of the Yangtze Delta stopped progading in the past decade and began to recede; wetlands above the 0-m isobath decreased by 19 % between 2001 and 2004 (Yang, S.L. *et al*., 2006). Delta subsidence, shoreline retreat, erosion of seawalls, and other subsequential problems may concur with wetland loss. All these may create serious problems in Shanghai, the most populous city in China with about 20 million inhabitants.

The Yangtze River provides a substantive amount of nutrients, nourishing rich fishing grounds on the inner continental shelf of the East China Sea. A decline of sediment supply also reduces the supply of nutrients, particularly silicates. For instance, between 1998 and 2003, the Si : N ratios dropped from 1.5 to 0.6 and primary production decreased by 86 % in the East China Sea (Gong *et al*., 2006). Due to Si-limitation, the phytoplankton community has shifted from diatom-dominated to flagellate-

dominated, thereby changing the ecological communities (Gong *et al*., 2006). After the TGD impoundment in June 2003, saltwater intrusion in the Yangtze Estuary appeared earlier and its duration lengthened (Xian *et al*., 2005). This saltwater intrusion has led to increased water temperature and salinity, which consequently stimulated several jellyfish blooms in the estuary in 2003 and 2004 (Xian *et al*., 2005). Since jellyfish can feed on fish eggs and larvae, these jellyfish blooms may also endanger coastal fishing resources.

29.8 CLIMATIC AND ANTHROPOGENIC IMPACTS ON OTHER GLOBAL RIVERS – THE MISSISSIPPI EXAMPLE

Owing to their inability to modulate basin-wide change, rivers draining small basins are generally more responsive to both sudden and long-term changes. Similarly, arid basins are more likely to feel the effects of climatic and anthropogenic change than rivers draining humid basins. For example, present-day runoff from the Yellow River is only about 15% of its 1950s levels owing to decreased precipitation and, more importantly, increased water consumption (Wang *et al*., 2006). Similarly, the impoundment by the Aswan High Dam and related downstream irrigation have decreased the Nile's water and sediment discharge to less than 10% of the pre-Aswan levels.

While low-runoff rivers seem more vulnerable to climatic and anthropogenic changes, high-runoff rivers also can be affected, as shown by the Yangtze in the present chapter. Another obvious example is the Mississippi River. While its drainage basin is nearly twice as large as the Yangtze's (3.3 vs 1.8×10^6 km^2), its pre-dam annual water and sediment discharges were not dissimilar (650 km^3 and 500 mt) to those of the Yangtze (900 km^3 and 480 mt). Moreover, both rivers are joined by high-runoff, low-sediment-yield tributaries in the south and east (the southern rivers in the Yangtze, and the Ohio-Tennessee in the Mississippi), and low-runoff, high-sediment-yield tributaries in the north-west and west (the northern and upstream rivers in the Yangtze, and the Missouri-Arkansas in the Mississippi) (Figure 29.12). The low-runoff Missouri and Arkansas occupy a larger percentage of the Mississippi drainage basin than do the north-western rivers in the Yangtze Basin, leading to a substantially lower runoff to the coastal waters.

Dam construction on the Mississippi accelerated in the 1930s for better navigation, flood control, and generation of hydroelectric power as well as in response to economic depression, much in the same way as it did on the Yangtze Basin after 1950. As with the Yangtze, Mississippi water discharge has not decreased despite the more than 50 000 dams throughout its watershed. In fact, between 1950 and 2000, discharge increased about 30% (Figure 29.13) in response to the Pacific Decadal Oscillation and the North Atlantic Oscillation (Hurrell, 1997; Lins and Slack, 1999). Despite the increased water discharge, however, sediment delivery of the Mississippi has decreased by about 75% since the early 1950s (Figure 29.13). Unlike the Yangtze, which has experienced several distinct episodes of decreased sediment delivery in response to climatic and land-use changes, however, the sharply decreased sediment discharge from the Lower Mississippi reflects primarily the construction of the Fort Randall and Gavins Point Dams in 1953 and the Garrison Dam in 1954 along the middle reaches of the Missouri River (Meade and Parker, 1985). Sediment delivery since the mid-1950s has shown only a slight decline even though dams have continued to be built (Figure 29.13).

Another impact from dam construction, combined perhaps with climate change, has been the change in seasonality of water discharges from both the Mississippi and Yangtze. Water discharges during high-flow months in both rivers have decreased in company with increased discharges during low-flow months (Figure 29.13). Although changes in seasonal precipitation may partially explain these variations, more likely are the releases of stored water from upstream reservoirs in response to hydroelectric and irrigation needs.

As with many other North American and European rivers, it seems doubtful that other large dams will be built on the Mississippi, at least in the foreseeable future; as any such significant change in Mississippi sediment discharge is likely to reflect landuse change rather than the river flow. By contrast, the number of large dams still planned for the Yangtze suggests that sediment delivery will continue to decline in the coming years in response to both changes in river flow and landuse.

29.9 CONCLUSION

From 1950 to 2005, construction of over 50 000 dams and consumption of 90 km^3 water have led to small variations in annual and monthly basin-wide water discharges from the Yangtze River. Regionally, runoff in the Yangtze northern sub-basin has declined much more than has precipitation owing to increased water consumption, whereas increased runoff in the southern Yangtze may reflect decreased evapotranspiration. Since the 1980s, however, Yangtze sediment discharge has decreased dramatically. In 2003–2005, the upper river (measured at Yichang) and lower reaches (Datong) transported only 17% and 38% of their natural sediment discharges in the 1950–1960s, respectively. Throughout the basin, the most striking sedi-

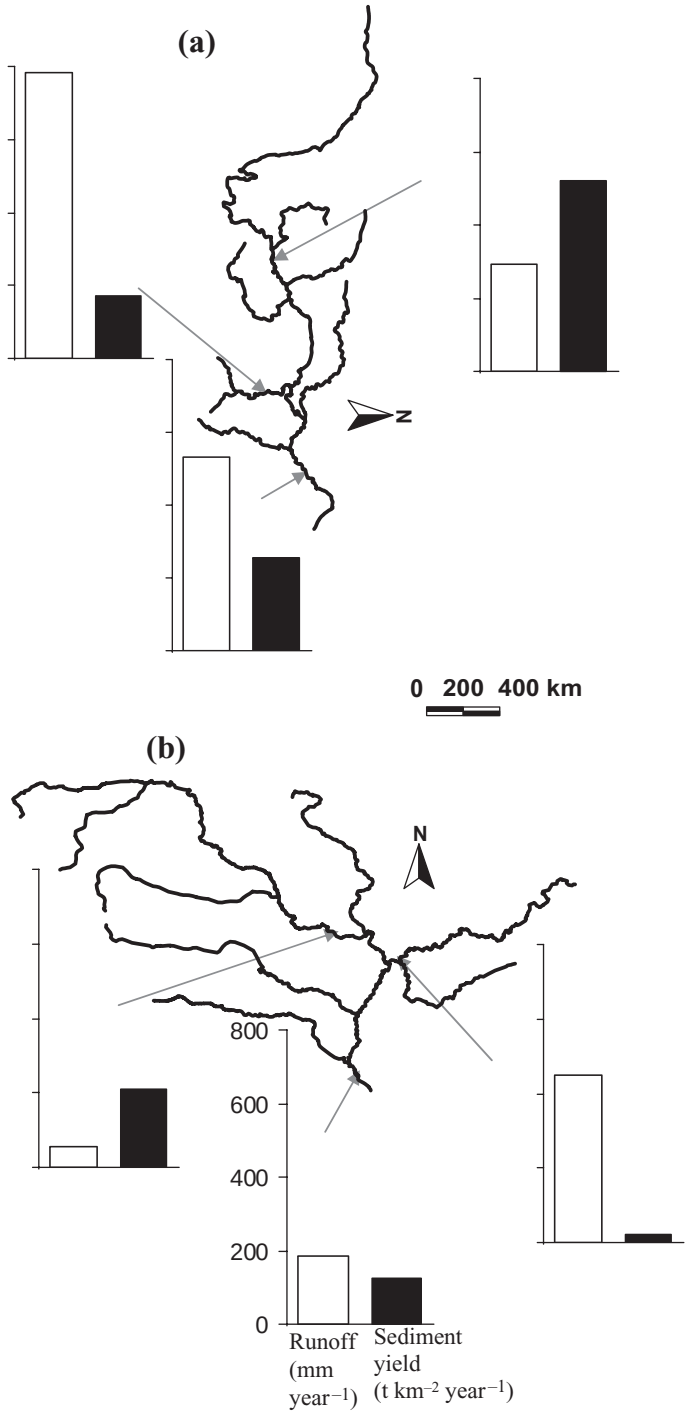

Figure 29.12 Spatial distribution of runoff and sediment yield in the (a) Yangtze and (b) Mississippi Rivers. Both rivers are characterized by high-runoff, low-sediment-yield tributaries to the south and east, respectively, counterbalanced by low-runoff, high-sediment-yield tributaries to the north-west and west

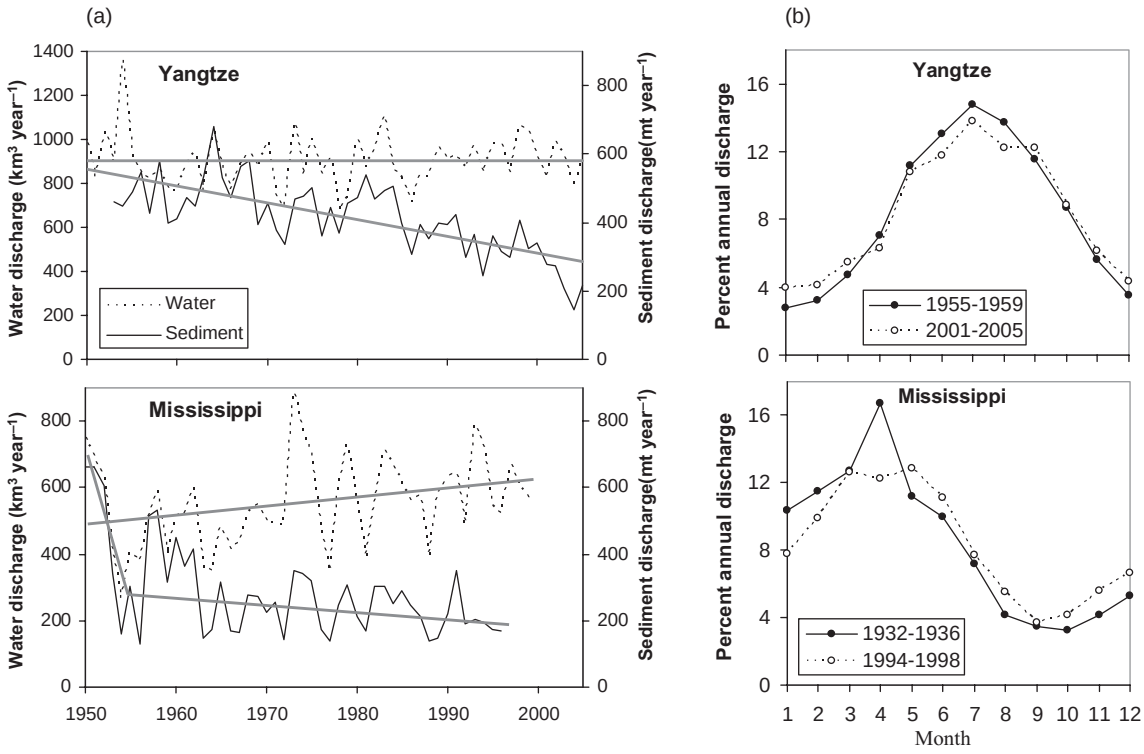

Figure 29.13 (a) 1950–2005 trends of water and sediment discharges from the lower reaches of the Yangtze and Mississippi Rivers. The Yangtze has experienced a small variation in water discharge but a gradual decrease in sediment discharge since 1986. In contrast, the Mississippi has experienced a 30% increase in water but a sharp decline in sediment after construction of three Missouri River dams in the early 1950s. (b) Monthly water discharges from the Yangtze and Mississippi Rivers during early and recent 5-year periods. Decreased water discharges during high-flow months and corresponding increased discharges during low-flow months may reflect changes in seasonality of precipitation and/or the release of reservoir-stored water for hydropower and irrigation during low-flow months

ment decreases (>80%) occurred in the Jialing and Han tributaries (mainly owing to dam construction), as well as in the two passages between the mainstem and Dongting Lake (owing to lake reclamation). The shrinking Dongting Lake now carries a much smaller percentage of the discharges passing Yichang, increasing the flood potential of the middle Yangtze. Given the proposed increase in the number of major dams and water diversions, sediment discharge from the Yangtze will probably continue to decline such that Yangtze delta and coastal areas could be severely impacted.

ACKNOWLEDGEMENTS

We are grateful to Drs Avijit Gupta and particularly our friend and colleague, Robert H. Meade, for their valuable comments and suggestions in improving and revizing the chapter. This research was supported by the US National Science Foundation (NSF) and Office of Naval Research (ONR) as well as the NSFC Project 90211022 of China. This chapter is Contribution No. 2810 of the Virginia Institute of Marine Science, the College of William & Mary.

REFERENCES

Bobrovitskaya, N.N., Zubkova, C. and Meade, R.H. (1996) Discharge and yields of suspended sediment in the Ob and Yenisey Rivers of Siberia. In: *Erosion and Sediment Yield: Global and Regional Perspectives* (D.E. Walling, and B.W. Webb, Eds.). International Association of Hydrological Sciences Publication 236, Wallingford, pp. 115–123.

Bulletin of Water Resources in China (1997–2005) Ministry of Water Resources of the People's Republic of China, website: http://sdinfo.chinawater.net.cn/index.asp (in Chinese).

Bulletin of Yangtze River Sediment (2000–2005) Press of Ministry of Water Resources of the People's Republic of China, website: http://www.cjh.com.cn/ (in Chinese).

Carriquiry, J.D., Sanchez, A. and Camacho-Ibar, V.F. (2001) Sedimentation in the northern Gulf of California after cessation of the Colorado River discharge. *Sedimentary Geology*, 144(1–2): 37–62.

Chen, J., Chen, X. and Chen, M. (2003) *Impacts and Countermeasurements of the South-to-North Water Diversion Projects on the Ecosystem and Environment of the Yangtze Estuary*. East China Normal University Press, Shanghai, pp. 277.

Chen, X., Zong, Y., Zhang, E., Xu, J. and Li, S. (2001) Human impacts on the Changjiang (Yangtze) River basin, China, with special reference to the impacts on the dry season water discharges into the sea. *Geomorphology*, 41(2–3): 111–123.

Chen, Z., Li, J., Shen, H. and Zhanghua, W. (2001) Yangtze River of China: historical analysis of discharge variability and sediment flux. *Geomorphology*, 41(2–3): 77–91.

Chu, Z.X., Sun, X.G., Zhai, S.K. and Xu, K.H. (2006) Changing pattern of accretion/erosion of the modern Yellow River (Huanghe) subaerial delta, China: based on remote sensing images. *Marine Geology*, 227(1–2): 13–30.

Cyranoski, D. (2005) Climate change: the long-range forecast. *Nature*, 438(7066): 275–276.

Dai, D. and Tan, Y. (1996) Soil erosion and sediment yield in the Upper Yangtze River basin. In: *Erosion and Sediment Yield: Global and Regional Perspectives* (D.E. Walling, and B.W. Webb, Eds.). International Association of Hydrological Sciences Publication 236, Wallingford, pp. 191–203.

Deng, X. and Huang, C. (1997) Analysis of transport characteristics and influence of human activities in the Jingsha River. *Journal of Sediment Research*, 4: 37–41 (in Chinese).

Du, Y., Cai, S., Zhang, X. and Zhao, Y. (2001) Interpretation of the environmental change of Dongting Lake, middle reach of Yangtze River, China, by ^{210}Pb measurement and satellite image analysis. *Geomorphology*, 41(2–3): 171–181.

EGRSTGP (Expert Group on River-borne Sediment of the Three Gorges Project) (2002) *Study on sediment of the Three Gorges Engineering Project (Book 8)*. Intellectual Property Press, Beijing (in Chinese).

Fuggle, R. and Smith, W. (2000) Large dams in water and energy resource development in the People's Republic of China (PRC). Country review paper prepared as an input to the World Commission on Dams, Cape Town, www.dams.org.

Gedney, N., Cox, P. M., Betts, R. A., Boucher, O., Huntingford, C. and Stott, P. A. (2006) Detection of a direct carbon dioxide effect in continental river runoff records. *Nature*, 439: 835–838.

Gleick, P.H. (1993) *Water in Crisis: A Guide to the World's Fresh Water Resources*. Oxford University Press, New York, pp. 504.

Gleick, P.H. (2000) *The World's Water 2000–2001: the Biennial Report on Freshwater Resources*. Island Press, Washington, DC.

Gong, G., Chang, J., Chiang, K., Hsiung, T., Hung, C., Duan, S. and Codispoti, L.A. (2006) Reduction of primary production and changing of nutrient ratio in the East China Sea: effect of the Three Gorges Dam? *Geophysical Research Letter*, 33, L07610, doi:10.1029/2006GL025800.

Heilig, G.K. (1999) Can China Feed Itself? A System for Evaluation of Policy Options. International Institute for Applied Systems Analysis, Laxenburg, Austria, pp.63, website: www.iiasa.ac.at.

Higgitt, D.L. and Lu, X. (1996) Patterns of sediment yield in the upper Yangtze basin, China. In: *Erosion and Sediment Yield: Global and Regional Perspectives* (D.E. Walling, and B.W. Webb, Eds.). International Association of Hydrological Sciences Publication 236, Wallingford, pp. 205–214.

Hurrell, J.W. (1997) Decade trends in the North Atlantic Oscillation: Regional temperatures and precipitation. *Science*, 269: 676–679.

Kendall, M.G. (1975) *Rank Correlation Methods*, 4th Edition. Charles Griffin, London.

Li, C., Yang, S., Fan, D. and Zhao, J. (2004) The change in Changjiang suspended load and its impact on the delta after completion of Three Gorges Dam. *Quaternary Sciences*, 24(5): 495–550 (in Chinese).

Lins, H.F. and Slack, J.R. (1999) Streamflow trends in the United States. *Geophysical Research Letters*, 26: 227–230.

Liu, B., Xu, M., Henderson, M. and Gong, W. (2004) A spatial analysis of pan evaporation trends in China, 1955–2000. *Journal of Geophysical Research*, 109, D15102.

Liu, Y. and Zhang, P. (1991) Soil erosion and sediment characters of the high sediment yield regions in the upper Yangtze River. *Hydrology*, 3: 6–12 (in Chinese).

Lu, X.X. and Higgitt, D.L. (1998) Recent changes of sediment yield in the Upper Yangtze, China. *Environmental Management*, 22(5): 697–709.

Ma, L., Zhang, M., Guo, H. and Shen, Y. (2002) Research on the change of runoff–sediment relationship due to soil and water conservation in Jialingjiang River basin. *Hydrology*, 22(1): 27–31 (in Chinese).

Mann, H.B. (1945) Non-parametric test against trend. *Econometrica*, 13: 245–259.

Meade, R.H. (1996) River-sediment inputs to major deltas. In: *Sea Level Rise and Coastal Subsidence* (J.D. Milliman, and B.U. Haq, Eds.). Kluwer Academic, Dordrecht, pp. 63–85.

Meade, R.H. and Parker, R.S. (1985) Sediment in rivers of the United States, in National Water Summary 1984. *US Geological Survey Water-Supply Paper* 2275, 49–60.

Meade, R.H., Bobrovitskaya, N.N. and Babkin, V.I. (2000) Suspended-sediment and fresh-water discharges in the Ob and Yenisey Rivers, 1960–1988. *International Journal of Earth Sciences*, 89: 461–469.

Menon, S., Hansen, J., Nazarenko, L. and Luo, Y. (2002) Climate effects of black carbon aerosols in China and India. *Science*, 297(5590): 2250–2253.

Milliman, J.D. and Meade, R.H. (1983) World-wide delivery of sediment to the oceans. *Journal of Geology*, 91(1): 1–21.

Milliman, J.D. and Syvitski, J.P.M. (1992) Geomorphic/tectonic control of sediment discharge to the ocean: the importance of small mountainous rivers. *Journal of Geology*, 100(5): 525–544.

Nilsson, C., Reidy, C.A., Dynesius, M. and Revenga, C. (2005) Fragmentation and flow regulation of the world's large river systems. *Science*, 308(5720): 405–408.

Pan, J. (1997) Study on sediment transport characteristics in Jinsha River basin. *Bulletin of Soil and Water Conservation*, 17(5): 35–39 (in Chinese).

Ren, L., Wang, M., Li, C. and Zhang, W. (2002) Impacts of human activity on river runoff in the northern area of China. *Journal of Hydrology*, 261(1–4): 204–217.

Roderick, M.L. and Farquhar, G.D. (2002) The cause of decreased pan evaporation over the past 50 years. *Science*, 298(5597): 1410–1411.

Saito, Y., Yang, Z.S. and Hori, K. (2001) The Huanghe (Yellow River) and Changjiang (Yangtze River) deltas: a review on their characteristics, evolution and sediment discharge during the Holocene. *Geomorphology*, 41(2–3): 219–231.

Shen, G. and Xie, Z. (2004) Three gorges project: chance and challenge. *Science*, 304(5671): 681b.

Shen, H. (2001) *Material Flux of the Changjiang Estuary*. China Ocean Press, Beijing, pp. 176 (in Chinese).

Shi, Y.L., Yang, W. and Ren, M.E. (1985) Hydrological characteristics of the Changjiang and its relation to sediment transport to the sea. *Continental Shelf Research*, 4(1–2): 5–15.

Shiklomanov, I.A. (1999) World Water Resources and Their Use. State Hydrological Institute (SHI), St Petersburg, website: http://espejo.unesco.org.uy/.

Shiklomanov, I.A. and Rodda, J.C. (2003) *World Water Resources at the Beginning of the Twenty-first Century*. International Hydrology Series. Cambridge University Press, Cambridge, pp. 435.

Smith, L.C. (2000) Trends in Russian Arctic river-ice formation and breakup, 1917 to 1994. *Physical Geography*, 20(1): 46–56.

Stanley, D.J. and Warne, A.G. (1998) Nile Delta in its destructional phase. *Journal of Coastal Research*, 14: 794–825.

Syvitski, J.P.M., Vorosmarty, C.J., Kettner, A.J. and Green, P. (2005) Impact of Humans on the Flux of Terrestrial Sediment to the Global Coastal Ocean. *Science*, 308(5720): 376–380.

Thomas, A. (2000) Spatial and temporal characteristics of potential evapotranspriration trends in China. *International Journal of Climatology*, 20, 381–396.

Vörösmarty, C. J., Meybeck, M., Fekete, B., Sharma, K., Green, P. and Syvitski, J. P. M. (2003) Anthropogenic sediment retention: major global impact from registered river impoundments. *Global and Planetary Change*, 39(1–2): 169–190.

Wang, H., Yang, Z., Saito, Y., Liu, J. and Sun, X. (2006) Interannual and seasonal variation of the Huanghe (Yellow River) water discharge over the past 50 years: connections to impacts from ENSO events and dams. *Global and Planetary Change*, 50(3–4): 212–225.

Wu, S. (2000) Counter-proposals for the environmental administration and sustainable development of the main source and upper reaches of the Changjiang River. *Yunnan Geographic Environment Research*, 12(2): 25–30 (in Chinese).

Xian, W., Kang, B. and Liu, R. (2005) Jellyfish Blooms in the Yangtze Estuary. *Science*, 307: 41c.

Xie, P., Wu, J., Huang, J. and Han, X. (2003) Three-Gorges Dam: risk to ancient fish. *Science*, 302(5648): 1149b–1151.

Xu, K.H. (2006) Linking Land to Ocean: Flux and Fate of Water and Sediment from the Yangtze River to the East China Sea. PhD Dissertation, The College of William & Mary, pp. 174.

Xu, K.H., Milliman, J.D., Yang, Z.S. and Wang, H.J. (2006) Yangtze sediment decline partly from Three Gorges Dam. *EOS Transactions, AGU*, 87(19): 185–190.

Xu, K.Q., Chen, Z., Zhao, Y., Wang, Z., Zhang, J., Hayashi, S., Murakami, S. and Watanabe, M. (2005) Simulated sediment flux during 1998 big-flood of the Yangtze (Changjiang) River, China. *Journal of Hydrology*, 313(3–4): 221–233.

Yang, S.L., Zhao, Q.Y. and Belkin, I.M. (2002) Temporal variation in the sediment load of the Yangtze river and the influences of human activities. *Journal of Hydrology*, 263(1–4): 56–71.

Yang, S.L., Zhang, J., Zhu, J., Smith, J.P., Dai, S.B., Gao, A. and Li, P. (2005) Impact of dams on Yangtze River sediment supply to the sea and delta intertidal wetland response. *Journal Geophysical Research*, 110, F03006, doi: 10.1029/2004JF000271.

Yang, S.L., Li, M., Dai, S.B., Liu, Z., Zhang, J. and Ding, P.X. (2006) Drastic decrease in sediment supply from the Yangtze River and its challenge to coastal wetland management. *Geophysical Research Letters*, 33, L06408, doi:10.1029/2005GL025507.

Yang, Z.S., Wang, H., Saito, Y., Milliman, J.D., Xu, X.K. and Shi, G. (2006) Dam impacts on the Changjiang (Yangtze River) sediment discharge to the sea: the past 55 years and after the Three Gorges Dam. *Water Resources Research*, 42, W04407, doi:10.1029/2005WR003970.

Zhang, R. (1995) Problems about sedimentation in Three Gorges Reservoir and its countermeasures. *China Three Gorges Construction*, 3: 18–19, 47 (in Chinese).

Zhang, X. and Wen, A. (2002) Variation of sediment in upper stream of Yangtze River and its tributary. *Shuili Xuebao*, 4: 56–59 (in Chinese).

Zhang, X. and Wen, A. (2004) Current changes of sediment yields in the upper Yangtze River and its two biggest tributaries, China. *Global and Planetary Change*, 41(3–4): 221–227.

30

Large River Systems and Climate Change

Michael. D. Blum

Department of Geology and Geophysics, Louisiana State University, Baton Rouge, LA 70803, USA

30.1 INTRODUCTION

Fluvial landforms and deposits provide a readily studied record of landscape evolution in response to Quaternary climatic and environmental change, and studies of the long-term dynamics of river systems and their responses to external controls, can play important roles in global change research. Moreover, modern fluvial environments are critical to human activities, ancient fluvial deposits are important repositories for hydrocarbons, groundwater and other resources, and river systems will play an important role in transferring the effects of future climate change to the Earth's surface. Studies of the long-term dynamics of fluvial systems therefore have a broad range of applications.

Large river systems are especially interesting in the context of climate change and other external forcing mechanisms, they integrate signals from large areas. Moreover, many large river systems discharge to marine basins, and have witnessed the direct impact of the high amplitude, high frequency glacio-eustatic sea-level changes that have characterized the Late Quaternary Period. This chapter provides a brief overview of the responses of large rivers to climate and sea-level change by: (a) developing a historical perspective and outlining a basic conceptual framework for the responses of fluvial systems to climate change; and (b) illustrating a range of responses to Late Quaternary climate and sea-level change with examples drawn from the recent literature on three large river systems. The chapter concludes by discussing some potential impacts of future climate change on large river systems.

30.2 A BRIEF HISTORY OF IDEAS

Several concepts from the late nineteenth and early twentieth centuries have played key roles in studies of fluvial response to climate and sea-level change, and are especially important in the context of large river systems as we view them today. Based on observations along the Colorado River of the western USA, Powell (1875) defined base level as the lower limit to which rivers can erode their valleys, with his 'grand' or ultimate base level corresponding to sea level. A second concept was that of the graded stream, which Gilbert (1877) suggested was adjusted in terms of channel slope, or longitudinal profile, so that the available discharge could transport the amount of sediment supplied by the drainage network. Mackin's (1948) later discussion of the graded stream is more detailed, but also focused on equilibrium long profiles that are adjusted to prevailing conditions of discharge and sediment load.

As recently as the 1950s and 1960s, the prevailing model for climate change focused on the glacial–interglacial scale, and was in large part derived from Penck and Brückner's (1909) study of terraces along tributaries to the Danube River in southern Germany. Prior to Penck and Brückner's (1909) work, Pleistocene glaciation was an established concept, but multiple glaciations were not yet widely accepted. However, Penck and Brückner (1909) differentiated four moraines that could be traced to four separate terraces. Each terrace contained a deep weathering profile and was separated from the next younger terrace by a period of valley incision. From these data, they inferred four Pleistocene glacial–interglacial cycles, with each consisting of a long glacial, a long interglacial,

Large Rivers: Geomorphology and Management, Edited by A. Gupta

and short transitions between end-member states. This 'square-wave' model for glacial–interglacial climate change (Figure 30.1a) remained dominant until the development of oxygen-isotope records from ocean basins in the 1950s–1980s.

Penck and Brückner's (1909) study also established an interpretive model that was to serve the community for years to come, when they linked fluvial aggradation to glacial-period sediment supply, and incision with terrace formation to interglacial periods (Figure 30.1b). As noted by Butzer (1980) among others, many early studies focused on this 'glacial' vs 'interglacial' dichotomy, and assumed that present floodplains represented the Holocene, the first terrace was from the last Pleistocene glacial period, the second terrace was from the previous glacial period, and so on. This model was influential in the development of the climatic geomorphology popular among many twentieth century European scientists, and established terraces and associated deposits as foci for the study of fluvial responses to climate change, especially at the glacial–interglacial scale. Correlation of terraces to glacial periods can be found through the literature today.

Fisk's (1944) study of the lower Mississippi valley of the USA was similarly important, but focused on sea-level change as a singular causal mechanism. According to Fisk (a) the valley was deeply incised to a point some 1000 km upstream due to increased channel gradients during sea-level fall and lowstand, (b) braided-streams formed when gradients decreased during late Pleistocene to middle Holocene sea-level rise, and (c) the transition to a meandering regime occurred during the late Holocene highstand (Figure 30.1c). From this reasoning, Fisk and subsequent workers correlated terraces of the lower Mississippi valley and Gulf of Mexico coastal plain to previous interglacial highstands (Figure 30.1d). Fisk's (1944) model was, of course, 180° out-of-phase with Penck and Brückner (1909), in that deposition occurred during interglacials, and incision with terrace formation occurred during glacials. However, Fisk's model was equally influential in that many workers in coastal regions assigned successively older terraces to successively older interglacials.

In the last five decades, records of climate and sea-level change, and interpretations of changes in fluvial systems over time, have become increasingly independent. With the development of ^{14}C dating in the 1950s, it became possible to develop chronological frameworks for climate change from palaeobiological and other indicators, and, independently, for fluvial deposits and landforms themselves. Also in the 1950s, Leopold and Maddock's (1953) hydraulic geometry studies initiated a generation of efforts that developed quantitative relations between discharge regimes, sediment load, and measures of channel geometry. Development of ^{14}C dating and the hydraulic geometry paradigm made it possible to move beyond counting terraces and inferring correlations with glacial stages. It became increasingly clear that direct correlations between glacial–interglacial cycles and fluvial landforms were more complicated, and, perhaps more importantly, that fluvial systems were more sensitive to Holocene-scale climate changes than previously recognized (Knox, 1976, 1983; Butzer, 1980). Pertinent to the present discussion, Knox (1976) used hydraulic geometry reasoning to suggest that Gilbert's (1877) and Mackin's (1948) concepts of the graded stream should be redefined, since long profiles actually change little over time (see also Leopold and Bull, 1979): he noted instead that for alluvial channels, cross-sectional and plan-view geometries scale to various measures of discharge, and respond rapidly to changes in discharge and sediment load over time. Hence, the concept of grade should be redefined to emphasize those variables.

New palaeobiological and geochemical data from ocean sediments and ice cores beginning in the 1960s led to acceptance of Milankovitch orbital forcing of climate and sea-level change (Hays *et al*., 1976; Imbrie *et al*., 1984; Chappell and Shackleton, 1986), and development of the marine oxygen isotope stage (hereafter MIS) nomenclature and timescale (Figure 30.2a). One particularly relevant concept that emerges from this body of literature concerns the nature of average Earth system conditions, and how they depart significantly from the old square-wave model. Full interglacials like the Holocene are relatively short-lived, as are full glacials (see Porter, 1989), and up to 80 % of any middle to late Pleistocene 100 ka glacial–interglacial cycle witnessed global temperatures that were intermediate in character (Figure 30.2a, b). Moreover, eustatic sea level would have been at −20 m or more for perhaps 90 % of the time. Hence, an average world would be one that is significantly different from today when measured in terms of climate, vegetation, slope stability, and sediment production. Presently submerged continental shelves would exist as subaerial extensions of present-day coastal plains, and the average base level to which river long profiles terminate would reside in mid-shelf or farther basinward positions (Figure 30.2c).

New models for climate and sea-level change raise a number of issues in the context of fluvial response to climate change, as does the concept of average Earth system conditions mentioned above. However, at the same time that new paradigms for climate and sea-level change were being developed, the temporal range of ^{14}C essentially limited the detailed study of fluvial activity to the last 20–30 ka, the last full-glacial maximum and the

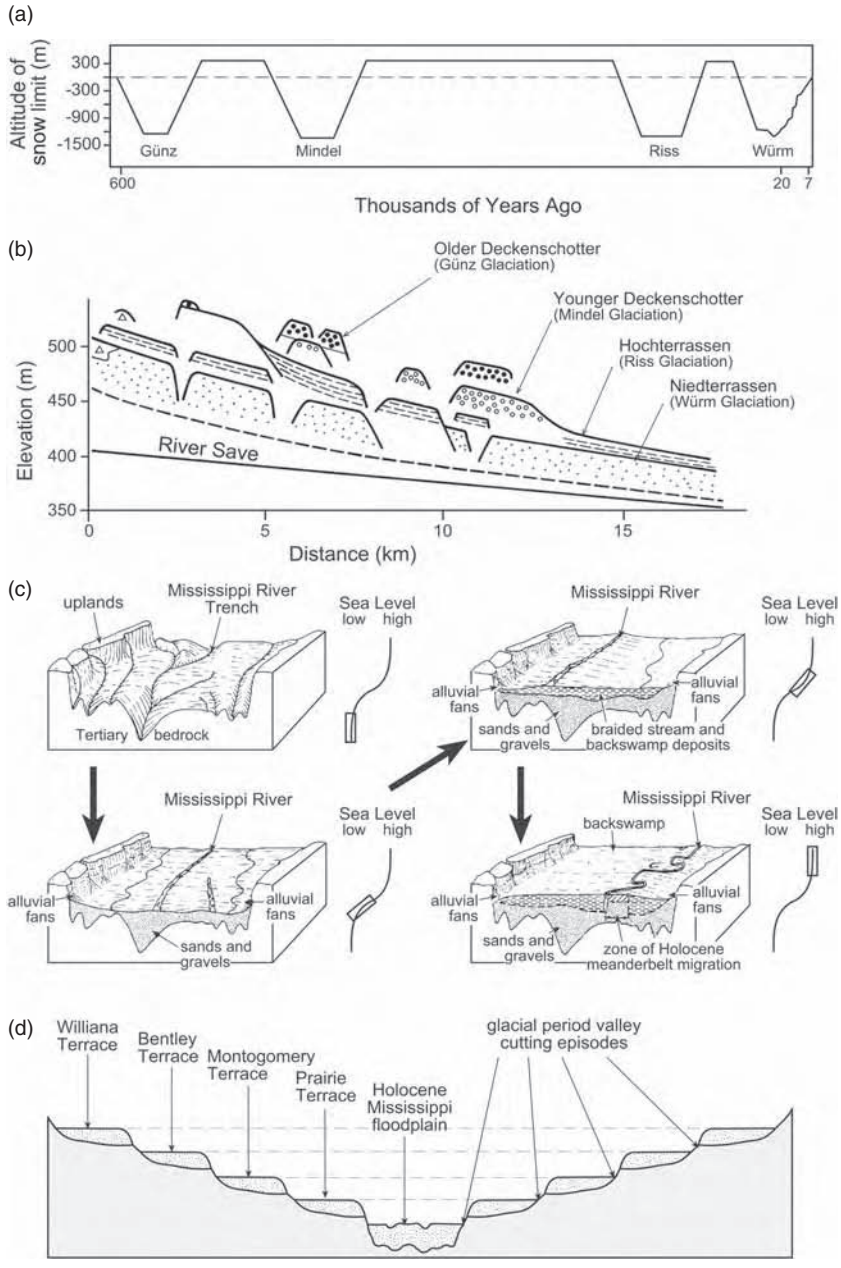

Figure 30.1 Historical ideas. (a) Rendition of original Penck and Bruckner (1909) square wave model for Quaternary glacial–interglacial cycles. (b) Penck and Bruckner's (1909) model for relationships between glacial moraines and outwash terraces in the Danube drainage of southern Germany. (c) Rendition of Fisk's (1944) model for Mississippi River response to sea-level change. (d) Fisk model for terraces of the Gulf of Mexico coast in Louisiana

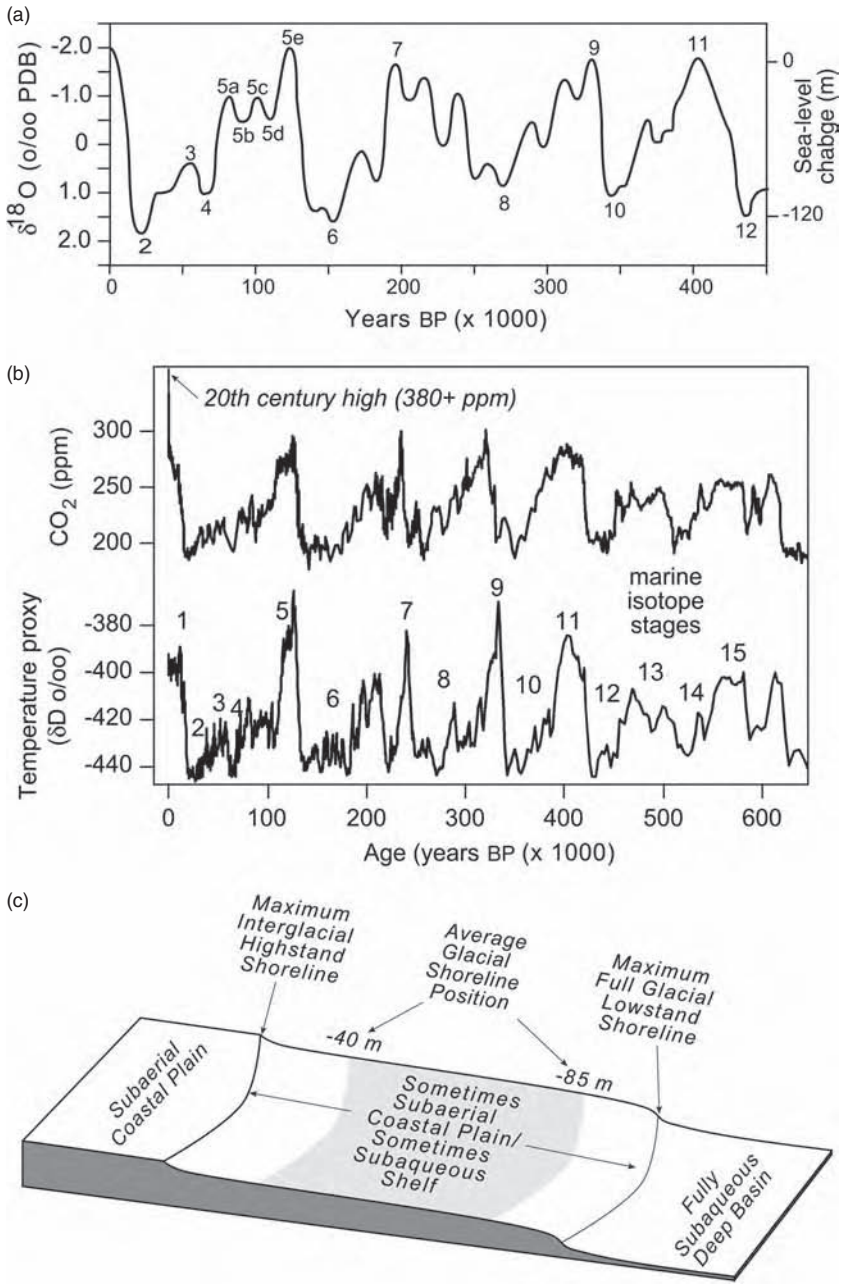

Figure 30.2 Quaternary climate and sea-level change. (a) Oxygen isotope record from ocean basins for the last 400 ka, illustrating 100 ka cyclicity in glacial–interglacial cycles and inferred glacio-eustatic component of sea-level change. (b) Carbon dioxide (CO_2) and deuterium (δD) records for the past 650 000 years from EPICA Dome C and other ice cores in Antarctica, correlated to marine isotope stage correlations. Deuterium is a proxy for air temperature, with more positive values indicating warmer conditions (adapted from Brook, 2005). For (a) and (b), note that most of the time, climate and sea-level positions are significantly different from the Holocene. (c) Schematic illustration of average shoreline positions to which rivers discharge over Quaternary timescales (adapted from Blum and Aslan, 2006)

Holocene. While this is an important time period in the Human context, it also represents only the last 20–30 % of a single 100 ka glacial–interglacial cycle, and is not in any way representative of the previous 70–80 %. Prior to the 1990s, re-examination of longer-term fluvial system evolution and response to climate change had been hampered by a paucity of geochronological methods that extend through at least one complete 100 ka glacial–interglacial cycle. Newer geochronological methods with longer time windows, for example the various luminescence techniques and cosmogenic radionuclides, have been applied to fluvial landforms and deposits beginning only in the last decade or so (e.g. Page *et al*., 1996; Phillips *et al*., 1997; Blum and Price, 1998; Hancock *et al*., 1999). Moreover the 1990s emergence of tectonic geomorphology, with its attention to long timescales, quantification of rates of erosion, and development of theory, has significantly raised the profile of fluvial landscape evolution to a new level, since terraces represent timelines in the landscape from which processes and rates of uplift can be measured and compared (e.g. Pazzaglia and Brandon, 2001).

30.3 FLUVIAL RESPONSE TO CLIMATE CHANGE: SOME GENERAL CONCEPTS

Several decades of theoretical, numerical and physical modelling, and empirical studies show that valley and channel gradients, as well as channel size, shape, and pattern, reflect rates of uplift or subsidence, prevailing discharge regimes (flood magnitude and frequency), and prevailing sediment loads (Figure 30.3a). Moreover, depositional processes, facies, and depositional systems are linked to channel geometry through the spatial distribution of depositional landforms and environments. Channels respond to changes in the relationship between discharge regimes and sediment supply through a series of morphological and sedimentary adjustments, and by storing or removing sediments from valley axes (Figure 30.3b; see Knox, 1983; Bull, 1991; Blum and Törnqvist, 2000; Bridge, 2003; Church, 2006). Although changes in discharge regimes and sediment supply can be forced by climate change and other external forcing mechanisms, a number of factors act as filters and make linkages between initial forcing and the subsequent response both nondeterministic and nonlinear (Figure 30.3c). As summarized in Schumm (1991), a number of complicating factors should be considered, including (a) spatial and temporal scale, (b) convergence of responses to different forcing mechanisms, (c) divergence of response following similar external inputs, (d) differential sensitivity, (e) complexity of response due to internal system dynamics, and (f) lag times between time of forcing and time of response.

Large river systems introduce two important complications that deserve additional mention. First, as shown in the various chapters within this volume, large river systems are most commonly polyzonal, and the lower reaches therefore integrate signals from different climatic and physiographic regions, each of which may have a different magnitude or direction of change in discharge regimes or sediment supply over time. Second, large river systems are major elements around which subcontinental-scale landscapes are organized. Most large river systems are organized around major structural grain, have long profiles that connect source regions in distal tectonic hinterlands to sinks within ocean basins (Potter, 1978; Miall, 2006), and all but one of the 50 largest drainage basins in the world have channel lengths that exceed 1000 km, with most of the top 25 exceeding 2000 km (Schumm and Winkley, 1994). What then are the timescales necessary to propagate signals of climate change or other forcing mechanisms through rivers with length scales measured in 10^3 km or more? Can we view large river systems as sensitive and faithful recorders of climate change?

Recent research in tectonic geomorphology suggests 10^5–10^6 years or more may be required for steady-state equilibrium conditions to be achieved in many landscapes (Whipple, 2001). Specific to fluvial systems, Dade and Friend (1998) argued that timescales required to reach equilibrium following a perturbation are related to the square of the length of the system, divided by diffusivity, which is, in itself, related to discharge and sediment transport. They calculated response times for the Mississippi and Brahmaputra Rivers at 65 and 85 ka, respectively. Castelltort and Van Den Driessche (2003) subsequently recalculated response times for these and other large systems using slightly different methods, however, their most conservative estimates for large river systems still exceed 40 ka (Table 30.1). Major elements of landscape geometry, for example the long profiles of large river systems, should therefore be adjusted to reflect mean conditions over timescales that approximate or exceed the characteristic response time. Hence, from the concept of the average world described above, many long-lived large river systems and their drainage basins should be adjusted, in terms of long profiles, slopes, and sediment production, to an average glacial world, and graded to sea-level positions on the mid-shelf or farther basinward. Moreover, from this reasoning, the characteristic response times for parameters such as long profiles in the lower reaches of large river systems will be relatively long compared with changes in discharge and sediment supply regimes driven by the 40 and 20 ka Milankovitch cycles, or the higher frequency changes typical of the Holocene, and may never reach equilibrium with such conditions.

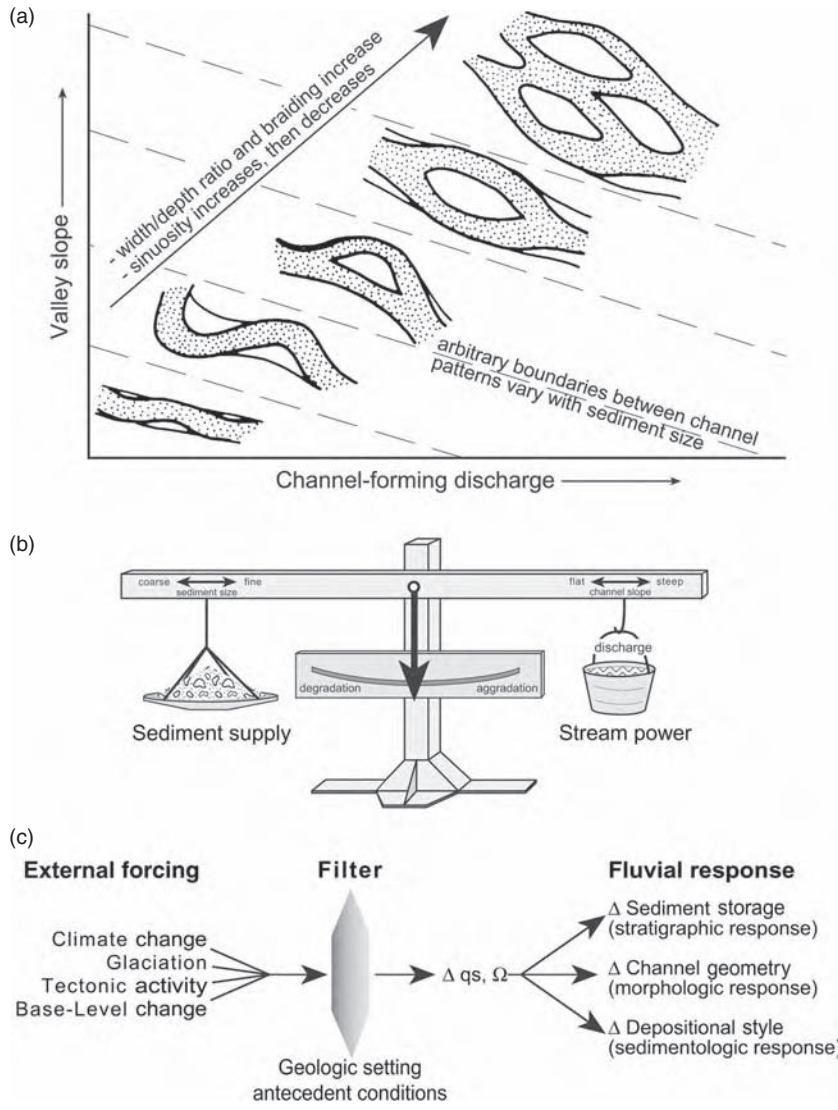

Figure 30.3 (a) General relationship between channel plan-view geometry, valley slope, and channel-forming discharge (modified from Bridge, 2003), indicating dependence of channel form on slope, discharge, and sediment load. (b) Balance model for aggradation and degradation of alluvial channels, emphasizing changes in the relationship between discharge and sediment supply. Channel beds aggrade when sediment supply exceeds transport capacity, and degrade when the reverse is true. Redrawn from an unpublished drawing by W. Borland of the US Bureau of Reclamation, based on an equation by Lane (1955; S.A. Schumm and F.G. Ethridge, personal communication, 1999). (c) Conceptual model for fluvial responses to external forcing. Forcing mechanisms, shown on the left, are passed through a filter that defines how they are actually translated into changes in stream power (Ω) and sediment supply (qs). Changes in Ω and qs then determine the direction and magnitude of fluvial stratigraphic, morphologic, and sedimentologic responses (adapted from Blum and Straffin, 2001)

Table 30.1 Drainage basin characteristics and equilbrium response times for river systems that discharge to ocean basins, and have drainage basin areas greater than 600 000 km^2. Modified from Castelltort and Van den Dreissche (2003; see discussion therein), based on data in Hovius (1998). Note that mean sediment discharge includes both the suspended and solute components (must be converted to volume for calculations, and the response time is calculated for the drainage basin as a whole, not just a specific reach. As calculated, the equilibrium time represents the time period over which the system will reshape surface topography

River	Total stream length, L (km)	Total drainage area, A (km^2)	Maximum relief, H (m)	Mean sediment flux, Q_s (10^6 m^3 year^{-1})	Mean water discharge, Q_m (m^3 s^{-1})	Mean slope, S (m m^{-1})	Mean estimated river mouth width, W (m)	Diffusivity coefficient, $K = Q_s/WS$ (10^6 m^2 year^{-1})	Equilibrium response time, $T_b = L^2/K$ (years)
Nile	6670	2 715 000	5110	53	317	0.0008	1648	42.0	1 060 000
Amazon	6299	6 150 000	6768	508.5	200 000	0.0011	2480	190.8	208 000
Mississippi	5985	3 344 000	4400	194.4	18 400	0.0007	1829	144.6	248 000
Ob	5570	2 500 000	4506	24.4	12 200	0.0008	1581	19.1	1 623 000
Yenisey	5550	2 580 000	3492	28.9	17 800	0.0006	1606	28.6	1 078 000
Yangtze	5520	1 940 000	6800	261.5	28 500	0.0012	1393	152.4	200 000
Huanghe	4670	980 000	5500	52.6	1 550	0.0012	990	45.1	483 000
Mekong	4500	810 000	6000	81.5	14 900	0.0013	900	67.9	298 000
Paraná	4500	2 600 000	6720	62.2	18 000	0.0015	1612	25.8	784 000
Amur	4416	1 855 000	2499	26.7	10 300	0.0006	1362	34.6	564 000
Lena	4400	2 430 000	2579	37	16 200	0.0006	1559	40.5	478 000
Congo	4370	3 700 000	4507	25.5	40 900	0.001	1924	12.8	1 487 000
Mackenzie	4240	1 448 000	3955	70	9 830	0.0009	1203	62.4	288 000
Niger	4160	1 112 700	2918	15.6	6 020	0.0007	1055	21.0	823 000
Murray	3490	910 000	2239	39	698	0.0006	954	23.6	516 000
Volga	3350	1 350 000	1638	38.1	8 400	0.0005	1162	67.1	167 000
Indus	3180	960 000	8611	107.8	7 610	0.0027	980	40.6	249 000
Yukon	3000	855 000	6194	34.8	6 180	0.0021	925	18.2	494 000
Rio Grande	2870	670 000	4295	11.9	95	0.0015	819	9.7	851 000
Danube	2860	815 000	3087	48.1	6 660	0.0011	903	49.4	166 000
Brahmaputra	2840	610 000	7736	215.2	19 300	0.0027	781	101.1	80 000
Orinoco	2740	945 000	5493	70	34 900	0.002	972	35.9	209 000
Zambezi	2660	1 400 000	2606	23.3	6 980	0.001	1183	20.1	352 000
Ganga	2510	980 000	8848	221.9	11 600	0.0035	990	63.6	99 000
Colorado (Cal.)	2333	640 000	4700	61.1	32	0.002	800	37.7	144 000
Columbia	1950	670 000	3748	18.5	7 930	0.0019	819	11.8	323 000
Orange	1860	1 020 000	3482	38.1	2 890	0.0019	1010	20.2	171 000

These issues have figured prominently in modelling fluvial responses to climate change, and raise questions regarding whether the upstream and downstream reaches of large river systems will respond in phase or out-of-phase with each other due to timescales required for signal transfer. Indeed, a number of modelling studies have suggested that responses in upstream and downstream reaches should be out-of-phase (Hancock and Anderson, 2002; Castelltort and Van Den Driessche; 2003). However, to a great extent these modelling efforts are conceptually driven by the downstream propagation of changes in sediment production: the Castelltort and Van Den Driessche (2003) study, for example, was specifically concerned with climate-driven changes in sediment supply within headwater source regions, and whether such signals could be discerned in the stratigraphic record of a distal sedimentary basin. By contrast, it might be argued that climate-driven changes in discharge regimes should be propagated through a large river system almost instantaneously, and should therefore be recorded by changes in channel morphologies and the resulting fluvial depositional and erosional record. This issue is addressed further with reference to specific case studies below.

30.3.1 Continental Interiors: Uplift, Subsidence, and Climate Change

Regardless of whether fluvial responses to climate change reaches a steady-state or not, the response should vary by position within a large and complex river system due to (a) local- to regional-scale rates of uplift or subsidence, the (b) resultant ability of fluvial systems to migrate laterally, incise, aggrade, and modulate sediment transfer and storage over various timescales, and (c) proximity to sea level and the influence of relative sea-level change (Blum and Törnqvist, 2000; Figure 30.4). The steep upper reaches of drainage networks within rapidly uplifting continental interiors typically have high stream powers, incising bedrock channels with discontinuous floodplains, minimal sediment storage capacity, and short residence times for sediment as a whole. Records of fluvial responses to climate change within rapidly incising bedrock valleys such as these tend to be fragmentary, and may extend only through the last glacial–interglacial period. For large river systems of the scale discussed in this volume, steep upper reaches are likely to be where systems are most directly coupled to climate change, in terms of both discharge regimes and sediment supply, however records may be poorly preserved.

By contrast, lower-gradient mixed bedrock-alluvial valleys (*sensu* Howard *et al*., 1994) are common to the extensive relatively low-relief continental interiors, and represent the conveyor belts for sediment delivery to ocean basins (Blum and Törnqvist, 2000). Mixed bedrock-alluvial valleys tend to have mostly continuous floodplains and longer sediment residence times, and, outside of the formerly glaciated regions of North America and Eurasia, may contain flights of terraces and associated fluvial deposits that record landscape evolution over time periods of 10^6 years or more (Figure 30.5a). Flights of terraces have served as focal points for the study of fluvial response to longer-wavelength climate change since the classic studies of Penck and Brückner (1909), and from a qualitative perspective, the formation of terraces is reasonably well known (Bull, 1991; Merritts *et al*., 1994; Hancock and Anderson, 2002). Periods of net bedrock valley incision reflect times when the concentration of sediments within channels is sufficiently low such that the entire sediment thickness can be mobilized during flood events, and bedrock can be incised by the mobile sediment load. By contrast, periods of channel-belt formation, lateral migration, and/or aggradation represent times when sediment concentration is sufficiently high that coarse sediment within the channel is not fully mobilized, and bedrock straths are not subject to abrasion and incision.

Tectonic geomorphologists have argued that long-term, time-averaged rates of valley incision within many continental interiors closely reflect rates of rock uplift, such that elevation differences between terraces with adequate chronological controls can be used to calculate incision

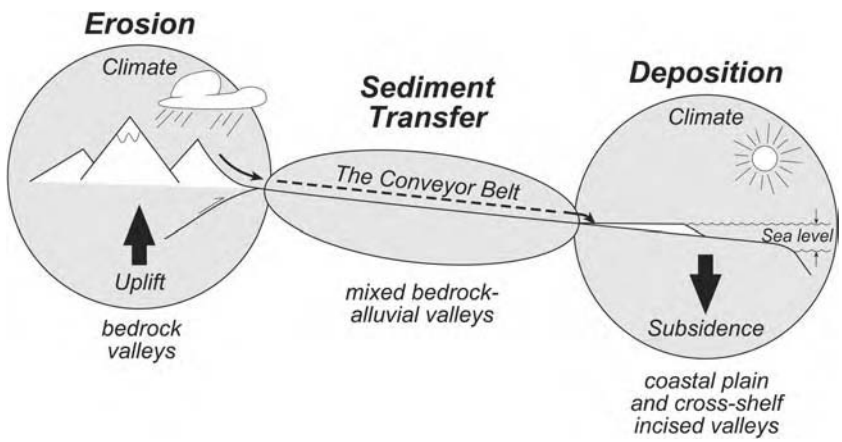

Figure 30.4 Conceptual model for large river systems from source-to-sink. In steep upper reaches, where sediment is produced, bedrock incision dominates, and terraces may be present, but the record will be fragmentary. Lower gradient mixed bedrock-alluvial valleys are the primary conveyor belts for sediment delivery to basin margins, and typically contain flights of terraces that may collectively record millions of years of landscape evolution. Coastal-plain incised valleys, as defined here, extend from the upstream limits of sea-level influence, to the highstand shoreline (highstand prism shown in white), whereas cross-shelf incised valleys extend from the highstand to lowstand shorelines, the horizontal distance over which sea-level falls during glacial periods (adapted and modified from Castelltort and Van Den Driessche, 2003)

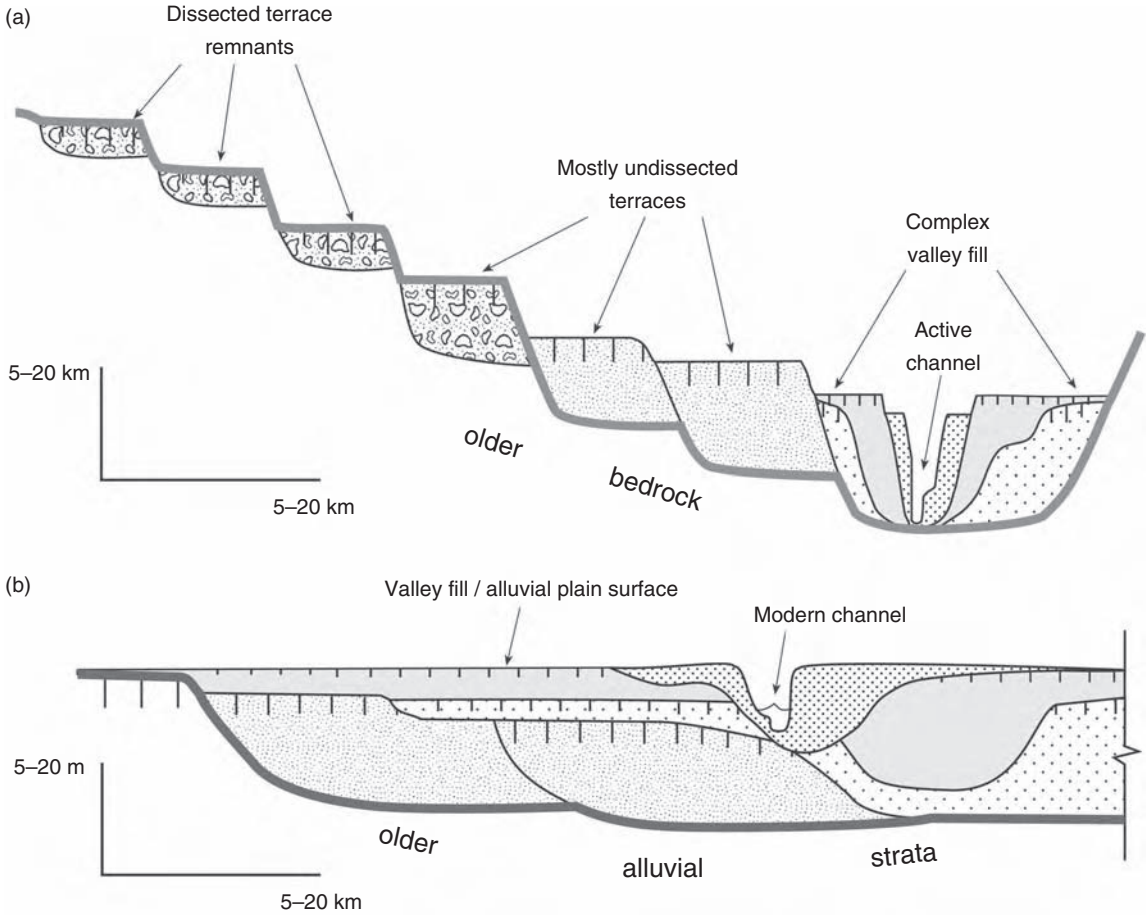

Figure 30.5 (a) Schematic model for mixed bedrock-alluvial valley setting, with flights of downward-stepping terrace surfaces and underlying fills, and a complex Holocene valley fill with multiple high-frequency stratigraphic units. Older and higher terraces are commonly discontinuous and dissected, with significant thicknesses of strata removed; they also may represent long periods of time, and multiple lateral migration, aggradation, and incision events within a limited elevation range that are not readily differentiated due to degree of preservation. Younger mostly intact terraces and the complex valley fill may represent the last glacial cycle (above thick gray line). Vertical hachures represent soil profiles, with the time for surface stability and soil development represented by length of hachure. (b) Schematic model for a coastal-plain incised valley, where a cycle of sea-level fall then rise results in a succession of downward-stepping then aggradational stratigraphic units bounded by palaeosols. The same model might apply to an alluvial valley within a subsiding continental interior basin, with incision and aggradation forced by climate change. The solid gray line encloses a single 100 ka glacial–interglacial cycle, and deposits above that line would correlate to deposits above the gray line in (a) (adapted from Blum and Törnqvist, 2000)

rates as a proxy for long-term time-averaged uplift rates (e.g. Pazzaglia and Brandon, 2001; Westaway *et al*., 2006). Even so, it is important to recognize that bedrock incision and terrace formation is not solely a tectonic story and a measure of tectonic control over fluvial systems. Rather, the ubiquitous presence of terrace flights clearly indicates that bedrock incision is highly unsteady when considered over timescales of 10^3–10^6 years, such that more geologic time may actually be represented by lateral migration and channel-belt construction. Accordingly, many workers have suggested that flights of terraces reflect climate-controlled unsteadiness in discharge regimes and sediment supply, superimposed on long-term trends of uplift-controlled bedrock valley incision (e.g. Bull, 1991; Blum and Törnqvist, 2000). Numerical modelling by Hancock and Anderson (2002) supports the view that climate change

can produce flights of terraces in this way, at least for relatively small river systems.

For mixed bedrock-alluvial valleys, it therefore seems likely that downward-stepping flights of terraces represent the primary response to climate change at Milankovitch timescales of 10^4–10^5 years. A number of studies have correlated long terrace sequences to the marine-based oxygen isotope records of glacial–interglacial cycles (e.g. Porter *et al*., 1992; Antoine, 1994; Bridgland *et al*., 2004), although river systems of the scale discussed in this volume have not figured prominently in this effort. Regardless, there remains no well-established general model that links periods of specific river behaviour to specific climate conditions or transitions, to the same degree attempted in the older work of Penck and Brückner (1909). Many records indicate the last major period of bedrock valley incision and terrace formation corresponds to the transition from the last glacial maximum to the beginning of the Holocene interglacial: for time periods prior to the last glacial maximum, the shortage of geochronological methods has severely limited understanding of the precise timing of lateral migration and deposition of fluvial deposits, or bedrock incision and terrace formation.

True alluvial valleys and alluvial plains, with fully alluvial channels, are common to subsiding basins, or valleys that have aggraded due to sea-level rise. Examples can be found in active foreland basins such as the Indo-Gangetic Plains of India and the Po plain of northern Italy, or the passive continental margins of the US Gulf Coast and the east coast of China. Alluvial valleys such as these may be net aggradational when considered over geologic time, and preserve a more complete record of fluvial system evolution than mixed bedrock-alluvial valleys, however, sediments delivered to subsiding basins are only preserved in the longer-term stratigraphic record when they subside below maximum depths of incision. Until that time they can be remobilized and transported out of the basin (continental interior forelands like the Indo-Gangetic plains), or elsewhere in the basin (both continental interior and continental margin basins), by externally forced cycles of incision and aggradation (Figure 30.5b). For continental margin systems, remobilization is especially important during glacial periods when river systems extend their courses to falling stage and lowstand shorelines, and develop incised valleys (see discussion of sea-level influences below).

Within individual mixed bedrock-alluvial or fully alluvial valleys, terrace surfaces commonly display differences in the morphology of formative channels. This is especially clear when comparing channel patterns from the last glacial period with those of modern interglacial rivers in the same valleys. Attention to morphological changes was a natural outcome of the hydraulic geometry paradigm, with early studies by Dury (1965) and Schumm (1968) discussing large-scale changes in channel geometry as a result of climate change in the US and Australia. Contrasts between braided glacial-age and sinuous single channel interglacial river systems are also well known from Europe (Starkel, 1991), where many present-day temperate regions experienced periglacial climates during glacial periods, or drained alpine glaciers or the Fennoscandian ice sheet. Few examples of this type of morphological change have been described from large river systems, with the notable exception of the lower Mississippi valley, where braided stream patterns from the last glacial period stand in sharp contrast to the meandering channel patterns of the Holocene.

As noted above, research spurred by the development of radiocarbon dating in the latter half of the twentieth century made it clear that fluvial systems are very sensitive to the high-frequency millennial-scale climate changes typical of the Holocene (e.g. Knox, 1983, 2000). Although the majority of work was completed on small river systems, it seems clear that fluvial responses to Holocene-scale climate rarely involved significant bedrock valley incision and generation of a partial flight of terraces, unless there are very high rates of uplift (Pazzaglia and Brandon, 2001). Instead, dominant themes include changes in channel morphology and rates of lateral channel migration, minor aggradation or incision through alluvial deposits themselves, increases or decreases in rates of overbank floodplain sedimentation, and repeated episodes of floodplain stability and soil formation followed by renewed overbank flooding and burial of soil profiles (e.g. Blum and Straffin, 2001; Macklin *et al*., 2005). As a result, Holocene valley fills can be stratigraphically complex (Figure 30.5a). Moreover, they are most commonly lithologically distinct from preceding glacial period deposits: thick successions of floodplain strata typical of Holocene alluvial sequences are not commonly found within units from the MIS 4-2 glacial period (Blum and Törnqvist, 2000; Blum and Straffin, 2001).

A variant on the theme of fluvial response to climate change – the response of floods to climate change – emerged from studies of slackwater deposits in canyon-confined bedrock streams of the western USA, which were designed to understand the magnitude and frequency of floods in the recent geologic past (Kochel and Baker, 1982; Baker *et al*., 2002; Chapter 5). Subsequent studies focused on reconstruction of palaeoflood magnitude and frequency from a variety of data sources, ranging from slackwater deposits that record the most extreme flood stages in bedrock canyons, to measures of palaeochannel geometry that record floods with recurrence intervals in the 1–10 year

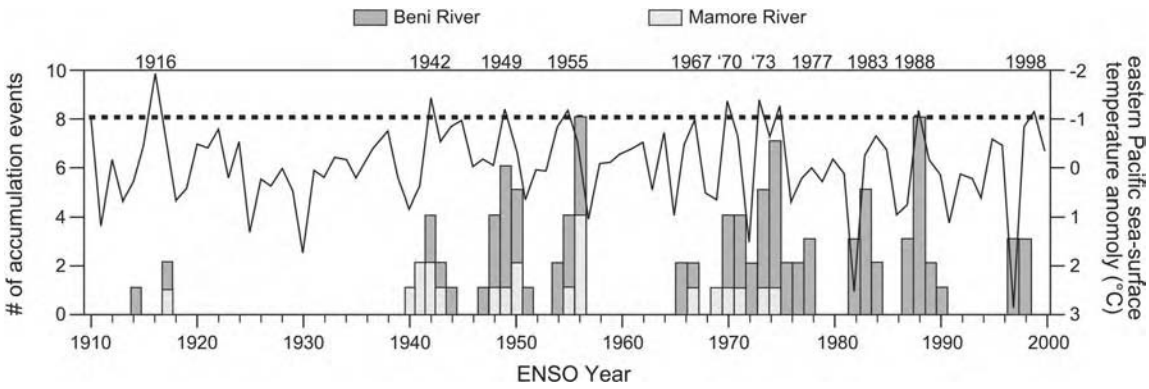

Figure 30.6 Inferred links between El Niño–Southern Oscillation events and floodplain deposition on Beni and Mamore river floodplains, tributaries to the Amazon in northern Bolivia. Number of floodplain accumulation events represented by bars. Sea surface temperature anomaly, represented by the solid line, is the anomaly for the eastern Equatorial Pacific from November to February, the early rainy season months for Bolivia. Noted years exhibit either sea-surface temperature anomalies <–1 °C (the La Niña threshold, marked by dashed line) or the accumulation of floodplain sediment (adapted from Aalto *et al*., 2003)

range in mixed bedrock-alluvial valleys (Knox, 1993, 2000). Most of these studies were conducted on river systems smaller than those discussed in the present volume, on the far upstream or tributary reaches of large river systems, or on extreme floods generated by nonmeteorologic causes (dam failures, glacial-lake outbursts, etc.; O'Conner *et al*., 2002). However, these and other studies illustrate that (a) atmospheric circulation changes through time have a direct impact on the magnitude and frequency of floods, (b) changes in flood magnitude and frequency are not directly proportional to increases or decreases in precipitation because of buffering by other variables that influence runoff rates, especially vegetation, and (c) relatively small changes in climate can significantly increase or decrease the magnitudes of floods over a range of recurrence intervals (Knox, 1993).

A recent development in high resolution studies of fluvial response to climate change has resulted from the application of radiogenic isotope geochronology (Goodbred and Kuehl, 1998), which has the potential to resolve annual rates and spatial variability of sediment transfer and deposition in floodplains over the last 100–150 years. Aalto *et al*. (2003), for example, described sedimentary facies and obtained ^{210}Pb profiles from a large number of cores throughout the Beni and Mamore river floodplains of northern Bolivia, which represent the principal sediment and water sources for the Madeira River, the largest sediment source for the Amazon. Through comparison with gauging station records, Aalto *et al*. (2003) show that major floodplain depositional events had mean recurrence intervals of ~8 years, and correspond to floods produced by the La Nina component of the El Nino–Southern Oscillation (ENSO) (Figure 30.6). Flooding occurs during both ENSO phases, however, La Nina floods produce rapid rates of rise in channel stage, which outpace local rain-generated water level rise in the floodplain, such that levees are breached and crevasse channels disperse sediments and prograde splays into the floodplain. Studies of this kind illustrate the sensitivity of large river systems to high-frequency changes in climate system forcing, as well as pave the way for linkages between the geologic record of fluvial response to climate change, which is regime-based, the record from the period of historical monitoring, which is event-based, and predictions regarding the effects of climate change on large river systems in the future.

30.3.2 Continental Margins: Importance of Relative Sea-Level Change

Most large river systems discussed in this volume discharge to marine basins. This is a fundamental issue, since it raises the question of the influence of relative sea-level change, which, for the Quaternary period is to a large extent forced by, and co-varies with, climate change. At some distance upstream from a maximum interglacial highstand shoreline, fluvial systems must become independent of the high-frequency (10^4–10^5 years) sea-level changes typical of the Quaternary period: the mixed bedrock-alluvial valleys described above fall into this category. However, there is no point moving in the downstream direction where the influence of climate-driven unsteadiness in discharge regimes can go to zero, and

evolution of the lower reaches of large river systems must therefore reflect the influence of both climate and sea-level change (Blum and Törnqvist, 2000).

Beginning in the 1960s, examination of shallow marine seismic data made it clear that glacial period fluvial systems had left behind an extensive record on the now-submerged continental shelves (Curray and Moore, 1964; Suter and Berryhill, 1985; Miall, 2002; Anderson *et al*., 2004). From four decades of studies in the offshore, and related field studies onshore, it is now clear that the sole deterministic fluvial response to the high rates of sea-level change typical of the Quaternary period is linked to regression and transgression of the shoreline to which river mouths terminate: sea-level fall forces channel extension across newly emergent shelves, whereas sea-level rise forces channel shortening and river mouth backstepping. Within this context, other responses are nondeterministic, and conditioned by alluvial valley, coastal plain, and shelf gradients, as well as by climate-controlled unsteadiness in discharge and sediment supply (Ethridge *et al*., 1998; Blum and Törnqvist, 2000). With that said, however, large river systems commonly construct low-gradient aggradational-progradational delta plains (e.g. the Mississippi), or shallow subaqueous deltaic clinoforms (e.g. the Amazon; Nittrouer *et al*., 1986), during sea-level highstand. When sea-level falls, channels will most commonly incise through this prism as they extend across the shelf (Figure 30.7a): extension and incision, in turn, serves to partition coastal-plain and cross-shelf incised valleys (Figure 30.7b), within which fluvial activity during the subsequent glacial period takes place (Blum and Törnqvist, 2000). Valley filling during sea-level rise and highstand then produces a landward-tapering wedge of deposits that onlap fluvial deposits from the glacial period (Figure 30.7c).

Blum and Törnqvist (2000) compiled data to illustrate the distances over which Late Quaternary sea-level change has influenced different river systems. For convenience of discussion, they defined the landward limit of the influence of sea-level rise as the onlap distance (see Figure 30.7a and c), and suggested this distance is inversely related to the gradient of the onlapped glacial period floodplain, and correlates to sediment supply. Accordingly, long low gradient river systems with large sediment loads will be affected very far upstream: for the Mississippi, this distance exceeds 4–500 km upstream from the highstand shoreline (Saucier, 1994; see discussion below). For the Amazon, present-day tidal influences are felt some 1000 km upstream from the mouth, and formerly incised tributaries are dammed by Holocene floodplain aggradation that far upstream, hence incision during the last sea-level lowstand extended at least that far (Archer, 2005). By contrast, the distances over which channels extend during lowstands reflect shelf width, among other factors. Of the systems discussed in this volume, the large Chinese rivers might represent one end-member, as they are thought to have extended some ~400 km across what is now the East China Sea (Wellner and Bartek, 2003). The Mississippi River might represent the opposite extreme: it now discharges to the shelf margin and continental slope, so if sea level were to fall to lowstand positions, it would not extend at all, just incise.

30.4 FLUVIAL RESPONSE TO PAST CLIMATE CHANGE: CONTRASTING EXAMPLES

The following discussion reviews recent research on three contrasting river systems discussed elsewhere in this volume, so as to more fully develop key themes discussed above.

30.4.1 The Colorado River in Grand Canyon, Western USA

The Colorado River, western USA, heads in the Rocky Mountains of Colorado, flows through the Colorado Plateau and Basin and Range physiographic and tectonic provinces, and eventually discharges into the Gulf of California and Pacific Ocean along the San Andreas transform margin (see Chapter 10). The Grand Canyon of Colorado River (Figure 30.8) is known for its dramatic splendor, as well as for the many grand ideas in geomorphology that were spawned during the early days of United States government-sponsored exploration of the western interior. As noted above, among the most important of these would be base level, as defined by Powell (1875) in reports that followed his famous trips down the Colorado River. Now, some 130 years later, geomorphological and geochronological studies of terraces and Holocene deposits in Grand Canyon provide examples of the response of a large polyzonal river within a midlatitude continental interior to climate change, as well as how trunk stream and tributary responses may be out-of phase with each other.

Total drainage area for the Colorado River system is some 640 000 km^2 (Hovius, 1998), roughly half of which is upstream from Grand Canyon. Headwaters for the Colorado River and its major tributaries, the Green and San Juan Rivers, lie within the Rocky Mountains of Wyoming and Colorado, respectively, are snow-covered for much of the year, and were modestly glaciated during the late Pleistocene MIS 6, 4, and 2 glacial periods. Prior to construction of large dams in the middle to late twentieth century, Rocky Mountain snowmelt sources supplied more than 50% of discharge to the Colorado mainstem and the Grand Canyon reach discussed here. By contrast, the

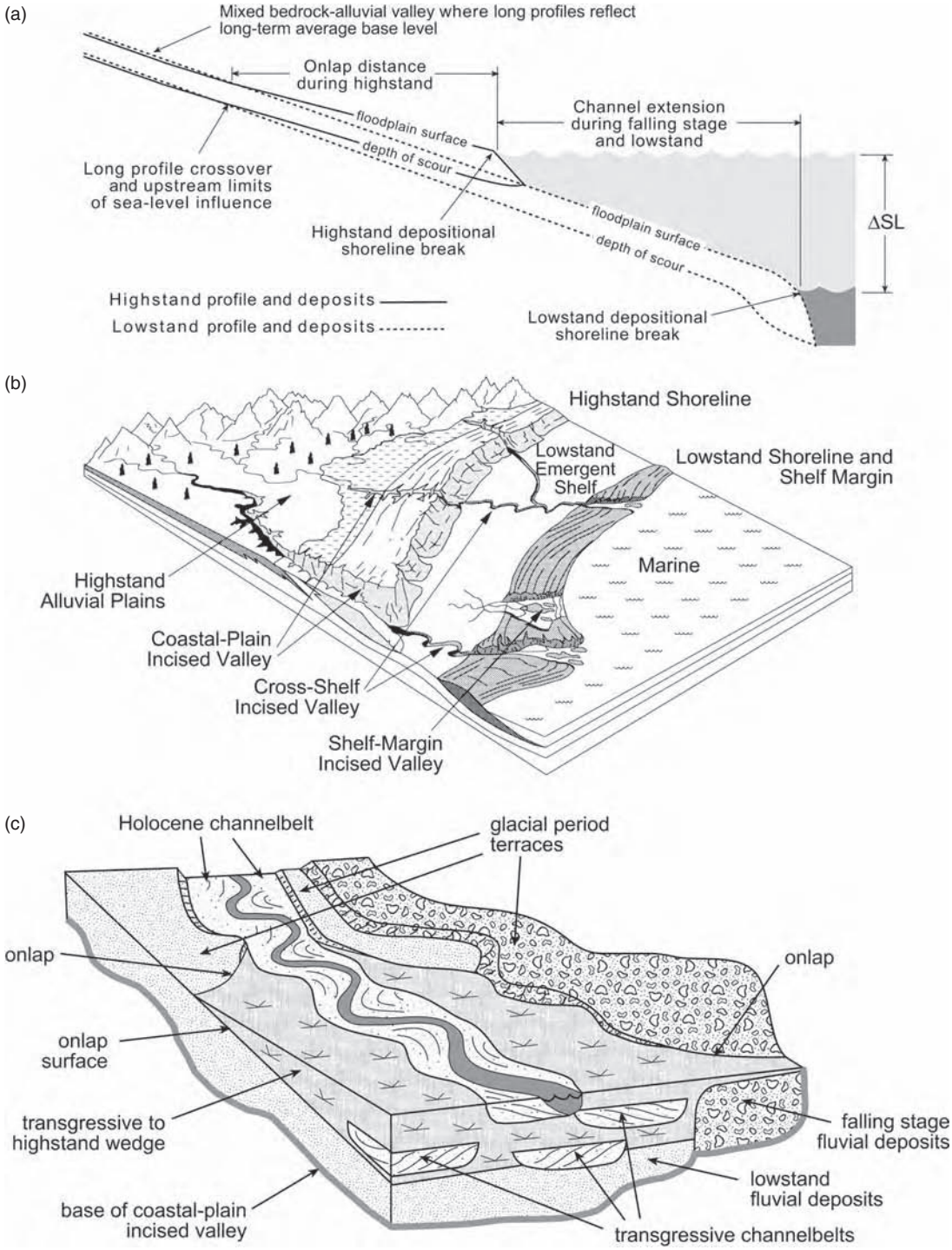

Figure 30.7 (a) Long profile model for fluvial response to sea-level change along low gradient continental margins where highstand deposition results in a distinct depositional shoreline break that must be cut through as channels extend across newly exposed shelfs during sea-level fall. Model illustrates differences between highstand and lowstand long profiles, definition of onlap distance, and definition of channel extension during sea-level fall (simplified from Blum and Törnqvist, 2000). (b) Schematic continental margin setting, where sea-level fall results in development of a coastal-plain and cross-shelf incised valley system that extends through the highstand shoreline, and across the emergent shelf to the lowstand shoreline (modified from Zaitlin *et al*., 1994). (c) Model for coastal plain incised valley fill, illustrating channel belts that represent the glacial period, when sea-level fell and channels extended across the shelf, and which are onlapped by estuarine, channel and floodplain facies associated with the transgression and highstand. Note that channel belts deposited during falling stage and lowstand occur as terraces updip from the onlap point, and are buried farther downdip (originally developed for the Gironde estuary, France; modified from Allen and Posamentier, 1993)

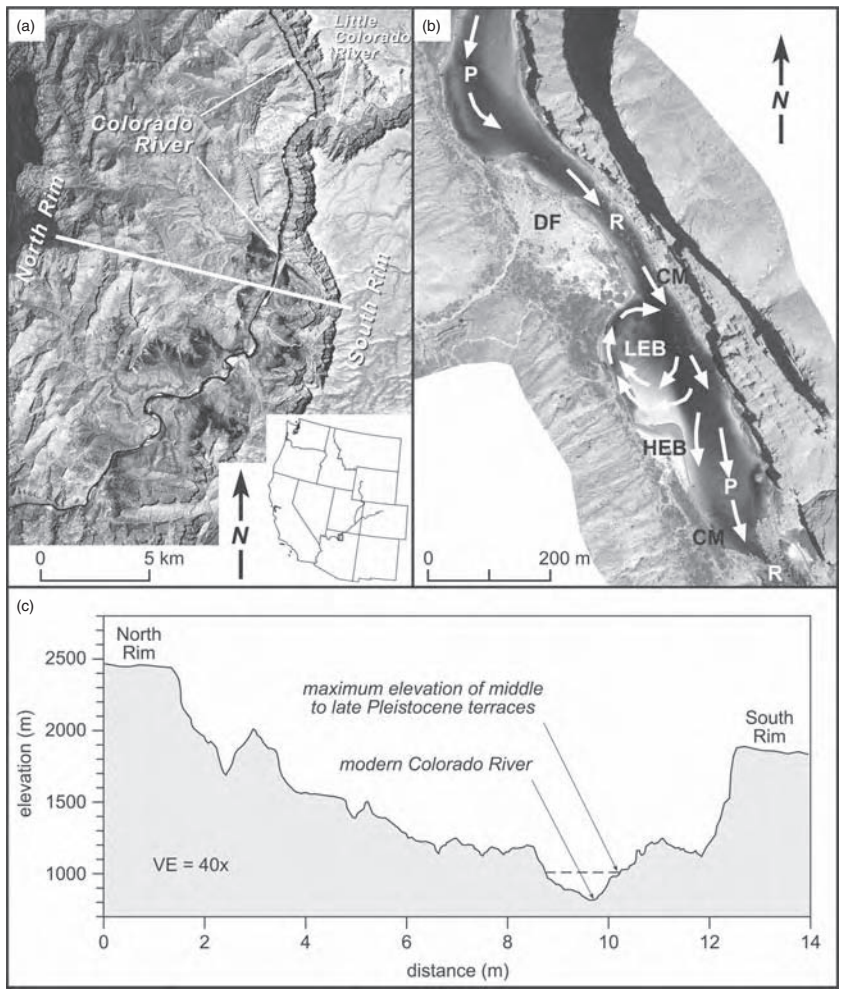

Figure 30.8 (See also colour plates.) (a) Landsat Thematic Mapper image of eastern Grand Canyon. Inset shows the Colorado River drainage basin within the western United States, with small box illustrating location of eastern Grand Canyon reach. (b) Panchromatic aerial photograph of Saddle Canyon, a typical fan–eddy–bar complex of the Colorado River in Marble Canyon. DF, tributary debris fan; R, rapid or riffle; P, main-channel pool; HEB, high-elevation eddy bar; LEB, low-elevation eddy bar; CM, channel-margin deposits. Arrows indicate flow direction. (Courtesy of J. Hazel Jr; adapted from Hazel *et al*., 2006). (c) Topographic profile across eastern Grand Canyon, from north rim to south rim, illustrating position of late Pleistocene terraces within the deeply incised canyon. Location of profile shown in (a). Taken from USGS 7.5 min DEMs

Colorado Plateau is semi-arid to arid, with minimal runoff, but tributaries that originate on the Colorado Plateau represent the dominant source for sediments to the mainstem within the Grand Canyon reach (see Chapter 10; Anders *et al*., 2005). Prior to trapping of sediments within reservoirs, most importantly Glen Canyon Dam and Lake Powell just upstream from Grand Canyon in the mid 1960s, the Colorado River was second in North America only to the Mississippi in terms of sediments delivered to ocean basins, and would have ranked in the top 10–12 systems in the world (Hovius, 1998).

The Colorado River within Grand Canyon is a bedrock to occasionally mixed bedrock-alluvial channel, with a Plio-Pleistocene trend of bedrock incision and canyon deepening that is the reason for its grandeur. Long-term average rates of bedrock incision vary spatially between the eastern (upstream) and western (downstream) reaches. However, they appear to be everywhere greater than

70 m Ma^{-1}, with estimates for some reaches of 400 m Ma^{-1} (Pederson *et al*., 2002; Chapter 10). Moreover, long-term incision of the canyon is well-documented, but occasional basaltic volcanic eruptions along canyon margins have created lava dams that ponded water for >100 km upstream: these dams eventually burst, and have generated peak discharges that rank among the 10 largest palaeofloods estimated for North America (Fenton *et al*., 2006). Finally, modern rapids and sandbars are localized to reaches where tributary streams deliver coarse bedload via debris flows, construct rapids, and create fan-eddy-bar depositional sites (Schmidt, 1990; Figure 30.8b): sites of potential net deposition are therefore highly localized and tethered to the deep canyon-confined tributary-trunk stream junctions, where coarse bedload is introduced, a trend that has likely characterized the past as well. For a variety of reasons, then, the potential preserved record of fluvial response to climate change is highly fragmentary.

Within this overall erosional context, a flight of middle to late Pleistocene terraces with underlying coarse graveliferrous deposits of varying thickness, and a sand-dominated succession of Holocene floodplain deposits have been recognized by a variety of researchers over the years. The oldest and highest terrace occurs some 175 m above present river level (Figure 30.8c), with a typical downward-stepping suite of successively younger terraces and associated graveliferrous deposits (Figure 30.9) at successively lower elevations (Machette and Rosholt, 1991). However, moderately firm relationships between episodes of fluvial deposition and terrace formation, and climate change or other forcing mechanisms, had remained elusive due to inadequate chronological controls. However, most recently, Anders *et al*. (2005) presented results from uranium-series, cosmogenic radionuclide, and optical luminescence dating of this flight of terraces in eastern Grand Canyon. For the more recent part of the record, they identify a thick aggradational succession of gravels that were deposited mostly during the penultimate glacial stage, MIS 6, a second succession deposited during the early part of the last 100 ka glacial cycle, MIS 4, and speculate that thick graveliferrous deposits from the last full-glacial maximum (MIS 2) reside below present river level (Figure 30.10a). By contrast, although the record is not as long, major phases of aggradation and sediment storage by debris flow-dominated tributary streams correspond with MIS 3 and the Holocene, and the last major episode of bedrock incision along tributaries corresponds with MIS 2 (Figure 30.10b).

From these data, Anders *et al*. (2005) infer that major episodes of Colorado mainstem aggradation and incision correspond to hydrologic changes triggered by glaciation and deglaciation in distal Rocky Mountain headwaters. Periods of glaciation correspond to periods of reduced snowmelt discharge, and produced the major episodes of aggradation and storage of coarse gravels in Grand Canyon, whereas periods of minimal ice volumes in headwaters correspond with increased discharges and episodes of net bedrock incision. They further infer that major phases of aggradation and incision by tributaries correspond with climate-driven changes in sediment production within proximal Colorado Plateau source regions, and dispersal to canyon floors via debris-flow processes. This apparent out-of-phase relationship between the Colorado mainstem, dominated by changes in discharge regimes from distal headwaters, and tributary streams, dominated by sediment supply and debris-flow processes within local tributaries, illustrates the inherent complexities of large polyzonal systems. Of equal importance, since Grand Canyon is some 600 km downstream from glaciated headwater source regions, the mainstem record also suggests

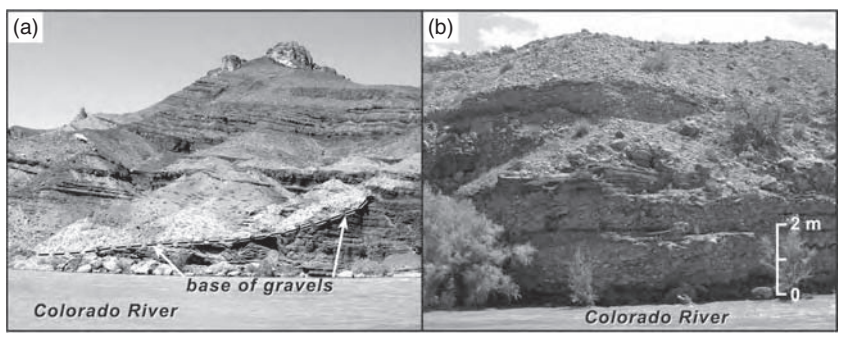

Figure 30.9 (a) Outcrop of graveliferrous late Pleistocene deposits of the Colorado River within eastern Grand Canyon, illustrating basal cut bedrock surface (strath). (b) Close-up view of graveliferrous late Pleistocene deposits of the Colorado River within eastern Grand Canyon. These deposits correspond to unit M3 of Anders *et al*. (2005; see Figure 30.10a)

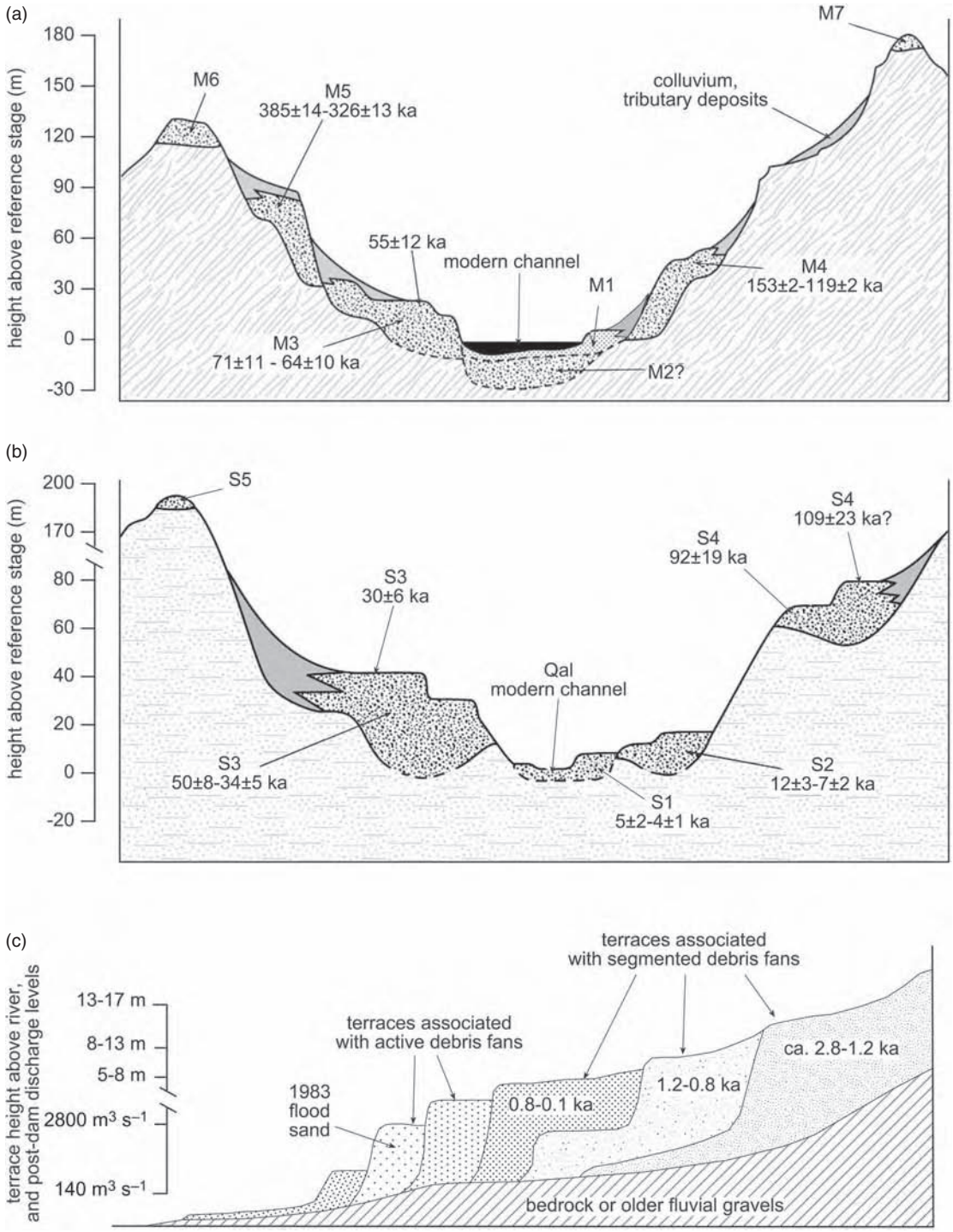

Figure 30.10 Stratigraphic framework for eastern Grand Canyon. (a) Schematic composite cross-section of the Colorado mainstem, illustrating relative heights of major terraces and colluvial deposits, as well as numerical age estimates (adapted from Anders *et al*., 2005). (b) Schematic composite cross-section of major tributary valleys, illustrating relative heights of major terraces and colluvial deposits, as well as numerical age estimates (adapted from Anders *et al*., 2005). (c) Schematic composite cross-section of the Colorado mainstem Holocene record, illustrating relative heights of major terraces and colluvial deposits, as well as numerical age estimates (adapted from Hereford *et al*., 1996). Subsequent work has shown that Holocene terraces are not strictly constructional fluvial landforms, but instead include aeolian and colluvial facies as well

that climate-controlled changes in discharge regimes can be transmitted throughout a large drainage system relatively rapidly at glacial–interglacial and stadial–interstadial timescales (10^4–10^5 years).

The Holocene record of Colorado River in Grand Canyon consists of three mappable terraces, with sand-dominated alluvial, colluvial, and aeolian deposits that rest on a composite bedrock and fluvial gravel surface (Hereford *et al*., 1996; Figure 30.10c). Radiocarbon ages plus archaeological data constrain deposition of all three units to the late Holocene (ca. 2.8–1.2, 1.2–0.8 and 0.8–0.1 ka) with erosional unconformities inferred to separate each unit from the next older unit. Detailed sedimentological analysis by Draut *et al*. (2005) at a number of archaeologically significant areas shows these deposits consist of overbank flood-deposited sand that interfingers towards canyon walls with colluvial materials, and is extensively reworked by aeolian processes in between flood events. Coeval channel-belt facies have not been identified, nor have deposits from the early to middle Holocene, and may be below present river level. Although similarly detailed records are not available for the Colorado mainstem farther upstream near the Rocky Mountain source, Hereford *et al*. (1996) note that the timing of late Holocene changes in fluvial behaviour corresponds to records elsewhere on the Colorado Plateau, and suggest that climate change is the causal mechanism. Regardless, the sandy, flood-dominated nature of Holocene deposits and the high-frequency millennial-scale signature in the stratigraphic record, render them distinct from older glacial period landforms and deposits. Similar sand-rich deposits have not been identified in the older record (Anders *et al*., 2005), perhaps because interglacial conditions similar to the Holocene are rare, and deposits from such time periods have a correspondingly decreased chance of preservation (Blum and Straffin, 2001).

In addition to the record of floodplain, colluvial, and aeolian deposition, and minor terrace formation, rock shelters in Grand Canyon contain slackwater deposits that provide insights into palaeoflood history (O'Conner *et al*., 1994). The largest peak discharge recorded by gauging stations prior to construction of the Glen Canyon Dam just upstream was ~4815 $m^3 s^{-1}$ in 1921, with estimates of ~5950 $m^3 s^{-1}$ for the flood of 1884, during the early days of US government exploration (Topping *et al*., 2003). O'Conner *et al*. (1994) identified and dated 15 floods since ca. 4500 years BP with estimated discharges exceeding 5600 $m^3 s^{-1}$, with 10 events in the last 2300 years that exceeded an estimated 6800 $m^3 s^{-1}$. The largest flood recorded by slackwater deposits occurred between 1600 and 1200 years BP, with an estimated discharge of 14 000 $m^3 s^{-1}$, more than twice that for any event during the period of historical observation and monitoring. Time series were not sufficient to draw conclusions regarding palaeoclimatic influences, but elsewhere in the southwestern US, Ely *et al*. (1993) note that changes in flood magnitudes through time reflect regional trends in climate change.

30.4.2 The Ganga-Brahmaputra System, India and Bangladesh

The Ganga-Brahmaputra system of India and Bangladesh drains the highest relief part of the Earth's surface, the Himalaya Mountains and Tibetan Plateau, and eventually discharges to the Indian Ocean through the Bengal Basin. The Ganga trunk stream gathers a number of large tributaries from the central Himalaya to the north, and from the Indian craton to the south, flows west to east through the Himalayan foreland basin, then south into the Bengal Basin and the Indian Ocean. The Brahmaputra, by contrast, flows east to west after emerging from the eastern Himalayas, then south to eventually merge with the Ganga. Although these two great rivers now flow together to the Indian Ocean, they have entered separately in the past (Goodbred, 2003).

Total drainage area for the combined Ganga-Brahmaputra system is some 1.6×10^6 km^2, the 11th largest drainage basin in the world. However, because of the extreme end-member high relief Himalayan and Tibetan Plateau source terrain, the combined Ganga-Brahmaputra system ranks second only to the Amazon in sediment delivered to ocean basins: in fact, the Ganga alone ranks second, with the Brahmaputra a close third (Hovius, 1998). The modern discharge regime is dominated by the Indian monsoon, such that some 80% of annual discharge originates during the wet summer months, with snowmelt runoff and other sources comprising the remaining 20%. Here again, the combined system ranks second only to the Amazon in mean annual peak discharges, and fourth in mean annual discharge. The Himalayan headwaters were more extensively glaciated during the various Pleistocene glacial periods, but more importantly, a range of modelling studies and empirical data indicate that the intensity of the annual monsoon cycle has varied significantly over time in association with the 23 kyr Milankovitch precessional cycle (Goodbred, 2003).

The Himalayan foreland, through which the Ganga and its major tributaries flow, consists of extensive low gradient alluvial plains within a subsiding continental interior foreland basin setting (Figure 30.11), the antithesis of the Grand Canyon described above, and therefore a very different style of long-term fluvial system evolution characterized by net aggradation. Recent studies by Shukla *et al*.

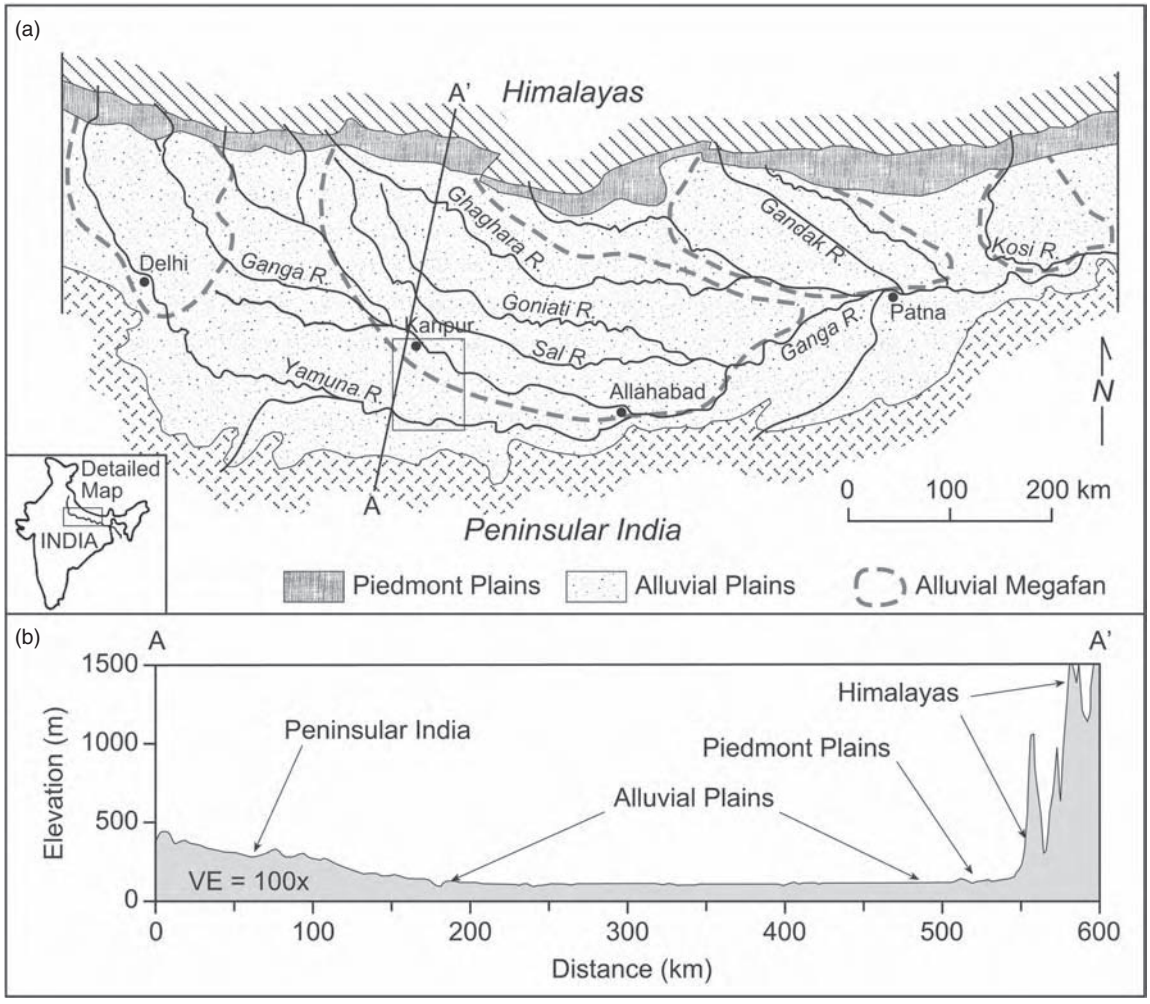

Figure 30.11 (a) Map of Gangetic plains, illustrating major rivers and the general extent of large megafans that have been identified by previous workers (adapted from Goodbred, 2003). Also shown are the locations of the Ganga and Yamuna Rivers, including the Gibling *et al*. (2005) study area. Inset shows location within India. (b) Topographic profile across Gangetic Plains, illustrating relief of the southernmost Himalayas, the relative flatness of the alluvial plains, which lie over the Himalayan foreland basin, and the low relief Indian cratonic region to the south (the peripheral forebulge). Taken from 30 m resolution SRTM DEMs

(2001), Singh (2004), Sinha *et al*., (2005), and Gibling *et al*. (2005) discuss the geomorphology and stratigraphic evolution of the Gangetic plains. As shown in Figure 30.11, alluvial plains have been interpreted as a series of low-gradient megafans emerging from the Himalayas. Shukla *et al*. (2001) indicate that alluvial megafans are constructed by widespread aggradation and avulsion, followed by periods of deep incision. The most recent cycle of aggradation and incision corresponds well to the precessional cycle: alluvial megafans accumulated more than 30 m of sediment during a cool and wet MIS 3, were largely inactive during the dry MIS 2 full glacial maximum, and were then deeply incised (20–30 m) during the wet late Pleistocene to early Holocene insolation maximum, forming broad valleys (Figure 30.12a).

Gibling *et al*. (2005) provide more detail on the sedimentological, stratigraphic, and geochronologic framework of interfluves between the Ganga and one of its major Himalayan tributaries, the Yamuna. Within their study area (location in Figure 30.11a), the Ganga and Yamuna are

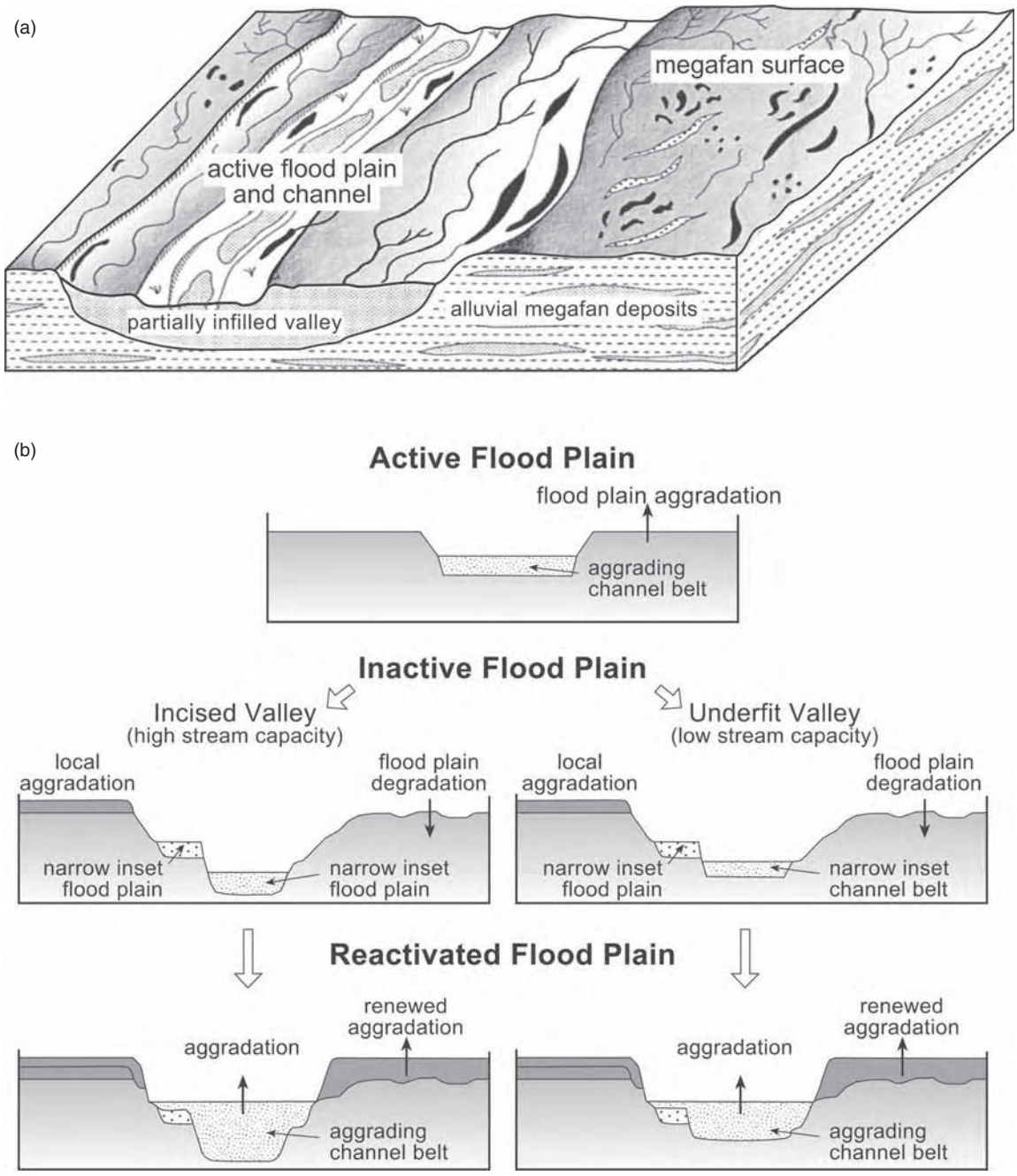

Figure 30.12 (a) Schematic view of Ganga megafan deposits illustrating an inferred sequence of aggradation, valley incision, and infilling. Megafan deposits are interpreted to comprise >30 m of sediment deposited during MIS 3, with deeply incised valleys forming during the wet late MIS-2 to early Holocene transition (adapted from Goodbred, 2003; see references therein). (b) Model for generation of floodplain sequences in the southern Gangetic Plains, reflecting variation through time in the frequency of floodplain inundation by the major rivers (modified from Gibling *et al*., 2005). Upper diagram represents time period when rivers are actively inundating broad floodplains, and accumulating thick floodplain muds. Middle block diagrams illustrate floodplain abandonment (referred to as 'detachment' by Gibling *et al*., 2005), which is interpreted to reflect deep incision due to increased discharge and sediment transport capacity (left block diagram), or to reductions in flood stage without major incision (Blum and Törnqvist, 2000) and development of an underfit valley (right block diagram). Although floodplains may be abandoned by major rivers, they may aggrade locally from small plains-fed rivers, lakes, and aeolian landforms (left side of each block diagram). Parts of floodplains not aggrading locally may be gullied (right side of each block diagram). In either case, renewed floodplain deposition by major rivers buries pre-existing surfaces and deposits (lower two block diagrams).

Table 30.2 Summary of Ganga system behavior over the late Quaternary (modified from Goodbred, 2003 and references therein)

	MIS 3 (58–24 ka)	MIS 2-LGM (24–18 ka)	Late MIS 2 and early Holocene (18–7 ka)	Mid–late Holocene (7 ka–present)
Regional climate	Cool, moderately wet	Cold, dry	Warmer, very Wet	Warm, wet
Sediment load (upper/ lower river basin)	High/moderate(?)	Low/low	High/very high	High/high
River discharge	Moderate	Low	Very high	High
Himalayan glacial valleys	Widespread glacier advance, valley aggradation	Limited glacier advance	Brief glacier advance (?), valley incision	Retreat (melt), mixed valley aggradation and incision
Megafans and alluvial plains	Widespread aggradation	Largely inactive, minor incision	Rapid, widespread incision	Slow aggradation
Bengal delta and shelf	Incision, local aggradation (?)	Inactive (incised)	Very rapid aggradation	Aggradation
Deep-sea Bengal fan	Aggradation (?)	Largely inactive (?)	Rapid aggradation	Slow aggradation

separated from each other by broad (~80 km) mostly undissected alluvial plain surfaces that are now occupied by minor streams. However, alluvial plains are underlain by thick successions of floodplain muds from the major rivers, interspersed with minor lacustrine and aeolian deposits, indicating widespread aggradation of alluvial plain surfaces in the past. Thick floodplain successions are capped by soil profiles, indicating nondeposition or very slow deposition by major rivers, although soil profiles are commonly veneered by deposits from local streams, aeolian deposits, and/or cultural debris. Geochronological data presented in Gibling *et al*. (2005) correspond to the model proposed by Shukla *et al*. (2001), and indicate the most recent extended period of widespread floodplain aggradation occurred from ca. 90–27 ka (late MIS 5, MIS 4 and MIS 3). Abandonment of alluvial plains as actively aggrading environments, with confinement of major rivers to their present incised courses, occurred during and after the last glacial maximum. Gibling *et al*. (2005) suggest this occurred initially by decreases in flood magnitudes without major channel incision from ca. 27–15 ka, forming underfit valleys, then by incision of channels followed by lateral migration and reworking of floodplains from ca. 13–9 ka, the late Pleistocene to early Holocene transition (Figure 30.12b). The Ganga and Yamuna remain confined today, at least in this study area, but stratigraphic data suggest an older period of areally widespread alluvial plain aggradation, perhaps followed by entrenchment into incised valleys, prior to and during MIS 5. Gibling *et al*. (2005) note that this part of the Gangetic Plains is too far upstream to have been affected by sea-level change, and link changes in fluvial activity over time to periods of climate change, especially changes in monsoon intensity driven by variations in the 23 ka precessional cycle.

Goodbred (2003) provides an important first synthesis of the Ganga system as a whole, from glaciated headwaters to the delta plain and beyond, over the last glacial – interglacial cycle, and reinforces the direct coupling between fluvial processes and changes in monsoon intensity forced by the 23 ka precessional cycle (Table 30.2). Peak glaciation in Himalayan headwaters was, for example, out-of-phase with the globally defined last glacial maximum, and instead occurred during MIS 4 and 3, with smaller ice volumes, reduced runoff, and reduced sediment transport during MIS 2 due to decreased monsoon intensity and moisture availability. By contrast, on the delta plain, at the other end of the terrestrial system, sediment supply and discharge maxima occurred during the early Holocene, as driven by climate change and precession-forced peak monsoon intensity. Sediment supply during this time was of sufficient magnitude to aggrade the delta plain and maintain the shoreline at roughly the same position even though rates of subsidence are fairly high, and this was a time period of rapid post-glacial sea-level rise (Goodbred and Kuehl, 2000). Most importantly, Goodbred (2003) notes that climate signals were propagated through this large system very rapidly, significantly more rapidly than that envisioned by the response times of Castelltort and Van Den Driessche (2003), such that response to climate change at the multi-millennial scale was essentially system-wide.

30.4.3 The Lower Mississippi River, South-central USA

The lower Mississippi River has long served as an icon in the fluvial geomorphology and sedimentology communities. The modern Mississippi is the fourth largest system

in the world when measured in terms of drainage area, and seventh largest when measured in terms of discharge or sediment load (Hovius, 1998). In its present interglacial state, the Mississippi drains an area of some 3.4×10^6 km^2 within the conterminous United States, between the Rocky and Appalachian mountain chains, and is a classic example of a complex polyzonal system that discharges to a passive continental margin. The Ohio River, which drains much of the humid eastern US, provides most of the water for the lower Mississippi, whereas the Missouri system, which drains the semi-arid central and northern Rocky Mountains, provides most of the sediment (see Chapter 9). In fact, the combined water and sediment discharge from the Upper Mississippi, Missouri, and Ohio Rivers represent more than 80% of total values, and the Lower Mississippi serves as a 1000 km long conveyor belt that transfers water and sediment to the Gulf of Mexico. However, during glacial periods, the drainage area was greatly enlarged to include much of southern Canada, and the lower Mississippi was also the conduit for meltwater and sediment routed from the southern margins of the ice sheet to the Gulf of Mexico (Figure 30.13). During the last glacial maximum, the Mississippi drainage would have been considerably larger, and inferred meltwater-dominated discharges for the period of deglaciation are comparable with those of the modern Amazon (Licciardi *et al*., 1999).

The extensive late Pleistocene and Holocene landforms and deposits of the lower Mississippi valley (LMV) therefore provide an example of the response of a large, long-lived, low-gradient fluvial system to changes between

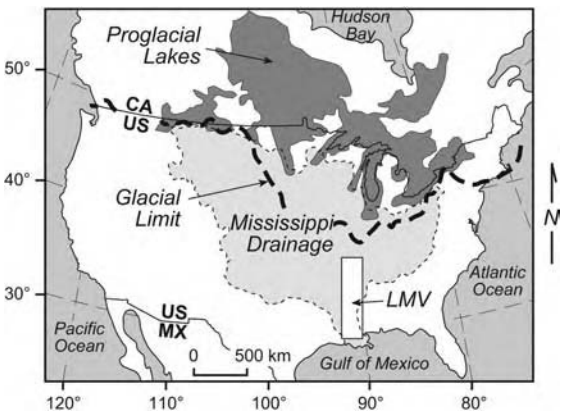

Figure 30.13 Drainage basin for the Mississippi River. Also shown is the Pleistocene glacial limit, the general extent of late Pleistocene proglacial lakes that discharged through the Mississippi into the Gulf of Mexico during deglaciation, and the location of the lower Mississippi valley shown in Figure 30.14a. (modified from Blum *et al*., 2000)

end-member states of continental-scale proglacial vs non-glacial discharge regimes and sediment supply. As noted above, an initial model for evolution of the LMV was developed in the landmark work of Fisk (1944), who recognized multiple braided stream surfaces, as well as multiple younger meander belts, and coupled valley evolution to glacio-eustasy and forced changes in gradient. Chronological and genetic aspects of Fisk's (1944) model were considerably revised by Saucier (1994), who assigned braided stream surfaces to the MIS 4-2 glacial period, and inferred that the transition to a meandering regime occurred in the earliest Holocene. Blum *et al*. (2000) then used stratigraphic relations between chronologically controlled loess units and subjacent fluvial deposits to further revise LMV history. They focused on the northern LMV, where deposits and landforms reside in two distinct bedrock-confined valleys, the Western and Eastern Lowlands (Saucier, 1994): they recognized the Eastern Lowlands contained three large-scale braided stream surfaces and underlying channel belts from the last glacial maximum and early deglacial period, which were constructed then incised in response to millennial-scale fluctuations in the delivery of meltwaters and outwash from the former ice margin and the drainage of large proglacial lakes. However, precise links between specific channel belts and specific meltwater events were not possible due to dating limitations.

Most recently, Rittenour *et al*. (2005) applied optical luminescence dating techniques to lower Mississippi valley deposits, which provides the first chronological framework from which the role of external forcing can be evaluated, and provided for some refinement of map units identified in Saucier (1994; Figure 30.14a). Key aspects of the northern LMV history can be summarized as follows:

1. During MIS 5, until ca. 85 ka, the Mississippi maintained a meandering channel planform. Shortly thereafter, the Mississippi channel was transformed into a braided pattern, and flowed mostly within the Western Lowlands through MIS 4, 3, and 2. Presumably, the ancestral Ohio River occupied the Eastern Lowlands, but records from this time period are not widely preserved.
2. Three major periods of Mississippi braid channel-belt construction and incision occurred within the Western Lowlands from ca. 65–25 ka. The Mississippi permanently abandoned the Western Lowlands, in favour of a course through the Eastern Lowlands Bell City-Oran Gap ca. 25–20 ka.
3. At least three large-scale channel belts with braided surface morphologies were constructed, incised and

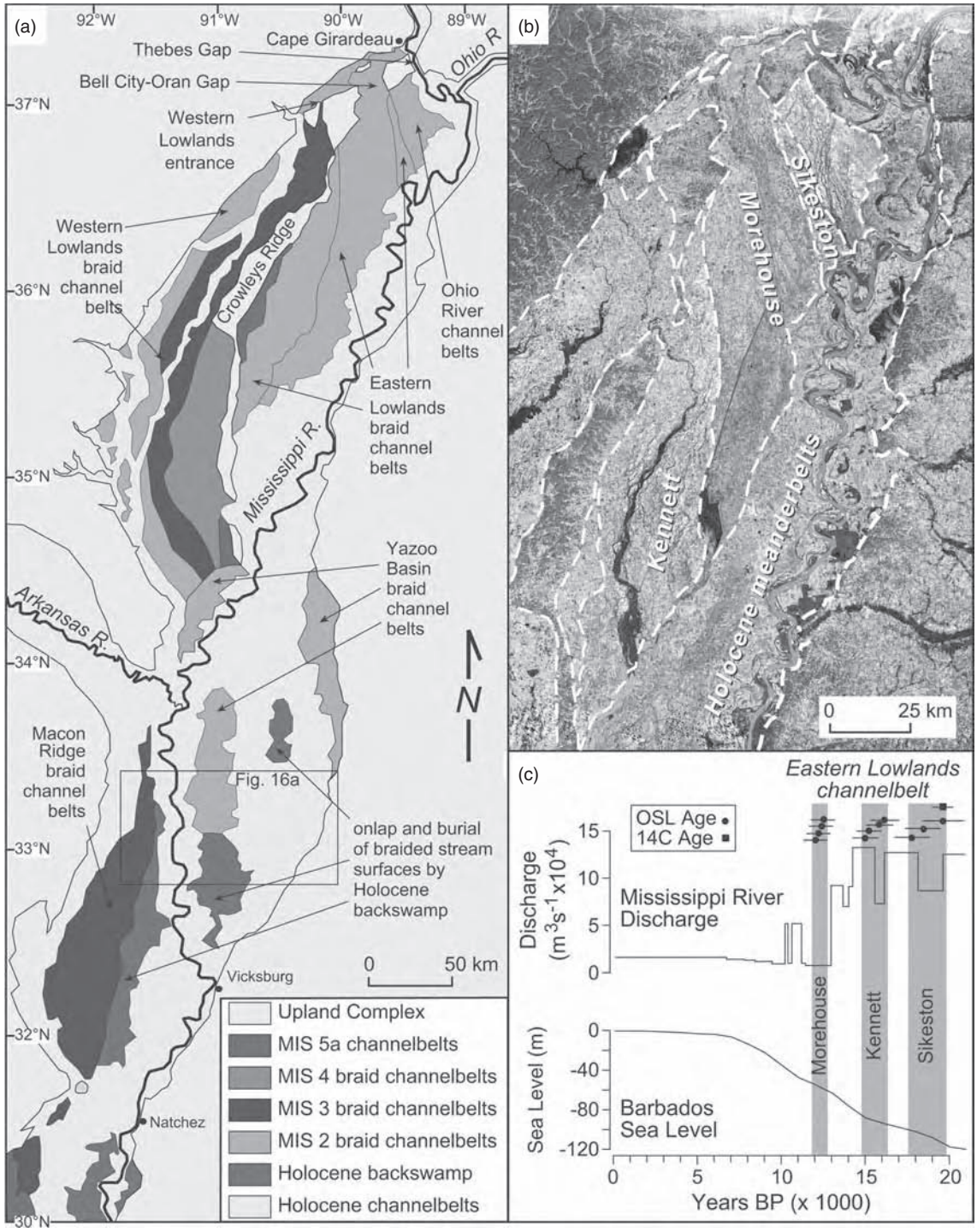

Figure 30.14 (See also colour plates.) The northern lower Mississippi valley and meltwater discharge. (a) Quaternary fluvial deposits and landforms of the lower Mississippi valley. Holocene channel belts are undifferentiated. Updated from Saucier (1994) to include results of optical luminescence dating by Rittenour *et al*. (2005). Area shown as Upland Complex includes both pre-Plio-Pleistocene bedrock, as well as Plio-Pleistocene fluvial gravels, sands, and loess. Late Pleistocene channel belts are also commonly veneered by loess. Deposits of the Arkansas valley are undifferentiated, and include areas of late Pleistocene channel belts as well (Saucier, 1994). (b) Landsat TM image of the northern lower Mississippi valley, illustrating distribution of braided stream surfaces from the last glacial maximum and subsequent period of deglaciation. (c) Correlations between time periods of braided channel-belt construction (orange), meltwater discharge through the lower Mississippi valley, and glacio-eustatic sea-level rise (modified from Rittenour, 2004). Mississippi River discharge estimates from Licciardi *et al*. (1999). Barbados sea-level record from Bard *et al*. (1990)

abandoned within the Eastern Lowlands Bell City-Oran Gap course during the period ca. 20–12 ka. The youngest of these is fully preserved and some 40 km wide, and formed during the period 12.5–12 ka (Figure 30.14b). Rittenour *et al*.'s (2005) OSL ages confirm previous inferences regarding millennial-scale adjustments to meltwater fluctuations, but also provide sufficient resolution to correlate periods of channel-belt formation with reduced meltwater routing through the Mississippi drainage, and periods of incision to meltwater peaks (Figure 30.14c).

4. The Mississippi occupied its present course through Thebes Gap by ca. 11.5 ka, and has joined the Ohio River just downstream from that point since that time. Shortly thereafter, the channel resumed a meandering planform, presumably in association with the loss of meltwaters and glacial sediment loads.

Detailed history of the southern LMV during the last glacial period remains less well known. Saucier (1994) recognized the Mississippi had not incised as far upstream as Fisk (1944) envisioned, but noted that braided stream surfaces are buried by Holocene backswamp in the lower half of the valley. Blum *et al*. (2000) recognized that major full- and late-glacial channel-belt construction and incision events in the northern LMV were contemporaneous with rapid glacio-eustatic sea-level rise, but the downstream extent of these events was not known. Rittenour *et al*. (2005) show that braided stream surfaces from MIS 3 are present at elevations above the modern floodplain at distances of only 200 km upstream from the present highstand shoreline (see Figure 30.14a), which indicates that incision did not propagate very far upstream during MIS 4 and 3, in spite of perhaps 80 m of total sea-level fall during that time. Blum and Lancaster (unpublished data) re-examined subsurface data from the southern LMV, and correlate buried surfaces in the lower alluvial valley with terraces farther upstream. Holocene backswamp facies onlap late Pleistocene braided stream surfaces some 5–600 km upstream from the highstand shoreline, defining the upstream limits of sea-level controls on valley aggradation. However, cross-sections and long profiles of the lower alluvial valley (Figure 30.15) illustrate three buried surfaces that are interpreted to correlate with the three full- and late-glacial periods of channel-belt formation and incision farther upstream. If correct, these data would indicate that meltwater-controlled millennial-scale periods of channel-belt formation and incision were transmitted far downstream over valley lengths of >800 km, in spite of rapid sea-level rise.

Little is known about lower Mississippi River response to climate change during the Holocene. Mapping by Saucier (1994) identified five distinct channel belts with meandering planforms in the Yazoo Basin that span the Holocene (Figure 30.16a), but the relative significance of climate change vs a series of wholly autogenic meander belt avulsions remains unclear. Farther downstream, the early Holocene record is deeply buried due to sea-level rise and forced valley aggradation, and only two to three distinct meander belts have been identified. Aslan and Autin (1999) suggest that early to middle Holocene channel belts in the Yazoo Basin gave way downstream to a rapidly aggrading, anastomosing channel and floodplain system with numerous poorly drained backswamps and lakes as the Mississippi responded to early to middle Holocene sea-level rise (Figure 30.16b). By contrast, the dominant late Holocene theme is one of linked channel belt and subdelta construction, avulsion and channel-belt relocation, and construction of a new subdelta lobe (Saucier, 1994; Törnqvist *et al*., 1996; Aslan *et al*., 2005). Knox (1996) argued that climate changes in the upper Mississippi valley and upper midwest of the US should be recorded in the lower alluvial valley and delta plain. However, links between channel-belt formation and avulsion, construction and abandonment, climate change, and the overall trend of valley filling in response to sea-level rise remain speculative, and should represent fertile topics for future research.

30.5 EPILOGUE: LARGE RIVERS AND CLIMATE CHANGE, PAST TO FUTURE

The discussion above focused on retrodicting responses of fluvial systems to climate and sea-level change, which requires detailed examination and documentation of the stratigraphic record, robust geochronological methods, and independently defined records of changes in forcing mechanisms. Even in the best of circumstances, there are perhaps no 'smoking guns' for any particular interpretive model, and interpretations may depend on predilection of the investigator for autogenic (everything is 'complex response') vs allogenic (everything is climate or sea-level change) controls (Blum and Törnqvist, 2000). Moreover, the standards for correlation of changes in alluvial successions to external forcing mechanisms tend to increase with decreasing age of the landforms or deposits in question: considerable debate can ensue regarding discrepancies of 10^1–10^2 years as the age of deposits approach the historical period, and correlations become event-based rather than regime-based. In the future, new geochronological and subsurface data collection methods, coupled with rapidly evolving modelling approaches, will serve to more precisely define relationships between surface processes and landscapes, the stratigraphic record of changes in fluvial systems

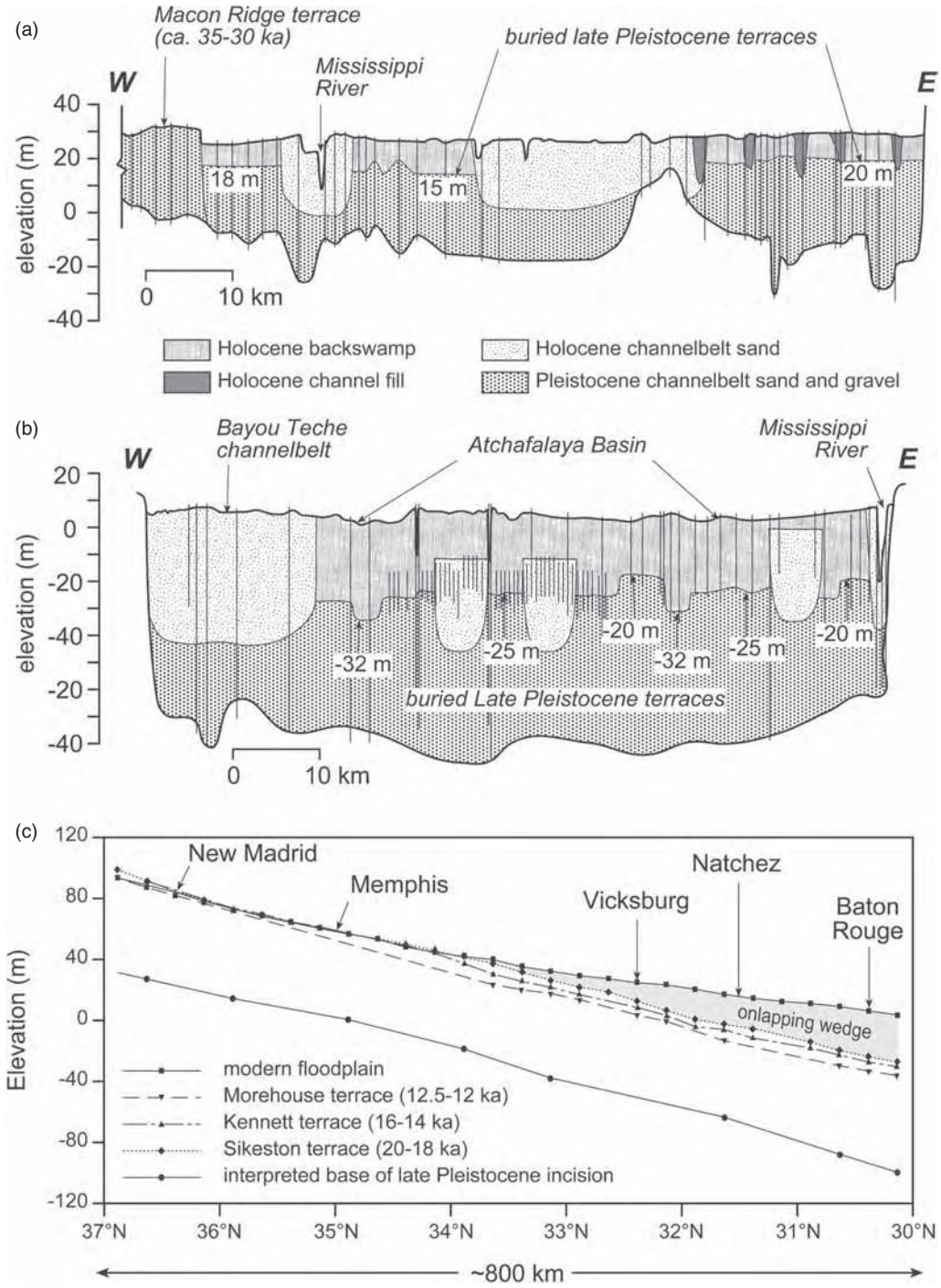

Figure 30.15 The southern lower Mississippi valley and interactions between meltwater discharge and sea-level change. (a) Valley cross-section in the central Yazoo Basin (~33° N latitude; see location in Figure 30.14a), illustrating basal gravels and sands of presumed late Pleistocene age, overlain by Holocene channel-belt sands and backswamp muds. (b) Valley cross-section in southernmost alluvial valley, between Baton Rouge and Lafayette, Louisiana (~30° N latitude), illustrating basal gravels and sands of presumed late Pleistocene age, overlain by Holocene channel-belt sands and backswamp muds. In each cross-section, thick backswamp muds occur in locations where Holocene channels have not migrated through, and are interpreted to have passively buried braided stream surfaces. (c) Long profiles of the Sikeston, Kennett, and Morehouse braided stream surfaces in the northern alluvial valley (see Figure 30.14b and c), with correlations to buried surfaces identified farther downstream These correlations indicate valley incision due to deglacial meltwater flooding propagated to the southernmost part of the alluvial valley, in spite of contemporaneous sea-level rise. Also shown is the onlapping wedge of Holocene sediments deposited during more recent sea-level rise and forced valley filling. Cross-sections and long profiles from M. Blum and R. Lancaster, unpublished, and based on compilation of US Army Corps of Engineers borehole data. Locations and depths of boreholes used in (a) and (b) shown with vertical bars

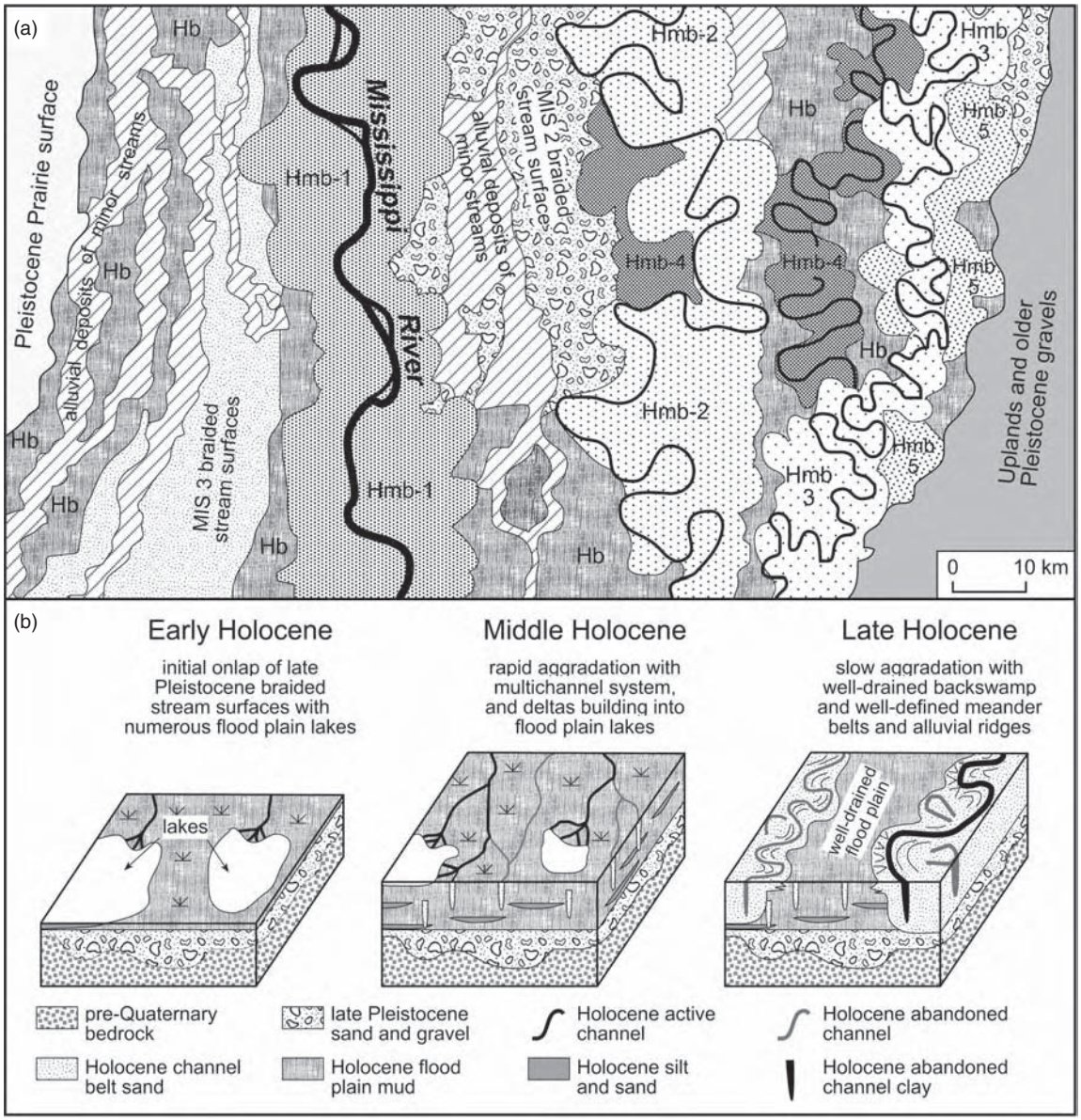

Figure 30.16 The lower Mississippi valley during the Holocene. (a) Surficial geologic map of the central Yazoo Basin, illustrating distribution of late Pleistocene braided stream surfaces, as well as the five distinct meander belts that have been identified, and the distribution of Holocene backswamp muds that onlap buried late Pleistocene braided stream surfaces. Location shown in Figure 30.14a. Hmb indicates Holocene meandering channel belt of Mississippi River: Hmb-1, the modern channel belt; Hmb-5, the oldest Holocene channel belt identified (adapted from Saucier, 1994). (b) Schematic block diagrams summarizing Holocene floodplain development in the southern lower Mississippi valley, near Natchez (see Figure 30.14a). The early Holocene floodplain was initially represented by lakes and poorly drained backswamps. Multichannel floodplain streams, crevasse splays, and lacustrine deltas filled the lakes and poorly drained backswamps as the floodplain aggraded rapidly in response to sea-level rise. Slower rates of floodplain aggradation after ca. 5 ka led to the development of continuous meander belts with raised alluvial ridges (modified from Aslan and Autin, 1999)

through time, and records of climate and/or sea-level change, and open up possibilities for developing quantitative and process-oriented source-to-sink understanding of fluvial systems. Large river systems are critical in this regard, because they integrate the effects of surface processes over subcontinental scales, and therefore play fundamental roles in landscape evolution and the flux of materials from erosional continental interiors to ocean basins.

The review above illustrates that Late Quaternary climate and sea-level changes have had a profound impact on river systems of all scales, and large river systems are no exception. Three themes deserve special mention:

1. The landscape and stratigraphic record of this impact is spatially differentiated. At one end of a spectrum, continental interior reaches, where bedrock and mixed bedrock-alluvial valleys predominate, likely reflect interactions between rates of uplift and climate-driven unsteadiness in discharge regimes and sediment supply. At the other end of the spectrum, subsiding continental margin reaches also clearly reflect the influence of relative sea-level change.
2. The dominant rhythms in large river systems appear to vary significantly, such that global correlations may be implausible, but continental to subcontinental signals are robust. The response of the Colorado River in Grand Canyon, driven by glacial–interglacial and stadial–interstadial cycles in distal Rocky Mountain headwaters contrasts markedly with the monsoon-driven signal in the Ganga system, and the signal of continental-scale glaciation to deglacial meltwater routing to nonglacial climates in the Mississippi system.
3. Response times for large river systems are surprisingly short. In cases examined above, signal transfer and production of a discernible morphologic and/or stratigraphic response occurred an order of magnitude or more faster than predicted by calculations of characteristic response times. This likely reflects sensitivity to changes in flood magnitudes and frequency, which can be transferred rapidly through large drainage basins, relative to the timescales required to transfer changes in sediment supply.

There is no longer much scientific debate regarding the reality of climate change, nor the impact that human activities have had in the recent past, and will continue to have in the near future (IPCC, 2001). The landscape and stratigraphic record provides the only actual empirical record of fluvial responses to past climate and sea-level change, and represents a set of already completed experiments. However, climate changes of the future, both natural and anthropogenically enhanced, represent Earth system experiments that are waiting to happen. Prediction of responses is an entirely different issue, one that has heretofore been almost entirely dependent on numerical models, and one that is therefore fraught with uncertainty on a number of completely different levels. Nevertheless, two fundamental issues ensure that large river systems must figure importantly in this regard. First, the hydrological cycle, of which large river systems are a major component, will play a key role in transferring the effects of future climate change to the land surface (IPCC, 2001). Second, the sensitivity of river systems to climate changes over a range of spatial and temporal scales ensures these changes will not go unnoticed: especially pertinent in this context is the observation that relatively modest changes in climate result in amplified changes in discharge regimes, especially flood magnitude and frequency (Knox, 1993).

Accordingly, model predictions of the effects of future climate change on river systems have devoted considerable attention to changes in water supplies and total runoff, as well as flood magnitude, frequency and seasonality (Arora, 2001; Arora and Boer, 2001; Nijssen *et al*., 2001; Wetherald and Manabe, 2002; Manabe *et al*., 2004). There is strong consensus that future climate changes will have significant impacts on precipitation patterns, especially decreases in the percentage of precipitation that falls as snow in high elevations, as well as the midlatitudes and farther poleward (IPCC, 2001). For example, one of the more robust general predictions is a direct manifestation of warmer temperatures in regions now dominated by snowmelt runoff during late spring and summer (Barnett *et al*., 2005): even without changes in precipitation amounts, intensity, and seasonality, warmer temperatures will lead to less precipitation stored on the landscape as snow, and migration of the seasonality of floods from late spring and early summer to late winter and early spring. There is also some consensus that many non snowmelt-dominated tropical to midlatitude regions will experience increases in the magnitude and frequency of extreme events, floods and droughts (IPCC, 2001). There is less consensus on other issues. Specific predicted effects vary regionally, and always track predicted changes in precipitation: however, predicted precipitation changes are themselves strongly dependent on the time period investigated, the climate change scenarios, and parameterizations of various physical processes in the models.

Arora and Boer (2001; see also Arora, 2001) and Wetherwald and Manabe (2002; see also Manabe *et al*., 2004), for example, tailored modelling approaches to estimation of future hydrological changes in major river systems, and illustrate the potentially conflicting results

that may reflect different model scenarios. Arora and Boer (2001) used a coupled atmosphere–ocean general circulation model with flow routing through major drainage basins, plus a quadrupling of atmospheric CO_2 relative to AD 1850, and simulated changes in mean annual discharge, mean annual flood, the magnitudes of 2, 5, 10, 25, and 50 year floods, and flow duration curves for the period AD 2071–2100 (Figure 30.17). Wetherwald and Manabe (2002) used a coupled atmosphere–ocean–land surface model structure, but with more conservative forcing by atmospheric CO_2, and focused on predicting changes in mean runoff and soil moisture for the 30 year period centred on AD 2050. The most comparable predictions between the two studies would be mean annual discharge from Arora and Boer (2001) and mean annual runoff from Wetherwald and Manabe (2002): there are a few cases where results agree closely, but in most cases predicted changes differ in magnitude by factors of 5–10, and roughly 50% of the cases examined differ in terms of the predicted direction of change. However, as noted in Arora (2001), model exercises may predict modern or control values of precipitation or various measures of discharge or runoff to within 20% of actual values less than 50% of the time, so lack of a more precise agreement between different model runs is no surprise.

Clearly, more work needs to be done in predicting the hydrological consequences of future climate change. However, as noted by IPCC (2001), the effects of future climate changes will be most profound on river systems that are in a relatively unmodified state, and highly modified systems will be somewhat buffered from future climate change, natural or anthropogenic. Nilsson *et al*. (2005) show the majority of the world's large river systems are significantly impacted by dam construction: globally, there are some 45 000 dams higher than 15 m, which are capable of retaining some 15% of global runoff. The pervasive impact of dam construction on the hydrology of large river systems is indeed staggering, and it seems clear that flow regime changes that have resulted from dam construction vastly exceed that expected from future climate change (Graf, 2005). Sediment retention in reservoirs is an equally important consequence of dam construction, and the impact on sediment supply has been equally profound. Syvitski *et al*. (2005) note that human activities, especially forest clearance and agricultural activities, have greatly increased rates of erosion of the landscape, but rates of sediment delivery to the coastal oceans have decreased due to sediment retention in reservoirs by as much as 10% on a global scale, with significantly higher values for selected regions. Large changes

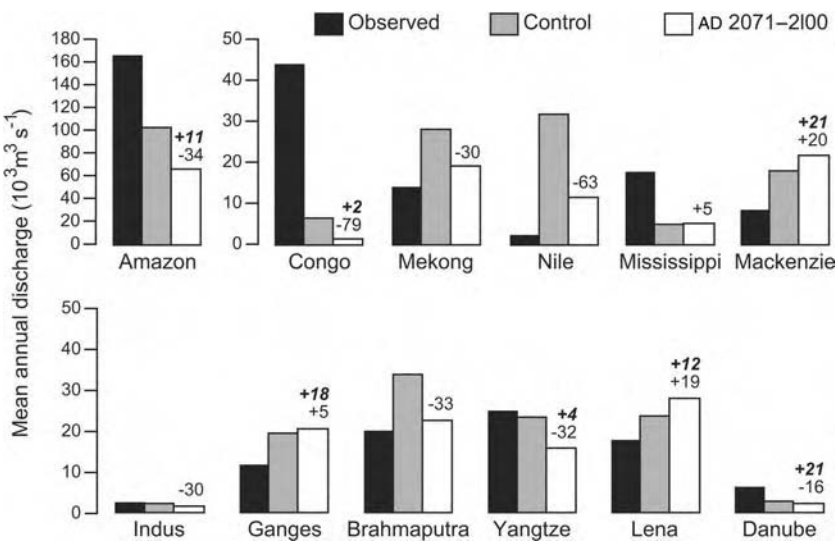

Figure 30.17 Model predictions of changes in discharge due to future climate change. Bar graphs illustrate predictions from Arora and Boer (2001) for a number of rivers discussed in this volume. Numbers above predicted changes in mean annual discharge indicate the percent change for Arora and Boer (2001), with percent change in mean rates of simulated runoff for the period 2035–2065 from Wetherwald and Manabe (2002) in bold italics, where available. Note that in some cases, observed values agree well with simulated control values, whereas in other cases, agreement is not good. Note the mixed results when comparing the two sets of model predictions

in flow regimes and sediment loads due to human activities clearly mean that coupling between highly modified large river systems and climate change will be significantly different in the future.

Many examples could be cited and discussed in this context, but the Colorado and Mississippi systems in the USA, discussed above and elsewhere in this volume, provide examples of how much of the near future will be tied to management of depleted sediment supplies in the face of climatic and other uncertainty. For the Colorado River in Grand Canyon (see Chapter 10), the sand bar components of the linked tributary fan–eddy–sand bar complexes (see Figure 30.8b) provide a critical resource for recreationalists, as well as critical habitats for a diversity of species. However, construction of Glen Canyon Dam and Lake Powell, just upstream, reduced sediment supply to the Grand Canyon reach by ~90%, and reduced peak flows considerably, while at the same time maintaining low flows above the threshold for sand transport. As a result, there has been significant depletion of sands previously stored in the channel, as well as a significant reduction in subaerial sand bar area and volume (Hazel *et al*., 2006: Figure 30.18). Accordingly, considerable effort has been directed towards constructing detailed sediment budgets, monitoring sediment inputs from tributaries, and development of experimental flow scenarios to utilize sediment inputs from tributaries for bar-building purposes (Rubin *et al*., 2002). To the extent that future climate changes are predicted to reduce total water supplies in the Colorado system (Christensen *et al*., 2004), this may become an increasingly complicated task with fewer degrees of freedom.

For the Mississippi River, the tragic strikes of Hurricanes Katrina and Rita in 2005 highlight the fragility of a naturally subsiding alluvial-deltaic plain that has been highly modified by human activities, and which is feeling the effects of rising sea levels. At present, the Mississippi system has ~39 000 dams of some type (Graf, 1999), and sediment supply to the lower river and delta plain has decreased by ~80% since 1850 as a result of dams and other river control structures (Kesel *et al*., 1992). To compound the issue, the lower Mississippi channel is flanked by a continuous levee system that prohibits dispersal of sediments into the floodplain and delta plain, and instead discharges sediments directly to the shelf margin and beyond. Coastal retreat in light of slowly rising sea level and reduced sediment delivery is a truly global problem (Syvitski *et al*., 2005), and for the Mississippi delta region,

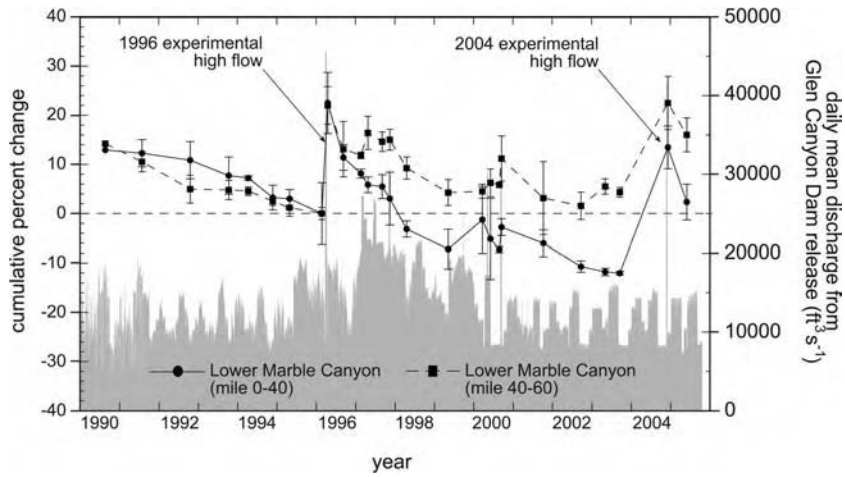

Figure 30.18 Graph illustrating changes in subaerial sand bar area within Marble Canyon, Grand Canyon National Park, Arizona (USA), from 1990 to 2005. Graph illustrates steady reduction in bar area for two reaches, measured with respect to distance downstream from Lees Ferry, located a few kilometers downstream from Glen Canyon Dam. Major depositional events occurred on bars in both reaches during experimental flows of 1996 and 2004, which were designed for this purpose. The 1996 experimental flows took place without a clear understanding of the mass balance of sand-sized sediment in the channel, whereas the 2004 flow followed a period of monitoring that demonstrated significant tributary input and stockpiling of sand in the mainstem. Post-flood erosion of bars is most significant in miles 0–40, but in each case the new sand deposited on bars appears to have a limited time span before it too is eroded and transported downstream (courtesy of J. Hazel Jr, Northern Arizona University). For a complete discussion of this set of issues, see Hazel *et al*. (2006) and references therein

the rates of coastal land loss are staggering (Figure 30.19): one-third of deltaic wetlands have disappeared in the last 100 years, at rates of ~100 km^2 $year^{-1}$, and there is a projected loss of an additional 1280 km^2 by the year 2050 (Barras *et al*., 2003). Efforts to reverse land loss trends, preserve ecologically critical wetlands, and restore the delta to serve as a buffer from storm surges of the future, will revolve around development of plans to manage the dispersal of available sediments to the delta plain. Model predictions of the hydrological consequences of future climate change are indeterminate for the Mississippi system, since they do not closely reproduce modern discharge regimes nor predict large changes in response to global warming (Arora, 2001; Arora and Boer, 2001). However, future climate controls on discharge regimes may not be significant when compared with the rates at which progress is made on managing sediments, and restoring the delta to serve as a buffer from future storm surges. Coupling between the lower Mississippi River and delta and future climate change therefore revolves around managing sediments so as to mitigate against the impact of future hurricane strikes that are predicted to be more intense in a warmer world.

In closing, linking past fluvial response to climate change with the future is a challenge, because of different timescales, empirical vs modelling approaches, human impact, and other factors. It has long been recognized that key periods of recent Earth history may represent useful analogs for climate conditions of the future, and the recent geologic past can serve as a key to the future. Documentation of past fluvial system responses to climate and sea-level change provides for delineation of the boundary

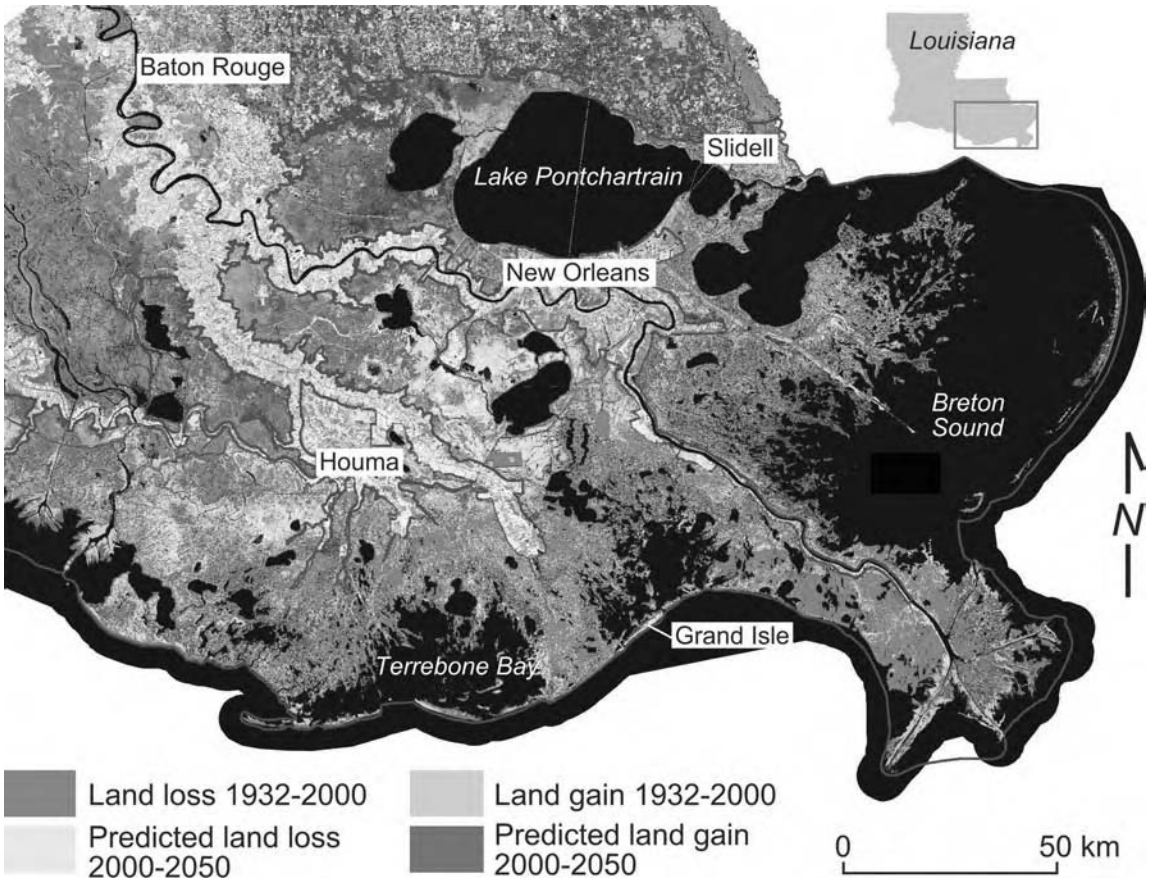

Figure 30.19 (See also colour plates.) Land surface gains and losses in lower Mississippi delta region, 1932–2000 and predicted for period 2000–2050. Blue line indicates limits of land change study area. Adapted from United States Geological Survey (2003) Map NWRC 2003-02-0373. See also Barras *et al*. (2003)

conditions, or context, within which modern systems operate, and the longer-term benchmark modes of behavior against which modern and future patterns and rates of change can be judged. Large river systems that are relatively unmodified by human activities will likely respond to climate changes of the near future as they have in the recent past, the late Holocene, for example, through minor changes in channel morphology and rates of lateral channel migration, minor aggradation or incision through alluvial deposits themselves, and/or increases or decreases in rates of floodplain sedimentation. However, for many large river systems, future climate change will be played out on a stage where the primary variables of discharge and sediment supply are fundamentally altered by human activities to a much greater degree than would be possible due to climate change alone. In such systems, coupling between river systems and climate change will be defined somewhat differently: key issues of interest will be the management of water supplies, so as to serve society's needs and retain or restore ecosystem function, and management of limited sediment volumes so as to maintain or restore key landscape and ecological elements that were once built naturally. Exciting challenges await at different ends of the temporal spectrum for those interested in large rivers and climate change.

REFERENCES

Aalto, R., Maurice-Bourgoin, L., Dunne, T., Montgomery, D.R., Nittrouer, C.A. and Guyot, J.-L. (2003) Episodic sediment accumulation on Amazonian floodplains influenced by El Niño/Southern Oscillation. *Nature*, 425: 493–497.

Allen, G.P. and Posamentier, H.W. (1993) Sequence stratigraphy and facies model of an incised valley fill: the Gironde Estuary, France. *Journal of Sedimentary Petrology*, 63: 378–391.

Anders, M.D., Pederson, J.L., Rittenour, T.M., Sharp, W.D., Gosse, J.C., Karlstrom, K.E., Crossey, L.J., Goble, R.J., Stockli, L. and Yang, G. (2005) Pleistocene geomorphology and geochronology of eastern Grand Canyon: linkages of landscape components during climate changes. *Quaternary Science Reviews*, 24: 2428–2448.

Anderson, J.B., Rodriguez, A.B., Abdullah, K., Fillon, R.H., Banfield, L., McKeown, H. and Wellner, J.S. (2004) Late Quaternary stratigraphic evolution of the northern Gulf of Mexico margin: a synthesis. In: *Late Quaternary Stratigraphic Evolution of the Northern Gulf of Mexico Margin* (J.B. Anderson and R.H. Fillon, Eds.). SEPM Special Publication, 64: 1–23.

Antoine, P. (1994) The Somme valley terrace system (northern France); a model of river response to Quaternary climatic variations since 800 000 BP. *Terra Nova*, 6: 453–464.

Archer, A.W. (1995) Review of Amazonian depositional systems. In: *Fluvial Sedimentology VII* (M.D. Blum, S.B. Marriott and S.F. Leclair, Eds.). International Association of Sedimentologists Special Publication, 35: 17–40.

Arora, V.K. (2001) Streamflow simulations for continental-scale river basins in a global atmospheric general circulation model. *Advances in Water Resources*, 24: 775–791.

Arora, V.K. and Boer, G.J. (2001) Effects of simulated climate change on the hydrology of major river basins. *Journal of Geophysical Research*, 106: 3335–3348.

Aslan, A. and Autin, W.J. (1999) Evolution of the Holocene Mississippi River floodplain, Ferriday, Louisiana: insights on the origin of fine-grained floodplains. *Journal of Sedimentary Research*, 69: 800–815.

Aslan, A. Autin, W.J. and Blum, M.D. (2005) Causes of river avulsion: insights from the late Holocene history of the Mississippi River, USA. *Journal of Sedimentary Research*, 75: 650–664.

Baker, V.R., Webb, R.H. and House, K. (2002) The scientific and societal value of palaeoflood hydrology. In: *Ancient Floods, Modern Hazards: Principles and Applications of Palaeoflood Hydrology* (P.K. House, R.H. Webb, V.R. Baker and D.R. Levish, Eds.). American Geophysical Union Press, Washington, DC: 1–19.

Bard, E., Hamelin, B., Fairbanks, R.G. and Zindler, A. (1990) Calibration of the ^{14}C timescale over the past 30 000 yrs using mass spectrometric U-Th ages from Barbados corals. *Nature*, 345: 405–410.

Barnett, T.P., Adam, J.C. and Lettenmaier, D.P. (2005) Potential impacts of a warming climate on water availability in snow-dominated regions. *Nature*, 438: 303–309.

Barras, J., Beville, S., Britsch, D., Hartley, S., Hawes, S., Johnston, J., Kemp, P., Kinler, Q., Martucci, A., Porthouse, J., Reed, D., Roy, K., Sapkota, S. and Suhayda, J. (2003) Historical and projected coastal Louisiana land changes, 1978–2050. United States Geological Survey, OFR 03-334: 39 p.

Blum, M.D. and Aslan, A. (2006) Signatures of climate vs. sea-level change within incised valley fill successions: Quaternary examples from the Texas Gulf Coast. *Sedimentary Geology*, 190: 177–211.

Blum, M.D. and Price, D.M. (1998) Quaternary alluvial plain construction in response to interacting glacioeustatic and climatic controls, Texas Gulf Coastal Plain. In: *Relative Role of Eustasy, Climate, and Tectonism in Continental Rocks* (K.W. Shanley and P.W. McCabe, Eds.). SEPM Special Publication, 59: 31–48.

Blum, M.D. and Straffin, E.C. (2001) Fluvial response to external forcing: examples from the Massif Central of France, the Texas Coastal Plain (USA), the Sahara of Tunisia, and the Lower Mississippi Valley (USA). In: *River Basin Sediment Systems: Archives of Environmental Change* (D. Maddy and M.A. Macklin, Eds.). Balkema Press, Lisse: 195–228.

Blum, M.D. and Törnqvist, T.E. (2000) Fluvial response to climate and sea-level change: a review and look forward. *Sedimentology*, 47(Suppl.): 1–48.

Blum, M.D., Guccione, M.J., Wysocki, D. and Robnett, P.C. (2000) Late Pleistocene evolution of the Mississippi valley, southern Missouri to Arkansas. *Geological Society of America Bulletin*, 112: 221–235.

Bridge, J.S. (2003) *Rivers and Floodplains: Forms, Processes, and the Sedimentary Record*. Blackwell Scientific Publishing, Oxford: 491 p.

Bridgland, D., Maddy, D. and Bates, M. (2004) River terrace sequences: templates for Quaternary geochronology and marine–terrestrial correlation. *Journal of Quaternary Science*, 19: 203–218.

Brook, E.J. (2005) Tiny bubbles tell all. *Science*, 310: 1285–1287.

Bull, W.B. (1991) *Geomorphic Responses to Climate Change*. Oxford University Press, Oxford.

Butzer, K.W. (1980) Holocene alluvial sequences: problems of dating and correlation. In: *Timescales in Geomorphology* (R.A. Cullingford, D.A. Davidson and J. Lewin, Eds.). John Wiley & Sons, Ltd, London: 131–142.

Castelltort, S. and Van Den Driessche, J. (2003) How plausible are high-frequency sediment supply-driven cycles in the stratigraphic record? *Sedimentary Geology*, 157: 3–13.

Chappell, J. and Shackelton, N.J. (1986) Oxygen isotopes and sea level. *Nature*, 324: 137–140.

Christensen, N.S., Wood, A.W., Voisin, N., Lettenmaier, D.P. and Palmer, R.N. (2004) The effects of climate change on the hydrology and water resources of the Colorado River Basin. *Climatic Change*, 62: 337–363.

Church, M. (2006) Bed Material transport and the morphology of alluvial river channels. *Annual Review of Earth and Planetary Science*, 34: 325–354.

Curray, J.R. and Moore, D.G. (1964) Pleistocene deltaic progradation of continental terrace, Costa De Nayarit, Mexico. In: *Marine Geology of the Gulf of California* (Van Andel, T.H. and Shor, G.G., editors.). SEPM Special Publication, M3: 193–215.

Dade, W.B. and Friend, P.F. (1998) Grain-size, sediment transport regime, and channel slope in alluvial rivers. *Journal of Geology*, 106: 661–675.

Draut, A.E., Rubin, D.M., Dierker, J.L., Fairley, H.C., Griffiths, R.E., Hazel Jr, J.E., Hunter, R.E., Kohl, K., Leap, L.M., Nials, F.L., Topping, D.J. and Yeatts, M. (2005) Sedimentology and stratigraphy of the Palisades, Lower Comanche, and Arroyo Grande areas of the Colorado River corridor, Grand Canyon, Arizona. *United States Geological Survey, Scientific Investigations Report* 2005–5072: 68 p.

Dury, G.H. (1965) Principles of underfit streams. *United States Geological Survey Professional Paper* 452-A.

Ely, L.L., Enzel, Y., Baker, V.R. and Cayan, D.R. (1993) A 5000-year record of extreme floods and climate change in the southwestern United States. *Science*, 262: 410–412.

Ethridge, F.G., Wood, L.J. and Schumm, S.A. (1998) Cyclic variables controlling fluvial sequence development: problems and perspectives. In: *Relative Role of Eustasy, Climate, and Tectonism in Continental Rocks* (K.W. Shanley and P.W. McCabe, Eds.). SEPM Special Publication, 59: 17–29.

Fenton, C.R., Webb, R.H. and Cerling, T.E. (2006) Peak discharge of a Pleistocene lava-dam outburst flood in Grand Canyon, Arizona, USA. *Quaternary Research*, 65: 324–335.

Fisk, H.N. (1944) *Geological Investigations of the Alluvial Valley of the Lower Mississippi River*. Mississippi River Commission, United States Army Corps of Engineers: 78 p.

Gibling, M.R., Tandon, S.K., Sinha, R. and Jain, M. (2005) Discontinuity-bounded alluvial sequences of the southern Gangetic plains, India: aggradation and degradation in response to monsoonal strength. *Journal of Sedimentary Research*, 75: 369–385.

Gilbert, G.K. (1877) *Report on the Geology of the Henry Mountains*. United States Geographical and Geological Survey of the Rocky Mountain Region.

Goodbred, S.L. (2003) Response of the Ganga dispersal system to climate change: a source-to-sink view since the last interstade. *Sedimentary Geology*, 162: 83–104.

Goodbred Jr, S.L. and Kuehl, S.A. (1998) Floodplain processes in the Bengal Basin and the storage of Ganga–Brahmaputra river sediment: an accretion study using ^{137}Cs and ^{210}Pb geochronology. *Sedimentary Geology*, 1998; 121: 239–258.

Goodbred, S.L. and Kuehl, S.A. (2000) The significance of large sediment supply, active tectonism, and eustasy on margin sequence development: Late Quaternary stratigraphy and evolution of the Ganga – Brahmaputra delta. *Sedimentary Geology*, 133: 227–248.

Graf, W.L. (1999) Dam nation: a geographic census of American dams and their large-scale hydrologic impacts. *Water Resources Research*, 35: 1305–1311.

Graf, W.L. (2005) Geomorphology and American dams: the scientific, social, and economic context. *Geomorphology*, 71: 3–26.

Hancock, G.S. and Anderson, R.S. (2002) Numerical modelling of fluvial strath-terrace formation in response to oscillating climate. *Geological Society of America Bulletin*, 114: 1131–1142.

Hancock, G.S., Anderson, R.S., Chadwick, O.A. and Finkel, R. C. (1999) Dating fluvial terraces with ^{10}Be and ^{26}Al profiles: application to the Wind River, Wyoming. *Geomorphology*, 27: 41–60.

Hays, J.D., Imbrie, J. and Shackleton, N.J. (1976) Variations in the Earth's orbit: pacemaker of the Ice Ages. *Science*, 194: 1121–1132.

Hazel Jr, J.E., Topping, D.J., Schmidt, J.C. and Kaplinski, M. (2006) Influence of a dam on fine-sediment storage in a canyon river. *Journal of Geophysical Research*, 111: F01025, doi: 10.1029/2004JF000193.

Hereford, R., Thompson, K.S., Burke, K.J. and Fairley, H.C. (1996) Tributary debris fans and the late Holocene alluvial chronology of the Colorado River, eastern Grand Canyon, Arizona. *Geological Society of America Bulletin*, 108: 3–19.

Howard, A.D., Dietrich, W.E. and Seidl, M.A. (1994) Modelling fluvial erosion on regional to continental scales. *Journal of Geophysical Research*, 99: 13971–13986.

Hovius, N. (1998) Controls on sediment supply by large rivers. In: *Relative Role of Eustasy, Climate, and Tectonism in Continental Rocks* (K.W. Shanley and P.W. McCabe, Eds.): SEPM Special Publication, 59: 3–16.

Imbrie, J.J., Hays, J.D., Martinson, D.G., McIntyre, A., Mix, A.C., Moreley, J.J., Pisias, N.G., Prell, W.L. and Shackleton, N.J. (1984) The orbital theory of Pleistocene climate: support from a revised chronology of the marine ∂^{18}O record. In: *Milankovitch and Climate – Part 1* (A.L. Berger, J.J. Imbrie, J. Hays, G. Kukla and B. Saltzman, Eds.). Reidel Publishing, Dordrecht: 269–306.

IPCC. (2001) *Climate Change 2001: Synthesis Report*. A Contribution of Working Groups I, II, and III to the Third Assessment

Report of the Integovernmental Panel on Climate Change (Watson, R.T. and the Core Writing Team, editors). Cambridge University Press, Cambridge and New York, NY: 398 p.

Kesel, R.H., Yodis, E.G. and McGraw D.J. (1992) An approximation of the sediment budget of the Lower Mississippi River prior to major human modification. *Earth Surface Processes and Landforms*, 17: 711–722.

Knox, J.C. (1976) Concept of the graded stream. In: *Theories of Landform Development* (W.N. Melhorn and R.C. Flemal, Eds.). State University of New York at Binghamton Publications in Geomorphology, Bunghampton, NY: 169–198.

Knox, J.C. (1983) Responses of river systems to Holocene climates. In: *Late Quaternary environments of the United States* (H.E. Wright and S.C. Porter, Eds.). Vol. 2, The Holocene. University of Minnesota Press, Minneapolis, MN: 26–41.

Knox, J.C. (1993) Large increases in flood magnitude in response to modest changes in climate. *Nature*, 361: 430–432.

Knox, J.C. (1996) Late Quaternary upper Mississippi River alluvial episodes and their significance to the lower Mississippi River system. *Engineering Geology*, 45: 263–285.

Knox, J.C. (2000) Sensitivity of modern and Holocene floods to climate change. *Quaternary Science Reviews*, 19: 439–457.

Kochel, R.C. and Baker, V.R. (1982) Palaeoflood hydrology. *Science*, 215: 353–361.

Lane, E.W. (1955) The importance of fluvial morphology in river hydraulic engineering. *Proceedings of the American Society of Civil Engineers*, 81: 1–17.

Leopold, L.B. and Bull, W.B. (1979) Base level, aggradation, and grade. *Proceedings of the American Philosophical Society*, 123: 168–202.

Leopold, L.B. and Maddock, T. (1953) The hydraulic geometry of stream channels and some physiographic implications. *United States Geological Survey, Professional Paper* 252: 57 p.

Licciardi, J.M., Teller, J.T. and Clark, P.U. (1999) Freshwater routing by the Laurentide ice sheet during the last deglaciation. In: *Mechanisms of Global Climate Change at Millennial Time Scales* (P.U. Clark, *et al*. Eds.). American Geophysical Union, Geophysical Monograph 112: 177–201.

Machette, M.N. and Rosholt, J.N. (1991) Quaternary geology of the Grand Canyon. In: *Quaternary Nonglacial Geology: Conterminous US* (R.B. Morrison, Ed.). Geological Society of America, Volume K-2, The Geology of North America: 397–401.

Mackin, J.H. (1948) Concept of the graded river. *Geological Society of America Bulletin*, 59: 463–512.

Macklin, M.G., Johnstone, E. and Lewin, J. (2005) Pervasive and long-term forcing of Holocene river instability and flooding by centennial-scale climate change. *The Holocene*, 15: 937–943.

Manabe, S., Milly, P.C.D. and Wetherald, R. (2004) Simulated long-term changes in river discharge and soil moisture due to global warming. *Hydrological Sciences-Journal des Sciences Hydrologiques*, 49(4): 625–642.

Merritts, D.J., Vincent, K.R. and Wohl, E.E. (1994) Long river profiles, tectonism, and eustasy: a guide to interpreting fluvial terraces. *Journal of Geophysical Research*, 99: 14031–14050.

Miall, A.D. (2002) Architecture and sequence stratigraphy of Pleistocene fluvial systems in the Malay Basin, based on seismic timeslice analysis. *American Association of Petroleum Geologists Bulletin*, 86: 1201–1216.

Miall, A.D. (2006) How do we identify big rivers? And how big is big? *Sedimentary Geology*, 186: 39–50.

Nijssen, B., O'Donnell, G.M., Hamlet, A.F. and Lettenmaier, D.P. (2001) Hydrologic sensitivity of global rivers to climate change. *Climate Change*, 50: 143–175.

Nilsson, C., Reidy, C.A., Dynesius, M. and Revenga, C. (2005) Fragmentation and flow regulation of the world's large river systems. *Science*, 308: 405–408.

Nittrouer, C.A., Kuehl, S.A., DeMaster, D.J. and Kowsmann, R. O. (1986) The deltaic nature of Amazon shelf sedimentation. *Geological Society of America Bulletin*, 97: 444–458.

O'Conner, J.E., Ely, L.L., Wohl, E.E., Stevens, L.E., Melis, T.S., Kale, V.S. and Baker, V.R. (1994) A 4500-year record of large floods on the Colorado River in the Grand Canyon, Arizona. *Journal of Geology*, 102: 1–9.

O'Conner, J.E., Grant, G.E. and Costa, J.E. (2002) The geology and geography of floods. In: *Ancient Floods, Modern Hazards: Principles and Applications of Palaeoflood Hydrology* (P.K. House, R.H. Webb, V.R. Baker and D.R. Levish, Eds.). American Geophysical Union Press, Washington, DC: 359–385.

Page, K., Nanson, G. and Price, D. (1996) Chronology of Murrumbidgee River palaeochannels on the Riverine Plain, southeastern Australia. *Journal of Quaternary Science*, 11: 311–326.

Pazzaglia, F.J. and Brandon, M.T. (2001) A fluvial record of long-term steady-state uplift and erosion across the Cascadia Forearc High, western Washington State. *American Journal of Science*, 301: 385–431.

Pederson, J., Karlstrom, K., Sharp, W. and McIntosh, W. (2002) Differential incision of the Grand Canyon related to Quaternary faulting – constraints from u-series and Ar/Ar dating. *Geology*, 30: 739–742.

Penck, A. and Brückner, E. (1909) *Die Alpen im Eiszeitalter*. Tauchnitz, Leipzig.

Phillips, F.M., Zreda, M.G., Gosse, J.C., Klein, J., Evenson, E.B., Hall, R.D., Chadwick, O.A. and Sharma, P. (1997) Cosmogenic ^{36}Cl and ^{10}Be ages of Quaternary glacial and fluvial deposits of the Wind River Range, Wyoming. *Geological Society of America Bulletin*, 109: 1453–1463.

Porter, S.C. (1989) Some geological implications of average Quaternary glacial conditions. *Quaternary Research*, 32: 245–262.

Porter, S.C., An, Z.S. and Zheng, H.B. (1992) Cyclic Quaternary alluviation and terracing in a non-glaciated drainage basin on the north flank of the Qinling Shan, Central China. *Quaternary Research*, 38: 157–169.

Potter, P.E. (1978) Significance and origin of big rivers. *Journal of Geology*, 86: 13–33.

Powell, J.W. (1875) *Exploration of the Colorado River of the West and its Tributaries.* United States Government Printing Office, Washington, DC: 291 p.

Rittenour, T.M., Goble, R.J. and Blum, M.D. (2005) Development of an OSL chronology for Late Pleistocene channelbelts in the lower Mississippi valley, USA. *Quaternary Science Reviews*, 24: 2539–2554.

Rubin, D.M., Topping, D.J., Schmidt, J.C., Hazel, J., Kaplinski, M. and Melis, T.S. (2002) Recent sediment studies refute Glen Canyon Dam hypothesis. *EOS Transactions* 83(25): 277–278.

Saucier, R.T. (1994) *Geomorphology and Quaternary Geologic History of the Lower Mississippi Valley*. Mississippi River Commission, Vicksburg, MS.

Schmidt, J.C. (1990) Recirculating flow and sedimentation in the Colorado River in Grand Canyon, Arizona. *Journal of Geology*, 98: 709–724.

Schumm, S.A. (1968) River Adjustment to Altered Hydrologic Regimen: the Murrumbidgee River and Palaeochannels, Australia. *United States Geological Survey Professional Paper* 598.

Schumm, S.A. (1991) *To Interpret the Earth: Ten Ways to be Wrong.* Cambridge University Press, Cambridge.

Schumm, S.A. and Winkley, B.R., editors. (1994) The character of large alluvial rivers. In: *The Variability of Large Alluvial Rivers*. American Society of Civil Engineers, New York, NY: 1–9.

Shukla, U.K., Singh, I.B., Sharma, M. and Sharma, S. (2001) A model of alluvial megafan sedimentation: Ganga Megafan. *Sedimentary Geology*, 144: 243–262.

Singh, I.B. (2004) Late Quaternary history of the Ganga Plain. *Journal of Geological Society India*, 64(4): 431–454.

Sinha, R., Jain, V., Prasad Babu, G. and Ghosh, S. (2005) Geomorphic characterization and diversity of the rivers of the Gangetic plains: morphology, processes and controls. *Geomorphology*, 70: 207–225.

Starkel, L. (1991) Long-distance correlation of fluvial events in the temperate zone. In: *Temperate Palaeohydrology* (L. Starkel, K.J. Gregory and J.B. Thornes, Eds.). John Wiley & Sons, Ltd, Chichester: 473–495.

Suter, J.R. and Berryhill, H.L. (1985) Late Quaternary shelf-margin deltas, northwest Gulf of Mexico. *American Association of Petroleum Geologists Bulletin*, 69: 77–91.

Syvitski, J.P.M., Vörösmarty, C.J., Kettner, A.J. and Green, P. (2005) Impact of humans on the flux of terrestrial sediment to the global coastal ocean. *Science*, 308: 376–380.

Topping, D.J., Schmidt, J.C. and Vierra Jr, L.E. (2003) Discharge of the Colorado River at Lees Ferry, Arizona, during the 1884 flood and between May 8, 1921, and September 30, 2000: construction and analysis of a continuous record of instantaneous discharge. *US Geological Survey Professional Paper* 1677.

Törnqvist, T.E., Kidder, T.R., Autin, W.J., Van der Borg, K., De Jong, A.F.M., Klerks, C.J.W., Snijders, E.M.A., Storms, J.E.A., Van Dam, R.L. and Wiemann, M.C. (1996) A revised chronology for Mississippi River subdeltas. *Science*, 273: 1693–1696.

United States Geological Survey. (2003) 100+ years of land change for southeast coastal Louisiana. Map NWRC 2003-02-0373.

Wellner, R.W. and Bartek, L.R. (2003) The effect of sea level, climate, and shelf physiography on the development of incised-valley complexes: a modern example from the East China Sea. *Journal of Sedimentary Research*, 73(6): 926–940.

Westaway, R., Bridgland, D. and White, M. (2006) The Quaternary uplift history of central southern England: evidence from the terraces of the Solent River system and nearby raised beaches. *Quaternary Science Reviews*, 25(17–18): 2212–2250.

Wetherald, R.T. and Manabe, S. (2002) Simulation of hydrologic changes associated with global warming. *Journal of Geophysical Research*, 107(D19): 4379.

Whipple, K.X. (2001) Fluvial landscape response time: how plausible is steady-state denudation. *American Journal of Science*, 301: 313–325.

Zaitlin, B.A., Dalrymple, R.W., and Boyd, R. (1994) The stratigraphic organization of incised-valley systems associated with relative sea-level change. In: *Incised-Valley Systems: Origins and Sedimentary Sequences* (R.W. Dalrymple, R. Boyd and B.A. Zaitlin, Eds.). SEPM Special Publication, 51: 45–60.

Index

italic used for figures, **bold** for tables

Large Rivers: Geomorphology and Management, Edited by A. Gupta

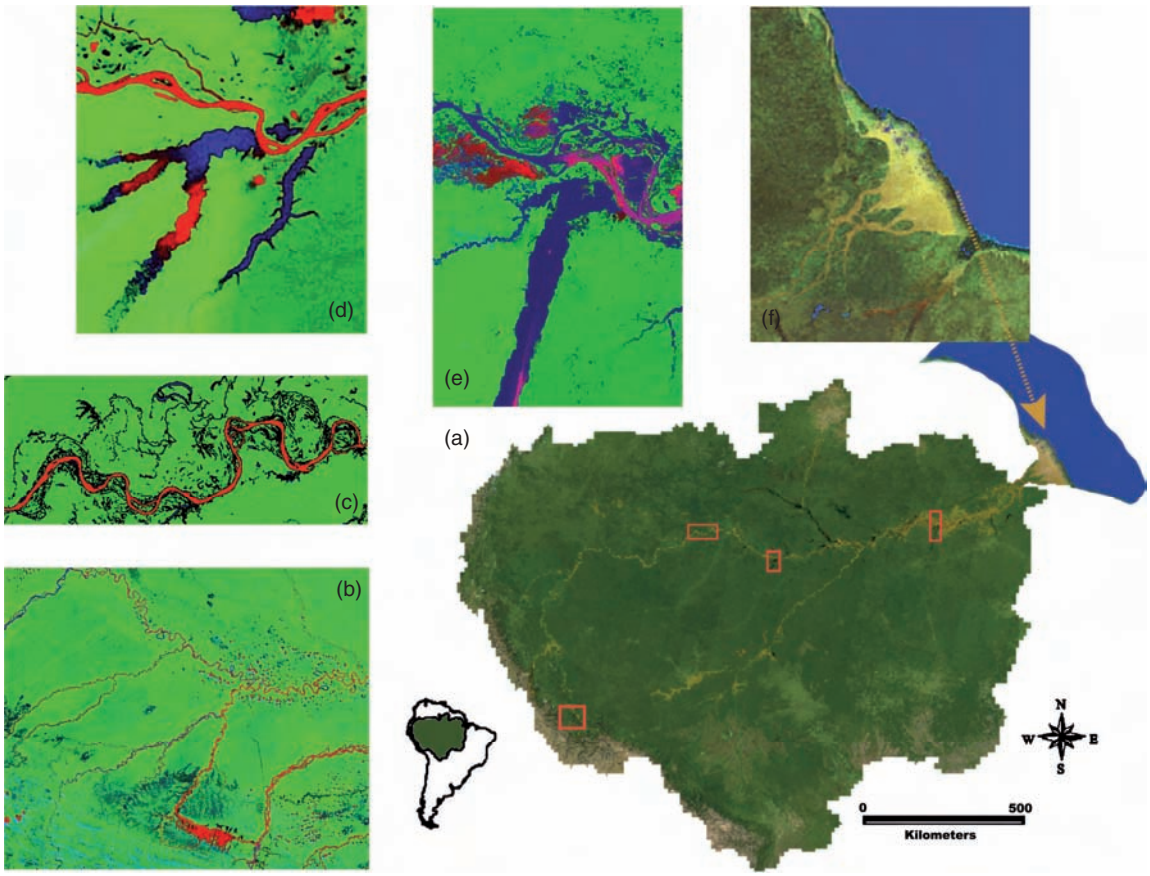

Figure 8.2 Regional patterns of channel-floodplain and coastal properties. Processed remote sensing images of Amazon Basin derived from MODIS (a and f) true-colour composite and Landsat TM and ETM (b–e). Processing for the Landsat data involved application of spectral mixture analysis (Adams *et al*., 1995) yielding landscape gradients among turbid water (red to purple), clear water (blue) and tropical forest (green and blue-green). (a) True-colour MODIS image shows the basin boundary and locations in clockwise rotation (downstream) from most western site for images (b)–(d). The confluence of the Negro River with the Solimões River creating the Amazonas River can be observed as the large black water river between the boxes delineating images (d) and (e). (b) Assembly of rivers flowing off the eastern slope of Andes. The large meandering tributary flowing NW to SE is the Madre de Dios River, one of the larger tributaries to the Beni River and eventually the Madeira River. Other rivers exhibit braiding and oxbow lakes associated with intensive bar formation and channel migration. The bright red colour indicates high turbidity in all of the channels. The large rectangular red area near the base of the mountain front indicates the location of extensive thinly vegetated or bare alluvium, probably in the form of substantial floodplain and fan deposits that extend for 10–20 km. (c) The most sinuous reach in the Brazilian Amazon (Mertes *et al*., 1996) showing remarkable large-amplitude bends and complex intersections of floodplain channels. The complex scroll topography is representative of large areas of the central Amazon floodplain in Brazil. In the north-central portion of the image the only oxbow on the central Amazon that is scaled to the main channel bend size (30–40 km across) can be observed as a very clear (blue) lake. An oxbow in the making is observed in the modern cutoff developing at the Fonte Boa bend, the most eastern meander on the image. The former floodplain channel on the south side of this bend has been actively capturing more water over at least the past 150 years according to historical accounts of the position and nature of this channel. Earlier accounts (Bates, 1864; Herndon, 1853) indicate that the main channel of the river flowed around the sharp bend and that the small town of Fonte Boá was 1.2 km from the main river on a narrow and slowly migrating side channel. The main channel has now migrated more rapidly towards the town and the side channel has widened, requiring dismantling of some of the Fonte Boa water front in the 1980s. (d) Coari Lake with the Amazon River cutting across the former mouth of the Coari River (at 4°8′S 64°50′W) due to an avulsion that formed the relatively sharp bend with the single island in the middle of the lake. The avulsion occurs at the eastern end of a south-trending tilted zone, first described by Tricart (1977). Turbid water can be observed entering the lake at the upstream ends of the three larger branches. The river is straighter in this section than upstream, the scroll-bar topography of the floodplain becomes smoother, and lakes increasingly become rounder downstream. (e) The mouth bay of the Tapajós River showing the NE–SW trending fracture pattern and also the tremendous size (tens of km across) of a ria lake. The surface sediment concentrations in the Amazon main channel are lower (darker red and tending towards purple) in this downstream image than in (b)–(d). The river is anastomosing through this reach and large round lakes on the floodplain can be differentiated from ria lakes and the smaller, narrower lakes observed upstream. (f) The delta region of the Amazon River showing the transfer of the sediment plume (orange-brown) nearly 100 km out to sea. Also visible is the northerly dispersion of the sediment plume due to tidal circulation and wave action. In the SW corner of the image a black rectangle indicates the location of the ria lake at the mouth of the Xingú River

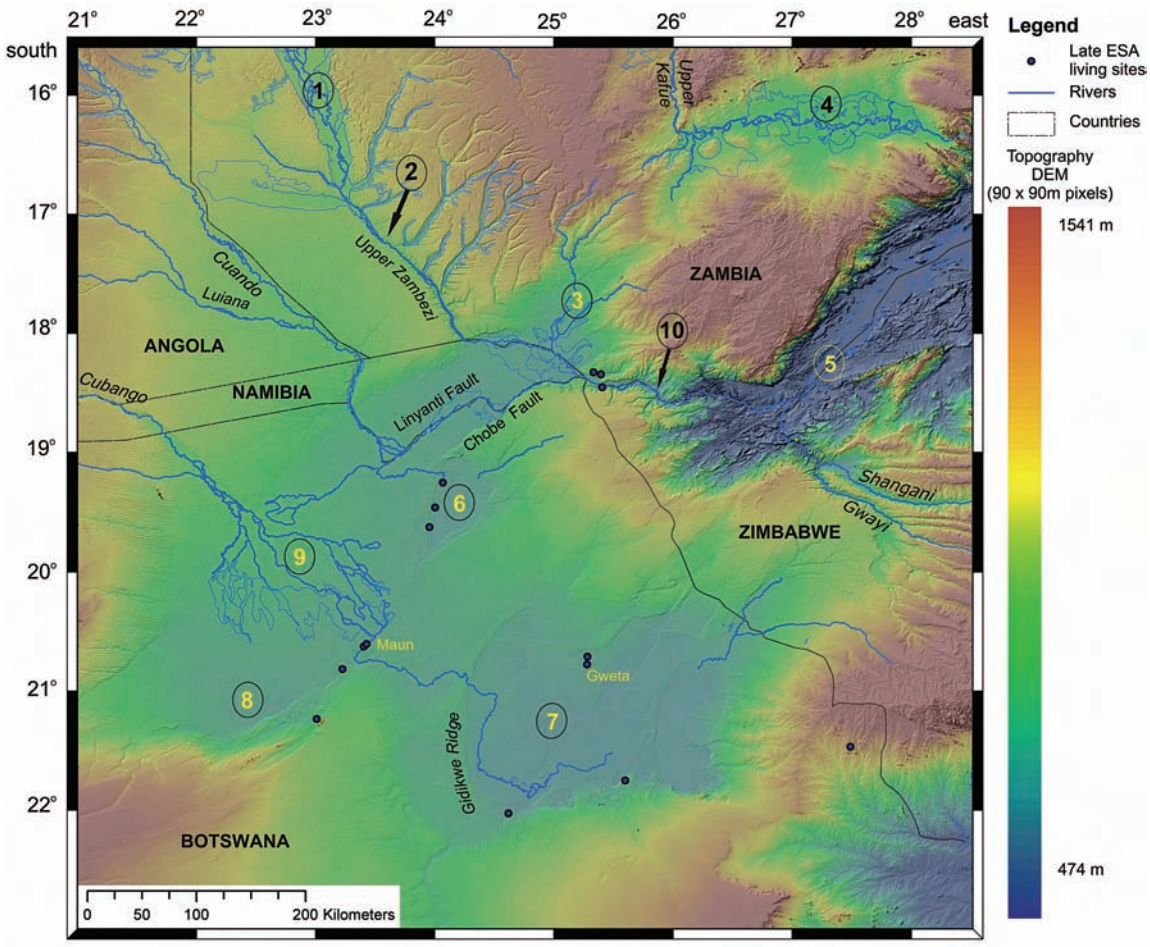

Figure 15.15 DEM image illustrating the subdued topography extending from the Machili Flats, across the line of the Upper Zambezi River, south-west into the area formerly covered by the greater Palaeo-Lake Makgadkigadi. This reflects alluvium supplied by the upper Chambeshi-Kafue system, which was formerly linked to the Upper Zambezi via the Machili Flats. Locations: 1, Barotse Floodplain; 2, Ngonye (Sioma) Falls; 3, Machili Flats; 4, Kafue Flats, formerly occupied by Pleistocene Lake Patrick; 5, Gwembe Trough (Lake Kariba); 6, Mababe depression, 7, Makgadikgadi depression; 8, Ngami depression; 9, Okavango Delta; 10, Victoria Falls. Early Stone Age (ESA) living sites (Robbins and Murphy, 1998; McFarlane and Segadika, 2001) in the Makgadikgadi Basin depicted by circles

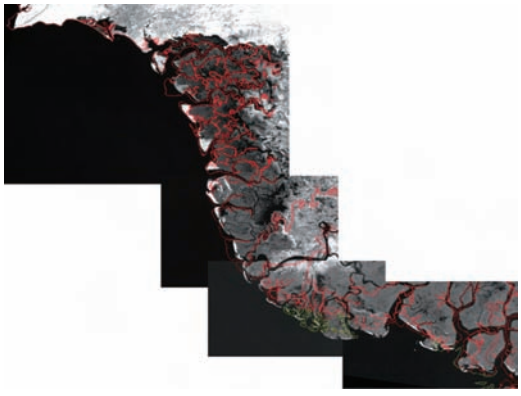

Figure 16.11 Satellite image of the Indus Delta in 2000 showing how the coast has changed since 1950. The coast in 1950 is shown as a red line, with yellow depicting sand bars developed near the mouth (unpublished, Stefan Constatinescu, University of Bucharest, Romania). (Image from NASA Visible Earth)

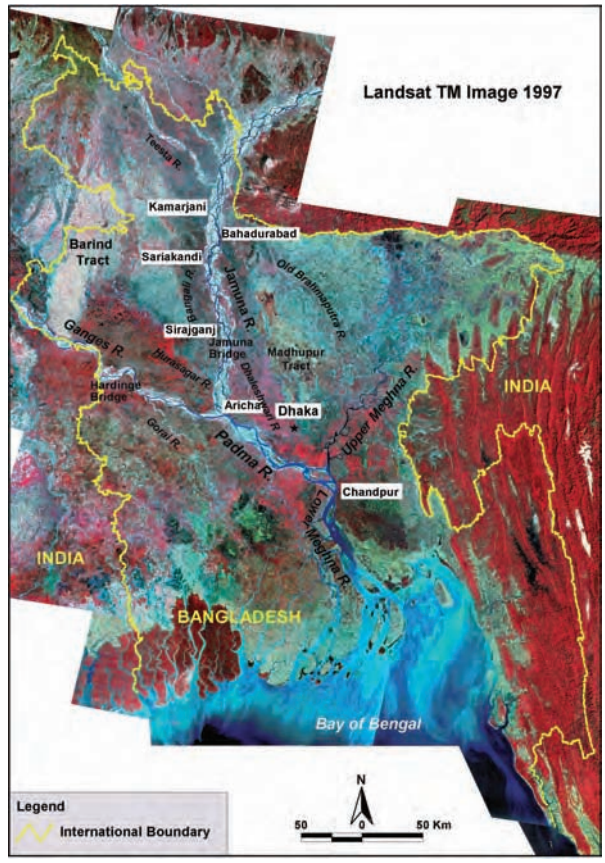

Figure 19.1 Landsat image of Bangladesh, showing the Brahmaputra-Jamuna, Ganges and Meghna Rivers, together with the major features and towns referred to in this chapter

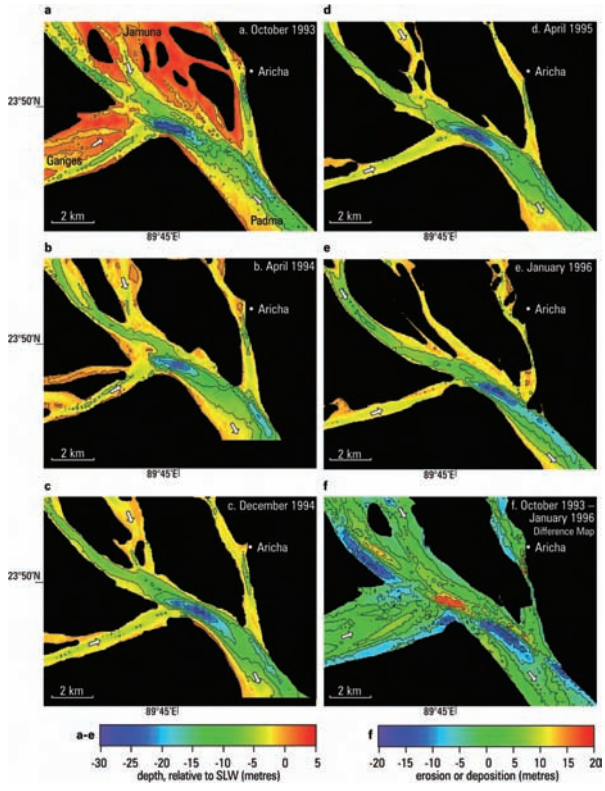

Figure 19.19 Plots of bed morphology and channel change at the junction of the Jamuna and Ganges Rivers. Reprinted by permission from Macmillian Publishers Ltd: Nature, Vol. 387, Best, J.L. and Ashworth, P.J., Scour in large braided rivers and the recognition of sequence stratigraphic boundaries, pp. 275–277, 1997

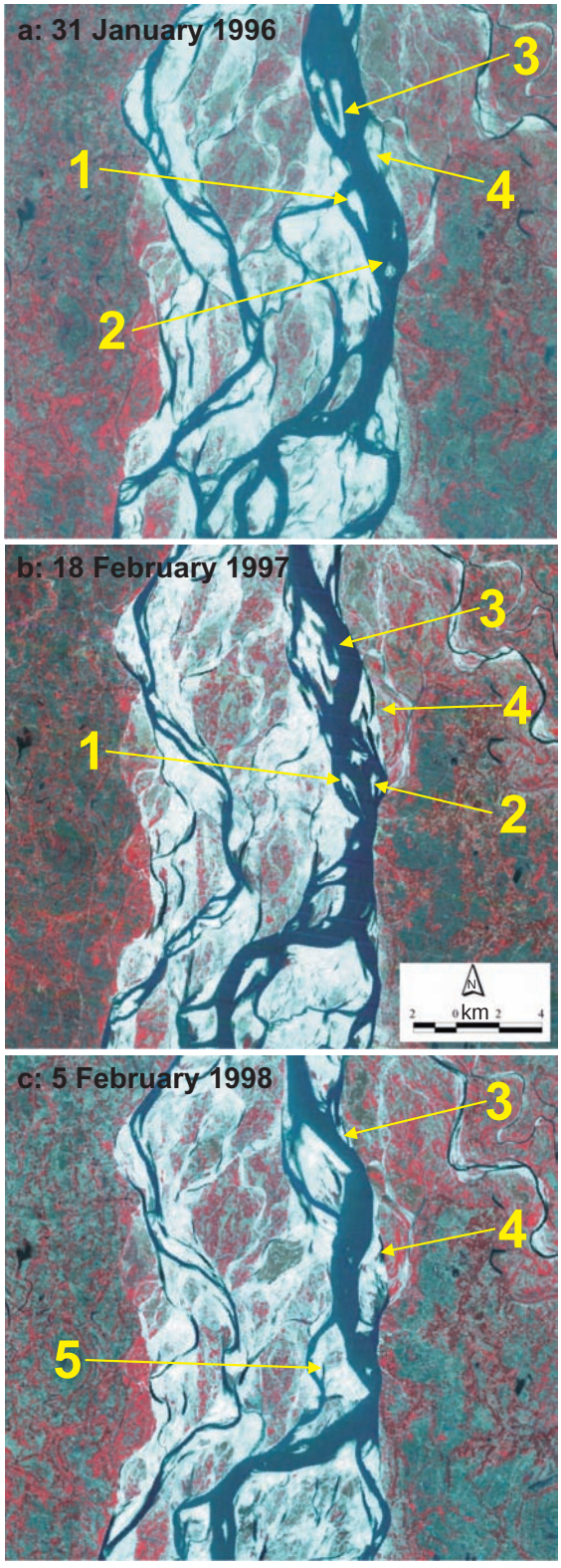

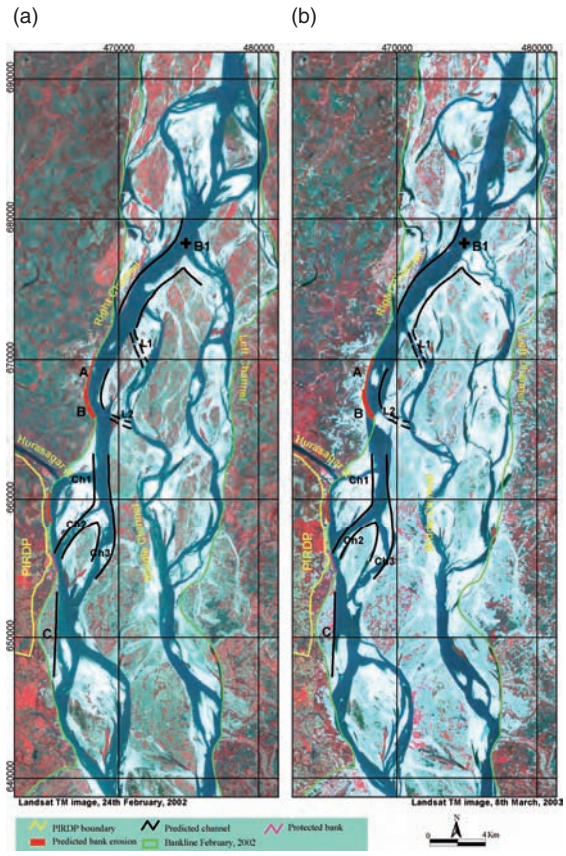

Figure 19.29 Satellite images of the Jamuna River at the PIRDP site near the confluence with Hurasagar River taken in (a) February 2002 and (b) March 2003, showing the predicted channel and bankline changes (a) and the resultant changes after the flood season (b) (see also Table 19.2). Reprinted from EGIS, Satellite images of the Jamuna River at the PIRDP site near the confluence with Hurasagar River taken in February 2002 and March 2003, showing the predicted channel and bankline changes and the resultant changes after the flood season, with permission from CEGIS

Figure 19.16 Morphological evolution of the reach studied by Ashworth *et al*. (2000) at Bahadurabad: (a) January 1996 (which represents stage 6 in Figure 19.15); (b) February 1997; (c) February 1998

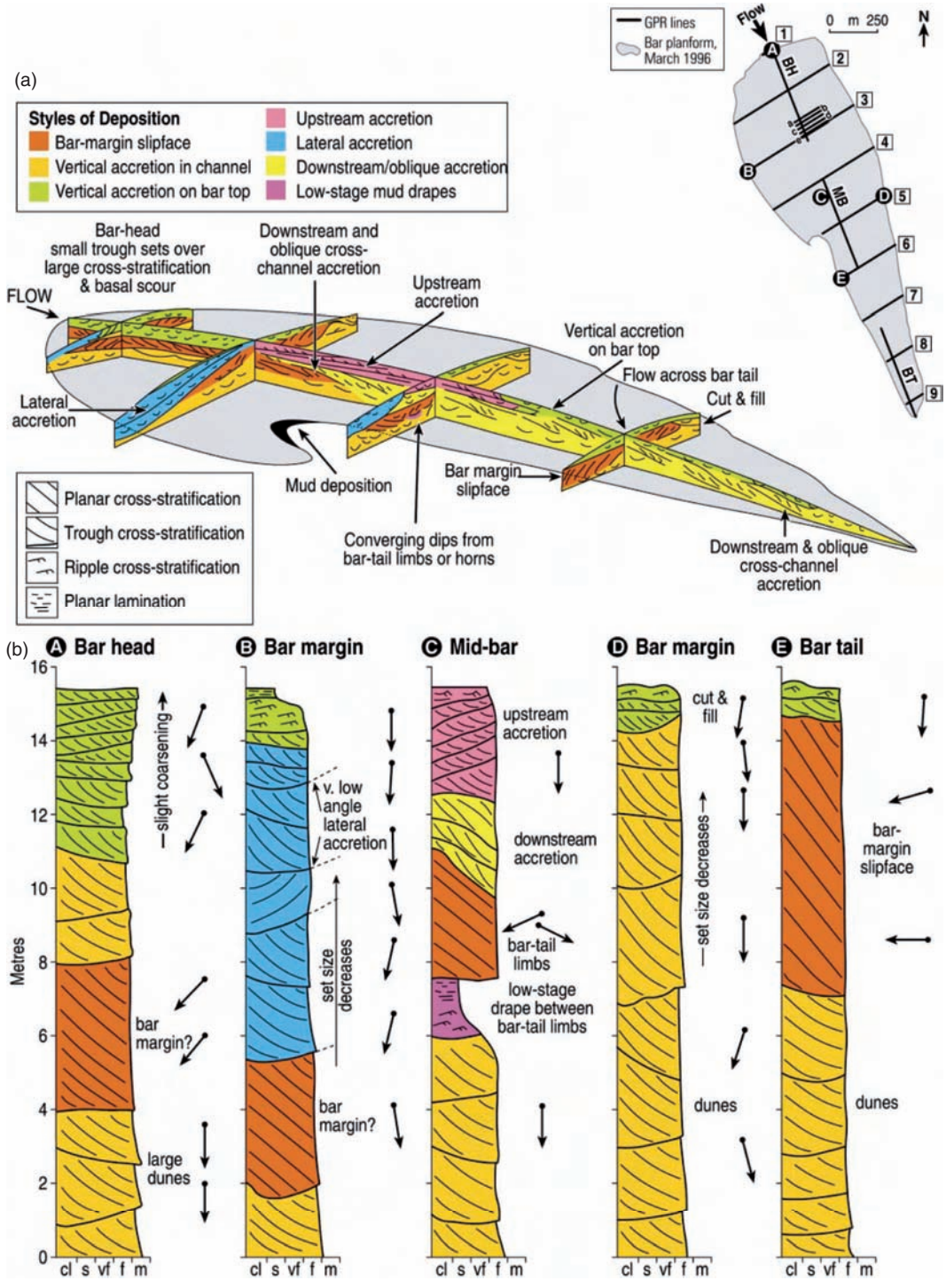

Figure 19.23 Styles of deposition and vertical facies profiles for a mid-channel bar in the Jamuna River. (a) Three-dimensional diagram of the principal styles of deposition quantified within the Jamuna braid-bar (see text for details). The scale of the bar is 3 km long, 1 km wide and 12–15 m high. The different styles of deposition are coloured and the main sedimentary structures are labelled. (b) Schematic sedimentary logs at five localities within the large braid bar (see inset for location), illustrating the characteristic sedimentary structures, large-scale bedding surfaces, and styles of deposition (see a). Arrows depict the approximate flow directions for sedimentary structures at various heights in each profile, with flow down the page (e.g., profile A, bar head at 2 m) indicating flow parallel to the mean flow direction (see arrow on inset location map). Deviations in flow from this direction are shown, such as the oblique, cross-channel movement of the bar-margin slipface (e.g. profile E, bar-tail at 8.5 m). Reprinted from Journal of Sedimentary Research, Vol. 73, Best *et al*. Three-dimensional sedimentary architecture of a large mid-channel sand braid bar, Jamuna River, Bangladesh, pp. 516–530, 2003, with permission from SEPM (Society for Sedimentary Geology)

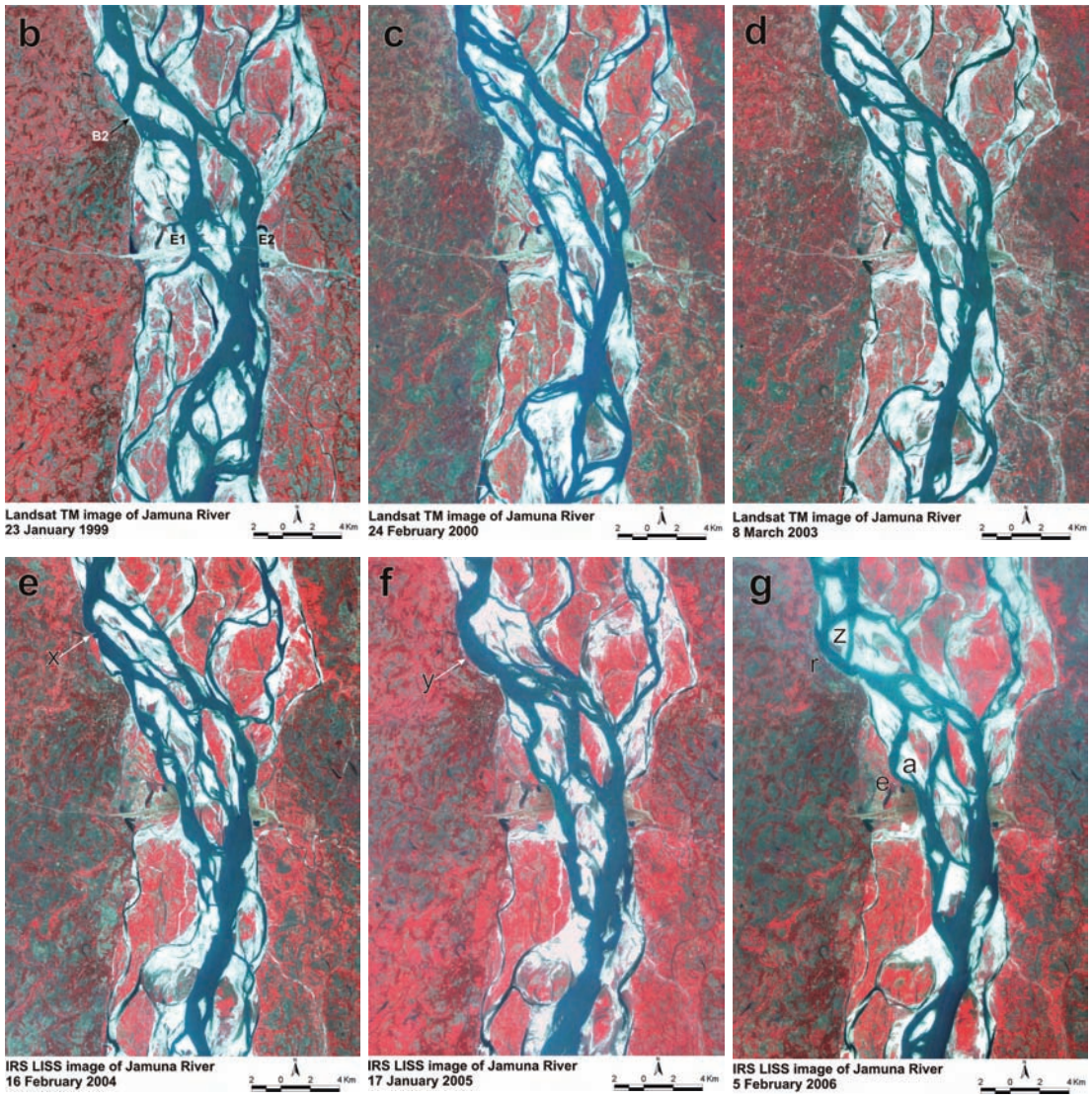

Figure 19.26 (b)–(f) The Bangabandhu Bridge site at (b) low flow 1999 after bridge completion; (c–f) development of the channel morphology during 2000–2005. In (b), labels E1 and E2 refer to the arcuate embankments, termed 'guide bunds', upstream of the Bangabandhu Bridge, and label B2 indicates the nose of the B2 hardpoint at Sirajganj. Label x in (e) points to the groyne at Shailabari that was eroded during the 2004 flood, and subsequently led to extensive erosion of the west bank in this vicinity (see label y in f). Label a in (g) and (h) indicates lateral accretion and bar growth that is causing erosion (labelled e) of the western channel bank. In (g) and (h), label z points to the mid-channel bar growth and lateral accretion upstream of the B2 structure that is causing bank erosion (labelled r)

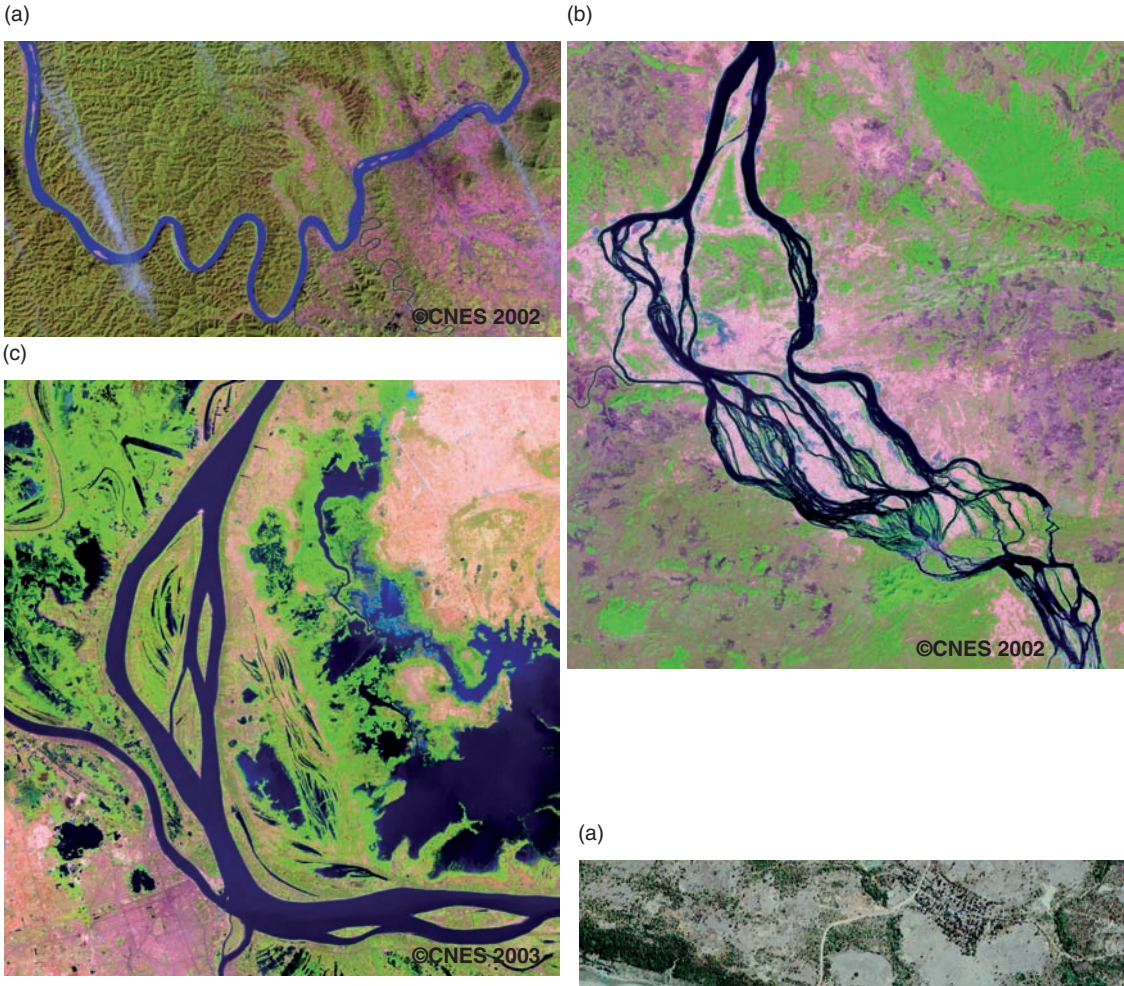

Figure 20.10 Illustrations of selected river units. (a), (b) and (c) from SPOT 5 images ©CNES and reproduced by CRISP (Singapore) under license from SPOT IMAGE ®. (a) Units 1b(left), 1c (middle) and 1d (right). Reprinted from Geomorphology, doi:10.1016/j.geomorph.2006.03.036, Avijit Gupta, S.C. Liew, 'The Mekong from satellite imagery', Copyright (2007), with permission from Elsevier. (b) Anastomosed channel in basalt, the 4000 islands, unit 5. Reprinted from Geomorphology, doi:10.1016/j.geomorph.2006.03.036, Avijit Gupta, S.C. Liew, 'The Mekong from satellite imagery', Copyright (2007), with permission from Elsevier. (c) Free-moving Mekong in unit 7. Reprinted from Geomorphology, doi:10.1016/j.geomorph.2006.03.036, Avijit Gupta, S.C. Liew, 'The Mekong from satellite imagery', Copyright (2007), with permission from Elsevier

Figure 20.12 (a) Satellite image of a large U-bend in the Mekong (unit 3). Reprinted from Geomorphology, doi:10.1016/j.geomorph.2006.03.36. Avijit Gupta, S.C. Liew, The Satellite imagery, Copyright (2007), with permission from Elsevier. (b) Map of the Mekong channel bend in unit 3 (from Gupta, 2004). Depths generalized from Mekong River Commission (1996–99), *Hydrographic Atlas*, Mekong River Commission, Bangkok

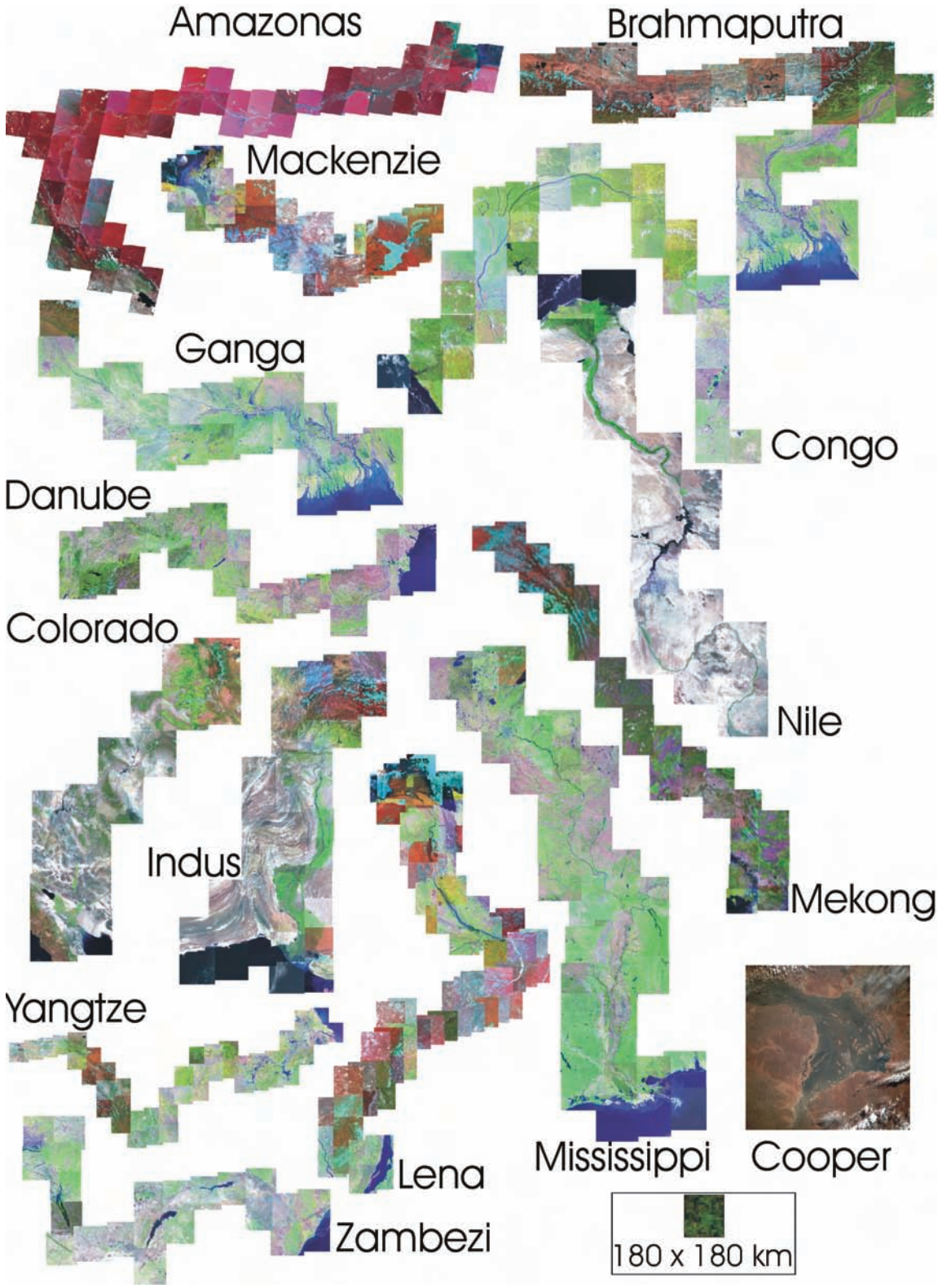

Figure 25.4 Landsat mosaics of 14 rivers showing valley configuration along the course of the main river channels. Each of the rivers represented in Figure 25.3 is shown here assembled from Landsat image colour composites. Each of the individual Landsat pieces is approximately 180 × 180 km. The mosaics were assembled by undergraduate students at the University of California, Santa Barbara. The Cooper River image (Australia) is a NASA space shuttle image showing flooding during November 1989. (Image courtesy of NASA)

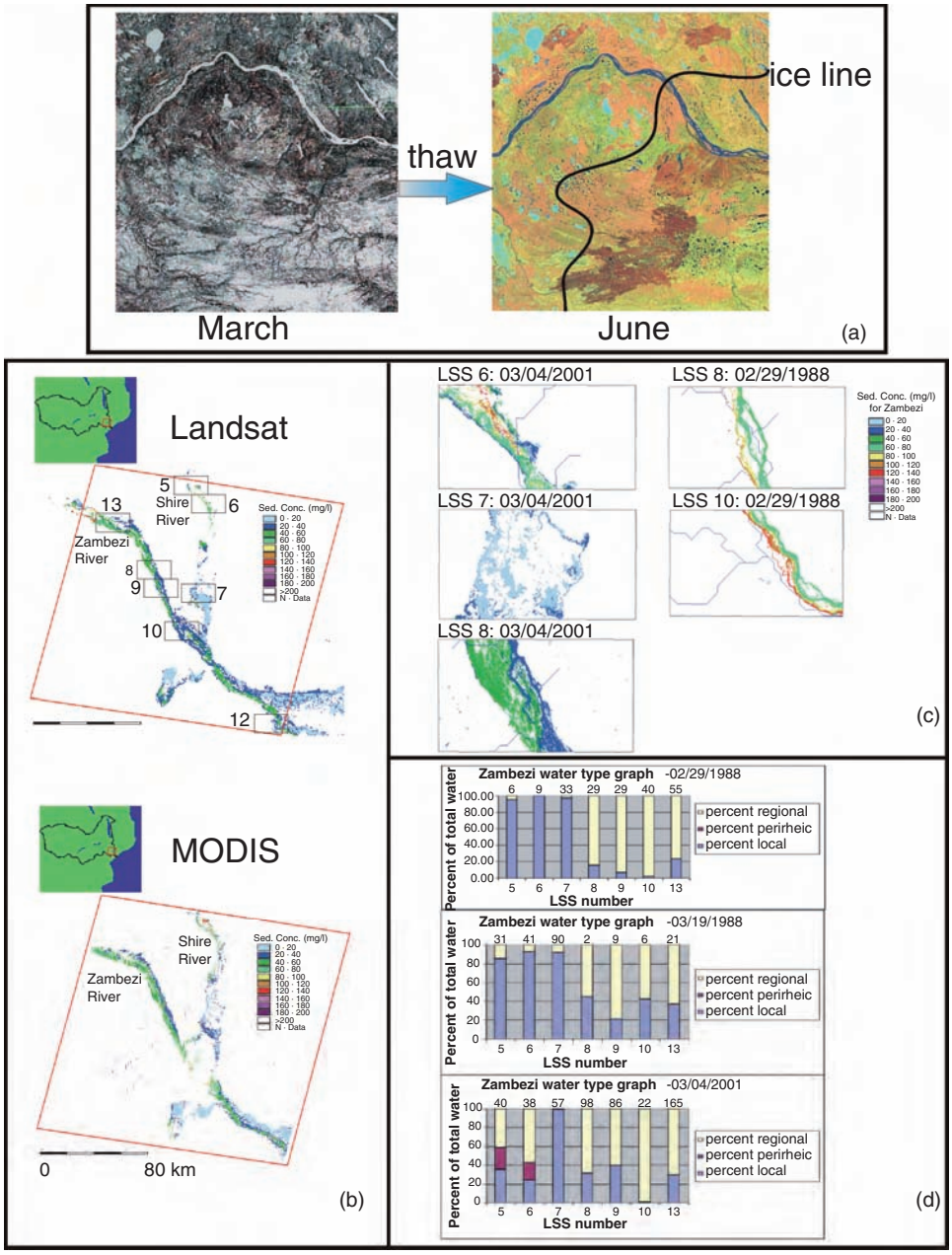

Figure 25.9 Examples of analyses of water properties using Landsat data. (a) Simple analysis of Landsat color composites to show progression of thaw across riverine landscape of Mackenzie River. Image on left shows winter conditions while June image on right (color composite of red, green, and blue applied to Landsat bands 5, 3, and 4, respectively) is used to show position of the ice line marked at the boundary between frozen lakes (light blue) and thawed lakes (dark blue). (b) Comparison of calculation of surface sediment concentration from Landsat and MODIS data for lower Zambezi River. Data shown for 4 March 2001 for both images and surface sediment concentrations are in milligrams per liter. The red box outlines the approximate extent of the Landsat image positioned at path/row 167/72. Numbered rectangles are locations of study sites for which data are shown in (c) and (d). Using the algorithm structure of spectral mixture analysis (Mertes *et al.*, 1993, 2004), these results show that with proper expression of laboratory data, sediment concentration results from different remote sensing instruments are identical. (c) Detail of areas shown in (b) for different dates as derived from Landsat images. Blue lines show the location of theoretical stream channels derived from a morphometric analysis of the GTOPO 30 DEM. (d) Water type graphs for three different flood periods for study sites 5–10 and 13 on Lower Zambezi River as derived from Landsat data. The range of concentrations are for the regional (>60 mg l^{-1}), perirheic (40–60 mg l^{-1}, only for 4 March 2001) and local water (0–60 mg l^{-1} except for 4 March 2001 when 0–40 mg l^{-1}). The study site (LSS) that each bar corresponds to is denoted on the x-axis. The number above each bar indicates the inundated area that was detected within the LSS (in km^2). The LSSs are all rectangular boxes with areas of between 350 and 550 km^2

(a) Stage 1

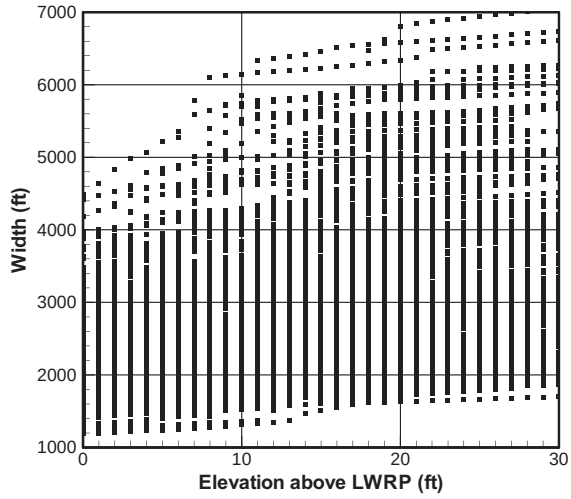

(b) Stage 2

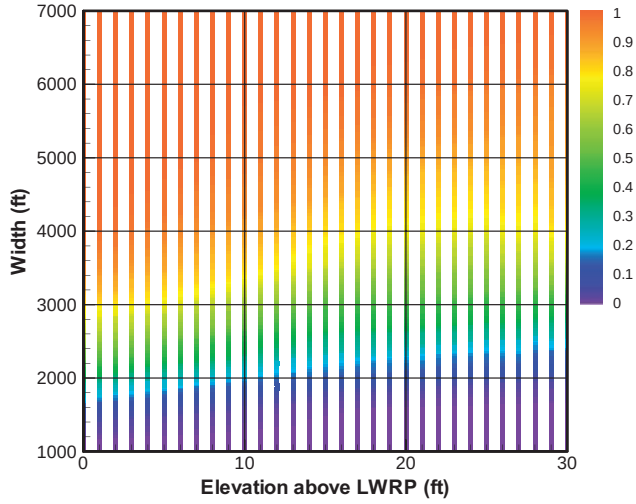

(c) Stage 3

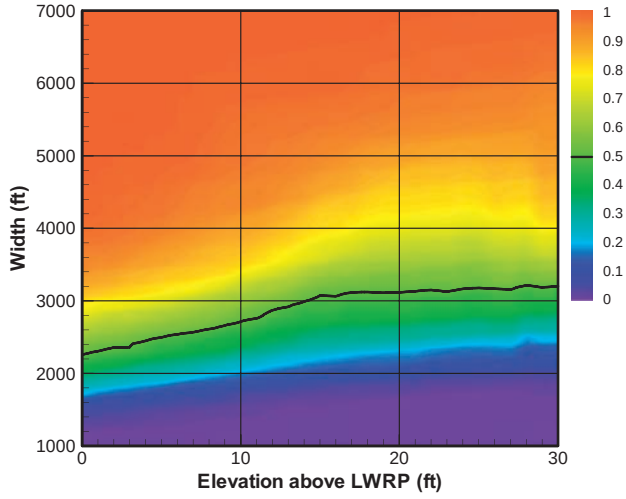

Figure 26.6 Development of cumulative frequency plots of channel geometry variability with elevation above LWRP. (a) Stage 1: plotting data values for each cross-section. (b) Stage 2: assigning probability (0 to 1) and interpolation along the y-axis. (c) Stage 3: interpolation of probability across the remainder of the grid, showing the 50% probability line. The example shown is for width in the 1997 survey

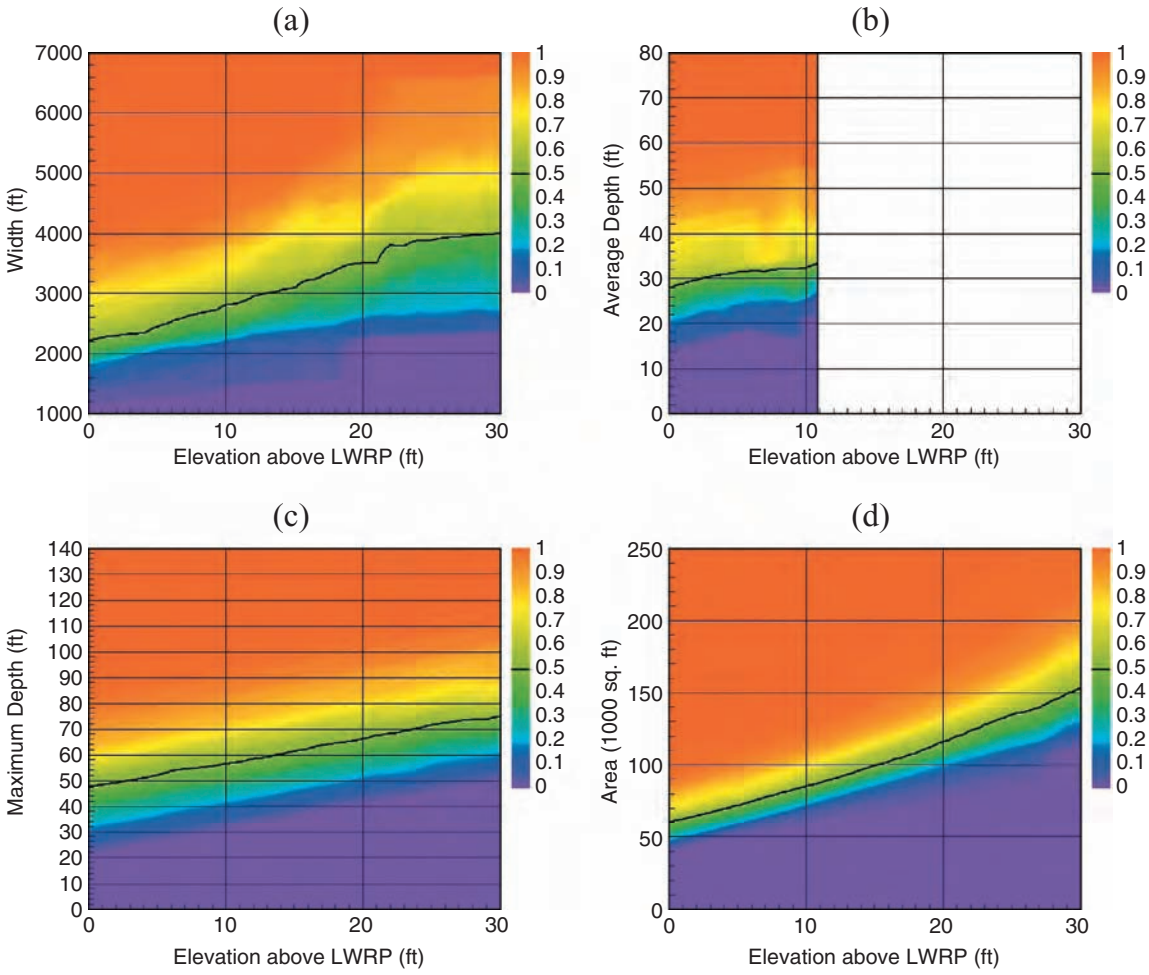

Figure 26.7 Sample results from the probability analysis: (a) width in 2001 for bends; (b) average depth in 1995 for crossings; (c) maximum depth for all sections in 2001; (d) cross-sectional area in 1997 for all sections

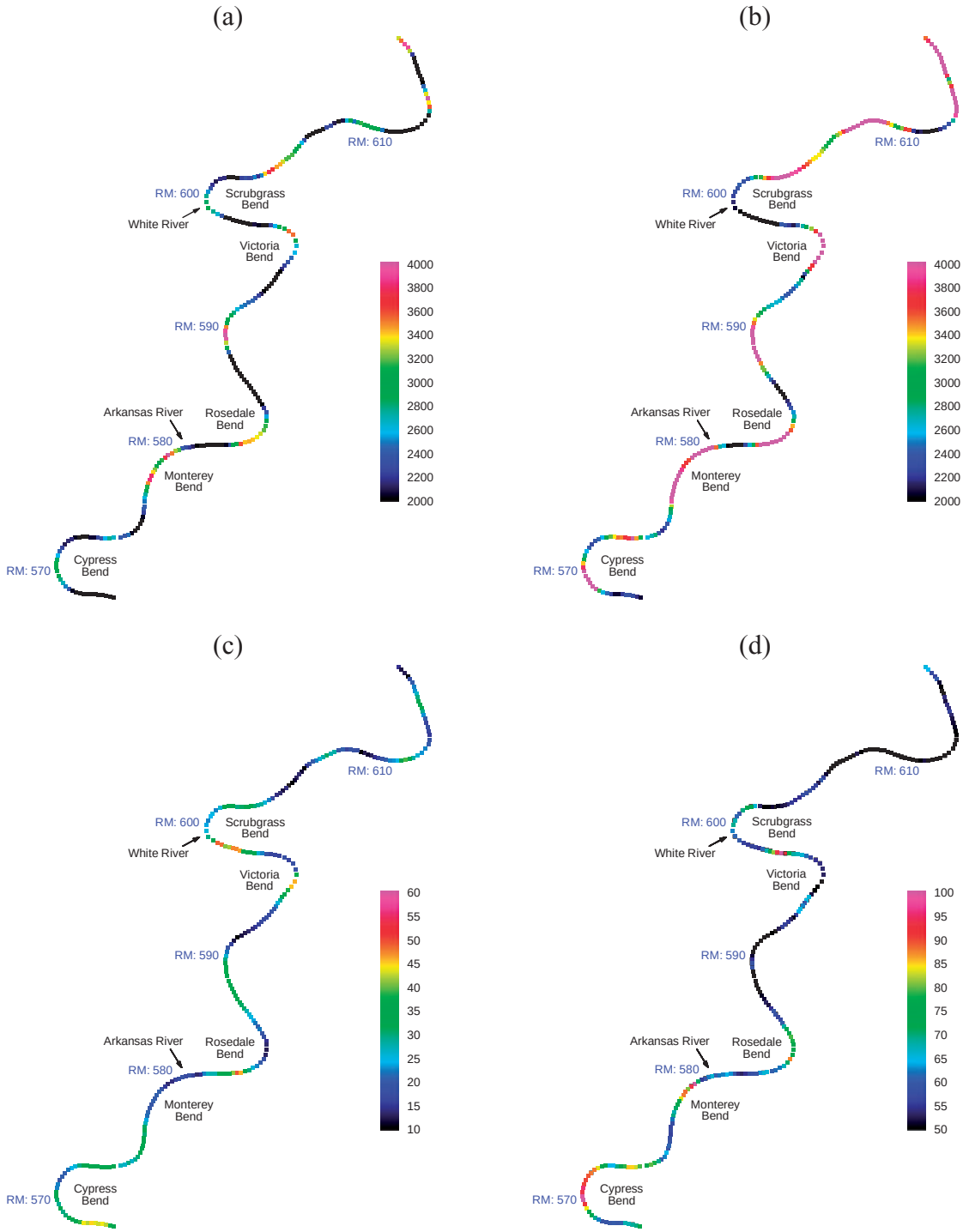

Figure 26.8 Example results from the spatial analysis: (a) width (ft) in 1997 at LWRP; (b) width (ft) in 1997 at 20 ft above LWRP; (c) average depth (ft) in 2001 at LWRP; (d) area (1000 ft^2) in 1996 at LWRP (this plot also shows interpolated values in white)

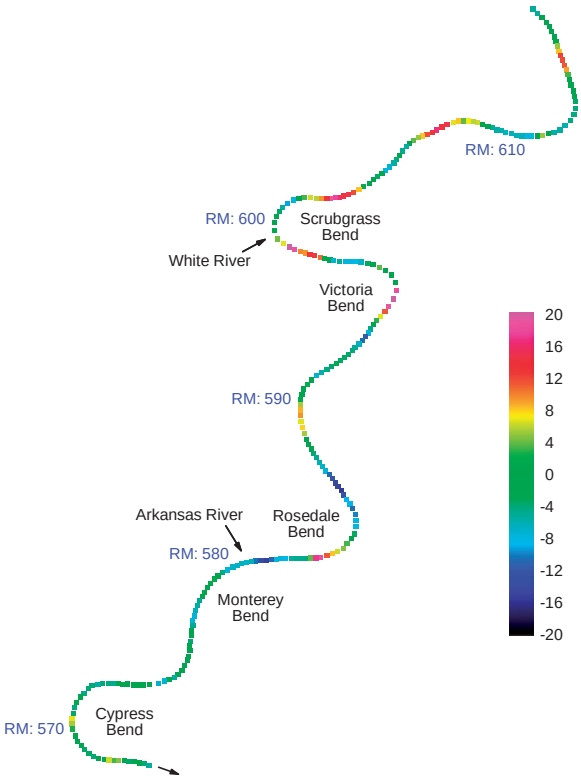

Figure 26.9 Changes in average depth (ft) between 1992 and 2001, indicative of aggradation and degradation

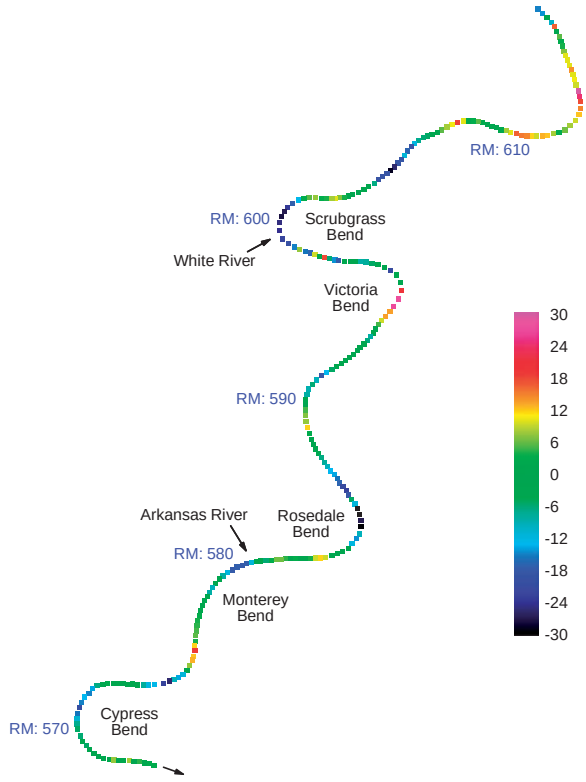

Figure 26.10 Changes in area (1000 ft^2) between 1992 and 2001, indicative of scour and fill

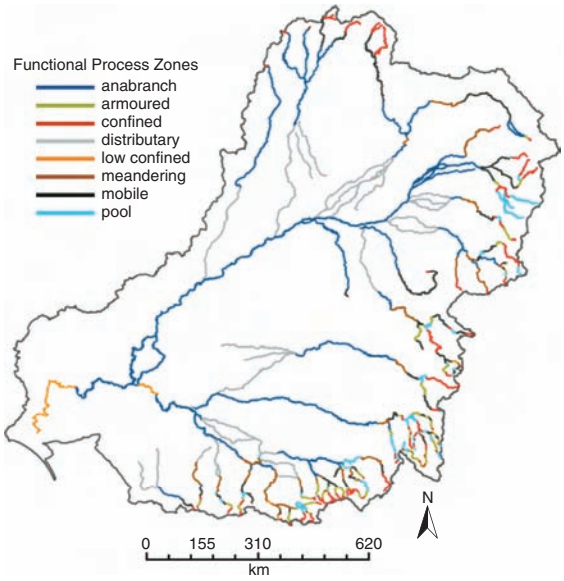

Figure 28.3 The spatial arrangement of functional process zones within the Murray-Darling Basin

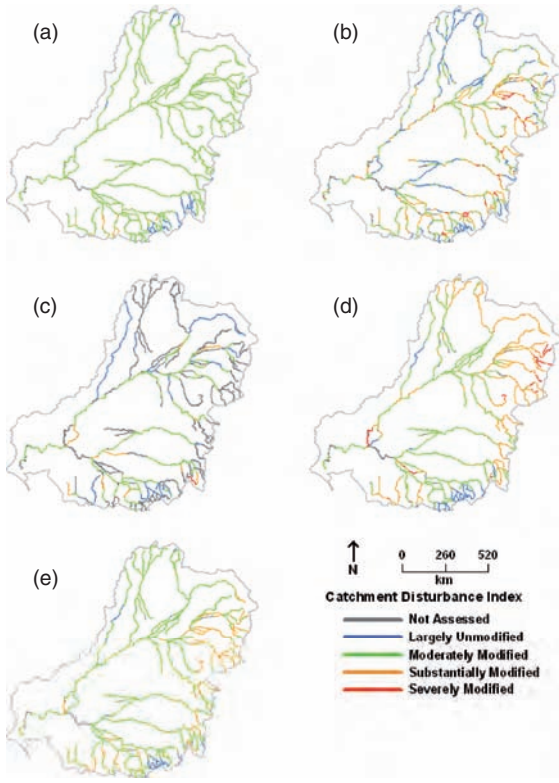

Figure 28.5 The physical condition of rivers within the Murray-Darling Basin according to function process zones: (a) the overall Environmental Index (ARC_e); (b) Catchment Disturbance Index (*CDI*); (c) Habitat Index (*HI*); (d) Hydrological Disturbance Index (*HDI*); (e) Sediment Transport of Nutrient Load Index (*SSNLI*)

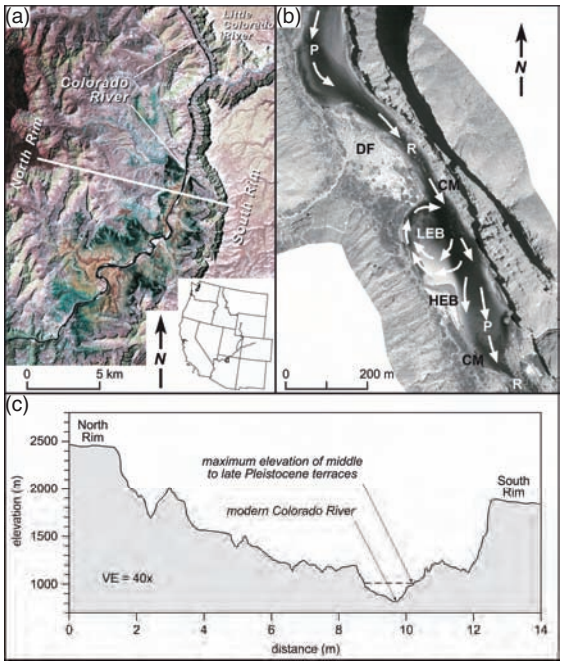

Figure 30.8 (a) Landsat Thematic Mapper image of eastern Grand Canyon. Inset shows the Colorado River drainage basin within the western United States, with small box illustrating location of eastern Grand Canyon reach. (b) Panchromatic aerial photograph of Saddle Canyon, a typical fan–eddy–bar complex of the Colorado River in Marble Canyon. DF, tributary debris fan; R, rapid or riffle; P, main-channel pool; HEB, high-elevation eddy bar; LEB, low-elevation eddy bar; CM, channel-margin deposits. Arrows indicate flow direction. (Courtesy of J. Hazel Jr; adapted from Hazel *et al*., 2006). (c) Topographic profile across eastern Grand Canyon, from north rim to south rim, illustrating position of late Pleistocene terraces within the deeply incised canyon. Location of profile shown in (a). Taken from USGS 7.5 min DEMs

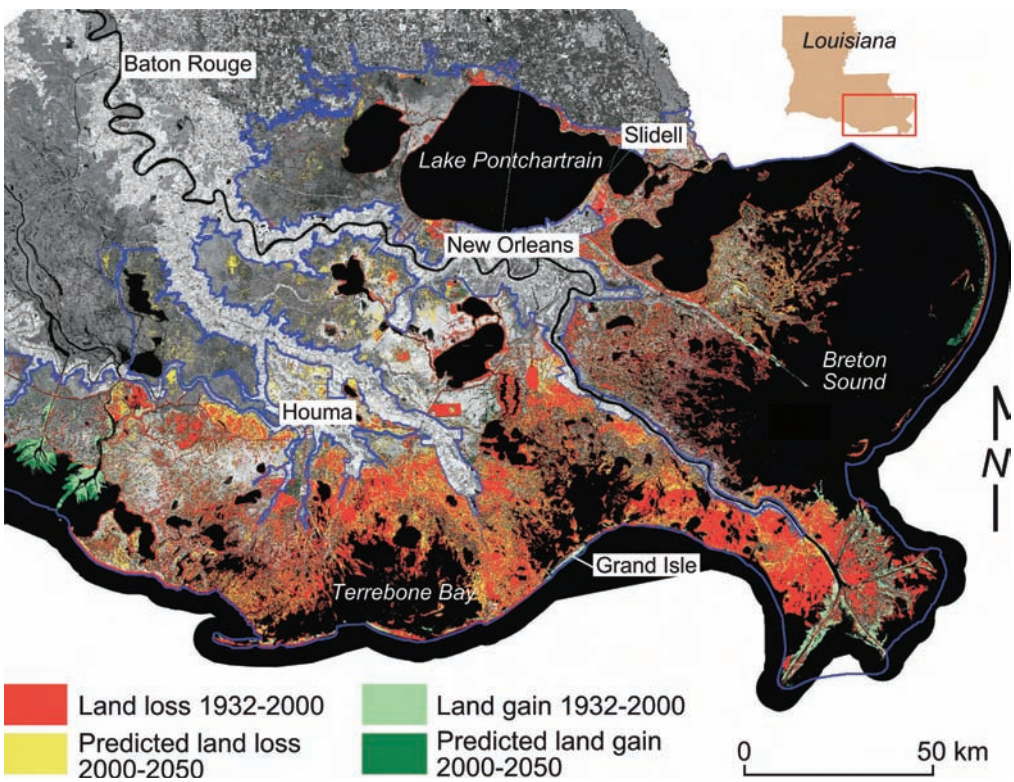

Figure 30.19 Land surface gains and losses in lower Mississippi delta region, 1932–2000 and predicted for period 2000–2050. Blue line indicates limits of land change study area. Adapted from United States Geological Survey (2003) Map NWRC 2003-02-0373. See also Barras *et al*. (2003)

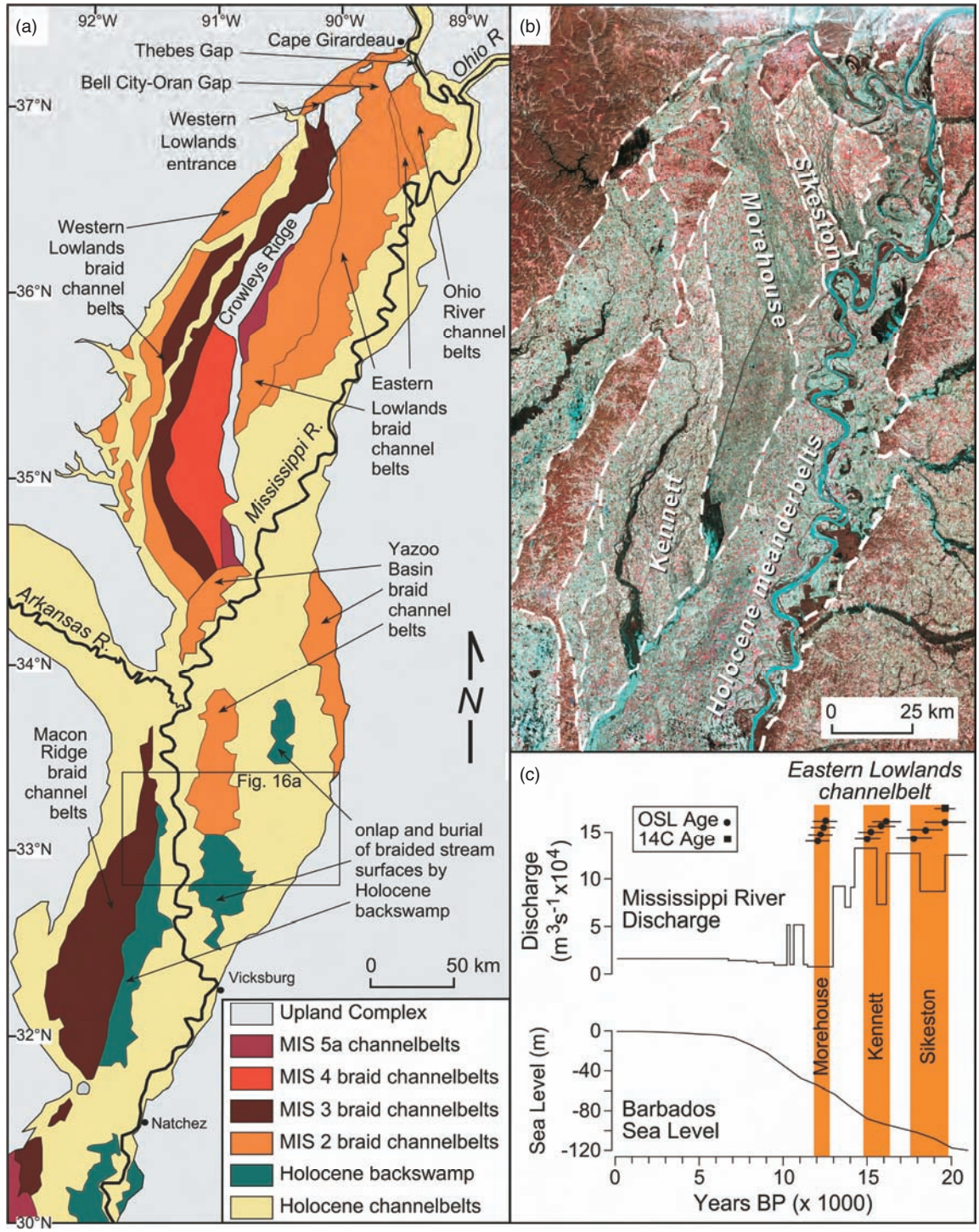

Figure 30.14 The northern lower Mississippi valley and meltwater discharge. (a) Quaternary fluvial deposits and landforms of the lower Mississippi valley. Holocene channel belts are undifferentiated. Updated from Saucier (1994) to include results of optical luminescence dating by Rittenour *et al*. (2005). Area shown as Upland Complex includes both pre-Plio-Pleistocene bedrock, as well as Plio-Pleistocene fluvial gravels, sands, and loess. Late Pleistocene channel belts are also commonly veneered by loess. Deposits of the Arkansas valley are undifferentiated, and include areas of late Pleistocene channel belts as well (Saucier, 1994). (b) Landsat TM image of the northern lower Mississippi valley, illustrating distribution of braided stream surfaces from the last glacial maximum and subsequent period of deglaciation. (c) Correlations between time periods of braided channel-belt construction (orange), meltwater discharge through the lower Mississippi valley, and glacio-eustatic sea-level rise (modified from Rittenour, 2004). Mississippi River discharge estimates from Licciardi *et al*. (1999). Barbados sea-level record from Bard *et al*. (1990)